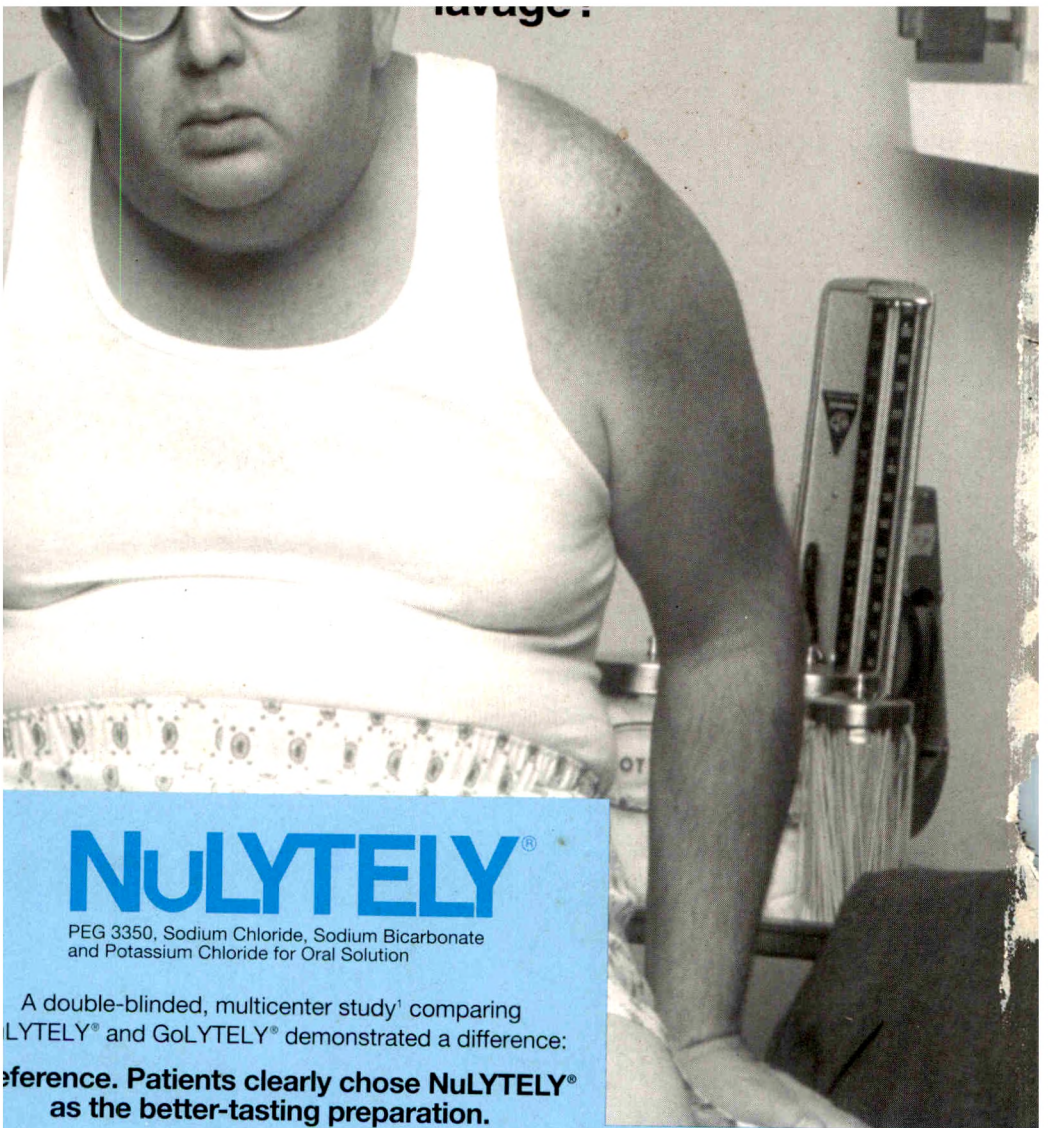
WX - H01766 - 40 - P024467

WCM

AJR

American
Journal of
Roentgenology

July 1992



NuLYTELY®

PEG 3350, Sodium Chloride, Sodium Bicarbonate and Potassium Chloride for Oral Solution

A double-blinded, multicenter study[1] comparing LYTELY® and GoLYTELY® demonstrated a difference:

eference. Patients clearly chose NuLYTELY® as the better-tasting preparation.

lete prescribing information.

ated for bowel cleansing prior

cated in patients with gastro-
ation, toxic colitis or toxic

ngs, should be added to the
atients with severe ulcerative

ag reflex, unconscious, or
gitation or aspiration should be
pecially if it is administered via
ating, distention or abdominal
discontinued until the symp-
on is suspected, appropriate
ons before administration of

ADVERSE REACTIONS: Nausea, abdominal fullness and bloating are the most common adverse reactions (occurring in up to 50% of patients) to administration of NuLYTELY. Abdominal cramps, vomiting, and anal irritation occur less frequently. These adverse reactions are transient and subside rapidly. Isolated cases of urticaria, rhinorrhea and dermatitis have been reported with a related drug (GoLYTELY®) which may represent allergic reactions.

CAUTION: Federal law prohibits dispensing without prescription.

STORAGE: Store in sealed container at 25° C. When reconstituted, keep solution refrigerated. Use within 48 hours. Discard unused portion. NDC 52268-0300-01

Manufactured for Braintree Laboratories, Inc. Braintree MA 02184 by Lyne Laboratories, Inc., Stoughton MA 02072.

Reference: 1. Data on file, Braintree Laboratories.

LABORATORIES · INC
Braintree

Official Journal of the American Roentgen Ray Society

AJR

American Journal of Roentgenology
Diagnostic Imaging and Related Sciences

Editor-In-Chief Robert N. Berk, *La Jolla, California*
University of California, San Diego
School of Medicine and Medical Center

Editor Emeritus Melvin M. Figley, *Seattle, Washington*

Associate Editor Karim Valji, *San Diego, California*

Consulting Editors A. James Barkovich, *San Francisco, California*
Edward A. Sickles, *San Francisco, California*

P 24,467

Statistician Charles C. Berry, *San Diego, California*

Editorial Board

Mark E. Baker
Lawrence W. Bassett
Michael A. Bettmann
Ethan M. Braunstein
Felix S. Chew
Horacio R. D'Agostino
N. Reed Dunnick
David K. Edwards
Ronald G. Evens
Sandra K. Fernbach
Richard H. Gold
Edward G. Grant
John R. Hesselink
Emanuel Kanal
Ray F. Kilcoyne
Carolyn Kimme-Smith
Melvyn T. Korobkin
Mark J. Kransdorf
Faye C. Laing
Thomas L. Lawson
Robert G. Levitt
Martin J. Lipton
Bruce L. McClennan
Richard P. Moser
Jeffrey H. Newhouse
Sven J. K. Paulin
David M. Paushter
Vassilios Raptopoulos
Donald L. Resnick
Charles A. Rohrmann, Jr.
Peter M. Ronai
Stuart S. Sagel
Sanjay Saini
Stefan C. Schatzki
William P. Shuman
Edward A. Sickles
Barry A. Siegel
M. Leon Skolnick
Edward T. Stewart
Murali Sundaram
Robert D. Tien

Director of Publications: Susan Brown Cappitelli **Editorial Staff:** Barbara Rose, *managing editor*; Katie L. Spiller, Barbara L. Halliburton, and Janine Anderson, *manuscript editors*; Nancy Rydbeck, *office manager*; Sheri Smith, *administrative assistant*; Linda J. Waggoner, *administrative secretary*

AJR, AMERICAN JOURNAL OF ROENTGENOLOGY (ISSN 0361 803X) is published monthly by the American Roentgen Ray Society, 1891 Preston White Dr., Reston, VA 22091. Annual dues include $50 for journal subscription. Second-class postage paid at Baltimore, MD, and at additional mailing offices. **POSTMASTER**, send address changes (Form 3579) to Subscription Fulfillment, AJR, 428 E. Preston St., Baltimore, MD 21202. Subscription rates $125 ($180 foreign); institutions $135 ($190 foreign); in training $25 ($80 foreign); single copy $18 ($22 foreign). The GST number for Canadian subscribers is 123394371. Airmail rates furnished on request. Indexed by *Current Contents* and *Index Medicus*. Copyright © 1992 by American Roentgen Ray Society.
0361–803X/92$3.00

PERSONAL COMPUTER/LASER VIDEODISC SYSTEM

to assist you in the

diagnosis of Skeletal Dysplasias

A unique collection of 400 Skeletal Syndromes
7000 Illustrations

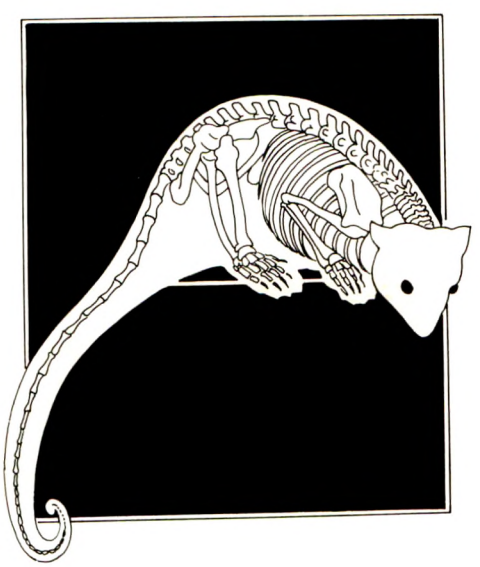
including

- *X-rays*
- *Clinical pictures*
- *Chondro-osseous histology*

OSSUM

AN ILLUSTRATED DATABASE OF SKELETAL DYSPLASIAS

SSUM



for further information contact:

Dr. Agnes Bankier – Medical Geneticist to the successful related POSSUM system.

PO Box 1100 Parkville Victoria 3052 Australia
Phone: (03) 345 5160 Fax: (03) 348 1391

E-Z-EM®

In studies of the colon, accurate, repeatable results are only achieved with precisely mixed, dependably consistent barium suspensions. Single-patient E-Z-DOSE™ kits give you that consistency and save time and money too. They eliminate mess and waste, while they simplify stocking and inventory control. And E-Z-DOSE comes with either a non-latex, silicone-cuffed *or* acorn-shaped retention tip. Discover the efficiency of single-patient liquids. Call your E-Z-EM Distributor or one of our Customer Service Specialists at 1-800-544-4624.

E-Z-EM, Inc.
717 Main Street
Westbury, NY 11590
Tel: 1-800-544-4624
Fax: 516-333-8278

E-Z-EM INTEGRITY • E-Z-EM DEDICATION • E-Z-EM INNOVATION
30 Years of Quality and Service to Radiology
E-Z-EM®

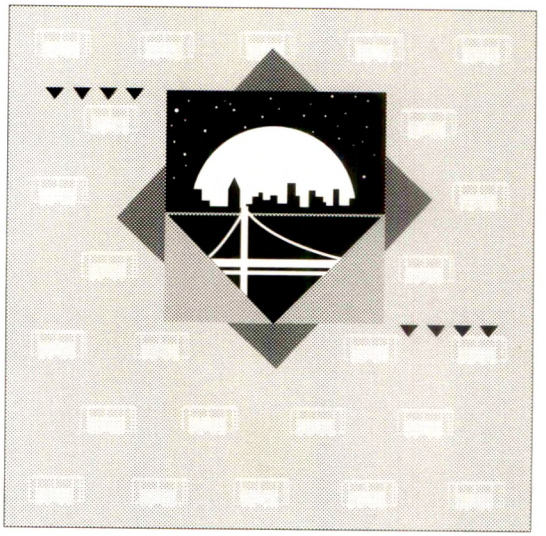
CONSISTENCY IS NO ACCIDENT.



E-Z-DOSE: Catalog Nos. P650PPS (silicone-cuffed tip) and P650PPR (acorn-shaped tip)

E-Z-EM stock is publicly traded on the NASDAQ National Market System under the symbol EZEM. For financial information, contact Investor Relations at 1-800-544-4624, ext. 345.

© E-Z-EM, Inc., 1992



San Francisco

American Roentgen Ray Society
93rd Annual Meeting
April 25–30, 1993

San Francisco Marriott • San Franciso, CA

Time to Renew?

To ensure uninterupted service, please renew your AJR subscription two months prior to the expiration of your current subscription. To avoid renewal notices and price increases, consider a multiyear subscription. Current prices are available for up to three years.

For assistance with your renewal, call TOLL-FREE

1-800-638-6423

(from anywhere in the U.S.)
Or write

AJR Subscription
Fulfillment Department
428 East Preston Street
Baltimore, MD 21202-3993



55th Annual Course

RADIOLOGY/92
Imaging & Intervention:
1992 and Beyond

September 19-23, 1992
(Saturday through Wednesday)
Minneapolis, Minnesota

Presented by
Department of Radiology
University of Minnesota

PROGRAM

Radiology/92 will be a comprehensive course emphasizing: vascular intervention, neuroradiology, musculoskeletal, body imaging, and ultrasound. In order to take advantage of Saturday night stay overs and resultant lower airfares, the course will be held Saturday through Wednesday.

GUEST SPEAKERS

Dennis M. Balfe (St. Louis); Guillermo F. Carrera (Milwaukee); J. William Charboneau (Rochester); George Y. El-Khoury (Iowa City); Glenn S. Forbes (Rochester); Derek C. Harwood-Nash (Toronto); John Huston (Rochester); Clifford R. Jack Jr. (Rochester); C. Daniel Johnson (Rochester); Herbert Y. Kressel (Philadelphia); Richard A. McLeod (Rochester); William D. Middleton (St. Louis); Gary M. Middleton (St. Louis); Gary M. Miller (Rochester); Donald E. Schwarten (Indianapolis).

FEES: $550
$300 (Resident/Fellow, Military, VA)

ACCREDITATION: 26.25 hours Category 1, AMA

DIRECT INQUIRIES TO: RADIOLOGY/92, Continuing Medical Education, University of Minnesota, 107 Radisson Hotel Metrodome, 615 Washington Avenue S.E., Minneapolis, Minnesota 55414; telephone (612) 626-7600; FAX: (612) 626-7766.

"Equal Educational Opportunity"

Keep It All Together

Easily and Conveniently With Bound Volumes of the *American Journal of Roentgenology*

Keeping up with scientific and technological advances in radiology is more important than ever, and that's why each issue of the *American Journal of Roentgenology* is packed with up-to-the-minute information crucial to you and your practice. **Keep this important resource together for easy reference in convenient and attractive bound volumes.**

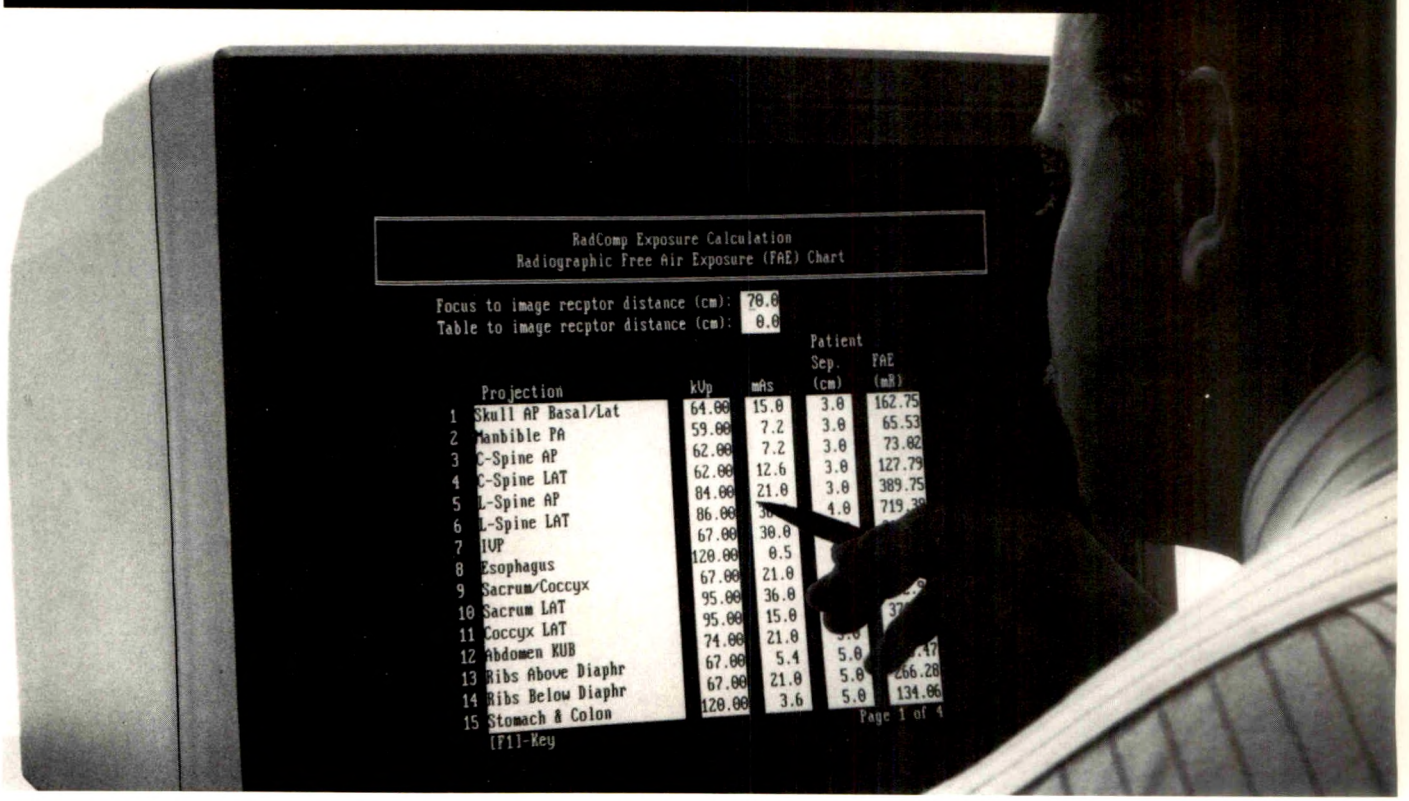


Each edition is imprinted with the year and volume number and contains six issues filled with the kind of vital research, commentary and analysis you've come to expect in the AJR.

For ordering information, contact AJR Subscription Fulfillment Department, 428 E. Preston St., Baltimore, MD 21202-3993, or call toll-free **1-800-638-6423.**

The Problem: HOW TO COMPLY WITH JCAHO REQUIREMENTS. QUICKLY. EASILY. ACCURATELY.

The Solution: THE NUCLEAR ASSOCIATES' RADCOMP X-RAY ENTRANCE SKIN EXPOSURE PROGRAM.



JCAHO Requirement D.R.2.2.10.2 states that you must maintain a table of patient doses (entrance skin exposure ESE) for all the common x-ray procedures you perform...in all of your x-ray rooms...including special procedures such as mammography, where the mean glandular dose should be included. Furthermore, JCAHO stipulates that the techniques employed must be based on measurements performed at a variety of kVp settings.

Now, with the RADCOMP X-Ray Entrance Skin Exposure Program, you can eliminate the enormous time-consuming job that your staff has to go through in order to comply with these requirements. The RADCOMP Skin Exposure Program, when linked with any IBM™ -compatible PC, will generate the required table of patient entrance skin exposures quickly, conveniently and accurately — so you and your staff can concentrate on what you do best... taking care of patients.

RADCOMP is available in two programs: one for x-ray, fluoroscopy, mammography and cine; and one for mammography exclusively. Extensively tested for over seven years, RADCOMP is easy to operate and so accurate that its output matches data published in NCRP 102, thus giving additional credibility to RADCOMP's accuracy.

For a limited time only, we are offering a FREE DEMONSTRATION DISK that shows you how to comply with JCAHO requirements, eliminate all of the tedious, time-consuming calculations you are now doing, and dramatically reduce measurement time.

Send in your request on your letterhead today for your free demonstration disk and Bulletin 4425-44

IBM™, International Business Machines, Inc.

NUCLEAR ASSOCIATES

VICTOREEN

Division of VICTOREEN, INC.
100 VOICE ROAD • P.O. BOX 349
CARLE PLACE, NY 11514-0349
(516) 741-6360 • FAX (516) 741-5414

AJR Guidelines for Authors

Address new and revised manuscripts, correspondence, and classified ads to the Editor:

AJR Editorial Office
2223 Avenida de la Playa, Suite 103
La Jolla, CA 92037-3218
Telephone: (619) 459-2229; FAX: (619) 459-8814

Inquiries regarding reprints or permission to republish *AJR* material should be addressed to the publisher:

Publications Department ARRS
1891 Preston White, Dr., Reston, VA 22091

The *AJR* publishes original contributions to the advancement of medical diagnosis and treatment. Submitted manuscripts should not contain previously published material and should not be under consideration for publication elsewhere.

Manuscript decisions are based on peer review. Reviewers receive manuscripts without title pages to ensure an unbiased review. Statements made in the article, including changes made by the Editor or manuscript editor, are the responsibility of the author and not of the *AJR* or its publisher. Authors will be sent the edited manuscript, galley proof, and proofs of illustrations. If the corresponding author will be unavailable to review galleys, arrangements should be made for a coauthor or colleague to read and return the proof.

The following guidelines are based on instructions set forth in the **Uniform Requirements for Manuscripts Submitted to Biomedical Journals** (*Ann Intern Med* **1988;**108:258–265). Articles will be edited, however, to conform to the individual style of *AJR*.

General Guidelines for Major Papers

Abstract. Clearly state (in 250 words or fewer) the purpose, methods, results, and conclusions of the study. Include actual data.

Introduction. Briefly describe the purpose of the investigation and explain why it is important.

Methods. Describe the research plan, the materials (or subjects), and the methods used, in that order. Explain in detail how disease was confirmed and how subjectivity in observations was controlled.

Results. Present results in a clear, logical sequence. If tables are used, do not duplicate tabular data in text, but do describe important trends and points.

Discussion. Describe the limitations of the research plan, materials (or subjects), and methods, considering both the purpose and the outcome of the study. When results differ from those of previous investigators, explain the discrepancy.

AUTHOR'S CHECKLIST

For priority handling, complete the following checklist, sign the copyright form on the reverse side of this page, and include both with the manuscript.

_____ Two copies of the manuscript (the original and a photocopy) and two complete sets of figures are submitted. One copy has been retained by the author.

_____ If appropriate, *AJR* Guidelines for case reports, technical notes, pictorial essays, or letters to the Editor have been followed. (See page A8.)

_____ The manuscript, including references, figure legends, and tables, is typed double-spaced on 8½ × 11 in. (21.6 × 27.9 cm) *nonerasable* paper. Right-hand margins are not justified.

_____ All manuscript pages are numbered consecutively beginning with the abstract. Authors' names do not appear on the manuscript pages.

_____ The manuscript is organized as follows: title page, blind title page (title only), abstract, introduction, methods, results, discussion, acknowledgments, references, tables, figure legends, and figures.

_____ Informed consent has been obtained from patients who participated in clinical investigations. If experiments were performed on animals, authors complied with NIH guidelines for use of laboratory animals.

_____ Use of unfamiliar acronyms and abbrevations is kept to a minimum. When abbreviations are used they are defined at first mention, followed by the abbreviation in parentheses.

_____ Metric measurements are used throughout, or the metric equivalent is given in parentheses.

_____ Names and locations (city and state only) of manufacturers are given for equipment and nongeneric drugs.

_____ Upon acceptance, final version is submitted on a 5 1/4-in. DOS-compatible diskette in Wordperfect or ASCII format.

Title Page

_____ The following information is given: title of article; names and complete addresses (including zip code) of all authors; current addresses of authors who have moved since study; acknowledgment of grant or other assistance. The corresponding author is clearly identified, and a current address, phone number, and FAX number are given.

_____ A blind title page is included in each copy of the manuscript, giving only the title (without the authors' names) for use in the review process.

Abstract

_____ An abstract of approximately one and one-half typewritten pages is organized into the following paragaphs.

Objective. In one or two sentences, indicate the specific goal or purpose of the article, and indicate why it is worthy of attention. Explain the hypothesis to be tested, the dilemma to be resolved, or the deficiency to be remedied. The objective stated here must be identical to the one given in the title and introduction of the paper.

Subjects (or materials) and methods. Describe succinctly the methods used to achieve the objective explained in the first paragraph, stating what was done, how it was done, how bias was controlled, what data were collected, and how the data were analyzed.

Results. The findings of the procedures described in the preceding paragraph are presented here. All results should flow logically from the methods described and not stray from the specific objective of the paper. Include as many specific data as possible within the overall length limitation of one typewritten page.

Conclusion. In one or two sentences, present the take-home message to be remembered when all else is forgotten. Describe the conclusion of the study, based solely on the

data provided in the body of the abstract. Conclusions must relate directly to the objective of the paper as defined in the title and first paragraph of the abstract.

_____ No abbreviations or reference citations are used.

References

_____ References (not to exceed 35) are typed double-spaced starting on a separate page and are **numbered consecutively in the order in which they appear in the text**.

_____ All references are cited in the text and are enclosed in brackets and typed on line with the text (not superscript).

_____ Unpublished data are not cited in the reference list, but are cited parenthetically in the text, for example, (Smith DJ, personal communication), (Smith DJ, unpublished data). This includes papers submitted, but not yet accepted, for publication.

_____ Papers presented at a meeting are not cited in the reference list, but are cited parenthetically in the text (e.g., Smith DJ et al., presented at the American Roentgen Ray Society meeting, May 1990). After first mention, use (Smith DJ et al., ARRS meeting, May 1990).

_____ Inclusive page numbers (e.g., 333–335) are given for all references.

_____ Journal names are abbreviated according to *Index Medicus*.

_____ Style and punctuation of references follow the format illustrated in the following examples (all authors are listed when six or fewer; when seven or more authors, the first three are listed, followed by "et al."):

Journal article

1. Long RS, Roe EW, Wu EU, et al. Membrane oxygenation: radiographic appearance. *AJR* **1986**;146:1257–1260

Book

2. Smith LW, Cohen AR. *Pathology of tumors*, 6th ed. Baltimore: Williams & Wilkins, **1977**:100–109

Chapter in a book

3. Breon AJ. Serum monitors of bone metastasis. In: Clark SA, ed. *Bone metastases*. Baltimore: Williams & Wilkins, **1983**:165–180

Tables

_____ Each table is typed double-spaced on a separate page without vertical or horizontal rules; each has a short, descriptive title. Tables do not exceed two pages in length and contain at least four lines of data.

_____ Tables are numbered in the order in which they are cited in the text.

_____ Abbreviations are defined in an explanatory note below each table.

_____ Tables are self-explanatory and do not duplicate data given in the text or figures.

_____ All arithmetic (percentages, totals, differences) has been double checked for accuracy, and tabular data agree with data given in the text.

Figures and Legends

_____ Two complete sets of original figures are submitted unmounted in labeled envelopes.

_____ Figures are clean, unscratched, 5 × 7 in. (13 × 18 cm) glossy prints with **white borders.** A separate print is submitted for each figure *part*.

_____ All figure parts relating to one patient have the same figure number.

_____ Each figure is labeled on the back with the figure number and an arrow indicating "top." For black-and-white figures, labeling is done on a gummed label, which is then affixed to the back of the print. **Never** use labels on **color** figures, but write figure number on the back lightly in pencil. *Never* use ink on front or back of any figures.

_____ Authors' names are *not* written on the backs of figures.

_____ Only removable (rub-on) arrows and letters are used on the figures. Symbols are uniform in size and style and are not broken or cracked.

_____ Images are uniform in size and magnification.

_____ Line drawings are done in black ink on a white background. They are professional in quality, and all use the same size type. (Only glossy prints are acceptable.)

_____ Written permission has been obtained for use of all previously published illustrations (and copies of permission letters are included), and an appropriate credit line is given in the legends.

_____ Legends are typed double-spaced, and figure numbers correspond with the order in which the figures are cited in the text.

Transfer of Copyright Agreement, Conflict of Interest Acknowledgment, Certification of Coauthors, and Exclusive Publication Statement

Complete copyright to the article entitled: _____

_____

is hereby transferred to the American Roentgen Ray Society (for United States government employees to the extent transferable), effective if and when the article is accepted for publication in the *American Journal of Roentgenology*. In the case of the authors who are officers or employees of the United States government, the American Roentgen Ray Society recognizes that works prepared by officers or employees of the United States government as part of their official government duties are in the public domain.

Authors reserve all proprietary rights other than copyright, such as patent rights and the right to use all or part of this article in future works of their own. The authors retain the right of replication, subject only to crediting the original source of publication and receiving written permission from the publisher.

Authors guarantee that this manuscript contains no matter that is libelous or otherwise unlawful, invades individual privacy, or infringes any proprietary rights.

Authors understand that they will receive no royalty or other compensation from the American Roentgen Ray Society.

Authors guarantee that the editor has been or will be informed of any proprietary or commercial interest or conflicts of interest the authors may have that relate directly or indirectly to the subject of this article.

All authors certify that they have made substantive and specific intellectual contributions to the article and assume public responsibility for its content.

Finally, the authors certify that none of the material in this manuscript has been published previously or is currently under consideration for publication elsewhere.

First author/date	Second author	Third author
Fourth author	Fifth author	Sixth author

This agreement must be signed by all authors in order for the manuscript to be published.

Case Reports

A case report is a brief description of a specia provides a message that transcends the individ

Format. There is no abstract. The introduct be a short paragraph giving the general backg the specific interest of the case. No more thar should be described in detail (similar ones ca tioned briefly in the discussion). Emphasis sh the radiologic aspects; clinical information mus to that necessary to provide a background for ogy. The discussion should be succinct and sh on the specific message and relevance of radio ods. A review of the literature is not appropriat

Length. Maximum of five double-spaced, pages, including the references but not the ti figure legends.

References. Maximum of eight.

Figures. Maximum of four, unless the text is accordingly. Legends must not repeat the text.

Tables and Acknowledgments. Not appropri reports.

Pictorial Essays

A pictorial essay is an article that conveys it through illustrations and their legends. Unlike articles, which are based on original researc essays serve primarily as teaching tools, like e scientific meeting. They are not encyclopedic ters. The abstract should be a short, introdu graph.

Length. Maximum of four double-spaced, pages, including the references but not the ti figure legends.

References. Maximum of four.

Figures. Maximum of 30 figure *parts*. Numbe as few as necessary to convey the message o

Tables and Acknowledgments. Not approp torial essays.

Opinions, Commentaries, and Perspectives

Opinions, commentaries, and perspectives articles dealing with controversial topics or iss cial concern to radiologists.

Format. Include a title page but no abstrac may be used to break up the text.

Length. Maximum of five double-spaced, pages.

References. Maximum of five.

Tables and Figures. Maximum of four.

All submissions to the *AJR* must be acco


OMNIPAQUE
(iohexol)
has a
new
image

Introducing

FLEXIPAK™ (Flexible Container)

A new package for OMNIPAQUE with safety, convenience and flexibility built in



The safety package

New FLEXIPAK makes it simple to purge air from the flexible container before hanging to help reduce the potential for air emboli. The easily spiked port eliminates the possibility of infusing microscopic rubber particles from glass-bottle stoppers. And you don't need an air vent because the soft sides collapse as OMNIPAQUE flows.

The convenience package

No more waste and messy cleanups from broken glass bottles. And, FLEXIPAK is ready and easy to hang, even on crowded IV poles. FLEXIPAK lightens the load from setup to administration and all points in between.

The flexibility package

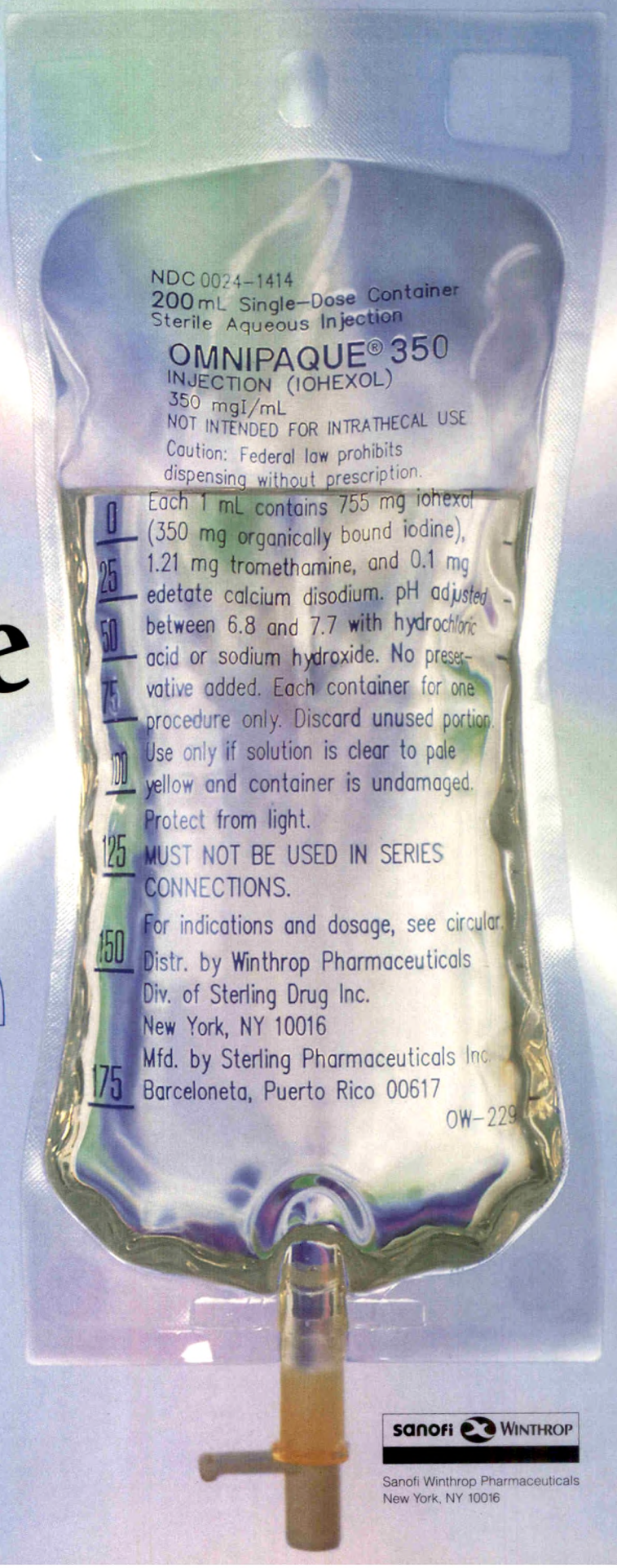
FLEXIPAK is flat and stackable for the best possible utilization of your storage space. And FLEXIPAK is available in the concentrations and sizes used most often.

	100 mL	150 mL	200 mL
OMNIPAQUE 240	X	X	X
OMNIPAQUE 300	X	X	
OMNIPAQUE 350	X	X	X

© 1991 Sanofi Winthrop Pharmaceuticals

It's all part of the package!

NONIONIC
OMNIPAQUE®
(IOHEXOL)



See last page for important product information concerning contraindications, warnings, adverse reactions, patient selection, and prescribing and precautionary recommendations.

All nonionic iodinated contrast media currently available inhibit blood coagulation, in vitro, less than ionic contrast media. Clotting has been reported when blood remains in contact with syringes containing nonionic contrast media. Therefore, meticulous intravascular administration technique is necessary to minimize thromboembolic events.

64-1121

sanofi WINTHROP

Sanofi Winthrop Pharmaceuticals
New York, NY 10016

OMNIPAQUE® 140 240 300 350

INJECTION (IOHEXOL)
INTRAVASCULAR

PLEASE CONSULT FULL PRODUCT INFORMATION BEFORE USING. A SUMMARY FOLLOWS:

DESCRIPTION: OMNIPAQUE is a sterile, pyrogen-free and preservative-free, nonionic, water-soluble radiographic contrast medium for intravascular administration in concentrations of 140, 240, 300, and 350 mgI/mL. OMNIPAQUE 140 contains 302 mg of iohexol equivalent to 140 mg of organic iodine per mL; OMNIPAQUE 240 contains 518 mg of iohexol equivalent to 240 mg of organic iodine per mL; OMNIPAQUE 300 contains 647 mg of iohexol equivalent to 300 mg of organic iodine per mL; and OMNIPAQUE 350 contains 755 mg of iohexol equivalent to 350 mg of organic iodine per mL. Each milliliter of iohexol solution contains 1.21 mg tromethamine and 0.1 mg edetate calcium disodium with the pH adjusted between 6.8 and 7.7 with hydrochloric acid or sodium hydroxide. Unused portions must be discarded. Iohexol solution is sensitive to light and should be protected from exposure.

CONTRAINDICATIONS: OMNIPAQUE should not be administered to patients with a known hypersensitivity to iohexol.

WARNINGS—General: Nonionic iodinated contrast media inhibit blood coagulation, in vitro, less than ionic contrast media. Clotting has been reported when blood remains in contact with syringes containing nonionic contrast media.

Serious, rarely fatal, thromboembolic events causing myocardial infarction and stroke have been reported during angiographic procedures with both ionic and nonionic contrast media. Therefore, meticulous intravascular administration technique is necessary, particularly during angiographic procedures, to minimize thromboembolic events. Numerous factors, including length of procedure, catheter and syringe material, underlying disease state, and concomitant medications, may contribute to the development of thromboembolic events. For these reasons, meticulous angiographic techniques are recommended including close attention to guidewire and catheter manipulation, use of manifold systems and/or three-way stopcocks, frequent catheter flushing with heparinized saline solutions and minimizing the length of the procedure. The use of plastic syringes in place of glass syringes has been reported to decrease but not eliminate the likelihood of in vitro clotting.

OMNIPAQUE should be used with extreme care in patients with severe functional disturbances of the liver and kidneys, severe thyrotoxicosis, or myelomatosis. Diabetics with a serum creatinine level above 3 mg/dL should not be examined unless the possible benefits of the examination clearly outweigh the additional risk. OMNIPAQUE is not recommended for use in patients with anuria.

Radiopaque contrast agents are potentially hazardous in patients with multiple myeloma or other paraproteinemia, particularly in those with therapeutically resistant anuria. Although neither the contrast agent nor dehydration has separately proven to be the cause of anuria in myeloma, it has been speculated that the combination of both may be causative factors. The risk in myelomatous patients is not a contraindication; however, special precautions are necessary. Partial dehydration in the preparation of these patients prior to injection is not recommended since this may predispose the patient to precipitation of the myeloma protein in the renal tubules. No form of therapy, including dialysis, has been successful in reversing the effect. Myeloma, which occurs most commonly in persons over age 40, should be considered before instituting intravascular administration of contrast agents.

Ionic contrast media, when injected intravenously or intra-arterially, may promote sickling in individuals who are homozygous for sickle cell disease.

Administration of radiopaque materials to patients known or suspected of having pheochromocytoma should be performed with extreme caution. If, in the opinion of the physician, the possible benefits of such procedures outweigh the considered risks, the procedures may be performed; however, the amount of radiopaque medium injected should be kept to an absolute minimum. The patient's blood pressure should be assessed throughout the procedure and measures for the treatment of hypertensive crisis should be readily available.

Reports of thyroid storm following the use of iodinated, ionic radiopaque contrast media in patients with hyperthyroidism or with an autonomously functioning thyroid nodule suggest that this additional risk be evaluated in such patients before use of any contrast medium.

Urography should be performed with caution in patients with severely impaired renal function and patients with combined renal and hepatic disease.

PRECAUTIONS—General: Diagnostic procedures which involve the use of radiopaque diagnostic agents should be carried out under the direction of personnel with the prerequisite training and with a thorough knowledge of the particular procedure to be performed. Appropriate facilities should be available for coping with any complication of the procedure, as well as for emergency treatment of severe reactions to the contrast agent itself. After parenteral administration of a radiopaque agent, competent personnel and emergency facilities should be available for at least 30 to 60 minutes, since severe delayed reactions have occurred (see ADVERSE REACTIONS: Intravascular—General).

Preparatory dehydration is dangerous and may contribute to acute renal failure in patients with advanced vascular disease, in diabetic patients, and in susceptible nondiabetic patients (often elderly with preexisting renal disease), infants, and small children. Dehydration in these patients seems to be enhanced by the osmotic diuretic action of urographic agents. It is believed that overnight fluid restriction prior to excretory urography generally does not provide better visualization in normal patients. *Patients should be well hydrated prior to and following administration of any contrast medium, including iohexol.*

Acute renal failure has been reported in diabetic patients with diabetic nephropathy and in susceptible nondiabetic patients (often elderly with preexisting renal disease) following excretory urography. Therefore, careful consideration of the potential risks should be given before performing this radiographic procedure in these patients.

Immediately following surgery, excretory urography should be used with caution in renal transplant recipients.

The possibility of a reaction, including serious, life-threatening, fatal, anaphylactoid or cardiovascular reactions should always be considered (see ADVERSE REACTIONS: Intravascular—General). It is of utmost importance that a course of action be carefully planned in advance for immediate treatment of serious reactions, and that adequate and appropriate personnel be readily available in case of any reaction.

The possibility of an idiosyncratic reaction in susceptible patients should always be considered (see ADVERSE REACTIONS: Intravascular—General). The susceptible population includes, but is not limited to, patients with a history of a previous reaction to contrast media, patients with a known sensitivity to iodine per se, and patients with a known clinical hypersensitivity: bronchial asthma, hay fever, and food allergies.

The occurrence of severe idiosyncratic reactions has prompted the use of several pretesting methods. However, pretesting cannot be relied upon to predict severe reactions and may itself be hazardous for the patient. It is suggested that a thorough medical history with emphasis on allergy and hypersensitivity, prior to the injection of any contrast media, may be more accurate than pretesting in predicting potential adverse reactions.

A positive history of allergies or hypersensitivity does not arbitrarily contraindicate the use of a contrast agent where a diagnostic procedure is thought essential, but caution should be exercised (see ADVERSE REACTIONS: Intravascular—General). Premedication with antihistamines or corticosteroids to avoid or minimize possible allergic reactions in such patients should be considered and administered using separate syringes. Recent reports indicate that such pretreatment does not prevent serious, life-threatening reactions, but may reduce both their incidence and severity.

Even though the osmolality of OMNIPAQUE is low compared to diatrizoate- or iothalamate-based ionic agents of comparable iodine concentration, the potential transitory increase in the circulatory osmotic load in patients with congestive heart failure requires caution during injection. These patients should be observed for several hours following the procedure to detect delayed hemodynamic disturbances.

General anesthesia may be indicated in the performance of some procedures in selected adult patients; however, a higher incidence of adverse reactions has been reported in these patients and may be attributable to the inability of the patient to identify untoward symptoms, or to the hypotensive effect of anesthesia, which can reduce cardiac output and increase the duration of exposure to the contrast agent.

Angiography should be avoided whenever possible in patients with homocystinuria, because of the risk of inducing thrombosis and embolism.

In angiographic procedures, the possibility of dislodging plaques or damaging or perforating the vessel wall should be borne in mind during the catheter manipulations and contrast medium injection. Test injections to ensure proper catheter placement are recommended.

Selective coronary arteriography should be performed only in those patients in whom the expected benefits outweigh the potential risk. The inherent risks of angiocardiography in patients with chronic pulmonary emphysema must be weighed against the necessity for performing this procedure.

When OMNIPAQUE is to be injected using plastic disposable syringes, the contrast medium should be drawn into the syringe and used immediately.

If nondisposable equipment is used, scrupulous care should be taken to prevent residual contamination with traces of cleansing agents.

Parenteral products should be inspected visually for particulate matter and discoloration prior to administration. If particulate matter or discoloration is present, do not use.

Information for Patients: Patients receiving injectable radiopaque diagnostic agents should be instructed to:

1. Inform your physician if you are pregnant.
2. Inform your physician if you are diabetic or if you have multiple myeloma, pheochromocytoma, homozygous sickle cell disease, or known thyroid disorder (see WARNINGS—General).
3. Inform your physician if you are allergic to any drugs, food, or if you had any reactions to previous injections of dyes used for x-ray procedures (see PRECAUTIONS—General).
4. Inform your physician about any other medications you are currently taking, including nonprescription drugs, before you are administered this drug.

Drug/Laboratory Test Interaction: If iodine-containing isotopes are to be administered for the diagnosis of thyroid disease, the iodine-binding capacity of thyroid tissue may be reduced for up to 2 weeks after contrast medium administration. Thyroid function tests which do not depend on iodine estimation, eg, T_3 resin uptake or direct thyroxine assays, are not affected. Many radiopaque contrast agents are incompatible in vitro with some antihistamines and many other drugs; therefore, no other pharmaceuticals should be admixed with contrast agents.

Carcinogenesis, Mutagenesis, Impairment of Fertility: No long-term animal studies have been performed to evaluate carcinogenic potential, mutagenesis, or whether OMNIPAQUE can affect fertility in men or women.

Pregnancy Category B: Reproduction studies have been performed in rats and rabbits with up to 100 times the recommended human dose. No evidence of impaired fertility or harm to the fetus has been demonstrated due to OMNIPAQUE. There are, however, no studies in pregnant women. Because animal reproduction studies are not always predictive of human response, this drug should be used during pregnancy only if clearly needed.

Nursing Mothers: It is not known to what extent iohexol is excreted in human milk. However, many injectable contrast agents are excreted unchanged in human milk. Although it has not been established that serious adverse reactions occur in nursing infants, caution should be exercised when intravascular contrast media are administered to nursing women. Bottle feedings may be substituted for breast feedings for 24 hours following administration of OMNIPAQUE.

Pediatric Use: Pediatric patients at higher risk of experiencing adverse events during contrast medium administration may include those having asthma, a sensitivity to medication and/or allergens, congestive heart failure, a serum creatinine > 1.5 mg/dL, or those less than 12 months of age.

ADVERSE REACTIONS

Intravascular—General: Adverse reactions following the use of OMNIPAQUE are usually mild to moderate in severity. However, serious, life-threatening, and fatal reactions, mostly of cardiovascular origin, have been associated with the administration of iodine-containing contrast media, including OMNIPAQUE. The injection of contrast media is frequently associated with the sensation of warmth and pain, especially in peripheral angiography; pain and warmth are less frequent and less severe with OMNIPAQUE than with many contrast media.

Cardiovascular System: Arrhythmias including PVCs and PACs (2%), angina/chest pain (1%), and hypotension (0.7%). Others including cardiac failure, asystole, bradycardia, tachycardia, and vasovagal reaction were reported with an individual incidence of 0.3% or less. In controlled clinical trials involving 1,485 patients, one fatality occurred. A cause and effect relationship between this death and iohexol has not been established.

Nervous System: Vertigo [including dizziness and lightheadedness] (0.5%), pain (3%), vision abnormalities [including blurred vision and photomas] (2%), headache (2%), and taste perversion (1%). Others including anxiety, blurred vision, fever, motor and speech dysfunction, convulsion, paresthesia, somnolence, stiff neck, hemiparesis, syncope, shivering, transient ischemic attack, cerebral infarction, and nystagmus were reported, with an individual incidence of 0.3% or less.

Respiratory System: Dyspnea, rhinitis, coughing, and laryngitis, with an individual incidence of 0.2% or less.

Gastrointestinal System: Nausea (2%) and vomiting (0.7%). Others including diarrhea, dyspepsia, cramp, and dry mouth were reported, with an individual incidence of less than 0.1%.

Skin and Appendages: Urticaria (0.3%), purpura (0.1%), abscess (0.1%), and pruritus (0.1%).

Individual adverse reactions which occurred to a significantly greater extent for a specific procedure are listed under that indication in full prescribing information.

Pediatrics: In controlled clinical trials involving 391 patients for pediatric angiocardiography, urography, and contrast-enhanced computed tomographic head imaging, adverse reactions following the use of OMNIPAQUE 240, OMNIPAQUE 300 and OMNIPAQUE 350 were generally less frequent than with adults.

Cardiovascular System: Ventricular tachycardia (0.5%), 2:1 heart block (0.5%), hypertension (0.3%), and anemia (0.3%).
Nervous System: Pain (0.8%), fever (0.5%), taste abnormality (0.5%), and convulsion (0.3%).
Respiratory System: Congestion (0.3%) and apnea (0.3%).
Gastrointestinal System: Nausea (1%), hypoglycemia (0.3%), and vomiting (2%).
Skin and Appendages: Rash (0.3%).

General Adverse Reactions to Contrast Media: Physicians should remain alert for the occurrence of adverse effects in addition to those discussed above. The following reactions have been reported after administration of other intravascular iodinated contrast media, and rarely with iohexol. *Reactions due to technique:* hematomas and ecchymoses. *Hemodynamic reactions:* vein cramp and thrombophlebitis following intravenous injection. *Cardiovascular reactions:* rare cases of cardiac arrhythmias, reflex tachycardia, chest pain, cyanosis, hypertension, hypotension, peripheral vasodilatation, shock, and cardiac arrest. *Renal reactions:* occasionally, transient proteinuria; and rarely, oliguria or anuria. *Allergic reactions:* asthmatic attacks, nasal and conjunctival symptoms, dermal reactions such as urticaria with or without pruritus, as well as pleomorphic rashes, sneezing, and lacrimation; and rarely, anaphylactic reactions. Rare fatalities have occurred due to this or unknown causes. *Signs and symptoms related to the respiratory system:* pulmonary or laryngeal edema, bronchospasm, dyspnea; or *to the nervous system:* restlessness, tremors, convulsions. *Other reactions:* flushing, pain, warmth, metallic taste, nausea, vomiting, anxiety, headache, confusion, pallor, weakness, sweating, localized areas of edema (especially facial cramps), neutropenia, and dizziness. Rarely, immediate or delayed rigors can occur, sometimes accompanied by hyperpyrexia. Infrequently, "iodism" (salivary gland swelling) from organic iodinated compounds appears 2 days after exposure and subsides by the sixth day.

In general, the reactions which are known to occur upon parenteral administration of iodinated contrast agents are possible with any nonionic agent. Approximately 95% of adverse reactions accompanying the use of water-soluble intravascularly administered contrast agents are mild to moderate in degree. However, severe, life-threatening anaphylactoid reactions, mostly of cardiovascular origin, have occurred. Reported incidences of death range from 6.6 per 1 million (0.00066%) to 1 in 10,000 (0.01%). Most deaths occur during injection or 5 to 10 minutes later, the main feature being cardiac arrest, with cardiovascular disease as the main aggravating factor. Isolated reports of hypotensive collapse and shock are found in the literature. The incidence of shock is estimated to be 1 out of 20,000 (0.005%) patients.

Adverse reactions to injectable contrast media fall into two categories: chemotoxic reactions and idiosyncratic reactions.

Chemotoxic reactions result from the physicochemical properties of the contrast media, the dose, and the speed of injection. All hemodynamic disturbances and injuries to organs or vessels perfused by the contrast medium are included in this category.

Idiosyncratic reactions include all other reactions. They occur more frequently in patients 20 to 40 years old. Idiosyncratic reactions may or may not be dependent on the amount of dose injected, the speed of injection, and the radiographic procedure. Idiosyncratic reactions are subdivided into minor, intermediate, and severe. The minor reactions are self-limited and of short duration; the severe reactions are life-threatening and treatment is urgent and mandatory.

The reported incidence of adverse reactions to contrast media in patients with a history of allergy is twice that in the general population. Patients with a history of previous reactions to a contrast medium are three times more susceptible than other patients. However, sensitivity to contrast media does not appear to increase with repeated examinations.

Most adverse reactions to injectable contrast media appear within 1 to 3 minutes after the start of injection, but delayed reactions may occur.

Regardless of the contrast agent employed, the overall estimated incidence of serious adverse reactions is higher with angiocardiography than with other procedures. Cardiac decompensation, serious arrhythmias, angina pectoris, or myocardial ischemia or infarction may occur during angiocardiography and left ventriculography. Electrocardiographic and hemodynamic abnormalities occur less frequently with OMNIPAQUE than with diatrizoate meglumine and diatrizoate sodium injection.

CONSULT PACKAGE INSERT FOR A MORE DETAILED DISCUSSION OF ADVERSE REACTIONS FOR INTRAVASCULAR USE OF OMNIPAQUE.

OVERDOSAGE: Overdosage may occur. The adverse effects of overdosage are life-threatening and affect mainly the pulmonary and cardiovascular systems. The symptoms include cyanosis, bradycardia, acidosis, pulmonary hemorrhage, convulsions, coma, and cardiac arrest. Treatment of an overdosage is directed toward the support of all vital functions and prompt institution of symptomatic therapy.

The intravenous LD_{50} values of OMNIPAQUE (in grams of iodine per kilogram body weight) are 24.2 in mice and 15.0 in rats.

DOSAGE AND ADMINISTRATION: Details are provided in the package insert.

THE RADIOLOGICAL SOCIETY OF NORTH AMERICA
Vanguard Flagship Scholar

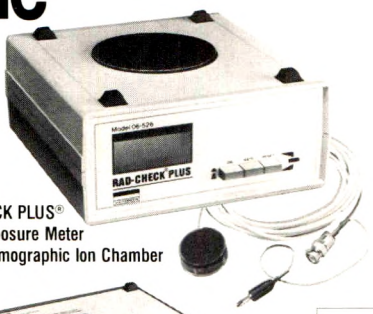
sanofi WINTHROP
Sanofi Winthrop Pharmaceuticals
New York, NY 10016

64-1079

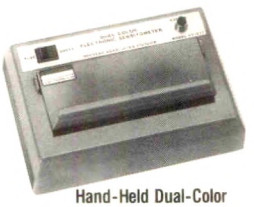
Comply with ACR, JCAHO and State Mammographic QC Requirements Quickly, Easily, Inexpensively!



Mammographic QC Phantoms



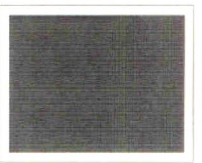
RAD-CHECK PLUS®
X-Ray Exposure Meter
with Mammographic Ion Chamber



Hand-Held Dual-Color Sensitometer



Mammographic Digital kVp Meter



Mammographic Screen-Film Contact Test Tool



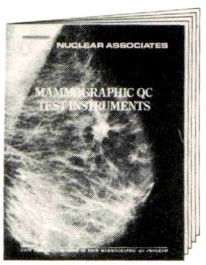
Hand-Held MINISCAN X-Ray Film Processor QC System



Hand-Held Digital Clamshell Densitometer



Mammography Focal Spot Test Stand



FREE MAMMOGRAPHIC QC CATALOG

Our extensive line of mammographic QC test instruments and accessories will help you implement an effective QC program in your facility.

Phone (516) 741-6360, FAX (516) 741-5414, or write and request your FREE Mammographic Catalog MM-44

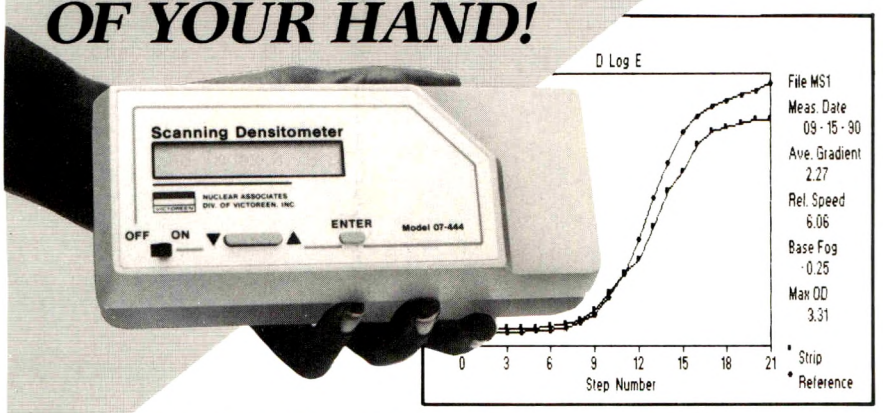
NUCLEAR ASSOCIATES

VICTOREEN

Division of VICTOREEN, INC.
100 VOICE ROAD • P.O. BOX 349
CARLE PLACE, NY 11514-0349 U.S.A.
(516) 741-6360
FAX (516) 741-5414

*Victoreen, Inc.

IMAGINE...X-RAY FILM PROCESSOR QC IN THE PALM OF YOUR HAND!



***IMAGINE...**performing daily film processor QC in seconds!*
***IMAGINE...**a compact, lightweight, portable scanning QC system that has more features and capabilities than you ever dreamed were possible!*

MINISCAN

You can use it WITH or WITHOUT a Computer!

MINISCAN is a...

- Standard high quality transmission densitometer.
- Scanning QC densitometer to measure, analyze and store data for up to 20 independent sensitometric strips in its own built-in memory (no external computer or software needed)!
- Complete film processor QC system (when combined with the Film Processor QC Software Package) to track and monitor the performance of a virtually unlimited number of film processors. PLUS generate comprehensive reports, control charts, and corrective action forms, and more!

MINISCAN...*More Than You Ever Imagined!*

For more details, request Bulletin 5011-44

NUCLEAR ASSOCIATES

VICTOREEN

Division of VICTOREEN, INC.
100 VOICE ROAD • P.O. BOX 349
CARLE PLACE, NY 11514-0349 U.S.A.
(516) 741-6360
FAX (516) 741-5414

For 25 years, the leading source for all clinically-proven quality control products for diagnostic imaging.

AJR Business and Subscriber Information

The American Roentgen Ray Society

AJR, American Journal of Roentgenology, is published monthly to disseminate research on current developments in the radiologic sciences and commentary on topics related to radiology. It is published by the American Roentgen Ray Society (ARRS), 1891 Preston White Dr., Reston, VA 22091; (703) 648-8992. Address inquiries regarding Society business, the annual ARRS meeting, and membership to the Society to the above address.

Correspondence regarding editorial matters should be addressed to Editorial Office, AJR, 2223 Avenida de la Playa, Ste.103, La Jolla, CA 92037-3218; telephone 1-800-348-4257 or (619) 459-2229; FAX (619) 459-8814. For information on manuscript submission, see Guidelines for Authors.

Subscriber Information

ARRS annual dues include $50 for journal subscription. Nonmember subscription rates are as follows: $125/year ($180 foreign); institutions, $135 ($190 foreign); in-training, $25 ($80 foreign). Single copies of the Journal may be purchased for $18 ($22 foreign). Airmail rates will be furnished on request. The GST number for Canadian subscribers is 123394371.

Call toll-free, 1-800-638-6423 (in Maryland call 1-800-638-4007), with subscription inquires or problems. Please have the mailing label from your latest issue available when you call.

Report changes of address to Subscription Fulfillment, AJR, 428 E. Preston St., Baltimore, MD 21202. Damaged or unreceived issues must be reported within 60 days of publication (90 days for foreign subscribers) for replacement.

Advertising Information

All advertising is subject to approval by the publisher. Acceptance of advertising does not indicate endorsement of the products or services advertised or the claims made. For display advertising information, contact Gary Walchli, National Sales Representative, AJR, 428 E. Preston St., Baltimore, MD 21202, (410) 528-4291.

For classified advertising information, contact the Publications Department, ARRS, Attn: Terry Fitterer, 1891 Preston White Dr., Reston, VA 22091; telephone (703) 648-8992; FAX (703) 264-8863.

Copyrights, Permissions, and Reprints

Contents of the *AJR* are copyrighted by the ARRS. No part of this publication may be reproduced without permission. Requests for such permission should be addressed to the Publications Department, ARRS, Attn: Terry Fitterer, 1891 Preston White Dr., Reston, VA 22091. For reprints of a particular article, please contact the author designated in the footnotes for that article.

Indexes

The *AJR* provides volume and yearly indexes (subject and author) in the June and December issues. *AJR* articles are also indexed in *Current Contents*, *Index Medicus*, and the cumulative index published by *Radiology*.

Fleischner Lecture

Imaging the Respiratory System in the First Few Years After Discovery of the X-Ray:
Contributions of Francis H. Williams, M.D.

Reginald Greene[1]

Imaging of the respiratory system developed with exceptional rapidity in North America during the spring of 1896, after Roentgen's discovery of X-rays in November 1895, largely because of the efforts of a unique physician, Francis H. Williams. With great zeal, this pioneer used fluoroscopy for early detection of tuberculosis and other life-threatening chest disorders. By the summer of 1896, he had accumulated more than 100 volumes containing tracings of clinical chest fluoroscopy. As a result of his extensive clinical experience, his dedication to patients' welfare, and his sense of scientific inquiry, several inventions and many landmark clinical observations were made in the first few years after the discovery of the X-ray. These included (1) the invention of a "densitometer" for standardized measurements of relative X-ray attenuation of the lung, (2) the invention of a "seehear" device to correlate auscultative findings and fluoroscopic observations, (3) the recognition that fluoroscopy was more accurate than percussion for estimating mediastinal displacement, (4) the discovery that clinically occult tuberculosis and congestive heart failure could be detected with fluoroscopy, (5) the documentation that unilateral chest disease caused decreased ipsilateral ventilatory compliance and increased contralateral ventilation, (6) the identification of the classical imaging characteristics of tuberculosis, pneumonia, pneumothorax, tension pneumothorax, pleural effusion, hydropneumothorax, emphysema, congestive heart failure, and air trapping. In April 1896, Dr. Williams described the "air bronchogram" in a radiograph of a patient with pneumonia.

AJR 159:1–7, July 1992

It is a great privilege to deliver this lecture, named for Felix Fleischner, a leading contributor to chest radiology in the 20th century and a mentor during my residency training at the Massachusetts General Hospital. I have chosen to speak on the legacy to respiratory imaging provided by the many discoveries that another exceptional physician, Francis H. Williams (Fig. 1), made shortly after Roentgen's discovery of the X-ray. Knowledge of this early period provides a historical context in which to view the significance of modern advances and future discoveries in chest imaging.

Transatlantic Dissemination of Roentgen's Discovery

Europe was the home of Roentgen's discovery and the site of many pioneering clinical applications of X-rays, but nowhere did chest imaging develop more rapidly or flourish with greater impact than in the United States. News of the December 28, 1895, publication of the great X-ray discovery was almost immediately received in America via transatlantic cable communication [1]. Only 3 days elapsed between the first newspaper account of Roentgen's discovery in the Viennese *Neue Freie Presse* (January 5, 1896) and its report in the *New York Sun* (January 8, 1896) [2]. Within a month, lead articles suggesting the potential medical applications of X-rays appeared in the *Boston Medical and Surgical Journal* (February 13, 1896), the

Received September 30, 1991; accepted after revision February 12, 1992.

Presented at the annual meeting of the Fleischner Society, Interlaken, Switzerland, May 1991.

[1] Department of Radiology, Massachusetts General Hospital, Fruit St., Boston, MA 02114. Address reprint requests to R. Greene.

0361–803X/92/1591–0001
© American Roentgen Ray Society

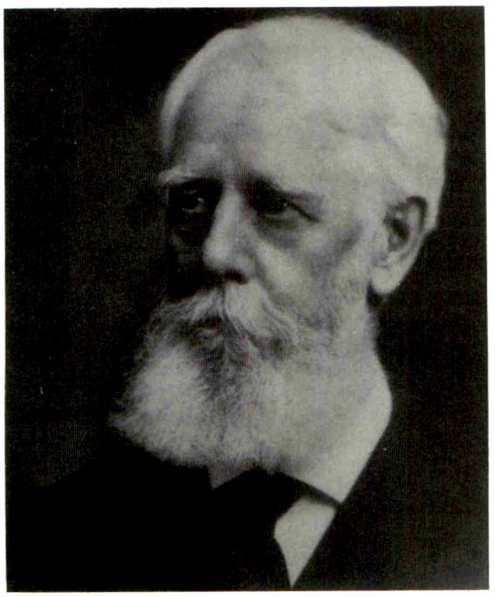


Fig. 1.—Francis H. Williams, M.D. Photograph of portrait made in 1924 marking Williams's 50th graduation reunion from the Massachusetts Institute of Technology (MIT) and 42 years as life member of the MIT Corporation. (Photograph reprinted with the permission of the MIT Museum.)

forerunner of the *New England Journal of Medicine*, and in the *Journal of the American Medical Association* (February 15, 1896) [3, 4]. The new world also was quick to reproduce Roentgen rays. A score of American physicists, who had previous experience with the Hittorf, Crookes, and Lenard tubes, produced anatomic X-ray images within the next few months, including a group at the Massachusetts Institute of Technology (MIT), whose machinery was to become an important vehicle for Francis Williams's experimental and clinical studies during the spring and summer of 1896 [5].

The Medical Milieu of 1896

Tuberculosis devastated everyday life before the turn of the century and exerted a pivotal influence on the rapid development of X-ray imaging of the chest. In 1896, this disease accounted for 15% of all reported deaths, and together with other infectious ailments, caused most deaths, half of which occurred in children less than 5 years old [6]. The tubercle bacillus was still a relatively recent discovery as the causative agent of consumption, and not all American physicians accepted its causal role [7, 8]. Advanced tuberculous disease was untreatable, and the ability to uncover minimal disease was limited.

The two great clinicians who were to become the progenitors of chest medicine and chest radiology in the United States, Edward Livingston Trudeau and Francis Williams, were brought together in clinical collaboration by their dedication to the cause against tuberculosis. There was high mutual respect between the two, who commonly exchanged the care of their tuberculous patients between their respective practices in Saranac Lake (NY) and Boston [8, 9].

Personal encounters with tuberculosis are the best illustrations of the tragic failures of early diagnosis and medical treatment in the late 19th century. In 1872, Trudeau learned of his own advanced tuberculosis, taking it as a virtual death sentence. The stethoscopic diagnosis of his disease was delayed until the disease advanced and caused fever and fatigue. He had previously suffered from undiagnosed tuberculous swelling of the cervical lymph nodes and cold abscesses of the thigh as a medical house officer in New York City. His younger brother had died of the disease in childhood, and his adolescent daughter subsequently died of tuberculosis in 1893.

Francis Williams was among those who were convinced that improved survival rates depended on recognition and treatment of tuberculosis while the disease was still in its early stages. It is no wonder that Williams saw in the discovery of the X-ray a potentially powerful method of saving lives through earlier diagnosis of tuberculosis. At 43 years of age, Dr. Williams was already a leader in medical therapeutics, the first in Boston to successfully use diphtheria antitoxin (1894), and the author of a regular series on medical therapeutics in the *Boston Medical and Surgical Journal (BMSJ)* [10–13]. He soon also became the central figure in the development of chest imaging in the United States, ultimately establishing one of the first hospital departments of radiology at Boston City Hospital.

The First Steps in Chest Imaging

Williams's early success with clinical X-ray imaging was partly attributable to his influence as a lifetime member of the MIT Corporation and the resulting access to a large physics laboratory [14]. Using relatively powerful X-ray equipment, Williams was able to begin a series of in vitro experiments and clinical studies with fluoroscopy and roentgenography by April 1896. The earliest record of clinical chest fluoroscopy dates from April 14, 1896, when he transported a patient from Boston City Hospital to the MIT physics laboratory. He most likely actually began clinical fluoroscopy before that date. Williams's first report on clinical use of X-rays to diagnose chest disease was made to the Suffolk Medical Society only 77 days after the first *BMSJ* description of Roentgen's discovery [15]. The *BMSJ* issues of 1896 not only contain many articles by Williams on medical therapeutics, they contain the announcement of Roentgen's discovery and Williams's own first report on the use of X-rays for medical diagnosis (April 25, 1896) [15]. On April 30, 1896, Williams reported to the prestigious Association of American Physicians on the successful fluoroscopic localization of tuberculosis, answering questions from the leading physicians of the era, including William Osler of Baltimore [16, 17]. In that same year, Williams reported the results of fluoroscopic examinations in 40 patients with tuberculosis [18]. By August 29, 1896, he had accumulated more than 100 volumes containing fluoroscopic drawings. The number of volumes increased to more than 400 by April 12, 1897. Like his noted European pioneering colleagues, Antoine Béclère of Paris and Guido Holzknecht of Vienna, Williams later organized his early X-ray

experience into a major text, much of which was devoted to the chest [9, 19, 20]. The first printing of Williams's book sold out in 3 months.

X-Ray Equipment

Unlike so many other pioneers who struggled with weak, unpredictable and unsafe X-ray machines, Williams benefited from the expertise of a team of MIT engineers, who provided him with the most powerful and up-to-date X-ray machines and tubes then in existence [9]. An inventive relative, Dr. William Rollins, devised high-output X-ray tubes for Williams, and enclosed them in a lead-lined collimator box to limit scatter. These engineering safeguards, and meticulous safety practices, helped Williams and his colleagues to avoid completely the radiation injuries so common in other pioneers.

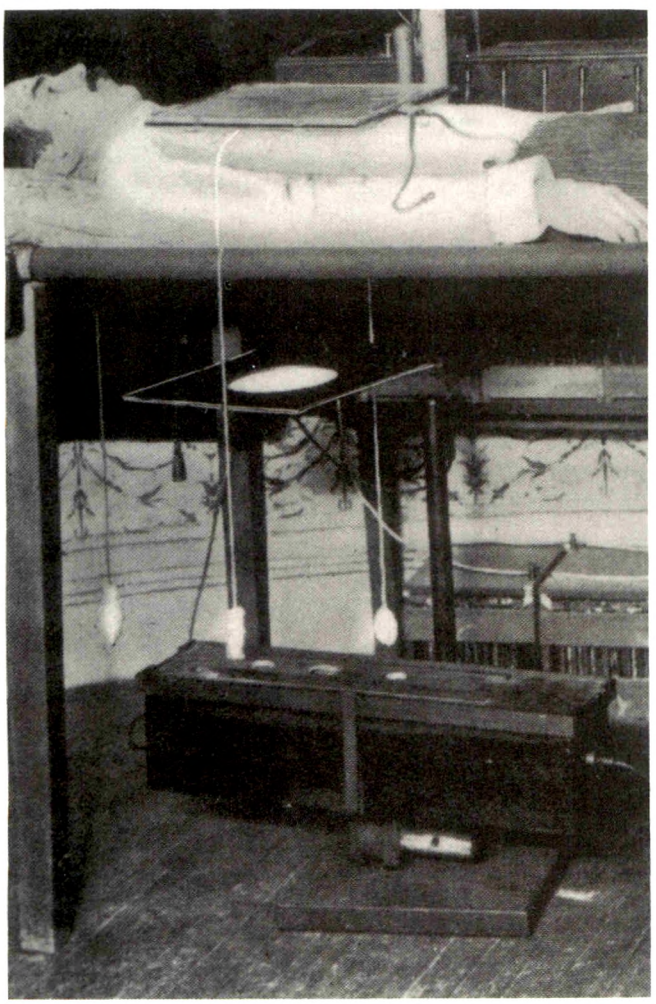


Fig. 2.—"Seehear" device acted as a large stethoscope for correlative studies of fluoroscopy and auscultation. A patient is shown lying on a stretcher with a flat boxlike seehear device on his chest just beneath a fluoroscopic screen. Earpieces connected to seehear are just visible, resting on patient's right arm. X-ray tube is enclosed in a lead-shielded box on the floor, with adjustable collimator holes. Plumb lines extend from the patient for accurate tube alignment. Additional collimating diaphragm is suspended from stretcher. (Reprinted from Williams [9].)

Auscultation, Percussion, and Fluoroscopy

The relatively low power of X-ray machines produced poor chest roentgenograms because of respiratory motion and required the X-ray pioneers to rely almost exclusively on fluoroscopy for chest diagnosis. The mandatory use for fluoroscopy was not without its benefits, lending authenticity to chest observations by providing supplementary functional insights. The beating of the cardiac chambers and the change in shape and position of the heart and lungs during breathing were recognized in the first fluoroscopic studies. The "seehear" was developed by Williams to assist in the correlation of fluoroscopy and auscultation (Fig. 2). The device was a flat vulcanite boxlike air space connected to earpieces that acted like a large stethoscope when it was placed on the chest in front of a fluoroscopic screen. By calling the device seehear, rather than "hearsee," Williams seems to have implied the preeminence of the new Roentgen ray over the stethoscope in respiratory diagnosis. With the aid of the seehear, Williams identified increased fluoroscopic luminance of the lungs during inspiration.

Differential X-Ray Attenuation

In the earliest in vitro experiments of equal volumes of tissue constituents in beakers, Williams showed that the X-ray absorptions of water, bone, fat, and gas were different [9]. Recognizing that absorption was based on tissue density and that the density of blood was slightly greater than that of water, Williams looked for a roentgenographic difference between the two. He was clearly disappointed to find that beakers of blood and water had only a very slightly perceptible difference in opacity, and he concluded that in vivo roentgenograms would not be sensitive enough to detect the 1/2000th

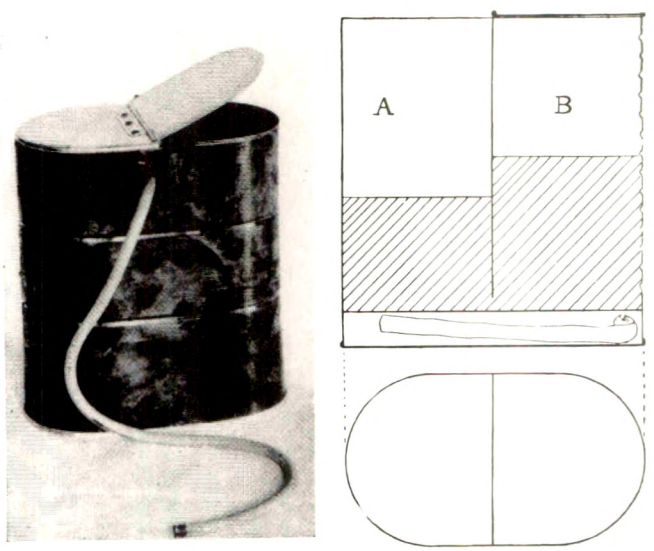


Fig. 3.—Photograph of densitometer shows an aluminum-bottomed canister with two water chambers connected by a rubber-tubed mouthpiece. Diagram shows layout of two water chambers that enable fluoroscopist to adjust water level to match attenuation of tissue being examined fluoroscopically. (Reprinted from Williams [9].)

difference in tissue density of blood and water. In further written analysis of these results, Williams illustrates his foresight, reminding us of CT and MR imaging, when he anticipates the future development of more sophisticated imaging techniques that might permit noninvasive testing of the physical and chemical composition of the body [9].

Williams studied the increased fluoroscopic luminance associated with inflation of the lung, devising a "densitometer" to standardize measurements of relative tissue density. The device, to be placed in the fluoroscopic field of view of the lung alongside the recumbent patient, consisted of an oval canister with a thin aluminum top and bottom, containing two water-filled chambers connected at the very bottom. By sucking or blowing air into the mouthpiece of tubing connected to the chambers, the operator could change the water level in a measurement chamber to match the fluoroscopic blackening of the organ under study (Fig. 3). Williams used this device to calculate the relative density of fully inflated excised lung, obtaining remarkably close agreement with calculations based on modern standard data. Williams also described the decreased transradiancy of the lung after expiration from full inspiration, observing that 2.5 cm of water visible during full inspiration became invisible after maximum expiration.

Diaphragmatic Motion

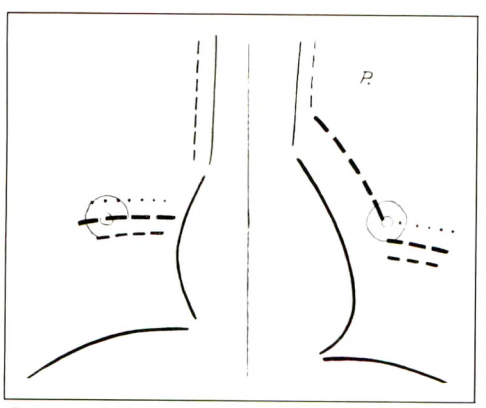
Williams made tracings to record his fluoroscopic observations permanently. For reference points, he placed a linear metal rod over the sternum and tiny metal fragments on the nipples. He then recorded his fluoroscopic observations with pencil marks on a reusable sheet placed over the fluorescent screen. The marks on the sheet were copied onto tracing paper, and later transferred onto half life-size anatomic blanks for a permanent record. Williams showed that diaphragmatic position correlated with the phases of respiration (Fig. 4). His observations of normal motion proved to be an important basis for subsequent observations of abnormal diaphragmatic motion in disease.

Airways Disease

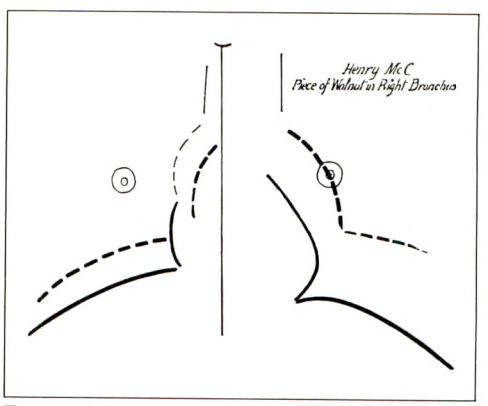
Williams's fluoroscopic observations of emphysema in the spring and summer of 1896 sound eerily similar to present-day textbook descriptions, and they undoubtedly served as the basis for many subsequent descriptions:

> The pulmonary area is more extensive and brighter than in health, and reaches not only lower down but higher up in the chest. The diaphragm is lower down in the thorax, and its excursion is restricted in the upper part of its usual movement. It sometimes happens that the diaphragm is so low down during full inspiration that it has a peculiar outline, this curve being made up of two curves on each side, instead of one, and following the organs directly under it. . . . The cardiac outline . . . stands out with unusual clearness on the fluorescent screen. . . . The heart . . .is lower down in the thorax . . . and its long axis is in a more vertical position. . . . The lower position of the diaphragm gives the axis of the heart . . . this vertical direction, and is one of the reasons why this organ when looked at from side to side, is at greater distance from the sternum in emphysema than in health [9].

Williams also noted that in emphysema the vertically oriented heart showed little of the variation in configuration that normally occurs during inspiration and expiration. Williams identified the effects of air trapping in central bronchial obstruction, noting decreased ipsilateral diaphragmatic movement, increased contralateral movement ventilation, and contralateral mediastinal displacement (Fig. 5).



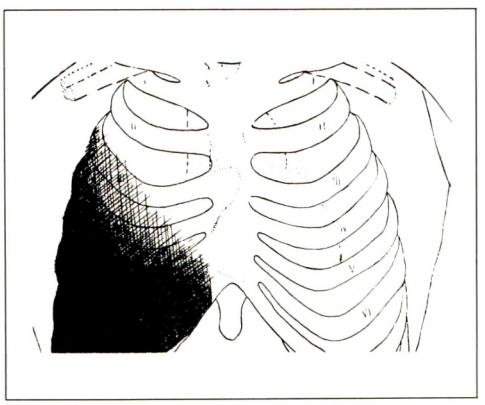
4



5

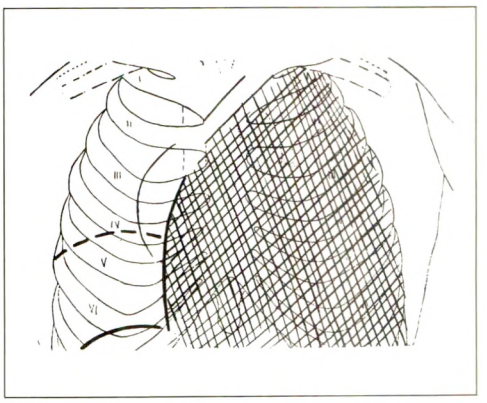
Fig. 4.—Normal diaphragmatic motion. A tracing made from fluoroscopic examination of normal chest shows diaphragmatic positions after full inspiration (*lowest solid lines*), after full expiration (*dotted lines*), after end-tidal inspiration (*light dashed lines*), and after end-tidal expiration (*heavy dashed lines*). Cardiac silhouette is shown to become more transverse and mediastinum to become wider as lungs deflate. Tracings were obtained by (1) placing metallic markers on sternal midline and nipples, (2) tracing points of reference from fluoroscopy onto a washable sheet placed over fluorescent screen, and (3) transferring cloth marks onto tracing paper. Permanent records were made by copying tracings onto half-size anatomic blanks of chest by dividing all measurements in half. (Reprinted from Williams [9].)

Fig. 5.—Air trapping. Fluoroscopic tracing of a 9-year-old boy with a walnut in right main bronchus shows right-sided air trapping. Decreased upward excursion of ipsilateral diaphragm and contralateral displacement of cardiac silhouette occur on expiration. (Reprinted from Williams [9].)



6

Fig. 6.—Fluoroscopic tracing from August 1896 shows that opacity of a large right-sided pleural effusion rises to a higher level along lateral margin of chest than it does more centrally. This appearance was attributed to greater thickness of fluid to be traversed by lateral part of X-ray beam. (Reprinted from Williams [9].)



7

Fig. 7.—Fluoroscopic tracing shows massive left-sided pleural effusion due to tuberculosis. Heart is shifted to right, and excursion of contralateral diaphragm between total lung capacity (*solid line*) and end-tidal expiration (*dashed line*) is increased. (Reprinted from Williams [9].)

Congestive Heart Failure

In 1896, Williams may have been the first to discover that asymptomatic patients with mitral stenosis might have increased opacity of the lung bases due to passive congestion and pulmonary edema, even when clinical signs and symptoms were absent [9]. He observed that these clinically occult fluoroscopic findings would resolve after administration of digitalis.

Pleural Disease

Modern descriptions of pleural effusion tend to reiterate Williams's original description, "the outline of the diaphragm. . . is less well defined, or obliterated altogether, according to the amount of fluid present. . . . The outline. . . may be seen to change. . . when the patient changes position" [9]. The shape of the pleural opacity along the lateral chest wall fascinated Williams, just as it interested Felix Fleischner 50 years later (Fig. 6). Williams attributed the greater opacity of the pleural fluid along the lateral chest wall to its greater projected thickness as compared with the more central fluid. He found that massive pleural effusion displaced the heart contralaterally and increased the excursion of the contralateral hemidiaphragm (Fig. 7). On expiration, the heart could be observed to displace farther to the contralateral side, reflecting the greater selective ventilation of the normal lung. Williams found that in large unilateral pleural effusion, percussion underestimated the degree of mediastinal shift shown by fluoroscopy. In pleurisy due to pleuritic adhesions, he found that diaphragmatic motion was restricted on the ipsilateral side and increased on the contralateral side (Fig. 8). The classical signs of pneumothorax were observed in 1896, and the difference between simple and tension conditions was recognized:

> The affected side is seen to be divided into two parts, the upper of which is unusually light and the lower very dark. The affected side of the chest is usually clear, and the light area in this region is larger than normal; the lung is retracted; the diaphragm is pushed low down in the chest and has little or no movement, and the organs on this side are displaced to the opposite side. The amount of displacement varies according to whether the air in the chest is or is not under greater than atmospheric pressure; if air is pumped in during the respiratory movement through a valve-like opening, and the pressure in that side of the thorax is thereby increased, the displacement of the organs may be very great [9] (Fig. 9).

The air-fluid interface of hydropneumothorax in the sitting position was observed as follows:

> The general appearance of this side may be likened to a tumbler partially filled with black ink; when the patient moves backward or forward, the level of the fluid changes; if he is taken by the shoulders and gently shaken, the surface is disturbed, and the splashing of the fluid is clearly seen. When the fluid is at a certain level, especially if the hydropneumothorax is in the left side, the pulsations of the heart disturb its surface, and the waves caused by the partially submerged and beating heart can be observed [9].

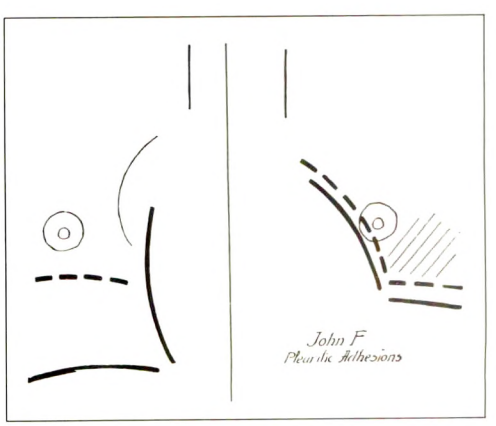


Fig. 8.—Pleuritic adhesions. Fluoroscopic tracing shows a patient with left-sided pleurisy. Excursion of ipsilateral diaphragm is restricted, and excursion of contralateral diaphragm is increased. (Reprinted from Williams [9].)

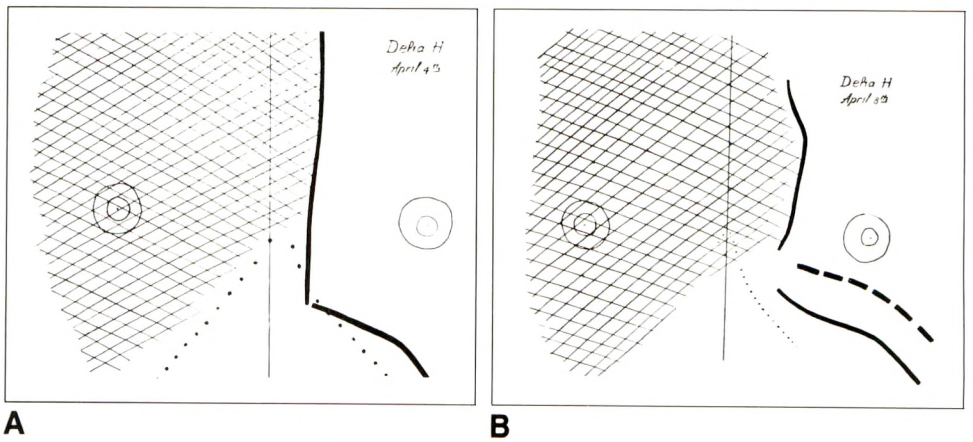


Fig. 9.—*A* and *B*, Tension pneumothorax. Fluoroscopic tracing (*A*) shows left-sided tension pneumothorax due to tuberculosis, and extensive right-sided tuberculous pneumonia. Pneumothorax was presumably due to invisible tuberculous focus in collapsed left lung. Left hemithorax was exceptionally bright on fluoroscopy, and left lung was not visible because of collapse. Left cardiac margin was displaced to right, and left hemidiaphragm was markedly depressed. Absence of a dotted line above left hemidiaphragm indicates negligible excursion during breathing. Because patient was in marked respiratory distress, 1 l of air was removed, which promptly relieved symptoms. Fluoroscopic tracing afterward (*B*) shows mediastinum moved back toward left side and hemidiaphragm resumed movement. (Reprinted from Williams [9].)

Tuberculosis, Pneumonia, and the "Air Bronchogram"

The common fluoroscopic findings of early tuberculosis were identified by Williams in the spring of 1896: (1) darkening of the diseased lung apex, (2) restriction in the excursion of the ipsilateral diaphragm, (3) displacement of the heart and mediastinum to the ipsilateral side because of restricted expansion of the diseased lung, and (4) increased diaphragmatic excursion on the normal side (Fig. 10). Hypertrophy of bronchial glands and miliary disease also were detected occasionally. Williams found that fluoroscopy sometimes revealed the location of tuberculosis "where and when it would otherwise have been unsuspected" [9]. He was supported by his Parisian colleague, Antoine Béclère, in the early conclusion that fluoroscopy could be used to detect tuberculosis when no clinical signs of disease were apparent [21]. Williams cautioned that normal findings on chest fluoroscopy did not exclude tuberculosis.

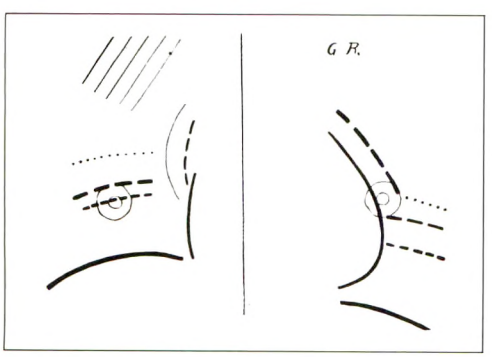


Fig. 10.—Early tuberculosis. Fluoroscopic tracing of minimal tuberculosis shows increased balancing in right upper lobe (*thin oblique lines*), elevation of *ipsilateral* hemidiaphragm after maximum inspiration (*solid lines*) and decreased tidal movement of diaphragm (i.e., between *heavy dashed line* of end-tidal expiration and *light dashed line* of end-tidal inspiration). Right hemidiaphragm was also higher after maximum expiration, and heart was slightly shifted to right. (Reprinted from Williams [9].)

Williams found that early pneumonia could be detected with fluoroscopy even when there were no signs of it by auscultation or percussion. The "visible bronchial tree" (or "air bronchogram" as it later became more popularly known) is a fundamental observation in pneumonia that is attributed to Felix Fleischner, who made its classical description in 1927 and elucidated its mechanism in 1948 [22, 23]. Records show that the visible bronchial tree was actually recognized in the first year after Roentgen's discovery. In 1896, Francis Williams described it in a postmortem lung roentgenogram of a patient who died of pneumonia: "The lightest portion is healthy; the darkest parts have been more affected by the pneumonic process than those that are less dark. It is noteworthy that the smaller bronchi show as light lines in the dark portions of the lungs" [9]. It is unfortunate that the photographic print of the radiograph leading to this historic observation is not of reproducible quality.

The Legacy of 1896

Looking back on the remarkable developments in respiratory imaging in the first few years after discovery of the X-ray, it is not difficult to identify the pivotal factors that account for them. Most of the pioneers learned almost immediately of Roentgen's discovery, but few possessed Williams's combination of scientific and medicine background and access to the expert engineering support. His respected position as a clinician and medical writer before 1895 lent credibility to his published observations. His prominent social position and influence at MIT assured him of the continuing engineering support necessary for clinical studies. The driving force for Williams's clinical discoveries, however, derives from a strong medical imperative to detect and cure early tuberculosis, a zeal he shared with his counterpart in chest medicine, Edward Livingston Trudeau. The unprecedented success of Williams's enterprise depended on attributes he shared with the latter-day chest radiologist, Felix Fleischner: a cultivated devotion

to observation, a well-nurtured habit of stochastic reasoning and analytical inquiry, and a meticulous attention to record-keeping. Present-day radiologists have much to learn from the character of this remarkable Bostonian who toiled at the dawn of radiologic discovery.

ACKNOWLEDGMENTS

Without the preservation of Williams's notes, drawings, and writings by the well-catalogued archives of the Rare Books Department of the Countway Medical Libarary of Harvard Medical School, the MIT Museum, and the Boston Athenaeum, much of this historical investigation would not have been possible.

REFERENCES

1. Röntgen WC. Über eine neue Art von Strahlen. Vorläufige Mittheilung, Sitzungsberichte der Wurzburger Physik-mediz Gesellschaft, December 28, **1895**
2. Grigg ERN. *The trail of the invisible light.* Springfield, IL: Thomas, **1965**: 9–19
3. X-rays (editorial). *Boston Med Surg J* **1896**:134:174–175
4. The Roentgen rays (editorial). *JAMA* **1896**;26:336
5. Goodwin HM. *A history of the department of chemistry and physics at the Massachusetts Institute of Technology, 1865–1933.* Cambridge, MA: The Technology Press, MIT, **1933**
6. Record of mortality. *Boston Med Surg J* **1896**;134:75
7. Koch R. Die Aetiologie der Tuberculose. *Berl Klin Wchnschr* **1882**;19: 221–230
8. Trudeau EL. *An autobiography.* New York: Lea & Febiger, **1915**:7–245
9. Williams FH. *The Roentgen rays in medicine and surgery.* New York: Macmillan, **1901**
10. Williams FH. Report on progress in therapeutics: new preparations of tuberculin. *Boston Med Surg J* **1897**;137:85–87
11. Williams FH. The prevention of the spread of diphtheria by means of the bacterial test. *Boston Med Surg J* **1896**;135:582
12. Williams FH. An epidemic of cerebrospinal meningitis caused by *Diplococcus intracellularis meningitidis. Boston Med Surg J* **1896**;136:498
13. Williams FH. Quinine in malaria. *Boston Med Surg J* **1896**;134:126–127
14. Prescott SC. Francis Henry Williams. *Proc Am Acad of Arts Sci* **1938**;134:399–402
15. A notable demonstration of the X-rays (editorial). *Boston Med Surg J* **1896**;134:447–448
16. Williams FH. Notes on X-rays in medicine. *Trans Assoc Am Physicians* **1896**;11:375–382
17. Williams FH. The X-rays in the diagnosis of chest troubles, with an exhibition of a fluorescope. *Boston Med Surg J* **1896**;134:621
18. Williams FH. A method for more fully determining the outline of the heart by means of the fluoroscope, together with other uses of the instrument of medicine. *Boston Med Surg J* **1896**;135:335–337
19. Béclère A. *Les rayons de Röntgen et la diagnostic de la tuberculose.* Paris: Baillière, **1899**
20. Holtzknecht G. Fortschritte auf dem Gebiete der Röntgenstrahlen. Ergandzungsband 6. In *Archiv und Atlas der normalen und pathologischen Anatomie.* Hamburg: Lucas Gräfe & Sille, **1901**
21. Petit LH. Les rayons X dans le diagnostic de lésions thoracique. *Rev Tuberculose* **1897**;5:103–104
22. Fleischner FG. Der sichtbare Bronchialbaum, ein differentialdiagnostisches Symptom in Röntgenbild der Pneumonia. *Fortschr Geb Röntgenstr* **1927**;36:319–323
23. Fleischner FG. The visible bronchial tree: a Roentgen sign in pneumonic and other pulmonary consolidations. *Radiology* **1948**;50:184–189



The Radiology Outreach Foundation (ROF) is a nonprofit corporation whose goal is to help disadvantaged countries improve their health care by providing radiology equipment, books, consultation, education, and training to their practitioners. This assistance is on an application basis that is independent of political, ethnic, or religious orientation of the grantee. It depends on the need of the people and the ability of the ROF to meet that need. The ROF is approved by the U.S. Internal Revenue Service as a tax-exempt organization. It is endorsed by the following radiologic societies:

American Association of Women Radiologists
American College of Radiology
American Roentgen Ray Society
Association of University Radiologists
Radiological Society of North America
Society of Chairmen of Academic Radiology Departments
Society for Pediatric Radiology
European Society of Pediatric Radiology

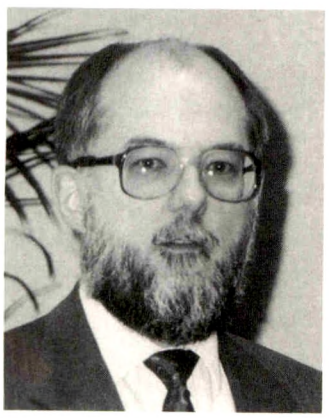
All donations to the ROF are tax deductible. Persons who would like to contribute financially to the ROF, would be interested in being a visiting professor, would like to send books or journals to any of the institutions supported by the ROF, or would like further information about the ROF should write to

Charles A. Gooding, M.D.
President
Radiology Outreach Foundation
3415 Sacramento St.
San Francisco, CA 94118 USA

Mallinckrodt 60th Anniversary Rededication Program

The Edward Mallinckrodt Institute of Radiology 60th Anniversary Rededication Program

William A. Murphy, Jr.[1]



The Edward Mallinckrodt Institute of Radiology celebrated its 60th anniversary September 12–14, 1991. In commemoration of this milestone and in recognition of the 100th anniversary of Washington University School of Medicine (1891–1991), the Institute invited its staff, alumni, and friends to a 3-day celebration that included scientific sessions, social events, and a program of rededication.

At Washington University, interest in the X-ray was already evident in the weeks immediately following Röntgen's discovery. In fact, Francis E. Nipher reported his investigations involving the photographic recording of an X-ray image directly from a calcium tungstate screen in the May 22, 1896, issue of *Science.*

Typical of the early days of radiology, X-ray imaging at Washington University was the responsibility of surgeons. These activities took place within the surgical clinics in the university's new medical department (founded in 1891). In 1910, when the current school of medicine organizational structure was adopted, a radiology service was formed within the department of surgery, and Russell D. Carman (1875–1926), a surgeon, was put in charge. Today, Carman is considered Washington University's first radiologist. Soon Carman was recruited to join the Mayo Clinic, and Ralph Walter Mills (1877–1924), an internist and expert in gastrointestinal radiology, replaced him as roentgenologist. During Mills's tenure (1912–1917), the Barnes Hospital was built, opened its doors (1914), and became the teaching hospital for the school of medicine. The new radiographic department consisted of one room for X-rays and another for photographs; the two rooms were connected by a darkroom.

The third director (1917–1949) of the radiology service was a surgeon trained in obstetrics and gynecology but infatuated with X-ray technology, Sherwood Moore (1880–1963). Under his stewardship, the radiologic enterprise grew and prospered and a substantial research foundation was laid. In 1922, Evarts Ambrose Graham (1883–1957), chairman of surgery, hypothesized that visualization of the gallbladder would be possible by X-ray methods. He assembled and led a team of clinical researchers, including Moore, and chemists from the Mallinckrodt Chemical Works. Their efforts resulted in successful opacification of the gallbladder in a dog (November 1923) and shortly thereafter in a human (January 1924). Cholecystography quickly became an indispensable medical test and was integral to abdominal imaging for more than 50 years until largely replaced by sonography and CT.

As a result of his company's successful collaboration with physicians at Washington University and in keeping with his high standard of philanthropy, Edward Mallinckrodt, Sr. (1845–1928), in 1927 funded the construction of a building to house an institute of radiology. When Mr. Mallinckrodt died

[1] Chairman, 60 Anniversary Celebration Committee, Mallinckrodt Institute of Radiology, 510 S. Kingshighway Blvd., St. Louis, MO 63110-1076. Address reprint requests to W. A. Murphy, Jr.

AJR **159:9–10, July 1992** 0361–803X/92/1591–0009 © American Roentgen Ray Society

before the building was completed, his son Edward, Jr. (1878–1967), continued and increased the family's commitment. The General Education Board of the Rockefeller Foundation provided matching endowment funds, and the Institute began routine operation in August 1931.

With founding of the Institute, radiology gained departmental status in the medical school, and Sherwood Moore became professor of radiology as well as the first director of the Institute. Under his guidance and that of the directors who succeeded him, Hugh M. Wilson (1949–1963), Juan M. Taveras (1963–1971), and Ronald G. Evens (1971 to present), the physicians and staff of the Institute made continuous contributions to its growth, the best patient care, education of leaders in the field, and advancement of the science.

Growth of radiology at Washington University has paralleled the growth of the specialty in general. A few facts about the Institute illustrate the point. The radiology service was created in 1910 with a single physician and one room of primitive equipment. Seventeen years later, at the time of the Mallinckrodt family grants, there were four radiologists, 16 other employees, and six rooms of equipment. By 1970, the final year of Dr. Taveras' term as director, the Institute consisted of 31 radiologists, 400 other employees, and 34 rooms of equipment. In 1990, the Institute had 77 radiologists, 780 other employees, and 74 rooms of equipment—more than double its 1970 size. By any measure, both radiology as a specialty and the Mallinckrodt Institute as an academic program have experienced remarkable success.

Hardly any major scientific or technologic advancement in diagnostic radiology, radiation oncology, or nuclear medicine has occurred without being influenced by the staff of the Institute. Examples of such developments since cholecystography include angiography, conventional tomography, CT, MR imaging, the linear accelerator, the medical cyclotron, positron emission tomography, sonography, computers in radiology, and many others.

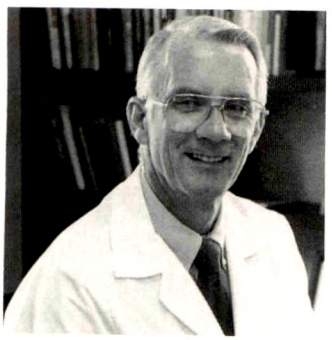
Currently, the Mallinckrodt Institute of Radiology counts radiologists and scientists from all 50 states and many countries among its more than 500 living alumni. Many of the Institute's trainees have joined other academic institutions and been influential in their successes. This legacy is of great pride to the Institute.

On Saturday morning, September 14, 1991, faculty, residents, alumni, friends, and guests gathered to reflect on what it means to be a physician in an academic institution and to focus on the missions and responsibilities ahead. It is apparent that as our society progresses through the 1990s, radiology will be faced with a series of rapidly emerging and difficult challenges. These protected moments of serious reflection were set aside to help understand, prepare for, and meet what might otherwise appear to be uncontrolled changes. The program rededicated the Institute's physical facilities and staff to the highest standards of professional achievement.

Six faculty and alumni addressed topics central to the life of radiology. While traditional subjects of clinical care, education, and research were reexamined, the session also included analysis of industrial partnerships, governmental initiatives, and ethics. At the conclusion of the lectures, a time capsule was prepared to await the 100th anniversary of the Institute in 2031. To all who attended, the rededication program was a highlight of a spectacular weekend. Four of the lectures from that program are reprinted in this special section of the *AJR*.

Government and Radiology During the Next 60 Years

Ronald G. Evens[1]



Our specialty of radiology began nearly 100 years ago in a time when political issues were of little importance to medicine and usually concerned conflicts between physicians and sometimes their hospitals. Governmental funding of clinical programs was nonexistent. Decades later, when the Mallinckrodt Institute of Radiology was established in 1931, the federal and state governments remained insignificant participants in medical care. The early Institute billed the patient directly, occasionally billed their employers, and never billed the government. Research was funded by the university, the General Education Board of the Rockefeller Foundation, or philanthropists, as best exemplified by the Mallinckrodt family. Teaching was the responsibility of teachers without review or certification by regulatory agencies.

The year 1991 presents a very different scenario. The government, whether federal or state, is a primary participant in clinical and academic activities. And, where government dollars flow, regulation soon follows. Regulation is increasingly more pervasive and complicated and not just restricted to the government. Another important aspect of regulation is nongovernmental and "self-induced" by physicians and medical societies. Examples include board certification, mammography accreditation, and various joint commissions. Both governmental and voluntary regulatory programs are historically recent, and their quality, quantity, and importance are increasing rapidly.

The Past

For many years the only major medical governmental regulating agency was the Food and Drug Administration (FDA). The Congress authorized the FDA in 1906 with the strong encouragement of most physicians and the American Medical Association because of several national scandals. Most were related to the food industry; a striking example was publicized by Upton Sinclair's novel *The Jungle* describing the terrible conditions in the meat-packing industry. The FDA had relatively little to do with medical practice until the 1930s [1]. Major revisions in the FDA's authority continued to follow additional crises and disasters. For example, in 1938 a pharmaceutical called elixir sulfonamide was formulated incorrectly and killed more than 100 people before discovered and reported. The subsequent 1938 revisions of the law added cosmetics and medical devices to FDA regulation for the first time. Another example is the thalidomide tragedy that resulted in a series of malformed infants and more stringent amendments to the law in the early 1960s that included the regulation of investigational new drugs for the first time. Another FDA milestone for radiologists was the 1968 Radiation Control and Health and Safety Act, which transferred radiation protection regulation from the Public Health Service to the FDA. Now radiation protection is an FDA issue, similar to all medications, cosmetics, food, additives, and devices. When the FDA is in the spotlight, so is radiology. In 1991 the FDA was under serious challenge from many fronts, some "activists" who wanted more stringent laws as well as some "pragmatists" who desired less regulation with its associated delays and cost.

Prior to World War II, the FDA was the only major governmental agency involved in medicine, but government involvement with medical issues expanded soon afterward. The National Institutes of Health (NIH) grew from a small Public Health Service laboratory on Staten Island into the primary funder of medical research. Beeson [2] reported on the importance of NIH and its growth in research spending from $750 million during the decade of the 1940s to more than $140 billion in the 1970s. The federal support of research is generally given high marks by everyone and certainly has had a significant impact on the academic medical center, as exemplified by Washington University. For example, in 1950 there were approximately 1000 full-time faculty positions in all United States medical schools. With federal support, by 1985 there were more than 12,000 faculty members and thousands of postdoctoral fellows and other trainees [2].

The expanding federal government interest in medical issues following World War II was broad based and affected

[1] Director, Mallinckrodt Institute of Radiology, Washington University School of Medicine, 510 S. Kingshighway Blvd., St. Louis, MO 63110-1076. Address reprint requests to R. G. Evens.

AJR **159:11–14, July 1992** 0361–803X/92/1591–0011 © American Roentgen Ray Society

nearly every part of medical practice. The government and politicians wanted to make major improvements in the public's access to medical care and the quality of care delivered. Lawrence Brown, a political scientist at the University of Michigan [3], suggests the multiplicity of federal laws and agencies falls into four general categories according to their prime method of motivating health care delivery: subsidy, financing, reorganization, and regulation.

The first step by the federal government to influence medical care was legislation oriented toward subsidy. Examples include legislation authorizing the NIH to subsidize research; the Hill-Burton legislation of 1946 creating major subsidies for hospital construction; and multiple legislative incentives to increase the number of physicians, nurses, and other health personnel during the 1950s. More recent examples of subsidy legislation are President Nixon's establishment of the National Cancer Advisory Board in 1971 and the Health Professions Educational Assistance Act of 1976 to increase the number of primary care physicians.

As subsidy programs failed to solve problems of the quality or access to medical care programs, the government next moved to direct financing of health care. The year 1965 was seminal for federal legislation, as President Lyndon Johnson and Congress established the Medicare and Medicaid programs against the strong opposition of the American Medical Association and most of organized medicine and individual physicians. The government soon found the bill for medical care was much more than expected. While federal/state financing of health programs was finally accepted by physicians, the dollars consumed continued to grow. Yet federal legislation continued to add financial responsibility to the government. Examples are the addition of disabled individuals and patients undergoing renal dialysis to the Medicare program in 1972 and the Child Health Assurance Program of 1984, which added pregnant women and some children to the Medicaid program.

Brown [3] outlines the expected pattern to be followed by the federal government when the political goals of the Congress are not met by subsidy and financing, and initiatives of Congress have resulted in continued high costs. According to Brown's thesis, as financial legislation created more economic problems than social value improvement, the next legislative step attempted to reorganize medicine. By the 1970s, President Kennedy had supported legislation to develop the National Health Service Corps and Congress had provided funds to encourage health maintenance organizations (HMOs), established the Health Care Financial Administration (HCFA) within Medicare, and established local Health Service Agencies (HSAs) and many other programs. None seemed to work, and many were abandoned during the Reagan administration. Finally, when subsidy, financing, and reorganization added costs but did not meet social goals, regulation was the next legislative step—the era currently in vogue.

The Present

Regulation started slowly with the FDA in 1906, but expanded with fervor after the Medicare and Medicaid legislation of 1965. Regulations became a part of almost every medical/political thrust, as exemplified by the HMO legislation in 1970, Certificate of Need legislation in 1974, physician service review organizations and HSAs in the mid 1970s, and every subsequent adjustment to Medicare authorizations.

In addition to the many agencies and rules directly related to medical care, the Congress of the 1960s, 1970s, and 1980s generated a series of agencies or specialty programs that indirectly affect medicine. To list a few, the Environmental Protection Agency has dramatically increased the cost of medical waste disposal as well as influenced the economic impact of certain work-related diseases such as pneumoconiosis, the Nuclear Radiation Council regulates the availability and use of isotopes, the Federal Aviation Agency regulates the transportation of isotopes, the Department of Agriculture regulates the use of animals in research, and the Equal Employment Opportunity Commission affects personnel policies in every business, including medicine [4].

Nongovernmental Regulation

Today, considerable regulation does not originate from the government, and many important regulatory agencies, boards, and commissions, are "voluntary." Examples familiar to most physicians include the Joint Commission of Accreditation of Health Organizations (JCAHO) [5], which was only founded in 1951 and now has considerable impact on how we practice medicine and the cost of care in hospitals and other facilities. The vast majority of physicians voluntarily submit to specialty board examinations such as the American Board of Radiology (ABR) (I wonder if our third- and fourth-year residents would agree that it is voluntary). While not required by law, these voluntary certifying examinations have great influence on the professional experience of radiologists, including obtaining hospital privileges, state licensure, and ability to bill certain third-party payers. Medical and residency training is certainly affected by the various residency review committees (RRCs) (a voluntary program of "joint ventures" by the American Medical Association, American Hospital Association, and specialty societies); examples include the Liaison Commission on Medical Education (LCME) for medical students and the Liaison Commission for Graduate Medical Education (LCGME) for postgraduate training. Some voluntary regulation programs have gained the force of law. The clinical chemistry laboratories were previously voluntarily certified by the JCAHO and the American College of Pathologists, but have been subjected to a series of federal clinical laboratory regulations since soon after Medicare enactment and the first Clinical Laboratory Improvement Amendment of 1967. The pattern has been increased involvement of physician-owned laboratories [6].

In 1991, probably the most active arena of voluntary regulation was the development of medical standards. This is taking a considerable amount of effort by most specialty organizations, including the American College of Radiology (ACR). Defining standards for practice is new—first initiated by the American Society of Anesthesiology in 1986. Standard setting is now "standard" practice, and in 1990 involved more than 15 specialty societies including the ACR. Currently the

standards are voluntary, but there is a strong possibility (and concern by many physicians) that standards will move from guidelines to rules and regulations, as is the case with the clinical laboratory. If this happens, physicians and their practices must meet the standards in order to practice and get paid for services. You can imagine the concerns and/or interest by various professionals—physicians, lawyers, regulators, and providers [7].

How do these affect the Institute and radiologists today? The answer is in nearly every way. Today, governments (through Medicare, Medicaid, Veterans Affairs, Champus, and state employee insurance) pay nearly 50% of all clinical bills and the percentage is rising. The recent act of Congress authorizing HCFA to develop a national payment system (the famous Relative Value Schedules) was the most important item of the ACR agenda in 1991. Federal agencies (notably the NIH, Department of Energy, Veterans Affairs, and Department of Defense) are the primary sponsors of biomedical research. Essentially every training program requires certification by someone, usually a voluntary organization such as the LCGME. While local political issues are important, the political playing field has moved to the state and national levels.

The Future

Do governmental programs influence the practice of radiology—of course! A few examples: (1) Concerns about cost encouraged secretary of health Joseph Califano in 1975 to decide that CT was "technology run wild," and it took more than 2 years for body CT to become accepted for payment by HCFA [8]. (2) Positron emission tomography (PET) is still not accepted for clinical use and there is debate on how its radiopharmaceuticals should be regulated and by what agency [9]. (3) The Mallinckrodt Institute must have state Certificate of Need committee approval before we can install and use new technology such as CT, MR imaging, and PET. (4) At least once a year we are reviewed by various regulatory councils, agencies, and groups. Within the last year, the Institute has been reviewed by the JCAHO (twice, once for Barnes and once for Children's), the RRC for radiology, the ACR for mammography, and the Joint Committee for Radiologic Technology (JCRT) for technology training in diagnosis and therapy; our medical school will be reviewed in October by the LCME. All of these are voluntary, but we have little choice if we want to participate in the training of physicians. Each of these review agencies strongly influences the manner in which we educate our students. For example, the procedures by which the ABR tests our residents dramatically influence how we practice and teach; just come around the Institute during the 3 months before boards and see what the residents are doing—intensely reviewing (and memorizing) 4 years of training.

What's the future? It's easy to predict that government action and regulation will not only continue but increase owing to the double problem of access and cost. Access to medical care continues to be a major problem, and the government has to take a leadership role in solutions to the problem. Most parties involved with medical care (i.e., insured patients, physicians, insurance carriers and third-party payers, and corporations) are interested in issues with a higher priority than providing care to the uninsured and underinsured. As David Axelrod, former New York State commissioner of health in the 1980s, stated: "Without government in the healthcare delivery process, economics and economic considerations will always determine who gets what and therefore leaving out those without economic power" [10]. The second driving power will continue to be concern about costs, and regulation will focus on the specialty of radiology. Today radiology is big business—approximately 300 million X-ray procedures a year, approximately 1.3 diagnostic examination per person per year in the United States, costing approximately $20 billion, and rising steadily [11]. "High tech" is now approximately 50% of all radiology charges, and most new technologies are expensive [12].

Let's not forget that each of the 50 states has regulatory mandates as well as the federal government. While some believe state health programs have been "eclipsed" [13], most physicians and administrators would debate that states have become more important [14]. States leading in regulatory enthusiasm (such as Massachusetts and Maryland) [15] develop their own programs in an attempt to control costs. Certificate of Need legislation in the state of Missouri has certainly affected the Mallinckrodt Institute, and considerable time, effort, and funds are required to obtain approval for major installations of equipment.

An Action Plan

What should we do? Medical care is not meeting the needs of many citizens, and nearly everyone agrees care costs too much. Somebody has to take leadership to solve the problems. Sam Thier, the most recent president of the National Institute of Medicine, tells us that physicians must lead because no one else is an expert on medical care [16]. But others should also be a part of the process, since expertise in many areas (business, the law, social sciences, etc.) will be necessary to find the best solution. Accordingly, we must learn to lead and cooperate with others. We must accept the fact that nearly everyone, including physicians, have self-interests—insurance companies want to keep their business going, employers want to reduce their costs, and physicians want to protect their practice and finances. Real leadership will recognize self-interest but emphasize the larger interests of the country and its citizens.

Is there a special position for the Mallinckrodt Institute of Radiology and its faculty and staff? Yes, this celebration of our first 60 years demonstrates how we have led in science, clinical care, and education. The challenge of the next 60 years will be to use our special expertise to continue caring for people *and* improving future medical care, but in addition we must play a new role in the political process. While politics is highly political, legislation is influenced by data— the best law does not come from a vacuum of knowledge but from facts and wisdom that the Institute's faculty can provide. We must not only care for patients, teach future physicians and technologists, and expand medical knowledge, but we also must influence the political process that will establish how medicine will be practiced in the next century.

It is possible that technology assessment and regulation can actually improve patient care as quality standards are raised and access is improved. The downside risk is the possibility of overregulation, "excessive paper," and loss of the innovative spirit that is currently a part of the practice of medicine and associated academic endeavors. The specialty of radiology and our Institute will be best served by recognizing that continued government involvement is inevitable, and rather than fighting, let's become leaders in the political process. The next 60 years will offer the opportunity to use our research skills and clinical expertise in many ways. Our challenge will be to consider political issues without adversely affecting our primary missions—taking care of patients, developing new knowledge, and training the leaders of the future.

REFERENCES

1. Hayes AH Jr. Food & Drug reputation after 75 years. *JAMA* **1981**;246:1223–1226
2. Beeson PB. One hundred years of American medicine. *Ann Intern Med* **1986**;105:436–444
3. Brown LD. The proper boundaries of the role of government. *Bull N Y Acad Med* **1986**;62:15–26
4. Keith SN, Bell RM, Swanson AG, Williams AP. Effects of affirmative action in medical schools. *N Engl J Med* **1985**;313:1519–1525
5. Kyes K. Performance assessment: a JCAHO perspective. *Decisions Imaging Economics* **1991**;4:13–18
6. Peddecord KM, Hammond HD. Clinical laboratory regulation under the Clinical Laboratory Improvement Amendments of 1988. Can it be done? *Clin Chem* **1990**;36:2027–2035
7. Boisaubin EV. Practice standards: implications for the internist. *Am J Med Sci* **1990**;300:173–177
8. Evens RG. Computed tomography—a controversy revisited. *N Engl J Med* **1984**;310:1183–1185
9. Tilyou S. Regulation of PET radiopharmaceuticals, NDA for ^{99m}Tc HMPAO, and the gastric emptying petition. *J Nucl Med* **1989**;30:137–140
10. Axelrod D. The state perspective. *Bull N Y Acad Med* **1986**;62:94–100
11. Sunshine JH, Mabry MR, Bansal S. The volume and cost of radiologic services in the United States in 1990. *AJR* **1991**;157:609–613
12. Evens RG, Evens RG Jr. Analysis of economics and use of MR imaging units in the United States in 1990. *AJR* **1991**;157:603–607
13. Rabe BG. The eclipse of health departments and local governments in American environmental regulation. *J Publ Health Policy* **1988**;9:376–392
14. Farmer HF. Government regulation—national or state: is one better than the other? *J Fla Med Assoc* **1989**;76:300–301
15. Fielding JE, Weiner S. Controlling hospital costs in Massachusetts. *N Engl J Med* **1978**;299:1249–1251
16. Thier SO. Health care reform: who will lead? *Ann Intern Med* **1991**;115:54–58

Research at the Mallinckrodt Institute of Radiology: A Strategic Plan for the 1990s

Michael W. Vannier[1]



Research at the Mallinckrodt Institute of Radiology is a source of pride in the institution. We think we are quite good; at the same time, we are sure we could be better. More than a year ago, the senior members of the department met and, over a period of time, formulated a strategic plan for the future of the Institute. In that strategic plan, goals for improved internal research administration and productivity were set. The report summarizes the strategies for our future research activities in terms of three goals: (1) improved research in imaging and associated sciences, (2) increased procurement of research funds, and (3) improved transfer of technology from research to clinical applications.

The first step in implementing this plan was assessment of the Institute's current research status. If we are ever to realize any improvement, we must know where we are now. In 1990, we received about $8.5 million in extramural funding.

We established criteria to measure our progress in achieving these goals, including financial performance, scientific productivity, and amount of faculty involvement. These criteria are under development in much the same way that the methods for achieving our goals are continuously refined and improved. Current funding levels, for example, are often not the best predictors of future performance. It is difficult to use crude aggregate scores (like total research funding) to recognize research opportunities and solve current problems. For this reason, it is imperative that we develop better measures for assessing our complex research environment.

Opportunities for Improvement

It is important that we recognize our weaknesses as well as our strengths in order to guide the allocation of resources available for research. The motivation to pursue extramural funding for research is not strong for many radiologists. The large investment of time (e.g., nights, weekends, travel, writing and rewriting proposals and reports, begging and borrowing special equipment or expertise, hiring and managing research staff, and managing problems associated with the use of experimental animal or human subjects) that is needed to be successful as independent (and funded) investigators does not translate into any obvious advantage for most faculty. Clearly, many members of our clinical staff have established their reputations, been promoted, and become widely recognized in the profession. This is true even though all their work is reported in clinically oriented, primarily descriptive publications and reviews. In most instances, the senior clinical faculty has had little involvement (or interest) in extramurally funded investigator-initiated peer-reviewed studies. Why then should junior faculty members deviate from this well-established norm to risk their careers on focused, difficult, time-consuming, demanding research projects that could compete effectively for extramural support? We currently do not have a completely satisfactory answer to this key question, but are committed to finding one. The solution may lie in recognition, encouragement, incentives, perks, or other rewards. We may have to try them all before we arrive at an effective solution.

The staff of the Institute (faculty and support personnel) is remarkably stable and cooperative. Resources are abundant, and virtually all of us are satisfied. Nevertheless, it is unusual for radiologists to work as teams. They are much more likely to work in isolation on their own projects. Other professionals may be acknowledged and listed as authors, but they make a limited contribution and have little influence on the work. Multidisciplinary studies that involve major commitments (extending over years) to a research problem by radiologists with other clinicians (surgeons, oncologists, internists, pathologists) or basic scientists or engineers are rarely attempted. As a consequence, most research projects are performed by a faculty member working in isolation, with only modest assistance from colleagues.

Radiologists are not inclined to take risks with the research projects they select. Radiologists usually undertake projects

[1] Director, Division of Radiology Research, Mallinckrodt Institute of Radiology, 510 S. Kingshighway Blvd., St. Louis, MO 63110-1076. Address reprint requests to M. W. Vannier.

AJR **159:15–17, July 1992** 0361–803X/92/1591–0015 © American Roentgen Ray Society

they can perform alone. They rarely consult experts regarding important elements of the research, such as experimental design, analytic techniques, and statistical analysis. If they do this at all, it is only when the project is nearing completion. They find it more productive, easier, and faster to do projects in which they are in complete control. Characteristically, such studies involve a simple retrospective review of images from specific groups of patients.

Commitment to Research

At its 60th anniversary celebration, the Mallinckrodt Institute of Radiology has renewed its dedication to research. A research committee, consisting of senior faculty members from all divisions of the Institute, has been formed to oversee the allocation and use of research resources, especially space and funds. One of its charges is to adopt a long-term perspective to ensure greater research productivity and quality. Until now, there has been little accountability for the use of research resources by faculty members. For example, although many diagnostic examinations are performed solely for research purposes without charge to patients or investigators, there has been no mechanism to determine how these studies are being used. Consequently, there has been no incentive for the faculty to use this resource as productively as possible. These studies may not have been wasted, although some surely were, but it is unclear how effectively they have been used. In the future, accountability will ensure that opportunities to accomplish important research will not be lost. The allocation of resources—personnel, space, funds, equipment, and gratis examinations—will be based on the scientific merit of research proposals submitted by the faculty as determined by peer review. Reviewers will include members of the research committee and consultants from other departments at Washington University. In selected instances, outside reviewers (established investigators from other institutions) will be asked to provide a written assessment of proposals (and be offered an honorarium for a formal mail review).

We recognize that investigators must have adequate time and resources to be productive in research. Other specialists usually have more time than radiologists to devote to research. Internists and surgeons, for example, often serve on clinical services only 3 or 4 months a year, whereas radiologists rarely have long periods free of clinical responsibilities. Research laboratories in medicine and surgery departments are often operated by investigators who have no obligations to patients. This is rarely the case in radiology.

In addition, internists have research laboratories (space, equipment, and personnel) that operate very independently of routine patient care. Although there are research laboratories in radiology, it is often true that no radiologists are present. Radiologists may complete their entire residency and fellowship and enter academic practice but never spend a day in or even visit the research laboratories of their own department, much less attempt an experimental project of their own. This tradition is counterproductive, and the establishment of laboratory facilities devoted to radiologists' research interests with provision of extensive related infrastructural resources is a major goal of our current and future research program. We have determined that provision of a research infrastructure is required for our long-term success, including equipment and personnel; biostatistical services; data base management (design, entry, retrieval services); custom computer programming for projects; computer network services; image manipulation and analysis; and administrative support to assist in formulating proposals, budgets, and personnel matters. The assignment and training of skilled support personnel who have the appropriate equipment and space with sufficient funding to handle incidental expenses (such as disposables and travel) is a key element in our long-term plan.

Radiology research projects often require specially designed equipment to quantify complex physical phenomena. Radiologists usually are not qualified to perform these studies without the assistance of physicists and engineers. To provide a mechanism for this type of support, we have consulted our engineering and basic science colleagues, provided them space, and stimulated collaboration on problems of immediate clinical significance as well as long-term development. Expensive equipment, such as CT and MR scanners, must be available to the faculty if they are to perform competent research. Scanners used both for patients and research are rarely satisfactory for research, because patients must take precedence and use of clinical scanners is invariably quite high. To find space for this equipment and pay for it, we have entered into long-term arrangements with basic scientists, pharmaceutical houses, and other clinical departments to form an imaging research center with enough extramurally supported projects to provide shared equipment for research and the distribution of costs over a broad base of sponsors and users.

Imaging systems are costly and in some cases, such as MR and CT, require specialized environments. Such systems are typically fully used for examining patients, and cannot be modified without introducing unacceptable risk to patients. If research is important, dedicated imaging equipment is essential. To provide an investigator with academic time but no instrumentation to perform a study is not a sufficiently high level of commitment to achieve our long-term goal of outstanding research quality. Therefore, we have made the move to provide extensive space and dedicated state-of-the-art instrumentation for research in radiology. An example of this is MR, where our best scanning equipment and greatest amount of space are used for imaging research.

Some obstacles to progress will always be present. We seek to remove impediments imposed by administrative or resource limitations. The process of identifying, prioritizing, and solving problems, and incrementally but continuously improving the research environment, is our commitment.

It is unrealistic to think that we can solve all problems at once. The research opportunities at any large medical center differ according to the presence of expert collaborators, populations of patients, knowledge and interest of the staff, and many other factors.

Transition

The transition from resident to fellow to assistant professor must not be the weak link in the Institute's goal of increasing research productivity. Residents and fellows will be taught the fundamentals of research, but most of the Institute's resources will be invested in equipping newly appointed assistant professors with the skills and motivation they need to be productive. In the future, mentors will be appointed for new faculty members to guide them in the proper direction, to stimulate their interest, and to expedite their progress. We no longer are satisfied with a career plan that includes writing case reports. The most important individual in the future development of the research program at the Mallinckrodt Institute of Radiology is a fully trained, newly appointed, and highly motivated assistant professor. We intend to teach residents and fellows about research but provide the most resources to individuals whose training is complete. We find that often the individuals who have recently joined the faculty have some relevant research experience already. We seek to build on this foundation by instituting a plan and selecting or nominating a mentor to assist in the difficult transition from recent postgraduate trainee to established independent investigator (with extramural support).

This transition is not inexpensive. We anticipate that it will cost upward of $350,000 and require 3 years or more to accomplish this transition. This money may be used for specialized equipment, support personnel, space, and related costs. This commitment on the part of the institution is firm and strong, but requires an equal commitment from the candidate to invest the time and effort and to make the sacrifices needed to achieve the goal of outstanding science and substantial independent support.

We define an independent investigator as one who has successfully applied for and been granted National Institutes of Health support through the traditional mechanisms (R01, R29, or similar). The candidate can expect to have a laboratory with dedicated support personnel and space and equipment devoted to his or her research program.

Training

Additional effort must be made to attract physicians from established M.D.–Ph.D. medical scientist training programs to apply for radiology residencies. We recognize that these people are a major resource for improving research in radiology. They are equipped with the specialized skills necessary to do research, and they have proved their commitment to research. In the future, the strong attraction of residencies in radiology will encourage applicants who have specialized research training. These individuals made the commitment to be medical scientists at the time they entered medical school. In many cases, this was 5 years or more before residency. M.D.–Ph.D. training programs are competitive, and they select candidates that show exceptional promise to become research scientists. Radiology can attract these candidates into residency and retain them as clinician-researchers. This is a major strategy for improving research in radiology over the long term.

Recently, we introduced a research track in the diagnostic radiology residency to accommodate candidates who are willing to commit an additional year (usually postgraduate year 2 or 3) or more to develop their research program under the mentorship of an established faculty member (not necessarily from radiology). The intent is to provide for simultaneous development of research and clinical skills. This is a new experience for both the residents and the staff.

Collaborations

We seek to increase the number and quality of research collaborations both intra- and extramurally. The most important intramural collaborators are clinician-researcher colleagues from medicine, surgery, pathology, and neurology as well as the biomedical basic sciences, engineering, and physics. The key extramural collaborators and sponsors of research include industry (equipment and pharmaceutical manufacturers) and institutions, universities, and government.

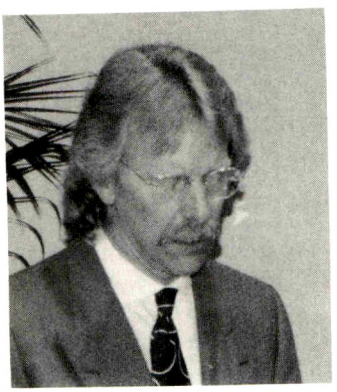
Future

We look to the future for continuous incremental improvement in our research environment and productivity. An imaging research center with combined MR and positron emission tomographic resources is planned. We will enhance our administrative structure for the management of projects, offer better peer review, and encourage increased communication among qualified investigators, with provision of incentives, increased visibility, and establishment of bench marks. Divisional, sectional and departmental research reports and a catalog of investigators will be created.

Winston Churchill said that we are closer to the end of the beginning than to the beginning of the end. There is much room for improvement, and we are committed to doing whatever is necessary to advance medical knowledge and strengthen the profession in service to our patients.

Radiology Ethics

John D. Armstrong II[1]



The ethical dimensions of our professional endeavors are central in these deliberations. Traditionally, Western ethics has sought to discover, and to guide us toward, what is "right," and make moral judgments about what is "good." Ethics has sought to discover the "ought," which is often in conflict with the "is." Ethics asks questions about the values that we hold, about how we ought to live and how humans ought to relate to one another and to the rest of nature. Insofar as one thinks critically about one's own moral views, or the moral values of others, or reflects on their justification, or compares them with rival attitudes, to that extent one is a moral philosopher.

In the first portion of this discussion, I will examine the Western philosophical tradition from which we descend. Second, I will examine a significant conflict in the modern medical paradigm. Third, I will speculate about the sort of new value system or new paradigm that might be needed if we are to appropriately meet the needs of our patients and society.

Western Philosophical Tradition

Prior to the Age of Enlightenment, the dominant world view in Europe was organic and the framework of science was based on the paradigms of Aristotle and the Church. With reason and faith as its main cornerstones, science endeavored to understand the meaning and significance of things. Subsequently, during the Scientific Revolution, major contributions were made in philosophy and science that changed the world view.

René Descartes, the founder of modern philosophy, experienced an illuminating vision. His vision was to construct a complete science of nature about which he could have absolute certainty. He began by doubting all traditional knowledge, the impressions of his senses, and even the fact of his body; until he reached the one thing he could not doubt, the existence of himself as a thinker. Thus, he arrived at his celebrated statement, "*Cogito, ergo sum*" ("I think, therefore I am"). From this, Descartes deduced that the essence of nature lies in thought. This view had the startling consequence that the world is made of two incompatible kinds of substance: mind (or consciousness) and matter, which is extended and divisible. Thus, we are, in his view, an incorporeal or disembodied mind mysteriously located in a mechanical extended body. In fact, Descartes compared the human body to a clock. In this view, a sick man may be compared to a poorly made clock and a healthy man to a well-made clock. Thus, Descartes gave scientific thought its general framework; that is, the view of nature as a perfect machine governed by exact mathematical laws. As matter, the material universe had no intrinsic purpose, life, or spirituality. Descartes also shared Bacon's view that the aim of science was the domination and control of nature [1].

In contradistinction to the Cartesian world view, a modern system's view of nature gives value to concepts like organic, holistic, and ecologic; however, the Cartesian paradigm (of the mechanistic view of life) dominates our attitudes toward health and illness. The so-called biomedical model, which forms the conceptual foundation of modern scientific medicine, is firmly grounded in Cartesian thought. It regards the human body as a machine that can be analyzed in terms of its parts; disease is the malfunction of biological mechanisms, which are studied from the point of view of cellular and molecular biology; we physicians then intervene physically or chemically to correct the malfunctioning of a specific mechanism. This analytic and reductionist approach of the biomedical model has difficulty with the phenomenon of healing, a concept often considered outside the scientific framework; the biomedical model cannot give an account of the social, environmental, psychological, or spiritual dimensions of the human condition [2, 3].

Conflict in the Medical Paradigm

I will briefly characterize a distinction that seems preeminent in modern life, medicine, and radiology. It may be called the humanity vs technology conflict.

Humanity

In significant measure, illness is a loss of humanity. When one becomes a patient, one is suffering and fears dying (or a

[1] Department of Radiology, University of Colorado Health Sciences Center, Campus Box A030, 4200 E. Ninth Ave., Denver, CO 80262-0030. Address reprint requests to J. D. Armstrong II.

AJR **159:18–20, July 1992** 0361–803X/92/1591–0018 © American Roentgen Ray Society

painful death) and one may no longer be free to order one's life; thus, one becomes dependent, vulnerable, and exploitable [4]. The fact of illness establishes our self-imposed obligation as physicians to act as moral agents, with particular sanctions to act in the patient's best interests, to relieve suffering. The patient is the beneficiary in the trust relation; we (physicians) are the trustees [5]. Our duty is to honor the patient's humanity and allow for one's individual uniqueness to be taken into account. We profess (or promise) competence, compassion, fidelity, and beneficience in that trust [6].

Technology

Advances in biology during the 19th century were accompanied by the rise of new technology. New diagnostic tools, like the stethoscope, were invented, and at the same time the attention of physicians gradually shifted from the patient to the disease. The mechanistic view of the human organism encouraged an engineering approach to health with an accompanying avoidance of the philosophical and existential issues that arise in every serious illness. An excessive emphasis on medical technology and the perception of it as the only, or most important, way to improve health results from this perspective. High technology, in which we are involved, has taken a central role in modern medical care. An examination of our increasing dependence on complex technologies reveals that technology has accelerated the trend toward specialization; has enforced the physician's tendency to look at particular parts of the body instead of the person with the illness; has shifted diagnostic evaluation to hospitals or high-technology centers; contributes to depersonalization, if not dehumanization, of patients, who often feel helpless and frightened; sharply increases health care costs; contributes to entrepreneurial medical practice and conflicts of interest (e.g., self-referral); causes unnecessary pain and suffering; contributes to "defensive medicine" and fear of litigation; contributes to the spellbinding mystique that surrounds the medical profession; and reflects the fact that our profession (like our society) denies death, the ultimate existential issue for humankind [2].

In the context of modern medicine's emphasis (and reliance) on high technology, to what extent do radiologists think of themselves as physicians and take responsibility for their role in the patient-physician relationship? I offer the following model of radiologic practice in its varied levels of function for our reflection.

At one level, the radiologist experiences physical proximity and psychosocial closeness to a patient, and perhaps to his or her family members, in a dialogue focused on the patient. The patient acknowledges the radiologist as an integral part of the health care delivery system and may remember the radiologist's name after several days. This level may correspond with the paradigm patient-physician relation.

At a second level, the radiologist has contact and discussion with a patient, perhaps during part of the informed consent process, but the interaction is brief and focused on a specific issue. The patient may not hear or remember the radiologist's name.

At a third level, the radiologist may have visual contact with the patient who is undergoing an imaging examination, perhaps a glance through the window of the CT or MR device, without interpersonal contact. At this distance, the radiologist probably lingers in the patient's mind as just another hospital employee. At this level, the radiologist may review the patient's chart for relevant information and/or make a note in the record about some aspect of the imaging data or patient care.

At a fourth level, the radiologist has no contact with the patient but engages in some form of dialogue with the patient's physician about the patient, the imaging data, or other aspect of the patient's care. This communication may take the form of a telephone call or face-to-face discussion.

At a fifth level, the radiologist may be concerned exclusively with current medical images, have no access to (or interest in) relevant clinical data or previous images, and have no contact with the patient or the physician other than through a written report.

At a sixth level, the consultative communication may take the form of "shadow"-based language that relies on words and phrases such as opacity, echo density, attenuation, or signal intensity. The radiologic report may remain descriptive, and important concepts such as anatomic designation, pathologic characteristics, likely diagnosis, and significance (of the findings) to the patient are not offered in the communication. Perhaps included at this level of function is the physical absence of the radiologist from the sites of the patient's examination and the interphysician dialogue; for example, because of telecommunication of images to the radiologist's residence.

Finally, a seventh level entails a view that the "patient" is merely an abstract entity, an object in the marketplace, a source of income. In this view, the patient-physician relation is perceived as a means; the end is perceived as material success, community prestige, or personal power.

In a culture in which the marketing orientation prevails, and in which material success may be the dominant value, there is little reason to be surprised that the patient-physician relation may follow a pattern of exchange wherein the patient is perceived as a commodity and the radiologist (or any physician) is remunerated for his or her skilled labor. This seven-level model, although imperfect and incomplete, represents a spectrum of separation or uncoupling between the patient and physician on which we all can be found, and it serves to illustrate the conflict between humanity and technology, as well as the conflicting values between a physician's obligation to the patient and self-interest.

New Paradigms

I assert that our dominant value system is inadequate and inappropriate for guiding our thinking about new ways to deal with current health care and societal crises. The problems that we have created cannot be resolved by the same mode of thinking with which we created them. A humorous story helps to introduce new thinking.

A customer at a restaurant is so well known as a borscht lover that whenever he comes in he is immediately served

borscht without having to order it. One day, after being served, he beckons to the waiter.

"Waiter," he says, "taste the borscht."

"You don't like it?"

"Taste it."

"Look, you don't like, so I'll change it."

"Taste it."

"Why do I have to taste? You don't like? So I'll give you a menu, you'll select something else, I'll bring anything at no extra charge. We only want to please you."

"Taste the borscht!"

"Look, I got 57 other customers here, I'm gonna taste everybody's borscht, I won't get any work done!"

The customer stands up.

"Will you sit *down* and *taste* the BORSCHT!"

The waiter sits down, looks around the table. He says, "So where's the spoon?"

The customer says, "Ahh!" [7]

The customer could have asked the waiter for a spoon. Instead he asked the waiter to examine a process, to participate for a moment in a different world view.

We are clearly in a paradigm shift—a profund transition in thoughts, perceptions, and values that form a vision of our reality. Systems theory looks at the world in terms of the interrelatedness and interdependence of all phenomena. In this framework, an integrated whole whose properties cannot be reduced to those of its parts is called a system [8]. Living beings, societies, and ecosystems are all systems. As living beings, we are self-organizing systems, intrinsically dynamic in nature. The principal dynamic phenomena that characterize self-organizing systems are self-renewal and self-transcendence. Self-renewal is the ability to continuously renew and recycle our components while maintaining the integrity of our overall structure. Self-transcendence is the ability to reach out creatively beyond physical and mental boundaries in the process of learning, development, and evolution [9].

Self-renewal and self-transcendence require that we think in new ways. New learning begins with curiosity and perhaps in seeing with new eyes. To whom should we listen in the process of acquiring this new thinking? In my view, we listen to persons who speak from different perspectives and in different voices. We listen to patients, lost in the system. We listen to women; the demise of patriarchy is in sight. We listen to children; they disarm us. We listen to our elders; they have a sense of what is important in the long view. We begin to examine the processes in which we are involved and perhaps question the very basis of the conceptual framework of our most cherished ideas.

Clearly, an organism that thinks only in terms of its own survival will invariably destroy its environment and, as we are learning from experience, will thus destroy itself [10].

The shift in our thinking from a world of objects to a world of relationships has far-reaching implications [11]. As we seek to become more holistic in our thinking, we integrate medical concerns with other societal concerns and see ourselves as part of a single moral community that is global in scope and extended in time. Another element of a new ethic concerns mindfulness and concentrates on mundane details of everyday life. We must be mindful of everything we do, because in a highly interconnected world almost nothing is done without effect. Mindfulness is part of a strenuous morality, one that sees moral content in many activities that have been seen traditionally as morally neutral [12]. Such morality can be empowering, for it gives enormous opportunity to make a difference even in our everyday lives. I believe the ultimate reason for living virtuous lives is not for the sake of being virtuous, but because such a life will have a long-term effect on the collective good.

In summary, I have briefly explored the mechanistic Cartesian world view as the basis of our biomedical model, reflected on the conflict between humanity and technology, and speculated about new values.

As spiritual beings we are unable to separate ourselves from our connections to one another. As moral philosophers our continued growth is an ongoing and open adventure whose outcome is inherently unpredictable. We have the opportunity to use our creative and moral imaginations to find the answers that ethics asks: How should we live, how should humans relate to one another in the human community, and how should the human community relate to the rest of nature? Finally, as radiological physicians, to what extent should we value our relatedness and interdependence with our patients, and to what extent do our contributions in patient care, education, and research turn on that connection?

ACKNOWLEDGMENTS

Thanks to Lois M. French Armstrong, Boulder County Mental Health, Boulder, CO: Stewart R. Reuter, Professor of Radiology, University of Texas Health Science Center at San Antonio, TX; Corey M. Franklin, Director of ICU, Cook County Hospital, Associate Professor of Medicine, University of Illinois Health Center, Chicago, IL; George F. Roggensack, Radiologist, St. Mary's Hospital, Madison, WI.

REFERENCES

1. Vrooman JR. *René Descartes*. New York: Putnam, **1970**
2. Capra F. The biomedical model. In: *The turning point*. New York: Bantam Books, **1982**:123–163
3. Laslow E. *Introduction to systems philosophy*. New York: Harper Torchbooks, **1972**
4. Tomasma D, Pelligrino E. Beneficience-in-trust. In: *For the patient's good*. Oxford: Oxford University Press, **1988**:51–58
5. Armstrong J. *Trust in the patient-physician relation: a conceptual analysis and elaboration of the necessary and sufficient conditions for trust* (thesis). Boulder, CO: University of Colorado, **1992**
6. Brody H. The physician-patient relationship. In: Veatch RM, ed. *Medical ethics*. Boston, MA: Jones and Bartlett, **1989**:65–91
7. Rosten L. *Encyclopedia of Jewish humor*. New York: Jonathan David, **1969**
8. vonBertalanffy L. *General systems theory*. New York: George Braziller, **1968**:3–53
9. Jantsch E. *The self-organizing universe*. New York: Pergamon, **1980**
10. Berry T. *The dream of the earth*. San Francisco, CA: Sierra Club Books, **1988**:50–69
11. Gilligan C. *In a different voice*. Cambridge, MA: Harvard University Press, **1982**
12. Jamieson D. Ethics, public policy and global warming. In: *Symposium on Science, Policy and Value, Issues in Global Environmental Change*. New Orleans: American Association for the Advancement of Science, **1990**

The Hidden Curriculum

P24467

Dixie J. Anderson[1]



Education, one of the most important strengths of an academic radiology department, tends to be taken for granted. The newest high-technology equipment and the basic and clinical research, not our educational programs, command our attention and seem to define academics. In addition to taking education for granted, we assume that our educational programs will always be there and will be even better than when we were the students. While it seems intuitive that effective transfer of knowledge requires constant attention to maintain quality and examination to define the most important specific methods, the science of education is often considered to be secondary to other types of research and the provision of clinical service. How does it happen that with a minimum of focused attention we continue to find quality educational programs in our academic centers? I believe it is because of our "hidden curriculum."

The educational experience may be divided into three facets: the physical structure, the fundamental knowledge, and the hidden curriculum. Successful education results from the seemingly effortless integration of these three components into the daily conduct of a radiology department.

Physical structure includes not just the facility and its equipment, but the schedule, the logistics, the structure of the day, and the frequency and number of conferences. This physical structure is the time, space, and resources that allow for a variety of learning opportunities. It is the scaffolding that supports protected time for asking questions and finding answers; time for education to occur. If we were discussing theater, the physical structure would be the set, the setting, and other elements like the length and form of the play.

Fundamental knowledge, the traditional curriculum, is the second facet. This is the part of education on which we all tend to focus, taking the first component, the physical structure, for granted and ignoring the third, the hidden curriculum. Continuing the theater analogy, this second component would be the script, the play itself. The curriculum, especially in a dynamic field like radiology, requires an ever-changing knowledge base. As new information, new technologies, and new procedures develop, we must make all of that easily accessible to learners. Fundamental knowledge is transferred in many ways, often dictated by the physical structure and, in the case of the diagnostic radiology residency, through a balanced mix of didactics, case discussion conferences, hands-on experience, and the stacks and stacks of studies interpreted over the 4 years of the residency.

The third facet, probably the most important of the three, is what I have chosen to call the hidden curriculum, and it is this component that I wish to emphasize, for it is the part of education that every member of an academic department will participate in and contribute to. The hidden curriculum can be defined as the indelible message, often nonverbal, that a person takes from an event or an experience. It is the essence, the soul, that which is remembered after the source is forgotten. In the theater, this component would be the production, the acting, how the lines are delivered, humorously or seriously, and the costumes.

I first started thinking about the power of the hidden curriculum when a friend related a story about her college professor. The professor said that when he went to kindergarten he learned a whole set of facts he had not known before, but these revelations were not part of the intended kindergarten curriculum. He learned that he was fat. He had not known that before. He learned that he was slower than his peers at almost everything they did. He also learned that he was poor. These ideas became more deeply ingrained than any other thing he learned that year. In fact, it took him many years to deal with those cumbersome, limiting messages, though he finally did and became a very effective, productive adult.

Well, you say to yourself, we don't deliver such self-defeating messages. But the idea that we may teach things that we do not necessarily intend to teach, just by the way things are done, by the issues we avoid confronting, by the way we cover certain topics, and by the priorities we give certain aspects of our operation, deserves broader recognition and discussion.

[1] Mallinckrodt Institute of Radiology, Washington University School of Medicine, 510 S. Kingshighway Blvd., St. Louis, MO 63110-1076. Address reprint requests to D. J. Anderson.

AJR **159:21–22, July 1992** 0361–803X/92/1591–0021 © American Roentgen Ray Society

Radiology is one of the most favored specialties today, and part of the reason for its positive profile is the mostly unstated message that medical students learn from clinical faculty—a message of respect for the radiologist, a message that there remains a great deal of satisfaction to be had in radiology at a time when satisfaction within other medical specialties is diminishing. Though unspoken, the reviews concerning our specialty are very powerful.

What are the unstated messages within our academic radiology departments, what do they say about education, and, more importantly, to what extent do each of us have some control over them? Think back to your first impression of your institution. Recall that feeling you had as you were introduced, your impression of the size of the place, the people who greeted you, the security, the way the place was dressed. And what were the first words you heard? Were they about money? Or did they convey a concern for patient care? Did they show disdain or respect for colleagues in other specialties? Was there an excitement concerning the experience?

One of my most memorable and formative early experiences was working with and being taught by two superb technologists who were not afraid to challenge the system when it was in the best interest of the patient. And when they had a question about the practical need for doing a particularly long or arduous procedure, I was impressed with how often their opinions were heard and were influential. That was an unintentional message: all members of the team are important and are treated with respect.

The hidden curriculum supercedes the lecture series. In fact, it begins long before the lecture starts and does not stop when the lights come on and the slides flick off. We are each a part of an educational process all the time. How we exchange information with each other and our clinical colleagues, the language we use, our intellectual honesty, and the respect we have for one another are important. Each of these things influences our teaching, our learning, and our effectiveness.

When the chief of the department makes teaching medical students a high priority or takes the time to sit with residents to discuss their concerns, it is a message of caring. When the person in charge of medical student education insists that we include students in our daily conferences, we have sent a strong signal of respect for our own beginnings and our own teachers. When one of my colleagues volunteers to help get the work done so that we all may attend a conference, that is a hidden curriculum—a message of support for education.

How we deal with uncertainty and with our mistakes is also very important. When we verbalize our uncertainties and when we search for and learn from our errors we announce our conscientious participation in patient care.

To be most effective, the hidden curriculum and the conventional curriculum should be concordant. Certainly the hidden curriculum can overpower the intended curriculum. For example, when your family physician claims to be concerned about your health and well-being, but does not take the time to listen to your story, the message is at odds with the words, belying a lack of real concern, although unintended.

What is the basis for success in education, particularly in promoting a strong, supportive hidden curriculum? Our success is based on individuals, role models who contribute to one or more of the three components of the educational process. These people are exemplified by chairpersons who make sure the physical structure is in place: state-of-the-art equipment, faculty, support staff, as well as time set aside for learning; and by many radiology faculty who embody fundamental knowledge, people who have dedicated themselves to becoming "walking textbooks of radiologic acumen"; and by those who contribute daily to the hidden curriculum.

In my personal experience, the latter are perhaps best exemplified by two radiologists and teachers who are no longer with us. One was the late Hy Senturia, whom I knew as the chief of radiology at Jewish Hospital in St. Louis and who had an unparalleled work ethic, the highest standards, and a strong sense of what it meant to be a whole person as well as a competent, caring radiologist. The other was Dan Biello, first a resident at the Mallinckrodt Institute and then a member of the Mallinckrodt nuclear medicine staff. Dan was an absolutely exemplary role model who taught us, even while he was dying of Hodgkin's disease, how to live. He was dedicated to the service of caring for patients, but at the same time he was able to take care of himself and give support to colleagues, friends, and family gathered around him. The dignity and integrity he portrayed will always be with me. The apprenticeship format of our teaching programs allows a powerful personal statement illustrating the integration of a demanding career within a fulfilling life.

People are the strength of our hidden curriculum, the main source of the hidden messages. Life is a contact sport. Each of us is constantly coming into contact with people, constantly having opportunities to make a difference in the lives of others. What we teach is not limited to what we say, but includes how we say it. Our teachings reflect our attitudes, prejudices, honesty, and humility. It is our example that will be remembered long after the differential diagnoses are forgotten. Our example, our hidden curriculum, must be considered, guarded, and used wisely.

Perspective

Radiologic Evaluation of a Renaissance Painting

Alan H. Robbins,[1,2] Steven M. Wetzner,[1,2] and Maurizio Marini[3]

The 16th century tempera-on-wood painting entitled *The Crucifixion of St. Peter* (Fig. 1A) was purchased in Spain in 1956 [1]. Recent investigation has confirmed that the painting hung for several centuries in a small Dominican convent outside Madrid until the late 1930s (Reinecker H, personal communication). The scene depicted in the painting is remarkably similar to, and is in most respects a nearly perfect scale model of, that depicted in the Pauline Chapel fresco in the Vatican (Fig. 1B), the last fresco ever painted by Michelangelo [2].

Some differences between the two works, however, are readily apparent: The painting shows St. Peter completely nude, without a loin cloth. No nails hold him to the cross. In the fresco, these details have been completed. In the painting, the head of the man in the background between the two spear holders is disproportionately large compared with the heads of those next to him, and neither of his legs is shown. In the fresco, the head is in proper proportion, and a leg has been included to complete the lower half of the figure. In addition, important differences are seen in the background hills and sky, in the tips of the spears held by the soldiers on the left, and in the area of St. Peter's left hand.

The painting has been attributed to Michelangelo by a number of scholars. It is presumed that it was created as the preliminary study (modèllo) for the fresco [1–3]. Other art historians have suggested that the painting was simply a copy of the fresco, probably painted by one of Michelangelo's contemporaries [4, 5]. The painting has recently undergone a series of tests to reassess the attribution. This article presents the radiographic findings obtained as part of that reassessment.

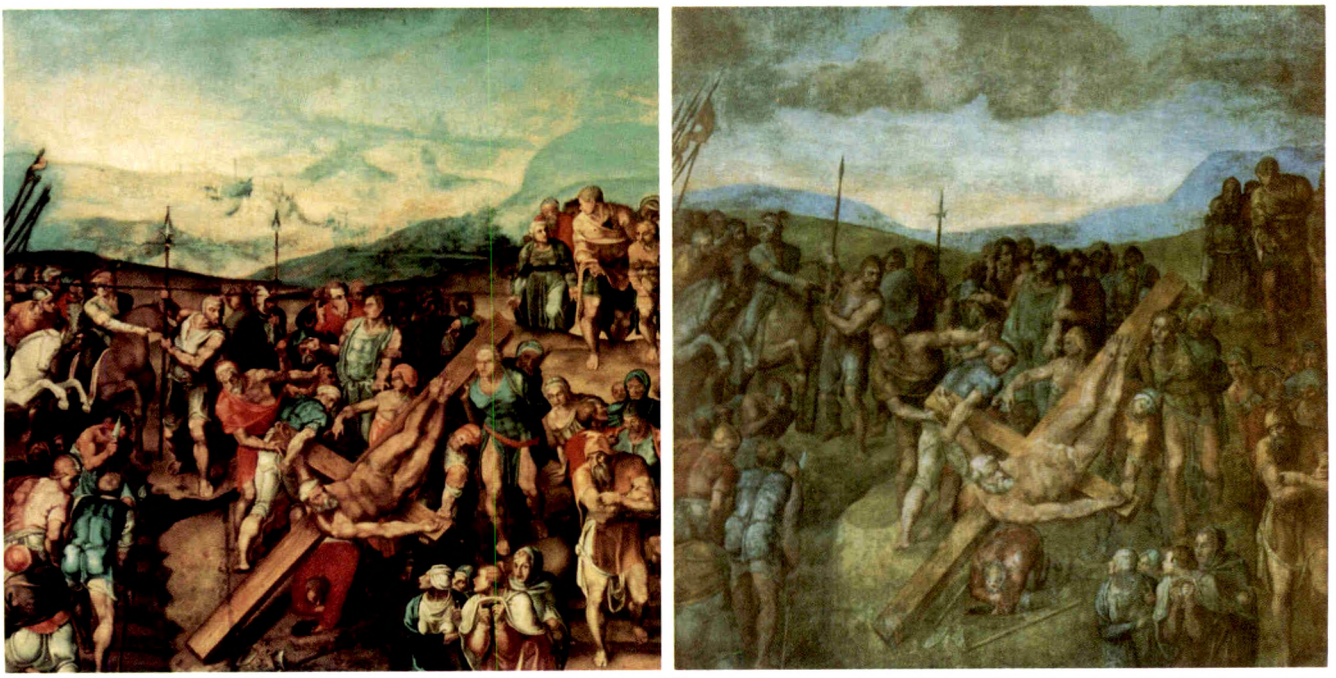
Methods

Radiographs of the painting were obtained by using high-resolution film (DuPont SR381) without intensifying screens [6]. Radiographic factors were 50 kV, 200 mAs, and 36-in. (91.4-cm) tube distance. (Initial standard radiographs were provided by the Fogg Museum, Harvard University. Others were obtained at New England Baptist Hospital, Boston.) Digital radiographic techniques were also used [7]. Primary digital radiographs of the painting were obtained with 40 kV and exposure times in the range of 12–16 msec. A constant potential generator and a 9-in. (22.9-cm) high-resolution image amplifier (Philips Medical Systems, Shelton, CT) were used in conjunction with a 1024 matrix computed angiographic system (Angiographic Devices Corp., Littleton, MA). Additionally, the standard radiographs were digitized by using an AVP Proscan laser film digitizer and viewed on AVP Telepro 2500 and Telepro 1280 workstations (Advanced Video Products, Littleton, MA). After windowing, magnification, and a variety of image processing maneuvers to provide zoom, sharpening, and edge enhancement, hard copies were obtained with both techniques.

The radiographs were studied carefully with the following goals: (1) To assess the underlying structure of the wood panel on which the work is painted. (2) To determine if evidence exists either of a grid drawn on the panel or of "punching" (a method of tracing) underlying the painting, either of which would indicate the work of a copyist [8]. (3) To detect the presence and characteristics of any underdrawing beneath the paint layer and, where possible, to compare the figures detected on the radiographs of the painting with their

Received December 26, 1991; accepted after revision January 30, 1992.
Presented in part at the annual meeting of the American Roentgen Ray Society, Boston, May 1991.
[1] Department of Radiology, New England Baptist Hospital, 125 Parker Hill Ave., Boston, MA 02120. Address reprint requests to A. H. Robbins.
[2] Department of Radiology, Tufts University School of Medicine, Boston, MA 02111.
[3] Via S. M. Dell'Anima 54-55, 00186 Rome, Italy.

 0361–803X/92/1591–0023 © American Roentgen Ray Society



A B

Fig. 1.—*A*, *The Crucifixion of St. Peter*, tempera on wood (actual size, 84 × 84 cm).
***B*, *The Crucifixion of St. Peter*, fresco, Pauline Chapel, the Vatican (actual size, 625 × 660 cm). (Courtesy of the Vatican Museums.)**
The painting is a nearly perfect scale model of the fresco. A number of important differences exist (see text).

counterparts in the fresco and with two other drawings done by Michelangelo as preparatory studies for the fresco. These are a surviving cartoon (life-sized line drawing) used to make the fresco, currently housed at the National Museum in Naples, Italy [9], and a line drawing depicting two of St. Peter's executioners [10], which is the property of the Ashmolean Museum, Oxford, England. (4) To detect the presence of radiographically demonstrable pentimenti, which are changes by the artist that reflect creative thought processes that occurred as the composition of the painting evolved and that would generally indicate the originality of a work.

Findings

Initial examination of the radiographs shows that the grain of the underlying wood panel is easily seen. A number of areas have been filled in with a heavy metallic material, probably lead, to cover defects in the surface. Two large cracks running transversely are both visible on the painting itself.

The radiographs show no evidence of a cross grid either drawn or incised into the wood panel. No evidence of any organized pinpricks is seen that would indicate that any of the figures were traced.

Many outlines of figures in the paintings are seen. Some are very sharp and easily seen, whereas others are barely visible. The radiodensity of the outlines of the sharply outlined figures is indicative of a carefully done, well-defined underlying drawing, probably one that was incised into the tempera-coated surface of the wood panel. The poor visibility of other figures indicates that they were created in a different manner, presumably painted directly, without a well-defined preliminary line drawing. Interestingly, this includes much of the body of St. Peter himself, which is seen extremely poorly (Fig. 2).

Some portions of the cross are seen as sharply defined lines. The extreme foot end of the cross is not sharply incised; the actual end of the cross, as seen in the painting, as well as another option tested by the artist, are both faintly visible as sketched lines in locations that are both positioned far short of the extremes to which the incised lines reach (Fig. 2).

The structure of the cross is not symmetric. The length of the left arm of the cross is only 90% of the length of the right; the length of the head end of the cross is only 90% of the length of the foot end. These ratios are significantly different from those found in the fresco, in which the arms of the cross are of equal length. Likewise, the top and bottom longitudinal segments are equal to one another in length.

Importantly, the lines of the cross are interrupted at a number of points, ending anywhere they intersect the figure of St. Peter. This indicates that the figure of St. Peter was painted onto the panel first and that the cross was drawn in afterward. This is in contradistinction to the outline of the large man seen supporting the cross on the right. This figure was apparently drawn and painted after the cross, because the line of the cross runs through the man's face (Fig. 2).

Among the figures that are particularly sharp in outline and that appear to have been carefully drawn are the large man and the group of women in the right foreground, the soldiers climbing the stairs in the left foreground, and the two men

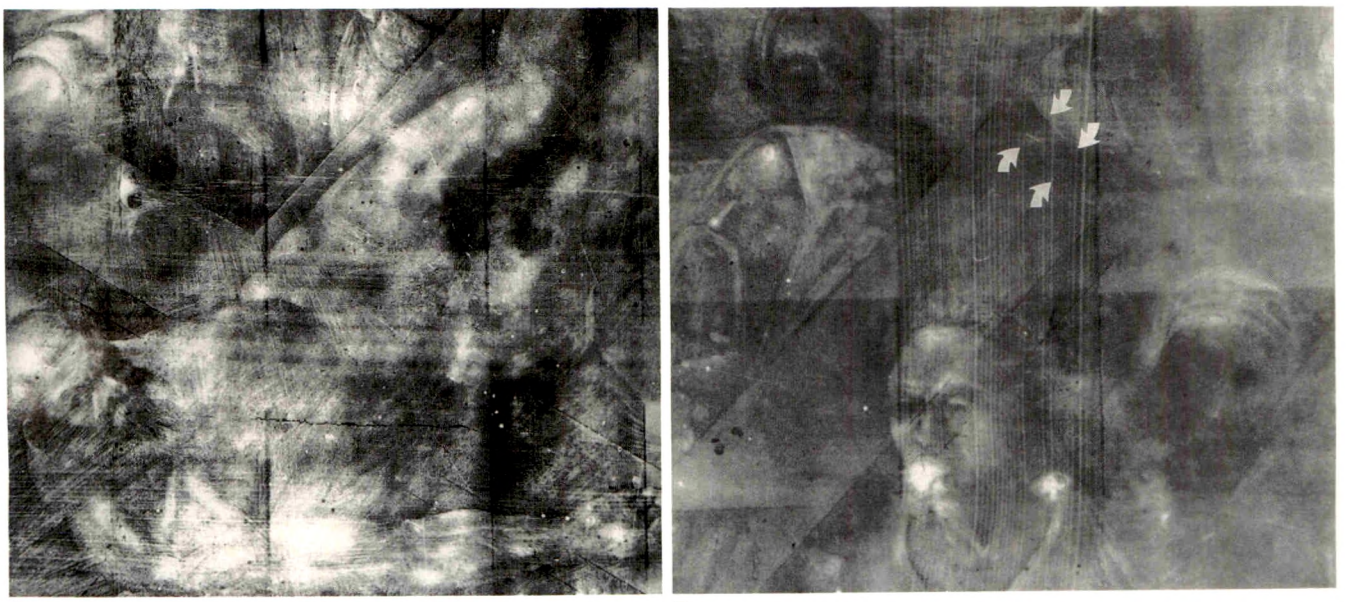


Fig. 2.—Digital radiographs of *The Crucifixion of St. Peter*.
***A*, Digitally enhanced radiograph of central part of painting. St. Peter's torso is difficult to see. Lines of the cross do not intersect his body at any point. (See text for detailed description.)**
***B*, Digital radiograph of large man supporting cross on right. The lines of the cross traverse his face. Note the two sketch lines outlining different lengths of cross (*arrows*).**

supporting the cross on the left. Comparison of the last two groups with known works by Michelangelo are particularly interesting.

A digital radiograph of the three soldiers climbing the stairs in the left foreground is shown in Figure 3. There is a remarkable congruence with the Capodimonte Museum cartoon, even though the cartoon is several feet high (263 × 156 cm) and the radiologically visible line drawing from the painting is only several inches high (28 × 18 cm). The drawing from the painting is virtually a perfect scale model of the line drawing in the cartoon. Indeed the degree of line-for-line congruity of the drawings is so perfect as to raise the question of whether it would even have been possible for a copyist to create such by viewing only the fresco.

The same striking comparability is noted when the radiograph of the painting showing the drawing of the two executioners supporting the left arm of the cross is compared with the Ashmolean Museum sketch of the same figures. It is with respect to this comparison that attention must be drawn to a particularly precise area of detail, which is depicted in Figure 4. The radiograph of the painting shows that the area around and including the left hand of St. Peter has been clearly sharply drawn. The end of the cross does not cover the top of the trousers of one of the men. The ruffled top of the trousers is sharply drawn, as is the position of St. Peter's fingers. Virtually identical details are visible on the Ashmolean sketch. However, examination of the same area in the fresco shows a much simpler design, wherein the cross completely covers the top of the pants. St. Peter's fingers are held at a distinctly different angle. Thus, these details on the painting could not possibly have been copied from the fresco. They were presumably part of what was originally planned and were illustrated in the Ashmolean sketch, and were for some reason abandoned in the final version of the fresco itself.

Pentimenti

The unsharpness of the figure of St. Peter and the extended sketch lines at the foot end of the cross indicate the initiative processes of the artist. The fact that the cross was apparently drawn in after the principal figure of St. Peter indicates the artist's greater concern for the principal subject as opposed to the cross to which he is affixed. On the other hand, the large man supporting the cross on the left, although an important figure, appears to have been added even later, probably because a strong figure was needed at this point to bear the immense weight of the cross.

Many other pentimenti can be detected. Two pairs of parallel lines and one pair of angled lines seen in the left central portion of the painting are not part of any figure visible in the painting. However, these lines do parallel the lines of the cross. Their location and orientation suggest that the artist started to sketch in the cross or portions thereof in different areas of the painting and then abandoned the idea.

Three compass-drawn partial circles of different sizes are present in the top left of the painting where only the sky is seen in the painting. Two sketch lines are visible, diverging from St. Peter's left knee, radiating to the right (Fig. 2). Visible also are similar lines defining both the direction faced and the line of gaze of the smaller man supporting the left arm of the cross. These are shown in part in Figure 4.

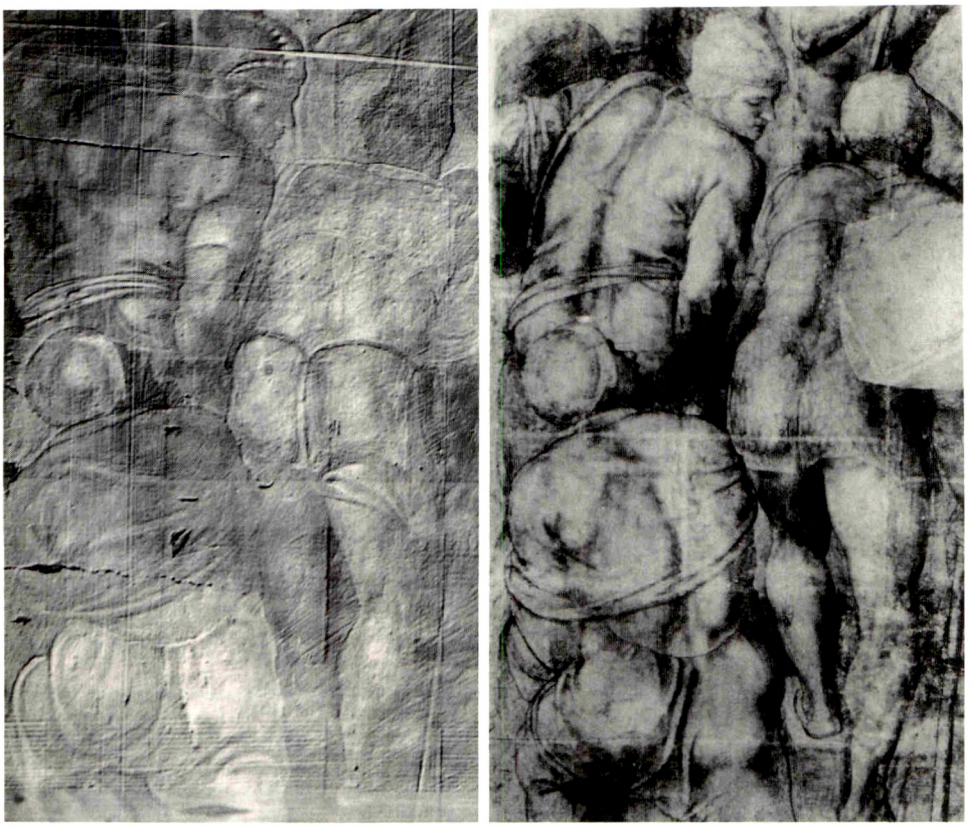


Fig. 3.—*A*, Digital radiograph of soldiers in left foreground of *The Crucifixion of St. Peter* painting (actual size, 28 × 18 cm).

***B*, Cartoon (line drawing) used by Michelangelo to produce the fresco (actual size, 263 × 156 cm). (Reprinted with permission from Museo Nazionale, Naples, Italy.)**

Underdrawing in painting is remarkably similar to cartoon.

The radiographic appearance of the group of women in the right foreground is shown in Figure 5. Three of the women are surrounded by compass-drawn circles, the central points of which are identifiable on the radiograph. These circles were apparently drawn to localize the general area for these figures. Other lines drawn were placed by the artist to define the line of gaze of one of the women.

Discussion

Radiography has proved to be of use in the evaluation of paintings, since underlying structure and images not apparent by surface inspection may be seen. These images may be useful to demonstrate prior use of the painted surface and can also give insights into the composition of the painting. We used digital techniques to augment traditional radiographic methods. They proved to be of value particularly for edge enhancement and for demonstration purposes. We did not recognize any images with digitization that were not otherwise visible.

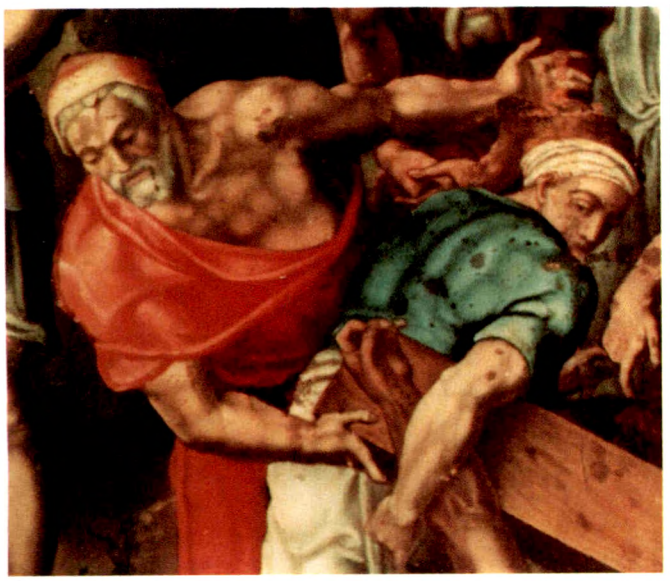
It should be stressed that radiographic techniques do not offer an absolute measure of truth as to the originality of a work or the lack thereof. The data obtained must be used as evidence to be weighed. In that regard, we have not found signs characteristic of a copyist, but have found signs characteristic of an original composition. Thus, we think we have sufficient evidence to prove that the painting was not copied from another work.

A most important observation is the absence of radiographic evidence of a grid. Without the use of a grid, many dimensions in a copy would be distorted compared with the fresco, which, without extensive scaffolding, can be viewed only at a considerable angle from below.

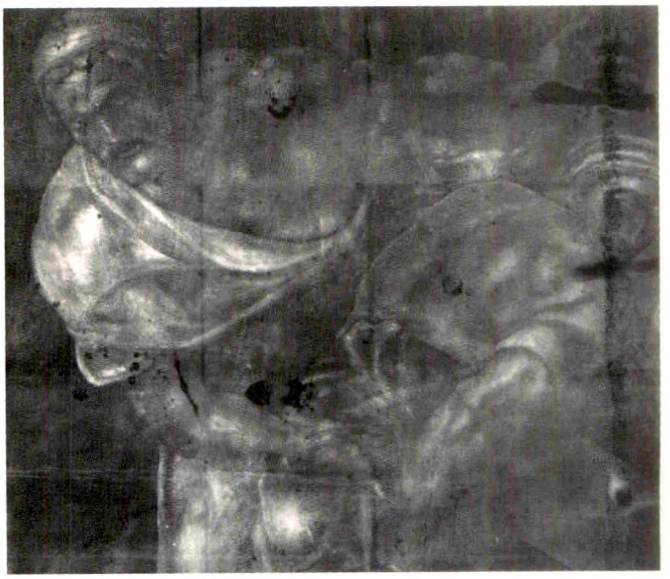
In the fresco, the outline of the cross is perfectly symmetric from top to bottom and side to side and is a most easy figure to copy. In the painting, however, the cross is asymmetric and significantly dissimilar from the fresco, an unlikely copying error. In addition, the radiographic findings on the painting indicate that the main figure of St. Peter was apparently painted first and the cross added afterward. This would be a rather illogical sequence for a copyist to follow. A more likely scenario would be that the copyist would draw the central geometric figure first (i.e., the cross), and then place the figure of St. Peter on it.

Radiographic evidence indicates that the artist was uncertain as to how long the foot end of the cross should be. Other evidence shows that the artist experimented with placing the cross in other areas. These are not the findings that would be expected with a copyist, who would know the exact dimensions of the cross and where to place this important and easily copied geometric figure.

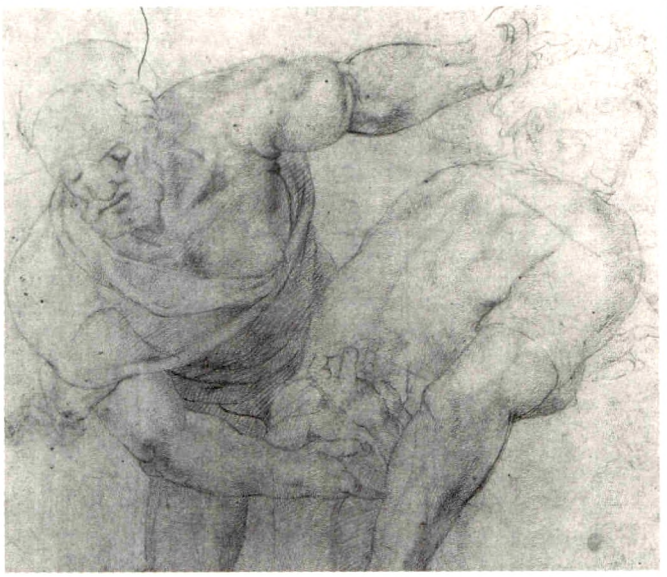
The large number of pentimenti seen on the radiographs are not characteristic of a copied composition. To the con-



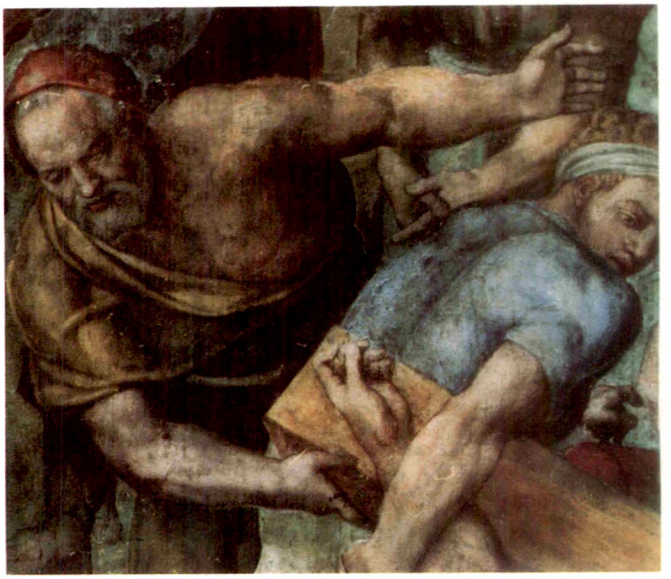
A



B



C



D

Fig. 4.—*A*, Detailed view of *The Crucifixion of St. Peter* painting shows two executioners supporting left arm of cross.
***B*, Radiograph of area shown in *A* reveals a sharp underdrawing outlining figures.**
***C*, Portion of preliminary study done by Michelangelo shows the same figures as in *A* and *B* (actual size, 255 × 160 mm). (Reprinted with permission from Ashmolean Museum, Oxford, England.)**
***D*, Same area as *A*–*C*, but from fresco. (Courtesy of the Vatican Museums.)**
Drawn figures in painting (*A* and *B*) show certain complex features that conform with those in preliminary sketch (*C*). Note bunched waistband of pants, position of end of cross, and position of St. Peter's fingers. Views of same area of fresco (*D*) show that fresco does not conform with Michelangelo's original concept (*C*). These findings make it highly improbable that the painting could have been copied from the fresco.

trary, they are indicative of the artist's apparent uncertainties and planning during the compositional phase of his work. As such, they are strong indicators that the work is an original effort.

The pentimenti are most numerous and complicated in the right lower quadrant of the painting, many in relation to the group of women in the right foreground. This finding correlates with two important observations made by recent scholars. In the fresco, this same group of women apparently constituted the last section of work to be finished [11]. It is also thought that this part of the fresco was hastily completed because of pressure to ready the chapel for the conclave of cardinals that was preparing to meet to select the successor to Pope Paul III [12]. If it is assumed that the composition of the painting was the working model for the fresco, it is ironic that the area that the artist found the most complex to create initially in the painting was the very same area that he was pressured to finish hastily in the fresco itself.



Fig. 5.—Computer-enhanced radiograph of *The Crucifixion of St. Peter* painting. Women in right foreground are well seen. At least two arcs localizing three of the figures are visible (*arrowheads*). The anticipated line of gaze of one of them is also seen (*solid arrows*). Converging lines on left (*open arrows*) represent direction faced by kneeling figure supporting right arm of cross. These pentimenti, as well as those elsewhere in the painting, some of which are illustrated in Fig. 2 (see text for description), are evidence that the composition of the painting was an original effort.

The near-perfect scale relationship of several of the drawn figures in the painting to other studies done by Michelangelo in preparation for his last fresco offers strong support that the painting was his own model. The presence of the same precise details in the radiographs of the painting and in the Ashmolean sketch, details not present in the fresco itself, is even a stronger indication that the painting actually represented the original design for the fresco, a design that was presumably modified during the completion of the fresco.

Conclusions

We conclude that the radiologic findings offer considerable argument against the hypothesis that the tempera-on-wood painting *The Crucifixion of St. Peter* is a copy of the Pauline Chapel fresco, as has been suggested by art historians. To the contrary, our findings offer strong evidence that the painting was created as an original effort by Michelangelo. As such, they provide a substantial body of evidence supporting the contention that the painting was the model for Michelangelo's last fresco.

REFERENCES

1. Meneses E. Ostra joya artistica sacada de Espana. *Blanco y Negro* (Madrid), July 27, **1963**
2. Goldscheider L. *Michelangelo's last painting*. Essay, privately printed, London, **1968**
3. Hardy C. *Michelangelo and the Pauline modello: art, document and odyssey*. New York: privately printed, **1992**:25–85
4. Cappel CB. Michelangelo's cartoon for the "Crucifixion of St. Peter" reconsidered. *Master Drawings* **1987**;5(2):131–142
5. De Tolnay C. *Michelangelo: the final period*. Princeton, NJ: Princeton University Press, **1960**:145
6. James AE Jr, Gibbs SJ, Falke THM, et al. Radiographic analysis of paintings. *Med Radiogr Photogr* **1987**;63(1):1–24
7. James AE Jr, Gibbs SG, Diggs J, et al. The use of digital radiographic techniques in the analysis of works of art with an emphasis upon painting. In: Price RR, Rollo FD, Monahan WG, James AE, eds. *Digital radiography: a focus on clinical utility*. New York: Grune & Stratton, **1982**:335–344
8. Marijnissen R. *Paintings: genuine · fraud · fake*. Brussels: Elsevier, **1985**:85–86
9. Steinmann E. Cartoni di Michelangelo. *Bollettino d'Arte* **1925**;5:3–16
10. Parker KT. *Catalogue of the collection of drawings in the Ashmolean Museum, II*, vol. 331. Oxford: Ashmolean Museum, **1956**:171
11. Baumgart F, Biagetti B. *Die fresken des Michelangelo L. Sabbatini und F. Zuccari in der Capella Paolina im Vatikan*. Vatican City: Tipografia Poliglotta Vaticana, **1934**:56
12. Steinberg L. *Michelangelo's last paintings*. London: Phaidon, **1975**:44–46

Value of Sonography in Determining the Nature of Pleural Effusion: Analysis of 320 Cases

Pan-Chyr Yang[1]
Kwen-Tay Luh[2]
Dun-Bing Chang[1]
Huey-Dong Wu[2]
Chong-Jen Yu[1]
Sow-Hsong Kuo[2]

To assess the value of sonography in determining the nature of pleural effusions, we prospectively analyzed the sonographic findings in 320 patients with pleural effusion of various causes (224 with exudates and 96 with transudates). The nature of the effusions was established on the basis of chemical, bacteriologic, and cytologic examination of pleural fluid; pleural biopsy; and clinical follow-up. All patients had high-frequency, real-time sonography performed by one of three sonographers who had no clinical information concerning the patients. The sonographer evaluated the images for internal echogenicity of the effusion, thickness of the pleura, and associated parenchymal lesions of the lung. The images were also printed out and interpreted a second time by the other two sonographers to reach a consensus. Our results showed that the two types of effusions could be distinguished on the basis of sonographic findings. Transudates were anechoic, whereas an anechoic effusion could be either a transudate or an exudate. Pleural effusions with complex septated, complex nonseptated, or homogeneously echogenic patterns were always exudates ($p < .01$). Sonographic findings of thickened pleura and associated parenchymal lesions in the lung also were indicative of an exudate ($p < .01$). Homogeneous echogenic effusions were due to hemorrhagic effusion or empyema. Sonographic evidence of a pleural nodule was a specific finding in patients with a malignant effusion.

We conclude that sonography is useful in determining the nature of pleural effusion.

***AJR* 159:29–33, July 1992**

Pleural effusions are classically divided into transudates and exudates [1]. A transudate is caused by systemic factors that influence the formation and absorption of pleural fluid. The pleural surfaces are not involved by the primary disease. An exudate is caused by diseased pleural surfaces. Differentiation between a transudate and an exudate may affect the diagnostic approach and the patients' management.

Although chest sonography has been useful for the diagnosis of pleural opacities [2–10], the main use of sonography is still limited to guiding aspiration of minimal effusions and loculated effusions. The success rate of sonographically guided thoracentesis is high, and the procedure is safe [11, 12]. Several recent studies extended the use of sonography to the examination of chest wall tumors [13], evaluation of pleural involvement by lung cancer [14], and guidance of a pleural biopsy for focal pleural involvement [15]. The usefulness of high-frequency, real-time sonography in determining the nature of pleural effusion has not been specifically assessed before.

Accordingly, we investigated the usefulness of sonographic findings, including the internal echogenicity and associated changes in the pleural and lung parenchyma, in determining the nature of pleural effusion.

Subjects and Methods

We prospectively analyzed the value of the sonographic pattern in predicting the nature of pleural effusion in 320 consecutive patients between June 1985 and December 1989 at

Received November 25, 1991; accepted after revision January 27, 1992.

[1] Department of Internal Medicine, National Taiwan University Hospital, No. 1, Chang-Te St., Taipei, Taiwan 100, Republic of China. Address reprint requests to P.-C. Yang.

[2] Department of Clinical Pathology, National Taiwan University Hospital, Taipei, Taiwan 100, Republic of China.

0361–803X/92/1591–0029
© American Roentgen Ray Society

National Taiwan University Hospital. Patients who had prior needle aspiration were excluded. The study included 189 male subjects and 131 female subjects, between 2 and 84 years old (mean age, 54 ± 16 years). Ninety-six patients (30%) had massive effusion that involved more than two thirds of the hemithorax on chest radiographs, 166 patients (52%) had moderate effusion, and 58 patients (18%) had minimal effusion.

The nature of the effusions in the 320 patients was established on the basis of chemical, bacteriologic, and cytologic examination of the pleural fluid and by pleural biopsy, as well as by various hematologic examinations and clinical follow-up. Each effusion was defined as a transudate, an exudate, or an empyema on the basis of the levels of sugar, lactate dehydrogenase (LDH), and total protein in the effusion and the results of cytologic examinations and bacterial cultures [16]. The pleural exudates met at least one of the following criteria, whereas pleural transudates met none: (1) pleural fluid protein level divided by serum protein level greater than 0.5, (2) pleural fluid LDH level divided by serum LDH level greater than 0.6, and (3) pleural fluid LDH level greater than two thirds the upper limit of the normal level of the serum LDH. Parapneumonic effusions are pleural effusions associated with bacterial pneumonia or lung abscess [17]. Empyemas are diagnosed when accumulations of pus are seen in the pleural space or when bacterial cultures of pleural fluid are positive. Hemorrhagic effusions are diagnosed when fluids obtained from thoracentesis appear bloody and incoagulable [17].

An effusion was defined as malignant if cytologic examination of the fluid showed malignant cells or histologic examination of specimens obtained from pleural biopsy or transthoracic needle aspiration biopsy showed evidence of a malignant neoplasm.

The underlying diseases were diagnosed on the basis of the results of chemical, bacteriologic, and cytologic examinations of the pleural effusions, chest radiographs, CT scans, biopsy from primary or metastatic sites, and clinical follow-up.

Table 1 shows the nature of fluid in 320 patients with pleural effusions. Ninety-six effusions were transudates, and 224 were exudates. Among the 224 exudates, 113 were malignant and 111 were not. Twenty-eight patients had parapneumonic effusions, 20 had empyemas, and 16 had hemorrhagic effusions.

All patients were examined with high-resolution sonographic units (Aloka SSD 630, SSD 650, Aloka, Tokyo; Toshiba 100A, Toshiba, Tokyo) with 3.5-, 5.0-, and 7.5-MHz linear and convex transducers. The sonography was performed by one of three sonographers who had no clinical information concerning the patients. The patients were examined while supine or sitting, with the transducer scanning through the intercostal space. The sonograms were first interpreted by the examiner for internal echogenicity of the effusion, pleural thickness, pleural nodules, and associated parenchymal lesions of the lung. The sonograms also were recorded on Polaroid film (Polaroid, Cambridge, MA) and interpreted by the other two sonographers. If the interpretations differed, the final sonographic diagnosis was the majority interpretation. The echogenicity of bile in the gallbladder was used as a reference for anechoic lesions. Echogenicity of the effusion was compared with echogenicity of the liver (hypoechoic, isoechoic, or hyperechoic).

The effusion was subclassified as anechoic, complex nonseptated, complex septated, or homogeneously echogenic. The effusion was defined as anechoic if echo-free spaces were present between visceral and parietal pleura, complex nonseptated if heterogeneous echogenic material was inside the anechoic pleural effusions, complex septated if fibrin strands or septa were floating inside the anechoic pleural effusions, and homogeneously echogenic if homogeneously echogenic spaces were present between visceral and parietal pleura (Fig. 1).

The parietal pleura was measured and arbitrarily defined as thickened if the pleural thickness was 3 mm or greater (Fig. 2). The pleural nodules were hypoechoic nodular lesions with defined margins located in the parietal or visceral pleura (Fig. 3), while focal pleural thickenings were echogenic areas of increased thickness in the parietal pleura that had poorly defined margins. The lesions in the lung parenchyma were subclassified into pulmonary consolidation, abscess, and tumor. Consolidation was seen as a wedge-shaped hypoechoic lesion with an air bronchogram in the lung parenchyma (Fig. 4). Lung abscess appeared as a hypoechoic cavity in a consolidated lung. Tumor was a homogeneously hypoechoic or echogenic mass in the consolidated lung parenchyma (Fig. 5). Associated lesions in the lung parenchyma shown on sonograms were confirmed either on chest radiographs or CT scans of chest.

Data were analyzed statistically with the chi-square test; a p value less than .05 was considered significant.

TABLE 1: The Nature of Pleural Effusions in 320 Patients

Nature of Effusion	No. of Patients
Transudate (n = 96)	
Congestive heart failure	36
Cirrhosis of liver	24
Nephrotic syndrome	20
Hypoalbuminemia	16
Nonmalignant exudate (n = 111)	
Parapneumonic effusion	28
Tuberculous pleurisy	24
Collagen diseases	20
Empyema	20
Hemothorax	16
Postpericardiotomy syndrome	3
Malignant exudate (n = 113)	
Lung cancer	58
Breast cancer	24
Lymphoma and leukemia	4
Esophageal cancer	4
Gastric cancer	3
Colonic cancer	4
Carcinoma of unknown primary	16

Results

The sonographic patterns and the nature of the pleural effusions in 320 patients are shown in Table 2. Four basic sonographic patterns of internal echogenicity of pleural effusions were seen. One hundred seventy-two effusions were anechoic, 50 were complex nonseptated, 76 were complex septated, and 22 were homogeneously echogenic. All pleural effusions with an internal sonographic pattern that was complex septated, complex nonseptated, and homogeneously echogenic were exudates ($p < .01$). The anechoic effusions could be either transudates or exudates. None of the internal sonographic patterns were specific for malignant effusion. Of 22 patients with homogeneously echogenic effusions, 10 patients had empyema and 12 had hemorrhagic effusions. Eight of the hemorrhagic effusions were malignant.

Seventy-six patients had pleural thickness of 3 mm or more. Only three of the effusions were transudates, the other 73 effusions were exudates ($p < .01$). Ten patients had pleural nodules on either the parietal pleura or visceral pleura detected with sonography. All of these patients had malignant effusions. Nine of the patients had effusions with cytologic

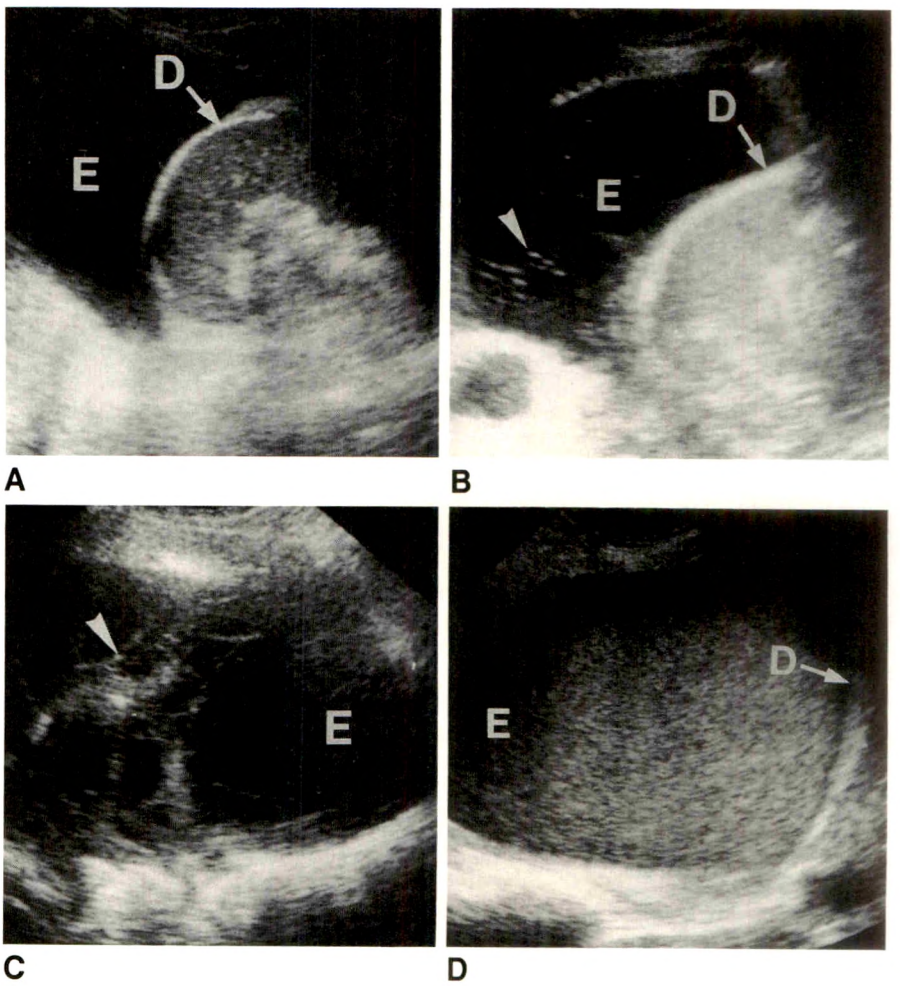


Fig. 1.—*A–D*, Sonograms show four typical patterns of pleural effusion: homogeneously anechoic (*A*), complex nonseptated with heterogeneously hyperechoic spots (*arrowhead*) inside effusion (*B*), complex septated with septa or fibrin strands (*arrowhead* in *C*), and homogeneously echogenic (*D*). E = effusion, D = diaphragm.

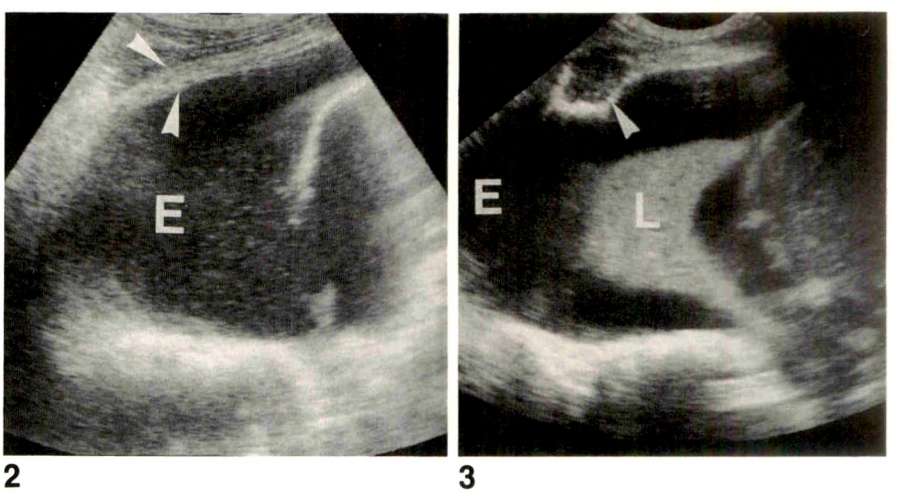
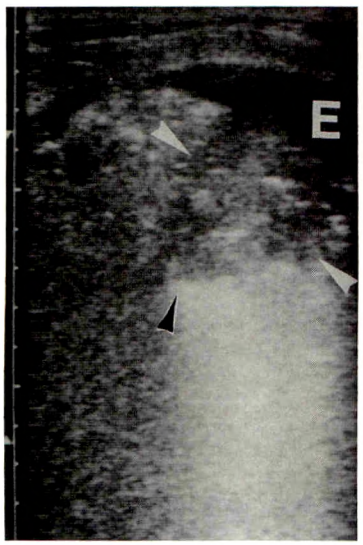


Fig. 2.—40-year-old man with adenoid cystic carcinoma in mouth and right-sided pleural effusion. Sonogram of chest shows massive effusion (E) with complex nonseptated pattern. Parietal pleura is 4–5 mm thick (*arrowheads*). Effusion study shows exudate, and cytologic examination confirmed malignant effusion.

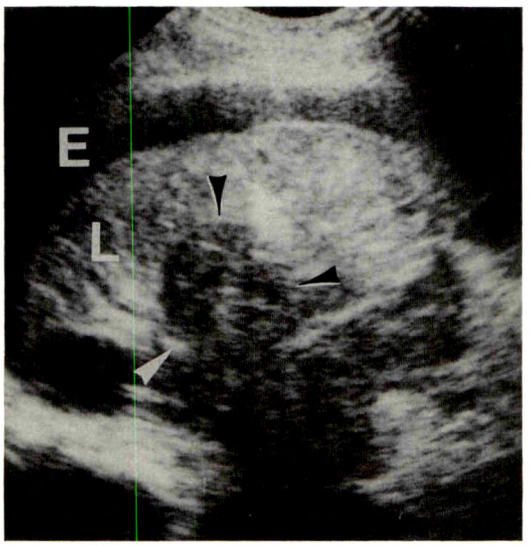
Fig. 3.—42-year-old man with nasopharyngeal carcinoma and right-sided, massive pleural effusion. Results of repeated cytologic examinations were negative for malignant cells. Sonogram of chest shows a 1.5-cm hypoechoic nodule at parietal pleura (*arrowhead*). Sonographically guided needle aspiration biopsy of nodule revealed squamous cell carcinoma. E = effusion, L = collapsed lung.

results positive for malignant cells. The other patient had malignant effusion confirmed by needle aspiration of the pleural nodule.

Fifty-four patients had pleural effusion with associated lung parenchymal changes; this included 40 patients with consolidations, four with lung abscesses, four with obstructive pneumonia, and six with tumor. In 32 patients with sonographic diagnosis of pulmonary consolidation, findings on chest radiographs confirmed the diagnoses. In the other 14 patients with lung abscesses, obstructive pneumonias, and consolidations,



4



5

Fig. 4.—30-year-old woman with right-sided pleural effusion. Sonogram of chest reveals a wedge-shaped consolidation (*arrowheads*) with pleural effusion (E), suggesting an exudate. This patient was finally proved to have pneumonia with parapneumonic effusion.

Fig. 5.—68-year-old woman with left-sided, massive pleural effusion. Cytologic examination of pleural effusion showed lymphocytosis and no malignant cells. Sonogram of chest reveals a hypoechoic tumor (*arrowheads*) in consolidated lung (L) in addition to effusion (E). Sonographically guided transthoracic needle aspiration of tumor confirmed diagnosis of squamous cell carcinoma.

TABLE 2: Sonographic Patterns and Nature of Pleural Effusion in 320 Patients

Effusions	Internal Echogenicity				Thickened Pleura ($n = 76$)	Pleural Nodule ($n = 10$)	Parenchymal Lesions ($n = 54$)
	Anechoic ($n = 172$)	Complex Nonseptated ($n = 50$)	Complex Septated ($n = 76$)	Homogeneously Echogenic ($n = 22$)			
Transudate ($n = 96$)	96	0	0	0	3	0	3
Exudate ($n = 224$)							
Nonmalignant ($n = 111$)	30	27	40	14	42	0	38
Malignant ($n = 113$)	46	23	36	8	31	10	13

the parenchymal lesions were confirmed by both chest radiography and CT of the chest. Fifty-one patients had exudates and three patients had transudates ($p < .05$). Two of the three patients with transudates had obstructive pneumonia, and one had a fibrotic infiltrate due to an inactive pulmonary tuberculosis.

Discussion

The value of sonography for the detection of pleural lesions is well known [2–12]. Sonography is useful in defining the nature of pleural masses [5, 8, 9, 18] and localizing loculated or minimal effusion before thoracentesis [5, 7, 11, 12]. Recently, chest sonography has been found useful in detecting pleural and pleurally based lesions [7], evaluating pleural involvement by lung tumor [13], assessing lesions in lung parenchyma, and guiding percutaneous transthoracic biopsy [15, 19, 20].

Previous studies on the use of sonography to determine the nature of pleural effusions are limited [2–9]. Most of the reported studies were done with contact B-scans [2, 3, 6–10, 21–23]. Use of high-frequency (3.5-, 5.0-, and 7.5-MHz), real-time, linear and sector transducers greatly improved the image resolution in the detection of pleural effusion. Not only can the internal echogenicity of a pleural effusion be visualized in more detail but the associated pleural and parenchymal changes can be clearly depicted [13, 15]. The internal echogenicity of pleural effusions can be anechoic, complex nonseptated, and complex septated [5]. Also, the echogenicity of pleural effusion can be homogeneous [11]. The sonographic observation of pleural thickness, pleural tumor, and associated lung parenchymal changes have not been considered together with the internal echogenicity of pleural fluid as criteria for determining the nature of pleural effusions [5, 11, 24].

Our results show that sonography can be used to determine the nature of pleural effusion. In addition to the basic effusion patterns (anechoic, complex nonseptated, and complex septated [5]), a pleural effusion can be homogeneously echogenic. Transudates are usually anechoic, whereas an anechoic effusion could be either a transudate or an exudate. Pleural effusions with complex septated, complex nonseptated, or homogeneously echogenic patterns are always ex-

udates ($p < .01$). An echogenic effusion may sometimes be confused with a solid lesion. However, if the lesion changes shape with respiration and tiny echogenic materials can be seen swirling, then the lesion is fluid [11]. In this series, the homogeneously echogenic effusions are seen in hemorrhagic effusions and empyema only. The echogenic nature is probably due to the presence of a high content of tissue debris or blood in the pleural cavity [11]. Patients with homogeneously echogenic effusions may need drainage via a chest tube. The associated thickened pleura and lung parenchymal changes are also indicative of exudates. The presence of a pulmonary consolidation or lung abscess may suggest an exudate of infectious origin. Presence of tumor in the consolidated lung may indicate a malignant lesion involved in the pathogenesis of effusion. The pleural nodules were seen only in patients with malignant effusions in this series.

Fibrin strands and septa within a hypoechoic space are useful signs serving to distinguish pleural fluid from a solid mass [6, 11, 24]. The fibrin strands tend to occur in effusions that are rich in protein [11]. The "winding bands" or fibrin strands also were reported to associate with tuberculous pleural effusions [24]. In this study, we found that fibrin strands and septa were commonly seen in all kinds of exudates, including empyema, hemothorax, parapneumonic effusions, and malignant pleural effusions. Sometimes the septa were so profuse that they had a honeycomb appearance.

In addition to the useful diagnostic information provided by the sonograms, chest sonography also can be used to guide a percutaneous transthoracic needle aspiration biopsy of the associated pleural and lung parenchymal lesions with high diagnostic yield [15, 19, 20].

We conclude that sonography is a useful diagnostic tool for determining the nature of pleural effusions.

REFERENCES

1. Paddock FK. The diagnostic significance of serous fluids in disease. *N Engl J Med* **1940**;223:1010–1015
2. Doust BD, Baum JK, Maklad NF, Doust VL. Ultrasonic evaluation of pleural opacities. *Radiology* **1975**;114:134–140
3. Laing FC, Filly RA. Problems in the application of ultrasonography for the evaluation of pleural opacities. *Radiology* **1978**;126:211–214
4. Rosenberg ER. Ultrasound in the assessment of pleural densities. *Chest* **1983**;84:283–285
5. Hirsch JH, Rogers JV, Mack LA. Real-time sonography of pleural opacities. *AJR* **1981**;136:297–301
6. Marks WM, Filly RA, Callen PW. Real-time evaluation of pleural lesions: new observations regarding the probability of obtaining free fluid. *Radiology* **1982**;142:163–164
7. Yang PC, Sheu JC, Luh KT, Kuo SH, Yang SP. Clinical application of real-time ultrasonography in pleural and subpleural lesions. *J Formosan Med Assoc* **1984**;83:646–657
8. Lipscomb DJ, Flower CDR. Ultrasound in the diagnosis and management of pleural disease. *Br J Dis Chest* **1980**;74:353–361
9. Hirsch JH, Carter SJ, Chikos PM, Calacurcio C. Ultrasonic evaluation of radiographic opacities of the chest. *AJR* **1978**;130:1153–1156
10. Ravin CE. Thoracocentesis of loculated pleural effusions using grey scale ultrasonic guidance. *Chest* **1977**;71:666–668
11. McLoud TC, Flower CDR. Imaging the pleura: sonography, CT, and MR imaging. *AJR* **1991**;156:1145–1153
12. Henschke CL. The pathogenesis, radiologic evaluation and therapy of pleural effusion. *Radiol Clin North Am* **1989**;27:1241–1255
13. Saito T, Kobayashi H, Kitamura S. Ultrasonographic approach to diagnosing chest wall tumors. *Chest* **1988**;94:1271–1273
14. Sugama Y, Tamaki S, Kitamura S, Kira S. Ultrasonographic evaluation of pleural and chest wall invasion. *Chest* **1988**;93:275–279
15. Chang DB, Yang PC, Luh KT, Kuo SH, Yu CJ. Ultrasound-guided pleural biopsy with tru-cut needle. *Chest* **1991**;100:328–333
16. Light RW, MacGregor MI, Luchsinger PC, Ball WC. Pleural effusions: the diagnostic separation of transudate and exudates. *Ann Intern Med* **1972**; 77:507–513
17. Light RW. *Pleural diseases*, 2nd ed. Philadelphia: Lea & Febiger, **1990**: 39–73
18. Wu HD, Yang PC, Kuo SH, Luh KT. Ultrasonography in complete chest x-ray opacification of hemithorax. *J Formosan Med Assoc* **1989**;88:694–699
19. Yang PC, Luh KT, Wu HD, et al. Lung tumors associated with obstructive pneumonitis: US studies. *Radiology* **1990**;174:717–720
20. Yang PC, Luh KT, Lee YC, et al. Ultrasonography and ultrasound-guided transthoracic aspiration of lung abscess. *Radiology* **1991**;180:171–175
21. Gryminski J, Krakowka P, Lypacewicz G. The diagnosis of pleural effusion by ultrasonic and radiographic techniques. *Chest* **1976**;70:33–37
22. Sandweiss DA, Hanson JC, Gosink BB, Moser KM. Ultrasound in diagnosis, localization, and treatment of loculated pleural empyema. *Ann Intern Med* **1975**;82:50–53
23. Joyner CR Jr, Herman RJ, Reid JM. Reflection ultrasound in the detection and localization of pleural effusion. *JAMA* **1967**;200:399–402
24. Martinez OC, Serrano BV, Romero RR. Real-time ultrasound evaluation of tuberculous pleural effusions. *JCU* **1989**;17:407–410

Videotape Review

RSNA Today Video, Vol. 5, No. 6. Oak Brook, IL: The Radiological Society of North America, 1991. $55; by subscription, 6 issues annually at $185 for RSNA members and $225 for nonmembers (VHS videotape)

This tape consists of three sections introduced by William J. Casarella. Jud W. Gurney presents the first section, "Diffuse Lung Disease: Radiologic and Physiologic Correlation." After an interesting initial explanation of the distribution of various physiologic parameters (e.g., ventilation, perfusion, lymph flow, oxygen concentration, pH), Dr. Gurney goes on to present illustrative cases for each parameter. Adding the expected physiologic patterns to classical anatomic patterns of disease (i.e., alveolar or interstitial) could, it seems, greatly enhance differential diagnosis of lung disease. An additional, rather interesting mechanical parameter, abiotrophy, can evidently also affect the distribution of disease in the lungs, and examples are presented that illustrate this point. This interesting presentation seems to beg a more comprehensive article combining both anatomic and physiologic distribution, perhaps including correlation with findings on high-resolution CT scans.

Next, Wende W. Logan-Young, director of the Breast Clinic of Rochester, presents a full discussion titled "Operating a Breast Imaging Center." After presenting her office layout, which is used to segregate patients having screening examinations from patients having other studies done, Dr. Logan-Young discusses several of the important aspects of running this type of imaging service. Training technologists, educating patients, and interacting with patients are discussed, and the importance of personally examining every "problem" patient (i.e., patients who are not at the center for screening mammography) is emphasized. Before any of the full range of ancillary tests available (e.g., sonography, biopsy, ductography) is performed, a complete film review with the patient is done. Also emphasized is the importance of maintaining the integrity of the doctor-patient relationship between the referring physician and the patient, especially in reference to the breast physical examination. Although greatly interesting in terms of a specific subspecialty type of practice in which high numbers of patients are seen (approximately 180 per day), easy correlation with the average general radiologic practice may be difficult.

Last, Robert A. Zimmerman presents "Imaging Insights: Differentiating Between Neoplasms and Infarcts in the Cerebral Hemisphere." Initially, correct emphasis is placed on the temporal evolution of a lesion as the primary differential point; tumors enlarge and infarction masses resolve. Subsequent refinement clarifies many of the confusing aspects of the differential diagnosis of neoplasm and infarction, including the use of contrast material, gray matter–white matter distribution of typical examples of both entities, and the concepts of vasogenic and cytotoxic edema. Reviewing one study in which 13% of clinical "strokes" actually represented metastatic foci, Dr. Zimmerman underscores the importance of his presentation and, in the end, presents a clear, concise six-point conclusion.

Hano A. Siegel
Mercy Hospital
San Diego, CA 92103

Case Report

Lung Torsion After Percutaneous Needle Biopsy of Lung

Ruffin J. Graham,[1] Robert L. Heyd,[1] Vikram A. Raval,[1,2] and Thomas F. Barrett[1,2]

Torsion of the lung is a rare event that can have serious consequences for the patient. We describe a case of pulmonary torsion that occurred after percutaneous needle biopsy of the lung in a patient with lung cancer. We think this is the first reported case of pulmonary torsion after this common procedure.

Case Report

An 81-year-old man was referred for CT to evaluate a mass in the left lung that had been detected on a chest radiograph. The CT scan (Fig. 1A) showed a relatively small central tumor posterior to the left main bronchus. The scan also showed a large area of consolidation, approximately 17 × 8 cm, involving the lingular segment of the left upper lobe; bilateral pleural thickening; and multiple calcified pleural plaques. The lingular bronchus was obstructed, with distal air resorption and parenchymal consolidation, giving the appearance of a "drowned lobe." No pneumothorax was present.

Bronchoscopy performed 2 weeks after the chest CT examination showed that the orifice of the left upper lobe bronchus was slitlike, with significant ribbing and erythema. Multiple samples obtained by endobronchial lavage and biopsy specimens from the left upper and lower lobes showed no evidence of a malignant tumor, although the bronchoscopist's impression was that the patient had bronchogenic carcinoma and that the bronchoscopy results were suboptimal because of bronchial narrowing. The patient tolerated the procedure well.

Several hours after the broncoscopic examination, the patient was admitted to the hospital because of a syncopal episode with confusion and ataxia. CT of the head showed metastatic disease with ring-enhancing lesions in the superior right and left parietal lobes. A chest radiograph (Fig. 1B) showed the atelectatic lingular segment of the left upper lobe detected on the CT scan 2 weeks earlier. No air bronchograms were seen. Both the cardiac and diaphragmatic silhouettes were obliterated.

Five days after admission, the patient had a fine-needle biopsy of the atelectatic lung to obtain specimens for cytologic examination. The patient was placed in the right lateral decubitus position. Under fluoroscopic guidance, the atelectatic lobe was localized in the left lower lung and a 22-gauge Chiba needle (Medi-Tech, Inc., Watertown, MA) was inserted at the seventh intercostal space along the midaxillary line. When the needle was inserted, no solid tissue was felt. Fluoroscopy showed that the atelectatic lobe was located entirely in the upper part of the left hemithorax instead of the left base. A chest radiograph (Fig. 1C), obtained with the patient supine and with the needle still in place, showed that the mass had shifted to the upper part of the left hemithorax. A small left-sided pneumothorax was also detected. The biopsy needle was withdrawn, placed at the midaxillary line over the upper left hemithorax, and reinserted. Three needle passes were performed, each yielding thick mucuslike fluid. Histologic examination of the fluid showed well-differentiated adenocarcinoma. Fluoroscopy at the end of the procedure showed that the mass remained in the upper part of the left hemithorax.

After the fine-needle biopsy, a tube was placed in the left side of the chest to reduce the pneumothorax. A chest radiograph (Fig. 1D) obtained after insertion of the chest tube and with the patient erect showed that the lobe had again shifted and was located at the left base, silhouetting the cardiac border.

Discussion

Pulmonary torsion is rare. A literature review by Moser and Proto [1] identified 21 reported cases, most associated with prior surgery (10 cases) or trauma (five cases). Of the other six cases reported, spontaneous pneumothorax was noted

Received December 6, 1991; accepted after revision January 22, 1992.
[1] Department of Radiology, Western Reserve Care System, 345 Oak Hill Ave., Youngstown, OH 44501. Address reprint requests to R. J. Graham.
[2] Department of Radiology, Northeastern Ohio Universities College of Medicine, State Rte. 44, Rootstown, OH 44272.

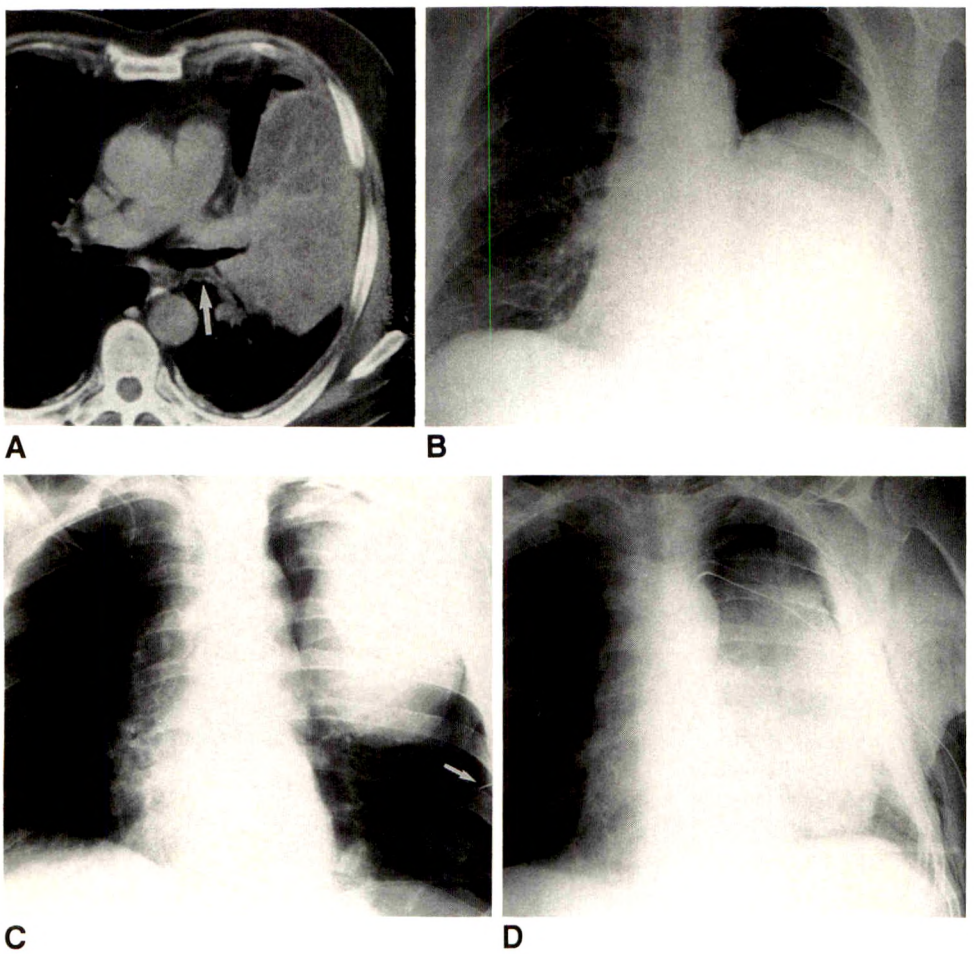


Fig. 1.—Lung torsion after percutaneous needle biopsy.

***A*, Axial CT scan of chest inferior to carina shows consolidation of lingula and small central tumor (*arrow*).**

***B*, Anteroposterior chest radiograph obtained with patient supine shows atelectasis of lingular segment of left upper lobe.**

***C*, Anteroposterior chest radiograph obtained with patient supine during needle biopsy shows collapsed lingular segment of left upper lobe in superior part of left hemithorax and apical pneumothorax. Biopsy needle (*arrow*) is in place.**

***D*, Anteroposterior chest radiograph obtained with patient erect and after insertion of chest tube shows atelectatic segment at base of left lung.**

in one and squamous cell lung cancer was present in another. Felson [2] has reported nine cases of pulmonary torsion and described five circumstances that favor its development: (1) an airless lobe, consolidated or atelectatic; (2) a long, free, lobar pedicle; (3) absence of parenchymal bridge between contiguous lobes; (4) pneumothorax or pleural effusion; and (5) transection of the inferior pulmonary ligament. Several of these factors were present in our patient: chest CT showed a consolidated lingular segment of the left upper lobe, a pleural effusion was present, the lobar pedicle was weakened by tumor (Fig. 1A), and pneumothorax occurred during the biopsy. Lateral decubitus positioning also may have predisposed the patient to torsion.

To our knowledge, lung torsion has not been previously reported as a complication of percutaneous needle biopsy. Pneumothorax, a common complication of transthoracic needle biopsy, is a factor that may favor the development of pulmonary torsion [2]. The lack of reports of pulmonary torsion complicating percutaneous needle lung biopsy may be due to several factors: the rarity of lung torsion, the presence of coincident pulmonary abnormalities that may obscure the diagnosis of torsion, and unfamiliarity with the radiographic features of pulmonary torsion. These signs, as enumerated by Felson [2], are (1) a collapsed or consolidated lobe occupying an unusual position, (2) hilar displacement in a direction inappropriate for the atelectatic-appearing lobe, (3) alteration in the normal course of pulmonary vasculature, (4) rapid opacification of an ipsilateral lobe after trauma or thoracic surgery (a finding frequently mistaken for pleural effusion), (5) a change in position of an opacified lobe on sequential radiographs (the major finding in our case), (6) bronchial cutoff or distortion (best seen on CT), (7) lobar air trapping, and (8) primary and secondary signs of lobar collapse.

The mechanism of torsion of the upper lobe of the lung in patients with pneumothorax has been clearly explained. According to Berkmen et al. [3], the weight of the lung is sustained in vivo mainly by negative pleural pressure, with each individual lobe additionally supported by the contiguous lobes. The hilar bronchi do not support the lung and show relatively little resistance to bending, despite considerable tensile strength. When a large pneumothorax is present, all external supports are eliminated, and the lung collapses because of its intrinsic elastic recoil. Separation of the lower lobe from the diaphragm is usually prevented by the pulmonary ligament. As a result, the lower lobe deviates posteriorly, medially, and downward, leaving the upper lobe supported by its bronchus only. Thus, the only force opposing the weight of the upper lobe is its bronchus, which bends under the

weight of the lobe. In our patient, the lingula was drawn superiorly together with the hilus.

In many cases of pulmonary torsion, the patient has undergone surgery either for definitive diagnosis of pulmonary torsion or for prevention of pulmonary infarction. However, because of the shifting position of the opacified lobe in our patient (diagnostic of pulmonary torsion) and because he was not a good candidate for surgery, thoracotomy was not indicated.

In conclusion, lung torsion must be kept in mind as a possible rare complication of percutaneous needle biopsy of the lung, especially in patients with multiple pulmonary abnormalities.

REFERENCES

1. Moser ES Jr., Proto AV. Lung torsion: case report and literature review. *Radiology* **1987**;162:639–643
2. Felson B. Lung torsion: radiographic findings in nine cases. *Radiology* **1987**;162:631–638
3. Berkmen YM, Yankelevitz D, Davis SD, Zanzonico P. Torsion of the upper lobe in pneumothorax. *Radiology* **1989**;173:447–449

AJR to Use Diskettes Instead of Hard-Copy Manuscripts for Editing and Printing

Beginning with the January 1993 issue, accepted papers to be published in the *AJR* will be edited and printed by using computer diskettes rather than hard copies of the manuscripts. This change will expedite the editing and publication process and result in less delay between submission of manuscripts and their appearance in the Journal. Also, with the new system, authors will receive page proofs rather than galleys before publication. This will enable them to see exactly what their final article will look like.

Effective immediately, upon *acceptance* of manuscripts for publication, authors will be asked to send a copy of their revised manuscript on a 5¼-inch DOS-compatible diskette in Wordperfect or ASCII format along with the hard copy of the revision. Articles will be edited directly on the diskettes. Changes will be highlighted electronically; as before, a hard copy of the edited manuscript and figure proofs will be mailed to authors for approval before publication. Note that hard copies of manuscripts will still be required for the peer-review and revision processes.

The *AJR* already takes great pride in the speed with which the peer-review process is accomplished (mean time, 3.4 weeks) and in the amount of time between submission of manuscripts and their final appearance in print (6 months). This is nearly twice as fast as many other journals. With the new system, these intervals will be even shorter. Authors will see their work in print faster, and the timeliness of the Journal will be greater than ever.

Robert N. Berk
Editor-in-Chief

Too Late

Stefan C. Schatzki[1]

Charles Arthur Fries was born in Hillsboro, OH, in 1854. He spent his youth in Cincinnati, where in 1875, he studied at the McMicken School of Design and, in 1874, possibly also with the famous American artist and teacher Frank Duveneck at the Ohio Mechanics Institute. He went to New York briefly to work in a lithography shop, and in 1877 he traveled to Europe for further study. On his return, he painted in both New York and Vermont until he moved to Southern California with his wife and daughter in 1896.

Fries never became very well known, and little information remains today of his career. He developed a local reputation for his landscapes of California mountains and deserts, and some repute for his illustrations that were published in *Leslie's Monthly Magazine* and in the *McGuffey Readers* and other school textbooks. He was actively involved in teaching art in San Diego.

As has been true of many painters who never achieve real success, Fries painted one hauntingly beautiful work entitled *Too Late*. This forceful painting, which illustrates the drama associated with the death of a child in a poor, bleak, austere setting, has a powerful effect on the onlooker. The physician has arrived "too late" on his mission of mercy. The subject of this painting was supposedly suggested to Fries when his daughter became ill while the family was living in the old Capistrano Mission near San Diego shortly after their arrival in California in 1896. "Too Late/Painted in the/Dining Room of the Capistrano/Mission/1896" is captioned on the back of the painting. Although her illness was serious, Fries's daughter recovered, unlike the child in the painting.

The remoteness felt by the displaced artist and his attempts to reconnect with his roots on the East Coast are illustrated in a series of letters between Fries and the famous New York art dealer Robert W. Macbeth. The Macbeth gallery had been devoted to "the permanent exhibition and sale of American pictures" since its opening in 1892. By 1914, it was perhaps the most important gallery dealing exclusively in American paintings and six years earlier, in 1908, had held the historic exhibition of a group of prominent American painters that is now known as "The Eight." In 1914, Fries wrote, "I have been out here for eighteen years and have not been in touch with the art world of the East as much as I would have liked. . . . I am originally from Cincinnati and was a fellow student with Robert Blum, Kenyon Cox, Twachtman, Ed Potthast [all prominent American artists], but I presume they are not familiar with my work now as I used to paint in a much lower key." Macbeth later wrote to Fries and, referring to some paintings that Fries had sent on approval, stated, "I have looked at them carefully on several occasions. . . . Should you see them here, I think you would agree with me that they do not hold up with the other things we are showing."

As late as 1912, Fries was still exhibiting *Too Late* at the Philadelphia Academy and at the Corcoran Gallery. Fries never sold the painting. Fortunately, his daughter, Alice Fries King, made her father's masterpiece available to a much wider audience when in 1967 she gave *Too Late* to the Corcoran Gallery of Art in Washington, DC.



Charles Arthur Fries (1854–1940). *Too Late*, 1896. Oil on canvas, 25 × 38 in. The Corcoran Gallery of Art, Washington, DC. Gift of Mrs. Alice Fries King in memory of her father.

[1] Department of Radiology, Mount Auburn Hospital, 330 Mount Auburn St., Cambridge, MA 02238.

I thank my secretary, Ruth McNeill, for her continuing valuable help in preparing this series of articles.

Pleuropulmonary Paragonimiasis: Radiologic Findings in 71 Patients

Jung-Gi Im[1]
Hee Young Whang[1]
Woo Sun Kim[1]
Man Chung Han[1]
Young-Soo Shim[2]
Seung-Yull Cho[3]

Pleuropulmonary paragonimiasis is a disease caused by lung flukes characterized by migration of a juvenile worm in the early stage and by formation of cysts around the worm later on. The purpose of this study was to describe the radiologic manifestations of pleuropulmonary paragonimiasis, with special emphasis on the worm cyst and worm migration track. We retrospectively studied 71 patients who had evidence of pleuropulmonary paragonimiasis on chest radiographs (n = 71) and CT scans (n = 17). The diagnosis was based on the detection of eggs or on positive antibody tests. On chest radiographs, 59 patients (83%) had pulmonary lesions and 43 patients (61%) had pleural lesions. Pulmonary findings included patchy air-space consolidation (n = 37) with or without cystic changes; ring shadows (n = 16); and peripheral linear opacities (n = 29), which were more prominent in patients with pleural effusion. Twelve patients (17%) had bilateral pleural effusions or pneumothoraces. On CT scans, round low-attenuation cystic lesions (5–15 mm), filled either with fluid (n = 5) or gas (n = 5), were characteristically seen within the consolidation. Peripheral linear opacities seen on radiographs were suggestive of worm migration tracks on CT scans. CT may reveal an intracystic worm.

Although the findings vary depending on the stage of the disease, findings on chest radiographs are usually typical of paragonimiasis. CT provides more specific information about the worm cyst and the worm migration track.

***AJR* 159:39–43, July 1992**

Paragonimiasis is a parasitic disease caused by the trematode *Paragonimus westermani* or other species of *Paragonimus*. Human infection occurs by ingestion of raw or incompletely cooked freshwater crab or crayfish infected with the metacercaria [1]. Paragonimiasis is endemic in certain areas of East and Southeast Asia [2–6]. Several case reports [7–10] of paragonimiasis in Indo-Chinese refugees in North America have been published. The features of pulmonary paragonimiasis shown on radiographs have been described in detail [2–4, 11], but peripheral linear shadows and pleural lesions were not emphasized. CT findings of pulmonary paragonimiasis have been described [12], but more detailed CT studies are needed.

The purpose of this report is to describe the findings on chest radiographs and CT scans in 71 patients with pleuropulmonary paragonimiasis.

Materials and Methods

We retrospectively studied 71 patients living in South Korea who initially had evidence of pulmonary or pleural lesions on radiographs and in whom pulmonary paragonimiasis was confirmed later. The diagnosis was based on positive serologic test for *Paragonimus*-specific antibody [13] (n = 47) or by detection of eggs either in sputum (n = 27) or in percutaneous needle aspirates (n = 4). In seven patients, the antibody test was positive and parasite ova were detected in sputum. Patients who had associated pulmonary tuberculosis or lung cancer were excluded from the study. The group comprised 38 men and 33 women 22–72 years old (mean, 43 years). The most frequent clinical manifestation was cough (n = 45), followed

Received December 9, 1991; accepted after revision February 11, 1992.

[1] Department of Radiology, Seoul National University, College of Medicine, 28 Yongon-Dong, Chongno-Gu, Seoul 110-744, Korea. Address reprint requests to J-G. Im.

[2] Department of Internal Medicine, Seoul National University, College of Medicine, Seoul 110-744, Korea.

[3] Department of Parasitology, College of Medicine, Chung-Ang University, 221 Hucksuck-Dong, Tongjak-Gu, Seoul 156-756, Korea.

0361–803X/92/1591–0039
© American Roentgen Ray Society

TABLE 1: Findings on Chest Radiographs in 71 Patients with Pleuropulmonary Paragonimiasis

Finding	No. of Patients (%)
Pulmonary lesions	
Air-space consolidation	
Focal patchy	32 (45)
Segmental lobar	5 (7)
Subtotal	37 (52)
Cyst(s)	33 (46)
Linear opacity	29 (41)
Nodule	18 (25)
Total	59 (83)[a]
Pleural lesions	
Effusion	
Unilateral	20 (28)
Bilateral	6 (8)
Subtotal	26 (37)
Hydropneumothorax	
Unilateral	6 (8)
Bilateral	6 (8)
Subtotal	12 (17)
Thickening	5 (7)
Total	43 (61)

[a] Total represents total number of patients with pulmonary lesions, not total number of findings.

by blood-tinged sputum (n = 43), dyspnea (n = 27), and chest pain (n = 27). Thirty-four patients had eaten pickled freshwater crab.

Seventeen patients were studied with CT. Scans were obtained on a GE 9800 scanner (General Electric Medical Systems, Milwaukee, WI) with contiguous 10-mm collimation after IV injection of contrast medium. In five patients, additional high-resolution CT scans were obtained with a 1.5-mm collimation, 140 kVp, 170 mA, and 3-sec exposure time. The scans were targeted retrospectively with a field of view of 20–22 cm.

Results

Findings on Chest Radiographs

Fifty-nine (83%) of 71 patients had pulmonary abnormalities on chest radiographs (Table 1). There was no predilection to any specific area of the lung. Thirty-seven patients (52%) had focal patchy or segmental lobar air-space consolidation (Fig. 1). Eight patients had masslike consolidation; these patients later had CT scanning or needle aspiration biopsy. Cystic lesions 5–30 mm in diameter were seen in 33 patients (46%), either with associated focal air-space consolidation (n = 17) (Fig. 2), or as thin-walled ring shadows (n = 16). Of 25 patients who had air-space consolidation on initial radiographs and were followed up, nine had cystic changes in 1–8 months. In four patients, several aggregated cysts had a typical soap-bubble appearance (Fig. 3). Peripherally located linear shadows, 2–4 mm thick and 2–7 cm long, were seen in 29 patients (41%) (Fig. 4). Those linear shadows frequently were adjacent to the consolidated lung and were more prominent in patients with pleural effusion. Focal consolidations and linear shadows frequently showed changes in size and position on follow-up examination. Nodular shadows were seen in 18 patients (25%).

Forty-three patients (61%) had pleural abnormalities, such as effusion (n = 26), hydropneumothorax (n = 12) (Fig. 4), and thickening (n = 5). Twelve patients (17%) had bilateral effusions or hydropneumothoraces. Residual pleural abnormalities on follow-up radiographs varied with the duration of the disease and with effective treatment. However, of 13 patients who had had pleural effusion or hydropneumothorax, and were followed up more than 3 months after treatment with praziquantel, seven had no evidence of pleural disease and six had minimal blunting of costophrenic sulci.

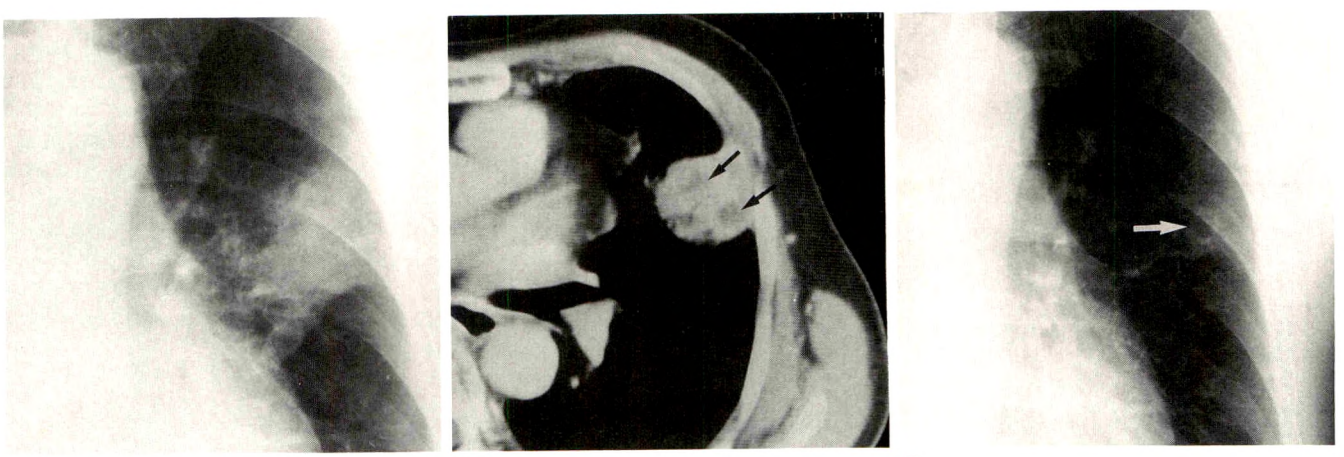


Fig. 1.—41-year-old man with pulmonary paragonimiasis showing sequential change of masslike consolidation.
***A*, Initial chest radiograph shows dense air-space consolidation in upper lobe of left lung.**
***B*, Contrast-enhanced CT scan obtained 5 days after *A* shows round masslike consolidation containing multiple round areas (*arrows*) of low attenuation.**
***C*, Chest radiograph obtained 7 weeks after *A*, 5 weeks after treatment with praziquantel, shows typical ring shadow (*arrow*) similar in size and shape to round lesions of low attenuation in *B*, suggesting that fluid within worm cysts in *B* has been evacuated through communicating airway.**

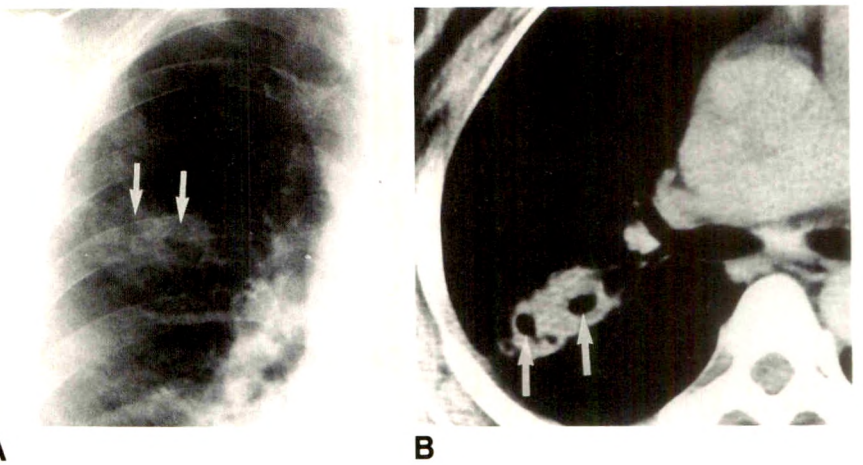


Fig. 2.—47-year-old woman with pulmonary paragonimiasis showing cysts within consolidation.

***A*, Chest radiograph shows relatively well defined patchy opacity in upper lobe of right lung that contains cystic cavities (*arrows*).**

***B*, CT scan shows air-filled cysts (*arrows*) within masslike consolidation, suggesting fluid in cysts has already been evacuated.**

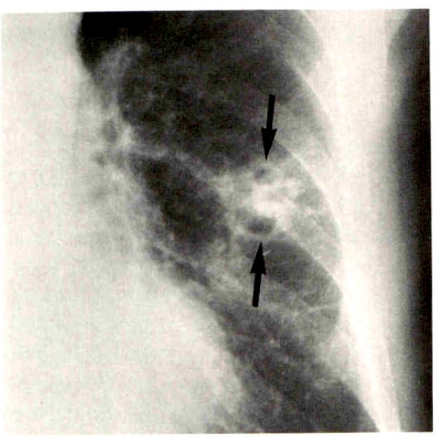


Fig. 3.—51-year-old man with pulmonary paragonimiasis. Chest radiograph shows aggregated, uniform-sized, thin-walled cysts (*arrows*) with a soap-bubble appearance in upper lobe of left lung.

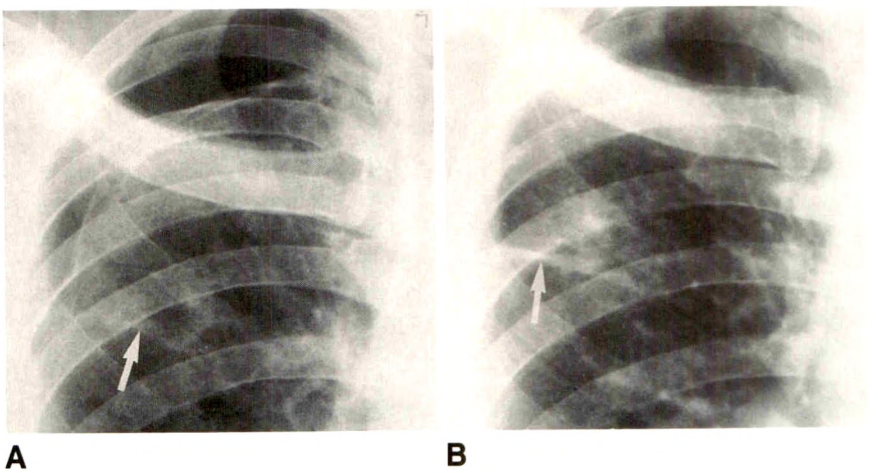


Fig. 4.—Pulmonary paragonimiasis in a 41-year-old man with pneumothorax and linear opacity.

***A*, Initial chest radiograph shows poorly defined infiltrations (*arrow*) in upper lobe of right lung. Note associated pneumothorax.**

***B*, Follow-up chest radiograph obtained 20 days after *A* shows linear bandlike opacity (*arrow*) abutting costal pleura. Note also small cystic shadow adjacent to linear opacity.**

Findings on CT Scans

Fourteen of 17 patients had air-space consolidation. In seven patients, the consolidated lung was well marginated, with a masslike appearance. Within the consolidated lung, round, cystic areas 5–15 mm in diameter and consisting either of fluid ($n = 5$) (Fig. 1B) or of gas ($n = 5$) (Fig. 2) were seen. Thin-walled cysts without adjacent air-space consolidation were seen in 10 patients. A cyst communicating with a dilated bronchus was seen in three patients (Fig. 5). In two patients, an ovoid structure with soft-tissue attenuation was seen within the cysts, suggesting the presence of a worm within the cyst (Fig. 6). Linear opacities, extending from the pleura to the lung, running differently from the course of the bronchovascular bundle, were seen in seven patients (Fig. 7). Other findings were variable-sized nodules ($n = 7$) and bronchiectasis ($n = 6$).

Discussion

P. westermani gains entrance to its human host as an encysted metacercaria within freshwater crabs and crayfish. Once ingested, the larvae escape from the cyst in the small intestine, penetrate the intestinal wall, and enter the peritoneal cavity. In 3–8 weeks, they penetrate the diaphragm and pleura and enter the lung. The larvae mature into adult flukes within the lung, and cystic cavities form around the flukes [1, 4]. On radiographs, during the process of pleural penetration by juvenile worms, pneumothorax or pleural effusion is seen, and during the process of larval migration within the lung, patchy migrating air-space consolidation appears [4].

The appearance of pulmonary lesions on radiographs varies with the stage of the infection and the surrounding tissue reaction. The initial finding is patchy air-space consolidation due to hemorrhagic pneumonia caused by the migrating

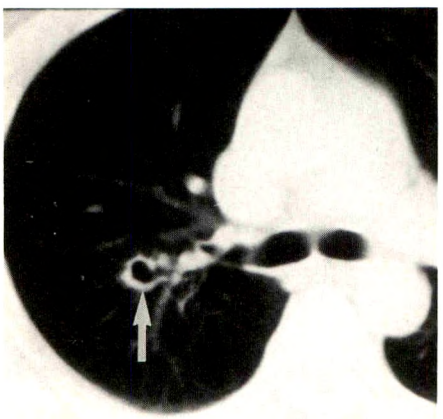


Fig. 5.—Pulmonary paragonimiasis with a cyst in a 36-year-old man with blood-tinged sputum. CT scan obtained just below tracheal carina shows round cystic lesion (*arrow*) that communicates with tubular structure, suggesting a dilated bronchus or a worm migration track.

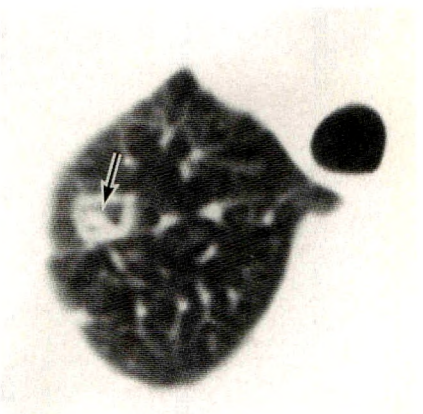


Fig. 6.—Pulmonary paragonimiasis in a 35-year-old woman. CT scan shows a thin-walled cavity in right apex. Ovoid structure (*arrow*) within cavity suggests a worm.

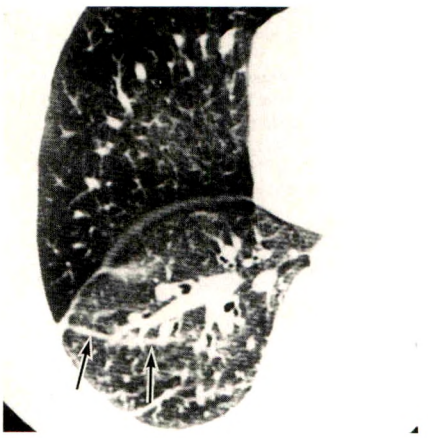


Fig. 7.—Pulmonary paragonimiasis in a 61-year-old man. High-resolution CT scan targeted to right lower quadrant of thorax shows linear bandlike area of increased attenuation (*arrows*) abutting major fissure. Course of linear lesion is different from that of bronchovascular bundle.

worm. At this stage, pleural effusion or pneumothorax is frequently seen. As juvenile worms mature into adults, they tend to settle down, and cysts form around them (worm cysts) [4]. Hypotheses for the mechanism of this formation include ischemic infarction after obstruction of an arteriole or a vein by a worm or by eggs [14] and expansion of the small airway by an intraluminal parasite [1]. When the cystic space is filled with hemorrhagic fluid and surrounded by pericystic air-space consolidation, it appears as a localized masslike consolidation on radiographs. Cysts that communicate with the adjacent bronchiole or bronchus appear as air cysts within the consolidated lung or as ring shadows.

On radiographs, peripheral linear shadows 2–4 mm thick and 3–7 cm long and invariably extending from the pleural surface (Fig. 4) suggest worm migration tracks or peripheral atelectasis caused by obstruction of small airways by the worm. However, high-resolution CT scans show clearly that the linear opacities run differently from the course of the bronchovascular bundle, suggesting a worm migration track (Fig. 7). Such linear opacities are most commonly and clearly seen in patients with pleural effusion, which suggests that interposition of the pleural fluid through the defect on the surface of the visceral pleura makes the track more prominent. Worm burrows or migration tracks could also appear as air-filled tunnels of various diameters, as reported by Singcharoen and Silprasert [12].

The prevalence of pleural effusion in patients with pleuropulmonary paragonimiasis varies from 2.9% [2] to 48% [9]. In our study, 38 (54%) of 71 patients had either pleural effusion or hydropneumothorax; 12 (17%) of these had bilateral lesions. Thus, unexplained bilateral pleural effusions or pneumothoraces are findings suggestive of paragonimiasis, especially in endemic areas. We think the higher prevalence of pleural effusion in our study is due to earlier diagnosis on the basis of the results of antibody tests done during the stage of active worm migration.

Adult *P. westermani* worms are bean shaped, 5–12 mm long, 3–6 mm wide, and 2–5 mm thick [15], a size that can be seen on radiologic images. However, no previous reports have described the radiologic appearance of the worm itself. To investigate the nature of the radiologic findings in paragonimiasis, we induced experimental paragonimiasis in 21 cats by intragastric infusion via nasogastric tube of 30 metacercariae of *P. westermani* that were isolated from freshwater crabs (Im J-G et al., presented at the Radiological Society of North America Meeting, November 1991). In this study, we clearly demonstrated that the eccentric thickening of the cyst wall (eclipse effect) on posteroanterior radiographs and the ovoid intracavitary nodule on plain images represent worm(s) within the cavity (Fig. 8). We think that the flat intracavitary lesions with soft-tissue attenuation seen on the CT scans in our study (Fig. 6) represent intracavitary worms, although this was not confirmed pathologically.

The worms tend to settle in the peribronchial area [1, 14, Im J-G et al., RSNA meeting, November 1991]. Thus, obstruction of the adjacent airway results in subsegmental atelectasis, as shown in five patients in our study (Table 1). The relationship between paragonimiasis and bronchiectasis has been discussed [3, 4, 6]. Suwanik and Harinsuta [3] showed dilated bronchi and worm tracks adjacent to worm cysts on bronchography. The CT scans in our series clearly showed a tubular structure communicating with a cyst (Fig. 5). The tubular structure could represent a dilated bronchus or a worm migration track. In a study of experimental paragonimiasis, Lee [16] showed that all the worms detected in the lungs of five dogs at 6 months of infestation were located within the cystic dilated peripheral bronchi or within the larger proximal bronchi.

The diagnosis of paragonimiasis is made either by detecting eggs in sputum, stool, fluid from bronchoscopic lavage, or biopsy specimens, or by a positive anti-*Paragonimus* antibody test. Although specific, egg detection rates have been re-

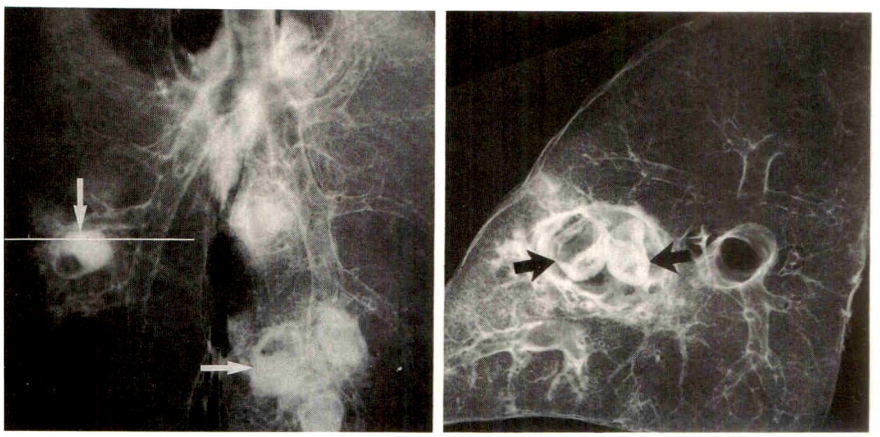


Fig. 8.—Experimental paragonimiasis in a cat studied 20 weeks after intragastric infusion of 30 metacercariae of *Paragonimus westermani* through nasogastric tube.

***A*, Radiograph of isolated fresh inflated lung shows multiple worm cysts with eccentric wall thickening (eclipse effect) (*arrows*).**

***B*, Radiograph of lung slice (4 mm thick) in transverse plane at level of white line marked in *A*, obtained after air-dried fixation by Heitzman's method. Worm cyst contains two dried worms (*arrows*).**

ported to be low (28–38%) [15]. Enzyme-linked immunosorbent assay [13] is highly sensitive (92%) and specific [15] in detecting antibodies. Antibody levels drop to normal range 4–24 months after successful treatment [15].

Distinguishing between paragonimiasis and tuberculosis is frequently difficult. Pulmonary infiltrates in paragonimiasis are usually poorly defined consolidations that change rapidly with time, whereas infiltrates in tuberculosis are nodular lesions that change slowly. Cysts in paragonimiasis invariably have a smooth inner margin and a thin wall, with a typical ring shadow. After treatment, residual fibrosis and emphysematous change are virtually absent in paragonimiasis, whereas these findings are usual in tuberculosis. Subpleural linear opacities are common in paragonimiasis, especially in the early stage, and are unusual in tuberculosis. In cases of pleurisy, residual pleural fibrosis is unusual in paragonimiasis, even with a long duration of the disease, whereas it is usual in tuberculosis.

In summary, typical findings of pleuropulmonary paragonimiasis on radiographs are patchy air-space consolidation with or without cysts, ring shadows, subpleural linear opacities, and bilateral pleural effusions. CT provides more specific information about the worm cyst and worm migration track.

REFERENCES

1. Yokogawa M. *Paragonimus* and paragonimiasis. *Adv Parasitol* **1965**;3: 99–158
2. Miller FL, Walker R. The roentgen characteristics of pulmonary paragonimiasis. *Radiology* **1955**;65:231–235
3. Suwanik R, Harinsuta C. Pulmonary paragonimiasis: an evaluation of roentgen findings in 38 positive sputum patients in an endemic area in Thailand. *AJR* **1959**;81:236–244
4. Yang S-P, Hunag C-T, Cheng C-S, Chiang L-C. The clinical and roentgenological courses of pulmonary paragonimiasis. *Chest* **1959**;36:494–508
5. Roque FT, Ludwick RW, Bell JC. Pulmonary paragonimiasis: a review with case reports from Korea and the Philippines. *Ann Intern Med* **1953**; 38:1206–1221
6. Sadun EH, Buck AA. Paragonimiasis in South Korea: immunodiagnosis, epidemiologic, clinical, roentgenologic and therapeutic studies. *Am J Trop Med Hyg* **1960**;9:562–569
7. Burton K, Yogev R, London N, Boyer K, Shulman ST. Pulmonary paragonimiasis in Laotian refugee children. *Pediatrics* **1982**;70:246–248
8. Taylor CR, Swett HA. Pulmonary paragonimiasis in Laotian refugees. *Radiology* **1982**;143:411–412
9. Johnson RJ, Johnson JR. Paragonimiasis in Indochinese refugees. *Am Rev Respir Dis* **1983**;128:534–538
10. Johnson JR, Falk A, Iber C, Davis S. Paragonimiasis in the United States: a report of nine cases in Hmong immigrants. *Chest* **1982**;82:168–171
11. Yang SP, Cheng CS, Ghen KM. Chest x-ray findings and some clinical aspects in pulmonary paragonimiasis. *Chest* **1955**;27:88–95
12. Singcharoen T, Silprasert W. CT findings in pulmonary paragonimiasis. *J Comput Assist Tomogr* **1987**;11:1101–1102
13. Cho SY, Hong ST, Rho YH, Choi S, Han YC. Application of micro-ELISA in serodiagnosis of human paragonimiasis. *Korean J Parasitol* **1981**; 19:151–156
14. Diaconita GH, Goldis GH. Investigations on pathomorphology and pathogenesis of pulmonary paragonimiasis. *Acta Tuberc Scand* **1964**;44:53–75
15. Shim Y-S, Cho S-Y, Han Y-C. Pulmonary paragonimiasis: a Korean perspective. *Semin Respir Med* **1991**;12:35–45
16. Lee O-R. A histopathologic study of the lungs infected with *Paragonimus westermani* in the dog. *Korean J Parasitol* **1979**;17:19–44

Book Review

Cardiac Imaging in Infants, Children, and Adults. By Larry P. Elliott. Philadelphia: Lippincott, 960 pp., 1991. $150

This text uses as its framework portions of volume 2 of the five-volume loose-leaf text on radiology edited by Juan M. Tavaras et al. Dr. Elliott has integrated the contributions of 50 well-known authors to produce a format that describes each cardiovascular disease in terms of the normal anatomy and physiology, pathophysiologic changes seen on plain radiographs, and noninvasive and invasive methods of imaging.

The book begins with an introduction on cardiac anatomy and physiology, with an emphasis on their relationship to findings on radiographs. Then, information is presented on nuclear cardiology, echocardiography, CT, ultrafast CT, MR imaging, and positron emission tomography. This material is as current as might be expected for a hardcover text. Newer techniques such as transesophageal echocardiography and technetium-bound isonitriles for cardiac imaging are included.

Cardiac disease in adults is divided into sections on valvular disease, abnormalities of the great vessels including aneurysms, pericardial disease, cardiac tumors, cardiomyopathies, and ischemic disease. Each section includes chapters on morphology, pathophysiology, plain radiography, and various other imaging techniques, including angiography where appropriate. Each chapter covers a very specific topic, so little overlap of material occurs. Differences in the authors's styles of writing make the transition from one topic to another a little uneven. However, the clarity and instructional quality of the chapters have not been compromised.

The next sections deal with the diagnosis of congenital heart disease in children, infants, and, where pertinent, adults. Dr. Elliott has written or collaborated on many of the chapters in these sections, which makes for a smoother transition between chapters. A separate part deals with the premature infant with heart disease and the infant with respiratory distress. Angiocardiography in both infants and adults and coronary angiography are addressed in special sections. A final part deals with pulmonary embolic disease, including strategies for the imaging workshop, elements of ventilation-perfusion scanning, pulmonary angiography, and discussion of the National Institutes of Health study on detection of pulmonary embolism and clinical trials with urokinase.

Several sections in the hardcover text have been added since the 1991 update to the loose-leaf edition. These include sections on MR imaging of various cardiac abnormalities, CT and ultrafast CT of the heart, and several sections on pathophysiologic changes. Of special note is a new chapter on abnormalities of the great arteries, which is clearly written and well illustrated with both drawings and radiologic images. Many chapters have been updated. Several of the sections on echocardiography have been significantly revised. A centralized section including images from color Doppler echocardiography has also been added.

Radiologic images, drawings, and charts are of uniformly high quality. Abundant labels and complementary artwork make the images easy to interpret.

The chapters by Elliott on congenital heart disease provide a major strength of this text. Here, Dr. Elliott has applied his "physiologic analysis" of plain radiographs, and the reader is shown to appreciate chest radiographs not as static pictures of bones and soft tissues but as surprisingly accurate indicators of complex hemodynamic processes. Radiology residents will appreciate chapter 15, which provides vascular-anatomic sets of differential diagnosis based on the pulmonary vascularity.

One surprising deficiency is the absence of a section on heterotaxic disorders. Asplenia is mentioned briefly, but the material is difficult to locate in the text, being tucked away in the chapter on cyanosis and decreased vascularity. The discussion of congenital anomalies of the coronary arteries and coronary fistulas is also incomplete and underemphasized. These are two areas in which knowledgeable cardiac radiologists can make a significant contribution to the interpretation of the coronary arteriogram, even in 1991.

The transition process from loose-leaf to hardcover has not been painless. Color Doppler echocardiograms and nuclear medicine images are welcome additions. However, these are centralized in a few pages, and this section is difficult to locate.

The list of contributors to this work has continued to grow, and the quality of the presentations has remained high. The cost ($150) is not trivial, particularly for someone in training. However, this book is comprehensive and is designed to be both an instructional and a reference text that will maintain its usefulness both during and after postgraduate training. I continue to refer to this work, and I recommend it to residents, fellows, and anyone who wishes to increase his or her knowledge of cardiac radiology.

John E. Aruny
Brigham and Women's Hospital
Harvard Medical School
Boston, MA 02115

Pictorial Essay

CT Evaluation of Poststernotomy Complications

Philip A. Templeton[1] and Elliot K. Fishman[2]

Complication rates after sternotomy are between 0.5% and 5% [1]. Mortality is high: 27% for mediastinal infection and 50% for diffuse mediastinitis [2]. More recent series report a 10–20% mortality rate if the diagnosis is made early and sternal debridement and antibiotic lavage are performed [3]. Predisposing factors for complication include repeat surgery for hemorrhage or to redo a coronary artery bypass, external cardiac massage, mechanical ventilation, tracheostomy, and error in surgical technique (e.g., off-centered sternal incision or inadequate sternal fixation). Imaging choices include plain film radiography, tomography, CT, scintigraphy, and sinography. CT plays a major role in the assessment of complication, depicting the extent and depth of the abnormality. The scans must be studied for abnormalities in the presternal, sternal, and retrosternal compartments. CT scans that

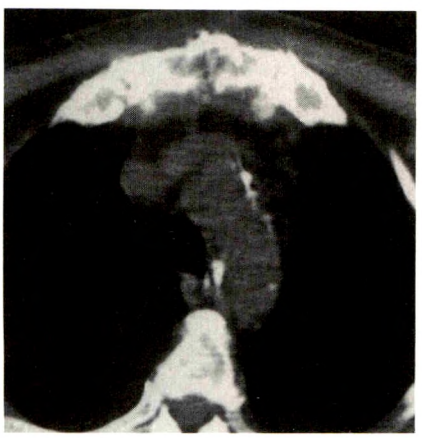


Fig. 1.—Edema: normal postoperative findings. CT scan shows minimal soft-tissue strands retrosternally and in anterior mediastinal fat. Minimal strands may be present for 2–3 weeks after surgery. Preserved mediastinal fat planes generally indicate that these changes are not significant. Dots of air also may be seen up to 7 days after surgery.

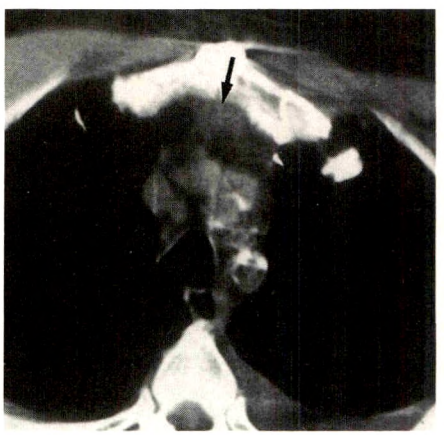


Fig. 2.—Focal retrosternal fluid collections: normal postoperative findings. CT scan shows small amounts of retrosternal fluid (*arrow*) with preserved fat planes. This can be seen for several days to weeks after surgery and removal of mediastinal drainage tubes. Such a finding in the first postoperative week or two is of uncertain significance. A similar finding, several weeks or months after surgery, would raise the possibility of an abscess or pseudoaneurysm.

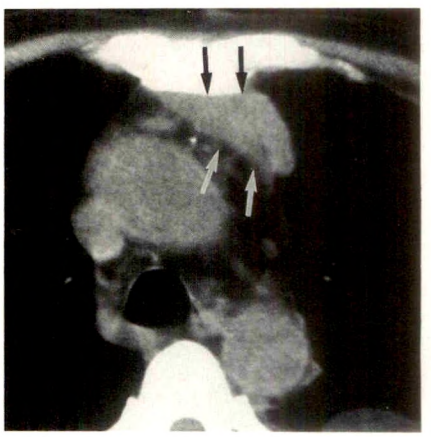


Fig. 3.—Hematoma. CT scan shows a well-circumscribed fluid collection (*arrows*) with high CT numbers, which suggests hematoma. If infection is suspected, bacteriologic confirmation must be obtained. If pseudoaneurysm is suspected, IV contrast enhancement, MR imaging, or angiography is necessary.

Received December 20, 1991; accepted after revision February 5, 1992.

[1] Department of Radiology, University of Maryland Medical System, 22 S. Greene St., Baltimore, MD 21201. Address reprint requests to P. A. Templeton.
[2] Department of Radiology and Radiological Science, Johns Hopkins Hospital, Baltimore, MD 21205.

AJR **159:45–50, July 1992** 0361–803X/92/1591–0045 © American Roentgen Ray Society

show no abnormalities are useful for reassurance: the presence of preserved mediastinal fat planes rules out infection requiring surgical intervention [4]. Detection of abnormalities on CT scans can be used to guide further evaluation, including the sampling of collections for culture, or may indicate the need for immediate surgery. Imaging and clinical findings should be compared closely.

Technique

CT scans should be obtained with IV contrast material when possible. In addition to standard 8- to 10-mm collimation scans, 4- to 5-mm collimation scans can be useful in evaluating the sternum. Scans should be viewed at settings appropriate for evaluation of the mediastinum, lungs, and sternum. If IV contrast material is not used initially, and a periaortic fluid collection is revealed, the possibility of a pseudoaneurysm must be evaluated by using IV contrast-enhancement, MR imaging, or angiography.

Normal Postoperative Appearance

Usual postoperative changes can persist for 2–3 weeks. These include minimal presternal and retrosternal soft-tissue infiltration with edema and blood (Fig. 1), focal retrosternal air and fluid (Fig. 2), localized hematoma (30–60 H) [3] (Fig. 3), postincisional bone defect (Fig. 4), minor sternal irregularities

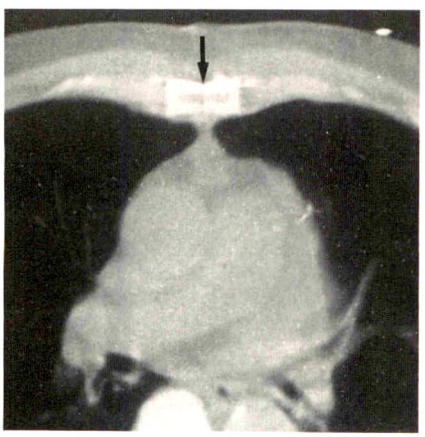


Fig. 4.—Postincisional bone defect: normal postoperative finding. CT scan shows midsternal lucency (*arrow*), which represents sternal incision.

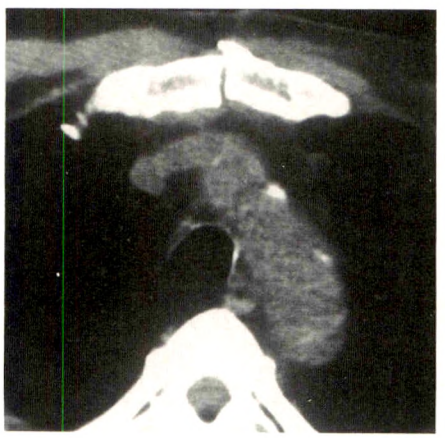


Fig. 5.—Minor sternal offset. CT scan shows minimal sternal irregularity or gaps, which may be normal findings. Defects in sternal closure are common, and correlation with clinical examination and symptoms is necessary to determine sternal stability.

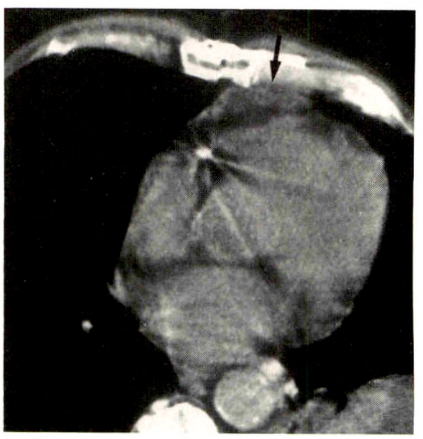


Fig. 6.—Pericardial thickening. CT scan shows small amount of anterior pericardial fluid or thickening (*arrow*), an expected finding in early postoperative period.

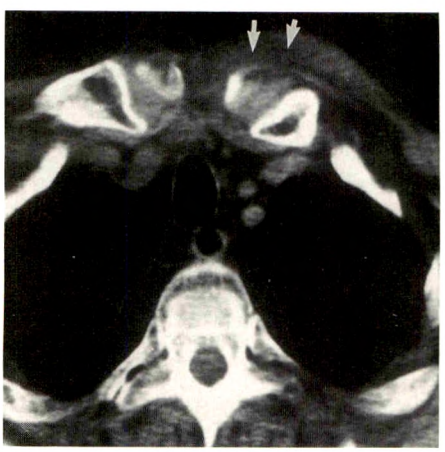
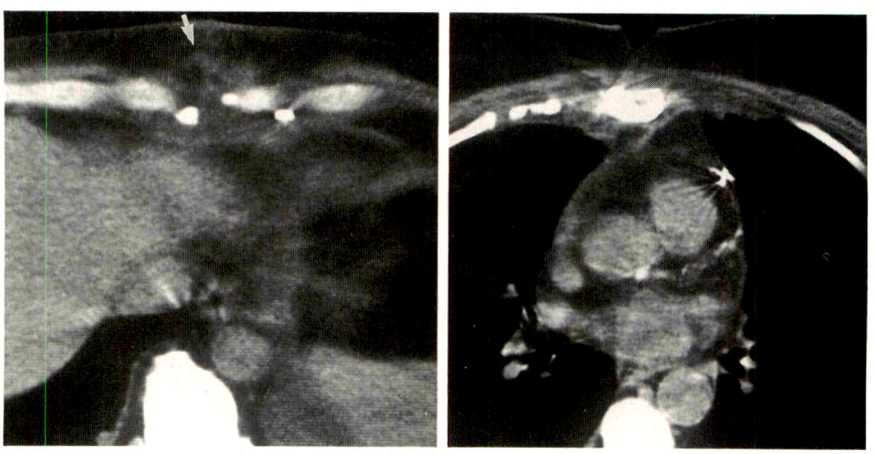


Fig. 7.—Sternal debridement with muscle flap. CT scan obtained 3 months after surgery shows left pectoralis muscle used to close sternal wound opening (*arrows*). Note clear fat planes and lack of fluid collections.



A **B**

Fig. 8.—Inflammation and drainage.
***A*, CT scan of patient with drainage from lower sternum shows minimal presternal inflammation (*arrow*) and no evidence of deep collection or osteomyelitis. Conservative management led to resolution without surgical intervention.**
***B*, CT scan of open anterior chest wound shows no drainable collection.**

or offset (Fig. 5), and minimal pericardial thickening (Fig. 6). Dots of mediastinal air, if present, usually resolve by 7 days after surgery, but can persist longer [1]. The postincisional bone defect is a normal midsternal lucency or line that can be seen on chest radiographs or CT scans, representing the sternal incision. If sternal debridement is performed for infection, the sternal defect is often closed with muscle flaps (e.g., pectoralis major or rectus abdominis muscle) (Fig. 7).

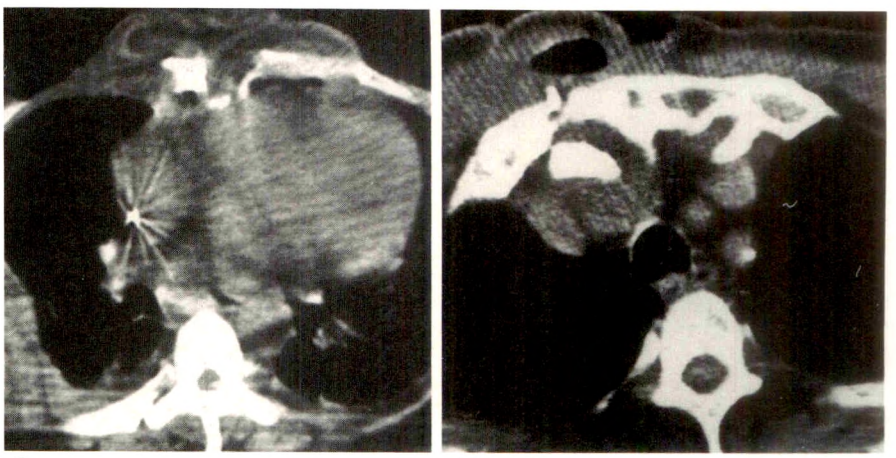


Fig. 9.—Major debridement. CT scan shows large open wound after debridement and placement of muscle flap. Right-sided pleural collection is present, but no mediastinal collection is seen.

Fig. 10.—Abscess. CT scan shows air-fluid level in anterior chest wall, with surrounding inflammation and sternoclavicular joint irregularity.

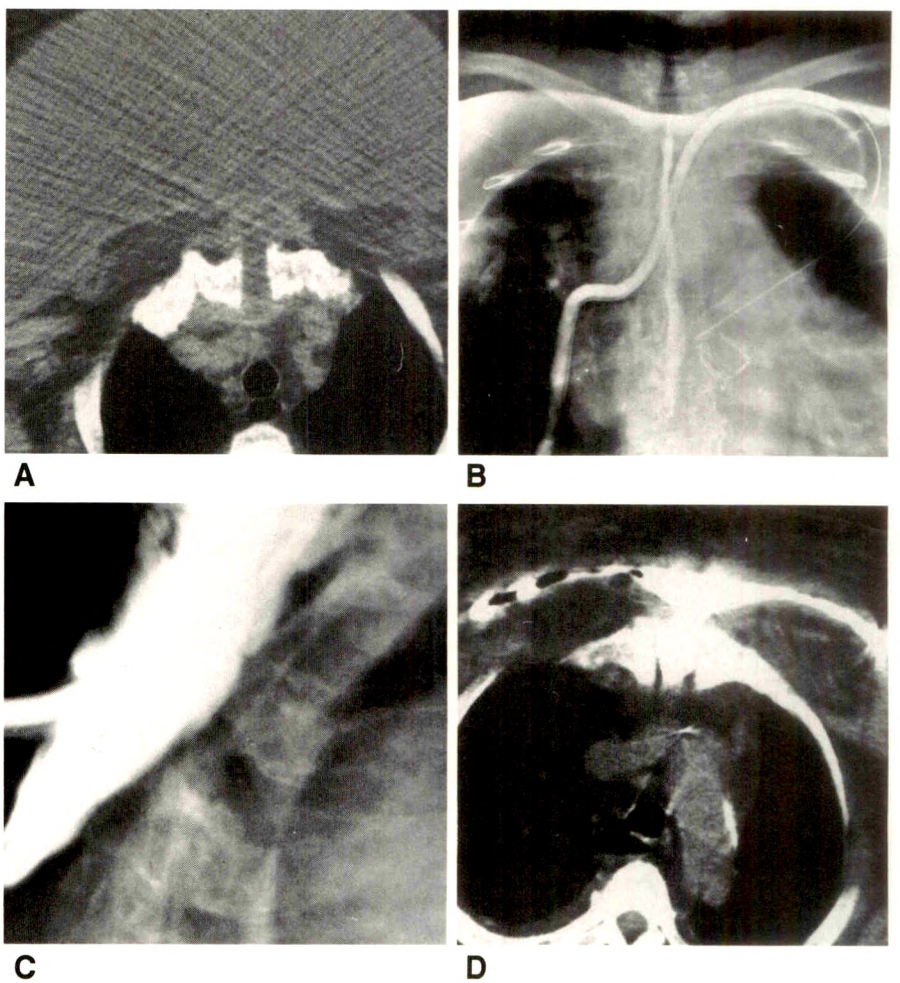


Fig. 11.—Sinus tracts and sinography.

***A*, CT scan shows massive fluid collection in anterior portion of chest extending to sternal dehiscence. No evidence of communication with mediastinum is seen.**

***B* and *C*, Posteroanterior (*B*) and lateral (*C*) chest radiographs after contrast injection into sinus tract show large triangular space filling anterior portion of chest and no definite connection with mediastinum.**

***D*, CT scan obtained after sinography shows air and contrast material in cavity, which extends to sternal dehiscence but does not communicate with mediastinum or pleura.**

Presternal Complications

Presternal soft tissues include the skin, subcutaneous tissues, and muscles. Most complications are due to inflammation or infection (Figs. 8 and 9), draining sinus tracts, or frank abscess formation (Fig. 10). CT depicts the extent of inflammatory changes and the presence of drainable collections. When a draining sinus tract is present, contrast sinography can be used to evaluate the extent of the collection. CT sinography is useful to determine the presence or extent of mediastinal communication (Fig. 11).

Sternal Complications

A variety of symptomatic problems can lead to CT examination of the sternum, including a sternal click, excessive incisional pain, sterile or purulent wound drainage, and sternal instability [4]. CT can aid in detection of minimal dehiscence, paramedian sternotomy incision, major dehiscence, and osteomyelitis. Defects in sternal closure do not necessarily indicate a significant clinical problem (Fig. 12). When CT findings are equivocal, clinical findings and additional studies such as the sequential use of ^{99m}Tc-phosphate and ^{67}Ga-citrate scintigraphy can be useful.

A paramedian sternotomy, with its off-centered incision, can cause dehiscence (Fig. 13). The thin side of the sternum frequently breaks. Defects in sternal closure require clinical correlation; the finding alone does not indicate sternal instability. Sternal dehiscence is usually clinically obvious. Imaging findings include rotation of the sternal wire, displacement or fracture, and progressive widening of the postincisional lucency (Fig. 14).

Early sternal osteomyelitis can be difficult to differentiate from minor sternal irregularities due to the bone saw and normal anatomic variants simulating abnormality. Eventually, frank bone destruction, severe demineralization, and dehis-

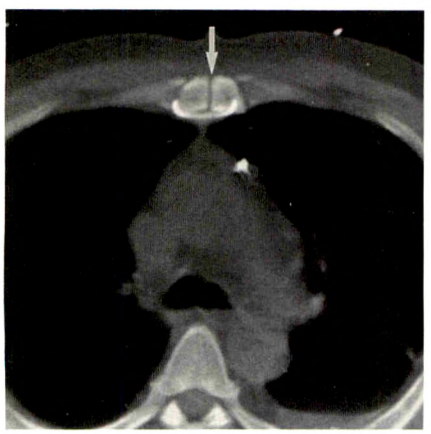


Fig. 12.—Minimal diastasis. CT scan shows a small sternal separation of no clinical significance (*arrow*).

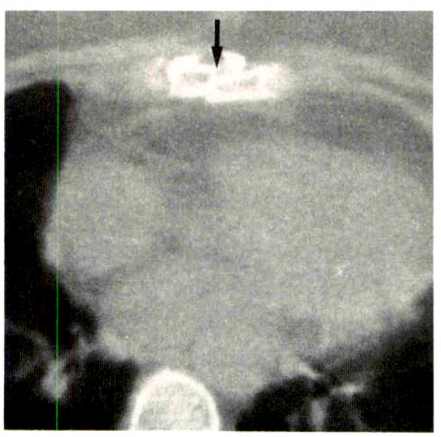


Fig. 13.—Paramedian sternotomy. CT scan shows sternal incision is uneven (*arrow*), with right half of sternum smaller than left half.

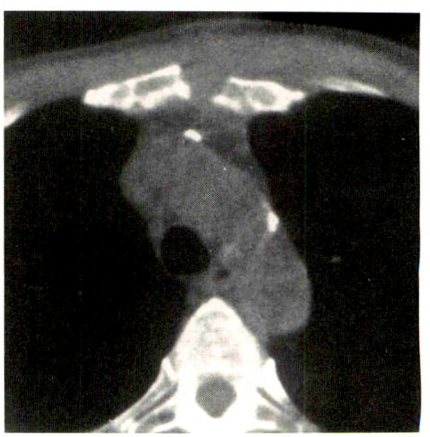
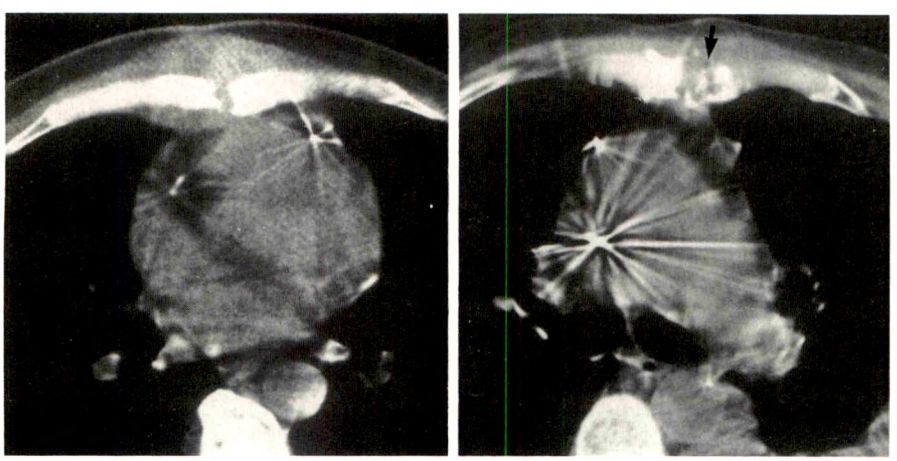


Fig. 14.—Sternal dehiscence. CT scan shows wide gap separating two sternal halves.



A **B**

Fig. 15.—Sternal osteomyelitis.
***A*, CT scan shows sternal irregularity, dehiscence, and soft-tissue collection from abscess around sternum.**
***B*, CT scan shows sternal bone irregularity and destruction (*arrow*).**

cence are universal in sternal osteomyelitis. CT can show subtle erosions, periosteal new bone formation, sharply marginated sclerosis, and adjacent soft-tissue swelling [4] (Fig. 15).

Retrosternal Complications

Retrosternal or deep complications can be life-threatening and include abscess, mediastinitis, pericardial effusion or hematoma, loculated effusion, and empyema. Uninfected mediastinal and pleural collections also are common (Fig. 16). Only bacteriologic analysis can exclude infection. Large pericardial effusions may develop postoperatively (Fig. 17). High-attenuation collections suggest hemopericardium. Marked pericardial thickening can lead to constriction.

Mediastinitis can be difficult to diagnose. Obliteration of mediastinal fat planes and diffuse soft-tissue infiltration with or without gas collections are suggestive. Frank abscess collections are usually of low density and may contain air also.

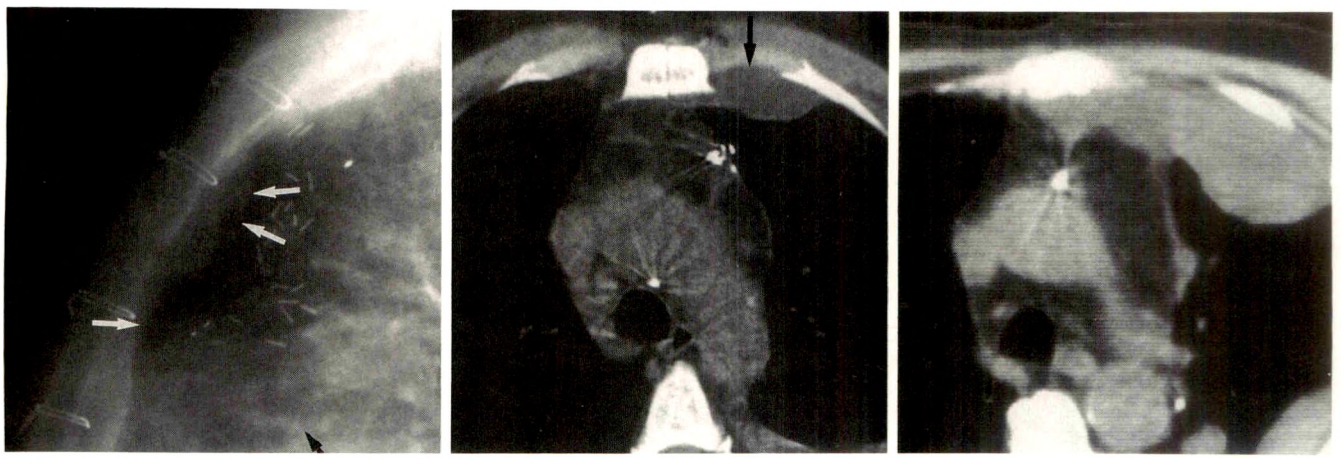


Fig. 16.—Fluid collections.
***A*, Lateral chest radiograph shows a retrosternal collection (*arrows*).**
***B*, CT scan shows low-density collection (*arrow*) and no definite evidence of infection (i.e., air in collection). Correlation with clinical situation is necessary in such cases to determine if aspiration is indicated. This collection resolved without treatment.**
***C*, CT scan in another patient shows complicated collection due to loculated hemothorax. Infection cannot be excluded in such postoperative collections. Clinical signs of infection help in the decision whether to aspirate such collections or to observe the patient and possibly obtain a follow-up CT scan.**

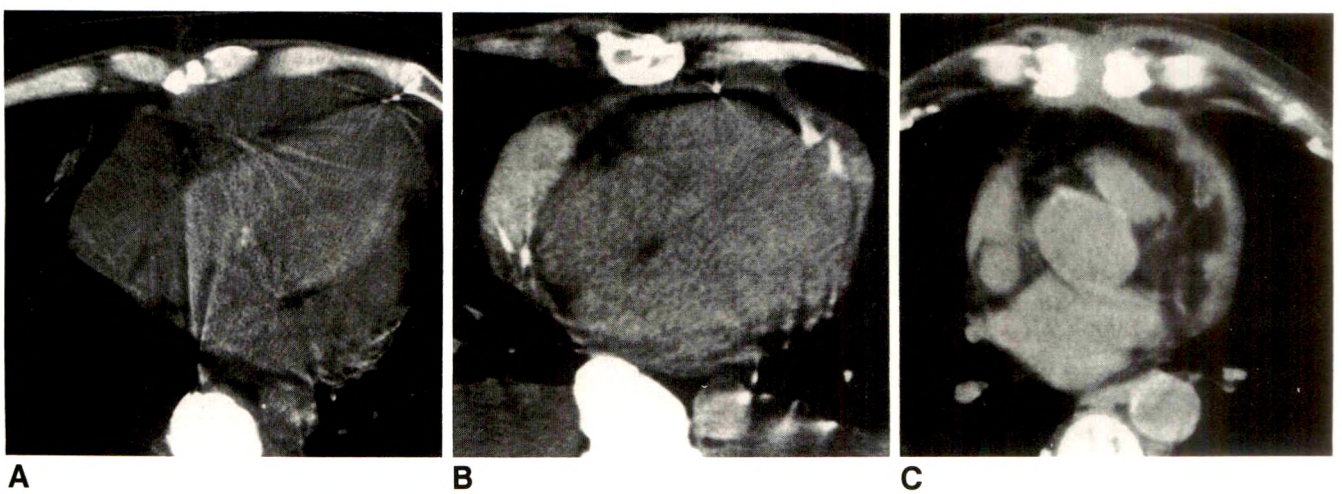


Fig. 17.—Pericardial effusion/hemopericardium.
***A*, CT scan shows large pericardial effusion that developed after surgery.**
***B*, CT scan shows high-attenuation collections with high CT numbers, suggesting hemopericardium.**
***C*, CT scan shows marked pericardial thickening.**

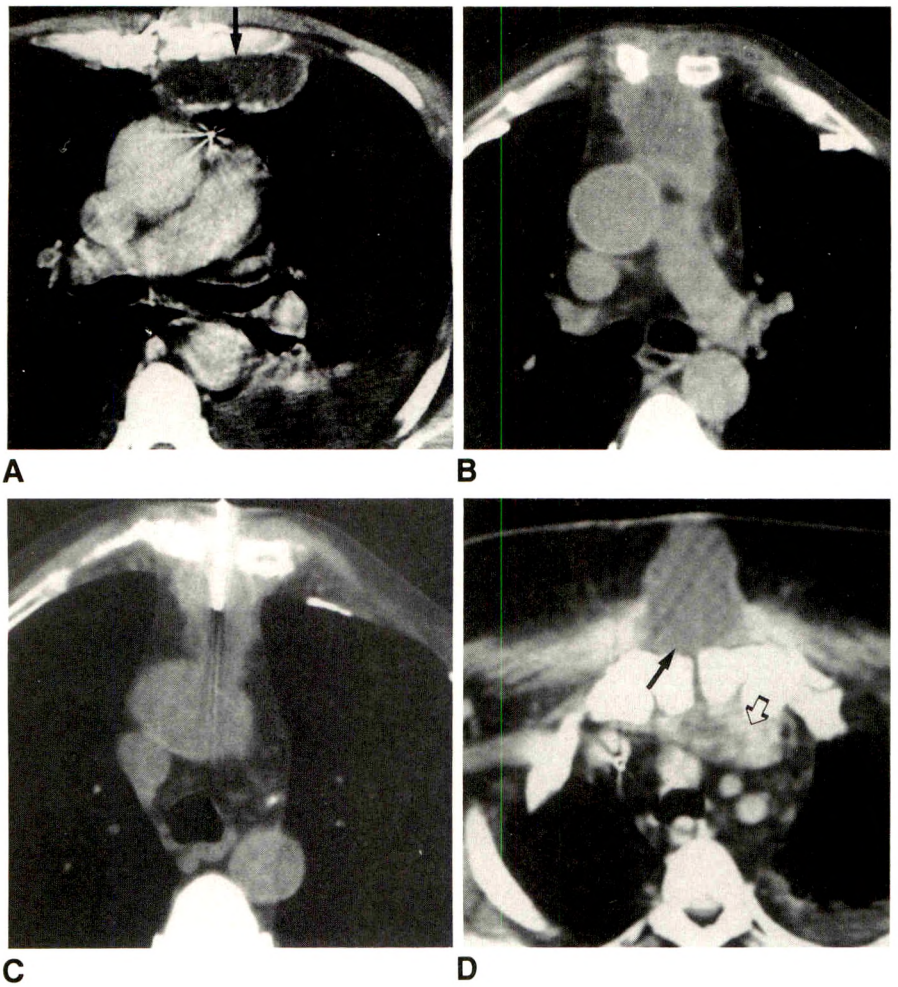


Fig. 18.—Mediastinitis/abscess.

***A*, CT scan shows enhancing rim of anterior mediastinal or medial pleural collection (*arrow*), which was drained and proved to be infected.**

***B* and *C*, CT scans show anterior mediastinal collection in a patient with sternal dehiscence, chest wall cellulitis, and pectoralis muscle flap. Contrast-enhanced CT excluded aortic pseudoaneurysm. CT-guided aspiration was performed, and infection was diagnosed.**

***D*, CT scan shows extensive presternal (*solid arrow*) and retrosternal (*open arrow*) abscess in a diabetic patient also being treated with steroids for hemolytic anemia. CT helped in evaluation of full extent of infection. Diffuse soft-tissue infiltration, fluid collections with/without air bubbles, and obliteration of normal mediastinal fat planes suggest diagnosis of mediastinitis or abscess.**

CT helps show the extent of the collection and can be used to guide aspiration and drainage (Fig. 18).

REFERENCES

1. Goodman LR, Kay HR, Teplick SK, Mundth ED. Complications of median sternotomy: computer tomographic evaluation. *AJR* **1983**;141:225–230
2. Carrol CL, Jeffrey RB Jr, Federle MP, Vernacchia FS. CT evaluation of mediastinal infections. *J Comput Assist Tomogr* **1987**;11:449–454
3. Culliford AT. Role of antibiotic lavage and radical debridement in the treatment of acute mediastinal wound infections following sternotomy. *Cardiac Surgery: State of the Art Reviews*, **1988**;12:459–473
4. Kay HR, Goodman LR, Teplick SK, Mundth ED. Use of computed tomography to assess mediastinal complications after median sternotomy. *Ann Thorac Surg* **1983**;36:706–714

Case Report

Mammographic Appearance of Loiasis

Cynthia A. Britton,[1] Jules Sumkin,[2] Manju Math,[3] and Scott Williams[4]

Few, if any, reports have been published on the mammographic appearance of parasitic disease within the breast, although the plain film findings of three parasitic diseases, dracunculiasis, cysticercosis, and loiasis, have been described [1–3]. Infection with any of these parasites can produce subcutaneous calcifications that are visible on plain films or mammograms. We describe a case of loiasis in the breast that had the mammographic appearance of indeterminate clustered microcalcifications associated with the *Loa loa* larvae.

Case Report

A 29-year-old woman had had a painful mass in the upper outer quadrant of her right breast for 2 weeks. She had no discharge from

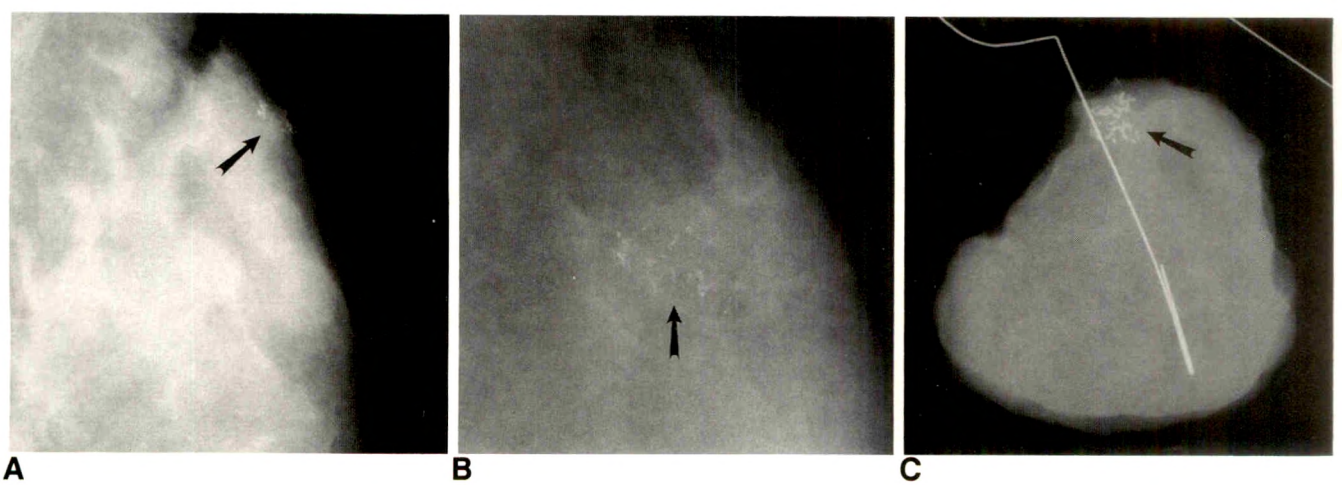


Fig. 1.—Loiasis mimicking malignant calcifications on mammography.
***A*, Mediolateral mammogram shows calcified larvae within a suspicious lesion (*arrow*) in upper outer quadrant of right breast.**
***B*, Magnified mammogram shows serpiginous calcifications (*arrow*) of *Loa loa* larvae.**
***C*, Radiograph confirms inclusion of calcified larvae (*arrow*) within biopsy specimen.**

Received November 22, 1991; accepted after revision January 9, 1992.
[1] Department of Radiology, University of Pittsburgh Medical Center, One Children's Pl., 3705 Fifth Ave., Pittsburgh, PA 15213. Address reprint requests to C. A. Britton.
[2] Department of Radiology, Magee-Women's Hospital, Forbes Ave. and Halket St., Pittsburgh, PA 15213.
[3] Department of Pathology, Magee-Women's Hospital, Forbes Ave. and Halket St., Pittsburgh, PA 15213.
[4] Department of Surgery, Magee-Women's Hospital, Forbes Ave. and Halket St., Pittsburgh, PA 15213.

the nipple, fever, or erythema. As a Peace Corps volunteer in Gabon, West Africa, in 1985, she became infected with the *L. loa*, or African eye worm, and had a history of multiple subcutaneous masses in her extremities associated with the infection. Her family history was significant for the death of a maternal grandmother at age 34 of breast cancer.

A mammogram showed serpiginous calcifications within a suspicious lesion in the upper outer quadrant of the right breast (Fig. 1A). A magnified view showed that the calcifications resembled neither typical benign nor malignant breast calcifications (Fig. 1B). An excisional biopsy was performed to confirm the presence of *L. loa* larvae and exclude carcinoma. The radiograph of the biopsy specimen confirmed the presence of the calcified larvae within the specimen (Fig. 1C). Histologic examination showed a giant-cell granulomatous reaction accompanying the worms.

Discussion

Loiasis is a tropical disease caused by the worm *L. loa*. Larvae enter the patient via the bite of the mango fly and reproduce in the subcutaneous tissue, usually in the extremities and in the subconjunctival tissues of the eye. The life cycle of the worm is completed when the infected human host is again bitten by the mango fly, and the microfilaria produced by the larvae become infective within the fly.

The mature larvae die and calcify within the subcutaneous tissue. Their serpiginous, filamentous appearance is suggestive of a parasitic infection and is unlike that of benign or malignant breast calcifications. They are usually accompanied by painful areas of intense inflammation called Calabar swellings, named for a West African town in which loiasis is endemic. This is seen most commonly in the extremities—the breast mass in this patient is an unusual example of a Calabar swelling located centrally within the body. When accompanied with an intense inflammatory reaction, the combination of a mass with microcalcifications on mammography may cause confusion in excluding a malignant tumor, as in this patient.

The diagnosis of loiasis is supported by a history of travel to an endemic area such as West Africa, the presence of immature worms or microfilariae in the blood, eosinophilia, and a history of Calabar swellings or subconjunctival worms.

REFERENCES

1. Reeder NM. Tropical diseases of the soft tissues. *Semin Roentgenol* **1973**;8:47–71
2. Johnstone RDC. Loiasis. *Lancet* **1947**;1:250–252
3. Resnick D, Niwayama G. *Diagnosis of bone and joint disorders*, 2nd ed. Philadelphia: Saunders, **1988**:2735–2736

Epithelioid Hemangioendothelioma of the Liver: Imaging Findings with Pathologic Correlation

William J. Miller[1]
Gerald D. Dodd III
Michael P. Federle
Richard L. Baron

Hepatic epithelioid hemangioendothelioma is a rare malignant neoplasm that has nonspecific clinical signs and symptoms and can be difficult to diagnose on the basis of biopsy results. Radiologists may suggest the diagnosis of this slowly progressive neoplasm by recognizing its characteristic radiologic features. We correlated images from CT (13), sonography (nine), and MR (six) with pathologic findings in resected whole livers (eight) and biopsy specimens (five) from 13 patients 25–58 years old. Gross pathologic examination showed a repetitive pattern of multiple solid tumor nodules, in a predominantly peripheral distribution, with coalescence as individual nodules exceeded 4 cm. Tumor nodules had a hyperemic rim. Lesions adjacent to the capsule often produced capsular retraction. These findings correlated well with imaging findings. On CT, the lesions were of low attenuation, peripherally based, and with capsular retraction or flattening in nine (69%) of 13 patients. Unenhanced CT scans showed superior conspicuity over contrast-enhanced CT scans (9/13, 69%) and showed the extent of lesions more accurately in all cases (13/13, 100%). In nine patients, lesions had a peripheral enhancement pattern of alternating attenuation values correlating with the hyperemic rim at pathologic evaluation. On sonograms, the tumors were solid and predominantly hypoechoic. On MR, tumor signal was low on T1-weighted and high on T2-weighted images, with a low-signal halo present around many of the lesions.

CT, sonographic, or MR findings of coalescent peripheral hepatic masses with capsular retraction are highly suggestive of hepatic epithelioid hemangioendothelioma.

AJR 159:53–57, July 1992

Hepatic epithelioid hemangioendothelioma (EHE) is a rare tumor of vascular origin that occurs almost exclusively in adults [1–6]. These tumors have a clinical course intermediate between that of benign cavernous hemangiomas and malignant angiosarcomas; most patients survive 5–10 years after diagnosis [1, 3]. Diagnosis of these tumors on clinical grounds is difficult because of their nonspecific signs and symptoms and misinterpretation of pathologic specimens [1, 3]. To date, only a few cases of hepatic EHE have been reported in the imaging literature [7–9]. In reviewing 13 cases of hepatic EHE treated at our hospital, we have detected a repetitive constellation of imaging characteristics highly suggestive of hepatic EHE. This report correlates the pathologic findings of hepatic EHE with the imaging studies.

Materials and Methods

Thirteen patients with pathologically proved hepatic EHE had imaging studies at our institution between 1985 and 1991. The patients consisted of nine men and four women (12 whites, one Hispanic) with a mean age of 39 years (range 25–58). The clinical signs and symptoms were nonspecific. Hepatomegaly and abdominal pain were the most common, but they were present in only seven patients. Liver enzymes were slightly elevated in four of 13 patients. Tests for α-fetoprotein and carcinoembryonic antigen were negative in the six

Received November 20, 1991; accepted after revision January 23, 1992.

Presented at the annual meeting of the Society of Gastrointestinal Radiologists, Carlsbad, CA, February 1991.

[1] All authors: Department of Radiology, University of Pittsburgh, School of Medicine, Presbyterian-University Hospital, DeSoto at O'Hara Sts., Pittsburgh, PA 15213. Address reprint requests to M. P. Federle.

0361–803X/92/1591–0053
© American Roentgen Ray Society

patients tested. Eight patients underwent hepatectomy and orthotopic liver transplantation, and five had biopsies of liver lesions.

Imaging studies were usually performed within 1 month (mean, 10 days) of transplantation or biopsy. Imaging studies included CT (13), sonography (nine), and MR imaging (six). CT scans were obtained with GE 8800 (four) and 9800 (nine) scanners (General Electric, Milwaukee, WI). Scans consisted of contiguous 1-cm sections through the liver without and with administration of 150 ml of IV contrast material. (Data are not available on four of the older studies, in which drip infusions may have been used; the more recent studies were done with power injectors at 1.5 ml per second with a 40-sec delay.) Sonographic studies were performed on an Acuson scanner (Acuson Corp., Mountain View, CA) with 2.5- and 3.5-MHz transducers.

MR images were obtained in the transverse plane by using a GE 1.5-T Signa system (five cases) and a Siemens 1.0-T system (Siemens Medical Systems, Iselin, NJ) (one case). Slice thickness was 10 mm with a 2-mm gap between planes, and a 128 × 256 matrix was used. Short TR/TE (400–800/20 [TR/TE]), long TR/short TE (>1800/20–30), and long TR/TE (>1800/80–100) spin-echo images were obtained. Respiratory compensation and spatial presaturation were used to decrease motion artifacts. IV gadopentetate dimeglumine (0.1 mm/kg) was used in conjunction with short TR/TE spin-echo imaging in four patients.

All radiologic studies were retrospectively reviewed for characterization of liver parenchymal abnormalities, liver contour, liver lobe size, and splenomegaly. In 11 patients, the imaging studies were compared with pathologic reports describing examination of the resected livers, photographs of the pathologic specimens, and liver biopsy results. Investigators directly correlated radiologic images with the pathologic findings of fresh hepatectomy specimens from two patients.

Results

Pathology

Gross pathologic examination of the total hepatectomy specimens from the eight patients who had liver transplantation showed a normal red brown capsular surface with multiple subcapsular tumor nodules. Serially sectioned liver specimens showed that the EHE tumors were multiple in all patients and mostly peripheral (Fig. 1). The tumor nodules were tan white and firm, and frequently caused capsular retraction (reported in all eight patients having transplantations) (Figs. 1 and 2). Individual tumor nodules ranged from less than 1 cm to 4 cm in diameter, often with a hyperemic periphery (Figs. 1 and 2). At larger sizes, the lesions were usually confluent, producing large aggregate masses (Fig. 2). In one case, nearly the entire liver parenchyma was replaced by tumor.

Histologically, the nodules were composed of a fibrous myxoid stroma with a relatively hypocellular center. The tumor

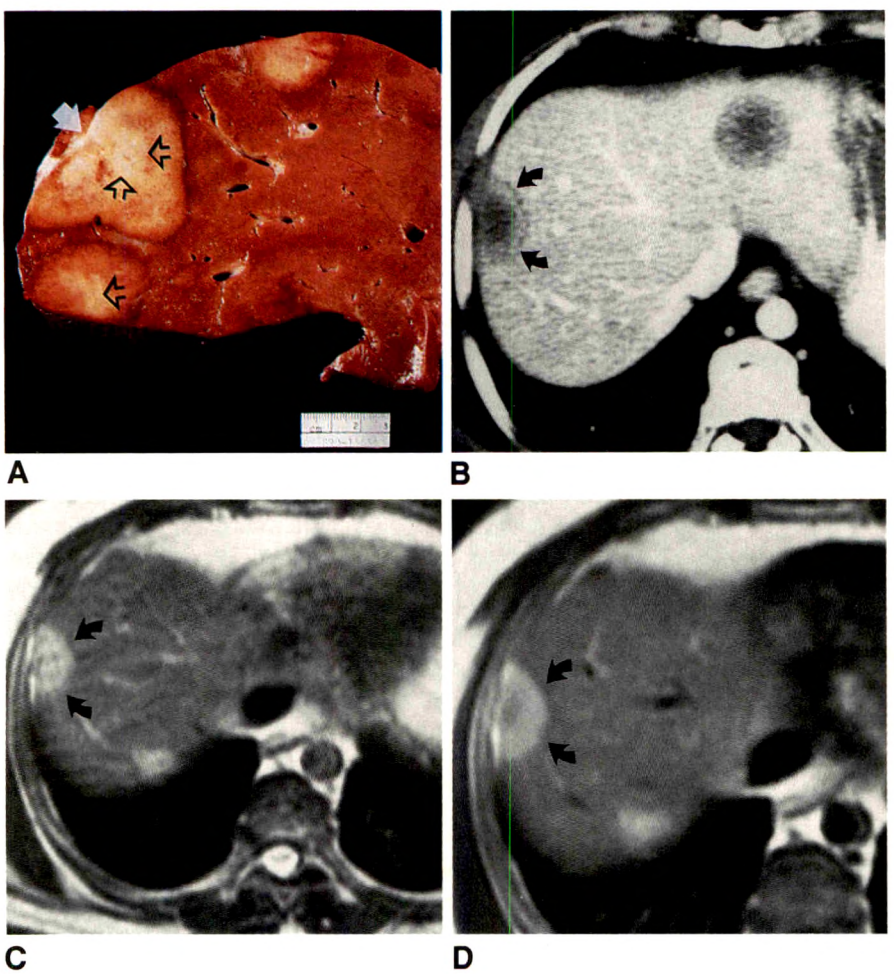


Fig. 1.—Hepatic epithelioid hemangioendothelioma with peripheral distribution of lesions and capsular retraction in a 42-year-old man.

***A*, Transverse (fresh cut) liver section through tumor nodules shows a white avascular central area (*black arrows*) surrounded by a hyperemic area. Note peripheral distribution of lesions and area of capsular retraction (*white arrow*).**

***B*, Enhanced CT scan shows tumor nodule with complex enhancement pattern consisting of a nonenhancing center, hyperemic inner rim, and low-attenuation outer halo (*arrows*).**

***C*, Long TR/TE spin-echo MR image shows high-intensity lesions, one with a thin, low-signal peripheral rim (*arrows*).**

***D*, Contrast-enhanced short TR/TE MR image shows lesion (*arrows*) with a complex enhancement pattern consisting of a hypointense (nonenhancing) central region, peripheral hyperemic zone of high signal intensity, and outermost hypointense avascular rim.**

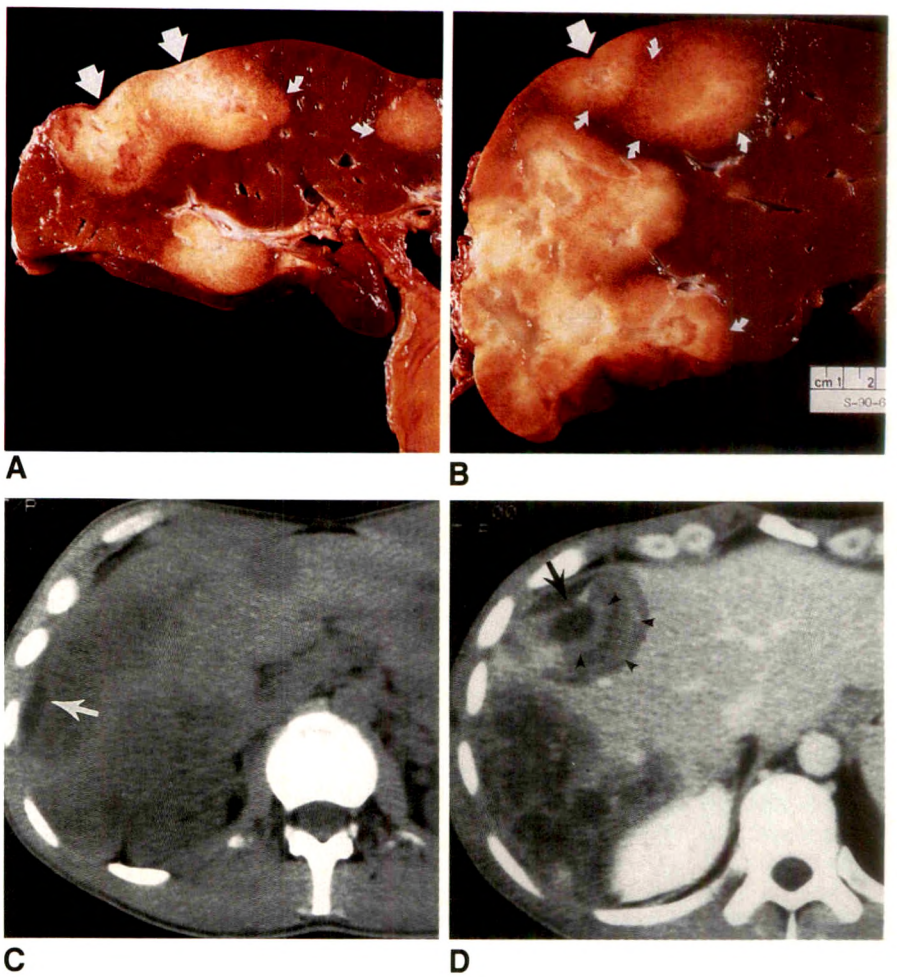


Fig. 2.—Epithelioid hemangioendothelioma of liver with coalescent tumor nodules and capsular retraction in a 29-year-old man.

***A* and *B*, Transverse (fresh cut) liver sections show peripheral distribution of confluent lesions and capsular retraction (*straight arrows*). Note also hyperemia of tumor nodule margins (*curved arrows*).**

***C*, Unenhanced CT scan at same level as *A* correlates well with liver specimen in showing peripheral confluent lesions with capsular retraction (*arrow*). A small amount of ascites is adjacent to capsular retraction.**

***D*, Enhanced CT scan at level similar to *B* correlates with liver specimen showing coalescent tumor nodules. One lesion shows capsular retraction (*arrow*) with adjacent ascites. Alternating zones of contrast enhancement (*arrowheads*) within medial segment of tumor are seen in pathologic specimen (*B*) as two confluent lesions with corresponding hyperemic zones.**

margins (periphery) showed increased cellularity with active proliferation of two cell types: dendritic and epithelioid. The epithelioid cells stained positive for factor VIII–related antigen in all 11 cases tested. At the margin of the nodules, tumor cells invaded the hepatic sinusoids, venules, and small portal vein branches, producing a narrow concentric avascular zone around the tumors.

CT

In all 13 patients, CT showed multiple liver lesions; more than 75% were peripheral and extended to the liver margin. Retraction of the liver capsule overlying tumor nodules was detected in nine patients (Figs. 1 and 2), but in less than 25% of the peripheral lesions. In no case did tumor cause a focal bulge in the liver contour. Compensatory hypertrophy of the uninvolved left lobe was seen in three patients.

Confluence of tumor nodules was seen in seven patients (Figs. 2 and 3). In all 13 patients, unenhanced CT scans showed the tumor nodules as areas of mostly homogeneous decreased attenuation compared with normal liver parenchyma. In two patients, the tumors contained calcifications (Fig. 4). Lesion conspicuity on unenhanced scans was better than or equal to that on enhanced scans in 10 of 13 cases, and the unenhanced scans were superior for showing the extent (size) of tumor involvement. In nine patients, CT with contrast material showed peripheral tumor enhancement surrounding central low attenuation. In seven of these patients, some lesions had a second, more peripheral hypodense rim that correlated with the thin avascular rim seen at pathologic examination (Figs. 1 and 2).

Sonography

Sonography showed intrahepatic lesions in eight of nine patients. Six of the eight patients had discrete, mostly peripheral, individual tumor nodules ranging in size from 2 to 4 cm. The other two patients had peripheral confluent tumor masses. The echogenicity of the tumors varied; six patients had hypoechoic masses (Fig. 3), one patient had hyperechoic masses, and one had both hypoechoic and isoechoic masses relative to liver. The hyperechoic and isoechoic masses had peripheral hypoechoic rims (Fig. 3). No correlation was found between echogenicity and the size of the tumors. The liver capsule directly overlying the tumor nodules was retracted or flattened in two patients.

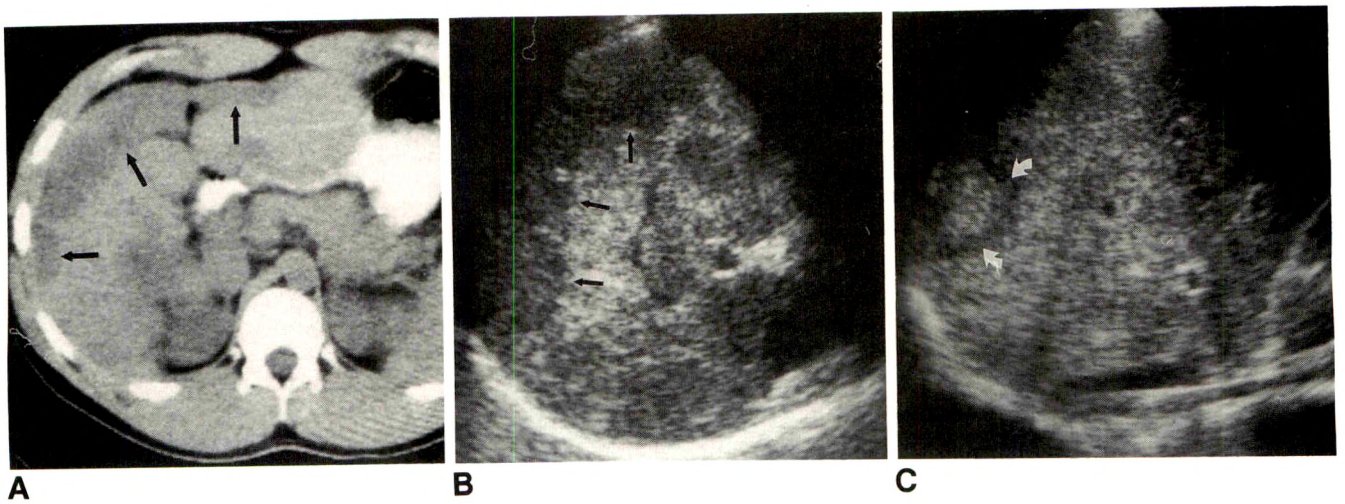


Fig. 3.—Hepatic epithelioid hemangioendothelioma with CT and sonographic correlation and different sonographic appearances in 25-year-old man.
***A*, Unenhanced CT scan shows coalescent peripheral tumor nodules (*arrows*).**
***B*, Transverse sonogram shows peripheral tumor is hypoechoic (*arrows*).**
***C*, Sagittal sonogram shows isoechoic tumor nodule with hypoechoic rim (*arrows*).**

MR Imaging

MR showed lesions in all six patients. As with CT and sonography, the lesions were multiple and located mostly in the liver periphery abutting the liver capsule. Capsular retraction or flattening, centered over the lesions, was detected in three patients.

The lesions had various signal characteristics on short TR/TE images. Three patients had low-intensity lesions, and two patients had low-intensity lesions centrally, with a thin peripheral dark rim. In one patient, the lesion had an isointense signal intensity in the center surrounded by a thin dark rim.

The long TR/TE images showed lesions of heterogeneously increased signal intensity in all six patients, five of whom also had masses with a thin peripheral dark rim (Fig. 1).

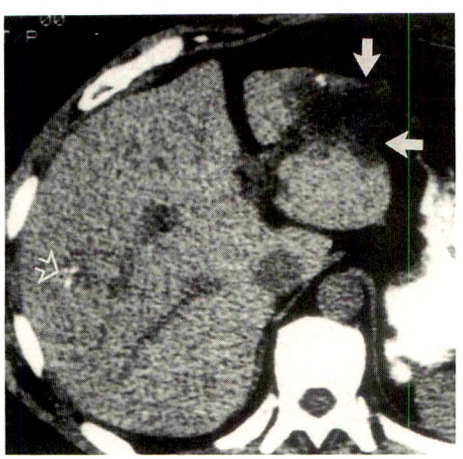


Fig. 4.—Epithelioid hemangioendothelioma of liver with tumoral calcifications and capsular retraction in a 58-year-old man. Unenhanced CT scan shows peripheral tumor nodule containing calcification and capsular retraction (*solid arrows*). Calcification is also seen in a more central liver lesion (*open arrow*).

On gadopentetate dimeglumine–enhanced short TR/TE spin-echo images, three patients had three concentric layers of alternating signal intensity. Similar to the findings on CT, lesions on MR had a hypointense central region surrounded by thick enhancement. The outer margin of the lesions showed a thin, nonenhancing hypointense rim (Fig. 1).

Discussion

The term *epithelioid hemangioendothelioma* was first coined by Weiss and Enzinger [1] in 1982 in a review of 41 patients who had similar soft-tissue tumors. The authors described a solid tumor of vascular origin that was primarily composed of epithelioid-appearing endothelial cells. Most of the tumors in their series had a clinical course between that of benign endothelial tumors (hemangiomas) and malignant angiosarcomas. Since their report, similar tumors have been detected in bone, liver, and lung [2–6]. The clinical course of hepatic EHE is identical to that of extrahepatic EHE; most patients survive 5–10 years after diagnosis [3].

EHE of the liver is usually found in young adults. The mean age of patients in this series was 39 years, and Radin et al. [8], in a review of the literature, reported a mean age of 45 years. Ishak et al. [3], in a series of 32 patients, reported that the clinical signs and symptoms and laboratory data of their patients were nonspecific. No risk factors or specific causes of hepatic EHE were identified. In several reports, cases were originally misdiagnosed as metastatic carcinoma, sclerosing hepatic carcinomas, and nonneoplastic disorders such as postnecrotic fibrosis or venoocclusive disease [3, 10, 11]. Because of the prolonged course and nonspecific clinical manifestations, the age of the patient at the time EHE is detected by biopsy or imaging studies may vary widely. More familiarity with the pathologic findings and better access to advanced imaging techniques may allow discovery of this tumor at earlier ages, as recent studies have shown [7, 8].

Furui et al. [7] and Radin et al. [8] reported on the imaging appearances of these lesions in two small series. The results of our series agree with their observations that on CT these lesions are mostly peripheral and of low attenuation, are most conspicuous on unenhanced scans, and occasionally have an enhancing peripheral rim and/or outer hyodense halo. Hypertrophy of unaffected liver regions is seen in advanced cases. Previous reports [7, 8] have shown sonographic appearances of EHE as hypodense with occasional foci of central increased echogenicity. In our series, we had similar findings; most of the lesions were hypoechoic.

The MR appearance of these tumors has been limited to one case described by Radin et al. [8]. In our series, the MR images had a distinctive appearance that in many ways correlated well with the CT appearance and the pathologic findings. The concentric alterations in signal intensity seen on short TR/TE, long TR/TE, and in particular on the contrast-enhanced spin-echo images appear to be consistent findings. Combined with the peripheral distribution and the proper clinical setting, these findings may suggest the diagnosis.

Although Furui et al. [7] described one case with "dimpling" of the margin of the liver, they concluded that these lesions generally do not alter the peritumoral hepatic contour. However, in our series, we found a much higher prevalence of liver capsular retraction centered over lesions (nine of 13 cases). This is an unusual feature of malignant lesions in the liver, as most large peripheral tumors cause a protrusion of the adjacent liver margin. Capsular retraction centered over a peripheral mass should thus be considered highly suggestive of EHE. However, lesions causing biliary obstruction can result in liver atrophy, which in some ways may simulate capsular retraction. Also, peripheral metastatic lesions treated with chemotherapy can cause an appearance similar to the retraction seen in EHE lesions, perhaps caused by a process of fibrosis similar to that seen in EHE. However, the mostly peripheral location of EHE lesions and the clinical history should allow differentiation of EHE from treated metastatic disease.

The radiologic findings seen in hepatic EHE correlate well with the pathologic findings. Macroscopically our patients with EHE had multiple, solid, firm nodules with a hyperemic periphery and dense fibrous center, similar to previously reported findings [3, 12]. Histologic findings showed that the tumor produces a fibrous myxoid stroma that is most dense in the center of the nodules, with increasing cellularity toward the periphery of the lesions. These findings account for their solid, firm consistency grossly and their hypovascular center. The actively proliferating, increased cellular periphery of the nodules accounts for the hyperemic outer portions seen on gross specimens. Tumor infiltration and occlusion of hepatic sinusoids and small vessels cause a narrow avascular zone between the tumor nodules and liver parenchyma. These findings correlate with the enhancement pattern on CT and MR, with the central portion of the nodules appearing hypodense and not enhancing to the same degree as the hyperemic periphery. The hyperemic periphery may not be hyperdense on CT; it may be isodense with normal liver parenchyma, and not detected. Thus, unenhanced CT often shows tumor conspicuity better and is more accurate in detecting tumor extent; this is in agreement with earlier reports [7, 8]. The outer, hypodense rim seen on CT and hypointense rim on MR correspond with the peripheral avascular zone, where vascular invasion is detected on pathologic examination. This may also be the reason for the halo appearance on sonography, although the peripheral hyperemic, cellular portions of the tumor may also contribute to the hypoechoic rim.

The capsular retraction or flattening seen on CT, sonography, and MR has been documented in the pathologic and surgical literature [3, 8, 12]. This retraction is most likely due to the tumor fibrous reaction, which distorts the tumor margin and adjacent liver capsule. The complete transverse imaging of CT and MR most likely explains why more cases of retraction were seen on CT and MR than on sonography. Retrospective review of sonograms also limited our ability to look for this finding, which may have been presented but not imaged.

With progression of this disease, the nodules often coalesce in the periphery of the liver. Because EHE replaces liver parenchyma slowly over years, compensatory enlargement of uninvolved portions of the liver can be seen [8, 10, 11]. This was seen in three of our patients, all of whom had extensive disease, and is a late finding in the course of the disease.

Calcification has occasionally been detected histologically, on abdominal radiographs [3], and on CT scans [7, 8]. Dense calcifications were detected on CT and sonography in two patients in our series, and is a less common finding.

REFERENCES

1. Weiss SW, Enzinger FM. Epithelioid hemangioendothelioma: a vascular tumor often mistaken for a carcinoma. *Cancer* **1982**;50:970–981
2. Dorfman HD, Tsuneyoshi M, Bauer T. Epithelioid hemangioendothelioma of bone (abstr). *Lab Invest* **1986**;45:17
3. Ishak WG, Sesterhenn IA, Goodman ZD, Rabin L, Stromeyer FW. Epithelioid hemangioendothelioma of the liver: a clinicopathological study of 32 cases. *Hum Pathol* **1984**;15:839–852
4. Dail D, Liebow A. Intravascular bronchioloalveolar tumor (abstr). *Am J Pathol* **1975**;78:6a–7a
5. Dail DH, Liebow AA, Gmelich JT, et al. Intravasular bronchiolar, and alveolar tumor of the lung (IVBAT): an analysis of twenty cases of a peculiar sclerosing endothelial tumor. *Cancer* **1983**;51:452–464
6. Weldon-Linne CM, Victor TA, Christ ML. Antigenic nature of "intravascular bronchioloalveolar tumor" (letter). *Arch Pathol Lab Med* **1981**;105:628
7. Furui S, Itai Y, Ohtomo K, et al. Hepatic epithelioid hemangioendothelioma: report of five cases. *Radiology* **1989**;171:63–68
8. Radin DR, Craig JR, Colletti PM, Ralls PW, Halls JM. Hepatic epithelioid hemangioendothelioma. *Radiology* **1988**;169:145–148
9. Lee KS, Rossleigh MS, Fernandes VB, Morris JG. Scintigraphic features of malignant epithelioid hemangioendothelioma. *Clin Nucl Med* **1989**; 14:501–503
10. Clements D, Hubscher S, West R, Elias E, Macmaster P. Epithelioid hemangioendothelioma of the liver: a case report. *J Hepatol* **1986**;2: 441–449
11. Eckstein RP, Ravich RMB. Epithelioid hemangioendothelioma of the liver: report of two cases histologically mimicking venoocclusive disease. *Pathology* **1986**;18:459–462
12. Iwatsuki S, Sheahan DG, Starzl TE. The changing face of hepatic resection. *Curr Probl Surg* **1989**;5:345–348

Gastric Leiomyosarcoma

David G. Disler[1] and Felix S. Chew

A 65-year-old man had a 3-day history of melena. CT showed a spherical 8-cm mass in the posterior wall of the gastric fundus with a small central ulceration, small flecks of calcification, and extensive regions of inhomogeneity (Fig. 1). The adjacent organs and structures, including the liver, omentum, and retroperitoneum, were uninvolved. Examination of the surgically resected specimen revealed a solid tumor with necrosis and hemorrhage. Microscopy showed whorled bundles of spindle cells with four mitotic figures per 50 high-power fields. The final pathologic diagnosis was low-grade malignant gastric stromal tumor (leiomyosarcoma).

Half of all gastrointestinal stromal tumors are gastric; approximately 80% of these are leiomyomas or leiomyosarcomas. Benign leiomyomas are common, and if small, are generally asymptomatic. Their malignant counterpart, leiomyosarcoma, is less common and accounts for only 1% of all malignant gastric neoplasms. The two may be difficult to distinguish from each other clinically and radiologically. Although both leiomyomas and leiomyosarcomas may present with ulcer, bleeding, pain, nausea and vomiting, weight loss, and palpable mass, signs and symptoms are more common in leiomyosarcomas. Also, leiomyosarcomas tend to be larger. Both grow submucosally in the gastric wall, leaving the luminal surface smooth. However, ulceration may be seen in up to 50% of cases; the ulcers tend to be small, even if the tumor itself is large [1, 2]. Foci of calcification are characteristic of both leiomyomas and leiomyosarcomas. Necrosis and hemorrhage are evident radiologically as an inhomogeneous appearance before and after contrast enhancement; these occur more commonly in malignant tumors [3]. Extragastric spread occurs with local extension and infiltration of contiguous structures, particularly the liver, omentum, and retroperitoneum, and with involvement of regional or distant lymph nodes. At presentation, extragastric spread is found in 50–67% of cases of leiomyosarcoma; CT is not reliable in detecting it [4]. Patients with leiomyosarcomas that are 8 cm or larger are more likely to have disseminated disease, and consequently they have a shorter mean survival time (15.5 months) than do patients with tumors that are smaller than 8 cm (83 months) [1]. The treatment is surgical, but because these lesions are asymptomatic until late in the clinical course, fewer than half are resectable.

REFERENCES

1. Berk JE, Haubrich WS, Kalser MH, Roth JL, Schaffner F, eds. *Bockus gastroenterology*, 4th ed. Philadelphia: Saunders **1985**:1273–1274
2. Mitros FA. *Atlas of gastrointestinal pathology*. New York: Gower Medical, **1988**;ch. 4:19–20
3. Megibow AJ, Balthazar EJ, Hulnick DH, Naidich DP, Bosniak MA. CT evaluation of gastrointestinal leiomyomas and leiomyosarcomas. *AJR* **1985**;144:727–731
4. Andaker L, Morales O, Hojer H, Backstrand B, Borch K, Larsson J. Evaluation of preoperative computed tomography in gastric malignancy. *Surgery* **1991**;109:132–135

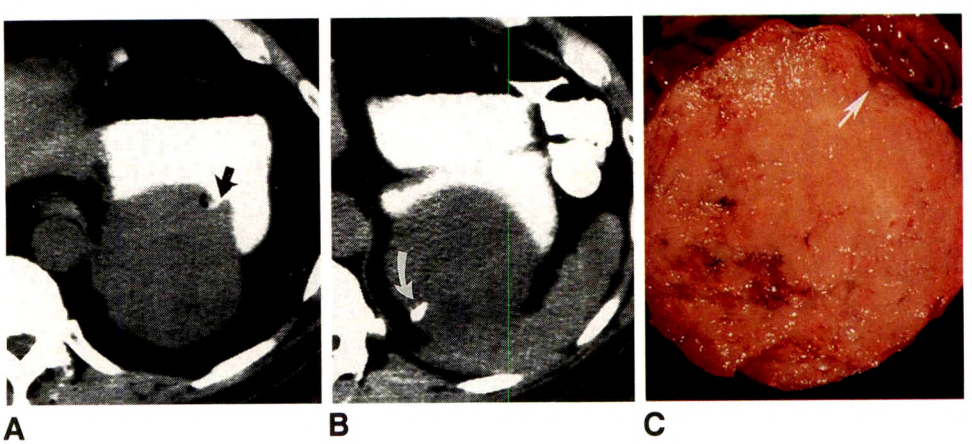


Fig. 1.—Gastric leiomyosarcoma.
***A* and *B*, Axial CT scans show exophytic mass straddling posterior gastric wall with a small central ulceration (*straight arrow*) and a focus of calcification (*curved arrow*). Lesion is heterogeneous in attenuation.**
***C*, Cut gross specimen shows a small ulceration (*arrow*) and regions of hemorrhage and necrosis. Mucosa is intact everywhere but at ulceration.**

From the weekly radiologic-pathologic correlation conferences conducted by Jack Wittenberg. Pathology editor: Andrew E. Rosenberg. Radiology editors: Felix S. Chew, William E. Palmer, Daniel P. Barboriak, Daniel I. Rosenthal.

[1] Both authors: Department of Radiology, Massachusetts General Hospital and Harvard Medical School, 32 Fruit St., Boston, MA 02114. Address reprint requests to F. S. Chew.

Case Report

Hereditary Hemorrhagic Telangiectasia: Findings in the Liver with Color Doppler Sonography

Philip W. Ralls,[1] Meade B. Johnson, D. Randall Radin, Kevin P. Lee, and William D. Boswell

Hereditary hemorrhagic telangiectasia (HHT), also known as Osler-Weber-Rendu disease, is a condition with autosomal dominant inheritance that occurs in all races with an estimated frequency of 1–2:100,000 [1]. It is characterized by telangiectases, arteriovenous fistulas, and aneurysms. The skin and mucosa, as well as blood vessels of the lung, liver, and CNS, may be involved [1, 2]. Although the angiographic abnormalities of the liver in HHT are well known [3–6], description of sonographic findings [3, 7–9] is limited. Doppler sonographic findings have been described in only one patient [10]. To our knowledge, this is the first report describing hepatic color Doppler sonographic findings in three patients with HHT.

Case Reports

Case 1

A 73-year-old man with known long-standing HHT presented with syncope, congestive heart failure, and a hematocrit of 0.14. Sonography showed that the celiac trunk and common, proper, and intrahepatic hepatic arteries were markedly enlarged. Color Doppler sonography revealed two large arteriovenous malformations, one in the right lobe (Fig. 1A) and one in the left. CT revealed enlarged arteries, but showed the arteriovenous fistulas less well than did the color Doppler sonogram (Fig. 1B). The patient's heart failure was attributed to both anemia and the large hepatic arteriovenous fistulas.

Case 2

Abdominal sonography of a 45-year-old woman at another hospital showed anechoic structures ventral to the portal veins; a diagnosis of Caroli's disease was suggested. At our facility, color and spectral Doppler sonography revealed enlarged arteries, consistent with HHT. Several tangled masses of vessels were detected and thought to represent tortuous enlarged arteries rather than large arteriovenous fistulas (Fig. 2). No arteriovenous fistulas were imaged.

Discussion

The major pathologic features of HHT are mucocutaneous and visceral vascular abnormalities: (1) telangiectases, dilated channels lined by a single layer of endothelium attached to a continuous basement membrane that originates from capillaries and postcapillary venules [1]; (2) arteriovenous fistulas, which occur mainly in the liver (30% of all patients), lungs (15–20%), and CNS (<10%); and (3) aneurysms that may involve any size vessel [1, 2]. Virtually all small vessels (arterioles, capillaries, and venules) may be dilated and intercommunicate extensively. Telangiectases of the lips, tongue, and fingertips (60–70% of patients) often suggest the diagnosis. Epistaxis (78%) and gastrointestinal bleeding (44%) [2] occur despite normal hemostatic factors.

Hepatic disease in HHT may be primary or related to complications of therapy [1, 2]. Increased blood flow through arteriovenous fistulas may cause hepatomegaly, pain in the right upper quadrant of the abdomen, or a pulsatile liver. Left-to-right shunting through liver fistulas may lead to high-output cardiac failure [1, 11]. Rarely, hepatic artery to portal vein shunts may lead to portal hypertension, with bleeding gastrointestinal varices and encephalopathy. Fibrovascular his-

Received November 5, 1991; accepted after revision January 7, 1992.

[1] All authors: Department of Radiology, University of Southern California School of Medicine and the Los Angeles County–USC Medical Center, 1200 N. State St., Box 631, Los Angeles, CA 90033. Address reprint requests to P. W. Ralls.

AJR **159:59–61, July 1992** 0361–803X/92/1591–0059 © American Roentgen Ray Society

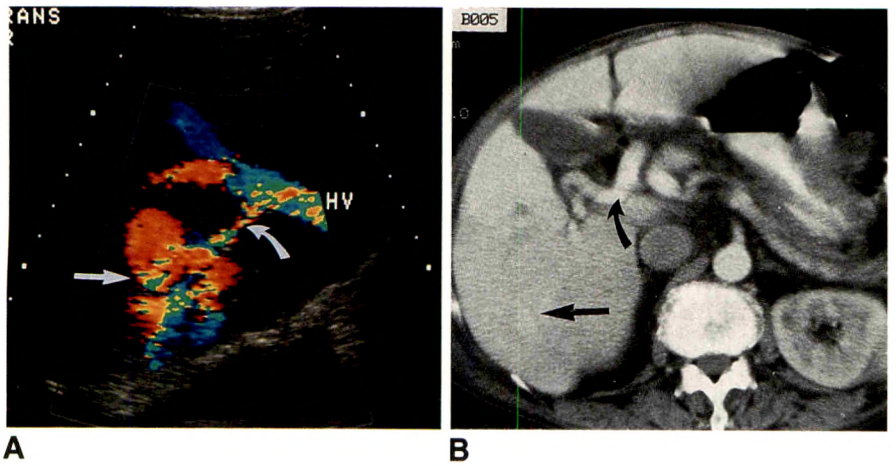


Fig. 1.—73-year-old man with hereditary hemorrhagic telangiectasia.

A, Transverse color Doppler sonogram through right lobe of liver shows large arteriovenous fistula (*straight arrow*) that exhibits complex flow. Draining hepatic vein (*curved arrow*) shows rapid, aliased flow. This was the only patient in whom large fistulas were noted.

B, CT scan obtained after mechanical injection of bolus of contrast medium shows fistula (*straight arrow*), although not as well as it was shown by color Doppler sonography. Note enlarged hepatic artery (*curved arrow*), which is another feature of hereditary hemorrhagic telangiectasia.

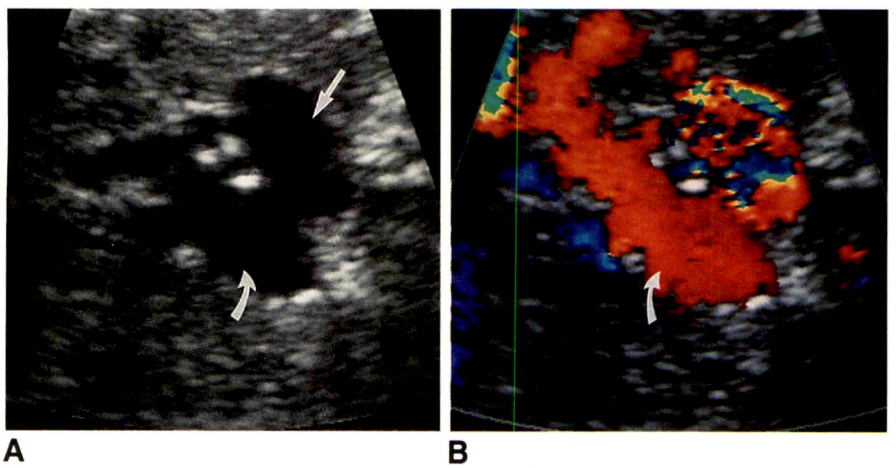


Fig. 2.—45-year-old woman with hereditary hemorrhagic telangiectasia.

A, Transverse sonogram near right portal vein (*curved arrow*) shows ventral anechoic structure (*straight arrow*), which was initially thought to be a dilated bile duct.

B, Transverse color Doppler sonogram shows this structure is a tangled mass of enlarged arteries. *Curved arrow* shows right portal vein.

tologic changes occur in the liver, but it is debatable whether these lead to cirrhosis or other clinically significant disease [2].

Secondary hepatic complications may be caused by hormonal therapy or by frequent blood transfusions. Hormonal therapy may cause peliosis hepatis, hepatic adenoma, or even hepatocellular carcinoma. Transfusion necessitated by hemorrhage may lead to hepatitis or iron deposition–related cirrhosis.

Reasons for performing liver sonography in patients with known HHT include jaundice, abdominal pain, hepatomegaly, to evaluate cirrhosis and its complications (portal hypertension and tumor), and to confirm the presence of suspected arteriovenous fistulas. As mucocutaneous telangiectases may be absent or few [12], HHT may be unsuspected before sonography, as in one of our patients.

In patients with HHT, sonography may reveal enlargement of the main hepatic and intrahepatic arteries. Increased echogenicity from fatty infiltration [8] and abnormal liver echogenicity from cirrhosis may occur. Complications of cirrhosis (collateral vessels, neoplasm) also might be encountered. To our knowledge, sonographic findings in HHT-related cirrhosis have not been described.

In addition to the two cases described, HHT was diagnosed in a 49-year-old woman with upper gastrointestinal bleeding. Color Doppler sonography revealed enlarged, tortuous arteries with high-velocity, aliased flow in both intra- and extrahepatic arteries in all three cases. Color Doppler sonography prevented confusion arising from the gray-scale appearance, which may mimic biliary dilatation. This problem occurred initially in two of three patients. Large hepatic arteriovenous fistulas were imaged in only one patient. Visualization of fistulas probably depends on their size. Tangled arterial masses related to the enlarged arteries, as occurred in one patient, may be difficult to differentiate from arteriovenous fistulas. Careful color Doppler tracing or spectral analysis of feeding arteries and draining veins should facilitate distinction. Spectral analysis should reveal arterial signal only in enlarged arteries, while arteriovenous fistulas should exhibit a spectrally broadened, mixed arterial and venous, high-amplitude pattern. We have examined several patients with HHT without liver involvement; all had normal findings on color Doppler sonograms of the liver.

Familiarity with color Doppler sonographic findings should make diagnosis of HHT straightforward in most cases. The markedly enlarged hepatic arteries in HHT are easily distin-

guishable from the prominent, corkscrew arteries sometimes imaged by color Doppler sonography in patients with cirrhosis [13]. On occasion, vascular liver tumors may cause arterial enlargement; we have seen this in focal nodular hyperplasia and hepatocellular carcinoma [14]. Conceivably, enlarged arteries might result with vasculitis, arteriovenous fistulas from any cause, or diffuse arterial abnormalities like Takayasu's disease. We suspect that the sonographic findings and clinical history would virtually always allow easy differentiation of HHT from these conditions.

Hepatic color Doppler sonography might prove useful in other related situations, such as in defining the extent of disease before therapeutic embolization [3] or in evaluating the results of therapy, possibly obviating repeat angiography. In children of HHT patients, color Doppler sonography might aid in the diagnosis so that appropriate genetic counseling could be planned. Liver biopsy guided by color Doppler sonography may be useful to avoid puncturing dilated arteries.

REFERENCES

1. Peery WH. Clinical spectrum of hereditary hemorrhagic telangiectasis (Osler-Weber-Rendu Disease). *Am J Med* **1987**;82:989–997
2. Reilly PJ, Nostrant TT. Clinical manifestations of hereditary hemorrhagic telangiectasis. *Am J Gastroenterol* **1984**;79:363–367
3. Bourgeois N, Delcour C, Deviere J, et al. Osler-Weber-Rendu disease associated with hepatic involvement and high output heart failure. *J Clin Gastroenterol* **1990**;12:236–238
4. Campbell EW, Jewson D, Gilbert E. Angiographic identification of enteric lesions. *Arch Intern Med* **1970**;125:705–707
5. Halpern M, Turner AF, Citron BP. Angiodysplasias of the abdominal viscera associated with hereditary hemorrhagic telangiectasia. *Radiology* **1967**; 102:783–789
6. Thomas ML, Carty H. Hereditary hemorrhagic telangiectasia of the liver demonstrated angiographically. *Acta Radiol* **1974**;15:433–438
7. Goes R, VanTussenbroeck F, Cattenie F, et al. Osler's disease diagnosed by ultrasound. *JCU* **1987**;15:129–131
8. Cloogman HM, DiCapo RD. Hereditary hemorrhagic telangiectasia: sonographic findings in the liver. *Radiology* **1984**;150:521–522
9. Danchin N, Thisse JY, Newmann JL, et al. Osler-Weber-Rendu disease with multiple intrahepatic arteriovenous fistulas. *Am Heart J* **1983**; 105:856–859
10. Vilgrain V, Menu Y, Nahum H. Doppler sonography in Osler-Weber-Rendu disease. *AJR* **1991**;157:413–414
11. Burckhardt D, St. Alder GA, Ludin H, et al. Arteriovenous fistulae lead to hyperdynamic circulation and heart failure. *Am Heart J* **1973**;85:797–800
12. Vase P, Grove O. Gastrointestinal lesions in hereditary hemorrhagic telangiectasia. *Gastroenterology* **1986**;91:1079–1083
13. Ralls PW. Color Doppler sonography of the hepatic artery and portal venous system. *AJR* **1990**;155:517–525
14. Ralls PW, Johnson MB, Lee KP, et al. Color Doppler sonography in hepatocellular carcinoma. *Am J Physiol Imaging* **1991**;6:57–61

AJR

AMERICAN JOURNAL OF ROENTGENOLOGY

MELVIN M. FIGLEY FELLOWSHIPS IN RADIOLOGY JOURNALISM 1993

The American Roentgen Ray Society announces four one-month fellowships in radiology journalism in the La Jolla editorial office of the *AJR*. Board-certified radiologists with special academic promise are invited to apply.

PURPOSE

The purpose of the fellowship is (1) to stimulate bright young radiologists to continue with an academic career, to accelerate their progress, and to stimulate their interest in good radiology journalism and (2) to improve the quality of radiology journals by teaching the fundamentals of medical journalism to academicians, training manuscript reviewers and future editors, and providing core teachers of medical journalism in radiology departments around the country.

CURRICULUM

Through hands-on experience in the editorial office, the fellows will be taught the fundamentals of medical writing, manuscript preparation, peer review, manuscript editing, the ethics of scientific journalism, and journal publication and printing in personal tutorials given by the *AJR* editors and editorial staff. They will visit the ARRS Publication office and Waverly Press in Maryland to observe the publication and printing process.

STIPEND

The successful candidates will each be awarded $10,000, which includes the cost of travel to La Jolla and Maryland, living expenses for the month, and an honorarium.

APPLICATIONS

Candidates should apply in writing to Robert N. Berk, M.D., Editor-in-Chief, *AJR* Editorial Office, 2223 Avenida de la Playa, Suite 103, La Jolla, CA 92037. Applications from senior candidates are welcome. The letter must include a curriculum vitae and a description of the candidate's goals during the fellowship. Letters of recommendation from his or her department chairman and one other senior person are required. Deadline for receipt of applications is Sept. 1, 1992. The successful candidates will be notified Oct. 1, 1992.

Case Report

Langerhans Cell Histiocytosis of the Liver: Imaging Findings

D. Randall Radin[1]

The term *Langerhans cell histiocytosis* refers to proliferation of a unique histiocyte, the Langerhans cell [1, 2]. According to the Writing Group of the Histiocyte Society [1], this term replaces the terms histiocytosis X, eosinophilic granuloma, Hand-Schüller-Christian disease, and Letterer-Siwe disease. Clinical manifestations of Langerhans cell histiocytosis are varied and depend on the sites and extent of involvement. Common sites of involvement include bone marrow, lung, skin, liver, spleen, and lymph nodes. More than 90% of patients with disseminated disease are less than 21 years old [2]. Sonographic, CT, and MR findings in an adult with Langerhans cell histiocytosis of the liver constitute the subject of this report.

Case Report

A 48-year-old woman had weakness, 7-kg weight loss, and intermittent abdominal pain, nausea, and diarrhea. Treatment for hypothyroidism was begun 6 weeks earlier. Serum level of bilirubin was elevated at 3.4 mg/dl (58 μmol/l; normal, 0.1–1.2 mg/dl [2–20 μmol/l]) and serum level of alkaline phosphatase was elevated at 1074 U/l (normal, 20–90 U/l). Sonography showed a large irregular area of increased echogenicity centrally within the liver (Fig. 1A) and a 3-cm round, well-circumscribed, homogeneous, hyperechoic lesion with enhanced through-transmission posteriorly in the right lobe.

Unenhanced CT showed a large irregular hypoattenuating lesion centrally in the liver (Fig. 1B); attenuation of the lesion was as low as −14 H. Several small hypoattenuating lesions were seen superiorly and posteriorly in the right lobe. A large, mostly isoattenuating, exophytic mass extended medially from the inferior aspect of the right lobe. A similar exophytic mass extended posteriorly from the lateral segment of the left lobe.

The hypoattenuating hepatic masses were moderately hyperintense on T1-weighted MR images (Fig. 1C) but only slightly hyperintense on T2-weighted images (Fig. 1D). The isoattenuating, exophytic right-sided hepatic mass was slightly hyperintense on T1-weighted images (Fig. 1E) and isointense on T2-weighted images. Although vessels were seen coursing through the masses, evidence of mass effect was present (Fig. 1C). A 3-cm mass located posteriorly in the right lobe of the liver, corresponding to the lesion shown by sonography, was hypointense on T1-weighted images and hyperintense on T2-weighted images (Figs. 1C and 1D).

Open liver biopsy was performed. Several hours after surgery, hypotension, hypernatremia, and obtundation developed. MR imaging of the brain showed an enhancing 8-mm mass in the tuber cinereum. Results of endocrinologic evaluation indicated a diagnosis of panhypopituitarism including diabetes insipidus. Information obtained at that time indicated that the patient had had polyuria and polydipsia for 2 years.

The results of a wedge biopsy of the liver were consistent with Langerhans cell histiocytosis. Hormonal replacement therapy was begun. Sonography of the liver 8 months after the first examination showed no change in the large, irregular, hyperechoic hepatic lesion.

Discussion

In the present case and two previous cases [3, 4] of Langerhans cell histiocytosis involving the liver in adults, sonography showed hyperechoic irregular and nodular lesions. In the present case and three previous cases [2–4], CT showed hypoattenuating irregular and nodular lesions. Attenuation of the lesions was consistent with fat in two cases. In the present case, the MR finding of hyperintense hepatic lesions on T1-weighted images, with lower signal

Received November 12, 1991; accepted after revision December 30, 1991.

[1] Department of Radiology, University of Southern California School of Medicine, Los Angeles County–USC Medical Center, 1200 N. State St., Los Angeles, CA 90033-1084.

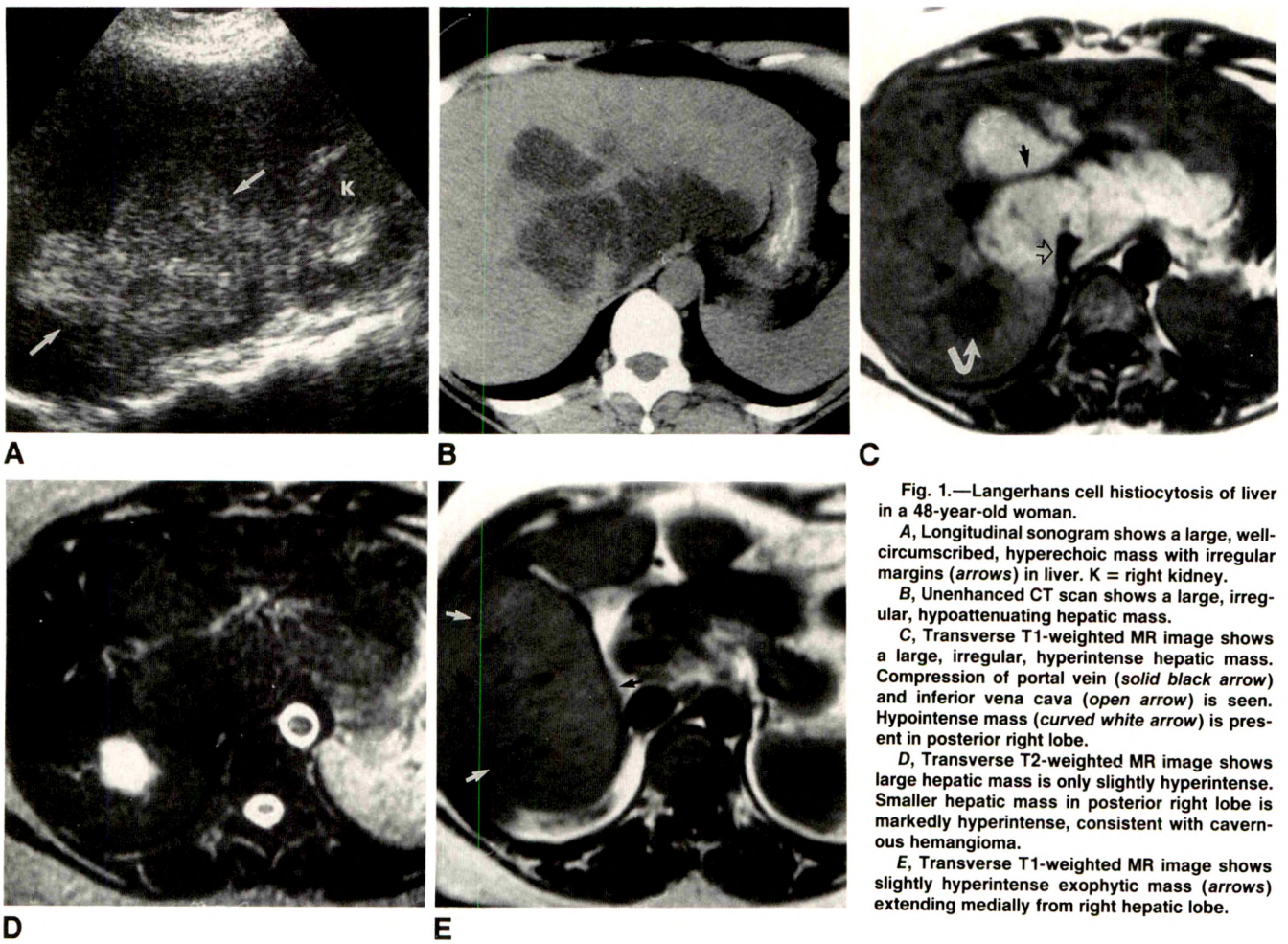


Fig. 1.—Langerhans cell histiocytosis of liver in a 48-year-old woman.

***A*, Longitudinal sonogram shows a large, well-circumscribed, hyperechoic mass with irregular margins (*arrows*) in liver. K = right kidney.**

***B*, Unenhanced CT scan shows a large, irregular, hypoattenuating hepatic mass.**

***C*, Transverse T1-weighted MR image shows a large, irregular, hyperintense hepatic mass. Compression of portal vein (*solid black arrow*) and inferior vena cava (*open arrow*) is seen. Hypointense mass (*curved white arrow*) is present in posterior right lobe.**

***D*, Transverse T2-weighted MR image shows large hepatic mass is only slightly hyperintense. Smaller hepatic mass in posterior right lobe is markedly hyperintense, consistent with cavernous hemangioma.**

***E*, Transverse T1-weighted MR image shows slightly hyperintense exophytic mass (*arrows*) extending medially from right hepatic lobe.**

intensity on T2-weighted images, also was consistent with fatty infiltration. However, the degree of mass effect in this case would be exceptional for focal fatty change. Hepatic masses that may have sonographic, CT, and MR findings consistent with fat include lipomas, angiomyolipomas, liver cell adenomas, myelolipomas, and hepatocellular carcinomas with fatty metamorphosis [5]. In addition, some small (<5 cm) hepatocellular carcinomas may be hyperintense on T1-weighted MR images because of accumulation of copper or copper-binding protein [6, 7]. However, these masses are hyperattenuating on unenhanced CT images [7]. The radiologic appearance of hepatic lesions in Langerhans cell histiocytosis is due to the lipid-rich nature of these distinctive histiocytes [2, 3].

Hepatic involvement is associated with a high mortality rate in patients with Langerhans cell histiocytosis [2]. Although this proliferation of cells is not thought to be a malignant neoplasm [1], reversal of hepatomegaly and improvement of hepatic function after chemotherapy have been reported [2, 4]. Spontaneous resolution of hepatomegaly and of multiple hypoattenuating hepatic lesions shown by CT also has been reported [2].

In conclusion, when sonography, CT, or MR imaging shows irregular or nodular hepatic lesions with features consistent with focal fatty infiltration or fat-containing tumor, the diagnosis of Langerhans cell histiocytosis should be considered, especially in the presence of typical cutaneous, osseous, or pulmonary lesions or evidence of diabetes insipidus or pituitary insufficiency.

REFERENCES

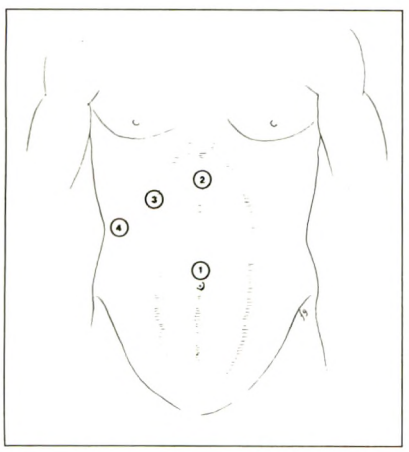
1. Chu T, D'Angio GJ, Favara B, Ladisch S, Nesbit M, Pritchard J. Histiocytosis syndromes in children. *Lancet* **1987**;1:208–209
2. Trochtenberg DS, Dessypris EN. Reversible hepatomegaly and diabetes mellitus in an adult with disseminated histiocytosis X. *Am J Med Sci* **1990**;299:179–184
3. Päivänsalo M, Mäkäräinen H. Liver lesions in histiocytosis X: findings on sonography and computed tomography. *Br J Radiol* **1986**;59:1123–1125
4. Iwai M, Kashiwadani M, Okuno T, Takino T, Koshikawa T. Cholestatic liver disease in a 20-year-old woman with histiocytosis X. *Am J Gastroenterol* **1988**;83:164–168
5. Yoshikawa J, Matsui O, Takashima T, et al. Fatty metamorphosis in hepatocellular carcinoma: radiologic features in 10 cases. *AJR* **1988**;151:717–720
6. Ebara M, Watanabe S, Kita K, et al. MR imaging of small hepatocellular carcinoma: effect of intratumoral copper content on signal intensity. *Radiology* **1991**;180:617–621
7. Kitagawa K, Matsui O, Kadoya M, et al. Hepatocellular carcinomas with excessive copper accumulation: CT and MR findings. *Radiology* **1991**;180:623–628

Pictorial Essay

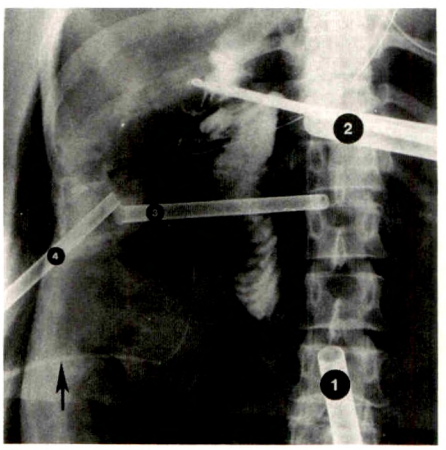
Operative Cholangiography in Patients Undergoing Laparoscopic Cholecystectomy: Unique Radiographic Findings

Suppiah Balachandran,[1] Philip Goodman,[1] Rami Saydjari,[2] Mark W. Hogge,[1] and Morton H. Leonard, Jr.[1]

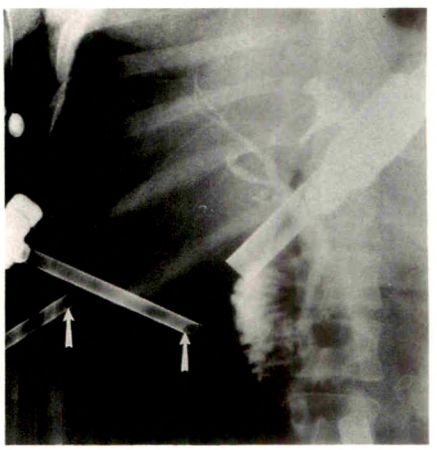
Laparoscopic cholecystectomy is a recent surgical innovation in which a cholecystectomy is performed through four ports in the anterior abdominal wall under direct vision via a laparoscope. Unlike conventional cholecystectomy, no abdominal incision is



1



2



3

Fig. 1.—Four abdominal ports are created during laparoscopic cholecystectomy. Port 1 is created for passage of the laparoscope. Final removal of the gallbladder also occurs through this port. Cannulas in remaining ports admit various surgical instruments for dissection, irrigation, and cholangiography.

Fig. 2.—Cholangiogram shows hardware used during laparoscopic cholecystectomy. All four plastic disposable cannulas have flush ends. Cannulas 1 and 2 are 10 mm in diameter and allow entry of laparoscope and surgical instruments, respectively. A metal clamp overlies cholangiographic catheter, which enters through port 2, upper midline port. Laparoscope that was inserted through lower midline umbilical port was withdrawn before film exposure. Cannulas 3 and 4 enter through lateral (subcostal) ports, are 5 mm in diameter, and are mainly intended for grasping and retracting gallbladder during dissection. A nasogastric tube is used in all cases to deflate stomach, which would otherwise obstruct operative field. Cholangiographic catheter usually is inserted into abdomen through Intracath sheath placed beside lower lateral cannula (*arrow*). Surgical instrument constantly present in operative field is cholangiographic clamp that is inserted through port 2. Jaws of clamp placed over cystic duct secure cholangiographic catheter and prevent leakage of contrast material.

Fig. 3.—Cholangiogram shows beveled metal cannulas (*arrows*) used during laparoscopic cholecystectomy. They are similar in size and have function identical to plastic cannulas. Use of metal rather than plastic cannulas is a personal preference of surgeon. Larger 10-mm plastic cannulas through ports 1 and 2 are also seen.

Received December 9, 1991; accepted February 5, 1992.
[1] Department of Radiology, University of Texas Medical Branch, 301 University Blvd., Galveston, TX 77550. Address reprint requests to S. Balachandran.
[2] Department of Surgery, University of Texas Medical Branch, Galveston, TX 77550.

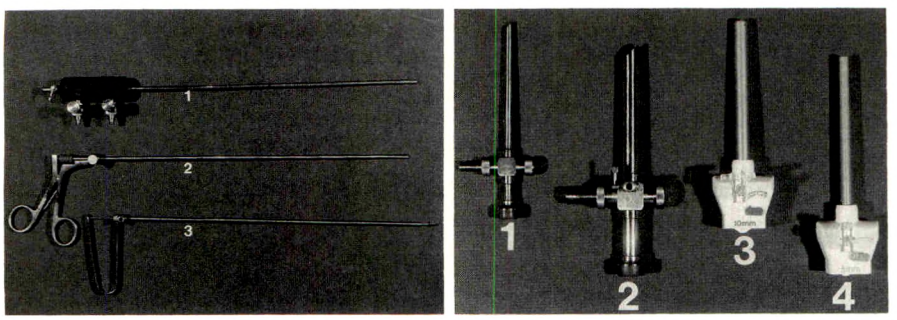
AJR **159:65–67, July 1992** 0361–803X/92/1591-0065 © American Roentgen Ray Society

made, the abdomen is distended with large amounts of carbon dioxide, and cholangiography is performed *before* the gallbladder is removed. These differences lead to several findings on operative cholangiograms that are not seen on cholangiograms obtained in patients undergoing conventional cholecystectomy. In patients having the laparoscopic procedure, the extensive pneumoperitoneum causes the falciform ligament and the gallbladder to be visible on operative cholangiograms. Subcutaneous emphysema can be seen on the cholangiogram if carbon dioxide leaks into the abdominal wall via the abdominal ports. Also, the instruments used in the laparoscopic procedure are visible on the cholangiograms because they must remain in the field when the radiographs are made.

The purpose of this essay is to illustrate these unique findings seen on operative cholangiograms obtained during laparoscopic cholecystectomy. Recognition of these differences is important to avoid mistaken impressions that abnormalities exist.

Operative Procedure

Laparoscopic cholecystectomy is performed in the operating room with the patient under general anesthesia [1]. After carbon dioxide is insufflated in the abdomen to create pneumoperitoneum, four puncture wounds (ports) are made in the anterior abdominal wall with trocars (Fig. 1). The first trocar is introduced supraumbilically. The remaining trocars are introduced under direct visualization by using the laparoscope. The trocars are withdrawn, and the cannulas are left in the abdominal ports to allow passage of instruments and the laparoscope (Figs. 2–5). Blunt dissection is used to find and isolate the cystic duct and cystic artery. The cystic artery is ligated with surgical clips and divided. The cystic duct is then partially transected by using microscissors. A 12-gauge sheath-over-needle catheter is introduced into the abdomen lateral to the second subcostal cannula under direct visualization. A cholangiogram catheter is introduced into the abdomen through this sheath. The catheter is grasped and directed into the opening in the cystic duct. A self-retaining clamp is used to hold the catheter in place, and cholangiograms are obtained. All other instruments are removed from the abdomen when the cholangiograms are obtained. After the radiographs are exposed, the catheter is withdrawn. The cystic duct is then ligated proximal and distal to the opening and divided by using microscissors. Electrocautery and blunt dissection are used to dissect the gallbladder from the liver.



A B

Fig. 4.—Photographs of hardware used in laparoscopic cholecystectomy. *A*, 1 = irrigator, 2 = atraumatic grasping forceps, 3 = cholangiographic clamp. *B*, 1 and 2 = metal cannulas, 3 and 4 = plastic cannulas.

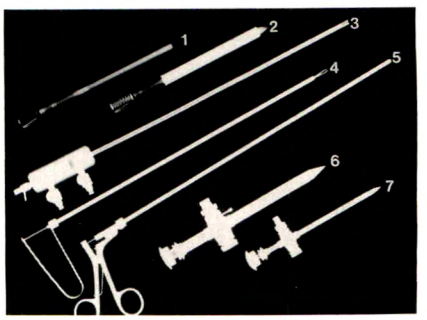
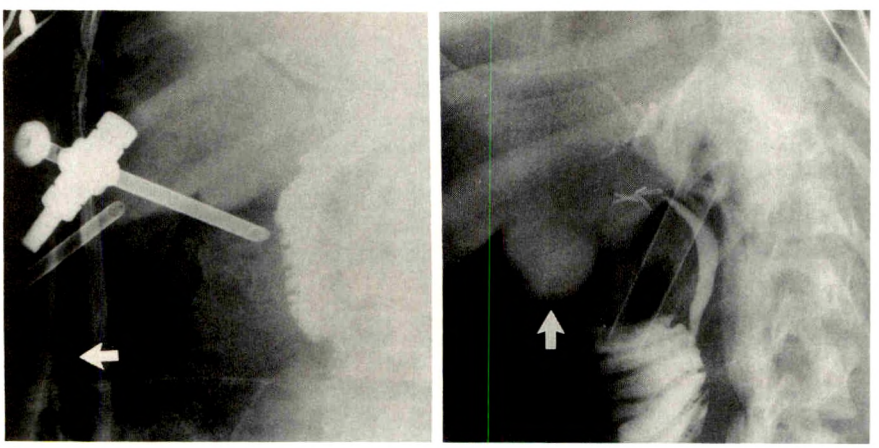


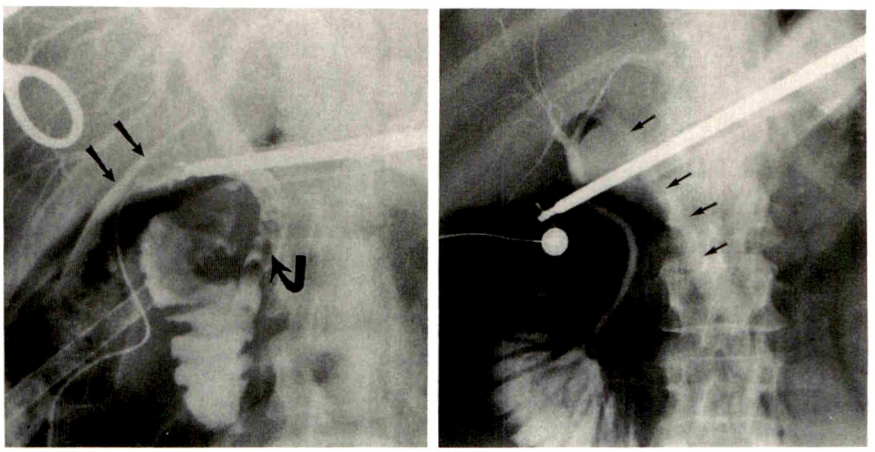
Fig. 5.—Radiograph of hardware used in laparoscopic cholecystectomy: 1 and 2 = trocars with plastic cannulas, 3 = irrigator, 4 = cholangiographic clamp, 5 = atraumatic grasping forceps, 6 and 7 = trocars with metal cannulas.



6 7

Fig. 6.—Subcutaneous emphysema. Cholangiogram obtained during laparoscopic cholecystectomy shows leakage of carbon dioxide at port, resulting in subcutaneous emphysema (*arrow*). This feature is unique to laparoscopic cholecystectomy and is not seen on cholangiograms obtained during open cholecystectomy. All four cannulas in their abdominal ports are visible. Cholangiogram catheter within its sheath is seen below arrow.

Fig. 7.—Cholangiogram obtained during laparoscopic cholecystectomy shows gallbladder as pear-shaped structure (*arrow*) with density of soft tissue. Contrast is provided by surrounding intense, artificial pneumoperitoneum. This feature is not readily appreciated on a cholangiogram during open cholecystectomy because pneumoperitoneum is naturally occurring, open, and less intense. Three plastic cannulas in their abdominal ports are visible. Cholangiogram catheter enters cystic duct.



8 9

Fig. 8.—Extravasation of contrast material. Cholangiogram obtained during laparoscopic cholecystectomy shows collection of extravasated contrast material in subhepatic space (*straight arrows*). Stones are seen in common bile duct (*curved arrow*). These features may also be seen on cholangiograms obtained during open cholecystectomy. Cholangiographic clamp is seen entering cannula in port 2. Two other cannulas are present, one each in ports 3 and 4.

Fig. 9.—Pneumoperitoneum. Cholangiogram obtained during laparoscopic cholecystectomy shows falciform ligament (*arrows*), which is easily visible because surrounding contained pneumoperitoneum is artificially introduced, and maintained throughout operative procedure by continuous flow of carbon dioxide. As pneumoperitoneum is open, naturally occurring, and not very intense, intraabdominal structures such as falciform ligament are not readily appreciated on cholangiograms obtained during open cholecystectomy. Cholangiographic clamp is seen entering cannula in port 2.

The gallbladder is usually removed intact via the supraumbilical port under direct vision. Bile and small gallstones in the gallbladder may be removed by suction to reduce the size of large or distended gallbladders before they are withdrawn through the abdominal port. The abdomen is irrigated with normal saline. The instruments and cannulas are removed, and the wounds are closed.

Discussion

Cholangiograms obtained during laparoscopic cholecystectomy have several features that are not commonly seen on cholangiograms obtained during an open cholecystectomy. These include unusual displays of pneumoperitoneum and subcutaneous emphysema (Fig. 6) and visualization of the unresected gallbladder (Fig. 7) and of unique hardware that must remain in the operative field during the film exposure. Findings seen on cholangiograms obtained during both types of procedures include extravasated contrast material (Fig. 8) and filling defects in the common bile duct.

The falciform ligament (Fig. 9) is frequently visible because of the large amount of carbon dioxide in the abdomen [2]. Because the pelvis is not included on intraoperative laparoscopic cholangiograms, the urachus [3] is not seen. Intraoperative laparoscopic cholangiograms help the surgeon correctly identify the common bile duct or its anatomic variations so that injury to the duct can be avoided or minimized [4]. On the basis of the cholangiographic findings, the surgeon may elect to proceed with the laparoscopic cholecystectomy, complete the laparoscopic cholecystectomy and later attempt endoscopic retrograde retrieval of stones through the common bile duct, or convert the laparoscopic cholecystectomy to an open cholecystectomy.

REFERENCES

1. Gradacz TR, Talamini MA. Traditional versus laparoscopic cholecystectomy. *Am J Surg* **1991**;161:336–338
2. Han SY. Variation in falciform ligament with pneumoperitoneum. *J Can Assoc Radiol* **1980**;31:171–173
3. Jelaso DV, Schultz EH Jr. The urachus: an aid to diagnosis of pneumoperitoneum. *Radiology* **1969**;92:295–296
4. Berci G. Sackier JM, Paz-Partlow M. Routine or selected intraoperative cholangiography during laparoscopic cholecystectomy? *Am J Surg* **1991**;161:355–360

Book Review

Ultrasound of Appendicitis and Its Differential Diagnosis. By Julien B. C. M. Puylaert. New York: Springer-Verlag, 118 pp., 1990. $59

Sonography of the bowel has not yet attained the diagnostic level of sonography of other parts of the gastrointestinal tract, primarily because air in the bowel limits the quality of the results. Puylaert, the author of *Ultrasound of Appendicitis and Its Differential Diagnosis*, has come up with a solution to this problem of air in the bowel, and he describes his methods in this excellent text. What Puylaert has perfected is a graded-compression technique that reduces the distance between the transducer and the bowel and also allows the use of high-frequency transducers; all of this serves to eliminate or reduce artifacts caused by air in the bowel, thereby resulting in a better quality study. What makes Puylaert's work significant is that it can help reduce both the morbidity rate and the number of unnecessary operations performed for appendicitis. Diagnosing appendicitis on the basis of sonographic findings can also help in achieving more expedient surgery when surgery is necessary.

Although the author has written numerous papers on this subject and related topics, this is the first time all the information has been presented together in one volume. The book is divided into seven chapters. It starts with an introduction and a review of the literature. It then covers examination techniques, normal anatomy of the right lower abdomen on sonography, the diagnosis of appendicitis on the basis of sonographic findings, differential diagnosis, and indications and clinical impact of the work. Puylaert also describes other imaging techniques that could be used in the diagnosis of appendicitis (e.g., plain film, barium enema, and CT) and even discusses percutaneous drainage for the nonsurgical management of appendiceal abscesses. Puylaert's research and methods have so far been confirmed by other authors, thus giving his work validity.

The text is clearly written and contains illustrations of good quality. Its value also comes from the fact that no other book has been written specifically on this topic, although other books have made brief mention of papers on this topic.

The book is useful not only to those radiologists who perform sonography of the acute abdomen but also to others in training and in practice. They will find it helps them comprehend the potential applications of sonography in patients with clinically suspected appendicitis. Because it has a generous clinical discussion on appendicitis, I also recommend this book to other physicians who deal with disorders of the right lower quadrant. All in all, Puylaert has written an excellent book on this subject.

Richard E. Rosenthal
Cooper Hospital/University Medical Center
Camden NJ 08103

Pictorial Essay

Mucocele of the Appendix: Imaging Findings

David Madwed,[1] R. Mindelzun, and R. B. Jeffrey, Jr.

Mucocele of the appendix, a cystic mass resulting from a dilated appendiceal lumen caused by abnormal accumulation of mucus, is a rare entity that often is not considered when problems of the right lower quadrant are assessed. Preoperative recognition of mucocele of the appendix is important because of the possibility of rupture at surgery with development of pseudomyxoma peritonei and to predict malignant transformation. The appearances of mucoceles of the appendix on sonography, CT, and barium studies are illustrated.

Mucocele of the appendix, a descriptive term that implies a dilated appendiceal lumen caused by abnormal accumulation of mucus, is a rare clinical entity; the reported prevalence in appendectomy specimens at surgery is 0.2–0.3% [1]. A correct preoperative diagnosis is rarely made on the basis of clinical examination or findings on conventional radiographs. Accurate diagnosis is essential in order to prevent rupture at surgery with development of pseudomyxoma peritonei and to predict malignant transformation. The advent of advanced imaging techniques, particularly CT and sonography, has been invaluable in the diagnosis of mucocele of the appendix. This report details the wide spectrum of findings of mucocele of the appendix on sonography, CT, and barium studies.

General Imaging Features

Mass Lesion

The typical imaging finding of an appendiceal mucocele is a cystic mass in the expected region of the appendix. Plain abdominal radiographs may show mass effect on the adjacent bowel or bladder. Sonography shows an oblong, heterogeneous cystic mass containing mucin that is both liquid and gelatinous and viscous (Fig. 1). The degree of internal echogenicity is related to the number of acoustic interfaces provided by the mucin [2]. Excellent through-transmission and posterior enhancement are usually present. The mass is well encapsulated unless rupture has occurred. The primary sonographic differentiation from uncomplicated acute appendicitis is the lack of appendiceal wall thickening of more than 6 mm. This distinguishing feature produces a characteristic target lesion, with an echogenic submucosal layer sandwiched by an edematous inner hypoechoic lamina propria–muscularis mucosa and outer hypoechoic muscular layer.

On CT, a low-attenuation, well-encapsulated mass with smooth regular walls is seen in the right lower quadrant (Fig. 2). Again the degree of attenuation depends on the amount of mucin in the mass. Adjacent bowel is displaced by the mass, but no periappendiceal inflammation or abscess is seen, key differential points in excluding acute appendicitis. It should be mentioned that an optimal CT examination depends on adequate opacification of the terminal ileum and cecum. Repeat examination with additional oral contrast material as well as thin sections may be necessary to delineate or exclude appendiceal disease. For instance, Figure 3 shows a right lower quadrant cystic mass that was thought to be an appendiceal mucocele but was surgically proved to be a fluid-filled terminal ileum loop. Repeat examination with additional contrast material would have been helpful in this case.

Barium examination shows an extrinsic impression on the cecum, terminal ileum, or sigmoid colon (Fig. 4). A classic

Received December 9, 1991; accepted after revision February 4, 1992.
[1] All authors: Department of Diagnostic Radiology, Stanford University Hospital, Stanford, CA 94305.

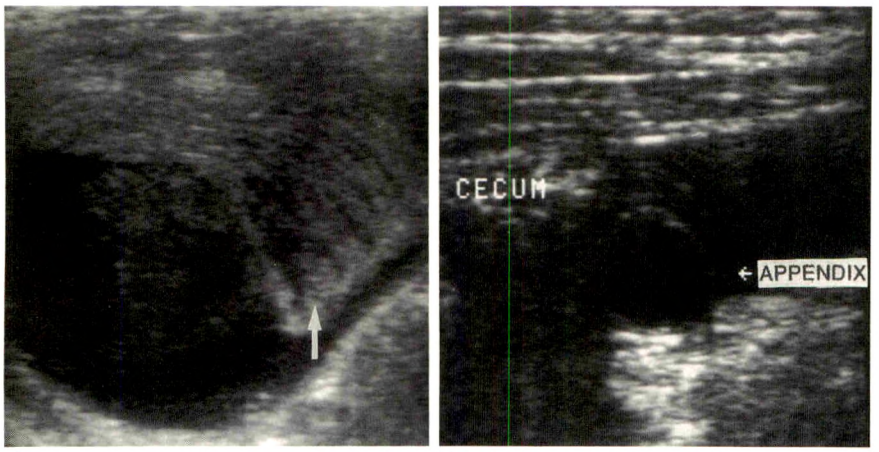


Fig. 1.—Transverse sonograms of right lower quadrant of a 55-year-old woman (*A*) and a 64-year-old man (*B*) show differences in mucocele appearance based on nature of cyst fluid. Heterogeneous echogenic mass in *A* is due to gelatinous and viscous composition of mucus (*arrow*), whereas anechoic cystic mass with enhanced through-transmission in *B* (appendix) is due to homogeneous liquid composition.

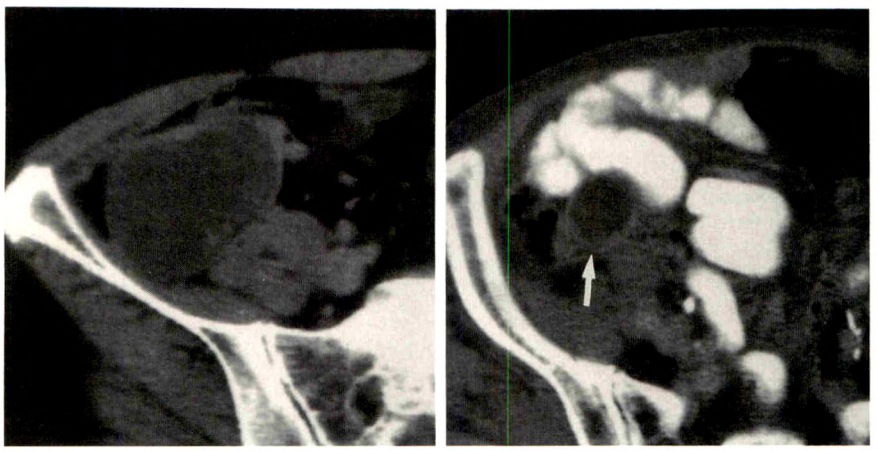


Fig. 2.—Abdominal CT scan of a 63-year-old woman with right lower quadrant pain shows typical appearance of appendiceal mucocele. Note well-encapsulated cystic mass and associated mass effect without surrounding inflammation. Lack of wall calcification broadens differential diagnosis, which would include abscess, old hematoma, pancreatic pseudocyst, and ovarian cyst.

Fig. 3.—Abdominal CT scan of a 49-year-old man with right lower quadrant pain shows well-encapsulated cystic mass (*arrow*) in expected region of appendix. Differential diagnosis would include mucocele, abscess, and normal fluid-filled terminal ileum loop. The patient was operated on for unrelated reasons, and the mass turned out to be a dilated but unobstructed loop of ileum. Repeat examination through this region with additional oral contrast material would have been helpful.

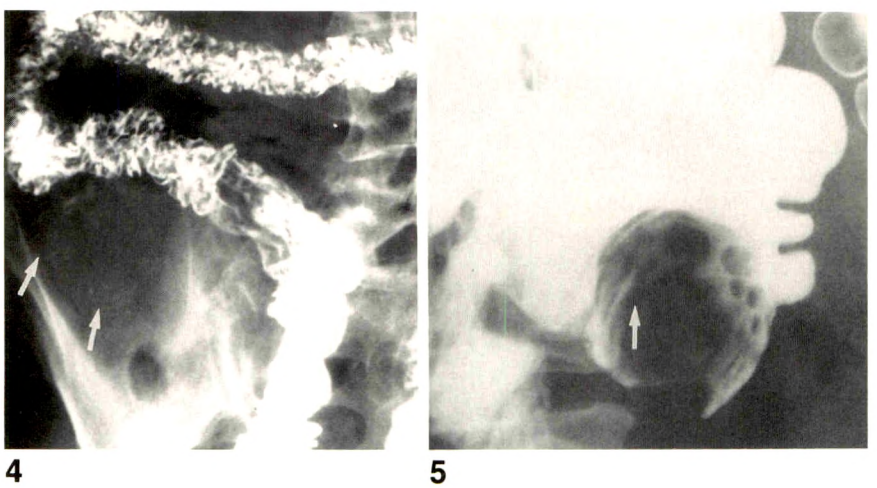


Fig. 4.—Postevacuation film from barium enema of a 58-year-old man shows calcified right lower quadrant mass with displacement of surrounding bowel, two key findings of appendiceal mucocele. The most important finding, subtle calcific spheres (*arrows*) within cavity lumen, is classic for myxoglobulosis.

Fig. 5.—Barium enema from a 69-year-old woman shows filling defect in region of cecum with classic vortical fold pattern representing radiating cecal folds (*arrow*) toward appendiceal lumen. Differential diagnosis includes any appendiceal mass lesion; for example, mucocele, carcinoid, carcinoma, and appendiceal abscess.

appearance is the "vortical fold" pattern described by Vorhaus; this represents a concentric ring appearance of the cecal mucosal folds directed toward the obstructed appendiceal orifice [1] (Fig. 5).

Calcification

The presence of curvilinear or punctate wall calcification in a right lower quadrant cystic lesion strongly suggests the

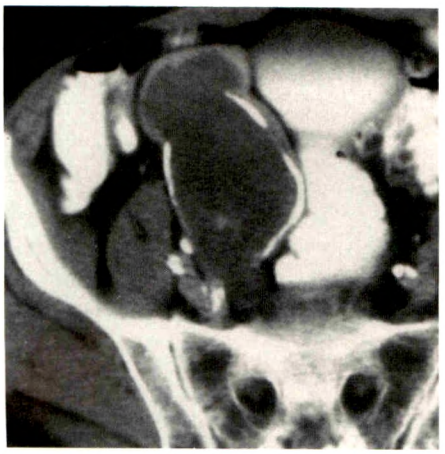


Fig. 6.—Abdominal CT scan of a 52-year-old man shows classic findings of appendiceal mucocele: well-encapsulated cystic mass in right lower quadrant, mass effect without surrounding inflammation, and curvilinear wall calcification.

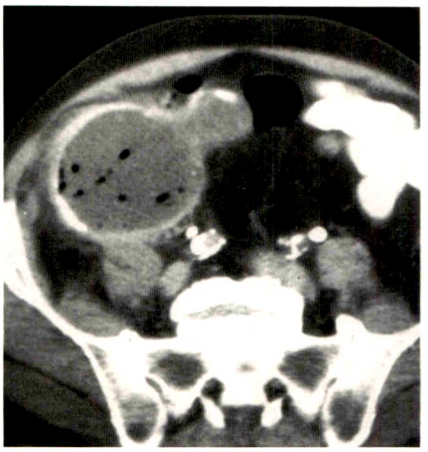


Fig. 7.—Abdominal CT scan of a 53-year-old woman shows a cystic well-encapsulated mass with intraluminal gas that proved to be an infected mucocele. Lack of surrounding inflammation and presence of curvilinear wall calcification would be unusual for abscess.

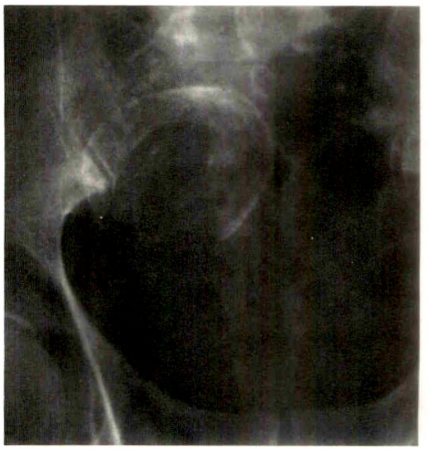


Fig. 8.—Plain film of abdomen of a 59-year-old man shows eggshell calcification of a porcelain appendix. Differential diagnosis would include hematoma and aneurysm.

diagnosis of mucocele of the appendix. This may be seen on plain films but is best appreciated on CT scans (Fig. 6). Furthermore, the presence of wall calcification in a right lower quadrant cystic mass with intraluminal gas allows one to differentiate an infected mucocele from an abdominal abscess cavity (Fig. 7). Sonography shows a highly echogenic wall with distal shadowing. The calcification is due to a dystrophic response to a chronic inflammatory process incited by the mucus in the appendiceal wall. This can ultimately lead to a "porcelain" appendix [1] (Fig. 8).

Myxoglobulosis

Myxoglobulosis, a variant of mucocele seen in 0.35–8.0% of cases, is characterized by an appendix filled with "translucent globules" or a cluster of "frog eggs" [1]. When these spheres calcify, they become evident on plain films, sonograms, and CT scans (Fig. 4). They may shift in the appendix with changes in body position. It has been hypothesized that the spheres represent a derivative of granulation tissue found in the wall of the mucocele that eventually breaks off, undergoes necrosis, and subsequently calcifies [1].

Intussusception

Intussusception of a mucocele of the appendix is extremely uncommon, with fewer than 30 reported cases in the literature. The appendiceal mass acts as the intussusceptum, providing the classic appearance of an enteroenteric intussusception. Barium studies show the classic "coiled spring" appearance, and CT shows a collapsed proximal segment ringed by a rim of mesenteric fat lying within the distal lumen (Fig. 9).

Pseudomyxoma Peritonei

Pseudomyxoma peritonei is characterized by implants of mucinous epithelium on the peritoneal surfaces and mucus accumulation within the peritoneal cavity. The pathophysiology of this process is a matter of controversy. Some have considered it a foreign-body peritonitis with a fibrotic response caused by spillage of mucus into the peritoneum. However, more recent studies [1, 2] indicate that pseudomyxoma occurs only in the presence of a malignant mucocele.

CT shows low-attenuation ascites with scalloping of the liver contour, corresponding to the peritoneal implants (Fig. 10). In addition, implants can be seen on serosal surfaces and as nidi within cavities reached by the usual routes of intraperitoneal flow dynamics (Fig. 10). These nodules may also

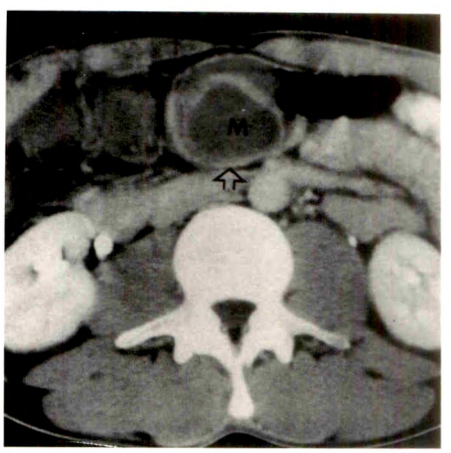
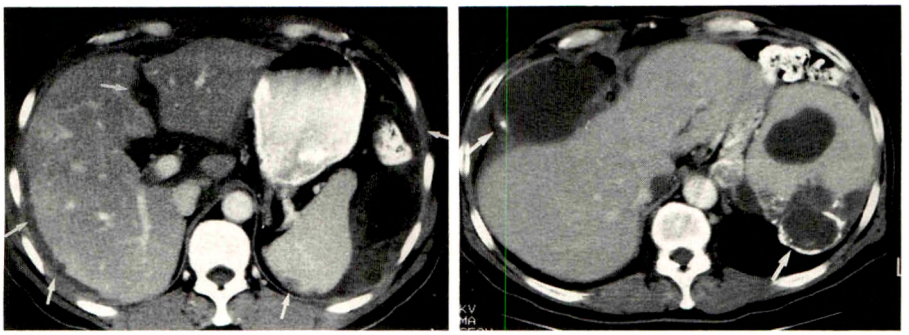


Fig. 9.—Abdominal CT scan shows enteroenteric intussusception caused by mucocele of appendix, with intussuscipiens (*arrow*) and central low-attenuation mass (M) representing mucocele, which acts as intussusceptum.



A B

Fig. 10.—Abdominal CT scans in two different patients show characteristic findings of pseudomyxoma peritonei.

A, 51-year-old man. Low-attenuation ascites and nodular contour (*arrows*) to hepatic and splenic capsules, ligamentum teres, and peritoneal cavity are compatible with serosal implants. Metastatic ovarian carcinoma can also have this appearance.

B, 44-year-old man. CT scan shows calcification (*arrow*) of serosal implants.



Fig. 11.—Abdominal CT scan of a 52-year-old woman. Low-attenuation cystic mass in right lower quadrant with wall nodularity and internal septations (*arrows*) was found to be an appendiceal cystadenocarcinoma at surgery. Although no reliable imaging findings are distinctive for malignant mucoceles, the presence of wall nodularity should raise the possibility of neoplasia.

calcify, usually in a rimlike fashion (Fig. 10). Adhesions and intestinal obstruction are the most frequent complications of this condition.

Mucinous Cystadenocarcinoma and Cystadenoma

It was once thought that the majority of mucoceles were the result of postinflammatory obstruction or other benign causes such as a fecalith followed by distal accumulation of mucus. More recent evidence [3, 4] from pathologic examinations suggests that mucosal atypia or neoplasia is the basis for mucocele formation. Currently, mucoceles of the appendix can be divided into three major categories: (1) retention mucocele with normal appendiceal mucosa, (2) cystadenoma mucocele with neoplastic epithelium similar to that seen in villous adenomas and adenomatous polyps of the colon, and (3) cystadenocarcinoma mucocele with neoplastic epithelium similar to that seen in adenocarcinomas of the colon. No unique imaging characteristics distinguish these groups other than the finding that cystadenomas and cystadenocarcinomas often are larger than retention mucoceles and spread to peritoneal surfaces more readily than do simple retention mucoceles (Fig. 11).

When pseudomyxoma peritonei is found in the setting of cystadenocarcinoma of the appendix, the prognosis is poor with a 20% 5-year survival rate [1]. Preoperative diagnosis is extremely helpful to the operating surgeon, for careful mobilization and resection without peritoneal contamination is essential for optimal results.

REFERENCES

1. Dachman A, Lichtenstein J, Friedman A. Mucocele of the appendix and pseudomyxoma peritonei. *AJR* **1985**;144:923–929
2. Gibbs M. Mucinous cystadenoma and cystadenocarcinoma of the vermiform appendix with particular reference to mucocele and pseudomyxoma peritonei. *J Clin Pathol* **1973**;26:413–421
3. Horgan J, Chow P, Richter J, Rosenfield A, Taylor K. CT and sonography in the recognition of mucocele of the appendix. *AJR* **1984**;143:959–962
4. Wolff M, Ahmed N. Epithelial neoplasms of the vermiform appendix. *Cancer* **1976**;37:2511–2521

Case Report

Bowel Ischemia and Perforation After Cocaine Use

Carmen Endress,[1] Denise G. K. Gray, and Gertraud Wollschlaeger

Bowel ischemia related to cocaine use is frequently overlooked in patients who come to the emergency department because of acute abdomen. Cocaine-induced abnormalities resemble other acute abdominal conditions. We describe two cases of bowel ischemia and perforation that occurred in patients who smoked crack cocaine.

Case Reports

Case 1

A 30-year-old woman was admitted because of pain in the lower abdomen localized to the right lower quadrant. The pain was crampy and associated with bloody diarrhea. The abdomen was diffusely tender with involuntary muscle rigidity. No fever or hypotension were found. She used cocaine regularly and had smoked crack cocaine heavily approximately 24 hr before the onset of the symptoms. Acute appendicitis or pelvic inflammatory disease was the suspected diagnosis. Findings on sonography of the pelvis were normal. However, abdominal sonography showed marked thickening of the walls of the large bowel from the transverse colon to the cecum (Figs. 1A and 1B). No peristalsis was observed. Peritoneal fluid was seen surrounding the abnormal walls of the colon. CT confirmed the sonographic findings (Fig. 1C).

Gastrografin enema performed to exclude perforation showed marked edema and lack of distensibility of the colon from the splenic flexure to the cecum (Fig. 1D). No perforation was detected. Two days later, colonoscopy and biopsy were performed. The colonoscopy showed marked submucosal edema and hemorrhages in the transverse and ascending colon. Biopsy of the ascending colon showed ulcerations and necrosis. The patient was treated symptomatically with IV fluids, pain medications, and suctioning via a nasogastric tube. The pain disappeared after 5 days. The patient was discharged with no medications and was to have follow-up in the gastrointestinal clinic.

Case 2

A 28-year-old man had abdominal pain in the right lower quadrant. This pain had developed 1 week earlier after he got "high smoking crack" cocaine. He remembered that at the time he had passed out for approximately 30 min. When he woke up, he felt severe abdominal pain. He continued to smoke cocaine on a daily basis, but the abdominal pain persisted. He had been smoking cocaine daily or every other day for 4 years.

On admission, the patient had a temperature of 39°C and tenderness in the right lower quadrant of the abdomen. He was admitted with the diagnosis of acute appendicitis. A single-contrast barium enema showed a mass in the right lower quadrant with deformity and displacement of the ileum and sigmoid colon. The appendix was not visualized (Fig. 2A). CT showed a large pelvic abscess (Fig. 2B). Surgery was performed with drainage of a pelvic abscess, small-bowel resection, and appendectomy. The pathologic examination of the resected specimen showed areas of hemorrhage and ulceration. The ileum had an area of perforation with part of the wall incorporated into the abscess. The periappendiceal serosa was inflamed, but the appendiceal mucosa was normal. The patient had no complications after surgery and was discharged 1 week later. One year later, he had recovered completely.

Discussion

Case reports of bowel ischemia after cocaine use have been published sporadically [1–5], but in our society, where cocaine abuse is increasing, this diagnosis deserves strong

Received November 27, 1991; accepted after revision January 22, 1992.

[1] All authors: Department of Radiology, Detroit Receiving Hospital, Wayne State University, 4201 St. Antoine, 3L-8, Detroit, MI 48201. Address reprint requests to C. Endress.

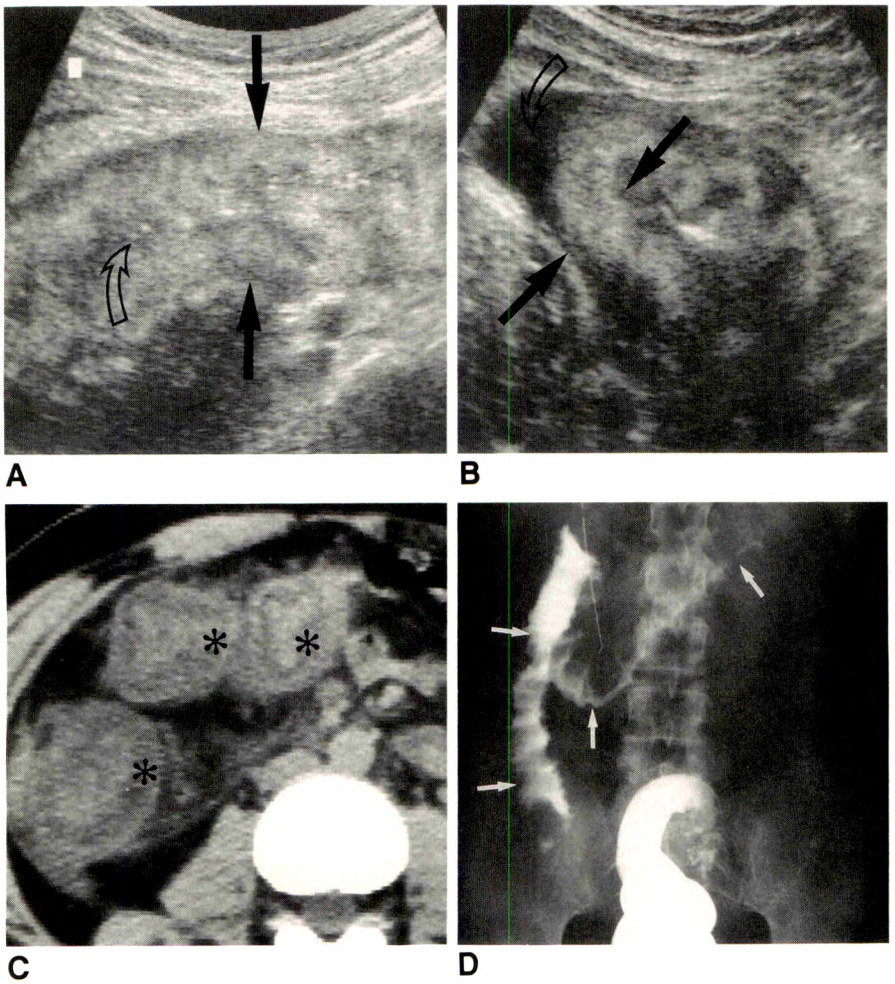


Fig. 1.—Bowel ischemia in a 30-year-old cocaine user.

***A*, Transverse sonogram of upper abdomen shows marked thickening of walls of transverse colon (*straight arrows*) and luminal narrowing (*curved arrow*) due to ischemia associated with increased accumulation of submucosal fluid.**

***B*, Sonogram through right lower quadrant of abdomen shows thickened cecal walls (*straight arrows*) and free fluid along superior aspect of right paracolic gutter (*curved arrow*).**

***C*, Mid abdominal CT scan shows marked submucosal edema (*asterisks*); attenuation values of colonic wall are close to values for water density.**

***D*, Radiograph after Gastrografin enema shows scalloped contours (*arrows*) of colonic walls from splenic flexure to cecum. Partially evacuated colon is due to colonic irritability.**

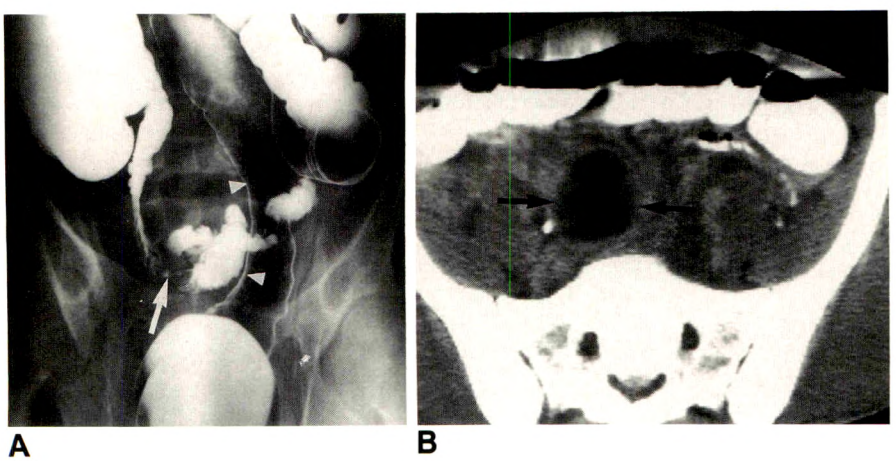


Fig. 2.—28-year-old chronic cocaine user with abdominal pain.

***A*, Radiograph after barium enema shows that sigmoid colon is displaced by a pelvic mass (*arrowheads*). Barium from ileum has extravasated into abscess cavity (*straight arrow*).**

***B*, CT scan at mid pelvic level shows a fluid-filled cavity with enhancing thick walls (*arrows*), which proved to be a large pelvic abscess.**

emphasis, especially in the major urban cities of the United States.

Cocaine produces severe vasoconstriction of the splanchnic circulation, leading to ischemia and possible infarction. Investigators [6, 7] have suggested that cocaine blocks the reuptake of released norepinephrine by the α-adrenergic receptors, abundantly found in the ileum and colon. This interrupts the termination of the catecholamine effect, thereby potentiating vasoconstriction and decreasing blood flow. Severe and prolonged ischemic episodes may eventually result in bowel necrosis, perforation, peritonitis, or abscess formation.

The pathologic effects of cocaine on the bowel include the following: petechial or focal hemorrhage, mucosal edema,

ulcerations, serosanguinous peritoneal fluid, necrosis, and perforation.

Our data and the experience of others indicate that patients are usually young adults with a history of long-term cocaine abuse. However, older patients may be affected, especially those who use cocaine sporadically. All our patients admitted that they had smoked cocaine just before the sudden development of crampy abdominal pain and bloody diarrhea.

The patients with bowel ischemia and perforation after cocaine use had no history of predisposing factors that make other causes of thrombosis or bowel ischemia likely. The ischemic effect of cocaine in the bowel may be transitory. One of our patients improved with conservative medical treatment. This finding indicates that cocaine-induced ischemic effects in the bowel are variable and could be reversible. The other patient had persistent pain and leukocytosis indicative of progressive ischemic effects, followed by necrosis, perforation, and abscess formation.

Initial plain radiographs of the abdomen show normal findings or a nonobstructive pattern of ileus [8]. CT and sonography are excellent imaging procedures for the assessment of abnormal thickening of the bowel wall, serosanguinous fluid around the thickened ischemic bowel, and perforation with abscess.

A recent appraisal [9] of the pathogenesis of ischemic injury points out that the initial event is an increase in mucosal permeability. This is followed by lifting of the mucosa and increased accumulation of fluid in the submucosa as shown on CT scans and sonograms in our patients (Figs. 1A and 1B). Bowel infarction related to the local effects of ingested cocaine when the ingested packets burst within the intestine has been reported [1]. The manifestation of intestinal ischemia with infarction can result from inhaled, ingested, or injected cocaine.

ACKNOWLEDGMENTS

We gratefully express our appreciation to our secretary, Janice Palonis.

REFERENCES

1. Nalbandian H, Sheth N, Dietrich R, Georgiou J. Intestinal ischemia caused by cocaine ingestion: report of two cases. *Surgery* **1985**;97:374–376
2. Riggs D, Weibley RE. Acute toxicity from oral ingestion of crack cocaine: a report of four cases. *Pediatr Emerg Care* **1990**;6:24–26
3. Yang RD, Han MW, McCarthy JW. Ischemic colitis in a crack abuser. *Dig Dis Sci* **1991**;36:238–240
4. Telsey AM, Merrit TA, Dixon SD. Cocaine exposure in a term neonate: necrotizing enterocolitis as a complication. *Clin Pediatr* **1988**;27:547–550
5. Gherardi R, Marc B, Alberti X, et al. A cocaine body packer with normal abdominal plain radiographs: value of drug detection in urine and contrast study of the bowel. *Am J Forensic Med Pathol* **1990**;11:154–157
6. Texter EC Jr, Chou CC, Merrill SL, Laureta HC, Frohlich ED. Direct effects of vasoactive agents on segmental resistance of the mesenteric and portal circulation. *J Lab Clin Med* **1964**;64:624–633
7. Gilman AG, Rall TW, Nies AS, Taylor P. *The pharmacological basis of therapeutics*, 8th ed. New York: Pergamon, **1990**:319–320
8. Beerman R, Nunez D Jr, Wetli CV. Radiographic evaluation of the cocaine smuggler. *Gastrointest Radiol* **1986**;11:351–354
9. Haglund U, Bulkley GB, Granger DN. On the pathophysiology of intestinal ischemic injury. *Acta Clin Scand* **1987**;152:321–324

Book Review

The Cystic Kidney. Edited by Kenneth J. Gardner, Jr., and Jay Bernstein. Boston: Kluwer, 444 pp., 1990. $145

In recent years, renal cysts and renal cystic diseases have been studied in depth by investigators from a wide range of disciplines, using sophisticated, evolving technologies. Studies of the structural and ultrastructural anatomy of the cells that make up the walls and basement membranes of cysts have clarified and criticized the earlier hypothesis that cysts form simply as a result of obstruction of nephrons. Animal models of renal cystic diseases have made possible in vivo investigation of the influence of chemical and humoral factors on cyst development. Murine metanephric organ cultures and cyst epithelial cell cultures have provided in vitro models in which cyst development and growth can be observed and examined. Molecular pathology of the inherited renal cystic diseases has been clarified in gene mapping studies that used recombinant DNA technology.

This book reviews, in a thoroughly documented and carefully organized way, what is currently known and what is currently under study about the diseases in which renal cysts are manifest. It consists of 17 chapters divided into four sections. The first two sections deal with cysts as structures, not as parts of diseases, and examine the fundamental nature of cysts. Newly evolved hypotheses of cyst genesis are proposed and examined. This is followed by a section that describes renal cystic diseases as they are dealt with by clinical disciplines. Chapters cover classification, radiologic findings, systemic manifestations, management of patients, and ethical problems. The final section presents renal cystic diseases in the traditional way, as disease entities. Chapters on each of the major diseases review prevalence, pathology, natural history, clinical manifestations, and complications.

The book is well written and edited to make it not just accessible but also interesting reading, even for someone who is not fluent in the lingo of some of the component disciplines. It is an example of the best use of the multiauthor format. It succeeds because it keeps a large amount of specialized material from a variety of points of view clearly directed at a central theme. Some repetition of information occurs with this format, but because the context and point of view are different in each chapter, the repetition adds to the reader's understanding.

Individual chapters are lean, but the information they contain is complete. Graphs, tables, diagrams, and radiologic and pathologic images are freely used, well reproduced, and carefully explained. An excellent index permits easy reference.

This is a book of concepts and philosophy as well as facts. It will appeal to anyone interested in catching up on renal cystic diseases and will be a valuable reference book for those who deal with the clinical or investigative problems posed by these diseases.

Morton Glickman
Yale–New Haven Hospital
New Haven, CT 06510

Calcified Renal Stones and Cyst Calcifications in Autosomal Dominant Polycystic Kidney Disease: Clinical and CT Study in 84 Patients

Errol Levine[1]
Jared J. Grantham[2]

Although renal calculi and cyst calcifications occur commonly in patients with autosomal dominant polycystic kidney disease (ADPKD), their true frequency is unknown because it is difficult to distinguish between the two with excretory urography and sonography. A detailed analysis of renal calcifications in ADPKD based on CT findings has not been performed. Accordingly, we retrospectively evaluated clinical and CT findings in 84 patients with ADPKD to determine the frequency of calculi and cyst calcifications, the relationship of these abnormalities to symptoms, and possible factors in their pathogenesis. Of the 84 patients, 53 had both IV contrast-enhanced and unenhanced CT scans and 31 had unenhanced scans only. We examined unenhanced CT scans of all 84 patients for renal calcifications. However, we classified renal calcifications into stones and cyst calcifications in only the 53 patients, because it is often difficult to distinguish between the two when only unenhanced scans are available. Of 84 patients, 18 (21%) had passed renal calculi or had stones treated surgically and 42 (50%) had renal calcifications on CT. Of the 53 patients who had both enhanced and unenhanced CT scans, 19 (36%) had renal calculi on CT. Patients with stones had significantly higher frequencies of previous flank pain (68% vs 35%) and of urinary tract infections (63% vs 18%) than did those without calculi. Cyst calcifications occurred in 13 (25%) of 53 patients and were probably a consequence of cyst hemorrhage. Cyst calcifications were found significantly more often in older patients with larger kidneys and worse renal function.

We conclude that renal stones have a high rate of occurrence among patients with ADPKD and are a significant cause of morbidity in this disorder. Cyst calcification is also common in patients with ADPKD, particularly those with more advanced cystic disease.

***AJR* 159:77–81, July 1992**

Patients with autosomal dominant polycystic kidney disease (ADPKD) frequently develop renal calcifications caused by either renal calculi or cyst calcifications [1, 2]. Differentiation between these two causes of calcifications based on excretory urography and sonography is often difficult [1, 3]. Consequently, the prevalences of calcified renal calculi and of cyst calcifications in ADPKD are not precisely known. CT performed with and without IV contrast enhancement is an excellent technique for detecting renal calcifications in ADPKD and for distinguishing calcified calculi from calcifications in cysts. However, to the best of our knowledge a detailed CT study of renal calcifications in ADPKD has not been performed. We retrospectively evaluated clinical and CT findings in 84 patients with ADPKD to determine (1) the frequency of renal calcifications, (2) whether the calcifications were in calculi or cysts, and (3) whether the calcifications were related to symptoms.

Materials and Methods

Eighty-four patients with ADPKD who had abdominal CT between January 1980 and June 1991 were identified by a review of radiology department and medical records. The diagnosis

Received December 9, 1991; accepted after revision January 23, 1992.

[1] Department of Diagnostic Radiology, 2-169 Bell Memorial Hospital, University of Kansas Medical Center, 3901 Rainbow Blvd., Kansas City, KS 66160-7234. Address reprint requests to E. Levine.

[2] Department of Medicine, Division of Nephrology, University of Kansas Medical Center, Kansas City, KS 66160-7234.

0361-803X/92/1591-0077
© American Roentgen Ray Society

of ADPKD was based on family history, clinical findings, and imaging criteria [4]. The patients consisted of 40 males and 44 females 13–71 years old (mean, 43 years). Indications for CT included assessment of disease extent in 28 patients, flank pain and/or macroscopic hematuria in 25, confirmation of a suspected diagnosis of ADPKD in 18, family screening in six, unexplained deterioration in renal function in four, and suspected renal cyst infection in three. In all patients CT was performed on a General Electric 8800 or 9800 scanner (General Electric Medical Systems, Milwaukee, WI) or a Siemens DRH or Somatom HiQ scanner (Siemens Medical Systems, Iselin, NJ). Contiguous 8- or 10-mm abdominal sections were obtained routinely. In 53 of 84 patients CT was performed both with and without IV contrast enhancement. Only unenhanced CT scans were obtained in 31 patients. Contrast-enhanced scans were obtained by using either 150 ml of meglumine diatrizoate (60%) or 150 ml of iohexol (300 mg I/ml) administered by drip infusion.

The following data were analyzed from medical records for each patient relative to the time of the CT scan: sex; age; urinary tract symptoms; presence of hypertension; treatment with dialysis; and serum creatinine, calcium, phosphorus, uric acid, and blood urea nitrogen levels.

Without knowledge of clinical data, we examined the unenhanced CT scans of all 84 patients for the presence, number, and size of renal calcifications. However, calcifications were classified as either calculi or cyst calcifications in only the 53 patients who had both IV contrast-enhanced and unenhanced CT scans because it is often difficult to distinguish between the two when only unenhanced scans are available. Calculi were diagnosed by their relationship to the opacified collecting system (Fig. 1). Cyst calcification was diagnosed by its relationship to cysts shown on contrast-enhanced scans, by its location outside the opacified renal collecting system, and by morphology (e.g., curvilinear calcification) (Fig. 2). Follow-up CT scans obtained in 12 patients at intervals ranging from 19 to 84 months after the first scans were evaluated for changes in renal calcification.

The presence and number of high-density cysts (Fig. 3) were also recorded for each patient. The length (l), width (w), and anteroposterior dimension (AP) were recorded for both kidneys in each patient. The volume (V) of each kidney was estimated according to the

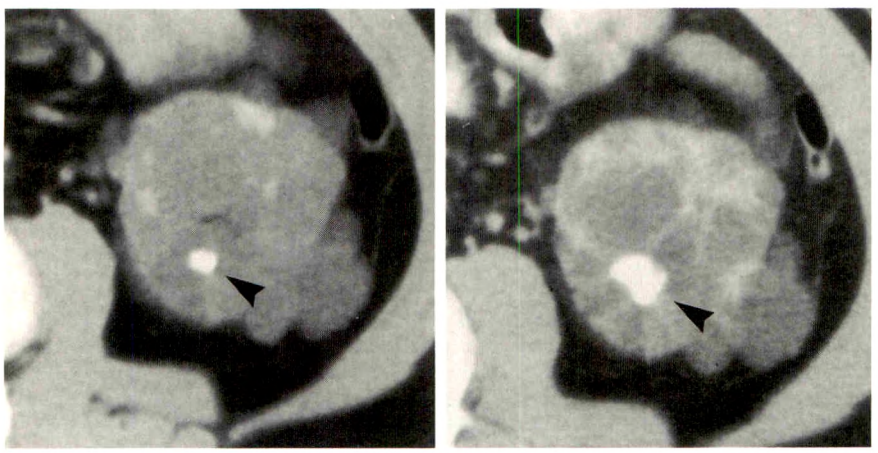


Fig. 1.—Polycystic kidney disease with calculus in lower pole of left kidney.
***A*, Unenhanced CT scan shows small rounded calcification (*arrowhead*).**
***B*, Contrast-enhanced CT scan reveals that calcification is located in opacified calix (*arrowhead*).**

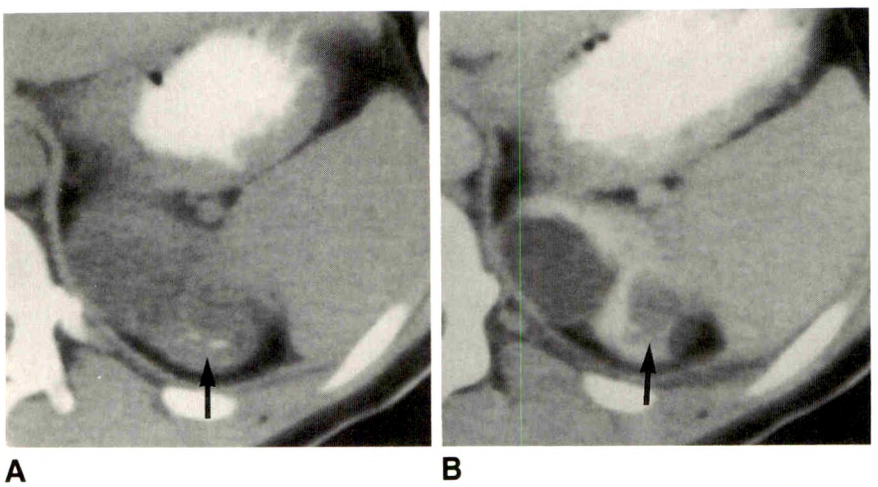


Fig. 2.—*A*, Unenhanced CT scan shows curvilinear calcification (*arrow*) in upper pole of left kidney.
***B*, Contrast-enhanced CT scan shows that calcification is located in wall of upper pole cyst (*arrow*) remote from opacified calices (*not shown*).**

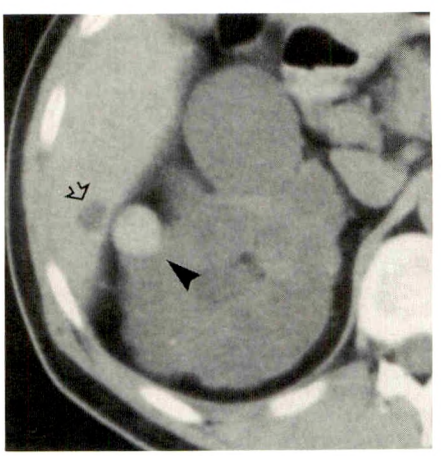


Fig. 3.—Unenhanced CT shows several fluid-filled cysts and subcapsular hemorrhagic cyst (*arrowhead*) (attenuation value = 64 H) in right kidney. Note small liver cyst (*open arrow*).

modified equation for an ellipsoid, namely, $V = 0.49 \times l \times w \times AP$. A mean renal volume was determined for each patient.

The Student's two-sample t test and the chi-squared test were used to test for statistical significance between means and frequencies, respectively.

Results

Renal Calculi

Renal calculi were detected in 19 (36%) of 53 patients having CT with and without IV contrast enhancement. Stones were often multiple; the mean number per patient was 2.1 (range, 1–4). They ranged in size from 3 to 20 mm (mean, 7.8 mm). Calculi were located only in the calices in 12 patients, in the calices and renal pelvis in four, and only in the renal pelvis in three. Stones were bilateral in 12 (63%) of 19 patients and were unilateral in seven (37%).

Patients with renal calculi had significantly higher frequencies of previous episodes of flank pain (68%) than those without stones (35%) (Table 1). No significant differences were found in mean age, sex, frequency of hypertension and hematuria, mean blood chemistry values, and mean renal volume between patients with and without calculi. Eighteen (34%) of 53 patients had histories of urinary tract infections, that is, acute pyelonephritis in eight and cystitis in 10. Urinary tract infections occurred in 16 (52%) of 31 females and in two (9%) of 22 males ($p = .001$, chi-squared test). Patients with stones had significantly higher frequencies of urinary tract infections (63% vs 18%) than those without calculi ($p = .001$, chi-squared test). Among eight patients with histories of acute pyelonephritis, six had renal calculi seen on CT, whereas six of 10 patients with cystitis had stones seen on CT. Of the two patients with acute pyelonephritis in whom acute cyst infections developed, both had ipsilateral renal calculi (Fig. 4).

Cyst Calcification

Thirteen (25%) of 53 patients in whom CT was performed with and without IV contrast enhancement were shown to have bilateral cyst calcifications on their first CT scans (Table 1). Cyst calcifications appeared as small flecks of calcification or curvilinear calcifications in cyst walls (Fig. 2) or, occasionally, as amorphous calcification of cyst contents. Patients with cyst calcifications were significantly older than those without calcifications and also had more severe cystic disease, as indicated by larger kidneys and worse renal function. Patients with cyst calcifications did not differ significantly from those without calcifications regarding sex; urinary tract symptoms; frequency of hypertension; frequency of high-density cysts; and mean serum calcium, phosphorus, and uric acid levels. Seven (13%) of 53 patients had both cyst calcifications and calculi. Evaluation of follow-up CT scans in 12 patients showed new or progression of cyst calcifications in eight (Fig. 5).

Total Renal Calcifications

CT analysis of the entire patient population (84 patients) showed renal calcifications (including cyst calcifications and calculi) in 42 (50%). Calcifications were bilateral in 30 patients

TABLE 1: Clinical, Renal Volume, and Blood Chemistry Data in 53 Patients with Autosomal Dominant Polycystic Kidney Disease Grouped According to the Presence or Absence of Renal Calculi and Renal Cyst Calcifications

Clinical, Renal Volume, and Blood Chemistry Data	Renal Calculi		Cyst Calcifications	
	Present ($n = 19$)	Absent ($n = 34$)	Present ($n = 13$)	Absent ($n = 40$)
Clinical data				
Age in years (mean ± SEM)	37 ± 3	39 ± 2	45 ± 4	36 ± 2[a]
Sex				
No. of men (%)	8 (42)	14 (41)	7 (54)	15 (38)
No. of women (%)	11 (58)	20 (59)	6 (46)	25 (63)
Signs and symptoms (no. of patients [%]):				
With current flank pain	12 (63)	14 (41)	9 (69)	22 (55)
With previous episodes of flank pain[b]	13 (68)	12 (35)[c]	–	–
With current or previous hematuria	9 (47)	11 (32)	7 (54)	13 (33)
With hypertension	13 (68)	25 (74)	11 (85)	27 (68)
Undergoing dialysis	0	0	0	0
With urinary tract infection	12 (63)	6 (18)[c]	4 (31)	14 (35)
With high-density cysts	11 (58)	19 (56)	10 (77)	20 (50)
Renal volume in cm^3 (mean ± SEM)[d]	431 ± 52	577 ± 80	743 ± 132	454 ± 56[a]
Blood chemistry data in mg/dl (mean ± SEM)				
Blood urea nitrogen	16.7 ± 1.5	16.1 ± 0.9	20.6 ± 1.8	14.9 ± 0.8[a]
Serum creatinine	1.1 ± 0.1	1.1 ± 0.1	1.3 ± 0.1	1.0 ± 0.1[a]
Serum calcium	9.7 ± 0.1	9.5 ± 0.1	9.7 ± 0.1	9.6 ± 0.1
Serum phosphorus	3.8 ± 0.1	3.8 ± 0.1	3.9 ± 0.2	3.8 ± 0.1
Serum uric acid	4.6 ± 0.4	5.4 ± 0.4	5.8 ± 0.8	5.0 ± 0.3

[a] Means of present and absent differ significantly ($p < .05$, two-sample t test).

[b] For patients with cyst calcifications, numbers for both current and previous flank pain are grouped under current flank pain.

[c] Frequencies of present and absent differ significantly ($p < .05$, chi-squared test).

[d] Normal renal volume = 330 ± 84 cm^3 (mean ± SD).

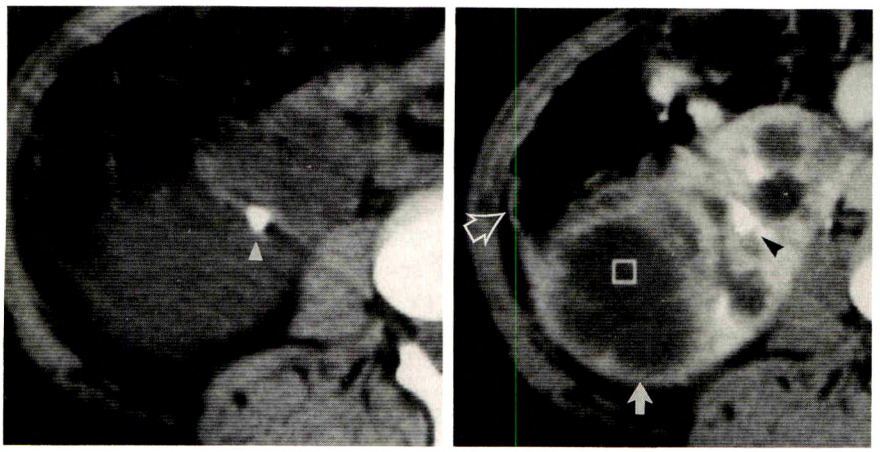


Fig. 4.—Acute pyelonephritis complicated by cyst infection in a 21-year-old woman with polycystic kidney disease and renal calculus.

***A*, Unenhanced CT scan reveals triangular calcification (*arrowhead*) in lower pole of right kidney.**

***B*, Contrast-enhanced CT scan shows calculus in opacified lower pole calix (*arrowhead*). Note lower pole cyst (*solid arrow*), which is larger than adjacent cysts. Cyst has irregular, thickened wall, and adjacent renal fascia (*open arrow*) is thickened. Patient responded to antibiotic therapy; follow-up sonogram showed absence of large cyst, suggesting rupture into collecting system.**

(71%) and unilateral in 12 (29%). Thirty-one patients (74%) with renal calcifications had histories of flank pain as compared with 21 patients (50%) without calcifications ($p < .05$, chi-squared test). Nineteen patients (45%) with renal calcifications had hematuria as compared with nine patients (21%) without calcifications ($p < .05$, chi-squared test). High-density cysts occurred in 53 (63%) of 84 patients. Eighteen (21%) of 84 patients had documented histories of passage of renal calculi and urinary recovery of calculi. Four patients (5%) required surgical management of calculi including pyelolithotomy in two, ureterolithotomy in one, and extracorporeal shock-wave lithotripsy in one.

Discussion

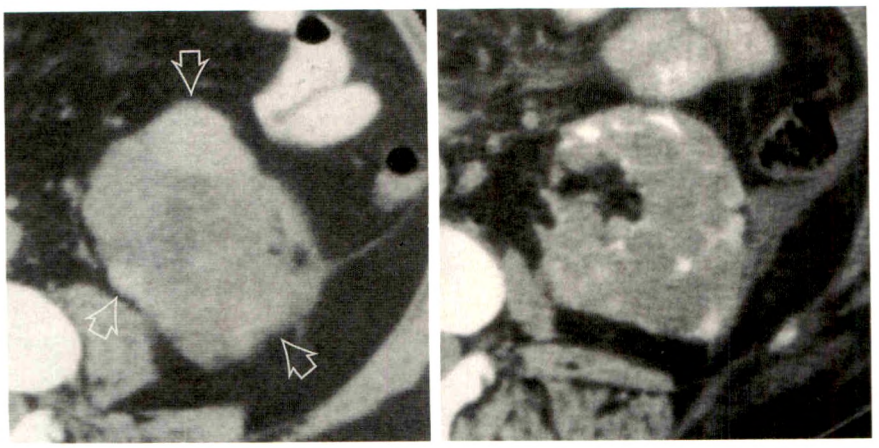
Flank pain and hematuria, which are often recurrent, severe, and disabling, are among the most important and common manifestations of ADPKD [3, 4]. About 62% of 84 patients in our study reported episodes of flank pain and 33% reported episodes of macroscopic hematuria. Acute flank pain and hematuria may result from cyst hemorrhage, renal calculi, cyst infection, and, rarely, renal neoplasm [4]. Differentiation among these complications is important for management purposes and is best achieved by CT [5].

Renal calcifications were seen on CT in 50% of our 84 patients. Our study shows that these are due to stones or cyst calcifications or to a combination of the two. CT performed with and without IV contrast enhancement provides an excellent method for detecting renal calcifications in ADPKD and for distinguishing between stones and cyst calcifications (Figs. 1, 2, and 4). About 57% of calculi that occur in ADPKD are composed predominantly of uric acid [1]. Pure uric acid calculi are radiolucent on conventional tomography. However, these calculi are reliably shown by CT as densities with attenuation values greater than 200 H [6, 7]. Differentiation between stones and cyst calcifications based on excretory urography and sonography is often difficult [1, 3].

Cyst calcification is related to a cyst wall or lumen (Fig. 2), while calculi lie within the opacified collecting system (Figs. 1 and 4). This is apparent on CT even when the calices are displaced by multiple cysts. If only unenhanced CT scans are obtained because of renal functional impairment, distinction between stones and cyst calcification is sometimes possible on the basis of the morphology of the calcification (Figs. 2 and 4–6). However, small rounded renal calcifications are common in ADPKD and are often impossible to localize when only unenhanced CT scans are studied (Fig. 6).

It is generally accepted that renal calculi occur more frequently in patients with ADPKD than in the general population [1, 3, 4]. Stones in patients with ADPKD may be due to metabolic abnormalities [1] or to stasis resulting from pressure on the renal collecting system caused by multiple cysts [3, 8]. The most comprehensive study to date based on clinical and urographic findings in 751 patients with ADPKD showed nephrolithiasis in 151 patients (20%) [1]. This frequency is somewhat lower than that of our smaller study, which revealed calculi in 36% of 53 patients with ADPKD. The difference is probably partly due to the greater sensitivity of CT than of excretory urography in showing small calculi and radiolucent uric acid calculi. However, since about 30% of our patients had CT because of flank pain or hematuria, the demonstrated prevalence of stones is probably higher than would have been encountered in an asymptomatic patient population with ADPKD.

The morbidity associated with renal calculi in patients with ADPKD is difficult to determine because cyst hemorrhage occurs in about 63% of patients and often results in clot colic that is indistinguishable from colic due to stone passage [3]. Among our 84 patients, about 21% had passed calculi that were recovered from the urine and 5% required surgical management of stones. However, these data may underestimate the frequency of symptomatic stones in patients with ADPKD. About 68% of patients in whom renal calculi were seen on CT had previous episodes of flank pain as compared with 35% of those without calculi, although the two groups did not differ in the frequency of high-density cysts (Table 1). It is likely, therefore, that flank pain in ADPKD is often due to ureteric passage of calculi that are not recovered from the urine.



A B

Fig. 5.—Development of cyst calcification in polycystic kidney disease.
***A*, Unenhanced CT scan displays several high-density cysts (*arrows*) in left kidney.**
***B*, Follow-up CT scan obtained 46 months after *A*. Multiple curvilinear calcifications have developed in cyst walls, some at location of previously noted hemorrhagic cysts.**

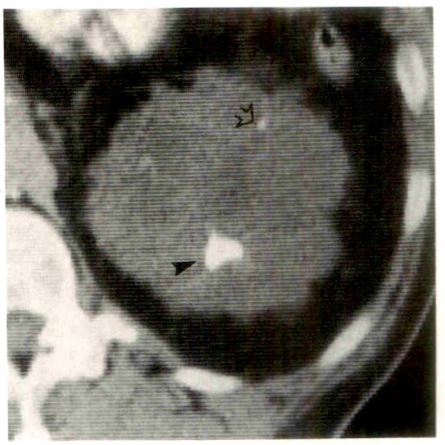


Fig. 6.—Unenhanced CT scan shows calculus (*arrowhead*) in lower pole of left kidney in patient with polycystic kidney disease. Concavity on posterolateral aspect suggests that stone formed on papilla and grew in calix. Differentiation from cyst calcification is possible without use of IV contrast medium. However, small anterior calcification (*arrow*) is indeterminate in nature and location.

As shown by our patients and other reported series, urinary tract infections occur commonly in patients with ADPKD and are significantly more common in women than in men [3, 9]. Such infections are usually due to gram-negative organisms such as *Escherichia coli* and may lead to serious complications including cyst infection, perinephric abscess, septicemia, and death [3, 9]. Although it is unlikely that calculi actually initiate urinary tract infections in patients with ADPKD, our study suggests that calculi may exacerbate such infections. In our subgroup of 53 patients, those with stones had significantly higher frequencies of infections (63% vs 18%) than those without calculi. Among eight patients with acute pyelonephritis, six had renal calculi. Two of the six had acute cyst infections and ipsilateral calculi (Fig. 4).

Renal cyst calcification is a common phenomenon in patients with ADPKD and was detected in 25% of our subgroup of 53 patients. It is generally believed to result from episodes of cyst hemorrhage [2]. However, because cyst calcification may require 3–5 years to develop in hemorrhagic cysts (Fig. 5), the lack of a significant correlation between them is not unexpected (Table 1). Among 53 patients, cyst calcifications were found more often in older patients with larger kidneys and worse renal function. This suggests that cyst calcification is a phenomenon associated with more advanced cystic disease, and it may indeed develop as part of the natural history of the disorder. Clinically significant renal cell carcinoma is a rare occurrence in large series of patients with ADPKD [10], and cyst calcification should not be considered as a sign of malignant neoplasm unless an associated soft-tissue mass also occurs.

In conclusion, renal calcifications occur commonly in patients with ADPKD. They may be due to stones or to cyst calcification or to a combination of the two. CT provides an excellent technique for detecting calcifications and for distinguishing renal calculi from cyst calcifications in patients with ADPKD. Stones occur frequently in patients with ADPKD and often produce morbidity by causing intermittent ureteric obstruction and by exacerbating renal infections. Cyst calcifications result from previous cyst hemorrhage, occur in patients with more advanced renal cystic disease, and are probably part of the natural history of the disorder.

REFERENCES

1. Torres VE, Erickson SB, Smith LH, Wilson DM, Hattery RR, Segura JW. The association of nephrolithiasis and autosomal dominant polycystic kidney disease. *Am J Kidney Dis* **1988**;11:318–325
2. Levine E, Grantham JJ. High-density renal cysts in autosomal dominant polycystic kidney disease demonstrated by CT. *Radiology* **1985**;154:477–482
3. Delaney VB, Adler S, Bruns FJ, Licinia M, Segel DP, Fraley DS. Autosomal dominant polycystic kidney disease: Presentation, complications, and prognosis. *Am J Kidney Dis* **1985**;5:104–111
4. Gabow PA. Autosomal dominant polycystic kidney disease—more than a renal disease. *Am J Kidney Dis* **1990**;16:403–413
5. Levine E, Grantham JJ. The role of computed tomography in the evaluation of adult polycystic kidney disease. *Am J Kidney Dis* **1981**;1:99–105
6. Segal A, Spataro RF, Linke CA, Frank IN, Rabinowitz R. Diagnosis of nonopaque calculi by computed tomography. *Radiology* **1978**;129:447–450
7. Federle MP, McAninch JW, Kaiser JA, Goodman PC, Roberts J, Mall JC. Computed tomography of urinary calculi. *AJR* **1981**;136:255–258
8. Amar AD, Das S, Egan RM. Management of urinary calculous disease in patients with renal cysts: review of 12 years of experience in 18 patients. *J Urol* **1981**;125:153–156
9. Schwab SJ, Bander SJ, Klahr S. Renal infection in autosomal dominant polycystic kidney disease. *Am J Med* **1987**;82:714–718
10. Gregoire JR, Torres VE, Holley KE, Farrow GM. Renal epithelial hyperplastic and neoplastic proliferation in autosomal dominant polycystic kidney disease. *Am J Kidney Dis* **1987**;9:27–38

Book Review

Échographie en Pratique Obstétricale. By B. Guérin du Masgenêt, Y. Ardaens, B. Bailleux, and D. Houzé de L'Aulnoit. Paris: Masson, 190 pp., 1991.

This 190-page book, in 10 chapters, has several authors and contributors. Ardaens and Coquel are radiologists, the others are gynecologists-obstetricians. This is an authoritative book, well balanced, carefully written, brief and concise, yet encyclopedic in scope. It is presented in a good format with superior production and easy legibility. The numerous illustrations are of high quality, and the accompanying legends are excellent. This is a pacemaker in the French medical literature.

This book is the result of extensive technical research and clinical study. Thus, echography (sonography) gives accurate detailed information that could never have been obtained with standard radiography of the abdomen and pelvis. The first chapter gives excellent detail of the techniques of sonography in gynecology and obstetrics. Subsequent chapters deal with the determination of the presence of pregnancy, stage of fetal development, anatomy of the developing fetus, detection of fetal malformations, and extrauterine pregnancy. Complete discussions are presented of the various types of pathologic conditions associated with pregnancy: ovarian cysts, fibromas, involvement of the biliary and urinary tracts, venous thrombosis, appendicitis, and disorders of the thyroid and mammary glands. Doppler evaluation of uterine and adnexial blood flow and the indications and complications of interventional procedures are included also.

Chapter 10 presents a novel approach to the psychological, ethical, and medicolegal aspects of prenatal diagnosis, a significant approach not taken by other authors in other books. The prenatal diagnosis of fetal abnormalities is traumatic for the mother, who fears having an abnormal child. In turn, the physician fears a missed diagnosis, a false-negative diagnosis, or misinterpretation of information given to the patient.

We have gone a long way since the early days of radiography of the maternal abdomen and pelvis with the possible hazards of radiation injury to the developing fetus. Sonography has become an indispensable technique in diagnostic radiology, especially in obstetrics and gynecology. This excellent book should be in the library of gynecologists and obstetricians and of radiologists who are particularly involved in this field, and who have adequate knowledge of the French language. For those who do not read French, this book can be an inducement to study and become acquainted with a beautiful and rich language. This carefully prepared book is a valuable addition to the rapidly advancing field of sonography and a significant addition to diagnostic radiology. I would welcome an English edition of this book.

William H. Shehadi
Greenwich, CT

Diagnosis of Placenta Previa During the Third Trimester:
Role of Transperineal Sonography

Barbara S. Hertzberg[1]
James D. Bowie
Barbara A. Carroll
Mark A. Kliewer
Therese M. Weber

Placenta previa can be difficult to diagnose with transabdominal sonography during the third trimester of pregnancy, because of difficulties in imaging the cervix late in pregnancy. Although transperineal sonography offers an additional view of the cervix, its value in the diagnosis of placenta previa has not been studied. Accordingly, we performed transperineal sonography on 164 patients who had had transabdominal scans that had shown placenta previa or had been inconclusive during the third trimester of pregnancy. Transabdominal sonograms had been inconclusive for placenta previa in 157 of these patients because the cervix was not visualized. The remaining seven patients had transabdominal scans that showed placenta previa. Transperineal sonography successfully visualized the internal surface of the cervix in all 164 patients, allowing determination of the presence or absence of placenta previa in all cases. Transperineal sonograms showed absence of placenta previa in 154 patients. At delivery, none of these patients had evidence of placenta previa. Transperineal sonography showed placenta previa in 10 patients. In nine of these patients, placenta previa was confirmed at delivery. The 10th patient did not have clinically significant placenta previa at delivery.

Our study shows that transperineal sonography is a valuable technique to complement transabdominal sonography for detection of placenta previa during the third trimester of pregnancy. Use of transperineal sonography should be strongly considered when a definitive diagnosis regarding placenta previa is not possible by transabdominal sonography because the cervix is not visualized. In such cases, transperineal sonography will usually show the internal surface of the cervix without overlying placental tissue, allowing confident exclusion of placenta previa. Occasionally, however, transperineal sonography will show a placenta previa that was not seen with transabdominal sonography.

***AJR* 159:83–87, July 1992**

Sonographic evaluation for placenta previa requires direct visualization of both the cervix and the lower edge of the placenta [1–3]. Although this is usually readily accomplished by transabdominal sonography during the second trimester, visualization of these structures becomes more difficult with advancing gestation. In the third trimester, the inferior edge of the posterior, midline placenta may be obscured by fetal parts; similarly, it is often impossible to depict the cervix by transabdominal sonography late in the third trimester [4, 5]. Because of these limitations, alternative techniques are needed to complement transabdominal sonography for the diagnosis of placenta previa. Although endovaginal sonography has been suggested [6–10], a transperineal approach provides another, more convenient means of imaging the cervix and lower uterus without requiring specialized equipment, vaginal penetration, or external fetal manipulation [11–14].

The goal of this study was to investigate the value of using transperineal sonography to complement transabdominal sonography in the diagnosis of placenta previa.

Received November 21, 1991; accepted after revision February 10, 1992.

Presented at the annual meeting of the American Roentgen Ray Society, Orlando, FL, May 1992.

[1] All authors: Department of Radiology (Box 3808), Duke University Medical Center, Durham, NC 27710. Address reprint requests to B. S. Hertzberg.

0361–803X/92/1591–0083
© American Roentgen Ray Society

Subjects and Methods

Transperineal sonography was used prospectively to evaluate 164 women for possible placenta previa. All patients were in their third trimester of pregnancy. The indications for sonography were diverse, and included determination of fetal age and presentation, size-dates discrepancy, placental location, fetal anomalies, adnexal mass, fetal growth, preterm labor, premature rupture of membranes, fetal presentation, vaginal bleeding, and multiple gestations. Patients were included in the study if results of their transabdominal sonography were either inadequate to exclude placenta previa (157 patients) or suggestive of placenta previa (seven patients) and if they subsequently delivered at our institution.

Transabdominal sonography was performed with a 3.5-MHz phased-array sector transducer (Acuson 128, Mountain View, CA) positioned on the lower portion of the abdomen and angled caudally, using the amniotic fluid as an acoustic window. The examination was performed with the mother's urinary bladder empty so as not to distort the configuration of the cervix or lower uterine segment.

For transperineal sonography, ultrasound gel was placed on the head of the transducer, which was draped with a protective covering (Hefty Baggies, Mobil Chemical Co., Pittsford, NY) secured with a rubber band. A scanning medium of KY Jelly (Johnson & Johnson, New Brunswick, NJ) was applied to the outer surface of the protective covering. The transducer was positioned directly on the perineum in a sagittal orientation, usually over but occasionally between the labia minora, with the center of the transducer typically posterior to the urethra and anterior to the vagina (Fig. 1). When the cervix and lower uterus were visualized on the sonogram, the transducer was slowly angled medially and laterally in order to image the entire internal surface of the cervix. Hard-copy films were obtained for both the transperineal and transabdominal sonograms.

Transabdominal sonograms were considered diagnostic of placenta previa if placental tissue was shown over any part of the cervix while the mother's urinary bladder was empty, in the absence of cervical or lower uterine contractions. Complete placenta previa was diagnosed if transabdominal sonograms showed placental tissue covering the entire surface of the internal os. Marginal placenta previa was defined as placental tissue covering part of the cervix without encroaching on the internal os, and partial placenta previa was defined as placental tissue covering a portion of the internal os without covering the entire os, but these two grades of placenta previa were grouped together for data analysis as they are frequently difficult to distinguish from each other by sonography. The transabdominal sonogram was considered inadequate to exclude placenta previa if the inferior margin of the placenta could not be imaged in its entirety or the cervix could not be visualized.

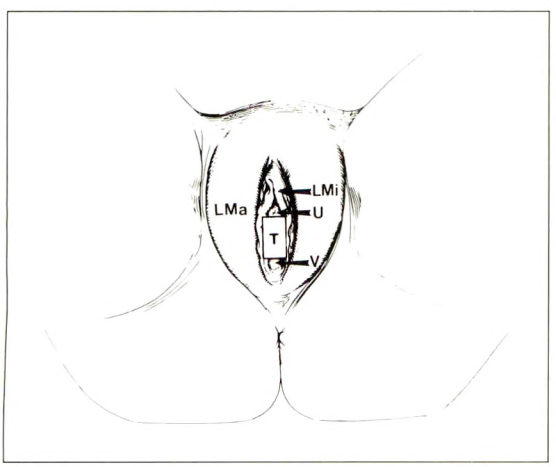


Fig. 1.—Transducer positioning for transperineal scanning. Schematic diagram of perineum shows transducer positioned on perineum in a sagittal orientation between labia majora (LMa). LMi = labia minora, U = urethra, T = transducer, V = vagina.

Placenta previa was diagnosed when transperineal sonograms showed placental tissue completely covering the internal os of the cervix (complete placenta previa) or overlying a portion of the cervix without completely covering the internal os (marginal or partial placenta previa). Placenta previa was excluded if transperineal sonograms showed at least one of the following: (1) direct transperineal visualization of both the lower edge of the placenta and the cervix, with the lower edge of the placenta seen separate from the cervix, (2) amniotic fluid between the presenting part and cervix without interposed placental tissue, or (3) the presenting part immediately overlying the cervix without space for intervening placental tissue. In patients with multiple transperineal sonograms, the examination that included the transperineal/transabdominal combination performed closest to delivery was the one used for analysis.

Medical records were reviewed to determine the presence or absence of placenta previa at delivery. Placenta previa was confirmed at delivery when placental tissue was visualized overlying the cervix during cesarean section or cesarean hysterectomy. Absence of clinically significant placenta previa at delivery was confirmed if no placental tissue was seen overlying the cervix at cesarean section or if successful vaginal delivery was accomplished without abnormal vaginal bleeding attributable to placenta previa.

Results

Transperineal sonography successfully depicted the internal surface of the cervix in all 164 patients in the study, allowing determination of the presence or absence of overlying placental tissue in all cases. The transperineal sonograms excluded placenta previa in 154 patients and showed placenta previa in the remaining 10.

Of the 154 patients in whom transperineal sonograms excluded placenta previa, the absence of previa was based on (1) visualization of the presenting part of the fetus immediately overlying the cervix without space for intervening placental tissue in 90 patients (58%, Fig. 2A), (2) visualization of amniotic fluid between the presenting part and the cervix without interposed placental tissue in 60 patients (39%, Fig. 2B), and (3) direct transperineal visualization of the lower edge of the placenta, separate from the cervix, in four patients (3%, Fig. 2C). Transabdominal sonograms were inconclusive for placenta previa in all 154 patients with transperineal sonograms that excluded placenta previa, because the cervix was obscured by the presenting part of the fetus. Delivery records confirmed that all 154 patients with transperineal sonograms excluding placenta previa had no evidence of placenta previa at the time of delivery.

Five of the 10 patients in whom transperineal sonography showed placenta previa had a complete placenta previa (Fig. 3), and five had a marginal or partial placenta previa. Of the 10 patients with transperineal sonograms that showed placenta previa, seven had transabdominal sonograms that showed placenta previa. For these seven, the sonographic appearance of placenta previa was similar, although the cervix

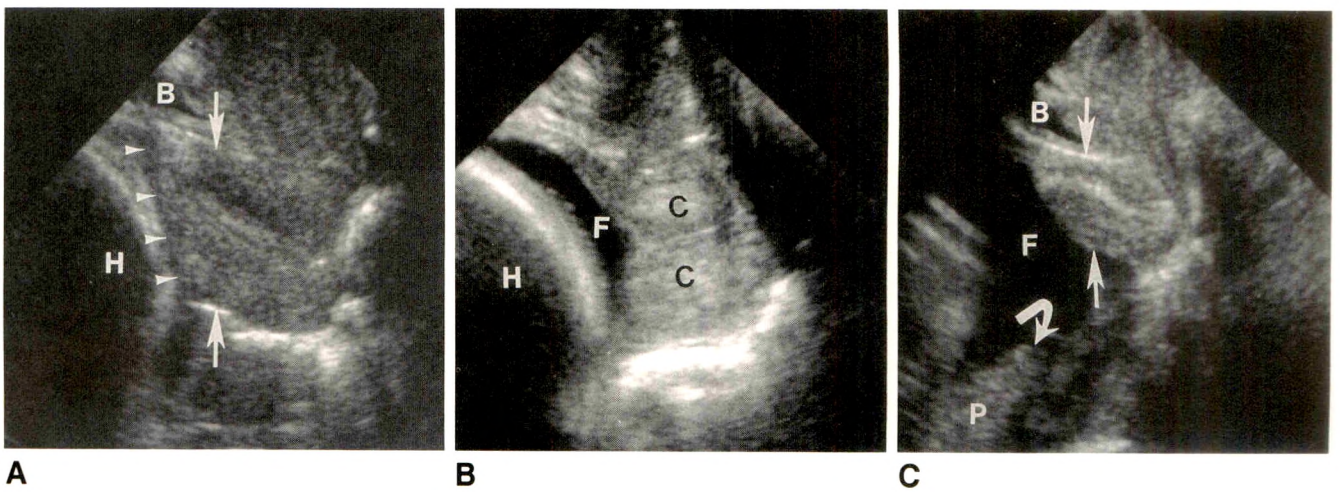


Fig. 2.—Transperineal sonograms show absence of placenta previa.
A, Sonogram shows head (H) of fetus directly abutting internal surface of cervix (*arrowheads*) without space for interposed placental tissue, thereby excluding placenta previa. B = maternal bladder, *arrows* = cervix.
B, Sonogram excludes placenta previa by showing amniotic fluid (F) between head of fetus (H) and cervix (C), without interposed placental tissue.
C, Sonogram shows inferior edge of placenta (*curved arrow*) separate from cervix (*straight arrows*), thereby excluding placenta previa. B = maternal bladder, F = amniotic fluid, P = placenta.

and placenta were depicted in different orientations by the two approaches (Fig. 4A–4E). In the other three patients with transperineal sonograms showing placenta previa, the transabdominal sonogram was inconclusive for placenta previa because overlying fetal parts obscured the cervix and the lower uterine segment. Cesarean section ($n = 7$) or cesarean hysterectomy ($n = 2$) was performed in nine of 10 patients with transperineal sonograms showing placenta previa, confirming the diagnosis in all nine. One result was false-positive, in a patient with an inconclusive transabdominal sonogram and a marginal placenta previa shown by transperineal sonography at 30 weeks' gestation who had an uncomplicated vaginal delivery at term.

During cesarean section, one of the patients with a marginal placenta previa diagnosed on the basis of both transperineal and transabdominal sonography also had a succenturiate lobe of the placenta with vasa previa. Both transabdominal and transperineal sonograms had revealed a membrane over the cervical os, but only the transabdominal study showed the succenturiate lobe. Color Doppler sonography was not done in this case.

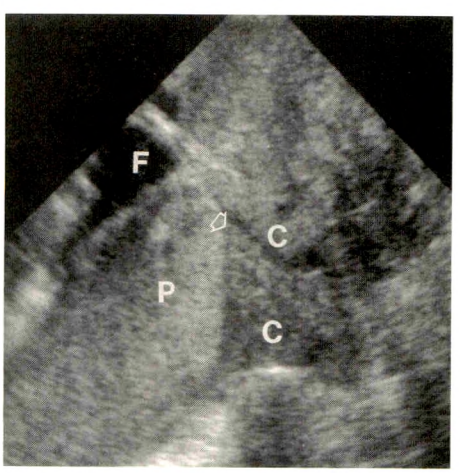


Fig. 3.—Transperineal sonogram shows placental tissue (P) covering entire internal os (*open arrow*), consistent with complete placenta previa. F = amniotic fluid, C = cervix.

Six patients had more than one transperineal sonogram obtained in the third trimester. Interpretations of the sonograms for the presence or absence of placenta previa were the same in all but one of these patients. In this case, a transperineal sonogram at 28.8 weeks' gestation showed a marginal placenta previa, but follow-up at 32.9 weeks' gestation revealed no placenta previa, and the patient had an uncomplicated vaginal delivery at term.

No complications were attributable to transperineal sonography, and the procedure was uniformly accepted by patients.

Discussion

Although sonography is considered the imaging procedure of choice in evaluating patients for placenta previa, there are several sources of potential errors in making a sonographic diagnosis. Sources of false-positive results include distortion of the lower uterine segment by a cervical or uterine contraction or an overdistended urinary bladder and the presence of a subchorionic hematoma overlying the cervix that simulates placental tissue [1, 3, 4, 15]. To avoid false-negative interpretations, one must visualize both the lower edge of the placenta and the cervix. Although visualization of the lower edge of the placenta at a point above the region of the cervix usually correlates with absence of placenta previa, the cervix itself must be directly visualized to exclude completely the possibility of an accessory lobe overlying the cervix. Moreover, although transabdominal sonography frequently localizes a segment of the inferior edge of the placenta cephalad to the

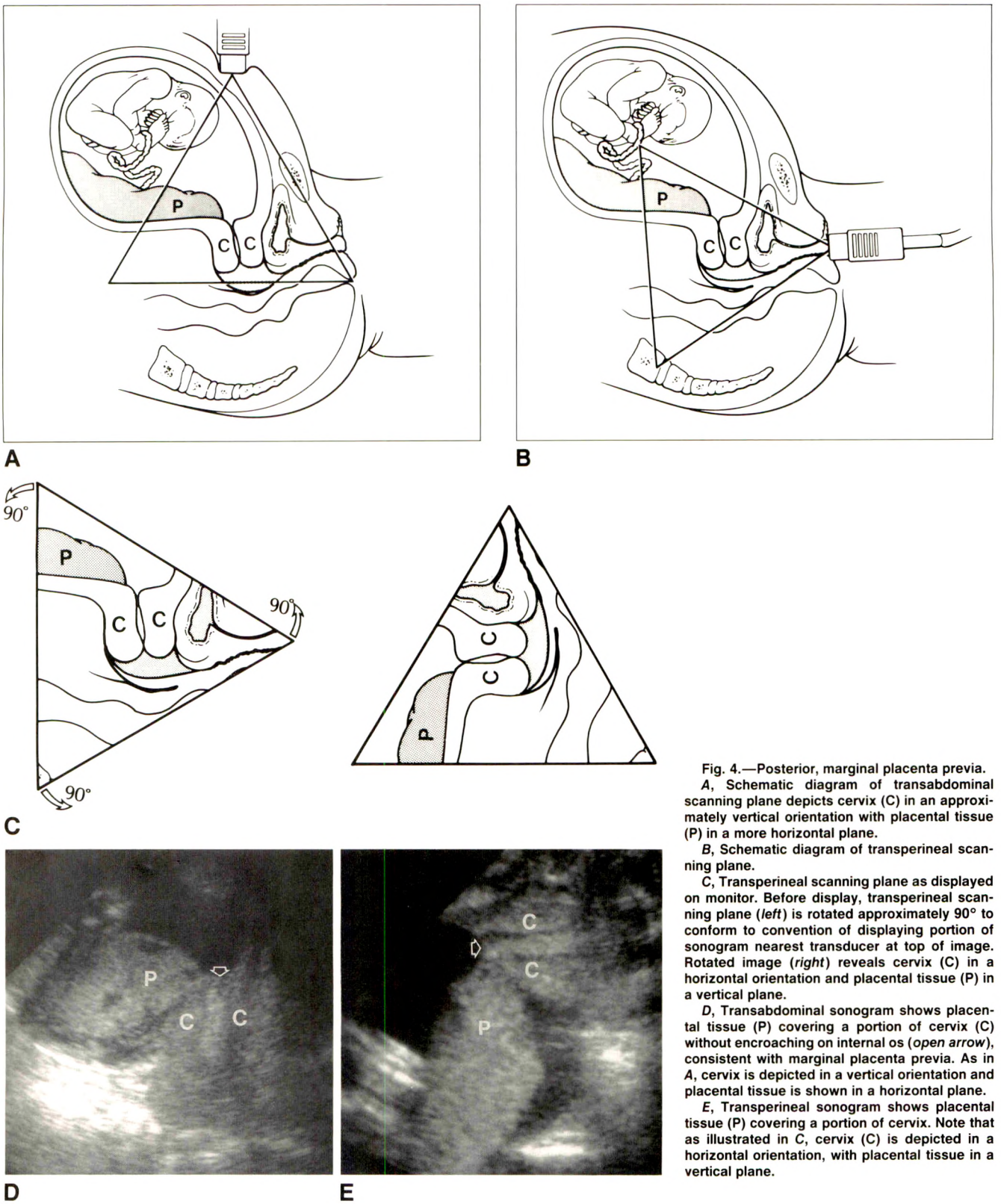


Fig. 4.—Posterior, marginal placenta previa.

A, Schematic diagram of transabdominal scanning plane depicts cervix (C) in an approximately vertical orientation with placental tissue (P) in a more horizontal plane.

B, Schematic diagram of transperineal scanning plane.

C, Transperineal scanning plane as displayed on monitor. Before display, transperineal scanning plane (*left*) is rotated approximately 90° to conform to convention of displaying portion of sonogram nearest transducer at top of image. Rotated image (*right*) reveals cervix (C) in a horizontal orientation and placental tissue (P) in a vertical plane.

D, Transabdominal sonogram shows placental tissue (P) covering a portion of cervix (C) without encroaching on internal os (*open arrow*), consistent with marginal placenta previa. As in *A*, cervix is depicted in a vertical orientation and placental tissue is shown in a horizontal plane.

E, Transperineal sonogram shows placental tissue (P) covering a portion of cervix. Note that as illustrated in *C*, cervix (C) is depicted in a horizontal orientation, with placental tissue in a vertical plane.

region of the cervix, other portions of the inferior placental edge may be obscured by fetal parts.

Although transabdominal sonography is usually successful in depicting the cervix during the first and second trimesters of pregnancy, visualization becomes progressively more difficult during the third trimester. Thus, an alternative technique is needed to complement transabdominal sonography during the third trimester. To this end, techniques have been devel-

oped to elevate the presenting part of the fetus from the pelvis, but these can be uncomfortable for the patient and are often unsuccessful late in the third trimester [2, 16]. Another approach has been to use endovaginal sonography [6–10]. Initial studies using endovaginal sonography have been promising, but the endovaginal probe must be inserted cautiously while directly visualizing the cervix, and further adjustments in the position of the probe also must be made with caution to minimize the possibility of inducing bleeding in the patient with possible placenta previa. Alternatively, transperineal sonography is a more convenient and possibly safer means of imaging the cervix and lower uterus because vaginal penetration is avoided, virtually eliminating the potential for inducing bleeding that is associated with endovaginal sonography.

Transperineal sonography has been used in other clinical situations, such as in imaging the cervix, evaluating vaginal atresia, or imaging the presenting part of the fetus [11–14, 17–20]. However, we are not aware of prior studies of the value of this technique in the evaluation of placenta previa. Although the presence of rectal gas obscuring the region of the external os is a potential difficulty with transperineal sonography, [12, 13], this does not pose a significant problem when evaluating patients for placenta previa because it is the internal surface of the cervix that is important when imaging to look for overlying placental tissue.

In the current study, the greatest value of transperineal sonography was in helping to exclude placenta previa in patients in whom the cervix was not seen on transabdominal sonography. Most patients with placenta previa shown by transperineal sonography also had it shown by transabdominal sonography. This may be attributed to placental tissue in the lower uterus elevating the presenting fetal part sufficiently to allow transabdominal visualization of the cervix during the latter stages of gestation, when this might not otherwise be possible. However, in a significant minority of patients with placenta previa, transperineal sonography was the only method that detected placental tissue overlying the cervix during the third trimester.

The relative lack of false-positive results in this study as compared with prior reports [1, 4, 15, 21] can be attributed to a number of factors. In this study, all images were obtained with the patient's urinary bladder empty, and only third-trimester patients were evaluated. The majority of false-positive results in prior studies tended to occur earlier in pregnancy when lower uterine contractions are more problematic and changes that occur in the cervix near term ("ripening") [22] have not yet taken place.

Accurate interpretation of transperineal sonograms requires the same precautions as in the evaluation of transabdominal sonograms. Sonograms should not be considered to show placenta previa unless the mother's urinary bladder is empty. Images must be obtained in the absence of lower uterine contractions, because a contraction may temporarily pull placental tissue into the lower uterine segment [3]. An echogenic subchorionic hematoma overlying the cervix can simulate placental tissue. Finally, the entire internal surface of the cervix must be scanned to avoid overlooking a marginal placenta previa positioned lateral to scans through the midportion of the cervix.

Our results show that transperineal sonography is a valuable procedure to complement transabdominal studies. Transperineal sonography should not replace transabdominal sonography in the evaluation of placenta previa. Sonography in these cases requires visualization of both the inferior edge of the placenta and the cervix. The cervix is almost always seen on transperineal sonograms, but the lower edge of the placenta is usually beyond the field of view. In such cases, transabdominal sonograms facilitate visualization of the lower edge of the placenta.

REFERENCES

1. Bowie JD, Rochester D, Cadkin AV, Cooke WT, Kunzmann A. Accuracy of placenta localization by ultrasound. *Radiology* **1978**;128:177–180
2. Jeffrey RB, Laing FC. Sonography of the low-lying placenta: value of Trendelenburg and traction scans. *AJR* **1981**;137:547–549
3. Artis AA, Bowie JD, Rosenberg ER, Rauch RF. The fallacy of placental migration: effect of sonographic techniques. *AJR* **1985**;144:79–81
4. Townsend RR, Laing FC, Nyberg DA, Jeffrey RB, Wing VW. Technical factors responsible for "placental migration": sonographic assessment. *Radiology* **1986**;160:105–108
5. Brown JE, Thieme GA, Shah M, Fleischer AC, Boehm FH. Transabdominal and transvaginal endosonography: evaluation of the cervix and lower uterine segment in pregnancy. *Am J Obstet Gynecol* **1986**;155:721–726
6. Farine D, Peisner DB, Timor-Tritsch HE. Placenta previa: is the traditional diagnostic approach satisfactory? *J Clin Ultrasound* **1990**;18:328–330
7. Farine D, Fox HE, Jakobson S, Timor-Tritsch HE. Vaginal ultrasound for diagnosis of placenta previa. *Am J Obstet Gynecol* **1988**;159:566–569
8. Farine D, Fox HE, Timor-Tritsch I. Vaginal ultrasound for ruling out placenta previa: case report. *Br J Obstet Gynaecol* **1989**;96:117–119
9. Farine D, Fox HE, Jakobson S, Timor-Tritsch HE. Is it really a placenta previa? *Europ J Obstet Gynecol Reprod Biol* **1989**;31:103–108
10. Leerentveld RA, Gilberts ECAM, Arnold MJCWJ, Wladimiroff JW. Accuracy and safety of transvaginal sonographic placental localization. *Obstet Gynecol* **1990**;76:759–762
11. Jeanty P, d'Alton M, Romero R, Hobbins JC. Perineal scanning. *Am J Perinatol* **1986**;3:289–295
12. Mahony BS, Nyberg DA, Luthy DA, Hirsch JH, Hickok DE, Petty CN. Translabial ultrasound of the third-trimester uterine cervix: correlation with digital examination. *J Ultrasound Med* **1990**;9:717–723
13. Hertzberg BS, Bowie JD, Weber TM, Carroll BA, Kliewer MA, Jordan SG. Sonography of the cervix during the third trimester of pregnancy: value of the transperineal approach. *AJR* **1991**;157:73–76
14. Zilianti M, Azuaga A, Calderon F, Redondo C. Transperineal sonography in second trimester to term pregnancy and early labor. *J Ultrasound Med* **1991**;10:481–485
15. Gallagher P, Fagan CJ, Bedi DG, Winsett MZ, Reyes RN. Potential placenta previa: definition, frequency, and significance. *AJR* **1987**;149:1013–1015
16. Lee TG, Knochel JQ, Melendez MG, Henderson SC. Fetal elevation: a new technique for placental localization in the diagnosis of previa. *JCU* **1981**; 9:467–471
17. Scanlan KA, Pozniak MA, Fagerholm M, Shapiro S. Value of transperineal sonography in the assessment of vaginal atresia. *AJR* **1990**;154: 545–548
18. Graham D, Nelson MW. Combined perineal-abdominal sonography in the evaluation of vaginal atresia. *JCU* **1986**;14:735–738
19. Sakamoto H, Takagaki K, Masaoka N, et al. Clinical application of the perineal scan: prepartum screening for cord presentation. *Am J Obstet Gynecol* **1986**;155:1041–1043
20. Weber TM, Hertzberg BS, Bowie MD. Transperineal ultrasound: alternative technique to improve visualization of the presenting fetal part. *Radiology* **1991**;179:747–750
21. Langlois SLP, Miller AG. Placenta previa: a review with emphasis on the role of ultrasound. *Aust N Z J Obstet Gynecol* **1989**;29:110–116
22. Anderson HF, Ansbacher R. Ultrasound: a new approach to the evaluation of cervical ripening. *Semin Perinatol* **1991**;15:140–148



San Francisco

American Roentgen Ray Society

93rd Annual Meeting

April 25–30, 1993

San Francisco Marriott • San Franciso, CA

Ovarian Cysts Are Common in Premenarchal Girls: A Sonographic Study of 101 Children 2–12 Years Old

Harris L. Cohen[1]
Peter Eisenberg[1]
Francine Mandel[2]
Jack O. Haller[3]

Previous studies of sonograms in premenarchal girls have reported the typical ovary to be homogeneous in echogenicity, with cysts an uncommon finding, particularly in children less than 6 years old. These studies found no macrocysts (cysts >9 mm in greatest length) in patients less than 11 years old. This information contradicts published pathology studies and our sonographic experience. The goal of this study was to determine the prevalence of cysts in the ovaries of premenarchal girls. The pelvic sonograms of 101 consecutive premenarchal girls between 2 and 12 years old, without known gynecologic or endocrinologic disease, were prospectively studied. One hundred fifty-five ovaries were adequately imaged in three dimensions. Ovaries were evaluated for the presence or absence of cysts (as defined by sonographic criteria), and the length of the cyst or of the largest cyst, if several were noted, was measured. Cysts were identified in 106 ovaries (68%). Cysts were seen in patients of all ages, particularly in the younger children (2–6 years old). Thirteen of the cysts, noted in 11 patients between 2 and 10 years old, were macrocysts.

The typical sonographic appearance of the ovary in premenarchal girls is not homogeneous. Cysts are common in premenarchal girls between 2 and 12 years old and are the cause of the typical heterogeneous image. Macrocysts can be seen in healthy girls less than 11 years old.

AJR 159:89–91, July 1992

Orsini et al. [1] and Salardi et al. [2], in the key sonographic studies of premenarchal girls, reported the typical ovary to be solid and homogeneous in echogenicity. The pattern of homogeneous echogenicity represents ovarian parenchyma without sonographically evident cysts. The identification of cysts in the ovaries of girls in this age group, particularly in children less than 6 years old, was considered unusual. Pathologic studies [3–6], however, suggest that ovarian cysts are common in infants and children. We analyzed the sonograms of 101 girls between 2 and 12 years old to determine the prevalence of ovarian cysts in this age group. Sonography is the imaging standard for ovarian cysts, and any well-marginated, echoless, circular or oval area found within the borders of an ovary of normal size and shape and without evidence of contained calcium, fat, or septa represents an ovarian cyst, whether functional or not.

Subjects and Methods

We prospectively studied 101 consecutive premenarchal girls between 2 and 12 years old who underwent pelvic sonography at North Shore University Hospital–Cornell University Medical College between January 1989 and September 1991.

The examinations were part of routine pelvic sonography performed for a variety of reasons, usually to determine the cause of abdominal or pelvic pain or to evaluate the urinary tract in girls who had bladder or kidney infections. Examinations were performed by a sonographer and a sonologist. All cases were reviewed a second time by one sonologist

Received January 14, 1992; accepted after revision February 11, 1992.

[1] Department of Radiology, North Shore University Hospital–Cornell University Medical College, 300 Community Dr., Manhasset, NY 11030. Address reprint requests to H. L. Cohen.

[2] Division of Biostatistics, Department of Research, North Shore University Hospital–Cornell University Medical College, 300 Community Dr., Manhasset, NY 11030.

[3] Department of Radiology, SUNY–Health Science Center at Brooklyn, 450 Clarkson Ave., Brooklyn, NY 11203.

0361–803X/92/1591–0089
© American Roentgen Ray Society

before the patient was discharged from the department. Any discrepancy between the interpretations of the sonographer, sonologist, or reviewing sonologist would have excluded the case. This did not occur. The longest cyst length measured by any of the examiners on a satisfactory sonogram was used.

Of 121 patients between 2 and 12 years old (note age distribution in Table 1) who had pelvic sonography, 17 were excluded because of a history of premature thelarche (bilateral breast development without any other sign of puberty in a child less than 8 years old) or premature adrenarche (the isolated appearance of pubic, and, at times, axillary hair without evidence of estogenization or virilization in a child less than 8 years old) [7]. Three patients with Turner's syndrome were excluded. No patient had a history or evidence of acute gynecologic abnormality, a known endocrinologic abnormality, or an ovarian mass, other than a cyst, which would have excluded them from this study of healthy patients. Two patients (an 8-year-old and a 10-year-old) had had a unilateral oophorectomy for benign teratoma.

Machines used were the ATL Ultramark 4 and 9 (Advanced Technology Laboratories, Bothell, WA) and the Acuson 128 (Acuson Corp, Mountain View, CA). The last two machines had a cineloop feature, which allows the recapture of a limited number of the immediately preceding images. Transducers used depended on the patient's size, with a 5.0-MHz transducer typically used in the young child or thinner older child. When necessary, 3.5-MHz transducers were used. If patients were old enough to cooperate, they were encouraged to drink water before the examination. No patient was catheterized to aid bladder filling.

The presence of ovarian cysts (defined as sharply marginated, completely sonolucent areas imaged within the confines of normal appearing adnexa that contained no evident fat or calcification) was noted. Cysts were measured according to their longest length. The measurement of the largest cyst in each ovary was used to determine average cyst size. Following the criteria of Salardi et al. [2], cysts with lengths greater than 9 mm were defined as macrocysts. An ovary was considered cystic whether it contained one or several cysts. No ovary was included for cyst analysis if it was not adequately imaged in three dimensions. Data were excluded if a cyst was seen but the ovary was not imaged in three dimensions.

Percentages of cysts within each age studied were computed mathematically. An analysis of variance was used to compare mean (longest) lengths of cysts for each age group (years 2–12). Fisher's exact test was used to compare the proportion of cystic ovaries for each age group studied.

A drawback to this study was the lack of follow-up other than that provided by our clinicians. No routine follow-up examinations were performed unless the clinical problem persisted. No patient was sent for another imaging study or surgery on the basis of our findings, and we therefore cannot report on imaging or surgical proof of our findings beyond the confirmation of the sonographer and sonologist's findings with the imaging technique we believe is the gold standard for evaluation of the normal ovary in children.

Results

One hundred fifty-five ovaries in 101 children were adequately imaged. Nine ovaries were excluded because they could not be imaged in three dimensions. Table 1 records the number of patients examined in each year of life and denotes the number of ovaries seen in three dimensions, the number and percentage of ovaries seen containing cysts, the range of the cyst diameters, and the number and percentage of ovaries with cysts greater than 9 mm (definition of a macrocyst from Salardi et al. [2]), for each of these years of life.

TABLE 1: Cysts Seen per Premenarchal Year

Age (yr)	No. of Patients	No. of Ovaries Imaged	No. (%) of Ovaries with Cysts	Cyst Size Range (mm)	No. (%) of Ovaries with Macrocysts[a]
2	14	17	12 (71)	2–9	0 (0)
3	12	20	12 (60)	3–17	4 (20)
4	11	11	9 (82)	3–12	1 (9)
5	11	21	17 (81)	2–14	4 (19)
6	9	12	8 (67)	2–10	1 (8)
7	2	2	2 (100)	6–7	0 (0)
8	17	30	21 (70)	2–15	3 (10)
9	7	13	8 (62)	3–7	0 (0)
10	7	11	7 (64)	2–6	0 (0)
11	2	3	2 (67)	5–7	0 (0)
12	9	15	8 (53)	3–15	2 (13)

[a] The numbers of patients with macrocysts were 4, 1, 3, 1, 2, and 2 for ages 3, 4, 5, 6, 8, and 12 years, respectively.

Cystic ovaries were seen in patients of all age groups. The prevalence of cystic ovaries among those adequately imaged was 68% (106 of 155 imaged). No age group showed less than a 53% prevalence. No statistically significant difference was noted with regard to the proportion of cystic ovaries noted per year ($p = .25$).

The average cyst was 6 mm with a standard deviation of 4 mm. No statistically significant difference was found in average cyst size at different ages ($p = .71$). The presence of multiple cysts in a single ovary was not rare. Macrocysts were seen in patients of several ages, particularly those between 3 and 8 years old. Thirteen macrocysts were seen in 11 patients less than 11 years old (Table 1).

Discussion

The most recent large real-time sonographic study of ovaries of children and adults was limited in its evaluation of premenarchal subjects because the average age of the subjects in this group was 9.5 years [8]. The most recent large real-time sonographic studies of the ovaries of premenarchal girls were those of Orsini et al. [1] and Salardi et al. [2]. They studied 114 premenarchal girls between 2 and 13 years old. Ovarian morphology was evaluated by the "presence or absence of cystic . . . structures" within the ovary and the separation of these ovaries into homogeneous and cystic groups. Cystic ovaries were further subdivided into those with microcysts (clearly outlined cysts no greater than 9 mm long and those with macrocysts (at least one cyst greater than 9 mm long [1, 2].

Salardi et al. [2] and Orsini et al. [1] found that virtually all patients less than 6 years old had a solid homogeneous ovary. Among those patients 6 years old or older, more ovaries with cysts were noted, but the homogeneous ovary remained characteristic in patients up to 11 years old. They theorized that as the girls neared menarche, ovaries enlarged and echogenicity became inhomogeneous because of the development of preovulatory follicles and corpora lutea due

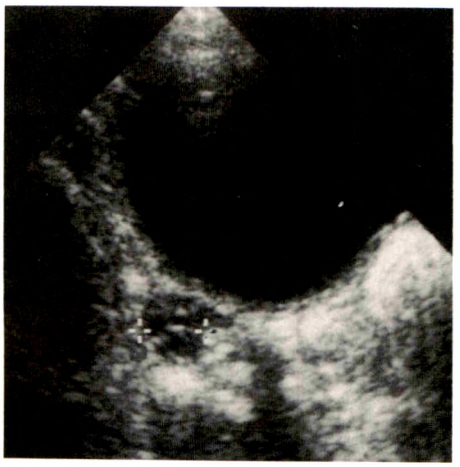


Fig. 1.—Transverse oblique sonogram of cystic right ovary. Ovary of this healthy 6-year-old is heterogeneous in echogenicity because of cysts, largest of which is 7 mm in greatest length.

to gonadotropin stimulation. Yet they also stated that ovarian maturation seemed influenced by age and not hormonal stimulation because, even in pubertal girls, ovarian volumes did not correlate with basal concentrations of sex hormones. Although they stated that microcysts may be normal even during the first years of life, their chart, republished in an adapted form as recently as 1991 [9], noted no microcysts in patients 2, 3, and 5 years old and less than a 25% prevalence among patients 4, 6, 7, and 8 years old. No patient less than 12 years old had a macrocyst [1, 2].

Our study notes microcysts (Fig. 1) in 72% of patients between 2 and 6 years old (58 cystic ovaries of 81 ovaries imaged) and 68% of patients between 7 and 10 years old (38 cystic ovaries of 56 imaged).

We imaged 13 macrocysts in girls between 2 and 10 years old, a group in which Salardi et al. found none. This may, in part, be happenstance because 9 mm was an arbitrary dividing point between microcyst and macrocyst. The probable key element in the greater number of macrocysts and microcysts imaged in our study than in their 1984 work is the improvement in sonographic technology. Salardi and Orsini's studies were performed with a mechanical 3-MHz transducer. Our work has taken advantage of higher frequency transducers, annular-array and curved linear-array transducers with electronic focusing, and cineloop recapture of images that could have been lost when the child being examined was uncooperative.

Our findings are most consistent with those reported by pathologists. In 1861, Rokitansky noted cystic follicles in the ovaries of children, neonates, and fetuses [3]. Peters et al. [4], in a study of the ovaries of 52 girls between 2 months and 11 years old who died of acute disease or accidental death, noted active follicular growth at all ages. The ovaries of 94% of their patients showed normal healthy follicles with normal oocytes and granulosa cells as well as cysts in various stages of atresia [4].

Polhemus [5], in a review of 171 cadavers of infants and children autopsied at Children's Hospital of Los Angeles, also noted extensive follicular growth as normal in childhood. Several cysts may be present at the same time. Follicles with intact granulosa layers averaged 3.5 mm in diameter. Other follicles that did not undergo ovulation but reached various stages of development before atresia often developed cysts that, instead of involuting, enlarged up to several centimeters. Polhemus's work refuted the accepted clinical opinion of his day that "ovarian follicle ripening" begins with puberty. Rather, ovarian follicles begin maturing at or before birth [5], and the child's ovary is a dynamic organ undergoing constant internal change [4].

Merrill [6] studied histologic sections of the ovaries of 98 children and also noted maturing follicles in girls of all ages. Among his 2-year-old patients, who had the largest percentage of cysts, he noted that 80% had gross cysts, a finding similar to that of our sonographic study. The lowest percentage of cysts (53%) was seen in his prepubertal patients. We noted a similar prevalence in our 12-year-old patients but, as with Merrill, we have no explanation for this finding.

In conclusion, contained cysts make the image of the typical ovary in the premenarchal girl between 2 and 12 years old sonographically heterogeneous rather than homogeneous. The cause of these cysts, noted in girls in all age groups, is unknown. The large percentage of cystic ovaries imaged in our study population is consistent with previous pathology reports. The presence of cysts in a premenarchal ovary in an otherwise healthy child does not suggest endocrinologic or other disease. The discrepancy from the results of Salardi et al. [2] may in part be related to improvements in transducer technology.

ACKNOWLEDGMENTS

We thank Cheryl Jacoby, Molly Pose, Lauri Federbush, Dara Muller, Maureen Parcell, and Maria Clifford for their sonographic expertise; Adam Cooper for his photographic work; and Sandra W. Cohen, Karl Drehobl, and Benjamin Adam Cohen for their computer consultations.

REFERENCES

1. Orsini L, Salardi S, Picu G, Bovicelli L, Cacciari E. Pelvic organs in premenarchal girls: real-time ultrasonography. *Radiology* **1984**;153: 113–116
2. Salardi S, Orsini L, Cacciari E, Bovicelli L, Tassoni P, Reggiani A. Pelvic ultrasonography in premenarchal girls: relation to puberty and sex hormone concentrations. *Arch Dis Child* **1985**;60:120–125
3. Spivack M. Polycystic ovaries in the newborn and early infancy and their relationship to the structure of the endometrium. *Am J Obstet Gynecol* **1934**;27:157–173
4. Peters H, Himelstein-Braun R, Faber M. The normal development of the ovary in childhood. *Acta Endocrinol* **1976**;82:617–630
5. Polhemus D. Ovarian maturation and cyst formation in children. *Pediatrics* **1953**;11:588–594
6. Merrill J. The morphology of the prepubertal ovary: relationship to the polycystic ovary syndrome. *South Med J* **1963**;56:225–231
7. Emans S, Goldstein D. *Pediatric and adolescent gynecology*, 3rd ed. Boston: Little Brown, **1990**;103:140–142
8. Cohen H, Tice H, Mandel F. Ovarian volumes measured by US: bigger than we think. *Radiology* **1990**;177:189–192
9. Surratt J, Siegel M. Imaging of pediatric ovarian masses. *RadioGraphics* **1991**;11:533–548

Book Review

Diagnostic Ultrasonics. Principles and Use of Instruments, 3rd ed. By W. N. McDicken. New York: Churchill Livingstone, 367 pp., 1991. $59

Although the radiologic literature—textbooks and journals alike—has been dominated recently by works on MR imaging, it would be unfortunate if practicing radiologists, sonographers, or radiology residents overlooked the pearl in the sonographic literature that is *Diagnostic Ultrasonics*. This is not a text on clinical sonography per se, but its value for the clinical ultrasound unit should not be underestimated. Do not be deceived by its relatively pedestrian-appearing title, for here is a wonderfully readable, comprehensive text that covers, in a superbly organized, lucid way, the physical principles of diagnostic sonography and practical aspects for optimal operation of sonographic imaging systems.

Written in a pedagogic style rare in medical texts, each of the book's 28 chapters is a concise but thorough discussion of one topic, organized in crisp outline form and summarized and referenced in equally concise fashion so that, at the end of each chapter, the reader retains a manageable number of useful gems directly applicable to the clinical ultrasound environment. Although the book has a logical progression of chapters, with each chapter building on the preceding chapters, even the novice in sonography will be comfortable reading chapters at random. Radiology residents beginning their sonographic training would, for example, be well served by spending an hour reading chapters 10–13 and 15 (fewer than 70 pages) detailing the design and use of real-time imaging systems and the causes of (and methods for elimination of) artifacts. Even experienced sonographers will find the text quite helpful as a reference, whether for a quick review of the physics of Doppler imaging or for a nice description of optimization of image quality that can be achieved by following clearly outlined steps in instrument adjustment.

The illustrations, paper, and binding are of top quality, particularly surprising given the relatively modest price for a hardcover medical text. I think that *Diagnostic Ultrasonics* is the most comprehensive, readable, and practically useful text on this subject available today. It is an indispensable introduction and reference text for any ultrasound section. I also recommend it highly to all radiology residents, if only for its outstanding sections on physics and instrument adjustments in clinical scanning.

H. Esterbrook Longmaid III
New England Deaconess Hospital
Boston, MA 02215

Case Report

Prolapsing Inverted Papilloma of the Prostatic Urethra: Diagnosis by Transrectal Sonography

Kathryn Occhipinti,[1] Rosalyn Kutcher,[1] and Ralph L. Gentile[2]

Diagnosis of obstructive lesions of the prostatic urethra on the basis of radiologic findings first became possible with the introduction of voiding cystourethrography.

In a 1970 review article, Downs [1] summarized 21 cases of congenital urethral polyps detected on voiding cystourethrograms and added these uncommon lesions to the differential diagnosis of obstruction of the bladder outlet in children. Since then, two reported cases of congenital urethral polyps in children have been diagnosed on the basis of transabdominal pelvic sonograms [2, 3]. In both cases, the polyps were visualized within the bladder lumen, and the true origin was confirmed with voiding cystourethrography and cystoscopy. Although an inverted papilloma of the bladder has been visualized with transabdominal pelvic sonography [4], we report the first case of this rare tumor of the prostatic urethra in an adult that was visualized during routine transrectal sonography for evaluation of prostatitis.

Case Report

The patient was a 40-year-old man with a 2-year history of perineal and urethral signs and symptoms attributed to chronic prostatitis. He had urethral pain after ejaculation, dull rectal and perineal pain, and occasional interruption of voiding associated with perineal pain. He had been treated with multiple antibiotics and antiinflammatory agents without improvement. Courses of prostatic massages and hot baths produced no benefit. Cultures of the urine and prostatic expressate were negative for bacteria. On physical examination, the prostate was slightly tender, but no fluid could be expressed. Transrectal sonography was performed with an Acuson 128 unit with 7.5-MHz transrectal transverse and longitudinal probes. The prostate was normal. A small polypoid mass 0.7 × 0.6 cm was seen at the bladder neck with a stalk extending into a slightly dilated prostatic urethra (Figs. 1A and 1B). Cystoscopy confirmed a polypoid structure arising from an extremely narrow, long stalk originating just to the left of the verumontanum. During instillation of fluid, this structure stretched proximally, extending to the neck of the bladder. It was removed endoscopically, and histologic examination showed that it was an inverted papilloma. No associated inflammation or malignant degeneration was evident.

The patient's signs and symptoms improved dramatically. He noted in particular a strong urinary stream, having assumed that his preoperative stream had been normal. He was able to ejaculate without any discomfort, and all other signs and symptoms progressively lessened.

Discussion

An inverted papilloma is a rare tumor of men 40–80 years old. The tumor has a predilection for the neck and trigone of the bladder, although less common areas of occurrence have been reported: the prostatic urethra, ureter, and renal pelvis. The origin of this tumor is debated, but a possible association with chronic infection or obstruction of the bladder outlet has been postulated [5]. In a review [6] of 50 patients at the Mayo Clinic who had inverted papilloma of the urinary tract, the most common symptoms were hematuria and obstruction of the bladder outlet.

Received November 12, 1991; accepted after revision December 26, 1991.

[1] Department of Radiology, Albert Einstein College of Medicine/Montefiore Medical Center, 111 E. 210th St., Bronx, NY 10467. Address reprint requests to R. Kutcher.

[2] Department of Urology, Albert Einstein College of Medicine/Montefiore Medical Center, 111 E. 210th St., Bronx, NY 10467.

AJR **159:93–94, July 1992** 0361–803X/92/1591–0093 © American Roentgen Ray Society

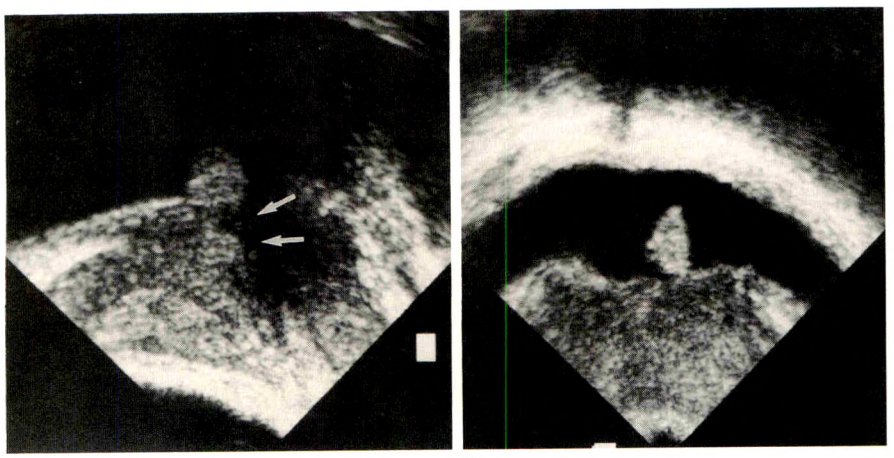


Fig. 1.—*A* and *B*, Longitudinal (*A*) and transverse (*B*) sonograms show a polyp along base of bladder at left posterior margin of neck of bladder. Polyp has a stalk (*arrows*) extending into prostatic urethra.

Histologically, these tumors show inversion of the usual structure of a papilloma, with complex invaginations of basal transitional epithelium and a fibrovascular stroma that is not central but is found only between the epithelial sheets. The lesion is covered by benign urothelium but may contain areas of cystitis cystica or squamous metaplasia [7]. Although inverted papillomas have been considered benign, one case of recurrence in the region of the prostatic urethra has been reported [6]. Other investigators have described an association with transitional cell carcinoma. Malignant transformation of papillomas located in the neck of the bladder and the renal pelvis also have been reported [8–10]. These cases show the prudence of considering inverted papillomas as low-grade transitional cell carcinomas and treating them with transurethral resection and periodic follow-up.

In our patient, the papilloma was discovered incidentally during transrectal scanning for symptoms of prostatitis. The papilloma was in a prolapsed position near the neck of the bladder, but the appearance of linear echogenic soft tissue suggested a stalk within the prostatic urethra. Previous transabdominal sonograms, which showed polyps within the bladder lumen, could not show a specific location because of limitations in resolution. Transrectal sonography of the prostate has gained acceptance in the diagnostic evaluation of prostatic malignancy, prostatic inflammation, and infertility. Transrectal sonography also can play an integral role in the evaluation of nonspecific perineal symptoms or obstruction of the bladder outlet. Detailed images of the neck of the bladder and the prostatic urethra enable better anatomic localization of pathologic changes. This may obviate further radiographic procedures, especially in the younger patient.

REFERENCES

1. Downs RA. Congenital polyps of the prostatic urethra. *Br J Urol* **1970**;42:76–85
2. Mueller B, Jequier S, Laberge I. Ultrasonographic diagnosis of an obstructive polyp of the bladder neck. *J Ultrasound Med* **1984**;3:521–522
3. Caro PA, Rosenberg HK, Synder HM III. Congenital urethral polyp. *AJR* **1986**;147:1041–1042
4. Govaerts J, Beelaerts W, Van Camp K. Inverted papilloma of the bladder: a report of two typical cases, including sonographic figures. *Acta Urol Belg* **1983**;51:504–509
5. Catalona WJ. Bladder cancer. In: Gillenwater JY, ed. *Adult and pediatric urology*. St. Louis: Mosby Year Book, **1991**:1139–1140
6. DeMeester LJ, Farrow GM, Utz DC. Inverted papillomas of the urinary bladder. *Cancer* **1975**;36:505–513
7. Kashgarian M, Rosai J. Urinary tract. In: Rosai J, ed. *Ackerman's surgical pathology*. St. Louis: Mosby, **1989**:901–902
8. Altaffer LF III, Wilkerson SY, Jordan GH, Lynch DF. Malignant inverted papilloma and carcinoma in situ of the bladder. *J Urol* **1982**;128:816–818
9. Uyama T, Shoosuke M. Inverted papilloma with malignant change of the renal pelvis. *Urology* **1981**;17:200–201
10. Lazarevic B, Garret R. Inverted papilloma and papillary transitional cell carcinoma of the urinary bladder. *Cancer* **1978**;42:1904–1911

Pictorial Essay

Diseases of the Lumbar Spine: Findings on Fat-Suppression MR Imaging

Robert D. Tien,[1] Erik M. Olson,[2] and Chi S. Zee[3]

Fat-suppression MR techniques have been useful in imaging both the head and neck and the orbit. The lumbar spine is not as complex as the head and neck and does not contain as much fat as the orbit. Nevertheless, high signal from epidural and marrow fat in the lumbar spine can make it difficult to detect and define pathologic processes. In addition, the administration of gadopentetate dimeglumine can cause some infectious and neoplastic lesions of the spine to become isointense with fat on T1-weighted images. Compared with conventional MR imaging without fat suppression, contrast-enhanced fat-suppression MR imaging can better differentiate these enhancing lesions from surrounding fat. In this essay, we illustrate the findings of fat-suppression MR imaging in a variety of diseases of the lumbar spine.

The multiplanar ability, superior resolution, and excellent tissue characterization of MR imaging makes this an extremely valuable technique in evaluating lumbar spine disease. Fat within the epidural space and bone marrow has high signal intensity on T1-weighted images (e.g., 800/20/2 [TR/TE/excitations]) and occasionally obscures lesions. Compared with conventional T1-weighted MR imaging, fat-suppression T1-weighted images better delineate lesions surrounded by fat and better detect abnormal enhancement adjacent to structures with a high fat content [1]. The fat suppression of our illustrations was achieved by either the ChemSat sequence or by the spectral presaturation with inversion-recovery (SPIR) sequence in a 1.5-T supraconducting magnet. In the absence of any gradients, the ChemSat sequence suppresses fat and excites it preferentially (compared with water) with a narrow-band pulse. It then dephases the fat's signal with added gradients and immediately continues with the imaging sequence [1]. The SPIR sequence begins with a narrow-bandwidth 180° fat-selective pulse that inverts only the magnetization of the protons on fat molecules. After a delay period (TI), which is chosen so that the longitudinal component of the magnetization of the fat protons equals zero, a conventional spin-echo pulse sequence is obtained [2]. Both techniques achieve excellent fat suppression, are easily affected by the magnetic field inhomogeneity, and provide highly comparable imaging qualities.

Clinical Applications

Postoperative Spine

In patients who have had prior lumbar spine surgery and recurrent pain, enhanced MR imaging helps differentiate avascular, unenhancing residual herniated disk or a free disk fragment from vascular, enhancing epidural fibrotic scar. With fat-suppression images, Bobman et al. [3] demonstrated improved delineation of contrast-enhancing scar adjacent to epidural fat, and we have found postoperative enhancement of intrathecal nerve roots to be more obvious (Fig. 1). However, unenhanced images without fat suppression are necessary to differentiate residual disk or free fragment from

Received July 29, 1991; accepted after revision January 22, 1992.
[1] Department of Radiology, Box 3808, Duke University Medical Center, Durham, NC 27710. Address reprint requests to R. D. Tien.
[2] Department of Radiology, University of California, San Diego, Medical Center, 225 Dickinson St., San Diego, CA 92103.
[3] Los Angeles County–University of Southern California Imaging Science Center, 1744 Zonal Ave., Los Angeles, CA 90033.

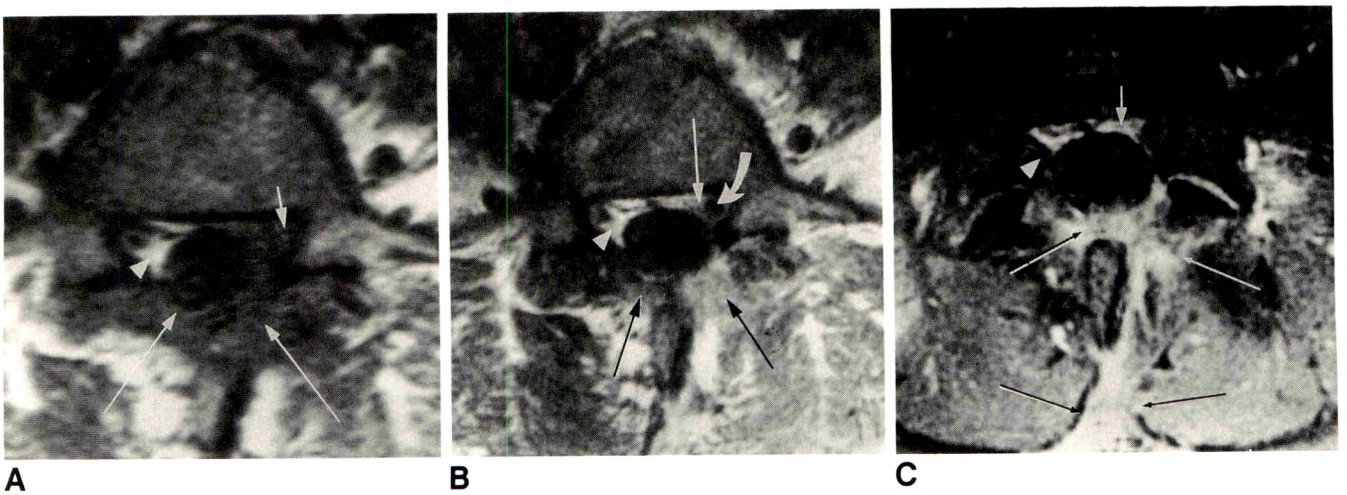


Fig. 1.—55-year-old man with previous left-sided hemilaminectomy and diskectomy who now had recurrent pain.
A, T1-weighted axial MR image (800/20/2) shows low-signal-intensity tissue filling left lateral recess (*short arrow*) and posterior epidural space (*long arrows*). High-signal fat is seen in right epidural space (*arrowhead*).
B, Low-signal-intensity tissue at epidural space mildly enhances (*straight arrows*) on T1-weighted axial image obtained after administration of contrast material. Unenhancing nerve root is clearly visible (*curved arrow*). However, enhanced anterior epidural tissue has high signal similar to that of epidural fat (*arrowhead*) and is not well differentiated.
C, Fat-suppression contrast-enhanced T1-weighted MR image successfully suppresses epidural fat signal (*arrowhead*) and can show enhancing scar tissue (*long arrows*) much better than images without fat suppression can. Enhancement at anterior epidural space (*short arrow*) is a mixture of enhancement of posterior vertebral venous plexus and scar. Artifact from gut motion is accentuated on fat-suppression images.

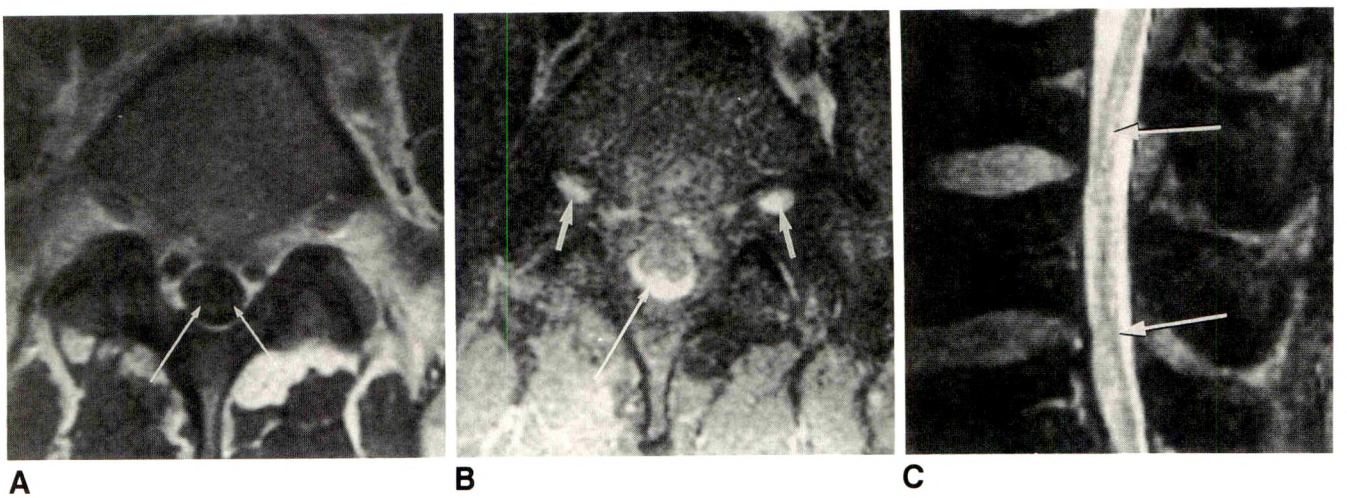
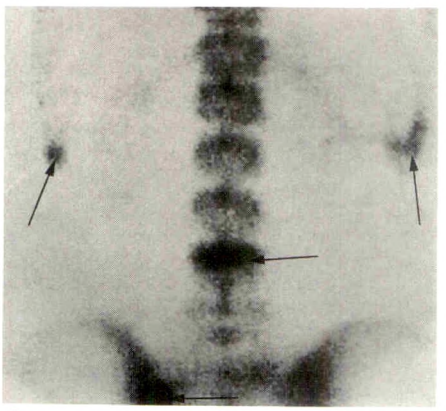


Fig. 2.—23-year-old man with back pain and previous myelographic procedures.
A, T1-weighted axial MR image (800/20/2) obtained after administration of contrast material only vaguely suggests abnormal enhancement of nerve roots (*arrows*).
B, Fat-suppression T1-weighted MR image obtained after administration of contrast material shows striking enhancement of clumped nerve roots within thecal sac (*long arrow*). Normally enhanced nerve root ganglia (*short arrows*) are also much brighter on fat-suppression image.
C, Gradient-recalled echo sagittal MR image (350/15/1) clearly shows abnormally thickened nerve roots (*arrows*). On the basis of imaging findings, arachnoiditis was diagnosed; CSF findings were in concurrence.

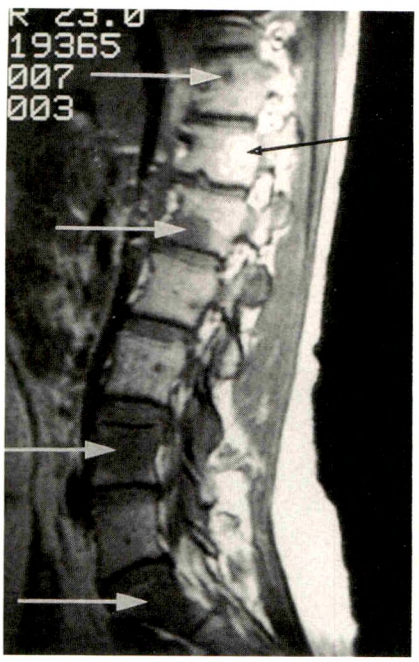
epidural fat, since both have low signal intensity on fat-suppression images.

Arachnoiditis

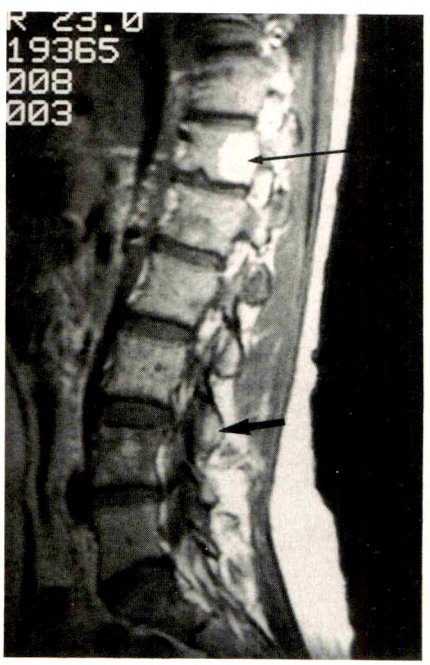
In patients with arachnoiditis, subtle contrast enhancement of the intrathecal nerve roots is more clearly visible on fat-suppression images than on regular enhanced T1-weighted images (Fig. 2). This improved clarity probably is due to a shift of the gray scale's dynamic range following fat suppression. Clustered, enhancing nerve roots could indicate a low-grade arachnoiditis and could explain the nonspecific post-operative pain some patients experience. It is important to note that enhancement occasionally is seen in patients who have not had back surgery or lumbar puncture.



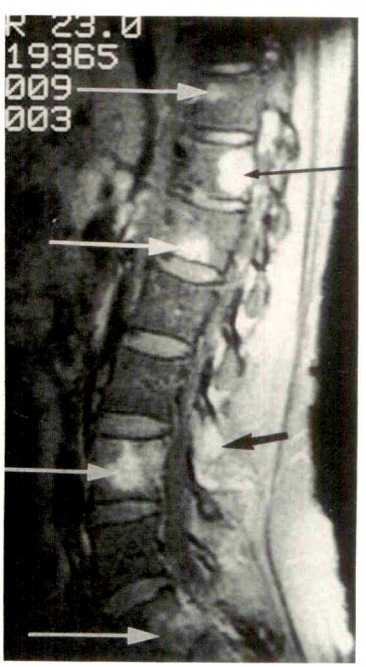
A



B



C



D

Fig. 3.—22-year-old woman with metastatic lung cancer.

***A*, ^{99m}Tc bone scan shows abnormal uptake in L4 vertebral body, ribs, and right sacroiliac joint (*arrows*).**

***B–D*, Sagittal MR images obtained 1 week after bone scan clearly show advantage of fat-suppression enhanced images. Unenhanced T1-weighted image (600/20/2) (*B*) shows areas of low signal intensity in sacrum and L4, L1, and T11 vertebral bodies (*white arrows*) and area of slightly increased signal intensity posteriorly within T12 vertebral body (*black arrow*). Enhanced T1-weighted image without fat suppression (*C*) shows decreased contrast between enhancing lesions and surrounding marrow. Lesion at T12 (*long thin arrow*) and spinous process of L3 also enhance. Contrast-enhanced T1-weighted image with fat suppression (*D*) clearly shows enhancing lesions. Sacrum; L3 spinous process; and L4, L1, and T11 vertebral body lesions (*white arrows*, *short black arrow*) all represent metastatic lung cancer, most of which cannot be seen on bone scan. T12 lesion (*long black arrow*), which has high T1 signal and enhances with contrast medium, most likely represents a hemangioma. Although bone scan did not show all spinal lesions, it can serve as a survey technique for entire body skeleton. MR can reveal more detailed information for a smaller area of interest**

Tumors

High-signal fatty bone marrow may be isointense with enhancing neoplasm on contrast-enhanced T1-weighted images and may potentially obscure or alter lesion size. Fat-suppression images eliminate possible confusion between which focal areas within the marrow are fat and which are metastatic lesions. In our cases of metastatic disease, fat-suppression enhanced images have shown better lesion discrimination and delineation (Fig. 3). Several enhanced areas of the posterior elements are also easier to discern on fat-suppression images. The gadopentetate dimeglumine–enhanced T1-weighted images without fat suppression provide nearly as much information as do the corresponding fat-suppressed images. Therefore, in the evaluation of metastatic disease, enhanced imaging without fat suppression could almost be eliminated except for the use of unenhanced T1-weighted imaging for the baseline study.

The fat-suppression technique also provides more descriptive enhanced images of lumbar ependymoma and schwannoma than do images without fat suppression (Figs. 4 and 5). The abnormally enhancing mass is clearly visible, and the margins between the lesion and bone marrow are more distinct and revealing.

Osteomyelitis, Diskitis, and Myositis

In patients with osteomyelitis, diskitis, or myositis, fat-suppression images show improved delineation and define the margins of infectious foci (Fig. 6). Enhanced infected areas are more conspicuous on these images than they are on images without fat suppression, and the epidural and paravertebral components of inflammatory tissues are more distinguishable on enhanced fat-suppression images.

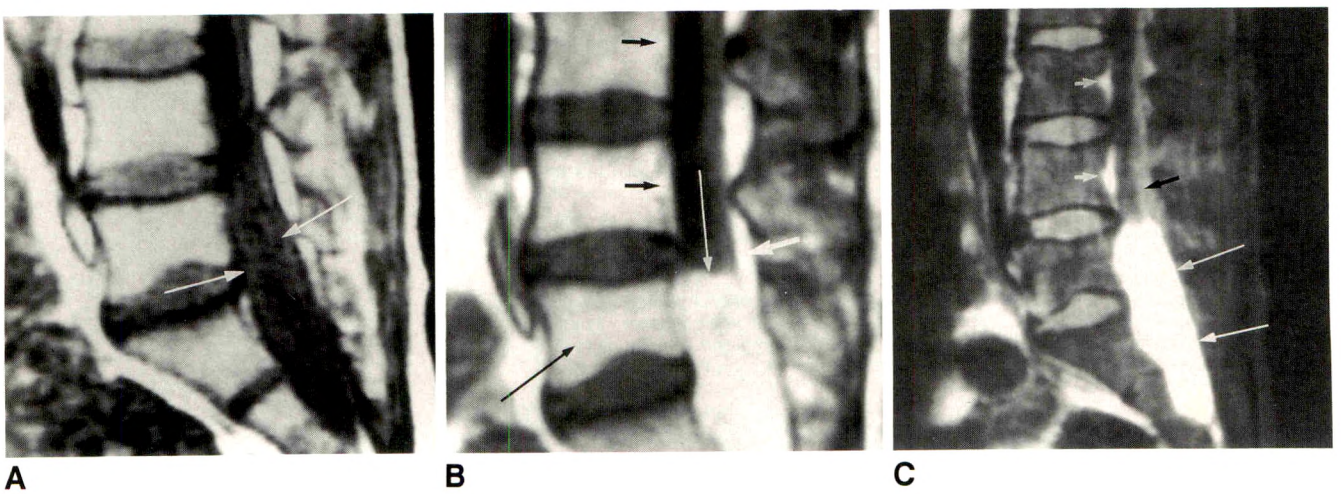


Fig. 4.—32-year-old man with ependymoma of lumbar spine.
A, T1-weighted sagittal MR image (800/20/2) shows relatively homogeneous mass in distal thecal sac (*arrows*), which is slightly hyperintense relative to CSF. Margins of mass are difficult to delineate.
B, On contrast-enhanced T1-weighted MR image, mass (*long white arrow*) enhances brightly, but is isointense with adjacent epidural fat (*short white arrow*) and slightly hyperintense relative to vertebral bodies (*long black arrow*). Epidural posterior vertebral venous plexus also enhances (*short black arrows*).
C, On fat-suppression contrast-enhanced T1-weighted MR image, not only is mass (*long white arrows*) exquisitely shown, but it is also easily distinguished from epidural fat (*black arrow*) and vertebral bodies. Enhanced epidural venous plexus at L3–L4 is more visible (*short white arrows*). However, anterior border of enhanced mass blends with enhanced epidural venous plexus at L5 and S1–S2.

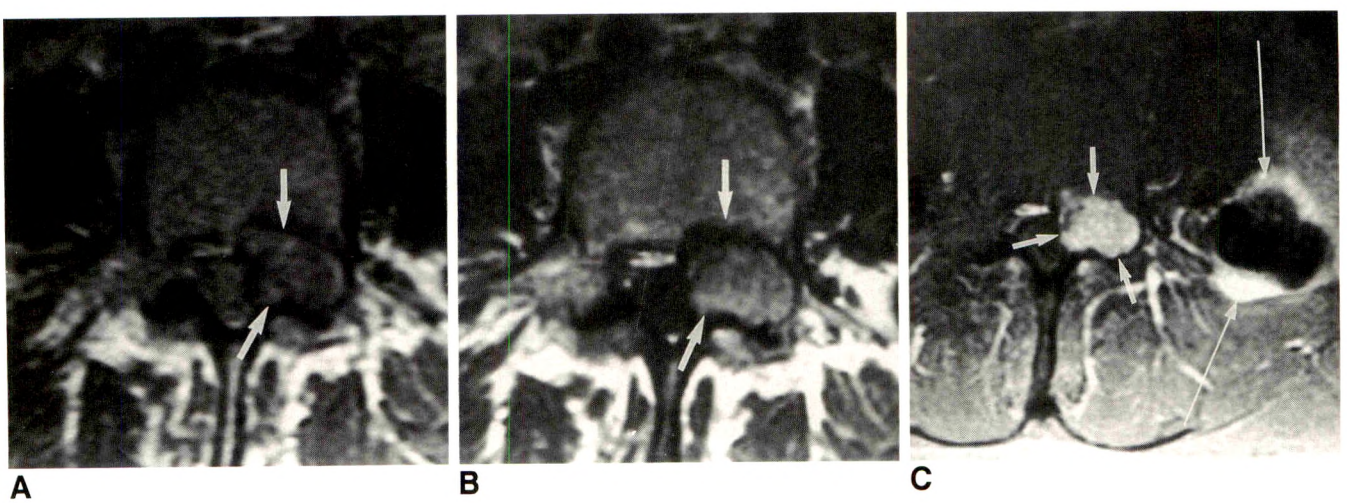


Fig. 5.—43-year-old man with left leg pain.
A, T1-weighted axial MR image (600/20/1) shows round mass (*arrows*) that is isointense but has margins that are not sharply delineated.
B, T1-weighted MR image after administration of contrast material shows mildly enhanced mass (*arrows*). Signal intensity of mass is still very similar to that of adjacent bone marrow.
C, Fat-suppression contrast-enhanced T1-weighted MR image shows enhancing mass (*short arrows*) extremely well. Margin of mass is clearly depicted. High-signal fat adjacent to bowel (*long arrows*) is not suppressed because of local magnetic field inhomogeneity caused by air in bowel. Pathologic diagnosis of this mass at surgery was schwannoma.

Congenital Lesions

In patients with spinal dysraphism, identifying the position of the tethered cord is important for planning therapy. In the case of lipomyelomeningocele, the high-signal intrathecal lipoma sometimes obscures the exact position of the tip of the posteriorly tethered cord on conventional T1-weighted MR images (Fig. 7). The fat-suppression technique suppresses the fat signal, and the resulting images successfully show the tip of the tethered cord and clearly define the extent of the lipoma.

Conclusions

Fat suppression requires excellent magnetic field homogeneity in order to prevent unequal fat suppression. The large

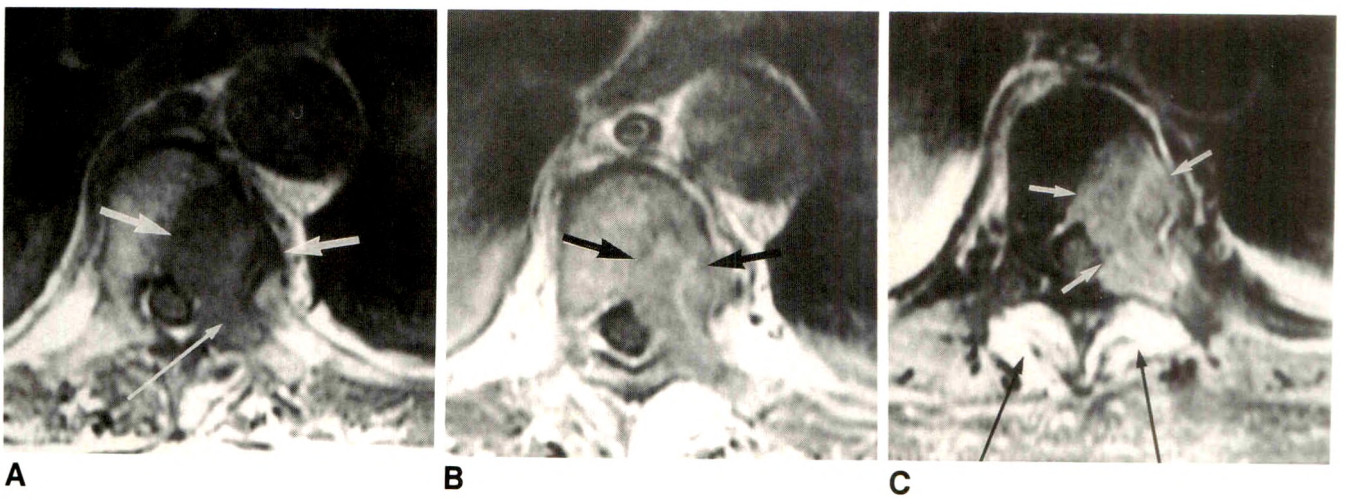


Fig. 6.—43-year-old woman with staphylococcal sepsis and back pain.

A, T1-weighted axial MR image (600/20/1) of thoracic spine shows low-signal-intensity area (*short arrows*) involving left vertebral body and left pedicle (*long arrow*).

B, T1-weighted axial MR image after administration of contrast material shows low-signal area enhances inhomogeneously (*arrows*). Lesion has signal similar to that of normal right vertebral bone marrow. Margin of lesion cannot be seen clearly.

C, Fat-suppression contrast-enhanced T1-weighted MR image clearly defines margin of enhancing lesion (*short arrows*). Also, enhancing tissue (*long arrows*) of paraspinous process is easily identifiable. On the basis of imaging findings, diagnosis was osteomyelitis with thecal sac compression and inflammatory myositis.

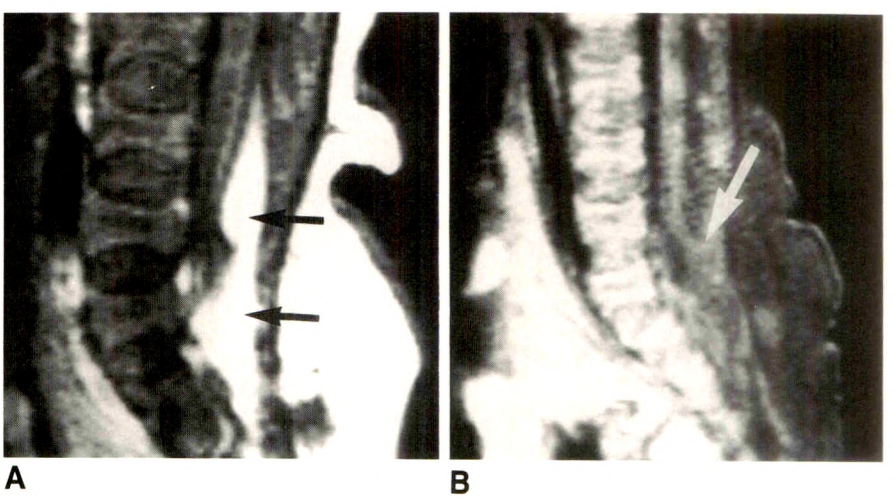


Fig. 7.—5-year-old boy with a lipomyelomeningocele of lumbar spine.

A, T1-weighted oblique sagittal MR image (800/20/2) shows intrathecal large bright mass (*arrows*), which may be contiguous with subcutaneous fat. Tip of lower cord is not well defined.

B, Fat-suppression T1-weighted midsagittal MR image obtained after patient was repositioned shows markedly suppressed signals of epidural fat and intrathecal mass. These results indicate that intrathecal mass is a lipoma. Because surrounding high signal was eliminated, lower end of cord, which was tethered at L4–L5 interspace (*arrow*), is clearly identifiable. This imaging finding was confirmed by surgery.

field of view required to image the lumbar spine increases the risk of magnetic field inhomogeneity. Bulk magnetic susceptibility artifacts, which can result in uneven fat suppression in areas of changing imaging volume such as the neck, are less of a problem in the lumbar spine [1]. However, magnetic susceptibility artifacts from foreign objects near the spine (e.g., metallic fixation devices of spines, intraspinal shunt tubing, or epidural electrodes) can seriously degrade fat-suppression images. Also, fat-suppression techniques cannot produce as many slices as can techniques without fat suppression, and they are more affected by patients' motion as well as motion from vascular pulsation. Despite these limitations, satisfactory-quality fat-suppression images of the lumbar spine can be obtained in most patients in a reasonable time frame.

REFERENCES

1. Tien RD. Fat-suppression MR imaging in neuroradiology: techniques and clinical application. *AJR* **1992**;158:369–379
2. Oh CH, Hilal SK, Cho ZH. Selective partial recovery (SPIR) in steady state for selective saturation magnetic resonance imaging (MRI). In: *Book of abstracts: Society of Magnetic Resonance in Medicine 1988*. Berkeley, CA: Society of Magnetic Resonance in Medicine, **1988**:1042
3. Bobman SA, Atlas SW, Listerud J, Grossman RI. Postoperative lumbar spine: contrast-enhanced chemical shift MR imaging. *Radiology* **1991**;179:557–562

Book Review

The Traumatized Hand and Wrist. Radiographic and Anatomic Correlation. By Louis A. Gilula. Philadelphia: Saunders, 235 pp., 1992. $65

Injuries to the hand and wrist are among the most commonly encountered traumas. This superb book is the compilation by Louis Gilula of more than a decade's experience. His seminal articles on posttraumatic ligamentous instabilities of the wrist (*Radiology* 1978;129:641) and the analytic approach to and case exercises in carpal injuries (*AJR* 1979;133:503) were immediately recognized as classic works of investigation and radiologic-pathologic correlation. The importance of the principles expounded by Dr. Gilula can be measured by noting the standing-room-only attendance at the many refresher courses he has given at annual meetings of the American Roentgen Ray Society and the Radiological Society of North America.

Dr. Gilula is the editor of this book and one of the authors of 10 of the 13 chapters. Six contributors (four radiologists and two orthopedic/hand surgeons) collaborated on the remaining three chapters. All are acknowledged authorities on hand injuries.

The book is organized into 13 chapters. The first six deal primarily with hand injuries, and the remaining seven concern injuries of the wrist. Chapter 1, "Imaging of the Hand and Wrist," is an overview of diagnostic imaging, including plain radiography, arthrography, CT (that may be performed in any desired imaging plane) and MR imaging. Notably absent from this chapter is any mention of polydirectional tomography. I find this technique useful, particularly in the examination of patients who are wearing casts. I hope that a future edition of the book will address this deficiency.

Chapter 2, "Radionuclide Bone Imaging in Surgical Problems of the Hand," describes the technique of three-phase bone scanning, which the author thinks is useful for detecting areas of abnormal activity that then can be studied further by using other imaging techniques. A variety of abnormalities are described. One topic that probably deserves greater attention is evaluation of acute scaphoid fractures before radiographs show any changes. In the author's view, bone scans show abnormalities within hours of the fracture in these patients. Chapter 3, "Soft Tissue Evaluation in Trauma," contains excellent photographs and line drawings. The tables on abnormalities of the various fat planes and soft-tissue regions of interest are extremely valuable. The two authors of this chapter were also coauthors of an excellent article on this subject published in the *AJR* (1984;142:781).

Chapter 4, "Anatomy Affecting the Metacarpal and Phalangeal Bones of the Hand," is an exceptionally detailed treatise on the subject. It is better organized than most anatomy books. Because of the extensive detail, many radiologists may prefer to skim this chapter and refer to it when specific questions of anatomy arise. This chapter may be of more interest to hand surgeons. Each section is subdivided into parts on bones, muscles and tendons, and joints. For bones, the articular surfaces of the base and head and the shaft are described. The muscles and tendons are each discussed as to origin, anatomic course, insertion, and function. The sections on the joints are further subdivided into general information, ligaments and joint capsules, and extracapsular support. Chapter 5, "Phalangeal Fractures and Dislocations," and Chapter 6, "Metacarpal Fractures and Dislocations," are organized into subsections that include introductory remarks and specific injuries. Each of the sections on specific injuries is further subdivided into general information, mechanism of injury, and anatomy. This approach is quite useful in establishing clinical-radiologic correlation.

Chapter 7, "Wrist Trauma: Roentgenographic Analysis," is a reiteration of the principles formulated by Gilula and expanded on in his lectures. The chapter discusses fractures, dislocations, and carpal instabilities. It repeats some of the information found in chapter 1. I think that in a subsequent edition of this book, this chapter should be placed near the beginning of the book with the general information. Chapter 8, "Wrist Ligament Anatomy and Biomechanics," contains excellent anatomic descriptions and illustrations. This chapter, too, appears out of place and should be near the front of the book. Chapters 9 through 13 describe isolated carpal fractures, multiple carpal fractures, fractures and fracture-dislocations of the distal radius and ulna with and without carpal fracture, carpal fracture-dislocations, and static carpal ligament instabilities, respectively. As with the chapters on phalangeal and metacarpal injuries, these are also divided into introductory remarks and specific remarks about the injury. They include general information; mechanism of injury; and associated injuries to the volar, dorsal, radial, ulnar, and intraarticular ligaments.

Despite the minor shortcomings of misplacement of the chapters on technique and principles and on the anatomy of the ligaments of the wrist, this is a superb book. The images and artwork are excellent. This book should become a standard reference for imaging of hand and wrist injuries, particularly in any department that examines large numbers of patients who have these injuries. In addition, orthopedic surgeons will find this book extremely useful. I highly recommend it.

Richard H. Daffner
Allegheny General Hospital
Pittsburgh, PA 15212

Case Report

Ewing's Sarcoma of the Hand

Eva M. Escobedo,[1] Ann G. Bjorkengren,[1] and Sheila G. Moore[2]

The hand is an uncommon location for Ewing's sarcoma [1–7]. When Ewing's sarcoma does occur in the hand or foot, its radiographic features often differ from the more typical appearance of this tumor in other locations [5]. We report a case of Ewing's sarcoma of the hand with unusual radiographic features and illustrate the findings from a second patient.

Case Report

A previously healthy 8-year-old girl presented 3 days after she had injured her right hand while playing on jungle gym bars. Although the immediate pain was mild, swelling at the base of the third finger was persistent.

Physical examination revealed a firm but nontender circumferential swelling about the proximal phalanx of the third finger of the right hand. The range of motion of adjacent metacarpophalangeal and proximal interphalangeal joints was slightly limited. No other abnormalities were noted. The leukocyte count was 6.2×10^9/l and the erythrocyte sedimentation rate was 6 mm/hr, both within normal limits.

A radiograph (Fig. 1) revealed a lytic, expansile lesion involving the entire proximal phalanx of the third finger with an associated circumferential soft-tissue mass. A pathologic fracture was noted near the base of the phalanx. Minimal periosteal reaction was present along the posterolateral border. A ^{99m}Tc-methylene diphosphonate bone scan showed increased uptake of radionuclide only in the abnormal phalanx. On the basis of the imaging studies, the differential diagnosis included an indolent infectious process such as tuberculosis, coccidioidomycosis, or chronic bacterial osteomyelitis; or a neoplastic disease such as Ewing's sarcoma, lymphoma, or, less likely, osteosarcoma.

An open surgical biopsy was performed. Microscopic examination of the specimen showed a tumor composed of tightly packed cells with small, round-to-oval, uniform nuclei with a stippled chromatin pattern and small nucleoli (Fig. 1B). Periodic acid–Schiff (PAS) stains with and without diastase predigestion showed abundant cytoplasmic glycogen. Immunohistochemical studies showed no reactivity for PD7 (common leukocyte antigen), synaptophysin, chromogranin, or keratin. The only positive immunostaining was for vimentin. The immunologic and histologic findings supported a diagnosis of Ewing's sarcoma.

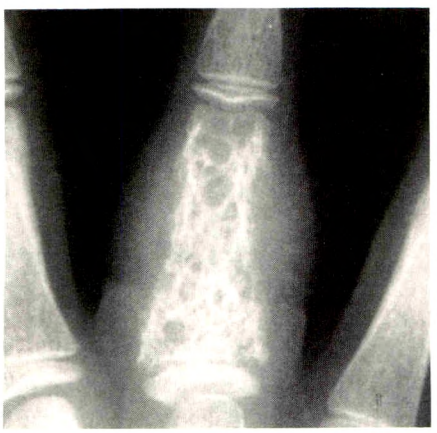
Discussion

Ewing's sarcoma is the second most common malignant primary bone tumor of childhood and adolescence. It may affect any bone, but is frequent in the femur, ilium, and tibia. Involvement of the hand is relatively rare, with (to our knowledge) only 27 cases of Ewing's sarcoma of the hand reported [1–7]. Of these, 11 cases involved a phalanx, 13 cases involved a metacarpal, and in three cases the tumor location within the hand was not specified. Only four of these 27 cases were reported in the radiologic literature.

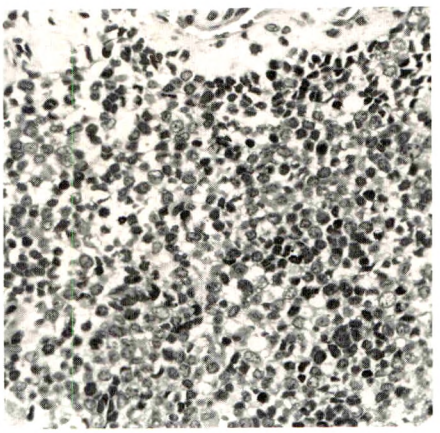
When it occurs in the hand, Ewing's sarcoma may have radiographic features that differ from the more characteristic findings of permeative bone destruction and laminated or spiculated periosteal reaction [5]. These features, shown in our patient (Fig. 1), include bony expansion, a cystic or honeycomb pattern, and lack of laminated or spiculated periosteal reaction. A second patient with Ewing's sarcoma of the hand (Fig. 2) also had marked bony expansion and absence of an aggressive periosteal reaction.

Received November 12, 1991; accepted after revision January 2, 1992.
[1] Department of Radiology, Stanford University Medical Center, Stanford, CA 94305.
[2] Department of Radiology, Lucille Salter Packard Children's Hospital, Stanford, CA 94305.

 0361–803X/92/1591–0101 © American Roentgen Ray Society



A



B

Fig. 1.—*A*, Anteroposterior radiograph of lesion in proximal phalanx. Expansile, "honeycomb" pattern involves full extent of bone distal to physis.

B, Photomicrograph of biopsy specimen shows sheets of undifferentiated, small, round cells. (H & E, original magnification ×200)



Fig. 2.—Anteroposterior radiograph of Ewing's sarcoma in fifth metacarpal of a 5-year-old boy.

In a report from the Intergroup Ewing Sarcoma Study, which included 377 patients, 10 with a lesion of the foot and two with a lesion of the hand, expansion, lack of laminated or spiculated periosteal reaction, and absence of cortical thickening (as seen in both our cases) was seen more commonly in Ewing's sarcoma of the hand or foot than in Ewing's sarcoma of other locations. Pathologic fracture, and a cystic or honeycomb pattern, as seen in one of our patients (Fig. 1), also was more common in the hand and foot. The combination of permeative destruction and irregular areas of sclerosis, seen in the other patient (Fig. 2), and the soft-tissue mass, as seen in both cases, was reported to be a common radiographic feature at all locations [5].

The differential diagnosis of this lesion includes osteomyelitis [8], particularly the spina ventosa of tuberculosis or coccidioidomycosis. In the proper clinical setting, such as in the hand-foot syndrome of sickle cell disease, bone infarction also could be considered; especially in the patient in whom no cortical destruction was noted. Knowledge of the often atypical radiographic appearance of Ewing's sarcoma of the hand is important in ensuring a prompt and accurate diagnosis, leading to the appropriate, usually surgical, therapy. The mistaken diagnosis of infection could lead to undesirable delays in treatment, potentially worsening the prognosis for the patient.

REFERENCES

1. Baird RJ, Krause VW. Ewing's tumor: a review of 33 cases. *Can J Surg* **1963**;1:136–140
2. Dahlin DC. *Bone tumors*, 3rd ed. Springfield, IL: Thomas, **1978**:274–287
3. Euler E, Wilhelm K, Permanetter W, Kreusser T. Ewing's sarcoma of the hand: localization and treatment. *J Hand Surg* **1990**;15:659–662
4. Netherlands Committee on Bone Tumors. *Radiological atlas of bone tumors*, vols. 1 and 2. Baltimore: Williams and Wilkins, **1966**(1):151 and **1973**(2):XII
5. Reinus WR, Gilula LA, Shirley SK, Askin FB, Siegal GP. Radiographic appearance of Ewing sarcoma of the hands and feet: report from the Intergroup Ewing Sarcoma Study. *AJR* **1985**;144:331–336
6. Resnick DK, Kyriakos M, Greenway GD. Tumors and tumor-like lesions of bone: imaging and pathology of specific lesions. In: Resnick DK, Niwayama G, eds. *Diagnosis of bone and joint disorders*, 2nd ed. Philadelphia: Saunders, **1988**:3845–3855
7. Strege DW, Hanel DP, Vogler C, Schajowicz F. Ewing sarcoma in a phalanx of an infant's finger. *J Bone Joint Surg [Am]* **1989**;71-A:1262–1265
8. Marcove RC, Charosky CB. Phalangeal sarcomas simulating infections of the digits: review of the literature and report of four cases. *Clin Orthop* **1972**;83:224–231

Three-Dimensional Time-of-Flight MR Angiography with a Surface Coil: Evaluation in 12 Subjects

Lloyd E. Hendrix[1]
Julie A. Strandt
David L. Daniels
Leighton P. Mark
Jessica A. Borne
Leo F. Czervionke
Victor M. Haughton
Alan L. Williams

We compared three-dimensional time-of-flight MR angiograms obtained with head coils and then with surface coils in five patients with intracranial vascular lesions and in seven normal volunteers to determine if imaging of intracranial vascular anatomy could be improved with the use of a surface coil. Visualization of small peripheral vessels was consistently better with a surface coil than with a head coil at identical small fields of view (FOVs). The surface-coil technique allowed small-FOV imaging of peripheral vascular lesions with higher spatial resolution and signal-to-noise ratio similar to that of large-FOV head-coil images. The use of a surface coil introduced the problem of signal falloff; centrally located vessels were visualized as well or better when a standard head coil was used.

We conclude that surface-coil MR angiography can serve as a useful adjunct to routine head-coil MR angiography in the evaluation of peripheral vascular abnormalities.

***AJR* 159:103–106, July 1992**

For MR angiography (MRA) to compare favorably with conventional angiography it must provide optimal spatial and contrast resolution, accurate portrayal of vascular morphology with minimal artifacts, and ideally some degree of selectivity of vessel visualization in various planes. An area of vascular anatomy that is of considerable clinical concern but that can be difficult to image with MRA is the intracranial circulation [1–6]. For imaging this anatomy, use of a small field of view (FOV) should increase spatial resolution; however, if the FOV is decreased and the number of pixels is unchanged (to increase resolution), the signal-to-noise ratio (SNR) decreases and increased signal averaging is required to retain the same SNR.

Since local coils have proved useful in small-FOV, high-resolution imaging [7], we investigated the use of a surface coil for MRA of intracranial vessels. To our knowledge, MRA with a surface coil has not been used previously to evaluate intracranial blood vessels.

Subjects and Methods

Twelve subjects (seven normal volunteers, three patients with arteriovenous malformations [AVMs], and two patients with venous angiomas) were examined with MR imaging at 1.5 T and commercially available software (Signa, General Electric Medical Systems, Milwaukee, WI). The diagnoses were based on results of conventional angiography in four patients (three patients with AVMs, one with a venous angioma) and on results of CT and conventional spin-echo (SE) MR imaging in one case of venous angioma.

All subjects were required to wear earplugs because of the high noise level during MRA sequences. Owing to the limits of small-FOV imaging, the patient was positioned so that the region of interest was placed as close to the isocenter of the gantry as possible. In normal subjects, the region of interest was considered to be the anterior or lateral half of the head at the level of the circle of Willis. A 3-in. (7.6-cm) planar surface coil (General Electric) was

Received December 2, 1991; accepted after revision February 10, 1992.

[1] All authors: Department of Radiology, Medical College of Wisconsin, Froedtert Memorial Lutheran Hospital, 9200 W. Wisconsin Ave., Milwaukee, WI 53226. Address reprint requests to L. E. Hendrix.

0361–803X/92/1591–0103
© American Roentgen Ray Society

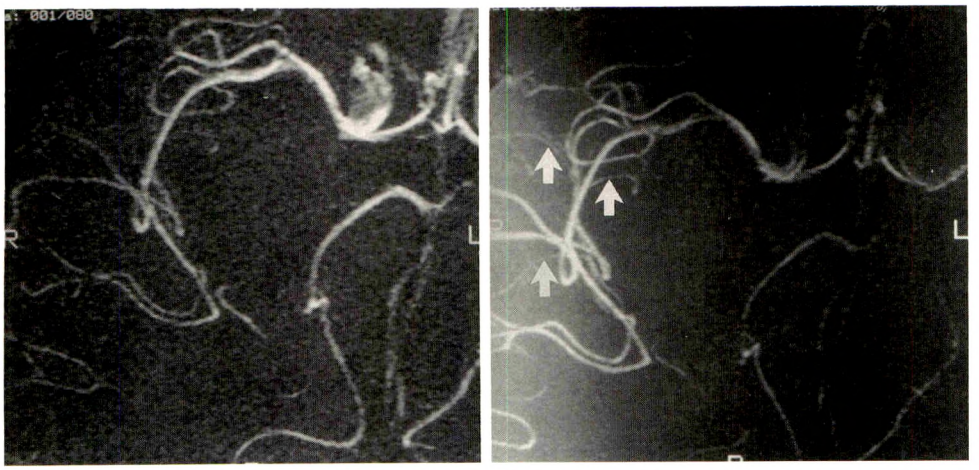


Fig. 1.—*A* and *B*, 8-cm field-of-view axial collapsed 3D time-of-flight imaging of head shows normal middle cerebral artery on images obtained with standard head coil (*A*) and with 3-in. (7.6-cm) surface coil placed over right temporal region (*B*). Visualization of small arterial branches (*arrows*) is improved in *B*. Conversely, deeper vessels are seen better with head coil (*A*). Because spatial resolution is identical, improved visualization of small vessels in *B* is a function of increased signal-to-noise ratio in near field.

placed over the temporal region or the orbit, or a 5-in. (12.7-cm) (General Electric) or 6-in. (15.2-cm) (Medical Advances, Inc., Milwaukee, WI) planar coil was placed over the midline of the face. In the patients with vascular lesions, the surface coil was placed over the head or face so as to lie as near as possible to the region of interest. A coronal SE T1-weighted localizer image, 300/20/1 (TR/TE/excitations), was obtained. A three-dimensional (3D) time-of-flight (TOF) angiography sequence consisting of 60 or 28, 1-mm-thick slices was then performed with the volume of axially acquired data containing the region of interest. All subjects were studied with both head and surface coils. For each normal volunteer, head- and surface-coil images were obtained with the same parameters. Imaging parameters included a TR of 40 msec (system specified minimum of 43 msec at 8-cm FOV), a system-selected TE (5–7 msec, depending on FOV and matrix), two excitations, a 20° flip angle, a 192 or 128 × 256 matrix, and an 8-, or 10-, or 12-cm FOV. Patients with vascular lesions were examined first with the standard head-coil technique by using a 22-cm FOV; these images helped determine optimal coil placement for surface-coil imaging at a 10- or 12-cm FOV. An antialiasing technique (for reduction of phase and frequency wraparound) and flow compensation were used for all sequences. Both patients with venous angiomas were imaged after IV administration of gadopentetate dimeglumine in a dose of 0.1 mmol/kg body weight. In four subjects, a spatial presaturation pulse was applied to diminish the signal intensity of extracranial tissues in the near field of the surface coil. Other techniques used to diminish the near-field signal intensity included shifting the FOV, filtration (Image Intensity Correction, General Electric), and postprocessing with volume-rendering software (General Electric). The acquisition time ranged from 7 to 16.5 min depending on the matrix size and number of slices.

From each sequence, a stack of axial images was obtained. This 3D data set was then subjected to a standard maximum-intensity-projection (MIP) algorithm [8] to create a "collapsed" axial image and a series of coronal and sagittal projections in various degrees of obliquity. All MR images were evaluated in a retrospective, nonblinded fashion.

Results

High-resolution images of the circle of Willis and especially of smaller, more peripheral vessels of normal subjects were obtained with each of the surface-coil placements. Surface-coil images of small peripheral vessels were consistently superior to those obtained with a standard head coil (Fig. 1). In some cases, small peripheral vessels could be seen only with surface-coil imaging. The anatomy of each of the AVMs and one venous angioma was seen in greater detail with appropriate surface-coil placement (Figs. 2 and 3). The other venous angioma, while identifiable on magnitude images (the individual axial images of the 3D data set) of series obtained with either the head or surface coil, was only faintly visible on the axial collapsed image of the head-coil series and was inapparent on the collapsed image of the surface-coil series.

In general, the signal intensity of flow within vessels diminished with increasing distance from the surface coil. We found that more centrally located intracranial vessels were seen as well or better when a standard head coil was used (Fig. 1).

The high signal of tissues closest to the surface coil (due to the greater sensitivity of the reception field near the coil) in some cases made it difficult to window/level images for viewing and filming and obscured intravascular signal in certain projections. We found this problem could be reduced by several imperfect methods. Repositioning the coil by distancing it slightly from the head surface reduced superficial signal intensity but, not surprisingly, also resulted in reduced signal intensity of the underlying anatomy of interest. We found it difficult to move the FOV so as to precisely exclude only tissues near the coil that were not of interest. Image intensity correction by means of filtering evened out signal intensity but at the cost of slight although visible increased background noise. We obtained only partial suppression of near-field high signal with application of a selective saturation pulse over the extracranial soft tissues nearest the surface coil. We found postprocessing (i.e., deletion of data outside the volume of interest from the 3D data set before MIP ray tracing) was effective for reprojected images.

Discussion

The MIP technique used to produce projection images provides excellent contrast but results in a slight false reduction in vessel size [9]. Nonetheless, flow within relatively small arteries was consistently well seen in our study. Our particular

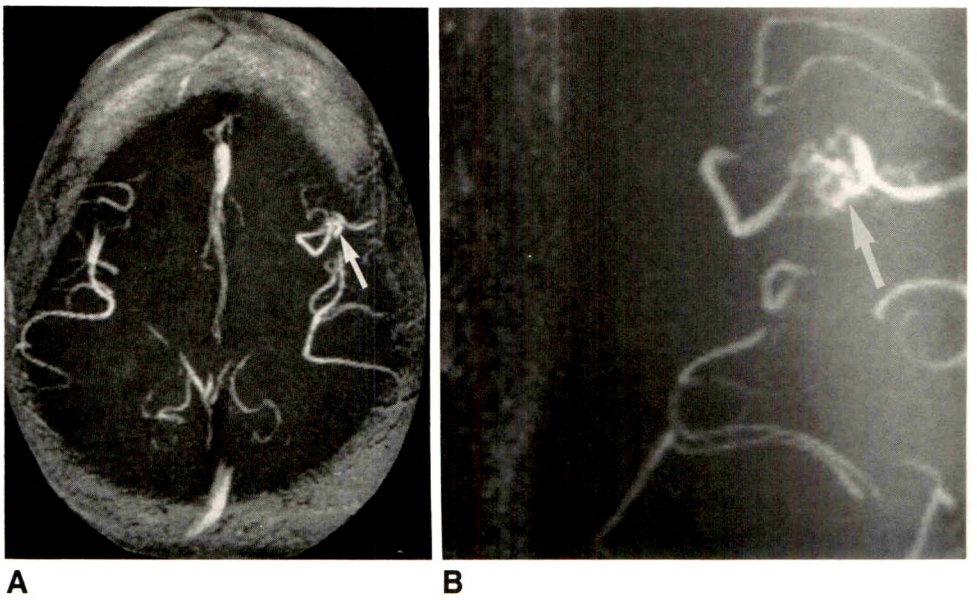


Fig. 2.—*A* and *B*, Axial collapsed 3D time-of-flight imaging of head shows small left frontal arteriovenous malformation nidus (supplied by middle cerebral artery) on images obtained with 22-cm field of view (FOV) and a head coil (*A*) and with 12-cm FOV and a 7.6-cm planar surface coil placed over left convexity (*B*). With surface coil, signal-to-noise ratio is comparable to that with head coil, and spatial resolution is increased. Nidus (*arrows*) is 1 cm in diameter and could be easily overlooked in *A*. This lesion was verified with conventional angiography.

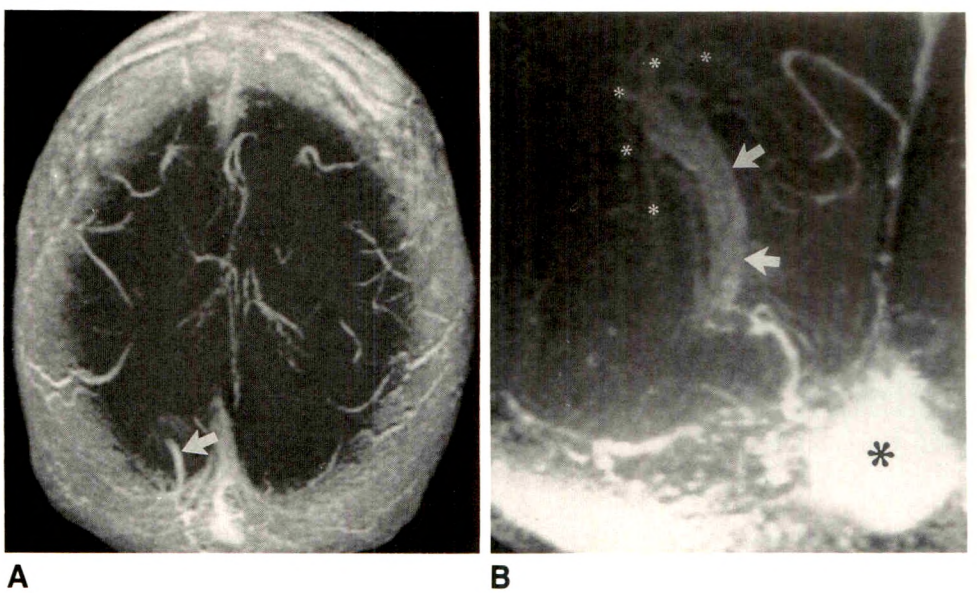


Fig. 3.—Gadopentetate dimeglumine–enhanced axial collapsed 3D time-of-flight imaging of head shows occipital venous angioma on images obtained with 22-cm field of view (FOV) and a head coil (*A*), and with 10-cm FOV and a surface coil placed over occiput (*B*). Caput medusae (*small asterisks*) and varix (*arrows*) are seen well. Lower signal intensity of lesion relative to arteries is probably caused by slower flow. Varix measures 2 cm in axial plane. *Large asterisk* = superior sagittal sinus.

imaging parameters were chosen with the intention of optimizing visualization of intracranial arterial anatomy [10]. Slow flow within aneurysms or diseased arteries might not be seen optimally without changing certain parameters (i.e., reducing the flip angle or increasing the TR), and flow within veins can be better seen when using TOF MRA or phase-contrast MRA with low-velocity encoding. Because the function of a surface coil is independent of these variables, the same advantages in spatial resolution and SNR are maintained irrespective of chosen parameters and pulse sequence.

In addition to the increase in SNR and spatial resolution, surface-coil imaging has the further benefit of decreasing the volume from which signal is detected, thereby reducing contributions to the signal from structures outside the region of interest. Image degradation due to "wraparound" and motion artifacts generated by extracranial structures are thus diminished [7].

The change in the sensitivity of the reception field of the surface coil as a function of distance from the coil resulted in certain limitations of our technique common to surface-coil imaging in general [7]. We made several conclusions regarding methods to diminish excessive near-field brightness. Distracting the coil away from high-signal, fatty superficial tissues is a straightforward although limited solution, in that moving a surface coil away from the region of interest tends to defeat the coil's purpose. Image intensity correction by filtering probably should be limited to situations in which considerable superficial fat is situated between the coil and the region of interest since this technique increases noise in the image. The shape and orientation of a saturation pulse (linear and orthog-

onal) do not correspond to the contour of the head. For this reason, only a portion of near-field brightness could be suppressed without extending the saturation pulse into the region of interest. In our experience, postprocessing was most effective in diminishing signal intensity of structures superimposed over the region of interest in reprojected images, although it was limited by software that could prescribe only a rectangular volume of interest.

Signal dropoff in the far field was also a limiting factor. On the basis of our findings, it is unlikely that imaging of deep midline lesions such as galenic AVMs or brainstem vascular malformations, for example, can be improved on by surface-coil support.

It is not entirely clear why one venous angioma failed to reconstruct with the MIP algorithm. A likely explanation is that along the projected rays traversing the lesion, the maximum-intensity voxels lay outside the lesion. Because only the maximum signal intensity along each projection ray can be taken to create a maximum-signal-intensity projection image, a lesion not of sufficiently greater signal intensity than background will fail to reconstruct [9, 11]. In this case, certain factors could have contributed to this scenario. The flow velocity (and thus the signal intensity) in the lesion was probably lower than in surrounding arteries. The lesion was in proximity to orbital and skull base fat, and the ambient signal intensity of near-field background tissues was high. In retrospect, filtration may have been useful. This case serves to underscore the need to examine the individual magnitude images making up the 3D data set since they may have information that is not apparent on the MIP reprojections.

A number of methods may potentially improve the technique of surface-coil MRA. Dedicated surface coils for various anatomic regions and improved coil design to minimize intrinsic coil noise could improve image quality. In particular, the advent of phased-array coils promises the SNR and resolution of a small surface coil over FOVs normally associated with whole head or body imaging with no increase in imaging time [12]. Study of these various methods is ongoing.

On the basis of our experience, we believe that surface-coil MRA can complement head coil MRA to better show peripheral vascular abnormalities.

ACKNOWLEDGMENTS

We thank General Electric Corporate Research and Development, C. L. Dumoulin, and S. P. Souza for use of their MIP program.

REFERENCES

1. Ruggieri PM, Laub GA, Masaryk TJ, Modic MT. Intracranial circulation: pulse-sequence considerations in three-dimensional (volume) MR angiography. *Radiology* **1989**;171:785–791
2. Edelman RR, Wentz KU, Mattle HP, et al. Intracerebral arteriovenous malformations: evaluation with selective MR angiography and venography. *Radiology* **1989**;173:831–837
3. Dumoulin CL, Cline HE, Souza SP, Wagle WA, Walker MF. Three-dimensional time-of-flight magnetic resonance angiography using spin saturation. *Magn Reson Med* **1989**;11:35–46
4. Ross JS, Masaryk TJ, Modic MT. Intracranial aneurysms: evaluation by MR angiography. *AJNR* **1990**;11:449–456
5. Marchal G, Bosmans H, Van Fraeyenhoven L, et al. Intracranial vascular lesions: optimization and clinical evaluation of three-dimensional time-of-flight MR angiography. *Radiology* **1990**;175:443–448
6. Edelman RR, Mattle HP, O'Reilley GV. Flow dynamics in the circle of Willis: evaluation by selective MRA. *Stroke* **1990**;21:55–56
7. Kneeland JB, Hyde JS. High-resolution MR imaging with local coils. *Radiology* **1989**;171:1–7
8. Rossnick S, Laub G, Braeckle R, et al. Three dimensional display of blood vessels in MRI. In: *Proceedings of the IEEE Computers in Cardiology Conference.* New York: Institute of Electrical and Electronic Engineers, **1986**:193–196
9. Anderson CM, Saloner D, Tsuruda JS, et al. Artifacts in maximum-intensity-projection display of MR angiograms. *AJR* **1990**;154:623–629
10. Turski PT, ed. *Vascular magnetic resonance imaging: Signa applications guide*, vol. 3. Milwaukee: General Electric Medical Systems, **1990**
11. Laub G. Displays for MR angiography. *Magn Reson Med* **1990**;14:222–229
12. Roemer PB, Edelstein WA, Hayes CE, Souza SP, Mueller OM. The NMR phased array. *Magn Reson Med* **1990**;16:192–225

MR Imaging of Symptomatic Peripheral Vascular Malformations

Kevin M. Rak[1]
Wayne F. Yakes[1,2]
Robin L. Ray[2]
James N. Dreisbach[2]
Steve H. Parker[2]
James M. Luethke[1]
A. Thomas Stavros[2]
Dick D. Slater[1]
Brian J. Burke[1]

We performed a retrospective study of symptomatic peripheral vascular malformations to determine if MR imaging can be used to distinguish slow-flow venous malformations from high-flow arteriovenous malformations and arteriovenous fistulas. Twenty-seven MR examinations in 25 patients with malformations outside the CNS were reviewed. Sixteen venous malformations, nine arteriovenous malformations, and two arteriovenous fistulas were included. In all cases, the MR findings were correlated with the results of angiography. The distinction between slow-flow venous malformations and high-flow arteriovenous malformations and arteriovenous fistulas was made primarily on T2-weighted MR images, which showed high signal intensity in venous malformations and flow voids in high-flow lesions. In addition to the previously described MR features of venous malformations (serpentine pattern with septations, associated muscle atrophy, and typical T1 and T2 signal intensities), several new MR features were apparent. Venous malformations had a propensity for multifocal involvement (37%), orientation along the long axis of extremities or affected muscles (78%), and adherence to neurovascular distributions (64%). Prominent subcutaneous fat was commonly seen adjacent to the malformation. MR images of arteriovenous malformations and arteriovenous fistulas also commonly showed muscle atrophy and subcutaneous fatty prominence.

Our results show that slow-flow venous malformations can be distinguished from high-flow arteriovenous malformations and fistulas on the basis of spin-echo MR signal characteristics. The associated imaging characteristics help in the differential diagnosis in problematic cases.

***AJR* 159:107–112, July 1992**

Symptomatic vascular malformations include venous malformations, arteriovenous malformations (AVMs), arteriovenous fistulas (AVFs), and mixed lesions. Historically, angiography and venography have provided the most specific diagnostic information, but MR has recently been shown to be useful in evaluating these lesions [1–7]. MR depicts the anatomic relationships between vascular malformations and adjacent organs, nerves, tendons, and muscles, thereby providing significant help in therapeutic planning, be it surgical or ethanol endosurgical ablation [8–13].

The goals of the study were twofold: (1) to evaluate the usefulness of MR in distinguishing slow-flow lesions (venous malformations) from high-flow lesions (AVMs and AVFs) and (2) to describe additional MR features of these various malformations that, to the best of our knowledge, have never before been published. Twenty-seven MR examinations in 25 patients with symptomatic peripheral malformations were reviewed. CNS lesions were not included. The MR findings were correlated with arteriographic findings in all cases and with venographic findings in 16.

Received April 5, 1991; accepted after revision February 4, 1992.

The opinions and assertions contained herein are the private views of the authors and are not to be construed as official or as reflecting the views of the Department of the Army or Department of Defense.

[1] Department of Radiology, Fitzsimons Army Medical Center, Aurora, CO 80045-5001. Address reprint requests to K. M. Rak.

[2] Radiology Imaging Associates, P. C., Swedish Medical Center, Englewood, CO 80110.

0361–803X/92/1591–0107
© American Roentgen Ray Society

Materials and Methods

Over a 20-month period, 25 patients (15 females, 10 males) 8–63 years old (mean, 23 years) were referred to our institutions for evaluation and treatment of vascular malformations outside the CNS. Sixteen venous malformations were studied: three in the upper extremity, two in the face or neck, and 11 in the lower extremity (two of which extended into the pelvis or buttocks). Nine AVMs were evaluated: three in the pelvis, two in the face or neck, two in the paraspinal region, one in the lower extremity, and one in the upper extremity. Both AVFs studied were in the lower extremity: one was a single congenital AVF and the other was in a patient who had numerous posttraumatic AVFs.

Twenty-seven MR examinations were performed; two patients had separate vascular malformations in anatomically unrelated regions, necessitating two angiographic and MR studies in each of these patients. Equipment included 1.5-T Signa (General Electric, Milwaukee, WI), 0.5-T Vista (Picker International, Highland Heights, OH), and 0.5-T Magnetom (Siemens, Iselin, NJ) imaging systems. In all but one of the examinations, at least two orthogonal planes of acquisition were used. Each lesion was imaged with spin-echo (SE) relative T1 weighting, 500–1000/15–20 (TR range/TE range), and more T2 weighting (1500–2500/20–90). Gradient-echo (GRE) sequences were obtained in 18 cases: 13 by using a single-slice technique, 20–50/11–15/10–30° (TR/TE/flip angle), and five by using a multiplanar technique (500–1000/20–30/10–30°).

Each vascular malformation was evaluated by using biplane selective arteriography. In addition, each of the 14 venous malformations localized to an extremity was studied by using closed-system venography, and two face and neck venous malformations were studied by using direct puncture venography. On the basis of angiographic criteria, the lesions were categorized as venous malformations, AVMs, or AVFs. Venous malformations were characterized arteriographically as having normal inflow arteries, a normal intervening capillary bed, and contrast pooling in dilated stagnant venous spaces in the late venous phase. AVMs were characterized arteriographically as having enlarged inflow arteries with prompt shunting into tortuous draining veins. No intervening capillary bed was present. AVFs likewise lack an intervening capillary bed, but usually have a single arteriovenous connection [13]. At our institutions, ethanol embolotherapy is the primary means of treatment for symptomatic vascular malformations; therefore, surgical correlation in all cases was not possible. However, in seven of the patients with venous malformations, biopsy was performed: in each case the histologic findings corresponded to the MR and angiographic interpretations.

The MR images were interpreted retrospectively by three radiologists who had full knowledge of the angiographic findings. The MR and angiographic studies were interpreted together, in hopes of delineating additional imaging characteristics that would make it possible to distinguish low-flow from high-flow vascular malformations, and expanding on differential diagnostic features. Subsequently, once the MR criteria were established for distinguishing venous malformations from AVMs and AVFs, all 27 MR examinations were reanalyzed by two other radiologists. These radiologists categorized the lesions on the basis of our previously described criteria, but were otherwise blinded, having no knowledge of angiographic results or clinical data.

Results

Of the 16 venous malformations evaluated, all had similar MR signal characteristics: predominantly decreased signal intensity compared with fat on T1-weighted images, hyperintense signal compared with fat on T2-weighted images, and increased signal intensity compared with skeletal muscle on both T1- and T2-weighted images (Fig. 1). With T1 weighting, scattered small foci of higher signal intensity, comparable to the intensity of fat, were commonly noted. GRE images in 10 lesions corresponded to long TR/TE SE sequences, with increased signal found in the abnormal vascular elements of the venous malformation. Low-signal linear striations were uniformly seen within the lesions with both SE and GRE sequences.

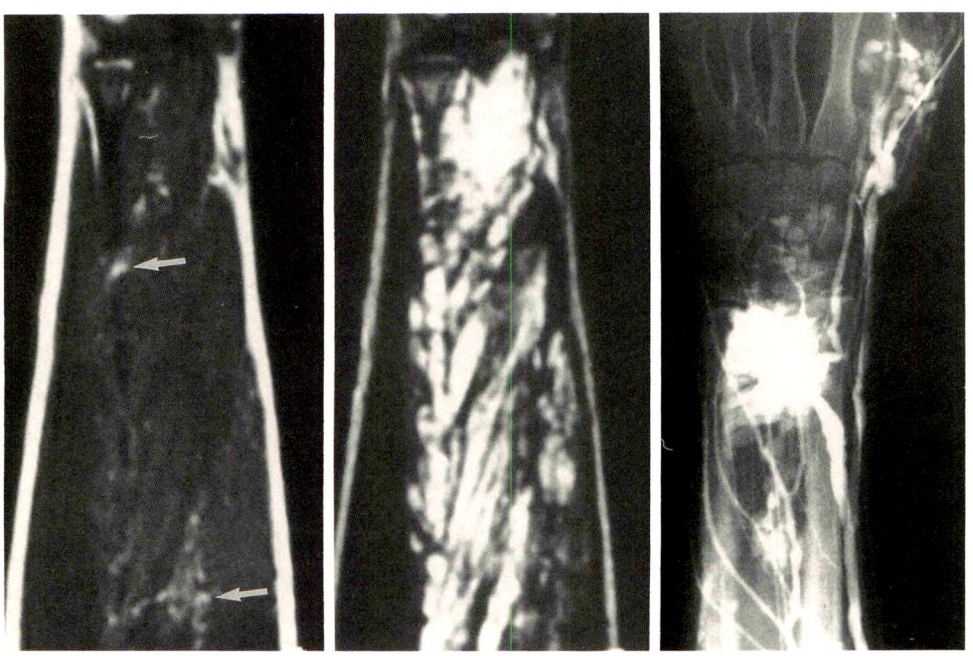


Fig. 1.—Typical MR characteristics of slow-flow venous malformation in forearm of 11-year-old boy.

***A*, T1-weighted SE (600/20) coronal MR image shows that involved area has signal intensity slightly higher than that of skeletal muscle but less than that of subcutaneous fat. Areas of higher T1 signal intensity may be related to fatty replacement (*arrows*).**

***B*, T2-weighted SE (2000/80) coronal MR image shows higher signal intensity of venous malformation relative to muscle and subcutaneous fat.**

***C*, Corresponding closed-system venogram shows extent of lesion is better defined with MR than with venography, because of incomplete contrast opacification of lesion.**

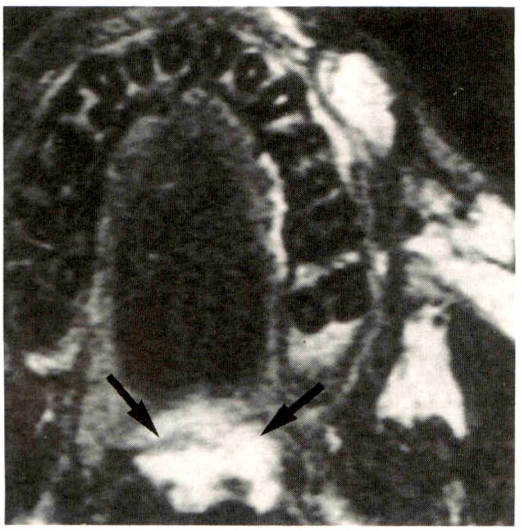


Fig. 2.—Multifocal venous malformation in a 23-year-old man. T2-weighted (2200/90) axial MR image shows anatomically separate focus in soft palate/uvula (*arrows*) that was not detected with arteriography. Also, note involvement of left gingiva.

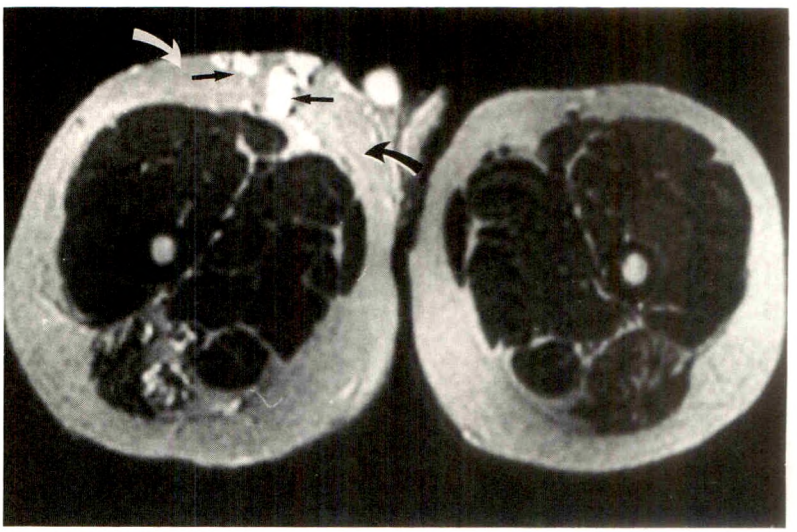


Fig. 3.—Asymmetric fatty prominence associated with venous malformation in a 47-year-old man. T2-weighted (2000/80) axial MR image of thighs shows normal left thigh and asymmetric prominence of subcutaneous fat (*curved arrows*) associated with venous malformation (*straight arrows*) in anterior subcutaneous fat of right thigh.

In five of the 16 cases, fatty infiltration or replacement in the involved or adjacent musculature was present. In no case was a prominent feeding artery or draining vein detected. In three cases, phleboliths were detected; these correlated with calcifications seen on plain films. In four cases, signal voids larger than typical linear striations were seen within the vascular elements and no corresponding phleboliths were detected on plain films. Thirteen of the 16 lesions had muscular or fascial involvement, whereas three lesions were limited solely to the subcutaneous fat. On MR imaging, two of the 13 lesions with muscular or fascial involvement also had infiltration of the associated tendons. One lesion had an intramedullary component within the femur, as noted on both MR and arteriography. In six of the 16 venous malformations, smaller, secondary sites of involvement were detected and shown to be anatomically separate from the primary focus. We determined that these venous malformations were multifocal in distribution (Fig. 2). Of the five venous malformations in which images of the contralateral extremity were available, hypertrophic subcutaneous fat was present on the affected side in four cases (Fig. 3).

Eleven of the 14 venous malformations in the extremities were oriented along the long axis of the extremity, paralleling fascial planes (Fig. 4). Of these 14 lesions, nine followed an identifiable neurovascular distribution (two along the radial distribution, two along the sciatic distribution [14], two along the anterior tibial distribution, two along the posterior tibial distribution, and one along the peroneal distribution). The adjacent vascular distributions were not involved (Fig. 4).

In nine of the 11 high-flow vascular malformations (AVMs and AVFs) imaged, the main MR feature on SE sequences was the presence of flow-related signal voids (Figs. 5A and 5B). An exception was in a patient with a paraspinal AVM. She had MR imaging after several unsuccessful operations and subsequent radiation therapy. These previous treatments

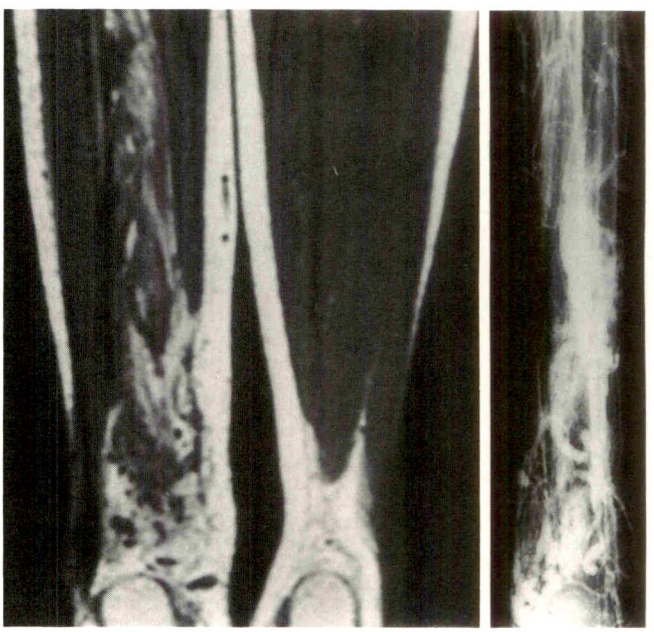


Fig. 4.—Ancillary characteristics of venous malformation in right calf of a 21-year-old woman.

A, T1-weighted (600/20) coronal MR image shows orientation of venous malformation along long axis of right lower extremity and strict adherence to peroneal venous distribution, sparing anterior and posterior tibial compartments. Subcutaneous fat is also asymmetrically prominent along medial aspect of affected limb.

B, Corresponding closed-system venogram shows adherence of venous malformation to peroneal venous distribution.

were thought to account for the lesion's atypical MR appearance: small central flow voids and a larger surrounding area of fibrous scar. In another patient, metallic artifacts from surgical clips obscured visualization of an arteriovenous fis-

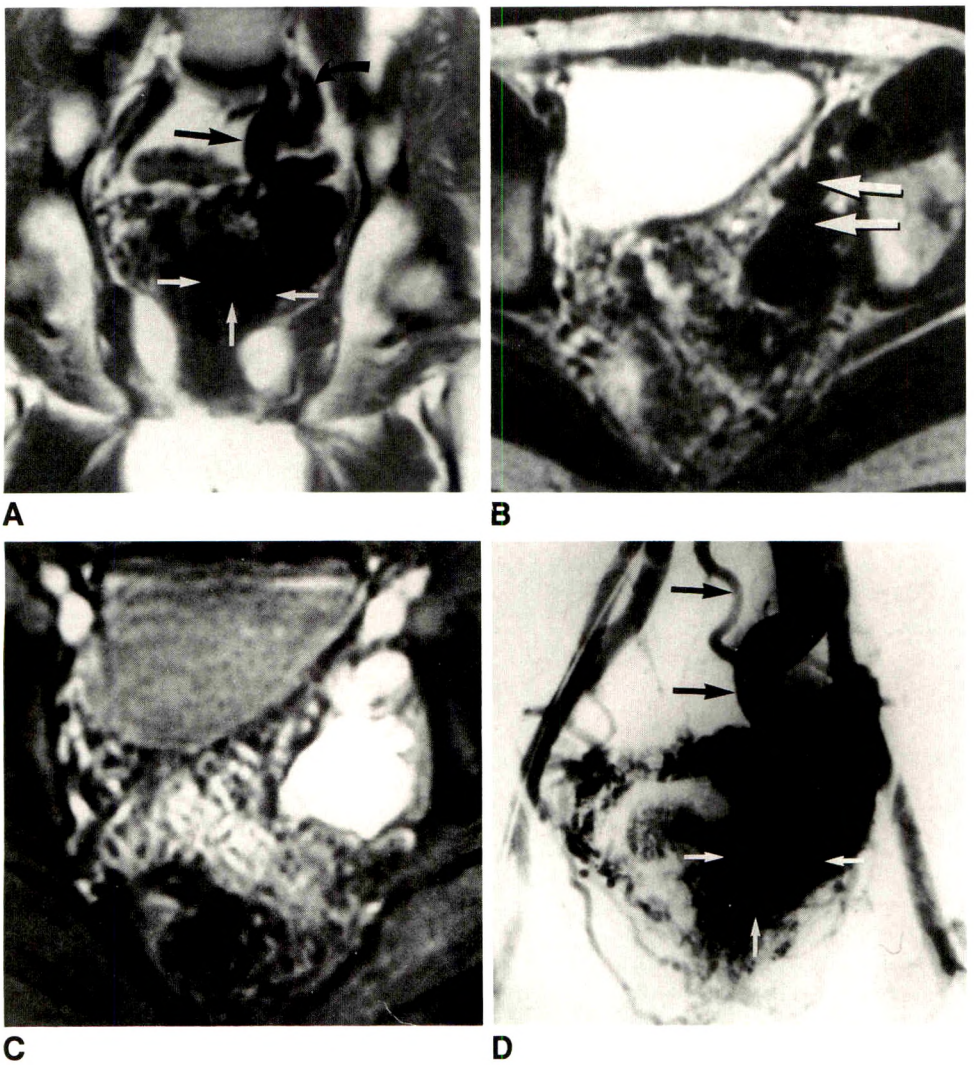


Fig. 5.—Typical MR characteristics of a high-flow lesion in a 50-year-old man with pelvic arteriovenous malformation.

***A*, T1-weighted SE (600/20) coronal MR image shows prominent flow voids in nidus (*white arrows*) of arteriovenous malformation, and tortuous feeding artery (*straight black arrow*) and dilated draining vein (*curved arrow*) proximal to nidus.**

***B*, T2-weighted (2500/80) axial MR image shows persistence of flow voids (*arrows*) within malformation.**

***C*, Corresponding gradient-echo (50/13/20°) axial MR image shows high signal intensity within areas of void on SE images, indicating that areas are flow related.**

***D*, Corresponding subtraction angiogram, arteriographic phase, shows enlarged arterial feeders (*black arrows*) and large vascular nidus (*white arrows*).**

tulous connection. In each of the remaining nine patients with AVMs or AVFs with no previous surgical intervention, prominent flow voids were seen on T1- and T2-weighted SE sequences. By contrast, in the eight patients in whom GRE images were obtained, these areas had higher signal intensity (Fig. 5C). Arteriographic correlation was provided in all cases (Fig. 5D). The single-slice and multiplanar GRE techniques were not used concurrently; thus, a direct comparison of these techniques was not possible.

In seven of the 11 patients with AVMs or AVFs, dilated feeding arteries and draining veins, commonly tortuous, were detected proximal to the abnormal vascular connections (Fig. 5A). Other than by following the larger inflow and outflow vessels to their site of origin or drainage, SE or GRE sequences could not be used to accurately distinguish the smaller arteries from veins. Although phase imaging was not used, this technique might be able to provide this information. Of four patients with AVMs or AVFs in the extremities, two had fatty infiltration of adjacent musculature. In nine patients with AVMs or AVFs in whom the contralateral extremity was also imaged, six had asymmetric prominence of subcutaneous fat on the affected side.

On the basis of these MR characteristics (T2 signal intensity, presence or absence of dilated feeding arteries or draining veins, orientation, multifocality), 26 of the 27 vascular malformations were correctly characterized by the second (blinded) group of the radiologists as being low flow or high flow. The only error was in the paraspinal AVM, which was atypical in appearance, presumably as a result of the patient's previous treatment.

Discussion

Symptomatic vascular malformations make up a spectrum of vascular anomalies. Venous malformations are postcapillary dilated venous spaces typified by stagnant flow, lack of normal venous valves, and absence of arteriovenous shunting. They have commonly been referred to in the literature as hemangiomas. However, on the basis of differences in cellular characteristics, endothelial hyperplasia and regression, and clinical behavior, we concur with the work of Mulliken et al. [15–17] and believe that hemangiomas of infancy and venous malformations are separate and distinct vascular anomalies.

Further, unlike venous malformations, on MR imaging, hemangiomas consistently have high-flow signal voids within the lesion. This has been observed by us and by others [7]. AVMs are also congenital lesions with arteriovenous shunting without an intervening capillary bed. AVFs may be congenital or posttraumatic and also have high-flow shunting similar to that of AVMs. In contrast to AVMs, usually only a single arteriovenous communication is present in AVFs. However, in a long-standing posttraumatic AVF, neovascular recruitment of multiple arteries can simulate an AVM near the arteriovenous connection [18, 19].

Our results show that slow-flow venous malformations can consistently be distinguished from the high-flow AVMs and AVFs on the basis of MR findings. All 16 venous malformations had predominantly high signal intensity on long TR/TE SE sequences. In contrast, all AVMs and AVFs that had not been treated before MR imaging had mainly signal voids on all SE sequences. These flow voids are attributed to both time-of-flight phenomena and turbulence-related dephasing.

On MR imaging, venous malformations have a characteristic serpentine pattern with internal striations and septations and associated focal muscle atrophy. The described signal intensity is greater than that of skeletal muscle on both T1- and T2-weighted images, but less than that of subcutaneous fat on T1 sequences and greater than that of fat on T2 sequences. Pathologically, these findings have been correlated with fibrofatty septa between endothelium-lined vascular channels. The high signal intensity seen on SE sequences with long TR/TE has been attributed to stagnant flow in these abnormal vascular spaces [2, 3, 5]. Newly described MR characteristics in our patients include a propensity for discontinuous multifocal involvement, a tendency for orientation along the long axis of affected extremities, a tendency to follow neurovascular distributions, occasional extension into tendon sheaths, and associated enlargement of adjacent subcutaneous fat. This suggests a more diffuse congenital tissue dysplasia rather than a dysplasia isolated to the malformed vascular spaces. Orientation along the long axis of the extremity, multifocality, and absence of dilated feeding arteries or draining veins are additional characteristics helpful in differentiating low-flow from high-flow lesions. Features shared by low-flow and high-flow vascular malformations include associated muscle atrophy and subcutaneous fatty prominence. Although not uniformly seen, these characteristics may be helpful in distinguishing vascular malformations from other soft-tissue masses. One caveat for our study is that only symptomatic malformations were evaluated (i.e., patients requiring therapy). As such, asymptomatic or less extensive vascular malformations might not have characteristics exactly like those we have described.

Four of the 16 venous malformations had areas of signal void larger than those associated with typical linear septations, but these were only a minor component of the malformation (making up only a small proportion of the lesion) as compared with being the dominant feature in AVMs and AVFs. Previously cited explanations for these areas of signal void in venous malformations on SE sequences are thrombosed vessels, phleboliths, and linear, fibrous striations cut in cross section [5]. In our series, angiography showed the presence of associated single AVFs in two of the 16 venous malformations. In one of these two cases, GRE images were obtained, and the corresponding area had higher signal intensity on the GRE images. We postulate, on the basis of these findings, that the presence of concurrent AVFs, although not common, might occasionally account for these atypical areas of signal void within venous malformations on SE imaging.

The multifocal nature of venous malformations, occurring in 37% of the patients in our series, is important information for planning treatment of these vascular malformations. The results of surgical treatment of venous malformations have historically been disappointing [6, 20]. With incomplete resection, the residual malformation becomes aggressive and symptomatic, commonly more so than it was preoperatively. The complete extent of the vascular malformation must be known before any treatment is initiated [8, 10, 13]. MR frequently will show the full extent of the malformation more accurately than can be achieved by using the combination of arteriography and venography (Fig. 1). Furthermore, as many venous malformations are multifocal, MR can be used to guide the angiographic evaluation of unsuspected areas of adjacent involvement, and to depict anatomic relationships to aid in therapeutic planning. In one patient with a facial venous malformation (Fig. 2), secondary foci in the soft palate and uvula were noted on MR and not detected with arteriography. The abnormal postcapillary vascular spaces of a venous malformation are better opacified with closed-system venography than with arteriography. In anatomic sites such as the face and neck, in which closed-system venography is difficult to perform, MR can show sites of involvement not detected by standard arteriography with delayed venous-phase imaging. Although it is not a substitute for venography, MR may be useful in localizing the site for direct-puncture venography.

The addition of GRE sequences in imaging vascular malformations is not essential, but it does increase the specificity of findings, particularly for high-flow lesions. Areas of signal void on SE sequences are not specific for flow, but are confirmed to be flow related by high signal intensity with GRE images (Fig. 5). However, the low-flow and high-flow lesions are not as readily differentiated on GRE images, because of the higher signal of each when flow-sensitive techniques are used.

In conclusion, we have documented the ability of MR to consistently distinguish slow-flow venous malformations from high-flow AVMs or AVFs with SE MR imaging. We have verified the typical MR features of vascular malformations, and have described new findings that should aid in their differential diagnosis.

REFERENCES

1. Levine E, Wetzel LH, Neff JR. MR imaging and CT of extrahepatic cavernous hemangiomas. *AJR* **1986**;147:1299–1304
2. Yuk WTC, Kathol MH, Sein MA, Ehara S, Chiu L. Hemangiomas of skeletal muscle: MR findings in five patients. *AJR* **1987**;149:765–768
3. Buetow PC, Kransdorf MJ, Moser RP, Jelinek JS, Berrey BH. Radiologic appearance of intramuscular hemangioma with emphasis on MR imaging. *AJR* **1990**;154:563–567
4. Cohen JM, Weinreb JC, Redman HC. Arteriovenous malformations of the

extremities: MR imaging. *Radiology* **1986**;158:475–479
5. Cohen EK, Kressel HY, Perosio T, et al. MR imaging of soft tissue hemangiomas: correlation with pathologic findings. *AJR* **1988**;150: 1079–1081
6. Pearce WH, Rutherford RB, Whitehill TA, Davis K. Nuclear magnetic resonance imaging: its diagnostic value in patients with congenital malformations of the limbs. *J Vasc Surg* **1988**;8:64–70
7. Meyer JS, Hoffer FA, Barnes PD, Mulliken JB. Biological classification of soft-tissue vascular anomalies: MR correlation. *AJR* **1991**;157:559–564
8. Yakes WF, Haas KD, Parker SH, et al. Symptomatic vascular malformations: ethanol embolotherapy. *Radiology* **1989**;170:1059–1066
9. Yakes WF, Luethke JM, Parker SH, et al. Ethanol embolization of vascular malformations. *RadioGraphics* **1990**;10:787–796
10. Yakes WF, Parker SH, Gibson MD, Haas DK, Pesner PH, Carter TE. Alcohol embolotherapy of vascular malformations. *Semin Intervent Radiol* **1989**;6:146–161
11. Yakes WF, Luethke JM, Merland JJ, et al. Ethanol embolization of arteriovenous fistulas: a primary mode of therapy. *J Vasc Intervent Radiol* **1990**;1:89–96
12. Yakes WF, Pesner P, Reed M, Donohue HJ, Ghaed N. Serial embolizations of an extremity arteriovenous malformation with alcohol via direct percutaneous puncture. *AJR* **1986**;146:1038–1040
13. Yakes WF, Parker SH. Diagnosis and management of vascular anomalies. In: Castaneda-Zuniga WR, Tadavarthy SM, eds. *Interventional radiology*, 2nd ed. Philadelphia: Williams & Wilkins, **1991**:152–189
14. McLellan GL, Morettin LB. Persistent sciatic artery: clinical, surgical and angiographic aspects. *Arch Surg* **1982**;117:817–822
15. Mulliken JB, Glowacki J. Hemangiomas and vascular malformations in infants and children: a classification based on endothelial characteristics. *Plast Reconstr Surg* **1982**;69:412–420
16. Upton J, Mulliken JB, Murray JE. Classification and rationale for management of vascular anomalies in the upper extremity. *J Hand Surg* **1985**;6:970–975
17. Finn MC, Glowacki J, Mulliken JB. Congenital vascular lesions: clinical application of a new classification. *J Pediatr Surg* **1983**;18:894–900
18. Lawdahl RB, Routh WD, Vitek JJ, McDowel HA, Groww GM, Keller PS. Chronic arteriovenous fistulas masquerading as arteriovenous malformations: diagnostic considerations and therapeutic implications. *Radiology* **1989**;170:1011–1015
19. Trout HH, Tievsky AL, Rieth KG, Drug EM, Giordano JM. Arteriovenous fistula simulating arteriovenous malformation. *Otolaryngol Head Neck Surg* **1987**;97:322–325
20. Szilagy DE, Smith RF, Elliot JP, Hageman JH. Congenital arteriovenous anomalies of the limbs. *Arch Surg* **1976**;111:423–429

American Roentgen Ray Society
Residents' Award Papers, 1993

The ARRS announces competition for the 1993 President's Award and two Executive Council Awards for the best papers concerning the clinical application of the radiologic sciences.

Awards

The winner of the President's Award will receive a certificate and a $2000 prize. The winners of the two Executive Council Awards will each be given a certificate and a prize of $1000. The winners will be announced on March 15, 1993. Winning papers will be presented at the ARRS annual meeting at the San Francisco Marriott, San Francisco, CA, April 25–30, 1993. Winning papers will be submitted for early publication in the *American Journal of Roentgenology*. All other papers will be returned to the authors.

Regulations

Eligibility is limited to residents or fellows in radiology who have not yet completed 4 years of approved training in a radiologic discipline. A letter from the resident's department chairman attesting to this status must accompany the manuscript. The resident must be the sole or senior author and be responsible for all or most of the project.

Submitted manuscripts must not exceed 5000 words and have no more than 10 illustrations. Four copies of the manuscript and illustrations are required. Submitted manuscripts should not contain previously presented or published material and should not be under consideration for publication elsewhere.

Deadline for submissions is February 12, 1993. Send papers to

Nancy O. Whitley, M.D.
Chairman, Committee on Education & Research
American Roentgen Ray Society
Department of Radiology
University of Maryland Medical Systems Hospital
22 S. Greene St.
Baltimore, MD 21201

Budd-Chiari Syndrome: Detection with Color Doppler Sonography

Philip W. Ralls[1]
Meade B. Johnson
D. Randall Radin
William D. Boswell, Jr.
Kevin P. Lee
James M. Halls

The value of color Doppler sonography in evaluating newly diagnosed Budd-Chiari syndrome in five patients was studied. Hepatic venous findings included absence of vessels (one patient), flow reversal (two patients), narrowing (four patients), and tortuosity (three patients). Detected collaterals included hepatic venous to hepatic venous (four patients), hepatic venous to subcapsular systemic venous (two patients), and portosystemic (three patients). Hepatic venous spectral Doppler waveforms were flat and essentially aphasic in four patients, indicative of distal hepatic venous compression. The inferior vena cava was markedly compressed in two patients and slightly compressed in one. Color Doppler sonography allowed more reliable and confident identification of irregular, compressed, or otherwise abnormal hepatic veins than did conventional sonography. Color Doppler sonography also showed collateral vessels that were undetected with conventional sonography or other imaging techniques.

Our results suggest that color Doppler sonography may be a valuable tool in the initial diagnosis and evaluation of suspected Budd-Chiari syndrome.

***AJR* 159:113–116, July 1992**

Budd-Chiari syndrome (BCS) describes a group of diseases characterized by obstruction or severe stenosis of all or some of the hepatic veins with or without obstruction or stenosis of the inferior vena cava (IVC) [1–3]. BCS is rare; its prevalence was 0.061% in one autopsy series [4]. In the past, BCS was diagnosed primarily by venography, liver biopsy, and scintigraphy [3, 5–8]. More recently, contrast-enhanced CT [9, 10], MR imaging [11], and sonography [8, 9, 12–15] enhanced by the use of Doppler techniques [16–19] have been used. Although its use has been reported in fewer than 30 cases in the English language literature, Doppler sonography is now generally recommended as the appropriate screening technique for BCS [6, 7, 12, 13, 16–20].

Color Doppler sonography (CDS), which displays color-coded flow information superimposed on gray-scale images, is more effective in imaging hepatic and perihepatic vascularity than is spectral Doppler imaging [21, 22]. The use of CDS in evaluating six cases of BCS has been reported [18, 20, 23]. However, the description of CDS findings in those cases was incomplete or limited to patients who had already undergone palliative surgery. We describe CDS findings in five patients with newly diagnosed BCS.

Materials and Methods

We performed a retrospective analysis of five cases of BCS that had been studied with CDS. No specific selection or exclusion criteria were used. The diagnosis was confirmed by biopsy in three patients and hepatic venography in two patients. CDS was performed by using a Quantum QAD-1 Angiodynography system (Quantum Medical Systems, Issaquah, WA) or an Acuson 128 computed sonography system and an Acuson XP system (Acuson,

Received September 27, 1991; accepted after revision January 28, 1992.

[1] All authors: Department of Radiology, University of Southern California School of Medicine, Los Angeles County/University of Southern California Medical School, 1200 N. State St., Box 631, Los Angeles, CA 90033.

0361–803X/92/1591–0113
© American Roentgen Ray Society

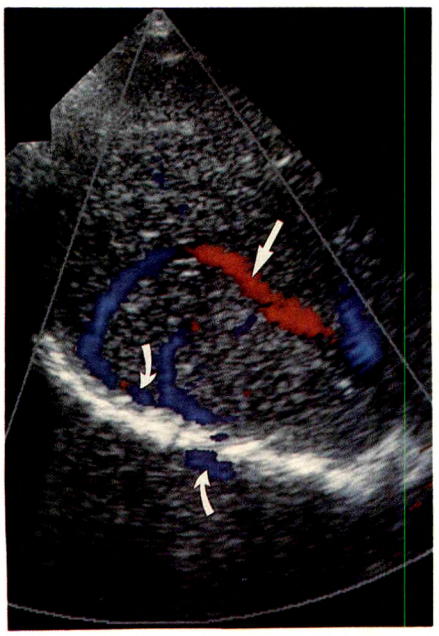


Fig. 1.—Hepatic venous to systemic subcapsular collateral veins. Transverse oblique color Doppler sonogram of right lobe of liver. Collateral pathway represents one route of egress for hepatic blood when hepatic venous stenosis is present. Flow reversal in hepatic venous collateral is coded red (*straight arrow*). Hepatic veins with flow reversal and collateral systemic veins (*curved arrows*) shown here were invisible on gray-scale images and were defined only when color Doppler imaging was used. Stenotic segment of right hepatic vein near inferior vena cava was evident on another image.

Mountain View, CA). Color Doppler images were optimized by using techniques previously described [21].

All examinations were analyzed for liver size, shape, and echo texture. Ascites was sought. Hepatic veins were evaluated for stenosis, tortuosity, flow direction, and spectral Doppler waveform. Three types of collateral vessels were specifically sought: (1) hepatic venous to hepatic venous ("spiderweb") collaterals, (2) portosystemic collaterals, and (3) hepatic venous to systemic venous collaterals.

Results

In two of the five cases, BCS was undiagnosed before CDS, even though other studies (CT in both, MR in one) had been performed before CDS. In three cases, the diagnosis was known before CDS examination. Two patients were found to have hypercoagulable conditions (polycythemia rubra vera, circulating lupus anticoagulant). No cause for BCS was found in the other three patients.

Liver morphology was abnormal on sonography in all patients. The right lobe was small in three patients and normal in two. The left lobe was enlarged in four patients and normal in one. The caudate lobe was enlarged in four patients and normal in one. Hepatic echogenicity was heterogeneous in three patients and normal in two. No hepatic veins were identified in one patient; at least one hepatic vein was imaged in the other four patients. Ascites was present in three of five patients. The IVC was normal in two patients, slightly compressed in one, and markedly compressed in two. In no patient was intraluminal thrombus detected in the hepatic veins or IVC on initial studies. A small IVC clot was noted on a follow-up study in one patient. Flow reversal in the hepatic vein was seen in two of the four patients in whom hepatic veins were visualized (Fig. 1). Narrowing of the hepatic vein was present in all four (Figs. 2 and 3), and tortuosity was noted in three of the four (Fig. 3).

Hepatic venous to hepatic venous collaterals (spiderweb) were noted in four of five patients, including two patients in whom they were invisible on gray-scale imaging (Fig. 4). Hepatic venous to systemic venous collaterals (subcapsular hepatic veins) were noted in two of five patients (Fig. 1). Portosystemic collaterals were noted in three of five patients. Interestingly, all three had flow reversal in the right portal vein with hepatofugal flow via an enlarged paraumbilical vein.

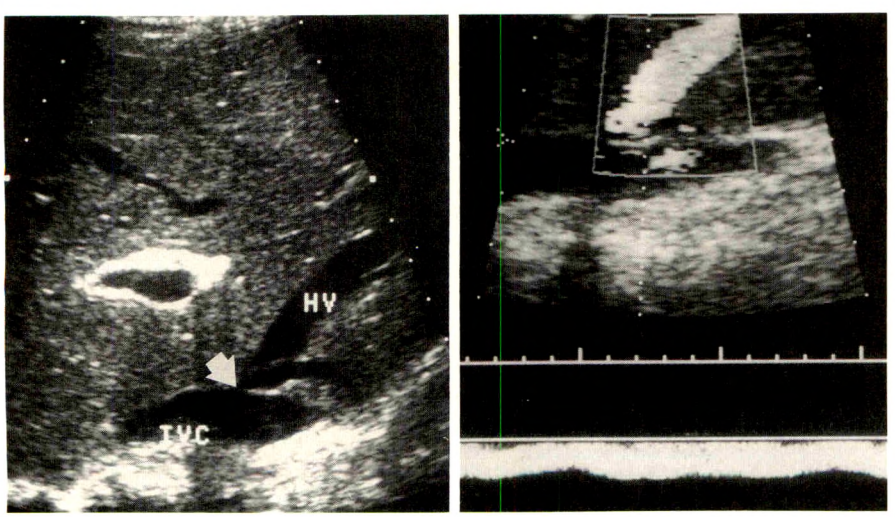


Fig. 2.—Enlarged hepatic vein (HV) draining caudate lobe.

***A*, In this patient, the only major hepatic vein that could be imaged was a markedly enlarged hepatic vein in caudate lobe. Normally, caudate lobe vein is either inapparent or tiny. Note narrowing at its junction with inferior vena cava (IVC) (*arrow*). Multiple intrahepatic hepatic venous collaterals drained into this vein.**

***B*, Spectral Doppler longitudinal color waveform and spectral Doppler sonogram (reproduced in black and white). Flat waveform lacks usual phasic pattern seen in normal hepatic veins, indicating compression of vein distally.**

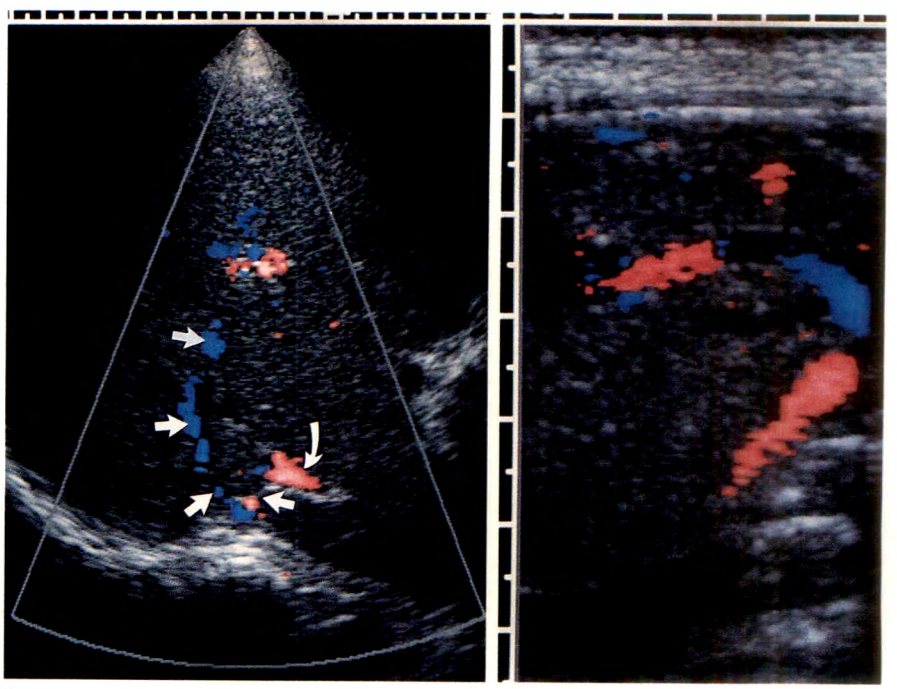


Fig. 3.—Narrowed and tortuous hepatic vein collateral on transverse color Doppler sonogram of liver. Inferior vena cava is compressed (*curved arrow*). Tortuous narrowed collateral (*straight arrows*) enters inferior vena cava dorsally rather than following typical direct course. It was invisible on gray-scale images.

Fig. 4.—"Spiderweb" hepatic venous to hepatic venous collaterals on transverse color Doppler sonogram of tip of right lobe of liver. Red- and blue-coded collaterals are part of network of hepatic venous to hepatic venous collaterals. This type of collateral (spiderweb) is generally considered diagnostic of Budd-Chiari syndrome. Collaterals displayed here were visible on gray-scale images. In two other patients, collaterals of this type were invisible on gray-scale images, and were detected only on color Doppler image.

3 4

Portal flow was normal in the other two patients. Spectral Doppler analysis in the four patients with visible hepatic veins revealed a flat, essentially aphasic waveform (Fig. 2B).

Discussion

Venous obstruction in BCS may be primary (related to congenital obstruction by webs or membranes that may represent residua of embryologic structures [24] such as the left umbilical vein and ductus venosus) or secondary (related to hypercoagulable states such as polycythemia rubra vera and sickle cell disease, trauma, neoplasm, medications, pregnancy, and other conditions). Obstruction by webs or membranes is common in Asia. In other regions, secondary BCS is more common. The cause is not known in the majority of patients [4, 6, 7].

Clinical features of BCS are variable and most often include ascites (93%); hepatomegaly (70%); and abdominal pain, edema, and superficial abdominal collateral veins (about 55% each) [4]. Clinical symptoms of BCS vary widely. Acute BCS typically is accompanied by acute pain and hepatosplenomegaly [12]. In addition, chronic BCS may be accompanied by complications of cirrhosis and portal hypertension [5, 10, 25]. Occasionally, patients with BCS are asymptomatic.

All patients with BCS share a common vascular abnormality; egress of blood via the major hepatic veins is blocked or markedly reduced. Hepatic blood must find collateral pathways to exit the liver. These pathways include hepatic vein to portal vein collaterals with portosystemic shunting (e.g., via enlarged paraumbilical veins, esophageal varices), hepatic veins to systemic veins (via capsular veins to the azygos, intercostal, and other systemic veins) (Fig. 1), and intrahepatic hepatic venous to hepatic venous collaterals (spiderweb collaterals) (Fig. 4).

The diagnosis of BCS is often confirmed by biopsy, which typically shows congestive changes associated with hepatic vein obstruction, or venography, which shows venous abnormalities and collaterals. Unfortunately, biopsy may be nondiagnostic owing to sampling errors or nonspecific findings [26, 27], and venography cannot show collaterals when hepatic venous catheterization is unsuccessful. Biopsy was nondiagnostic in two of the five cases reported here.

Sonography has gained favor in the diagnosis of BCS because it is effective and noninvasive. Hepatic venous gray-scale findings in BCS include absence, stenosis, dilatation, irregularity, or abnormal or absent junction with the IVC. Less specific changes include parenchymal inhomogeneity and morphologic changes such as caudate hypertrophy and atrophy or enlargement of the other lobes and segments. Although sonography may show the underlying cause of secondary BCS, such as neoplasia or thrombosis, it is less successful in diagnosing primary BCS because IVC and hepatic vein webs are not reliably imaged.

Absent or reversed hepatic venous flow and intrahepatic hepatic venous to hepatic venous spiderweb collaterals are diagnostic of BCS. A flat hepatic vein waveform, lacking the normal phasic fluctuation, indicates distal compression and, although nonspecific, supports the diagnosis of BCS. This hepatic vein waveform pattern occurs when distal compression shields the more proximal hepatic vein from the usual triphasic fluctuations caused by cardiac contractility. It is interesting that all three patients having decompression via portosystemic collaterals had hepatofugal flow via the same type of collateral, a recanalized paraumbilical vein.

CDS improves the sonographic detection of BCS by automatically adding flow information otherwise undetectable, or detectable only with great effort. In essence, CDS combines the ability of sonography to display morphology with the ability of venography to display flow. In this series, CDS allowed more reliable and confident identification of irregular or compressed hepatic veins and collateral hepatic veins and showed flow reversal clearly. Collateral vessels including spiderweb hepatic vein to hepatic vein channels, were easily detected and clearly displayed with CDS. These findings may be missed with conventional Doppler sonography and other imaging techniques, as occurred in several patients in this series.

In these five patients, CDS revealed flow information equivalent or superior to that obtained with venography, without the invasiveness or technical limitations of venography. However, CDS has limitations; for example, retroperitoneal collaterals may be obscured by overlying bowel gas. Although not conclusively proved by our study, we believe that CDS may become the preferred initial imaging technique in the examination of patients suspected to have BCS.

REFERENCES

1. Cho KJ, Geisinger KR, Shields JJ, et al. Collateral channels and histopathology in hepatic vein occlusion. *AJR* **1982**;139:703–709
2. Maguire R, Doppman JL. Angiographic abnormalities in partial Budd-Chiari syndrome. *Radiology* **1977**;122:629–635
3. Kreel L, Freston JW, Clain D. Vascular radiology in the Budd-Chiari syndrome. *Br J Radiol* **1967**;40:755–759
4. Parker RGF. Occlusion of the hepatic veins in man. *Medicine* (Baltimore) **1959**;38:369–402
5. Deutsch V, Rosenthal T, Adar R, et al. Budd-Chiari syndrome: study of angiographic findings and remarks on etiology. *AJR* **1972**;116:430–439
6. Stanley P. Budd-Chiari syndrome. *Radiology* **1989**;170:625–627
7. Murphy FB, Steinberg HV, Shires GT III, et al. The Budd-Chiari syndrome (review). *AJR* **1986**;147:9–15
8. Powell-Jackson PR, Karani J, Ede RJ, et al. Ultrasound scanning and 99mTc sulphur colloid scintigraphy in diagnosis of Budd-Chiari syndrome. *Gut* **1986**;27:1502–1506
9. Becker CD, Scheidegger J, Marincek B. Hepatic vein occlusion: morphologic features on computed tomography and ultrasonography. *Gastrointest Radiol* **1986**;11:305–311
10. Mathieu D, Vasile N, Menu Y, et al. Budd-Chiari syndrome: dynamic CT. *Radiology* **1987**;165:409–413
11. Stark DD, Hahn PF, Trey C, et al. MRI of the Budd-Chiari syndrome. *AJR* **1986**;146:1141–1148
12. Gentil-Kocher S, Bernard O, Brunelle F, et al. Budd-Chiari syndrome in children: report of 22 cases. *J Pediatr* **1988**;113:30–38
13. Makuuchi M, Hasegawa H, Yamazaki S, et al. Primary Budd-Chiari syndrome: ultrasonic demonstration. *Radiology* **1984**;152:775–779
14. Menu Y, Alison D, Lorphelin JM, et al. Budd-Chiari syndrome: US evaluation. *Radiology* **1985**;157:761–764
15. Park JH, Lee JB, Han MC, et al. Sonographic evaluation of inferior vena caval obstruction: correlative study with vena cavography. *AJR* **1985**; 145:757–762
16. Hosoki T, Kuroda C, Tokunaga K, et al. Hepatic venous outflow obstruction: evaluation with pulsed duplex sonography. *Radiology* **1989**;170: 733–737
17. Ohnishi K, Terabayashi H, Tsunoda T, et al. Budd-Chiari syndrome: diagnosis with duplex sonography. *Am J Gastroenterol* **1990**;85(2):165–169
18. Bolondi L, Gaiani S, LiBassi S, et al. Diagnosis of Budd-Chiari syndrome by pulsed Doppler ultrasound. *Gastroenterology* **1991**;100:1324–1331
19. Gupta S, Barter S, Phillips GWL, et al. Comparison of ultrasonography, computed tomography and 99m Tc-liver scan in diagnosis of Budd-Chiari syndrome. *Gut* **1987**;28:242–247
20. Grant EG, Perrella R, Tessler FN, et al. Budd-Chiari syndrome: the results of duplex and color Doppler imaging. *AJR* **1989**;152:377–381
21. Ralls PW. Color Doppler sonography of the hepatic artery and portal venous system. *AJR* **1990**;155:517–525
22. Tessler FN, Gehring BJ, Gomes AS, et al. Diagnosis of portal vein thrombosis: value of color Doppler imaging. *AJR* **1991**;157:293–296
23. Sukigara M, Kimura S, Adachi H, et al. Primary Budd-Chiari syndrome: demonstration by real-time two-dimensional Doppler echography. *JCU* **1989**;17:615–621
24. Hirooka M, Kimura C. Membranous obstruction of the hepatic portion of the inferior vena cava. *Arch Surg* **1970**;100:656–663
25. Wang Z, Zhu Y, Wang S, et al. Recognition and management of Budd-Chiari syndrome: report of one hundred cases. *J Vasc Surg* **1989**;10: 149–156
26. Tisnado J, Cho SR, Carithers RL, Jr, et al. The Budd-Chiari syndrome: angiographic pathologic correlation. *RadioGraphics* **1983**;3(1):155–181
27. Khuroo MS, Dataa DV. Budd-Chiari syndrome following pregnancy. *Am J Med* **1980**;68:113–121

Extrinsic Compression of the Superficial Femoral Artery at the Adductor Canal: Evaluation with Intravascular Sonography

Salem H. K. The[1,2]
Richard A. Wilson[1]
Elma J. Gussenhoven[1,2]
Herman Pieterman[3]
Klaas Bom[1,2]
Jos R. T. C. Roelandt[1]
Hero van Urk[4]

Balloon angioplasty of the superficial femoral artery was performed in 15 consecutive patients with obstructive atherosclerotic disease near the adductor hiatus. After angioplasty, extrinsic compression of the femoral artery at the adductor hiatus was shown on intravascular sonograms in five patients (33%). In retrospect, this inward deformation of the arterial wall was thought to be present in only one case before angioplasty.

After angioplasty, intravascular sonography was used successfully to differentiate between residual stenosis due to residual plaque and that due to extrinsic compression of the wall of the femoral artery near the adductor hiatus. We conclude that intravascular sonography may be a useful adjunct to angiography for determining the cause of residual stenosis.

AJR 159:117–120, July 1992

The distal femoral artery and vein pass through the adductor canal and exit the canal in the lower third of the thigh to enter the popliteal fossa [1, 2]. The high prevalence of acute [3, 4] and chronic [5–11] atherosclerotic disease in this region is well known. External mechanical factors that intermittently compress the femoral artery have been used to explain the localization of the disease in this particular region of the artery [2–12]. In a recent study, external sonography was used to localize the adductor hiatus [2]. However, to the best of our knowledge, intravascular sonographic evidence for external forces at the adductor hiatus that compress the femoral artery has not been reported. We describe the use of intravascular sonography to show such external compression on the femoral artery in the adductor canal.

Subjects and Methods

Intravascular sonography and angiography were performed in 15 consecutive patients with atherosclerotic disease of the distal femoral artery near the adductor canal, 8–13 cm craniad to the popliteal fossa [2]. Patients with symptoms of disabling claudication were selected for this study on the basis of preangioplasty arteriographic findings of a stenotic or obstructed superficial femoral artery. The study population included 13 men and two women 49–83 years old (mean age, 66 years).

A 7-French introducer sheath was placed by percutaneous or direct puncture of the common femoral or superficial femoral artery. Percutaneous studies ($n = 9$) were performed by using local anesthesia only; intraoperative studies ($n = 6$) were performed with the patient under general anesthesia. An angiographic catheter was advanced distally in the femoral artery under fluoroscopic guidance. All patients received 5000 IU of heparin IV. A radiopaque ruler was placed under the leg throughout the study to allow reproducible registration of both angiograms and sonograms before and after intervention. A 100-mm spot-film angiogram was obtained after administration of approximately 15 ml of Iopamiro 370 (Dagra, Diemen, the Netherlands).

A 5-French echocatheter (Du-MED, Rotterdam, the Netherlands) was advanced under fluoroscopic guidance across the region of the stenosis. Use of the echocatheter has been

Received November 7, 1991; accepted after revision January 29, 1992.

This work was supported by the Interuniversity Cardiology Institute of the Netherlands, the Netherlands Technology Foundation, the Dutch Ministry of Economic Affairs, and National Institutes of Health Fogarty Senior International Fellowship Grant 1F06 TWO1633-01.

[1] Department of Thoraxcenter, University Hospital Dijkzigt, Erasmus University (Ee 2312), P. O. Box 1738, 3000 DR Rotterdam, the Netherlands. Address reprint requests to E. J. Gussenhoven.

[2] Interuniversity Cardiology Institute of the Netherlands.

[3] Department of Radiology, University Hospital Dijkzigt, Erasmus University, 3000 DR Rotterdam, the Netherlands.

[4] Department of Vascular Surgery, University Hospital Dijkzigt, Erasmus University, 3000 DR Rotterdam, the Netherlands.

0361–803X/92/1591–0117
© American Roentgen Ray Society

described in detail previously [13–15]. Briefly, the echocatheter contains a 1-mm-diameter, 30-MHz, single-element transducer at its tip. The transducer is mechanically rotated by a flexible drive shaft and is covered by an acoustically transparent dome. Axial resolution of the system is 80 μm, and the lateral resolution is better than 225 μm at a depth of 1 mm. The catheter is connected to a prototype instrument providing continuous real-time cross sections of the vessel (up to 16 images per second). The sonograms are displayed on a monitor by means of a video-scanned memory of 512 × 512 pixels with 256 shades of gray.

If sonography showed definite invagination of part of the arterial wall that remained unaltered during injection of saline under pressure, extrinsic compression of a length of 1–2 cm near the adductor hiatus was judged to be present. Angioplasty was done with a 6-mm-diameter, 4-cm-long balloon (Cordis Corp., Miami, FL) with inflation pressures between 4 and 10 atm (4–10 × 10^5 Pa). Angiographic evidence of successful dilatation of the stenotic region was defined as a decrease in narrowing of the lumen diameter to less than 50%.

Results

Intravascular sonograms were of excellent quality, with clear visualization of intimal thickening, calcification, and medial thickness. Sites of stenosis shown angiographically before intervention were accurately verified with intravascular sonography. The use of the radiopaque ruler was essential for this purpose.

Intravascular sonography could be used to differentiate among various types of residual stenosis. Generally, obstruction was caused by residual plaque inside the vessel lumen; evidence of extrinsic compression of the femoral artery in the adductor canal was seen in five (33%) of the 15 studies (Figs. 1–4). In two patients, mild compression (≤25% and ≤50%) resulting in minimal lumen reduction was confirmed by angiography (Fig. 2). In three other patients, the compression resulted in a significant lumen reduction (50–90%) (Figs. 3 and 4). The angiographic data were consistent with residual stenosis: 50% or less in two patients and 50–90% in one patient.

Surgical evidence of extrinsic compression at the adductor canal was obtained in one patient. In this patient, an attempt at laser ablation in the femoral artery resulted in perforation. Surgery confirmed the location of the adductor hiatus, as indicated earlier by intravascular sonography (Fig. 3).

The reproducibility of this typical inward deformation was noted in another patient. Five months after angioplasty, this patient had angioplasty again because of recurrence of claudication symptoms. Just before the second angioplasty, intravascular sonography revealed a significantly reduced arterial

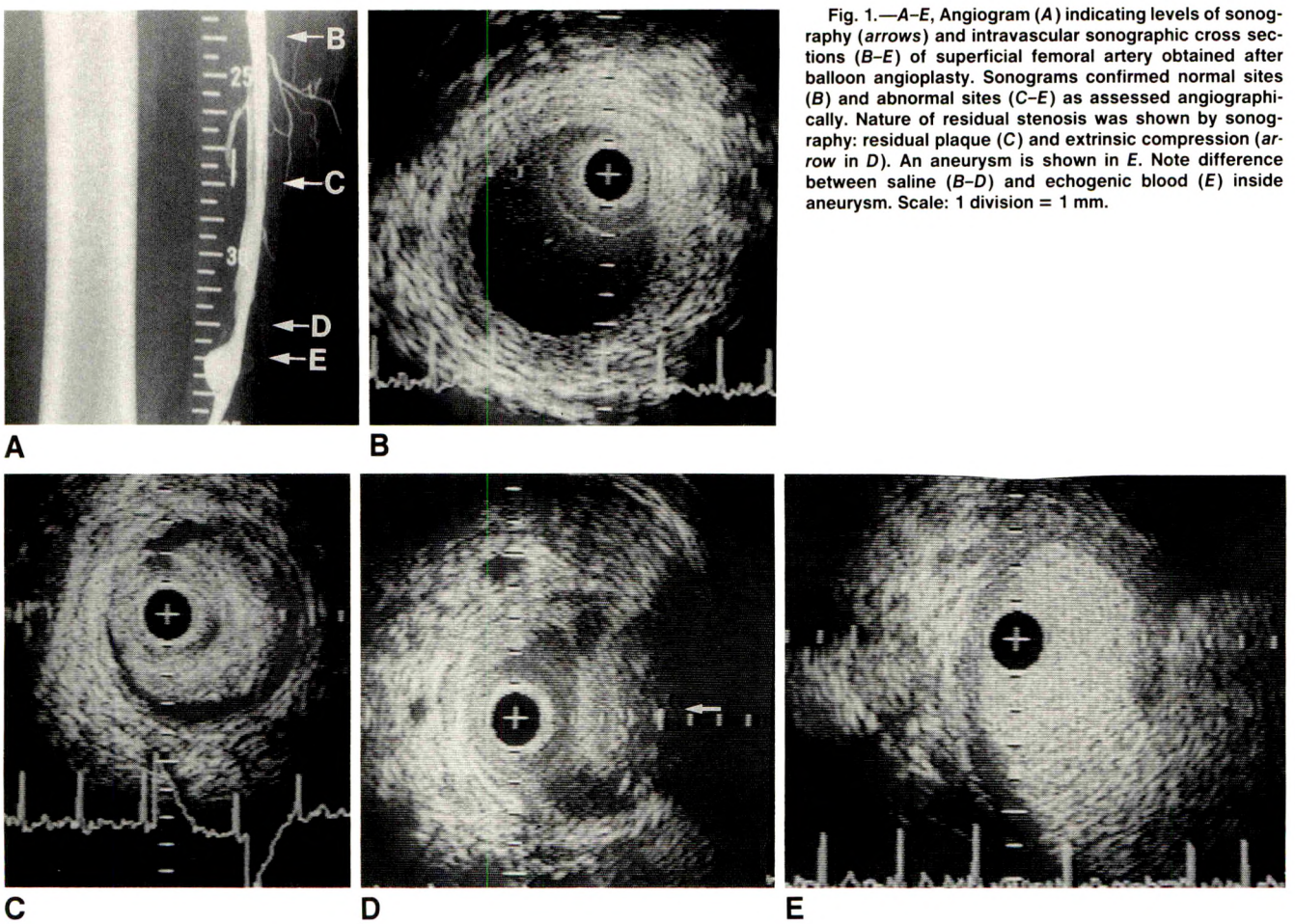


Fig. 1.—*A–E*, Angiogram (*A*) indicating levels of sonography (*arrows*) and intravascular sonographic cross sections (*B–E*) of superficial femoral artery obtained after balloon angioplasty. Sonograms confirmed normal sites (*B*) and abnormal sites (*C–E*) as assessed angiographically. Nature of residual stenosis was shown by sonography: residual plaque (*C*) and extrinsic compression (*arrow* in *D*). An aneurysm is shown in *E*. Note difference between saline (*B–D*) and echogenic blood (*E*) inside aneurysm. Scale: 1 division = 1 mm.

Fig. 2.—Intravascular sonogram after angioplasty shows mild extrinsic compression. Arterial wall is partially compressed into lumen (*arrow*), suggesting that external forces exceed intraluminal pressure.

Fig. 3.—Intravascular sonogram after angioplasty shows moderate extrinsic compression, with arterial wall partially compressed into lumen (*arrow*).

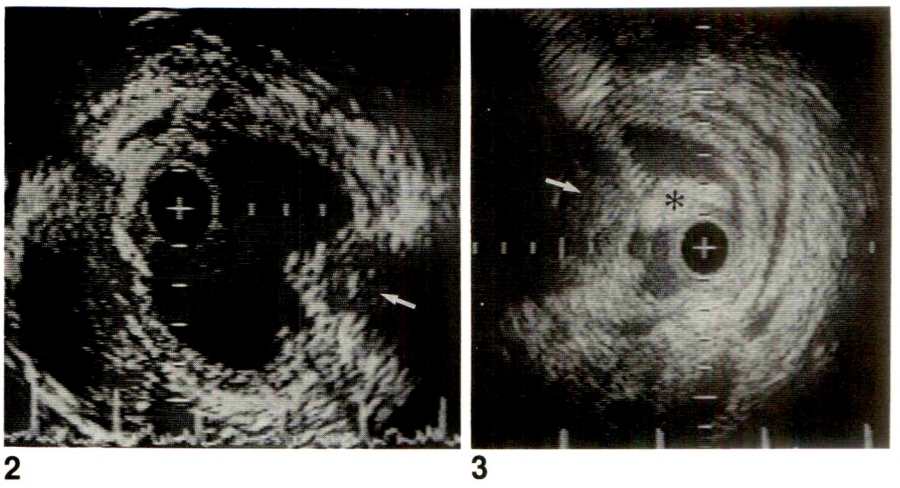
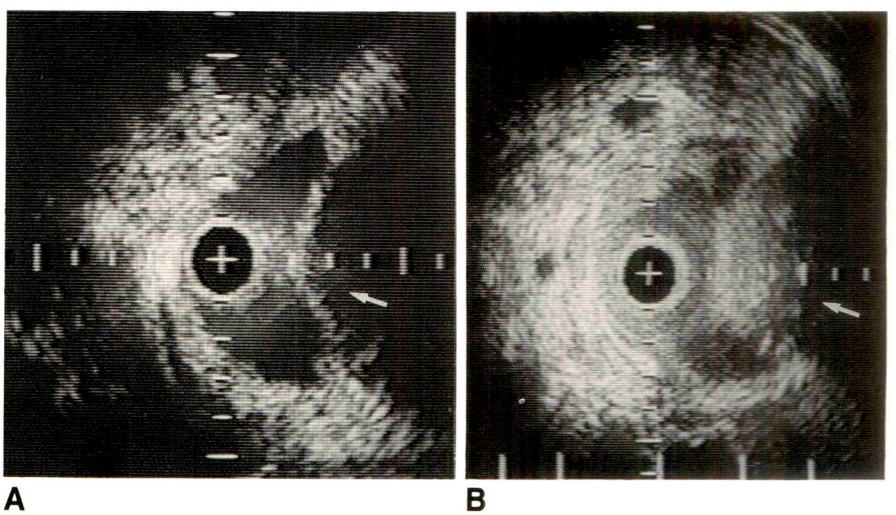


Fig. 4.—*A* and *B*, Intravascular sonograms obtained at initial angioplasty (*A*) and when angioplasty was repeated 5 months later (*B*) show soft-tissue lesion (*arrow*) partially filling lumen. Scale: 1 division = 1 mm.



lumen. After angioplasty, angiograms showed equivocal indications of extrinsic compression but the intravascular sonograms showed definite invagination of the arterial wall consistent with external compression (Fig. 4B).

Discussion

Previous studies have shown that atherosclerotic disease involving the femoral artery occurs most often near the adductor hiatus [9]. It is also believed that restenosis occurs more frequently in this region and could partially explain the higher success rate for balloon angioplasty in the iliac artery compared with the femoral artery [16].

Femoral vessels pass through the adductor canal between thigh muscles. The adductor canal is triangular on transverse section, bounded anteriorly and laterally by the vastus medialis muscle; posteriorly by the adductor longus and adductor magnus; and superiorly by an aponeurosis of these muscles, which extends across the femoral vessels to the vastus medialis muscle [1]. It is postulated that the predilection for obstructive disease in this region may be related to external mechanical factors that result in repetitive microtrauma and, consequently, damage to the vessel wall [2–11] with intimal fissuring [3–5] and intimal proliferation [6].

In this study, the intravascular sonograms obtained before angioplasty showed diffuse intimal thickening proximal to the site of extrinsic compression, but no calcified lesions, intimal tears, or dissection were observed near the adductor canal. With intravascular sonography, the specific location of the adductor canal could not be determined before intervention. However, all lesions were in the distal third of the thigh at the level of the adductor hiatus.

In five cases, intravascular sonography showed localized invagination of the arterial lumen that was not evident with angiography. Compared with intravascular sonography, the angiographic significance of the stenosis was less clearly shown in two patients. The technique was routinely performed in a single-plane (anteroposterior) direction. Additional angiographic views might have defined the degree of narrowing more precisely. Intravascular sonography provides tomographic cross sections of the vessel and can image the constituents of the arterial wall [17, 18]. This is an advantage,

especially in those cases with significant vessel wall compression that might otherwise be considered residual plaque [15]

Stretching and damage of the arterial wall after angioplasty appeared to allow external forces to exceed internal distending pressure, with consequent partial deformation of the vessel wall toward the center of the lumen. However, other explanations for the postangioplasty luminal deformity must be considered. Luminal encroachment did not mimic an intimal flap, which might be misinterpreted as external compression. No blood flow was observed around the deformity to suggest an intimal tear or localized dissection in any of the studies, and injection of saline under pressure had no effect on the inward deformation. Spasm of the artery or elastic recoil are unlikely alternative explanations for luminal deformity, as these events generally involve the entire circumference of the artery. Patients were not treated with nitroglycerin or other vasodilators.

Although angiography was considered the reference method in this study, intravascular sonography provided valuable additional information [14, 15]. The results of this study may have clinical implications: if the arterial wall has been weakened by the angioplasty [19] and has partially invaginated into the lumen, then care must be taken to avoid more aggressive recanalization with atherectomy or laser devices. In addition, such partially invaginated vessels may be more effectively treated with intravascular stents or bypass surgery.

ACKNOWLEDGMENTS

The authors thank G. P. Gerritsen, W. P. T. M. Mali, and C. Di Mario for their suggestions.

REFERENCES

1. Warwick R, Williams PL. *Gray's anatomy*, 35th ed. London: Longman, **1973**:674–675
2. Scholten FG, Mali WPTM, Hillen B, van Leeuwen MS. US location of the adductor canal hiatus: morphologic study. *Radiology* **1989**;172:75–78
3. Balaji MR, DeWeese JA. Adductor canal outlet syndrome. *JAMA* **1981**;245:167–170
4. Verta MJ, Vitello J, Fuller J. Adductor canal compression syndrome. *Arch Surg* **1984**;119:345–346
5. Dunlop GR, Dos Santos R. Adductor canal thrombosis. *N Engl J Med* **1957**;256:557–580
6. Palma EC. Hemodynamic arteriopathy. *Angiology* **1959**;10:134–143
7. Novotny H. Splitting of the adductor canal: a method of improving locally collateral circulation in thromboangiitis obliterans. *Acta Chir Scand* **1950**;99:332–340
8. Linhart J, Dejdar R, Prerovsky I, Hlavova A. Location of occlusive arterial disease of lower extremity. *Invest Radiol* **1968**;3:188–198
9. Watt JK, Origin of femoro-popliteal occlusions. *BMJ* **1965**;2:1455–1459
10. Mavor GE. The pattern of occlusion in atheroma of the lower limb arteries. *Br J Surg* **1956**;43:352–358
11. Lindbom A. Arteriosclerosis and arterial thrombosis in the lower limb. *Acta Radiol* **1950**;80[suppl]:1–80
12. Wagner M, Ricciardi J. A correlative anatomic study of degenerative occlusive disease of the arteries of the lower extremities. *Angiology* **1966**;17:574–582
13. Gussenhoven EJ, The SHK, Gerritsen P, et al. Real-time intravascular ultrasonic imaging before and after balloon angioplasty (case report). *J Clin Ultrasound* **1991**;19:294–297
14. Van Urk H, Gussenhoven EJ, Gerritsen GP, et al. Assessment of arterial disease and arterial reconstructions by intravascular ultrasound. *Int J Card Imaging* **1991**;6:157–164
15. The SHK, Gussenhoven EJ, Du Bois NAJJ, et al. Femoropopliteal vein bypass grafts studied by intravascular ultrasound. *Eur J Vasc Surg* **1991**;5:523–526
16. Becker GJ, Katzen BT, Dake MD. Noncoronary angioplasty. *Radiology* **1989**;170:921–940
17. Gussenhoven EJ, Essed CE, Lancée CT, et al. Arterial wall characteristics determined by intravascular ultrasound imaging: and in vitro study. *J Am Coll Cardiol* **1989**;14:947–952
18. Potkin BN, Bartorelli AL, Gessert JM, et al. Coronary artery imaging with intravascular high-frequency ultrasound. *Circulation* **1990**;81:1575–1585
19. Lyon RT, Zarins CK, Lu C-T, Yang C-F, Glagov S. Vessel, plaque, and lumen morphology after transluminal balloon angioplasty: quantitative study in distended human arteries. *Arteriosclerosis* **1987**;7:306–314

Insertion of Hickman Central Venous Catheters by Using Angiographic Techniques in Patients with Hematologic Disorders

J. F. Cockburn[1]
C. A. Eynon[2,3]
N. Virji[1]
J. E. Jackson[1]

During a 9-month period, 69 Hickman catheters were successfully inserted by using angiographic techniques in 59 patients with hematologic disorders. A pneumothorax, which did not require drainage, developed in one patient. No other significant complications occurred at the time of insertion. Eighteen catheters were removed electively, 15 are still in situ, six were removed for thrombosis, and five were accidentally removed. Infection precipitated removal in six subjects. Ten patients died with the catheter in place. Five catheters were removed in patients with refractory septicemia of unknown origin. One catheter burst during an injection and had to be removed. Three patients were lost to follow-up. There were 3.24 infectious episodes per 1000 days of catheterization, more than twice the rate found in some other series.

The results of this study are compatible with the growing body of evidence in favor of the angiographic insertion of Hickman catheters. The apparently high rate of infection is ascribed to factors other than insertion in the angiography suite, including the high proportion of bone marrow transplantation patients.

AJR 159:121–124, July 1992

Hickman catheters [1] provide safe long-term venous access for administration of chemotherapeutic agents and antibiotics, total parenteral nutrition, and repeated blood sampling. Traditionally, these catheters have been inserted by surgeons in the operating room. Nowadays, however, many Hickman catheters are inserted by radiologists, who do so quickly, safely, with minimal delays, and with a sepsis rate comparable to that associated with placement in sterile operating rooms [2–6]. Since October 1990, all Hickman catheter insertions in patients with hematologic disorders at our hospital have been performed by a radiologist using standard angiographic techniques. Most of these patients were undergoing bone marrow transplantation. We chose to examine the outcome in these patients, who are at high risk because of myelosuppression, to assess whether such placement was associated with an acceptably low rate of complications. This article presents data collected from the consecutive placement of 69 Hickman catheters inserted by using angiographic techniques in 59 patients during a 9-month period in the Hammersmith Hospital Department of Diagnostic Imaging. It emphasizes common difficulties encountered during insertion and ways to overcome them.

Subjects and Methods

Between October 1990 and June 1991, we monitored the progress of 59 patients referred to our department for placement of an indwelling central venous catheter. Sixty-nine Hickman catheters were inserted in the angiography suite. Thirty-seven patients had chronic myeloid leukemia, and 12 had acute myeloid leukemia. Other leukemias were present in three patients, and multiple myeloma was the diagnosis in two patients. The remaining diagnoses were Gaucher's disease, thalassemia major, myelodysplasia, non-Hodgkin's lymphoma, and aplastic anemia. The patients' age range was 17–65 years (median, 39 years). Bone marrow

Received October 28, 1991; accepted after revision January 22, 1992.

[1] Department of Diagnostic Radiology, Royal Postgraduate Medical School, Hammersmith Hospital, Du Cane Rd., London W12 0HS, Great Britain.

[2] Department of Hematology, Royal Postgraduate Medical School, Hammersmith Hospital, Du Cane Rd., London, W12 0HS, Great Britain.

[3] Present address: Department of Infectious Diseases, Churchill Hospital, Headington, Oxford, OX3 7LJ, Great Britain.

0361–803X/92/1591–0121
© American Roentgen Ray Society

transplantation was the most common reason for catheter insertion (56 catheters). Administration of chemotherapeutic agents accounted for a further 11. The remaining two catheters were required for long-term antibiotic administration and blood transfusion. Patients without hematologic disorders were excluded from the study as they constitute a small proportion of our caseload and are a very heterogeneous group. Triple-lumen Hickman catheters were used in 46 patients; our clinicians prefer the increased access, and placement is easier because of the catheters' increased rigidity. Vancomycin (500 mg) was administered by IV infusion 1 hr before or during the procedure. Premedication was not routine, and rarely administration of IV benzodiazepine was required to reduce a patient's anxiety during the insertion.

Technique

Where practicable, a left-sided puncture was planned (for reasons discussed later). Venography of the arm was performed via a winged cannula placed in the patient's left hand; 20 ml of iohexol (300 mg/ml) and digital imaging were used to confirm patency of the subclavian vein. The technique of percutaneous insertion of semipermanent catheters has been well described [2, 7–9], and a brief summary follows. Under aseptic conditions, an entry site 2 cm below the junction of the medial two thirds and the lateral one third of the clavicle is infiltrated with 2% lidocaine. An 8-mm stab incision is made at the entry site and is deepened by blunt dissection to the level of the posterior surface of the clavicle. Initial access to the subclavian vein is achieved by using a Neff percutaneous puncture set (William Cook Europe, Bjaeverskov, Denmark). The subclavian vein is punctured with a 22-gauge Chiba needle, through which a 0.018-in. (0.046 cm) mandril wire with a platinum tip is introduced. The track is dilated and the mandril wire is exchanged for a 0.038-in. (0.097 cm) J guidewire, over which a peel-away sheath is introduced. The size of the sheath varies between 9- and 13-French, depending on the number of channels in the catheter. A subcutaneous track is created by using the tunneling instrument provided in the Hickman kit (Davol Inc., Cranston, RI). The central catheter is cut to an appropriate length under fluoroscopic guidance, by placing it on the patient's anterior chest wall over the course of the 0.038-in. wire lying with its tip in the right atrium. The catheter tip is fed into the superior vena cava via the sheath. Fluoroscopy is used to monitor the positions of needle tip and wires. A posteroanterior chest radiograph shows the final position of the catheter and excludes the immediate development of complications such as pneumothorax and hemothorax.

Results

All catheter placements were successful. Thirty-one of the 69 catheters were inserted by one radiologist. Thirty-eight catheters were placed by one of seven other radiologists. Catheters remained in place for a total of 4015 days. Duration of continuous catheterization ranged from 6 to 211 days, with a mean of 58 days. On a number of occasions, difficulties were encountered at the time of insertion. A venogram of the arm could not be obtained in one patient who was an IV drug abuser. Blind puncture of the subclavian vein was performed, and the Hickman catheter was introduced as previously described. Radiologists who were learning the procedure occasionally had difficulty negotiating the space between the clavicle and the first rib. With experience, this ceased to be a problem. The introducer sheath buckled during insertion in four cases, necessitating use of a new sheath in one. For 18 catheters introduced on the right side, the mean time taken for insertion was 56 min (range, 25–120 min). For 51 introduced on the left side, the mean insertion time was 39 min (range, 25–70 min). In one patient, an apical pneumothorax that did not require treatment developed. Three thrombocytopenic patients had prolonged oozing of blood from the exit site, but this was not copious, and stopped after 36 hr in the worst case (a patient with a platelet count of 19×10^9/l). A hematoma formed at the insertion site in one patient but resolved without further treatment.

The calculated infection rate was 3.24 per 1000 days of catheterization. Five catheters were removed because of septicemia refractory to antibiotics and antifungal agents. No pathogen was isolated from the exit site or the catheter tip in these patients. Thirteen catheters became infected as shown by positive cultures for microorganisms. Of these 13 infections, two occurred in patients who did not receive transplants. Seven involved only the exit site, and six of these were treated without removal of the catheter. The seventh progressed rapidly to gram-negative septicemia, and the catheter was withdrawn. Five tunnel infections (erythema and induration greater than 1 cm proximal to the exit site) necessitated removal of the catheter. In one patient, the catheter was removed because of subclavian vein thrombosis, and culture of material from the tip was positive for *Streptococcus faecalis* in the absence of overt infection. *Staphylococcus epidermidis* was cultured in nine cases. *Staphylococcus aureus*, *Pseudomonas*, and *Streptococcus salivarius* infections accounted for the remainder. Six of the infections at the exit site responded to antibiotics without removal of the catheter. The five tunnel infections required removal of the catheter to effect cure.

Elective removal was undertaken in 18 cases, 10 patients died with the catheter in situ, and 15 patients still had a catheter in place at the end of the study period. Five Hickman catheters were pulled out by accident because they snagged on drip stands and other clinical equipment. In one catheter, a channel burst during the administration of an IV bolus, which necessitated removal of the catheter. Six catheters became blocked because of venous thrombosis that occurred between 13 and 65 days after insertion (mean, 41 days). No evidence suggested that catheter insertion had been more traumatic in these cases. Follow-up could not be obtained in three patients.

Discussion

Insertion of Hickman catheters has traditionally been performed by surgeons, who use either a percutaneous approach or a cut-down on the subclavian or jugular vein. Insertion is usually uncomplicated, but occasionally initial venous access or final positioning of the catheter is difficult, and such problems are often compounded by poor fluoroscopic facilities in the operating room. In addition, surgeons are unfamiliar with guidewire techniques that may be useful in such circumstances. Because of problems in positioning catheters in a number of patients for a short time in our hospital, we decided to offer percutaneous placement in the angiography suite.

The initial results have been so successful that placement by radiologists is now the method of choice.

A number of problems can occur during placement of central venous catheters: failure to traverse the gap between the first rib and the clavicle, kinking of the introducer sheath, and increased difficulty during right-sided insertions. The first is liable to happen when the initial incision is made more medially than we have described. The needle must then be introduced more steeply in order to pass underneath the clavicle and is often brought to a halt by the first rib. Redirection more superficially is required in this instance, but a second more lateral incision may be necessary to allow the more oblique approach. Conversely, the clavicle is hit when the needle is directed too superficially; this is usually easily recognized and remedied.

It is generally taught that for insertion of a Hickman catheter, the peel-away sheath should be introduced only a short distance into the subclavian vein, but the reasons for this are not well known. The natural tendency is to push the sheath in too far, to ensure that its tip is intraluminal before the dilator and guidewire are removed. Inexperienced operators prefer to place the tip of the sheath in the superior vena cava, thinking that subsequent insertion of the catheter will be easier and misplacement less likely. It became clear early in our experience, however, that this technique is associated with a number of problems, the most serious of which is the sometimes severe pain experienced by the patient during insertion of the sheath. This occurs because the relatively rigid sheath and its dilator push against the opposite wall of the superior vena cava and distort the mediastinal structures (Fig. 1). Nearly all patients described having a severe dragging and choking sensation during this manipulation.

We also found that when the distal end of the sheath is in the superior vena cava, the sheath almost invariably kinks, especially when a right-sided approach is used. This makes subsequent insertion of the catheter extremely difficult. The sheath must then be partially withdrawn, without removing it completely from the subclavian vein, until the kink is abolished. This is not always simple, particularly as the sheath is poorly radiopaque, and its tip is difficult to visualize.

In view of these problems, we have altered our insertion technique. First, we prefer to use a left-sided approach; kinking is less likely because of the more obtuse angle between the left brachiocephalic vein and the superior vena cava. Second, we introduce the sheath only a short distance into the vein so that its intraluminal course is straight. Care is taken to ensure that the sheath tip is intraluminal before the dilator is removed. Although this might be expected to make correct positioning of the catheter tip in the superior vena cava more difficult, we have not found this to be the case. Since we have begun performing insertions in this manner, the procedure has been much better tolerated, and patients' discomfort has been minimized. Kinking of the sheath was the major cause of the greater mean time required to perform right-sided catheterizations. Interestingly, no increase in the number of infections, thromboses, or other delayed complications was associated with right-sided insertion.

During this study, 3.24 infections occurred per 1000 days of catheterization. This figure compares unfavorably with the rate of 1.37 infections per 1000 days of catheterization calculated from a total of 694,852 days in the study by Clarke and Raffin [10]. Neutropenia at the time of catheter insertion was present in only three of the 13 patients with subsequent infections and thus cannot be held responsible for our rate of sepsis. We think that our high number of marrow transplantation patients (50 of 59) is at least partly responsible for the increased frequency of infection. Press et al. [11] observed that this group had a rate of infection from placement of Hickman catheters that was twice that of other groups, although this observation was not statistically significant. The use of high-dose chemotherapy and the prolonged immunosuppression used to prevent graft-vs-host disease are factors that may predispose this group to infection. Factors other than contamination in the angiography suite probably are

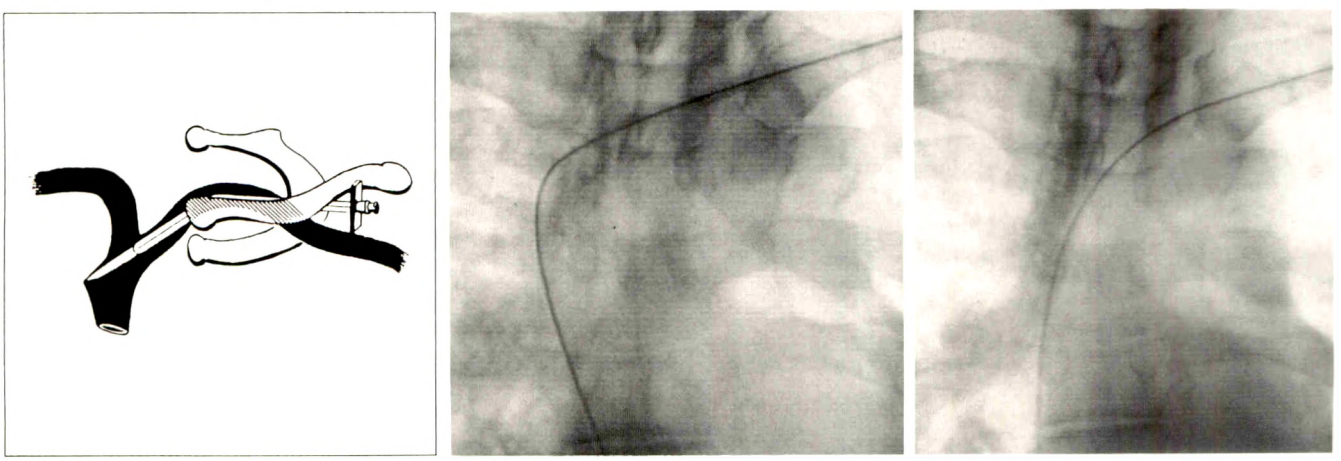


Fig. 1.—Placement of Hickman catheter.

A and *B*, Line drawing (*A*) and radiograph (*B*) taken during insertion of peel-away sheath and its dilator show distortion that occurs when sheath is introduced too far.

C, Radiograph shows sheath and its dilator have been partially withdrawn, so that vessel is no longer distorted.

responsible for most infections. Inasmuch as ablative chemotherapy is started within 24 hr of catheter insertion in most of our patients, and the cellular nadir occurs 10 days after this, it could be argued that any organisms introduced by the radiologist should proliferate during the first period of host defenselessness. Only two of our infections occurred within the first 4 weeks (at 6 and 16 days). We recognize that deducing the cause of infections from their timing is inexact, and we cannot fully exonerate the radiologist in the development of late infections. Considerable evidence has accumulated, however, that indicates that sepsis associated with a Hickman catheter is much more related to routine care of the catheter than to contamination at the time of insertion. The appointment of a specialist nurse dedicated to monitoring and educating patients and staff with respect to good catheter care may help in reducing a high rate of sepsis [12].

In conclusion, we think that placement of Hickman catheters by radiologists using angiographic techniques has several advantages. First, although most insertions are uncomplicated, difficulties in venous access or correct positioning of the catheter tip in the superior vena cava will occur occasionally, and these are often easily overcome by using guidewire techniques and good-quality fluoroscopy. Second, visualization of the course of the subclavian vein with preliminary venography of the arm, which is easily performed in the angiography suite, allows a rapid and confident venous puncture. Venous thrombosis or stenosis can be detected before venous catheterization is attempted, and an alternative route can be chosen if necessary. Furthermore, arterial puncture should occur less commonly if the course of the vein has been shown by venography. Inadvertent puncture of the subclavian artery is a recognized complication of the percutaneous approach, and severe bleeding may occur. We think that the use of a 22-gauge Chiba needle is likely to minimize the risk of significant hemorrhage should the artery be entered. Finally, angiography time is less costly than operating room time, and because insertion is almost always on the day the request is made, delays are generally shorter.

REFERENCES

1. Hickman RO, Buckner CD, Clift RA, Sanders JE, Stewart P, Thomas ED. A modified right atrial catheter for access to the venous system in marrow transplant recipients. *Surg Gynecol Obstet* **1979**;148:871–875
2. Robertson LJ, Mauro MA, Jaques PF. Radiologic placement of Hickman catheters. *Radiology* **1989**;170:1007–1009
3. Page AC, Evans RA, Kaczmarski R, Mufti GJ, Gishen P. The insertion of chronic indwelling central venous catheters (Hickman lines) in interventional radiology suites. *Clin Radiol* **1990**;42:105–109
4. Andrews JC, Walker-Andrews SC, Ensminger WD. Long-term central venous access with a peripherally placed subcutaneous infusion port: initial results. *Radiology* **1990**;176:45–47
5. Pulido-Duque JM, Fernando C, Reves R, et al. Percutaneous Hickman catheter placement in the radiology suite. *Semin Intervent Radiol* **1991**;8: 82–84
6. Lambiase RE, Dorfman GS, Cronan JJ, Paolella LP, Caldwell ME. Percutaneous alternatives in nutritional support: a radiological perspective. *J Parenter Enteral Nutr* **1988**;12:513–520
7. Kirkemo A, Johnston MR. Percutaneous subclavian placement of the Hickman catheter. *Surgery* **1989**;91:349–351
8. Linos DA, Mucha P Jr. A simplified technique for the placement of permanent central venous catheters. *Surg Gynecol Obstet* **1982**;154:248–250
9. Hawkins J, Nelson E. Percutaneous placement of Hickman catheters for prolonged venous access. *Am J Surg* **1982**;144:624–626
10. Clarke DE, Raffin TA. Infectious complications of indwelling long-term central venous catheters. *Chest* **1990**;97:966–972
11. Press OW, Ramsey PG, Larson EB, Fefer A, Hickman RO. Hickman catheter infections in patients with malignancies. *Medicine* **1984**;63: 189–200
12. Reed WP, Newman KA, DeJongh C, et al. Prolonged venous access for chemotherapy by means of the Hickman catheter. *Cancer* **1983**;52: 185–192

Case Report

Atherectomy of the Distal Aorta Using a "Kissing-Balloon" Technique for the Treatment of Blue Toe Syndrome

Richard A. Clugston,[1] Andrew C. Eisenhauer, and Ray V. Matthews

The blue toe syndrome occurs when microembolization from a proximal source causes digital ischemia or infarction of one or both feet while peripheral pulses remain intact. Effective use of catheter-based atherectomy has recently been described for lesions of the superficial femoral artery in this clinical setting [1], but its use has not been reported for lesions of the abdominal aorta. We describe successful atherectomy of a distal aortic lesion in a patient with blue toe syndrome.

Case Report

A 36-year-old woman became aware of paresthesia and bluish discoloration of the toes of the right foot and later of the left foot 6 weeks before admission. She initially sought medical attention after progression of paresthesia, further discoloration, and the onset of nocturnal rest pain. Claudication of the calf, thigh, or buttock was not experienced at any stage. Abdominal aortography revealed a severe stenosis of the distal abdominal aorta, with heaped-up plaque encroaching into the aortic lumen from the anterior wall (Figs. 1A and 1B), probably associated with thrombus formation. IV heparin was begun and the patient was transferred to our hospital for further evaluation. On examination, the femoral, popliteal, dorsalis pedis, and posterior tibial pulses were palpable bilaterally, and a bruit was heard in the lower abdomen. The toes of both feet had bluish discoloration of various degrees. The patient smoked, had an elevated serum level of cholesterol, and was taking an estrogen-containing contraceptive preparation. Blue toe syndrome due to recurrent small-vessel microembolization was diagnosed. After 4 days of heparin therapy, aortoiliac arteriography was repeated and showed only limited resolution of the lesion, consistent with partial dissolution of the thrombus. The residual severe stenosis of the distal aorta involved the origin of both iliac arteries. The iliac and infrainguinal vessels were otherwise free of disease. Six- and 9-French sheaths were placed in a retrograde fashion in the right and left femoral arteries, respectively, and a 9-French directional atherectomy device (Atherocath, Devices for Vascular Intervention, Mountain View, CA) was passed via the left femoral artery to the lesion, and atherectomy was attempted. This was unsuccessful because the Atherocath would not adequately engage the anteriorly located lesion within the relatively capacious aorta. The caliber of the iliofemoral vessels was judged to be too small to accept an 11-French sheath safely, precluding the use of an 11-French device.

Satisfactory engagement of the device with the plaque was achieved by simultaneously inflating a 7-mm balloon (advanced from the right side of the groin) posterior to the balloon of the atherectomy device, thereby buttressing the cutting chamber against the lesion ("kissing-balloon" atherectomy; Fig. 1C). Precise relative positioning of the atherectomy cutter, atherectomy balloon, and posteriorly located angioplasty balloon was critical to enable safe atherectomy. This was accomplished easily with the aid of fluoroscopy in the anteroposterior and lateral planes, paying attention to bony landmarks. Multiple slivers of atheromatous debris were then retrieved, and their nature was later confirmed histologically. A postatherectomy, preangioplasty angiogram showed a readily recognizable but suboptimal reduction in the degree of aortic stenosis. Adjunctive kissing-balloon angioplasty was therefore performed at the aortic bifurcation by using 7- and 8-mm balloons, in order to obtain an optimal reduction in the degree of stenosis without exposing the patient to the risk of vessel perforation from additional attempts to achieve total plaque removal by atherectomy. A satisfactory final angiographic result was obtained (Figs. 1D and 1E). No pressure gradient existed from the central aorta to either common femoral

Received October 11, 1991; accepted after revision December 18, 1991.
[1] All authors: Hospital of the Good Samaritan, 616 S. Witmer St., Los Angeles, CA 90017. Address reprint requests to A. C. Eisenhauer.

 0361–803X/92/1591–0125 © American Roentgen Ray Society

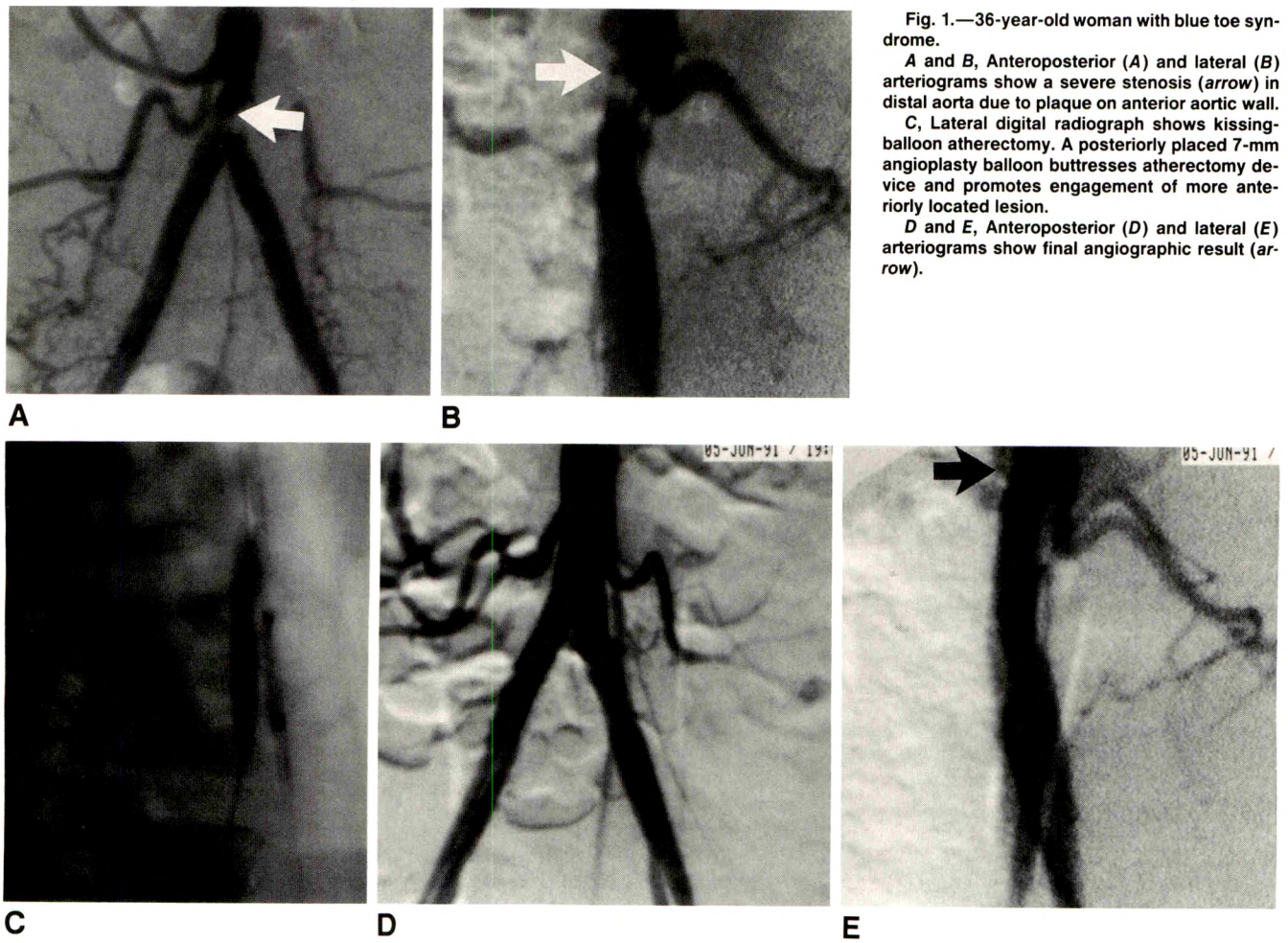


Fig. 1.—36-year-old woman with blue toe syndrome.

***A* and *B*, Anteroposterior (*A*) and lateral (*B*) arteriograms show a severe stenosis (*arrow*) in distal aorta due to plaque on anterior aortic wall.**

***C*, Lateral digital radiograph shows kissing-balloon atherectomy. A posteriorly placed 7-mm angioplasty balloon buttresses atherectomy device and promotes engagement of more anteriorly located lesion.**

***D* and *E*, Anteroposterior (*D*) and lateral (*E*) arteriograms show final angiographic result (*arrow*).**

artery at the conclusion of the procedure. Further microembolization was not precipitated, and digital amputation was not required. At discharge, the patient's regimen included aspirin, Coumadin (Du Pont Pharmaceuticals, Wilmington, DE), and lovastatin. She had an uncomplicated convalescence with prompt healing of the feet and was without recurrence of symptoms at 3 months' follow-up.

Discussion

The blue toe syndrome is caused by microembolization and occlusion of digital vessels by proximal arterial lesions situated typically within the aorta, aortoiliac, or femoropopliteal segments supplying the affected foot. Aneurysms, or more commonly ulcerated, complicated plaques, release emboli that may be composed of fibrinoplatelet-thrombus aggregates, or less often of predominantly cholesterol-rich fragments of atheroma [2]. Recurrent signs and symptoms are usual [3] but tissue or digit loss is not.

An ideal management strategy has not been defined. Surgical bypass with exclusion of the lesion, or endarterectomy, is effective [2, 3] but invasive. Antiplatelet therapy, anticoagulation, or both may be useful for fibrinoplatelet emboli [4], but would not be expected to be beneficial for cholesterol fragment emboli. It has been postulated that anticoagulants might even favor recurrent embolization by preventing thrombus formation and healing of an eroded plaque [5]. Because shear forces generated by the increased velocity at a stenosis appear critical in promoting platelet aggregation [6], restoration of arterial continuity by balloon angioplasty has been advocated and used successfully [7]. The need for anticoagulation preceding angioplasty is controversial, as initial angioplasty followed by antiplatelet therapy also has been effective [8].

Percutaneous, catheter-based directional atherectomy has recently been reported in the treatment of embologenic lesions in the superficial femoral artery [1]. However, to our knowledge, it has not been used for embologenic aortic lesions. It is less invasive than bypass surgery or endarterectomy and may be superior to balloon angioplasty because the surface of the underlying lesion is removed. Theoretically, actual removal of potentially embologenic fibrinoplatelet aggregates, thrombus, or cholesterol-rich deposits at the lesion surface might be expected to reduce the frequency of further embolic events. Moreover, material retrieved may provide insight into pathophysiologic mechanisms in the individual case and aid in guiding subsequent therapy.

Currently available peripheral atherectomy catheters have been used extensively and with success in occlusive and more distal peripheral vascular disease, but generally not for aortic lesions because the devices available for percutaneous introduction are considerably undersized with respect to the aortic lumen [9]. We describe here a simple method for eliminating this discrepancy in size. Safe engagement of the cutter housing on the aortic lesion was facilitated by kissing-balloon atherectomy, with a buttressing angioplasty balloon passed from the contralateral femoral artery and inflated between the opposite aortic wall and the balloon of the atherectomy device. The cutter must be positioned carefully to ensure that the angioplasty balloon does not abut the cutter in order to avoid balloon perforation.

In this patient, catheter-based atherectomy and adjunctive angioplasty was an effective treatment of the blue toe syndrome occurring consequent to recurrent aortic microembolization and thereby precluded more invasive surgical intervention.

REFERENCES

1. Dolmatch BL, Rholl KS, Moskowitz LB, et al. Blue toe syndrome: treatment with percutaneous atherectomy. *Radiology* **1989**;172:799–804
2. Karmody AM, Powers SR, Monaco VJ, Leather RP. "Blue toe" syndrome: an indication for limb salvage surgery. *Arch Surg* **1976**;111:1263–1268
3. Brenowitz JB, Edwards WS. The management of atheromatous emboli to the lower extremities. *Surg Gynecol Obstetr* **1976**;143:941–945
4. Morris-Jones W, Preston FE, Greaney M, Chatterjee DK. Gangrene of the toes with palpable peripheral pulses: response to platelet suppressive therapy. *Ann Surg* **1981**;193:462–466
5. Kempczinski RF. Lower extremity arterial emboli from ulcerating atherosclerotic plaques. *JAMA* **1979**;241:807–810
6. Sixma JJ. Role of blood vessel, platelet and coagulation interactions in haemostasis. In: Bloom AL, Thomas DP, eds. *Haemostasis and thrombosis*. New York: Churchill Livingstone, **1981**:252–267
7. Brewer ML, Kinnison ML, Perler BA, White RI. Blue toe syndrome: treatment with anticoagulants and delayed percutaneous transluminal angioplasty. *Radiology* **1988**;166:31–36
8. Kumpke DA, Zwerdlinger S, Griffin DJ. Blue digit syndrome: treatment with percutaneous transluminal angioplasty. *Radiology* **1988**;166:37–44
9. Simpson JB, Selmon MR, Robertson GC, et al. Transluminal atherectomy for occlusive peripheral vascular disease. *Am J Cardiol* **1988**;61:96–101

LIST OF BOOK AND VIDEOTAPE REVIEWS

34 **RSNA Today Video, Vol. 5, No. 6.** *The Radiological Society of North America*
44 **Cardiac Imaging in Infants, Children, and Adults.** *Elliott LP*
68 **Ultrasound of Appendicitis and Its Differential Diagnosis.** *Puylaert JBCM*
76 **The Cystic Kidney.** *Gardner KJ Jr, Bernstein J*
82 **Échographie en Pratique Obstétricale.** *du Masgenêt BG, Ardaens Y, Bailleux B, de L'Aulnoit DH*
92 **Diagnostic Ultrasonics. Principles and Use of Instruments, 3rd ed.** *McDicken WN*
100 **The Traumatized Hand and Wrist. Radiographic and Anatomic Correlation.** *Gilula LA*
128 **Echocardiography.** *Craig M, ed*
136 **A Practical Guide to Ultrasound of Fetal Anomalies.** *Hegge FN*
148 **Radiology of the Extremities.** *Baker N*
160 **Head and Neck Radiology.** *Noyek A*
176 **Pediatric Orthopedic Radiology, 2nd ed.** *Ozonoff MB*

Book Review

Echocardiography. Edited by Marveen Craig. (Vol. II in Diagnostic Medical Sonography. A Guide to Clinical Practice.) Philadelphia: Lippincott, 416 pp., 1991. $85

Marveen Craig has had significant experience as a sonographer and teacher and is highly respected in the field of echocardiography. In addition, she has solicited the expertise of other sonographers, who are equally prominent, as contributors. The first three chapters (part I) offer a thorough review of the normal anatomy and physiology of the heart. The following five chapters (part II) are about the fundamentals of echocardiography. Chapter 4 is a complete review of the basic physical principles and instrumentation used. Chapters 5 and 6 present the standard two-dimensional imaging planes and practical hints to obtain optimal M-mode and two-dimensional images. Chapter 7 presents basic M-mode formulas used for volumes and ejection fraction, recommended by the American Society of Echocardiography. Chapter 8 gives useful tips on managing an ultrasound laboratory.

Chapters 9–21 (parts III–V) are about specific clinical applications of echocardiography and Doppler imaging. They include sections on mitral and tricuspid valve disease, aortic and pulmonic valve disease, cardiomyopathies, coronary artery disease, pericardial disease, inflammatory disease, cardiac trauma, prosthetic heart valves, transesophageal and intraoperative echocardiography, cardiac embryology, and congenital heart disease. All of the sections have examples of the most common findings in all of these diseases. The last chapter is about the role of the sonographer and the training guidelines for physicians and sonographers who perform echocardiography.

The chapter on transesophageal and intraoperative echocardiography lacks the basic imaging scan planes and up-to-date information. Another weakness of the book is the lack of high-quality figures, making it difficult to illustrate many of the points adequately as single-stop frames. Also, more color figures would enhance the overall strength of the book.

We recommend this book mainly for beginning cardiologists and sonographers who want to begin performing and interpreting two-dimensional and Doppler echocardiography.

Nancy Dalton
David J. Sahn
University of California, San Diego, Medical Center
San Diego, CA 92103

Technical Note

Wallstent Misplaced During Transjugular Placement of an Intrahepatic Portosystemic Shunt: Retrieval with a Loop Snare

Robert B. Sanchez,[1] Anne C. Roberts, Karim Valji, Steven Lengle, and Joseph J. Bookstein

Expandable metallic stents are important tools in the bronchial [1], biliary [2, 3], urinary [4], and vascular systems [5, 6], although their use in these systems is still investigative, and their efficacy has yet to be proved. Transjugular intrahepatic portosystemic shunt (TIPS) procedures have become feasible since the advent of these stents [6, 7]. As with any procedure, complications may occur, and migration of these stents during placement is possible. We describe the use of a right-angled loop snare to retrieve a Wallstent that was misplaced during a TIPS procedure.

Case Report

A TIPS procedure was performed in a 43-year-old man with a history of IV drug and alcohol abuse and portal hypertension. A single episode of esophageal variceal bleeding caused a decrease in his hematocrit to 0.22. The patient was not a surgical candidate because he was a Jehovah's Witness, which precluded perioperative blood transfusions.

After gaining access to the portal venous system via the jugular approach by using a Ring transjugular portography set (Cook, Bloomington, IN), we dilated a tract through the liver and placed two Wallstents (Schneider U.S. Stent Division, Minneapolis, MN). After dilatation to 10 mm, the stents failed to overlap, and a third stent was deployed. After dilatation to 10 mm, the third stent migrated cephalad along the guidewire, completely overlapping the second stent and no longer covering the gap between the first two stents. A fourth stent was deployed to bridge the gap. During the placement of the fourth stent, the third stent migrated farther cephalad along the guidewire into the right atrium (Fig. 1A).

A right-angled loop snare (Microvena, Vadnais Heights, MN) was used to retrieve the stent. The loop of the snare was placed over the guidewire, and the catheter containing the snare (except for the protruding loop) was inserted along the side of the guidewire into the 9-French sheath in the jugular vein. The snare was opened and placed around the stent. The loop was then tightened, compressing the stent against the guidewire (Fig. 1B). The stent was then pulled back firmly against the distal end of the sheath. The guidewire was removed while firm tension was applied on the loop to prevent escape of the stent. By pulling firmly on the snare, we were able to fold the stent into the access sheath and completely remove it from the patient (Fig. 1C).

Discussion

TIPS is the equivalent of a portacaval shunt that is placed percutaneously. Although the procedure is in its infancy, initial results are favorable, and in experienced hands, the procedure appears to be safe even for patients with liver failure and coagulopathy [6, 7]. One of the potential complications is stent misplacement or migration. The ability to percutaneously retrieve misplaced stents improves the safety and efficacy of TIPS procedures.

Received November 18, 1991; accepted after revision January 2, 1992.

[1] Department of Department of Radiology (H-756), University of California, San Diego, Medical Center, 225 Dickinson St., San Diego, CA 92103. Address reprint requests to R. B. Sanchez.

AJR 159:129–130, July 1992 0361–803X/92/1591–0129 © American Roentgen Ray Society

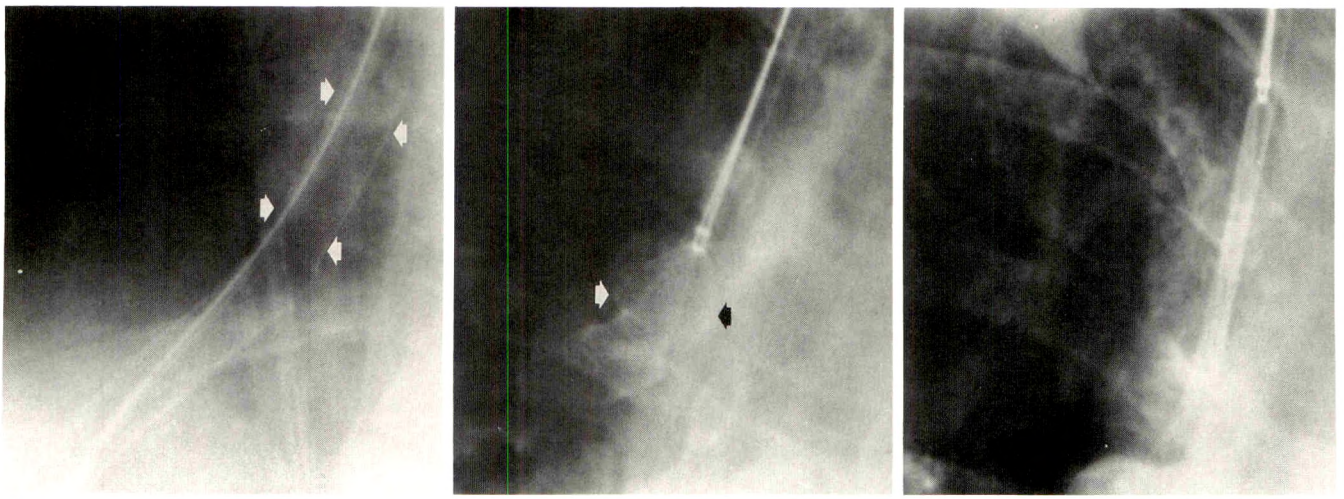


Fig. 1.—Radiographs show removal of stent during transjugular placement of an intrahepatic portosystemic shunt.
***A*, Two stents can be seen in liver. Third stent is misplaced in right atrium (*arrows*), but guidewire is still through stents.**
***B*, After guidewire removal, stent (*arrows*) is doubled over as it is removed by snare.**
***C*, Stent has been pulled back into sheath and is doubled over and compressed.**

It is useful to consider the possible causes of the stent misplacement. We suspect that the inner of two concentric stents will slide relatively easily, while the outer stent is much more restrained by invaginations of hepatic parenchyma. The migration of the third stent occurred despite its having been fully dilated to 10 mm within the stents that had previously been dilated to 10 mm. Thus, the original overlap of the third stent over the first and second stents was lost as the inner third stent migrated easily within the outer first two. We believe that the third stent migrated because no tissue retained it in place. The same event probably explained the ease with which this stent migrated farther until it was entirely within the right atrium, while the fourth stent was being placed. Before migration, the distal end was within the second stent, and the stent was probably loose proximally within a large hepatic vein. Although one of us has previously placed many biliary Wallstents, this event occurred early in our experience with vascular placement, and the possibility of a technical error cannot be completely excluded.

Without the guidewire in place, the stent could have embolized into the heart or lungs. We initially considered manipulating the stent over a balloon into the jugular or iliac veins; however, the recipient vein would have been susceptible to thrombosis, and the stent could have been lost during repositioning.

Technically, snaring and removing the stent by means of snare-loop-over-the-wire technique was quite simple. Because the Wallstent is so flexible and compressible, it was easily pulled back into the sheath and removed. Maintaining the guidewire across the stent was critical in preventing complete escape of the third stent and in facilitating passage of the snare loop around the stent. When it was finally necessary to remove the guidewire so that the stent could be folded into the sheath, great care was exercised to maintain a tight loop.

In conclusion, it is possible to have stent migration during a TIPS procedure. It is important to visualize the position of the stent before the guidewire is removed. If stent migration has occurred, the flexibility of the Wallstent allows snaring and removal via a sheath.

REFERENCES

1. Simonds AK, Irving JD, Clarke SW, Dick R. Use of expandable metal stents in the treatment of bronchial obstruction. *Thorax* **1989**;44:680–681
2. Lammer J. Biliary endoprostheses. Plastic versus metal stents. *Radiol Clin North Am* **1990**;28:1211–1222
3. Neuhaus H, Hagenmuller F, Griebel M, Classen M. Percutaneous cholangioscopic or transpapillary insertion of self-expanding biliary metal stents. *Gastrointest Endosc* **1991**;37:31–37
4. Donald JJ, Rickards D, Milroy EJ. Stricture disease: radiology of urethral stents. *Radiology* **1991**;180:447–450
5. Palmaz JC, Kopp DT, Hayashi H, et al. Normal and stenotic renal arteries: experimental balloon-expandable intraluminal stenting. *Radiology* **1987**; 164:705–708
6. Richter GM, Noeldge G, Roessle M, et al. Transjugular intrahepatic portosystemic stent shunt (TIPS). *Radiology* **1990**;174:1027–1030
7. Roberts JP, Ring E, Lake JR, Sterneck M, Ascher NL. Intrahepatic portocaval shunt for variceal hemorrhage prior to liver transplantation. *Transplantation* **1991**;52:160–162

Occult Glove Perforations:
Frequency During Interventional Radiologic Procedures

Margaret E. Hansen[1]
Donald D. McIntire[2]
George L. Miller III[1]

Because the intact surgical glove is an important barrier against exposure to blood and other body fluids, occult glove perforations occurring during procedures may have implications for infection control and protection of health care workers. Although the frequency of occult glove perforations during surgery has been studied, no such data have been reported for interventional radiology. This study was designed to determine the frequency of occult glove perforations in interventional radiology. Gloves used during interventional radiologic procedures were collected and tested for occult perforations according to previously accepted methods. The frequency of occult defects in unused gloves was also determined. A form completed for each pair of gloves indicated length of use, awareness of perforations, and information about the procedure. The anatomic distribution of perforations was also studied. Occult perforations were found in 49 (10%) of 492 used gloves. The frequency of defects in unused gloves was 1% (2/160). Gloves worn fewer than 2 hr had a perforation rate of 7% (29/406), and those worn 2 hr or longer had a rate of 23% (20/86; $p < .0001$). Perforations were noticed by the wearer in only three (6%) of the 49 perforations. The perforation rate for inner gloves of a double-glove set was 3% (1/34; the corresponding outer glove also was perforated).

Although the 10% rate of occult glove perforation during interventional radiologic procedures found in this series is lower than rates described with surgical procedures, it is not insignificant. The significant increase in the rate of perforation when gloves are worn more than 2 hr suggests that gloves should routinely be changed at or before 2 hr of wear, particularly in procedures involving high-risk patients.

AJR 159:131–135, July 1992

Concern about transmission of infectious agents between health care workers and patients is rising, particularly with regard to HIV. This is due in part to widespread publicity surrounding a case in which an HIV-positive dentist is thought to have transmitted HIV to five of his patients [1]. Less well publicized is the number of health care workers who may have acquired HIV infection from occupational exposure, perhaps because in some such cases it is difficult to document how or when infection occurred [2–7]. Although the risk of occupational HIV infection is quite low, it is not zero. The overall risk of occupational hepatitis B virus transmission is of similar concern [8–10].

The Centers for Disease Control (CDC) have recommended the use of universal precautions for all health care workers whenever they may be exposed to patients' blood or other body fluids [11, 12]. Interventional radiologic procedures probably pose little risk of physician to patient transmission of infection, but could result in physicians being exposed to infectious agents. Universal precautions as endorsed by the CDC include the use of gloves, masks, goggles, and impermeable gowns where appropriate. Surgical gloves are certainly the most universally used of these barriers in interventional radiology, serving to maintain asepsis and to protect both patient and operator from transmission of infectious agents. The frequency of glove perforations occurring during interventional radiologic procedures is therefore im-

Received January 7, 1992; accepted after revision February 13, 1992.

[1] Department of Radiology, University of Texas Southwestern Medical Center, 5323 Harry Hines Blvd., Dallas, TX 75235-9071. Address reprint requests to M. E. Hansen.

[2] Academic Computing Services, University of Texas Southwestern Medical Center, Dallas, TX 75235-9071.

0361–803X/92/1591–0131
© American Roentgen Ray Society

portant. Although the frequency of occult glove perforations occurring during surgical and dental procedures has been studied [13–22], no such data have been reported for interventional radiology. This study was designed to determine the frequency of occult glove perforations during interventional radiologic procedures.

Materials and Methods

Surgical gloves used during interventional radiology procedures were collected over a 4-week period. Ultraderm (brand A) and Triflex (brand B) gloves (Baxter Healthcare Corp., Valencia, CA) and Spectra gloves (brand C) (Becton-Dickinson, Franklin Lakes, NJ) were used. Each pair of gloves was accompanied by a completed form indicating the length of time worn; the wearer's awareness of leaks, perforations, or needle sticks; the type of procedure being done; the wearer's experience level and dominant hand; and a subjective estimation of the patient's risk for HIV infection. Gloves were inspected for gross perforations and then were filled with water to check for occult perforations (Fig. 1) according to the method described by Skaug [13]. One hundred sixty unused gloves (brand A), taken from the supply of surgical gloves available in the interventional radiology procedure rooms, were evaluated in the same manner.

Data were analyzed by using the SAS statistical package (SAS Institute Inc., Cary, NC). The chi-squared test was used for data comparing perforation rates across categories. In some cases, such as the comparison across risk categories, Fisher's exact test was used because the chi-squared approximation was not optimal for these small sample sizes.

Results

Two occult perforations were found in 160 unused gloves (perforation rate, 1%). Both were in the right glove, one on the second finger and one on the third finger. Used gloves were designated as "single" when only one glove was worn on each hand. "Double-outer" and "double-inner" designated outer and inner gloves when two gloves were worn on each hand. Single and double-outer gloves were considered as one group; double-inner gloves were considered separately.

Forty-nine perforations (10%) were found in 492 single or double-outer gloves. Two were grossly visible before filling the gloves with water; neither perforation was recognized by the wearer. Forty-seven perforations were detected only after the gloves were filled with water. Only one glove had more than one perforation; in this case, only one of the two perforations was tabulated.

One perforation was found in 34 double-inner gloves (3%); the corresponding outer glove also had a perforation, and the surface of the inner glove was contaminated with blood. No perforations were found in double-inner gloves when the corresponding outer gloves were intact (0/33).

Only three of the 49 perforations were recognized by the wearers. In one case, a perforation resulted from nicking the left thumb with a scalpel blade. No bleeding occurred, and the blade was discarded without further use. No specific cause could be identified for the other two recognized perforations. In both cases, the wearers noticed fluid leaking through the glove onto their skin during the procedure or after removal of the gloves.

The anatomic distribution of glove perforations is shown in Figure 2. Dominant and nondominant hands were equally involved (53% and 47%, respectively; $p = .668$ [chi squared]). Gloves were grouped by length of time worn, and perforation rates were calculated for each group (Fig. 3): eight (6%) of 130 gloves in the 0–29 min group had perforations, nine (11%) of 86 gloves in the 30–59 min group had perforations,

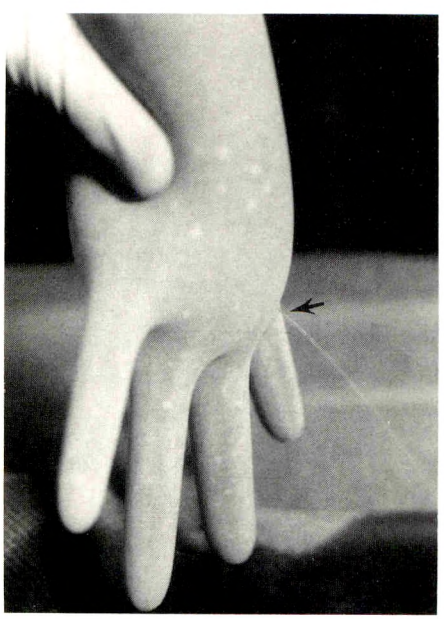


Fig. 1.—Method of glove testing. Holes are shown by fine jets of water (*arrow*) spraying from glove.

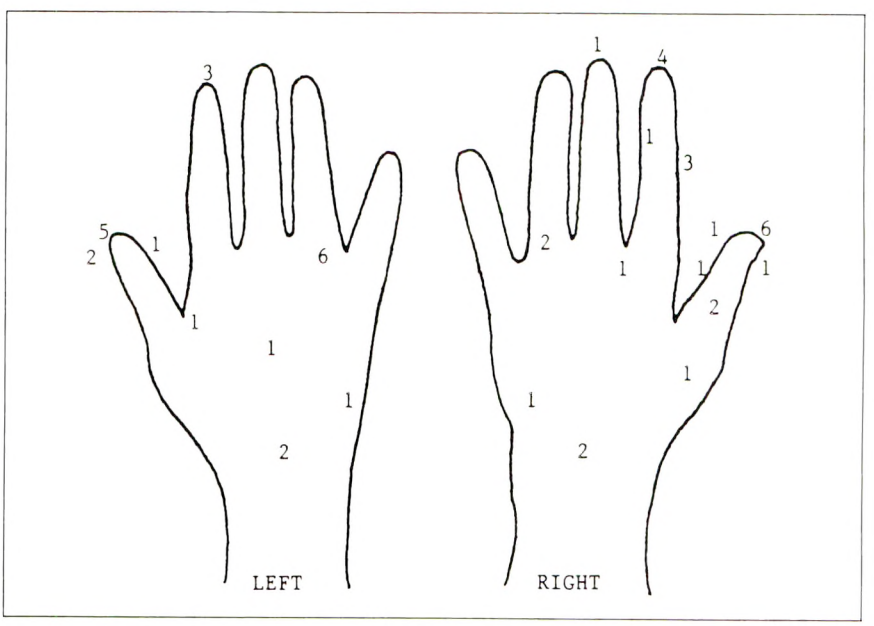


Fig. 2.—Drawing shows anatomic distribution of perforations. Palmar surface is shown, as most perforations were in palm area.

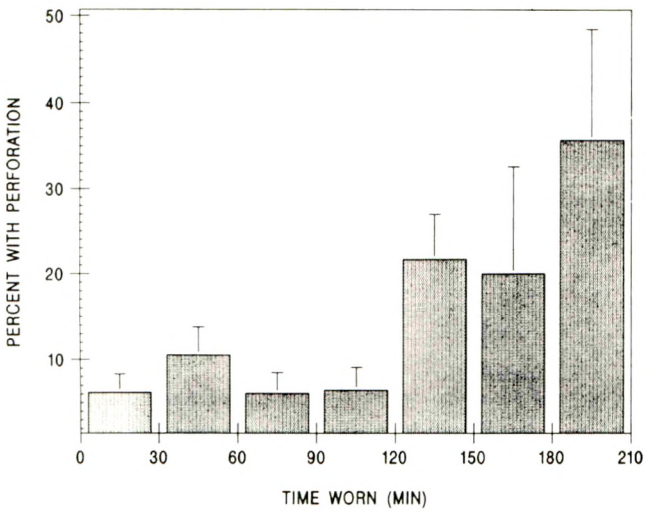


Fig. 3.—Graph shows relationship between frequency of glove perforations and length of time gloves were worn.

six (6%) of 98 gloves in the 60–89 min group had perforations, six (7%) of 92 gloves in the 90–119 min group had perforations, 13 (22%) of 60 gloves in the 120–149 min group had perforations, two (20%) of 10 gloves in the 150–179 min group had perforations, and five (36%) of 14 gloves in the 180–209 min or more group had perforations. No perforations were found in two gloves worn for more than 210 min. Perforation rates increased significantly ($p < .0001$) for gloves worn 2 hr or more. The number of gloves worn 3 hr or more was too small to determine whether the perforation rate in this group (5/16, 31%; $p = .402$ [chi squared]) was significantly higher than the rate for the 2–3 hr group. No significant difference was found in perforation rates for different types of procedures, but numbers in many of these subgroups were small. Twelve perforations (9%) were found in 136 gloves used in neuroangiography, 27 perforations (11%) were found in 242 gloves used in visceral angiography, and 10 perforations (9%) were found in 114 gloves used in nonvascular interventional procedures. No significant difference was found in perforation rates for different levels of wearer experience, but numbers in several of these subgroups were small. No perforations were found in 10 gloves worn by technologists, 30 perforations (10%) were found in 300 gloves worn by junior residents, 15 perforations (14%) were found in 108 gloves worn by senior residents, three perforations (6.5%) were found in 46 gloves worn by fellows, and one perforation (4%) was found in 28 gloves worn by faculty members.

In five cases, both right and left gloves of a pair had perforations. The duration of the procedure in these cases ranged from 5 to 180 min (mean, 114; median, 130). In four of these cases, the wearers commented on the survey form on the difficulty of the procedure. In the fifth case, the gloves were changed after 5 min because the wearer nicked one finger with a scalpel blade.

Of the 492 single or double-outer gloves, 218 (44%) were used in emergency procedures and 274 (56%) in elective cases. The frequency of perforations was 10% in both groups (22/218 and 27/274, respectively). No significant difference was found between these groups ($p = .930$, chi squared).

Patients were considered at high risk for HIV infection in six cases, at uncertain risk in 136 cases, and at low risk in 104 cases. The frequencies of perforations in these three groups were 8% (1/12), 8% (22/272), and 13% (27/208), respectively; the differences among the groups were not significant ($p = .177$, Fisher's exact test). Operators chose to wear double gloves in three (50%) of six high-risk cases, 12 (9%) of 136 uncertain-risk cases, and two (2%) of 104 low-risk cases.

Most of the used gloves were brand A (444, 90%); few B (36, 7%) and C (12, 3%) brand gloves were used. Glove selection was based on the wearer's preference in most cases; very large (size 8.5) or very small (size 6 or smaller) gloves were only stocked in brand B. The frequencies of perforations were 9% (42/444), 14% (5/36), and 17% (2/12) for brands A–C, respectively. These numbers are too small to show statistical significance ($p = .356$, Fisher's exact test; the probability of detecting a difference of three percentage points between the perforation rates for gloves B and C is only .08 with this sample size).

Discussion

The overall frequency of surgical glove perforations found in this study is lower than rates previously reported for surgical and dental procedures, which have ranged from 11% to 37.5% [13–23]. Interventional radiologic procedures involve much less handling of sharp instruments than surgical or dental procedures do, so this finding was not unexpected. Moreover, when sharp instruments are used during interventional radiologic procedures, both of the operator's hands are generally in full view rather than positioned within a body cavity, where they may be at greater risk of injury. The occult perforation rate of 10% may be greater than many interventional radiologists would expect, however, given the relatively low frequency of reported needle sticks and other recognized injuries during interventional radiologic procedures. An explanation for these occult glove injuries may lie in the types of stresses placed on gloves during interventional radiologic procedures. Pinching glove material between catheter hub and the power-injector connector is a common occurrence, as is catching a glove on a stopcock. Handling of guidewires, some of which may have sharp back ends, may also lead to occult perforations. Forceful hand injection of saline or contrast material may contribute to glove damage as well.

Some authors [17, 24] have advocated routine double gloving as a means of reducing the risk of skin contamination during surgical procedures. The number of double-glove sets in our series was too small to assess the value of this approach for interventional radiologic procedures. In addition, only one double-outer perforation occurred in our series, and the corresponding inner glove was also perforated. In this case, the perforated inner glove was contaminated with blood on the outside, indicating that it did not protect against skin contamination. The low frequency of perforations in unused

gloves (1%) indicates that routine double gloving is not warranted, although this precaution may be indicated if the wearer has a recent cut, abrasion, or other area of nonintact skin on one or both hands, or if the procedure involves a high-risk patient. In our series, operators wore double or single pairs of gloves according to personal preference. Some indicated that they routinely double gloved, even for patients estimated to be at low risk for HIV infection; others used double gloving for high-risk patients only. Most of our cases were estimated to be of uncertain risk (55%); relatively few were considered high risk (2%).

The anatomic distribution of perforations in our series, with almost equal involvement of dominant and nondominant hands, differs from that reported previously [6, 16, 21, 22]. Surgical perforations are more common on the left-hand gloves of right-handed surgeons; the left index finger is the most common site. This may be due to suturing techniques in which the left hand is used to palpate or retract tissue while suture material is passed with the right, or the needle is grasped with the fingers of the left hand after passing suture material through the tissue. In interventional radiologic procedures, both left and right hands are used about equally in many maneuvers, and should be equally at risk for glove perforations. Two obvious exceptions are administration of local anesthetics and arterial (or venous) puncture; both are maneuvers in which one hand may be used to palpate the pulse while a needle is advanced with the other [25].

The increased number of perforations in gloves worn 2 hr or longer is in agreement with previous surgical reports, which found higher rates of glove perforation or accidental injury during operations that lasted longer than 1 hr [21, 23]. Interventional radiologic procedures that last 2 hr or more are often complex or difficult. Several catheter and guidewire manipulations or exchanges may be necessary. A larger number of angiographic runs may need to be performed, with more frequent connections of the catheter to the power injector. Similarly, several hand injections may be required to follow progress or determine the position of a catheter during such a case. All of these factors could contribute to the increased frequency of perforations.

Only three of the 49 perforations in our series were recognized by the wearer of the gloves. This agrees with previous studies [14, 16, 18, 21]. Numbers in our series were too small to determine if different types of interventional radiologic procedures carry greater or lesser risk of glove perforations. However, the perforation rates for neuroangiography, visceral angiography, and nonvascular interventional procedures were fairly similar.

Operator experience may be a factor in the frequency of glove perforations, as suggested by surgical studies [13, 19, 23] in which more experienced operators incurred fewer glove perforations or accidental injuries than inexperienced operators did. Numbers in several of our subgroups are too small to show significant differences, but they do suggest a trend in this direction. However, other factors must be considered. Most interventional procedures at our institution are performed by residents, who are supervised by fellows and faculty members. Direct participation by fellows or faculty members is necessary in a minority of cases, thus accounting for the small number of used gloves from these two groups. When fellows or faculty members become directly involved, it is often for only a portion of the procedure, and they may change gloves more frequently as other tasks require attention. Thus, fellows and faculty members rarely wear a single pair of gloves for 2 hr or longer, and their gloves may not be exposed to the same stresses as those worn by residents. In addition, fellows or faculty members rarely perform catheter-injector hookups, arterial punctures, or suturing; these tasks are most often done by residents. This too may account for a reduced frequency of glove perforations for more experienced operators in our series.

The lack of a significant difference in perforation rates for emergency and elective interventional radiologic procedures agrees with the results of surgical studies, in which differences between these groups were marginal or nonexistent [16, 23]. The number of brand B or C gloves in our series was too small for us to detect significant differences in perforation rates among the three brands, all of which meet current standards for surgical gloves [26]. Further study of various glove types would be necessary to determine whether significant differences exist.

It is important to emphasize that the overall rate of glove perforation during interventional radiologic procedures is low compared with the rate for surgical procedures. It is of some concern, however, that most perforations were unrecognized by the wearer of the glove, raising the possibility of prolonged skin exposure to blood or other body fluids. Although interventional radiologic procedures do pose some risk of occupational transmission of HIV, this risk is probably quite low. Studies of surgeons and dentists have shown very low occupational risk of infection [6, 7], and risk to interventional radiologists is unlikely to be significantly higher. The risk of occupational transmission of hepatitis B virus (and hepatitis C) is greater for both patients and health care workers [8–10]. It may be prudent, especially when high-risk patients are involved, to change gloves at or before 2 hr of wear, even if the wearer is not aware of any leaks or perforations. The number of glove perforations due to needle sticks or other sharp injuries is low in interventional radiologic procedures, but all efforts should be made to reduce such injuries.

Interventional radiologic procedures do not generally involve large open incisions or work within a confined body cavity, and exposure to blood or other body fluids is usually minimal. Opportunity for contamination of the patient's wound with the operator's blood following injury is likewise small. In addition, the rate of sharp injuries in interventional radiologic procedures is low. In our series, only one injury occurred during 219 person-procedures (case exposure rate, 0.5%; 95% confidence interval, 0.01–2.5%). This is much lower than the surgical injury rate, which can be as high as 21% (Tokars J et al., presented at the VII International Conference on AIDS, June 1991). In no case from our series was a patient known to be exposed to the blood or other body fluid of an operator, either directly or via a contaminated instrument. Data from other institutions would be useful to confirm the safety of interventional radiologic procedures for both operators and patients, so that a rational approach to infection control in interventional radiology may be taken.

ACKNOWLEDGMENTS

We thank our residents and fellows for help with glove and data collection.

REFERENCES

1. Update: transmission of HIV infection during an invasive dental procedure—Florida. *MMWR* **1991**;40:21–27, 33
2. Update: acquired immunodeficiency syndrome and human immunodeficiency virus infection among health-care workers. *MMWR* **1988**;37: 229–239
3. Becker CE, Cone JE, Gerberding J. Occupational infection with human immunodeficiency virus (HIV): risks and risk reduction. *Ann Intern Med* **1989**;110:653–656
4. Beekmann SE, Fahey BJ, Gerberding JL, Henderson DK. Risky business: using necessarily imprecise casualty counts to estimate occupational risks for HIV-1 infection. *Infect Control Hosp Epidemiol* **1990**;11:371–379
5. Marcus R, CDC Cooperative Needlestick Surveillance Group. Surveillance of health care workers exposed to blood from patients infected with the human immunodeficiency virus. *N Engl J Med* **1988**;319:1118–1123
6. Lowenfels AB, Wormser GP, Jain R. Frequency of puncture injuries in surgeons and estimated risk of HIV infection. *Arch Surg* **1989**;114: 1284–1286
7. Klein RS, Phelan JA, Freeman K, et al. Low occupational risk of human immunodeficiency virus infection among dental professionals. *N Engl J Med* **1988**;318:86–90
8. Weber DJ, Hoffmann KK, Rutala WA. Management of the healthcare worker infected with human immunodeficiency virus: lessons from nosocomial transmission of hepatitis B virus. *Infect Control Hosp Epidemiol* **1991**;12:625–630
9. Snydman DR, Bryan JA, Dixon RE. Prevention of nosocomial viral hepatitis, type B (hepatitis B). *Ann Intern Med* **1975**;83:838–845
10. Welch M, Webster M, Tilzey AJ, Noah ND, Banatvala AD. Hepatitis B infections after gynaecologic surgery. *Lancet* **1989**;1:205–207
11. Recommendations for prevention of HIV transmission in health-care settings. *MMWR* **1987**;36(S2):1S–18S
12. Update: universal precautions for prevention of transmission of human immunodeficiency virus, hepatitis B virus, and other bloodborne pathogens in health-care settings. *MMWR* **1988**;37:377–382, 387–388
13. Skaug N. Micropunctures of rubber gloves used in oral surgery. *Int J Oral Maxillofac Surg* **1976**;5:220–225
14. Church J, Sanderson P. Surgical glove punctures (letter). *J Hosp Infect* **1980**;1:84
15. Brough SJ, Hunt TM, Barrie WW. Surgical glove perforations. *Br J Surg* **1988**;75:317
16. Matta H, Thompson AM, Rainey JB. Does wearing two pairs of gloves protect operating theatre staff from skin contamination? *BMJ* **1988**;297:597–598
17. Gerberding JL, Littell C, Tarkington A, Brown A, Schecter WP. Risk of exposure of surgical personnel to patients' blood during surgery at San Francisco General Hospital. *N Engl J Med* **1990**;322:1788–1793
18. Devenish EA, Miles AA. Control of *Staphylococcus aureus* in an operating-theatre. *Lancet* **1939**;1:1088–1094
19. Penikett EJK, Gorrill RH. The integrity of surgical gloves tested during use. *Lancet* **1958**;2:1042–1043
20. Shouldice EE, Martin CJ. Wound infections, surgical gloves and hands of operating personnel. *Can Med Assoc J* **1959**;81:636–640
21. Russell RT, Roque FE, Miller FA. A new method for detection of the leaky glove. *Arch Surg* **1966**;93:245–249
22. McCue SF, Berg EW, Saunders EA. Efficacy of double-gloving as a barrier to microbial contamination during total joint arthroplasty. *J Bone Joint Surg [Am]* **1981**;63-A:811–813
23. Hussain SA, Latif ABA, Choudhary AAAA. Risk to surgeons: a survey of accidental injuries during operations. *Br J Surg* **1988**;75:314–316
24. Gerberding JL, Schecter WP. Surgery and AIDS: reducing the risk (editorial). *JAMA* **1991**;265:1572–1573
25. Williams DM, Marx MV, Korobkin M. AIDS risk and risk reduction in the radiology department (commentary). *AJR* **1991**;157:919–921
26. Standard specification for rubber surgical gloves (D3577). In: *Annual book of ASTM standards*, vol. 9.02. Philadelphia: American Society for Testing and Materials, **1991**:344–346

Book Review

A Practical Guide to Ultrasound of Fetal Anomalies. By Frederick N. Hegge. New York: Raven, 242 pp., 1992. $39

Dr. Hegge's book is easily lost to view when placed on a shelf with other texts on obstetric ultrasound. However, this guide is unlikely to stay on the shelf of anyone who does obstetric ultrasound; it will probably be on the counter of the reading room, as mine is. The first 48 pages of this pocket-sized book contain eight succinct chapters giving an overview of fetal scanning technique and ultrasound's impact on detection of fetal anomalies. The last 181 pages form a pictorial atlas of fetal anomalies organized by organ system.

The first section gives a brief overview of congenital fetal anomalies, including rates, relative frequencies, associations, and detectability by ultrasound. Much of the information is presented in tabular form. A particularly useful table (Table 1-7) lists 76 drugs and chemicals to which pregnant women may be exposed and the fetal anomalies associated with such exposure. Chapters 4 through 7 describe the recommended fetal survey protocols of the American College of Obstetrics and Gynecology and the American Institute of Ultrasound in Medicine. The author outlines a complete fetal survey and shows normal anatomy as well as anomalies that might be found in each part of the survey during each trimester of pregnancy.

Regrettably, the book has no discussion of screening maternal serum for α-fetoprotein. Abnormalities of the cord, placenta, cervix, and uterus are not described; Dr. Hegge presumably thought these topics were outside the scope of his book. A short table (Table 1-8) lists the characteristics of eight named syndromes. The common chromosomal abnormalities and their associated ultrasound findings are depicted in chapter 25.

The second section of the book is a superb atlas of fetal anomalies. It is organized by organ systems and parallels the anatomic survey outlined in the first section. The illustrations are of generally high quality, although a little small. Text is kept to a minimum to make room for the illustrations. Included are fine examples of almost every common detectable anomaly. The section on the fetal heart and thorax is especially helpful. It describes in detail an expanded cardiac examination including the outflow tracts of the ventricles and shows many cardiac abnormalities that can be found by using this technique.

Not included are examples of megalocystis–microcolon–intestinal hypoperistalsis, fetal goiter, schizencephaly, and iniencephaly. Also, the association of asymmetric cephalocele with amniotic bands is not shown. In the sections on amniotic bands, it would be useful to discuss and show examples of amniotic sheets, which are much more common and may be confused with amniotic bands. Finally, one illustration (page 64) shows a transverse image through the fetal head above the corpus callosum. Bright echoes paralleling the falx are labeled as ventricular walls. These look more like the well-described echogenic lines thought to be white matter tracts or vessels.

This pocket guide is recommended for sonographers and radiologists in training to give a quick overview and serve as a handy reference during fetal surveys with ultrasound. This type of image-intensive teaching source would lend itself well to distribution on CD-ROM for use as a computerized text-atlas.

Chris Sistrom
University of Virginia
Charlottesville, VA 22908

Review Article

CNS Complications of Cocaine Abuse: Prevalence, Pathophysiology, and Neuroradiology

Eugene Brown,[1,2] Jordan Prager,[1] Hsin-Yi Lee,[1] and Ruth G. Ramsey[1]

The United States is facing an epidemic of cocaine use by adolescents and young adults from all socioeconomic backgrounds. Epidemiologic data suggest that the use of the drug continues to increase on a year-by-year basis. This is a serious public health problem because cocaine is highly addictive and is associated with a variety of serious complications. In the CNS, these include stroke, intracerebral hemorrhage, vascular spasm, and possibly vasculitis. Seizures and sudden death have been reported. Cocaine use during pregnancy may be associated with fetal hypoxia, intracerebral hemorrhage, and possibly congenital malformations in the neonate. Many of these complications have been recognized only in the last 5–10 years. For example, ischemic changes in the brains of chronic cocaine abusers have been reported only recently. Because even further increases in cocaine use are predicted by drug enforcement officials, it is expected that radiologists will encounter its complications more frequently in the future. Therefore, radiologists should become familiar with the radiologic manifestations of the drug's effects. This article describes the drug's pathophysiology and complications and discusses the evolving role of imaging procedures.

Prevalence and Background Information

It is estimated that 30–40 million Americans have some experience with cocaine and that one of every two persons between the ages of 25 and 30 years has used the drug [1]. Its use is common among 18- to 25-year-olds. Data from the National Survey on Drug Abuse showed that 19% of the respondents in this age group had used cocaine within the prior year, and one third of these persons reported they had used cocaine during the previous month [2]. Although recent data indicate a small but steady increase in use by the younger population, the prevalence of use continues to increase among all Americans as new cohorts of present users begin and continue to use this drug as they move into the older age groups [2]. Moreover, the drug has become more available in recent years. Once considered a drug of the rich, the availability and relative purity of cocaine have increased since the early 1970s, while the price has dropped. For example, from 1982 to 1984 the price of a gram of cocaine decreased to the pre-1977 level of $85 and the relative purity increased [3]. Data from the federally sponsored Drug Abuse Warning Network (DAWN) show that between 1986 and 1989 the number of times cocaine was mentioned in emergency department admission reports more than doubled, suggesting that the use and abuse of this drug continue to increase [4].

The data on the increasing use and wide prevalence of cocaine use are disturbing for several reasons. First, cocaine is a dangerous drug. It is associated with a variety of complications, including subarachnoid hemorrhage, cerebral infarction, cerebral ischemia, intraparenchymal hemorrhage, seizures, cerebral vasculitis, cerebral arterial spasm, and death [5]. The worst complication can occur the first time a person uses cocaine. A tragic example is Len Bias (Boston Celtics' draft choice in 1986) who had no history of drug use and was in excellent heath. He died 48 hr after being picked for the draft, when he was celebrating the signing of his contract.

Received September 10, 1991; accepted after revision February 5, 1992.

[1] Department of Radiology, Box 429, The University of Chicago Hospitals, 5841 S. Maryland Ave., Chicago, IL 60637-1470. Address reprint requests to J. Prager.

[2] Present address: Department of Radiology, Harvard Medical School and The Massachusetts Eye and Ear Infirmary, 243 Charles St., Boston, MA 02114.

AJR **159:137–147, July 1992** 0361–803X/92/1591–0137 © American Roentgen Ray Society

Cocaine use by pregnant women is associated with cerebral infarction in infants. A variety of cardiovascular complications, including myocardial infarction, coronary artery thrombosis, cardiac arrythmias, and episodes of transient hypertension, have been either attributed to or associated with cocaine use. These are important because they may be the cause of secondary CNS complications such as hypoxic brain injury and embolization. Various systemic complications have been described, and many patients with patterns of heavy cocaine abuse report symptoms of insomnia, lack of appetite, feeling physically run down, and lack of sexual interest [6].

Second, cocaine is a highly addictive drug. Animal studies have shown that the drug has strong reinforcing properties [7]. The short biological half-life of cocaine, coupled with its ease of use and reinforcing properties, may produce a pattern of compulsive use. One survey of callers to a toll-free hotline for cocaine users showed that between 66% and 83% reported addictive patterns of use, including loss of control over use and inability to stop using cocaine, despite repeated attempts. In addition, more than 90% of the callers reported adverse physical and psychological consequences associated with the use of cocaine [8]. The drug produces a short-lived but intense euphoria, with feelings of elation, increased energy and alertness, and decreased appetite and fatigue. The high may be followed by a dysphoric "crash" minutes later, leading to the compulsion of repeated administration and eventually addiction.

Finally, as the demand for cocaine has grown in the United States, so has a subculture of smugglers and suppliers who import the drug from its sites of production in northern South America. In these countries, cocaine affects society on many levels: from local peasants who chew the plant leaves for their stimulant effect to entire nations (most notably Colombia, where cocaine trade is the leading source of foreign exchange) that depend on it as a source of wealth and economic growth. It is reported that approximately 400,000 acres are devoted to the illegal cultivation of coca [9]. It is apparent that the medical, behavioral, and economic impact of cocaine is immense.

Until recently, relatively little information was available about the complications associated with cocaine abuse. In fact, in the early 1970s, even drug experts concluded that cocaine was a relatively harmless drug. The National Commission on Marijuana and Drug Abuse in 1973 stated that "little social cost related to cocaine has been verified in this country" [8]. At the same time, the Strategy Council on Drug Abuse stated that the morbidity associated with cocaine use did not appear to be great [8]. Today, we know better. In this review, we examine the effects of cocaine on the CNS and review the neuroradiologic features of CNS complications of cocaine abuse.

Pharmacology and Usage

The pharmacologic effects of cocaine can be understood by examining its three major sites of action. First, cocaine provides local anesthesia, and the drug was initially introduced in 1884 for this purpose. The local anesthetic effect is due to the blockage of propagation of electrical impulses within nerve cells by preventing rapid depolarization of the cell membrane and the rapid influx of sodium ions [10]. The systemic effects of cocaine, in contrast, are mediated by alterations in synaptic transmission. The drug blocks the presynaptic reuptake of norepinephrine and dopamine. As a result, the concentration of these transmitters at the postsynaptic receptor site increases. This leads to activation of the sympathetic nervous system, with the production of tachycardia, increased systolic blood pressure, mydriasis, and other sympathomimetic effects [10, 11]. The effect of cocaine on the dopaminergic neuronal systems in the brain is thought to be mediated by short-term blockage of dopamine reuptake. However, it is thought that long-term use causes depletion of dopamine at these sites. This may be the mechanism by which alterations in dopaminergic transmission occur, leading to dysphoria and craving for more of the drug.

Cocaine is an alkaloid that occurs within the leaves of the shrub *Erythroxylon coca*, which is indigenous to Peru and Bolivia. The leaves can be chewed directly, or the drug can be prepared in more concentrated forms. The most common form is cocaine hydrochloride, which is prepared by dissolving the alkaloid in hydrochloric acid. A water-soluble salt is formed, which is most often ground to a fine powder. On the street, this is often diluted with talc, procaine, or sugar. This mixture can then be snorted or applied to mucous membranes, where it is absorbed into the bloodstream. The hydrochloride form is unsuitable for smoking, however, because it decomposes on heating and melts at 195°C.

Free base and crack (alkaloidal free base of cocaine hydrochloride) can be smoked. Many users prepare their own free base from the hydrochloride form by extracting cocaine with an alkaline solution. A solvent such as ether can then be added. The mixture separates into two layers; the top layer contains the cocaine. The solvent can then be evaporated, leaving relatively pure cocaine. The process can be hazardous because of the ether, which is quite volatile [12]. Crack is prepared by combining cocaine hydrochloride with baking soda and water and then heating the mixture to remove the water. Crack has different chemical properties from cocaine hydrochloride. It melts at 98°C and vaporizes at higher temperatures; thus, it can be smoked. The name crack comes from the popping sound the drug makes when it is heated.

Neurovascular Complications

Although a relatively large and varied group of CNS complications in patients who abuse cocaine has been described, most patients primarily have either ischemic manifestations, intraparenchymal hemorrhage, or subarachnoid hemorrhage. Table 1, a compilation of several studies, shows the profile of neurovascular complications. When neurologic signs are present, imaging studies show findings associated with neurologic abnormalities in nearly 80% of cases. Hemorrhage occurs about twice as frequently as ischemia does. Table 2 shows the causes of hemorrhage. When hemorrhage is present, a preexisting vascular abnormality is shown on angiograms in approximately half the cases.

TABLE 1: Neurovascular Complications of Cocaine Abuse

Study	No. of Patients	No. with Abnormal Imaging Findings	Percentage of Patients with Neurologic Signs and Abnormal Imaging Findings	No. with Infarct	No. with Hemorrhage
Gean-Marton et al.[a]	48	37	77	10	27
Jacobs et al. [13]	16	14	87	6	8
University of Chicago (unpublished)	8	8[b]	8	5	3
Nolte and Gelman [14]	27	—[c]	—[c]	8	19
Total	99			29	57

[a] Presented at the American Roentgen Ray Society meeting, May 1991.
[b] The University of Chicago study included only patients with abnormal imaging findings.
[c] Imaging results are not known for each patient.

TABLE 2: Hemorrhage Associated with Cocaine Abuse

Study	Number of Patients				
	Total	With Aneurysm	With Arteriovenous Malformation	With Tumor/Other	With No Angiography or with Normal Angiographic Findings
Gean-Marton et al.[a]	27	10	2	2	14
Jacobs et al. [13]	8	2	1	0	5
University of Chicago (unpublished)	3	2	1	0	0
Nolte and Gelman [14]	19	5	2	1	11
Total	57	19	6	3	30

[a] Presented at the American Roentgen Ray Society meeting, May 1991.

Cerebral Ischemia

Jacobs et al. [13] surveyed a population of more than 3700 drug abusers. Fifty-four percent of the patients (mean age, 34 years) with radiologic abnormalities had ischemic complications. The rest of the patients were equally divided between those with subarachnoid hemorrhage (23%) and those with intracerebral hemorrhage (23%). Of the patients with ischemic manifestations, the vast majority (83%) had infarctions involving the distribution of the right or left middle cerebral artery. The infarctions were generally subcortical, although one of the patients had an infarct that involved the cortex as well. We have seen similar cases and patients with single and multiple infarcts (Figs. 1 and 2). Three of the patients in the study of Jacobs et al. had angiography. Findings included occlusion of both the anterior cerebral arteries and the posterior branches of the left middle cerebral artery and stenosis of the M1 segment of the left middle cerebral artery.

Although ischemic effects of cocaine are now known to be a complication of cocaine abuse, they may be far more common than is generally appreciated. A study by Tumeth et al. [15] that used single-photon emission computed tomography (SPECT) included 12 cocaine abusers, 11 of whom had focal perfusion deficits. The defects were most often scattered throughout the frontal and temporal lobes. None of the patients were HIV-seropositive, and a control group of five patients all showed normal findings on SPECT. Tumeth et al. found that the severity of the defects seen on SPECT correlated with the frequency of use and dose of cocaine as reported by the users. Defects were seen with CT in only three of the 12 cocaine abusers. These same patients had the most severe abnormalities on SPECT. In contrast, nine patients with mild or moderate cocaine use and moderate defects shown by SPECT had no corresponding defects on CT scans. This raises the possibility that a large amount of subclinical ischemic disease in cocaine users is not detected by conventional imaging (CT). It would certainly be of interest to examine MR images of similar patients to see if areas of ischemia are shown more commonly on MR images than on CT scans. Volkow et al. [16] detected abnormal cerebral blood flow in 14 of 20 cocaine addicts who had positron emission tomography (PET). Interestingly, however, the authors found abnormal cerebral blood flow in seven of 24 control subjects, thus raising questions about the specificity of PET scanning.

Cerebral vasculitis.—The mechanism for cocaine-induced cerebral ischemia is poorly understood, but some have suggested that it might be cerebral vasculitis. For example, Kaye and Fainstat [17] reported a case of a 22-year-old man with cocaine-induced "vasculitis." Two radiographs provided with their study showed marked constriction of the supraclinoid carotid artery and the M1 segment of the middle cerebral

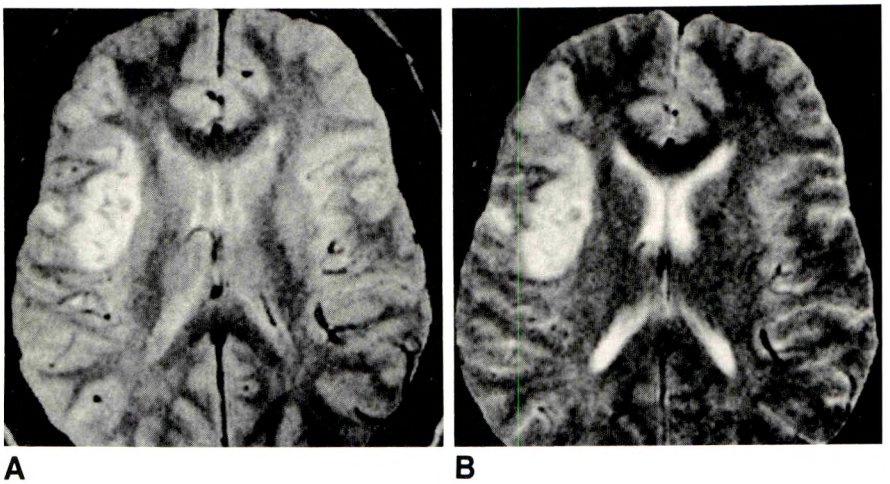


Fig. 1.—Ischemic infarction. 36-year-old man woke up with left hemiparesis after having snorted cocaine previous evening.
A and *B*, Intermediate (*A*) and T2-weighted (*B*) MR images show increased signal intensity of lesion in insula and frontotemporal lobe cortex.

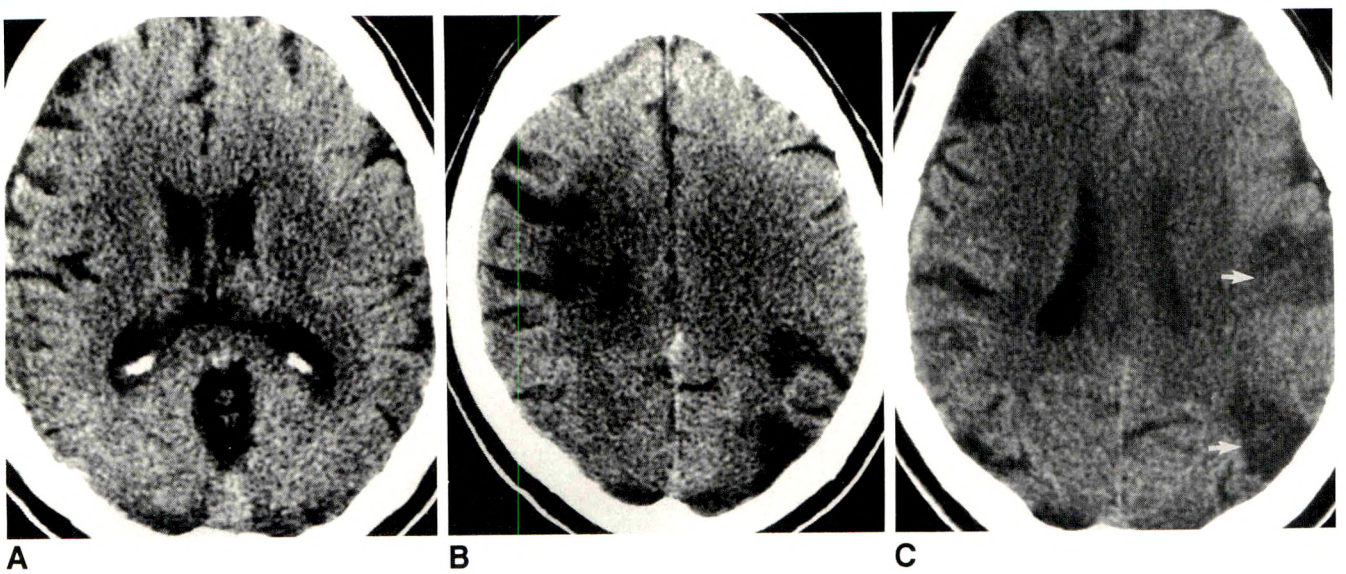


Fig. 2.—Multiple ischemic infarcts. 42-year-old chronic cocaine user with headache.
A and *B*, CT scans show multiple bilateral cortical and subcortical infarcts. Note normal appearance of left temporofrontal region in *A*.
C, CT scan obtained 2 days after *A* and *B* shows new left frontotemporal cortical infarcts (*arrows*).

artery. No evidence of peripheral involvement was seen, and the erythrocyte sedimentation rate was at the upper limit of the normal range. No biopsy was done, although the patient reportedly improved when treated with prednisone. Classically, cerebral vasculitis involves a characteristic pattern of narrowing and dilatation of the small and medium-sized vessels. This pattern has been seen with the vasculitis associated with use of amphetamines and phenylpropanolamine. However, the pattern of involvement in the case reported by Kaye and Fainstat mainly involved the large vessels at the base of the brain, and this pattern has also been reported by others [13]. This may simply represent an example of cocaine-induced vasospasm and not a true vasculitis. Others [18, 19] have suggested vasospasm as a diagnosis in the Kaye and Fainstat case and have attributed the abnormality to associated subarachnoid hemorrhage. One case of biopsy-proved vasculitis associated with cocaine use has been reported, but it appears that this is a rare event [20, 23]. This is in contrast to cases associated with use of amphetamines, which cause an inflammatory vasculopathy with necrosis of the vessel wall potentially leading to rupture and hemorrhage [20, 22].

Cerebral vasospasm.—Another possible mechanism for cocaine-induced cerebral ischemia may involve the induction of spasm (Fig. 3). Intuitively, this seems reasonable because it is well known that cocaine induces spasm of the coronary arteries [23] and potentiates contraction of vascular smooth muscle. This appears to be a direct effect of cocaine and may be independent of α-adrenergic stimulation because it has been shown to occur in tissues that lack sympathetic innervation [24]. Also, it has been shown in vitro and in vivo that this effect is not blocked by pretreatment with prazosin or phentolamine but is consistently blocked by pretreatment with

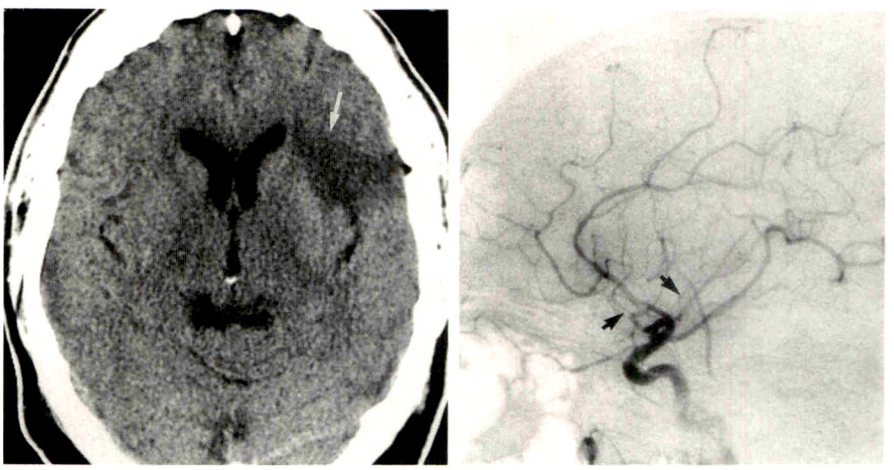


Fig. 3.—Spasm-induced infarction. 34-year-old crack user with acute onset of right hemiparesis and slowed speech.

***A*, CT scan shows cerebrovascular accident (*arrow*) in left frontotemporal region.**

***B*, Angiogram shows spasm of small vessels from middle cerebral artery (*arrows*) and overall paucity of vessels in frontal region.**

diltiazem [24, 25]. This suggests that the potentiating effect of cocaine on the contraction of vascular smooth muscle may be a direct result of the drug's action on calcium channel flux. Moreover, although most of these in vivo and in vitro data have been obtained from studies of the coronary arteries, the direct vasconstrictive effect of cocaine on cerebral vessels has recently been shown in a cat model [26]. Wang et al. [27] have shown that in rabbits, cocaine or methamphetamine alone failed to produce significant basilar artery spasm, whereas the combination of the two drugs produced definite basilar artery vasospasm. The observed vasoconstrictive effect was synergistic, representing a far greater response than that of either drug alone.

Indeed, these results are a departure from the classically held views about the drug's mode of action. It appears that the vasospastic effects of cocaine in the cerebral vasculature may be due to both direct effects on calcium channels and sympathomimetic effects. The potentiation of vasospasm by the coadministration of cocaine and amphetamines is of interest because cocaine available on the street is often impure and may be cut with amphetamine [28]. Recently, the use of calcium channel blockers has been advocated in the treatment of acute cocaine poisoning; they reduce both the clinical effects of the drug and the subjective effects of the poisoning [29].

Although it appears that pharmacologically induced vasospasm may be a prime contributor to the ischemic toxic effects of cocaine, other mechanisms have been proposed, including vasospasm related to acute hypertension. This is based on the observation that the pattern of subcortical and lacunar infarcts seen in systemic hypertension is indistinguishable from that seen with cocaine [13]. Presumably, this is based on the transient rise in systolic blood pressure that is seen shortly after cocaine is ingested. In fact, cocaine-induced ischemia may be multifactorial in origin, with both the adrenergic stimulant effects and the direct effects on vascular smooth muscle contributing to the toxic effects [25].

Cerebral thrombosis.—Cocaine affects hemostasis by directly enhancing platelet aggregation via the drug's effect on arachidonic acid and thromboxane [30]. Cocaine also may have direct procoagulant effects mediated by depletion of antithrombin III and protein C in patients with cocaine-related arterial thromboses [25]. The effects of cocaine on the clotting system and platelet aggregation have been described in studies of the coronary circulation; whether these effects contribute significantly or directly to cocaine-induced cerebral ischemia is unclear.

Secondary complications.—Finally, ischemic complications in the CNS also may be produced as the result of cocaine's effects on other organ systems. The well-known cardiovascular complications of cocaine include myocardial infarction, acute coronary artery thrombosis, cardiac arrhythmias, asystole, and respiratory arrest [5, 31]. Any of these complications could theoretically affect the CNS by causing either decreased perfusion or embolization of blood products. In addition, impurities such as talc or sugar in street cocaine could find their way into the cerebrovascular system (especially with IV injection) and cause embolization. Perhaps this is related to the increased frequency of hemorrhagic ischemic events seen in IV drug users.

Intraparenchymal Hemorrhage

Intraparenchymal hemorrhage, one of the two main types of intracerebral hemorrhage seen with cocaine use, is a well-known and frequent complication (Figs. 4 and 5). For example, Nolte and Gelman [14] reviewed the literature from 1977 through 1989 and found 18 cases of intracranial hemorrhage associated with cocaine use. Of these, seven patients had intraparenchymal hemorrhage without any predisposing factor. Along with their literature review, the authors included a case report of an intracerebral hemorrhage in a 29-year-old woman who died after having abused cocaine for many years. An autopsy showed "no evidence of infarction, neoplastic infiltration, vascular malformation or vasculitis. There were no deposits of amyloid, and the arteriolar walls were not thickened or sclerotic and did not suggest chronic hypertension."

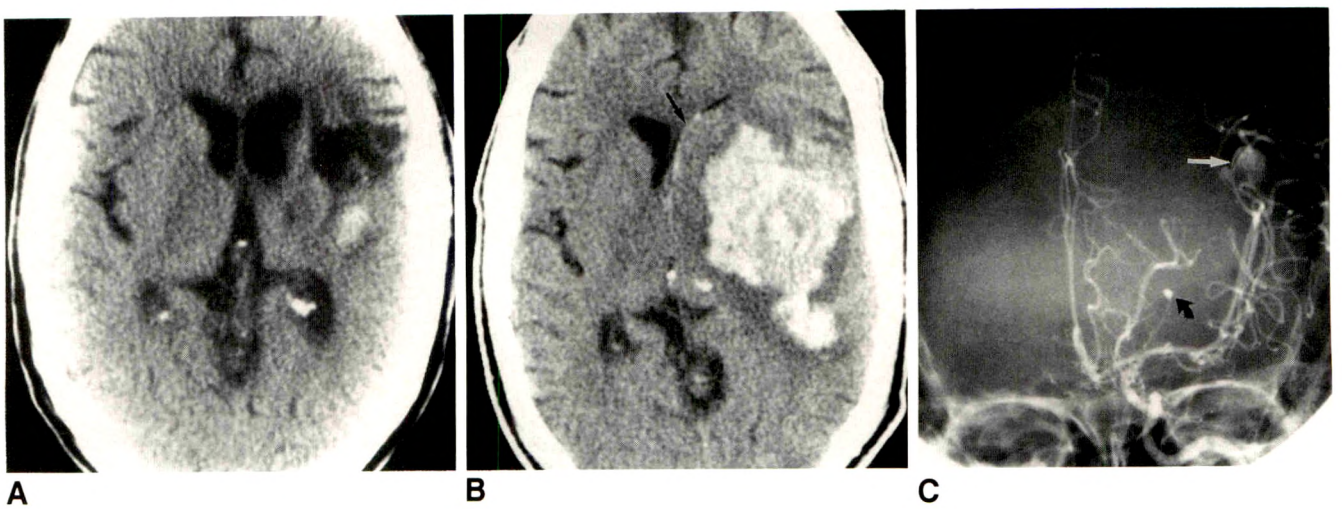


Fig. 4.—Intraparenchymal hemorrhage due to aneurysm.

A, CT scan obtained because of complaint of headache in 46-year-old chronic crack abuser shows increased-attenuation lesion in left frontal lobe and enlarged sylvian fissure and frontal horn. High-attenuation lesion is probably unruptured aneurysm. A small hemorrhage around aneurysm also is suggested.

B, CT scan obtained 2 days later because of increasing headache and neurologic signs shows large hematoma with intraventricular hemorrhage (*arrow*). Left lateral ventricle is markedly compressed and midline is shifted.

C, Angiogram shows two aneurysms, a larger one (*white arrow*) in branch of middle cerebral artery and a smaller one (*black arrow*) with associated spasm from a lenticulostriate artery.

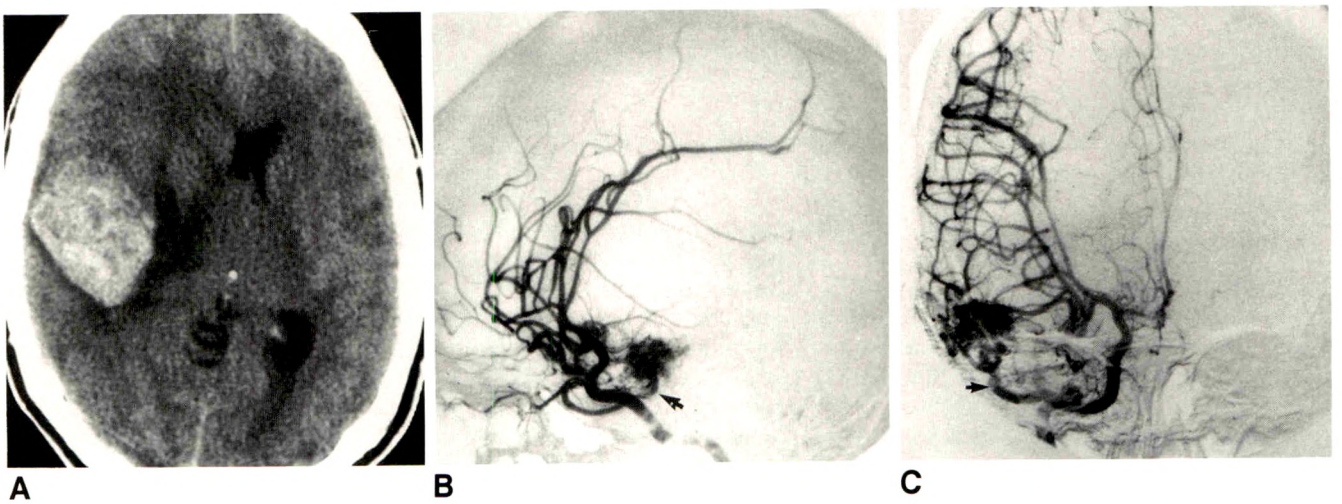


Fig. 5.—Intraparenchymal hemorrhage from arteriovenous malformation. Acute onset of headache and left hemiplegia in 40-year-old chronic cocaine abuser.

A, CT scan shows right temporal hemorrhage with edema and mass effect.

B and *C*, Angiograms show collection of abnormal vessels in anterior temporal lobe with an early draining vein (*arrow*).

Jacobs et al. [13] reviewed the records of more than 3700 drug abusers and found that four had had intracerebral hemorrhage. The intraparenchymal hemorrhages were most often central, in the region of the putamen or thalamus. One patient with a temporal parietal hemorrhage had an underlying vascular malformation. Wojak and Flamm [32] described six patients with intracranial hemorrhage, three of whom had intraparenchymal hemorrhage. Of these, one had an underlying arteriovenous malformation and one had an astrocytoma. The third patient had no vascular abnormality.

It is apparent that cocaine-induced intraparenchymal hemorrhage varies in appearance and location. It may or may not be associated with underlying vascular malformations or tumors. Although in some cases hemorrhage appears to be related to underlying ischemia, many cases do not show evidence of underlying disease. This raises questions about the relationship between ischemic disease and hemorrhagic disease in these patients. Some authors have suggested that hemorrhagic strokes are more common than "bland" strokes in cocaine users [33]. Several mechanisms could account for

these findings. Hemorrhages may be occurring in areas that are already ischemic. As previously noted, both direct effects of cocaine on vascular smooth muscle and local sympathomimetic effects of the drug may contribute to this phenomenon. Reperfusion of temporarily ischemic areas might then lead to hemorrhage. Alternatively, systemic effects such as the transient increase in the systolic blood pressure might be involved. The appearances of cocaine-induced intraparenchymal hemorrhages and hemorrhages seen in hypertensive patients are strikingly similar. (This refers to the hemorrhages that tend to be centrally located and unassociated with underlying vascular malformations. Previously, we noted the similarity in the patterns of subcortical infarcts in these same two groups of patients.) Despite the radiologic similarities of appearance, it remains unclear whether hypertension is involved in the pathogenesis of intraparenchymal hemorrhage in the cocaine users. Certainly, this mechanism has been postulated [13]. Embolization from the heart related to cocaine-induced arrhythmias, asystole, or myocardial infarction also may produce hemorrhagic cerebral infarctions in some patients.

Subarachnoid Hemorrhage

The second group of patients with intracranial hemorrhage is made up mostly of patients who have subarachnoid hemorrhage, although some patients with intraparenchymal hemorrhage may fall in this group also. Primarily, these patients have underlying vascular abnormalities. Berry aneurysms of the circle of Willis are a common finding (Fig. 6); however, arteriovenous malformations or tumors may be seen as well. Rarely, superior sagittal sinus thrombosis with hemorrhagic venous infarction, dural arteriovenous fistula, rupture of multiple mycotic aneurysms, and large-vessel thrombosis have been described (Gean-Marton AD et al., presented at the American Roentgen Ray Society meeting, May 1991). In patients with subarachnoid hemorrhage but no lesion shown by CT or angiography, MR should be considered because some angiographically occult vascular malformations may then be detected.

Cocaine-induced stroke in patients with underlying vascular malformations is thought to be due to the transient elevation of blood pressure that occurs after cocaine ingestion [13, 32, 34]. Hemorrhage may occur within seconds of cocaine use or may lag use by as much as 12 hr. In many cases, however, it occurs within a few minutes. This corresponds well with the known transient period of increased systolic blood pressure seen in these patients [11]. The cases in which hemorrhage is delayed are more problematic from a mechanistic point of view. The increased systolic pressure is known to last less than an hour in almost all cases.

The patients who have these hemorrhages and infarctions are generally young and have an otherwise low prevalence of stroke. Most cocaine-induced strokes occur in patients less than 50 years old [35], and in one series, the mean age was 34 years [13]. Although these patients may have other unspecified risk factors, such as underlying hypertension or alcohol abuse, the high prevalence of stroke is impressive. In a study of all patients between 17 and 44 years old who were treated for stroke in a 9-year period at San Francisco General Hospital [36], 34% of the strokes were associated with recreational drug use. In the patients 35 years old or younger, the association was stronger and was found in 47%. Cocaine was the most common drug used by these patients. In view of these data, it may be prudent to consider cocaine use as a possible cause whenever stroke or hemorrhage is seen in patients less than 40 years old.

Other CNS Complications

Cerebral Atrophy

Cerebral atrophy has recently been described as a complication of chronic cocaine abuse [37]. Pascual-Leone et al. compared the CT scans of 35 habitual cocaine abusers with scans of a group of first-time users and a large group of headache patients. The authors found a statistically significant

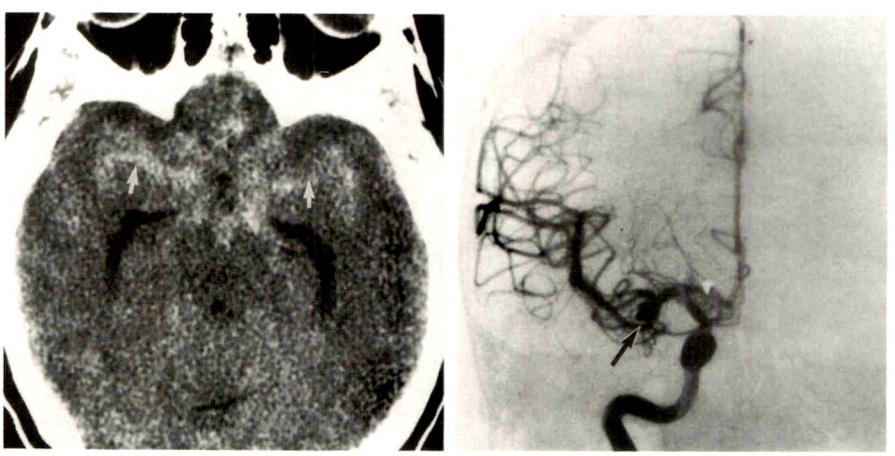


Fig. 6.—Subarachnoid hemorrhage. 39-year-old with acute onset of headache while snorting cocaine.

***A*, CT scans show subarachnoid hemorrhage (*arrows*) in sylvian and interhemispheric fissures.**

***B*, Angiogram shows lobulated aneurysm (*arrow*) of middle cerebral bifurcation.**

increase in the indexes of atrophy in the chronic abuser group. The atrophy mainly affected the frontal lobes. These results agree with those of Tumeth et al. [15], who detected multiple areas of ischemic changes in a frontotemporo parietal distribution in chronic cocaine users imaged with SPECT. The correlation between the data in these two studies suggests that the underlying mechanism for the development of atrophy in these patients may be ischemic. The authors [37] were unable to correlate any significant behavioral changes with these findings.

Seizures

Another common complication of cocaine abuse is seizures. Lowenstein et al. [38] reported that seizure was the most common complication of cocaine encountered in their survey of 1130 visits to the emergency department at San Francisco General Hospital. The prevalence of seizures may be even higher than suspected. User surveys have indicated much higher prevalences than those reported in the DAWN data [4]. This might, in part, reflect the fact that many users might not seek medical attention. Alternatively, the cause of some seizures may be misdiagnosed because the patient says he or she does not use cocaine or because toxicology screening may not be performed. The mechanism of cocaine-induced seizures has long been thought to be related to the local anesthetic action of the drug. Like lidocaine, cocaine lowers the seizure threshold and can block nerve cell conduction [39]. Seizures are one of the few complications of cocaine use in which a direct relationship with dose has been shown [35]. All routes of administration are associated with seizures, and seizures can be induced in some persons by small quantities of the drug [40]. Although most cocaine-induced seizures are benign and self-limiting, seizures may be due to other more severe complications, such as infarction and intracranial hemorrhage.

Rare CNS Complications

Severe cocaine overdose rarely may be associated with a symptom-free interval of up to 1 hr followed by the sudden onset of generalized seizures, respiratory collapse, and death [41].

Other rarely reported complications include hyperthermia; hypothalamic involvement with increased appetite, kleptomania, and personality changes; transient ischemic attacks; lateral medullary syndrome; partial motor seizures; transient hemiparesis; and fungal cerebritis [5, 35, 41, 42]. Psychiatric complications include depression, suicidal ideation, paranoia, hallucination, and catatonia [5, 41]. In most of these cases, the mechanism and relationship to underlying cerebrovascular abnormalities are poorly understood. In many of these cases, a temporal association with cocaine use is the only factor that links them to cocaine. This, of course, does not necessarily imply causality.

In our review of the literature, we found only two reported cases of involvement of the spinal cord from acute cocaine poisoning. In one of these, quadriplegia developed in a 31-year-old man after he snorted cocaine [43]. Unfortunately, no pathologic proof was obtained, and the results of MR imaging were described as "inconclusive due to technical difficulties." We conclude that although involvement of the spinal cord and anterior artery has been reported as a rare CNS complication of cocaine abuse, relatively few well-documented cases have been reported and this area deserves further study.

Head and Neck Complications

In the head and neck, the common complications of cocaine use are related primarily to irritation of the respiratory mucosa of the nose or mouth, depending on the route of administration. In users who apply cocaine directly to the gums, lacerations of the gingival mucosa may occur [44]. These patients also may have a higher prevalence of decayed or missing teeth, as well as advanced periodontal disease. In users who snort the drug, nasal irritation, stuffiness, rhinorrhea, and atrophy of the nasal mucosa may occur [45]. This may lead to necrosis of the nasal mucosa and turbinates. Epistaxis, crust formation, ischemia, and perforation of the nasal septum may occur with chronic intranasal use. Significant structural damage to the nasal cavity may follow, with disintegration of

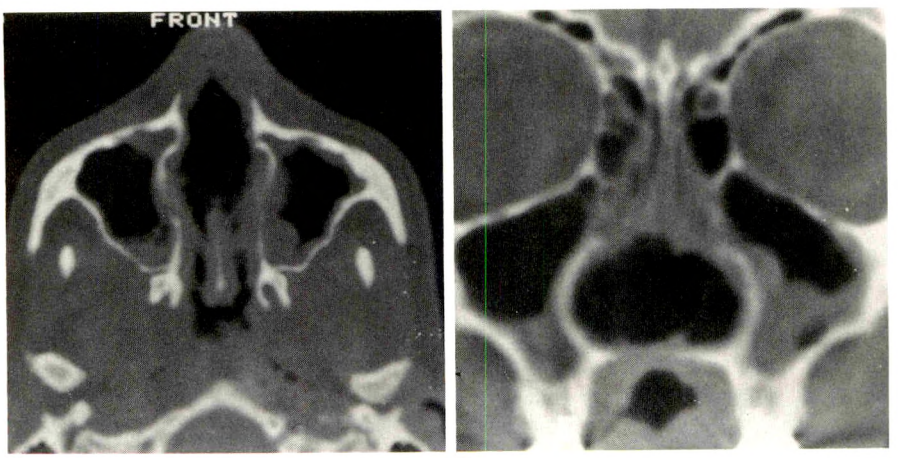


Fig. 7.—Perforated septum. 44-year-old with chronic cocaine abuse by snorting who had epistaxis.

***A* and *B*, Axial (*A*) and coronal (*B*) CT scans show destruction of nasal septum and turbinates.**

the nasal cartilages and loss of the structural integrity of the nasal cavity (see Fig. 7). Chronic osteolytic sinusitis may occur and may result in invasion of the adjacent orbits in rare cases [46]. Although anosmia is common among chronic users, a recent study [47] suggested that most users, even those with heavy use and intranasal damage, do not develop permanent olfactory damage.

Fetal CNS Complications

Obstetric complications associated with cocaine use include abruptio placenta, spontaneous abortion, fetal death, and premature labor [5, 48, 49]. Abnormalities of the CNS may be seen in babies born to cocaine users. The neonates delivered from such pregnancies tend to be small for gestational age, have low birth weights, and have a decreased head circumference [35, 48]. Also, microcephaly (head circumference less than 10th percentile) is a common finding that may be seen in up to 21%, and intrauterine growth retardation may be seen in 25% [50, 51]. Such infants show increased irritability, which may last for several weeks after birth [52].

Cocaine crosses the placenta, and increased blood levels of cocaine are found in the fetuses [53], who are often addicted to cocaine at birth [54]. Also, the pathways for cocaine metabolism may be underdeveloped in fetuses, leading to the accumulation of the cocaine metabolite benzoylecgonine. Benzoylecgonine does not cross the placenta because of the metabolite's ionic charge, and fetal renal excretion is poor [53]. The accumulation of cocaine and its metabolites may be in part responsible for the sympathomimetic effects observed in the fetus after maternal administration of the drug. However, the effect on fetal oxygenation, blood pressure, and heart rate is significantly more severe after maternal administration than it is if the fetus is injected directly [55]. This suggests that cocaine effects in fetuses may be more dependent on uterine oxygenation and vascular clamping than on sympathomimetic effects.

Prenatal exposure to cocaine may result in significant CNS lesions in the fetus [35, 54]. Sonographic findings may be abnormal in up to 35% of infants exposed to the drug in utero, similar to the prevalence in infants at risk for hypoxic-ischemic injury [56]. Intraventricular hemorrhage, intraparenchymal hemorrhage, and hemorrhage in unusual locations such as the posterior fossa may occur [54, 56]. Periventricular leukomalacia, deep brain cysts, and perinatal infarction also are seen [33, 35, 44, 54]. These findings are thought to be associated with fetal hypoxia and its effects on the regulation of cerebral blood flow; they are similar to those seen in low-birth-weight premature infants who were not exposed to cocaine [57].

Spasm of the uterine artery may be the mechanism by which cocaine induces fetal hypoxia. Cocaine causes increased maternal blood pressure with an increase in uterine vascular resistance. This is associated with decreased uterine and placental blood flow, with resultant fetal hypoxia [35]. Interestingly, uterine arteries lack sympathetic innervation. The effects on uterine arteries are thought to be direct effects of cocaine on calcium channels in vascular smooth muscle, with secondary arterial vasospasm [24].

The possible teratogenicity of cocaine in humans is controversial. It is well known that temporary ligation of the uterine arteries at midgestation produces congenital anomalies in rats [58]. Recently, Webster and Brown-Woodman [59] showed that similar results could be produced by administering cocaine to pregnant rats at midgestation. The teratogenicity of cocaine in humans is not well known. Some studies of large populations of cocaine-exposed women have found increased rates of malformations in the women's infants. These have included skull defects, encephaloceles, and eye malformations [60]. Other researchers have shown that specific brain and ocular abnormalities are increased in these infants. For example, Dominguez et al. [61] studied a large population of infants exposed to cocaine prenatally and found an increased prevalence of schizencephaly, callosal agenesis, septooptic dysplasia, and porencephaly. They attributed these findings to prenatal exposure to cocaine and other street drugs. They also postulated that the type of malformation may vary with the stage of gestation during which drug exposure occurs. These findings are quite recent and need to be confirmed in other studies.

Recent evidence suggests that a number of CNS lesions, including those causing malformations, may be increased in infants exposed to cocaine in utero. This is disturbing in view of the increased prevalence of use of cocaine, especially among pregnant women. For example, 12% of the mother-infant pairs at San Francisco General Hospital tested positive for cocaine use in 1987 [35]. Chasnoff et al. [62] found that approximately 14% of pregnant women in Pinellas County, FL, tested positive on toxicologic screenings for illicit drug use. These results did not correlate with race and socioeconomic status and suggest that illicit drug use during pregnancy is common. The public health implications of these data are alarming.

Summary

With the increasing frequency of cocaine use in the United States, the number of cocaine-related complications is destined to increase. Common cerebrovascular complications include ischemic disease, intraparenchymal and subarachnoid hemorrhage, atrophy, and seizures. When neurologic signs are present, imaging studies are abnormal in more than 75% of cases. Hemorrhage is more frequently reported than ischemia, and when hemorrhage is present, underlying vascular abnormalities are seen in nearly half the cases. However, SPECT data suggest that in chronic users subclinical ischemia is more common than formerly suspected. Cocaine-induced complications also are seen in the infants of cocaine-addicted mothers. Cocaine affects other organ systems, most notably the cardiovascular system, and CNS complications may result from the induction of myocardial infarction, arrhythmias, and coronary artery thrombosis. Secondary complications of transient hypertension, hypotension, and embolization also may cause strokes, hemorrhages, and small ischemic lesions in

the CNS. When snorted, cocaine can ulcerate and eventually erode through the nasal septum.

Our understanding of the genesis of cocaine-related complications is growing; however, much remains to be learned. Cocaine-related vasospasm appears to be one of the central mechanisms by which the drug's effects are mediated and may have a significant impact on the genesis of many complications. Recent evidence suggests that cocaine affects flux in calcium channels, directly producing arterial spasm, and, at least in some organs (notably uterine arteries), these effects may be independent of sympathetic innervation. Also, cocaine has been shown to affect the clotting mechanism and platelet aggregation. This is in addition to its well-known local anesthetic effects and effects on the adrenergic and dopaminergic systems. It is likely that the genesis of many cocaine-related complications are multifactorial. Complications are produced by all methods of administration, and in first-time users, even small doses may produce significant, life-threatening complications.

The role of imaging procedures in the detection of cocaine-related complications continues to evolve. Recent SPECT data suggest that cerebral blood flow is disordered and that chronic users have a high level of subclinical ischemic disease. The amount of such disease appears to be underestimated on CT scans, and further studies with MR imaging may confirm and expand these findings. With the high prevalence of cocaine abuse, radiologists should be alert for the possibility of cocaine use as an explanation for strokes, hemorrhages, and seizures in young adults.

REFERENCES

1. Shick JFE, Senay EC. Diagnosis and management of cocaine abuse. In: *Directions in psychiatry*, part I, vol. 7. New York: Hatherleigh Co., **1985**:lesson 5, 3–7
2. Abelson HI, Miller JD. A decade of trends in cocaine use in the household population. *NIDA Res Monogr* **1985**;61:35–49
3. Siegel RK. Cocaine smoking. *J Psychoactive Drugs* **1984**;14:271–343
4. Barnett PM. Data from hospitals underestimate role of cocaine in trauma, study concludes. *Wall Street Journal*, May 28, **1991**, p. B5
5. Cregle LL, Mark H. Medical complications of cocaine abuse. *N Engl J Med* **1986**;315:1495–1500
6. Chitwood DD. Patterns and consequences of cocaine use. *NIDA Res Monogr* **1985**;61:111–129
7. Bozarth MA, Wise RA. Toxicity associated with long-term intravenous heroin and cocaine self-administration in the rat. *JAMA* **1985**;254:81–83
8. Adams EH, Durell J. Cocaine: a growing public health problem. *NIDA Res Monogr* **1984**;50:9–14, **1985**;61:9–13
9. White PT. An ancient Indian herb turns deadly coca. *National Geographic* January **1989**;175:3–47
10. Ritchie JM, Greene NM. Local anesthetics. In: Gilman AG, Goodman LS, et al. *The pharmacological basis of therapeutics*. New York: Macmillan, **1985**:309–310
11. Fischman MW, Schuster CR, Resnekov L, et al. Cardiovascular and subjective effects of intravenous cocaine administration in humans. *Arch Gen Psychiatry* **1976**;33:983–989
12. Jekel JF, Allen DF, Podlewski H, Clarke N, Dean-Patterson S, Cartwright P. Epidemic free-base cocaine abuse: case study from the Bahamas. *Lancet* **1986**;1:459–462
13. Jacobs IG, Roszler MH, Kelly JK, Klein MA, Kling GA. Cocaine abuse: neurovascular complications. *Radiology* **1989**;170:223–227
14. Nolte KB, Gelman BB. Intracerebral hemorrhage associated with cocaine abuse. *Arch Pathol Lab Med* **1989**;113:812–814
15. Tumeth SS, Nagel JS, English RJ, Moore M, Holman BL. Cerebral abnormalities in cocaine abusers: demonstration by SPECT perfusion brain scintigraphy. *Radiology* **1990**;176:821–824
16. Volkow NA, Mullani N, Gould LK, Adler S, Krajewski K. Cerebral blood flow in chronic cocaine users: a study with positron emission tomography. *Br J Psychiatry* **1988**;152:641–648
17. Kaye BR, Fainstat M. Cerebral vasculitis associated with cocaine abuse. *JAMA* **1987**;258:2104–2106
18. Weingarten K. Cerebral vasculitis associated with cocaine abuse or subarachnoid hemorrhage. *JAMA* **1988**;259:1648–1649
19. Levine SR, Welch KMA, Brust JCM. Cerebral vasculitis associated with cocaine abuse or subarachnoid hemorrhage. *JAMA* **1988**;259:1648
20. Levine SR, Brust JCM, Futrell N, et al. Cerebrovascular complications of the use of the "crack" form of alkaloidal cocaine. *N Engl J Med* **1990**; 323:669–704
21. Kredel DA, Ditter SM, Frankel MR, Ross WK. Biopsy-proven cerebral vasculitis associated with cocaine abuse. *Neurology* **1990**;40:1092–1094
22. Citron BP, Halpern M, McCarron M, et al. Necrotizing angitis associated with drug abuse. *N Engl J Med* **1970**;283:1003–1011
23. Lange RA, Cigarroa RG, Yancy CW Jr, et al. Cocaine-induced coronary artery vasoconstriction. *N Engl J Med* **1989**;321:1557–1562
24. Chokshi SK, Gal D, Whelton JA, Isner JM. Evidence that fetal distress in newborns of cocaine users is due to vascular spasm and may be attenuated by pre-treatment with diltiazem (abstr 737). *Circulation* **1989**; 80[suppl II]:II–185
25. Isner JM, Chokshi SK. Cocaine and vasospasm. N Engl J Med **1989**; 321:1604–1606
26. Powers RH, Madden JA. Vasoconstrictive effects of cocaine, metabolites and structural analogs on cat cerebral arteries (abstr). *FASEB J* **1990**;4: A1095
27. Wang AM, Suojanen JN, Colucci VM, Arumbaugh CL, Hollenberg NK. Cocaine- and methamphetamine-induced acute cerebral vasospasm: an angiographic study in rabbits. *AJNR* **1990**;11:1141–1146
28. Johnson CE, Fischman MW. The pharmacology of cocaine related to its abuse. *Pharmacol Rev* **1989**;41:3–52
29. Jaffe GH. Drug addiction and drug abuse. In: Goodman AG, Gilman AG, et al. *The pharmacological basis of therapeutics*. New York: Pergamon, **1990**:522–574
30. Togna G, Tempesta E, Togna AR, Dolci N, Cebo B, Caprino L. Platelet responsiveness and biosynthesis of thromboxane and prostacyclin in response to in vitro cocaine treatment. *Haemostasis* **1985**;15:100–107
31. Nanji A, Filipenko J. Asystole and ventricular fibrillation associated with cocaine intoxication. *Chest* **1985**;85:132–133
32. Wojak JC, Flamm ES. Intracranial hemorrhage and cocaine use. *Stroke* **1987**;18:712–715
33. Klonoff D, Andrews B, Obana W. Stroke associated with cocaine use. *Arch Neurol* **1987**;46:989–993
34. Lichtenfeld PJ, Rubin DB, Feldman RS. Subarachnoid hemorrhage precipitated by cocaine snorting. *Arch Neurol* **1984**;41:223–224
35. Rowbotham MC, Lowenstein DH. Neurologic consequences of cocaine use. *Annu Rev Med* **1990**;41:417–422
36. Kaku DA, Lowenstein DH. Recreational drug use: a growing risk factor for stroke in young people. *Neurology* **1989**;39[suppl 1]:161
37. Pascual-Leone A, Dhuna A, Anderson D. Cerebral atrophy in habitual cocaine abusers: a planimetric CT study. *Neurology* **1991**;41:34–38
38. Lowenstein DH, Collins SD, Massa SM, McKinney HE Jr, Benowitz N, Simon RP. The neurologic complication of cocaine abuse (abstr). *Neurology* **1987**;37[suppl 1]:195
39. Ritchie JM, Greene NM. Local anesthetics, In: Goodman AG, Gilman AG, et al. *The pharmacological basis of therapeutics*. New York: Pergamon, **1990**:311–320
40. Alldredge B, Lowenstein DH, Simon RP. Seizures associated with recreational drug abuse. *Neurology* **1989**;39:1037–1039
41. Wetil CV, Wright RK. Death caused by recreational cocaine use. *JAMA* **1979**;241:2519–2522
42. Mody CK, Miller BI, McIntyre HB, Mendoza R, Goldberg MA. Neurologic complications of cocaine abuse (abstr). *Neurology* **1987**;37[suppl 1]:193
43. Sawaya GR, Kaminski MJ. Spinal cord infarction after cocaine use (letter). *South Med J* **1990**;83:601–602
44. Lee CY, Mohammadi H, Dixon RA. Medical and dental implications of cocaine abuse. *J Oral Maxillofac Surg* **1991**;49:290–293

45. Chaudhry RM, Abadir AR, Ginautienne K, et al. Effect of cocaine abuse on nasal mucosa, septum and turbinates. *Proc West Pharmacol Soc* **1990**; 33:249–251
46. Goldberg RA, Weisman JS, McFarland JE, Krauss HR, Hepler RS, Shorr N. Orbital inflammation and optic neuropathies associated with chronic sinusitis of intranasal cocaine abuse: possible role of contiguous inflammation. *Arch Ophthalmol* **1989**;107:831–835
47. Gordon AS, Moran DT, Jafek VW, Eller PM, Strahan CR. The effect of chronic cocaine abuse on human olfaction. *Arch Otolaryngol Head Neck Surg* **1990**;116:1415–1418
48. Acker D, Sachs BP, Tracey KJ, Wise WE. Abruptio placentae associated with cocaine use. *Am J Obstet Gynecol* **1983**;146:220–221
49. MacGregor SN, Keith LG, Chasnoff IJ, et al. Cocaine use during pregnancy: adverse perinatal outcome. *Am J Obstet Gynecol* **1987**;157:686–690
50. Hadeed AJ, Siegal SR. Maternal cocaine use during pregnancy: effect on the newborn infant. *Pediatrics* **1989**;84:205–210
51. Cabral H, Timperi R, Buchner H. Effects of maternal marijuana and cocaine use on fetal growth. *New Engl J Med* **1989**;320:762–768
52. Doberczak TM, Shanzer S, Senie RT, Kandall SR. Neonatal neurologic and electroencephalographic effects of intrauterine cocaine exposure. *J Pediatr* **1988**;113:354–358
53. Meeker JE, Reynolds PC. Fetal and newborn death associated with maternal cocaine use. *J Anal Toxicol* **1990**;14:379–382
54. Spires MC, Gordori EF, Choudhuri M, Maldonado E, Chan R. Intracranial hemorrhage in a neonate following prenatal cocaine exposure. *Pediatr Neurol* **1989**;5:324–326
55. Woods JR, Plessinger MS, Clark KE. Effect of cocaine on uterine blood flow and fetal oxygenation. *JAMA* **1987**;257:957–961
56. Dixon SD, Bejar R. Encephalographic findings in neonates associated with maternal cocaine and methamphetamine use: incidence and clinical correlates. *J Pediatr* **1989**;115:770–778
57. Volpe JJ. Current concepts of brain imaging in the premature infant. *AJR* **1989**;153:243–251
58. Brent RL. Editorial comment: relationship between uterine vascular clamping, vascular disruption syndrome and cocaine teratogenicity. *Tetralogy* **1990**;41:757–760
59. Webster WS, Brown-Woodman PD, Lipson AH. Teratogenic properties of cocaine in rats (abstr). *Tetralogy* **1990**;41:689–697
60. Bingol N, Magdelena F, Diaz V, Stone RK, Gromisch DS. Teratogenicity of cocaine in humans. *J Pediatr* **1987**;100:93–96
61. Dominguez R, Vila-Coro AA, Slopis JM, Bohan TP. Brain and ocular abnormalities in infants with in utero exposure to cocaine and other street drugs. *Am J Dis Child* **1991**;145:688–695
62. Chasnoff IJ, Landress HJ, Barrett ME. The prevalence of illicit drug or alcohol use during pregnancy and discrepancies in mandatory reporting in Pinellas County, Florida. *New Engl J Med* **1990**;322:1202–1206

New Format for Abstracts

Beginning immediately, the *AJR* will publish abstracts of articles in a different format, much like the ones recently adopted by the *New England Journal of Medicine* and the *Journal of the American Medical Association*. The purpose of the new design is to have abstracts present the essential elements of articles more clearly and concisely. The contents, organization, and length of the abstracts will be the same as before; however, rather than being all one paragraph except for the conclusion, abstracts will now be divided into four paragraphs, each with a title: objective, subjects (or materials) and methods, results, and conclusion. Please read the article on pages 207–208 of this issue for a detailed explanation of how to prepare abstracts in this new format.

In addition, the *AJR* Guidelines for Authors, which appears at the front of every issue of the Journal, has been revised to help you write abstracts in this new format. Authors should familiarize themselves with these guidelines and incorporate them into all manuscripts submitted for publication.

Robert N. Berk
Editor-in-Chief

Book Review

Radiology of the Extremities. By Nancy Baker. Philadelphia: Lippincott, 125 pp., 1991. $49.95

Radiology of the Extremities is a small book, with most of its 125 pages dedicated to images, charts, and drawings. The text portion of the book is extremely terse. Chapter 2, for example, contains only two discussions. The first of these is on primary bone tumors and fills less than half a page. The other discussion is on metastasis and consists of about 90 words. Many major topics are dealt with in 100 or fewer words, and often the discussion concerns nonradiologic information. The book has six chapters. The first five deal with infection, tumor, arthritis, osteopenia, and osteonecrosis. Chapter 6 is titled "Miscellaneous Orthopedic Conditions," but the only topics discussed are clubfoot, congenital hip dysplasia, and spondylolysis. Paget's disease and acromegaly are included in the chapter on osteopenia, although marrow disorders are ignored, as are other major topics throughout the book.

The entire bibliography consists of 22 entries. It lists primarily textbooks, most of which are either out of print or out of date. The book has numerous mistakes and inconsistencies. The coned-down radiograph of the knee on the cover is upside-down. Despite the title, the spine and axial skeleton are dealt with regularly throughout the book. In Figure 1.2, "b" and "c" are switched. In Figure 2.1, a chart of primary bone tumors, nontumors such as simple bone cyst, aneurysmal bone cyst, and eosinophilic granuloma are included, but legitimate neoplasms such as chondromyxoid fibroma, parosteal osteosarcoma, chordoma, and adamantinoma are omitted. Osteochondroma is listed as an osseous neoplasm, and malignant fibrous histiocytoma is said to arise from marrow elements. These types of errors persist throughout the book.

Although the book has three CT scans, CT as a technique is essentially ignored. MR imaging is neither mentioned nor illustrated, despite a chapter dedicated to osteonecrosis.

I do not recommend this book. Other texts currently available are more authoritative, accurate, and up-to-date.

Richard A. McLeod
Mayo Clinic
Rochester, MN 55095

Review Article

MR Imaging of the Spinal Cord: Current Status and Future Advances

Gordon Sze[1]

The advent of MR imaging has dramatically altered the evaluation of suspected myelopathy. MR is far less invasive than traditional imaging techniques and often offers a degree of understanding of an abnormality not previously possible. These achievements have closely followed recent technologic advances, such as the development of contrast agents and the introduction of sequences that permit a reduction in both imaging time and artifacts. The current role of MR in the imaging of spinal cord disorders, including intramedullary tumors, infectious and inflammatory myelitis, demyelinating diseases, vascular lesions, trauma, syringomyelia/hydromyelia, and neurodegenerative disorders, is reviewed. While further improvements will undoubtedly occur, the field of spinal MR imaging appears to be entering a maturing phase.

The advent of MR imaging has permitted direct visualization of the spinal cord for the first time [1]. Although the presence or absence of cord lesions could be inferred on myelography and postmyelographic CT by the shape of the surrounding contrast column, MR imaging allows specific assessment of the cord parenchyma itself. This review focuses on the MR imaging findings in diseases of the spinal cord, including tumors, cysts, demyelinating diseases, infections, vascular diseases, and trauma. The article concludes with a discussion of recent advances in the techniques available for MR imaging of the cord.

Technique

Technically, assessment of the spinal cord presents one of the greatest challenges in the use of MR to evaluate the neuraxis. Early images were markedly degraded by motion artifacts, especially from respiration, cardiac pulsation, and CSF pulsation [2, 3]. Several techniques have evolved to compensate for involuntary motion, and high-quality images of the cord are now obtained routinely.

For the evaluation of a suspected, and possibly small, intramedullary lesion, both short TR (e.g., 600/30 [TR/TE]) and long TR (e.g., 2200/30,80) sagittal images are essential. Short TR sagittal sequences generally contain excellent morphologic detail. Long TR sagittal sequences often show subtle lesions that are not visualized on the short TR sagittal sequences, and also provide further characterization of lesions. These acquisitions are best obtained with cardiac gating and/or gradient-moment nulling techniques in order to decrease the effect of flow artifacts, especially on high-field-strength units [2, 3]. For both short TR and long TR images, it is necessary to obtain sufficiently thin sections, preferably 3 mm or less with minimal interslice gaps. The use of a higher matrix improves resolution and helps to reduce the effect of the Gibbs artifact, which may produce a thin linear longitudinal line down the center of the cord that can be mistaken for a syrinx [4].

Received December 6, 1991; accepted after revision February 3, 1992.
Presented at the annual meeting of the American Roentgen Ray Society, Boston, May 1991.
[1] Department of Diagnostic Radiology, Yale University School of Medicine, 333 Cedar St., P.O. Box 3333, New Haven, CT 06510. Address reprint requests to G. Sze.

Although much of the information in an MR study of the cord is obtained in the sagittal plane, axial images can also be vital. In general, if further morphologic detail is desired, axial short TR sections are usually acquired. If further characterization of lesions or if confirmation of a subtle lesion seen on the long TR sagittal images is desired, then short TR sequences are not optimal. Rather, gradient-echo (e.g., 800/35/20° [TR/TE/flip angle]) or long TR axial sections may be necessary. In the cervical spine, volumetric gradient-echo sequences that allow one to obtain sections as thin as 1 mm are used. These sequences are very sensitive to subtle disturbances of the cord parenchyma, such as multiple sclerosis (MS) plaques.

Intramedullary Tumors

The advent of MR has tremendously increased the ability to detect and characterize tumors of the cord. Short TR sagittal sequences readily disclose the marked cord widening often associated with intramedullary neoplasms. Long TR sagittal scans reveal high signal within the substance of the cord, consistent with either tumor or surrounding edema. Because of MR's sensitivity to hemorrhage, areas of bleeding are easily detected. A number of different appearances may be seen. If hemorrhage into a tumor cyst occurs, fluid levels may result. Owing to the evolution of hemoglobin breakdown products and to other factors, the relative signal intensities of the inferior and superior components may vary. In addition, hemorrhagic cord tumors are often associated with hemosiderin deposition, which appears as peripheral marked hypointensity on long TR sequences.

While unenhanced MR images generally can be used to detect tumors of the cord accurately, gadopentetate dimeglumine can help in further characterization and delineation [5–9]. Enhancement with gadopentetate dimeglumine is most useful in cases of focal masses, especially hemangioblastomas and metastases [6] (Fig. 1). Both of these lesions tend to be fairly well circumscribed and produce extensive surrounding edema. Because of this, cord swelling far beyond the region of the actual tumor is often seen. The use of gadopentetate dimeglumine can be very effective in pinpointing the exact location of the lesion [5, 6]. Although the area of cord enlargement can be extensive, the actual lesion may be small, less than one vertebral body in height.

Results with primary cord gliomas are less dramatic. First, as in the brain, it is likely that areas of enhancement do not coincide with the actual boundaries of these infiltrative tumors. Second, unlike that seen with hemangioblastomas and metastases, enhancement is often variable. It does appear, however, that primary tumors tend to enhance in the cord much more often than in the head [6–9].

In gliomas of the cord, enhancement again tends to be fairly focal [5–9] (Fig. 2). Areas of enhancement may be representative of more active tumor and good areas for biopsy, as is the case in the brain. Often, these tumors are associated with cysts. Cysts can be either intratumoral or rostral and caudal. Rostral and caudal cysts tend to be benign [10, 11]. Even though the fluid within them might be proteinaceous or hemorrhagic, these cysts are usually not lined by tumor nor do they contain tumor cells. Unlike tumor cysts, they do not require excision but are merely drained at surgery. Contrast enhancement has proved useful in identifying the nature of cysts associated with tumors [6–9]. Tumor cysts are generally surrounded by enhancement, while the walls of benign cysts lack associated contrast uptake.

Although 40–50% of gliomas of the brain do not enhance, the large majority of gliomas of the cord do, regardless of grade [5–9]. In fact, unenhancing gliomas of the cord are unusual, although they have been documented. Even very low-grade tumors tend to show some enhancement. Of the 55 reported cases of cord glioma in which contrast-enhanced MR was used, enhancement was seen in 54 [5–9, 12]. Because of this, the use of contrast material can be helpful in differentiating suspected neoplasms from other disorders, for

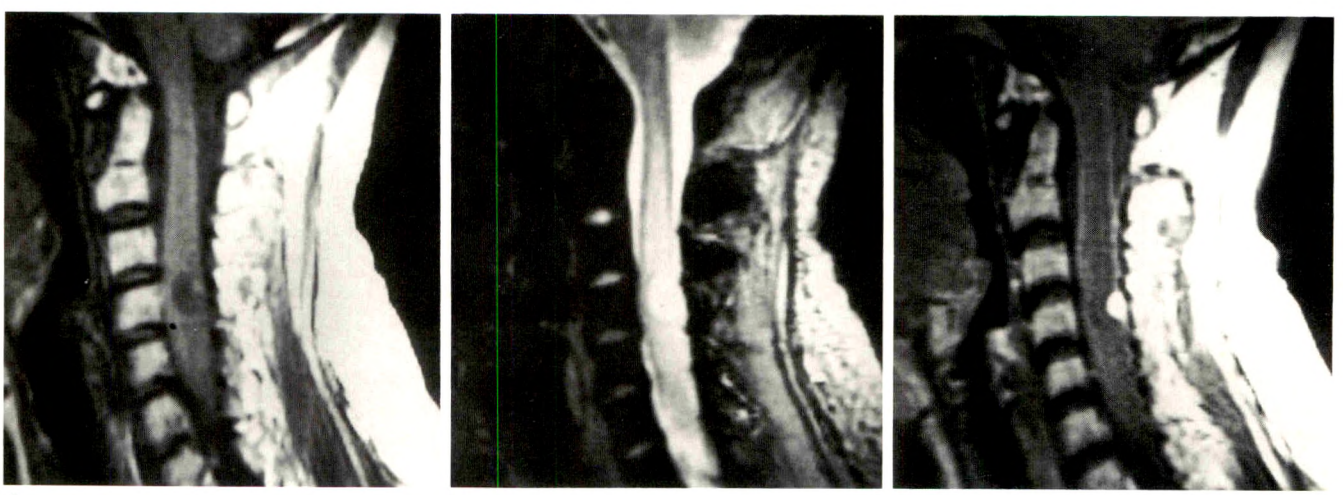


Fig. 1.—Spinal cord hemangioblastoma.
***A* and *B*, Short TR (600/30) and gradient-echo (800/35/20°) sagittal MR images show an enlarged cervical cord with central cystic cavity and surrounding edema. A small nodule is noted along wall of cystic cavity posteriorly.**
***C*, Short TR (600/30) sagittal MR image after administration of contrast material shows enhancing nodule along posterior aspect of cyst.**

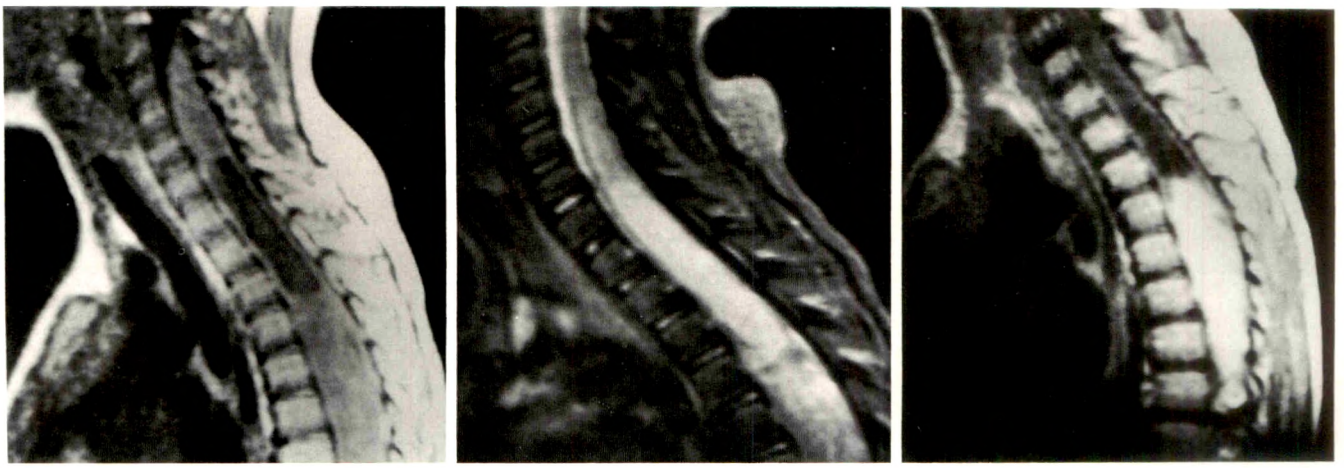


Fig. 2.—Cord astrocytoma.
A, Short TR (600/20) sagittal MR image shows a diffusely expanded cord. In addition, area of cystic change is noted in upper portion of thoracic cord.
B, Long TR (2136/80) sagittal MR image confirms superior cyst. Also noted is area of heterogeneity within cord inferior to cyst.
C, Short TR (600/20) sagittal MR image after administration of contrast material shows marked enhancement of main tumor nidus, with rostral cyst.

example, infection or benign syrinx. If no enhancement is seen, the likelihood of a glioma of the cord is significantly reduced.

Infectious and Inflammatory Myelitis

As with the brain, multiple infectious agents can affect the cord and cause myelopathic symptoms, including bacterial, granulomatous, viral, and even parasitic diseases. As a rule, however, inflammatory diseases that affect the cord tend to be seen earlier than those in the brain. Therefore, certain lesions that require time to develop, such as the well-formed abscess capsule, are comparatively unusual in the cord.

Viral agents are probably the most common ones to directly involve the cord. Often, the exact virus may be difficult to determine. Regardless of the specific agent, the response of the cord parenchyma is stereotypical [13, 14]. An inflammatory cellular infiltrate, usually composed of lymphocytes and plasma cells, predominates, although neutrophils may be numerous early in the disease. Edema, both vasogenic and cytotoxic, occurs. Cellular destruction may be limited to individual neurons and small foci, or it may be extensive and fail to respect anatomic boundaries. Vessel thrombosis may lead to secondary ischemia. Short TR images generally reveal mild enlargement of the cord, often quite extensive. Long TR images show high intensity within the cord, often extending beyond the area that might be expected from the degree of cord swelling. The presence of a skip area separating multiple regions of enlarged cord is strongly suggestive of an inflammatory condition rather than tumor [15]. After the administration of contrast material, enhancement may be nodular and resemble that of tumor. Alternatively, enhancement may be diffuse, peripheral, or even punctate and speckled [15] (Fig. 3). All of these patterns of enhancement are unusual for tumor.

Granulomatous diseases, such as tuberculosis or sarcoid, also affect the cord. In these cases, short and long TR images generally show focal enlargement of a limited segment of the cord. After the administration of contrast material, nodular enhancement is usually seen [15]. This pattern strongly resembles that of tumor, and differentiation between the two may be difficult.

Demyelinating Diseases

MS is the most common demyelinating disease to affect the cord. Eighty percent of cases involve the cord, and 20–33% show symptoms referable to the cord alone [16]. Lesions may involve any region of the cord, regardless of anatomy, although the cervical cord is involved more often. Devic's disease, also known as neuromyelitis optica, represents the association of transverse myelitis with acute visual loss due to optic neuritis.

Pathologically, the typical regions of demyelination are seen [16]. In acute plaques, the axons are relatively preserved while the myelin is fragmented. These changes are often associated with microglial and perivascular lymphocytic infiltration. In chronic plaques, dense fibrillary gliosis is typical. In severe cases, atrophy is common. The majority of patients with cord lesions documented with the use of MR imaging will also have brain lesions, although these lesions may have occurred at different times. Therefore, a screening head examination may be performed in lieu of a spinal examination if the diagnosis is in doubt [17]. However, if evaluation of the cord is desired, MS plaques in the cord can be detected. Good-quality cardiac-gated long TR images, with flow-compensation techniques, are essential for the visualization of cord plaques in the sagittal plane. In the axial plane, gradient-echo images are often very sensitive in showing MS plaques that disrupt the otherwise easily visualized border between gray and white matter in the cord.

As in the head, MS plaques generally appear of high intensity compared with the remainder of the cord on long TR or gradient-echo images. Large and acute plaques may have

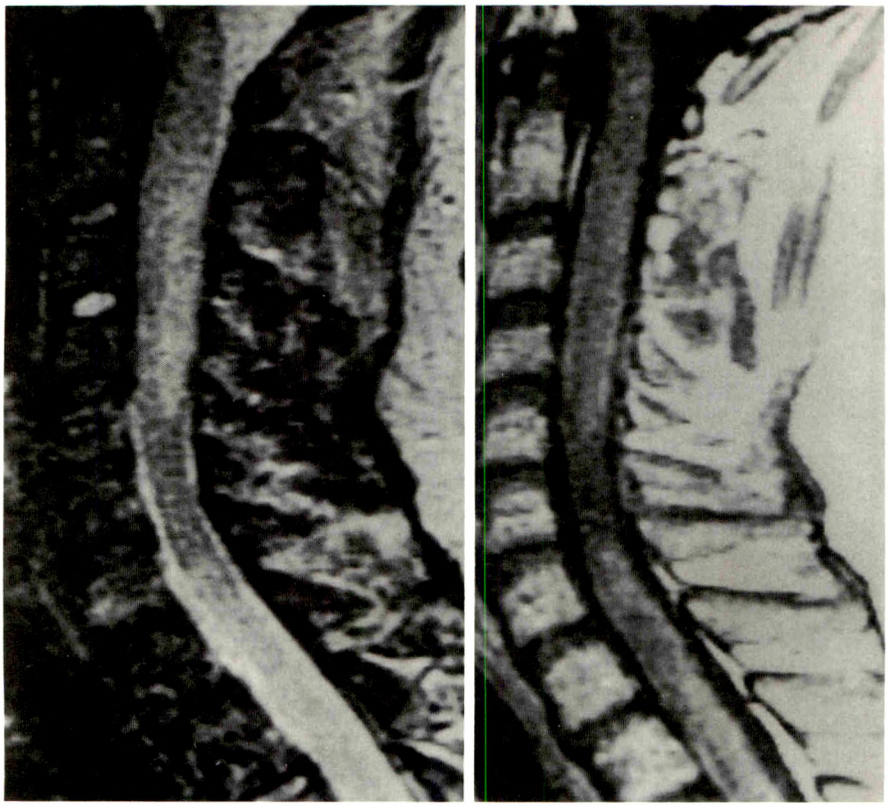


Fig. 3.—Inflammatory myelitis.
A, Swollen areas of spinal cord show diffuse high signal on long TR (2200/80) MR image.
B, After contrast administration, long TR (2200/80) MR image shows diffuse enhancement with unenhancing skip area. This pattern is unlike that usually seen in tumor.

mass effect and resemble tumors. Acute plaques generally enhance after the administration of contrast material while chronic plaques do not [18] (Fig. 4). While the natural history of plaques in the brain has been described both without and with treatment, this research has not been done in the spine. Presumably, acute cord plaques also enhance for several weeks initially before repair of the blood-brain barrier takes place.

Radiation change is another entity that may cause myelopathy. The development of myelopathy is dependent on the dose of radiation received, the interval at which the radiation was administered, and the number of fractions [19–23]. Radiation myelopathy may be divided into acute and chronic forms. The acute form is best known as the transient myelopathy of Lhermitte and is manifested by shocklike sensations down the back when flexing the neck. It usually occurs 3 months after radiation treatment and resolves spontaneously. Findings on MR imaging are normal.

Chronic radiation myelopathy has been described in three forms [19–23]. First, lower motor neuron disease can occur as a result of injury to the anterior horn cells. Second, acute paraplegia due to radiation-induced vascular changes and secondary cord ischemia has been seen. Third, and by far the most common, is chronic progressive radiation myelopathy. It primarily involves the lateral columns. These patients have sensory or motor changes and frequently Brown-Séquard syndrome. Symptoms are often slowly progressive and may result in death. The cause of these changes is unclear, but they may result from either radiation-induced vascular change or primary neuronal damage. Chronic radiation myelopathy of all types usually occurs approximately 1 year after radiation therapy and has been described as late as 13 years after irradiation.

As with MS, radiation myelopathy may have a variety of appearances on MR [24]. When it is fulminant, chronic progressive radiation myelopathy often can be seen as an area of focal cord swelling on short TR images with associated high intensity on long TR images. In particularly severe cases, contrast enhancement can occur [24]. The appearance can markedly resemble that of tumor. In the late stage of chronic radiation myelopathy, the cord may appear totally normal on both short TR and long TR images or may even appear atrophic.

Acute disseminated encephalomyelitis, also known as postvaccinal or postinfectious encephalomyelitis, typically occurs several weeks after an antecedent innoculation or viral syndrome. Patients have focal lesions, often in the white matter; as in MS, these lesions appear random in distribution [16]. Pathologically, although the syndrome is associated with previous infection, no infectious agents can be found. Most often, one sees a perivascular lymphocytic infiltration, associated with areas of demyelination that follow the course of the vessels. In severe cases, hemorrhage may occur. The reaction is presumed to be immune in nature, possibly owing to antigen-antibody deposition, complement-mediated endothelial damage, and vasculitis. The brain is most often involved, but a very small proportion of cases involve the cord.

Imaging findings, in general, resemble those seen in the acute phase of MS. Short TR images may show a normal cord or a slightly enlarged cord. Long TR images show corresponding areas of high signal intensity (Fig. 5). In more severe cases, enhancement may be seen. Since acute dis-

seminated encephalomyelitis is a monophasic disease, unlike MS, it has been speculated that the enhancement pattern should also be monophasic, unlike MS, in which different lesions may enhance, subside, and reenhance at different intervals.

Vascular Lesions

Vascular lesions of the cord can be separated into infarcts and malformations. Cord infarcts generally present acutely. Although they may have a wide array of causes, they are most often associated with surgery for aortic aneurysms [25]. As in the head, mass effect on short TR images and high signal on long TR images is generally seen. In the subacute phase, contrast enhancement, generally diffuse in nature, can be demonstrated. Presumably, the time course of enhancement reflects that seen in brain infarcts, although there is a lack of research on this topic. Early exaggerated enhancement due to incomplete ischemia has not been described in the cord.

Many types of malformations may involve the cord, including intramedullary arteriovenous malformations (AVMs), cavernous hemangiomas, and extramedullary vascular malformations [26]. Intramedullary AVMs generally occur in young adults, are fed most often by the anterior spinal artery, and present acutely as cord hemorrhage or as subarachnoid hemorrhage [26]. The thoracic cord is involved most often. Short TR and long TR images may reveal a normal or swollen cord, often with areas of hemorrhage. Serpiginous signal voids representing the nidus are seen in the cord, consistent with the actual malformation [27, 28] (Fig. 6). Large serpiginous signal voids may also be present in the subarachnoid space owing to feeding and draining vessels. Atrophy or syrinx formation can be caused by the AVM. Hemosiderin deposition is usually present, indicative of previous hemorrhage. Cobb syndrome is a metameric angiomatosis associated with an intramedullary AVM, an epidural AVM, vertebral or superficial angiomas, or any combination of these abnormalities.

Extramedullary arteriovenous fistulas, also known as dural arteriovenous fistulas or as radiculomeningeal fistulas, generally occur in older patients, especially men, and are due to a fistula between a dural branch of a radicular artery and the perimedullary veins [26]. These fistulas are generally fed by the posterior circulation, and symptoms are usually those of cord claudication or a progressive myeloradiculopathy, often a conus medullaris syndrome. These lesions can be very difficult to visualize on MR (Fig. 7). Conus enlargement and intramedullary high signal on long TR images may be present. Scalloping of the posterior surface of the cord may be caused by the enlarged perimedullary veins. If gadopentetate dimeglumine is given, punctate enhancement of the posteriorly draining medullary veins can be seen along the surface of the cord in about one fourth of cases [29, 30] (Fig. 7). On delayed scans, diffuse cord enhancement has been reported, possibly due to venous engorgement and secondary ischemia.

Finally, cryptic vascular malformations of the cord may occur, as in the head; the most common of these, cavernous hemangiomas, are seen with increasing frequency [31]. Their appearance in the cord is similar to their appearance in the head (Fig. 8). Generally, these lesions appear either as a central focus of high signal intensity, surrounded by a low-intensity rim, due to the breakdown products of blood, or, in smaller lesions, as low intensity due to hemosiderin deposition. Mass effect is unusual unless they have recently bled. In general, very little contrast enhancement is seen.

Trauma

Pathologic changes that occur in the injured spinal cord can be divided into acute and chronic [32]. Acutely, the trauma can result in a wide spectrum of injury, ranging from mild cord contusion to severe disruption of cord architecture and hemorrhage. Secondary edema can lead to vascular compromise of adjacent areas. Most of these changes occur in the first few days following trauma. After the first week, the subacute phase begins, as the body attempts to heal from the results of the injury. Macroscopically, edema and the smaller areas of hemorrhage are resorbed. The acute infiltrate is replaced by mononuclear cells. Astrocytic gliosis may also be seen at the periphery of the injury. Chronically, fibrous tissue fills in the regions of necrosis and hemorrhage. Secondary atrophy of the cord may be present.

In the acute setting, MR imaging permits the visualization of changes in the traumatized cord directly as long as the patient is sufficiently stable and cooperative to be imaged [33, 34]. Imaging may be particularly important when the trauma is incomplete, that is, when some motor and/or sensory function below the level of the injury persists [32]. In these cases, aggressive treatment may be indicated in order to

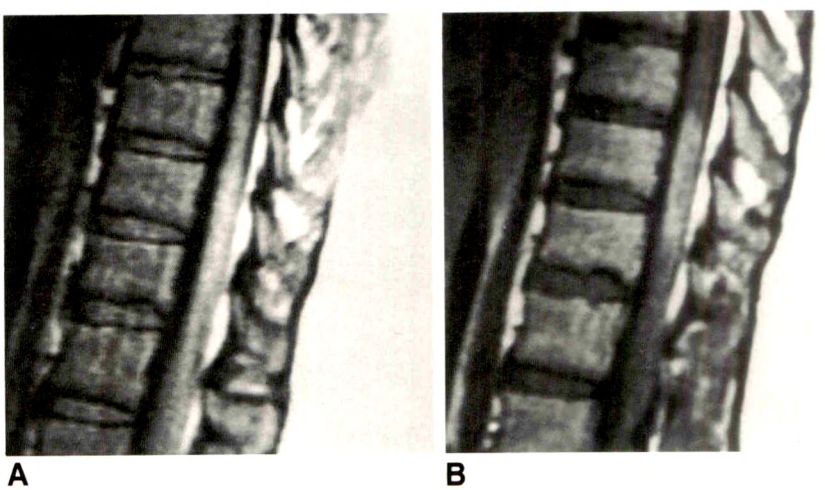


Fig. 4.—Multiple sclerosis.
***A*, Long TR (2235/30) sagittal MR image shows high intensity in cord over a short segment.**
***B*, Short TR (500/12) sagittal MR image after administration of contrast material shows enhancement.**



Fig. 5.—Acute disseminated encephalomyelitis.

A, Long TR (1333/80) sagittal MR image shows focal high intensity at C6–C7.

B, Short TR (600/30) sagittal MR image after administration of contrast material shows focal and marked enhancement of lesion.

prevent further deterioration. These incomplete injuries may be characterized by varying clinical characteristics. The central cord syndrome is often seen in elderly patients with cervical spinal stenosis, in which even minor trauma can result in hemorrhage into the central gray matter of the cord. These patients have decreased function in the upper extremities but relatively normal function in the lower extremities. Other incomplete cord injuries may present as Brown-Séquard syndrome, anterior cord syndrome, or mixed motor and sensory deficits.

The MR characteristics of the acutely injured spinal cord reflect the clinical symptoms. If the injury is mild, with only temporary neurologic dysfunction, MR imaging may show a normal cord. With increasing cord injury, short TR images may be normal or may reveal cord swelling [32]. The long TR images, however, are the most sensitive in showing cord edema, which is seen as areas of high signal intensity within the substance of the cord (Fig. 9). Areas of hypointensity on both short TR and long TR images, with later evolution to hyperintensity, peripheral at first, are typical of hemorrhagic regions. The presence of hemorrhage has been associated with a poor prognosis [33]. Also important to note are any retropulsed bone fragments or disk fragments that may impinge on the cord. Rarely, rapidly ascending spinal necrosis can result from thrombosis of the anterior spinal artery or other interruption in the blood supply. In cases of penetrating injury of the spinal cord, such as in knife or gunshot wounds, actual transection of the cord may be visualized.

In the chronic stage, an imaging examination may be indicated if new or progressive signs of neurologic dysfunction

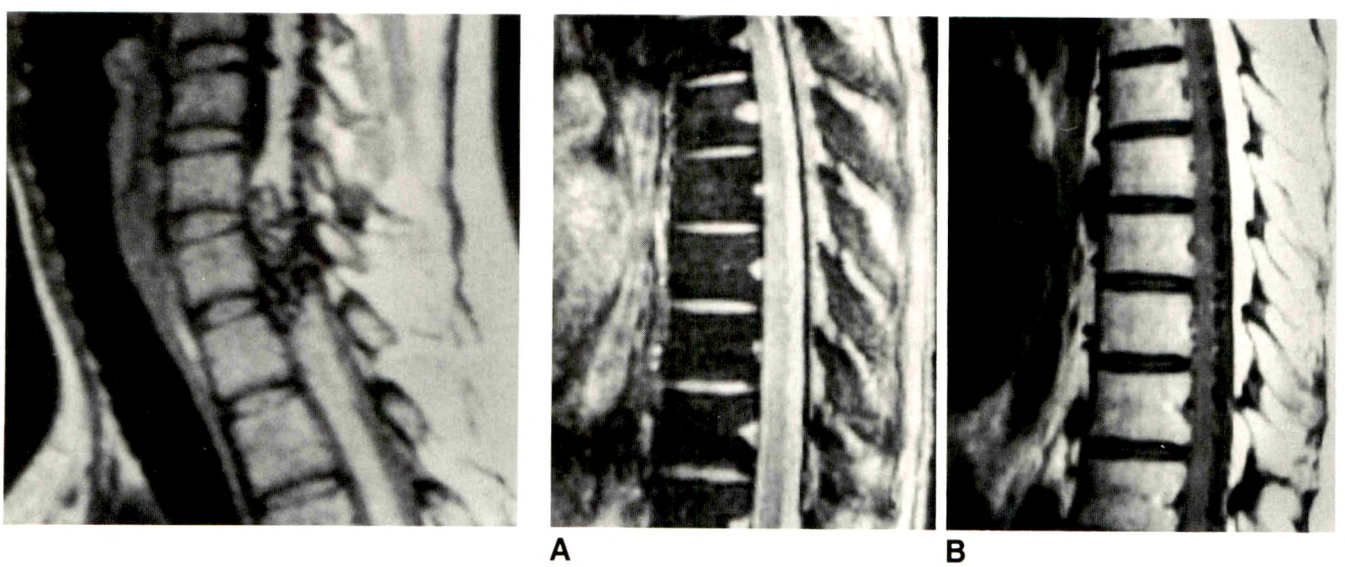


Fig. 6.—Arteriovenous malformation of cord. Short TR (600/20) sagittal MR image shows marked serpiginous signal voids permeating substance of cord, especially visible at C7 and on axial image (*not shown*). In addition, marked large serpiginous signal voids are present along cord periphery superiorly, consistent with large draining veins.

Fig. 7.—Dural arteriovenous fistula.

A, Gradient-echo (367/15/15°) sagittal MR image of thoracic spine shows subtle scalloping of posterior surface of cord.

B, Short TR (550/20) sagittal MR image after administration of contrast material shows subtle punctate enhancement of some focal and serpiginous hypointensities posterior to cord.



A B

Fig. 8.—Cryptic vascular malformation of distal thoracic cord in a patient with long-standing fluctuating conus symptoms.

***A*, Short TR (600/20) sagittal MR image obtained during a period of exacerbation shows focal high signal intensity in conus, consistent with evolving products of hemorrhage. Also seen are areas of mixed increased and decreased signal intensity extending superiorly, representing hemorrhage at other stages of evolution and extension of the bleeding.**

***B*, Long TR (2368/70) sagittal MR image again shows multiple areas of mixed signal intensity within cord, consistent with evolving hemorrhage. In this case, because of acute nature of hemorrhage, high signal intensity is also noted in surrounding cord, probably because of edema.**

occur [32, 35]. In these cases, the development of intramedullary cysts, myelomalacia, or adhesions may be treated. Areas of cord injury or transection are well demonstrated (Fig. 10). Myelomalacia is generally visualized as a poorly defined area of low intensity within the cord on short TR images [32]. Long TR images disclose high intensity in the corresponding regions. Progression to a well-defined cyst can be detected on MR by the presence of a well-defined low-intensity region on short TR images, with a sharp interface between the surrounding normal cord and the cyst itself. The cyst contents appear uniformly hypointense or may show evidence of flow, unlike in myelomalacia. If the lesion is extensive, then a cyst is more likely, since myelomalacia is characterized by relatively short segments of involvement. Clearly, the differentation is clinically important, since myelomalacia cannot be treated with shunting. Those cysts in which flow artifacts appear especially prominent are particularly good candidates for treatment, since active pulsations within the cyst may predispose to further extension.

Syringomyelia/Hydromyelia

Although cord cysts may be commonly associated with trauma or neoplasm, true syringomyelia or hydromyelia is usually found related to Chiari malformation or is idiopathic in origin [13]. Hydromyelia is due to congenital dilatation of the central canal. Syringomyelia represents a cavity in the cord itself. The pathogenesis is highly debatable. The dysraphic theory suggests that a closure defect of the neural tube at the level of the posterior raphe is responsible. The hydrodynamic theory maintains that disturbances of CSF outflow from the fourth ventricle leads to hydromyelia, followed by syringomyelia as a result of rupture of the dilated ependymal canal. Occasionally, syrinxes can also occur as a result of arachnoid adhesions with secondary alteration in CSF flow [36–38]. These cases typically involve the thoracic region, unlike other syrinxes, which are usually located in the cervical cord. Symptoms depend on the location of the syrinx. Pathologically, syrinxes may be lined by fibrous astrocytosis.

On MR, short TR images accurately show the morphology of the cyst. Typically, there is a sharp interface between the normal cord and the syrinx itself. Metameric haustrations are typical of Chiari-associated hydromyelia. The syrinx itself is often well defined and smooth, but occasionally septa are detected. If arachnoiditis is present, extensive adhesions may blur the interface between the cord and the surrounding CSF [36]. If the cyst shows any suspicious features at all, such as loss of definition in a focal region, then contrast enhancement is indicated to ensure that a neoplasm is less likely.

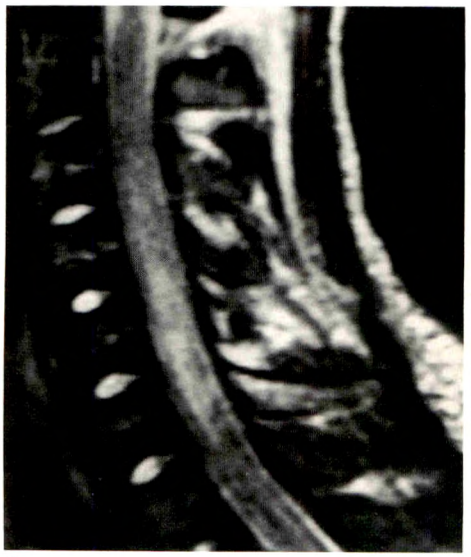
Neurodegenerative Disorders of the Spinal Cord

A small number of neurodegenerative disorders involve the cord [13]. Different disorders involve different tracts, and involvement of structures other than the cord, such as the cerebellum or other parts of the brain, is frequently associated. The pathogenesis of most of these disorders is unknown. Pathologically, these diseases are typified by very little inflammatory reaction and by progressive, symmetric breakdown of cells, usually neurons.

Friedreich's ataxia is believed to be due to a mutation on chromosome 9 and occurs in both autosomal recessive and dominant inheritance patterns [39]. Patients are typically adolescents or young adults and present with a mixed clinical picture of gait ataxia, upper extremity clumsiness, and dysarthria. Pathologically, myelin loss and gliosis focused on the posterior columns, spinocerebellar tract, and corticospinal tract are seen, with secondary atrophy. MR imaging reveals an atrophic spinal cord with normal signal intensity [40].

While Friedreich's ataxia is the prototypical progressive ataxia, several other degenerative disorders of the cord can also occur. These include hereditary spastic paraplegia (Strümpell-Lorain disease) and hereditary posterior column ataxia (Biemond syndrome) [41]. Other syndromes may involve the brain, especially the cerebellum, as well as the cord and include olivopontocerebellar atrophy and Shy-Drager syndrome.

Other types of neurodegenerative disorders primarily involve the motor neurons. Of these, the prototype is amyotrophic lateral sclerosis. Although most cases are sporadic, occurring in elderly patients, the disease is transmitted in an autosomal dominant fashion in approximately 5% of cases



9

Fig. 9.—Posttraumatic cord contusion in patient with bullet wound to soft tissues of neck and secondary quadriparesis. Long TR (2308/80) sagittal MR image shows diffuse high intensity in enlarged region of cord.



10

Fig. 10.—Chronic disruption of cord after direct stab wound. Short TR (600/20) sagittal MR image shows disruption of distal thoracic cord with significant atrophy both above and below area of trauma.

[42]. The clinical triad consists of atrophic weakness of the distal upper extremities, mild spasticity of the lower extremities, and generalized hyperreflexia. Innervation atrophy affects the muscles.

Pathologically, degeneration of the corticospinal tract and lower motor neurons is seen [13, 14]. Because corticospinal tract degeneration can extend superiorly to involve the cerebral peduncles, posterior portion of the posterior limb of the internal capsule, and corona radiata, MR reports have focused on the hyperintense foci seen on long TR sequences in the brain. However, the cord may also appear to be atrophic and flattened in its anterior and lateral portions owing to loss of motor neurons in the anterior horns in corticospinal tracts. Hyperintense foci in the cord have not been reported.

Other more unusual forms of motor neuron disease have been described clinically but not by imaging. One exception is juvenile amyotrophy of the distal upper extremity, also known as monomelic amyotrophy or benign focal amyotrophy. Characteristic unilateral muscular atrophy in the distal upper extremity due to selective anterior horn cell involvement in the lower cervical cord is seen. Unlike amyotrophic lateral sclerosis, this disease usually occurs in boys and stabilizes after a few years. Focal atrophy of the cervical cord, often limited to the anterior horn cell region, has been described [43].

Miscellaneous

Clinically, most metabolic and toxic disorders affect the brain far more than the cord. A very few, however, target the cord. Subacute combined degeneration of the cord occurs in patients with pernicious anemia due to vitamin B_{12} deficiency, but has also been associated with many other malnutritive and malabsorptive conditions [13, 14]. Pathologically, degeneration of myelin results in demyelination of the white matter, especially the dorsal and lateral columns.

Subacute necrotizing myelopathy accompanies malignancy, usually a lung carcinoma [13, 14]. Necrosis of myelin sheaths and axons occurs, usually in the thoracic cord. The syndrome resembles transverse myelitis.

Recent Advances in MR Imaging of the Cord

Although the appearance of tumors and other lesions of the cord has been well studied, several recent technologic innovations, including new pulse sequences, phased-array coil technology, and new methods of image display, have continued to expand the scope and versatility of MR imaging of the cord.

New Pulse Sequences

Often, cord lesions, especially subtle lesions such as MS plaques, are first detected with long TR images. Unfortunately, long TR images of the cord are often time-consuming and marred by motion artifacts. Recently, fast spin-echo (FSE) techniques have been developed that promise to provide images with a sensitivity to pathology comparable to that of long TR images, but in a much shorter time. These techniques are all variants of the original RARE (rapid acquisition with relaxation enhancement) sequence devised by Hennig et al. in 1986 [44–47]. Modification of the original sequence allows adaptation for clinical use [48, 49].

Although many variations exist, all of the FSE sequences consist of a single 90° pulse, followed by multiple 180° refocusing pulses. Each refocusing pulse is associated with its own phase-encoding gradient. The TE occurs where the lowest-order phase encodes, responsible for contrast, are placed.

The length of the echo train is crucial in determining the time of the acquisition, the number of sections, the image contrast, and the presence or absence of certain artifacts typical of the FSE sequences, such as blurring [49]. The length of the interecho spacing is also important and similarly contributes to the number of sections, the image contrast,

and the presence of certain artifacts. Thus, in specifying FSE acquisitions, new parameters, such as the length of the echo train and the interecho spacing, become important in addition to the familiar TR, TE, matrix size, and number of excitations.

FSE images strikingly resemble the routine long TR spin-echo images (Fig. 11). One crucial difference involves the persistent high signal intensity of lipid on FSE images, even when parameters apparently similar to those of routine spin echo are used. This persistent high signal intensity of lipid has been explained by the homonuclear coupling interaction of adjacent protons [49]. Early reports indicate that the FSE sequences are as sensitive in the detection of intramedullary disease as routine spin-echo sequences are [50]. MR imaging of the spine is characterized by long acquisition times and susceptibility to motion artifacts, factors that are less of a problem in brain imaging. Therefore, FSE images offer tremendous potential in the spine. Early reports on the evaluation of extradural disease suggest that FSE sequences are equivalent to gradient-echo sequences in the sagittal plane but are still inferior in the axial plane (Sze G, unpublished data).

The rapidity of the FSE sequences also makes a three-dimensional volumetric approach possible. Since the time of a volumetric acquisition is equal to $(TR \times N \times S_t \times S_s)/P$, where N is the number of excitations, S_t is the number of phase-encoding steps, S_s is the number of slice select steps, and P is the number of phase-encoding steps per TR, in routine spin echo, a volumetric acquisition would be prohibitive in the time required. However, with the FSE sequences, the volumetric acquisition can be obtained in a reasonable length of time [51]. Preliminary clinical evidence indicates that these sequences are also sensitive in the detection of intramedullary lesions.

A small number of disadvantages do exist with the FSE sequences: (1) FSE sequences introduce new artifacts. The effect of these artifacts, however, can be minimized with optimization of all the parameters. (2) The number of sections that can be obtained in a given acquisition is less than that of routine spin-echo imaging for a given TR. In MR imaging of the spine, the limited number of sections is not a clinical problem. (3) There is a theoretical loss of small object definition. Preliminary reports indicate that in the spine, detection of even small lesions, such as MS plaques, has not been compromised. The theoretical loss of small object definition applies to extremely small objects (two pixels), which also have short T2 relaxation times, a phenomenon very different from the majority of cord lesions. (4) Motion compensation techniques, such as gradient-moment nulling, are more difficult to apply in FSE imaging owing to the very short interecho spacing. Nevertheless, gradient-moment nulling can be applied to FSE imaging with slight limitations of other parameters, such as interecho spacing or TE.

Phased-Array Coils

Increasingly, clinicians request scans of the entire cord. Imaging of the length of the cord may be indicated to assess a diffuse process, such as tumor, MS, or inflammatory or infectious disease, or in cases of myelopathy in which exact localization is difficult. Both unenhanced and enhanced scans may be necessary. These clinical demands lead to a need for increased capability in spinal MR imaging. Either individual sequences must be performed more rapidly or large portions of the cord must be imaged on one acquisition, limiting patient imaging time.

In the past, only one surface coil could be used at a time, permitting only a limited field of view (FOV) in each acquisition [52, 53]. Increasing the FOV invariably led to decreased signal-to-noise ratio (SNR), particularly at the extremes near the end of the coil. Increasing the size of the surface coil reduced the advantages of the surface coil and decreased SNR. A single surface coil, therefore, could not always meet clinical demands.

With phased-array coils, several surface coils can be used together, combining the benefits of the small surface coil with the large FOV. These surface coils are arranged in a linear fashion. Coupled together to act as one, they markedly increase the length of the FOV, up to 48 cm (Fig. 12). The advantages of the phased-array coils are thus twofold: a larger FOV and increased SNR. With phased-array coils, one can routinely image the entire cord in a single acquisition (Fig. 12).

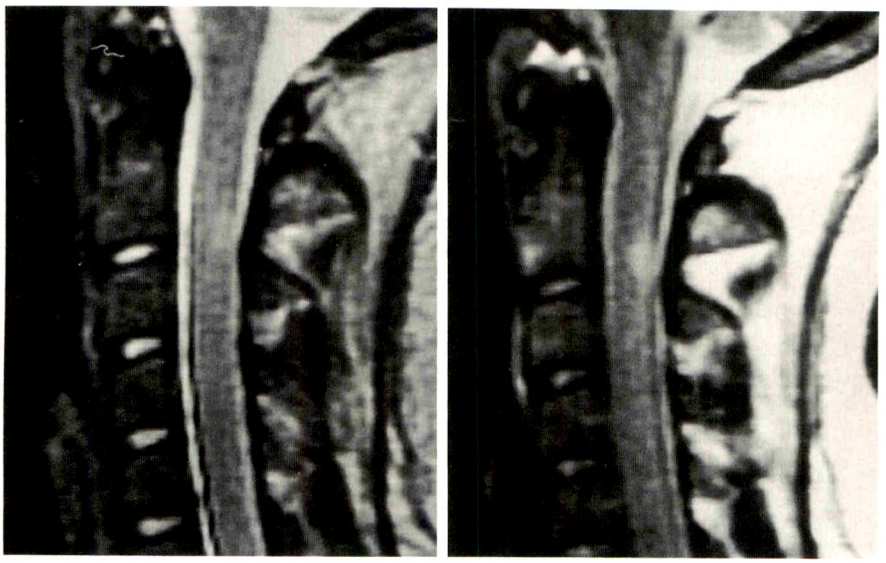
The multiple surface coils are matched by an equal number of receivers and memory boards. Each coil feeds into a separate receiver. The information from a particular coil is processed at this receiver and stored in one of the memory boards associated solely with the particular processing receiver. The information from the multiple surface coils is thus processed and stored. Because each receiver only processes signal from one specific coil, the noise heard by a particular receiver is limited to that transferred by a single surface coil. This allows for less noise coupling at the level of the receiver, resulting in increased SNR. The information from all receivers and memory boards is then coupled together by using a recombination type of algorithm.

Because of their advantages, phased-array coils will likely prove the most versatile of all coils for routine scanning of the spine. If a large FOV is required, such as a scan of the entire cord to evaluate an extensive syrinx, phased-array coils are clearly the method of choice. However, if only a limited FOV is required, phased-array coils still can be used because they provide better SNR and resolution than a single surface coil. Phased-array coils, therefore, are extremely versatile in their capabilities.

Image Display

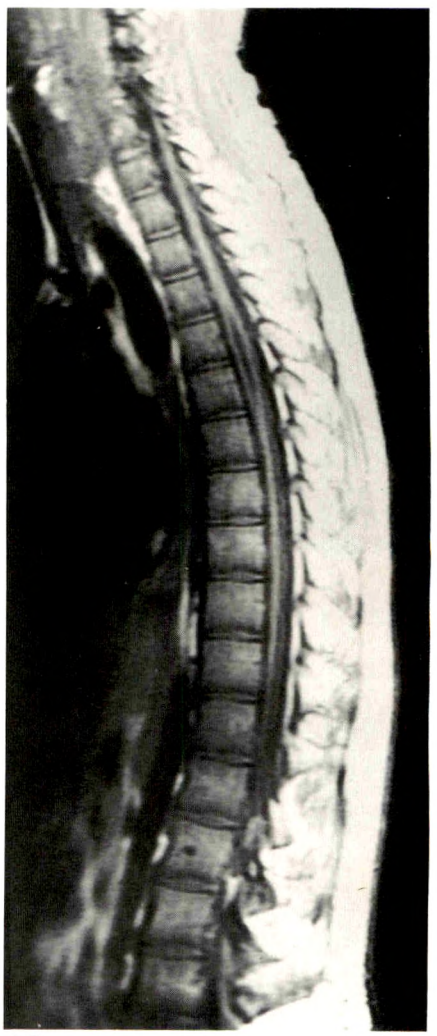
Significant advances have been made recently in the field of image display. The development of three-dimensional reformations promises to be one of the most important advances in MR imaging of the cord [54]. The ability to acquire very thin sections with gradient-echo sequences has permitted data acquired in one plane to be reconstructed and displayed in other planes. If isotropic voxels are obtained, minimal distortion or artifact exists in the reconstructions.

Three-dimensional reconstructions can be combined with enhancement with gadopentetate dimeglumine, particularly when spoiled gradient-echo sequences that display information in a "T1-weighted" fashion are used. One major question



A B

Fig. 11.—Multiple sclerosis.
A, Long TR (2188/80) cardiac-gated sagittal MR image of cervical spine, obtained in 12 min 48 sec, shows a small high-intensity lesion consistent with multiple sclerosis plaque.
B, Fast spin-echo (2000/112) MR image obtained in 3 min 12 sec also shows lesion.



12

Fig. 12.—Syrinx. Short TR (500/12) sagittal MR image with phased-array coils shows small focal area of low signal intensity within cord, consistent with a syrinx.

still must be addressed, namely, the sensitivity of spoiled gradient-echo sequences to contrast enhancement. Although spoiled gradient-echo sequences appear markedly T1 weighted, it has been noted that these sequences do not appear to show contrast enhancement after the administration of gadopentetate dimeglumine as clearly as short TR spin-echo sequences do (Augenstein HM et al., presented at the Radiological Society of North America meeting, November 1990; Rand SD et al., presented at the American Society of Neuroradiology meeting, June 1991).

Cine MR is another recent advance in the assessment of the cord and may be used to assess the pulsatility of cord cysts and to evaluate cord motion itself [55, 56]. As mentioned, cord cysts that are pulsatile are often considered better candidates for surgery, since persistent pulsatility may be associated with cyst expansion. These changes are optimally imaged with the use of a cardiac-gated gradient-echo technique, displayed in cine. In addition, myelomalacia can be readily differentiated from true cyst formation, since it fails to display pulsatility or turbulence. Use of this technique may also facilitate understanding of the origin of syringomyelia. Although it has been suggested that congenital syrinxes are connected to the fourth ventricle by the obex, a continuous flow void from the ventricle to the syrinx has not been observed.

Cord motion can be assessed with similar techniques. In these studies, a cardiac-gated spin-echo pulse sequence can be used to obtain phase information [56]. Peak caudal velocity of the cord has been noted to occur in early systole and to be 12.4 mm/sec. These velocities are decreased in patients with tethered cord or spinal cord compression, but not in those with intrinsic cord tumors.

REFERENCES

1. Norman D, Mills C, Brant-Zawadzki M, Yeates A, Crooks LE, Kaufman L. Magnetic resonance imaging of the spinal cord and canal: potential and limitations. *AJNR* **1984**;5:9–14

2. Rubin JB, Enzmann DR. Imaging of spinal CSF pulsation by 2DFT MR. *AJNR* **1987**;8:297–306
3. Rubin JB, Enzmann DR, Wright A. CSF-gated MR imaging of the spine: theory and clinical implementation. *Radiology* **1985**;167:225–232
4. Bronskill MG, McVeigh ER, Kucharczyk W, Henkelman RM. Syrinx-like artifacts on MR images of the spinal cord. *Radiology* **1988**;166:485–489
5. Bydder G, Brown J, Niendorf HP, et al. Enhancement of cervical intraspinal tumors in MR imaging with intravenous gadolinium-DPTA. *J Comput Assist Tomogr* **1985**;9:847–851
6. Sze G, Krol G, Zimmerman RD, Deck MDF. Intramedullary disease of the spine: diagnosis using gadolinium-DPTA enhanced MR imaging. *AJNR* **1988**;9:847–858
7. Valk J. Gadolinium-DPTA in MR of spinal lesions. *AJNR* **1988**;9:345–350
8. Dillon WP, Norman D, Newton TH, Bolla K, Mark A. Intradural spinal cord lesions: Gd-DPTA–enhanced MR imaging. *Radiology* **1989**;170:229–237
9. Parizel PM, Balériaux D, Rodesch G, et al. Gadolinium-DPTA–enhanced MR imaging of spinal tumors. *AJNR* **1989**;10:249–258
10. Goy AMC, Pinto RS, Raghavendra EN, et al. Intramedullary spinal cord tumors: MR imaging, with emphasis on associated cysts. *Radiology* **1986**;161:381–386
11. Poser CM. The relationship between syringomyelia and neoplasm. In: *American Lecture Series*, #262: *American Lectures in Neurology*. Springfield, IL: **1956**:28–32
12. Breger RK, Williams AL, Daniels DL, et al. Contrast enhancement in spinal MR imaging. *AJNR* **1989**;10:633–637
13. Okazaki H. *Fundamentals of neuropathology*. New York: Igaku-Shoin, **1983**:61–184
14. Rosenberg R, Grossman R, Schochet S Jr, Heinz E, Willis W Jr. *The clinical neurosciences*. New York: Churchill Livingstone, **1983**
15. Gero B, Sze G, Sharif H. MR imaging of intradural inflammatory diseases of the spine. *AJNR* **1991**;12:1009–1019
16. Helgason CM, Arnason BGW. Demyelinating diseases affecting the spinal cord. In: Davidoff RA, ed. *Spinal cord handbook*, vol. 4. New York: Dekker, **1986**:345–366
17. Edwards M, Farlow M, Stevens J. Cranial MR in spinal cord MS: diagnosing patients with isolated spinal cord symptoms. *AJNR* **1986**;7:1003–1005
18. Larsson EM, Holtas S, Nilsson O. Gd-DPTA–enhanced MR of suspected spinal multiple sclerosis. *AJNR* **1989**;10:1071–1076
19. Boden G. Radiation myelitis of the cervical spinal cord. *Br J Radiol* **1948**;21:464–469
20. Kim YH, Fayos JV. Radiation tolerance of the cervical spinal cord. *Radiology* **1981**;139:473–478
21. Maier JF, Perry RH, Saylor W, Sulak MH. Radiation myelitis of the dorsolumbar spinal cord. *Radiology* **1969**;93:153–160
22. McCunniff AJ, Liang MK. Radiation tolerance of the cervical spinal cord. *Int J Radiat Oncol Biol Phys* **1989**;16:675–678
23. Reagan TJ, Thomas JE, Colby MY. Chronic progressive radiation myelopathy. Its clinical aspects and differential diagnosis. *JAMA* **1968**;203:128–132
24. Zweig G, Russell EJ. Radiation myelopathy of the cervical spinal cord: MR findings. *AJNR* **1990**;11:1188–1190
25. Mawad ME, Rivera V, Crawford ES, Ramirez A, Breitbach W. Spinal cord ischemia after resection of thoracoabdominal aortic aneurysms: MR findings in 24 patients. *AJNR* **1990**;11:987–991
26. Hurth M, Houdart R, Djindjian R, Rey A, Dhindjian M. Arteriovenous malformations of the spinal cord. *Prog Neurol Surg* **1978**;9:238–266
27. Dormont D, Gelbert F, Assouline E, et al. MR imaging of spinal cord arteriovenous malformations at 0.5 T: study of 34 cases. *AJNR* **1988**;9:833–838
28. Minami S, Sagoh T, Nishimura K, et al. Spinal arteriovenous malformation: MR imaging. *Radiology* **1988**;169:109–115
29. Terwey B, Becker H, Throm A, Vahldiek G. Gadolinium-DPTA enhanced MR imaging of spinal dural arteriovenous fistulas. *J Comput Assist Tomogr* **1989**;13:30–37
30. Gaensler EHL, Jackson DE, Halback VV. Arteriovenous fistulas of the cervicomedullary junction as a cause of myelopathy. *AJNR* **1990**;11:518–520
31. Fontaine S, Melanson D, Cosgrove R, Bertrand G. Cavernous hemangiomas of the spinal cord: MR imaging. *Radiology* **1988**;66:839–842
32. Quencer RM. The injured spinal cord. Evaluation with magnetic resonance and intraoperative sonography. *Radiol Clin North Am* **1988**;26:1025–1045
33. Kulkarni MV, Bondurant FJ, Rose SL, Narayana PA. 1.5 Tesla magnetic resonance imaging of acute spinal trauma. *RadioGraphics* **1988**;8:1059–1082
34. Mirvis SE, Geisler FH, Jelinek JJ, Joslyn JN, Gellad F. Acute cervical spine trauma: evaluation with 1.5-T MR imaging. *Radiology* **1988**;166:807–816
35. Yamashita Y, Takahashi M, Matsuno Y, et al. Chronic injuries of the spinal cord: assessment with MR imaging. *Radiology* **1990**;175:849–854
36. Mark AS, Andrews BT, Sanchez J, Manelfe C, Peck W, Norman D. MRI of syringomyelia secondary to arachnoid adhesions (arachnoiditis) with emphasis on associated arachnoid cysts. In: *Book of Abstracts: Society of Magnetic Resonance in Medicine*. Berkeley, CA: Society of Magnetic Resonance in Medicine, **1987:** 251
37. Barnett JHM. Syringomyelia associated with spinal arachnoiditis. In: Barnett HJM, Foster JB, Hudgson P, eds. *Syringomyelia*. London: Saunders, **1973**:220–243
38. Barnett JHM. The pathogenesis of syringomyelic cavitation associated with arachnoiditis localised to the spinal canal. In: Barnett HJM, Foster JB, Hudgson P, eds. *Syringomyelia*. London: Saunders, **1973**:245–259
39. Chamberlain S, Shaw J, Rowland A, et al. Mapping of mutation causing Friedreich's ataxia to human chromosome 9. *Nature* **1988**;334:248
40. Wessel K, Schroth G, Diener HC, Muller-Forell W, Dichgans J. Significance of MRI-confirmed atrophy of the cranial spinal cord in Friedreich's ataxia. *Eur Arch Psychiatry Neurol Sci* **1989**;238:225–230
41. Schoene WC. Degenerative diseases of the central nervous system. In: Davis RL, Robertson DM, eds. *Textbook of neuropathology*. Baltimore: Williams & Wilkins, **1985**:788–823
42. Adams RD, Victor M. *Principles of neurology*, 4th ed. New York: McGraw-Hill Information Services Co., Health Professions Div., **1989**:35–77, 334–346, 488–500, 921–967
43. Biondi A, Dormont D, Weitzner I Jr, et al. MR imaging of the cervical cord in juvenile amyotrophy of distal upper extremity. *AJNR* **1989**;10:263–268
44. Hennig J, Naureth A, Friedburg H. RARE imaging: a fast imaging method for clinical MR. *Magn Reson Med* **1986**;3:823–833
45. Hennig J, Friedburg H, Strobel B. Rapid nontomographic approach to MR myelography without contrast agents. *J Comput Assist Tomogr* **1986**;10:375–378
46. Hennig J, Friedburg H, Ott D. Fast three-dimensional imaging of cerebrospinal fluid. *Magn Reson Med* **1987**;5:380–383
47. Hennig J, Friedburg H. Clinical applications and methodological developments of the RARE technique. *Magn Reson Imaging* **1988**;6:391–395
48. Mulkern RV, Wong STS, Winalski C, Jolesz FA. Contrast manipulation and artifact assessment of 2D and 3D RARE sequences. *Magn Reson Imaging* **1990**;8:557–566
49. Melki PS, Mulkern RV, Panych LP, Jolesz FA. Comparing the FAISE method with conventional dual-echo sequences. *J Magn Reson Imaging* **1991**;1:319–326
50. Sze G, Merriam M, Oshio K, Jolesz F. Fast spin echo imaging in the evaluation of intramedullary spinal lesions. *AJNR* (in press)
51. Oshio K, Jolesz F, Melki PS, Mulkern RV. T2-weighted thin slice imaging with multi-slab 3D RARE. *J Magn Reson Imaging* **1991**;1:695–700
52. Carlson JR, Arakawa M, Kaufman L, McCarten BM, George C. Depth-focused radio-frequency coils for MR imaging. *Radiology* **1987**;165:251
53. Kneeland JB, Hyde JR. High resolution MR imaging with local coils. *Radiology* **1989**;171:1–4
54. Sherry CS, Harms SE, McCroskey WK. Spinal MR imaging: multiplanar representation from a single high resolution 3D acquisition. *J Comput Assist Tomogr* **1987**;11:859–864
55. Quencer RM, Post MJ, Hinks RS. Cine MR in the evaluation of normal and abnormal CSF flow: intracranial and intraspinal studies. *Neuroradiology* **1990**;32:371–391
56. Levy LM, DiChiro G, McCullough D, Dwyer AJ, Johnson D, Yang S. Fixed spinal cord: diagnosis with MR imaging. *Radiology* **1988**;169:773–778

Book Review

Head and Neck Radiology. By Arnold Noyek. Philadelphia: Lippincott, 115 pp., 1991. $49.95

Complex anatomy, diverse pathologic changes, and multiple imaging techniques have made head and neck imaging one of the most difficult areas for understanding and interpretation. This book provides a pictorial atlas of pathologic processes in each anatomic region within the head and neck and a brief description of radiologic techniques useful in each of these anatomic regions.

The book is divided into 17 chapters as follows: temporal bone, paranasal sinuses, nasopharynx, orbital extension of diseases of the nasal cavity and paranasal sinuses, skull base, intracranial relationships of otorhinologic disorders, maxillofacial skeleton, temporomandibular joints and mandible, major salivary glands, thyroid gland, parathyroid glands, superior mediastinum, larynx and cervical trachea, upper digestive tract, vascular lesions of the head and neck, nonvascular soft-tissue lesions of the head and neck, otolaryngologic manifestations of systemic disease.

Each chapter begins with a brief description of radiologic studies used for the evaluation of that region. This is followed by a description of major findings and then illustrative cases to demonstrate the imaging techniques and a spectrum of pathologic changes in that region. Illustrations are labeled to show subtle changes or are accompanied by line drawings, and a brief description of the findings is provided.

A wide range of pathologic changes is illustrated, and image quality is satisfactory. However, the book suffers from a lack of descriptive information on normal anatomy, pathologic changes, and clinical signs of the various regions and entities illustrated, and it provides little in the way of differential diagnosis based on the radiologic appearances. A second deficiency is the almost complete absence of information on MR imaging of the head and neck, apart from occasional references to the technique and three images.

As a pictorial atlas for a quick review of pathologic changes that affect the head and neck, this book suffices. The images are of reasonable quality and a wide spectrum of diseases is illustrated. However, the lack of description of normal anatomy, pathologic changes, and differential diagnosis makes this text unsuitable as a primary reference text for residents or radiologists.

Mary Ann Johnson
University of Alberta Hospital
Edmonton, Alberta, Canada T6G 2B7

Review Article

MR Imaging in the Management of Extracranial Malignant Tumors of the Head and Neck

Patricia A. Hudgins[1] and Gerald S. Gussack[2]

Methods of treating malignant tumors of the extracranial portion of the head and neck have become more sophisticated. Cross-sectional imaging is extremely important in the evaluation of patients with a tumor in the head or neck. Although the complexities of head and neck radiology may be overwhelming, a uniform approach that first determines the location and extent of the primary tumor and then examines the nodal chains for metastatic adenopathy takes much of the mystery out of the process. MR imaging allows improved soft-tissue contrast and direct multiplanar acquisition of data, two advantages over CT. This review describes the current role of imaging in the clinical assessment of a patient with a malignant tumor in the head and neck, including the questions that must be answered before surgery and when MR imaging is the preferred technique.

The examination of patients with neoplasms of the head and neck has evolved significantly in the past decade. Although physical examination and endoscopy remain important diagnostic techniques, cross-sectional imaging has had an increasingly important role in both initial evaluation and follow-up care. CT or MR imaging complements the physical and endoscopic examinations, giving the surgeon information about the extent of the lesion and associated adenopathy, thus contributing to important treatment decisions. Ninety percent of head and neck neoplasms are epithelial and begin as superficial mucosal lesions. The clinician often uses endoscopy first to visualize and then to do a biopsy on the suspected abnormality [1]. Information about the location of the lesion, presence or absence of palpable adenopathy, and even the histology of the lesion is frequently available to the radiologist before the CT or MR examination. With this knowledge, the radiologist can decide on either CT or MR and perform a high-quality examination with special attention to the area in question.

The radiologist has two important goals in aiding decisions about therapy and management: to describe the tumor and to detect any pathologic adenopathy. Characteristics of the primary lesion that directly determine prognosis and aid in treatment planning include its epicenter or site of origin, size, presence of necrosis, invasion of adjacent structures, extension across the midline, involvement of bone or laryngeal cartilage, and status of the carotid artery or jugular vein. Preoperative demonstration of tumor margins is essential, as rates of localized control are improved when the tumor is completely excised. Clinically important nodal characteristics in the head and neck include the size, location, and number of metastatic ipsilateral and contralateral nodes to the primary lesion, presence or absence of necrosis, and extranodal spread with fixation to adjacent structures.

Imaging Technique

The extremely complex anatomy and many small structures in the head and neck make superior resolution and the highest signal-to-noise ratio (SNR) important goals of MR imaging of

Received November 25, 1991; accepted after revision January 17, 1992.
Some figures provided courtesy of a grant from Berlex Laboratories, Inc., Wayne, NJ.
[1] Department of Radiology, Section of Neuroradiology, Emory University School of Medicine, 1364 Clifton Rd., N.E., Atlanta, GA 30322. Address reprint requests to P. A. Hudgins.
[2] Department of Radiology, Section of Otolaryngology, Emory University School of Medicine, Atlanta, GA 30322.

 0361–803X/92/1591–0161 © American Roentgen Ray Society

the head and neck. Surface coils are necessary to optimize these examinations [2]. The best surface-coil design for the head and neck is a combined head and neck coil, which allows contiguous images to be obtained both high at the skull base and low at the thoracic inlet. However, if such a coil is not available for the machine in use, the study may be done with two different coils. Lesions high in the roof of the nasopharynx, paranasal sinuses, or skull base are best studied with a standard head coil, whereas a cervical neck coil can be used for the evaluation of the middle and lower cervical node groups. Careful planning is required to coordinate the use of two different coils and the pulse sequences needed for unenhanced and enhanced T1- and T2-weighted images.

Occasionally, but more commonly than in other areas of the body, the MR images are inadequate because of the patient's motion. Patients with lesions in the head and neck often have difficulty with secretions, which results in coughing, swallowing, or choking. Furthermore, these patients may have associated chronic pulmonary disease, with shortness of breath and coughing when supine. We have found that educating the patient before scanning greatly contributes to the success of the examination. The MR technologist emphasizes the need for remaining still, encourages shallow steady abdominal breathing, and pauses between sequences to allow coughing, deep breathing, or suctioning. The patient should be positioned with the neck in a neutral or slightly flexed position, as hyperextension makes swallowing more difficult [3].

The techniques and parameters used depend on the location of the tumor. The axial plane is most commonly imaged, as radiologists are more familiar with the neck's anatomy in this plane. Coronal images are important for examining lesions in the skull base and to confirm perineural, orbital, or extradural disease. Coronal images can be used to assess the laryngeal ventricle and detect infraglottic extension in laryngeal lesions. The coronal plane also should be considered for lesions in the tongue, floor of mouth, and external auditory canal or for matted nodal masses that extend over a long distance. T1-weighted images are most useful for defining anatomic detail in the neck, and T2-weighted images may allow distinction of normal from abnormal tissue on the basis of signal intensity. The optimal slice thickness for T1-weighted images through the primary tumor is 3 mm, and 5-mm thickness is adequate for assessing the nodes. Nasopharyngeal lesions are best studied with thin slices beginning at the roof of the nasopharynx and extending to the hard palate. Oral cavity and oropharyngeal lesions should be studied with sections 3 mm thick extending from the hard palate to the free edge of the epiglottis and valleculae. Laryngeal or hypopharyngeal lesions are imaged with thin sections beginning at the epiglottis and extending to at least 1 cm beneath the true vocal cords. Two "packages" or contiguous groups of T1-weighted images may be acquired, because the area that must be covered often exceeds the usual length of a single acquisition. The repetition time (TR) should be kept less than 800 msec, with an echo time (TE) less than 30 msec, to optimize evaluation of bony intramedullary disease, especially for lesions at the skull base. T2-weighted sequences (2000–2500/30–90) are generally slightly thicker, ranging from 4 to 6 mm. These sequences should cover both the primary lesion and the draining nodal groups.

Artifact suppression techniques, including gradient moment nulling, flow compensation, cardiac gating, and presaturation pulses, are currently available to minimize motion artifacts from swallowing and cardiac and respiratory movements and should be routinely used for neck studies. Phase-encoding gradients should be placed in the anteroposterior direction [3]. Parameters such as number of signal averages and matrix size depend on equipment as well as personal preference; however, the examination may be lengthy and all efforts should be directed toward speed.

The routine use of paramagnetic contrast agents, such as gadopentetate dimeglumine (Berlex, Wayne, NJ) in the evaluation of malignant lesions in the extracranial part of the head and neck remains controversial; however, in certain situations, contrast administration unequivocally improves lesion conspicuity [4–8]. Because it is impossible to predict which lesions will be better seen with contrast enhancement, we routinely obtain T1-weighted images enhanced with gadopentetate dimeglumine through the primary tumor and nodal masses. Many of the compartments in the neck are composed of fat and have high signal intensity on T1-weighted images. Enhancing lesions may become isointense with fat, and, therefore, less conspicuous, unless signal from fat can be suppressed. Early evidence suggests that fat-suppression sequences are superior to routine enhanced T1-weighted images [9, 10]. Therefore, at least one enhanced T1-weighted sequence through the primary tumor is obtained with fat suppression.

General Imaging Characteristics

MR is superior to CT for imaging many malignant lesions in the head and neck because of its superb soft-tissue contrast. Lesion conspicuity, interface between tumor and normal tissue, and local extension are best seen on MR, especially when the tumor is located in the oropharynx, nasopharynx, skull base, or neck [11]. Malignant tumors are generally isointense or hyperintense relative to muscle and hypointense relative to fat on T1-weighted images and slightly hyperintense relative to both muscle and fat on T2-weighted images. Some degree of enhancement is seen in most malignant tumors in this region, resulting in increased conspicuity of tumor boundaries at muscle interfaces, but enhancement may obscure tumor borders at tumor-fat interfaces unless fat-suppression sequences are used. Peripheral enhancement with lack of central enhancement suggests necrosis either in the primary tumor or metastatic nodes. This is important preoperative information, as the surgeon will use particular care in excising these lesions to avoid puncture of the tumor and potential spillage and seeding of the surgical bed. Gadopentetate dimeglumine–enhanced images also are important for defining perineural, intracranial, and extradural disease [4].

Tumors of the Skull Base

Skull base involvement or intracranial extension of tumor, dramatic manifestations of malignant tumors in the head and

neck, carry grave prognoses and usually portend advanced disease. The surgical extirpation of intracranial disease is complex, necessitating a combined craniofacial approach by the neurosurgeon and otolaryngologic surgeon. Skull base surgery has opened new frontiers for the treatment of malignant lesions with deep invasion, which had been thought to be inoperable. Accurate and thorough preoperative detection of the complete extent of disease is essential, guiding the resection and adjuvant radiotherapy to ensure the longest disease-free interval. A Le Fort I osteotomy approach to the nasopharynx, which gives wide exposure to the central skull base, has recently gained popularity for surgery in this region [12].

Malignant tumors originating in the paranasal sinuses and nasopharynx, because of their proximity to the skull base, are the most common neoplasms of the head and neck that involve the skull base. These include squamous cell carcinoma, tumors of salivary gland origin (e.g., adenoid cystic carcinoma), and lymphoma. Intracranial disease may spread either by direct extradural extension, through the foramina of the skull base, or by perineural spread [13–16].

MR is superior to CT for evaluating involvement of the skull base by head and neck lesions in most cases [13]. Unenhanced T1-weighted images are the most sensitive sequences for detecting bony intramedullary disease, which has low signal intensity, in sharp contrast to the high signal intensity of the normal fat within the marrow space of the skull base [17] (Fig. 1). Gadopentetate dimeglumine–enhanced T1-weighted images are always indicated, as perineural spread of tumor and epidural disease are best seen after contrast enhancement [4, 5, 18] (Fig. 2). Occasionally, thin-section direct coronal CT, which is superior to MR for cortical bone detail, may be necessary to detect or confirm subtle cortical disease [19].

Malignant perineural spread, characteristic of poorly differentiated squamous cell carcinoma and adenoid cystic carcinoma, extends in a retrograde manner along cranial nerves through the basal foramina into the intracranial compartment. Perineural spread, especially when associated with intracranial spread, implies advanced disease with a poor prognosis [20], and such extension greatly affects treatment. For example, an adenoid cystic carcinoma of the parotid gland with

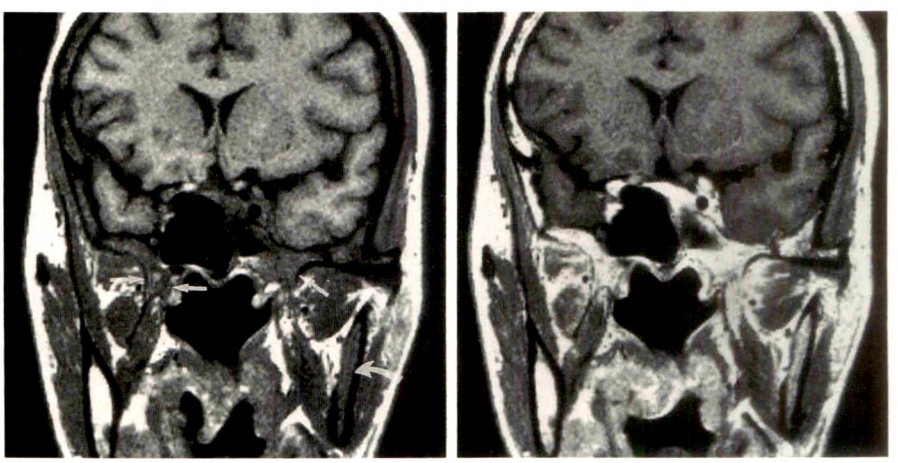


Fig. 1.—Diffuse involvement of bone marrow, skull base, and mandible in a patient with leukemia.

***A*, Coronal T1-weighted (500/20/2) MR image shows diffuse abnormal low signal within marrow of calvaria, skull base, and facial bones, including pterygoid plates (*straight arrows*) and left mandible (*curved arrow*). Right mandible is normal, with expected high signal intensity within marrow.**

***B*, Gadopentetate dimeglumine–enhanced T1-weighted MR image reveals enhancement of abnormal marrow, which has become nearly isointense with normal fatty marrow. Unenhanced T1-weighted images are the most sensitive for marrow disease and are always acquired before contrast material is administered to detect involvement of skull base by malignant tumors of head and neck.**

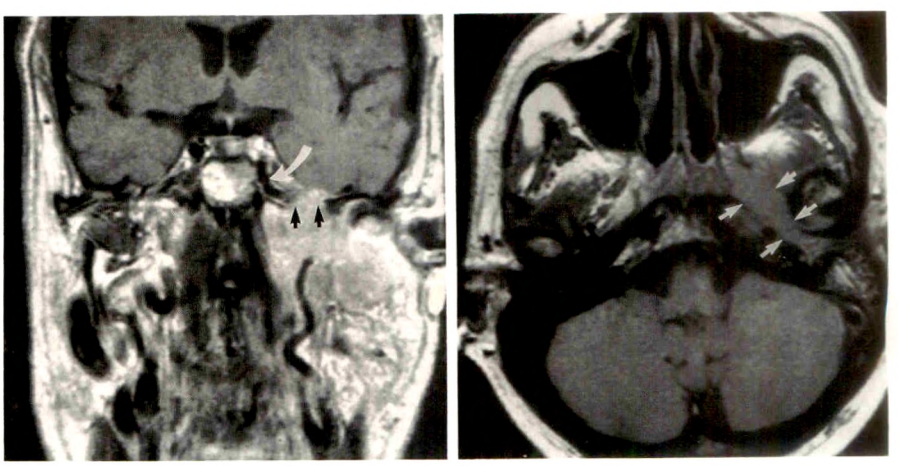


Fig. 2.—Squamous cell carcinoma of nasopharynx with involvement of skull base. Enhanced T1-weighted (800/30/2) coronal MR image shows destruction of skull base (*black arrows*) with associated intracranial epidural tumor. Notice large enhancing mass in nasopharynx that involves masticator and parapharyngeal spaces and is wrapping around cervical portion of internal carotid artery. However, vessel is patent, as evidenced by normal signal void in distal cavernous portion of artery (*white arrow*).

Fig. 3.—Squamous cell carcinoma extending through eustachian tube. Unenhanced T1-weighted (800/30/2) transverse MR image shows tumor extending from nasopharynx to middle ear (*arrows*), along course of left eustachian tube.

perineural spread requires additional resection of the temporal bone to obtain a clean margin at the facial nerve. Extension of a malignant neoplasm in the maxillary sinus into the foramen ovale requires an infratemporal fossa resection and a total maxillectomy.

MR is more sensitive than CT for evaluating perineural spread of tumor, especially when the disease is at the skull base, in the cavernous sinus, or extending into the cisternal portion of the cranial nerves [18]. The cranial nerves most commonly involved are the maxillary and mandibular divisions (V2 and V3) of the trigeminal nerve and the facial nerve (VII). Tumor will be seen extending into the foramen rotundum, ovale, or stylomastoid, respectively. Any foramina of the skull base, however, including the carotid canal, foramen lacerum, hypoglossal canal, jugular foramen, or eustachian tube (Fig. 3), is a potential pathway for intracranial spread. Thin-section T1-weighted images routinely show the major cranial nerves. Perineural thickening and enhancement with widening of the foramina are the hallmarks of tumor spread [4, 14, 15, 18]. Perineural extension commonly involves the nerves of the cavernous sinus, characterized by a mass within the sinus, lateral bowing of the dura, which forms the wall, and/or narrowing or displacement of the cavernous carotid artery. Cavernous sinus involvement was at one time deemed inoperable. Recent surgical advances and interventional neurovascular procedures, including temporary or permanent carotid occlusion, have allowed surgical resection of the cavernous sinus to be done safely [21].

Tumors of the Nasopharynx

The nasopharynx forms the cephalad portion of the aerodigestive tract; its boundaries are the skull base, including the sphenoid bone and clivus (basisphenoid) superiorly, the lower clivus (basiocciput) and first two cervical vertebral bodies posteriorly, the nasal fossa anteriorly, and the soft palate inferiorly. The deep extent of the nasopharynx is defined by the pharyngobasilar fascia, a tough fascial layer that inserts on the medial pterygoid plates laterally, and on the pharyngeal tubercle of the basiocciput centrally. The most common malignant neoplasm of the nasopharynx is squamous cell carcinoma, which frequently arises in the lateral pharyngeal recesses [22]. Other lesions that occur in the nasopharynx include lymphoma, adenocarcinoma, adenoid cystic carcinoma, plasmacytoma, and various sarcomas, including rhabdomyosarcoma. Deep spaces that surround and may be involved by nasopharyngeal malignant tumors include the fat-filled triangular parapharyngeal space laterally, the carotid space posterolaterally, the masticator space inferolaterally, the eustachian tube, the retropharyngeal space posteriorly, and the prevertebral space and skull base posterior to the retropharyngeal space.

Artifacts from swallowing are not a serious problem in the nasopharynx, as movement is minimal. The area is limited in extent, and the superb soft-tissue contrast on MR makes it the technique of choice for accurately defining the boundaries of any nasopharyngeal malignant neoplasm [2, 6, 22–24]. MR easily differentiates a mass from the surrounding muscle (Fig. 4). Involvement of the skull base, particularly the clivus, results in replacement of the normal high signal intensity of the medullary bone and obliteration of the normal thin line of signal void of the cortical bone. A common finding in a patient with a nasopharyngeal malignant lesion is ipsilateral opacification of the mastoid air cells or middle ear caused by tumor involvement of the eustachian tube. Any adult with unilateral serous otitis media or mastoiditis should have a careful evaluation of the nasopharynx.

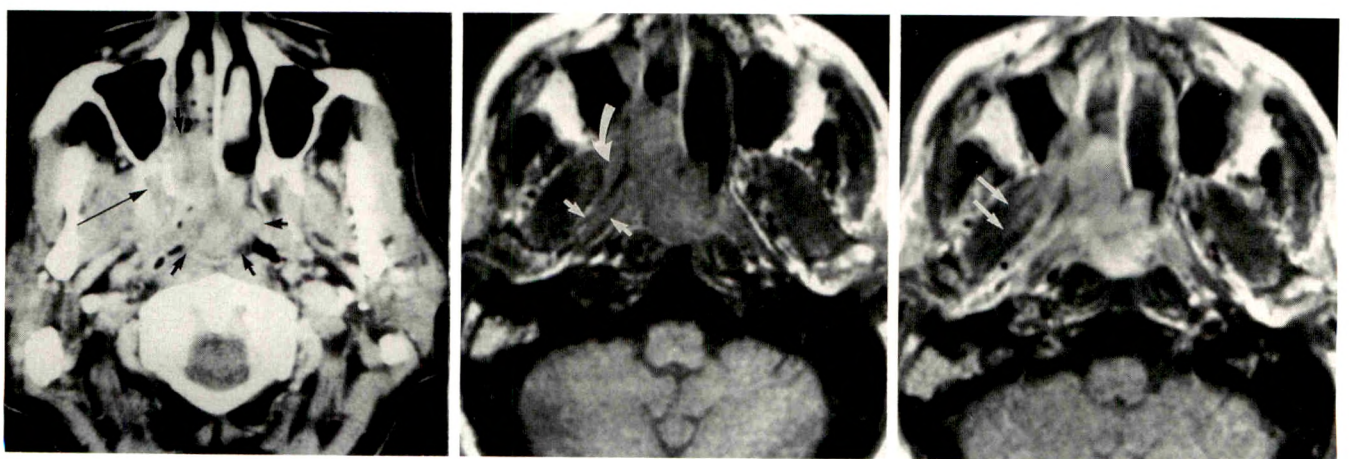


Fig. 4.—Adenoid cystic carcinoma, originating in nasopharynx.

A, Axial CT scan obtained with IV contrast material shows mass filling nasopharynx and posterior right nasal fossa (*short arrows*). Distortion of normal anatomy in medial masticator space and pterygoid fossa (*long arrow*) on right side suggests deep extension.

B, Unenhanced T1-weighted (800/30/2) axial MR image obtained at same level as *A*. Mass is slightly hyperintense relative to normal muscle. Deep extension into anteromedial aspect of lateral pterygoid muscle (*curved arrow*) and along tensor palatini muscle (*straight arrows*) is more conspicuous than on CT. Notice opacification of ipsilateral mastoid air cells, a frequent finding in malignant tumors of nasopharynx owing to eustachian tube dysfunction.

C, Gadopentetate dimeglumine–enhanced T1-weighted (800/30/2) MR image shows diffuse enhancement of lesion. Tumor extension into posterior aspect of lateral pterygoid muscle is better seen (*arrows*), because infiltrating tumor enhances and normal muscle enhances only minimally.

Although the mucosal lining of the nasopharynx can be examined clinically, malignant lesions often infiltrate deep to the mucosa, and the full extent of the disease is not visible by direct or fiberoptic examination [2, 25]. The mucosal surface is nearly isodense with the surrounding musculature on CT and, therefore, difficult to evaluate. On T2-weighted images it is hyperintense relative to muscle, and it enhances diffusely with gadopentetate dimeglumine. Ulcerating mucosal lesions are similar to normal mucosa in signal intensity and enhancement patterns; thus the role of MR in the detection of superficial lesions is limited. MR is essential, however, to show deep invasion or infiltration. Newer therapeutic techniques are dependent on accurate tumor delineation. Stereotaxic radiosurgery with the gamma knife is now being used for small, confined malignant lesions that were previously treated solely with irradiation or chemotherapy. This unit directs 201 cobalt-60 sources in a hemispheric array, which allows treatment of previously unresectable lesions with an accuracy of 1 mm [26]. Preoperative knowledge of involvement of the clivus, fossa of Rosenmuller, and cavernous sinus directs both the standard surgical and radiosurgical resections [12].

The major role of MR in the nasopharynx, therefore, is to determine the extent of deep disease, specifically, involvement of surrounding deep spaces, the prevertebral muscles, and skull base.

Tumors of the Oral Cavity and Oropharynx

The oral cavity extends from the lips to the circumvallate papillae of the tongue, while the oropharynx includes the base of the tongue to the vallecula and the posterior and lateral pharyngeal walls to the level of the soft palate. The most common malignant lesion of the oral cavity and oropharynx, squamous cell carcinoma, is commonly found on the ventral and lateral mobile tongue, retromolar trigone, floor of the mouth, alveololingual sulcus, tonsillar sulcus, and base of the tongue [27]. The superficial ulcerated portion of these lesions is well seen on physical examination and endoscopy, but deep invasion and involvement of adjacent compartments and structures is difficult to determine by physical examination (Fig. 5). MR is less affected by dental amalgam than is CT, and is the method of choice for evaluating lesions in this region [2, 7, 28, 29].

Local resection is the treatment for lesions of the oral cavity and oropharynx, and a complete resection with histologically normal margins is the goal. Surgical planning is aided by accurate preoperative knowledge of the extent of disease in the tongue and floor of the mouth. Local unilateral disease may be treated with a hemiglossectomy, and the surgical defect can be reconstructed primarily or with a myocutaneous flap [27]. Disease that extends across the midline must be detected preoperatively, because total glossectomy may be required. This more extensive procedure is associated with significant morbidity because of laryngeal aspiration of secretions and may even require a laryngectomy or extensive reconstruction. Invasion of the mandible or its periosteum should be determined to best plan for surgical resection and reconstruction of the jaw. Lesions in the base of the tongue and lateral pharyngeal walls may extend caudally to involve the larynx, requiring a supraglottic or horizontal laryngectomy as part of the surgical treatment. Extension upward to the soft palate is not rare. Failure to detect the full extent of disease may result in incomplete resection with early local recurrence and a shorter disease-free interval.

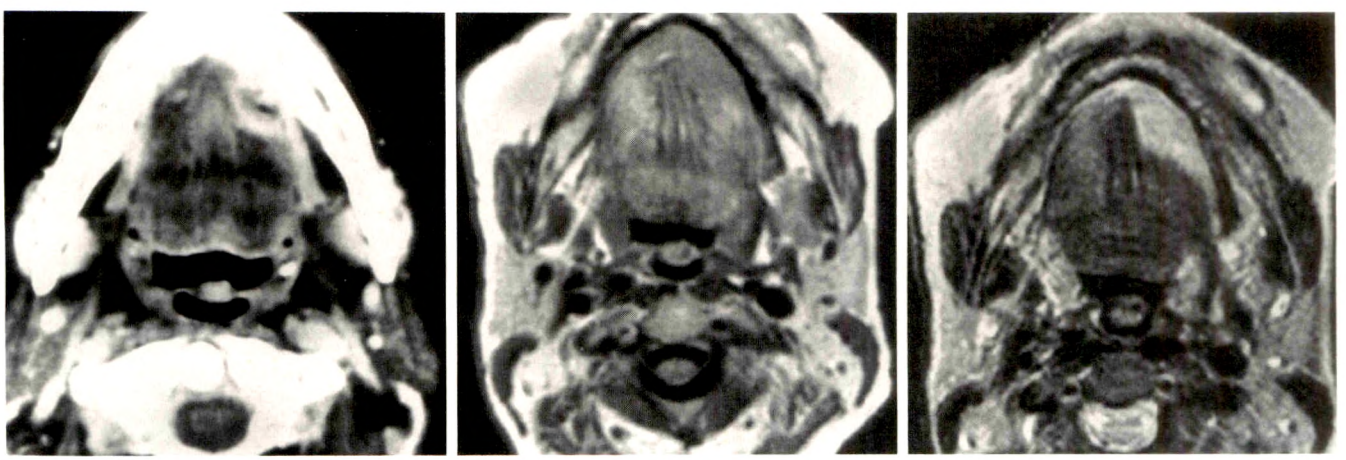


Fig. 5.—Squamous cell carcinoma, floor of mouth. Patient had shallow mucosal ulceration in gingivolingual sulcus, but deep extent of lesion was impossible to determine by physical examination.

***A*, Contrast-enhanced CT scan reveals a small necrotic lesion in left side of floor of mouth.**

***B*, Mass is isointense with muscle on this unenhanced T1-weighted (800/30/2) axial MR image and is seen only because it has distorted normal anatomic structures in floor of mouth. Decreased signal intensity seen in mandible adjacent to lesion, suggesting tumor involvement, was not confirmed on other sequences or at surgery, and is due to partial-volume artifact.**

***C*, T2-weighted (2000/90/1) MR image better shows precise boundaries of lesion, confirming lesion does not extend across midline or into tongue base.**

Tumors of the Paranasal Sinus

Malignant neoplasms of the paranasal sinuses make up only 3% of all cancers of the upper aerodigestive tract. Approximately 80% of these are squamous cell carcinomas; adenocarcinoma, tumors of salivary gland origin, and melanoma and metastases are the remaining lesions [30]. The presenting signs and symptoms of malignant tumors of the paranasal sinus (nasal obstruction, sinusitis, and epistaxis) mimic those of benign diseases; thus, these lesions are often advanced when diagnosed.

The three major goals of imaging lesions of the paranasal sinuses are to predict whether the lesion is benign or malignant, to define the extent of tumor outside the sinus cavity, and to distinguish tumor boundaries from the inflammatory changes. These goals are complicated by extensive debris that commonly accumulates within the sinus as the tumor obstructs the sinus ostium. CT accurately reveals destruction of the bony walls of the paranasal sinus, but the boundary between tumor and normal structures or inflammatory benign sinus contents may be indeterminate. For this reason, MR is more accurate in the preoperative assessment of malignant lesions of the paranasal sinuses.

Som et al. [31, 32] observed that 95% of tumors of the paranasal sinuses are intermediate in signal intensity on T2-weighted images; the remaining hyperintense tumors include mostly minor tumors of the salivary gland. Most inflammatory disease is hyperintense on T2-weighted images and is easily differentiated from tumor (Fig. 6). However, the signal intensity of benign inflammatory disease depends on many factors, including the presence of fungal infection, mucocele, or inspissated dry secretions [33–37]. Bone erosion is most often seen with malignant lesions, and the associated soft-tissue tumor is generally homogeneous in signal intensity, with a flat, broad-based interface with brain [38]. Extensive chronic inflammatory disease, particularly fungal infection, may erode bone and extend intracranially. Typically, the benign lesion is inhomogeneous in signal intensity with a polypoid rather than a flat interface with brain [38].

The decision for and extent of surgical resection depends on involvement of surrounding structures. Surgical options include maxillectomy with ethmoidectomy, exenteration of the orbit, or craniofacial resection [30, 39].

Tumors of the Hypopharynx and Larynx

MR is limited in imaging lesions in this region because of the mobility of the larynx and image degradation due to motion artifacts. Squamous cell carcinoma, which accounts for over

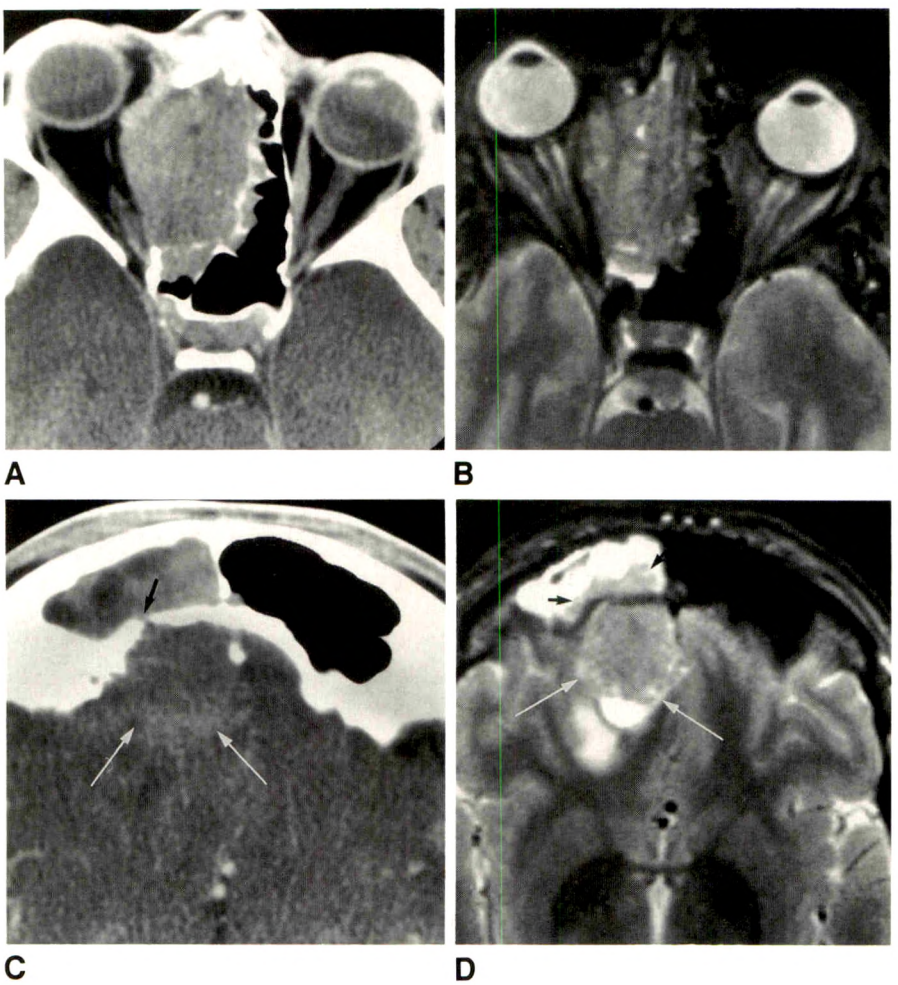


Fig. 6.—Squamous cell carcinoma, right ethmoidal sinus.

***A*, Large mass originating in right ethmoidal sinus with erosion through lamina papyrecea into orbit. Mass is intermediate in density on this contrast-enhanced CT scan.**

***B*, T2-weighted (2200/80/1) MR image obtained at same level as *A* shows mass is intermediate in signal intensity, characteristic of malignant disease of paranasal sinus.**

***C*, Contrast-enhanced CT scan obtained at a slightly higher level than *B* reveals opacification of right frontal sinus by soft tissue that is similar in density to tumor in ethmoidal sinus. Posterior wall of frontal sinus (*black arrow*) is eroded and a poorly defined intracranial mass (*white arrows*) is noted.**

***D*, T2-weighted MR image obtained at same level as *C* shows frontal sinus is filled with both benign secretions and tumor. Benign secretions are predominantly hyperintense and have accumulated as a result of obstruction of sinus ostium. Soft tissue in posterior sinus (*black arrows*), intermediate in signal intensity, is tumor. Intracranial mass (*white arrows*) is well seen.**

90% of malignant lesions, frequently occurs with advanced bulky disease, and the patients are uncomfortable and unable to cooperate during the examination. Thin-section (3 mm) CT is, therefore, the initial study performed, because images degraded by motion can easily be repeated. T1-weighted coronal MR is complementary to CT for detecting involvement of the laryngeal ventricle, true cords, and infraglottic spread of disease. The paralaryngeal and preepiglottic spaces are filled with fat and tumor extending into these deep spaces is hypointense and well seen. As faster sequences are developed, MR may play a greater role in imaging malignant tumors in the larynx and hypopharynx.

The surgical treatment for advanced laryngeal carcinoma is usually a total laryngectomy (Fig. 7). A less radical voice-sparing procedure, such as a vertical hemilaryngectomy or a supraglottic laryngectomy, can be performed for limited disease. Requirements for vertical hemilaryngectomy, a procedure performed primarily for isolated vocal cord lesions, are that the tumor be confined to the vocal cord with little or no involvement of the contralateral cord, have less than 1 cm of subglottic extension, not cross the ventricle, and have no gross involvement of the ipsilateral cricoarytenoid joint. Also, the involved vocal cord must not be fixed (Fig. 8) [40]. Supraglottic lesions that do not cross the ventricle, involve the thyroid cartilage, or are associated with a fixed vocal cord can be treated with supraglottic laryngectomy [40]. MR is especially helpful in ensuring that these requirements are met when conservation therapy is being considered. Cord mobility can be assessed clinically, but the status of the laryngeal ventricle and supraglottic or subglottic extension is accurately determined with direct coronal MR images [3, 41, 42]. Another contraindication for voice-sparing procedures is cartilage invasion by tumor. This is seen as hypointensity in the normally ossified, high-signal-intensity fatty marrow on T1-weighted images and relative hyperintensity of the marrow on T2-weighted images [43]. MR is more sensitive than CT for detecting cartilage invasion, although cartilage ossification can be normally asymmetric, making detection of tumor difficult [43]. The single best sign of cartilage involvement is tumor extension to the outer side of the cartilage [3].

Hypopharyngeal lesions may extend posteriorly to abut the pharyngeal musculature, and tumor and muscle may be isodense on CT. Tumor is easily differentiated from surrounding soft tissues, especially muscle, on MR.

Cervical Lymph Nodes

The presence of metastatic adenopathy in a patient with a primary malignant tumor of the head and neck is of enormous prognostic significance, reducing the expected survival by 50% if ipsilateral, and by an additional 50% if contralateral to the primary lesion [44]. MR or CT are more sensitive than the physical examination for detecting early cervical adenopathy [45–50] and will increase the cancer stage of the neck from 20% to 55% of the time [48].

Cervical lymph nodes, both benign reactive and metastatic, are intermediate in intensity on T1-weighted images and hyperintense relative to fat and muscle on T2-weighted images. Detection of central necrosis, the hallmark of squamous cell carcinoma, is unreliable unless enhanced T1-weighted images are obtained. A necrotic node appears heterogeneous, with a peripheral rim of enhancement and a nonenhancing central portion (Fig. 9). Contrast is also important for determining capsular integrity; an interruption in the enhancing peripheral rim is characteristic of extracapsular tumor spread. If the node is surrounded by fat, such as in the posterior triangle, the enhancing node may become isointense with fat

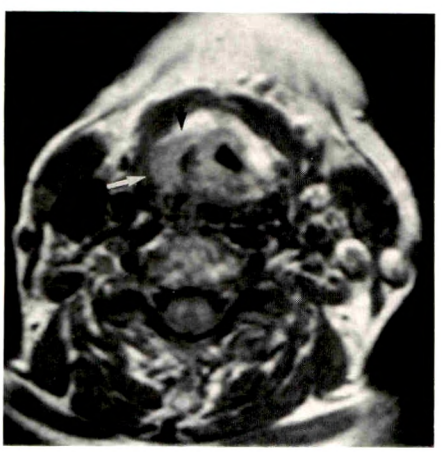
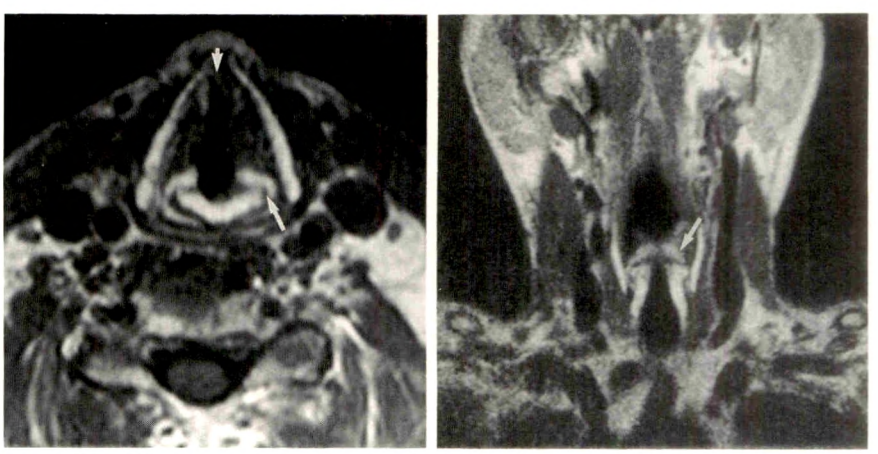


Fig. 7.—Supraglottic laryngeal squamous cell carcinoma, advanced. Axial T1-weighted (800/15/2) MR image shows large carcinoma on right side involving paralaryngeal space both anterolaterally (*black arrow*) and posteriorly (*white arrow*), replacing normal high-signal-intensity fat within paralaryngeal space. Laryngeal surface of aryepiglottic fold also is involved with tumor.



A B

Fig. 8.—Glottic carcinoma that meets all criteria for vertical hemilaryngectomy, a limited voice-sparing procedure.

A, T1-weighted (800/15/2) axial MR image obtained at level of true vocal cords reveals left cord thickened with tumor. Right cord is normal, ipsilateral cricoaretynoid articulation (*long arrow*) shows no tumor involvement, and anterior commissure is normal (*short arrow*).

B, Coronal T1-weighted MR image confirms normal cricoaretynoid articulation (*arrow*) ipsilateral to glottic tumor.

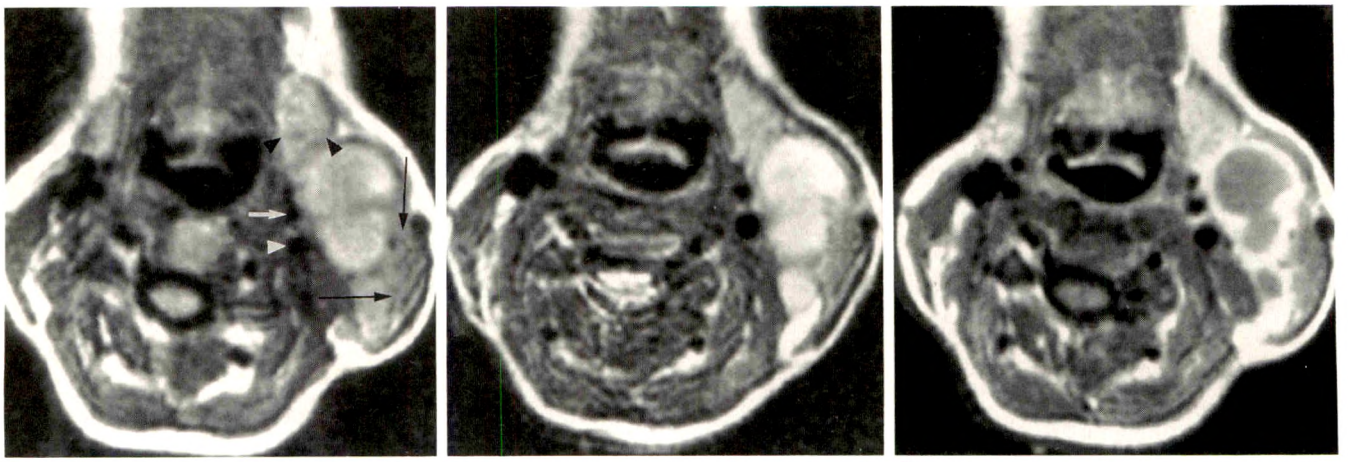


Fig. 9.—Necrotic metastatic high jugular chain nodes due to squamous cell carcinoma of nasopharynx.
***A*, Bulky adenopathy is seen in left high jugular chain nodal region on this T1-weighted (800/30/2) MR image. Submandibular gland (*black arrowheads*) is deviated anteriorly, internal carotid artery (*white arrow*) and jugular vein (*white arrowhead*) are compressed medially, and sternocleidomastoid muscle (*black arrows*) is displaced posterolaterally. Nodes are heterogeneous, with a low-intensity rim and a relatively higher intensity central portion.**
***B*, Nodes are homogeneously hyperintense on proton density–weighted (2500/50/1) MR image.**
***C*, Necrosis is confidently diagnosed on basis of gadopentetate dimeglumine–enhanced T1-weighted MR image, which reveals peripheral rim enhancement and no enhancement centrally.**

and may not be detected. Unenhanced images or fat-suppression sequences will overcome this problem.

Unfortunately, intensities of nodes on MR are not histologically specific, and reactive nodes are indistinguishable from nonnecrotic small metastatic nodes. The CT criteria for predicting metastatic disease, which include size, shape, presence of necrosis, and extracapsular spread, also are useful with MR. Lymph nodes in the high jugular and the submandibular chains can normally be up to 1.5 cm in maximum diameter, whereas nodes elsewhere in the neck are normally up to 1.0 cm in diameter. Any node larger than this should be considered clinically suggestive of metastasis, especially in a patient with known cancer. Central necrosis is always pathologic and characteristic of nodal spread from carcinoma, although inflammatory or lymphomatous nodes may occasionally become necrotic. Extracapsular spread of disease, especially with fixation to surrounding structures, carries an extremely poor prognosis [51]. It should be suspected when normal fat or fascial planes around the lymph nodes are obliterated. The relationship of nodal disease to the carotid artery should be reported, although frequently adenopathy, which appears on MR to involve the carotid artery, can be gently peeled off the artery during surgery.

Conclusion

MR imaging plays an important role in the preoperative assessment of the patient with a malignant lesion in the extracranial portion of the head and neck. Decisions about treatment, including type and extent of surgery, as well as the need for primary or adjuvant chemotherapy or radiotherapy, are directly affected by the findings on MR. The superior soft-tissue contrast and superb resolution of MR imaging make it the preferred technique for examining malignant lesions of the skull base, paranasal sinuses, nasopharynx, and oropharynx. Lesions in the larynx and hypopharynx are more difficult to study with MR because of the normal physiological mobility of laryngeal structures and the advanced stage of these lesions when they become apparent.

The complex anatomy in this region may be intimidating. An orderly methodical approach to interpretation of the images is helpful; first, determine the location and extent of the primary tumor, then look along nodal chains for metastatic adenopathy. The study must be well-planned and carefully monitored, with additional sequences used as needed to ensure complete visualization of the disease.

REFERENCES

1. Ariyan S, Cuono CB. Etiology, pathophysiology, diagnosis, workup, and staging of head and neck cancer. In: Ariyan S, ed. *Cancer of the head and neck.* St. Louis: Mosby, **1987**:142–152
2. Lufkin R, Hanafee W. MRI of the head and neck. *Magn Reson Imaging* **1988**;6:69–88
3. Curtin HD. The larynx. In: Som PM, Bergeron RT, eds. *Head and neck imaging.* St. Louis: Mosby–Year Book, **1991**:593–692
4. Crawford SC, Harnsberger HR, Lufkin RB, Hanafee WN. The role of gadolinium-DTPA in the evaluation of extracranial head and neck mass lesions. *Radiol Clin North Am* **1989**;27:219–242
5. Robinson JD, Crawford SC, Teresi LM, et al. Extracranial lesions of the head and neck: preliminary experience with Gd-DTPA-enhanced MR imaging. *Radiology* **1989**;172:165–170
6. Vogl T, Dresel S, Bilaniuk LT, Grevers G, Kang K, Lissner J. Tumors of the nasopharynx and adjacent areas: MR imaging with Gd-DTPA. *AJR* **1990**;154:585–592
7. Vogl T, Bruning R, Grevers G, Mees K, Bauer M, Lissner J. MR imaging of the oropharynx and tongue: comparison of plain and Gd-DTPA studies. *J Comput Assist Tomogr* **1988**;12:427–433
8. Lanzieri CF, Shah M, Krauss D, Lavertu P. Use of gadolinium-enhanced MR imaging for differentiating mucoceles from neoplasms in the paranasal sinuses. *Radiology* **1991**;178:425–428
9. Tien RD, Hesselink JR, Chu PK, Szumowski J. Improved detection and

delineation of head and neck lesions with fat suppression spin-echo MR imaging. *AJNR* **1991**;12:19–24
10. Barakos JA, Dillon WP, Chew WM. Orbit, skull base, and pharynx: contrast-enhanced fat suppression MR imaging. *Radiology* **1991**;179:191–198
11. Schaefer SD, Purdy PD. Comparison of computed tomography versus magnetic resonance imaging of the head and neck. In: Cummings CW, Fredrickson JM, Harker LA, Krause CJ, Schuller DE, eds. *Otolaryngology-head and neck surgery. Update I.* St. Louis: Mosby, **1989**:3–27
12. Sasaki CT, Lowlicht RA, Astrachan DI, Friedman CD, Goodwin WJ, Morales M. Le Fort I osteotomy approach to the skull base. *Laryngoscope* **1990**;100:1073–1076
13. Teresi LM, Lufkin RB, Vinuela F, et al. MR imaging of the nasopharynx and floor of the middle cranial fossa. Part II. Malignant tumors. *Radiology* **1987**;164:817–821
14. Laine FJ, Braun IF, Jensen ME, Nadel L, Som PM. Perineural tumor extension through the foramen ovale: evaluation with MR imaging. *Radiology* **1990**;174:65–71
15. Laine FJ, Nadel L, Braun IF. CT and MR imaging of the central skull base. Part 2. Pathologic spectrum. *RadioGraphics* **1990**;10:797–821
16. Ballantyne AJ, McCarten AB, Ibanez ML. The extension of cancer of the head and neck through peripheral nerves. *Am J Surg* **1963**;106:651–667
17. West MS, Russell EJ, Breit R, Sze G, Kim KS. Calvarial and skull base metastases: comparison of nonenhanced and Gd-DTPA-enhanced MR images. *Radiology* **1990**;174:85–91
18. Parker GD, Harnsberger HR. Clinical-radiologic issues in perineural tumor spread of malignant diseases of the extracranial head and neck. *RadioGraphics* **1991**;11:383–399
19. Virapongse C, Mancuso A, Fitzsimmons J. Value of magnetic resonance imaging in assessing bone destruction in head and neck lesions. *Laryngoscope* **1986**;96:284–291
20. Braun IF, Nadel L. The central skull base. In: Som PM, Bergeron RT, eds. *Head and neck imaging.* St. Louis: Mosby–Year Book, **1991**:876–924
21. Anand VK, Al-Mefty O. Craniofacial lesions and resection. In: Al-Mefty O, ed. *Surgery of the cranial base.* Boston: Kluwer, **1989**:167–191
22. Dillon WP. The pharynx and oral cavity. In: Som PM, Bergeron RT, eds. *Head and neck imaging.* St. Louis: Mosby–Year Book, **1991**:407–466
23. Dillon WP, Mills CM, Kjos B, DeGroot J, Brant-Zawadzki M. Magnetic resonance imaging of the nasopharynx. *Radiology* **1984**;152:731–738
24. Braun IF. MRI of the nasopharynx. *Radiol Clin North Am* **1989**;27:315–330
25. Weber AL, Kiwak MG. Radiology of the pharynx, neck, and esophagus. In: Lee KJ, ed. *Textbook of otolaryngology and head and neck surgery.* New York: Elsevier, **1989**:543–577
26. Kondziolka D, Lunsford LD. Stereotactic radiosurgery for squamous cell carcinoma of the nasopharynx. *Laryngoscope* **1991**;101:519–522
27. Ariyan S, Chicarilli ZN. Cancer of the oral cavity. In: Ariyan S, ed. *Cancer of the head and neck.* St. Louis: Mosby, **1987**:197–250
28. Unger JM. The oral cavity and tongue: magnetic resonance imaging. *Radiology* **1985**;155:151–153
29. Lufkin RB, Wortham DG, Dietrich RB, et al. Tongue and oropharynx: findings on MR imaging. *Radiology* **1986**;161:69–75
30. Anand VK. Malignant diseases of the nose and paranasal sinuses. In: Lee KJ, ed. *Textbook of otolaryngology and head and neck surgery.* New York: Elsevier, **1989**:304–312
31. Som PM, Shapiro MD, Biller HF, Sasaki C, Lawson W. Sinonasal tumors and inflammatory tissues: differentiation with MR imaging. *Radiology* **1988**;167:803–808
32. Som PM. Sinonasal cavity: tumor and tumorlike conditions. In: Som PM, Bergeron RT, eds. *Head and neck imaging.* St. Louis: Mosby–Year Book, **1991**:169–227
33. Zinreich SJ, Kennedy DW, Malat J, et al. Fungal sinusitis: diagnosis with CT and MR imaging. *Radiology* **1988**;169:439–444
34. Van Tassel P, Lee Y-Y, Jing B-S, De Pena CA. Mucoceles of the paranasal sinuses: MR imaging with CT correlation. *AJR* **1989**;153:407–412
35. Dillon WP, Som PM, Fullerton GD. Hypointense MR signal in chronically inspissated sinonasal secretions. *Radiology* **1990**;174:73–78
36. Som PM, Dillon WP, Fullerton GD, Zimmerman RA, Rajagopalan B, Marom Z. Chronically obstructed sinonasal secretions: observations on T1 and T2 shortening. *Radiology* **1989**;172:515–520
37. Som PM, Dillon WP, Curtin HD, Fullerton GD, Lidov M. Hypointense paranasal sinus foci: differential diagnosis with MR imaging and relation to CT findings. *Radiology* **1990**;176:777–781
38. Som PM, Dillon WP, Sze G, Lidov M, Biller HF, Lawson W. Benign and malignant sinonasal lesions with intracranial extension: differentiation with MR imaging. *Radiology* **1989**;172:763–766
39. Van Tuyl R, Gussack G. Prognostic factors in craniofacial surgery. *Laryngoscope* **1991**;101:240–244
40. Shumrick KA. Malignant lesions of the larynx. In: Lee KJ, ed. *Textbook of otolaryngology and head and neck surgery.* New York: Elsevier, **1989**:647–657
41. Curtin HD. Imaging of the larynx: current concepts. *Radiology* **1989**;173:1–11
42. Teresi LM, Lufkin RB, Hanafee WN. Magnetic resonance imaging of the larynx. *Radiol Clin North Am* **1989**;27:393–406
43. Castelijns JA, Gerritsen GJ, Kaiser MC, et al. Invasion of laryngeal cartilage by cancer: comparison of CT and MR imaging. *Radiology* **1987**;166:199–206
44. Som PM. Lymph nodes of the neck. *Radiology* **1987**;165:593–600
45. Lydiatt DD, Markin RS, Williams SM, Davis LF, Yonkers AJ. Computed tomography and magnetic resonance imaging of cervical metastasis. *Otolaryngol Head Neck Surg* **1989**;101:422–425
46. Johnson JT. A surgeon looks at cervical lymph nodes. *Radiology* **1990**;175:607–610
47. Close LG, Merkel M, Vuitch MF, Reisch J, Schaefer SD. Computed tomographic evaluation of regional lymph node involvement in cancer of the oral cavity and oropharynx. *Head Neck* **1989**;11:309–317
48. Hillsamer J, Schuller DE, McGhee RB, Chakeres D, Young DC. Improving diagnostic accuracy of cervical metastases with computed tomography and magnetic resonance imaging. *Otolaryngol Head Neck Surg* **1990**;116:1297–1301
49. Friedman M, Mafee MF, Pacella BL Jr, Strorigl TL, Dew LL, Toriumi DM. Rationale for elective neck dissection in 1990. *Laryngoscope* **1990**;100:54–59
50. Mancuso AA, Maceri D, Rice D, Hanafee W. CT of cervical lymph node cancer. *AJR* **1981**;136:381–385
51. Snyderman NL, Johnson JT, Schramm VL Jr, Myers EN, Bedetti CD, Thearle P. Extracapsular spread of carcinoma in cervical lymph nodes. *Cancer* **1985**;56:1597–1599

Books and Videotapes Received

Receipt of books is acknowledged as a courtesy to the sender. Books considered of sufficient interest are reviewed as space permits. If the book has been reviewed in the *AJR*, the date of its review is given in parenthesis.

Diagnostic Techniques in Urology. Edited by Patrick H. O'Reilly, Nicholas J. R. George, and Robert M. Weiss. Philadelphia: Saunders, 640 pp., 1990. $175 (4/92)

Transvaginal Ultrasound. By Melvin G. Dodson. New York: Churchill Livingstone, 273 pp., 1991. $65 (4/92)

Ultrasonography of the Urinary Tract, 3rd ed. Edited by Martin I. Resnick and Matthew D. Rifkin. Baltimore: Williams & Wilkins, 502 pp., 1991. $95 (4/92)

Handbook of Pediatric Imaging. Edited by Lori L. Barr. New York: Churchill Livingstone, 428 pp., 1991. $115 (4/92)

Principles and Practice of Cardiovascular Imaging. Edited by Gerald M. Pohost and Robert A. O'Rourke. Boston: Little, Brown, 880 pp., 1991. $175 (5/92)

MRI of Brain Tumors, parts 1 and 2. By Murray A. Solomon. (Part of Murray Solomon's Magnetic Resonance Video Review.) Burlingame, CA: Magnetic Resonance Video Review, MRI Learning Center, (408) 925-8328, 1991. Single tape, $125; both tapes, $250; series of 6 tapes, $545 (VHS videotape) (5/92)

Color Doppler Flow Imaging. By W. Dennis Foley. Boston: Andover, 175 pp., 1991. $125 (5/92)

FRCR Part 1. By Paul Butler, Charles G. Blakeney, Alan Brooks, and Robert Speller. New York: Springer-Verlag, 174 pp., 1991, softcover (5/92)

MRI of the Head and Neck. Edited by Robert B. Lufkin and William N. Hanafee. (One of 10 volumes in The Raven MRI Teaching File. Series editors: Robert B. Lufkin, William G. Bradley, Jr., and Michael Brant-Zawadzki.) New York: Raven, 254 pp., 1991. $60 (5/92)

Orthopaedic MRI. A Teaching File. By Stephen J. Pomeranz. Philadelphia: Lippincott, 434 pp., 1991, $89.50 (5/92)

Musculoskeletal Imaging. MRI, CT, Nuclear Medicine, and Ultrasound in Clinical Practice. Edited by John A. Markisz. Boston: Little, Brown, 397 pp., 1991. $125 (5/92)

MRI of the Brain III. Neoplastic Disease. Edited by Anton N. Hasso, Miyuki Shakudo, and Edla Chadrycki. (One of 10 volumes in The Raven MRI Teaching File. Series editors: Robert B. Lufkin, William G. Bradley, Jr., and Michael Brant-Zawadzki.) New York: Raven, 216 pp., 1991. $60, softcover (5/92)

MRI of the Spine. Edited by Robert M. Quencher. (One of 10 volumes in The Raven MRI Teaching File. Series editors: Robert B. Lufkin, William G. Bradley, Jr., and Michael Brant-Zawadzki.) New York: Raven, 240 pp., 1991. $60 (5/92)

Gastrointestinal Radiology. By Jack Farman. Philadelphia: Lippincott, 191 pp., 1991. $59.95 (5/92)

Cardiac Imaging. A Companion to Braunwald's Heart Disease. Edited by Melvin L. Marcus, Heinrich R. Schelbert, David J. Skorton, and Gerald L. Wolf. Philadelphia: Saunders, 1344 pp., 1991. $110 (6/92)

Quality Assurance in Radiotherapy Physics. Proceedings of an American College of Medical Physics Symposium, May 1991. Edited by George Starkschall and John Horton. Madison, WI: Medical Physics Publishing, 387 pp., 1991. $55 (6/92)

MRI of the Shoulder. By Michael B. Zlatkin. New York: Raven, 174 pp., 1991. $89 (6/92)

RSNA Today Video, Vol. 5, No. 4. Oak Brook, IL: The Radiological Society of North America, 1991. $55; by subscription, 6 issues annually at $185 for RSNA members and $225 for nonmembers (VHS videotape) (6/92)

Computed Tomography and Magnetic Resonance of the Thorax, 2nd ed. By David P. Naidich, Elias A. Zerhouni, Stanley S. Siegelman, and Jerald P. Kuhn. New York: Raven, 606 pp., 1991. $125 (6/92)

Magnetic Resonance Test and Syllabus. Section chairman: William G. Bradley, Jr. Reston, VA: American College of Radiology, 658 pp., 1991. Residents, $90; ACR members, $110; nonmembers, $175 (6/92)

Pediatric Cardiovascular Imaging. By Ina Lynn Dyer Tonkin. Philadelphia: Saunders, 288 pp., 1992. $85 (6/92)

Abdominal Sonography. By Mordecai Koenigsberg and Janet Hoffman-Tretin. Philadelphia: Lippincott, 143 pp., 1991. $49.95 (6/92)

Radiology of Trauma. By Salvatore J. A. Sclafani. Philadelphia: Lippincott, 155 pp., 1991. $59.95 (6/92)

RSNA Today Video, Vol. 5, No. 5. Oak Brook, IL: The Radiological Society of North America, 1991. $55; by subscription, 6 issues annually at $185 for RSNA members and $225 for nonmembers (VHS videotape) (6/92)

Principles and Practice of Radiation Oncology, 2nd ed. By Carlos A. Perez and Luther W. Brady. Philadelphia: Lippincott, 1568 pp., 1992. $195

Radiation Injury. By David S. Gooden. (American Jurisprudence. Proof of Facts, 3rd series.) Rochester, NY: Lawyers Cooperative Publishing, 239 pp., 1991. $26.95

Oncology Reviews. Soviet Medical Reviews Section F, vol. 3, part 5. Edited by N. N. Blokhin and N. N. Trapeznikov. Philadelphia: Harwood, 146 pp., 1991. $50

When Is a Dose Not a Dose? By Victor P. Bond. (NCRP Lecture No. 15). Bethesda: National Council on Radiation Protection and Measurements, 40 pp., 1991. $20

Evolution of White Matter Lesions in Neurofibromatosis Type 1: MR Findings

Robert J. Sevick[1,2]
A. James Barkovich[1,3,4]
M. S. B. Edwards[3]
T. Koch[4]
B. Berg[4]
T. Lempert[5]

To characterize further the evolution of white matter lesions in neurofibromatosis type 1, we reviewed 68 MR images in 43 patients (age, 1–31 years), including 25 follow-up studies (mean interval, 27 months). Lesion number, location, morphology, signal characteristics, and contrast enhancement were assessed. Lesion characteristics and changes thereof were correlated with the patients' ages. Thirty-four patients (79%) had white matter lesions. These lesions were hyperintense on T2-weighted images, were isointense on T1-weighted images, and showed no mass effect or contrast enhancement in 31 patients; in three patients, T1-prolongation was observed (one with significant mass effect). None of the lesions evolved into a glioma. The most common locations were the cerebellum (49%), brainstem (22%), and internal capsule (19%). Nineteen patients had white matter lesions and follow-up studies. Lesions decreased in size or number in seven patients (average age, 13 years), showed no change in three (average age, 12 years), increased in size or number in four (average age, 5 years), and showed a mixed pattern (increased/decreased size/number) in four (average age, 7 years).

White matter lesions in neurofibromatosis type 1 frequently increase in size or number early in childhood; this did not indicate neoplasia in our study. The lesions tend to resolve with increasing age. Lesion progression in a child more than 10 years old warrants close follow-up to rule out a neoplasm.

AJR 159:171–175, July 1992

Received November 22, 1991; accepted after revision January 22, 1992.

Presented at the annual meeting of the Western Neuroradiological Society, Laguna Niguel, CA, October 1991.

This work was supported in part by a clinical fellowship from the Alberta Heritage Foundation for Medical Research.

[1] Department of Radiology, University of California, San Francisco, 545 Parnassus Ave., San Francisco, CA 94143.

[2] Present address: Department of Radiology, Foothills Hospital and the University of Calgary, 1403 29th St., N.W., Calgary, Alberta T2N 2T9, Canada.

[3] Department of Pediatric Neurosurgery, University of California, San Francisco, 545 Parnassus Ave., San Francisco, CA 94143.

[4] Department of Pediatric Neurology, University of California, San Francisco, 545 Parnassus Ave., San Francisco, CA 94143.

[5] Magnetic Imaging Affiliates, 5730 Telegraph Ave., Oakland, CA 94609.

0361–803X/92/1591–0171
© American Roentgen Ray Society

Recent reports [1, 2] have emphasized the existence of at least two distinct forms of neurofibromatosis: type 1 (Recklinghausen's disease) and type 2 (bilateral acoustic neurofibromatosis). These diseases have distinct clinical manifestations and have been mapped to different chromosomes. Type 2 (associated with abnormality of chromosome 22) is characterized by the presence of multiple tumors of the meninges and Schwann cells. Type 1 (chromosome 17) is characterized by optic nerve gliomas, parenchymal gliomas, and foci of increased signal intensity on T2-weighted MR images of the cerebellum, pons, midbrain, internal capsules, and basal ganglia [2–6]. The exact nature of these lesions is unknown. The basal ganglia lesions may have accompanying mass effect and show hyperintensity on T1-weighted images [7], whereas the lesions confined to white matter are generally isointense on T1-weighted images and have no mass effect. The basal ganglia lesions may represent a separate entity, as their morphology and signal characteristics are different from those of white matter lesions [2].

Possible pathologic explanations for white matter lesions include low-grade tumor, heterotopia, foci of abnormal myelination, and hamartomas [1, 2, 8, 9]. Although a number of studies have described the MR appearance of these lesions, analysis of their temporal evolution has been limited. Knowledge of their normal temporal evolution is critical in characterizing the lesions, as growing lesions are generally considered neoplastic. We retrospectively reviewed MR images in 43 patients with an established clinical diagnosis of neurofibromatosis type 1, including

25 with follow-up studies, in an attempt to characterize further the white matter lesions of this disease.

Materials and Methods

Sixty-eight MR images were retrospectively reviewed in 43 patients. These patients had a clinical diagnosis of neurofibromatosis type 1 established by standard criteria [10]. Twenty-five patients had follow-up imaging 4–69 months (mean, 27 months) after the initial MR study. Patients were seen in clinic at 6-month intervals, and a complete neurologic examination was performed by a pediatric neurologist or neurosurgeon. The patients were 1–31 years old (mean, 10 years). Sixteen patients were 5 years old or younger when initially imaged; 12 were 6–10 years old, 12 were 11–15 years old, and three were more than 16 years old. Twenty-four patients were male, and 19 were female.

All MR images were obtained with a 1.5-T unit (Signa, General Electric Medical Systems, Milwaukee, WI). Standard T1- and T2-weighted spin-echo images in the sagittal and axial planes, respectively, were obtained in all patients. Additional T1- or T2-weighted coronal images were obtained in some patients. Gradient moment nulling (flow compensation) was used in all images obtained after 1988 (n = 40). IV contrast material (gadopentetate dimeglumine, Berlex, Wayne, NJ) was administered in 22 of 43 patients.

The MR images were reviewed by two radiologists with specific reference to the following: lesion number, location, morphology, signal characteristics on T1- and T2-weighted images, and presence or absence of contrast enhancement. Lesions partially or completely located within the basal ganglia were excluded.

Results

White matter lesions were observed in 34 patients (79%) who had an average age of 7 years. Twenty-two of these patients had gadopentetate dimeglumine–enhanced MR images. Eighteen white matter lesions were located in the medulla or pons (22%), 30 in the middle cerebellar peduncles (36%), 11 in the deep cerebellar white matter (13%), eight in the mibdrain (10%), and 16 in the supratentorial white matter (19%). Ten of the patients with white matter lesions also had optic nerve gliomas. The average age of patients without white matter lesions was 11 years.

In 31 of the 34 patients with white matter lesions, the lesions were hyperintense on T2-weighted images, were isointense on T1-weighted images, and showed no mass effect or contrast enhancement (Fig. 1). In the three remaining patients, prolonged T1 relaxation was observed, with no contrast enhancement or mass effect in two. One lesion showed moderate mass effect (Fig. 2). Maximum lesion diameter was 25 mm.

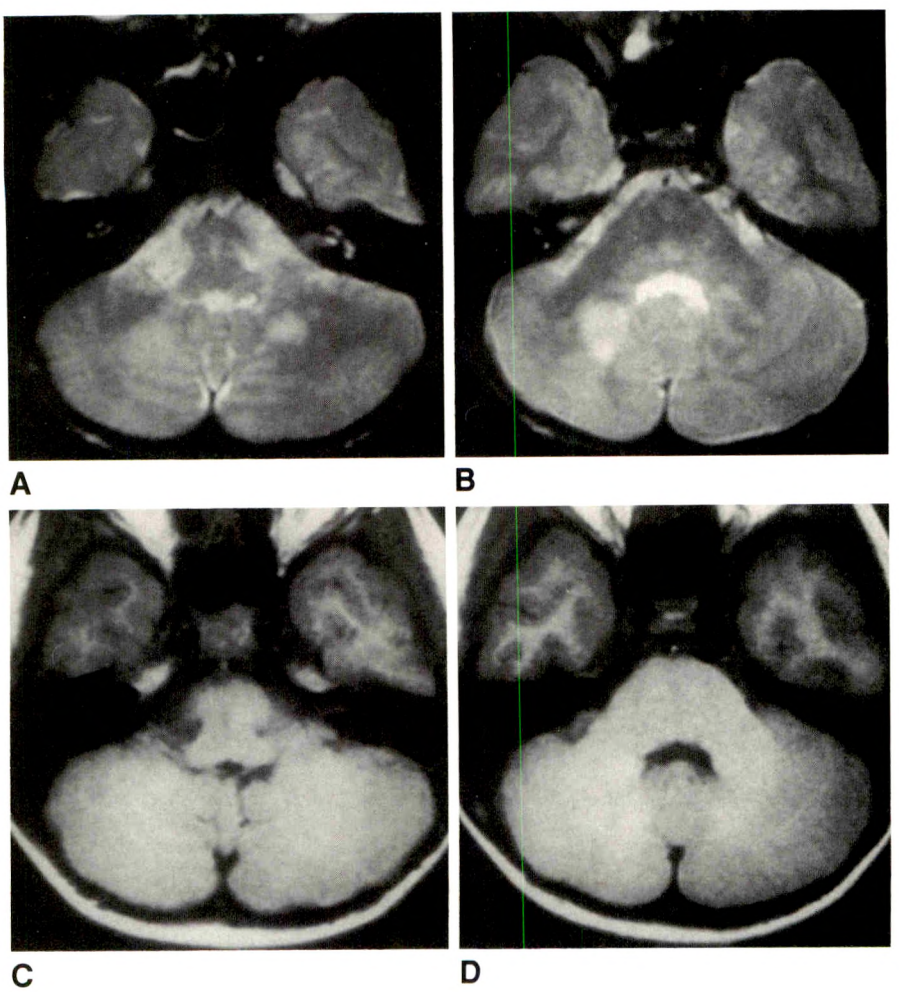


Fig. 1.—Typical white matter lesions in a 3-year-old boy with neurofibromatosis type 1.

***A* and *B*, Axial T2-weighted (2300/80) MR images through posterior fossa show white matter lesions with prolonged T2 relaxation in pons and cerebellum.**

***C* and *D*, Corresponding T1-weighted (600/20) MR images show that areas of hyperintense signal on T2-weighted images appear isointense, with no mass effect.**

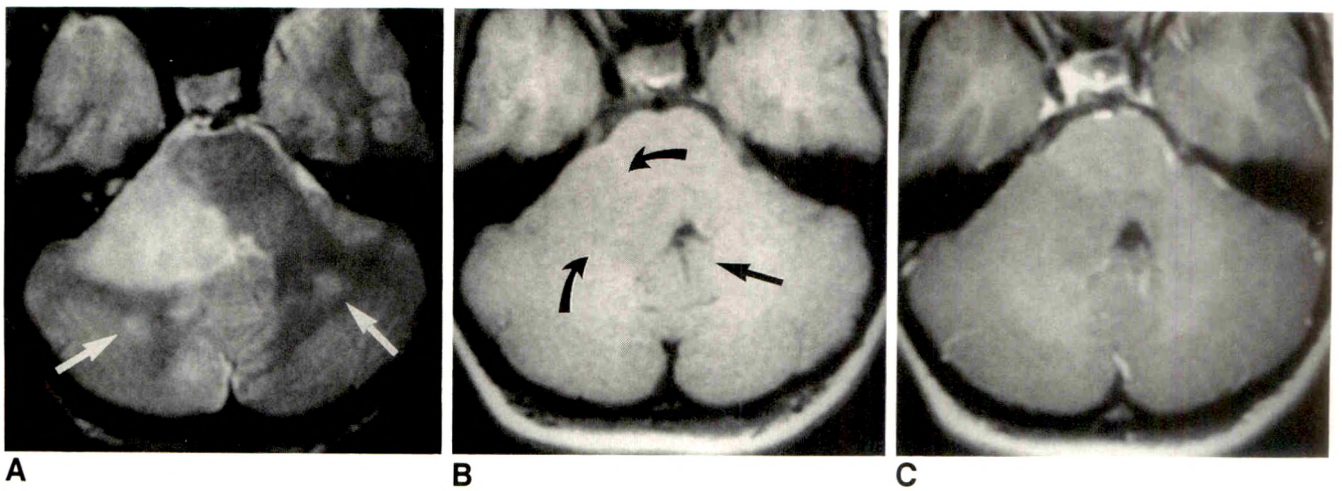


Fig. 2.—Atypical appearance of white matter lesions in 15-year-old girl with neurofibromatosis type 1.

A, Axial T2-weighted (2300/80) MR image at level of middle cerebellar peduncles shows a relatively large lesion with prolonged T2 relaxation, involving pons and middle cerebellar peduncle on right side. Smaller lesions (*arrows*) are evident in cerebellar white matter.

B, Unenhanced T1-weighted (600/20) MR image shows that area of prolonged T2 relaxation also has mildly prolonged T1 relaxation (*curved arrows*). Moderate mass effect is seen, evident as effacement of fourth ventricle (*straight arrow*).

C, Contrast-enhanced T1-weighted MR image shows findings similar to those on *B*. No contrast enhancement is evident. No change in imaging or clinical findings has been seen in 2 years of follow-up.

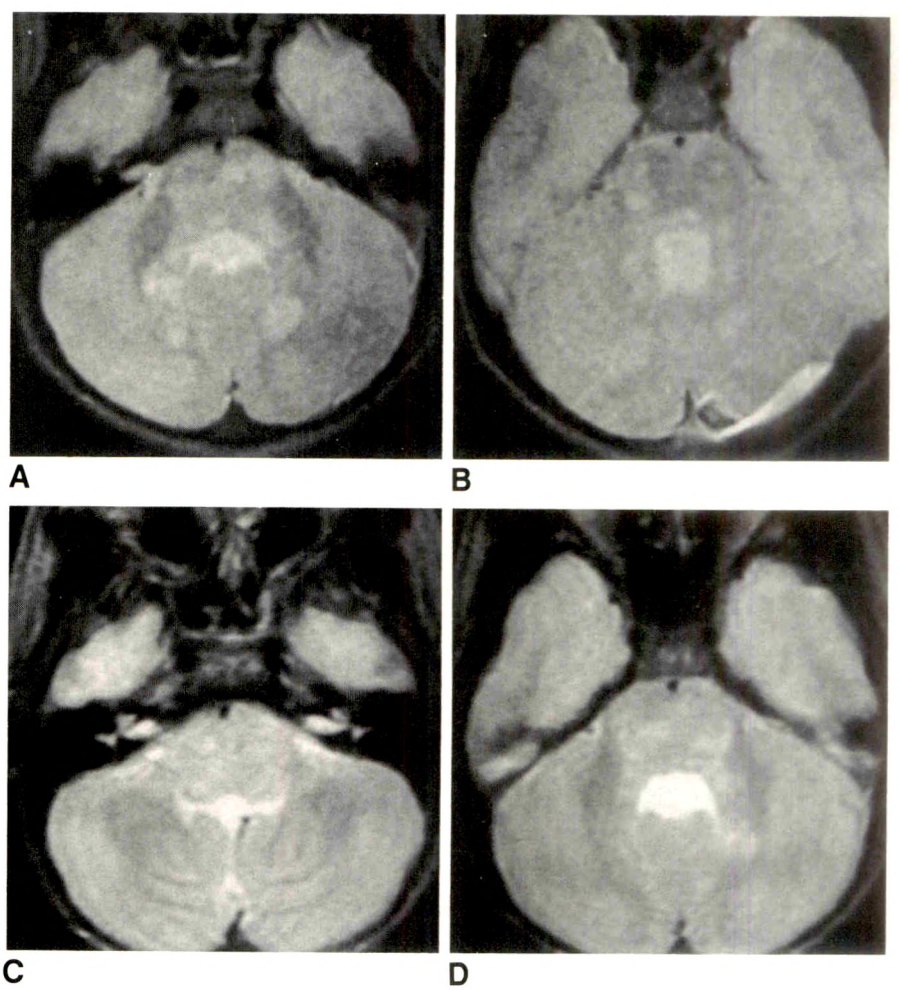


Fig. 3.—6-year-old boy with neurofibromatosis type 1.

A and *B*, Axial T2-weighted (2300/80) MR images through posterior fossa show multiple white matter lesions in pons and middle cerebellar peduncles.

C and *D*, MR images obtained 33 months after *A* (axial levels selected to show greatest extent of lesions) show resolution of lesions in right middle cerebellar peduncle.

Nineteen patients with white matter lesions had follow-up studies (16 of these patients received gadopentetate dimeglumine). None of the patients had focal neurologic signs or symptoms related to a white matter lesion. Imaging changes were correlated with the patient's age at the time of the follow-up study. One patient with a follow-up study was excluded because areas of T2 prolongation developed close to a known parenchymal glioma. Among these remaining patients, lesions improved (decreased size or number) in seven patients (average age, 13 years; Fig. 3), lesions showed no change in three (average age, 12 years), lesions worsened (increased in size or number) in four (average age, 5 years; Fig. 4), and lesions showed a mixed pattern (increased or decreased size or number) in four (average age, 7 years). None of the worsening lesions developed mass effect, T1 prolongation, or contrast enhancement.

Of the nine patients less than 10 years old, eight showed either worsening or a mixed pattern. One 10-year-old patient showed a mixed pattern. This was the oldest patient in whom worsening was observed. The remaining patients (>10 years old) all showed improvement ($n = 6$) or no change ($n = 2$) in white matter lesions. The youngest age at which improvement was seen was 6 years.

Discussion

Neurofibromatosis type 1 is characterized on MR imaging by optic nerve gliomas, parenchymal gliomas, and foci of prolonged T2 relaxation involving the brainstem, cerebellum, midbrain, internal capsule, and basal ganglia [2]. The precise cause and histologic features of white matter lesions with prolonged T2 relaxation are unknown. Numerous reports [2, 3, 5–7, 9] have proposed a variety of possible pathologic entities, including heterotopias, hamartomas, foci of abnormal myelination, and low-grade neoplasms. A stereotaxic biopsy of a white matter lesion in one patient showed normal brain tissue (Schorry EK, presented at the Annual Clinical Care Conference of the National Neurofibromatosis Foundation, October 1988). Although histologic features cannot be determined by using MR imaging, the determination of whether white matter lesions change over time is critical in establishing whether these lesions are benign or malignant.

The observed prevalence of white matter lesions in our series (79%) is slightly higher than figures previously reported [3, 11–13]. However, some of these reports [3, 11, 13] did not distinguish between type 1 and type 2 neurofibromatosis. Typical signal characteristics have been described [2, 6]; the

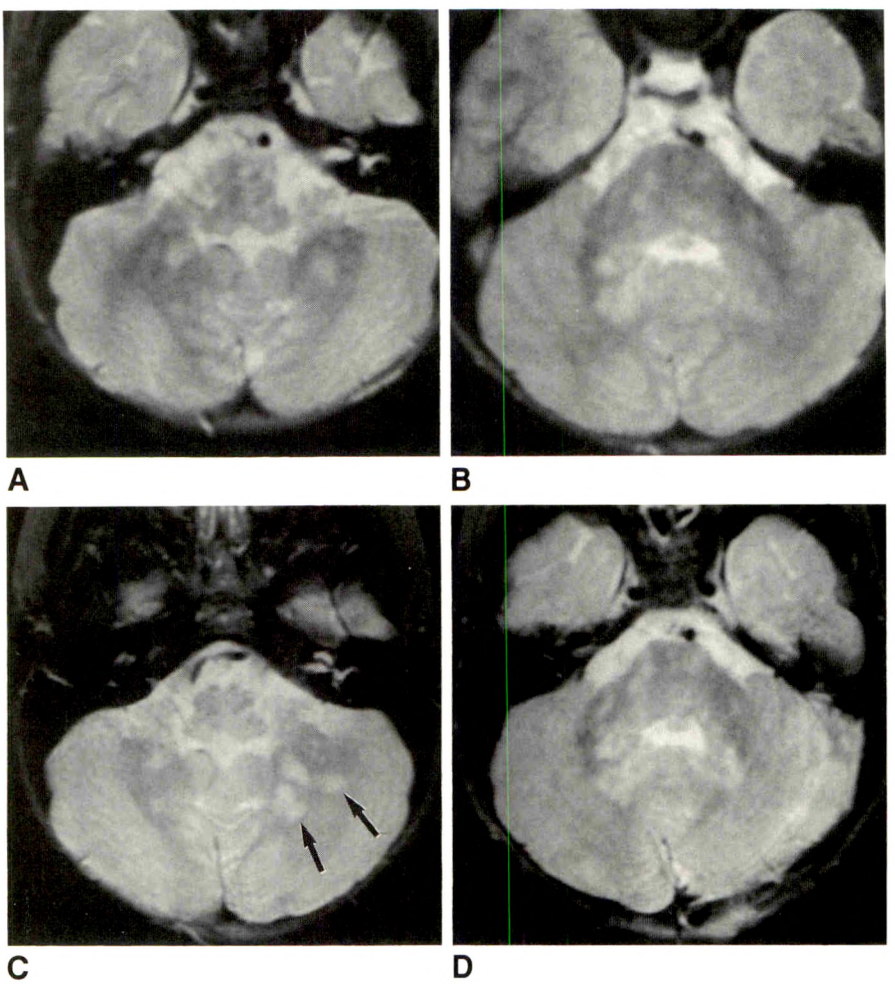


Fig. 4.—3-year-old girl with neurofibromatosis type 1.

***A* and *B*, Axial T2-weighted (2300/80) MR images through posterior fossa show multiple areas of prolonged T2 relaxation in pons and cerebellum.**

***C* and *D*, MR images obtained 6 months later show two new lesions (*arrows*) in white matter of left cerebellar hemisphere.**

lesions show prolonged T2 relaxation without T1 signal abnormality, mass effect, or contrast enhancement. Some lesions in the basal ganglia have associated T1 shortening and mild mass effect [2, 7]; such lesions may represent a histopathologic entity different from the typical white matter lesion [2] and were excluded from our study.

Three of our patients had lesions that had prolonged T1-relaxation times. No contrast enhancement was observed. One of the lesions showed mild mass effect. During 2 years of follow-up, no clinical or imaging change has developed in any of these cases to indicate that the lesions represent neoplasms. However, as lesions with T1 prolongation are uncommon, particularly in combination with mass effect, close clinical and imaging follow-up (including contrast-enhanced images) seems prudent, as these lesions may represent slowly growing glial neoplasms.

Previous reports of imaging follow-up in patients with white matter lesions and neurofibromatosis type 1 have been limited. Aoki et al. [2] reported follow-up in 13 patients; 12 showed no change, two showed a mild decrease in size of the lesion, and one had a new lesion in the globus pallidus. These authors noted that with increasing age, the lesions tend to resolve and are rarely seen in patients more than 20 years old [2]. Duffner et al. [11] reported follow-up of up to 2 years in 18 patients, only two of whom showed any change; correlation with patients' age at the time of scanning was not mentioned. We found that younger patients often have an increase in either size or number of white matter lesions. As these changes were quite common in patients less than 10 years old, and no T1 prolongation, mass effect, or contrast enhancement developed in any of the lesions, such changes are unlikely to be indicative of neoplasia in this age group. However, inasmuch as progression of lesions (increased size or number) was not seen in any patient more than 10 years old in our study, any worsening of white matter lesions in this age group warrants close clinical and imaging follow-up, including gadopentetate dimeglumine–enhanced imaging.

These observations, combined with the lack of transformation of any white matter lesion without mass effect or long T1 relaxation time into clinically or radiologically apparent glioma in any of our patients, suggests that most white matter lesions in neurofibromatosis type 1 are benign. Their exact histologic features remain obscure. Developmental anomalies such as hamartomas, heterotopias, or benign or malignant proliferation of glial cells or neurons would not be expected to have reversible signal abnormalities. A possible explanation might be the formation of chemically abnormal myelin that is subsequently broken down by normal metabolic processes, to be replaced by myelin with a more stable conformation. The answer awaits further research.

REFERENCES

1. Mulvihill JJ, Parry DM, Sherman JL, Pikus A, Kaiser-Kupfer MI, Eldridge R. NIH Conference: Neurofibromatosis 1 (Recklinghausen disease) and neurofibromatosis 2 (bilateral accoustic neurofibromatosis). *Ann Intern Med* **1990**;113:39–52
2. Aoki S, Barkovich AJ, Nishimura K, et al. Neurofibromatosis types 1 and 2: cranial MR findings. *Radiology* **1989**;172:527–534
3. Bognanno JR, Edwards MK, Lee TA, Dunn DW, Roos KL, Klatte EC. Cranial MR imaging in neurofibromatosis. *AJR* **1988**;151:381–388
4. Brown EW, Riccardi VM, Mawad M, Handel S, Goldman A, Bryan RN. MR imaging of optic pathways in patients with neurofibromatosis. *AJNR* **1987**;8:1031–1036
5. Goldstein SM, Curless RG, Donovan Post MJ, Quencer RM. A new sign of neurofibromatosis on magnetic resonance imaging of children. *Arch Neurol* **1989**;46:1222–1224
6. Hurst RW, Newman SA, Cail WS. Multifocal intracranial MR abnormalities in neurofibromatosis. *AJNR* **1988**;9:293–296
7. Mirowitz SA, Sartor K, Gado M. High-intensity basal ganglia lesions on T1-weighted MR images in neurofibromatosis. *AJNR* **1990**;10:1159–1163
8. Rosman NP, Pearce J. The brain in multiple neurofibromatosis (Von Recklinghausen's disease): a suggested neuropathological basis for the associated mental defect. *Brain* **1967**;90:829–838
9. Hoyt WF, Baghdassarian SA. Optic glioma of childhood. *Br J Ophthalmol* **1969**;53:793–798
10. Listernick R, Charrow J. Neurofirbomatosis type 1 in childhood. *J Pediatr* **1990**;116:845–853
11. Duffner PK, Cohen ME, Seidel G, Shucard DW. The significance of MRI abnormalities in children with neurofibromatosis. *Neurology* **1989**;39:373–378
12. Barkovich AJ, Aoki S, Nishimura K, Norman D. Cranial MR imaging of neurofibromatosis I and II: two distinct diseases (abstr). *AJNR* **1989**;10:878
13. Duffner PK, Cohen ME, Seidel G, Shucard D. Significance of magnetic resonance imaging abnormalities in children with neurofibromatosis. *Ann Neurol* **1988**;24:305–306

Book Review

Pediatric Orthopedic Radiology, 2nd ed. By M. B. Ozonoff. Philadelphia: Saunders, 816 pp., 1992. $125

The second edition of Dr. Ozonoff's book has been long awaited. It considerably adds to and updates the previous edition, which is still considered an authoritative and standard textbook for pediatric orthopedic radiology.

The text is divided into the same 10 chapters as was the first edition. The first five contain discussions of diseases specific to anatomic distribution under the following headings: spine, upper extremity, hip, lower extremity, and foot. The next three chapters are disease oriented, namely "Generalized Orthopedic Diseases of Childhood," Neuromuscular Disease," and "Skeletal Trauma." The last two chapters are devoted to orthopedic procedures and to special radiologic techniques, measurements, and calculations, respectively. References appear at the end of each subsection within every chapter; the bibliography is extensive and up-to-date, including materials published as recently as 1991.

As this entire work is that of one author, the style is uniform. The writing is clear and concise. The book is easily readable, and the images are opposite the relevant discussion, continuing when necessary onto the immediately ensuing pages. More than 1200 radiologic images are used liberally throughout, as well as several explanatory sketches and diagrams. Image quality is excellent, and the collection of cases is outstanding. The book has many images from the previous edition, including many arthrograms. As arthrography has a lesser role nowadays in pediatric radiology, it might have been more useful if some of the arthrograms had been replaced with examples obtained with current imaging techniques. However, discussions on CT, MR imaging, and sonography do appear in each section.

The level of the text is for a reader who has more than basic knowledge of radiology, and this fine book has much to offer all radiologists and orthopedic surgeons who work with children. The book addresses almost every orthopedic condition that may be encountered in a radiology department, and it will be of exceptional help to radiology trainees. The chapter on trauma is especially likely to be appreciated by residents on call. Like the previous edition, the book has excellent descriptions of normal bone positions and their anatomic relationships. The determination of positional abnormality and malalignment is clearly explained with the aid of simplified diagrams. These simplified diagrams and explanations are especially valuable in the chapter on the foot. The section on orthopedic techniques is informative and useful, particularly to anyone who may encounter evidence of unfamiliar techniques and instrumentation in patients. The collection of tables and standards at the end of the book is useful in clinical practice.

In summary, the second edition of *Pediatric Orthopedic Radiology* was worth waiting for. I think the book is outstanding, and I fully recommend this new edition to all radiology and orthopedic departments that serve children as their patients.

Ronald B. J. Glass
Children's National Medical Center
Washington, DC 20010-2970

Cerebellar and Cerebral Abnormalities in Rett Syndrome: A Quantitative MR Analysis

James W. Murakami[1]
Eric Courchesne[1, 2]
Richard H. Haas[2, 3]
Gary A. Press[4]
Rachel Yeung-Courchesne[1]

Rett syndrome is a neurodegenerative disease of young girls that begins in early childhood with autismlike behavior and loss of language skills, and progresses with marked deterioration of the motor system in the second decade of life. The purpose of this study was to determine if neuroanatomic changes detected with MR imaging could help to explain the clinical presentation and progression of signs and symptoms in these patients. Accordingly, computer-assisted planimetry was used to measure various dimensions of cerebral, cerebellar, and brainstem structures on sagittal and transverse MR images of 13 patients with Rett syndrome and 10 healthy volunteers. Dimensions of the cerebrum, basal ganglia, cerebellum, and brainstem were measured on transverse images. Areas of cerebellar vermian lobules, the fourth ventricle, the pituitary gland, and the corpus callosum were measured on sagittal images. Fourteen dimensions and areas were measured in each patient and each control subject; according to two-tailed Student's t tests, all but two values were significantly smaller in the patients with Rett syndrome than in control subjects. Graphing the measurements against age by using simple linear regression revealed progressive cerebellar atrophy without evidence of atrophy of the brainstem or cerebrum.

Our results indicate that patients with Rett syndrome have global hypoplasia of the brain and progressive cerebellar atrophy increasing with age. Cerebellar atrophy with age may contribute to the deterioration of the motor system seen in older patients with Rett syndrome.

AJR 159:177–183, July 1992

Received September 16, 1991; accepted after revision February 5, 1992.

This work was supported by NINDS grant 5-R01-NS19855 awarded to E. Courchesne, NIH CIDA grant K08-N501024 and a March of Dimes grant awarded to R. H. Haas, and the General Clinical Research Center (NIH M01-RR00827) of the University of California at San Diego.

[1] Neuropsychology Research Laboratory, Children's Hospital Research Center, 8001 Frost St., San Diego, CA 92123.

[2] Department of Neurosciences, School of Medicine, University of California, San Diego, La Jolla, CA 92093. Address reprint requests to E. Courchesne.

[3] Department of Pediatrics, School of Medicine, University of California, San Diego, La Jolla, CA 92093.

[4] Department of Radiology, Section on Magnetic Resonance, Kaiser Hospital, 4647 Zion Ave., San Diego, CA 92120.

0361–803X/92/1591–0177
© American Roentgen Ray Society

Rett syndrome, originally described by Andreas Rett in 1966 [1, 2], is estimated to affect 8000 girls in the United States. The estimated prevalence of this syndrome is approximately the same as that of phenylketonuria: one in 10,000 live female births [3]. Rett syndrome is a degenerative neurologic disease characterized by the appearance of autismlike behaviors, loss of purposeful hand use, and loss of language skills after apparently normal development. In most patients, the syndrome progresses, with the development of stereotypic hand movements, breathing abnormalities, seizures, and marked deterioration of the motor system in the later years. The clinical staging system of Hagberg and Witt-Engerstrom [4] classifies a progression through four stages in Rett syndrome; the onset of stage 4, commonly during teenage or early adult life, is defined by difficulty walking. Even the ambulatory older patients have deterioration of the motor system with hypotonia, ataxia, and pathologically brisk tendon reflexes.

CT and MR findings in patients with Rett syndrome are commonly reported as normal, with a small percentage of the patients described as having "mild" or "minimal" cortical atrophy [2, 5–12]. To determine whether any neuroanatomic changes correlated with clinical findings in Rett syndrome, we measured the dimensions and areas of structures of the cerebellum, cerebrum, and brainstem on MR images in 13 patients with Rett syndrome and 10 control subjects.

Materials and Methods

Patients with Rett Syndrome

Thirteen female patients with Rett syndrome were recruited from the University of California (San Diego) Rett Syndrome Clinic. Eleven patients had classic Rett syndrome according to the Rett Syndrome Diagnostic Criteria Work Group [13]. Two patients were atypical in that they had a higher level of function; nevertheless, they met most of the diagnostic criteria for Rett syndrome. Neither of the two atypical patients had any signs or symptoms that would exclude the diagnosis of Rett syndrome. Necessary diagnostic criteria for Rett syndrome include apparently normal prenatal and perinatal period, apparently normal psychomotor development through the first 6 months, deceleration of head growth between ages 5 months and 4 years, development of severely impaired expressive and receptive language, and stereotypic hand movements such as hand wringing or squeezing [13]. Supportive diagnostic criteria for Rett syndrome include breathing dysfunction, abnormalities on electroencephalograms, seizures, spasticity, and peripheral vasomotor disturbances [13]. Criteria for excluding Rett syndrome as a diagnosis include intrauterine growth retardation, signs of storage disease, microcephaly at birth, and other identifiable metabolic or progressive neurologic disorders [13]. Thirteen patients between 5 and 25 years old (12.0 ± 6.3 years, mean ± SD) were imaged in the transverse plane; 12 were imaged also in the sagittal plane. Rett syndrome ranged from stage 2 to stage 4. Head circumference was less than the 50th percentile for all 13 patients and less than the second percentile for eight of the 13 patients. Eleven of 13 patients had seizures. All patients with seizures were being treated with antiseizure medications; only four patients had been treated at some time with phenytoin.

Control Subjects

The control group consisted of 10 female volunteers between 6 and 27 years old (15.4 ± 7.5 years, mean ± SD). All 10 were imaged in the transverse plane; eight were imaged in the sagittal plane also. None had a history of neurologic or systemic illness.

MR Imaging Protocol

After informed consent was obtained, sagittal and transverse MR images were acquired with a 1.5-T magnet (GE Signa, General Electric Medical Systems, Milwaukee, WI). The control subjects were imaged without sedation; the patients with Rett syndrome were sedated with chloral hydrate (50–60 mg/kg body weight).

Sagittal images were acquired with a 256 × 256 matrix and a field of view of 16–24 cm after two to four excitations. A sagittal multisection T1-weighted spin-echo sequence was used with a repetition time (TR) of 600–800 msec and an echo time (TE) of 20–25 msec. Sagittal images were obtained only after the patient was adequately positioned (verified with preliminary transverse and sagittal images) to ensure that a true midsagittal image of the brain would be obtained. The sections were 5 mm thick; consecutive slices were separated by a 2.5-mm gap.

Transverse images were acquired with a 256 × 192 or 256 × 256 matrix and a field of view of 20–24 cm after one to two excitations. A multisection spin-echo axial sequence was used with a TR of 2000–3000 msec and TEs of 30 msec and 70–80 msec. The transverse images were obtained immediately after the sagittal images. The sections were 5.0 mm thick; consecutive slices were separated by a 2.5-mm gap.

Qualitative Assessment of the Images

All MR images were subjectively assessed by a neuroradiologist who reviewed the films with knowledge of the patients' diagnoses.

Image Quantification Protocol

Measurements of the brain on sagittal images were made in accordance with our previous report [14]. Areas were calculated by using a method of computer-assisted planimetry in which magnified images permitted differentiation of regions of interest from surrounding structures (Fig. 1). All sagittal measurements were made on the midsagittal image. The measurements included the area of vermian lobules I–V, vermian lobules VI–VII, vermian lobules VIII–X, the fourth ventricle, the ventral pons, the corpus callosum, and the pituitary gland. The boundaries between the vermian lobules were assigned in accordance with a previous report [15]: the boundary between vermian lobules I–V and VI–VII was defined as the line joining the anterior aspect of the primary fissure to the apex of the fourth ventricle; the boundary between vermian lobules VI–VII and VIII–X was defined as the line joining the anterior aspect of the prepyramidal fissure to the apex of the fourth ventricle. The fourth ventricle was designated as the area of CSF extending from the inferior aspect of

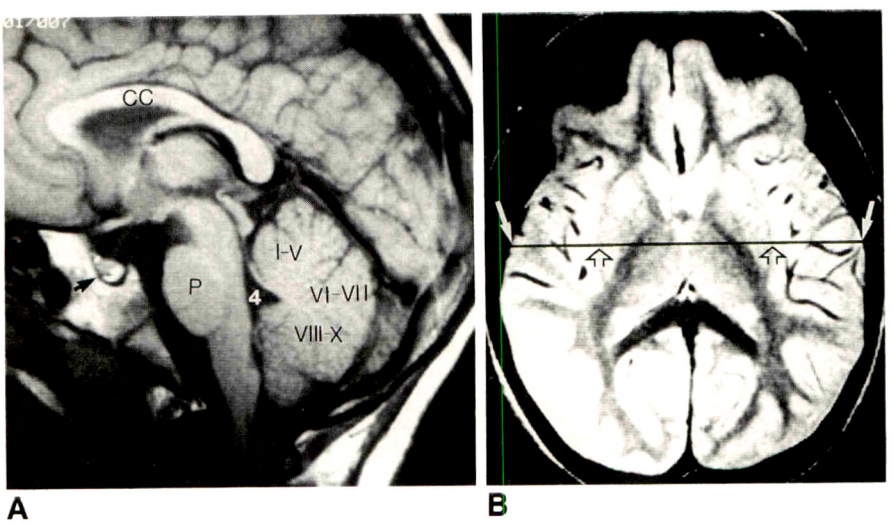


Fig. 1.—*A* and *B*, Midsagittal (*A*) and transverse (*B*) MR images from a 5-year-old with Rett syndrome. Areas measured on *A*: cerebellar vermian lobules I–V, VI–VII, and VIII–X, fourth ventricle (4), ventral pons (P), pituitary gland (*black arrow*), and corpus callosum (CC). Width of basal ganglia (*open arrows*) and lateral width of cerebrum (*white arrows*) at level of basal ganglia were measured on *B*.

the quadrigeminal plate to the obex, bounded anteriorly by the posterior aspect of the brainstem and posteriorly by the medullary velum, cerebellar vermis, and cerebellar tonsils. The area of the ventral pons is bounded anteriorly by CSF and posteriorly by the ventral aspect of the medial lemniscus, as described by Carpenter [16], Hayakawa et al. [17], and Hsu et al. [18]. The areas of the pituitary gland and the corpus callosum (measured from rostrum to splenium) were measured by using a previously described method [17]. Sagittal measurements were made independently by two observers. The observers were not blinded to the subjects' group designations. Midsagittal measurements of the two observers for the control subjects correlated well (r = .923–.994). Likewise, the two observers were in good agreement (r = .956–.991) on all seven measurements in the patients with Rett syndrome. All quantitative data presented here are from one observer.

Measurements made on transverse images included the cerebellar width, the widths of the inferior olives, the anteroposterior dimension of the cerebrum, the lateral width of the basal ganglia, and the lateral width of the cerebrum at the level of the basal ganglia. The cerebellar width, as described in a previous report [14], was the greatest transverse dimension of the cerebellum shown on a transverse image. The widths of the inferior olives were determined by choosing the image that showed the brainstem at the level of the inferior olivary nuclei, bisecting the brainstem into lateral halves, and measuring the distance from the midline to the lateral aspect of the brainstem through the left and right inferior olives. The anteroposterior length of the brain was the greatest anteroposterior dimension of the cerebrum shown on a single transverse image. The lateral width of the basal ganglia was determined by first choosing the transverse slice that best showed the putamen and globus pallidus and then measuring the distance perpendicular to the midline of the brain from the lateral aspect of the putamen of one hemisphere to the lateral aspect of the putamen of the opposite hemisphere, with the measurement line crossing the midline adjacent to the mamillothalamic tracts (Fig. 1). This "basal ganglia" line begins at the lateral aspect of one putamen, passes sequentially through that putamen, the corresponding globus pallidus, the midline of the brain adjacent to the mamillothalamic tracts, the globus pallidus of the opposite hemisphere, and finally the putamen of the opposite hemisphere (Fig. 1). By dividing the width of the basal ganglia by the cerebral width, we created a ratio of basal ganglia width to brain width. Transverse measurements were made by a single observer who knew the groups' designations.

As cachexia is common in older patients with Rett syndrome, we correlated our brain measurements with several body measurements (height, weight, head circumference) in the patients with Rett syndrome.

Statistical analysis of the data included two-tailed Student's t tests (statistical significance was $p \leq .05$) and simple linear regression analyses (statistical significance was $p \leq .01$).

Results

Subjective Assessment

The MR data for the patients with Rett syndrome were qualitatively assessed by a neuroradiologist who knew the patients' diagnoses when viewing the films. His impressions of the MR images from the 13 patients with Rett syndrome were (1) normal findings in eight cases (Fig. 2); (2) decreased cerebral volume, primarily in the frontal lobe, in three patients 6, 12, and 14 years old but not in any of the older patients; and (3) decreased cerebellar volume without cerebral abnormality in the two oldest patients, but not in any of the younger patients. The two oldest patients were a 25-year-old with mildly decreased vermian volume and a 23-year-old with severely decreased vermian and hemispheric volumes (Fig. 3).

Objective Measurements

Posterior fossa and pituitary gland.–Measurements of cerebellar width, cerebellar vermian lobules I–V, fourth ventricle, inferior olives, and pituitary gland were all significantly smaller (by 13–45%) in the patients with Rett syndrome than in the control subjects (see statistical results in Table 1). Measurements of the areas of the ventral pons and vermian lobules VI–VII and VIII–X also were smaller in the patients with Rett syndrome, but these differences were not statistically significant.

In the control group, no significant age-related changes were found in measurements of posterior fossa structures and the pituitary gland. Conversely, with increasing age the patients with Rett syndrome showed a statistically significant reduction in the area of vermian lobules I–V, VI–VII, and VIII–X (for each area; n = 12, $r \geq .738$, $p \leq .005$) and a trend toward enlargement in the area of the fourth ventricle (n = 11, r = .665, p = .024). For example, the area (mean ± SD) of vermian lobules VI–VII in the younger patients with Rett syndrome (5–10 years old, n = 8) was 265.5 ± 38.1 mm^2 whereas in the older patients with Rett syndrome (13–25 years old, n = 4) this area was 188.2 ± 46.3 mm^2. The ventral pons, inferior olives, and pituitary gland had no significant age-related changes in the patients with Rett syndrome.

Cerebrum and basal ganglia.—Quantitative analyses showed that measurements of cerebral width and length, basal ganglia width, and corpus callosum area were all significantly smaller (by 10–27%) in the patients with Rett syndrome than in the control subjects (see statistical results in Table 1). The widths of the basal ganglia and cerebrum were similarly reduced in the patients with Rett syndrome (see basal ganglia ratio in Table 1). No significant age-related changes were found in any measurement of supratentorial structures in either the Rett or the normal group.

Anthropometric data.—No statistically significant ($p \leq .01$) linear correlations were found between any of the measurements of the posterior fossa, pituitary gland, and supratentorial structures made on MR images and any of the anthropometric measurements (height, weight, head circumference).

Discussion

Nearly all measurements of length and area of the cerebellum, brainstem, basal ganglia, and cerebrum were significantly smaller than normal in our 5- to 25-year-old patients with Rett syndrome (Table 1). This evidence suggests that a variety of neural structures are similarly affected and that Rett syndrome may involve widespread brain hypoplasia. In addition, the area of the cerebellar vermis decreased with age and the area of the fourth ventricle increased with age. These findings indicate a progressive loss (i.e., atrophy) of the cerebellar parenchyma with age; measurement of other brain regions did *not* show age-related loss. Unlike the finding of widespread

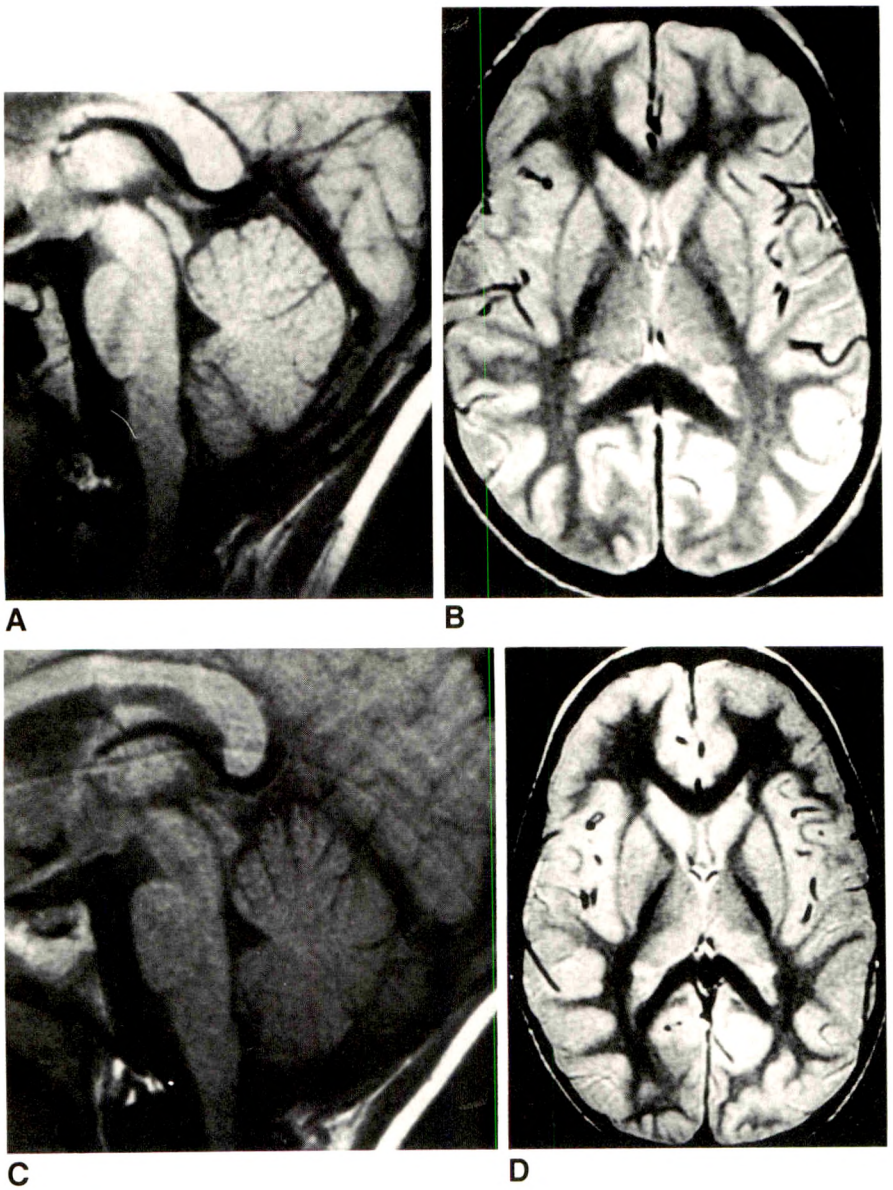


Fig. 2.—*A–D*, Midsagittal and transverse MR images from an 8-year-old patient with Rett syndrome (*A* and *B*) and a 6-year-old control subject (*C* and *D*) show no *qualitative* differences, but *quantitative* differences exist (Table 1).

hypoplasia, the latter results suggest that significant atrophy in Rett syndrome may be localized to the posterior fossa.

Cerebellar and Brainstem Findings

MR imaging indicated that two processes seem to affect the cerebellum in Rett syndrome: hypoplasia and late-onset atrophy. On MR images, hypoplasia (undergrowth) was evidenced by the significantly reduced width of the cerebellar hemispheres and reduced midsagittal area of the anterior vermis; the posterior vermis also was insignificantly smaller. These size reductions appeared in young patients who had no sign of atrophy (e.g., no increased sulcal widening) and in older patients. These quantitative MR findings are consistent with those of qualitative autopsy studies: Oldfors et al. [19] reported that the cerebellum appeared small in their 7- to 30-year-old patients with Rett syndrome, and Bauman and Kemper [20] reported increased cell packing density (a sign of arrested development) in the cerebellum in one 12-year-old patient. In the youngest of the autopsy cases in the study by Oldfors et al., no atrophy of the cerebellum was visible on macroscopic examination.

In the older patients with Rett syndrome but *not* in the younger ones, atrophy (evidenced by large increases in sulcal width) was shown on MR images of the cerebellar vermis and hemispheres (Fig. 3). Measurement of the vermis and fourth ventricle confirmed the presence of an age-related decline in the size of the cerebellum. These MR results parallel the autopsy data of Oldfors et al. [19], who reported macroscopic evidence of cerebellar atrophy in older but not younger patients with Rett syndrome. Autopsy data indicate that in the cases with the most severe atrophy, gliosis was found in molecular, Purkinje, and granular layers and in the white matter, accompanied by loss of neurons in the molecular and

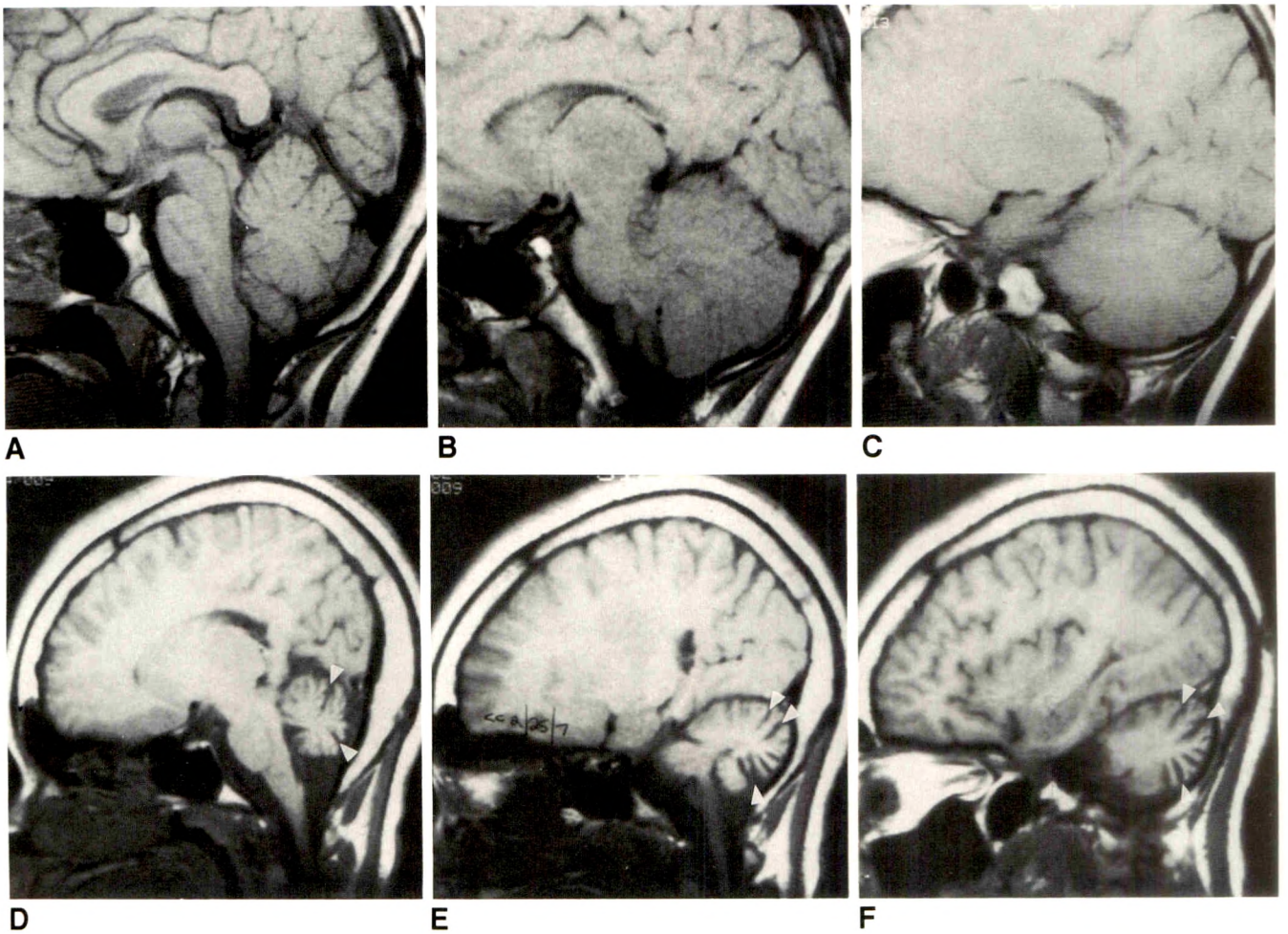


Fig. 3.—*A–F*, Representative sagittal MR images from a 9-year-old (*A–C*) and a 23-year-old (*D–F*) with Rett syndrome. In older patient, cerebellar vermian and hemispheric fissures are markedly widened (thought to represent cerebellar atrophy); *arrowheads* point to several such widened fissures. *A* and *D* are midsagittal images, *B* and *E* are 7.5 mm lateral to midsagittal, and *C* and *F* are 15 mm lateral to midsagittal.

Purkinje cell layers and in the dentate nucleus. Bauman and Kemper [20] did not report loss of neurons in their one 12-year-old patient. Thus, in Rett syndrome, loss of neurons apparently begins in childhood or adolescence and progresses for many years.

The cerebellar atrophy found in Rett syndrome may be an integral part of the disorder and would be consistent with the degeneration of the motor system seen clinically in patients with stage 3–4 Rett syndrome. Alternatively, it may be related to the poor nutritional status typical of these patients (e.g., seven of our 13 patients were less than the fifth percentile for weight). However, in the patients with Rett syndrome in the present study, no significant ($p \leq .01$) correlations between height, weight, and head circumference and cerebellar measurements were found. This does not rule out poor nutrition as a contributing factor in the cerebellar atrophy, but this factor seems less likely to be one of the more important factors. The cerebellar neuronal loss and gliosis and attendant atrophy might instead be related to the presence of seizure disorders, which is also typical of patients with Rett syndrome (e.g., seen in 11 of our 13 patients) or to the use of anticonvulsant medications (11 of our 13 patients have taken anticonvulsants; four have received phenytoin). This age-related cerebellar atrophy warrants further study.

These characteristics of cerebellar abnormalities distinguish Rett syndrome from several other developmental disorders involving the cerebellum, such as infantile autism, fragile X syndrome, and Down's syndrome. For example, in infantile autism, hypoplasia occurs but later atrophy does not; hypoplasia is limited to posterior vermis and hemispheres (including the flocculonodular lobe) and does not involve the anterior vermis; loss of Purkinje neurons is prenatal or perinatal, not late in childhood or adolescence; no cerebellar cortical gliosis or gliosis and loss of myelin in white matter occurs; and no loss of neurons in the dentate nucleus occurs [21, 22]. Thus, although patients with early stages of Rett syndrome have some of the behavioral features of classic infantile autism, the radiologically and microscopically observed spectra of cerebellar involvement in these two groups of patients differ markedly. As another example, in Down's syndrome, cerebellar hypoplasia without progressive atrophy is seen during childhood and adolescence; granule cell dysgenesis occurs

TABLE 1: Quantitative Measurements on MR Images in Control Subjects and in Patients with Rett Syndrome

Measurement	Control Subjects	Patients with Rett Syndrome	% Size Reduction in Patients with Rett Syndrome	*p* Value
Posterior fossa				
Vermis I–V (mm^2)	393.9 ± 36.4 (8)	343.1 ± 51.4 (12)	13	.027
Vermis VI–VII (mm^2)	276.5 ± 53.1 (8)	239.8 ± 54.4 (12)	13	.152
Vermis VIII–X (mm^2)	287.9 ± 43.0 (6)	241.4 ± 68.9 (11)	16	.157
Cerebellar width (mm)	101.0 ± 3.1 (10)	89.6 ± 6.4 (13)	12	<.001
Fourth ventricle (mm^2)	178.6 ± 59.4 (8)	122.1 ± 30.7 (11)	31	.034
Ventral pons (mm^2)	325.2 ± 35.1 (8)	294.0 ± 32.8 (12)	10	.058
Inferior olive width (right) (mm)	7.8 ± 0.9 (8)	6.5 ± 0.8 (13)	17	.003
Inferior olive width (left) (mm)	7.6 ± 0.8 (8)	6.6 ± 0.6 (13)	13	.012
Supratentorium				
Cerebral anteroposterior length (mm)	163.6 ± 5.0 (9)	144.8 ± 7.0 (13)	12	<.001
Cerebral lateral width (mm)	116.6 ± 6.4 (8)	103.0 ± 6.0 (13)	11	<.001
Corpus callosum (mm^2)	589.9 ± 93.5 (8)	430.9 ± 102.6 (12)	27	.002
Basal ganglia width (mm)	60.7 ± 2.5 (8)	54.6 ± 3.0 (13)	10	<.001
Basal ganglia ratio	0.52 ± 0.02 (8)	0.53 ± 0.02 (13)		.286
Pituitary gland (mm^2)	46.2 ± 17.6 (8)	25.5 ± 5.1 (10)	45	.012

Note.—Measurements are presented as mean ± SD, followed in parentheses by the number of subjects. The *p* values were calculated from pooled variances when Levene's F-test showed variances to be insignificantly different ($p \geq .1$) and from separate variances when variances were shown to be significantly different ($p \leq .1$).

but not dysgenesis or later loss of Purkinje cells. As a last example, in fragile X syndrome the posterior vermis is reduced in size but the anterior vermis is not [23].

Measurements of the transverse width of the cerebellar hemispheres and measurements of brainstem structures interconnected with the cerebellum (ventral pons and inferior olives) did not closely reflect the amount of cerebellar atrophy seen in the patients with Rett syndrome. A lack of such correlations has been noted in other disorders. For example, in a patient with progressive cerebellar degeneration [24], even though the vermis and cerebellar hemispheres were reduced in size by 85% and 42%, respectively, the width of the cerebellum, the widths of the inferior olives, and the midsagittal area of the ventral pons were reduced by only 4%, 2%, and 13%, respectively.

Supratentorial Findings

MR imaging showed clear evidence of hypoplasia of the cerebrum and the basal ganglia in Rett syndrome but no evidence of atrophy. For instance, cerebral length and width and measurements of the corpus callosum were reduced 10–27%, but no evidence of abnormal signal intensities or sulcal widening was found. In a recent MR report, Casanova et al. [25] also found the cerebral hemispheres and caudate nuclei in patients with Rett syndrome to be smaller than those in control subjects. However, they did not find a difference in a measurement of the corpus callosum, perhaps because their control subjects were patients rather than healthy volunteers.

These abnormal measurements of the cerebrum and basal ganglia from MR images are consistent with the microcephaly seen in other studies of Rett syndrome [2, 5, 6, 10–12] and in most of our patients. In patients with Rett syndrome the head circumference is usually normal at birth, but its growth rate decelerates after the age of 5–6 months [26, 27]. This deceleration occurs in the midst of a rapid and critical phase of human postnatal brain growth: for instance, from birth to 2 years, the number of synapses in the cerebrum nearly doubles [28], and the weight of the human brain normally more than doubles, from 384 to 961 g (see Table 111 in Blinkov and Glazer [29]) [30]. The rate of growth thereafter is significantly slower, but growth continues into the third decade of life [29].

Autopsy evidence is also consistent with MR evidence of cerebral hypoplasia and arrest of development without significant age-related global atrophy in patients with Rett syndrome. For example, recent autopsy findings in a 12-year-old patient with Rett syndrome [20] included signs of developmental arrest such as increased cell packing density throughout the cerebral cortex, basal ganglia, thalamus, hippocampus, amygdala, and cerebellum. In addition, the mean weight of the brain in 14 6- to 30-year-old patients with Rett syndrome from three studies [19, 20, 31] is 945 g, a weight comparable to the normal weight in 2-year-olds and 26% smaller than the normal weight in 6- to 30-year-old females [29, Table 111]. Moreover, the mean brain weight of the three youngest patients reported in the literature (6, 7, and 8 years old [19, 31]) differs by only 4% from the brain weight of the three oldest patients in the literature (18, 20, and 30 years old [19, 31]). Additionally, the mean brain weight of the eight youngest Rett cases reported in the autopsy literature (6–12 years old) is only slightly smaller than that of the six oldest cases (13–30 years old) (920 vs 978 g) [19, 31].

It is uncertain if atrophy of the cerebral cortex occurs in Rett syndrome. Some autopsy and imaging studies of the brain have stated that in a minority of patients with Rett

syndrome, the cerebral cortex show signs of "slight" atrophy [2, 5–7, 9–12, 31]. Unfortunately, these studies generally failed to maintain a clinically meaningful distinction between hypoplasia, defined as incomplete development or underdevelopment, and atrophy, defined as a wasting away, loss, or dimunition of previously established brain parenchyma. In developmental disorders, hypoplasia can result from atrophy of some parenchymal element (e.g., during early development, previously established Purkinje neurons may die, which then leads to cerebellar hypoplasia, as in infantile autism). None of the brain imaging or autopsy studies that did report atrophy in Rett syndrome provided the evidence necessary to draw this conclusion. On the contrary, the weight of evidence leans toward hypoplasia (e.g., arrest of brain weight, increased cell packing density, no age-related increase in sulcal width, no age-related changes in cerebral width or length, mild to absent evidence of cortical or white matter gliosis in the cerebrum) [19, 29, 31, this study].

The abnormality of the basal ganglia detected with MR imaging [25, this study] and at autopsy in patients with Rett syndrome is compatible with other indexes of dysfunction of the basal ganglia in this disorder. For example, patients with Rett syndrome have dysfunction of the extrapyramidal motor system, including abnormal hand-wringing behavior, gait apraxia, and truncal ataxia [4, 32]. Moreover, positron emission tomography showed evidence of decreased D_2-dopamine receptor binding in the caudate nucleus of a 25-year-old patient with Rett syndrome [33]. Finally, "isolated abnormal neurites and reactive or degenerative axonal swellings" have been seen at autopsy in the caudate nucleus of patients with Rett syndrome [31].

A final implication of the present study has to do with the clinical neuroradiologic examination of neurologically or developmentally impaired patients. Findings on neuroimaging studies of patients with Rett syndrome are commonly interpreted as normal [6–9]. A neuroradiologist interpreted qualitative findings on MR images as normal in eight of our patients with Rett syndrome. However, the quick, accurate, and simple *quantitative* analyses used in this study revealed that these normal images were markedly abnormal in all supratentorial and posterior fossa regions measured. Quantitative analyses are an important complement to routine radiologic interpretation of neuroimaging studies, particularly in children.

ACKNOWLEDGMENT

We thank Jeanne Townsend for assistance with the statistical analyses.

REFERENCES

1. Rett A. Uber ein eigenartiges hirnatrophisches Syndrom bei Hyperammoniamie in Kindesalter. *Wien Med Wochenschr* **1966**;116:723–738
2. Rett A. Cerebral atrophy associated with hyperammonemia. In: Vinken PJ, Bruyn GW, eds. *Handbook of clinical neurology*, vol. 29. Amsterdam: North-Holland, **1977**:305–329
3. Trevathan E, Adams MJ. The epidemiology and public health significance of Rett syndrome. *J Child Neurol* **1988**;3[suppl]:S17–S20
4. Hagberg B, Witt-Engerstrom I. Rett syndrome: a suggested staging system for describing impairment profile with increasing age towards adolescence. *Am J Med Genet* **1986**;24:47–59
5. Hagberg B, Aicardi J, Dias K, Ramos O. A progressive syndrome of autism, dementia, ataxia, and loss of purposeful hand use in girls: Rett syndrome. Report of 35 cases. *Ann Neurol* **1983**;14:471–479
6. Naidu S, Murphy M, Moser HW, Rett A. Rett syndrome: natural history in 70 cases. *Am J Med Genet* **1986**;24:61–72
7. Wu X, Zhao D, Ling Q, et al. Rett syndrome in China: report of 9 patients. *Pediatr Neurol* **1988**;4:126–127
8. Burd L, Gascon G, Kerbeshian J. Rett syndrome: case reports and management strategies. *Neurosci Biobehav Rev* **1988**;12:283–287
9. Krageloh-Mann I, Schroth G, Niemann G, Michaelis R. The Rett syndrome: magnetic resonance imaging and clinical findings in four girls. *Brain Dev* **1989**;11:175–178
10. Suzuki H, Matsazuka T, Hirayama Y, et al. Rett's syndrome: progression of symptoms from infancy to childhood. *J Child Neurol* **1986**;1:137–141
11. Nomura Y, Segawa M, Hasegawa M. Rett syndrome: clinical studies and pathophysiological consideration. *Brain Dev* **1984**;6:475–486
12. Moeschler JB, Charman CE, Berg SZ, Graham JM Jr. Rett syndrome: natural history and management. *Pediatrics* **1988**;82:1–10
13. The Rett syndrome Diagnostic Criteria Work Group (Trevathan E., Chairman). Diagnostic criteria for Rett syndrome. *Ann Neurol* **1988**;23:425–428
14. Murakami JW, Courchesne E, Press GA, et al. Reduced cerebellar hemisphere size and its relationship to vermal hypoplasia in autism. *Arch Neurol* **1989**;46:689–694
15. Courchesne E, Yeung-Courchesne R, Press GA, et al. Hypoplasia of cerebellar vermal lobules VI and VII in autism. *N Engl J Med* **1988**; 318:1349–1354
16. Carpenter MB. *Human neuroanatomy*. Baltimore: Williams & Wilkins, **1976**:322–325
17. Hayakawa K, Konishi Y, Matsuda T, et al. Development and aging of brain midline structures: assessment with MR imaging. *Radiology* **1989**;172:171–177
18. Hsu M, Yeung-Courchesne R, Courchesne E, Press GA. Absence of pontine abnormality in infantile autism. *Arch Neurol* **1991**;48:1160–1163
19. Oldfors A, Sourander P, Armstrong DL, et al. Rett syndrome: cerebellar pathology. *Pediatr Neurol* **1990**;6:310–314
20. Bauman ML, Kemper TL. The neuropathology of Rett syndrome is pervasive throughout the brain. *Neurology* **1991**;41:306–308
21. Arin DM, Bauman ML, Kemper TL. The distribution of Purkinje cell loss in the cerebellum in autism. *Neurology* **1991**;42:307
22. Bauman ML. Microscopic neuroanatomic abnormalities in autism. *Pediatrics* **1991**;87:791–796
23. Reiss AL, Patel S, Kumar AJ, Freund L. Preliminary communication: neuroanatomical variations of the posterior fossa in men with the fragile-X (Martin-Bell) syndrome. *Am J Med Genet* **1988**;31:407–414
24. Akshoomoff NA, Courchesne E, Press G, Iraqui V. Contribution of the cerebellum to neuropsychological functioning: evidence from a case of cerebellar degeneration. *Neuropsychologia* **1991** (in press)
25. Casanova MF, Naidu S, Goldberg TE, et al. Quantitative magnetic resonance imaging in Rett syndrome. *J Neuropsych Clin Neurosci* (in press)
26. Trevathan E, Naidu S. The clinical recognition and differential diagnosis of Rett syndrome. *J Child Neurol* **1988**;3[suppl]:S6–S16
27. Burd L, Gascon G. Rett syndrome: review and discussion of current diagnostic criteria. *J Child Neurol* **1988**;3:263–268
28. Huttenlocher PR. Morphometric study of human cerebral cortex development. *Neuropsychologia* **1990**;28:517–527
29. Blinkov SM, Glezer II; Haigh B, trans. Weight, volume, and linear dimensions of the brain. In: *The human brain in figures and tables: a quantitative handbook*. New York: Basic Books and Plenum, **1968**:123–136
30. Dobbing J, Sands J. Quantitative growth and development of human brain. *Arch Dis Child* **1973**;48:757–767
31. Jellinger K, Armstrong D, Zoghbi HY, Percy AK. Neuropathology of Rett syndrome. *Acta Neuropathol* **1988**;76:142–158
32. Hagberg B. Rett syndrome: clinical peculiarities, diagnostic approach, and possible causes. *Pediatr Neurol* **1989**;5:75–83
33. Harris JC, Wong DF, Wagner HN, et al. Positron emission tomography study of D_2 dopamine receptor binding and CSF biogenic amine metabolites in Rett syndrome. *Am J Med Genet* **1986**;24:201–210

American Roentgen Ray Society:
Officers, Committees, and Membership Information

Officers

President: A. Everette James, Jr.
President-elect: Andrew K. Poznanski
1st Vice-president: George R. Leopold
2nd Vice-president: Ralph J. Alfidi
Secretary: Joseph T. Ferrucci, Jr.
Treasurer: Beverly P. Wood

Executive Council: R. J. Alfidi, R. N. Berk, M. P. Capp, W. J. Casarella, D. O. Davis, N. R. Dunnick, J. T. Ferrucci, Jr., A. E. James, Jr., J. A. Kirkpatrick, Jr., A. M. Landry, Jr., G. R. Leopold, J. E. Madewell, T. C. McLoud, A. A. Moss, A. K. Poznanski, R. J. Stanley, J. H Thrall, N. O. Whitley, B. P. Wood, K. H. Vydareny, chair

Committees

Editoral Policy: R. N. Berk, E. Buonocore, M. M. Figley, R. G. Levitt, C. R. B. Merritt, K. Valji, W. J. Casarella, chair

Education and Research: G. M. Glazer, R. R. Hattery, C. B. Higgins, R. J. Stanley, W. M. Thompson, N. O. Whitley, chair

Finance and Budget: D. J. Anderson, R. K. Gedgaudas-McClees, J. E. Madewell, A. A. Moss, J. H. Thrall, chair

Nominating: M. P. Capp, C. A. Rohrmann, Jr., J. E. Madewell, chair

Publication: E. Buonocore, R. G. Levitt, C. R. B. Merritt, W. J. Casarella, chair

Membership: D. O. Davis, J. E. Madewell, T. C. McLoud, A. A. Moss, chair

Representatives to Other Organizations

American Board of Radiology: W. J. Casarella, J. A. Kirkpatrick, Jr., L. F. Rogers

American College of Radiology: J. E. Madewell, B. L. McClennan, R. J. Stanley, N. H. Messinger

American Medical Association: R. A. Gagliardi, delegate; R. G. Evens, alternate; K. L. Kidd, CPT Advisory Committee

American National Standards Institute: M. E. Haskin

National Council on Radiation Protection and Measurements: F. D. Miraldi, E. L. Saenger

Armed Forces Institute of Pathology: J. E. Madewell

Meeting Arrangements

Annual Meetings: April 25–30, 1993, Marriott San Francisco, San Francisco, CA; April 24–29, 1994, New Orleans Hilton, New Orleans, LA

Annual Meeting Committee: J. K. Crowe, N. R. Dunnick, R. R. Lukin, N. H. Messinger, R. J. Stanley, R. D. Steele, Jr., A. M. Landry, Jr., chair

Instructional Courses: B. L. McClennan, associate chair, R. J. Stanley, chair

Scientific Program: P. H. Arger, W. R. Brody, G. D. Fullerton, D. C. Kushner, W. M. Thompson, J. H. Thrall, A. K. Poznanski, chair

Scientific Exhibits: J. R. Haaga, D. S. Hartman, N. R. Dunnick, chair

ARRS Membership

An application form is printed in the January issue of the Journal. Qualified applicants will be admitted quarterly. Send completed forms to American Roentgen Ray Society, 1891 Preston White Dr., Reston, VA 22091. Active members are graduates of an approved medical or osteopathic school or hold an advanced degree in an allied science. They must practice radiology or work in an associated science in the United States or Canada and be certified by the American Board of Radiology, American Osteopathic Board of Radiology, or Royal College of Physicians of Canada or otherwise adequately document training and credentials. International members are foreign radiologists or scientists who are active in radiology or an allied science. Members-in-training are residents or fellows in radiology or postgraduate students in an allied science. Additional application forms can be obtained from the ARRS offices in Reston, VA.

Business Office

Paul R. Fullagar, Executive Director, American Roentgen Ray Society, 1891 Preston White Dr., Reston, VA 22091; (703) 648-8992; 1-800-438-2777.

High-Signal Foci on MR Images of the Brain: Observer Variability in Their Quantification

F. Zerrin Yetkin[1]
Victor M. Haughton[1]
Mary E. Fischer[2]
R. Anne Papke[1]
David L. Daniels[1]
Leighton P. Mark[1]
Lloyd E. Hendrix[1]
Russell J. Asleson[1,3]
Johan Johansen[1,4]

Foci of high signal in the cerebral white matter are common incidental findings on MR images of the brain of control subjects or patients with a variety of diseases. Although the number of foci has been reported to correlate with age and several risk factors, the degree of observer variability in quantifying foci has not been reported. We used kappa statistics to determine radiologists' agreement in counting high-signal-intensity foci on MR images obtained in healthy volunteers and in patients with hypertension. Before interpreting the images, one pair of radiologists studied 30 routine MR images and reached consensus on differentiating high-signal foci from other foci of high intensity caused by normal structures (e.g., deep gyri or Virchow-Robin spaces). These two observers then independently determined the number of foci in the study group. Using their own criteria, other radiologists independently counted the foci. Agreement between observers was determined with the kappa statistic. The results showed fair agreement between the radiologists who first reached a consensus in counting foci of hyperintensity and poor agreement between the other observers.

We conclude that in order to compare the frequency of foci of hyperintensity in different groups of patients, observer variability must be controlled. Studies without proper control subjects may lead to incorrect conclusions regarding the correlation of focal hyperintensities and various risk factors.

AJR 159:185–188, July 1992

Foci of abnormally high signal intensity in cerebral white matter are found incidentally on MR images in up to 20% of patients or control subjects. These foci of hyperintensity are also referred to as leukoaraiosis, periventricular hyperintensities, white matter hyperintensities, and "unidentified bright objects." The prevalence of foci of hyperintensity in patients with hypertension, migraine, and dementia and in asymptomatic control subjects has been studied [1–7]. Foci of hyperintensity have been reported to correlate with some demographic or medical factors. To our knowledge, the effect of observer variability on the number of foci of hyperintensity detected on MR images has not been studied. Accordingly, we measured the degree of observer variability in determining the number of high-signal foci found on MR images in healthy volunteers.

Materials and Methods

Radiologists independently interpreted MR images obtained in control subjects (313 studies), patients with multiple sclerosis (43 cases), patients with dementia of the Alzheimer type (32 cases), and patients with hypertension (63 cases). The patients with multiple sclerosis fulfilled the criteria of Schumacher et al. [8] for establishing the diagnosis. The patients with hypertension were selected from a group undergoing treatment for essential hypertension; none of them had neurologic signs or symptoms. The diagnosis in patients with dementia was documented by standard neurologic and neuropsychological testing.

Each MR study included a sagittal localizer image obtained with 500/20 (TR/TE) followed by a series of 40 axial images (2000/20,70) with a 5-mm slice thickness and 1-mm gap,

Received July 22, 1991; accepted after revision February 4, 1992.

[1] Department of Radiology, The Medical College of Wisconsin, Froedtert Memorial Lutheran Hospital, 9200 W. Wisconsin Ave., Milwaukee, WI 53226. Address reprint requests to V. M. Haughton.

[2] Biostatistics & Clinical Epidemiology, Medical College of Wisconsin, Milwaukee, WI 53226.

[3] Present address: Colorado Springs Radiologists, Colorado Springs, CO 80919.

[4] Present address: Department of Radiology, Akershus Central Hospital, Nordbyhagen, Norway.

0361–803X/92/1591–0185
© American Roentgen Ray Society

cardiac gating, 256 × 256 matrix, and two excitations obtained with a 1.5-T scanner (Signa, General Electric Medical Systems, Milwaukee, WI). The studies were placed in random sequence and assigned a number. All alphanumeric information on the images was obscured. Neuroradiologists with at least 2 years experience in MR imaging were recruited to interpret the images. One radiologist, designated as observer 1, interpreted 412 studies (mixture of patients and control subjects). Three radiologists reviewed portions of the entire collection (patients and control subjects mixed) without first conferring with one another on the criteria for distinguishing and enumerating foci of hyperintensity. The results are grouped under the heading of observer 2. Then observer 1 (designated observer 4 for this session) and another observer (designated observer 3) reviewed together 30 of the MR studies that were not included in the study sample to reach a consensus on distinguishing foci of hyperintensity from sulci or other normal structures. Then they reviewed independently 193 studies (mixture of patients and control subjects). All observers interpreted the designated studies independently without any knowledge of the patients' gender, age, or history. All observers determined the number of small (less than 5 mm) and large (5 mm or larger) foci of hyperintensity per case, provided a radiologic interpretation for the study (normal, abnormal, specific disease), and commented on the images or findings if they wished. Observer 1 interpreted the studies a third time 6 months later to determine intraobserver agreement.

The numbers of foci of hyperintensity found by each of the radiologists on images of each of the control subjects and the patients with hypertension were tabulated. The patients with multiple sclerosis and dementia were not included for this tabulation. Observers 1 and 2 were compared to determine agreement between radiologists who had not reached consensus. Observers 1, 2, and 3 were also compared to determine agreement in a larger group of radiologists who had not reached consensus. The second interpretations of observer 1 (labeled as observer 4) were compared with those of observer 3 to determine agreement between radiologists who had reached a consensus. The second and third interpretations of observer 1 were compared to determine intraobserver error. The first and second interpretations of observer 1 were compared to determine the agreement between interpretations made with and without a preliminary consensus session.

Agreement between observers was measured by using the kappa statistic, which is a measure of agreement adjusted for the agreement due to chance alone. If there is complete agreement between observers, kappa equals 1. For evaluation purposes, a kappa greater than .75 indicates excellent agreement, a kappa between .40 and .75 indicates fair agreement, and a kappa below .40 indicates poor agreement [9, 10].

Results

Of the 451 MR studies enrolled for this study, 356 were interpreted twice by one radiologist to determine intraobserver agreement; 293 were reviewed by both observers 3 and 4 (who reached a consensus); and 191 were reviewed by observers 1, 2, and 3 (with no consensus). Control subjects and patients were mixed randomly in each group of studies.

Agreement between observers 1 and 2 was poor or fair (Table 1). Agreement was fair for seven or more small foci of hyperintensity, for no large foci of hyperintensity, and for more than two large foci of hyperintensity; it was poor for all other comparisons. The kappa statistics were between .106 and .531 for small foci of hyperintensity and between .300 and .657 for large foci of hyperintensity.

TABLE 1: Comparison of Observers 1 and 2 for the Detection of High-Signal Foci in the Cerebral White Matter on MR Images

Size of Foci/ No. Detected	% of Total		Agreement	Kappa (95% CI)
	Observer 1	Observer 2		
Small (<5 mm)				
0	22	41	Poor	.270 (.141, .399)
1–2	27	15	Poor	.106 (.000, .250)
3–6	30	19	Poor	.147 (.002, .292)
7+	21	25	Fair	.531 (.389, .673)
Mean			Poor	.263 (.174, .352)
Large (>5 mm)				
0	72	73	Fair	.657 (.536, .778)
1–2	12	15	Poor	.300 (.114, .486)
3+	16	12	Fair	.542 (.370, .714)
Mean			Fair	.530 (.415, .645)

Note.—CI = confidence interval.

TABLE 2: Comparison of Observers 1, 2, and 3 for the Detection of High-Signal Foci in the Cerebral White Matter on MR Images

Size of Foci/No. Detected	% of Total			Agreement	Kappa
	Observer 1	Observer 2	Observer 3		
Small (<5 mm)					
0	22	41	63	Poor	.227
1–2	27	15	22	Poor	.005
3–6	30	19	11	Poor	.063
7+	21	25	5	Poor	.348
Mean				Poor	.162
Large (>5 mm)					
0	72	73	85	Fair	.530
1–2	12	15	9	Poor	.266
3+	16	12	6	Fair	.461
Mean				Fair	.440

Agreement among observers 1, 2, and 3 was poor or fair (Table 2). No small foci of hyperintensity were found in 22% of the studies by observer 1, in 41% by observer 2, and in 63% by observer 3. Detection of foci 5 mm or larger was less variable (Table 1). Observer 1 reported that 72% of studies showed no large foci of hyperintensity, observer 2 reported 73%, and observer 3 reported 85%. Agreement among the observers as measured by the kappa statistic for small foci of hyperintensity was poor (kappa, .005–.348); for large foci of hyperintensity, agreement was somewhat better (kappa, .266–.530). Each table is based on slightly different sample sizes, hence the discrepancies between tables.

Agreement between observers 3 and 4, who first reached agreement on diagnostic criteria of foci of hyperintensity, was fair (Table 3). Observer 3 reported no small foci of hyperintensity in 72% of MR studies, and observer 4 reported no small foci of hyperintensity in 70%. The percentage of studies with no large foci of hyperintensity was 90% for both observers. The kappa statistics were between .527 and .734 for small foci of hyperintensity and between .416 and .730 for large foci of hyperintensity. The difference between the results of observer 3 in Tables 2 and 3 is a result of the different sample sizes and random distribution of cases between these

samples (i.e., one group had more cases without foci of hyperintensity).

Agreement was poor or good between the results of observer 1 with and without benefit of the session to reach consensus. Kappa statistics were between .016 and .283 for small foci of hyperintensity and .193 to .592 for large foci of hyperintensity (Table 4).

Intraobserver agreement was excellent. Kappa for the presence of foci of hyperintensity was .891 between the first and second reviews by the same observer.

The MR studies in control subjects were in general classified as "normal" despite the presence of foci of hyperintensity. MR studies in control subjects or volunteers with multiple foci of hyperintensity were interpreted as "possible deep cerebral infarctions" or, rarely, as "suggestive of multiple sclerosis." The interpretations in the multiple sclerosis patients are not analyzed in this article (see [11] for analysis).

Discussion

No gold standard exists for the detection of foci of hyperintensity because usually anatomic verification is not obtained. Even when anatomic verification is obtained, the correlation between the pathologic and MR findings is not exact [12, 13]. Therefore, the accuracy of MR imaging in disclosing foci of hyperintensity—that is, the percentage of actual lesions that are correctly identified—cannot be assessed. The purpose of this study was to measure the variability between radiologists in determining the number of foci of hyperintensity. The results show that generally agreement is poor between observers unless they have first reached a consensus on identifying foci of hyperintensity (Fig. 1). Observers who had not reached a consensus had greater interobserver variation.

The multiple sclerosis and dementia cases were included to minimize bias in the interpretation process. The patients with multiple sclerosis presumably had demyelinating plaques rather than incidental foci of hyperintensity. The patients with dementia may have had foci of hyperintensity or deep infarctions. Therefore, these studies were not included in the tabulations of foci of hyperintensity. Observer bias was minimized by presenting the observer with studies that did and did not show pathologic changes (patients vs controls) and by blinding the observer to medical and demographic information. Studies of control subjects and of patients were mixed randomly to minimize over- and underinterpretation of cases. We instructed two observers to try to distinguish foci of hyperin-

TABLE 3: Comparison of Observers 3 and 4 for the Detection of High-Signal Foci in the Cerebral White Matter on MR Images

Size of Foci/ No. Detected	% of Total		Agreement	Kappa (95% CI)
	Observer 3	Observer 4		
Small (<5 mm)				
0	72	70	Fair	.734 (.647, .820)
1–2	18	15	Fair	.527 (.396, .658)
3–6	7	12	Fair	.559 (.396, .722)
7+	3	3	Fair	.544 (.262, .825)
Mean			Fair	.630 (.546, .715)
Large (>5 mm)				
0	90	90	Fair	.606 (.453, .760)
1–2	6	8	Fair	.416 (.215, .616)
3+	4	3	Fair	.730 (.504, .956)
Mean			Fair	.557 (.406, .708)

Note.—CI = confidence interval.

TABLE 4: Comparison of Observers 1 and 4 for the Detection of High-Signal Foci in the Cerebral White Matter on MR Images

Size of Foci/ No. Detected	% of Total		Agreement	Kappa (95% CI)
	Observer 1	Observer 4		
Small (<5 mm)				
0	33	73	Poor	.283 (.223, .343)
1–2	24	12	Poor	.016 (−.102, .071)
3–6	22	11	Poor	.159 (.054, .265)
7+	21	4	Poor	.270 (.163, .376)
Mean			Poor	.186 (.147, .225)
Large (>5 mm)				
0	78	89	Good	.592 (.491, .693)
1–2	9	7	Poor	.193 (.043, .342)
3+	13	5	Good	.485 (.345, .625)
Mean			Good	.466 (.387, .545)

Note.—CI = confidence interval.

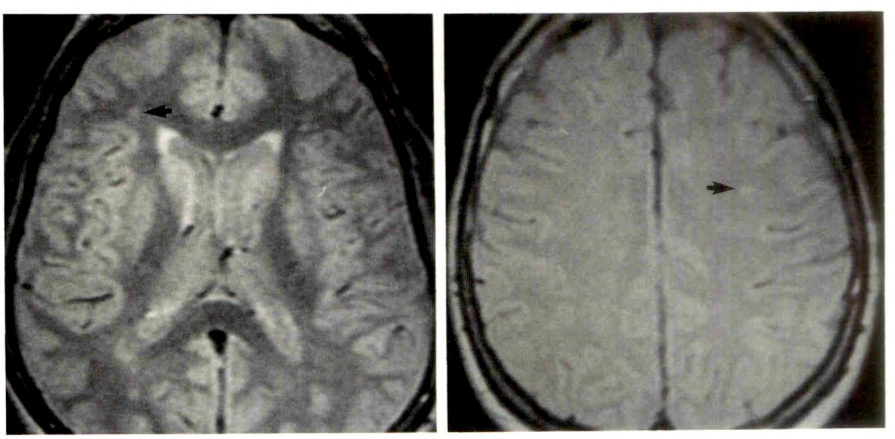


Fig. 1.—*A* and *B*, Examples of questionable foci of hyperintensity on proton density–weighted MR images in two volunteers. Areas marked with *arrows* were designated as foci of hyperintensity by some observers and as deep gyri by others.

tensity from normal structures such as deep gyri or sulci and from Virchow-Robin spaces. We eliminated Virchow-Robin spaces from the enumeration because they are common and are not usually counted as foci of hyperintensity. Criteria for distinguishing foci of hyperintensity are difficult to offer, because in our study anatomic verification was not possible. Our data show that greater precision can be obtained in enumerating foci of hyperintensity by using observers who have had practice in identifying foci of hyperintensity and by counting large rather than small foci of hyperintensity.

The enumeration of foci of hyperintensity is variable and somewhat arbitrary. Differences between observers and differences between MR imagers may play a role. Our data indicate that the number of foci of hyperintensity found in one study cannot be compared with the number in another, unless a consensus has been reached between observers.

REFERENCES

1. Awad IA, Spetzker RF, Hodak JA, Catherine A, Awad RN, Williams F Jr. Incidental lesions noted on magnetic resonance imaging of the brain: prevalence and clinical significance in various age groups. *Neurosurgery* **1987**;20:222–227
2. Soges LJ, Cacayosin ED, Petro GR. Migraine: evaluation by MR. *AJNR* **1988**;9:425–429
3. Erkinyuntti K, Ketoren L, Sulkava R. Do white matter changes on MRI and CT differentiate vascular dementia from Alzheimer's disease? *J Neurol Neurosurg Psychiatry* **1987**;50:37–42
4. Fazekas F, Chawluk JB, Alavi A, Hurtig HI, Zimmerman RA. MR signal abnormalities at 1.5 T in Alzheimer's dementia and normal aging. *AJR* **1987**;149:351–356
5. Kobari M, Meyer JS, Ichijo M, Oravez WT. Leukoaraiosis: correlation of MR and CT findings with blood flow, atrophy, and cognition. *AJNR* **1990**;11:273–281
6. Hendrie HC, Farlow MR, Austrom MG, Edwards MK, Williams MA. Foci of increased T2 signal intensity on brain MR scans of healthy elderly subjects. *AJNR* **1989**;10:703–707
7. Drayer BP. Imaging the aging brain. Part I: Normal findings. *Radiology* **1988**;166:785–796
8. Schumacher GA, Beebe G, Kibler RF, et al. Problems of experimental trials of therapy in multiple sclerosis: report by the panel on the evaluation of experimental trials of therapy in multiple sclerosis. *Ann N Y Acad Sci* **1965**;122:552–568
9. Fleiss JL. *Statistical methods for rates and proportions*, 2nd ed. New York: Wiley, **1981**:212–232
10. Landis JR, Koch GG. The measurement of observer agreement for categorical data. *Biometrics* **1977**;33:159–174
11. Yetkin Z, Haughton VM, Papke R, Fischer ME, Rao SM. Multiple sclerosis: specificity of MR for diagnosis. *Radiology* **1991**;178:447–451
12. Braffman BH, Zimmerman RA, Trojanowski JQ, Gonatas NK, Hickey WF, Schlaepfer WW. Brain MR: pathologic correlation with gross and histopathology. 2. Hyperintense white-matter foci in the elderly. *AJNR* **1988**;9:629–636
13. Marshall VG, Bradley WG, Marshall CE, Bhoopat T, Rhodes RH. Deep white matter infarction: correlation of MRI imaging and histopathologic findings. *Radiology* **1988**;167:517–522

Case Report

Iatrogenic Air in the Cavernous Sinus

Mark Adams,[1] Douglas J. Quint,[1] and O. Petter Eldevik[2]

Air in the cavernous sinus may be caused by trauma, surgery, or infection. We report a case that occurred in association with IV injection of contrast material through a catheter into a scalp vein.

Case Report

A 4-month-old girl with increasing irritability, symptoms of an upper respiratory tract infection, and a temperature of 39.4°C was admitted to the hospital for evaluation of possible sepsis and meningitis. Physical and neurologic examinations were unremarkable. Lateral radiographs of the neck, made to exclude a retropharyngeal abscess, were interpreted as suggestive of a retropharyngeal mass. CT per- showed no evidence of a retropharyngeal mass. However, gas was detected bilaterally in the cavernous sinuses on the contrast-enhanced scan (Fig. 1). Although this gas was initially considered consistent with infection, review of the unenhanced CT scan, which had been obtained minutes before the enhanced scan, showed no gas in the cavernous sinuses. As the contrast material had been administered through a scalp vein, the gas was thought to have been unintentionally introduced during the IV injection of the contrast material.

The ultimate diagnosis in this child was Kawasaki disease. No complications attributable to the air in the cavernous sinuses occurred.

Discussion

Gas in the cavernous sinus has been reported in association with infection, trauma, and surgery [1–3]. This gas has been confused with normal fat in the cavernous sinus [4]. Imaging of gas in the cavernous sinus was first reported by Curnes et al. [1] in 1987 in a patient in whom this condition was associated with septic cavernous sinus thrombosis. In 1988, Bartynski and Wang [2] described a patient with air in the cavernous sinus after traumatic fracture of the skull base. To the best of our knowledge, air in the cavernous sinus as a complication of administration of IV contrast material has never been reported.

Iatrogenically introduced air is the most likely source of the gas found in the cavernous sinus in our patient. She had no signs of cavernous sinus thrombosis [1, 5], no history of trauma, and no secondary signs of trauma to the skull base. Gram stains, cultures, and viral indexes of blood, urine, and CSF were negative for infection. The ultimate source of the child's fever was thought to be Kawasaki disease.

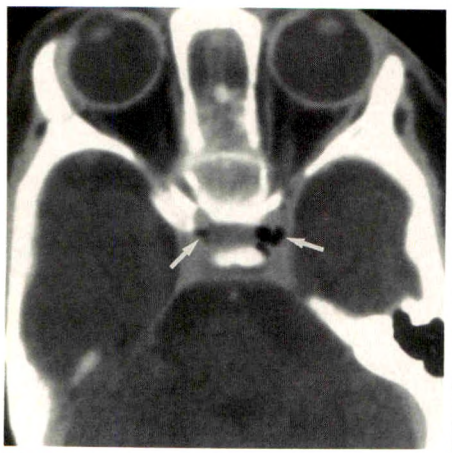
The veins of the head do not have valves, and therefore blood and its contents can travel unimpeded in either direction. The veins of the scalp, forehead, and face and their anastomoses with the cavernous sinuses are well described [6]. In our patient, the most likely pathway for the air embolus introduced through the catheter in the scalp vein was through the anterior superficial temporal veins to the frontal vein to the nasofrontal vein to the superior ophthalmic vein to the cavernous sinus. In another patient with contrast material injected through a scalp vein, we have seen dramatic opacification of this pathway (Fig. 2).

Finally, with inappropriate (i.e., too narrow) windowing of the CT scans at the console or during photography, fat, which

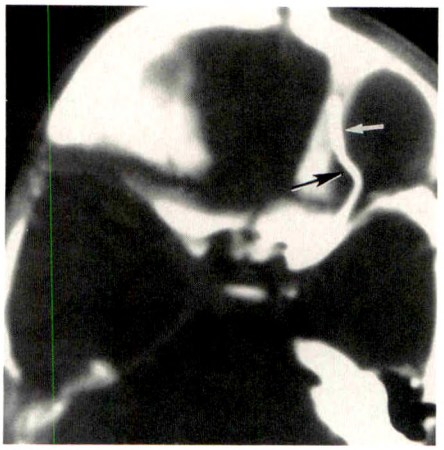
Received November 18, 1991; accepted after revision December 16, 1991.

[1] Department of Radiology, Box 30, Neuroradiology (B1D530H), University of Michigan Hospitals, 1500 E. Medical Center Dr., Ann Arbor, MI 48109-0030. Address reprint requests to D. J. Quint.

[2] Department of Radiology, Ulleval Hospital, Oslo, Norway.



1



2

Fig. 1.—4-month-old girl with fever due to Kawasaki disease. Contrast-enhanced CT scan of head shows gas in cavernous sinuses (*arrows*). Contrast material had been injected through a venous catheter in left side of scalp. Unenhanced scan obtained approximately 20 min earlier showed no cavernous sinus abnormalities.

Fig. 2.—Neonate being evaluated for seizures. CT scan obtained after injection of contrast material through a venous catheter in scalp shows opacification of left superior ophthalmic vein (*arrows*), confirming a route that air may travel from a scalp vein to the cavernous sinus.

can normally be seen in the region of the cavernous sinus in some patients [7], can be mistaken for air [4].

Gas within the cavernous sinus can have serious implications. It can suggest a fracture of the skull base or an infection that requires rapid and definitive management. However, if gas is seen in the cavernous sinus and no clinical explanation is apparent, the study should be repeated within several days before invasive therapy is initiated. This should be done to confirm the finding, as accidentally injected air (i.e., gas not associated with a disease) should be absorbed during this interval.

The finding of iatrogenically introduced air adds to the differential diagnosis of gas in the cavernous sinus and reemphasizes the importance of meticulous technique when contrast material is injected IV.

REFERENCES

1. Curnes JT, Creasy JL, Whaley RL, Scatliff JH. Air in the cavernous sinus: a new sign of septic cavernous sinus thrombosis. *AJNR* **1987**;8:176–177
2. Bartynski WS, Wang AM. Cavernous sinus air in a patient with basilar skull fracture: CT identification. *J Comput Assist Tomogr* **1988**;12: 141–142
3. Frost EAM. Some inquiries in neuroanesthesia and neurological supportive care. *J Neurosurg* **1984**;60:673–686
4. Navarrete ML, Galindo J, Pellicer M, Barcelona S. Cavernous sinus air bubble. *Ear Nose Throat J* **1990**;69:771–772
5. Hirsch WL, Roppolo HMN, Hayman LA, Hinck VC. Sella and parasellar regions: pathology. In: Latchaw RE, ed. *MR and CT imaging of the head, neck, and spine,* 2nd ed. St. Louis: Mosby, **1991**:717
6. Gray H. *Gray's anatomy,* 29th ed. Philadelphia: Lea and Febiger, **1973**: 683–695
7. Stricof DD, Gabrielsen TO, Latack JT, Gebarski SS, Chandler WF. CT demonstration of cavernous sinus fat. *AJNR* **1989**;10:1199–1201

Perspective

Current Role of Cerebral Angiography in the Diagnosis of Cerebrovascular Diseases

Samuel M. Wolpert[1] and Louis R. Caplan[2]

The role of cerebral angiography in the diagnosis of cerebrovascular disease is currently being questioned because of the increasing availability of MR angiography. The purpose of this essay is to place the use of cerebral angiography in perspective in light of these new developments. In patients with atherosclerotic cerebrovascular disease, MR angiography can almost entirely supplant cerebral angiography as a screening procedure in the evaluation of the carotid bifurcation. However, detection of "pseudoocclusion" still requires cerebral angiography for accurate diagnosis. Atherosclerotic stenosis or occlusion of the major intracranial vessels at the base of the brain can be detected with MR angiography, but not as accurately as with cerebral angiography. Furthermore, for detection of more distal occlusions, cerebral angiography is still needed. A number of erroneous concepts about the risks and value of cerebral angiography have prevented its optimal use for patients with cerebrovascular disease. These myths can be countered by applying several rules to optimize the use of cerebral angiography. Subarachnoid hemorrhage is best evaluated with CT followed by detailed cerebral angiography, although MR angiography can be used as a screening test for aneurysms 3 mm or larger. Cerebral angiography is still necessary to confirm the diagnosis of cerebrovascular malformations, although MR angiography is a useful screening test. Cerebral angiography is required for the definitive diagnosis of arteritis, arterial dissection, or fibromuscular dysplasia.

The purpose of this essay is to analyze the current use of conventional cerebral angiography in the diagnosis and management of vascular diseases of the brain. Angiographic technique and the role angiography has in interventional neuroradiology are not considered. Emphasis is given to comparisons between conventional and MR angiography, now that the availability of MR angiography has brought the use of conventional angiography under scrutiny.

Atherosclerotic Cerebrovascular Disease

In patients with atherosclerotic cerebrovascular diseases, much forethought and many hypotheses should precede imaging studies in order to maximize the information provided by the procedure so that effective treatment can follow. Clinicians should classify patients in one of three groups: those with ischemia in the anterior circulation, those with ischemia in the posterior circulation, or those thought to have penetrating artery ischemic disease (lacunar infarction). The vascular occlusive lesions in patients in the first two categories might be intracranial or extracranial, but in the lacunar infarct group the lesions are always intracranial. The probability of extracranial or intracranial disease can be estimated by using demographic variables, medical history, findings from clinical neurovascular examination, and sonography (Table 1). Having determined the arteries likely to be affected, and after careful and detailed consultation, the radiologist and neurophysician make decisions about which vessel should be studied and in which sequence.

Received October 30, 1991; accepted after revision February 3, 1992.
Presented at the annual meeting of the American Roentgen Ray Society, Orlando, FL, May 1992.
[1] Department of Radiology, New England Medical Center Hospitals, Inc., 750 Washington St., Boston, MA 02111. Address reprint requests to S. M. Wolpert.
[2] Department of Neurology, New England Medical Center Hospitals, Inc., Boston, MA 02111.

AJR **159:191–197, July 1992** 0361–803X/92/1591–0191 © American Roentgen Ray Society

TABLE 1: Information Used to Predict the Type of Lesion Before Cerebral Angiography Is Performed

Source of Information	Information Obtained
Demographic data	Race, sex, age
General history	Occurrence of hypertension, diabetes, coronary disease, peripheral vascular disease, and hyperlipidemia
Neurologic history	Nature of symptoms
Vascular examination	Presence of bruits, absent pulses
Neurologic examination	Brain localization
CT and MR imaging	Localization of infarcts
Sonography	Findings on carotid and vertebral artery duplex and continuous-wave and transcranial Doppler imaging

What Information Do Clinicians Seek from Cerebral Angiography and Why?

So that effective therapy can be prescribed, the major goal of cerebral angiography is to place the arterial lesion into one of three groups: complete vascular occlusion, presumably caused by thrombotic formation; severe flow-reducing stenosis; or normal or minor stenosis of a vessel that does not impede flow. Atherosclerotic ulceration can accompany any of these groups. Most atherosclerotic lesions occur in proximal arteries in the intra- and extracranial systems. Currently, we guide treatment differently, depending on the type and location of the disease. For normal or nonstenosing lesions, aspirin or other agents that alter platelet function are prescribed; for tightly stenosed arteries, warfarin sodium (Coumadin) or surgery is used, depending on the location and severity of the neurologic deficit and the condition of the patient. For occluded arteries, thrombolytic therapy or short- or long-term treatment with warfarin sodium is recommended, depending on the time elapsed since occlusion and whether occlusion is embolic or occurs locally in an area of preexisting severe stenosis.

Atherosclerotic disease in the carotid artery contributes to cerebral ischemia or infarction either by diminishing blood flow distal to a carotid stenosis or as a result of embolization of material from the site of stenosis or ulceration [1]. The location of lesions causing cerebrovascular disease in the carotid circulation is usually the carotid bifurcation, but it can vary from the origin of the brachiocephalic arteries to the terminal branches of the intracerebral arteries. The lesions can consist of smooth atheromatous plaques, ulcerated plaques, or mural thrombi; stenoses or occlusions may occur. Although angiography can accurately show stenosis or occlusion, it may not be as accurate in showing ulceration. In one series, ulcers were detected angiographically in only 60% of carotid bifurcations that showed ulceration at surgery [2]. Vertebrobasilar disease contributes to medullary, pontine, or cerebellar ischemia or infarction by causing a decrease in blood flow or by embolization from atheromatous lesions of the vertebral arteries or basilar artery [3].

In two closely allied circumstances, an accurate determination of the status of the internal carotid artery at the bifurcation is critical for immediate management. The first is a decrease of 70–99% in the diameter of the internal carotid artery in patients with recent hemispheric or retinal transient ischemic attacks. In these patients, carotid endarterectomy has been shown to reduce the prevalence of stroke [4]. The second scenario is correctly distinguishing angiographically between occlusion and pseudoocclusion of the internal carotid artery [5]. In patients with pseudoocclusion, the artery appears occluded but actually is patent, a condition called the "string sign" and diagnosed by trickle angiography (the administration of a relatively large volume of contrast medium over approximately 16 sec). Successful endarterectomy in these patients prevents the subsequent development of a stroke. Whereas in both instances carefully performed carotid angiography can show the lesion, it is the severely stenotic but patent internal carotid artery that may be missed on MR angiography.

Atherosclerotic cerebrovascular disease may also occur intracranially, involve the major vessels at the base of the brain or their distal branches, and be present with extracranial carotid disease. Cerebral angiography can show these abnormalities and also focal alterations in cerebral blood flow such as retrograde collaterals, focal areas of slow flow, and reactive hyperemia. Such changes in flow have been seen in 40% of patients with focal cerebral infarction and in 25% of patients with episodes of transient brain ischemia [6]. Some of these changes may be present even without angiographic evidence of an occluded artery.

Many myths and unsubstantiated dogma have affected the use of cerebral angiography for the diagnosis of cerebrovascular diseases and have prevented its optimal use. Understanding these myths can lead to a better understanding of the current role of cerebral angiography. Much of what follows recently appeared in part in the *American Journal of Neuroradiology* in a special article [7] on the use of angiography in patients with occlusive cerebrovascular disease and therefore is only summarized here.

Myths Surrounding the Use of Cerebral Angiography in Atherosclerotic Cerebrovascular Disease

Myth 1: Angiography is indicated only as a prelude to surgery. If surgery is not considered, angiography should not be performed.—Angiography is a diagnostic test and, like all diagnostic tests, is used to help determine what is wrong with the patient. It should be performed when the diagnosis is unclear and the degree of brain damage is not so severe that

any treatment would be futile. If the diagnosis can be established as accurately with less invasive technology (e.g., CT, MR imaging, sonography, or hematologic and cardiac tests), then angiography is unnecessary. Rational treatment depends on accurate diagnosis. When the diagnosis is uncertain, physicians must guess at the best choice of therapy; they might err by omitting a treatment that may be helpful or use treatments that are not indicated and could be harmful.

Myth 2: The cranial circulation is an open net. All the large extracranial arteries must be visualized in patients with ischemia, because disease at any one locus can lead to ischemia in any other.—In general, the hemodynamic theory of brain ischemia has been deemphasized by an accumulation of data that show that most brain infarcts are due to thromboembolism. Ringelstein et al. [8] were able to show that most patients with occlusions of the internal carotid artery in the neck had infarcts due to emboli. Angiography often showed "occlusio supra occlusionem," that is, distal artery-to-artery emboli. Fieschi et al. [9] showed that early angiography (within 6 hr of the onset of signs and symptoms) in patients with acute ischemic strokes showed complete arterial occlusions in 76% of patients, and most of the lesions (66%) were intracranial. In a study on the use of tissue plasminogen activator in patients with acute brain ischemia, angiography showed arterial occlusions thought to be due to atherosclerotic disease in 112 (80%) of 139 patients studied within 8 hr after the onset of signs and symptoms [10]. Most ischemic strokes were due to artery-to-artery or to cardiac-origin embolisms, a conclusion also evident from prospective series of cases collected by the Harvard Stroke Registry [11] and the Stroke Data Bank [12].

With neuroimaging tests now able to show the ischemic region in the brain, clinical and imaging information usually is sufficient to locate the arterial system involved. Clinicians need detailed information about the arteries supplying this ischemic region in order to make therapeutic decisions. Occlusive lesions at other sites are nearly always incidental. In selected cases, it may be useful to opacify other arteries, but routine opacification of all the large arteries is not warranted. Sonography (or MR angiography) can help supply information about other sites, and ordinarily should be performed before angiography if the condition is not acute.

Myth 3: The aortic arch must be opacified in all patients with ischemia in order to see all arteries and ensure that proximal occlusive lesions near the arch are not missed.—The two main reasons not to routinely study the arch are because detection of clinically significant lesions is extremely low and an added systemic risk exists with arch opacification, which uses large volumes of contrast medium. When Akers et al. [13] studied the results of arch and four-vessel angiography in 1000 consecutive patients, only six patients had hemodynamically significant intrathoracic vascular disease. Three of these lesions likely would have been discovered had selective angiography alone been performed. The risks involved in arch injections are not negligible. An arch injection is usually performed with 40–50 ml of contrast material (a lower volume is adequate if digital subtraction angiography is used). Cardiac overload and renal toxic effects can result. The details of the risks are reported in our previous article [7].

Myth 4: Angiography is not indicated for patients with vertebrobasilar disease. There are no surgical or treatment implications, and the study is dangerous.—A wide variety of surgical procedures have been performed on the posterior circulation arteries in patients with ischemic disease of the posterior circulation [14]. These include bypass procedures at the origin of the vertebral artery and endarterectomy and bypass procedures for lesions in the distal extracranial vertebral artery and in the proximal intracranial vertebral artery. Anticoagulation is also frequently prescribed and should be used only for certain vascular lesions such as severe stenosis of the main vertebral or basilar arteries [3, 15]. Analysis of clinical signs, MR imaging, and continuous-wave and transcranial Doppler (TCD) sonography can provide considerable useful data about occlusive lesions of the posterior circulation, but all have limitations [16]. Angiography by selective catheterization of the subclavian or vertebral arteries with imaging of the intracranial vertebral and basilar arteries often is needed to make important therapeutic decisions.

Angiographers are reluctant to study patients with vertebrobasilar disease because coma, quadriparesis, or even a locked-in state develops in some patients within days or hours after angiography. However, no data are available to support the inference that vertebral angiography is more risky than carotid angiography if soft 4- or 5-French catheters are used.

Myth 5: Patients should not have angiography in the acute stage of ischemic stroke because the risk associated with the procedure is higher at that time. Patients with deficits, especially if severe, have a higher risk. Angiography should be delayed, especially in ill patients.—We know of no data to support the idea that arteriography performed during acute stages of stroke is more dangerous or that complications are related to the severity of neurologic deficit. We disagree with the concept that angiography should not be carried out in the setting of an acute stroke. We have already cited the studies of Fieschi et al. [9] and del Zoppo et al. [10] that documented the high percentage of occluded arteries after angiography during the first 6–8 hr after the onset of signs and symptoms. In the report of the Harvard Stroke Registry, most emboli were no longer visualized 48 hr after the onset of stroke [11]. Treatment decisions often need to be made quickly. If thrombolytic agents are to be used, they need to be given within 8 hr and probably sooner.

When and How to Use Cerebral Angiography in Atherosclerotic Cerebrovascular Disease

Having dealt with some of the myths of cerebral angiography in patients with cerebrovascular diseases, we set out seven rules for proper study. Some of this material has been previously published in a book chapter [17]: (1) Angiography is indicated only when it is likely to answer clinically relevant questions. (2) Neuroimaging (CT and/or MR) and noninvasive sonography should be performed first. (3) During angiography, first study the vessel supplying the ischemic zone. (4)

Decisions on imaging or opacifying a vessel should be made sequentially. (5) Minimize the amount of contrast material injected during angiography and the length of the procedure. (6) Studies that provide optimal and clinically useful data require close cooperation between the clinicians and the angiographers. (7) Examine the patient frequently between injections in order to detect problems or complications as soon as possible.

MR Angiography vs Cerebral Angiography in Patients with Atherosclerotic Cerebrovascular Disease

What is the role of MR angiography in examining patients with suspected extracranial atherosclerotic carotid disease? MR angiography is still not as good as cerebral angiography for showing ulceration or plaque formation. When vessel tortuosity, turbulence, or very slow flow is present, artifacts may cause problems, although significant improvements in the technique are decreasing their frequency [18]. Studies on MR angiography of patients with atherosclerotic lesions of the carotid bifurcation have shown agreements of between 70% [19] and 100% [20, 21] when findings on MR angiograms are correlated with those on cerebral angiograms. Thus, we think that MR angiography can be considered an excellent screening test for patients with suspected cervical carotid disease (the addition of duplex extracranial carotid sonography and TCD imaging improves the accuracy of the noninvasive evaluation [22]). Although MR angiography can show stenotic and occlusive lesions of the vertebrobasilar system, studies comparing it with vertebral angiography have not yet been done.

MR angiography has also been shown to be useful in the evaluation of intracranial atherosclerotic disease; intracranial occlusions or severe stenoses of major vessels supplying areas of infarction have been seen with the three-dimensional time-of-flight technique [23], and either two-dimensional time-of-flight studies with presaturation sequences [24] or three-dimensional phase-contrast studies [25] can show alterations in flow direction and velocities in different arteries at the base of the brain. More distal occlusions involving smaller arteries are difficult to detect with MR angiography because of spatial resolution problems. In patients with acute stroke in whom accurate visualization of occlusion of the intracranial (and extracranial) arteries is necessary before IV thrombolytic agents can be administered, MR angiography has shown occlusions of the major intracranial arteries [23], but the number of detected stenosed or occluded arteries is not as high as that in patients examined with cerebral angiography [10]. Rapid arteriovenous shunting (which may follow an acute stroke) can also be detected by phase-angiographic techniques [25], but the determination of leptomeningeal collateral circulation remains a problem. Thus, the usefulness of MR angiography is continuing to approach that of carotid angiography. However, the extracranial arteries and all the intracranial arteries cannot be imaged by MR angiography in a reasonable time, artifacts still occur, and in tortuous systems overlapping arteries may be a problem. Considerations of technology, personnel, and time therefore will limit the number of patients with cerebrovascular disease that can be studied and the time available for each patient. Catheter angiography thus remains a key investigative test to detect, localize, and quantify most atherosclerotic cerebrovascular lesions.

Aneurysms

What Information Is Needed by the Neurosurgeon for Adequate Treatment of Patients?

Although cerebral ischemia is usually the province of the neurologist, in the United States, patients with intracranial hemorrhage are most often admitted to neurosurgical units. Needless to say, the level of cooperation between the neurosurgeon and radiologist must be equivalent to that between the neurologist and radiologist. Many of the rules and guidelines given here for treatment of the patient with ischemia also apply to patients with intracranial hemorrhage caused by ruptured aneurysms; however, the angiographic requirements are often more explicit. When patients are admitted to the hospital with a suspected brain hemorrhage, CT is the first and most appropriate imaging test to show the presence of hemorrhage. If the scan shows no abnormality, a lumbar puncture should be done to detect either a small subarachnoid hemorrhage (SAH) or meningitis. If a SAH is present, and as long as the patient is not comatose, immediate cerebral angiography is usually advised. The CT scan may show more subarachnoid blood in one location than in another or may show an intracerebral hematoma in addition to the SAH, information that the angiographer can use to decide which vessel should be injected first. The pattern of SAH should influence the thoroughness of the angiographic evaluation and the probability of detecting an aneurysm. For instance, if blood is found in the interhemispheric fissure, an aneurysm, usually from the anterior communicating artery, is almost certainly present. If the pattern of blood is more diffuse or is localized to the perimesencephalic cistern, an aneurysm is less likely to be found [26, 27].

Angiography of the anterior and posterior circulation (if the patient's condition permits) should continue until all potential sources of bleeding have been adequately opacified. If the results of four-vessel angiography (together with oblique views) are normal (an aneurysm will be seen in approximately 85% of patients with SAH after high-quality four-vessel angiography [28]), we generally advise that angiography be repeated 2 weeks later as a certain small percentage of aneurysms (depending on the thoroughness of the initial angiography) will be found on the second angiogram. We rarely repeat angiography more than once. We have found that aneurysms are detected on the second angiogram in less than 5% of patients (others have found them in 16% of patients [27, 29]), but we nevertheless obtain a second angiogram because of the devastating effects of allowing patients with treatable aneurysms to be left untreated. Even when one aneurysm is found, a search for other aneurysms is mandatory because multiple aneurysms occur in approximately 20% of patients. Once an aneurysm has been defined, oblique views to show the neck of the aneurysm so that effective surgical clipping can follow may be needed. An

aneurysm may not be seen for several reasons: (1) arterial spasm, which temporarily seals off the neck; (2) inadequate technique [30] (oblique views should also be obtained in the workup when abnormalities are questionable); (3) thrombosis of the aneurysm, providing a spontaneous cure; and (4) observer error, particularly with multiple lesions or tortuous vessels.

When an aneurysm is detected at the circle of Willis, the patency of all components of the circle should be studied. For instance, the patency of the anterior communicating artery can indicate whether one A1 segment of the anterior cerebral artery can be safely surgically occluded, and the knowledge that the posterior communicating arteries are patent can help the surgeon decide whether the P1 segment can be safely surgically occluded. Some of this information can be obtained only by using angiography with manual compression of one or other carotid artery and injection of the opposite carotid or vertebral arteries. If the vertebrobasilar circulation is compromised by vascular disease, knowledge of the internal and external carotid contributions to the basilar artery is critical before surgery for aneurysms in the posterior circulation is done [31, 32].

If moderate or severe spasm is seen on the initial angiogram, whether an aneurysm is seen or not, we delay further angiography because the patient is not an immediate surgical candidate and angiography will have to be repeated later. Depending on the patient's condition, we advise that additional studies be done after approximately 2 weeks. If spasm is not present, angiography is completed.

Usually we do not repeat angiography to assess the effectiveness of clip placement except after difficult surgery, in which case angiography may be necessary to confirm adequate clipping of the aneurysmal neck. Unusual oblique views may have to be devised to overcome the obscuring effects of the clip if the clip overlies the neck of the aneurysm. Angiography will also have to be done if inadvertent surgical occlusion of a major artery or branch is suspected, and also if multiple aneurysms or associated arteriovenous malformations (AVMs) are present and only the primary offender has been treated. Follow-up angiography will also be necessary if, after surgery, vasospasm is suspected; in these cases MR imaging or MR angiography is contraindicated unless a nonferromagnetic clip has been applied. TCD imaging or single-photon emission CT (SPECT) can be useful in examining patients during their clinical course. Vasospasm causes increased blood-flow velocities, which can be detected with TCD imaging, and stable xenon-enhanced CT or SPECT shows decreased blood flow when vasoconstriction is present [33–36].

Role of MR Angiography in Examining Patients with Cerebral Aneurysms

Although time-of-flight MR angiography can show cerebral aneurysms greater than approximately 3–4 mm in diameter, it does not show aneurysms with extremely slow flow, and the size of aneurysms containing turbulent flow is underestimated [37]. Three-dimensional phase-contrast angiography can also show aneurysms as small as 3 mm in diameter and is better than time-of-flight studies for the detection of slow flow [25]. Although most ruptured aneurysms are larger than 3 mm in diameter, even tiny aneurysms can cause devastating hemorrhages [38]. No studies have been done yet on the comparative values of MR angiography and cerebral angiography in the evaluation of patients with SAH and suspected intracranial aneurysms, and until such data are known, cerebral angiography should continue to be used. MR angiography can then be used as a screening test for suspected aneurysms in patients without SAH.

Cerebral Vascular Malformations

One of the most significant benefits of MR imaging has been in the diagnosis and classification of angiomatous malformations that can cause brain hemorrhage. In addition to angiomas such as AVMs, venous angiomas and cavernous angiomas can be diagnosed on the basis of MR imaging. Once an angioma is suggested on the basis of MR imaging, either by direct visualization of the lesion or by the presence of an intracerebral hemorrhage, treatment will depend on the accuracy of the diagnosis and further studies may become necessary. AVMs can be diagnosed on the basis of findings on MR imaging, MR angiography, or cerebral angiography. Three-dimensional time-of-flight MR angiography can accurately define the nidus but incompletely depicts the hyperdynamic afferent arteries [39]; three-dimensional phase-contrast MR angiography can show blood velocity in different vessels and also directly depict collateral flow to vascular lesions [25]. Angiography on the other hand is used to confirm the presence of an AVM; accurately show the AVM's angioarchitecture and its location; and guide therapy such as surgical excision, interventional angiographic obliteration, or radiotherapy. Angiography also is used to show the size and location of the AVM nidus, define the venous drainage, and detect associated aneurysms (either on the primary feeding arteries of the AVM or in the circle of Willis; seen in up to 16% of patients [40]). When cerebral angiography is performed, all potential arterial feeders to the AVM must be examined. The location of the lesion on CT or MR images will guide the angiographer in deciding the order in which the arteries need to be opacified. Also any AVM on the surface of the brain may have a supply partly or exclusively arising from the external carotid system, and therefore selective external carotid angiography will be necessary. Some AVMs are not seen on angiography and thus are considered occult or cryptic. This is probably because of their small size or thrombosis within the malformation [41].

Most cavernous angiomas usually do not opacify on angiography, although early or widened veins; stains, puddling, or blushes; or slight neovascularity have been reported [42]. Surgical excision of cavernous angiomas has been recommended for patients with intractable seizures and for those with previous gross hemorrhage because the lesions are likely to hemorrhage again; the outcome is more favorable if the patients are treated surgically than if they are treated conservatively [43]. Venous angiomas, however, are less likely

to bleed and should not be resected because surgery may also compromise vital intracerebral venous drainage [44]. Nevertheless, angiography may be needed for patients with suspected venous angiomas to confirm the medullary veins and venous tributaries.

Other Vascular Lesions

Cerebral angiography can show regions of focal arterial narrowing that are associated with arteritis, migraine, and drug abuse. Arteritis can be due to collagen vascular disease or radiation damage or be present in patients who have phakomatoses [45]. The affected arteries may be narrowed or dilated, and the abnormalities are focal, multifocal, or disseminated. In cranial arteritis, the supraclinoid segments of the internal carotid artery and adjacent proximal anterior, middle, and posterior cerebral arteries are narrowed; a moyamoya appearance or a vascular telangiectatic mesh of arteries is a frequent accompaniment. Meningitis usually involves the basal arteries, which become narrowed. Young women who use high-estrogen oral contraceptive agents may have arterial abnormalities, including occlusions of large and small intracranial vessels and luminal changes. The collagen vascular diseases can affect both the basal and the leptomeningeal arteries. In patients with lupus erythematosus, periarteritis nodosa, and temporal (giant-cell) arteritis, multiple peripheral aneurysms may be seen in addition to luminal irregularities. Radiation-induced arteritis usually involves the small arteries and may not be evident on arteriography. However, large-vessel stenoses with or without a moyamoya pattern and diffuse arteritis may occur and can be shown by angiography [46].

Not all patients with stroke have atheromatous thromboembolic disease; in some patients, carotid or vertebral arterial dissections, fibromuscular dysplasia, or aneurysms with emboli may be the cause of the ischemic event. Carotid or vertebral artery dissections can be suggested on the basis of CT or MR findings, but cerebral angiography is the definitive confirmatory test, which characteristically shows a tapering stenosis with or without an aneurysmal pouch [47]. Rapid angiography at five frames per second or faster may be necessary to accurately show the extremely rapid flow through a caroticocavernous fistula or aneurysm of the vein of Galen.

MR angiography is an excellent technique for the demonstration of sinovascular occlusive disease. If, however, any uncertainty develops about the patency of the dural venous sinuses, cerebral angiography may still be necessary. This is particularly important in patients with tumors at the skull vertex, for which surgical planning depends on the patency of the sagittal sinus.

Although in this essay interventional neuroradiology has not been considered, certain diseases, such as intractable epistaxis, can be treated most effectively by simple endovascular techniques that can be used by noninterventionalists. Furthermore, thrombolytic therapy for acute brain ischemia may in the future be carried out best through the intraarterial delivery of thrombolytic agents such as tissue plasminogen activator, streptokinase, or urokinase [48]. Early research on this type of treatment has yielded favorable results, and, if ultimately the treatment is found to be beneficial, the need for catheter angiography will increase, and it will probably be carried out by both interventional and noninterventional neuroradiologists.

Clearly, cerebral angiography still has many indications. The technical challenge, the skills of performance, and the art of diagnosis still exist. Cerebral angiography has not yet followed pneumoencephalography into the folklore and history of neuroradiology. Undoubtedly MR angiography will continue to improve, and the need for cerebral angiography will continue to decline in the 1990s. Some prophesy that in the future cerebral angiography will be needed only for interventional neuroradiology. We think that day has not yet arrived, and although we wish we could dispense with our lead aprons, we are not yet ready to abandon or forsake our catheters, needles, and guidewires.

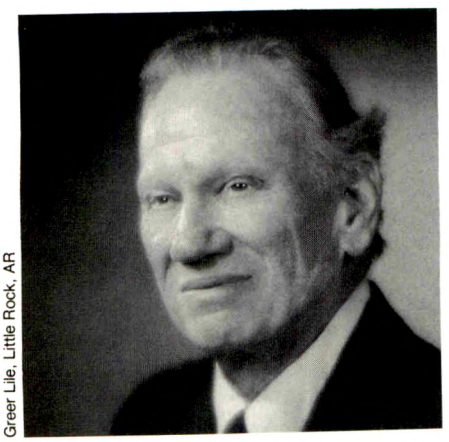
REFERENCES

1. Health and Public Policy Committee, American College of Physicians. Diagnostic evaluation of the carotid arteries. *Ann Intern Med* **1988**;167:119–123
2. Edwards JH, Kricheff II, Riles T, Imparato A. Angiographically undetected ulceration of the carotid bifurcation as a cause of embolic stroke. *Radiology* **1979**;132:369–373
3. Caplan LR. Vertebrobasilar disease: time for a new strategy. *Stroke* **1981**;12:111–114
4. North American Symptomatic Carotid Endarterectomy Trial Collaborators. Beneficial effect of carotid endarterectomy in symptomatic patients with high-grade stenosis. *N Engl J Med* **1991**;325:445–453
5. Ammar AD, Turrentine MW, Farha SJ. The importance of arteriographic interpretation in occlusion or pseudo-occlusion of the carotid artery. *Surg Gynecol Obstet* **1988**;167:119–123
6. Houser OW, Sundt TM, Holman CB, et al. Atheromatous disease of the carotid artery: correlation of angiographic, clinical, and surgical findings. *J Neurosurg* **1974**;41:321–331
7. Caplan LR, Wolpert SM. Angiography in patients with occlusive cerebrovascular disease: views of a stroke neurologist and neuroradiologist. *AJNR* **1991**;12:593–601
8. Ringelstein EB, Zeumer H, Angelou D. The pathogenesis of stroke from internal carotid artery occlusion: diagnostic and therapeutical implications. *Stroke* **1983**;14:867–875
9. Fieschi C, Argentino C, Lenzi GL, et al. Clinical and instrumental evaluation of patients with ischemic strokes within the first six hours. *J Neurol Sci* **1989**;91:311–322
10. Del Zoppo GJ, Poeck K, Pessin MS, et al. Recombinant tissue plasminogen activator in acute thrombotic and embolic stroke. *Ann Neurol* **1992** (in press)
11. Mohr JP, Caplan LR, Melski J, et al. The Harvard Cooperative Stroke Registry: a prospective registry. *Neurology* **1978**;28:754–762
12. Foulkes MA, Wolf PA, Price TR, et al. The Stroke Data Bank: design, methods, and baseline characteristics. *Stroke* **1988**;19:547–554
13. Akers DL, Markowitz IA, Kerstein MD. The value of aortic arch study in the evolution of cerebrovascular insufficiency. *Am J Surg* **1987**;154:230–232
14. Berguer R. Surgical indications for reconstruction of vertebral arteries. In: Berguer R, Caplan LR, eds. *Vertebrobasilar arterial disease.* St. Louis: Quality Medical, **1992**:201–210
15. Caplan LR. Anticoagulation for cerebral ischemia. *Clin Neuropharmacol* **1986**;9:399–414
16. Tettenborn B, Estol C, DeWitt LD, et al. Accuracy of transcranial Doppler in the vertebrobasilar circulation. *J Neurol* **1990**;237:159
17. Caplan LR, Wolpert SM. Conventional cerebral angiography in occlusive cerebrovascular disease. In: Wood JH, ed. *Cerebral blood flow: physiolog-*

ical and clinical aspects. New York: McGraw-Hill, **1987**:356–384
18. Masaryk TJ, Modic MT, Ruggieri PM, et al. Three-dimensional (volume) gradient-echo imaging of the carotid bifurcation: preliminary clinical experience. *Radiology* **1989**;171:801–806
19. Litt AW, Eidelman EM, Pinto RS, et al. Diagnosis of carotid artery stenosis: comparison of 2DFT time-of-flight MR angiography with contrast angiography in 50 patients. *AJNR* **1991**;11:449–456
20. Masaryk AM, Ross JS, DiCello MC, Modic MT, Paranadi L, Masaryk TJ. 3DFT MR angiography of the carotid bifurcation: potential and limitations as a screening examination. *Radiology* **1991**;179:797–804
21. Heiserman JE, Drayer BP, Fram EK, et al. Evaluation of carotid stenosis: clinical efficacy of two dimensional time-of-flight MR angiography. *Radiology* **1992**;182:761–768
22. Polak JF, Bajakian RL, O'Leary DH, Anderson MR, Donaldson MC, Jolesz FA. Detection of internal carotid artery stenosis: comparison of MR angiography, color Doppler sonography, and arteriography. *Radiology* **1992**;182:35–40
23. Warach S, Li W, Rinthal M, Edelman RR. Acute cerebral ischemia: evaluation with dynamic contrast-enhanced MR imaging and MR angiography. *Radiology* **1992**;182:41–47
24. Edelman RR, Mattle HP, O'Reilly GV, et al. Magnetic resonance imaging of flow dynamics in the circle of Willis. *Stroke* **1990**;21:56–65
25. Huston J, Rufenacht DA, Ehman RL, Wiebers DO. Intracranial aneurysms and vascular malformations: comparison of time-of-flight and phase-contrast MR angiography. *Radiology* **1991**;181:721–730
26. Rinkel GJE, Wijdicks EFM, Vermeulen M, et al. Nonaneurysmal perimesencephalic subarachnoid hemorrhage: CT and MR patterns that differ from aneurysmal rupture. *AJNR* **1991**;12:829–834
27. Iwanaga H, Kakai S, Ochia C, et al. Ruptured cerebral aneurysms missed by initial angiographic study. *Neurosurgery* **1990**;27:45–51
28. Kassell NF, Torner JC, Jane JA, et al. The international cooperative study on the timing of aneurysm surgery. Part 2: Surgical results. *J Neurosurg* **1990**;73:37–47
29. Perret G, Nishioka H. Report on the cooperative study of intracranial aneurysms and subarachnoid hemorrhage. Section 4: Cerebral angiography, an analysis of the diagnostic value and complications of carotid and vertebral angiography in 5,484 patients. *J Neurosurg* **1966**;25:98–114
30. Perrett LV, Bull JWD. The accuracy of radiology in demonstrating ruptured intracranial aneurysms. *Br J Radiol* **1959**;32:85–92
31. Pelz DM, Vinuela F, Fox AJ, Drake CG. Vertebrobasilar occlusion therapy of giant aneurysms: significance of angiographic morphology of the posterior communicating arteries. *J Neurosurg* **1984**;60:560–565
32. Pritz MB. Evaluation and treatment of aneurysms of the vertebral artery: different strategies for different lesions. *Neurosurgery* **1991**;29:247–256
33. Fayad PB, Brass LM. Single photon emission computed tomography in cerebrovascular disease. *Stroke* **1991**;22:950–954
34. Yonas H, Good WF, Gur D, et al. Mapping cerebral blood flow by xenon-enhanced computed tomography: clinical experience. *Radiology* **1984**; 152:435–442
35. Caplan LR, Brass LM, De Witt LD, et al. Transcranial Doppler ultrasound: present status. *Neurology* **1990**;40:696–700
36. Aaslid R, Huber P, Nornes H. A transcranial Doppler method in the evaluation of cerebrovascular spasm. *Neuroradiology* **1986**;28:11–16
37. Edelman RR, Mattle HP, Atkinson DJ, Hoogewoud HM. MR angiography. *AJR* **1990**;154:937–946
38. Weir B. Anatomy. In: Weir B, ed. *Aneurysms affecting the nervous system.* Baltimore: Williams & Wilkins, **1987**:308–363
39. Marchal G, Bosmans H, Van Fraeyenhoven L, et al. Intracranial vascular lesions: optimization and clinical evaluation of three-dimensional time-of-flight MR angiography. *Radiology* **1990**;175:443–448
40. Miyasaka K, Wolpert SM, Prager RJ. The association of intracerebral aneurysms, infundibula, and intracranial arteriovenous malformations. *Stroke* **1982**;13:196–203
41. Becker DH, Townsend JJ, Kramer RA, Newton TH. Occult cerebrovascular malformations: a series of 18 histologically verified cases with negative angiography. *Brain* **1979**;102:249–287
42. Simard JM, Garcia-Bengochea F, Ballinger WE, Mickle JM, Quisling RG. Cavernous angioma: a review of 126 collected and 12 new clinical cases. *Neurosurgery* **1986**;18:162–172
43. Robinson JR, Awad IA, Little JR. Natural history of cavernous angioma. *J Neurosurg* **1991**;75:709–714
44. Garner TB, Del Curling O, Kelly DL, Laster DW. The natural history of intracranial venous angiomas. *J Neurosurg* **1991**;75:715–722
45. Burrows EH, Leeds NE. Vascular abnormalities. In: Burrows EH, Leeds NE, eds. *Neuroradiology.* New York: Churchill-Livingstone, **1981**:75–117
46. Brant-Zawadzki M, Anderson M, DeArmond SJ, et al. Radiation-induced large intracranial vessel occlusive vasculopathy. *AJR* **1980**;134:51–55
47. Anson J, Crowell RM. Cervicocranial arterial dissection. *Neurosurgery* **1991**;29:89–96
48. Zeumer H, Grzyska U, Freitag HJ, Neunzig HP. Local intraarterial fibrinolysis in acute vertebrobasilar occlusion: recent results and technical developments. *Neuroradiology* **1989**;31:331–336

Memorial

Edwin F. Gray, 1912–1991



Greer Life, Little Rock, AR

On June 1, 1991, Edwin F. Gray was killed in a tragic aircraft accident, which also resulted in the deaths of his wife, Ruth; his daughter, Jan Love; and his daughter's husband, Earl Love.

Ed received his medical degree from the University of Arkansas School of Medicine and served his residency in radiology at Columbia-Presbyterian Hospital in New York, studying with Ross Golden. He became a diplomate of the American Board of Radiology in 1940. After 2 years of private practice, 1 in Terre Haute, IN, and 1 in Flint, MI, Ed began a long tour of army duty during World War II (1942–1946). Much of this time was spent in the Pacific arena.

After his tour of duty, he returned to his home in Little Rock, AR, to begin a career in private practice. I joined Ed in private practice in 1950, and we remained together until his retirement in 1985. By this time, the practice had grown to an 18-person group.

Ed was active in medical affairs. He was a member of the Pulaski County Medical Society, the Arkansas Medical Society, the American Medical Association, the Radiological Society of North America, the Arkansas chapter of the American College of Radiology, and the American Roentgen Ray Society. He was elected to fellowship in the American College of Radiology in 1950 and served as president of the Pulaski County Medical Society in 1955.

Ed and Ruth took part in many civic organizations and functions. He was particularly active in Kiwanis Club, serving as president of the Little Rock club and as lieutenant governor of the Missouri-Arkansas district.

An important bond in the Grays' lives was their love of flying. Both Ed and Ruth were accomplished pilots, holding advanced ratings. Ed was an active member in the Flying Physicians Club. Another bond stemmed from their love of tennis.

Friends and relatives will long remember the warmth and enthusiasm that Ed and Ruth unfailingly demonstrated. All who knew them grieve over the loss of this lovely, close-knit family.

Joseph D. Calhoun
Little Rock, AR 72205

Computers in Radiology

A PACS-Based Interactive Teaching Module for Radiologic Sciences

Shantanu Sinha,[1] Usha Sinha, Hooshang Kangarloo, and H. K. Huang

This article describes an interactive teaching module, linked to a picture archiving and communications system (PACS) data base, for teaching radiology. The module is currently tailored to MR images but can be adapted to any other imaging technique. An algorithm has been developed that allows the use of MR images acquired with routine clinical protocols and stored in the data base to yield, in real time, images at any other arbitrary TE and TR. In the browse mode, the user can study either the effect of different scan parameters or clinical cases on synthesized or acquired images. The quiz mode has multiple-choice questions and answers, accompanied by images. In the teaching mode, the instructor has access to the clinical data base and WRITE privileges for setting up the browse or quiz mode.

The module achieves considerable flexibility when linked to the PACS, with access to all archived images and the ability to subsequently synthesize MR images at arbitrary TE and TR values in real time. The module is also "dynamic" in character, in that the instructor can easily add new cases and comments to the teaching files, both to enhance its clinical aspects and to reflect advances in technology.

Training and education in radiology depends to a large extent on visual presentations. The traditional methods of classroom instruction are based on imparting information to students, usually without significant interaction between student and instructor. Self-instruction of residents through the use of teaching files relies on self-motivation and does not guide the student through the learning process. An additional problem facing radiology departments is that immediate readouts, required for optimum patient care, prohibit gathering them into one or two sessions per day for the purpose of teaching residents. Another issue of concern is the rapid growth of technology, which requires teaching new and changing material to students on an ongoing basis. The advent and growth of MR imaging is a case in point. It is a rapidly evolving methodology, and its continuously improving technology is a challenge in terms of training residents. The problem is compounded by the fact that time on the MR scanner is at a premium, and availability for purposes of instruction is limited.

Several attempts have been made to introduce computers and computer graphics for the implementation of instructional modules to enhance teaching radiology. Starkschall et al. [1] developed a computer-aided instructional module for teaching radiation therapy physics, presenting the student first with the instructional material then with a set of multiple-choice questions. A similar module was written by Goldberg et al. [2], with the added facility of showing a limited set of radiologic images of sufficiently good quality on easily available hardware. Posteraro et al. [3] implemented the MR-Tutor, in which the user, on entering the desired value of TE, TR, and TI, is shown graphically the relative MR signal intensities of two tissues in a spin-echo and inversion-recovery sequence. A hand-held teaching aid illustrating similar MR concepts as above has been developed by Malko and Nelson [4]. Rundle et al. (presented at the International Society for Optical Engineering meeting, February 1990) have a more comprehensive MR tutorial, in which contrast variation is shown by synthesizing images from an original data set of spin echoes at user

Received October 29, 1991; accepted after revision February 12, 1992.

[1] All authors: Department of Radiological Sciences, PU54, School of Medicine, University of California, Los Angeles, Center for the Health Sciences, 10833 Le Conte Ave., Los Angeles, CA 90024-1721. Address reprint requests to S. Sinha.

AJR **159:199–205, July 1992** 0361–803X/92/1591–0199 © American Roentgen Ray Society

set values of TE, TR, and flip angle. Clinical images were not used in the tutorial, possibly because the module was not linked to a picture archiving and communications system (PACS), and contrast variation studies were therefore confined to normal tissues.

We describe the design and development of an interactive teaching module (ITM) for radiologic purposes with the following three objectives. First, the teaching module should require no additional scans other than the routine clinical examinations (for demonstrating contrast variation by using image synthesis), thus eliminating additional time and expense. We developed an algorithm that allows us to determine the exact solution for intrinsic MR image parameters T1, T2, and proton density (hereafter referred to as parametric images) from an original set of source images acquired under routine clinical protocol. The analytic nature of the solutions kept to a minimum the computational time required to determine the parametric images, from which the program could subsequently synthesize MR images at arbitrary TE and TR values set by the student. Second, the module should allow interaction between the student and the computer by using images stored in a digital format and be comprehensive enough to eliminate the need for duplicative analog films. These requirements necessitate connecting the ITM to a large PACS data base, which contains a variety of teaching material with pathologic conditions. Since our algorithm does not need other than routine images, we could tap into the very large data base of clinical images that are stored in our departmental PACS. Finally, the module should be "dynamic" in character. It should be easy to edit and update teaching files, both in terms of pathologic cases as well as normal images (used for illustration of the physical principles underlying the constantly evolving technology of MR). The instructor should even be able to expand the module to include other radiologic imaging techniques.

System Description

ITM for radiologic imaging is written in C language and runs on a SUN 4/370 computer (Sun Microsystems Inc., Mountain View, CA), operating in a UNIX environment. The 16-bit MR images are displayed on the SUN 8-bits per pixel, gray-scale monitor; text and the user interface (a control panel) are simultaneously displayed on two subwindows. The computer is linked by the Ethernet communication protocol to the PACS system; that is, to the data base servers (where all text information is stored) and to two Kodak (Eastman Kodak Co., Rochester, NY) ADL 6800 optical disk libraries (where images are stored). It is possible for both text and image data to be retrieved from the PACS through the PACS data base management system and shown directly from the module. However, to increase the speed of retrieval of images and to provide a stand-alone basis for the tutorial, the required images are retrieved from the global PACS system and stored in a local magnetooptical disk. The PACS system has been discussed in detail elsewhere [5].

The ITM supports two types of users: the "student" with only read privileges to the local data base, and the "instructor/radiologist" with both READ and WRITE privileges to the local data base and read privileges to the global data base. Both of these users have access to the browse and quiz modes of the module; where the instructional material and questions based on that material are stored. The instructor has access to the teach mode, where the contents of the first two modes can be updated or modified. Details on these modes are described later.

Image Synthesis

A brief description of the method of image synthesis used by us is included since it is a central aspect of our tutorial. A detailed description is awaiting publication (Sinha S, Sinha U, Kangarloo H, Huang HK, unpublished data). The intensity of each pixel of an MR image is determined by the inherent intrinsic parameters, T1 (the spin-lattice relaxation time), T2 (the spin-spin relaxation time), proton density, and the operator-set extrinsic parameters: TE and TR. Our aim was to acquire the source data set (required for synthesis) with scan parameters (TE and TR) used in routine clinical settings. From these source images, the intrinsic parameters of an MR image, T1, T2, and proton density, can be calculated at each pixel. Having generated these parametric images, one would then, in the browse mode, be able to synthesize images at any arbitrary TE and TR for a number of clinical cases.

The solution for T2 is relatively straightforward and is given by the division of the signal intensities at each pixel location of two images acquired at the same TR, TR_1, but two different TEs, TE_1 and TE_2. The calculation for T1 is not as straightforward, since a solution is not obtained by a simple division, as in the case of T2. Earlier methods involved the use of least-square fitting techniques, which obviously do not yield exact solutions for T1 and took substantial computational time. However, a judicious choice of TRs such that $(TR_1 - TE_1) = 3(TR_3 - TE_3)$, where TR_1 and TR_3 are the TRs of two different images acquired with the same TE ($TE_1 = TE_3$), yields an analytic solution of T1. This alternative method of computing T1 yields both exact solutions and decreases the computational time. The source data set consists of a double and single spin-echo sequence with scan parameters for the double echo typically set at $TE_1 = 20$ msec, $TE_2 = 80$ msec, $TR_1 = 2120$ msec; for the single echo scan parameters are set at $TE_3 = TE_1 = 20$ msec and $TR_3 = 720$ msec. These parameters simultaneously satisfy the conditions that $(TR_1 - TE_1) = 3(TR_3 - TE_3)$ and that the acquired images be of clinical utility.

In addition to spin-echo image synthesis, an option for gradient-echo image synthesis is also available. Earlier tutorials have used a source set of spin echoes (Rundle DA et al., ISOE meeting, February 1990). We use a source set of gradient echoes, generated by RF-spoiled GRASS sequences, to synthesize images at arbitrary TEs, TRs, and flip angles. These generate images more representative of the acquired gradient-echo images since the effects of T2* are taken into account and can be acquired in a much shorter scan time. Three gradient-echo images were needed for the purpose: two with different flip angles but the same TR and

TE (for calculating T1) and two with different TEs but the same TR and flip angle (for T2*) with one scan common between the two sets. These yield analytic solutions for the parametric sets (i.e., T1, T2, and proton density) just as in the case of spin echoes, with the same advantages as mentioned previously.

Program Description

The three modes of the interactive teaching program—browse, quiz, and teach—are described in the following sections. Our initial development has focused on MR, but the module uses images from other imaging techniques as well.

Browse

The browse mode flow chart is shown in Figure 1. The choices offered in this mode are either the study of contrast variation between normal tissues as a function of the scan parameters (essentially to understand the physics of this technology) or the study of clinical cases.

The images required for the normal contrast variation study are the parametric images (T1, T2, and proton density) obtained from a source set of spin- and gradient-echo images. All the parametric images needed for image synthesis as well as all the text are stored in the local optical disk. The operator (i.e., the student) can choose the TE, TR (and flip angle in the case of gradient echoes) first slice number, and number of slices to be shown. Once these parameters are set, the program synthesizes the desired image and displays both the image as well as the text associated with the image. The user-interface screen for this mode is described in the Results and Discussion section. The process of image selection and text (diagnosis) entry by the instructor is discussed in the teach mode. Aside from spin- and gradient-echo synthesis, a third choice is *Comparison*. This displays 16 synthesized images, starting with an initial default set of TEs and TRs and slice number. The operator can then choose any of these 16 frames and change not only the TE and TR but also the slice number. This panel was created to compare, in one display screen, the appearance of the same slice in different domains of T1, T2, or proton-density weighting.

On choosing the clinical study, the user is presented with a list of teaching files. Each teaching file is associated with a radiologic subspecialty. On selecting a particular file, any clinical case included by the radiologist in the teaching file can be accessed by the user. Further, any clinical study that has the source image set required for synthesis can be used in that mode. The list of clinical cases appears along with a brief description of the pathology, whether the study can be used for synthesis, and whether the original data set is spin or gradient echo. If synthesis is possible, then the user is provided with the TE and TR (and flip angle) sliders. The image is displayed along with the comments relevant to the diagnosis as entered by the instructor in the teach mode (all retrieved from the local disk).

Quiz

In the quiz mode, all questions are displayed along with multiple-choice answers. On selecting any choice (right or wrong answer), a brief explanation and images (either synthesized or original) are displayed, if appropriate. All the questions and accompanying answers are stored in separate files in the quiz subdirectory of the local optical disk. Images accompa-

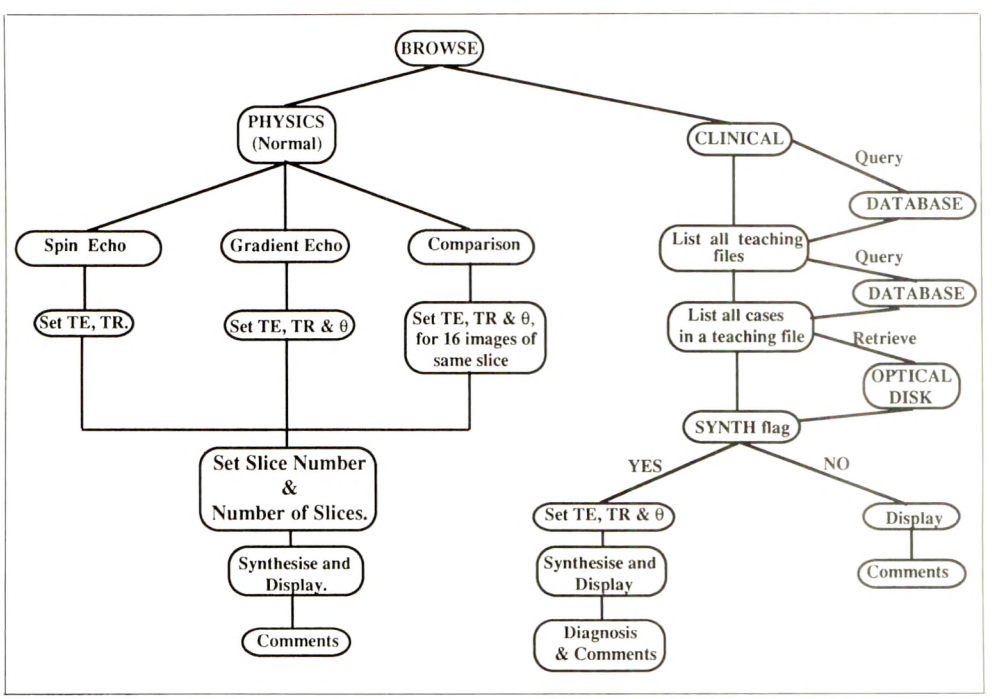


Fig. 1.—Flow chart for browse mode. The student can choose to study either the physics or clinical division. The first is set up to show different aspects of physics of MR imaging, while the second emphasizes clinical aspects. Both are capable of showing either synthesized or acquired images. All data used in this mode are stored in local data base, in a local magnetooptical disk.

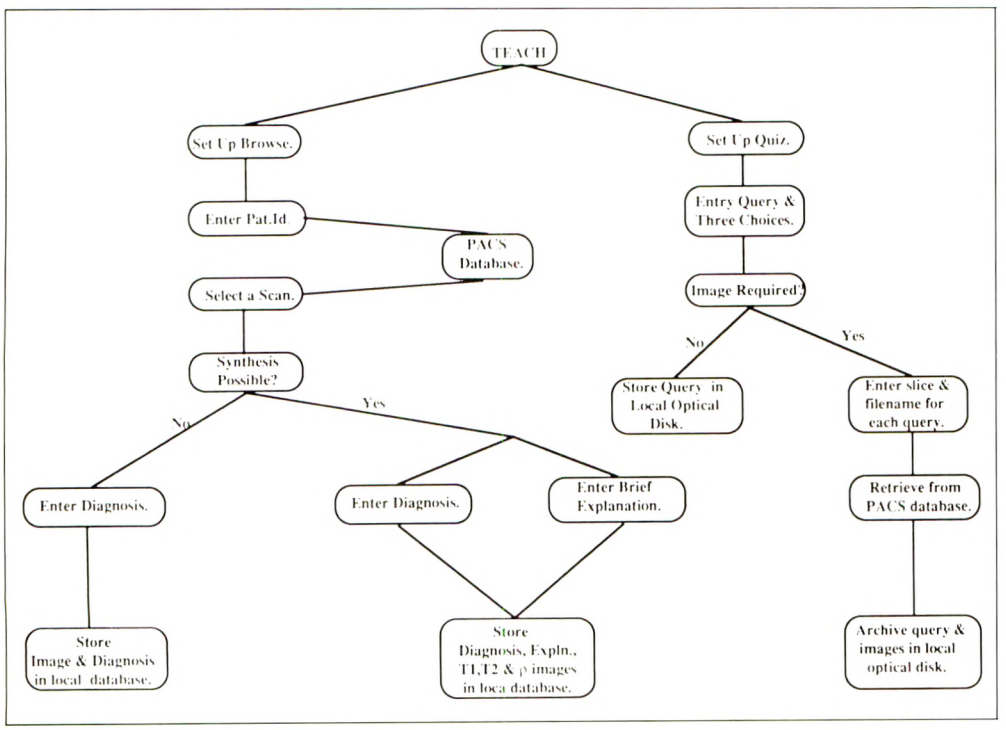


Fig. 2.—Flow chart for teach mode. Teach mode allows continuous update of all aspects of both browse and quiz modes. Images are retrieved from global PACS data base; proper comments and/or question-answer sets are typed in; and T1, T2, and proton-density matrices are calculated if necessary. Everything is finally stored in local data base. The entire process is menu-driven with no knowledge of programming required.

nying either a question or an answer are also stored in the local data base. These images had been retrieved from the PACS system in the teach mode and stored in the local optical disk. Whenever necessary, images from other techniques have been included in these question-answer sets in order to enhance the instructional impact of the module.

Teach

The teach mode is the workhorse of the module. All new cases and questions are added by the instructor/radiologist from this mode. The flow chart is shown in Figure 2. The teach mode has two options, set up browse and set up quiz, which add to the browse and quiz modes, respectively. To add cases to the browse mode, the instructor is prompted for the patient identification number. The information for all images for the same patient (retrieved from the global PACS data base) is displayed on the monitor. Choosing the image of interest results in the image being retrieved from the PACS optical disk and displayed on the screen. If image synthesis is not desired for that particular case, the instructor enters the diagnosis in a text subwindow and can then save both image and text on the local optical disk. The study is then accessible from the browse mode. If image synthesis is possible and desired, the instructor enters the correct scan numbers for the relevant set of double- and single-echo images. The data set is retrieved from the PACS optical disk, and the parametric images required for synthesis are first calculated and then stored in the local optical disk. The original images need not be stored, since they can be reproduced exactly if needed from the parametric images (since both T1 and T2 are analytic solutions). Only the values of TE and TR need to be stored. The instructor is also prompted to enter brief explanations in different ranges of TE and TR. The user can now synthesize images at arbitrary TEs and TRs for that particular clinical study.

In the set up quiz mode, the radiologist is prompted for the question and the three answers. If no images accompany either question or answers, then it is a simple process of entering a question and the three choices. These are stored in the quiz subdirectory of the local optical disk. If images are also to be displayed, then both the slice(s) of interest as well as the image file name have to be entered by the radiologist. These images are then retrieved from the PACS optical disk and stored along with the question in the local disk.

Results and Discussion

Figure 3 shows the spin-echo screen of the browse mode. At the top is the control panel, where the TE and TR can be set arbitrarily to change the contrast as easily as the mean and window level to obtain the optimum brightness. The number of slices to be displayed as well as the first slice number can also be set as desired. The middle panel displays either the text relevant to the TE and TR chosen or the diagnosis if in the clinical browse mode. A maximum of eight images, of consecutive slices, are displayed in the bottom panel, with the correct TE/TR at the bottom of each frame. A similar screen shows the contrast in synthesized field echoes. Both the contrast as well as susceptibility artifacts characteristic of field-echo images are correctly visualized, since these images have been generated from field-echo source sets. An extra slider is in the control panel, allowing the user to change the flip angle as well.

Figure 4 shows the comparison screen. If the auto button is selected, TEs and TRs are set at default values, with T1

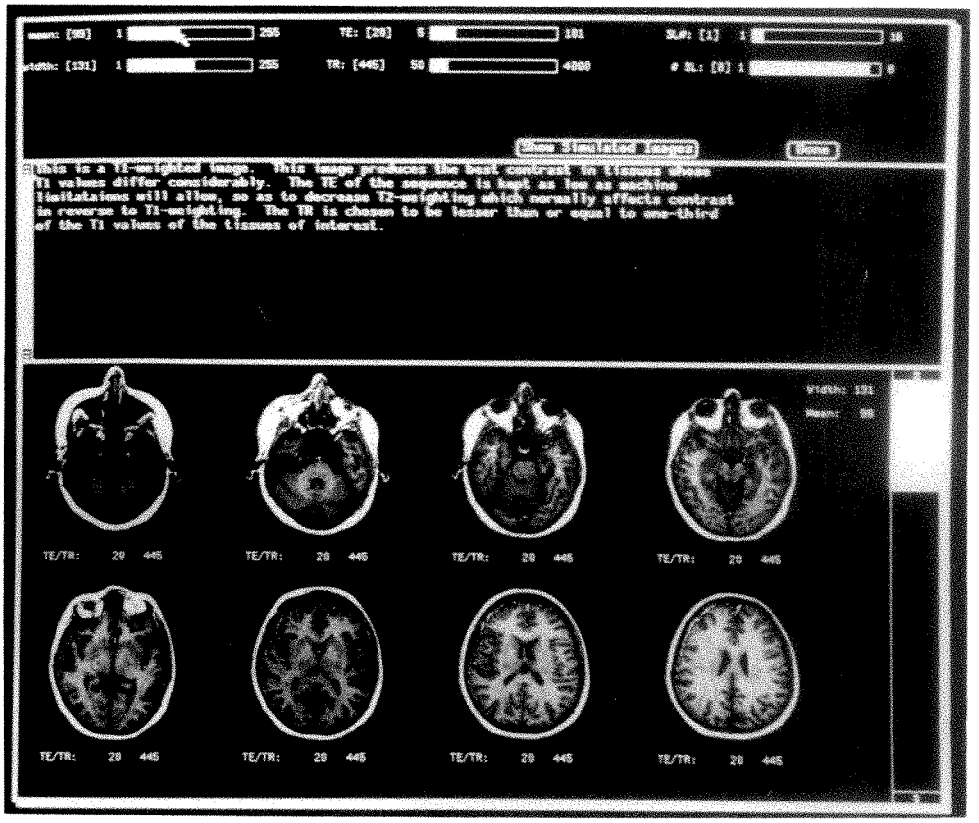


Fig. 3.—Spin-echo screen of browse mode. At top is control panel, where TE and TR at which images are chosen to be synthesized can be set as easily as mean and width. First slice number and number of slices can be set as desired. Middle panel shows appropriate explanatory text previously typed in by instructor. Lowest panel displays images, with chosen TE/TR appended at bottom.

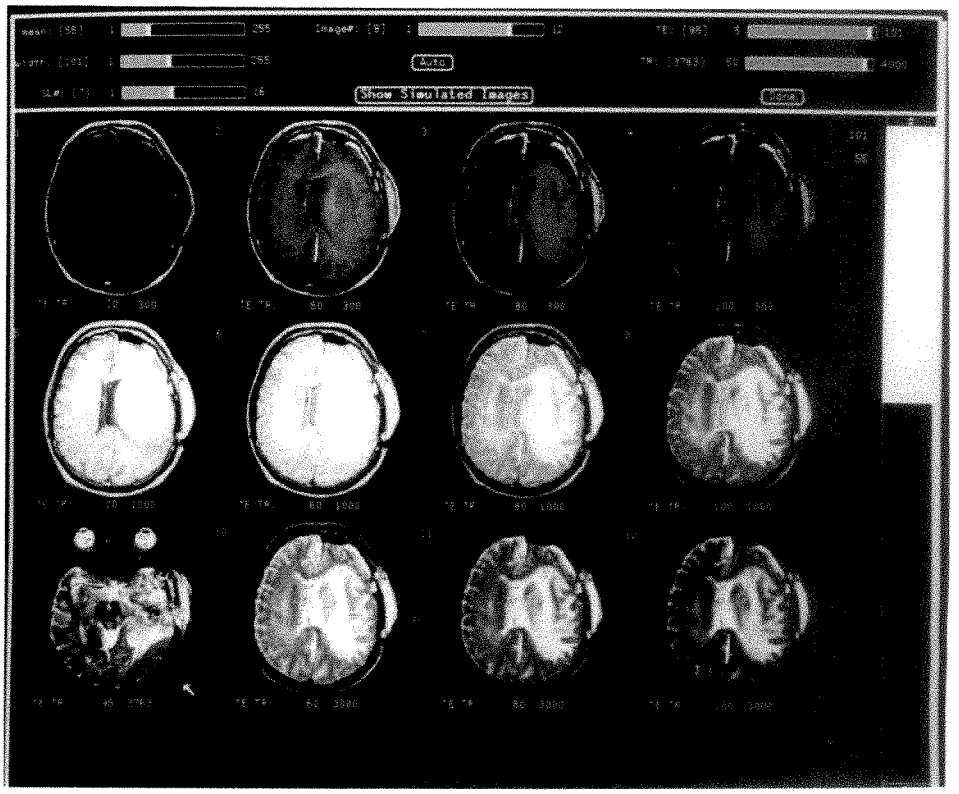


Fig. 4.—Comparison screen of browse mode. When *Auto* button is chosen, images are synthesized at a default set of TE/TRs, with T1-weighted images at top left, T2 at lower right, and proton density along diagonal. User can then choose to display, in any particular frame, any desired slice at any other value of TE/TR.

weighting in the upper left corner, T2 weighting in the lower right, and proton density in the lower left. The frame number and the TE/TR for that frame number are also displayed with each image. Subsequently, any particular frame can be chosen to show any desired slice at any selected TE and TR.

Figure 5 shows the quiz screen. The top panel displays the question as set by the instructor in the teach mode, along with the multiple-choice answers. The student has to select the answer in the next panel by clicking on any one of the choices. This panel also allows the image window to be set correctly. The next panel shows the text, and informs the user as to the correctness of the response. Images, synthesized or original and from any technique, are shown in the bottom panel.

The module has a fast response time for image and text display, making it truly interactive. Display of acquired images (as in clinical browse or in a clinical query mode) requires less than 40 msec for 16 slices. The text accompanying the images appears on the screen in less than 10 msec. Synthesis and subsequent display of images take about 270 msec for each slice. Responses to brightness and contrast adjustments are also around 10 msec.

The teach mode has proved to be particularly easy to use with respect to incorporating teaching material into the module. It has been structured such that the diagnostic text or the question-and-answer sets can be entered, and images from the PACS retrieved, by technical staff on instructions by the radiologist. Further, the PACS proved to be very valuable and effective in allowing images from techniques other than MR, such as CT and sonography, to be incorporated into either the browse or quiz mode whenever necessary. It takes about 2–5 min to retrieve a case from the main data base in the departmental PACS into the local optical disk, depending on the volume of traffic in the network. The robustness and portability of the module has been checked by installing it on other stand-alone Sun computer systems. Teaching modules are envisioned in all sections of the department responsible for teaching. (The department has 11 sections according to organ and age orientation.) The first module is located in the pediatric radiology section, where faculty have used PACS for several years.

We have not performed a formal receiver-operating-characteristic study to evaluate the level of satisfaction for each component of the ITM. It is clear from the initial reaction of the faculty and students, however, that the speed of display and function of both quiz and browse modes are extremely satisfactory. The teach mode requires almost the same amount of time that it would take to place copies of films in the analog teaching file. The process of image retrieval from the PACS is relatively lengthy, but less frequently used than the browse and quiz modes.

At present, an attempt is under way to incorporate several features into this module that will further enhance its capability as a radiologic instructional tool. Primary on this list is the use of hot spots or regions of interest that can be annotated by the instructor in the teach mode and stored along with the parametric images and finally displayed in the browse mode, indicating to the student the exact location of the abnormality.

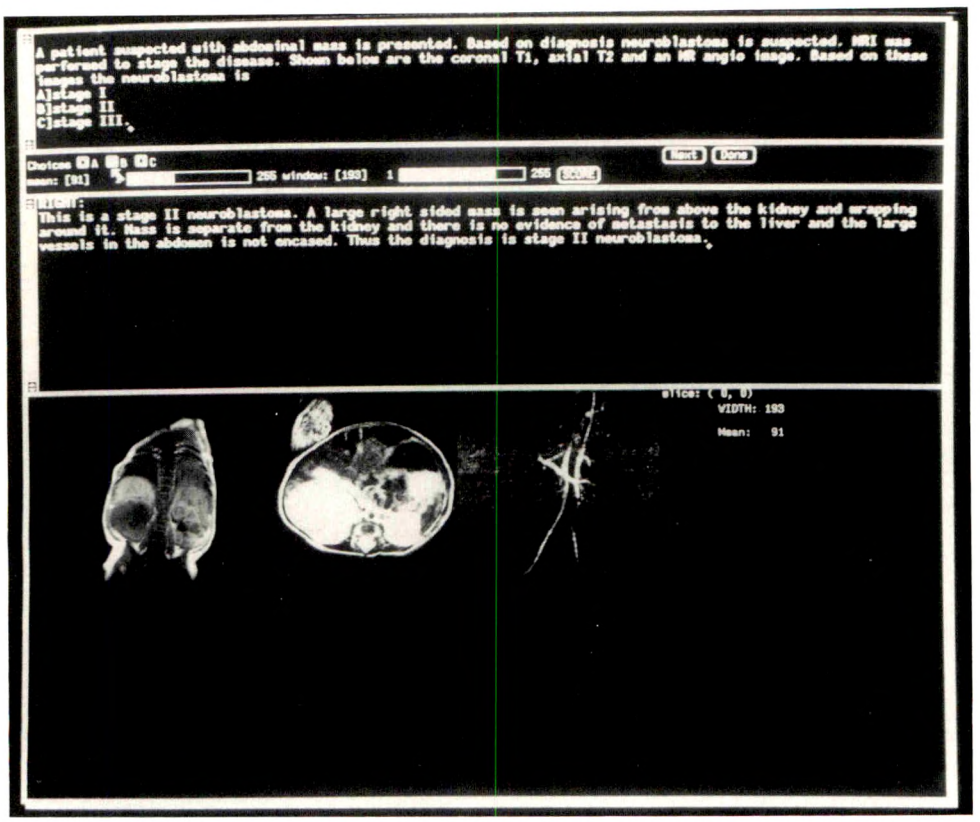


Fig. 5.—Screen for quiz mode. Top panel shows question with multiple-choice answers. User can choose answer in second panel. Text response and synthesized images appropriate to choice made are then displayed in lower two panels. User can then go to next question or opt out of quiz mode by choosing either *Next* or *Done* buttons in second panel, which also provides sliders for choosing right mean and window.

Zoom modes for better visualization and cine modes for more specialized uses are also being implemented. But the main thrust is in the steady development of the bank of teaching files, covering as large and comprehensive a range of teaching material as needed, together with the increase in the number and range of questions. The link to the departmental PACS is imperative for this effort. The modular nature of the programming of this project allows considerable flexibility in the developmental efforts. Thus, for example, the choice list in the browse mode or the structure of the question-answer image set can all be changed relatively easily if found necessary on future use.

In summary, the large number of images stored in the PACS system makes the teaching module very comprehensive. The dynamic nature of the module makes the unit interesting and interactive to the user. The radiologist has to spend some time to add a new case or a query, but no specific computer skill is required. All menus are self-explanatory, and the greatest effort for the instructor will be entering the diagnosis or questions. Thus, our program offers an easy way to include new clinical cases to the browse/quiz mode. The teaching module is currently being evaluated by both radiologists and student users with respect to ease of operation and efficacy.

REFERENCES

1. Starkschall G, Riggs JD, Lowther JR. A computer-aided instructional module for radiological physics. *Int J Radiat Oncol Biol Phys* **1986**;12:421–426
2. Goldberg HI, Fell S, Joseph MH, Taylor RC. A computer-assisted, interactive radiology learning program. *Invest Radiol* **1990**;25:947–951
3. Posteraro R, Blinder R, Herfkens R. MR-Tutor: a program for teaching the interdependence of factors which influence signal intensity in magnetic resonance imaging. *Comput Med Imaging Graph* **1989**;13:393–406
4. Malko JA, Nelson RC. Hand-held electronic teaching-aid for demonstrating MRI concepts. *Invest Radiol* **1989**;24:927–931
5. Taira RK, Stewart BK, Sinha U. PACS data base architecture and design. *Comput Med Imaging Graph* **1991**;15:171–176

Forthcoming Articles

REVIEW ARTICLES

Stress fractures: current concepts. *Daffner RH, Pavlov H*

Infertility in women: diagnostic evaluation with hysterosalpingography and other imaging techniques. *Krysiewicz S*

CARDIOPULMONARY RADIOLOGY

Pulmonary artery disease in Takayasu arteritis: angiographic findings. *Yamada I, Shibuya H, Matsubara O, et al.*

CT evidence of the "osseous pinch" mechanism for traumatic aortic injury. *Cohen AM, Crass JR, Thomas HA, Fisher RG, Jacobs DG*

Pictorial essay. High-resolution CT of bronchioloalveolar carcinoma. *Adler B, Padley S, Miller RR, Müller NL*

Pictorial essay. Intrathoracic neurogenic tumors: MR-pathologic correlation. *Sakai F, Sone S, Kiyono K, et al*

Case report. Transesophageal echocardiography for the evaluation of atherosclerosis of the thoracic aorta. *Singer RA, Karalis DG, Procacci PM, Naide D, Ross JJ Jr, Chandrasekaran K*

BREAST RADIOLOGY

Interval carcinomas in the Malmo mammographic screening trial: radiographic appearance and prognostic considerations. *Ikeda DM, Andersson I, Wattsgård C, Janzon L, Linell F*

Evaluation of mammographic image quality: a pilot study comparing five methods. *Caldwell CB, Fishell EK, Jong RA, Weiser WJ, Yaffe MJ*

GASTROINTESTINAL RADIOLOGY

Duodenal neoplasms: predictive value of CT in determining malignancy and tumor resectability. *Kazerooni EA, Quint LE, Francis IR*

Pictorial essay. CT findings in patients with small-bowel transplants. *Bach DB, Levin MF, Vellet AD, et al.*

Persistence of portosystemic collaterals and splenomegaly on CT after orthotopic liver transplantation. *Chezmar JL, Redvanly RD, Nelson RC, Henderson JM*

Calcification in the portal venous system: comparison of plain films, sonography, and CT. *Ayuso C, Luburich P, Vilana R, Bru C, Bruix J*

Abnormalities of the gallbladder detected by sonography and oral cholecystography 6 weeks to 6 months after ESWL: incidence in 174 patients. *Torres WE, Baumgartner BR, Casarella WJ*

Disappearing "gallstones": biliary pseudolithiasis complicating ceftriaxone therapy. *Kirejczyk WM, Crowe HM, Mackay IM, Quintiliani R, Cronin EB*

Case report. Thickened bile duct wall on sonography simulating duct dilatation. *Middleton WD, Surratt RS*

Case report. Splenosis: superparamagnetic iron oxide–enhanced MR imaging. *Storm BL, Abbitt PL, Allen DA, Ros PR*

GENITOURINARY RADIOLOGY

The seminal tract in patients with ejaculatory dysfunction: endorectal surface-coil MR imaging. *Schnall MD, Pollack HM, Van Arsdalen K, Kressel HY*

Case report. Transperineal hydrosonovaginography for demonstration of an incomplete vaginal septum. *Folio L, Rosenberg HK, Frishmuth GJ*

MUSCULOSKELETAL RADIOLOGY

Pictorial essay. Radiologic findings of diseases involving the maxilla and mandible. *Underhill TE, Katz JO, Pope TL, Dunlap CL*

Injuries of the superior portion of the glenoid labrum involving the insertion of the biceps tendon: MR imaging findings in nine cases. *Hodler J, Kursunoglu-Brahme S, Flannigan B, Snyder SJ, Karzel RP, Resnick D*

Width of the articular cartilage of the hip: quantification by using fat-suppression spin-echo MR imaging in cadavers. *Hodler J, Trudell D, Pathria MN, Resnick D*

The cruciate ligaments of the knee: correlation between MR appearance and gross and histologic findings in cadaveric specimens. *Hodler J, Haghighi P, Trudell D, Resnick D*

Pictorial essay. Knee effusion: normal distribution of fluid. *Schweitzer ME, Falk A, Berthoty D, Mitchell M, Resnick D*

PEDIATRIC RADIOLOGY

Diagnosis of liver disease in children: value of MR angiography. *Hubbard AM, Meyer JS, Mahboubi S*

NEURORADIOLOGY

Review. Neoplastic disease affecting the central skull base: CT and MR imaging. *Ginsberg LE*

Review. Diffusion MR imaging: clinical applications. *Le Bihan D, Turner R, Douek P, Patronas N*

Pictorial essay. Cystic masses of the head and neck: pitfalls in CT and MR interpretation. *Miller MB, Rao VM, Tom BM*

Value of acute-phase angiography to detect vascular injuries after gunshot wounds to the head: analysis of 12 cases. *Jinkins JR, Dadsetan RM, Sener RN, Desai S, Williams RG*

MR angiography of the head and neck: value of two-dimensional phase-contrast projection technique. *Applegate GR, Talagala SL, Applegate LJ*

MR of the pituitary stalk: size, shape, and enhancement pattern. *Simmons GE, Suchnicki JE, Rak KM, Damiano TR*

Hypertensive encephalopathy: findings on CT, MR, and SPECT in 14 cases. *Schwartz RB, Jones KM, Kalina P, et al.*

Gadopentetate dimeglumine–enhanced MR imaging of the postoperative lumbar spine: comparison of fat-suppressed and conventional T1-weighted images. *Mirowitz SA, Shady KL*

Case report. Tortuous vertebral artery: MR and CT demonstration. *Kricun R, Levitt LP, Winn HR*

Case report. Ganglioglioma with leptomeningeal and subarachnoid spread: results of CT, MR, and PET imaging. *Tien RD, Tuori SL, Pulkingham N, Burger PC*

Pictorial essay. Fast spin-echo high-resolution MR imaging of the inner ear. *Tien RD, Felsberg GJ, Macfall J*

Case report. Primary orbital endodermal sinus tumor. *Appignani BA, Jones KM, Barnes PD*

Case report. Diagnosis of von Hippel-Lindau disease in a patient with blindness resulting from bilateral optic nerve hemangioblastomas. *Ginzburg BM, Montanera WJ, Tyndel FJ, et al.*

INTERVENTIONAL RADIOLOGY

Influence of the stopcock in the efficiency of percutaneous drainage catheters: laboratory evaluation. *D'Agostino HB, Park Y, Moyers JP, et al.*

Acute lower gastrointestinal hemorrhage: treatment by superselective embolization with polyvinyl alcohol particles. *Guy GE, Shetty PC, Sharma RP, Burke MW, Burke TH*

Case report. Percutaneous extraction of biliary stones: value of endoluminal sonography. *Lossef SV, Garra BS, Barth KH, Zeman RK*

STATISTICS IN RADIOLOGY

Perspective. Strategies for improving power in diagnostic radiology research. *Beam CA*

ECONOMICS

Desperately seeking reimbursement. *Dickes L*

MEMO TO READERS

Report of the editor, 1991. *Berk RN*

MEETING NEWS

The American Institute of Ultrasound in Medicine: 36th annual convention. *Whalen E*

Memo to Authors

The Composition of Abstracts for *AJR* Articles

Robert N. Berk[1]

Few people will argue that the abstract is the most important part of articles published in the *AJR* or in any other medical journal [1]. Because it is so crucial, the abstract warrants *special* consideration by authors in the process of writing manuscripts for publication. Many readers use the information in the abstract to decide if they want to read the article in its entirety. Others, lacking the time or interest to read the article in detail, rely on the abstract to give them the essence of the paper. For people doing a computerized search of the literature or culling abstract indexes, the abstract may be the *only* part of the paper available to them. For all these reasons, it is prudent for authors to compose the abstract properly. To do this, they must have a clear understanding of the purpose of the abstract and keep the Journal's guidelines for writing abstracts firmly in mind [2–4].

The abstract should be a succinct and accurate summary of the contents of the paper. It should be a miniature of the article, constructed in the same way as the body of the manuscript: introduction, subjects (or materials) and methods, results, and conclusion. It should not be longer than one and one-half double-spaced typewritten pages (250 words), and it should contain no abbreviations or references. Of the various types of articles published in the *AJR*, only major articles have abstracts. In case reports, technical notes, pictorial essays, reviews, and commentaries, the introduction serves as the abstract.

With this issue, the *AJR* will begin to publish abstracts of articles in a different format, much like the ones recently adopted by the *New England Journal of Medicine* and the *Journal of the American Medical Association*. The purpose of the new design is to have abstracts present the essential elements of articles more clearly and concisely. It is for the convenience of readers, to make it simple for them to grasp the essence of articles by scanning the abstract. The contents, organization, and length of the abstracts are the same as before. However, rather than being all one paragraph except for the conclusion, abstracts will now be divided into four paragraphs, each with a title (objective, methods, results, and conclusions). The new requirement for writing abstracts encourages authors to include the appropriate information in a succinct and logical sequence. A properly designed abstract will provide readers with a trim, unambiguous message.

Objective

The first paragraph of the abstract should include a succinct statement of the specific goal or purpose of the article and indicate why it is worthy of attention. It should make the focus, premise, or central thesis of the paper clear. The paragraph should explain the author's motivation; that is, the hypothesis to be tested, the dilemma to be resolved, or the deficiency to be remedied. The objective stated here must be identical to the one given in the title and in the introduction of the paper. This paragraph should not be more than one or two sentences long; details belong in the introduction to the paper or in the discussion.

Subjects (or Materials) and Methods

The second paragraph should describe the methods used to achieve the objective explained in the first paragraph. It should include an explanation of how patients qualified to be included in the study, how they were selected, what abnor-

[1] Editor-in-Chief, *American Journal of Roentgenology*, 2223 Avenida de la Playa, Ste. 103, La Jolla, CA 92037. Address reprint requests to R. N. Berk.

AJR 159:207–208, July 1992 0361–803X/92/1591–0207 © American Roentgen Ray Society

malities they had, and what gold standard was used to confirm the diagnoses. There should be a succinct description of what was done, how it was done, how bias was controlled, what data were collected, and how the data were analyzed. (Use "Subjects and Methods" if patients were studied prospectively; use "Materials and Methods" if only records were studied.)

Results

The findings of the procedures described in the preceding paragraph are presented here. Descriptions of the methods and the results must not be intertwined. All results should flow logically from the methods described, and they must not stray from the specific objective of the paper. As many specific data as possible should be included within the overall length limitation of one and one-half pages, making the abstract substantive and able to stand alone. Promissory notes, such as "will be discussed" or "will be reviewed," are not appropriate.

Conclusion

The last paragraph should describe the conclusion of the study in one or two sentences. This must be based solely on the data provided in the body of the abstract, and it must relate directly to the objective of the paper as defined in the title and in the first paragraph of the abstract. It should anticipate such questions as, "So what?" or "Who cares?" It should give the take-home message to be remembered when all else is forgotten.

A good abstract provides readers with a specific message; one that is stated succinctly, accurately, and is simple to grasp. To achieve this goal, the abstract must be organized correctly, be of the proper length, and contain the appropriate information. Obviously, to accomplish all this in less than two typewritten pages is a daunting challenge for authors. However, it is well worth the effort. Writing the abstract properly is the best way authors have to ensure that readers will understand their message and grasp its importance. A good abstract guarantees that articles will receive the attention they deserve and serves as a major convenience for readers in the process.

REFERENCES

1. Huth EJ, *How to write and publish papers in the medical sciences*. Philadelphia: ISI Press, **1982**
2. Whalen E. An author's guide to the guidelines for authors. *AJR* **1989**;152:195–198
3. Berk RN, Preparation of manuscripts for radiology journals: advice to first-time authors. *AJR* **1992**;158:203–208
4. Siegelman SS. Advice to authors. *Radiology* **1988**;166:278–280

Meeting News

The Society of Gastrointestinal Radiologists: 21st Annual Meeting, February 1992

Elizabeth Whalen[1]

The 21st annual meeting of The Society of Gastrointestinal Radiologists (SGR) was held February 16–21, 1992, at the Hyatt Regency Grand Cypress, Orlando, FL. Among the activities offered were the annual Walter B. Cannon lecture, presentations of 34 scientific papers, 36 workshops, six parallel focus sessions, a categorical course on frontiers in gastrointestinal radiology, a radiology-pathology mini-course, 24 poster presentations, and an "unknown" film panel. Regrettably, *AJR* space limitations do not allow complete coverage of the entire program, but we have tried to include here a wide range of topics and types of presentations.

Among the awards presented, Joseph T. Ferrucci (Boston, MA) received the annual Walter B. Cannon Medal, and John H. C. Ransom (New York, NY) presented the Cannon Lecture. Three prizes were given for excellence in scientific presentations. The Roscoe E. Miller Award for the best scientific paper was presented to Lars G. Crabo and coauthors (P. C. Freeney, D. O. Graney, D. M. Conley; Seattle, WA) for "Venous Drainage of the Pancreatic Head: Contrast-Enhanced CT Appearance" (described later: see the section on scientific presentations, pancreas and liver subsection). Gerald D. Dodd (Pittsburgh, PA) was the winner of the Memorial Award, which recognizes the best presentation by a first-time presenter at an SGR meeting. Dr. Dodd's paper by himself and three coauthors (W. J. Miller, R. L. Baron, S. R. Confer) concerned sonographic screening of cirrhotic livers (described later: see the section on scientific presentations, pancreas and liver subsection). Dana Premer and colleagues (D. L. Day, J. Crowe, B. Carpenter; Minneapolis, MN) won an award for their poster presentation, "Imaging of Abdominal Manifestations of Cystic Fibrosis."

Scientific Presentations

Esophagus

Malpositioned nasal enteric feeding tubes.—Shayle Patzik (Chicago, IL) presented a study performed by himself and C. Smith concerning the prevalence of malpositioned nasal enteric feeding tubes at their institution, clinicians' awareness of the problem, and the guidelines in place concerning use of feeding tubes. These flexible, small-bore, polyurethane tubes, often inserted at bedside, carry potential complications due to misplacement. Care must be taken in the placement of these tubes and in follow-up studies to ensure against such complications. In a review of chest/abdominal radiographs of 100 consecutive patients with nasal enteric feeding tubes, these researchers found 19% were not in the optimal location—this figure is more than 100% higher than previously reported; moreover, approximately 8 hr after tube insertion, 21% of the clinicians involved in the cases were unaware that tests had shown the tubes had been malpositioned. The problem appears to be unrecognized at teaching institutions; of the eight institutions contacted for this study, none had developed guidelines for either tube placement or follow-up. To avoid complications from tube malpositioning, these researchers recommend imaging-guided tube placement whenever possible, limiting "blind tube" placement to trained and

[1] Contributing editor, *American Journal of Roentgenology*, Ste. 103, 2223 Avenida de la Playa, La Jolla, CA 92037.

Editor's note.—"Meeting News" articles report the highlights of important national radiology meetings. The articles will not undergo the peer review usually required of *AJR* publications, nor will they offer a critique of the information provided. The sole purpose of the series is to provide Journal readers with succinct, substantive, and accurate reviews of topics of current interest, written in a readable fashion and published promptly after the meeting.

***AJR* 159:209–216, July 1992** 0361–803X/92/1591–0209 © American Roentgen Ray Society

qualified personnel, and obtaining a radiograph immediately after the procedure to check tube placement.

Gastroesophageal reflux.—The role of barium studies in detecting gastroesophageal reflux was discussed by J. Keith Thompson (Birmingham, AL). He and his coauthors (R. E. Koehler, J. E. Richter) had observed that, although barium studies are generally held in low regard because of presumed low sensitivity in detecting gastroesophageal reflux, radiology departments receive many referrals to assess this diagnosis. Moreover, the water siphon test is also held in low regard because of its presumed *over*sensitivity. In this study, all patients were referred for either barium swallow or upper gastrointestinal studies, and reflux as seen on images was graded on a scale of 0 to 5 (clearance time also was recorded). All 83 patients had both barium studies and 24-hr pH monitoring within a period of 14 days; elicitation maneuvers were used in all patients. The 24-hr pH testing (despite its admitted problem with reproducibility values between 80% and 85%) was used as the gold standard to determine reflux. According to this standard, 55% of the patients did have gastroesophageal reflux.

When results of barium studies were considered without the water siphon results, the success of barium studies in detecting reflux was as follows: sensitivity, 44%; specificity, 89%; positive predictive value, 84%; and negative predictive value, 53%. When the water siphon results were considered along with the barium study results, the success in detecting gastroesophageal reflux was as follows: sensitivity, 65%; specificity, 80%; positive predictive value, 82%; and negative predictive value, 62%. These results suggest that barium studies are reasonable screening tests for gastroesophageal reflux; they yield fair sensitivity and high positive predictive value when elicitation maneuvers are used, and addition of the water siphon test increases sensitivity significantly with only minimal effects on positive predictive values.

Michael Y. M. Chen (Winston-Salem, NC) presented an investigation of the correlation of esophageal pH testing and radiographic findings in gastroesophageal reflux (coauthors: D. J. Ott, W. C. Wu, J. W. Sinclair, D. W. Gelfand). They studied 112 consecutive patients who had undergone both pH monitoring and multiphasic esophagography. For pH studies, the investigators recorded the percentage of time during which pH was less than 4, the number of reflux episodes, the duration of reflux episodes, and the symptoms. Cases of gastroesophageal reflux were categorized as mild, moderate, or severe on the basis of total acid exposure. In 62 patients, pH monitoring results showed no reflux; in six (10%) of these, however, reflux was diagnosed radiographically. Of the 50 patients with abnormal results on pH tests, reflux was diagnosed radiographically in 15 (30%). Detection rates of gastroesophageal reflux by radiography increased with severity of the disease: mild, 25%; moderate, 27%; and severe, 57%. On the basis of these findings, radiographic findings do not correlate with gastrointestinal reflux found by pH monitoring, particularly in patients with mild or moderate disease.

Pancreas and Liver

Contrast-enhanced CT appearance of venous drainage of the pancreatic head.—Lars G. Crabo (Seattle, WA) was awarded the Roscoe E. Miller Award for his and his coworkers' (P. C. Freeney, D. O. Graney, D. M. Conley) study on CT of the pancreatic head. They wanted to investigate the clinical significance of anatomic findings on CT of the small pancreatic veins because CT is currently the most widely used diagnostic test for pancreatic adenocarcinoma. However, when this imaging method is used, the number of *resectable* pancreatic tumors is overestimated by 36–62%. CT of these pancreatic veins may improve results because these veins *are* abnormal in pancreatic cancer. Studying CT scans from 100 consecutive patients without evidence of pancreatic disease, these investigators found ranges in size as follows: anterior pancreaticoduodenal veins (APDVs), 1–4 mm; posterior pancreaticoduodenal veins (PPDVs), 1–4 mm; and gastrocolic venous trunk (GCT), 3–7 mm. In their dynamic CT study of venous anatomy, they found that the APDVs and PPDVs lie just within the parenchyma on the anterior and posterior surfaces of the head of the pancreas, and the GCT joins the superior mesenteric vein anterior to the uncinate process. The frequencies of visualization of small pancreatic veins on contrast-enhanced CT were as follows: APDV, 98%; PPDV, 88%; and GCT, 89%. Dynamic CT can show the APDVs, the PPDVs, and the GCT; CT can help reassess patients with pancreatic head carcinoma; and CT evaluation of pancreaticoduodenal vein involvement may be useful in staging pancreatic cancer.

Sonographic screening for hepatic malignancies in cirrhotic livers.—In a presentation that won him the Memorial Award, Gerald D. Dodd (Pittsburgh, PA) presented the preliminary results of a prospective study by himself and his coauthors (W. J. Miller, R. L. Baron, S. R. Confer). They investigated sonographic detection of malignant tumors in 200 consecutive liver transplant recipients. Although several previous studies have investigated associated applications of hepatic imaging, these studies have been limited by three factors: their retrospective nature, limited pathologic correlation, and nonscreening protocol. In this study, sonograms were obtained in all 200 patients before liver transplantation to check for number, size, and location of tumors; state-of-the-art equipment was used; and staff radiologists interpreted all the images. About 86% of the sonographic examinations were performed within 120 days before the transplantation, and the sonographic criteria for tumor included heterogeneity and focal mass.

The preoperative sonograms yielded low sensitivity but very high specificity for malignant tumor; most of the tumors missed were small (≤1 cm), and the largest tumor missed was a diffusely infiltrating lesion that could not be seen even retrospectively. Previous studies have shown higher detection rates for sonography in patients with cirrhosis. The differences may be explained by the prospective nature of this study, the whole-liver correlations available after transplantation, the end-stage cirrhosis of the patients in this study, and different body habitus (North American in this study vs Oriental). These preliminary results indicate that, although sonography is not a sensitive screening device for detecting malignant tumors in cirrhotic livers, its specificity is so high that any lesion shown by sonography in a cirrhotic liver should be considered malignant until proved otherwise.

MR detection of hepatocellular carcinoma in patients with liver cirrhosis.—Ruedi F. Thoeni (San Francisco, CA) dis-

cussed a study in which he and his coauthors (G. Sicca, P. Shyn), who had no knowledge of the diagnosis beforehand, assessed the MR images of 29 patients with proved liver cirrhosis to evaluate the accuracy of MR imaging in detecting hepatocellular carcinoma (HCC). Five patients without cirrhosis also were imaged; four of these had HCC. In these 34 patients, the diagnosis of HCC was proved by surgery in nine patients, biopsy in 13, transplantation in 10, and 7- and 9-year follow-up (respectively) in two. Several MR sequences were used (including T1-weighted spin-echo, T2-weighted spin-echo, and contrast-enhanced gradient-recalled echo sequences); for all imaging procedures, glucagon was administered to the patient, and fat-saturation and respiratory-compensation techniques were used. MR criteria for liver cirrhosis included shrunken liver, nodular surface, inhomogeneity, splenomegaly, varices, and ascites. For HCC, MR criteria included inhomogeneity, vascular invasion, steatosis, presence of capsule, irregularity of margins, and extent beyond the capsule.

In the subgroup of patients thought to have liver cirrhosis, MR imaging yielded excellent results in detecting cirrhosis: 90% for sensitivity, 100% for specificity and positive predictive value, and 63% for negative predictive value. In detecting HCC, MR imaging accuracy was lower: sensitivity, 65%; specificity, 83%; positive predictive value, 92%; and negative predictive value, 45%. Investigating the relatively high numbers of false-negative results revealed that one false-negative was a missed lesion, eight false-negatives were additional lesions (in patients with multiple lesions), two false-negatives were interpreted as abscesses, and one false-negative was called a regenerating nodule. The two false-positives consisted of one regenerating nodule and one focal fatty infiltration. The researchers concluded that in this subgroup of patients at risk, MR imaging was very accurate in detecting moderate to advanced cirrhosis, but not sensitive enough to discern the extent of HCC in these patients. They recommend that additional tests be done when MR does not show HCC in patients at risk or in patients with elevated α-fetoprotein levels.

CT of hepatocellular carcinoma.—Using contrast-enhanced CT, W. Ross Stevens and colleagues (C. D. Johnson, D. H. Stephens, K. P. Batts; Rochester, MN) investigated the CT appearance of HCC in patients with alcohol-related disease and in other patients with HCC (e.g., those with viral hepatitis). Their study group consisted of 100 consecutive patients with pathologically proved HCC: this report described the results of the review of these patients' CT scans. On these CT scans, HCC was seen as a single mass in 47 (47%) of the cases, as multifocal masses in 46 (46%), and as a diffusely infiltrating lesion in four (4%). Most of the tumors appeared as heterogeneously hypodense masses with mixed vascularity. In 28 cases, CT showed portal vein involvement, and in 29 cases, it showed metastases or local extension of tumor. Tumor invasion of portal or hepatic veins was seen in 55% of alcoholic patients but in only 20% of patients with viral hepatitis. Tumor capsule was more common in patients with viral hepatitis: 33% of these scans showed tumor capsule, but tumor capsule was seen in only 12% of patients with disease related to alcohol. The findings from this retrospective review indicate four features that may help CT diagnosis of HCC: central scar, necrosis, vascular invasion (more commonly seen in larger, high-grade tumors from alcohol-related disease), and capsule (seen more commonly in patients with viral hepatitis).

Gallbladder

Complications of laparoscopic cholecystectomy.—As pointed out by Ellen Ward (Rochester, MN), laparoscopic cholecystectomy has been used since 1987 and has been preferred to traditional surgery for gallbladder removal—partially because of a lower complication rate due to less traumatic and less lengthy surgery. However, some complications have been reported in patients who have undergone laparoscopic cholecystectomy. Dr. Ward and colleagues (A. J. LeRoy, C. E. Bender, J. H. Donohue, R. W. Hughes) studied 29 patients with such complications, including injury of the bile duct (15), choledocholithiasis (seven), leaking of the cystic duct stump (four), bowel perforation (two), intraabdominal abscess (two), and intraperitoneal gallstones (two).

Among the patients with bile duct injuries (none of whom had bile duct abnormalities), endoscopic retrograde cholangiography was the first diagnostic test done and showed obstruction in nine of 11 cases; transhepatic cholangiography was used to see the proximal extent of the strictures. Of the bile duct injuries, 18% were classified as Bismuth I. The seven patients in whom choledocholithiasis developed after laparoscopic cholecystectomy were rehospitalized, and one patient underwent surgery; endoscopic retrograde cholangiography was used to diagnose the complication in these patients (two thirds also had sonographic examinations). In the four patients who suffered the complication of a leak in the cystic duct stump, cholangiography was necessary to distinguish this complication from injury of the bile duct. The leak was found to be aggravated by obstruction in 50% of these patients. Abdominal radiographs showed bowel perforations (one fatal) in two patients, and CT appeared to be most useful in recognizing both intraabdominal abscesses and calcification (indicating intraperitoneal gallstones, which are clinically significant only if infected). These results suggest that imaging studies can be helpful in identifying the complications of laparoscopic cholecystectomy and in planning treatment. In answer to a question, Dr. Ward mentioned that, in this study, the complication rate decreased as the experience of the surgical team performing the procedure increased.

Pericholecystic fluid collection as a prognostic indicator for percutaneous cholecystostomy.—David L. Harshfield (Little Rock, AK) discussed this evaluation of 50 patients with pericholecystic fluid collections. The study's coauthors were S. K. Teplick, E. F. Ferris (Little Rock, AK), and S. A. Teefey (Seattle, WA). In 10 of the 50 patients, percutaneous cholecystostomy had been performed for acute cholecystitis. Three types of pericholecystic fluid collections were defined: type I, very mild to moderate, not associated with perforation; type II, moderate to mild to somewhat complex, almost always associated with perforation; and type III, so complex that the gallbladder cannot be delineated, almost always associated with perforation.

Type I pericholecystic fluid collections are amenable to treatment by percutaneous cholecystostomy; these are identified on sonograms by sonolucence, crescent shape, and small size (<1 cm). Sonographic appearance of type II pericholecystic fluid collections included the following characteristics: size greater than 1 cm, usually an anechoic appearance, a thick wall, debris, septa, and sometimes a complex nature with nonvisible gallbladder. Some of the less severe type II collections were treated successfully by using percutaneous cholecystostomy alone. On sonograms, the type III pericholecystic fluid collections were always complex and encompassed the gallbladder; all type III collections required surgical cure—the percutaneous procedure served only as a temporizing measure. The division of pericholecystic fluid collections into three sonographic classes allowed quicker, more effective therapy decisions in these patients. Percutaneous cholecystostomy cured all type I collections and some type II collections; however, the more severe type II collections and the type III collections eventually required surgery, although percutaneous cholecystostomy did provide temporary improvement.

Colon and Small Intestine

Colonic contractions, pain, and cholecystokinin.—In introducing this study, Ger H. Ritsema (Rotterdam, the Netherlands) noted that many patients with irritable bowel syndrome have pain after eating a meal and that cholecystokinin is released endogenously after a meal and does cause colonic contractions. This study sought to answer three questions: (1) Can postprandial pain be caused by colonic contractions? (2) Can these contractions be visualized on barium enema studies? (3) Do patients recognize the same pain and site of pain for these contractions? In 20 patients with postprandial pain for which no organic cause had been found, barium examination without glucagon administration resulted in no visualization of contractions and no indication of pain by the patient. After informed consent had been obtained, these patients underwent another barium examination in which the enema was immediately followed by IV administration of cholecystokinin. Intermittent fluoroscopy was performed, but the patients could not see the fluoroscopic screen. In 18 (90%) of patients, fluoroscopy showed strong, circular, segmental colonic contractions; simultaneously, the patients reported the usual postprandial pain at the usual site. Dr. Ritsema concluded that colonic contractions (e.g., those caused by endogenous cholecystokinin) can cause postprandial pain; that such contractions can be seen when IV cholecystokinin is administered after barium enema; and that patients can be trusted to identify the cholecystokinin-related pain as the usual pain at the usual site.

Abdominal radiographic evaluation of childhood intussusception.—Intussusception is common in children and is easily confused with gastroenteritis and other diseases; the usual workup for suspected intussusception includes plain films and contrast enema (including air contrast). Delay of diagnosis is significant in these patients. Bernadette L. Koch presented a study performed by herself and colleagues (W. E. Shiels, C. K. Maves, N. D. Johnson, R. Rupich, D. R. Kirks; Cincinnati, OH) that addressed the question of whether plain radiography can be used as an effective screening tool for pediatric intussusception (i.e., does it have the required low false-negative rate?). In 141 patients with suspected intussusception, they evaluated the sensitivity and specificity of the following plain radiographic findings: air-filled cecum, soft-tissue mass, subhepatic angle, small-bowel obstruction, and paucity of bowel gas; they also assessed interobserver variability.

Air-enema studies showed intussusception in 51 patients and had normal results in 90 patients. These results were compared with the findings in a three-film series, including supine anteroposterior, prone posteroanterior, and left lateral decubitus views. The most sensitive radiographic findings for intussusception were nonvisualization of air-filled cecum (89%) and paucity of bowel gas (67%), and the most specific findings were small-bowel obstruction (98%) and soft-tissue mass (92%). A high false-negative rate (2–22%; interobserver variability, 10–20%) resulted when a distended small bowel was misinterpreted as an air-filled cecum. Anteroposterior and left lateral decubitus views showed the cecum in all cases with normal air-enema results and also showed soft-tissue masses in 93% of cases in which the air-enema study proved intussusception and the presence of such a mass. On the basis of these data, prone films seem unnecessary in assessing suspected intussusception in children. More importantly, according to Dr. Koch, "visualization" of the cecum is insufficient for exclusion of intussusception, and liberal use of air-enema examinations is recommended when the entire cecum cannot be visualized on plain films.

New Technology in Gastrointestinal Radiology

Imaging-directed percutaneous fine-needle aspiration biopsy vs fine-needle core biopsy.—W. J. Miller (Pittsburgh, PA) and coworkers (A. Dekker, E. L. Reyna, F. L. Thaeta, M. P. Federle) studied the biopsy results of 75 patients (62 with malignant lesions and 13 with nonmalignant lesions). Results from both fine-needle aspiration biopsy (FNAB) and fine-needle core biopsy (FNCB) were assessed for adequacy of sample obtained and sensitivity of findings for malignancy. The researchers used a 20-gauge spinal needle attached to a 20-ml syringe for FNAB and a Bard Biopty gun and a 20-gauge Biopty needle for FNCB procedures. In 61 patients, CT was used to guide the biopsy; sonography was used to guide the biopsy in 14 patients. For immediate interpretation of biopsy specimens, several slide smears and touch-prep slides were analyzed for FNAB and FNCB, respectively. Later processing of specimens involved cell blocks from FNAB (aspirated samples centrifuged to form pellets) and fixated and stained core biopsy samples from FNCB.

The percentages of biopsies yielding adequate samples for each type of procedure and analysis were as follows: FNAB immediate slides, 20%; FNAB aspirated cell block, 64%; FNCB immediate touch prep, 55%; FNCB fixated and stained core, 76%. For FNAB samples, the sensitivity of analysis of immediate slides (87%) was not significantly different from the sensitivity of aspirated cell block (78%). In sample ade-

quacy, the FNCB touch-prep immediate analysis yielded a significantly higher percentage of adequate samples than did immediate FNAB slides, which indicates that use of immediate FNCB (rather than immediate FNAB) results may obviate additional biopsies.

Aqueous gastrointestinal contrast agent for ultrafast MR imaging.—A study by Peter F. Hahn (Boston, MA) and colleagues (S. Saini, M. S. Cohen, P. Reimer, P. R. Mueller) investigated the use of Readicat 2 (E-Z-EM), a widely available contrast material, for use in echoplanar, T2-weighted, Instascan MR imaging of the abdomen. The oral contrast material (450 ml of dilute barium material) was given to 13 patients (four with malignant lesions, nine with extrahepatic upper abdominal masses, none with benign liver abscesses) and to four volunteers (whose imaging findings were normal before and after contrast administration). For further comparison, no oral contrast material was given in MR studies in 36 patients (12 with malignant liver lesions, 19 with benign liver lesions, five with extrahepatic upper abdominal masses). MR parameters included 10-mm slice thickness, 128 × 128 matrix, 20 × 40 cm field of view, slice acquisition time of 60 msec, echo time of 26 or 50 msec, and one excitation per slice. In evaluating the images, readers compared bowel marking and distension, image noise, and lesion conspicuity.

These researchers found that the administration of Readicat 2 before ultrafast MR imaging markedly increased bowel signal intensity, decreased signal-to-noise ratio by about 10% (not a significant difference), and improved lesion conspicuity (signal from gut lumen was at least 25% greater than signal from disease). This dilute barium sulfate suspension is a positive contrast agent that will increase signal from bowel lumen on T2-weighted images (however, barium should not be used in patients with perforation). Dr. Hahn emphasized that the effective contrast material for this application is the aqueous carrier, *not* the 2% barium. Preventing bowel motion artifacts is a significant advantage of ultrafast MR imaging, and this aqueous gastrointestinal contrast agent can increase the signal of normal lumen and improve lesion conspicuity on ultrafast imaging; furthermore, administration of Readicat 2 would enable patients to undergo MR imaging and CT scanning during the same visit.

Categorical Course: Frontiers in Gastrointestinal Radiology

Bowel Wall Enhancement Patterns on CT

Alec J. Megibow (New York, NY), who organized and moderated the categorical course for the meeting, presented a discussion of bowel wall enhancement patterns on CT. The rapid CT scanning capabilities at his institution and judicious use of contrast media have made possible the extraction of the information he presented. Hyperattenuating patterns may indicate scirrhous carcinoma, Crohn's disease, acute appendicitis, or ischemia; hypoattenuating patterns are characteristic of edema, fat, and mucin. If the target sign (a low-attenuation ring) is seen within the bowel wall, it probably represents submucosal edema and requires bolus-enhanced CT for visualization. One advantage of contrast-enhanced CT is that the target sign rules out neoplastic disease; the differential diagnosis then includes infectious disease (Crohn's disease, radiation enteritis) and vascular disease, and correlation with clinical symptoms helps make the diagnosis. On CT scans of the colon, the target sign may indicate diagnoses that include Crohn's disease, inflammatory disease, and pseudomembranous infections. When small-bowel obstruction is present, surgeons are most concerned about whether strangulation is present and whether treatment should be conservative or surgical. Interpretation of CT scans can sometimes answer these questions; for example, if the bowel appears gangrenous or at least compromised (resulting in focal ischemia), the radiologist can recommend immediate surgery.

CT of Acute Abdomen

In his talk, Emil J. Balthazar (New York, NY) discussed the life-threatening syndrome of acute abdomen that requires rapid and precise diagnosis, accurate evaluation, and emergent treatment. Indications of life-threatening acute abdominal pain include gastrointestinal perforations; intraperitoneal abscesses; acute inflammatory disease, such as appendicitis, diverticulitis, and colitis; spontaneous hemorrhage, ischemia, and infarction; strangulating internal obstruction; and abdominal trauma. For gastrointestinal perforations, CT can be helpful in detecting extraluminal air, the perforation site, and the cause of the perforation. CT has a better sensitivity than does radiography in the detection of free intraluminal air; Dr. Balthazar recommends reviewing images with wide (lung) windows (1500–2000 H) and notes that the air is usually in the anterior surface of the liver, along the falciform ligament. In finding the site of perforation, CT can help by showing focal abnormalities adjacent to intestinal segments, including collections of gas bubbles, inflammatory reactions, abscesses, extravasation of contrast material, and opaque foreign bodies. The cause of the perforation can be suggested by the CT appearance of the abnormal intestinal segment (including length and location of involvement, degree of wall thickening, and configuration and pattern of enhancement). In evaluating cases of peritonitis, however, the CT findings are often nonspecific. However, they may include a prominent, thick omentum and mesenteric folds; ascites with intraperitoneal air; loculated ascites; and thickening of the parietal peritoneum.

Intraoperative Sonography in Hepatic Resections

Robert A. Kane (Concord, MA) discussed the potential of intraoperative sonography in gastrointestinal applications. For example, this type of imaging could be used in the liver for the localization of occult lesions for biopsy or drainage, surveys for occult tumors or metastases, evaluation of lobar and segmental anatomy, assessment of tumor resectability, and guidance for wedge resection or cryotherapy. Dr. Kane emphasized that, in any one patient, multiple tumor nodules will look similar to one another; therefore, if two different-appearing lesions are seen, the radiologist should consider the possibility that the lesions are different, such as a heman-

gioma and a liver tumor. Intraoperative sonography may show more lesions than were seen in preoperative images and may delineate vascular invasion more clearly. To determine how intraoperative sonography of the liver affected lesion detection rate in patients undergoing surgery for hepatic metastases, we prospectively compared this imaging method with CT, MR imaging, and preoperative sonography in 50 cancer patients (tumors included colonic carcinoma in 42 patients, hepatoma in three, cholangiocarcinoma in two, and other primary tumors in three).

Of the 152 lesions seen on intraoperative sonograms, CT showed 89 (59%), MR imaging showed 100 (66%), and preoperative sonography showed 101 (66%); combining the results of two of these three methods increased the detection rate to only about 70%. All preoperative imaging methods failed to show a significant number of lesions that were shown by intraoperative sonography. To assess the impact of intraoperative sonography on treatment of patients, we studied 43 cases of cancer (28 colorectal cancer, six hepatoma, and nine other—including two benign lesions). The use of intraoperative sonography resulted in no change in treatment in 46% of cases, an alteration in surgical treatment in 16%, and the cancellation of surgery in 37%. A total of 53% of treatment decisions were affected by intraoperative sonography. Four statements summarize why it is a good idea for radiologists to perform intraoperative sonography: It improves patients' care; it provides excellent image quality; it helps to "sell" the importance of radiology services to surgical colleagues; and if radiologists do not perform intraoperative sonography, eventually surgeons will.

MR Imaging of Pediatric Abdomen and Pelvis

During the pediatric radiology session of the categorical course, George S. Bisset III (Cincinnati, OH) spoke about the techniques, indications, protocols, and outlook for the use of MR studies in pediatric abdominal imaging. Recommended techniques to prepare a child for abdominal MR imaging include allowing nothing to be taken orally by the patient for 4–8 hr before the examination (which helps avoid motion and risk of aspiration), administration of glucagon (which decreases bowel peristalsis and gives an ancillary sedative effect due to hyperglycemia), and possible use of a gastrointestinal contrast agent (the advantages of which must be weighed against the risk of aspiration in any child who must be sedated). Sedation may be required in children less than 8 years old; in 14,000 patients so far in Dr. Bisset's institution, 98% success has been achieved using oral chloral hydrate (50–100 mg/kg body weight) in patients less than 18 months old and IV pentobarbital sodium (2–3 mg/kg body weight; maximum total dose, 8 mg/kg) in children 18 months to 8 years old. The 2–3% of children who did not become sedated included those who were severely mentally retarded, those who were receiving chronic anticonvulsive therapy, or those who had other problems (e.g., increased liver metabolism). In these cases, an anesthesiologist can use an MR-compatible anesthesia cart to administer general anesthetics. All patients who cannot communicate directly should be monitored during MR imaging; this monitoring can be performed effectively by radiologic nursing personnel and includes measuring heart rate and pulse oximetry.

Indications for performing abdominal MR imaging in children include problem solving (coronal or sagittal images can help define the origin or extent of a mass, and signal characteristics can be assessed); imaging in patients who are allergic to contrast material or who have multiple metallic clips throughout the abdomen; and evaluation of primary abdominal masses (the role of MR imaging for this purpose is still not clear). The typical protocol for imaging evaluation of an abdominal mass in a child is as follows: plain film studies are followed by sonographic studies. If both results are normal, no further imaging studies are needed. If either radiographic or sonographic results are abnormal, then either MR images or CT scans may be requested—the request somewhat depends on institutional policies. MR imaging does offer advantages over CT in evaluating these masses; it improves visualization of intraspinal involvement, vessel invasion or displacement, bone marrow disease, and the nature of adjacent structures. However, CT is better than MR imaging for detecting calcification and assessing gross physiologic function (i.e., perfusion); furthermore, no contrast agent has yet been proved ideal for MR gastrointestinal imaging, and the longer period of sedation needed for MR studies is a disadvantage in pediatric imaging. The specific applications for abdominal and pelvic MR imaging in children include evaluation and follow-up of abdominal masses, assessment of end-stage liver disease before transplantation, the preoperative and postoperative examination of anorectal anomalies in patients with fecal incontinence, and localization of undescended testes that cannot be visualized on sonography.

Looking toward the future, Dr. Bisset quoted the anonymous sage who said, "Today's facts are tomorrow's fallacies" and pointed out that the higher spatial resolution and ultrafast techniques of MR imaging may speed evaluation of physiologic processes, allow real-time fluoroscopy for interventional procedures, and increase throughput of patients. Other developments that may dramatically affect the use of MR studies in pediatric abdominal imaging include MR angiography, magnetopharmaceutical products (including organ-specific contrast agents), and MR spectroscopy (allowing automatic acquisition and analysis with metabolic imaging as the ultimate goal).

Parallel Focus Session: New Gastrointestinal Interventions

Biliary Interventions

In the first talk of this session, Robert L. Vogelzang (Chicago, IL) emphasized both the ongoing utility and the progress being made currently in biliary interventions and specifically discussed percutaneous cholecystectomy, percutaneous gallstone treatment, and metallic endoprostheses.

The primary indication for percutaneous cholecystectomy is management of acute cholecystitis, but it is also being used for biliary decompression in ductal obstruction, diagnostic cholangiography, and access for interventional procedures.

In 22 high-risk patients with suspected acute cholecystitis, percutaneous cholecystectomy confirmed the diagnosis in 17 and excluded it in five. Dr. Vogelzang strongly recommends the use of percutaneous cholecystectomy in biliary decompression because its performance is easy and very quick (10–15 min), its portable nature allows the procedure to be performed at the patient's bedside, it can enhance performance of percutaneous biliary drainage (both reducing septic complications and allowing the interventionist to "bail out" in unsuccessful cases), it provides controlled biliary opacification to permit targeting of certain ducts, and it yields complete filling of the pancreas.

If percutaneous cholecystectomy is not an option, other percutaneous methods are available for gallstone elimination. MTBE, a colorless, low-viscosity solvent, has provided very rapid dissolution of gallstones. Regarding administration of MTBE via a pump developed by Baxter, national experience in 23 patients has shown that 10 of 15 with noncalcified stones are free of stones, one of seven with calcified stones are free of stones, and cholecystectomy has been performed in six. Another nonsurgical treatment for gallstones, the rotary gallstone lithotrite, is a high-speed rotating propeller that pulverizes gallstones and has shown some promise (through 1991, phase II clinical trials show 16 of 23 patients to be free of stones). Perhaps the easiest, most user-friendly new device, a flexible choledochoscope, is now being used at Mallinckrodt. After a 2-mm working channel has been provided by the insertion of this 15-French scope, the interventionist can use fluoroscopic guidance and direct visualization to localize gallstones. Localization is followed by a combination of imaging-guided basketing, crushing, and lithotripsy to rid the patient of the gallstones. Initial results have been very successful. The future of gallstone treatment may well be a multitechnique approach including laparoscopic cholecystectomy as well as some simple form of gallstone extraction with gallbladder ablation followed by medical gallbladder therapy.

The topic of metallic biliary endoprostheses is somewhat controversial. Advantages include ease of insertion (a single-day procedure), their small track size, and their very large internal lumen. However, use of these stents is somewhat limited because they cost so much (up to $1000/stent), they cannot be removed, and they probably provide no more patency than does a plastic stent. In 12 patients with complex biliary problems, 19 procedures with the metallic endoprostheses were performed; sepsis occurred in only three cases and hemorrhage in one. Primary patency was achieved in 58% of cases (average follow-up, 7 months), and secondary patency was achieved in 100% of cases (average follow-up, 3–30 months). These results suggest that metallic biliary endoprostheses may offer much promise, especially for patients with complex biliary hilar lesions.

Alcohol Ablation: New Nonsurgical Therapy for Liver Tumors

In his introductory remarks, Joseph T. Ferrucci mentioned the three main curative techniques for hepatic tumors: local resection, local/regional ablation, and liver transplantation (which, he mentioned in an interesting side note, is—for some unknown reason—never performed in Japan). Interventional radiologists are examining many possible methods for nonsurgical tumor ablation, including the older techniques of radiation and chemoembolization therapies, as well as more recent methods such as alcohol injection, laser photocoagulation, microwave hyperthermia, cryotherapy, RF electrocauterization, and high-intensity ultrasound treatments. Of the newer techniques, alcohol ablation is the only local/regional technique that has achieved significant clinical acceptance. This method, percutaneous ethanol injection (PEI), is being used for treatment of hepatocellular carcinoma (HCC) and colorectal metastases. In order for PEI to be effective for HCC, the disease must be localized, encapsulated, and in an early stage; tumors less than 3–4 cm have been treated with PEI only, and larger tumors have been treated with a combination of PEI and transarterial embolization. Studies in Japan and Italy have shown PEI survival to be greater than that after resection in patients with comparable disease (e.g., lesion size and number, Child's classification). With simple and inexpensive equipment and standard imaging guidance, alcohol can be injected into these tumors for cure. The mechanism of action is immediate cell death due to local dehydration, protein coagulation, and vascular thrombosis.

Dr. Ferrucci described his clinical trials in 21 lesions so far, in which 8–10 ml of alcohol were injected per session (for lesions averaging 2–3 cm). The imaging studies performed in these tumors included sonography in seven, CT in 11, and intraoperative imaging in one (twice); also direct vision was used to assess three cases in which the lesion was palpable and visible. How does the interventionalist know when the PEI procedure is completed? Four criteria are used: (1) The patient can no longer tolerate side effects such as pain or fever; (2) imaging studies show how the lesion is responding; (3) serum assay provides information on tumor status; and (4) results of fine-needle aspiration biopsy indicate whether any viable tumor remains. If internal septa are present and poor diffusion occurs around the tumor periphery, the procedure is probably failing and should be terminated. Complications of PEI include puncture-related complications (e.g., bleeding) and alcohol-related complications (e.g., fever, pain, venous thrombosis, and alcohol intoxication). In metastatic disease, the criteria for use of PEI include no gross extrahepatic disease on imaging workup (radiography, CT, sonography); fewer than three lesions; and lesion size less than 3 cm. As a rationale for PEI use in colorectal metastases, the procedure may prove to be primary curative therapy for poor surgical candidates, a debulking procedure to enhance effectiveness of systemic chemotherapy, or an adjunct to hepatic resection (either pre- or postoperative control of lesions beyond the bounds of the surgical resection).

In summary, the advantages of PEI of liver tumor are the relative lack of complications, lack of damage to normal tissue, reproducible results, and low cost and wide availability. The problem for future research is clinical assessment to develop criteria for selection of patients and to determine the results and efficacy of this approach. Both MR imaging and positron-emission tomography could be helpful in assessing PEI and other new nonsurgical methods for treating liver tumor.

The Walter B. Cannon Lecture: Recognition and Management of Severe Acute Pancreatitis

John H. C. Ranson (New York, NY) delivered the 20th annual Walter B. Cannon Lecture, and he began his talk by noting that Ambroise Paré made the first attempt in 1579 to explain the pathogenesis of pancreatitis. The diagnosis of acute pancreatitis is primarily clinical, and initial elevation of the serum amylase level is seen in 95% of these patients (vs 5% of patients with acute abdomen). In 15% of cases of acute pancreatitis, the CT findings will be normal; signs in the remaining cases include pancreatic enlargement, obliteration of the fat plane, and fluid in the pararenal space. An upper gastrointestinal series may be helpful in radiologic diagnosis. Although the differentiation between acute pancreatitis and acute biliary disease is very difficult, it also is usually not very important because these two entities call for the same conservative treatment; however, when the patient is extremely ill, the differentiation is important, and the radiologist should use cholangiography to make as exact a diagnosis as possible. In all patients, the recommended management of acute pancreatitis involves close observation, maintenance of intravascular volume, cessation of oral feedings, and respiratory monitoring and support. Dr. Ranson mentioned that studies flawed by the sins of too few patients total or too many patients with mild disease have resulted in flawed recommendations for management. Early surgical measures for acute pancreatitis included sump drainage (increased respiratory and septic complications, not used now); pancreatic resection (no demonstrable benefit); debridement of necrotic tissue; biliary procedures (>60% of patients with gallstones have little or no gross pancreatitis); and peritoneal lavage.

In acute pancreatitis, overall prognosis is correlated with the occurrence of pancreatic sepsis, and there is a relationship between the number of adverse prognostic signs (Ranson's criteria) and death of pancreatic sepsis. Identification of high-risk patients early in the course of their disease could indicate which patients require specific and aggressive treatment. In collaboration with Dr. Emil Balthazar and colleagues at New York University, Dr. Ranson developed a system based on CT findings that describes five classes of infection risk, from lowest risk to highest: A, normal pancreas; B, enlarged pancreas; C, local inflammation; D, one fluid collection; E, more than one fluid collection. A good relationship has been shown between early CT classification and later development of infection. Peritoneal lavage is helpful: Research has shown that peritoneal lavage for 7 days reduces the frequency of peritoneal sepsis and of deaths from pancreatic sepsis; death from abscess also were shown to decrease significantly with long-term (7-day) peritoneal lavage. Therefore, CT appears to be extremely useful in suggesting infection by detecting fluid collections and in helping make the diagnosis of acute pancreatitis when significant clinical uncertainty exists. CT can also be used for progressive assessment of the disease (with or without bolus contrast material), including early identification of any local complications and follow-up of patients who have undergone surgery to assess adequacy of debridement and to identify new fluid collections.

Letters

It's Not as Bad as They Say

(For my friend, Bill Winslade, on turning 50)

They say that when you turn 50
Your mind turns to mush
And your memory declines beyond recalling.
Your mental productions become as tasty as cooked yellow squash,
And new ideas are just a memory (to the extent that you can remember at all).
All of that is true,
But it's not as bad as they say.

They say one's sexual life declines
Or at least becomes seriously selective at age 50.
They also say that men become more attractive as they age
And that young women notice them more.
Everything they say is true,
But it's not as bad, or as good, as they say.

Physical fragmentation that commenced years before
Becomes obvious and palpable at age 50.
They say it takes a bit longer to get the machinery going in the morning,
And the midday nap during the seminar becomes a compulsory health measure.
All of that is true,
But it's not as bad as they say.

Moral forgetfulness and spiritual poverty,
Things that all of us have been working to achieve all our lives, finally becomes easy at age 50
When rationalization finally exceeds ambition.
It's true, it's true,
But it's not as bad as people say.

What people don't say about being 50 is this:

Most of the venom is gone,
And friendliness, tolerance, and kindness become more natural.
Having long been the recipient of many acts of kindness,
One now finds it a lot easier
To accept the stupid foibles of others.

On the whole, turning 50 is a curious experience:

You can still say you're middle-aged,
But you can't say you're young any more.
You observe, when you shave in the morning,
How much more you look like your father,
But you also observe that other people are aging much faster than you are.

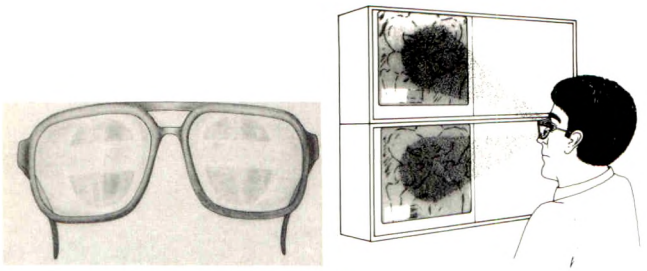
They say that turning 50 causes one to ponder his mortality
And the fact that fewer years remain than have already passed.
They say that's scary,
And while that's partly true,
It's not as bad as they say.

Melvyn H. Schreiber
University of Texas, Medical Branch at Galveston
Galveston, TX 77555-2774

Triple Vision: A Modification of Bifocal Lenses for Radiologists

It is common to see radiologists in front of a double-bank view box making all kinds of gestures in order to interpret the radiologic image accurately. This is especially apparent with radiologists who need bifocal eyeglasses. They may move their heads up and down constantly, trying to obtain the most precise image within their eyes' range. Or, they may constantly move their bifocals up and down in order to use the two magnifications in the lenses needed for far and close detailed vision. Or, they may constantly remove one pair of eyeglasses used for general vision and replace that pair with another pair used for magnified vision [1]. Although all these processes work so that the radiologic image can be interpreted accurately, long- and short-term problems may result. The constant movement of the head and neck may contribute to the development of degenerative arthritis of the cervical spine, and the perpetual replacement or adjustment of the eyeglasses may be annoying and uncomfortable. Radiologists can avoid all these problems and enjoy greater efficiency, accuracy, and comfort while working by using a different type of bifocal, or even trifocal, eyeglasses. These lenses let the radiologist see the image on the top of the double-bank view box just as clearly as the image on the bottom of the view box.

In this modified set of bifocals (Fig. 1), magnification lenses have been placed at both the top and the bottom of the eyeglasses. In the center are the prescription lenses needed for general vision. Eyeglasses such as these have been used by plasterers and painters, who, like radiologists, need to look at working areas that are above



1 2

Fig. 1.—Drawing shows modified bifocal eyeglasses. Top and bottom lenses have same magnification power. Middle lens is for general and long-distance use. Lenses can be blended so that lines are not visible.

Fig. 2.—Drawing shows how modified bifocal lenses are used. Additionally, different strengths may be appropriate for upper and lower lenses when distance from reader's eyes to top of view box is greater than that to bottom of view box.

the head. We could find no articles on the use of these eyeglasses for radiologists. Yet, these eyeglasses may be just as helpful for radiologists as for painters or plasterers.

The glasses can be altered to suit the needs of radiologists. For example, some may want to use a higher magnification for the upper lenses than for the lower lenses [1] so that they can adjust for different reading distances involved in looking at images on the top and the bottom of the view box (Fig. 2). The eyeglasses can be prepared by most opticians and can have three separate lenses or can have the lenses blended together as one smooth surface so that no distinction between the lenses is apparent.

Other modifications of eyeglasses that might be useful include low-reflectance lenses [2] and photochromic eyeglasses [3]. In addition, radiologists, like other practicing physicians, should have regular tests of visual acuity. They can compensate for any deterioration in visual acuity by using corrective lenses or by having their present prescription for corrective lenses adjusted [4].

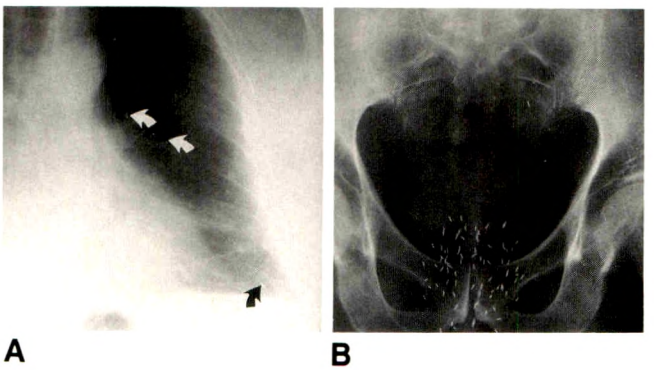
Alysa Beth Krain
Tulane University, Sophie Newcomb College
New Orleans, LA 70118
Louis A. Gilula
Mallinckrodt Institute of Radiology
Washington University, School of Medicine
St. Louis, MO 63110

REFERENCES

1. Revak CS. Viewing glasses as an alternative to bifocals. *Radiology* **1990**;174:578–579
2. Revak CS. Low-reflectance eyeglass lenses: a viewing aid to radiologists. *Radiology* **1979**;131:793–794
3. Balter S, Janower ML. The use of photochromic eyeglasses by radiologists. *Radiology* **1975**;116:450
4. Straub WH, Gur D, Good BC. Visual acuity testing of radiologists: is it time? *AJR* **1991**;156:1107–1108

Pulmonary Embolization of Iodine-125 Implants

A 65-year-old man with a history of asbestos exposure and cigarette smoking had follow-up examinations because of abnormal findings on a chest radiograph. Serial chest radiographs, which had shown no changes over several years, showed calcified pleural plaques, pleural thickening, and mild bibasilar interstitial thickening consistent with pulmonary fibrosis. The patient also had prostatic cancer and had iodine-125 radiation implants placed in the prostate.



A B

Fig. 1.—Pulmonary embolism of iodine-125 prostatic implants.
***A*, Posteroanterior chest radiograph shows embolized ^{125}I seeds (*arrows*) in left lung. Note also pleural plaques and basilar interstitial thickening.**
***B*, Abdominal radiograph shows multiple ^{125}I seeds implanted in prostate.**

A follow-up chest radiograph obtained 7 months after placement of the implants showed at least three short metallic rods in the left lung (Fig. 1A). An abdominal radiograph showed the ^{125}I implants in the prostate (Fig. 1B).

Exogenous embolic materials of all types have been reported, especially as related to IV drug abuse or bullet fragments from gunshot wounds. Iatrogenic emboli such as polyvinyl tubing, lymphangiographic oil, air, silicone antifoam agents, Swan-Ganz catheter tips, and, of course, materials used in embolic therapy have all been reported [1]. To our knowledge, embolization of ^{125}I implants has not been reported in the radiologic literature.

Since their introduction in 1956, ^{125}I implants have been commonly used in the treatment of prostatic cancer [2]. They may be placed by a suprapubic or transperineal approach. Steinfeld et al. [2] recently reported a case of pulmonary embolization of ^{125}I seeds as an unusual complication of therapy. In our case, the patient has had no apparent side effects, although some long-term effects are possible, such as cancer in the adjacent lung. The frequency of such embolization is unknown, but the complication may be more common than is reflected by the literature. Erosion into the paraprostatic venous plexus is the presumed mechanism, so increasing the number of seeds implanted may increase the likelihood of embolization to the lungs. Routine follow-up chest radiographs may be warranted in patients who have such implants.

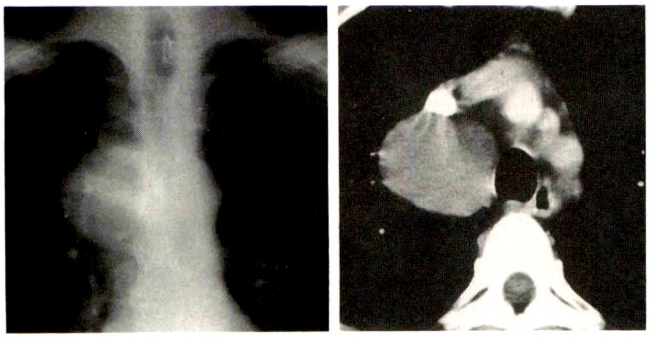
Gregory J. Welle
Kevin Quinn
Madigan Army Medical Center
Tacoma, WA 98431

REFERENCES

1. Pope CF, Sostman HD. Venous thrombosis and pulmonary embolism. In: Putman CE, Ravin CE, eds. *Textbook of diagnostic imaging*. Philadelphia: Saunders, **1988**:584
2. Steinfeld AD, Donahue BR, Plaine L. Pulmonary embolization of iodine-125 seeds following prostate implantation. *Urology* **1991**;37:149–150

Mediastinal Lymphangioma

Lymphangiomas are an uncommon neoplasm and are rare in the mediastinum. Two types of mediastinal lymphangiomas occur. The more common form extends from the neck into the mediastinum (cystic hygroma) and typically occurs in infants. The other form is confined to the mediastinum and frequently occurs in adults [1]. The



A B

Fig. 1.—Mediastinal lympangioma in a 52-year-old man.
***A*, Posteroanterior chest radiograph shows large, well-defined, low-density mass in superior mediastinum. No displacement or extrinsic compression of adjacent structures is present.**
***B*, CT scan with IV contrast material shows mass is nonenhancing, homogeneous, and of low density, with well-defined margins.**

radiologic findings are often sufficiently characteristic to suggest that a mediastinal mass is a lymphangioma.

A 52-year-old man had a routine medical examination. He had no specific complaints or symptoms, and he said he had not had dyspnea, dysphagia, or chest pain. Physical examination showed no evidence of stridor, wheeze, or jugular venous distension. A chest radiograph (Fig. 1A) showed a large, well-defined mass lesion of low density in the superior mediastinum. The mass did not cause any displacement or extrinsic compression of mediastinal structures despite its large size. CT scans with IV contrast material showed a large, well-defined mass in the superior mediastinum adjacent to the right lateral wall of the trachea (Fig. 1B). The mass was homogeneous and of low density (0–24 H) and showed no contrast enhancement. No evidence of displacement or compression of the trachea, superior vena cava, or other adjacent mediastinal structures was seen. The patient subsequently had a thoracotomy with complete resection of the mediastinal mass, which was diagnosed as a cystic mediastinal lymphangioma.

Lymphangioma confined to the mediastinum is a rare cause of a mediastinal mass. A review [2] of 1064 mediastinal mass lesions evaluated at the Mayo Clinic during a 40-year period found that only five were diagnosed as lymphangiomas. As in our case, the tumor usually is detected incidentally on chest radiographs, which most often show a large, well-defined mass without displacement or compression of adjacent mediastinal structures. CT scans show a low-density, homogeneous, well-defined mass that may envelop adjacent mediastinal structures without causing displacement or compression of these structures. Lymphangiomas do not show enhancement with IV contrast material. In one case [3], a mediastinal lymphangioma opacified during lymphangiography, indicating communication with the lymphatic system.

These radiologic findings are not entirely specific; similar findings may be seen with bronchogenic and enteric duplication cysts. However, bronchogenic and duplication cysts are more likely than lymphangiomas to cause displacement and compression of adjacent mediastinal structures. Thus, the finding of a large, well-defined, low-density mass that does not show enhancement with contrast material and does not displace or compress mediastinal structures should suggest the diagnosis of mediastinal lymphangioma.

Michael Baker
D. William Sherrick
Memorial Medical Center
Southern Illinois University School of Medicine
Springfield, IL 62781

REFERENCES

1. Fraser P. *Diagnosis of diseases of the chest*, 3rd ed. Philadelphia: Saunders, **1989**:1622–1623, 2854–2857
2. Wychulis AR, et al. Surgical treatment of mediastinal tumors: a 40 year experience. *J Thorac Cardiovasc Surg* **1971**;3:379–392
3. Pilla TJ, Wolverson MK, Sundaram M, Heiberg E, Shields JB. CT evaluation of cystic lymphangiomas of the mediastinum. *Radiology* **1982**;144:841–842

American College of Radiology Mammography Accreditation Program

The recent article by McLelland et al. [1] on the American College of Radiology (ACR) Mammography Accreditation Program points out the objectives of this program. Certainly the program was initiated with good intentions of improving the quality of mammography in the United States. It is unfortunate that the program has implications beyond quality assurance that I have not seen addressed in the literature.

Discussion on the subspecialization of radiology continues, questioning the future of general diagnostic radiology as a specialty. It is ironic that the death knell for general diagnostic radiology may have come from our own ACR.

Quickly the accreditation program has been embraced by the media, to the point that national network news programs have stated adamantly that a woman should not have mammography performed at an institution that is not accredited. Medicare has adopted guidelines virtually identical to those of the ACR program as a condition for reimbursement. Others are sure to follow.

Unfortunately, the ACR guidelines go beyond surveys of equipment and technical performance. Along with the technical survey come requirements for previous training and continuing medical education (CME) in mammography as a requirement for accreditation. Are we now expected to accrue a certain number of hours of CME in chest medicine each year in order to be allowed to interpret chest radiographs? The concept of examination-specific CME as a prerequisite for interpreting each examination represents an impossible task. It is conceivable that if this trend continues I could find myself ineligible to interpret radiographs of the spine because I had not completed enough CME on spinal disorders. Reading the literature and attending general educational meetings such as those of the American Roentgen Ray Society and the Radiological Society of North American and other selected specialty meetings no longer seems to be acceptable for continuing education. It is unrealistic to demand that a general radiologist accrue 15 hr or more of CME credit every 3 years for each specific examination he or she performs.

Those of us in private practice already face an enormous burden of regulation and paperwork. It is unfortunate that the ACR has opened the gates for a flood of accreditation paperwork for those of us who practice general radiology.

Richard E. Barlow
Pontchartrain Radiology Associates
Slidell, LA 70458

REFERENCE

1. McLelland R, Hendrick RE, Zinninger MD, Wilcox PA. The American College of Radiology Mammography Accreditation Program. *AJR* **1991**;157:473–479

Reply

As Dr. Barlow has pointed out, the intention of the voluntary American College of Radiology (ACR) Mammography Accreditation Program is to improve the quality of mammography in the United

States. Evidence indicates that the program is succeeding. The program evaluates image quality; radiation dose; quality control procedures; and personnel qualifications, including the continuing medical education (CME) of radiologists.

The requirements for previous training and for CME were included because many radiologists did not receive adequate training in mammography when they were residents. Because of increasing demands for mammography, radiologists without specialized training were being asked to interpret mammograms. The CME requirements were an attempt to overcome these problems and to advance expertise among radiologists in mammography.

The educational requirements of the program are hardly ominous. Fifteen hours of mammography-specific CME every 3 years amounts to only 5 hr every year. Contrary to Dr. Barlow's statement, the CME requirements can be obtained by attending mammography-specific category 1 refresher courses and scientific sessions at the annual meetings of the American Roentgen Ray Society or the Radiological Society of North America. Category 1 CME requirements can also be met without leaving home by means of the ACR Mammography Home Study Course, the Breast Imaging Self-evaluation Syllabus, and the ACR Video Disc on Breast Imaging. Category 1 CME credit is also granted for attendance at the ACR Symposia on Mammography and the ACR National Conference on Breast Cancer, as well as for attendance at many other mammography courses offered across the United States. Category 2 CME activities also meet the educational requirements of the ACR program. Category 2 CME credits specific to mammography can be obtained by reading or preparing mammography-related journal articles, attending or presenting mammography lectures that do not carry category 1 credit, preparing and presenting lectures to medical students or residents, or viewing videotapes on mammography. Five hours per year of such activities is far fewer hours than any radiologist who interprets mammograms is likely to obtain to stay current in the field.

Whether we like it or not, mammography is a high-profile procedure that is increasingly requested. This is partly because of mammography's capacity to detect breast cancer earlier, when the disease is more curable, and partly because it is a difficult examination to perform properly, leading to errors and, in some cases, litigation. Quality mammograms, accurately interpreted, can reduce these errors and the menace of litigation.

The concept of mammography accreditation was a response to clearly identified problems of quality in mammography. Acceptance and endorsement of the program by a wide variety of medical organizations, government, and the public support the view that such a program was needed. Accreditation is a constructive process meant to improve mammography by providing national standards and a program that individual sites can use to compare their performance to those standards. It is hoped that the program will reduce the number of unqualified individuals, including nonradiologists, who attempt to perform mammography.

We can appreciate Dr. Barlow's aggravation with the increasing "burden of regulation and paperwork" in radiology. However, the scenario he describes of "examination-specific CME as a prerequisite for interpreting" other diagnostic radiologic examinations is unlikely. However the ACR Council did adopt the CME standard for mammography. The ACR has not implemented, nor is it currently considering implementation of, accreditation programs for other techniques or examination-specific areas of radiology.

The ACR Mammography Accreditation Program is unique in radiology. It has arisen to resolve clearly identified problems of quality in mammography. It is an example of a voluntary program whose benefits far exceed its burden on the radiologist.

Robert McLelland
University of North Carolina
Chapel Hill, NC 27599-7510
R. Edward Hendrick
University of Colorado Health Sciences Center
Denver, CO 80262

Dirofilariasis of the Breast Mimicking Carcinoma on Mammography

Rarely, *Dirofilaria repens* organisms are found in humans as subcutaneous nodules, sometimes located in the breast. To the best of our knowledge, a case of *D. repens* nodules mimicking carcinoma on mammography has not been previously reported.

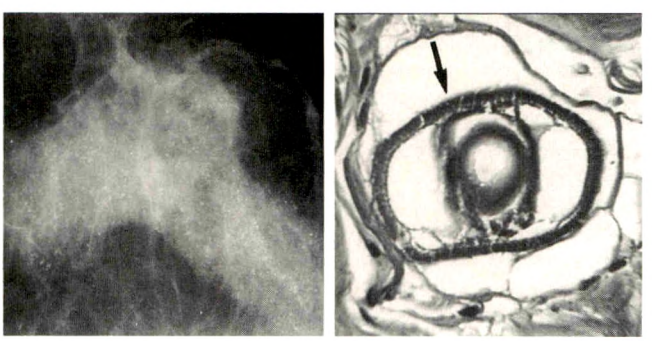
An 83-year-old woman had a mass in her left breast clinically suggestive of a malignant tumor. No palpable mass was detected in the right breast. Mammograms showed a 3-cm nodule with indistinct borders in the left breast and a large cluster of microcalcifications in the upper outer quadrant of the right breast (Fig. 1A). The microcalcifications were variable in size, shape, and density; some were linear, suggesting an intraductal location. Initial diagnosis was probable intraductal carcinoma. The leukocyte count was 5600/μl, without eosinophilia. The left breast and the right upper outer quadrant of the right breast were removed. Histologic examination showed a typical medullary carcinoma in the left breast and fibrocystic changes and rare lymphocytes in the right breast. The calcifications seen in the right breast on mammography were located in the ducts and lymphatics and were atypical calcospherites with an unusual "cylindrical" shape (Fig. 1B). Histologic examination showed that the calcospherites were fossilized *Dirofilaria* with a thick, layered cuticle and outer fine transverse striations (cuticular ridges). Inner structures corresponding to intestine and reproductive tube were characteristic of adult *D. repens*. The patient lived in a nonendemic area for *D. repens* but had a dog and had vacationed in the south of France, an endemic area for the parasite.

Dirofilaria are nematodes usually transmitted to humans by mosquitoes. Two types of zoonotic infections due to *Dirofilaria* are recognized: pulmonary and cutaneous. The pulmonary type is due to *Dirofilaria immitis* (the dog heartworm) and occurs mainly in the southern United States. Subcutaneous nodules, which may be located in the breasts, are typical of the cutaneous variety.

Dirofilariasis has no characteristic serologic finding; antifilarial antibodies may or may not be present. The genus *Dirofilaria* can be distinguished histologically by several features [1]. The diameter of the parasites varies from 100 to 600 mm. The organisms have a thick, multilayered cuticle that either is smooth or has longitudinal ridges, which resemble the spokes of a wheel.

These nematodes invade the subcutaneous tissues of dogs and cats, both wild and domestic, in Europe, Asia, and Africa. In humans, the infection can cause subcutaneous or conjunctival swelling with pain and inflammation or can be asymptomatic, as in our patient.

In endemic areas or occasionally in nonendemic areas in immigrant populations, filarial parasites may produce breast nodules. Twenty-



A **B**

Fig. 1.—83-year-old woman with histologically proved dirofilariasis of breast.

***A*, Craniocaudal mammogram of right breast shows a large cluster of granular microcalcifications of various sizes, shapes, and densities, suggestive of carcinoma.**

***B*, Photomicrograph of pathologic specimen shows a duct with calcification (*arrow*) due to fossilized *Dirofilaria*. (H and E, original magnification ×250)**

five cases of breast nodules subsequently proved to be *Dirofilaria* [1–4] have been reported; most occurred in the Mediterranean basin.

Numerous microcalcifications are also found in comedocarcinoma, but they are usually denser than those associated with dirofilariasis and occur in V and Y patterns. Nevertheless, the shape of some of the microcalcifications was highly suggestive of an intraductal location, and the initial diagnosis should have been a malignant lesion even if contralateral cancer had not been present. As shown in our patient, dirofilariasis is another cause for intraductal microcalcifications and can mimic breast cancer on mammography.

Christophe Frouge
Daniel Vanel
Institut Gustave Roussy
94805 Villejuif, France
Henri Tristant
Cabinet de Radiologie
75007 Paris, France
and colleagues

REFERENCES

1. Gutierez Y, Paul M. Breast nodule produced by dirofilaria tenuis. *Am J Surg Pathol* **1984**;8:463–465
2. Conly JM, Sekla LH, Low DE. Dirofilariasis presenting as a breast lump. *J Can Med Assoc* **1984**;130:1575–1576
3. Gupta IM. A subcutaneous nodule of the breast due to an adult filarial worm. *Am J Trop Med Hyg* **1964**;13:306–310
4. Gutierez Y. Diagnostic features of zoonotic filariae in tissue sections. *Hum Pathol* **1984**;15:514–525

Subpectoral Mass Mimicking a Malignant Breast Mass on Mammography

Lipomas arise from any soft tissue that contains fat and can be found in the extremities, thorax, and breast [1]. When lipomas occur in the breast, an encapsulated mass with a density typical of fat is seen. We describe a case of an unusual subpectoral lipoma that mimicked a malignant breast mass on mammograms. The large size of the lipoma caused compression of the breast parenchyma against the skin, producing the appearance of skin thickening on mammograms.

A 20-year-old woman had had a progressively enlarging hard mass in her left breast for 4 years. Mammograms showed a 16 × 20 cm mass with a density like that of fat occupying the entire breast (Fig. 1A). The remaining breast parenchyma was compressed against the skin, simulating skin thickening. The pectoralis muscle was also compressed against the skin, and a thin piece of atrophic pectoralis muscle could be seen extending anteriorly from the chest wall (Fig. 1B). At surgery, it was evident that the mass was originated from the chest wall and did not lie within the breast tissue as the mammogram suggested. Marked atrophy of the breast parenchyma due to chronic compression was present.

The differential diagnosis in this young woman would include lipoma, because the density of the mass was like that of fat. However, the hardness of the mass and the apparent skin thickening seen on mammography suggested the mass might be malignant, such as a sarcoma. In retrospect, it was apparent that compression of breast parenchyma against the otherwise normal skin caused by the subpectoral lipoma produced the appearance of skin thickening. The combination of the overlying pectoralis muscle and the lipoma explained why the lipoma was firm to palpation.

Recognition of the displaced pectoralis muscle on mammograms may allow correct identification of the origin of retropectoral lipomas such as this one and thus explain the inconsistency between the density of the lipoma on mammography and the hardness of the tumor on physical examination.

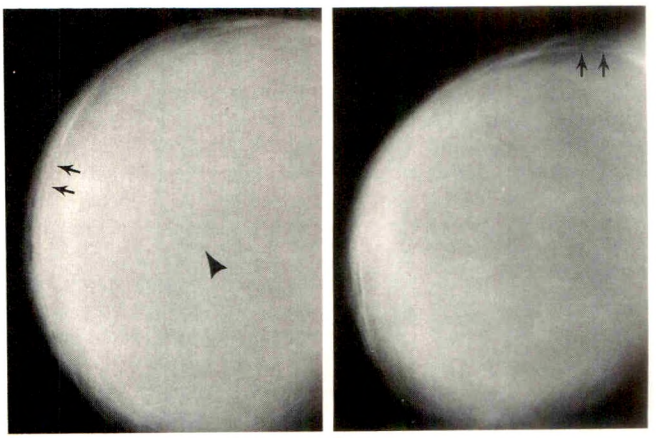


Fig. 1.—Subpectoral lipoma in a 20-year-old woman.
***A*, Craniocaudal mammogram of left breast shows a large, radiolucent mass (*arrowhead*) occupying entire breast. Note apparent skin thickening (*arrows*).**
***B*, Mediolateral mammogram shows atrophic displaced pectoralis muscle (*arrows*).**

Cynthia A. Britton
University of Pittsburgh Medical Center
Pittsburgh, PA 15213

REFERENCE

1. Haagensen CD. *Diseases of the breast*, 2nd ed. Philadelphia: Saunders, **1971**:305–307

Color Doppler Sonography in Afferent Loop Syndrome

We describe three patients in whom color Doppler images were a useful addition to sonograms for diagnosis of afferent loop syndrome. In two patients, the cause of the syndrome was recurrent cancer; in the third, it was an internal hernia. In all three patients, color Doppler images showed that the dilated afferent loop was behind the mesenteric vessels and in front of the aorta (Fig. 1).

Dong Ho Lee
Jae Hoon Lim
Young Tae Ko
Kyung Hee University Hospital
Seoul 130-702, Korea

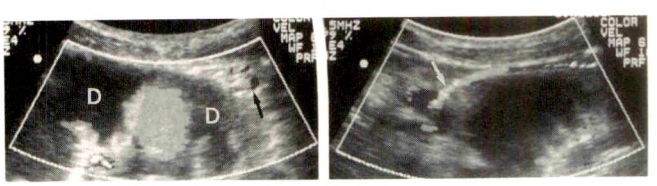
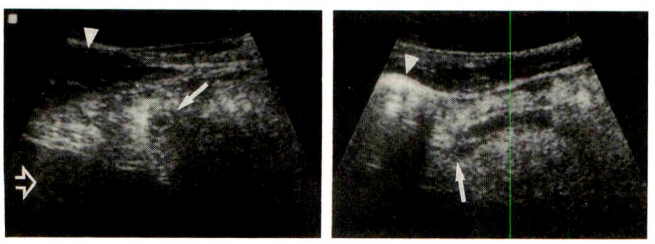


Fig. 1.—Color Doppler sonograms (shown here in black and white) of 57-year-old man with afferent loop syndrome caused by internal hernia.
***A*, Transverse view shows dilated afferent loop (D) between abdominal aorta and superior mesenteric vessels (*arrow*).**
***B*, Longitudinal view shows dilated afferent loop is behind superior mesenteric artery (*arrow*).**

Diagnosis of Epigastric Appendicitis Based on Sonographic Findings

Sonography has come to play an important role in the diagnosis of acute appendicitis [1–3]. It is also well known that the appendix can be found in unusual locations because of mobility of the cecum, excessive length of the appendix, or malrotation of the bowel [4]. We describe a case in which sonography played a pivotal role in the diagnosis of appendicitis in a patient whose appendix was located in the epigastrium.

A 32-year-old man had had burning epigastric pain, nausea, and vomiting for 2 days. His abdomen was diffusely tender, particularly in the epigastric area, and he had involuntary guarding and rebound. Results of laboratory tests were normal except for a leukocyte count of 22,900/μl. Plain films of the abdomen were normal.



A B

Fig. 1.—Epigastric appendicitis.

***A*, Transverse sonogram through epigastrium shows a 1.2-cm round structure (*solid arrow*) that represents appendix in cross section. Structure has hypoechoic outer rim, echogenic inner ring, and hypoechoic center. *Open arrow* = liver, *arrowhead* = rectus abdominis muscle.**

***B*, Oblique sonogram through epigastrium shows a tubular structure that represents appendix in longitudinal section. Structure has hypoechoic center surrounded by an echogenic layer and an outer hypoechoic rim. Note small amount of fluid (*arrow*) surrounding appendix and connection between appendix and cecum. *Arrowhead* = gas in cecum.**

Sonograms showed a thick-walled tubular structure in the epigastrium (Fig. 1). The structure was 1.0 cm in diameter and was surrounded by fluid. Its cephalic end connected with a part of the gastrointestinal tract that contained gas and was thought to represent the cecum. Caudally, the tubular structure ended blindly. The patient reported that the area was tender when it was scanned. The diagnosis was acute appendicitis with periappendicitis in the epigastrium. At surgery, an acutely inflamed appendix adjacent to the anterior abdominal wall and anterior to the liver was found and resected. A phlegmon involving the appendix and several loops of bowel prevented exploration of the abdomen. The patient did well, and no further investigations were done.

Anastasios Boubalos
Patrice Bret
Montreal General Hospital
McGill University
Montreal, Quebec, Canada H3G 1A4

REFERENCES

1. Vignault F, Filiatrault D, Brandt ML, Garel L, Grignon A, Quimet A. Acute appendicitis in children: evaluation with US. *Radiology* **1990**;176:501–504
2. Puylaert JBCM. Acute appendicitis: US evaluation using graded compression. *Radiology* **1986**;158:355–360
3. Jeffrey RB Jr, Laing FC, Townsend RR. Acute appendicitis: sonographic criteria based on 250 cases. *Radiology* **1988**;167:327–329
4. Schwartz SI, Ellis H. *Maingot's abdominal operations*. 8th ed. Norwalk, CT: Appleton-Century-Crofts, **1985**:1255–1258

Visceral Calcifications in Patients with AIDS

We read with interest the two cases reported by Towers et al. [1] as examples of visceral calcifications in AIDS patients caused by infections with organisms other than *Pneumocystis carinii* and appreciate the citation of our case report [2] of disseminated *P. carinii* infection. At first glance, it might seem that the two papers contradict each other, or that the cases and conclusions of Towers et al. supersede ours. This is not the case. However, a critical question is raised: What constitutes sufficient radiologic-pathologic correlation?

We previously stated [2] that infections other than disseminated *P. carinii* infection might result in focal calcifications. However, the evidence that this has happened, as provided by Towers et al., is circumstantial. Regarding the first case reported by Towers et al., we asked several pathologists to review Figure 1C. In their opinions, the calcifications shown in that autopsy specimen are not the result of necrotizing cytomegalovirus nephritis, which would be primarily localized to the renal parenchyma and associated with areas of visible inflammation. The calcifications shown appear to reside within the renal tubules and are more correctly termed tubular microliths, which are nonspecific, can be seen in any case of old or active tubular renal injury, and frequently are found at autopsy. Tubular microliths of the size shown would normally be too small to be visible as discrete echogenic foci on sonograms. Therefore, the cause of the sonographic abnormality remains in question, but we think it more likely represents healed residua of disseminated *P. carinii* infection that occurred during the second episode of *P. carinii* pneumonia that developed while the patient was receiving aerosolized pentamidine prophylactically. We have seen similar findings develop in several cases of disseminated *P. carinii* infection.

The second case of Tower et al. reminds us of a patient we saw recently. *P carinii* pneumonia developed in an AIDS patient who also had disseminated *Mycobacterium avium-intracellulare* infection. Abdominal CT scans obtained during therapy for the pneumonia showed hepatic calcifications similar to the ones shown in Figure 2B in the paper by Towers et al. The calcifications became more dense as treatment proceeded. The mycobacterial infection was not being treated at the time. The patient ultimately died, and autopsy showed widespread visceral mycobacterial infection, with extensive involvement of the hepatic reticuloendothelial system. However, most of the hepatic calcifications were localized to rather small foci of foamy exudate containing *Pneumocystis* organisms, diagnostic of disseminated *P. carinii* infection. A few scattered hepatic calcifications were not associated with any localized inflammation and were probably the residua of *P. carinii* organisms killed during therapy. Similarly, the adrenal glands had extensive involvement by cytomegalovirus; however, all adrenal microcalcifications occurred in foci of *Pneumocystis* organisms similar to the foci found in the liver. A needle biopsy of the liver, which was not done, probably would have shown infection with *M. avium-intracellulare*, as in the case of Towers et al., and the small, scattered, calcified foci associated with disseminated *P. carinii* infection would have gone undetected. We present this as a possible scenario, especially as no calcifications are evident in the mycobacterial granulomas in the paper by Towers et al.

The initial establishment of a radiologic-pathologic correlation requires evidence that the radiologic finding (the calcification) is directly within or intimately associated with the pathologic lesion (focus of necrotizing infection), as we showed in our published case report [2] and in the case of this AIDS patient who had the mycobacterial infection. Anything less is inconclusive. Towers et al. did not provide convincing radiologic-pathologic correlation. Nor did Falkoff et al. [3], who did not report any mycobacterial granulomas or calcifications in renal biopsy specimens from an AIDS patient who had *M. avium-intracellulare* infection. This is usually a diffuse infection, and blood cultures are usually positive for the organism. It is not clear how to

interpret the findings when tissue cultures are positive for mycobacteria in a patient such as the one described by Falkoff et al. Recovery of colonizing or circulating organisms from biopsy specimens without convincing demonstration of the actual radiologic or pathologic lesion is not sufficient proof of radiologic-pathologic correlation. In such instances, the results of the biopsy may be misleading and less informative than changes in the lesion shown by radiologic follow-up during specific therapy.

Even if we ignore these problems and accept these findings as calcifications associated with processes other than *Pneumocystis* infections, it would not alter our overall approach to the management of patients with disseminated *P. carinii* infection. We have treated six cases of disseminated *P. carinii* infection, with similar findings (i.e., calcifications) on radiographs, all in patients who had pathologically proved, active *P. carinii* pneumonia. Because such patients must be treated for the pneumonia anyway, we do not think that an invasive procedure is warranted to histologically show the presence of disseminated organisms. We still think that if a patient has pathologically proved, active *P. carinii* infection (especially if the patient has been receiving aerosolized pentamidine), characteristic disseminated lesions on CT scans or sonograms, and no overriding clinical process that mandates biopsy, then the lesions can be considered part of the *P. carinii* pneumonia, and the patient should have treatment of the pneumonia and close radiologic and clinical follow-up. In cases such as those reported by Towers et al. in which no active pneumonia with *P. carinii* was shown, percutaneous biopsy can be done as clinically indicated. For clinical decision making, and for purposes of publication, the notion that biopsy is mandatory and all informative should be reexamined. The chronologic improvement of lesions at clinical and radiologic follow-up during treatment of *Pneumocystis* infections is as good as, and occasionally might be better than, biopsy findings for diagnosing disseminated *P. carinii* infection.

Irwin M. Feuerstein
James M. Pluda
Mark Raffeld
Sarah K. Barksdale
Georgetown University
Washington, DC 20007
National Institutes of Health
Bethesda, MD 20892

REFERENCES

1. Towers MJ, Withers CE, Hamilton PA, Kolin A, Walmsley S. Visceral calcification in patients with AIDS may not always be due to *Pneumocystis carinii*. *AJR* **1991**;156:745–747
2. Feuerstein IM, Francis P, Raffeld M, Pluda J. Widespread visceral calcifications in disseminated *Pneumocystis carinii* infection: CT characteristics. *J Comput Assist Tomogr* **1990**;14:149–151
3. Falkoff GE, Rigsby CM, Rosenfield AT. Partial combined cortical and medullary nephrocalcinosis: US and CT patterns in AIDS-associated MAI infection. *Radiology* **1987**;162:343–344

Reply

We thank Dr. Feuerstein and his colleagues for their comments, and for the opportunity to clarify the message in our case report [1]. Our aim was not to contradict or supersede their previous report [2], but to illustrate a clinical and radiologic problem we encountered in two patients with AIDS and visceral calcifications. A sick patient with visceral calcifications may not have disseminated *Pneumocystis carinii* infection. The calcifications may be inactive residua of such an infection, or as we have suggested, other agents may be responsible for the illness and the calcifications. The point we wish to make is that without pathologic or microbiologic proof we do not know. Our cases illustrate this possibility. Certainly, most patients with visceral calcifications and *P. carinii* detected, for example, in the lungs, can be considered to have disseminated infection, and these patients do not need biopsies. However, many patients with these calcifications do not have active *P. carinii* pneumonia, and we think that biopsy should be done more often than it currently is.

Our evidence that *Mycobacterium avium-intracellulare* and cytomegalovirus caused the visceral calcifications in our patients is not conclusive, but we were careful not to claim it is. Definitive radiologic-pathologic correlation in AIDS patients is difficult, but knowledge of these infections will not advance if correlation is not attempted. Editing for the case-report format did not allow a full discussion of the pathologic findings. We agree that the calcifications shown in the histologic section of renal tissue from our first patient are tubular microliths. The purpose of the illustration is to show that the kidney was the site of a postinflammatory calcific process. Cytomegalovirus causes an interstitial nephritis, and inclusions may be found in the epithelial cells of proximal tubules [3]. The cause of tubular microliths is unknown, but it is not inconceivable that they could be caused by cytomegalovirus. Specimen radiography and dissection showed amorphous clumps of calcification 2–3 mm in diameter that were consistent with the echogenic foci seen on sonograms. The results of immunohistochemical staining with monoclonal antibodies against *P. carinii* in multiple sections were negative. Tubular microliths such as those illustrated would certainly not be seen as discrete abnormalities on sonograms.

It is possible that the calcifications in our patients represent healed residua of disseminated *P. carinii* infection, but without the information obtained from the biopsies, both patients would have been treated inappropriately for that infection. Our second patient had normal findings on sonograms of the abdomen 18 months and 2 years, respectively, after her previous *P. carinii* pneumonia, and she received no specific treatment other than prophylactic aerosolized pentamidine (it is recognized that such prophylaxis is associated with dissemination of *P. carinii* because serum levels of the drug are low). After sonograms showed the calcifications, she did not receive any specific treatment for *P. carinii* infection and was not compliant with further prophylaxis with aerosolized pentamidine. She survived for 12 months after biopsy. We think it is unlikely that this patient had an episode of disseminated *P. carinii* pneumonia that resolved without treatment other than aerosolized pentamidine, and that the timing of her previous *P. carinii* pneumonia and the follow-up sonograms excluded that infection as the cause of the calcifications. Another case remarkably similar to this one has been reported recently [4], and the authors make the same conclusion about the need for biopsy. It is not known how frequently these calcifications occur asymptomatically in patients receiving aerosolized pentamidine. In most cases, imaging is performed because of a clinical or biochemical abnormality.

We do not propose that patients who have proved, active *P. carinii* infection and visceral calcifications need biopsy, but those without such proof do, unless the calcifications are known to be healed residua of previous disseminated *P. carinii* infection.

Mark J. Towers
Cynthia E. Withers
Paul A. Hamilton
Arnost Kolin
Sharon Walmsley
Sunnybrook Health Science Centre
University of Toronto
Toronto, Ontario, Canada M4N 3M5

REFERENCES

1. Towers MJ, Withers CE, Hamilton PA, Kolin A, Walmsley S. Visceral calcifications in patients with AIDS may not always be due to *Pneumocystis carinii*. *AJR* **1991**;156:745–747
2. Feuerstein IM, Francis P, Raffeld M, Pluda J. Widespread visceral calcifications in disseminated *Pneumocystis carinii* infection: CT characteristics. *J Comput Assist Tomogr* **1990**;14:149–151
3. Colvin RB, Fang LST. Interstitial nephritis. In: Tisher C, Brenner B, eds. *Renal pathology*. Philadelphia: Lippincott, **1989**:735–736
4. Bray HJ, Lail VJ, Cooperberg PL. Tiny echogenic foci in the liver and kidney in patients with AIDS: not always due to disseminated *Pneumocystis carinii*. *AJR* **1992**;158:81–82

Small-Bowel Perforation After Preoperative High-Dose-Rate Intraluminal Brachytherapy for Rectal Carcinoma

In the treatment of rectal cancer, preoperative radiotherapy has been reported to increase local control [1]. We have treated 71 cases of rectal cancer by using preoperative high-dose-rate intraluminal brachytherapy. In two patients, small-bowel perforation occurred after irradiation.

Both patients received a total of 80 Gy preoperatively via a remote afterloader (RAL-303, Toshiba, Tokyo). The radiation was given in two fractions over 6 days for one patient and in four fractions over 12 days for the other. Treatment time per fraction was 23.2 min to a 13-cm length of the rectum for the first patient and 15.4 min to a 9-cm length for the second. The source of radiation was cobalt-60, with an activity of 2.53 Ci (93.6 GBq). The dose rate was 320 R (8.3×10^{-2} C/kg) per min at a point 1 cm from the source. The dose at a point 5 mm below the mucosa was calculated by using a computer (Varian-Ro7).

Both patients had sphincter-preserving surgery 2 weeks after brachytherapy was completed. Histologic examination showed that loss of viable cancer cells and necrosis involved more than 75% of the tumor volume in both cases. At 4.5 months (the first patient) and 4 months (the second patient) after the initial operation, generalized peritonitis associated with perforation of the distal ileum developed. Resection of distal ileum and ileostomy were performed in both cases. Examination of surgical specimens showed multiple acute ulcers penetrating into the muscularis propria and serosal thickening (Fig. 1), findings compatible with radiation-induced ileitis. The first patient recovered, but the second died of the disease.

Damage to the small bowel that requires surgical intervention occurs in 0.5–16.0% of patients after radiotherapy for pelvic neoplasms [2]. The prevalence of small-bowel injury after external-beam irradiation was higher than that after intracavitary irradiation in patients with gynecologic tumors. High-dose-rate intraluminal brachytherapy allows massive irradiation concentrated on the malignant tissue to be applied over a short time [3]. However, because it appears to have a low therapeutic ratio, the safe dose limit must be defined carefully [3]. The time-dose factors for the rectum calculated by using the standard procedure [4] were 528.3 and 391.3 in these cases. In other cases, we subsequently administrated more moderate doses of radiation (30–40 Gy) at the same dose rate. The calculated time-dose factors were reduced to a range of 127.2–198.7 with this modification. With the new regimen, we have not experienced any similar fatal complication. Understanding the severity of the complications of preoperative high-dose-rate intraluminal brachytherapy can lead to safer application of this procedure with appropriate doses and treatment volumes, thus providing better clinical results.

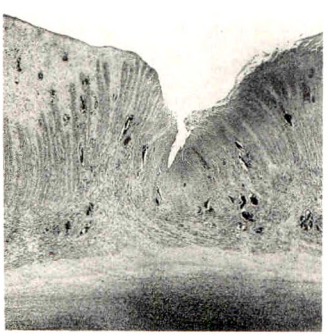


Fig. 1.—Small-bowel perforation after preoperative high-dose-rate intraluminal brachytherapy in rectal carcinoma. Photomicrograph of section of resected small bowel shows deep ulcer penetrating muscularis propria. Note also telangiectasia with cellular infiltration and fibrous thickening of serosa. (H and E, original magnification ×20)

Hidenori Yanagi
Masato Kusunoki
Norihiko Kamikonya
and colleagues
Hyogo College of Medicine
Nishinomiya, Hyogo 663, Japan

REFERENCES

1. Cummings BJ. A critical review of adjuvant preoperative radiation therapy for adenocarcinoma of the rectum. *Br J Surg* **1986**;73:332–338
2. Miholic J, Schlappack O, Klepacto W, et al. Surgical therapy of radiation-induced small bowel lesions: report of 34 cases with a high share of patients with combined chemotherapy. *Arch Surg* **1987**;122:923–926
3. Arai T, Morita S, Kusutani Y, et al. Relationship between total isoeffect dose and number of fractions for the treatment of uterine cervical carcinoma by high dose-rate intracavitary irradiation. *Br J Radiol* **1986**;17:89–92
4. Orton CG. Time-dose factors (TDFs) in brachytherapy. *Br J Radiol* **1974**;47:603–607

Detection of Hepatic Masses in Patients with Carcinoma

The relatively low sensitivity and specificities for MR imaging in detection of hepatic lesions in the study by Wernecke et al. [1] can be attributed in part to the suboptimal scanning techniques used by the authors. A TR of 2000 msec and a TE of 70 msec give a suboptimal T2 weighting; a TR/TE of 2500–3000/80–90 will give better contrast-to-noise ratios at high field strengths. The mixed spin-echo sequences of 800/70 could hardly be called T2 weighted. The lesion-to-liver contrast-to-noise ratio on T1-weighted images will also be improved by reducing TR and TE (TR reduced from 800 to 300–400) to decrease the spin-density component, which has little contrast for detection of hepatic lesions at 1.5 T.

The authors do not mention reduction of phase-ordered respiratory motion, and failure to reduce this motion would be a substantial limitation in imaging the abdomen. In addition, they used 10-mm-thick slices with, presumably, a 10–20% gap, which is equivalent to using 12-mm-thick slices, considerably higher than the 9-mm slices used for CT. From the images presented, it appears that in-plane resolution has been sacrificed to some extent in order to obtain more averages. Hence, the difference between CT and MR imaging in the detection of smaller lesions may be attributed in part to simple volume averaging. In my community hospital, 7-mm-thick slices and a 1.2-mm gap are routinely used for MR evaluation of the liver for metastases. In addition, cardiac pulsations and gastric motion compromise evaluation of the left lobe of the liver, which could be partially reduced by using first-order gradient moment nulling and various methods to decrease peristalsis (e.g., fasting, glucagon).

The simple techniques mentioned here for improving detection of hepatic lesions have been well known and commercially available for

several years and do not require improvement in current technology. State-of-the-art studies that compare efficacy of competing imaging techniques are important in our cost-conscious environment. The potential adverse effects of a study like the one by Wernecke et al. is that nonmedical third-party payers and physicians not trained in imaging technology will quote it and similar studies to justify using suboptimal technology because the cost is less. This may result in unnecessary surgery or duplication of imaging studies in order to confirm equivocal findings. There may be two additional reasons to select MR imaging over CT: the ability to distinguish between focal fatty infiltration and metastases with MR (e.g., after chemotherapy) and the risks of allergy and renal toxic reactions associated with use of iodinated contrast material.

Andrew Yang
Baltimore, MD 21239

REFERENCE

1. Wernecke K, Rummeny E, Bongartz G, et al. Detection of hepatic masses in patients with carcinoma: comparative sensitivities of sonography, CT, and MR imaging. *AJR* **1991**;157:731–739

Reply

We appreciate Dr. Yang's comments on our article [1]. Some of the issues he mentions are addressed in our article, but we discuss them in greater depth here.

First, we agree that the spin-echo pulse sequences (800/15, 800/70, and 2000/70) used in our study were only moderately T1 and T2 weighted. However, at the time of the study, these were the optimal pulse sequences available for liver imaging on our MR system (1.5 T). Before starting the study, we optimized the liver-to-spleen contrast on T1-weighted images obtained at 1.5 T by using different T1- and T2-weighted pulse sequences in volunteers who had MR imaging of the liver. Our early results showed no significant improvement in spleen-to-liver contrast-to-noise ratios when TR was reduced from 800 msec to 400 or 300 msec. Therefore, in order to scan the entire liver in one acquisition, we decided to use a TR of 800 msec (four excitations). A short TR/short TE (<300/<20) T1-weighted spin-echo pulse sequence with multislice capability was not available at the time. However, the highest lesion-to-liver contrast on T1-weighted images was with the T1-weighted gradient-echo pulse sequence (GRE 100/6/60°), which was used in our study routinely. These results are in agreement with recent data published by Saini et al. [2], who found similar lesion-to-liver contrast on T1-weighted images with short TE T1-weighted spin-echo and gradient-echo pulse sequences.

For T2-weighted imaging, the spin-echo 2000/70 pulse sequence was selected to provide lesion-to-liver contrast as well as good anatomic detail needed for tumor staging. Although more heavily T2-weighted images may provide higher lesion-to-liver contrast of "non-solid" tumors, our initial optimization of pulse sequences showed no significant differences in liver-to-spleen contrast (used as a model for "solid" tumors) for the 2000/70, 2000/90, and 2500/90 spin-echo pulse sequences. Inasmuch as our goal was to detect and to stage focal liver lesions, not to characterize them, we used a TR/TE of 2000/70 because imaging time was shorter and anatomic resolution was better than with a TR/TE of 2500/90. However, we agree that the pulse sequences used in our study are not useful in the differential diagnosis of malignant and benign (cysts, hemangiomas) hepatic lesions.

We used several techniques to reduce motion artifacts. In order to reduce artifacts resulting from respiratory or gastric motion and pulsatile flow, first- and second-order phase reordering were used routinely. Furthermore, presaturation pulses with a slice thickness of 5 cm each were used above and below the liver in order to reduce artifacts from pulsatile flow within the aorta and vena cava. Other methods to reduce gastric motion and bowel peristalsis, such as fasting or glucagon injections, were not used.

The MR imaging matrix used in our study was 128 × 256, yielding an in-plane resolution of 1.4 × 2.8 mm. MR images were obtained with a slice thickness of 10 mm and without interslice gaps (interleaved mode) because thinner slices most likely would have resulted in lower signal-to-noise ratios and poorer image quality. The slice thickness used for CT scans (9 mm) and MR images (10 mm) were almost the same, so it is unlikely that the difference between these two techniques was caused by volume averaging.

Although we used the optimal imaging techniques available with our MR system when our study was started, we agree that more recent technical developments in MR imaging may improve the detection rate of small hepatic lesions. However, the same may also hold true for the technical development in CT (fast CT scanning and spiral volume imaging). Thus, evaluation of these new imaging techniques in prospective clinical trials is required.

K. Wernecke
E. Rummeny
P. Vassallo
P. E. Peters
University of Münster Medical School
D-4400 Münster, Germany

REFERENCES

1. Wernecke K, Rummeny E, Bongartz G, et al. Detection of hepatic masses in patients with carcinoma; comparative sensitivities of sonography, CT and MR imaging. *AJR* **1991**;157:731–739
2. Saini S, Li W, Wallner B, Hahn PF, Edelmann RR. MR imaging of liver metastases at 1.5 T: similar contrast discrimination with T1- and T2-weighted pulse sequences. *Radiology* **1991**;181:449–453

Extrastiff Plastic-Coated Guidewire for Percutaneous Biliary Procedures

Percutaneous placement of biliary endoprostheses has become a common interventional procedure, and the availability of a hydrophilic plastic-coated guidewire (Glidewire; Terumo; Tokyo) has made catheterization of biliary stenosis easier than it was before. The major drawbacks of the Glidewire, which was proposed for use in angiography [1], are (1) a loss of tactile sensation and (2) the flexibility of the device. After the J-shaped part of the Glidewire is positioned securely beyond the stenosis, a catheter must be moved over the Glidewire into the stenotic area. Then the Glidewire must be removed and replaced by a rigid guidewire such as a 0.038-in. (0.97 mm) Amplatz extrastiff guidewire (Cook Co.; Bloomington, IN) for dilatation and placement of the stent. Because the use of two sequential guidewires increases the cost of the procedure, we recently evaluated the usefulness of a new extrastiff plastic-coated guidewire (Meditech/Boston Scientific; Watertown, MA; Fig. 1). The new guidewire is 0.038 in. in diameter and 150 cm long. Its surface is coated with a hydrophilic polymer, and it must be moistened with saline before it is used.

The study group consisted of 10 patients, six men and four women, 48–75 years old (mean, 65), with malignant (nine) or benign (one)

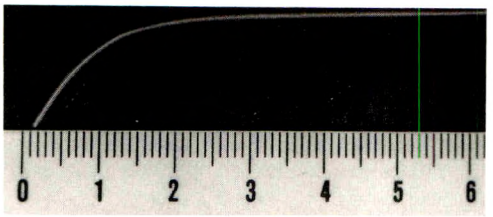


Fig. 1.—Photograph shows new 0.038-in. (0.97 mm) extrastiff plastic-coated guidewire. Distal end is J-shaped.

biliary obstruction who had percutaneous placement of an endoprosthesis. We used a balloon expandable metallic endoprosthesis (Strecker; Medi-tech/Boston Scientific) in three patients, a self-expandable stainless prosthesis (Gianturco; Cook Co.) in five, and a plastic stent (Roche; Cook Co.) in two.

After percutaneous transhepatic cholangiography, the most appropriate segmental bile duct was punctured with a Lunderquist 5-French sheath needle (Meadox-Surgimed; Olstykke, Denmark; a J-shaped one is recommended), and the new guidewire was inserted. After catheterization of the stenotic area, the guidewire was advanced to the ligament of Treitz. The stenotic area was then dilated, and the endoprosthesis or stent was positioned across the area of obstruction and left in place.

For each patient, all procedures were performed under sonographic and fluoroscopic guidance and in one session. The new extrastiff plastic-coated 0.038-in. guidewire was used successfully for catheterization, dilatation, and placement of the prosthesis in all but one patient. In that patient, who had cholangiocarcinoma of the left lobe invading the biliary confluence, a 0.035-in. (0.89 mm) Glidewire was needed for catheterization; the new 0.038-in. guidewire (Medi-tech) was used for dilatation and placement of the prosthesis.

It is dangerous to attribute "ideal" characteristics to a guidewire, because the technology and technique must be tailored to each case. However, with the development of endoscopic biliary procedures, percutaneous placement of biliary endoprostheses is becoming more difficult. Usually, percutaneous placement is used after endoscopic procedures have been unsuccessful, which often implies severe obstruction.

We found that the new extrastiff plastic-coated guidewire was highly reliable for use in percutaneous biliary procedures. The number of manipulations can be reduced, which leads to an increase in the success rate and has financial implications. Previously, when a catheter could not be passed beyond the obstruction, an external biliary drainage was left in place and a new attempt made several days later [2], which increased the cost of treatment. Another advantage of the new guidewire compared with the conventional extrastiff guidewire is the former's hydrophilic surfaces, which makes progression into the small bowel easy.

Philippe Soyer
Hospital Louis Mourier
92701 Colombes, France
Serge Derhy
Institut Gustave Roussy
94805 Villejuif, France

REFERENCES

1. Takayasu K, Muramatsu Y, Moriyama N, Ohtsu T, Catapia FC. Plastic-coated guidewire for hepatic arteriography. *Radiology* **1988**;166:545–546
2. Ferrucci JT Jr, Mueller PR, Harbin WP. Percutaneous transhepatic biliary drainage: technique, results, and applications. *Radiology* **1980**;135:1–13

Radiologic Abnormalities at the Harvest Site in Patients Undergoing Bone Marrow Transplantation

Bone marrow transplantation, a procedure that is being performed with increasing frequency, creates a wide range of radiologic findings [1]. Characteristic abnormalities occur at the site where the bone marrow is harvested, which should not be confused with metastatic disease.

Bone marrow is obtained from the pelvis with the patient prone [2]. The harvest needle is inserted into each posterior superior iliac spine, just penetrating the outer cortex. Bone marrow is aspirated several times at each site; the needle is advanced after each aspiration until the inner cortex is reached. Several sites along the medial posterior iliac crests are used.

We retrospectively reviewed findings on radiographs, CT scans, and bone scintigrams in 37 patients who had autologous bone marrow transplants. Changes on plain radiographs consisted of four to eight round to oval radiolucent lesions approximately 3 mm in diameter in the posterior iliac crests (Fig. 1A). The radiolucencies were usually surrounded by a 1- to 3-mm margin of sclerosis. The sclerosis is a normal healing response to osteonecrosis caused by the boring and rotational motions of the harvest needle, similar to the sclerosis seen after orthopedic drilling procedures [3].

CT scans showed intramedullary sclerosis confined to the iliac crests (Fig. 1B). Radiolucent lines 3 mm wide with sclerotic margins extended from the outer to the inner cortex of the iliac crests. Occasionally, the sacrum was involved. Periosteal reaction was rare.

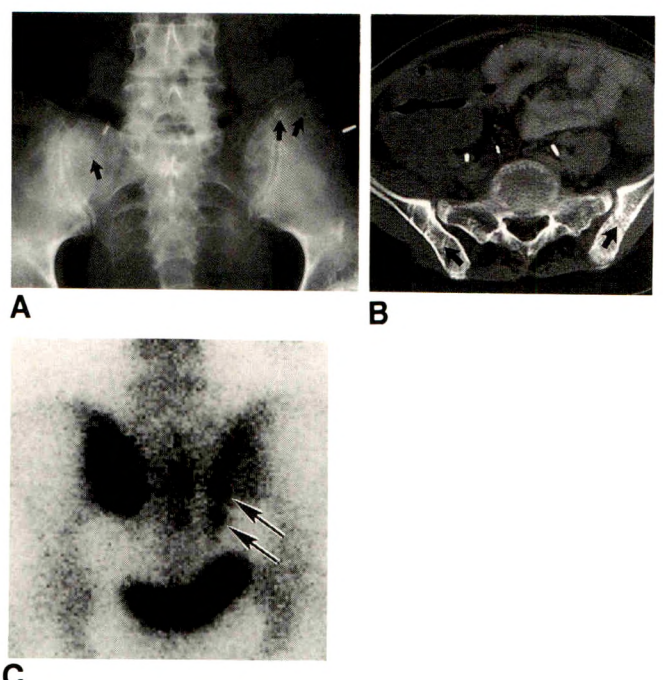


Fig. 1.—54-year-old woman with breast cancer. Bone marrow was harvested from posterior iliac crests.

***A*, Radiograph shows bilateral, multiple, round to oval radiolucencies (*arrows*) in iliac bone, surrounded by sclerosis.**

***B*, CT scan shows linear abnormalities (*arrows*) in posterior iliac crests at harvest sites.**

***C*, Scintigram (posterior view) obtained 2 months after harvest of bone marrow shows increased uptake of radionuclide (^{99m}Tc-methylene diphosphonate) in both iliac crests, including several punctate areas (*arrows*) in right crest.**

Hematomas in the soft tissues were sometimes seen in the period immediately after harvest.

The findings on bone scintigrams depended on the degree of osteoblastic activity. Increased uptake of radionuclide was confined to the posterior iliac crests and sacrum. Punctate areas of increased uptake corresponding to the individual harvest sites (Fig. 1C) were observed in some patients.

In one of our patients, a 16-year-old boy in complete remission from acute lymphocytic leukemia, CT showed resolution of the abnormalities 6 months after the marrow was harvested. Other patients have shown no change in the aspiration site over 2 years. Most have shown various degrees of resolution. It is during resolution that the site is most easily confused with metastatic disease.

Joseph E. Fondriest
Michael J. Pitt
Walter H. Williams
William S. Dalton
University of Arizona, University Medical Center
Tucson, AZ 85724

REFERENCES

1. Patzik SB, Smith C, Kubicka RA, Kaizer H. Bone marrow transplantation: clinical and radiographic aspects. *RadioGraphics* **1991**;11:601–610
2. Thomas ED, Storb R. Technique for human marrow grafting. *Blood* **1970**;36:507–515
3. Matthews LS, Green C, Goldstein SA. The thermal effects of skeletal fixation-pin insertion in bone. *J Bone Joint Surg [Am]* **1984**;66-A:1077–1083

Radiation-Induced Fracture of the Sacrum: Findings on MR

Insufficiency fractures of the sacrum may be associated with postmenopausal or corticosteroid-induced osteoporosis and with radiation therapy [1]. Pain is the presenting symptom and may suggest local tumor recurrence or metastatic disease to the osseous pelvis in patients who have had radiation therapy for malignant pelvic tumors.

A 66-year-old woman had resection of the rectum to treat a locally advanced squamous cell carcinoma of the anus. Tumor recurrence in the vagina was treated with external irradiation (10-MV photons; 2 Gy per session for 25 sessions) from the perineum to the L5–S1 disk. A complete remission was obtained. Five months after radiation therapy ended, pain developed in the patient's buttocks and lower limbs. She said that no trauma had preceded the pain, which subsided gradually and completely during the next 15 months. MR imaging 2 months after the onset of pain showed decreased signal intensity of the sacrum on T1-weighted images (Fig. 1A) and increased signal intensity on short TI inversion recovery images. On follow-up images obtained when the patient was asymptomatic, the abnormalities were markedly reduced (Fig. 1B). Sagittal images showed a healed fracture at S2.

Fracture is a common complication involving irradiated bone. Most fractures in the irradiated pelvis are not associated with metastasis and occur because of stress on weight-bearing atrophic bones that have decreased elastic resistance [2]. The sacrum and the sacroiliac joints are the major weight-bearing structures of the body. CT is the definitive technique for showing fractures in these areas, but in our patient, the fracture was shown by MR also. The additional signal abnormalities reflected prolongation of T1 and T2 relaxation times, which probably were related to an increased amount of free water [3]. It is reasonable to assume that this reflected edema associated with the fracture. We found no signs of infection and no evidence of locally recurrent tumor at clinical follow-up. No mass was evident on MR images to suggest tumor. Also, signal abnormalities resolved without treatment and in parallel with the clinical improvement.

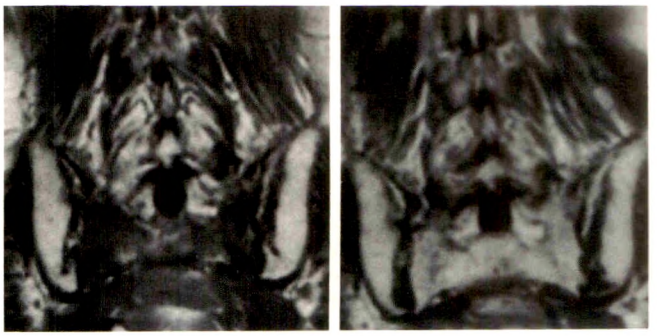


Fig. 1.—Radiation-induced fracture of sacrum.
***A*, Coronal T1-weighted (800/20) MR image shows low signal in sacrum, compatible with edema.**
***B*, Follow-up MR image (600/20) obtained when patient was symptom-free shows reduction of edema and normal postirradiation fat.**

Radiation-induced fractures of the sacrum often go unrecognized on conventional radiographs [1]. As it becomes more available, MR probably will play an increasing role in the examination of patients who have irradiation for pelvic tumors. It is therefore important to be aware of the possibility of a radiation-induced fracture of the sacrum and of the high sensitivity of MR for showing the concomitant edema. An erroneous diagnosis of metastasis to the sacrum could lead to further irradiation or aggressive chemotherapy, which could be harmful to the patient.

Hans H. Lien
Viggo Blomlie
Kristian Talle
Kjell M. Tveit
The Norwegian Radium Hospital
Oslo 3, Norway

REFERENCES

1. Cooper KL, Beabout JW, Swee RG. Insufficiency fractures of the sacrum. *Radiology* **1985**;156:15–20
2. Howland WJ, Loeffler RK, Starchman DE, Johnson RG. Postirradiation atrophic changes of bone and related complications. *Radiology* **1975**; 117:677–685
3. Mitchell DG, Burk DL, Vinitski S, Rifkin MD. The biophysical basis of tissue contrast in extracranial MR imaging. *AJR* **1987**;149:831–837

Duplex Sonography of the Cerebral Arteries

I enjoyed the comprehensive article on duplex sonography of the cerebral arteries by Zweibel [1]. However, I am confused by the use of the term "cerebral arteries" in the title, whereas the text refers almost exclusively to examination of the carotid arteries. Indeed, the author points out that "sonography is not very effective in providing a 'global' perspective of the cerebral vasculature, because only the cervical portion of the carotid arteries can be examined in detail." Does this review article reflect a change in nomenclature? If so, is this new terminology generally accepted? Am I missing something?

Ferris M. Hall
Beth Israel Hospital
Harvard Medical School
Boston, MA 02215

REFERENCE

1. Zweibel WJ. Duplex sonography of the cerebral arteries: efficacy, limitations, and indications. *AJR* **1992**;158:29–36

Reply

With respect to the inquiry of Dr. Hall regarding the title chosen for my recent article [1], the term "cerebral arteries" was chosen because the article includes material on duplex sonography of the vertebral arteries. The content of the article principally concerns the carotid arteries, as pointed out by Dr. Hall. Perhaps this term should have been used in the title rather than cerebral arteries. No alteration in nomenclature is suggested by the use of the term cerebral arteries.

William J. Zwiebel
University of Utah Medical Center
Salt Lake City, UT 84132

REFERENCE

1. Zwiebel WJ. Duplex sonography of the cerebral arteries: efficacy, limitations, and indications. *AJR* **1992**;158:29–36

Letters are published at the discretion of the Editor and are subject to editing.

Letters to the Editor must not be more than two *double-spaced*, typewritten pages. One or two figures may be included. Abbreviations should not be used. Limit the number of authors to four, or we will list only the first three and add "and colleagues" to the end of the list. See Author Guidelines.

Material being submitted or published elsewhere should not be duplicated in letters, and authors of letters must disclose financial associations or other possible conflicts of interest.

Letters concerning a paper published in the *AJR* will be sent to the authors of the paper for a reply to be published in the same issue. Opinions expressed in the Letters to the Editor do not necessarily reflect the opinions of the Editor.

Review of Current Literature

Initials and addresses of corresponding authors are provided in parentheses for each article so that the reader can obtain reprints directly. Abstracts are printed verbatim from each journal.

The New England Journal of Medicine

Long-term risk of colorectal cancer after excision of rectosigmoid adenomas. Atkin WS, Morson BC, Cuzick J (JC, Dept. of Mathematics, Statistics, and Epidemiology, Imperial Cancer Research Fund, P.O. Box 123, Lincoln's Inn Fields, London, WC2A 3PX, United Kingdom). *N Engl J Med* 326:658–662, March 1992

Background and Methods. Surveillance by repeated colonoscopy is currently recommended for patients with colorectal adenomas. We assessed the long-term risk of colorectal cancer after rigid-instrument sigmoidoscopy and polypectomy in 1618 patients with rectosigmoid adenomas (tumors of the rectum or distal sigmoid colon) who did not undergo surveillance. A total of 22,462 person-years of observation were accrued (mean, 14 years per patient).

Results. The incidence of subsequent rectal cancer in these patients was similar to that in the general population (standardized incidence ratio, 1.2; 95 percent confidence interval, 0.7 to 2.1). Most rectal cancers developed in patients whose adenomas had been inadequately removed; the risk was very low after complete removal.

The risk of subsequent colon cancer depended on the histologic type, size, and number of adenomas in the rectosigmoid. Among 842 patients with a rectosigmoid adenoma that was tubulovillous, villous, or large (≥1 cm), colon cancer developed in 31 patients. The standardized incidence ratio was 3.6 overall (95 percent confidence interval, 2.4 to 5.0) and 6.6 (95 percent confidence interval, 3.3 to 11.8) if there were multiple rectosigmoid adenomas. Among the remaining 776 patients with only small, tubular adenomas (whether single or multiple), colon cancer developed in only 4 patients. The standardized incidence ratio in this group was 0.5 (95 percent confidence interval, 0.1 to 1.3).

Conclusions. Follow-up colonoscopic examinations may be warranted in patients with tubulovillous, villous, or large adenomas in the rectosigmoid, particularly if the adenomas are also multiple. In patients with only a single, small tubular adenoma that is only mildly or moderately dysplastic (43 percent of our series), however, surveillance may not be of value because the risk of cancer is so low.

Biliary sludge as a cause of acute pancreatitis. Lee SP, Nicholls JF, Park HZ (SPL, Dept. of Medicine [111G1], VA Medical Center, 1660 S. Columbian Way, Seattle, WA 98108). *N Engl J Med* 326(9):589–593, 1992

Background. In about 20 to 40 percent of cases of acute pancreatitis, no cause can be found, and these are labeled idiopathic. In this study, we sought to determine the frequency with which patients with acute idiopathic pancreatitis have biliary sludge, a suspension of cholesterol monohydrate crystals or calcium bilirubinate granules that is found predominantly in the gallbladder.

Methods. Between 1980 and 1988, we prospectively studied 86 patients who had acute pancreatitis. In patients with no known cause of pancreatitis and no ultrasonographic evidence of gallstones or dilatation of the biliary ducts, we determined how often biliary sludge was present and its subsequent fate by repeated microscopical examinations of bile samples and abdominal ultrasonography. The outcome of patients treated by cholecystectomy or papillotomy was compared with that of untreated patients.

Results. The pancreatitis was considered idiopathic in 31 of the 86 patients (36 percent), of whom 23 had microscopical evidence of biliary sludge. Biliary sludge was detected by ultrasonography in only 11 of the 23 patients (48 percent). The sludge detected by ultrasonography was composed of calcium bilirubinate granules in 10 and cholesterol monohydrate crystals in 1 ($P = 0.003$). Calcium bilirubinate granules were found more frequently in men (nine men vs. four women, $P < 0.001$). Of the 21 patients in whom biliary sludge was the only finding (2 patients also had dilated bile ducts when restudied), the 6 treated by cholecystectomy and the 4 treated by papillotomy had fewer recurrences of acute pancreatitis during follow-up (up to seven years) than the 11 untreated patients ($P = 0.011$). The presence of biliary sludge appeared to increase the likelihood of recurrent attacks of pancreatitis ($P = 0.020$).

Conclusions. Biliary sludge is an underestimated cause of acute idiopathic pancreatitis.

Effects of concomitant cisplatin and radiotherapy on inoperable non–small-cell lung cancer. Schaake-Koning C, van den Boogaert W, Dalesio O, et al. (CS-K, Dept. of Radiotherapy, the Netherlands Cancer Institute, Plesmanlaan 121, 1066 CX Amersterdam, the Netherlands). *N Engl J Med* 326:524–530, Feb. 1992

Background and Methods. Cisplatin (*cis*-diamminedichloroplatinum) has been reported to enhance the cell-killing effect of radiation, an effect whose intensity varies with the schedule of administration. We randomly assigned 331 patients with nonmetastatic inoperable non–small-cell lung cancer to one of these treatments: radiotherapy for two weeks (3 Gy given 10 times, in five fractions a week), followed by a three-week rest period and then radiotherapy for two more weeks (2.5 Gy given 10 times, five fractions a week); radiotherapy on the same schedule, combined with 30 mg of cisplatin per square meter of body-surface area, given on the first day of each treatment week; or radiotherapy on the same schedule, combined with 6 mg of cisplatin per square meter, given daily before radiotherapy.

Results. Survival was significantly improved in the radiotherapy–daily-cisplatin group as compared with the radiotherapy group ($P = 0.009$): survival in the radiotherapy–daily-cisplatin group was 54

percent at one year, 26 percent at two years, and 16 percent at three years, as compared with 46 percent, 13 percent, and 2 percent, respectively, in the radiotherapy group. Survival in the radiotherapy–weekly-cisplatin group was intermediate (44 percent, 19 percent, and 13 percent) and not significantly different from survival in either of the other two groups. The survival benefit of daily combined treatment was due to improved control of local disease ($P = 0.003$). Survival without local recurrence was 59 percent at one year and 31 percent at two years in the radiotherapy–daily-cisplatin group; 42 percent and 30 percent, respectively, in the radiotherapy–weekly-cisplatin group; and 41 percent and 19 percent, respectively, in the radiotherapy group. Cisplatin induced nausea and vomiting in 86 percent of the patients given it weekly and in 78 percent of those given it daily; these effects were severe in 26 percent and 28 percent, respectively.

Conclusions. Cisplatin, given daily in combination with the radiotherapy described here to patients with nonmetastatic but inoperable non–small-cell lung cancer, improved rates of survival and control of local disease at the price of substantial side effects.

The use of transcranial ultrasonography to predict stroke in sickle cell disease. Adams R, McKie V, Nichols F, et al. (RA, Dept. of Neurology, HB-2060, Medical College of Georgia, Augusta, GA 30912). *N Engl J Med* 326(9):605–610, 1992

Background. Stroke, especially cerebral infarction, is a major cause of morbidity and mortality in children with sickle disease. Primary prevention of stroke by transfusion therapy may be feasible if there is a way to identify the patients at greatest risk. Transcranial Doppler ultrasonography can measure flow velocity in the large intracranial arteries. The narrowing of these arteries, which leads to cerebral infarction, is characterized by an increased velocity of flow.

Methods. Using transcranial Doppler ultrasonography, we prospectively measured the velocity of cerebral blood flow in children and young adults being followed because of sickle cell disease. The results were classified as either normal or abnormal on the basis of the highest velocity of flow in the middle cerebral artery. Abnormal velocity was defined as a flow $\geq$170 cm per second, a definition determined by post hoc analysis to maximize the predictive success of the test. The end point was a clinically apparent first cerebral infarction.

Results. Two hundred eighty-three transcranial ultrasound examinations were performed in 190 patients with sickle cell disease (age at entry, 3 to 18 years). After an average follow-up of 29 months, cerebral infarction was diagnosed in seven patients. In 23 patients the results of the ultrasound examinations were abnormal, and in 167 patients they were normal. The clinical and hematologic characteristics of the two groups were similar, but six of the seven strokes occurred among the 23 patients with abnormal ultrasound results ($P < 0.00001$ by Fisher's exact test). In this group, the relative risk of stroke was 44 (95 percent confidence interval, 5.5 to 346).

Conclusions. Transcranial ultrasonography can identify the children with sickle cell disease who are at highest risk for cerebral infarction. Periodic ultrasound examinations and the selective use of transfusion therapy could make the primary prevention of stroke an achievable goal.

Cancer

A prospective trial of early detection of pancreatic cancer by ultrasonographic examination combined with measurement of serum elastase 1. Nakaizumi A, Tatsuta M, Uehara H, et al. (AN, Dept. of Gastrointestinal Oncology, The Center for Adult Diseases, Osaka, 3-3, Nakamichi 1-chome, Higashinari-ku, Osaka 537, Japan). *Cancer* 69:936–940, 1992

The accuracy of ultrasonographic examination combined with measurement of elastase 1 levels for early detection of pancreatic cancer was evaluated prospectively. Abdominal ultrasonographic examination and measurement of serum elastase 1 levels were done with 2 weeks after the initial visit to the clinic in a total of 2098 patients older than 35 years of age with symptoms suggesting pancreatic disease. Those in which one or both of these examinations had abnormal results underwent additional tests such as endoscopic retrograde cholangiopancreatography and computed tomography. Of those with pancreatosonograms with abnormal results with or without abnormally high serum elastase 1 levels, 19 patients eventually were found to have pancreatic cancer. No patients with pancreatic cancer, a normal level of serum elastase 1, and a pancreatosonogram with normal results were found, but follow-up studies revealed one pancreatic cancer in 189 patients after technically unsatisfactory ultrasonographic examination. In 9 (45%) of the 20 cases detected in this study, the pancreatic cancers were resectable, and two (10%) were less than 2.0 cm in longest diameter. These findings indicate that this combined examination is useful for early detection of pancreatic cancer. However, no pancreatic cancer was found in patients with abnormally high serum elastase 1 levels without a pancreatosonogram with abnormal results. Moreover, a combination of ultrasonographic examination and measurement of the elastase 1 level did not raise the diagnostic accuracy over that of ultrasonographic examination alone. These findings indicate that ultrasonographic examination alone is useful in screening for early pancreatic cancer.

Reprinted by permission from the American Cancer Society.

Circulation

Intracoronary stenting for acute and threatened closure complicating percutaneous transluminal coronary angioplasty. Roubin GS, Cannon AD, Agrawal SK, et al. (GSR, University of Alabama at Birmingham, Lyons-Harrison Research Bldg., 1919 Seventh Ave. S., Ste. 310, UAB Station/Birmingham, AL 35294). *Circulation* 85:916–927, 1992

Acute closure remains a significant limitation of percutaneous transluminal coronary angioplasty (PTCA) and underlies the majority of ischemic complications. This study details the clinical and angiographic characteristics of a series of patients receiving an intracoronary stent device to manage acute and threatened closure and presents the early clinical results.

Methods and Results. From October 1989 through June 1991, 115 patients undergoing PTCA received intracoronary stents to treat acute or threatened closure in 119 vessels. Sixty-three percent had multivessel coronary disease, 33 (29%) had undergone prior coronary artery bypass grafting (CABG), and 52 (45%) had had previous PTCA. Using the American College of Cardiology/American Heart Association (ACC/AHA) classifications, 15% of lesions were class A, 55% were class B, and 30% were class C. Eight patients were referred with severe coronary dissection and unstable angina after PTCA at other institutions. Acute closure was defined as occlusion of the vessel with TIMI (Thrombolysis in Myocardial Infarction) 0 or 1 flow immediately before stent placement. Threatened closure required two or more of the following criteria: 1) a residual stenosis greater than 50%, 2) TIMI grade 2 flow, 3) angiographic dissection comprising extraluminal dye extravasation and/or a length of greater than 15 mm, 4) evidence of clinical ischemia (either typical angina or ECG changes). Twelve vessels (10%) met the criteria for acute closure, and 87 vessels (73%) satisfied the criteria for threatened closure. Twenty vessels (17%) failed to meet two criteria. Stenting produced optimal angiographic results in 111 vessels (93%), with mean diameter stenosis ($\pm$1 SD) reduced from 83 $\pm$ 12% before to 18 $\pm$ 29% after stenting. Overall, in-hospital mortality was 1.7% and CABG was required in 4.2%; Q wave myocardial infarction (MI) occurred in 7% and non–Q wave MI in 9%. Stent thrombosis occurred in nine patients (7.6%). For the 108 patients who presented in the catheterization laboratory without evolving MI, Q wave MI occurred in 4% and non–Q wave MI occurred in 7%. Angiographic follow-up has been performed in 81 eligible patients (76%), and 34 patients (41%) had a lesion of $\geq$50%.

Conclusions. This stent may be a useful adjunct to balloon dilatation in acute or threatened closure. Randomized studies comparing this stent with alternative technologies are required.

Gastroenterology

Esophagoglottal closure reflex: a mechanism of airway protection. Shaker R, Dodds WJ, Ren J, Hogan WJ, Arndorfer RC (RS, Dept. of Medicine, Medical College of Wisconsin, Milwaukee, WI). *Gastroenterology* 102:857–861, 1992

Abrupt esophageal distention occurs commonly during gastroesophageal reflux, thereby generating a circumstance favorable to esophagopharyngeal regurgitation and laryngeal aspiration of gastric refluxate. The aims of the present study were to examine the glottal response to esophageal distention by air and regional esophageal distention by a balloon. Fifteen healthy volunteers (age, 25 ± 5 years) were studied while they were in an upright position. Using concurrent videoendoscopy and manometry, glottal and upper esophageal sphincter (UES) responses to abrupt esophageal distention by air injection (10–60 mL) and balloon distention (1.5, 2.0, and 2.5 cm) were recorded simultaneously. In addition, 6 subjects were studied with concurrent synchronized videofluoroscopy. Results showed that esophageal distention by air at a threshold volume of 10–60 mL caused vocal cord closure. The UES response to this threshold volume was variable. Volumes larger than the threshold value caused complete UES relaxation and belching. In addition to vocal cord closure, belching was accompanied by anterior movement of the glottis. On videofluoroscopy, the hyoid bone moved anteriorly in association with belching, but not with vocal cord closure without belching. Proximal esophageal distention by the balloon also provoked vocal cord closure. This response was less consistent for balloon distention in the middle and distal esophagus. It is concluded that (a) esophageal distention by either air or a balloon evokes a glottal closure mechanism, thereby suggesting the existence of an esophagoglottal reflex; (b) this reflex is elicited most easily by distention of the proximal esophagus; (c) glottal and UES responses to esophageal distention are independent from each other; and (d) the esophagoglottal closure reflex may play an important role in preventing laryngeal aspiration of acid due to gastroesophageal reflux accompanied by acid regurgitation into the pharynx.

Reprinted with permission by the American Gastroenterological Association.

Noninvasive therapy of gallbladder calculi with a radiopaque rim. Sackmann J, Pauletzki J, Delius M, et al. (JS, Dept. of Medicine II, Klinikum Grosshadern, University of Munich, Munich, Germany). *Gastroenterology* 102:988–993, 1992

Safety and efficacy of shock-wave lithotripsy and bile acid dissolution therapy of patients with gallbladder calculi with a radiopaque rim were evaluated. Eight-six patients with symptomatic solitary stones were treated by this noninvasive therapy and were followed up to 18 months. Three different lithotripsy treatment modalities were used. Up to 1600 shock wave discharges were applied. Patients in group A (n = 20) were treated with an electrohydraulic water-bath lithotripter at a discharge voltage of 18 ± 1 kV (mean ± SD), group B patients (n = 25) were treated with an electrohydraulic water-cushion lithotripter at 19 ± 2 kV, and group C patients were treated (n = 41) with the same lithotripter at 22 ± 2 kV. Five to eight months after lithotripsy, 15% in group A were free of fragments compared with only 4% in group B (NS vs. group A), and 38% in group C had no stones (NS vs. group A; $P = 0.007$ vs. B). Thirteen to eighteen months after lithotripsy, the respective results were 59% in group A, 37% in group B (NS vs. group A), and 68% in group C (NS vs. group A; $P = 0.05$ vs. group B). Patients with fragments of ≤3 mm in diameter showed significantly better fragment clearance than those with larger fragments. The frequency of adverse effects was not significantly different between the three groups. Biliary colic occurred in 43% of the patients and mild biliary pancreatitis in 3 patients. Endoscopic sphincterotomy was required in 1 patient, and elective cholecystectomy was performed in 6 patients. Using a water-cushion lithotripter at high-power setting, selected patients with solitary gallbladder stones with a radiopaque rim may be treated safely and successfully by shock-wave lithotripsy combined with bile acid dissolution therapy.

Reprinted with permission by the American Gastroenterological Association.

Digestive Diseases and Sciences

Splenic and portal venous obstruction in chronic pancreatitis: a prospective longitudinal study of a medical–surgical series of 266 patients. Bernades P, Baetz A, Lévy P, Belghiti J, Menu Y, Fékété F (PB Service de Gastroentérologie, Hôpital Beaujon, 92118 Clichy Cedex, France). *Dig Dis Sci* 37(3):340–346, March 1992

The aim of this study was a prospective search for splenoportal venous obstruction (SPVO) in a medical–surgical series of 266 patients with chronic pancreatitis who were followed up a mean time of 8.2 years. SPVO was systematically searched for using ultrasonography and then confirmed by angiography or computed tomography. SPVO was found in 35 patients (13.2%) but was symptomatic in only two. Initial obstruction involved the splenic vein in 22 patients, the portal vein in 10, and the superior mesenteric vein in three. Since venous obstruction extended from the splenic to the portal vein in five patients, the prevalence of portal obstruction was 5.6% (15/266). Acute pancreatitis and pseudocysts were the probable cause of SPVO in 91.4% of our cases. Half the cases of splenic venous obstruction were related to pseudocysts of the caudal pancreas. Esophageal varices were found in two patients and gastric varices in four at the time of diagnosis and during follow-up. At the end of follow-up, 12 patients had undergone splenopancreatectomy ($N = 11$) or splenectomy ($N = 1$). Only one patient was operated on for massive esophageal variceal bleeding, and another patient died due to intractable colic variceal bleeding. In four of six patients operated on with portal vein obstruction, surgery was difficult due to venous collaterals. Ten patients were not operated on and 13 patients operated on were not treated for SPVO. The mean follow-up after diagnosis of SPVO for these final 23 patients was 28.9 months. None of these patients bled. We concluded that in chronic pancreatitis: (1) the prevalence of SPVO is 13.2%; (2) SPVO should be systematically searched for in patients with acute pancreatitis or pseudocysts, especially if therapeutic decisions would be modified by a diagnosis of SPVO; (3) the risk of digestive variceal bleeding is lower than previously reported; and (4) portal vein obstruction seems to be riskier than splenic vein obstruction, especially if surgery is needed.

Esophageal strictures following endoscopic variceal sclerotherapy: antecedents, clinical profile, and management. Kochhar R, Goenka MK, Mehta S (reprints not available). *Dig Dis Sci* 37(3):347–352, March 1992

We have evaluated 169 patients with portal hypertension receiving endoscopic variceal sclerotherapy in order to assess the predisposing factors, clinical profile, and treatment response of sclerotherapy-induced esophageal strictures. Of the 129 patients included in the final analysis, 20 (15.5%) developed persistent esophageal stricture. No significant difference was found with respect to age, nature of sclerosant (absolute alcohol, ethanolamine oleate, or sodium tetradecyl sulfate), etiology of portal hypertension. Child's class, initial variceal score, or intensity of sclerotherapy schedule between the patients who developed strictures and those who did not. However, female sex ($P < 0.01$) and persistent esophageal ulceration ($P < 0.05$) did predispose to stricture formation. Sclerotherapy-induced strictures presented with a variable grade of dysphagia, were always solitary, and were localized to the lower end of esophagus. Most of these could be diluted rapidly using Eder-Puestow metal olives (3.15 ± 0.80 dilatation sessions per patient). Stricture formation did interrupt an effective sclerotherapy program but only temporarily, and successful variceal obliteration could be obtained after stricture dilatation.

The Journal of Bone and Joint Surgery

The Scottish Rite abduction orthosis for the treatment of Legg-Perthes disease: a radiographic analysis. Meehan PL, Angel D, Nelson JM (PLM, Section of Orthopaedic Surgery, Emory Clinic, 1365 Clifton Rd., N.E., Atlanta, GA 30322). *J Bone Joint Surg [Am]* 74-A:2–12, Jan. 1992

We evaluated a consecutive series of thirty-four patients who had had Legg-Perthes disease to determine the results of treatment with the Scottish Rite weight-bearing abduction orthosis. All patients had been older than six years at the time of the onset of the symptoms, had been in the fragmentation phase of the disease when they were first seen, and had had Catterall group-III or IV involvement. Although comparison of this series with those reported previously is difficult due to the variability of the presentation of data in the literature, this orthosis does not appear to offer an advantage compared with other methods of management, or with no treatment, for patients such as those whom we studied.

Clinical Orthopaedics and Related Research

A histopathologic study of late aseptic loosening of cemented total hip prostheses. Williams RP, McQueen DA (RPW, Dept. of Orthopaedics, St. Francis Regional Medical Center, 929 N. St. Francis, Wichita, KS 67214). *Clin Orthop* 275:174–179, Feb. 1992

Eighteen patients being treated for revision total hip arthroplasty for aseptic loosening an average of 9.5 years after primary cemented hip arthroplasty were studied. The patients were found to have been symptomatic an average of one year before revision. Review of the roentgenograms at the time of revision revealed that most patients had moderate to severe loosening of the prostheses by Charnley's criteria. These findings were confirmed at surgery. Study of the tissue surrounding the prostheses suggests that the prominent particles were methylmethacrylate "pearls" caused by cement fragmentation. These particles were surrounded by histiocytes that were actively synthesizing and releasing protein. Cement fragmentation and not polyethylene wear may be the major cause of late aseptic loosening of cemented hip prostheses.

The Journal of Urology

Potential for inter-observer and intra-observer variability in x-ray review to establish stone-free rates after lithotripsy. Jewett MAS, Bombardier C, Caron D, et al. (MASJ, Division of Urology, The Wellesley Hospital, University of Toronto, Toronto, Ontario, Canada). *J Urol* 147:559–562, March 1992

The potential for variability among observers interpreting diagnostic tests is well known but has not been well established for radiological imaging of urolithiasis. We measured the inter-observer and intra-observer variability in the reporting of plain abdominal films and tomograms from patients who had undergone extracorporeal shock wave lithotripsy (ESWL*). Unlabeled copies of the plain abdominal films and tomograms from 58 patients were individually submitted to 3 different radiologists. Selected films from 25 patients were resubmitted to the same radiologists. We found differences among radiologists reporting plain abdominal films alone 52% of the time and even by the same radiologist rereading the films 24% of the time. Tomograms alone decreased the uncertainty but differences still occurred among radiologists 24% of the time and with themselves 16% of the time. When plain abdominal films and tomograms were read together there were differences among radiologists 28% of the time and with themselves 7% of the time but these were usually minor. We concluded from this study that the plain abdominal film alone was frequently difficult to interpret, resulting in uncertainty about the presence or absence of residual stone fragments. Tomograms alone or a plain abdominal film plus tomograms is superior to a plain abdominal film alone. Finally, radiological assessment with all modalities probably overestimates stone-free rates after ESWL even without consideration of the potential for reporting variability among observers.

The Journal of Pediatrics

Stroke in a cohort of patients with homozygous sickle cell disease. Balkaran B, Char G, Morris JS, Thomas PW, Serjeant BE, Serjeant GR (GRS, Medical Research Council Laboratories [Jamaica], University of the West Indies, Kingston 7, Jamaica, West Indies). *J Pediatr* 120:360–366, 1992

Strokes occurred in 17 of 310 children with homozygous sickle cell disease who were followed from birth, representing an incidence of 7.8% by the age of 14 years. Two children had subarachnoid hemorrhage, one having resolution of symptoms after aneurysm surgery and another dying of a presumed second hemorrhage 14 days later. The remaining 15 strokes were presumed to be cerebral infarction, although autopsy, angiographic, or computed tomographic evidence was available in only 8 children. There were 6 deaths, 2 in the acute event and 4 after recurrence, which occurred in 6 (46%) of 13 patients who survived the initial episode. There were 10 recurrent episodes at a median interval of 9 months after the initial event. Steady-state hematologic data revealed significantly higher leukocyte counts than in control subjects without strokes at age 1 year and in the last study preceding the stroke. The initial stroke coincided with an acutely lowered hemoglobin value in 5 patients (3 aplastic crises, 1 acute splenic sequestration, 1 probable pulmonary sequestration) and with painful crises in another 7 patients. We conclude that a high leukocyte count and an acute decrease of hemoglobin are risk factors for stroke in patients with homozygous sickle cell disease.

Evaluation of renal scars by technetium-labeled dimercaptosuccinic acid scan, intravenous urography, and ultrasonography: a comparative study. Shanon A, Feldman W, McDonald P, et al. (WF, Division of General Pediatrics, Hospital for Sick Children, 555 University Ave., Toronto, Ontario M5G 1X8, Canada). *J Pediatr* 120:399–403, 1992

The objective of our prospective study was to compare the sensitivity and specificity of ultrasonography, intravenous pyelography, and dimercaptosuccinic acid scan in detecting scarred kidneys. Twenty-seven consecutive subjects with recurrent urinary tract infections, vesicoureteral reflux, scarred kidneys, or a combination of these problems had all three imaging procedures performed. With the total number of scars serving as the gold standard, the sensitivity (94%) and specificity (100%) in identifying renal scars in children were highest for the DMSA scan. Intraobserver (95%) and interobserver (90%) reliability were also high for the DMSA scan. However, the clinical interpretation of the increased sensitivity of the DMSA scan is unknown. Changes on the scan not identified by intravenous urography may not represent true scars. Research into the long-term significance of these scars is indicated.

Limitations of the Glasgow Coma Scale in predicting outcome in children with traumatic brain injury. Lieh-Lai MW, Theodorou AA, Sarnaik AP, Meert KL, Moylan PM, Canady AI (MWL-L, Division of Critical Care Medicine, Children's Hospital of Michigan, 3901 Beaubien Ave., Detroit, MI 48201). *J Pediatr* 120:195–199, Feb. 1992

Objective: To study the hypothesis that, in the absence of an ischemic-hypoxic state, children with severe traumatic brain injury and with unfavorable Glasgow Coma Scale scores may have good recovery.

Design: Retrospective, observational, cross-sectional study with factorial design.

Setting: Inpatient population in a university hospital.

Patients: Seventy-nine children with traumatic brain injury admitted to the intensive care unit.

Interventions: All patients received close monitoring and strict control of intracranial pressure (<20 mm Hg) and cerebral perfusion pressure (>60 mm Hg).

Measurements and results: Admission Glasgow Coma Scale score, survival, need for cardiopulmonary resuscitation, presence of shock, peak intracranial pressure, duration of coma, Glasgow Outcome Scale score, and the results of neuropsychologic tests were analyzed. Of 79 children, 70 (89%) survived. Although the mortality rate was higher among patients with Glasgow Coma Scale scores of 3 to 5, 14 (64%) of 22 of these children survived. Nonsurvivors had a significantly higher incidence of shock and need for cardiopulmonary resuscitation. Except for two patients who had prolonged hypoxemia, all children, including those with Glasgow Coma Scale scores of 3 to 5, had a satisfactory outcome (Glasgow Outcome Scale scores of 4 or 5). Neuropsychologic outcome was not significantly different in the survivors with Glasgow Coma Scale scores of 3 to 5 and those with Glasgow Coma Scale scores of 6 or more.

Conclusions: A low Glasgow Coma Scale score does not always accurately predict the outcome of severe traumatic brain injury; in the absence of hypoxic-ischemic injury, children with traumatic brain injury and Glasgow Coma Scale scores of 3 to 5 can recover independent function.

Surgery Gynecology & Obstetrics

Outpatient open cholecystectomy. Saltzstein EC, Mercer LC, Peacock JB, Dougherty SH (ECS, Texas Tech University School of Medicine, 4800 Alberta Ave., El Paso, TX 79905). *Surg Gynecol Obstet* 174(3):173–175, March 1992

A prospective study to evaluate discharge of patients from the hospital the day of open cholecystectomy was performed. Patients were selected for outpatient operation if they were less than 55 years of age, did not undergo exploration of the common bile duct and had no significant co-morbidity.

During a six month period, 94 consecutive patients underwent cholecystectomy. Forty-four of 64 eligible patients were discharged the day of operation. Patients were walking and receiving oral liquids soon after operation. Marcaine® (bupivacaine hydrochloride) was injected subfascially in all patients and vertical incisions were used in 34 of 44. One patient required readmission for 12 hours, three days after operation. The satisfaction rate was high and the patients returned to their usual activity in seven to 21 days. Outpatient open cholecystectomy is safe and appropriate therapy and the data established a standard with which to compare that of laparoscopic cholecystectomy.

Gastrointestinal Radiology

Clinical and videofluoroscopic evaluation of swallowing in 41 patients with neurologic disease. Chen MYM, Peele VN, Donati D, Ott DJ, Conofrio PD, Gelfand DW (MYMC, Dept. of Radiology, Bowman Gray School of Medicine, Medical Center Blvd., Winston-Salem, NC 27157-1088). *Gastrointest Radiol* 17:95–98, 1992

Forty-one patients with neurologic disease (ND) were evaluated by clinical and videofluoroscopic examination of the oral cavity and pharynx to assess location and severity of swallowing dysfunction using various bolus consistencies. Four different materials were given to each patient, and included low- and high-viscosity barium suspensions, barium paste, and paste-coated cookie. Thirty-five patients had abnormalities of both oral and pharyngeal function. Four patients had pharyngeal dysfunction only, and two patients were normal. Mild swallowing difficulties occurred in five patients (12%), moderate dysfunction in 29 patients (71%), and severe dysfunction in 29 patients (71%) and severe dysfunction in five patients (12%). Thirty-two patients had pharyngeal stasis, which was symmetric in 30 patients (94%) and asymmetric in two. Site of stasis was not related to the type of neurologic disease. Fifteen patients aspirated, most of them (13 of 15) with the low-viscosity barium suspension. The predominance of aspiration with the low-viscosity liquid emphasizes the importance of clinical and videofluoroscopic evaluation of swallowing in dysphagic patients with ND for appropriate feeding recommendations. Thus, videofluoroscopy complemented the clinical examination and defined the type and severity of swallowing abnormalities and aspiration, when present.

Value of CT and sonography in the conservative management of acute splenoportal and superior mesenteric venous thrombosis. Rahmouni A, Mathieu D, Golli M, et al. (DM, Dept. of Radiology, Henri Mondor Hospital, 51 Avenue du Marechal de Lattre de Tassigny, F-94010 Creteil, France). *Gastrointest Radiol* 17:135–140, 1992

Acute splenoportal and superior mesenteric venous thrombosis were diagnosed on sonography and computed tomography (CT) in six patients. Sonography demonstrated the presence of echoic material filling the involved vessels in all patients. Precontrast CT scans demonstrated an increased, intra luminal density of the clots in four patients with splenoportal thrombosis. However, in two cases of superior mesenteric venous thrombosis, no hyperdensity was observed within the lumens. Nevertheless, the clots were always visualized as low-density regions in the vessel lumens after bolus injection. Intravenous anticoagulant therapy was started immediately after the diagnosis. All patients were evaluated twice a week with sonography and/or CT until recanalization occurred. The patency of the previously involved vessels was assessed from 6 days to 4 weeks after the acute episode (average time of recanalization: 17 days) without development of collateral pathways. It is concluded that, in the absence of clinical signs of a life-threatening process, a conservative management of acute splanchnic thrombosis can be successfully achieved by (1) early diagnosis, (2) efficacious intravenous anticoagulant therapy, (3) careful imaging follow-up of these patients by sonography and/or CT during the acute phase and, finally, (4) by an extensive search for a hypercoagulable state.

News

Workshop on New Devices for the Cardiac and Peripheral Vascular Laboratory

Pittsburgh Vascular Institute and Pittsburgh Heart Institute of Shadyside Hospital are sponsoring a hands-on workshop on new devices for cardiac and peripheral vascular laboratories, July 1–3, at Disney's Yacht and Beach Club Resort, Walt Disney World, Lake Buena Vista, FL. Instruction will be given in applications of intravascular stents, atherectomy devices, angioscopes, endovascular sonographic probes, and lasers. In addition, new balloon and wire technology and thrombolytic therapy will be reviewed. Program directors: James D. O'Toole and Mark H. Wholey. Category 1 credit: 14 hr. Fee: physicians, $500; nurses and technologists, $300. Information: Shadyside Hospital, New Devices Technology Workshop, 5230 Centre Ave., Pittsburgh, PA 15232; (412) 623-1051.

Imaging on Lake Coeur d'Alene

The Depts. of Radiology, University of Washington, Seattle, and Sacred Heart Medical Center, Spokane, are cosponsoring the 6th annual Imaging on Lake Coeur d'Alene: A Summer Radiology Meeting, July 15–18, at the Coeur d'Alene Resort, Coeur d'Alene, ID. The course is designed primarily for general diagnostic radiologists. Topics will include neuroradiology, abdominal imaging, diagnostic sonography, and mammography. Course cochairmen: Marvin J. Gottschall and Stephen. I. Marglin. Guest faculty: E. S. de Paredes, J. Destouet, N. R. Dunnick, J. G. Letourneau, and G. W. Nixon. Category 1 credit: 20 hr. Fee: up to July 1, $475; after July 1, $525. Information: Kathy Fischer, Course Secretary, Dept. of Radiology, Sacred Heart Medical Center, TAF-C9, Spokane, WA 99220; (509) 455-3352 or 455-3330.

ARDMS Exam Preparation Courses

Exam preparation courses for the American Registry of Diagnostic Medical Sonographers will be held in August, September, and October as follows: Ultrasound and Doppler Physics: presented by Frederick W. Kremkau; Aug. 28–29, Sheraton National Hotel, Washington, DC; Sept. 18–19, Doubletree Marine Beach Hotel, Los Angeles; Sept. 26–27, Hyatt Atlanta Airport Hotel, Atlanta; and Oct. 2–3, Radisson Hotel at O'Hare, Chicago. OB/GYN Ultrasound: presented by Dale R. Cyr; Aug. 30, Sheraton National Hotel, Washington, DC; Sept. 20, Doubletree Marine Beach Hotel, Los Angeles; and Oct. 4, Radisson Hotel at O'Hare, Chicago. Vascular Technology: presented by Cynthia B. Burnham and M. Lee Nix; Aug. 30–31, Sheraton National Hotel, Washington, DC; Sept. 20–21, Doubletree Marina Beach Hotel, Los Angeles; and Oct. 4–5, Radisson Hotel at O'Hare, Chicago. Information: Office of Postgraduate and Continuing Medical Education, Yale University School of Medicine, 333 Cedar St., P. O. Box 3333, New Haven, CT 06510; telephone: (203) 785-4578; fax: (203) 785-3083.

Radiology in County Kerry

Sharon Hospital, Sharon, CT, is sponsoring Radiology in County Kerry, Sept. 6–9, at the Great Southern Hotel, Parknasilla, County Kerry, Ireland. Topics to be discussed include body and obstetric sonography, body CT, MR imaging and CT of the head, and MR imaging of bone. Program chairman: D. Beatty Crawford. Program directors: Bob Birchenough and Betsy Birchenough. Registration will be limited to 65. Faculty: C. A. Helms, M. Hill, and R. Quencer. Category 1 credit: 24 hr. Fee: $650. Information: "Radiology in County Kerry," 93 Highwood Dr., Manchester, CT 06040; Dr. Beatty Crawford, telephone and fax: (203) 491-4611; or Betsy Birchenough, telephone: (203) 649-9119, fax: (203) 643-4549.

Sonography Update

The University of California, San Diego, is sponsoring the 8th annual Sonography Update, Sept. 9–11, at the Hotel Del Coronado, San Diego. Program directors: Barbara B. Gosink and Sandra Hagen-Ansert. Category 1 credit: 23.5 hr. Fee (through Aug. 16/after Aug. 16): physicians in practice, $350/$400; residents, fellows, and technologists, $250/$300. Information: Dawne Ryals, Ryals and Associates, P. O. Box 1925, Roswell, GA 30077-1925; telephone: (404) 641-9773; fax: (404) 552-9859.

Organ Imaging Review 1992

The University of Toronto is sponsoring its annual intensive general radiology course, Organ Imaging Review 1992, Sept. 14–18, at the Four Seasons Hotel, Toronto. Clinical-radiologic and radiologic-pathologic correlations will be emphasized. Appropriate use of conventional and advanced imaging techniques; assessment of specific areas, including chest, breast, musculoskeletal system, and CNS; abdominal imaging, and sonography will be discussed. Guest faculty: E. Fishman, F. Laing, E. Mendelson, R. Moser, and R. Pugatch. Category 1 credit: 30 hr. Fee ($U.S./$Canadian): physicians, $550/

$650; residents, fellows, and technologists, $400/$470. Information: Edward E. Kassel, M.D., Dept. of Radiology, University of Toronto, Faculty of Medicine, Rm. 127, FitzGerald Bldg., Toronto, Ontario, Canada M5S 1A8; telephone: (416) 978-6801; fax: (416) 978-6915.

Seminar in Diagnostic Ultrasound

The Dept. of Radiology, The University of Michigan Medical School, is sponsoring the 14th annual Seminar in Diagnostic Ultrasound, Sept. 17–19, at the Towsley Center, University of Michigan Medical Center, Ann Arbor. Course director: Terry M. Silver. Guest faculty: B. Goldberg, E. A. Lyons, M. L. Manco-Johnson, P. Ralls, and C. C. Reading. Category 1 credit: 14 hr. Information: Noceeba Southern, Towsley Center for Continuing Medical Education, Dept. of Postgraduate Medicine, The University of Michigan Medical School, P. O. Box 1157, Ann Arbor, MI 48106-9869; (313) 764-1422.

Neurologic Complications of Pregnancy

Neurologic Complications of Pregnancy will be presented at NYU Medical Center, New York City, Sept. 17–19. The course will address the needs of all health care professionals, including radiologists, involved in the care of pregnant women. Topics will include epilepsy, cerebrovascular disease, eclampsia, headache, back pain, multiple sclerosis, movement and neuromuscular disorders associated with pregnancy, neuropsychiatric manifestations of connective tissue diseases and psychiatric disorders, infections, neurooncology, head trauma, and drug abuse. The safety of diagnostic studies and the legal implications of the neurologic disorders of pregnancy will also be addressed. Category 1 credit: 13 hr. Fee: $300. Information: NYU Medical Center, Post-Graduate Medical School, 550 First Ave., New York, NY 10016; telephone: (212) 263-5295; fax: (212) 263-5293.

Western Neuroradiological Society Annual Meeting

The annual meeting of the Western Neuroradiological Society will be held at the Ritz-Carlton San Francisco, San Francisco, Oct. 1–4. Program director: Michael Brandt-Zawadzki. Category 1 credit is pending. Information: Dawne Ryals, Ryals and Associates, P. O. Box 1925, Roswell, GA 30077-1925; telephone: (404) 641-9773; fax: (404) 552-9859.

International Symposium on Vena Cava Filters

International Symposium on Vena Cava Filters will be held at the Congress Center, Le Futuroscope, Poitiers, France, Oct. 9–10. The program will include lectures and workshops. Topics will include thromboembolism, imaging of the inferior vena cava and its thromboses, interruptions of the inferior vena cava, the ideal vena caval filter, filter materials and insertion, alternative and associated treatments, indications and contraindications for filters, and case studies. Guest faculty: A. Dibie-D. Musset, R. F. Dondelinger, G. Emmanualli, L. Greenfield, R. W. Gunther, F. Joffre, P. Marrache, D. Midy, M. Simon, R. Vogelzang, F. C. Taylor, and S. Wallace. Information: Symposium International Filtres Cave, Madame Danielle Renaud, Service de Radiologie A, Hôpital La Milétrie, BP 577, 86021 Poitiers Cedex, France; telephone: (33) 49 44 39 11; fax: (33) 49 44 39 12.

Michigan Fall Radiology Conference

The Dept. of Radiology, William Beaumont Hospital, Royal Oak, MI, will present Michigan Fall Radiology Conference, Oct. 16–17, at the Townsend Hotel, Birmingham, MI. The conference is intended to be a refresher course as well as an update in practical aspects of diagnostic radiology, including modern imaging techniques. Guest faculty: N. R. Dunnick, D. M. Ikeda, and S. M. Wolpert. Category 1 credit: 14 hr. Fee: physicians, $175; residents, $75. Information: Miss Mary Anne Smith, Program Coordinator, William Beaumont Hospital, 3601 W. Thirteen Mile Rd., Royal Oak, MI 48072-2793; (313) 551-6199.

Breast Imaging Seminar

The Medical Imaging Service, Memorial Sloan-Kettering Cancer Center, New York City, will present Breast Imaging Seminar with Therapy Update, Oct. 19–21, at the center. The course is designed to improve skills in interpretation of mammograms, present technical factors important for obtaining optimal mammograms, and update quality assurance methods. Category 1 credit: 17 hr. Fee: physicians, $375; technologists and students (letter required): $200. Information: CME Office, Memorial Sloan-Kettering Cancer Center, 1275 York Ave., New York, NY 10021; telephone: (212) 639-6754; fax: (212) 717-3140.

Musculoskeletal Imaging

The University of California, San Diego, is sponsoring Musculoskeletal Imaging, Oct. 24–25, at the Hotel Del Coronado, San Diego. Program director: Donald Resnick. Category 1 credit (pending): 9 hr. Fee: physicians, $250; residents, fellows, and technologists, $150. Information: Dawne Ryals, Ryals and Associates, P. O. Box 1925, Roswell, GA 30077-1925; telephone: (404) 641-9773; fax: (404) 552-9859.

Postgraduate Radiology Course

The University of California, San Diego, is sponsoring the 17th annual Postgraduate Radiology Course, Oct. 26–30, at the Hotel Del Coronado, San Diego. Program director: David S. Feigin. Category 1 credit (pending): 25.25 hr. Fee: physicians, $600; residents, fellows, and technologists, $400. Information: Dawne Ryals, Ryals and Associates, P. O. Box 1925, Roswell, GA 30077-1925; telephone: (404) 641-9773; fax: (404) 552-9859.

Dysphagia Research Society Inaugural Meeting

The inaugural meeting of the Dysphagia Research Society will be held in Milwaukee, Nov. 6–8. The goals of the society are to enhance focused research pertinent to dysphagic conditions, encourage interdisciplinary research in dysphagia, provide a forum for research in dysphagia and interdisciplinary communication, and foster new methods and instrumentation for research and treatment of dysphagia. Abstracts of research on the physiology and pathophysiology of swallowing and on dysphagia-related topics are requested. The deadline for submission is Sept. 1. Abstract forms are available from Dysphagia Research Society, Organizing Office, c/o Reza Shaker, M.D., GI Section/111C, VA Medical Center, 5000 W. National Ave., Milwaukee, WI 53295; telephone: (414) 384-2000, ext. 6943; fax: (414) 384-8480. Steering committee: D. Bieger, W. Dodds, M. Donner, D. Castell, W. Hogan, B. Jones, G. Logemann, C. Sasaki, B. Sonies, K. Schulze, and R. Shaker. Information on the meeting: Reza Shaker, M.D., Division of Gastroenterology, Froedtert Memorial Lutheran Hospital, 9200 W. Wisconsin Ave., Milwaukee, WI 53226; telephone: (414) 259-3037; fax: (414) 384-8480.

The American Board of Radiology Examinations

Written examinations for the American Board of Radiology (ABR) are scheduled for Oct. 1–2, 1992, and Sept. 23–24, 1993. Oral examinations will be held at the Executive West Hotel in Louisville, KY, June 7–10, 1993. The ABR will accept applications for admission to the examinations after July 1, but not later than Sept. 30, in the year *preceding* the year in which the examination is to be taken. For application forms and further information: Office of the Executive Director, The American Board of Radiology, 2301 W. Big Beaver Rd., Ste. 625, Troy, MI 48084.

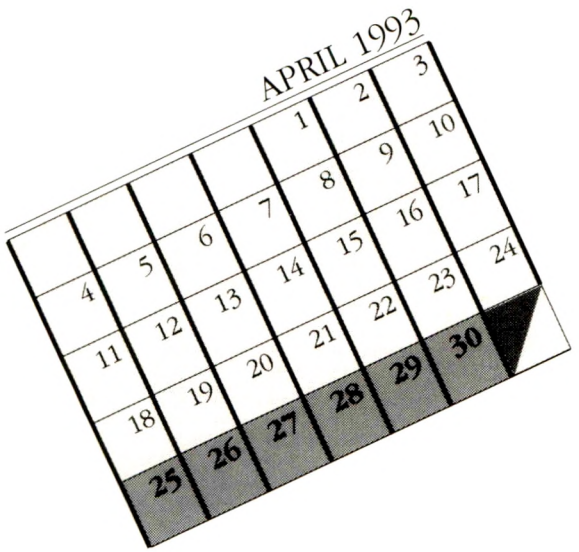
Meeting and Course Review

For the reader's convenience, a summary of upcoming meetings and courses is provided. Detailed listings are given in the *AJR* issue given in parentheses.

Practicum in Breast Imaging, times arranged, Baltimore (Aug 1991)
Magnetic Resonance Imaging in Spain and Morocco, June 28–July 1, Barcelona, and July 3–5, Casablanca (April)
1992 Marie Curie Award, deadline for nominations, July 1 (June)
Workshop on Vascular Anomalies, July 1–3, Denver (March)
Imaging Courses at Sea, breast imaging, July 4–11; MR imaging–musculoskeletal imaging, July 11–18 (May)
Paediatric Imaging Update, July 5–10, Port Douglas, Australia (March)
Symposium on Breast Disease, July 12–15, Grand Traverse Resort, MI (June)
Course on Body Imaging, July 13–17, Santa Fe, NM (March)
Diagnostic Imaging Seminar, July 13–17, Edgartown, MA (Martha's Vineyard) (April)
Vascular Imaging and Intervention for the 90s, July 17–19, San Francisco (April)
Diagnostic Imaging Update, July 20–22, San Francisco, and July 23–26, Carmel, CA (March)
Clinical Imaging for Non-Radiologists, July 20–24, San Diego (March)
The Sharper Image in MRI, July 27–31, Colorado Springs, CO (April)
MRI and Musculoskeletal Imaging, July 27–Aug. 1, Laguna Niguel, CA (March)
Courses on Prostate Ultrasound, July 31–Aug. 1 and Oct. 16–17, Albany, NY (June)
Mackinac Island Imaging Conference, Aug. 3–6, Mackinac Island, MI (May)
Midwest Interventional Radiology Seminar, Aug. 7–9, Peoria, IL (June)
Northern Imaging 1992 Radiology Seminar, Aug. 7–10, Knee Lake Lodge, Manitoba (June)
Symposium on Diagnostic Imaging, Aug. 8–12, Newport, RI (June)
Contemporary Medical Imaging IX, Aug. 12–16, Hilton Head Island, SC (April)
Summer Practicum, Aug. 16–20, Keystone, CO (April)
Barcelona 1992 Post-Games Imaging Conference, Aug. 17–21, Barcelona (April)
European Symposium on Uroradiology, Aug. 24–27, Herlev, Denmark (Aug 1991)
International Skeletal Society Refresher Course, Aug. 26–29, Stockholm (March)
Congress of Asian Federation of Societies for Ultrasound in Medicine and Biology, Aug. 30–Sept. 3, Seoul, Korea (Feb)
Cardiovascular and Interventional Radiological Society of Europe Annual Meeting and Postgraduate Course, Aug. 30–Sept. 3, Sitges (Barcelona), Spain (May)
Radiation, Physics, and Biology, Aug. 31–Sept. 4, New York City (May)
Ultrasound Angiography 92, Sept. 2–4, University of Southampton, United Kingdom (Feb)
Mammography Update, Sept. 7–11, Santa Fe, NM (June)
Pacific Northwest Diagnostic Ultrasound: OB/GYN Symposium, Sept. 10–12, Seattle (May)
Pittsburgh Breast Imaging Seminar, Sept. 10–13, Pittsburgh (May)
Symposium on Transrectal Ultrasound, Sept. 11–13, Chicago (May)
Ultrasound and Cardiovascular Technology Review Conference, Sept. 11–13, San Diego (June)
Vancouver Imaging Update 1992, Sept. 13–17, Vancouver, B.C. (May)
Mammographic Interpretation, Sept. 14–17 and Oct. 26–29, Boston (April)
MRI Visiting Fellowships at UCLA, Sept. 14–18, Oct. 5–9, and Dec. 7–11, Los Angeles (Sept 1991)
Dose, Time, and Fractionation in Radiation Oncology, Sept. 16–19, Madison, WI (May)
Musculoskeletal and Neuroradiological MRI, Sept. 21–26, Hilton Head Island, SC (June)
Practicum in Mammography for Technologists, beginning dates, Sept. 28 and Oct 19, San Diego (May)
Update in Film Screen Mammography, Sept. 30–Oct. 2, Richmond, VA (May)
Fall Foliage Imaging Seminar, Oct. 9–11, Burlington, VT (May)
Practical Radiology, Oct 12–15, Charlottesville, VA (June)
Nuclear Cardiology Symposium and Workshop, Oct. 14–16, Milwaukee (June)
Progress in Magnetic Resonance, Oct. 15–17, Locarno, Switzerland (June)
Society of Radiologists in Ultrasound Postgraduate Course, Oct. 23–25, Chicago (June)
International Course on MR Imaging, Oct. 25–28, Riyadh, Kingdom of Saudi Arabia (March)

AJR carries announcements of courses, symposia, and meetings of interest to its readers if received a minimum of 5 months before the event. There is no charge; receipt of items by the *AJR* Editorial Office is not acknowledged. Submit items for publication typed double-spaced. Provide title, date, location, brief description, sponsor, course directors, fees, category I credit, and address and telephone number for additional information. Faculty from the host institution will not be listed. Guest faculty names will appear **only** if initials are provided. Mail news items to *AJR* Editorial Office, 2223 Avenida de la Playa, Suite 103, La Jolla, CA 92037-3218.

Mark Your Calendar Now!



The American Roentgen Ray Society will return to San Francisco in 1993, and plans are already underway for what promises to be an educationally fulfilling and socially enjoyable week in the city by the bay. Look for the San Francisco logo in the next several issues of the *AJR* for updated meeting information.

Call for Papers

Abstracts of papers to be considered for the scientific program must be submitted by November 1, 1992. Abstract forms and instructions for submission are included in this issue and will also appear in the July through October issues. The *AJR* has first rights to all papers accepted for presentation at the ARRS meeting.

Call for Scientific Exhibits

The deadline for submission of abstracts to be considered for scientific exhibits is November 1, 1992. Abstract forms and instructions for submission are included in this issue and will also appear in the July through October issues.

Categorical Course

The topic of the 1993 Categorical Course is Ultrasound. A summary of topics and faculty for this course will appear in the February 1993 issue of the *AJR*.

Refresher Courses

Plans are underway to present at least 60 instructional courses on various topics of interest to the radiology community. A summary of these courses will be included in the February *AJR*. Early registration is strongly suggested, as these courses fill up quickly.

Resident Award Papers

The society offers three cash awards for the best scientific papers prepared by residents in radiology. The President's Award has a cash prize of $2,000, and there are two Executive Council Awards with a cash prize of $1,000 each. The winners of these three awards are invited to present their papers during the opening ceremonies at the annual meeting. Papers must be submitted by February 12, 1993, for consideration in this competition. Additional information on these awards will be mailed to all residency program directors in July.

Local Arrangements

The San Francisco area offers many opportunities for sightseeing, shopping and entertainment. Check the February *AJR* for detailed information on local tours developed especially for ARRS meeting attendees.

Registration and Hotel Reservations

All meeting activities will take place in the beautiful new San Francisco Marriott, centrally located on Market Street. The society has negotiated special room rates for meeting attendees, and the February *AJR* will contain meeting registration and hotel reservation forms. As in previous years, early registration is strongly suggested.

Travel

The society will make arrangements with United Airlines and a major car rental firm for preferred rates for meeting attendees. Taking advantage of these special rates benefits both you and the society – you save money on your reservations, and the society receives discounts to send staff and supplies to the meeting. Plan now to check the February issue of the *AJR* for details.

Classified Advertisements

Positions Available

GADSDEN RADIOLOGY ASSOCIATES is a 3-member radiology group seeking a fourth board-certified/eligible radiologist. Gadsden Radiology covers Baptist Memorial Hospital, a 250-bed hospital performing more that 55,000 radiologic exams/yr. All radiologic modalities are available, including state-of-the-art CT, SPECT, nuclear medicine, special procedures, and MRI. Gadsden Radiology Associates also covers their private office, imaging center, and a breast center. Teleradiography is used for call. Gadsden, AL, is a safe, clean city centrally located on the Coosa River approximately 1 hour from Birmingham, 90 Min. from Chattanooga, and 2 hours from Atlanta, GA. Salary and vacation are excellent. Health insurance and malpractice is paid. Interested candidates contact Homer A. Spencer, M.D., 401 Bay Street, Gadsden, AL 35999; (205) 543-3200, or fax (205) 546-7908. 7-1ap

ABDOMINAL RADIOLOGIST, THOMAS JEFFERSON UNIVERSITY HOSPITAL—The Dept. of Radiology at Jefferson has an immediate opening for an abdominal radiologist at either the junior or senior faculty level. Clinical responsibilities include GI fluoroscopy body, CT, and/or ultrasound. Jefferson has a large and well-equipped dept. performing 220,000 exams/yr, as well as extensive teaching and research programs. There are 5 modern fluoro rooms, 3 CT scanners, 30 ultrasound scanners, and 4 MRI units. All faculty members have dedicated academic time, and salary and benefits are excellent. Interested candidates should contact David C. Levin, M.D., Chairman, Dept. of Radiology, Thomas Jefferson University Hospital, 11th & Walnut Streets, Philadelphia, PA 19107; (215) 955-7264. An equal opportunity/affirmative action employer. 7x

COASTAL FLORIDA, IMMEDIATE OPENING FOR BC DIAGNOSTIC RADIOLOGIST to join 2-man group in single-site practice at well-equipped 110-bed hospital in small east coast community 60 miles from Orlando and Disney World. Relaxed practice includes all aspects of general radiology, including MRI. Excellent fringe benefits and early partnership. Contact Alan J. Stern, M.D. or Joseph E. Godard, M.D., P.O. Box 933, New Smyrna Beach, FL 32170; (904) 427-3401. 7-10ap

PEDIATRIC RADIOLOGISTS—Full-time faculty positions, Dept. of Radiology, Children's Hospital, Boston, MA, at the academic rank of assistant professor to professor, Dept. of Radiology, Harvard Medical School, available July 1, 1992. Salary and fringe benefits are highly competitive; salary is based on academic rank and experience. Candidates must be certified in diagnostic radiology by the American Board of Radiology or its equivalent, must have completed a fellowship in pediatric radiology, and must be eligible for active membership in The Society for Pediatric Radiology. Duties include clinical service, teaching, and research. Professional coverage includes conventional pediatric radiology, ultrasonography, computed tomography, MRI, nuclear medicine, vascular/interventional radiology, and digital radiography. The candidate must have a demonstrated interest and qualifications in basic and/or clinical pediatric imaging research. Children's Hospital and Harvard Medical School are affirmative action/equal opportunity employers. Address inquiry and CV to Donald R. Kirks, M.D., Radiologist-in-Chief, Dept. of Radiology, Children's Hospital, 300 Longwood Avenue, Boston, MA 02115; (617) 735-6291. 7a

CHIEF RADIOLOGIST—VAMC, Muskogee, Oklahoma, is recruiting a board-certified radiologist to serve as chief for a modern diagnostic imaging service, affiliated with OU/College of Medicine, Tulsa. Responsibilities include a Tulsa satellite clinic. For additional information, send CV to Gayle Harris, MD, COS, VAMC, Honor Heights, Muskogee, OK 74401. 7a

FACULTY POSITIONS IN RADIOLOGY—The Dept. of Radiology and Radiological Sciences of Vanderbilt University School of Medicine has openings in the following areas: neuroradiology, chest, musculoskeletal, and pediatric radiology. Research opportunities are exceptional. Candidates must be board-certified. Please send CV to C. Leon Partain, M.D., Ph.D., Professor and Chairman, Dept. of Radiology and Radiological Sciences, Vanderbilt University, Nashville, TN 37232-2675. An equal opportunity/affirmative action employer. 7-8a

BC/BE RADIOLOGIST—Busy clinic- and hospital-based practice is seeking to add additional BC/BE radiologists to its staff of 2 neuroradiologists and 7 general radiologists. Special skills or training in pediatrics, MRI, or nuclear medicine would be beneficial. Physician will join a 270-physician multi–specialty group representing over 50 specialities. Fargo Clinic is affiliated with St. Luke's Hospitals, a 400-bed level III care center with a NACHRI designated Children's Hospital. Fargo-Moorhead is a tri-college community of 130,000 which supports an opera company, symphony, community theater, and various athletic events. Year-round recreational opportunities abound. Guaranteed first year salary and competitive compensatory arrangements are available. Respond to Kathleen Toft, Physician Recruitment Director, 737 Broadway, Fargo, ND 58123; (800)-437-4010, ext. 2151. 7-10xa

THE UNIVERSITY OF CALIFORNIA, IRVINE, COLLEGE OF MEDICINE seeks candidates for the tenured position of professor and chair, Dept. of Radiological Science. The candidate must be an accomplished investigator, clinician, and teacher with vision to lead a major university dept. Send CV plus names and addresses of 3 references to Samuel E. Wilson, M.D., Professor and Chair, Dept. of Surgery, Chair of Search Committee, c/o Janet Nash, College of Medicine, Room 246, Irvine Hall, UCI, Irvine, CA 92717. UCI is an affirmative action, equal opportunity employer., Women and minorities are encouraged to apply. 7a

DIAGNOSTIC RADIOLOGIST ON THE ISLAND OF KAUAI with 45 doctors in multispecialty group. Three radiologists in clinic and hospital depts., BC radiologist to perform diagnostic radiology, CT scan, ultrasound, mammography, nuclear medicine, no angiography. Strong FNA service. Island of 50,000 people with moderate subtropical climate. All outdoor sports–scuba, snorkeling, fishing, golf, tennis, biking, etc. Incentive formula on becoming stockholder after 1 year, excellent benefits. Congenial group with quality care emphasis. CV by mail or fax (808) 246-1625 welcomed, or call Rex D. Couch, M.D., Medical Director, Kauai Medical Group, Inc., 3420-B Kuhio Highway, Lihue, HI 96766; (808) 245-1077. 7-8a

RADIOLOGIST—Angiography, interventionalist with experience in CT and ultrasound preferred to join active suburban Philadelphia 8-man hospital practice. Contact Richard B. Levine, M.D., Chairman, (215) 663-6078, eve. (215) 884-1523. 7ap

INTERVENTIONAL NEURORADIOLOGIST, COASTAL VIRGINIA — A 32-physician private radiology group which practices in 6 hospitals and several offices is seeking an interventional neuroradiologist who is eligible for senior membership in the American Society of Neuroradiology. The individual's clinical responsibilities would be primarily limited to a 644-bed tertiary-care center with level 1 trauma status. Diagnostic equipment includes 2 state-of-the-art Signa 1.5-T GE MR scanners (4.79 software and angio package), a DFP 60A bi-plane bi-digital 1024 matrix Toshiba DSA system (with digital stereo capabilities), and a Siemens DRH as well as a GE 9800 CT scanner. Some time would be spent at a 250-bed hospital with a Hitachi MRP-5000 0.2-T MR unit and a GE 9800 CT scanner with Hi-Light advantage software. Two (2) year fellowship trained neuroradiologists are already on staff. The practice is affiliated with a medical school and residency program which allows the pursuit of academic interests. The practice is located in a coastal resort area with a temperate climate and all water sports available. Interested persons should send a CV or contact Carl V. Bundschuh, M.D., Director of Neuroradiology and MRI, Medical Center Radiologists, Inc., 6161 Kempsville Circle, Ste. 330, Norfolk, VA 23502; (804) 466-0089. 7ap

DIAGNOSTIC RADIOLOGIST —Large private multi-hospital group in a coastal city of Virginia seeks a radiologist with special interests in all aspects of mammography. The practice includes a tertiary-care hospital which is affiliated with both a medical school and a radiology residency training program, thereby offering the benefits of both private practice and academics. The position would include directorship of future mammography clinics. Additional aptitude in other aspects of diagnostic radiology with specialized and/or fellowship training preferred. Interested applicants please send CV or inquiries to Medical Center Radiologists, Halifax Building, Ste. 330, 6161 Kempsville Circle, Norfolk, VA 23502; (804) 466-0089. 7ap

MARYLAND—The Dept. of Radiology, University of Maryland Medical System/Hospital in Baltimore, is seeking additional faculty members for the sections of pediatric radiology, ultrasound, nuclear (doubled boards desired), gastrointestinal, mammography, neuroradiology, vascular/interventional and skeletal radiology. Fellowship training or equivalent experience desired. Also, a Ph.D. imaging physicist is needed. ABR certification required or equivalent where appropriate. The medical center is an 800-bed acute-care hospital and tertiary referral center with an active and varied practice. A new affiliated VA hospital with 324 beds is now under construction and will be adjacent to and connected to the university in the Spring of 1992. The duties of new faculty members will include research and teaching. Academic rank and salary commensurate with experience. The radiologists are organized as a professional corporation offering excellent fringe benefits. Baltimore is a superb place in which to live and work. It has all the amenities of a large metropolitan center, yet is small enough to avoid most of the problems (traffic, inflated property values, etc.) of our largest cities. Washington, Philadelphia, and New York are readily accessible. Only 3 hrs. from Ocean City, MD. Submit CV to Gerald S. Johnston, M.D., Dept. of Diagnostic Radiology, 22 S. Greene St, Baltimore, MD 21201; (800) 866-8667 ext. 3477. Affirmative action equal opportunity employer and encourages applications from members of minority groups.7ap

LEBANON, NEW HAMPSHIRE, DARTMOUTH-HITCHCOCK MEDICAL CENTER is seeking an academic interventional radiologist at assistant professor level. Individual should have heavy commitment to academic practice with emphasis on teaching at the fellowship and resident level, including classroom instruction at the medical school level. Specific teaching and patient care interests in interventional treatment of complex liver disease including portal hypertension are highly desirable. 115,000 exams/yr, 15 staff members, 12 residents, and 2 fellows. Dept. with affiliated VA constitutes full-time faculty of Dartmouth Medical School and staff of new state-of-the-art dept. within new medical center campus. Board-certified or eligibility required. Write to Peter K. Spiegel, M.D. Dept. of Radiology, Dartmouth-Hitchcock Medical Center, One Medical Center Dr. Lebanon, NH 03756. AAEOE. 7ap

NEURORADIOLOGIST—Unique opportunity to join expanding N.Y.C. area practice. Board-certified radiologist with 2-yr fellowship in neuroradiology needed to head section of neuroradiology. This well-established university affiliated practice includes 9 board-certified radiologists practicing in a 487-bed teaching hospital and 2 private offices performing approximately 110,000 procedures/yr. State-of-the-art imaging equipment including 1.5-T GE Signa. Competitive salary leading to full equal partnership. Contact Jorge G. Pardes, M.D/William G. Wolff, M.D. Booth Memorial Medical Center; (718) 670-1594 or 1050. 7-10ap

DIAGNOSTIC RADIOLOGIST, NORTHEAST MICHIGAN—Excellent practice opportunity available for a diagnostic radiologist to commence in the autumn of 1992. Alpena Radiology, P.C,. seeks a BC/BE radiologist to complete our 3-man group. We offer excellent income, early partnership and idyllic lifestyle. We require a friendly, hard-working individual who will be a team player. The ability to work well with us and our excellent medical staff is a must. Alpena General Hospital is a modern 175-bed facility located on the shores of Lake Huron. The hospital provides all radiology equipment including: new R&F equipment (G.E.), Siemens CT, SPECT nuclear imaging, color flow Doppler, DSA, ACR accredited mammography. Siemens mobile MRI will commence shortly. The hospital administration is very supportive. The Alpena area is a sportsman's paradise. Sailing, boating, golf, fishing, hunting, skiing, etc. are all minutes away. Our moderate winters and Mediterranean summers are ideal. For more information please contact Steven Zweig, M.D. or James Weeks, M.D., Dept. of Radiology, Alpena General Hospital, 1501 W. Chisholm Street, Alpena, MI 49707; (517) 356-7520. 7-9a

MRI CLINICAL RESEARCH DIRECTOR—Roswell Park Cancer Institute is seeking an MRI clinical research director with interest in oncologic imaging. The Radiology Dept. includes a recently built GE MRI and research center linked with 2 new GE Hi-Light Advantage CT systems. This is part of an MRI, CT, SPECT Cancer Imaging and Research Center. PET collaboration with a nearby university is also possible. At this renowned comprehensive cancer center, opportunity for research and academic activity is outstanding. A faculty appointment will be at the School of Medicine and Biomedical Sciences, State University of New York at Buffalo, according to the level of professional qualifications. Please send CV to Andrew A. Gage, M.D., Deputy Institute Director, Roswell Park Cancer Institute, Elm and Carlton Streets, Buffalo, NY 14263. EOE M/F/H/V. 7-10a

DIAGNOSTIC RADIOLOGY AND BREAST IMAGING—Roswell Park Cancer Institute is seeking board-certified radiologists with interests in oncologic and general radiology, CT/MRI, ultrasound, and breast imaging. The modernization of the entire Radiology and Nuclear Medicine Depts. includes a new multidisciplinary Breast Imaging Center, a new MRI Center, and new CT, ultrasound and flouroscopy suites. At this renowned comprehensive cancer center, opportunity for multimodality clinical diagnostic imaging, research and academic activity is outstanding. A faculty appointment will be at the School of Medicine and Biomedical Sciences, State University of New York, according to the level of professional qualifications. Please send CV to Andrew A. Gage, M.D., Deputy Institute Director, Roswell Park Cancer Institute, Elm and Carlton Streets, Buffalo, NY 14263. EOE M/F/H/V. 7-10a

BC DIAGNOSTIC RADIOLOGIST—Affluent practice. Excellent salary, benefits, and partnership. Investigate now before socialized medicine becomes a reality! This 395-bed hospital, second largest in the beautiful state of Delaware, is centrally located on the East Coast. This is a rapidly expanding, high-powered group practice. Subspecialty training in interventional, imaging, or mammography desired. Open to F/M with 1–2 yr of postgrad experience. Send resume to or contact Ben Hollander, M.D., Dept. of Radiology, St. Francis Hospital, 7th & Clayton Sts., Wilmington, DE 19805; (302) 421-4304. 6–8ap

GOOD LIFE, GOOD MONEY—Radiologist needed for growing practice that covers 2 hospitals as well as 2 free-standing clinics. Modalities include R&F, general, mammography, CT, MRI, nuclear medicine, SPECT, and special procedures. Denton, population 60,000, located 30 mi. north of Dallas/Fort Worth, has 2 recreational lakes within 15 mi. and 2 major universities. Attractive financial and benefit packages are offered. Contact Family Radiology with CV at 1614 Scripture, Ste. 2, Denton, TX 76201; (817) 387-6159. 7a

RADIOLOGY FACULTY POSITIONS—The University of Tennessee, Memphis, in conjunction with UT Medical Group, Inc., is actively recruiting radiologists in diagnostic radiology, pediatric radiology, ultrasonography, angiography and interventional radiology, and magnetic resonance. Applicant must be board-certified or eligible. Competitive salaries, excellent benefits, and research/clinical opportunities. Blacks, women, handicapped, and other minorities are encouraged to apply. The University of Tennessee, Memphis, is an equal opportunity/Title IX/Section 504/ADA affirmative action employer. Send CV to Barry Gerald, M.D., Chairman, Dept. of Radiology, The University of Tennessee, Memphis, 800 Madison Ave., Memphis, TN 38163. 6–7a

CT/ULTRASOUND/MRI, VASCULAR/INTERVENTIONAL, NEURORADIOLOGISTS—The Medical College of Pennsylvania is seeking BC/BE radiologists with expertise in the above specialty areas. Responsibilities involve clinical work, teaching (resident and medical students), and research as desired. Competitive salary and benefits. Immediate full/part-time openings. Please contact Mindy M. Horrow, M.D., Dept. of Radiologic Sciences, Medical College of Pennsylvania, 3300 Henry Ave., Philadelphia, PA 19129; (215) 842-6578. 6–7a

PART-TIME PEDIATRIC/GENERAL RADIOLOGIST, CENTRAL MASSACHUSETTS—Radiologist sought with special competence in pediatric radiology to join an 11-member group. We serve a 550-bed medical center that includes the regional 40-bed neonatal intensive care unit. Position involves sharing general responsibilities including CT, ultrasound, and mammography. Part-time position may become full-time. Please send CV to Richard Danford, M.D., Worcester Radiologists, 121 Lincoln St., Worcester, MA 01605; (508) 753-8151. 6–8ap

VASCULAR/INTERVENTIONAL RADIOLOGIST—Temple University Hospital and School of Medicine is seeking a board-certified vascular/interventional radiologist with fellowship training for a faculty position at the assistant professor rank in the academic yr 1992–1993. This position involves responsibilities in patient care and teaching. Additionally, those candidates with research skills would be preferred. Applicants should contact Francis J. Shea, M.D., Deputy Chairperson, Dept. of Diagnostic Imaging, Temple University Hospital, 3401 N. Broad St., Philadelphia, PA 19140. Temple University Hospital and School of Medicine is an affirmative action/equal opportunity employer. 7xa

RADIOLOGIST—Established northeastern PA radiology practice seeking fifth radiologist for hospital and private practice. Applicant should have experience in CT, MRI, ultrasound, mammography, nuclear medicine, angiography, and interventional radiology. Potential for partnership. Candidate should be board-certified/eligible and licensed in PA. Address inquiries and current CV to Box E60, AJR (see address this section). 6–8ap

RENO, NEVADA—Opportunity exists for a board-certified diagnostic radiologist at the VA Medical Center. This is a full-time joint position with the University of Nevada- Reno School of Medicine. Competence in all areas of diagnostic imaging is required with special competence in MR imaging preferred. Experience in teaching, research, and clinical skills is advantageous. The dept. includes a GE 9800 CT scanner, ultrasound equipment. Including the availability of color Doppler and a SPECT nuclear imaging camera. The Special Procedure Suite is brand new. Essentially, all current interventional work is performed on a routine basis. Teaching responsibilities center predominantly on medical student education and to a lesser extent on instruction of non-radiology students. While the emphasis is on teaching and clinical work the potential for research with recruitment of this position will be excellent. Excellent salary and benefits. New special pay bonus package offered. The area offers the best in entertainment, sporting activities and location. San Francisco, Napa Valley, Lake Tahoe are within convenient driving distance. Nevada has no state income tax. CV and inquiries to Thomas C. Barcia, M.D., Chief, Diagnostic Imaging Service, VA Medical Center, 1000 Locust Street, Reno, NV 89520; (702) 328-1446. 7a

EXCITING RADIOLOGY OPPORTUNITIES NATIONWIDE!— Now is the time to make your move! Absolutely no cost to you. We specialize in radiology, so we understand your needs. Both group and private practice opportunities are available. We give you the inside tracks! Fax your CV to (214) 258-1092 or mail to Snelling Search Medical Group, 1301 Walnut Hill Ln., Ste. 103, Irving, TX 75038. For information on specific positions, call toll free (800) 259-5973. 6–7a

IMMEDIATE OPENING FOR BC/BE DIAGNOSTIC RADIOLOGIST, NEW ENGLAND, to join a 6-member group, leading to partnership, in an active community, university-affiliated hospital. Over 100,000 exams/yr. Practice includes CT, ultrasound, nuclear medicine, MRI, angiography, and interventional. Locum needed in interval. Located in New England close to boating and skiing, 1 hr from Boston. Contact Allan M. Deutsch, M.D., Dept. of Radiology, The Miriam Hospital, 164 Summit Ave., Providence, RI 02906; (401) 331-8500, ext. 4400. 6–8ap

CENTRAL WISCONSIN—Established radiology group in independent practice is seeking 2 additional radiologists for growing practice in central Wisconsin. All imaging modalities. Competitive first yr salary with full partner status available second yr. Full benefits. Excellent schools, recreation, and quality of life. Contact David E. Enerson, M.D., 900 Illinois Ave., Stevens Point, WI 54481; (715) 346-5140 or Andrew M. Lucas, M.D., 410 Dewey St., Wisconsin Rapids, WI 54495-8080; (715) 423-6060. 7xa

MRI/CT/ULTRASOUND—The State University of New York/Health Science Center at Brooklyn seeks a board-certified/eligible physician to join the faculty in cross-sectional imaging. The medical center is a 1,700-bed facility including Kings County Hospital and the State University Hospital. The medical center performs over 250,000 diagnostic procedures/yr. Currently, we have 4 state-of-the-art CT scanners with a fifth to be installed shortly. A GE Signa was recently installed and a second is planned. Seventeen ultrasound units are in clinical use. Research time and facilities are available. The 2 hospitals are connected with a PACS system via a microwave link. Rank and salary are commensurate with qualifications. CV should be addressed to Joshua A. Becker, M.D., Professor and Chairman, Dept. of Radiology, SUNY/Health Science Center at Brooklyn, 450 Clarkson Ave., Brooklyn, NY 11203. Equal opportunity employer. 6–7ap

NEURORADIOLOGIST—A faculty position is available in the Dept. of Radiology at the University of Rochester Medical Center, Strong Memorial Hospital, a 725-bed university hospital. An appointment as assistant professor or higher is available at a level appropriate to experience. A fellowship is required. The neuroradiology section consists of 5 faculty members and 1–2 fellows. Research and teaching opportunities are available in a strong academic dept. with state-of-the-art radiologic equipment. Contact John C. Wandtke, M.D., Acting Chair, Dept. of Radiology, Box 648, University of Rochester Medical Center, Rochester, NY 14642; (716) 275-2733. EO/AA/M-F. 6–8a

PEDIATRIC RADIOLOGY—The Medical College of Georgia seeks a general pediatric radiologist and a pediatric radiologist with expertise in pediatric imaging. These individuals will provide general and specialized pediatric radiology services, guide the integration of imaging services within pediatric radiology, and help plan and implement pediatric radiology services for the upcoming 175-bed Children's Medical Center. Tenured or nontenured positions are available at assistant, associate, or full professor levels. The senior appointee will become head of the Pediatric Radiology Section. Call or write Dr. Charles G. Howell, Jr., Pediatric Radiology Search Committee, Pediatric Surgery Section, Medical College of Georgia, Augusta, GA 30912-4070; (404) 721-3941. MCG is an equal opportunity/affirmative action employer. 7a

MAMMOGRAPHY FACULTY POSITION—The Dept. of Radiology at the University of Rochester Medical Center has a faculty position available in mammography. The mammography practice is in Strong Memorial Hospital and 2 private offices. One of the offices has over 30,000 exams/yr. The section offers a strong potential for academic growth with emphasis on original research and teaching. Academic time is available for faculty interested in developing a strong academic career. Support, resources, and opportunities are available for research. The radiologist can also participate in other aspects of radiology. Academic rank and salary will be determined by previous experience. Contact John C. Wandtke, M.D., Acting Chair, Dept. of Radiology, Box 648, University of Rochester Medical Center, Rochester, NY 14642; (716) 275-2733. EO/AA/M-F. 6–8a

DIRECTOR OF PEDIATRIC RADIOLOGY—The Division of Pediatric Radiology, Oregon Health Sciences University, Portland, OR, invites applications for a section director. Completion of an approved fellowship in pediatric radiology and ABR certification is required. Please send CV to Frederick Keller, M.D., Oregon Health Sciences University, Diagnostic Radiology, L340, 3181 S.W. Sam Jackson Park Rd., Portland, OR 97201-3098; (503) 494-4498. The OHSU is an affirmative action, equal opportunity employer. 6–8a

DIAGNOSTIC RADIOLOGIST—Private practice opportunity with 2 radiologists. Senior partner retiring. Excellent salary and early partnership. All imaging modalities including MRI. Angio experience desired. University community of 100,000 with abundant outdoor recreation. CV to Dan Davidson, M.D., 3000 W. Deborah Dr., Monroe, LA 71201; (318) 388-7810. 6–9ap

ISRAEL, DIAGNOSTIC RADIOLOGY—Opportunities for 3- to 4-wk or longer working vacations in a number of Israeli medical centers, on a volunteer basis. Positions varied, arrangements flexible. For information contact Jonathan H. Fish, M.D., 1844 San Miguel Dr., #302, Walnut Creek, CA 94596; (510) 947-0560. 5–7xa

PARTNERSHIP POSITION IN PALM SPRINGS, CA—Well-established, 9-member group has openings for 2 board-certified radiologists. A physician with a strong background in MRI is sought as director of the section of MRI. The other position requires a physician with mammography experience to direct imaging in the breast health section of a new comprehensive cancer center. The group covers a 350-bed hospital and 2 offices in a desirable, rapidly expanding area of southern California. MRI facilities include 1.5-T Picker Vista HPQ with MRA package, ViStar imaging computer, and 1.5-T GE Signa. Other equipment includes 3 CT, a Cemax image processor, 2 Acuson color-flow Doppler ultrasound, 4 nuclear cameras including 2 SPECT, and all other diagnostic modalities. Ground has just been broken on a new 25,000 sq. ft. radiology wing, which will be furnished with state-of-the-art equipment. New trauma center, cancer center, and rehab hospital being built. Excellent compensation and benefits package leading to full partnership. Beaches and large-city amenities of Los Angeles only 2 hr away. Yr-round sunny weather. Ample free time to enjoy southern California and the unparalleled recreational opportunities offered by the resort community of Palm Springs. Direct inquiries to Marvin J. Friedenberg, M.D., Desert Hospital, Dept. of Radiology, 1150 N. Indian Canyon Dr., Palm Springs, CA 92262. 7xa

BOSTON—Expanding private-practice group. night or evening call. Need experience in ma mography. Great lifestyle. Salary leading to eq partnership. Send letter and CV to Box E49, A (see address this section). 5–10a

NORTHERN CALIFORNIA—The Permaner Medical Group, Inc., is seeking a BC radiolog with multimodality interests and fellowship traini in MR to join a 12-person group serving a 337-b acute-care hospital and 2 outpatient clinics. Teac ing opportunities are available with residents subspecialty services on rotation from Stanfc University Hospital, as well as our own medical re idents. We have sited a GE 1.5-T MRI syste Competitive salary and excellent benefits. Plea send inquiries and CV to Bruce Baker, M.D., Chi Dept. of Radiology, Kaiser Permanente Medi Center, 900 Kiely Blvd., Santa Clara, CA 950 (408) 236-4444. EOE. 5–7a

DIAGNOSTIC RADIOLOGIST, ABDOMINAL I AGING—The University of Missouri–Columl Hospital and Clinics is seeking a radiologist w expertise in abdominal imaging (GI, CT, ult sound, and MRI). Board-certification required. F lowship desirable. Tenure and nontenure trac available at assistant and associate professor le els. Address inquiries to Robert J. Churchill, M. Dept. of Radiology, University of Missouri–Colu bia Hospital and Clinics, One Hospital Dr., Colu bia, MO 65212. An equal opportunity/affirmati action employer. 5–10ap

HOSPITAL-BASED, BC/BE RADIOLOGI needed to join newly-planned subregional medi center (campus). Must be proficient in general agnostic radiology, ultrasound, nuclear medicir CT, and MRI. Excellent opportunity plus attracti financial package. Located in east central Monta along the Yellowstone River. Great outdoors recreation, hunting, and fishing. Excellent educ tion system. Lifestyle is rural and family-oriente Send CV to Vice-President, Business Servic Holy Rosary Hospital, 2101 Clark, Miles City, M 59301. 5–7ap

BC/BE GENERAL DIAGNOSTIC RADIOLOGI needed to join 3 radiologists in 70-physician mu specialty clinic. Also responsible for radiology s vices at 250-bed hospital connected to clinic. radiology modalities available, including CT a MR. Competitive first-yr guarantee with excelle benefit package. Eligibility for shareholdership af 1 full fiscal yr. Community of 52,000 in beaut Mississippi River Valley. Send CV to P. Steph Shultz, M.D., Medical Director, Skemp Clinic, L 800 West Ave., S., La Crosse, WI 54601; (6(782-9760, ext. 6329. 5–7ap

RADIOLOGIST—A 4-physician group seeks a fi to join our well-established and growing practi We are located in east-central Illinois, with a 4 college, Jr. college, and a farming economy e hanced by numerous growing industries. We se a rural but very modern 230-bed hospital ($25 n lion expansion underway) and several other sit performing more than 80,000 exams/yr. Mattoc Charleston is a great place to raise a family wh still having access to big-city amenities. Please BC/BE, skilled in interventional or MRI, and able handle general diagnostic modalities competen Please reply to Bruce Fluesmeier, Lakeland Ra ologists, Ltd., 1221 Broadway, Mattoon, IL 619 (800) 745-7701. 3–8ap

FULL-TIME BC/BE DIAGNOSTIC RADIOLOGIST needed to replace retiring senior partner in a friendly, cooperative, 4-person group in south-central Idaho. 165-bed hospital with GE Signa 1.5-T MR, GE 9800 Quick CT, Acuson XP, and good technical staff. General radiology including angio, interventional, and nuclear medicine. Good income and vacation schedule, 1 yr to partnership. Nice community with extensive nearby skiing, hunting, fishing, etc., 80 mi. from Sun Valley, 4-hr drive from Yellowstone. Send CV and references to Dr. Evan Thomas, Southern Idaho Radiology, P. O. Box AB, Twin Falls, ID 83303. 5–7ap

DIRECTOR, DIVISION OF ULTRASOUND—The Dept. of Radiology, The University of Texas Medical Branch, is looking for a director of diagnostic ultrasound at the associate professor or professor entry level. The Division of Ultrasound, in our dept., is poised for growth and expansion. We require a leader with drive, initiative, and vision, and one who is still in his or her growing career phase. The University of Texas Medical Branch employs more than 8,400 employees, and Dept. of Radiology performs more than 200,000 exams/yr. The campus provides a fertile environment for those wishing to pursue an academic career. The clinical material and academic support are excellent. The dept. boasts many peer-reviewed publications and textbooks resulting from an inherent feature of the institution that allows one to pursue academic interests with freedom. Galveston is a very comfortable community with few large-city problems. It has an extremely pleasant climate, with the Gulf breeze making it exceptionally attractive throughout the yr. Outdoor activities abound, including boating, sailing, fishing, and tennis. The winters are extremely mild. More than half of the present faculty have lived in this area for 15 yrs or more. The dept. and institution are quite stable and have proved an excellent place for many of us to pursue academic careers. The position we offer has the foundation for the development of a truly superior academic career. Interested persons should send their CV to Leonard E. Swischuk, M.D., Chairman Ad-Interim, Dept of Radiology, The University of Texas Medical Branch, Galveston, TX 77550. UTMB is an equal opportunity, affirmative action employer, M/F/H/V. UTMB hires only individuals authorized to work in the United States. 5–7a

SUPERB PARTNERSHIP POSITION IN LAS VEGAS—Rapidly expanding 7-member group practice covering 2 full-service imaging centers and a small hospital has an immediate opening. We are looking for an additional board-certified radiologist with an uncommon dedication to excellence in patient care. Our outpatient facilities include 2 MR, 2 CT, angio with a 4-bed recovery area, 5 ultrasound, 5 mammography, 3 SPECT, plus R&F. This is an excellent opportunity for a partnership position with a well-respected group in a growing community. Please send CV to Dr. Mark Winkler, SDMI, 2950 S. Maryland Pkwy., Las Vegas, NV 89109. 3–2ap

IMMEDIATE OPENING—BC/BE radiologist to join 2 board-certified radiologists at a 130-bed community hospital and outpatient dept. located 25 mi. east of Palm Springs, CA. Excellent salary, fringe benefits, early partnership, no buy-in, and generous vacation time. All imaging modalities including SPECT ANGER camera, MRI, and angio/interventional. Reasonable housing in resort atmosphere. Contact Stephen J. Curtis, M.D., Radiology Director, J.F.K. Memorial Hospital, 47-111 Monroe St., Indio, CA 92201; (619) 775-8066. 4–7ap

DIAGNOSTIC RADIOLOGIST FOR TOP-5 CITY (MONEY MAGAZINE OCTOBER '91)—Progressive, well-established group of 9 board-certified radiologists has position immediately available for a recently trained BC diagnostic radiologist. Fellowship training preferred, but will consider qualified individual with special expertise in body imaging; angiographic experience is optional. Practice includes 2 tertiary hospitals (850 and 350 beds), private office, and 2 imaging centers. State-of-the art equipment includes 2 GE 1.5-T MRI units; ATL, Toshiba, and Acuson duplex color ultrasound; and 5 GE 9800 CT. High plains offer moderate climate, and surrounding area is ideal for outdoor interests, including skiing, hunting, boating, and fishing. Excellent compensation and benefits package leading to full partnership. Please reply with CV to Todd R. Samuels, M.D., Lubbock Radiology Associates, 3707 21st St., Lubbock, TX 79410. 5–8ap

DIAGNOSTIC RADIOLOGIST, TOLEDO, OH—Expanding 23-radiologist group seeks BC radiologist with 1 or more yrs fellowship experience. Interest/expertise in pediatric radiology, mammography, or nuclear medicine would be helpful. Position requires no special procedures and leads to equal partnership. Our group values quality of work as well as personal time and offers an excellent salary with very generous time off. Coverage includes 850-bed tertiary hospital, 350-bed suburban hospital, and 3 outpatient offices with more than 240,000 exams/yr. All modalities are represented. Excellent family-oriented community with great schools. Send CV to Drs. David Parker or Keith Wilson, Roemer Bldg., 3912 Sunforest Ct., Toledo, OH 43623; (419) 471-4438 days. 5–7ap

DIAGNOSTIC RADIOLOGIST needed for expanding practice in 200-bed, well-equipped community hospital in Troy, MI. Must have expertise in CT, ultrasound, and mammography. Very competitive salary and benefits. Send CV to Thomas Verhelle, M.D., Troy-Beaumont Hospital, 44201 Dequindre Rd., Troy, MI 48098. 4–7ap

ASSISTANT PROFESSOR, MR RADIOLOGIST—The Dept. of Radiology at The University of Texas Medical School at Houston and the Hermann Hospital are recruiting for a full-time MRI radiologist at the assistant professor level, beginning July 1, 1992. Preference will be given to candidates with fellowship training in MRI, body imaging, neuroradiology, or 1 yr of academic MRI experience. ABR certification is required. Responsibilities will include monitoring and interpretation of both body and neuro MRI, as well as medical student, resident, and fellow teaching. Extensive clinical and basic science research opportunities are available. The dept.'s MR facilities are state-of-the-art and located in a beautiful, spacious setting, which includes a 1.5-T GE Signa unit with proton spectroscopic capability. A second 1.5-T GE System, with MR angiography, fast spin echo (FSE), and phased array coils, will be installed in the first quarter of 1992. The dept. also has an active basic science research program; research facilities include a small bore MRI system with spectroscopy capabilities. The University of Texas at Houston is an equal opportunity employer. Women, minorities, and the disabled are encouraged to apply. Please send CV and 3 references to Bharat Raval, M.D., Professor and Interim Chairman, Dept. of Radiology, The University of Texas Medical School–Houston, 6431 Fannin, Suite 2.132, Houston, TX 77030. 2–7ap

FAIRBANKS, AK—Four diagnostic radiologists seek fifth partner for diversified practice including general radiology, ultrasound, nuclear medicine, MRI (GE 1.5-T), and CT (GE 9800). Hospital and office practice. Desirable lifestyle advantages in a university town. Unlimited access to the outdoors. Excellent salary, benefits, retirement, and vacation. One yr to full partnership. Contact Douglas Hutchinson, M.D., 1919 Lathrop #5, Fairbanks, AK 99701; (907) 452-5092. 2–7ap

DIRECTOR OF BREAST IMAGING—The Brigham and Women's Hospital/Harvard Medical School, Dept. of Radiology, is seeking a full-time diagnostic radiologist to head the Breast Imaging Section. This hospital-based facility has 4 mammographic rooms, 2 with ultrasound. In addition, there is a mammo-test unit for performance of large core breast biopsies. More than 12,000 mammograms, 1,000 preoperative wire localizations, 500 guided aspirations, and 150 core biopsies are performed annually. This wealth of clinical material coupled with an excellent clinical staff provides unlimited opportunity for collaborative clinical investigation. Candidates must have board certification. Please contact Jack E. Meyer, M.D., Director of Diagnostic Radiology, Brigham and Women's Hospital, 75 Francis St., Boston, MA 02115; (617) 732-6269. Brigham and Women's Hospital/Harvard Medical School is an affirmative action/equal opportunity educator and employer. 2–7a

NEURORADIOLOGIST—Senior ASNR member needed for excellent hospital and imaging center position in Tucson, AZ. Early partnership opportunity. Send CV to Arizona State Radiology, 7250 E. Ventana Canyon Dr., Tucson, AZ 85715. 8–7ap

THE DEPT. OF RADIOLOGY AT BROOKE ARMY MEDICAL CENTER, SAN ANTONIO, TX, is recruiting academic radiologists for several divisions of the dept., including ultrasound, chest, skeletal, neuroradiology, general diagnostic, interventional radiology, and mammography. Our dept. offers a fully accredited residency program with 24 residents and 16 attending full-time staff. Numerous consultants from across the country lecture on a continuing and regular basis. The hospital is a modern, tertiary-care center serving Texas, Oklahoma, and Louisiana. A strong residency program, interesting patient population, excellent equipment, teleradiology and digital radiology implementations underway, coupled with a south Texas lifestyle are positive aspects of the practice. Academic credentials and/or experience are necessary. Recently graduated fellows are encouraged to apply. Board certification is mandatory. Candidates should be particularly interested in patient care, teaching, and research. Salary and benefits are competitive and generous. Brooke is an EO/EEO employer. Please contact Dr. Billy E. Cunningham, COL, MC, Assistant Chief, Dept. of Radiology, Brooke Army Medical Center, Fort Sam Houston, TX 78234-6200; (512) 221-8418/8218. 8–7a

TWO DIAGNOSTIC RADIOLOGISTS, WASHINGTON—Prominent, 100-physician multispecialty clinic in Pacific Northwest seeks both a diagnostic radiologist and an interventional radiologist. Interventional radiologist should have fellowship training and/or extensive experience in interventional radiology. Diagnostic radiologist should have general radiology experience to include all full-scope imaging services. Guaranteed salary and partnership track available. Excellent benefit package. Abundant 4-season recreational opportunities. Send CV to Fred Bockenstedt, M.D., P. O. Box 489, Wenatchee, WA 98807. 5-10ap

THE RADIOLOGY DEPT. AT DWIGHT DAVID EISENHOWER ARMY MEDICAL CENTER is recruiting academic radiologists. The dept. provides a full range of services including angiography, ultrasound, CT (with a new GE 9800 Advantage system), and MRI (with a new 1.5-T GE Signa system). Development is underway for the installation of a digital teleradiology link to area medical facilities. The dept. is also beginning a radiology residency program in affiliation with the program at the Medical College of Georgia in Augusta. With this growth, the dept. has generated a need for several academic diagnostic radiologists. Board-certified diagnostic radiologists with academic credentials and/or experience are urged to apply. Fellowship training is desired, especially in interventional radiology and/or angiography, however candidates at all levels will be considered. Candidates should be particularly interested in patient care, teaching, and research. The medical center is located on Fort Gordon, GA, adjacent to Augusta, and is the tertiary-care hospital supporting 9 Army community hospitals of the southeastern region and Puerto Rico. The hospital supports fully accredited residency programs in family practice, general surgery, medicine, orthopedics, pathology, and psychiatry. Salary and benefits are competitive and generous. The medical center is an EO/EEO employer. Please contact Dr. Thomas M. Ralston, LtC., Chief, Radiology Dept., Eisenhower Army Medical Center, Fort Gordon, GA; (404) 791-6245. 8–7a

THE DEPT. OF RADIOLOGY AT WALTER REED ARMY MEDICAL CENTER is recruiting academic radiologists. We need board-certified radiologists to work in this famous and modern health-care center. Our dept. has a residency program consisting of 24 residents and several fellows. Subspecialists are needed in ultrasound, chest, mammography, genitourinary, gastrointestinal, pediatric, CT, MRI, and interventional radiology, as well as general radiology. Excellent opportunity to live in the nation's capital and also become an integral part of a large teaching program. Salaries are competitive and generous. Highly motivated applicants should contact Col. Mark F. Hansen, Radiology Consultant to the Army Surgeon General, Dept. of Radiology, TAMC, HI 96859-5000; (808) 433-6393. 8–7a

VETERANS AFFAIRS MEDICAL CENTER, AUGUSTA, GA, is seeking a physician board-certified/eligible in radiology. Subspecialty interest in chest, skeletal, GI or interventional radiology is desirable but not essential. This 1,142-bed tertiary-care medical center is affiliated with the Medical College of Georgia. Faculty appointment commensurate with qualifications and experience. Augusta enjoys a moderate climate, reasonable cost of living, numerous recreational facilities and institutions of higher learning. An equal opportunity employer. For additional information, contact George T. Jamarik, M.D. Chief, Radiology Service, at (404) 823-2236. 7a

RADIOLOGIST—Onslow Memorial Hospital is a 133-bed progressive non-profit hospital located in Jacksonville, North Carolina. We presently seek a full-time radiologist for our state-of-the-art dept. which includes SPECT nuclear medicine camera, CT scanner, 2 general rooms, 2 flouro rooms and .5-T MRI machine. Applicant must be capable of performing diagnostic interventional and angiographic radiology. Numerous beaches and recreational areas nearby. Interested individuals should forward a resume to Administrator, Onslow Memorial Hospital, P.O. Box 1358, Jacksonville, NC 28541. EOE M/F. 7a

SAN ANTONIO, TEXAS—Large group covering multiple hospitals and outpatient facilities seeks radiologists with angiography skills. Send CV to Search Committee, M&S X-Ray Associates, P.O. Box 15920, San Antonio, TX 78212-9510. 7-12ap

DIAGNOSTIC RADIOLOGIST—Board-certified radiologist with 1 yr neuro or MRI fellowship (or equivalent experience) to join 6-person hospital-based group in coastal Carolina city. Opportunity to pursue interest in spinal/neuro MRI in a highly desirable locale. Compensation competitive and negotiable. Send CV to AJR Box 70. (see address this section) 7ap

SOUTH CENTRAL FLORIDA—Immediate opening for board-certified (or eligible with intention to certify), Florida licensed general diagnostic radiologist. Four radiologists are now covering 3 hospitals totaling 250 beds as well as private diagnostic office with mammography. Onsite MRI at 1 hospital and mobile unit at another. Expertise in all modalities including interventional and angiography. Competitive package including early partnership. Send CV to Lawrence S. Ross, M.D., Radiology Consultants, P.A., 114 Medical Center, Sebring, FL 33870. 7xa

DIRECTOR OF IMAGING CENTER—The Dept. of Radiology at Graduate Hospital is looking for an experienced, board-certified radiologist to direct its imaging center. Fellowship training or extensive experience in body imaging is advantageous although not an absolute requirement, but experience in managing an outpatient imaging center is essential. The successful applicant will join a 13-physician radiology group in Center City Philadelphia at a tertiary-care hospital affiliated with the University of Pennsylvania. The 2-yr-old imaging center, located adjacent to the hospital and connected by a bridge, has state-of-the-art equipment including 2 GE 1.5-T MR scanners with phased array coils, endorectal MR, and MRA. Ultrasound includes color flow Doppler and there is an Elscint 2400 Elite CT scanner. Inquiries and CV's should be addressed to Jerome G. Jacobstein, M.D., Chairman, Dept. of Radiology, Graduate Hospital, One Graduate Plaza, Philadelphia, PA 19146, (215) 893-2050. 7ap

PEDIATRIC RADIOLOGIST—The University of California, Davis, School of Medicine has a full-time faculty position available in the Diagnostic Division of the Dept. of Radiology. Appointment will be at the assistant, associate, or full professor level. Candidates must be board-certified in diagnostic radiology, eligible for licensure in California, and have an academic background in pediatric radiology. Please forward a CV, a letter outlining background and interests in teaching/research, and the names and addresses of 5 references to Richard W. Katzberg, M.D., Chair, Dept. of Radiology, University of California, Davis, 2516 Stockton Boulevard, Ticon II, Sacramento, CA 95817. This position will be "Open Until Filled", but not later than October 31, 1992. The University of California is an equal opportunity/affirmative action employer and encourages applications from members of minority groups and women. 7a

CALIFORNIA, CENTRAL COAST (POP 60K)—BC radiologist sought for a small hospital with an active outpatient service. Routine radiology with mammography and ultrasound. Solo position. Relief coverage available. Generous salary. Full-time or 6-8 mo/yr. Write Box D44, AJR (see address this section). 7-8a

CHIEF, IMAGING SERVICE, VA MEDICAL CE TER, WASHINGTON, D.C—This tertiary-ca medical center has 590 operating beds and is af iated with Georgetown, George Washington, a Howard University Schools of Medicine. We a seeking a chief with strong clinical and administr tive skills. Board certification is required. The se vice consists of sections of diagnostic radiolo and nuclear medicine. A full range of services provided including general radiology, angiograph interventional radiology, ultrasound, computeriz axial tomography, and MRI. The candidate shou have teaching interests and would be expected qualify for an academic appointment at one of o affiliates. Please send CV's to L. Joseph Daghe M.D., Chief of Staff, VA Medical Center, 50 Irvi St., N.W., Washington, D.C. 20244. EOE. 7a

MEDICAL COLLEGE OF VIRGINIA - DEPAR MENT OF RADIOLOGY—Chief of section a section member, angiography/interventional radi ogy. An excellent opportunity is available for a d namic individual interested in building an o standing program already established on a stro foundation. Currently there are 2 full-time facu members in the section plus the services of ad tional faculty members equaling a third full-tir faculty equivalent. We are seeking to add anot fellowship-trained full-time junior faculty memb and a section chief to form a 5-faculty section charge of angiography/interventional radiology the Medical College of Virginia and its affiliat Hunter Holmes McGuire VA Medical Center. T gether the 2 institutions comprise 1,800-bed ABR certification or eligibility required. Individu should have experience working in a culturally verse environment. Academic rank and sala commensurate with experience. Anyone interest should send CV to or phone Anthony V. Pro M.D., Professor and Chairman, Dept. of Radiolo P.O. Box 470, Richmond, VA 23298-0470; (80 786-7212, fax (804) 371-6129. VCU/MCV is equal opportunity/affirmative action employ Women and minorities are encouraged to apply. 8a

FACULTY POSITION IN ABDOMINAL IMA ING—Dartmouth-Hitchcock Medical Center seeking a faculty member at the senior assista full professor level with experience and interest abdominal imaging. Clinical responsibility will be an entirely new 420-bed clinical facility opening Oct. 1991 with state-of-the-art instrumentatic Position will involve responsibility for residen training in GI/GU area. Proven record of acaden performance including research and teaching w an interest in providing academic guidance for e ergetic staff of younger radiologists. Interest candidates write with CV to Peter K. Spiegel, M. Chairman, Dept. of Diagnostic Radiology, Da mouth-Hitchcock Medical Center, Hanover, N 03756. AA/EOE. 7-9ap

CENTRAL NEW JERSEY, IMMEDIATE OPE ING—Radiologist with fellowship training or equ alent experience in vascular/interventional and in MR imaging to join 6-member group. Must willing to do other aspects of diagnostic radiolo mammography, ultrasound, CT, and nuclear me cine. Practice includes a 340-bed community h pital, a private radiology office, and an MRI facil Area is within a 10-mi. radius of Princeton and near New York City and Philadelphia. Competiti salary, excellent benefits, and partnership oppor nity. Send CV or call Margaret M. Beck, Busine Manager, 2127 Hamilton Ave., Trenton, NJ 086 (609) 587-9410. 7xa

WATERTOWN, NY—Two diagnostic radiologists wanted for full-time positions at military base in Upstate New York. Positions commence Oct. 1, 1992. Hours: Mon-Fri 7:30 am to 4:00 pm; No holidays; Rotating on-call. Must be BC/BE in diagnostic radiology, minimum 2-yrs experience. BLS required. Must have current license in any state. For further information contact Donna Troiano, National Emergency Services, 255 Executive Dr., Ste 204, Plainview, NY 11803; (800) 645-4848, (516) 349-0100. 7ap

THE DEPT. OF RADIOLOGY, VIRGINIA COMMONWEALTH UNIVERSITY/MEDICAL COLLEGE OF VIRGINIA, AND THE MCGUIRE VA MEDICAL CENTER, RICHMOND, VIRGINIA seek faculty for positions in diagnostic radiology (chest, GI, mammography, CT/US/MR, musculoskeletal, ER, angio/interventional, neuroradiology). MCV is a 1,058-bed facility and a level 1 trauma center. The McQuire VAMC is an 800-bed facility. ABR certification or eligibility required. Individual should have experience working in a culturally diverse environment. Academic rank and salary commensurate with experience. For position description, or to submit CV, write or phone A.V. Proto, M.D., Dept. of Radiology, MCV Box 470, Richmond VA, 23298-0470; (804) 786-7212. VCU/MCV is an equal opportunity/affirmative action employer. Women and minorities are encouraged to apply. 7-8a

MAMMOGRAPHER—Dartmouth-Hitchcock Medical Center is seeking radiologist to lead mammographic program with strong interest in new techniques and teaching. Dept. consists of 18 staff, 12 residents, 2 fellows, with a full range of modern radiologic practice. A new dept. in a new 420-bed medical center. Separate mammography section with state-of-the-art equipment. Opportunity exists to collaborate with Jack Wennberg in Outcomes Research. Seeking senior assistant, full professor level to be member of a 200-physician academic multispecialty group which forms the clinical faculty of Dartmouth Medical School. Write to Peter K. Spiegel, M.D. Chairman, Dept. of Diagnostic Radiology, Dartmouth-Hitchcock Medical Center, One Medical Center Dr., Lebanon, NH 03756. 7-9ap.

LIVE WHERE YOU CAN PLAY, THE SMOKY MOUNTAINS OF WESTERN NC—A 5-person group seeks a BC/BE diagnostic radiologist with experience in all modalities. Special interest in angio/interventional or nuclear medicine desired. Competitive salary leading to early full partnership. State-of-the-art equipment. Friendly, small-town atmosphere in 75,000+ population county. Plentiful amenities and diverse recreational activities in the immediate area. Moderate 4-season climate. Position available at this time, but would hold for suitable candidate. Send CV or call Dr. Ronald Liljedahl, Hendersonville Radiological Consultants, 807 N. Justice, Hendersonville, NC 28739; (704) 696-1045, work; (704) 697-6741, home. 6-9ap

Fellowships and Residencies

FELLOWSHIP IN IMAGING/ANGIO-INTERVENTIONAL—A 1-yr fellowship program at Lehigh Valley Hospital in Allentown, PA, is available. LVH is a 492-bed acute-care, university affiliated hospital. The fellowship program offers training in CT (head and body), ultrasound, MR, angiography, and interventional radiology. For further information contact Robert Kricun, M.D., Dept. of Radiology, Lehigh Valley Hospital, P.O. Box 689, Allentown, PA 18105-1556. 7-9c

FELLOWSHIP POSITIONS—The Dept. of Radiology and Radiological Sciences of Vanderbilt University School of Medicine is offering fellowship positions for 1993–94 in angiography, neuroradiology, chest, and pediatric radiology. Research opportunities are available and encouraged. Candidates must be board-certified or board-qualified in diagnostic radiology and must obtain a Tennessee medical license. Address inquiries and CV to Martin P. Sandler, M.D., Director, Fellowship Programs, Dept. of Radiology and Radiological Sciences, Vanderbilt University, Nashville, TN 37232-2675. An equal opportunity/affirmative action employer. 6–7c

FELLOWSHIPS AT THOMAS JEFFERSON UNIVERSITY HOSPITAL—The Dept. of Radiology at Thomas Jefferson University Hospital in Philadelphia offers the following fellowship programs each yr: (1) Ultrasound/CT/MRI—Jefferson's ultrasound division is one of the largest in the world and performs all currently available exams, including obstetric, vascular, lithotripsy, invasive, and endoluminal. We also operate 4 GE 1.5-T MRI units and 3 CT scanners. Contact Barry Goldberg, M.D., regarding this program. (2) Cardiovascular/interventional—This division is housed in a new suite containing Philips angio units with DSA and performs the full range of vascular and nonvascular interventional procedures. Contact Geoffrey Gardiner, Jr., M.D. (3) Neuro/ENT radiology—very active clinical services supply a wealth of material to this division, which is housed in a neurosciences imaging center containing all imaging modalities. Contact Carlos Gonzales, M.D. (4) Breast imaging—Jefferson's new breast-imaging center performs approximately 85 studies/day including ultrasound and needle localizations. Contact Stephen Feig, M.D. (5) Chest—includes biopsies and CT. Contact Robert Steiner, M.D. (6) MRI—a dedicated body MRI program including excellent research opportunities in addition to a large clinical case load. Contact Donald Mitchell, M.D. (7) Ultrasound—a dedicated ultrasound program. Contact Barry Goldberg, M.D. (8) Musculoskeletal—includes MRI of the musculoskeletal system. Contact David Karasick, M.D. All program directors listed above can be contacted at the Dept. of Radiology, Thomas Jefferson University Hospital, Philadelphia, PA 19107. Jefferson is an equal opportunity/affirmative action employer. 7xc

FELLOWSHIPS AT ALBANY MEDICAL CENTER—The newly-renovated and equipped Dept. of Radiology at the Albany Medical College and Center in Albany, NY, offers the following fellowship positions each yr: (1) Abdominal Imaging—This fellowship encompasses all aspects of MRI, ultrasound, CT, and other advanced techniques in imaging the abdomen. Four state-of-the-art MRI and 4 CT scanners as well as 5 color Doppler ultrasound units are utilized daily. Contact James C. Peters, M.D., regarding this program. (2) Neuroradiology—This fellowship encompasses the full range of advanced neuro imaging including MRI, CT, angiography, and myelography. Contact William A. Wagle, M.D. (3) Angiography and interventional radiology—Three advanced angiographic suites are utilized daily for a full range of vascular and interventional procedures. Contact Mohammad S. Sarrafizadeh, M.D. All program directors listed above may be contacted at the Dept. of Radiology, A-113, Albany Medical Center, Albany, NY 12208; (518) 445-3277 or contact Matthew D. Rifkin, M.D., Chairman, Dept. of Radiology, A-113, at the above address. Albany Medical Center is an equal opportunity/affirmative action employer. 1–12c

ONCORADIOLOGY/MAMMOGRAPHY FELLOWSHIP—The Dept. of Radiology at the Dana-Farber Cancer Institute and Brigham and Women's Hospital, which are Harvard Medical School affiliates, offers a 1-yr fellowship position beginning July 1, 1993. All imaging modalities involved in the diagnosis, staging, and follow-up of patients with malignant disease are integrated into this program. An additional feature is a concentrated experience in the performance of interventional breast diagnostic procedures. Please contact Jack E. Meyer, M.D., Director of Diagnostic Radiology, Brigham and Women's Hospital and Dana-Farber Cancer Institute, 75 Francis St., Boston, MA 02115; (617) 732-6269. Brigham and Women's Hospital/Dana Farber Cancer Institute/Harvard Medical School is an affirmative action/equal opportunity educator and employer. 5–4c

INTEGRATED CHEST RADIOLOGY FELLOWSHIP AT JOHNS HOPKINS UNIVERSITY HOSPITAL—The Dept. of Radiology, Division of Thoracic Imaging, Johns Hopkins University, is offering a 1- to 2-yr academically-oriented fellowship in chest radiology. The fellowship offers an integrated experience in cross-sectional imaging including more than 4,000 chest CT exams/yr and 1,000 thoracic MRI exams/yr. Strong research interests in high-resolution CT, MRI, and interventional thoracic radiology offer the potential candidate an exciting working environment. The fellowship is available starting July 1, 1993. Contact Janet E. Kuhlman, M.D., Director of Chest Radiology, Dept. of Radiology, Johns Hopkins Hospital, Baltimore, MD 21205; (410) 955-4419. 5–7cp

ADVANCED IMAGING FELLOWSHIP—The Dept. of Radiology and The Graduate Hospital Imaging Center are offering a 1-yr advanced imaging fellowship to include MR, CT and ultrasound. A position is available for July 1993. MR and CT imaging time will be spent performing both body and neuro studies. Facilities include 2 state-of-the-art GE 1.5-T MR scanners with phased array coils, endorectal MR and MRA. Ultrasound includes color flow Doppler. CTs include Elscint 2400 Elite and GE 9800. Candidates must have completed an approved 4-year residency prior to commencing the fellowship. Board-eligibility is a requirement. Salary will be at a PGY-5 level. Interested candidates should apply to Jerome G. Jacobstein, M.D., Chairman, Dept. of Radiology, The Graduate Hospital, One Graduate Plaza, Philadelphia, PA 19146; (215) 893-2050. 7-8cp

IMAGING (ULTRASOUND, BODY CT, AND MRI) FELLOWSHIP TO BEGIN JULY 1993—The Dept. of Radiology at The Western Pennsylvania Hospital (a 578-bed advanced, tertiary-care teaching hospital), Pittsburgh, PA, offers a 1-yr imaging fellowship. The fellowship emphasizes diagnostic ultrasound with rotations in body magnetic resonance imaging and computed body tomography. Examinations in all areas of sonography are performed and include obstetrics and gynecology, vascular/Doppler, abdominal, prostate, pediatrics, breast, and small parts. State-of-the-art equipment in all areas of the dept.Fellows will participate in procedures guided by ultrasound and computed tomography. Fellows have ample opportunity to participate in conference presentations and research projects, many of which culminate in publications. Inquiries should be addressed to Marcela Bohm-Velez, M.D., Director of Imaging Fellowship Program, Dept. of Radiology, The Western Pennsylvania Hospital, 4800 Friendship Ave., Pittsburgh, PA 15224. 5–12c

ACCREDITED FELLOWSHIPS IN PEDIATRIC RADIOLOGY AND PEDIATRIC NEURORADIOLOGY—Dept. of Radiology, Children's Hospital Medical Center, Cincinnati, OH, offers 1- or 2-yr accredited (Residency Review Committee for Radiology of ACGME) fellowships in pediatric radiology beginning July 1, 1994. A 1-yr pediatric neuroradiology fellowship program is also offered and may be taken separately or combined with 1 yr of adult neuroradiology fellowship at the University of Cincinnati Medical Center. Children's Hospital Medical Center (CHMC) is a 355-bed institution. The dept. performs over 105,000 radiological exams/yr in the largest children's hospital and ambulatory practice in the U.S. The dept. has 14 full-time faculty pediatric radiologists, 1 full-time research faculty, 7 fellows, and many resident trainees. Six pediatric radiology and 1 pediatric neuroradiology fellowship positions are available annually. Training includes all aspects of pediatric imaging neonatal radiology; neuroimaging; musculoskeletal radiology; cardiovascular and thoracic imaging; abdominal imaging; oncologic imaging; ultrasonography; nuclear medicine; computed tomography; MRI; and vascular/interventional procedures. The dept. has an active clinical service with state-of-the-art equipment as follows: digital fluoroscopy; Acuson and ATL ultrasound units with Doppler and color flow Doppler capabilities; planar SPECT gamma cameras; GE 9800 Quick CT scanner; 1.5-T GE MRI with spectroscopy, and cardiac catheterization/angiographic suite with digital vascular imaging. The fellowship provides a broad clinical experience in pediatric radiology as well as numerous opportunities to participate in both clinical and basic research. Candidates must be board-certified or board-qualified in diagnostic radiology and must obtain an Ohio medical license. Salary and fringe benefits are highly competitive. Applications are due prior to February 1993 with interviews scheduled during the fall and winter of 1992-93. There are numerous career opportunities in pediatric radiology and pediatric neuroradiology in both academic and private practice settings. To receive more information about the fellowships at CHMC or careers in pediatric radiology, please contact Director, Dept. of Radiology, Children's Hospital Medical Center, Cincinnati, OH 45229-2899; (513) 559-8058. Children's Hospital Medical Center and the University of Cincinnati College of Medicine are affirmative action/equal opportunity employers. 7-1cp

PEDIATRIC RADIOLOGY FELLOWSHIP—The Vanderbilt University Children's Hospital offers a 1-yr fellowship, with an option for a second yr, in pediatric radiology beginning July 1, 1992. This is a 210-bed facility with a staff with strong clinical and academic interests. It is both a primary care center and a tertiary referral facility; it is the only pediatric hospital in middle Tennessee with a catchment area extending into southern Kentucky. Training includes conventional radiography, digital fluoroscopy, computerized tomography, MRI, and all aspects of pediatric sonography. Flexible opportunities to participate in either clinical or basic research will be available. The Dept. of Radiology presently has 3 CT scanners, 3 MRI units, and a PET facility. Candidates must be board-certified or board-eligible in diagnostic radiology and must obtain a Tennessee medical license. Address all correspondence to Dr. Richard M. Heller, Dept. of Radiology, Medical Center North, Vanderbilt University Medical Center, Nashville, TN 37232-2675. An equal opportunity/affirmative action employer. 6–7c

FELLOWSHIP IN NEURORADIOLOGY—One fellowship position in neuroradiology is available July 1, 1993, in the Dept. of Radiology at New England Medical Center Hospitals, Boston, MA. The hospital is the teaching unit of Tufts University School of Medicine. The program is for 1 or 2 yrs and includes both adult and pediatric case material. The fellowship is accredited by the Accreditation Council for Graduate Medical Education. The fellow will be trained in the technique and interpretation of carotid and vertebral angiography as well as myelography. Computed tomography and MRI of the head and spine form major components of the neuroradiology service, as does interventional neuroradiology. Neuroradiological services at the New England Medical Center Hospitals are carried out in liaison with the Depts. of Neurology, Neurosurgery, and Pediatric Neurology. Joint radiological and clinical conferences are held frequently and, within a short time, the applicants will have considerable exposure to an array of neuroradiological material. The Dept. of Neuropathology also runs conferences, allowing correlation to be made between radiological interpretation and pathology. Interested applicants should call (617) 956-6333, or write to Samuel M. Wolpert, M.D., Professor of Radiology & Neurology, Director, Neuroradiology Fellowship Program, Dept. of Radiology, 750 Washington St., Boston, MA 02111. 7-8cp

FELLOWSHIP POSITIONS—The Dept. of Radiology of the Brigham and Women's Hospital-Harvard Medical School has 1- or 2-yr fellowship positions in the following areas: (1) cardiovascular and interventional, (2) neuroradiology, (3) CT/ultrasound/MR/interventional, (4) oncoradiology, (5) chest, (6) bone, (7) nuclear medicine, and (8) computer science. For more information, please send CV specifying your area of interest to B. Leonard Holman, M.D., Chairman, Dept. of Radiology, Brigham and Women's Hospital, 75 Francis St., Boston, MA 02115. Harvard Medical School and Brigham and Women's Hospital are equal opportunity, affirmative action employers. 5–4c

FELLOWSHIP PROGRAM IN INTERVENTIONAL RADIOLOGY—The fellowship offered is a 1-yr training program in interventional radiology. A high volume of studies provides excellent experience for the fellowship training program. The 1-yr appointment is intensive, supervised, and allows for graded responsibility in performance and interpretation of studies including angioplasty, atherectomy, arterial and biliary stents, and all drainage procedures. The fellowship training involves performance of interventional procedures under sonographic and CT guidance as well as fluoroscopy. Inquiries should be addressed to Gordon K. McLean, M.D., Director, Interventional Radiology, The Western Pennsylvania Hospital, 4800 Friendship Ave., Pittsburgh, PA 15224. 5–12c

MRI FELLOWSHIP—One-yr position is available in 1993 for fellow in MRI. The fellowship encompasses all phases of MR (musculoskeletal, body and neuro) as well as magnetic resonance angiography (including phase contrast, time-of-flight and magnitude phase contrast MRA). Over 12,000 MRIs are performed and interpreted annually as a part of this fellowship with direct one-on-one supervision. The fellowship also includes 20-30% CT; additionally, the option to obtain independent, full American Board of Nuclear Medicine certification is available. MR studies are divided between approximately 45% neuro and 55% body and musculoskeletal, including all joints and body parts. For further information contact Stephen J. Pomeranz, M.D., at (513) 281-3400, and ask for Chris or Jill. 7-9cp

VASCULAR/INTERVENTIONAL RADIOLO FELLOWSHIP—Temple University Hospital a School of Medicine has available a 1-yr fellows beginning July 1, 1992. The candidate will have posure to all areas of vascular and interventic radiology including noninvasive techniques a MRI/A. Applicants should contact, David S. E D.O., Chief, Section of Vascular/Interventional I diology, Dept. of Diagnostic Imaging, Temple U versity Hospital, 3401 N. Broad Stre Philadelphia, PA 19140. Temple University Hos tal and School of Medicine is an affirmative acti equal opportunity employer. 7-9c

FELLOWSHIP POSITION: WOMEN'S IMA ING—High-volume breast imaging (mammog phy, breast ultrasound, interventional procedur and ultrasound with emphasis on obstetrical a gynecologic sonography. State-of-the-art mamr graphic and sonographic equipment including s eotactic table and digital capability. Using s eotactic, ultrasound, or mammographic guidar all breast interventional procedures are perform including fine needle and core biopsies, cyst a rations, presurgical localizations, and galactog phy. Elective time in MRI, CT, and related clin specialties (surgery, pathology, obstetrics-gyne ogy). One-year fellowship to start in July 1993. F lows also have the opportunity to participate teaching, conference presentations, and resea projects, many of which culminate in publicatic Inquiries should be addressed to Ellen B. Menc son, M.D., Chief, Mammography and Women's aging, The Western Pennsylvania Hospital, 4 Friendship Ave., Pittsburgh, PA 15224. 5–12c

Tutorials/Courses

KONA, HAWAII 1992—Seventeenth Annual In national Body Imaging Congress, Oct. 10– CME 1. Mauni Lani Bay Hotel. Contact Med Seminars International, Inc., 18981 Ventura Bl Ste. 303, Tarzana, CA 91356; (818) 774-9077, (818) 774-0244. 5–10d

MUSCULOSKELETAL MRI, SECOND ANNU LOS ANGELES CONFERENCE, SEPT. 19– 1992—Faculty: Drs. Bradley, Brant-Zawadzki, etrich, Friedman, Harms, Resnick, Schlesin Medical Seminars International, Inc., 18981 Ve ra Blvd., #303, Tarzana, CA 91356; (818) 7 9077, fax (818) 774-0244. 4–9d

New Business Office for AJR

All inquires and correspondence regarding classified ads should be sent to:

AJR Classifieds
1891 Preston White Drive
Reston, VA 22091
Attn: Terry Fitterer
Phone: (703) 648-8992
FAX: (703) 264-8863

Final No.

Call for Scientific Papers

Date Received

Tracking No.

American Roentgen Ray Society
1993 Annual Meeting
April 25 – 30, 1993
San Francisco, CA

ADDRESS OF PRESENTING AUTHOR

Department

Institution

Street

City State Zip

Phone

Type title, authors, and abstract in the space provided below. (Instructions are on reverse side of this page. Abstract should not exceed 300 word

Select one category: ❑ Angio/Interventional ❑ Breast ❑ Sonography ❑ CT ❑ Gastrointestinal Tract ❑ Genitourinary Tract ❑ Neuroradiology ❑ Skeletal ❑ Chest ❑ MR ❑ Pediatrics ❑ Medical Physics

Projection Requirements: ❑ 35mm– single or double (circle one) ❑ 16mm silent film ❑ VHS (½") ❑ VHS (¾")

Has this been presented elsewhere? ❑ Yes ❑ No If yes, where? _____

Instructions for Scientific Paper Abstracts

1. Type information single-spaced. Underline the name of the presenting author. Append as a last line of the abstract any research grant support, if applicable (e.g. Supported by USPHS Grant HE-80144). If the abstract is accepted, it will appear in the program book exactly as typed. Use the following format:

MR IMAGING OF THE SPINE AND NECK
F.S. Lau, M.D., A.N. Kirk, M.D., R.A. Beck, Ph.D.
University of California, Bakersfield, Bakersfield, CA 92338

2. Abstracts should include four paragraphs devoted sequentially to the following topics: (1) object or purpose of the study; (2) materials, methods and procedures; (3) results; and (4) significance of the results and conclusions. The text should not exceed 300 words. Specific data are essential. The abstract should be a succinct summary of work done rather than a promissory note.

3. The Scientific Program Committee will grade each abstract and determine acceptance. Letters indicating acceptance or rejection will be mailed to all applicants in mid-January, together with meeting registration information.

Deadline for submission of abstracts is November 1, 1992. Mail **one** copy of abstract to

ARRS President-Elect
c/o Susan Roberts, Projects Manager
American Roentgen Ray Society
1891 Preston White Drive
Reston, VA 22091

Although mail submission is preferable, abstracts will be accepted by fax at (703) 264-8863. When faxing an application, **do not** mail a confirmation copy, as this results in unnecessary duplication of paper work.

Call for Scientific Exhibits

Final No.	
Date Received	Tracking No.

American Roentgen Ray Society
1993 Annual Meeting
April 25 – 30, 1993
San Francisco, CA

ADDRESS OF PRESENTING AUTHOR

Department

Institution

Street

City State Zip

Phone

Type title, authors, and abstract in the space provided below. (Instructions are on reverse side of this page.)

Select one category: ❑ Cardiovascular ❑ Breast ❑ Sonography ❑ Gastrointestinal ❑ Genitourinary ❑ Chest ❑ Neuroradiology ❑ Bone ❑ Pediatric ❑ Nuclear medicine ❑ Medical physics

What Type of Exhibit is Proposed? (Check one and fill in all appropriate blanks.)

_____ **Free-standing.** This is a self-contained display created in total by the exhibitor. It may be a fold-open unit, a unit shipped in cases and assembled on site, or a tabletop unit. Standard free-standing space is 10' x 10'. Indicate linear feet required_____.

_____ **Poster Board (Backboard panels).** Backboard panels are 4 x 8 ft. (1.2 x 2.5m). Number of panels required _____. If two panels are needed, there will be a ¼-in. frame separating the panels, thus requiring a separation in the presentation.

_____ **Viewbox.** Mounted materials (radiographs and other transparencies) for display on the society's illuminators. Each illuminator is 39.5 x 59.5 in. (100 x 151 cm). Number of illuminators required _____. Materials should not be glass mounted.

Instructions for Scientific Exhibit Abstracts

1. Type information single-spaced. Underline the name of the presenting author. Append as a last line of the abstract any research grant support, if applicable (e.g. Supported by USPHS Grant HE-80144). If the abstract is accepted, it will appear in the program book exactly as typed. Use the following format:

    MR IMAGING OF THE SPINE AND NECK
    F.S. Lau, M.D., A.N. Kirk, M.D., R.A. Beck, Ph.D.
    University of California, Bakersfield, Bakersfield, CA 92338

2. The abstract should be a brief paragraph that states the purpose, principal information and conclusions of the exhibit. Promissory statements are not acceptable. Brevity is desirable but not at the expense of specific information. Exhibits will be chosen on the basis of the quality of the abstract and exhibit space available. Poster board exhibits are encouraged as they do not require a viewbox or electricity.

3. The Scientific Exhibits Committee will grade each abstract and determine acceptance. Letters indicating acceptance or rejection will be mailed to all applicants in mid-January, together with meeting registration information. Exhibitors will receive instructions for exhibit preparation.

Deadline for submission of abstracts is November 1, 1992. Mail **one** copy of abstract to

N. Reed Dunnick, M.D.
Chairman, Scientific Exhibits Committee
c/o Susan Roberts, Projects Manager
American Roentgen Ray Society
1891 Preston White Drive
Reston, VA 22091

Although mail submission is preferable, abstracts will be accepted by fax at 703-264-8863. When faxing an application, **do not** mail a confirmation copy, as this results in unnecessary duplication of paper work.

Announcing

The American Roentgen Ray Society

1992 Categorical Course on Neuroradiology

ARRS

Neuroradiology

Categorical Course Syllabus

Editor:
Michael S. Huckman, M.D.
Co-Editors:
Derek C. Harwood-Nash, M.B., Ch.B.
Glenn S. Forbes, M.D.

Topics include:

Imaging of Complications of AIDS
Sonography in Neuroradiology
Lesions of the Skin and Brain
Brain Tumors
Back Pain in Children
Meninges in the Head and Spine
Evaluation of the Seizure Patient
Supratentorial Brain Neoplasms

To order call 1-800-227-7762 • Price $50 per book

Volume 159 American Journal of Roentgenology July 1992

FELIX FLEISCHNER LECTURE

1 **Imaging the respiratory system in the first few years after discovery of the X-ray: contributions of Francis H. Williams, M.D.** *Greene R*

MALLINCKRODT SYMPOSIUM

9 **The Edward Mallinckrodt Institute of Radiology 60th anniversary rededication program.** *Murphy WA Jr*
11 **Government and radiology during the next 60 years.** *Evens RG*
15 **Research at the Mallinckrodt Institute of Radiology: a strategic plan for the 1990s.** *Vannier MW*
18 **Radiology ethics.** *Armstrong JD II*
21 **The hidden curriculum.** *Anderson DJ*

SPECIAL ARTICLE

23 **Perspective. Radiologic evaluation of a Renaissance painting.** *Robbins AH, Wetzner SM, Marini M*

CARDIOPULMONARY RADIOLOGY

29 **Value of sonography in determining the nature of pleural effusion: analysis of 320 cases.** *Yang P-C, Luh K-T, Chang D-B, Wu H-D, Yu C-J, Kuo S-H*
35 **Case report. Lung torsion after percutaneous needle biopsy of lung.** *Graham RJ, Heyd RL, Raval VA, Barrett TF*
39 **Pleuropulmonary paragonimiasis: radiologic findings in 71 patients.** *Im J-G, Whang HY, Kim WS, Han MC, Shim Y-S, Cho S-Y*
45 **Pictorial essay. CT evaluation of poststernotomy complications.** *Templeton PA, Fishman EK*

BREAST RADIOLOGY

51 **Case report. Mammographic appearance of loiasis.** *Britton CA, Sumkin J, Math M, Williams S*

GASTROINTESTINAL RADIOLOGY

53 **Epithelioid hemangioendothelioma of the liver: imaging findings with pathologic correlation.** *Miller WJ, Dodd GD III, Federle MP, Baron RL*
59 **Case report. Hereditary hemorrhagic telangiectasia: findings in the liver with color Doppler sonography.** *Ralls PW, Johnson MB, Radin DR, Lee KP, Boswell WD*
63 **Case report. Langerhans cell histiocytosis of the liver: imaging findings.** *Radin DR*
65 **Pictorial essay. Operative cholangiography in patients undergoing laparoscopic cholecystectomy: unique radiographic findings.** *Balachandran S, Goodman P, Saydjari R, Hogge MW, Leonard MH Jr*
69 **Pictorial essay. Mucocele of the appendix: imaging findings.** *Madwed D, Mindelzun R, Jeffrey RB Jr*
73 **Case report. Bowel ischemia and perforation after cocaine use.** *Endress C, Gray DGK, Wollschlaeger G*

GENITOURINARY RADIOLOGY

77 **Calcified renal stones and cyst calcifications in autosomal dominant polycystic kidney disease: clinical and CT study in 84 patients.** *Levine E, Grantham JJ*
83 **Diagnosis of placenta previa during the third trimester: role of transperineal sonography.** *Hertzberg BS, Bowie JD, Carroll BA, Kliewer MA, Weber TM*
89 **Ovarian cysts are common in premenarchal girls: a sonographic study of 101 children 2–12 years old.** *Cohen HL, Eisenberg P, Mandel F, Haller JO*
93 **Case report. Prolapsing inverted papilloma of the prostatic urethra: diagnosis by transrectal sonography.** *Occhipinti K, Kutcher R, Gentile RL*

MUSCULOSKELETAL RADIOLOGY

95 **Pictorial essay. Diseases of the lumbar spine: findings on fat-suppression MR imaging.** *Tien RD, Olson EM, Zee CS*
101 **Case report. Ewing's sarcoma of the hand.** *Escobedo EM, Bjorkengren AG, Moore SG*

VASCULAR RADIOLOGY

103 **Three-dimensional time-of-flight MR angiography with a surface coil: evaluation in 12 subjects.** *Hendrix LE, Strandt JA, Daniels DL, et al.*
107 **MR imaging of symptomatic peripheral vascular malformations.** *Rak KM, Yakes WF, Ray RL, et al.*
113 **Budd-Chiari syndrome: detection with color Doppler sonography.** *Ralls PW, Johnson MB, Radin DR, Boswell WD Jr, Lee KP, Halls JM*
117 **Extrinsic compression of the superficial femoral artery at the adductor canal: evaluation with intravascular sonography.** *The SHK, Wilson RA, Gussenhoven EJ, et al.*
121 **Insertion of Hickman central venous catheters by using angiographic techniques in patients with hematologic disorders.** *Cockburn JF, Eynon CA, Virji N, Jackson JE*
125 **Case report. Atherectomy of the distal aorta using a "kissing-balloon" technique for the treatment of blue toe syndrome.** *Clugston RA, Eisenhauer AC, Matthews RV*
129 **Technical note. Wallstent misplaced during transjugular placement of an intrahepatic portosystemic shunt: retrieval with a loop snare.** *Sanchez RB, Roberts AC, Valji K, Lengle S, Bookstein JJ*

INTERVENTIONAL RADIOLOGY

131 **Occult glove perforations: frequency during interventional radiologic procedures.** *Hansen ME, McIntire DD, Miller GL III*

NEURORADIOLOGY

137 **Review. CNS complications of cocaine abuse: prevalence, pathophysiology, and neuroradiology.** *Brown E, Prager J, Lee H-Y, Ramsey RG*
149 **Review. MR imaging of the spinal cord: current status and future advances.** *Sze G*
161 **Review. MR imaging in the management of extracranial malignant tumors of the head and neck.** *Hudgins PA, Gussack GS*
171 **Evolution of white matter lesions in neurofibromatosis type 1: MR findings.** *Sevick RJ, Barkovich AJ, Edwards MSB, Koch T, Berg B, Lempert T*
177 **Cerebellar and cerebral abnormalities in Rett syndrome: a quantitative MR analysis.** *Murakami JW, Courchesne E, Haas RH, Press GA, Yeung-Courchesne R*
185 **High-signal foci on MR images of the brain: observer variability in their quantification.** *Yetkin FZ, Haughton VM, Fischer ME, et al.*
189 **Case report. Iatrogenic air in the cavernous sinus.** *Adams M, Quint DJ, Eldevik OP*
191 **Perspective. Current role of cerebral angiography in the diagnosis of cerebrovascular diseases.** *Wolpert SM, Caplan LR*

COMPUTERS IN RADIOLOGY

199 **A PACS-based interactive teaching module for radiologic sciences.** *Sinha S, Sinha U, Kangarloo H, Huang HK*

MEMO TO AUTHORS

207 **The composition of abstracts for *AJR* articles.** *Berk RN*

MEETING NEWS

209 **Meeting news. The Society of Gastrointestinal Radiologists: 21st annual meeting, February 1992.** *Whalen E*

OTHER CONTENT

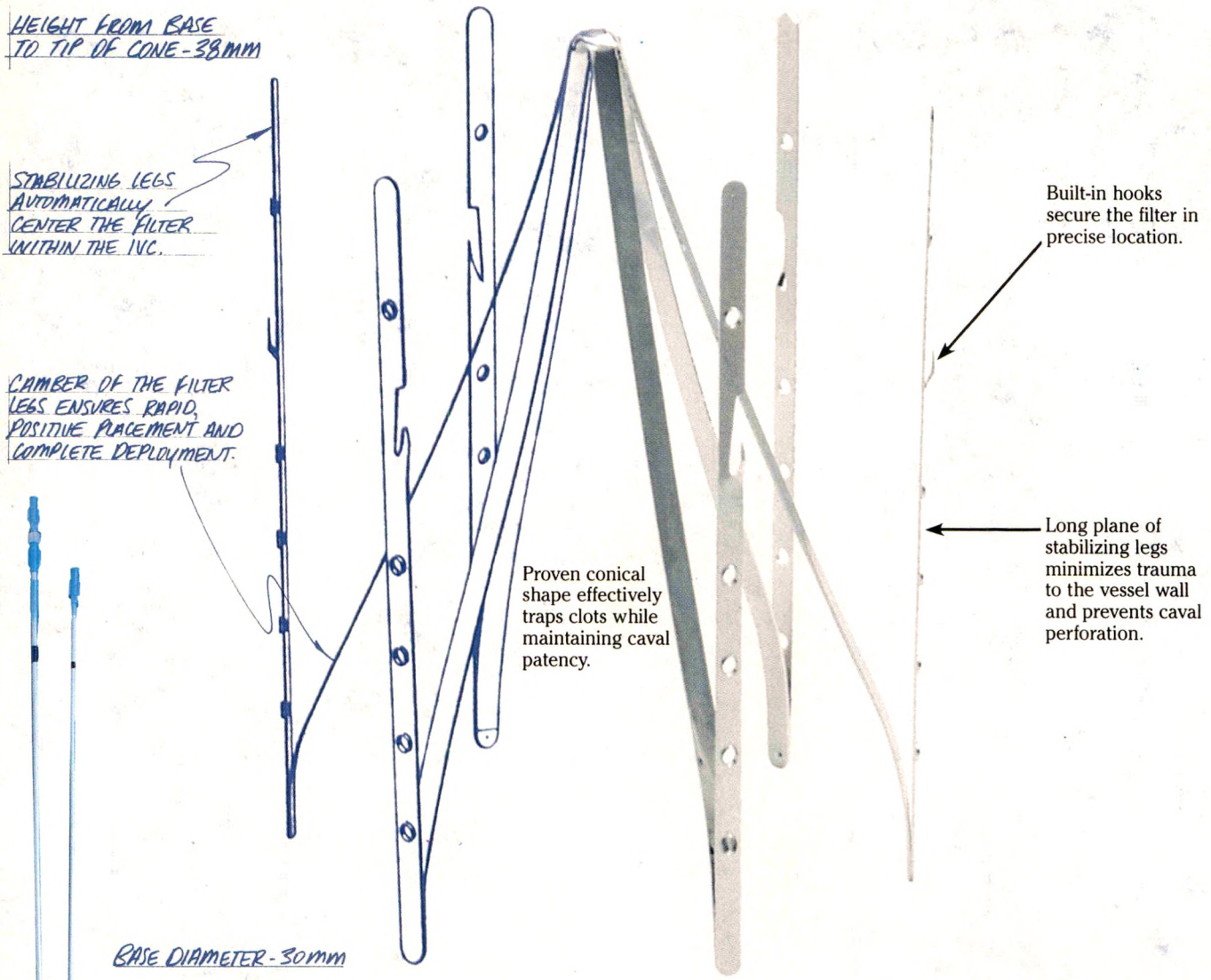
38 **Medicine in American art**
58 **Radiologic-pathologic conference**
62 **Figley Fellowship announcement**
112 **ARRS 1993 residents' award papers information**
127 **List of book and videotape reviews**
170 **Books and videotapes received**
184 **American Roentgen Ray Society information**
198 **Memorial. Edwin F. Gray**
206 **Forthcoming articles**
217 **Letters**
229 **Review of current literature**
234 **News**
237 **1993 ARRS meeting information**
238 **Classified advertisements**
Call for papers and exhibits for 1993 ARRS meeting
A6 **Guidelines for authors**
A14 ***AJR* business and subscriber information**

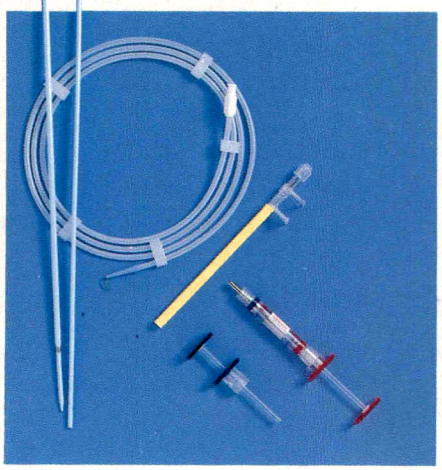
AJR

American
Journal of
Roentgenology

August 1992

The IVC filter designed the way you'd want it to be.





A flexible introducer facilitates the insertion procedure.

Finally, there's an IVC filter that does just what it's supposed to do.

Prevent recurrent pulmonary embolism. Maintain caval patency. And minimize procedural complications.

The Vena Tech™-LGM™ filter does it all because it's designed for success, with a proven-effective conical shape and longer stabilizing legs that ensure complete deployment. Best of all, the filter is deployed through a 10-French (ID) introducer. . . giving you and your patient a safer, easier insertion procedure.

The Vena Tech-LGM filter comes with everything you need for filter placement. And, with our unique 30D system, it can be placed from either the jugular or femoral approach.

See for yourself how easy it is. In just under ten minutes, our free video will show you how easy it is to place the Vena Tech-LGM filter. After you've seen it, you'll understand why we say the Vena Tech-LGM filter is the perfect fit—for both patient and physician.

So call 1-800-443-VENA today to receive your free video on the Vena Tech-LGM—the IVC filter that's designed for success.

B. Braun Vena Tech
1840 Oak Ave.
Evanston, IL 60201
(800) 443-VENA or (708) 866-1833
B.Braun of America Company

B.BRAUN

Official Journal of the American Roentgen Ray Society

AJR

American Journal of Roentgenology
Diagnostic Imaging and Related Sciences

Editor-In-Chief Robert N. Berk, *La Jolla, California*
University of California, San Diego
School of Medicine and Medical Center

Editor Emeritus Melvin M. Figley, *Seattle, Washington*

Associate Editor Karim Valji, *San Diego, California*

Consulting Editors A. James Barkovich, *San Francisco, California*
Edward A. Sickles, *San Francisco, California*

Statistician Charles C. Berry, *San Diego, California*

Editorial Board

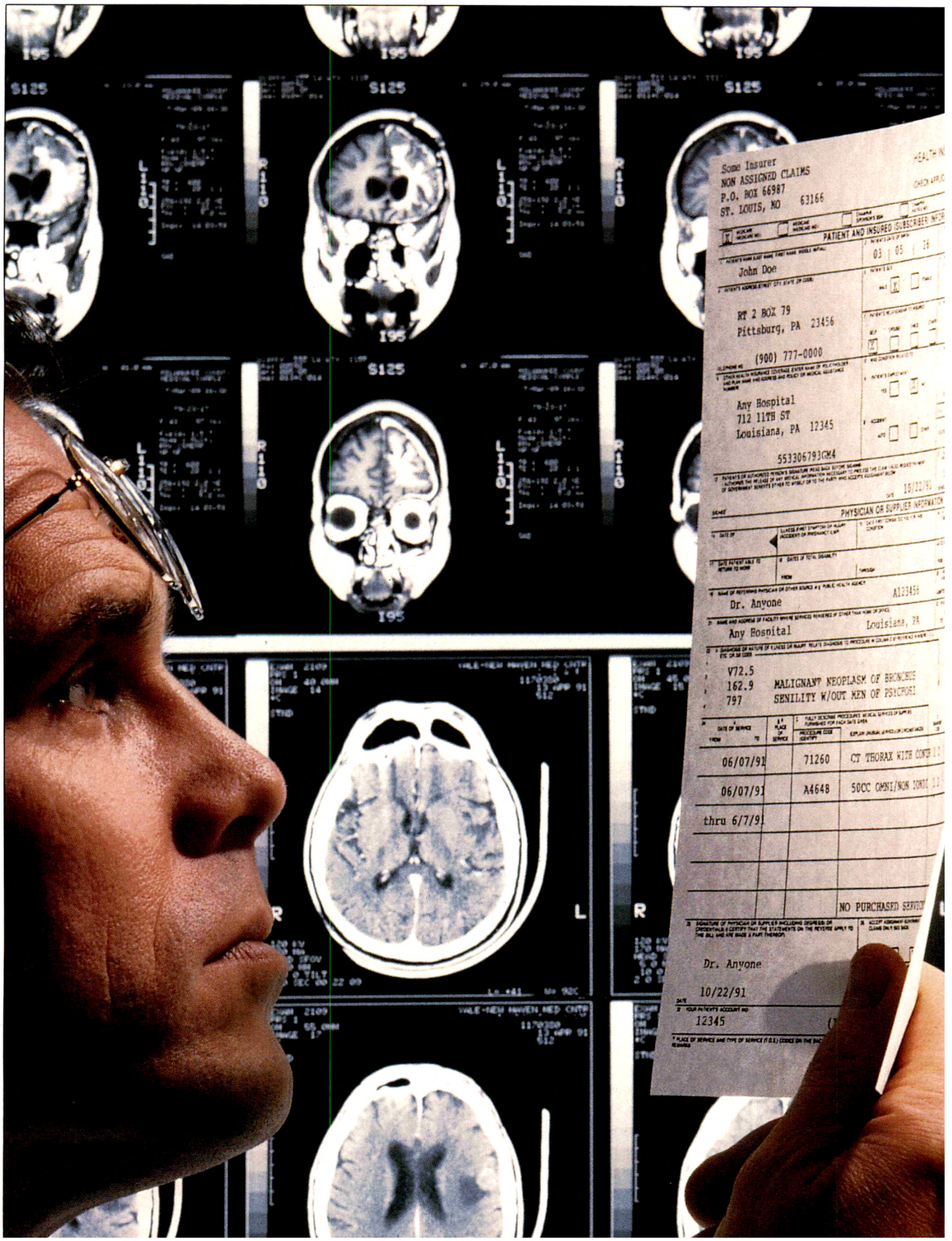
Mark E. Baker
Lawrence W. Bassett
Michael A. Bettmann
Ethan M. Braunstein
Felix S. Chew
Horacio R. D'Agostino
N. Reed Dunnick
David K. Edwards
Ronald G. Evens
Sandra K. Fernbach
Richard H. Gold
Edward G. Grant
John R. Hesselink
Emanuel Kanal
Ray F. Kilcoyne
Carolyn Kimme-Smith
Melvyn T. Korobkin
Mark J. Kransdorf
Faye C. Laing
Thomas L. Lawson
Robert G. Levitt
Martin J. Lipton
Bruce L. McClennan
Richard P. Moser
Jeffrey H. Newhouse
Sven J. K. Paulin
David M. Paushter
Vassilios Raptopoulos
Donald L. Resnick
Charles A. Rohrmann, Jr.
Peter M. Ronai
Stuart S. Sagel
Sanjay Saini
Stefan C. Schatzki
William P. Shuman
Edward A. Sickles
Barry A. Siegel
M. Leon Skolnick
Edward T. Stewart
Murali Sundaram
Robert D. Tien

Director of Publications: Susan Brown Cappitelli **Editorial Staff:** Barbara Rose, *managing editor*; Katie L. Spiller, Barbara L. Halliburton, and Janine Anderson, *manuscript editors*; Nancy Rydbeck, *office manager*; Sheri Smith, *administrative assistant*; Linda J. Waggoner, *administrative secretary*

AJR, AMERICAN JOURNAL OF ROENTGENOLOGY (ISSN 0361 803X) is published monthly by the American Roentgen Ray Society, 1891 Preston White Dr., Reston, VA 22091. Annual dues include $50 for journal subscription. Second-class postage paid at Baltimore, MD, and at additional mailing offices. **POSTMASTER**, send address changes (Form 3579) to Subscription Fulfillment, AJR, 428 E. Preston St., Baltimore, MD 21202. Subscription rates $125 ($180 foreign); institutions $135 ($190 foreign); in training $25 ($80 foreign); single copy $18 ($22 foreign). The GST number for Canadian subscribers is 123394371. Airmail rates furnished on request. Indexed by *Current Contents* and *Index Medicus*. Copyright © 1992 by American Roentgen Ray Society.
0361–803X/92$3.00

THE *OMNI*℠ REIMBURSEMEN

C L E A R I N



INFORMATION PROGRAM

T H E W A Y

Because you have more important things to read.

The *OMNI*℠ Reimbursement Information Program is dedicated to helping you obtain maximum reimbursement with minimal investment of your valuable time. Sponsored by the leader in nonionic contrast media support, the *OMNI* range of services includes:

1-800-767-*OMNI* Reimbursement Hot Line
for informed answers on claim submissions and expert guidance on resubmissions and appeals.

Policy Update Bulletins
on up-to-the-minute changes that affect your billings.

Payer Advocacy Efforts
that urge insurers to maintain competitive levels of payment and service.

Special Programs
for more in-depth analysis at your facility are also available.

Enroll your facility today.
Because insurers' policies are ever changing, timely information is the key to maximum payment. We're here to help. So call the *OMNI* Reimbursement Hot Line — 1-800-767-6664 — to enroll your facility. It could be the most rewarding decision you make today.

sanofi WINTHROP

LEADERSHIP IN NONIONIC CONTRAST MEDIA *REIMBURSEMENT*

© 1992 Sanofi Winthrop Pharmaceuticals
66-1212D

AJR Business and Subscriber Information

The American Roentgen Ray Society

AJR, American Journal of Roentgenology, is published monthly to disseminate research on current developments in the radiologic sciences and commentary on topics related to radiology. It is published by the American Roentgen Ray Society (ARRS), 1891 Preston White Dr., Reston, VA 22091; (703) 648-8992. Address inquiries regarding Society business, the annual ARRS meeting, and membership to the Society to the above address.

Correspondence regarding editorial matters should be addressed to Editorial Office, AJR, 2223 Avenida de la Playa, Ste.103, La Jolla, CA 92037-3218; telephone 1-800-348-4257 or (619) 459-2229; FAX (619) 459-8814. For information on manuscript submission, see Guidelines for Authors.

Subscriber Information

ARRS annual dues include $50 for journal subscription. Nonmember subscription rates are as follows: $125/year ($180 foreign); institutions, $135 ($190 foreign); in-training, $25 ($80 foreign). Single copies of the Journal may be purchased for $18 ($22 foreign). Airmail rates will be furnished on request. The GST number for Canadian subscribers is 123394371.

Call toll-free, 1-800-638-6423 (in Maryland call 1-800-638-4007), with subscription inquires or problems. Please have the mailing label from your latest issue available when you call.

Report changes of address to Subscription Fulfillment, AJR, 428 E. Preston St., Baltimore, MD 21202. Damaged or unreceived issues must be reported within 60 days of publication (90 days for foreign subscribers) for replacement.

Advertising Information

All advertising is subject to approval by the publisher. Acceptance of advertising does not indicate endorsement of the products or services advertised or the claims made. For display advertising information, contact Gary Walchli, National Sales Representative, AJR, 428 E. Preston St., Baltimore, MD 21202, (410) 528-4291.

For classified advertising information, contact the Publications Department, ARRS, Attn: Terry Fitterer, 1891 Preston White Dr., Reston, VA 22091; telephone (703) 648-8992; FAX (703) 264-8863.

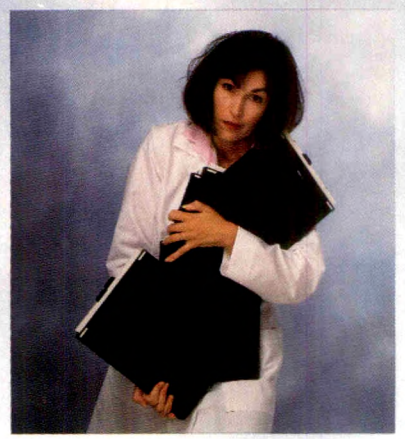
Copyrights, Permissions, and Reprints

Contents of the *AJR* are copyrighted by the ARRS. No part of this publication may be reproduced without permission. Requests for such permission should be addressed to the Publications Department, ARRS, Attn: Terry Fitterer, 1891 Preston White Dr., Reston, VA 22091. For reprints of a particular article, please contact the author designated in the footnotes for that article.

Indexes

The *AJR* provides volume and yearly indexes (subject and author) in the June and December issues. *AJR* articles are also indexed in *Current Contents*, *Index Medicus*, and the cumulative index published by *Radiology*.

There are a handful of reasons you should use the 3M Digital Imager System.



This is just one.



Now you have a choice of how to store 80 ultrasound images.

On the one hand … or in both hands … you've got five film cassettes.

On the other hand … or between index finger and thumb… you have the compact 3M Digital Imager Disk. And that leaves plenty of fingers for counting the benefits of the 3M Digital Imager System.

It's easy to use. You don't have to lug around film cassettes or load and unload them in the darkroom. You can store and review up to 80 diagnostic images on a single disk, play them back, edit them, and print on film only the images you need.

With the 3M Digital Imager System you can print up to 99 originals at the touch of a button. No more costly duplication. No more sacrificing resolution with second generation copies.

The highest resolution on the market. Built-in reliability. Professional support.

A handful of benefits instead of a handful of cassettes.

That's the advantage of the 3M Digital Imager System.

To find out more about the 3M Digital Imager System, call 1-800-328-1684 ext. 340. Or write: 3M Medical Imaging Systems Division, P.O. Box 33050, St. Paul, MN 55133-3050. In Canada, write: 3M Canada Inc., P.O. Box 5757 Terminal A, London, Ontario, Canada N6A 4T1.

© 3M 1990

Innovation working for you™

3M

PERSONAL COMPUTER/LASER VIDEODISC SYSTEM

to assist you in the

diagnosis of Skeletal Dysplasias

A unique collection of 400 Skeletal Syndromes
7000 Illustrations

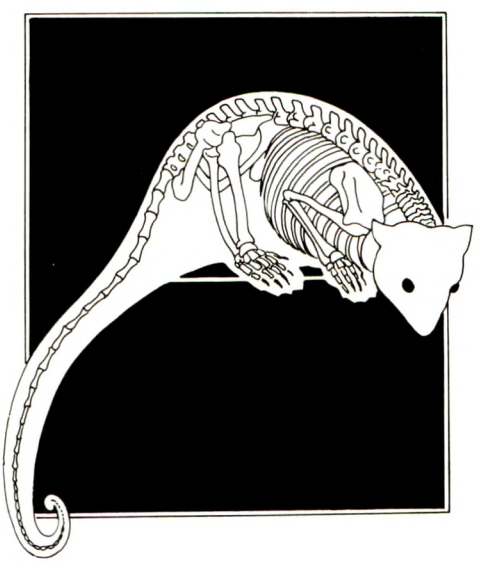
including

- *X-rays*
- *Clinical pictures*
- *Chondro-osseous histology*

OSSUM

AN ILLUSTRATED DATABASE OF SKELETAL DYSPLASIAS

SSUM



for further information contact:

Dr. Agnes Bankier – Medical Geneticist to the successful related POSSUM system.

PO Box 1100 Parkville Victoria 3052 Australia
Phone: (03) 345 5160 Fax: (03) 348 1391

Change of Address?

You won't miss a single issue if you notify us at least eight weeks in advance. Send your mailing label or account number along with your new address and the date the change is to take effect to:

AJR Subscription Fulfillment Dept.
428 East Preston Street
Baltimore, MD 21202-3993
or call TOLL-FREE
1-800-638-6423

Keep It All Together

Easily and Conveniently With Bound Volumes of the *American Journal of Roentgenology*

Keeping up with scientific and technological advances in radiology is more important than ever, and that's why each issue of the *American Journal of Roentgenology* is packed with up-to-the-minute information crucial to you and your practice. **Keep this important resource together for easy reference in convenient and attractive bound volumes.**

Each edition is imprinted with the year and volume number and contains six issues filled with the kind of vital research, commentary and analysis you've come to expect in the AJR.

For ordering information, contact AJR Subscription Fulfillment Department, 428 E. Preston St., Baltimore, MD 21202-3993, or call toll-free **1-800-638-6423.**

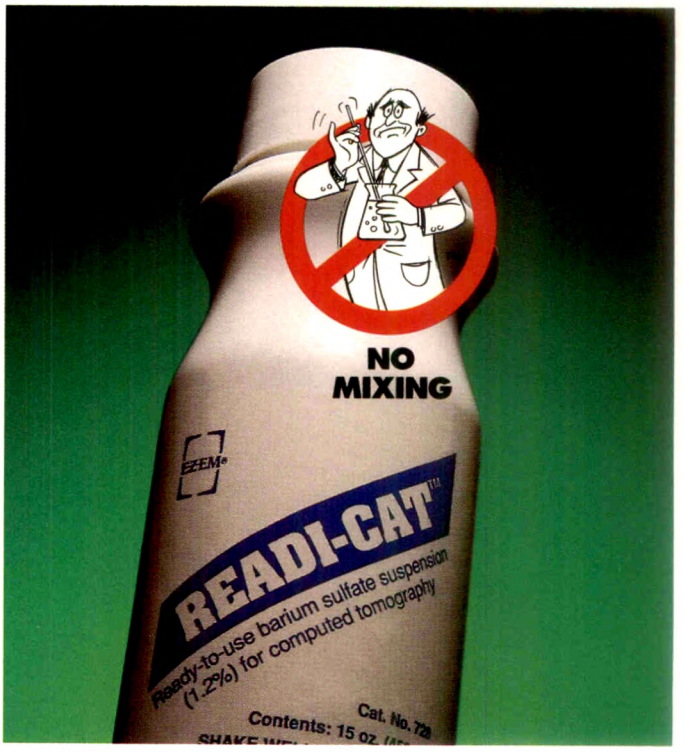
E-Z-EM®

Shake, drink and throw away. Single-patient bottles of Readi-CAT™ provide excellent contrast for CT studies of the GI tract, with the inherent safety and accuracy of barium sulfate. Since there's no mixing, there's no mess or waste. Stocking and inventory are easier too, and you get the ideal consistency every time, for consistently ideal results. In single-patient bottles or multi-dose jugs, Readi-CAT can make your life easier. Call your E-Z-EM Distributor or one of our Customer Service Specialists at 1-800-544-4624.

E-Z-EM, Inc.
717 Main Street
Westbury, NY 11590
Tel: 1-800-544-4624
Fax: 516-333-8278

E-Z-EM INTEGRITY • E-Z-EM DEDICATION • E-Z-EM INNOVATION
30 Years of Quality and Service to Radiology
E-Z-EM®

THIS CAT HAS ONLY ONE LIFE.



Readi-CAT (1.2% w/v): Catalog Nos. 728 (450 ml), 721 (900 ml), 724 (1900 ml), and Readi-CAT 2 (2% w/v): Catalog Nos. 723 (450 ml), 729 (900 ml), 726 (1900 ml)

E-Z-EM stock is publicly traded on the NASDAQ National Market System under the symbol EZEM. For financial information, contact Investor Relations at 1-800-544-4624, ext. 345.

© E-Z-EM, Inc., 1992

Seventeenth Annual

International BODY IMAGING CONGRESS

Mauna Lani Bay Hotel, Kona, Hawaii

October 10-17, 1992 (Sessions October 11-15)

The seventeenth edition of this highly regarded multimodality imaging conference will be held at the **Mauna Lani Bay Hotel**,on the island of Kona, Hawaii. This spectacular resort was featured in "Lifestyles of the Rich and Famous." A renowned invited faculty, including Drs. M. Bernardino, W. D. Boswell, W. G. Bradley, R.B. Dietrich, R.J. Friedman, H. Kressel, D. Kumpe, A. Lurus, M. L. Manco-Johnson, C. L. Partain, R. M. Quencer, T. Stavros, R. Townsend and F. Winsberg, will present topics in Computed Tomography, Ultrasonography, Magnetic Resonance Imaging, Interventional Radiology and correlative modalities. Special focus section on **Neuro Imaging, Interventional Radiology, and Helical CT Scanning** will be included. **The Congress has been approved for 30 Category I CME credits by the American Institute of Ultrasound in Medicine.**

Michael L. Manco-Johnson, M.D.
University of Colorado Health Sciences Center
Program Coordinator

Ronald J. Friedman, M.D.
University of Southern California
Meeting Coordinator

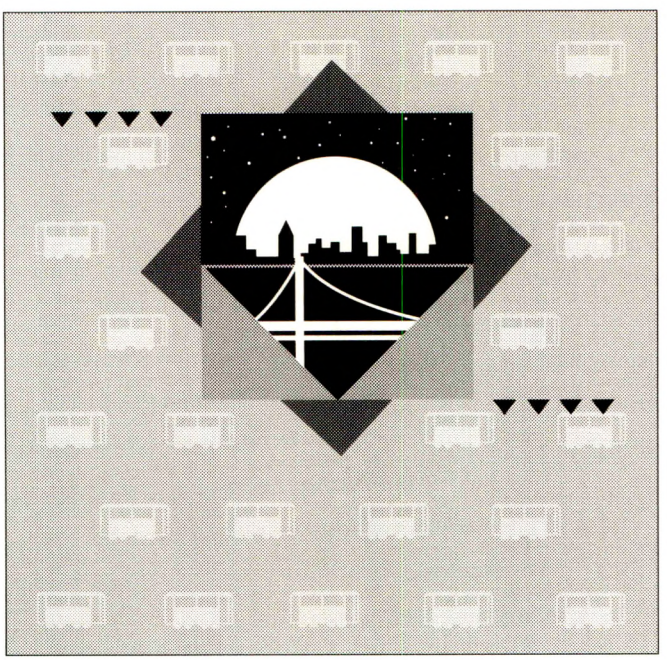
Registration Information: US $595 (Fellows, Residents, Interns, Technicians and Nurses with letter may deduct US $100.) All fees payable in **US DOLLARS** drawn on a **US BANK.**

For further travel information:

Pacifica Plaza Travel, Inc., 5839 Green Valley Circle, Suite 202, Culver City, CA 90230
(800) 927-4778, (310) 649-6677 FAX (310) 568-0402

For registration and further meeting information:

Medical Seminars International, Inc.
18981 Ventura Blvd.,Suite 303, Tarzana, CA 91356
(818) 774-9077 FAX (818) 774-0244



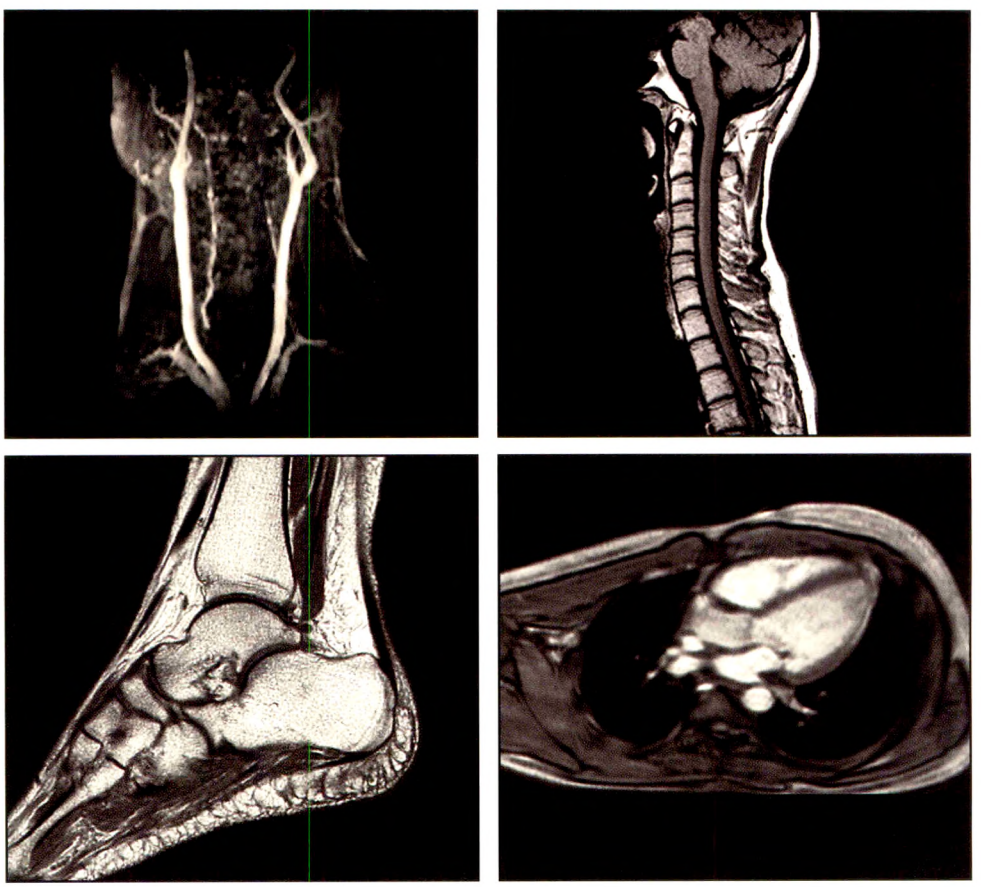
San Francisco

American Roentgen Ray Society

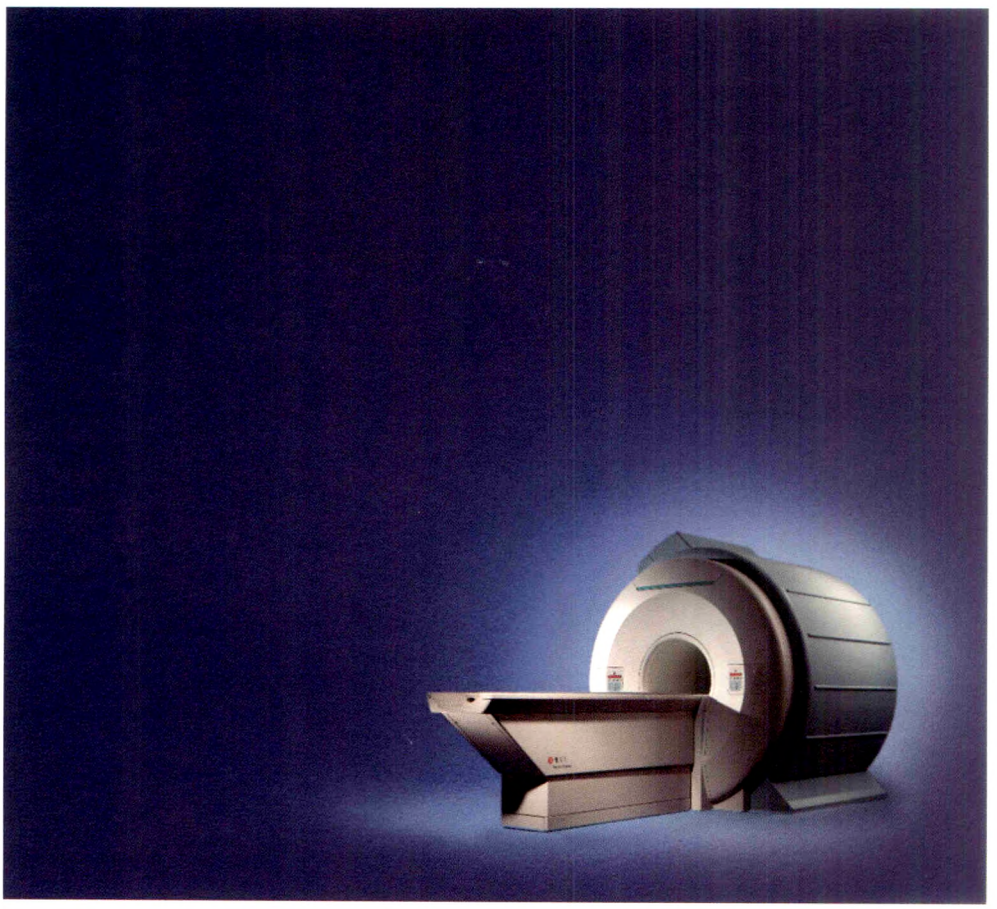
93rd Annual Meeting
April 25–30, 1993

San Francisco Marriott
San Francisco, CA

GET THE BIG PICTURE



IN A SMALL SPACE.



Now there's no reason to sacrifice image quality for size.

Not when the Picker Vista® Q active shield 1.0T system delivers images this clear, this detailed. Vista Q offers you the industry's highest homogeneity magnet, the only 60 cm patient aperture, and the only quadrature body and surface coils in a 1.0T MR system.

Vista Q is setting industry standards in image acquisition too – offering angio and cardiac imaging, 512^2 resolution, and volume imaging with submillimeter accuracy.

Yet with its small footprint, Vista Q is easy to site. Operating costs are low too. Vista Q's helium-only magnet requires just two refills a year.

So if you thought high field performance in an economical system was years away, think again. The Vista Q from Picker is here now.

For more information on Vista Q, call us at 1-800-323-0550. Or write Picker International, Inc., 595 Miner Road, Dept. CC, Cleveland, Ohio 44143.

PICKER

MORE THAN IMAGES. INSIGHT.

© 1992 Picker International, Inc.

When you give blood
you give another birthday,
another anniversary,
another day at the beach,
another night under the stars,
another talk with a friend,
another laugh,
another hug,
another chance.



American Red Cross

Please give blood.

Ad Council

AJR Guidelines for Authors

Address new and revised manuscripts and correspondence to the Editor:

AJR Editorial Office
2223 Avenida de la Playa, Suite 103
La Jolla, CA 92037-3218
Telephone: (619) 459-2229; FAX: (619) 459-8814

Inquiries regarding classified ads, reprints, or permission to republish *AJR* material should be addressed to the publisher:

ARRS Publications Department
1891 Preston White, Dr., Reston, VA 22091

The *AJR* publishes original contributions to the advancement of medical diagnosis and treatment. Submitted manuscripts should not contain previously published material and should not be under consideration for publication elsewhere.

Manuscript decisions are based on peer review. Reviewers receive manuscripts without title pages to ensure an unbiased review. Statements made in the article, including changes made by the Editor or manuscript editor, are the responsibility of the author and not of the *AJR* or its publisher. Authors will be sent the edited manuscript, galley proof, and proofs of illustrations. If the corresponding author will be unavailable to review galleys, arrangements should be made for a coauthor or colleague to read and return the proof.

The following guidelines are based on instructions set forth in the **Uniform Requirements for Manuscripts Submitted to Biomedical Journals** (*Ann Intern Med* **1988;**108:258–265). Articles will be edited, however, to conform to the individual style of *AJR*.

General Guidelines for Major Papers

Abstract. Clearly state (in 250 words or fewer) the purpose, methods, results, and conclusions of the study. Include actual data.

Introduction. Briefly describe the purpose of the investigation and explain why it is important.

Methods. Describe the research plan, the materials (or subjects), and the methods used, in that order. Explain in detail how disease was confirmed and how subjectivity in observations was controlled.

Results. Present results in a clear, logical sequence. If tables are used, do not duplicate tabular data in text, but do describe important trends and points.

Discussion. Describe the limitations of the research plan, materials (or subjects), and methods, considering both the purpose and the outcome of the study. When results differ from those of previous investigators, explain the discrepancy.

AUTHOR'S CHECKLIST

For priority handling, complete the following checklist, sign the copyright form on the reverse side of this page, and include both with the manuscript.

_____ Two copies of the manuscript (the original and a photocopy) and two complete sets of figures are submitted. One copy has been retained by the author.

_____ If appropriate, *AJR* Guidelines for case reports, technical notes, pictorial essays, or letters to the Editor have been followed. (See page A8.)

_____ The manuscript, including references, figure legends, and tables, is typed double-spaced on 8½ × 11 in. (21.6 × 27.9 cm) *nonerasable* paper. Right-hand margins are not justified.

_____ All manuscript pages are numbered consecutively beginning with the abstract. Authors' names do not appear on the manuscript pages.

_____ The manuscript is organized as follows: title page, blind title page (title only), abstract, introduction, methods, results, discussion, acknowledgments, references, tables, figure legends, and figures.

_____ Informed consent has been obtained from patients who participated in clinical investigations. If experiments were performed on animals, authors complied with NIH guidelines for use of laboratory animals.

_____ Use of unfamiliar acronyms and abbrevations is kept to a minimum. When abbreviations are used they are defined at first mention, followed by the abbreviation in parentheses.

_____ Metric measurements are used throughout, or the metric equivalent is given in parentheses.

_____ Names and locations (city and state only) of manufacturers are given for equipment and nongeneric drugs.

_____ Upon acceptance, final version is submitted on a 5 1/4-in. DOS-compatible diskette in Wordperfect or ASCII format.

Title Page

_____ The following information is given: title of article; names and complete addresses (including zip code) of all authors; current addresses of authors who have moved since study; acknowledgment of grant or other assistance. The corresponding author is clearly identified, and a current address, phone number, and FAX number are given.

_____ A blind title page is included in each copy of the manuscript, giving only the title (without the authors' names) for use in the review process.

Abstract

_____ An abstract of approximately one and one-half typewritten pages is organized into the following paragaphs.

Objective. In one or two sentences, indicate the specific goal or purpose of the article, and indicate why it is worthy of attention. Explain the hypothesis to be tested, the dilemma to be resolved, or the deficiency to be remedied. The objective stated here must be identical to the one given in the title and introduction of the paper.

Subjects (or materials) and methods. Describe succinctly the methods used to achieve the objective explained in the first paragraph, stating what was done, how it was done, how bias was controlled, what data were collected, and how the data were analyzed.

Results. The findings of the procedures described in the preceding paragraph are presented here. All results should flow logically from the methods described and not stray from the specific objective of the paper. Include as many specific data as possible within the overall length limitation of one typewritten page.

Conclusion. In one or two sentences, present the take-home message to be remembered when all else is forgotten. Describe the conclusion of the study, based solely on the

data provided in the body of the abstract. Conclusions must relate directly to the objective of the paper as defined in the title and first paragraph of the abstract.

_____ No abbreviations or reference citations are used.

References

_____ References (not to exceed 35) are typed double-spaced starting on a separate page and are **numbered consecutively in the order in which they appear in the text**.

_____ All references are cited in the text and are enclosed in brackets and typed on line with the text (not superscript).

_____ Unpublished data are not cited in the reference list, but are cited parenthetically in the text, for example, (Smith DJ, personal communication), (Smith DJ, unpublished data). This includes papers submitted, but not yet accepted, for publication.

_____ Papers presented at a meeting are not cited in the reference list, but are cited parenthetically in the text (e.g., Smith DJ et al., presented at the American Roentgen Ray Society meeting, May 1990). After first mention, use (Smith DJ et al., ARRS meeting, May 1990).

_____ Inclusive page numbers (e.g., 333–335) are given for all references.

_____ Journal names are abbreviated according to *Index Medicus*.

_____ Style and punctuation of references follow the format illustrated in the following examples (all authors are listed when six or fewer; when seven or more authors, the first three are listed, followed by "et al."):

Journal article

1. Long RS, Roe EW, Wu EU, et al. Membrane oxygenation: radiographic appearance. *AJR* **1986**;146:1257–1260

Book

2. Smith LW, Cohen AR. *Pathology of tumors*, 6th ed. Baltimore: Williams & Wilkins, **1977**:100–109

Chapter in a book

3. Breon AJ. Serum monitors of bone metastasis. In: Clark SA, ed. *Bone metastases*. Baltimore: Williams & Wilkins, **1983**:165–180

Tables

_____ Each table is typed double-spaced on a separate page without vertical or horizontal rules; each has a short, descriptive title. Tables do not exceed two pages in length and contain at least four lines of data.

_____ Tables are numbered in the order in which they are cited in the text.

_____ Abbreviations are defined in an explanatory note below each table.

_____ Tables are self-explanatory and do not duplicate data given in the text or figures.

_____ All arithmetic (percentages, totals, differences) has been double checked for accuracy, and tabular data agree with data given in the text.

Figures and Legends

_____ Two complete sets of original figures are submitted unmounted in labeled envelopes.

_____ Figures are clean, unscratched, 5 × 7 in. (13 × 18 cm) glossy prints with **white borders.** A separate print is submitted for each figure *part*.

_____ All figure parts relating to one patient have the same figure number.

_____ Each figure is labeled on the back with the figure number and an arrow indicating "top." For black-and-white figures, labeling is done on a gummed label, which is then affixed to the back of the print. **Never** use labels on **color** figures, but write figure number on the back lightly in pencil. *Never* use ink on front or back of any figures.

_____ Authors' names are *not* written on the backs of figures.

_____ Only removable (rub-on) arrows and letters are used on the figures. Symbols are uniform in size and style and are not broken or cracked.

_____ Images are uniform in size and magnification.

_____ Line drawings are done in black ink on a white background. They are professional in quality, and all use the same size type. (Only glossy prints are acceptable.)

_____ Written permission has been obtained for use of all previously published illustrations (and copies of permission letters are included), and an appropriate credit line is given in the legends.

_____ Legends are typed double-spaced, and figure numbers correspond with the order in which the figures are cited in the text.

Transfer of Copyright Agreement, Conflict of Interest Acknowledgment, Certification of Coauthors, and Exclusive Publication Statement

Complete copyright to the article entitled: _____

_____

is hereby transferred to the American Roentgen Ray Society (for United States government employees to the extent transferable), effective if and when the article is accepted for publication in the *American Journal of Roentgenology*. In the case of the authors who are officers or employees of the United States government, the American Roentgen Ray Society recognizes that works prepared by officers or employees of the United States government as part of their official government duties are in the public domain.

Authors reserve all proprietary rights other than copyright, such as patent rights and the right to use all or part of this article in future works of their own. The authors retain the right of replication, subject only to crediting the original source of publication and receiving written permission from the publisher.

Authors guarantee that this manuscript contains no matter that is libelous or otherwise unlawful, invades individual privacy, or infringes any proprietary rights.

Authors understand that they will receive no royalty or other compensation from the American Roentgen Ray Society.

Authors guarantee that the editor has been or will be informed of any proprietary or commercial interest or conflicts of interest the authors may have that relate directly or indirectly to the subject of this article.

All authors certify that they have made substantive and specific intellectual contributions to the article and assume public responsibility for its content.

Finally, the authors certify that none of the material in this manuscript has been published previously or is currently under consideration for publication elsewhere.

First author/date	Second author	Third author
Fourth author	Fifth author	Sixth author

This agreement must be signed by all authors in order for the manuscript to be published.

Case Reports

A case report is a brief description of a special case that provides a message that transcends the individual patient.

Format. There is no abstract. The introduction should be a short paragraph giving the general background and the specific interest of the case. No more than one case should be described in detail (similar ones can be mentioned briefly in the discussion). Emphasis should be on the radiologic aspects; clinical information must be limited to that necessary to provide a background for the radiology. The discussion should be succinct and should focus on the specific message and relevance of radiologic methods. A review of the literature is not appropriate.

Length. Maximum of five double-spaced, typewritten pages, including the references but not the title page or figure legends.

References. Maximum of eight.

Figures. Maximum of four, unless the text is shortened accordingly. Legends must not repeat the text.

Tables and Acknowledgments. Not appropriate in case reports.

Pictorial Essays

A pictorial essay is an article that conveys its message through illustrations and their legends. Unlike other *AJR* articles, which are based on original research, pictorial essays serve primarily as teaching tools, like exhibits at a scientific meeting. They are not encyclopedic book chapters. The abstract should be a short, introductory paragraph.

Length. Maximum of four double-spaced, typewritten pages, including the references but not the title page or figure legends.

References. Maximum of four.

Figures. Maximum of 30 figure *parts*. Number should be as few as necessary to convey the message of the paper.

Tables and Acknowledgments. Not appropriate in pictorial essays.

Opinions, Commentaries, and Perspectives

Opinions, commentaries, and perspectives are special articles dealing with controversial topics or issues of special concern to radiologists.

Format. Include a title page but no abstract. Headings may be used to break up the text.

Length. Maximum of five double-spaced, typewritten pages.

References. Maximum of five.

Tables and Figures. Maximum of four.

Technical Notes

A technical note is a brief description of a specific technique or procedure, modification of a technique, or equipment of interest to radiologists.

Format. No abstract, headings, or subheadings are required. If headings are used, they should be a combination of "Case Report," "Materials and Methods," "Results," and "Discussion." A brief one-paragraph introduction should be included to give the general background. Discussion should be limited to the specific message, including the uses of the technique or equipment. Literature reviews and lengthy case reports are not appropriate.

Length. Maximum of five double-spaced, typewritten pages, including the references but not the title page or figure legends.

References. Maximum of eight.

Figures. Maximum of two, unless the text is shortened accordingly.

Tables and Acknowledgments. Not appropriate in technical notes.

Letters to the Editor and Replies

Letters to the Editor and Replies should offer objective and constructive criticism of published articles. Letters may also discuss matters of general interest to radiologists. Material being submitted or published elsewhere should not be duplicated in letters, and authors must disclose financial associations or other possible conflicts of interest.

Format. All letters should be typed double-spaced on nonletterhead paper, with no greeting or salutation. Titles for letters should be short and pertinent. The title for a reply is simply "Reply." Do not use abbreviations in the title or the text. Authors' names and affiliations should appear at the end of the letter. Do not end a letter with a hand-written signature.

Number of authors. Maximum of four.

Length. Maximum of two double-spaced, typewritten pages, including references.

References. Maximum of four.

Figures. Maximum of two figures *or* one figure with two parts.

Tables and Acknowledgments. Not appropriate in Letters to the Editor and Replies.

Computer Page Articles

Articles published on the computer page deal with practical computer applications to radiology.

Format. Include a title page and an abstract.

Length. Maximum of eight double-spaced, typewritten pages.

References. Maximum of five.

Figures and Tables. Maximum of five. Computer printouts are not acceptable. Figures must be submitted as 5 × 7 in. glossy prints.

All submissions to the *AJR* must be accompanied by a completed copy of the Author's Checklist and the signed Copyright agreement.



When timing is critical, there's no time for guesswork

Comprehensive healthcare information in just minutes ...anytime you need it

As emergencies arise, you have to know what to treat, prevent, and look for immediately. Get the answers you need in just minutes through computer access to the National Library of Medicine, the largest, most complete healthcare information resource in the world.

The Friends of the NLM—a nonprofit organization—wants you, and all health professionals, to find out more about this unique link to the world's healthcare knowledge. To do so, simply use the coupon provided. You owe it to yourself and your patients.

The more you know, the better you heal

FRIENDS OF THE NLM NATIONAL LIBRARY OF MEDICINE

Friends of the NLM
1529 Wisconsin Avenue N.W.
Washington, D. C. 20007

☐ Please send me more information about the NLM and the services it offers.

☐ Please enroll me in the Friends of the National Library of Medicine. My tax-deductible check for $35.00 (member) or $100.00 (sponsor) is enclosed.
(Institutional and corporate memberships are also available.)

Name_____

Address_____

City_____ State_____ Zip_____

Review Article

Stress Fractures: Current Concepts

Richard H. Daffner[1] and Helene Pavlov[2]

Stress fractures are extremely common lesions that occur in specific areas and are related to specific activities. They are caused by increased muscular activity on bones that are not yet ready to take the increased pull of the involved muscles. The insufficiency type of stress fractures found in patients with bone of diminished mineral content is being recognized more often as increasing numbers of middle-aged and elderly persons are becoming more physically active. A variety of imaging studies can be used to diagnose stress fractures. Radionuclide bone scanning and MR imaging often show abnormalities early in the course of the injury. However, when radiographs appear normal, findings on scintigrams may be more suggestive of the proper diagnosis. In patients with suspected stress injury, radiographs should be obtained a second time, 1–2 weeks after the initial study. Biopsy should be avoided until evidence is clear-cut that the lesion has not changed over a short time.

Stress fractures are a group of skeletal injuries that occur in all age groups. They are common and are specific both in location and in regard to the activity that produced them [1–3]. Over the years, they have intrigued and confused clinicians and radiologists because trauma often was not considered as the cause. In the last decade, however, greater attention has been given to stress fractures because of the increased interest in physical fitness activities [4–10]. In addition, interest is now greater in the insufficiency type of stress fracture, which often is more confusing than the fatigue type. This review presents the pertinent aspects of stress fractures, emphasizing the types commonly encountered, and discusses the role of conventional and newer diagnostic imaging techniques, notably MR imaging. Additional attention is given to insufficiency fractures in the elderly and in patients with osteoporosis.

Definitions

A stress fracture is the result of repetitive, prolonged muscular action on a bone that has not accommodated itself to that action. Devas [1] observed that stress fractures occur in non–weight-bearing bones and showed that stress fractures do not result from impact on a bone. In most instances, persons who have stress fractures are engaged in vigorous activity that is either totally new or to which they have not yet become conditioned. From an etiologic standpoint, two types of stress fractures are encountered: fatigue fractures and insufficiency fractures. A *fatigue fracture* is caused by the application of abnormal muscular stress or torque to a bone that has normal elastic resistance. The following triad is associated with most fatigue fractures: the activity is (1) new or different for the person, (2) strenuous, and (3) repeated with a frequency that ultimately produces signs and symptoms [1–3, 11]. An *insufficiency fracture* occurs when normal or physiologic muscular activity stresses a bone that is defi-

Received January 14, 1992; accepted after revision February 28, 1992.
Presented at the annual refresher course of the International Skeletal Society, San Diego, CA, September 1991.
[1] Department of Diagnostic Radiology, Allegheny General Hospital and the Medical College of Pennsylvania, Allegheny Campus, 320 E. North Ave., Pittsburgh, PA 15212-4772. Address reprint requests to R. H. Daffner.
[2] Department of Radiology, Hospital for Special Surgery, New York, NY 10021.

AJR **159:245–252, August 1992** 0361–803X/92/1592–0245 © American Roentgen Ray Society

cient in mineral or elastic resistance. The term *pathologic fracture* should be restricted to any situation in which preexisting neoplasm or infection has weakened the bone [12].

Etiology

Stress fractures result from a variety of activities, and, as mentioned, the sites of occurrence are activity related. For example, both recreational and competitive runners are prone to stress fractures of the proximal medial posterior surface of the tibia [2, 12–14], the distal shaft of the fibula [1, 2], the navicular bone of the foot [7, 8, 15], and the neck of the femur. Dancing (e.g., ballet, aerobic dancing) is associated with stress fractures of the metatarsus, the anterior shaft of the tibia [16–18], and the neck and shaft of the femur [15]. Leaping activities such as may occur in basketball and ballet similarly can cause cortical stress fractures of the anterior tibia [16, 17] and the calcaneus. Recently, fatigue-type stress fractures in the sacrum in runners [4] and in patients engaged in vigorous aerobics [19] have been reported. Other activities and the common locations of associated fatigue fractures are listed in Table 1.

Insufficiency fractures occur in a variety of conditions in which the mineral content or the elasticity of bone is abnormal. These injuries occur most often in elderly women who have postmenopausal osteoporosis [21, 23–27]. They also occur in patients with osteoporosis of any cause, including use of corticosteroids, rheumatoid arthritis [22, 28–30], and diabetes mellitus [31]. They may also occur in the distal tibia and foot in patients with healing gross fractures of the more proximal tibia and fibula who begin weight bearing [32, 33]. Table 2 lists conditions predisposing to insufficiency fractures.

Stress fractures are also more likely to occur in normal bones at the sites of previous surgical screw holes [34], or at the sites of excision of bone. They also occur in patients who have had muscle or tendon transfers that result in a new balance of the musculoskeletal force on the bones. The most common examples are stress fractures in the second and third metatarsals associated with bunion surgery [20, 35, 36].

Biomechanics

Bone is a dynamic architectural substance that responds to changes in the muscular activity imposed on it. Increased muscular activity results in an increase in the strength of both muscles and bone [37, 38]. Conversely, a decrease in activity or muscular atrophy results in muscular and bony atrophy. Under normal circumstances, the muscles tone up at a faster rate than the bones do, and the result is a mechanical imbalance [5]. The novice recreational runner, for example, will experience positive cardiovascular effects within the first few days after beginning to run. Within a week, muscle tone and strength will be increased to the point that the runner will feel capable of extending the distance run. Unfortunately, the increase in muscle tone has not been accompanied by an equal increase in skeletal strength, and thus, extending the distance will prolong muscular pull on bones that are not yet ready to accept the added stress [1, 3, 5, 13]. Fatigue of opposing muscle groups that usually prevent one group of muscles from having an overexerting effect on the bone may result in a further imbalance and lead to bone failure [5].

Bone is a solid material, and its response to stress is similar to the responses of other structural materials, such as metal, wood, ceramics, and plastic. From an architectural standpoint, when they are stressed, all these materials behave according to Wolff's law [39, 40]. This is illustrated in Figure 1, which shows the deformity relationship of a bone to increasing stress. As the amount of stress on a bone is increased, progressive deformity occurs throughout the bone's elastic range. As long as the deformity remains within the elastic range, when the deforming force ceases, the bone will return to its original configuration. Beyond the elastic range, further

TABLE 1: Locations by Activity, of Common Fatigue Types of Stress Fractures

Location	Activity
Lower limb	
Metatarsus	Marching [1], ballet [16], weight bearing after bunionectomy [20]
Navicular bone	Marching [1], running [8, 15]
Calcaneus	Jumping [1]
Tibia, proximal shaft	Walking [21, 22], running [5, 13]
Tibia, mid and distal shaft	Running [5, 13], leaping (basketball, ballet, aerobic dancing) [17]
Fibula, distal shaft	Running [4]
Patella	Hurdling [1]
Femur, shaft	Ballet [16], running [1]
Femur, neck	Ballet [16]
Trunk	
Sacrum	Running [4], aerobics [19]
Pelvis, obturator ring	Bowling [1], gymnastics [1]
Lumbar vertebra (pars interarticularis)	Ballet [16], running [1], gymnastics [3]
Upper limb	
Humerus, distal shaft	Throwing a ball [1]
Ulna, shaft	Pitching a ball [10], propelling wheelchair [1]

TABLE 2: Conditions Predisposing to Insufficiency Fractures

Osteoporosis of any cause
Rheumatoid arthritis
Osteomalacia or rickets
Diabetes mellitus
Fibrous dysplasia
Paget disease
Pyrophosphate arthropathy
Healing gross tibial fracture
Osteogenesis imperfecta
Osteopetrosis
Hyperparathyroidism
Scurvy
Irradiation

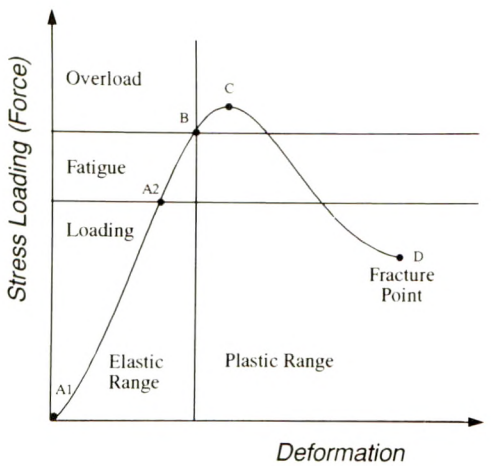


Fig. 1.—Wolff's law. Graph shows that as stress loading force increases, deformity on structure also increases. As long as force does not exceed amount corresponding to level B, the structure will return to its original configuration without evidence of damage (elastic range). Once fatigue level has been exceeded, however, further stress produces permanent deformity. Microfractures begin at point C, and ultimate failure occurs at point D.

stress causes plastic deformity. In this stage, permanent deformity occurs as the result of microfractures within the bone. Chamay and Tschants [39] and Wright and Hayes [40] verified this change in experiments with animal and human cadaveric specimens. As the number of microfractures increased, small cortical cracks occurred, and as the amount of stress increased, the cracks progressed. The fracture was propagated by the initiation of subcortical infractions ahead of the main crack [40]. Eventually, as the fracture point is exceeded, structural failure and complete or catastrophic fracture occur [41].

Daffner et al. [5] have suggested additional factors that contribute to the increased muscular pull, producing overload on stressed bones. The first, poor posture, typically causes a change in the center of gravity for which the body compensates. This increases the effect of direct muscular pull and also leads to fatigue of opposing muscle groups. A second factor is the operating conditions in which the activity is practiced. To a runner, changes in terrain, running surface, or equipment can cause a change or an increase in muscular pull on the bones of the leg. Running up or down a hill increases the forces by a factor of seven [5]. Changing from a grass surface to a hard surface may lead to protective curling of the feet to cushion the footfall, as suggested by Devas [1]. Improperly fitting shoes may cause sufficient discomfort so that a change in footfall occurs. All of these factors can result in increased muscular pull on the leg bones and subsequent fatigue of opposing muscle groups [1, 5].

Clinical Features

The classic clinical feature of a stress fracture is pain associated with a particular activity. The pain is relieved by rest and becomes worse when the activity is continued. In many instances, the activity will be new to the person [1, 2, 13]. The patient may have had a dramatic change in some facet of how he or she performs a particular activity. For example, a recreational runner who has been running 2 miles a day decides to increase the distance to 5 miles; the result is a tibial stress fracture [5]. Even conditioned professional athletes may have stress fractures when they have broken training or decided to increase the amount of effort involved in performing their particular athletic feat.

The clinical history is paramount in the diagnosis of a stress fracture. The patient must be questioned closely about the sequence of events leading to the sudden onset of pain in the affected limb. Furthermore, patients with a nonathletic habitus should be asked about any new physical activity. Recreational walking is a low-impact activity with excellent aerobic cardiovascular effects. Many middle-aged and elderly persons are now engaged in this activity, a fact that accounts for the increasing number of insufficiency-type stress fractures that are encountered [21, 24, 26, 27].

It is important that stress fractures be recognized so that the patient can abstain from the activity that produced the injury. Continued activity when a bone has been compromised (particularly in a leg) may result in a complete or catastrophic fracture, in distraction of the bone fragments from that bone, in a fracture of another bone in the same limb, or in a fracture of the same bone in the opposite limb as the person shifts his or her body weight to the opposite side [1, 2].

Patients with rheumatoid arthritis are at increased risk of insufficiency fractures because of osteopenia caused by the disease itself, disuse of the affected limbs, and use of corticosteroids [28, 29]. Furthermore, patients with rheumatoid arthritis who have recently had total joint replacement of a hip or a knee often have stress fractures in the affected limb as the result of increased ambulation made possible by the prosthesis [29].

Imaging Findings

Savoca [42] described stress fractures as compression or distraction fractures. Compression fractures generally occur in cancellous bone such as the neck of the femur, the proximal shaft of the tibia, and the calcaneus. Distraction fractures occur more commonly in compact bone. The exact radiologic appearance, however, depends on the amount of time between the onset of injury and the imaging examination and

on whether the patient continued participation in the activity despite pain. In the early phase, on radiographs, a fracture in the shaft of a long bone may appear as a lucency through the cortex without any periosteal reaction or callus (Figs. 2 and 3). In cancellous bone, the first manifestation may be a focal linear area of sclerosis perpendicular to the trabeculae (Fig. 4). As the bone heals, solid or thick lamellar periosteal reaction occurs (Fig. 5). Often, this occurs on the endosteal surface as well as on the periosteal surface [42]. The degree of reactive bone is generally confined to a small area of cortex (Fig. 6) and usually involves only one of the cortical surfaces. Ultimately, the area of periosteal reaction thickens, and the fracture line, if actually seen previously, disappears. Devas [14] described an unusual variety of stress fracture that was longitudinal and involved up to half the length of the tibia or femur.

Radionuclide bone imaging has been used for some time in patients with suspected stress fractures [43–45]. The bone scan can be used to distinguish between an actual bony lesion and a nonskeletal abnormality. This is important when the plain radiograph appears normal, particularly in competitive athletes or in persons for whom ceasing a particular

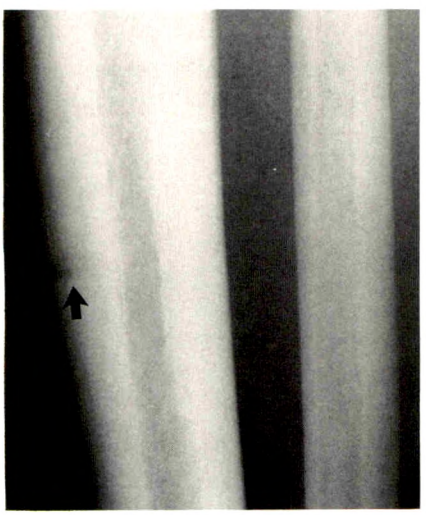


Fig. 2.—Radiograph shows anterior tibial stress fracture (*arrow*) in a basketball player.

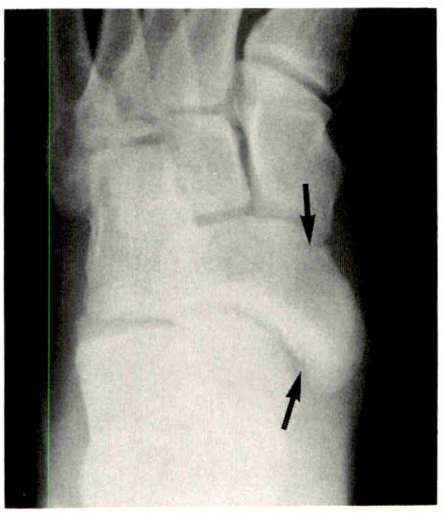


Fig. 3.—Radiograph shows tarsal navicular stress fracture (*arrows*) in a runner.

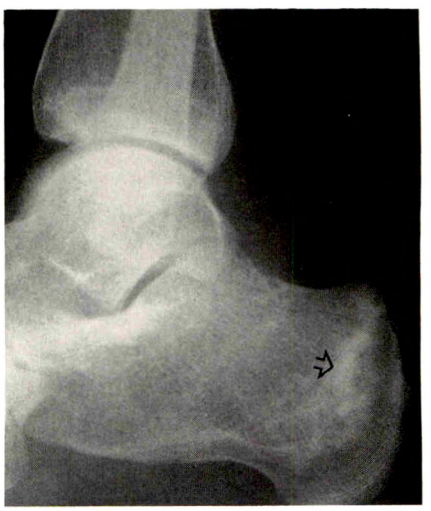


Fig. 4.—Radiograph shows insufficiency-type stress fracture (*arrow*) of calcaneus in a patient with postmenopausal osteoporosis. Note cortical thickening.

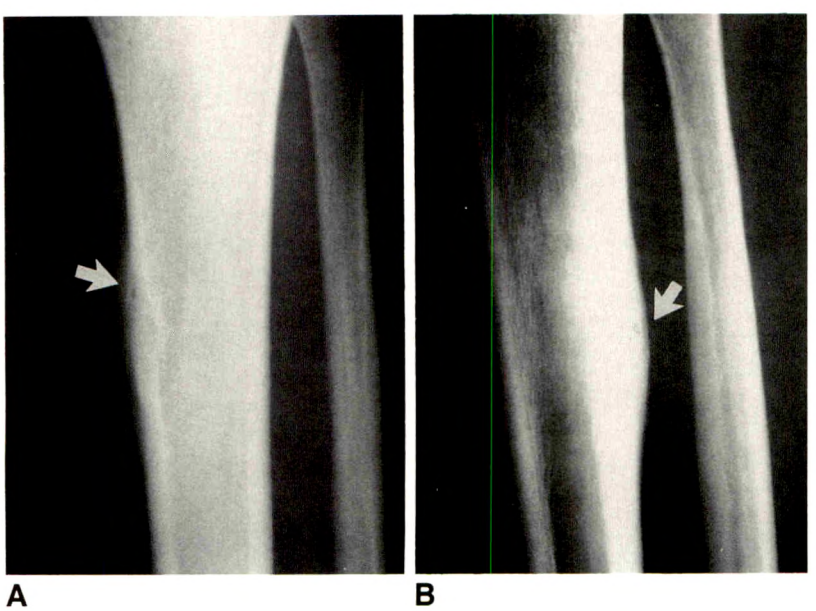


Fig. 5.—Typical location of tibial stress fracture in a recreational runner. *A* and *B*, Frontal (*A*) and lateral (*B*) radiographs show an area of cortical and endosteal reaction (*arrows*) on medial and posterior aspects of proximal tibia.

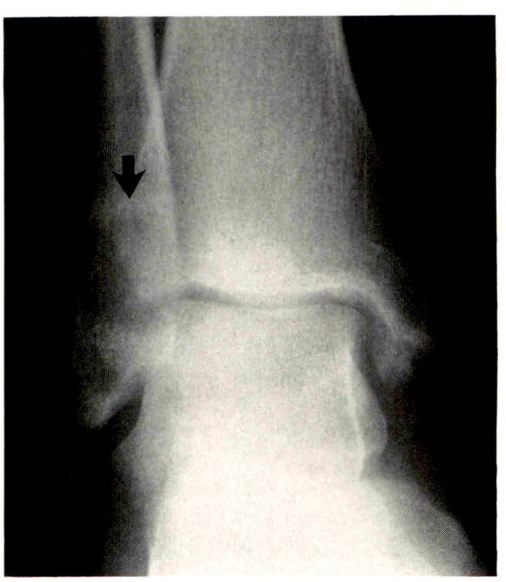


Fig. 6.—Radiograph shows stress fracture (*arrow*) of distal fibula in a long-distance runner.

activity could be detrimental to their livelihood. In these persons, increased uptake of radionuclide within a bone typically subject to stress fracture from a particular activity is highly diagnostic [44, 46, 47].

Scintigrams show abnormalities early in the course of the stress fracture. In the earliest stage, the image will show a slightly increased uptake of radionuclide. This eventually progresses to well-marginated areas of increased uptake. Scintigrams show evidence of stress fractures days to weeks before the radiographs do [43–45, 47].

Radionuclide scanning is also extremely useful in patients with insufficiency fractures. Scintigraphy is often used to search for metastatic lesions in patients in whom stress fractures are not considered. In insufficiency fractures of the sacrum, the pattern is considered diagnostic if the scintigram shows a vertical increase in the uptake of radionuclide (Fig. 7A) or in those patients with bilateral fractures, an H-shaped distribution ("Honda sign") (Fig. 8) [48, 49]. Patients who have these patterns should have follow-up CT scans through the sacrum in order to confirm the diagnosis.

Occasionally, the bone scan will appear normal early in the course of a stress injury. Milgrom et al. [50] recommend repeating the scan if the patient participates in an activity associated with stress fractures.

CT scanning has been used to diagnose stress fractures [51, 52]. With the exception of sacral stress fractures, however, the findings may be inconclusive in showing areas of periosteal and endosteal new bone as well as the fracture lines. CT should be used only as an ancillary examination, particularly in the sacrum (Fig. 7B) to confirm a diagnosis suggested by another imaging study [19, 24, 26, 27, 53].

MR imaging in patients with stress fractures has been described [19, 54–61]. MR findings parallel those found on scintigrams. If the patient is imaged within days after he or she becomes symptomatic, MR images will show low signal in the marrow areas on T1 weighting [57] (Fig. 7C). The signal is increased on T2 weighting, after injection of gadopentetate dimeglumine (Fig. 7D), and with short tau inversion recovery (STIR) sequences [58, 61]. The findings are nonspecific and represent the edema in the marrow or in the soft tissues surrounding the fracture. The findings can easily be confused with those seen in transient osteoporosis [62, 63], neoplasm, or infection. If the patient is imaged much later, linear areas of low signal may be seen on T1-weighted images [55, 57] (Fig. 9). These linear abnormalities have low signal on T2-weighted images and represent the callus and new bone formation at the fracture site and are suggestive of the diagnosis. Usually at this point, however, the radiographs or

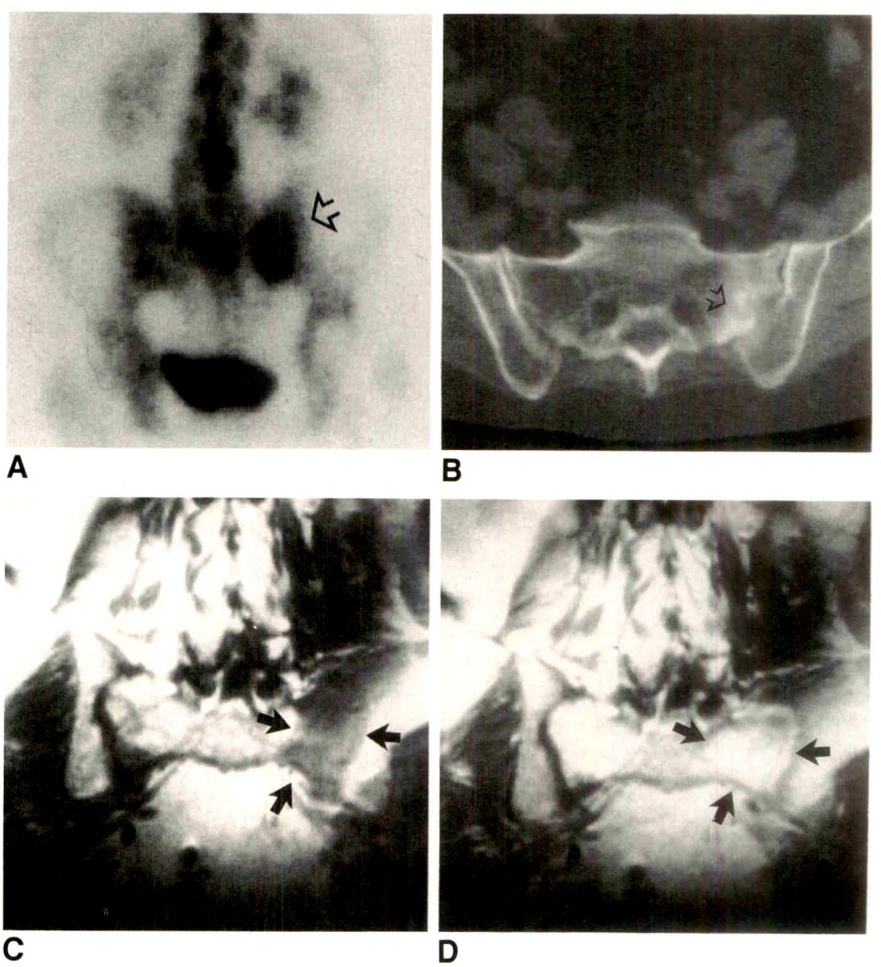


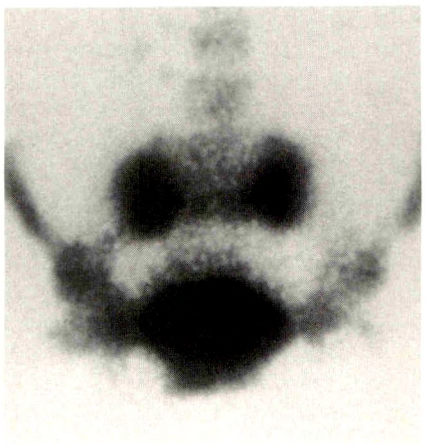
Fig. 7.—Patient with a unilateral sacral insufficiency fracture.

A, Scintigram shows increased uptake (*arrow*) of radionuclide on left side.

B, CT scan shows unilateral area of bone repair in left sacral wing (*arrow*).

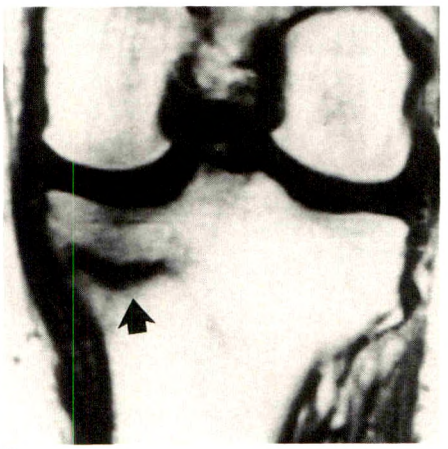
C, Coronal T1-weighted MR image shows unilateral area of signal loss (*arrows*) in sacrum on left side.

D, Contrast-enhanced coronal T1-weighted MR image shows increased signal (*arrows*) in area of abnormality on left side.



8

Fig. 8.—Bilateral sacral insufficiency fractures. Scintigram shows typical H-shaped areas of increased uptake of radionuclide ("Honda sign"). CT scan (*not shown*) confirmed that abnormality was caused by fractures.



9

Fig. 9.—Coronal T1-weighted MR image shows linear appearance of stress fracture (*arrow*) of proximal medial tibia. (Courtesy of T. Berquist, Ft. Lauderdale, FL.)

CT scans show the true nature of the lesion. The MR appearance parallels the scintigraphic appearance in that it is nonspecific early in the evolution of the stress fracture and more suggestive later [55, 57].

Figure 10 represents the continuum of bone response to increases in stress loading and the relationship of various imaging studies to that continuum. Note the parallel between abnormal findings on scintigrams and MR images.

Differential Diagnosis

The diagnosis of stress fractures should be readily apparent when a specific activity can be associated with the onset of signs and symptoms of a lesion in an area typical for stress fracture [1, 2]. Unfortunately, in many instances, the patient cannot recall a specific activity that can be associated with the onset of signs and symptoms. If any possibility exists that a bone lesion may represent a healing stress fracture, biopsy should be avoided unless evidence is clear-cut that the appearance of the lesion on radiographs has not changed over several weeks. A biopsy specimen of a stress fracture may contain immature bone cells, which are part of the healing fracture process but which may be misinterpreted by an inexperienced pathologist as representing a bone sarcoma.

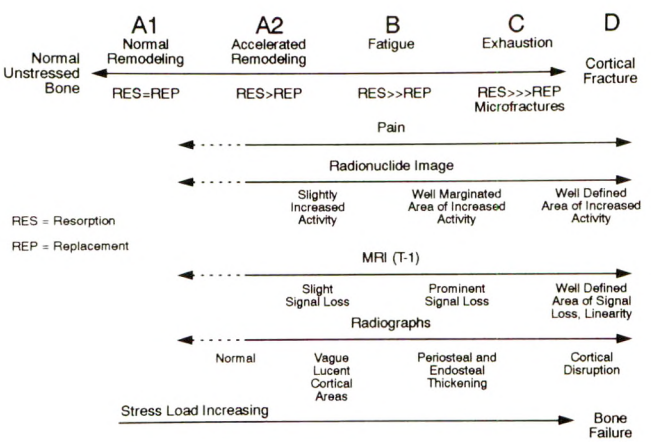


Fig. 10.—Continuum of bone response to increases in stress loading. Letters at top correspond to points on graph of Wolff's law (Fig. 1). Patient generally becomes symptomatic at point of accelerated remodeling (A2). Scintigrams and MR images show abnormalities much earlier than radiographs do. (Modified from Roub et al. [45].)

The differential diagnosis of stress fractures includes osteoid osteoma, chronic sclerosing osteomyelitis, osteomalacia, metastasis, osteogenic sarcoma, and Ewing's tumor. Patients with osteoid osteoma often have pain that is worse at night and is relived by aspirin or other analgesics. This is in contradistinction to stress fractures, which are characteristically made worse by activity and relieved by rest. On radiographs, the typical osteoid osteoma has a dense sclerotic area surrounding a lucent nidus (Fig. 11). It may be necessary to resort to tomography or CT to detect the nidus. Both osteoid osteomas and stress fractures may be eccentric; stress fractures occasionally involve both sides of the shaft of the affected bone. As a rule, however, stress fractures affect only one of the cortical surfaces. Periosteal reaction is often absent with an osteoid osteoma and is quite common in a stress fracture (Fig. 5). The sclerosis associated with an osteoid osteoma is much greater than the reactive change seen in a stress fracture.

Chronic sclerosing osteomyelitis (of Garré) has a dense sclerotic appearance and often no associated lucency on radiographs. The lesion usually involves the entire circumference of the bone and is much more widespread than a stress fracture (Fig. 12). The thinner linear sclerotic appearance of a stress fracture (Fig. 5) should be characteristic enough to distinguish the two lesions. Serial radiographs generally show little or no change within a short time in sclerosing osteomyelitis. A typical stress fracture, however, has a rapidly evolving course over several weeks.

Looser's zones or osteoid seams are insufficiency types of stress fractures often seen in patients with osteomalacia [64, 65]. They are more common in adults than in children. Patients with Looser's zones may have the characteristic findings of osteomalacia/renal osteodystrophy such as decreased mineralization, coarsened texture of the bones, "rugger-jersey" appearance of the spine, and, occasionally, bowed long

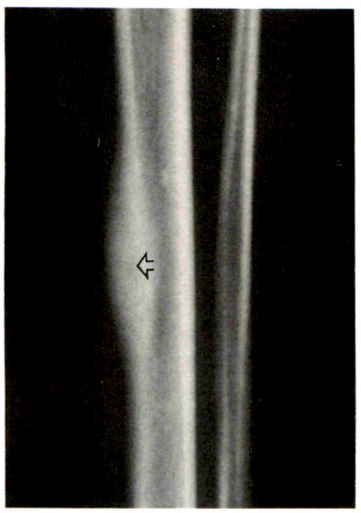


Fig. 11.—Osteoid osteoma. Frontal radiograph shows fusiform swelling of distal medial aspect of tibia. Extent of involvement is greater than that seen in a typical stress fracture. Central nidus (*arrow*) is faint. Compare with Fig. 5.

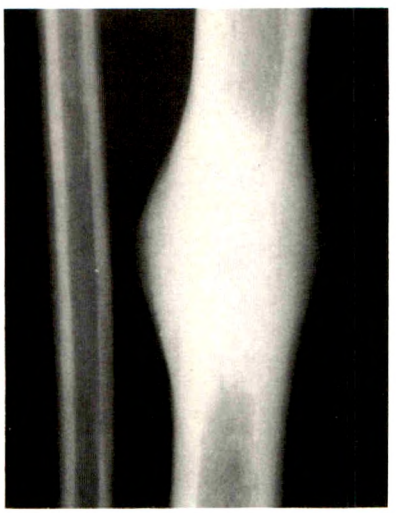


Fig. 12.—Sclerosing osteomyelitis. Frontal radiograph shows intense sclerosis involving both sides of midshaft of tibia and faint lucent nidus of infection centrally.

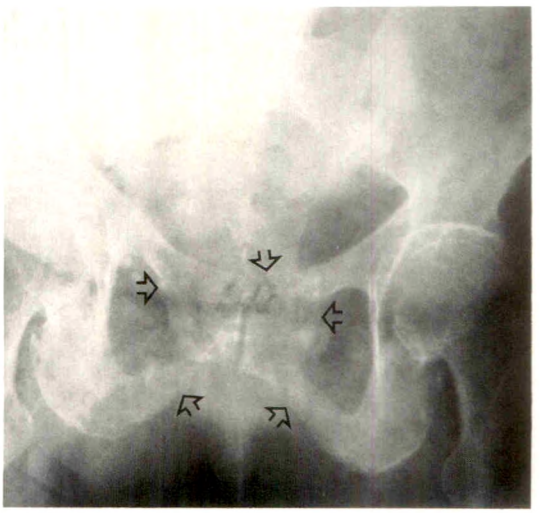


Fig. 13.—Radiograph shows pelvic insufficiency fractures (*arrows*) resembling malignant destruction of pubic bone. Multiplicity and symmetry of lesions in this woman with osteoporosis should suggest diagnosis.

bones. Most of these patients have chronic renal disease. In 1934, Milkman [64] believed he was describing a new disease when he published a report of a case of osteomalacia with "multiple" spontaneous idiopathic symmetric fractures. We now know these are insufficiency fractures.

Insufficiency fractures of the sacrum and pelvis may be confused with metastatic lesions, especially if bony resorption occurs at the fracture ends [23, 26, 66] (Fig. 13). Quite often, these injuries occur in patients with known malignant disease who have a sudden onset of pain in the lower back, hip, or groin. They may occur with normal activities such as walking. Often MR is the first imaging study ordered, and the findings may mislead the radiologist and clinician into thinking the changes are due to metastases.

Osteogenic sarcoma (and occasionally Ewing's tumor) is often included in the differential diagnosis of stress fractures, particularly in children or adolescents [67, 68]. The appearance of these neoplasms are usually sufficiently characteristic, but they should not be confused with a stress fracture. Osteogenic sarcomas are generally located within the metaphysis of the involved bone. The lytic pattern is generally of the moth-eaten variety. Periosteal reaction, when present, is that of an aggressive lesion and consists of spiculation; thin, irregular laminations; and, occasionally, Codman's triangles. These lesions do not change in a short time. The lytic destructive appearance of Ewing's tumor, particularly in the diaphysis of the long bones, should be sufficient to convince the observer of the correct diagnosis.

If a stress fracture is suspected, but imaging studies do not show an abnormality, radiographs should be obtained again in 1–2 weeks. Tomography and, occasionally, CT may be necessary to establish the diagnosis. Once the patient ceases the activity that produces the injury, evidence of healing within 1–2 weeks is sufficient to establish the proper diagnosis. In most instances, a delay of that short a time will not be detrimental. Biopsies should be avoided until radiographs clearly show that no healing has occurred, suggesting that a lesion other than stress fracture may be present.

REFERENCES

1. Devas MB. *Stress fractures*. London: Churchill Livingstone, **1975**
2. Daffner RH. Stress fractures: current concepts. *Skeletal Radiol* **1978**;2:221–229
3. Matheson GO, Clement DB, McKenzie DC, Taunton JE, Lloyd-Smith DR, MacIntyre JG. Stress fractures in athletes: a study of 320 cases. *Am J Sports Med* **1987**;15:46–58
4. Czarnecki DJ, Till EW, Minikel JL. Unique sacral stress fracture in a runner (letter). *AJR* **1988**;151:1255
5. Daffner RH, Martinez S, Gehweiler JA Jr, Harrelson JM. Stress fractures of the proximal tibia in runners. *Radiology* **1982**;142:63–65
6. Goergen TG, Venn-Watson EA, Rossman DJ, Resnick D, Gerber KH. Tarsal navicular stress fractures in runners. *AJR* **1981**;136:201–203
7. Pavlov H, Torg JS, Hersh A, Freiberger RH. The roentgen examination of runner's injuries. *RadioGraphics* **1981**;1:17–34
8. Pavlov H, Torg JS, Freiberger RH. Tarsal navicular stress fractures: radiographic evaluation. *Radiology* **1983**;148:641–645
9. Shelbourne KD, Fisher DA, Rettig AC, McCarroll JR. Stress fractures of the medial malleolus. *Am J Sports Med* **1988**;16:60–63
10. Tanabe S, Nakahira J, Bando E, Yamaguchi H, Miyamoto H, Yamamoto A. Fatigue fracture of the ulna occurring in pitchers of fast-pitch softball. *Am J Sports Med* **1991**;19:317–321
11. Wilson ES, Katz FN. Stress fractures: an analysis of 250 consecutive cases. *Radiology* **1969**;92:481–486
12. Pentecost RL, Murray RA, Brindley HH. Fatigue, insufficiency, and pathologic fractures. *JAMA* **1964**;187:1001–1004
13. Devas MB. Stress fractures of the tibia in athletes or "shin soreness." *J Bone Joint Surg [Br]* **1958**;40-B:227–239
14. Devas MB. Longitudinal stress fractures: another variety seen in long bones. *J Bone Joint Surg [Br]* **1960**;42-B:508–514
15. Towne LC, Blazina ME, Cozen LN. Fatigue fracture of the tarsal navicular. *J Bone Joint Surg [Am]* **1970**;52-A:376–378
16. Schneider HJ, King AY, Bronson JL, Miller EH. Stress injury and developmental change of lower extremities in ballet dancers. *Radiology*

1974;113:627–632
17. Daffner RH. Anterior tibial striations. *AJR* **1984**;143:651–653
18. Micheli LJ, Sohn RS, Solomon R. Stress fractures of the second metatarsal involving Lisfranc's joint in ballet dancers. *J Bone Joint Surg [Am]* **1985**;67-A:1372–1375
19. Hoang T-A, Nguyen TH, Daffner RH, Lupetin AR, Deeb ZL. Case report 491: stress fracture of the right sacrum. *Skeletal Radiol* **1988**;17:364–367
20. Ford LT, Gilula LA. Stress fractures of the middle metatarsals following the Keller operation. *J Bone Joint Surg [Am]* **1977**;59-A:117–118
21. Satku K, Kumar VP, Chacha PB. Stress fracture around the knee in elderly patients: a cause of acute pain in the knee. *J Bone Joint Surg [Am]* **1990**;72-A:918–922
22. Manco LG, Schneider R, Pavlov H. Insufficiency fractures of the tibial plateau. *AJR* **1983**;140:1211–1215
23. Casey D, Mirra J, Staple TW. Parasymphyseal insufficiency fractures of the os pubis. *AJR* **1984**;142:581–586
24. Cooper KL, Beabout JW, Swee RG. Insufficiency fractures of the sacrum. *Radiology* **1985**;156:15–20
25. Lourie H. Spontaneous osteoporotic fracture of the sacrum: an unrecognized syndrome of the elderly. *JAMA* **1982**;248:715–717
26. DeSmet AA, Neff JR. Pubic and sacral insufficiency fractures: clinical course and radiologic findings. *AJR* **1985**;145:601–606
27. Rawlings CE III, Wilkins RH, Martinez S, Wilkinson RH Jr. Osteoporotic sacral fractures: a clinical study. *Neurosurgery* **1988**;22:72–76
28. Miller B, Markheim HR, Towbin MN. Multiple stress fractures in rheumatoid arthritis. *J Bone Joint Surg [Am]* **1967**;49-A:1408–1414
29. Schneider R, Kaye JJ. Insufficiency and stress fractures of the long bones occurring in patients with rheumatoid arthritis. *Radiology* **1975**;116:595–600
30. Rappoport AS, Sosman JL, Weissman BN. Spontaneous fractures of the olecranon process in rheumatoid arthritis. *Radiology* **1976**;119:83–84
31. Kathol MH, El-Khoury GY, Moore TE, Marsh JL. Calcaneal insufficiency avulsion fractures in patients with diabetes mellitus. *Radiology* **1991**;180:725–729
32. Zlatkin MB, Bjorkengren A, Sartoris D, Resnick D. Stress fractures of the distal tibia and calcaneus subsequent to acute fractures of the tibia and fibula. *AJR* **1987**;149:329–332
33. Schultz E. Case report 624: stress fracture of distal portion of tibia associated with previously incurred gross fracture of more proximal segment of tibia. *Skeletal Radiol* **1990**;19:391–393
34. Brooks DB, Burstein AH, Frankel WH. The biomechanics of torsional fractures: the stress concentration of a drill hole. *J Bone Joint Surg [Am]* **1970**;52-A:507–514
35. Danon G, Pokrassa M. An unusual complication of the Keller bunionectomy: spontaneous stress fractures of all lesser metatarsals. *J Foot Surg* **1989**;28:335–339
36. Crotty JG, Berlin SJ, Donick II. Stress fracture of the first metatarsal after Keller bunionectomy. *J Foot Surg* **1989**;28:516–520
37. Jones HH, Priest JD, Hayes WC, Tichenor CC, Nagel DA. Humeral hypertrophy in response to exercise. *J Bone Joint Surg [Am]* **1977**;59-A:204–208
38. Kuusela T, Kurri J, Virtama P. Stress response of the tibial cortex: a longitudinal radiographic study. *Ann Clin Res* **1984**;16[suppl 40]:14–16
39. Chamay A, Tschants P. Mechanical influence in bone remodeling: experimental research on Wolff's law. *J Biomech* **1972**;5:173–180
40. Wright TM, Hayes WC. The fracture mechanics of fatigue crack propagation in compact bone. *J Biomed Mater Res* **1976**;7:637–648
41. Carter DR, Caler WE. Cycle-dependent and time-dependent bone fracture with repeated loading. *J Biomech Eng* **1983**;105:166–170
42. Savoca CL. Stress fractures: a classification of the earliest radiographic signs. *Radiology* **1971**;100:519–524
43. Geslien GE, Thrall JH, Espinosa JL, Older RA. Early detection of stress fractures using 99m Tc-polyphosphate. *Radiology* **1976**;121:683–687
44. Wilcox JR, Moniot AL, Green JP. Bone scanning in the evaluation of exercise related stress injuries. *Radiology* **1977**;123:699–703
45. Roub LW, Gumerman LW, Hanley EN Jr, Clark MW, Goodman M, Herbert DL. Bone stress: a radionuclide imaging perspective. *Radiology* **1979**;132:431–438
46. Bellah RD, Summerville DA, Treves ST, Micheli LJ. Low-back pain in adolescent athletes: detection of stress injury to the pars interarticularis with SPECT. *Radiology* **1991**;180:509–512
47. Norfray JF, Schlachter L, Kernahan WT Jr, et al. Early confirmation of stress fractures in joggers. *JAMA* **1980**;243:1647–1649
48. Schneider R, Yacovone J, Ghelman B. Unsuspected sacral fractures: detection by radionuclide bone scanning. *AJR* **1985**;144:337–341
49. Ries T. Detection of osteoporotic sacral fractures with radionuclides. *Radiology* **1983**;146:783–785
50. Milgrom C, Chisin R, Giladi M, et al. Negative bone scans in impending tibial stress fractures. *Am J Sports Med* **1984**;12:488–491
51. Murcia M, Brennan RE, Edeiken J. Computed tomography of stress fracture. *Skeletal Radiol* **1982**;8:193–198
52. Allen GJ. Longitudinal stress fractures of the tibia: diagnosis with CT. *Radiology* **1988**;167:799–801
53. Stroebel RJ, Ginzburg WW, McLeod RA. Sacral insufficiency fractures: an often unsuspected cause of low back pain. *J Rheumatol* **1991**;18:117–119
54. Stafford SA, Rosenthal DI, Gebhardt MC, Brady TJ, Scott JA. MRI in stress fracture. *AJR* **1986**;147:553–556
55. Lee JK, Yao L. Stress fractures: MR imaging. *Radiology* **1988**;169:217–220
56. Deutsch AL, Mink JH, Waxman AD. MR imaging of occult fractures of the proximal femur. *Radiology* **1989**;170:113–116
57. Deutsch AL, Mink JH. Magnetic resonance imaging of musculoskeletal injuries. *Radiol Clin North Am* **1989**;27:983–1002
58. Mink JH, Deutsch AL. Occult osseous and cartilaginous injuries about the knee: MR assessment, detection, and classification. *Radiology* **1989**;170:823–829
59. Brahme SK, Cervilla V, Vint V, Cooper K, Kortman K, Resnick D. Magnetic resonance appearance of sacral insufficiency fractures. *Skeletal Radiol* **1990**;19:489–493
60. Laroche M, Rousseau H, Jacquemier J-M, Joffre F, Arlet J, Mazieres B. Unusual stress fracture on the roof of the acetabulum: magnetic resonance imaging. *J Rheumatol* **1991**;18:115–116
61. Meyers SP, Wiener SN. Magnetic resonance imaging features of fractures using the short tau inversion recovery (STIR) sequence: correlation with radiographic findings. *Skeletal Radiol* **1991**;20:499–507
62. Alarcon GS, Sanders C, Daniel WW. Transient osteoporosis of the hip: magnetic resonance imaging. *J Rheumatol* **1987**;14:1184–1189
63. Bloem JL. Transient osteoporosis of the hip: MR imaging. *Radiology* **1988**;167:753–755
64. Milkman LA. Multiple spontaneous idiopathic symmetrical fractures. *AJR* **1934**;32:622–634
65. North KAK. Multiple stress fractures simulating osteomalacia. *AJR* **1966**;97:672–679
66. Goergen TG, Resnick D, Riley RR. Posttraumatic abnormalities of the pubic bone simulating malignancy. *Radiology* **1978**;126:85–87
67. Davies AM, Carter SR, Grimer RJ, Sneath RS. Fatigue fractures of the femoral diaphysis in the skeletally immature simulating malignancy. *Br J Radiol* **1989**;61:893–896
68. Horev G, Korenreich NZ, Grunebaum M. The enigma of stress fractures in the pediatric age: clarification or confusion through the new imaging modalities. *Pediatr Radiol* **1990**;20:469–471

Review Article

Infertility in Women: Diagnostic Evaluation with Hysterosalpingography and Other Imaging Techniques

Susan Krysiewicz[1]

This article examines the current roles of hysterosalpingography and other imaging studies used in the diagnostic assessment and treatment of infertility in women. The advantages and limitations of hysterosalpingography, transabdominal or transvaginal sonography, and MR imaging in detecting abnormalities of the uterus (congenital anomalies, intrauterine adhesions, myometrial and endometrial derangements) and tubal and peritubal disease are presented. The use of sonography to evaluate cyclical endometrial changes, to assess development of the follicle and corpus luteum, to determine whether ovulation has occurred, and to detect dysfunctional ovulatory dynamics is described, as is the role of this technique in improving the prognostic value of the postcoital test for assessing the quality of cervical mucus. With the development and availability of newer and improved methods for the treatment of infertility disorders in women, comprehensive and detailed evaluation to determine the precise underlying cause or causes of the infertility is important to allow formulation of the most appropriate therapeutic plan. With careful and thorough assessment, the cause of infertility can be identified in 90–95% of couples evaluated.

Infertility is defined as failure to conceive after 1 year during which no contraception is used. This definition is derived from a demonstrated fecundability or conception rate (i.e., percentage of women attaining pregnancy) of 20–25% per cycle, which results in approximately 94% of couples who are having regular unprotected intercourse conceiving by the end of 1 year. Infertility is estimated to occur in 10–15% of couples; the prevalence has increased in the last decade or so, in large part because of an increase in sexually transmitted diseases resulting in pelvic inflammatory disease and because of an increasing tendency to delay childbearing [1–4].

Considerable progress has been made in the understanding of reproductive physiology and in the development of newer and increasingly sophisticated methods to treat infertility. This has resulted in increasing numbers of couples seeking evaluation of their infertility. Because of the significant role of imaging techniques in this assessment, the radiologist must understand the use of imaging in the diagnosis and management of infertility in women.

Causes of Infertility

Many things affect fertility: the patient's age (maximum reproductive ability for a woman occurs between ages 21 and 24), frequency of coitus (more frequent intercourse leads to higher conception rates), duration of infertility (fecundability declines as the duration of the infertility increases, irrespective of age or coital frequency), certain drugs and medications, and nutritional and emotional factors [2, 4, 5].

Any infertility evaluation should begin with a complete history and physical examination of both partners. The following six factors should then be assessed, because they are responsible for most of the basic underlying causes of infertility: (1) male factor, (2) cervical factor, (3) endometrial-uterine factor, (4) tubal factor, (5) peritoneal factor, and (6) ovulatory factor [1, 2, 4, 5]. The distribution of the different causes will vary among centers, partly because of differences in the referral populations (Table 1). Also, in a significant number of patients, infertility will have multiple causes, and thus every couple must have a complete evaluation even if one problem area is readily identified.

Received August 7, 1991; accepted after revision February 25, 1992.
[1]Department of Radiology, Beth Israel Medical Center, 1st Ave. at 16th St., New York, NY 10003. Address reprint requests to S. Krysiewicz.

 0361–803X/92/1592–0253 © American Roentgen Ray Society

TABLE 1: Factors Responsible for Infertility

Factor	Estimated Percentage of Cases
Male	20–50
Cervical	5–10
Endometrial-uterine	2–5
Tubal	
As a single cause	10
As a contributing cause	25–40
Peritoneal	20–25
Ovulatory	10–20
Other	5–10

Diagnostic Evaluation of Infertility in Women

For each potential cause of infertility, a different set of diagnostic procedures is appropriate (Table 2).

Cervical Factor

The cervical factor with respect to fertility relates to the physical and chemical properties of cervical mucus that promote and maintain sperm penetrability and survival. The interaction between sperm and cervical mucus is evaluated by using the "postcoital test," in which the cervical mucus is evaluated 6–8 hr after intercourse to assess whether the number of motile spermatozoa is adequate. This test is done as close as possible to ovulation, when the mucus should have its optimal physical and chemical properties for penetration and survival of sperm. A persistently negative (abnormal) test result indicates an abnormality of the cervical mucus or oligoasthenospermia.

The most common cause of a negative test result is inappropriate timing [1, 2]. Because timing of ovulation by clinical determinants such as basal body temperature can be somewhat inaccurate, sonography has been advocated to monitor development of ovarian follicles and to detect ovulation, increasing the reliability and value of the postcoital test. Use of sonography in this way reduces the number of false-negative and false-positive results and adds an element of standardization to the procedure [6–8].

Endometrial-Uterine Factor

The endometrial-uterine factor refers to the function the uterus plays in the reproductive process. This includes transport of sperm, implantation and gestation of the embryo, and parturition. Uterine contractions help disperse sperm in the uterine cavity and transport them to the oviduct. Implantation requires an endometrium that is physiologically conditioned and hospitable for the fertilized oocyte. After implantation, the uterus must then foster the growth and development of the fetus. Anatomic abnormalities of the uterus such as congenital anomalies, intrauterine adhesions, and other myometrial abnormalities (e.g., myomata) or endometrial derangements (e.g., endometritis, underdeveloped or out-of-phase endometrium as present in luteal phase defects) may interfere with the normal function of the uterus. Diagnostic approaches to evaluate uterine-endometrial factors include endometrial sampling, hysteroscopy, hysterosalpingography, sonography, and MR imaging.

Intrauterine synechiae most often are caused by infection and trauma, such as dilatation and curettage in the recently pregnant uterus, and are seen only rarely after diagnostic dilatation and curettage or myomectomy [1–3, 5]. The adhesions partially or completely obliterate the endometrial cavity or can even obstruct the cervical canal. The infertility is attributed to an unfavorable endometrium for sperm migration and embryo implantation. Intrauterine adhesions can be diagnosed at hysteroscopy or on the basis of the characteristic findings of irregular, serpiginous, and angular filling defects within the endometrial cavity on hysterosalpingograms (Fig. 1). Synechiae may occasionally be seen as echogenic, serpiginous endometrial bridges on transvaginal sonograms, although no published reports have systematically compared the limitations and advantages of these two techniques. At present, sonography is not used to detect and determine the extent of adhesions.

The precise mechanism by which leiomyomas cause infer-

TABLE 2: Diagnostic Procedures for Evaluation of the Infertile Woman

Factor	Procedure
Cervical	Postcoital test
Endometrial-uterine	Hysterosalpingography
	Sonography
	MR imaging
	Hysteroscopy/laparoscopy
Tubal	Hysterosalpingography
	Color Doppler sonography with transcervical injection of echocontrast material
	Laparoscopy/chromopertubation
Peritoneal	Hysterosalpingography
	Sonography
	MR imaging
	Laparoscopy
Ovulatory	Clinical assessment/endocrine studies
	Sonography
	Endometrial biopsy

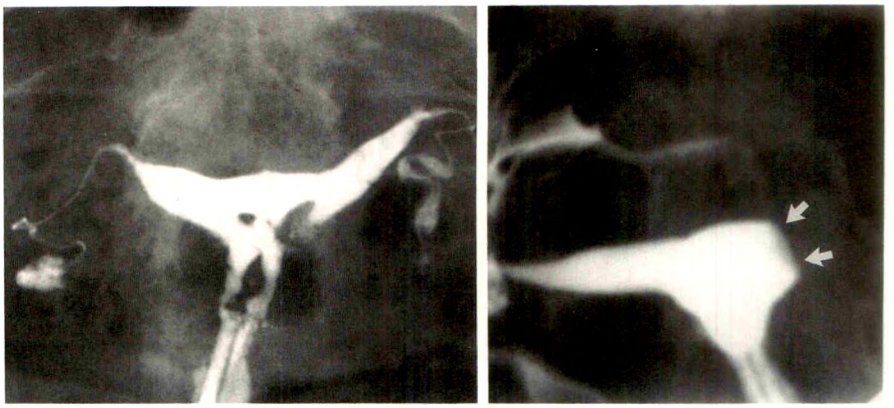


Fig. 1.—Hysterosalpingogram shows characteristic filling defects of intrauterine adhesions.

Fig. 2.—Hysterosalpingogram shows a leiomyoma (*arrows*) that has occluded intramural portion of left fallopian tube.

1 2

tility is not known. It is speculated that interference with reproductive capability is most likely a function of the size and location of these tumors. They can impair the patency of the reproductive tract by occluding the cervical canal or the intramural portion of the fallopian tubes (Fig. 2). They can distort the isthmic or ampullary portions of the oviduct and interfere with the relationship of this structure to the ovary, causing changes in oocyte transport (Fig. 3). Additionally, the enlarged and distorted uterus may result in poor transport of sperm [1–4].

Although uterine myomata can be detected on pelvic examination or by hysterosalpingography and sonography, small lesions can be missed with any of these methods, and additionally, precise localization of these tumors is difficult. It should nevertheless be remembered that the detection of small fibroids is only significant clinically for those lesions that impinge on the endometrium or alter tubal transit and affect fertility.

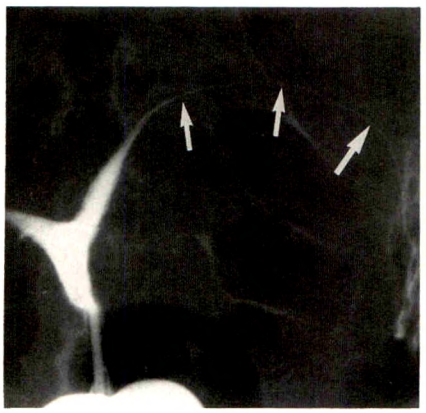
On hysterosalpingograms, leiomyomas, unless calcified, can be detected only when they enlarge and distort the uterine cavity. Subserosal myomata are frequently inapparent unless they result in obvious displacement of the uterus or tubal structures. Although enlargement of the uterine cavity, as may result from intramural myomas, is a reliable sign of the presence of these tumors, without accompanying filling defects in the uterine cavity, no indication of the location of the lesions is apparent. Although submucosal myomas produce filling defects on the endometrial contour, occasionally the defects may be obscured by introduction of larger amounts of contrast material, so early films are often diagnostically important.

Sonography provides a rapid and easy means to screen for the presence of uterine leiomyomata. The characteristic findings are uterine enlargement, contour abnormalities, and focal masses with an echogenicity different from that of the normal myometrium (Fig. 4). Nonetheless, small tumors or lesions that have only minimal differences in echogenicity from normal tissue can be missed on sonograms. Additionally, patient and technical factors may result in a suboptimal study. Transvaginal sonography is generally better than transabdominal sonography for the detection and localization of myomata [9]; however, MR imaging is currently the most accurate imaging technique available for this purpose. Small lesions are detected more often with MR imaging, and this technique is more sensitive and accurate than either sonography or hysterosalpingography in showing which uterine segments are involved with these tumors. Dudiak et al. [10], in a limited series comparing the findings on MR imaging, sonography, and hysterosalpingography with surgical and histological findings, reported an 85% sensitivity and 94% accuracy for MR imaging for detecting and localizing uterine myomata, vs a 69% sensitivity and 87% accuracy for sonography. When comparing MR imaging with hysterosalpingography, the sensitivity was 91% and the accuracy was 96% for MR imaging vs 18% sensitivity and 72% accuracy for hysterosalpingography. The specificities of the three imaging techniques were not shown to be significantly different; they were 100%, 97%, and 98% for MR imaging, sonography, and hysterosalpingography, respectively [10].

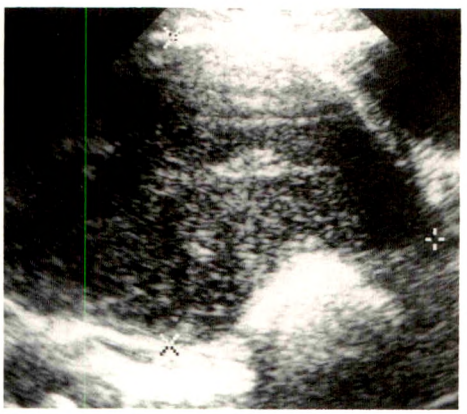
On MR images, although the relative signal intensity of leiomyomata can vary, most uncomplicated lesions have low signal intensity relative to normal myometrium on T2-weighted images. T1-weighted images are usually not as useful as T2-weighted images are for either the detection or the delineation of these tumors.

Because leiomyomas alone are rarely the primary cause of infertility, before myomatous disease is considered as a source of the patient's infertility, a complete evaluation of the infertile couple is always necessary to exclude other factors that may result in reproductive failure [1–4]. Should it be suspected after the infertility evaluation that uterine myomata are indeed the primary source of the infertility, and myomectomy is indicated, MR imaging is recommended for preoperative surgical planning to determine which uterine segments are involved, because of its superior accuracy in this regard and its excellent depiction of anatomic relationships [10].

Congenital uterine malformations are rarely the primary cause of infertility; however, approximately 20% of recurrent abortions are reportedly due to such developmental defects [1, 4]. Spontaneous abortion is more often associated with unicornuate, bicornuate, and septate uteri, but not arcuate or didelphic uteri. Septate uteri have the highest prevalence of habitual abortion; vascular deficiencies in the septum here are implicated as the cause of early fetal wastage [2–4].



3



4

Fig. 3.—Hysterosalpingogram shows displacement and draping of left fallopian tube (*arrows*) over subserosal fibroid.

Fig. 4.—Longitudinal sonogram shows enlarged, lobulated, inhomogeneous uterus characteristic of leiomyomatous disease. Although the exact mechanism by which fibroids cause reproductive failure is not known, it is postulated that in a case such as this, lesions can enlarge and distort the uterine cavity, which may impair sperm transport; they may distort the oviduct and interfere with normal oocyte migration; and large myomata may impair endometrial vascularity, which could adversely affect implantation. Because leiomyomata rarely are the primary cause of a patient's infertility, other causes must be fully investigated and excluded before myomectomy is considered.

Although uterine malformations may be suspected on the basis of history and physical examination, further evaluation is needed to determine the diagnosis precisely. Hysterosalpingography, sonography, MR imaging, and laparoscopy are techniques used to detect the various anomalies. Although hysterosalpingography is frequently used to determine the presence of congenital defects, a major drawback is its inability to show the external morphology of the uterus. Thus, for example, it may be difficult by hysterosalpingography alone to distinguish a bicornuate uterus from a septate or subseptate uterus. Visualization of the external contour can help in making this distinction, because a bicornuate uterus has a bilobed fundal configuration, whereas a septate uterus has a normal appearance. Nonetheless, on hysterosalpingograms, the presence of two uterine horns with convex lateral margins and wide separation between the horns (obtuse intercornual angle) suggests a bicornuate uterus, whereas two cavities with an angle of less than 75% between them suggest a septate or subseptate uterus [3, 5, 11–13] (Fig. 5). However, the ranges of intercornual angles for these two entities overlap somewhat, contributing to errors in diagnosis and resulting in a diagnostic accuracy of only roughly 55% [5, 12]. Additionally, noncommunicating uterine cavities or horns are not opacified during hysterosalpingography and are thus underdiagnosed when this procedure is used.

For visualization of the external uterine contour, various cross-sectional imaging studies can be used (Fig. 6). Sonography, for example, allows visualization of the external uterine contour, and combining the results of sonography and hysterosalpingography can improve the diagnostic accuracy in defining uterine anomalies to about 90% [12, 13]. Nonetheless, sonography has its diagnostic limitations. Myomata and adnexal masses can be confused with a duplicated uterine horn, an intrauterine septum can be missed, and in certain cases, physical and technical considerations limit the clear delineation of the external uterine configuration [3, 11, 13, 14]. Transvaginal sonography may be better for delineating external uterine contour and detecting such anomalies, although its precise diagnostic accuracy in this regard has not been determined [11].

Preliminary data suggest that MR imaging is currently the most accurate technique for the diagnosis of uterine congenital malformations [11, 13, 15]. T2-weighted spin-echo images generally have been shown to delineate normal uterine anatomy best, with the optimal imaging plane determined by individual uterine orientation, although transverse and coronal sections tend to be most helpful. MR imaging, for example, can be used to distinguish a septate from a bicornuate uterus. A bicornuate uterus is seen on T2-weighted images as two high-signal-intensity endometrial regions, each of which is surrounded by a low-signal juctional zone. In turn, each junctional zone is surrounded and separated by a medium-signal myometrial band (Fig. 7). In a septate uterus, the medium-signal myometrium is not present between the two cavities, and thus only a low-intensity zone is seen between the structures. Fibrous tissue, which primarily composes the septum, contributes most to the low signal [11, 14, 15]. Certain diagnostic difficulties may still be encountered with MR imaging (e.g., the differentiation of a duplicated cervix from a low septum), and thus clinical correlation remains important for the accurate interpretation of these studies [11].

Uterine malformations must be diagnosed accurately so that appropriate treatment is instituted and unnecessary surgery is avoided. In certain cases, laparoscopy for evaluation of the uterine configuration may be needed for a definitive diagnosis, although MR imaging may eventually replace this procedure [12, 14].

Tubal Factor

Tubal factors are a contributing cause of infertility in 25–40% of patients [1, 16–18]. Infection, endometriosis, and fibrotic reaction can all lead to tubal damage and occlusion, which interfere with the normal transport of the ovum to the uterine cavity.

Hysterosalpingography is important in the diagnostic evaluation of tubal factors because it provides information about internal tubal architecture and tubal patency. For example, salpingitis isthmica nodosa can be readily diagnosed on the basis of hysterosalpingographic findings, namely, by showing multiple irregular tubal diverticula (Fig. 8). It is thought to be the result of either pelvic inflammatory disease or tubal endo-

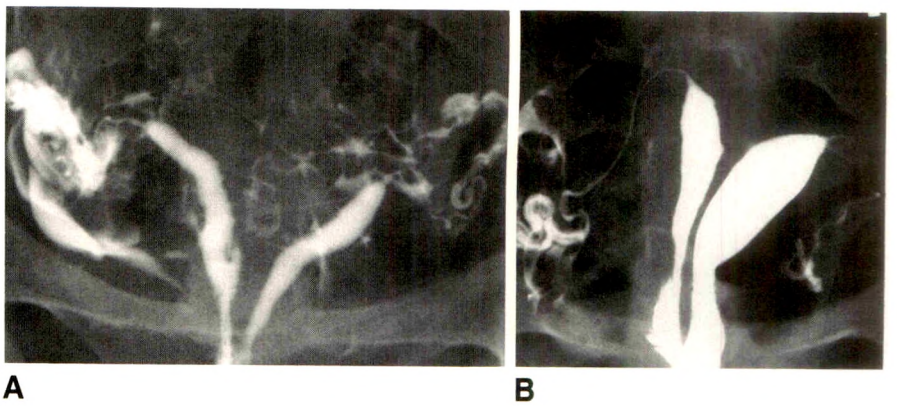


Fig. 5.—*A* and *B*, Hysterosalpingograms show bicornuate (*A*) and septate (*B*) uteri. Note obtuse intercornual angle of bicornuate uterus vs acute angle of septate uterus.

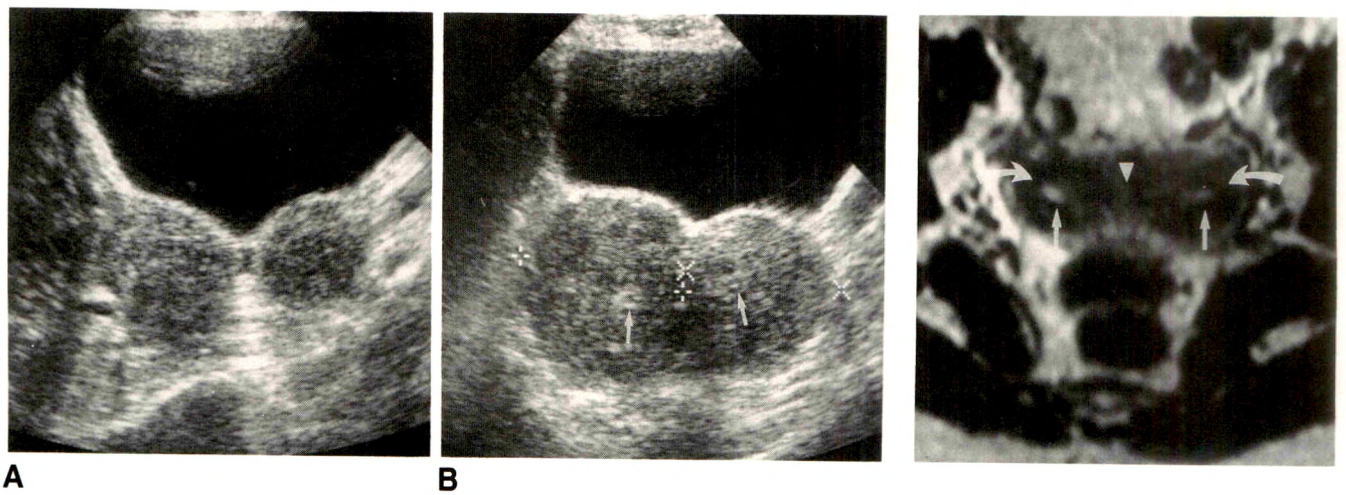


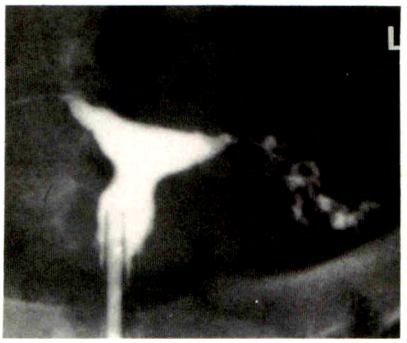
Fig. 6.—*A* and *B*, Transverse sonograms through uterine fundus (*A*) and through uterine body of a bicornuate uterus (*B*) show bilobed external uterine contour and two endometrial cavities (*arrows*).

Fig. 7.—T2-weighted axial MR image through bicornuate uterus shows two endometrial cavities (*straight arrows*) surrounded by low-signal junctional zones (*curved arrows*), which are then surrounded and separated by myometrium (*arrowhead*). A septate uterus would lack medium-signal myometrial band between endometrial cavities.

metriosis and is associated with a high rate of infertility (approximately 37%) and ectopic pregnancy (approximately 9%) [3].

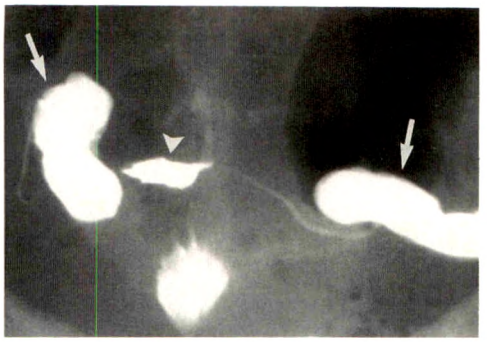
Tubal occlusion also is primarily due to the consequences of pelvic inflammatory disease and endometriosis. A few cases are the result of adhesions from previous surgery, and fewer still are due to obstructing lesions such as myomata. Tubal obstruction can be readily diagnosed during hysterosalpingography when no free intraperitoneal spillage of contrast material is seen. Although tubal occlusion with normal-appearing tubes may occasionally occur with peritubular disease, most often dilatation of the ampullary portions of the tubes (hydrosalpinx) without free spillage is seen (Fig. 9). If a proximal tubular obstruction is shown, selective salpingography can be used to deliver contrast material directly into the fallopian tube behind the occlusion to delineate the distal anatomy [3, 16, 17]. Finally, great care should always be exercised to avoid diagnosing tubal blockage on the basis of findings on a hysterogram when spasm results in false-positive obstruction. Spasm is most frequently related to pain during the examination and should be suspected when the proximal portion of a tube is occluded. A gentle technique should always be used, and delayed films should be obtained to rule out this possibility. Currently, none of the various available antispasmodic medications has been reliably shown to diminish or reverse such tubal spasm [3].

Although hysterosalpingography is the study most commonly used to show tubal patency, other techniques have been used. These include visualizing fluid in the cul-de-sac after transcervical injection of fluid during sonographic examination [19] and detecting radionuclide in the peritoneal cavity after the radionuclide is placed in the vaginal fornix ("radionuclide hysterogram") [20]. Neither of these methods can be used to show intratubal anatomy, and furthermore, they ultimately can be used only to predict unilateral tubal patency. Imaging of flow within the fallopian tubes with color



8

Fig. 8.—Hysterosalpingogram shows left tubal diverticula diagnostic of salpingitis isthmica nodosa.



9

Fig. 9.—Delayed view from a hysterosalpingogram shows bilateral hydrosalpinx (*arrows*). Endometrial cavity has only a small amount of residual contrast material (*arrowhead*).

Doppler sonography after transcervical injection of saline or an echocontrast agent has been reported recently with promising results [21–23]. Schlief and Deichert [22] found a sensitivity of approximately 92% and a specificity of 100% when comparing color Doppler sonography with hysterosalpingography and laparoscopy for detecting tubal patency. Peters and Coulam [23] showed an 81% sensitivity and 94% specificity of this technique when comparing the results with those of chromopertubation at laparoscopy. Overall agreement of the sonographic results with observations at laparoscopy was 86% vs 71% agreement between the results of hysterosalpingography and those of chromopertubation at laparoscopy. This difference, however, was not statistically significant [23]. The sensitivity and specificity for hysterosalpingography in their study were 65% and 82%, respectively. Agreement in the observations found at hysterosalpingography and laparoscopic chromopertubation have been reported to be on the order of 55–70% [22]. These data suggest that color Doppler sonography after injection of saline or an echocontrast agent is comparable to hysterosalpingography for detecting patency of the fallopian tubes and correlates well with laparoscopic findings. Because this technique does not require use of ionizing radiation or iodinated contrast material, it may eventually replace hysterosalpingography as the screening method to detect tubal occlusion. Further investigation, however, is still needed before the place of such examinations in an infertility work-up can be established [21–23].

In the past, definitive diagnosis and treatment of tubal occlusion had required laparoscopy or laparotomy with tubal reconstruction. Currently, selective salpingography and fluoroscopically guided procedures for fallopian tube recanalization are emerging as the initial interventional procedures for patients with proximal tubal occlusions, with success rates for overcoming the obstruction and showing distal tubal anatomy on the order of 76–95% [16, 17]. Tubal reocclusion rates have been estimated at 15–30% and ectopic pregnancy rates at 10% after such procedures [17]. It should be noted, however, that large-scale randomized controlled studies comparing fluoroscopic tubal recanalization with microsurgical techniques have not been published. Nonetheless, because of its proved success and because this procedure results in less morbidity than tubal microsurgery does, it is recommended as the initial therapy for patients with proximal tubal occlusion, with the more invasive treatments recommended for those with distal tubular disease and those in whom tubal recanalization is unsuccessful [17].

Peritoneal Factor

The peritoneal factor responsible for infertility relates to the presence of pelvic adhesions from previous infection, endometriosis, or surgery that may cause reproductive failure by interfering with tubal mobility, altering the relationship of the ovary to the tube (interfering with oocyte pickup), and causing tubal occlusion.

With hysterosalpingography, the presence of peritubular adhesions and endometriosis is underdiagnosed, with reported sensitivities ranging from 34% to 75% [3–5, 24]. Peritubular adhesions are suggested if loculated spillage of contrast material in the peritoneal cavity, ampullary dilatation, and a convoluted or vertical fallopian tube are seen [3, 24] (Fig. 10). Nonetheless, it is frequently difficult to distinguish a hydrosalpinx from a peritubular loculation, although the clinical implication of both here is the same.

Sonography, particularly transvaginal sonography, also may allow detection of pelvic adhesions and loculated fluid collections. Adhesions may be suggested by the en masse (aggregate) movement of the organs under investigation when pressure is applied simultaneously by the operator's hand transabdominally and by the probe transvaginally [25].

Patients with endometriosis have a high rate of infertility, reportedly in the range of 30–40% [2]. Endometriosis can be detected sonographically; complex adnexal or cul-de-sac masses (endometriomas) are shown, although cystic or solid endometriomas may be seen (Fig. 11). At times, it may be difficult to distinguish endometriomas from other hemorrhagic ovarian cysts, complex cystic neoplasms, or tuboovarian abscesses, although the clinical history should be helpful. MR imaging also can be used to diagnose endometriomas when the lesions have areas with the signal characteristics of hemorrhage. Just as with sonography, hemorrhagic cysts may be indistinguishable from an individual endometrioma; however, the finding of multiple, complex, hemorrhagic, multiloculated, tethered masses suggests endometriosis [13]. Generalized disease also may be difficult to diagnose accurately because it may produce nonspecific findings such as poor definition

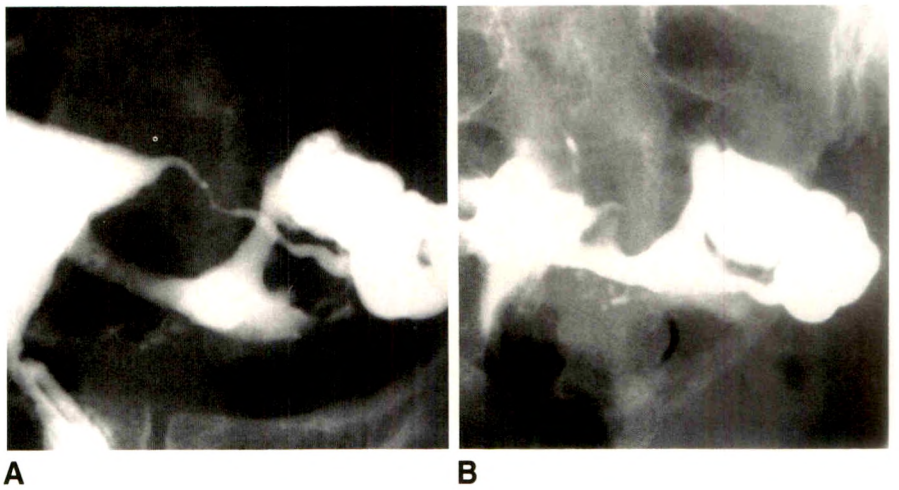


Fig. 10.—*A* and *B*, Filled (*A*) and delayed (*B*) films from hysterosalpingogram show irregular puddles of contrast material in pelvis, which persist unchanged on delayed views. These findings suggest peritoneal adhesions.

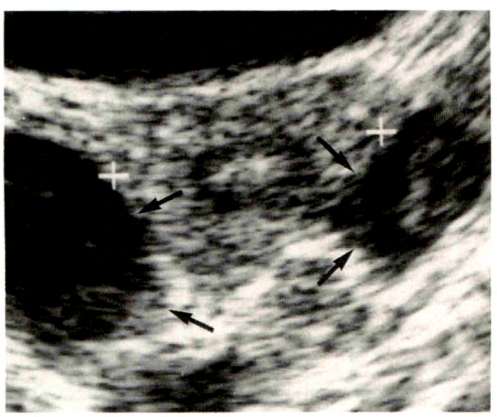


Fig. 11.—Transverse sonogram through pelvis shows bilateral complex adnexal masses (*arrows*) representing endometriomas. Bilateral hemorrhagic ovarian cysts or complex cystic neoplasms and tuboovarian abscesses could have a similar appearance and should be considered in the appropriate clinical situation.

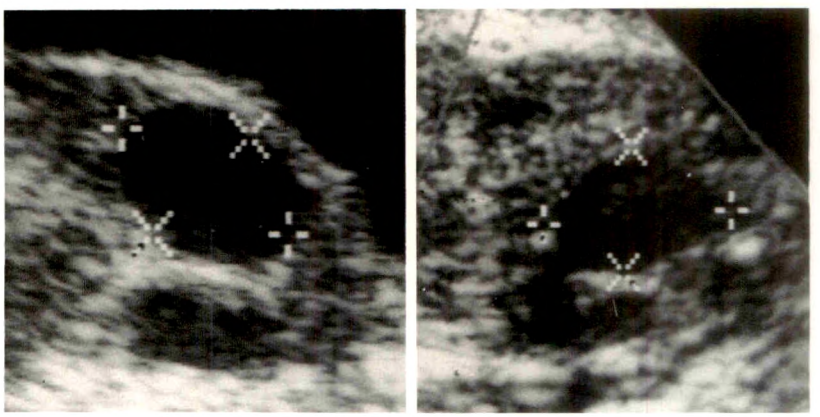


Fig. 12.—*A*, Longitudinal sonogram through an ovary shows a preovulatory follicle 15.2 × 20.3 mm.

B, Follow-up transvaginal sonogram obtained 2 days after *A* shows follicle now has internal echoes and has decreased in size to 6.4 × 9.8 mm. These changes imply ovulation has occurred.

(i.e., obliteration of margins) between pelvic structures and, on sonography, a generalized increase in echogenicity [3, 26].

Although cross-sectional imaging studies may be useful in supporting clinical findings that suggest endometriosis and in providing additional information about intrapelvic structures, they remain primarily ancillary for the diagnosis of endometriosis [18]. It is important to remember that small amounts of abnormal endometrial tissue and adhesions, which are usually not visualized by sonography or MR imaging, may cause infertility. Thus, neither of these techniques is sensitive enough for the diagnosis and staging of endometriosis [14, 26]. Diagnostic laparoscopy remains the gold standard for the visualization and evaluation of adnexal adhesions [24].

Ovulatory Factor

Normal ovarian follicular development, ovulation, and formation of a functional corpus luteum are needed for adequate reproductive function, and these represent the ovulatory factor that must be evaluated in an infertility investigation. Dysfunctional ovulatory dynamics are estimated to be responsible for 10–20% of cases of infertility [1, 2, 4, 27].

Both clinical and sonographic findings can be used to evaluate ovulation. Sonography is a vital tool for monitoring women in whom ovulation is being induced and those undergoing in vitro fertilization. Transabdominal or transvaginal sonography can be used, although the transvaginal approach is generally preferable because of the improved resolution associated with a higher frequency transducer, which can be used in transvaginal sonography because the pelvic structures are closer to the probe. Although the pelvic field of view is limited with the transvaginal approach, this is not a limitation when ovulatory dynamics only are being evaluated, unless anatomy prevents adequate delineation of the structures being examined. Additionally, interference by surrounding bowel loops is less likely than it is with transabdominal

scanning. Nonetheless, sonographic evaluation should be coupled with clinical findings and endocrine studies to provide proper and accurate information on follicular maturation or luteal function [1, 2, 5, 9, 28, 29].

Sonography during the ovarian cycle is used to show (1) growth of follicles, with measurement of their size and number; (2) intrafollicular structures, such as the cumulus oophorus and corpus luteum; and (3) endometrial reaction to follicle growth and to development of the corpus luteum [26, 30]

Sonography is well suited for showing and monitoring physiologic follicular growth (Fig. 12A). Normal follicular growth is linear; the average dimension of the follicle increases 2–3 mm/day [5, 18]. The average dimension of the mature follicle is 18–27 mm, with some differences in the measured size related to different measurement techniques or other factors, such as whether the patient is on an ovulation induction regimen and, if so, which one [5, 18, 26, 30]. For measurement, it is considered best to determine maximum diameter longitudinally and transversely and then use the mean as the index number [5]. In most women, although more than one follicle may appear and enlarge during a cycle, only one typically becomes fully mature and dominant.

For patients on ovulation induction regimens, sonography is important to assess timing of the pharmacologic protocols and to detect complications quickly, such as the premature appearance of several large follicles, which suggests hyperstimulation [5, 26, 31].

Although the oocyte itself cannot be visualized sonographically, the cumulus oophorus occasionally may be shown. The cumulus, the cluster of granulosa cells that contains the oocyte, is visualized as an echogenic, approximately 1-mm, eccentrically located mural protrusion within the follicle [5, 26, 31]. Visualization of the cumulus indicates maturity of the follicle, and it has been reported that its visualization means that ovulation will occur within 36 hr [18, 26, 30]. Still, no reproducible sonographic signs have been definitively shown to predict imminent ovulation reliably [5, 32].

The sonographic indications of ovulation are the sudden collapse of the growing follicle; the development of central echoes within the follicle and/or crenation of the follicular wall, accompanied by a decrease in size of the follicle; and visualization of fluid (not previously seen) in the cul-de-sac (Fig. 12B). Subsequently, with the formation of the corpus luteum, the internal area of the follicle will eventually fill in and become isoechoic with respect to the surrounding ovary [5, 26, 32].

Abnormal follicular dynamics, such as absence of or poor follicular development, rupture of small immature follicles, or continuous enlargement of the follicular cyst, signal ovulatory dysfunction and can be diagnosed on the basis of sonographic findings [25, 27, 29]. Sonography also is used to guide follicular aspiration for oocyte collection and embryo transfer for in vitro fertilization programs, and it may replace laparoscopic techniques for catheterization of the fallopian tube [25, 30, 31, 33].

Changes in the endometrium that occur during the menstrual cycle can be monitored by sonography and used to determine endometrial stage. Transvaginal sonography is particularly suited for this, delineating the endometrial alterations better than transabdominal sonography can [18]. The cyclical morphologic changes that are seen have been well documented and are not detailed here [5, 25, 33–36]. Lack of change in the endometrium, or an endometrial appearance out of phase with changes in the ovary (which may indicate a luteal phase defect when the endometrial response to support implantation is inadequate), may be suggested by sonographic findings and confirmed by hormonal assay and endometrial biopsy [1, 2, 35, 37]. Nonetheless, no morphologic features of the endometrium detectable by sonography can be used to predict whether pregnancy will occur [25, 33].

Conclusion

It is clear that imaging studies contribute greatly to the diagnosis and management of infertility in women. Hysterosalpingography remains the first-line radiologic examination for most women undergoing an infertility investigation. It can show intrauterine synechiae, abnormalities of tubal morphology such as salpingitis isthmica nodosa or hydrosalpinx, and tubal occlusion. Hysterosalpingographic findings may suggest uterine leiomyomas and congenital anomalies, although cross-sectional imaging techniques delineate these derangements better; MR imaging is the most accurate examination for detection and localization of myomata and characterization of congenital malformations. This is clinically important because the location, number, and size of myomata affect the treatment of these lesions, and the correct classification of a developmental abnormality can prevent unnecessary laparoscopy and aid in appropriate surgical management. Sonography plays a vital role in monitoring ovarian follicular development in spontaneous and induced cycles and is invaluable as a guidance procedure in reproductive techniques such as oocyte collection and gamete transfer in in vitro fertilization programs. It also can be used to increase the reliability of the postcoital test for assessing the quality of cervical mucus and to determine occlusion of the fallopian tubes. Although endometriosis can be diagnosed on the basis of findings on sonography or MR imaging, laparoscopy remains the standard for determining the presence and extent of pelvic adhesions, particularly with respect to the diagnosis and staging of endometriosis.

REFERENCES

1. Hammond MG, Talbert LM, eds. *Infertility: practical guide for the physician*, 2nd ed. Oradell, NJ: Medical Economics, **1985**
2. Moghissi K, ed. Current concepts in infertility. *Clin Obstet Gynecol* **1989**;22:9–189
3. Yoder IC. Hysterosalpingography and pelvic ultrasound: imaging in infertility and gynecology. Boston: Little, Brown, **1988**
4. Clark RL, Keefe B. Infertility: imaging of the female. *Urol Radiol* **1989**;11:233–237
5. Winfield AC, Wentz AC. *Diagnostic imaging of infertility*. Baltimore: Williams & Wilkins, **1987**
6. Hamilton CJCM, Evers JLH, de Haan J. Ultrasound increases the prognostic value of the postcoital test. *Gynecol Obstet Invest* **1986**;21:80–88
7. Daly DC, Reuter K, Cohen S, Mastroianni J. Follicle size by ultrasound versus cervical mucus quality: normal and abnormal patterns in spontaneous cycles. *Fertil Steril* **1989**;51:598–603
8. Check JH, Chase JS, Wu C-H, Goldberg BB, Adelson HG, Rankin A.

Diagnosis and treatment of the cervical factor. II. Employment of pelvic sonography in diagnosis. *Int J Fertil* **1986**;31:362–364
9. Mendelson EB, Bohm-Velez M, Joseph N, Neiman HL. Gynecologic imaging: comparison of transabdominal and transvaginal sonography. *Radiology* **1988**;166:321–324
10. Dudiak CM, Turner DA, Patel SK, Archie JT, Silver B, Norusis M. Uterine leiomyomas in the infertile patient: preoperative localization with MR imaging versus US and hysterosalpingography. *Radiology* **1988**;167:627–630
11. Mintz MC, Grumbach K. Imaging of congenital uterine anomalies. *Semin Ultrasound CT MR* **1988**;9:167–174
12. Reuter KL, Daly DC, Cohen SM. Septate versus bicornuate uteri: errors in imaging diagnosis. *Radiology* **1989**;172:749–752
13. McCarthy S. Magnetic resonance imaging in the evaluation of infertile women. *Magn Reson Q* **1990**;6:239–249
14. Carrington BM, Hricak H, Nuruddin RN, Secaf E, Laros RK, Hill EC. Mullerian duct anomalies: MR imaging evaluation. *Radiology* **1990**;176:715–720
15. Mintz MC, Thickman DI, Gussman D, Kressel HY. MR evaluation of uterine anomalies. *AJR* **1987**;148:287–290
16. Kumpe DA, Zwerdlinger SC, Rothbarth LJ, Durham JD, Albrecht BH. Proximal fallopian tube occlusion: diagnosis and treatment with transcervical fallopian tube catheterization. *Radiology* **1990**;177:183–187
17. Thurmond AS. Selective salpingography and fallopian tube recanalization. *AJR* **1991**;156:33–38
18. Blumenfeld Z, Yoffe N, Bronshtein M. Transvaginal sonography in infertility and assisted reproduction. *Obstet Gynecol Surv* **1990**;46:36–49
19. Rasmussen F, Larsen C, Justesen P. Fallopian tube patency demonstrated at ultrasonography. *Acta Radiol* **1986**;27:61–63
20. Angtuaco TL, Boyd CM, London SN, et al. Technetium-99m hysterosalpingography in infertility: an accurate alternative to contrast hysterosalpingography. *RadioGraphics* **1989**;9:115–128
21. Deichert U, Schlief R, van de Sandt M, Juhnke I. Transvaginal hysterosalpingo-contrast-sonography (Hy-Co-Sy) compared with conventional tubal diagnostics. *Hum Reprod* **1989**;4:418–424
22. Schlief R, Deichert U. Hysterosalpingo-contrast sonography of the uterus and fallopian tubes: results of a clinical trial of a new contrast medium in 120 patients. *Radiology* **1991**;178:213–215
23. Peters AJ, Coulam CB. Hysterosalpingography with color Doppler ultrasonography. *Am J Obstet Gynecol* **1990**;164:1530–1534
24. Karasick S, Goldfarb AF. Peritubal adhesions in infertile women: diagnosis with hysterosalpingography. *AJR* **1989**;152:777–779
25. Itskovitz J, Boldes R, Levron J, Thaler I. Transvaginal ultrasonography in the diagnosis and treatment of infertility. *JCU* **1990**;18:248–256
26. Hackeloer BJ. Follicular size assessment by ultrasound. In: Sanders RC, James AE Jr, eds. *The principles and practice of ultrasonography in obstetrics and gynecology*, 3rd ed. Norwalk, CT: Appleton-Century-Crofts, **1985**:517–596
27. Daly DC. Treatment validation of ultrasound-defined abnormal follicular dynamics as a cause of infertility. *Fertil Steril* **1989**;51:51–57
28. Bonilla-Musoles F, Pardo G, Perez-Gil M, Serra V, Pellicer A. Abdominal ultrasonography versus transvaginal scanning: accuracy in follicular development evaluation and prediction for oocyte retrieval in stimulated cycles. *JCU* **1989**;17:469–473
29. Eissa MK, Sawers RS, Docker MF, Lynch SS, Newton JR. Characteristics and incidence of dysfunctional ovulation patterns detected by ultrasound. *Fertil Steril* **1987**;47:603–612
30. Hackeloer BJ. The role of ultrasound in female infertility management. *Ultrasound Med Biol* **1984**;10:35–50
31. Mendelson EB, Friedman H, Neiman HL, Calenoff L, Vogelzang RL, Cohen MR. The role of imaging in infertility management. *AJR* **1985**;144:415–420
32. Zandt-Stastny D, Thorsen MK, Middleton WD, et al. Inability of sonography to detect imminent ovulation. *AJR* **1989**;152:91–95
33. Fleischer AC, Herbert CM, Hill GA, Kepple DM. Transvaginal sonography: applications in infertility. *Semin Ultrasound CT MR* **1990**;11:71–81
34. Forrest TS, Elyaderani MK, Muilenburg MI, Bewtra C, Kable WT, Sullivan P. Cyclic endometrial changes: US assessment with histologic correlation. *Radiology* **1988**;167:233–237
35. Fleischer AC, Mendelson EB, Bohm-Velez M, Entman SS. Transvaginal and transabdominal sonography of the endometrium. *Semin Ultrasound CT MR* **1988**;9:81–101
36. Yoshimitsu K, Nakamura G, Nakano H. Dating sonographic endometrial images in the normal ovulatory cycle. *Int J Gynecol Obstet* **1989**;28:33–39
37. Brandt TD, Levy EB, Grant TH, Marut E, Leland J. Endometrial echo and its significance in female infertility. *Radiology* **1985**;157:225–229

Fetching the Doctor

Stefan C. Schatzki[1]

American sculptor John Rogers was born on October 30, 1829, in Salem, MA. Although a descendent of a distinguished Massachusetts family, he was sent to Boston English High School after his father's financial losses precluded his going to college. Leaving school at the age of 17, Rogers spent the next 11 years as a machinist and draftsman, primarily in the Northeast, but also in Hannibal, MO. At about the age of 20, Rogers began to model small clay figures and genre subjects for his own amusement. It was not until 1858 that he finally decided to become a sculptor. He first went to Paris and then Rome but found the neoclassical style of his teachers distasteful and in conflict with his natural narrative style. After only several months, he returned to America to work as a draftsman in Chicago. However, within a short time his clay group *Checker Players* was so well received at a church bazaar that he decided to try his luck as a sculptor in New York, where he moved in the fall of 1860, and thus at the age of 31 began his remarkable career.

For more than the next quarter century, Rogers's groups became the most popular sculptures in the history of this country. Each plaster group consisted of two or more figures enacting episodes from everyday life. Events related to the Civil War were the subjects of his early successes, and he later depicted scenes from literature and American history. His works were rich in anecdotal detail, local color, and human interest. He popularized sculpture to a degree that has never been equaled and with a success that rivaled the colored lithographs of his contemporaries, Currier and Ives. More than 80,000 plaster groups were sold. He stated that the groups were "not intended for rich people's parlors, but more for common houses and the country." While Rogers was a superb storyteller, his work required exceptional technical skill and a great deal of originality.

Rogers began by carefully sculpting the group of figures in clay and then having his workmen pour a newly discovered gelatinous glue over the model. When the glue firmed it was removed and used as a mold for the subsequent plaster groups. All the plaster groups were painted the same tan color, and the designs were patented. Rogers, however, soon found that the clay models required constant repair because of the large number of plaster groups that were needed (for example, 5000 copies of *Checkers Up at the Farm* were sold). He therefore changed to bronze models. Although plaster Rogers' groups are occasionally available in antique stores today, and also are represented in many museum collections, the bronze models are very rare, largely belonging to the New York Historical Society.

Rogers developed a remarkable acumen in advertising and selling his works. Business expanded rapidly, he established a factory, and his groups sold widely throughout the United States and abroad. Referring to the group entitled *Fetching the Doctor*, which was first cast in 1881, the 1894 catalog of the Rogers Statuary Company stated, "The boy has been sent in haste for the country doctor, who has ventured to return seated behind him on the horse, his box of medicines in some danger of being spilled as well as himself." The cost of this group, which was very popular in physician's offices, was $10. Rogers frequently used his wife, children, and friends as models, and his sketchbook indicates that the boy in *Fetching the Doctor* was modeled after his 9-year-old son, Derby Rogers. *The First Ride*, *Slave Auction*, *The Fugitive's Story*, *Going for the Cows*, *The Matter of Opinion*, *Weighing the Baby*, and *Faust and Marguerite/Their First Meeting* are just some of the titles of the 80 groups that Rogers produced between 1863, when he was elected to the National Academy, and 1894, when he retired.

In addition to his popular small groups, Rogers produced two life-size statues, one that stands at the entrance of City Hall in Philadelphia, and one of Abraham Lincoln, for which he won a medal at the 1893 Columbian Exposition in Chicago, and that is now in Manchester, NH. Rogers died after a long illness at New Canaan, CT, on July 26, 1904. John Rogers, perhaps as much as any other 19th century American artist, was responsible for bringing original fine art into the homes of everyday Americans.



John Rogers (1829–1904). *Fetching the Doctor* 1881. Bronze, 16½ × 15 × 5½ in. The New York Historical Society, New York, NY.

[1] Department of Radiology, Mount Auburn Hospital, 330 Mount Auburn St., Cambridge, MA 02238.

AJR **159:262, August 1992** 0361–803X/92/1592–0262 © American Roentgen Ray Society

Pulmonary Artery Disease in Takayasu's Arteritis: Angiographic Findings

Ichiro Yamada[1]
Hitoshi Shibuya[1]
Osamu Matsubara[2]
Isao Umehara[1]
Tomoko Makino[1]
Fujio Numano[3]
Soji Suzuki[1]

One hundred sixteen arteriographic examinations in 98 patients with Takayasu's arteritis were studied retrospectively to evaluate the extent of aortic and pulmonary disease. Stenosis was the most frequent finding in the aorta and its branches, but occlusion, dilatation, and aneurysms were also seen. Adventitial vascular structures, consistent with dilated vasa vasorum, were observed in five patients (5%) and systemic artery–pulmonary artery communication was seen in six (6%). Twenty-one (70%) of 30 patients who had pulmonary arteriography were shown to have pulmonary artery involvement. Upper lobe pulmonary arterial branches showed abnormalities most frequently; segmental branches, followed by subsegmental branches, were most often involved. The frequency of abnormal findings on pulmonary arteriograms correlated with the number of involved brachiocephalic vessels. Stenotic lesions in the aorta and its branches progressed in five (45%) of 11 patients, and those in the pulmonary artery progressed in one (33%) of three cases.

Takayasu's arteritis characteristically involves the systemic and pulmonary arteries, and the extent of arteritis in the major branches of the aortic arch appears to correlate with pulmonary arterial involvement. Both thoracic and abdominal aortographic studies and pulmonary arteriography are necessary to properly diagnose the extent of the disease, and angiography should be repeated for appropriate patient follow-up.

***AJR* 159:263–269, August 1992**

Takayasu's arteritis is a primary arteritis of unknown cause that commonly affects the thoracic and abdominal parts of the aorta and its main branches [1]. Although it is seen more often in the Orient, the disease has a worldwide distribution [2–5]. It usually affects young women, and its prevalence in females is about 10 times that in males [1, 2].

Recent literature has reported that Takayasu's arteritis often affects the pulmonary artery as well as the aorta and its branches [6–8]. However, only a few reports have analyzed the pulmonary arteriographic findings in a large number of cases [9, 10]. No report has yet described the progression of disease seen angiographically. We reviewed the angiographic findings in 98 patients with Takayasu's arteritis to evaluate the relationship between the systemic and the pulmonary arterial diseases and to elucidate its progressive nature.

Materials and Methods

Ninety-eight cases of Takayasu's arteritis were seen at Tokyo Medical and Dental University Hospital between November 1965 and September 1990. The disease was diagnosed on the basis of guidelines established by the Aortitis Syndrome Research Committee of Japan [11], which included clinical symptoms and signs, laboratory findings, and angiographic findings. Ninety-one of these patients were women and seven were men. Their ages at the onset of symptoms ranged from 11 to 61 years (average, 28 ± 12 years). Their ages at time of examination ranged from 12 to 72 years (average, 39 ± 14 years).

A total of 116 arteriographic examinations were performed in these patients: 77 studies

Received October 21, 1991; accepted after revision February 25, 1992.

[1] Department of Radiology, Faculty of Medicine, Tokyo Medical and Dental University, 1-5-45 Yushima, Bunkyo-ku, Tokyo 113, Japan. Address reprint requests to I. Yamada.

[2] Department of Pathology, Faculty of Medicine, Tokyo Medical and Dental University, Tokyo 113, Japan.

[3] Department of Internal Medicine, Faculty of Medicine, Tokyo Medical and Dental University, Tokyo 113, Japan.

0361–803X/92/1592–0263
© American Roentgen Ray Society

TABLE 1: Correlation of Extent of Brachiocephalic Vessel Involvement and Findings on Pulmonary Arteriography in Patients with Takayasu's Arteritis

No. of Involved Brachiocephalic Vessels	No. of Patients	Pulmonary Arteriography: Abnormal Findings/ No. of Studies (%)
0	3	0/0
1	9	1/4 (25)
2	24	3/6 (50)
3	14	2/3 (67)
4	17	6/7 (86)
5	14	5/6 (83)
6	6	2/2 (100)
7	8	2/2 (100)
Total	95	21/30 (70)

were by conventional film-screen angiography and 39 were by IV digital subtraction angiography. Both thoracic and abdominal aortographic studies were performed in 84 patients, thoracic aortography alone in 11 patients, and abdominal aortography alone in three patients. Pulmonary arteriography was performed in 30 patients; pulmonary angiographic studies were done routinely only in the most recent cases. All pulmonary arteriograms were obtained with the film-screen technique with injection of contrast medium into the main pulmonary artery. Aortograms and pulmonary angiograms were reviewed independently for this study.

The 84 thoracic and abdominal aortographic studies were categorized into four types on the basis of the Nasu classification [12]: type 1, involvement of the branches of the aortic arch only; type 2, involvement of the thoracic aorta and its branches only; type 3, involvement of the abdominal aorta and its branches only; and type 4, extensive involvement of the entire length of the aorta and its branches.

The 95 thoracic aortographic studies were classified into eight groups, according to the number (0–7) of involved vessels seen among the seven brachiocephalic vessels (the brachiocephalic, the right and left subclavian, the right and left vertebral, and the right and left common carotid arteries), for the purpose of quantifying the extent of arteritis in the branches of the aortic arch.

We used Spearman's rank correlation test to examine a possible correlation between the number of involved brachiocephalic vessels and the frequency of abnormal findings on pulmonary arteriograms.

Autopsies were performed in three of the 98 patients; special attention was directed to the major blood vessels and lungs.

Results

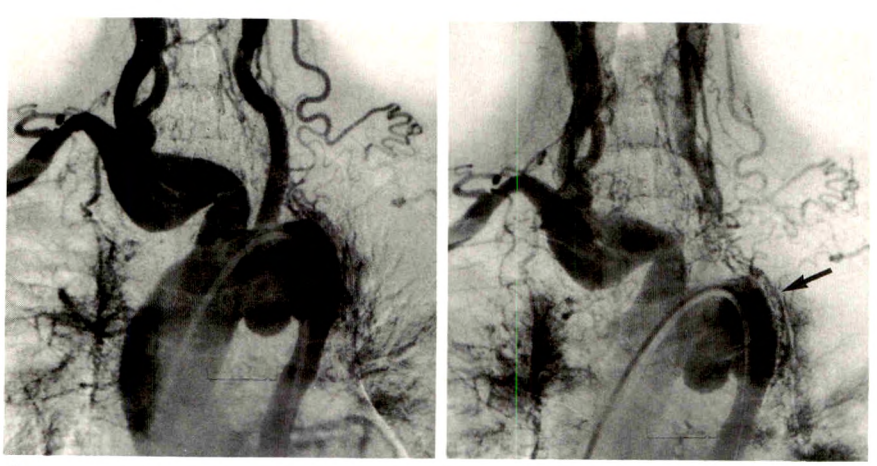
Abnormalities of the Aorta and Its Branches

The distribution of patients who had both thoracic and abdominal aortographic studies by Nasu classification was as follows: type 1, 19 patients (23%); type 2, nine patients (11%); type 3, three patients (4%); and type 4, 53 patients (63%). Thus, extensive disease that involved both the thoracic and abdominal portions of the aorta was the most prevalent type, whereas the classic pulseless disease, confined to the thoracic aorta and/or its branches, constituted only about one third of the cases.

The extent of disease in the brachiocephalic vessels in the 95 patients having thoracic aortography is shown in Table 1. The average number of involved vessels was 3.5 ± 1.8, and most patients (73%) had involvement of two to five vessels. Extensive involvement that included all of the brachiocephalic vessels was found in eight cases (8%).

The thoracic aortograms (95 patients) and abdominal aortograms (87 patients) from the 98 patients were analyzed. Stenosis was the most frequent finding in the aorta. Long-segment stenoses occurred commonly in the descending thoracic aorta (44%) and the abdominal aorta (51%) (Fig. 1), but never in the ascending aorta and very rarely in the aortic arch (3%). Complete occlusion of the aorta was not seen. Dilatation, more than 4 cm in diameter in the ascending aorta and more than 3 cm in diameter in the descending and abdominal portions [13], was seen less often than stenotic lesions, but when seen was usually in the ascending aorta (9%). A saccular aneurysm was seen in three patients: one in the aortic arch (Fig. 1), one in the descending aorta, and one in the abdominal aorta.

Aortic regurgitation was found in 27 (28%) of 95 patients; six (22%) of these patients had dilatation of the ascending aorta. This frequency of aortic dilatation in patients with aortic regurgitation was significantly higher than in the 68 patients



A B

Fig. 1.—Serial thoracic aortograms in a 24-year-old woman with Takayasu's arteritis.

***A*, Early arterial phase. Descending thoracic aorta is diffusely narrowed, and a saccular aneurysm is noted in lower aspect of aortic arch. Left subclavian artery is occluded at its origin, and right subclavian artery shows a proximal fusiform dilatation and distal stenosis.**

***B*, Late arterial phase. Fine serpentine vascular structures (*arrow*), presumably enlarged vasa vasorum, are seen in thickened wall of descending thoracic aorta (adventitial vascular structures).**

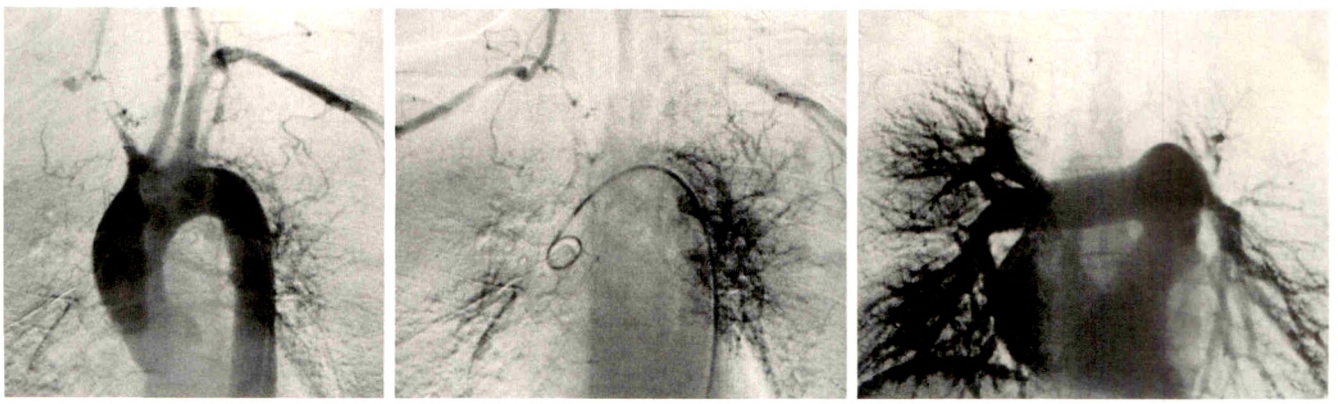


Fig. 2.—Thoracic aortograms in a 51-year-old woman with Takayasu's arteritis.
***A*, Thoracic aortogram, early phase. Occlusions can be seen in brachiocephalic trunk, right subclavian artery, and right common carotid artery.**
***B*, Thoracic aortogram, late phase. Visualization of pulmonary arterial branches in left upper and right middle lobes suggests systemic artery–pulmonary artery communication. Late opacification of right vertebral artery and distal right subclavian artery is seen, indicating subclavian steal phenomenon.**
***C*, Pulmonary arteriogram. Occluded branches of pulmonary artery in left upper and right middle lobes correspond to vessels opacified by systemic artery–pulmonary artery shunt in *B*.**

who did not have evidence of aortic regurgitation (three patients, 4%) ($p < .05$, Fisher's exact test).

In the branches of the thoracic aorta, stenosis was the most common finding, followed by occlusion (Figs. 1 and 2). Stenotic lesions most commonly involved the left subclavian artery (85%), the right subclavian artery (58%), and the left common carotid artery (50%). Dilatation was less common than stenotic lesions, but when seen was usually in the brachiocephalic trunk (5%) and in the proximal right subclavian artery (6%). Also, the left subclavian, common carotid, and vertebral arteries had a significantly higher rate of abnormalities than the respective right-sided vessels ($p < .001$, $p < .05$, and $p < .001$, respectively, χ^2 test). Further, 64 (78%) of 82 lesions in the left subclavian artery occurred proximal to the origin of the vertebral artery, whereas 18 (29%) of 62 lesions in the right subclavian artery were proximal to the origin of the vertebral artery, this difference being statistically significant ($p < .001$, χ^2 test). Additionally, a subclavian steal phenomenon with late opacification of the vertebral artery and the distal subclavian artery was noted in 11 cases (12%) (Fig. 2).

Of the branches of the abdominal aorta, the renal artery was involved most often (left, 36%; right, 31%), followed by the superior mesenteric artery (11%) and celiac trunk (8%).

Adventitial vascular structures consistent with dilated vasa vasorum were seen in the wall of the proximal descending aorta in five patients (5%) (Fig. 1). Four of these patients had been classified as having type 4 disease and the remaining patient classified as having type 2. Four patients had involvement of five brachiocephalic vessels; in the fifth patient, six brachiocephalic vessels were involved. Further, four cases had evidence of a pulmonary arterial abnormality; pulmonary arteriography was not performed in the fifth case.

A systemic to pulmonary artery communication was seen in six patients (6%) (Fig. 2). In all cases, pulmonary vessels that had been opacified on aortography were found to be occluded more proximally on pulmonary arteriography.

Abnormalities of the Pulmonary Artery

Of 30 cases in which pulmonary arteriography was performed, 21 (70%) of the arteriograms revealed abnormal findings (Fig. 2), and the distribution of these findings is summarized in Tables 2 and 3. Abnormalities were seen in both lungs in 13 cases, in the right lung in six cases, and in the left lung in two cases. The upper lobe pulmonary artery branches were more frequently involved than lower lobe vessels (Table 2). Further, the segmental branches were the most frequent site, followed by the subsegmental branches (Table 3).

The frequency of pulmonary arterial involvement significantly increased as the extent of abnormality in the brachiocephalic vessels increased, as is shown in Table 1 ($p < .01$, Spearman's rank correlation test). Further, pulmonary arterial abnormalities were present in all patients who had evidence of extensive involvement of the brachiocephalic vessels. However, the frequency of pulmonary arterial abnormalities showed no correlation with the extent of aortic disease.

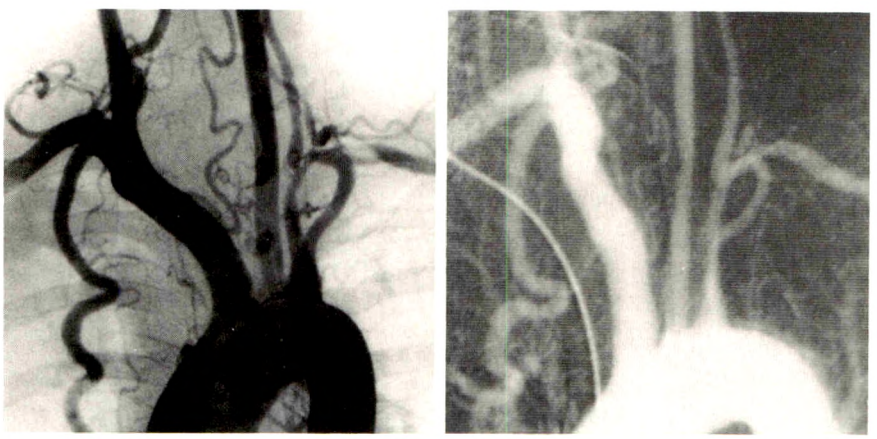
TABLE 2: Summary of Pulmonary Arteriographic Findings in 30 Patients with Takayasu's Arteritis

Artery	No. of Lesions by Type			
	Stenosis	Occlusion	Dilatation	Total
Pulmonary trunk	0	0	1	1
Right pulmonary	2	1	0	3
Upper lobe branches	9	23	0	32
Middle lobe branches	1	2	0	3
Lower lobe branches	0	2	0	2
Left pulmonary	1	0	0	1
Upper lobe branches	3	13	0	16
Lingular branches	5	7	0	12
Lower lobe branches	4	5	0	9
Total	25	53	1	79

TABLE 3: Distribution of Stenotic Pulmonary Arterial Lesions in 30 Patients with Takayasu's Arteritis

Region	No. of Lesions			
	Main Branch	Lobar Branch	Segmental Branch	Subsegmental Branch
Right lung	3			
Upper lobe		6	20	6
Middle lobe		0	3	0
Lower lobe		0	2	0
Left lung	1			
Upper lobe[a]		0	11	5
Lingular segments		0	9	3
Lower lobe		0	9	0
Total	4	6	54	14

[a] Exclusive of lingular segments.



A **B**

Fig. 3.—Initial and follow-up thoracic aortograms in a 29-year-old woman with Takayasu's arteritis.

***A*, Initial thoracic aortogram shows marked stenosis in left subclavian artery.**

***B*, Follow-up thoracic aortogram (IV digital subtraction angiography) obtained 2.5 years after diagnosis shows moderate stenosis in left common carotid artery and left subclavian artery stenosis.**

Time-Interval Change in Abnormalities of the Systemic and Pulmonary Arteries

Eleven patients had more than one examination: eight patients were examined twice, one patient three times, one patient four times, and one patient five times. In five (45%) of these 11 patients, the stenotic lesions progressed over an interval that ranged from 6 months to 8 years (Fig. 3). Progression occurred in the common carotid artery in two patients, in the subclavian artery in two other patients, and in the subclavian and inferior mesenteric arteries in the remaining patient. Further, in one patient a saccular aneurysm in the proximal descending aorta developed over a 3-year interval (Fig. 4).

Three patients had more than one pulmonary arteriographic examination during the study period: two patients had two and one patient had five. In one of these three patients, stenotic lesions in the pulmonary arterial branches had progressed over an interval of 3 years (Fig. 5).

Pathology of the Aorta and Lungs

In the postmortem inspection of three patients, close correlation was found between the angiographic studies and the macroscopic autopsy findings. Microscopic inspection of a dilated aortic wall showed marked thinning of the media, marked disruption of the elastic fibers, pronounced fibrotic thickening of the adventitia, and slight intimal thickening (Fig. 6A). In contrast, in an aortic wall that showed luminal narrowing, marked, circumferential, fibrous thickening of the intima was noted along with marked fibrosis of the adventitia and thinning of the media. In addition, the vasa vasorum were conspicuously prominent in the aortic wall and were increased in number. Scattered foci of lymphoplasmocytic infiltration in the media and adventitia were seen also.

Similarly, the pulmonary artery truncus and the extrapulmonic pulmonary artery branches showed microscopic changes that resembled those seen in the aortic wall. Stenotic or occluded lesions of the intrapulmonary elastic arteries were frequently observed in the segmental, subsegmental, and more peripheral branches. The microscopic features of these lesions were marked intimal fibrosis with several small vascular channels within the main lumen (a "vessel-in-vessel" appearance) (Fig. 6B); eccentric intimal fibrotic thickening (Fig. 6C); and complete occlusion by loose fibrous tissue within the lumen (Fig. 6D). The vascular channels in the occluded lumen of the pulmonary elastic artery demonstrated very unusual features. Further, most of these channels had well-developed muscular and elastic coats, which appeared to be muscular arterial walls.

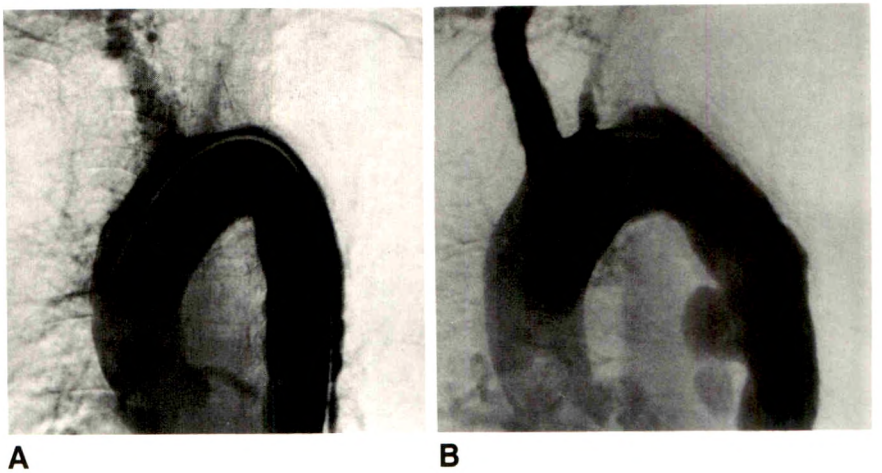


Fig. 4.—Initial and follow-up thoracic aortograms in a 44-year-old woman with Takayasu's arteritis.

A, Initial thoracic aortogram shows extensive occlusive change in brachiocephalic vessels and irregular contour in descending aorta.

B, Follow-up thoracic aortogram obtained almost 3 years after diagnosis shows development of irregularly shaped saccular aneurysm in proximal portion of descending thoracic aorta.

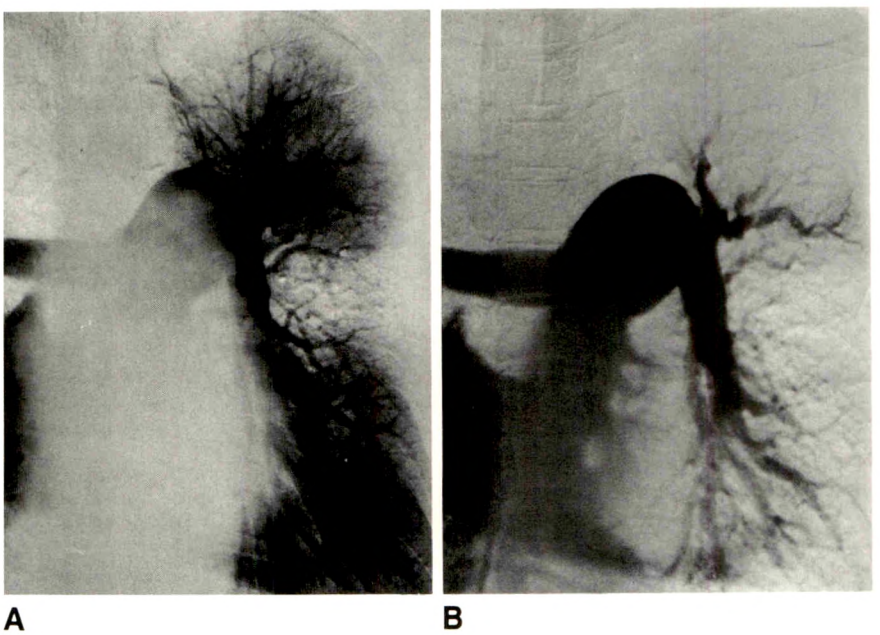


Fig. 5.—Initial and follow-up pulmonary arteriograms in a 47-year-old woman with Takayasu's arteritis.

A, Initial pulmonary arteriogram shows pulmonary arterial branch occlusion in left apical, posterior, and lingular segments.

B, Follow-up pulmonary arteriogram 3 years after diagnosis shows progression of occlusive lesions in pulmonary arterial branches of left upper lobe, as compared with those in *A*.

Discussion

Our angiographic examinations of patients with Takayasu's arteritis revealed that stenosis was the most common finding in the aorta and its branches, but that occlusion, dilatation, and aneurysms were not uncommon. The most frequent site of stenosis was the descending thoracic and abdominal portions of the aorta and the subclavian, common carotid, and renal arteries, whereas dilatation occurred most often in the ascending aorta and in the right-sided brachiocephalic and subclavian arteries. These findings are consistent with previous radiologic reports [1–5], and such a characteristic distribution might be accounted for partly by hemodynamic influences in the aorta and its branches.

Adventitial vascular structures noted in the aortic wall in such patients have been thought to represent enlarged vasa vasorum of the aorta [9, 14], and on thoracic aortography we observed such vascular structures in five (5%) of 95 patients. These adventitial vascular structures may be a collateral pathway to either the pulmonary or systemic circulation, since these patients had extensive occlusive changes in both the pulmonary and systemic arteries. Our pathologic examination also revealed that the vasa vasorum of the aortic wall became conspicuously enlarged and increased in number in one such patient.

The systemic to pulmonary artery communication in Takayasu's arteritis was first described by Ishikawa [15], and through the use of thoracic aortography we also observed such a communication in six (6%) of 95 patients. Further, the pulmonary vessels that had been opacified by the systemic to pulmonary artery shunt corresponded to the distal extent of vessels seen to be occluded more proximally on pulmonary arteriography. In this regard, it has been reported that when the pulmonary arterial pressure becomes diminished, the bronchial artery may enlarge to serve as collaterals [16]. Thus, visualization of a systemic to pulmonary artery shunt appears

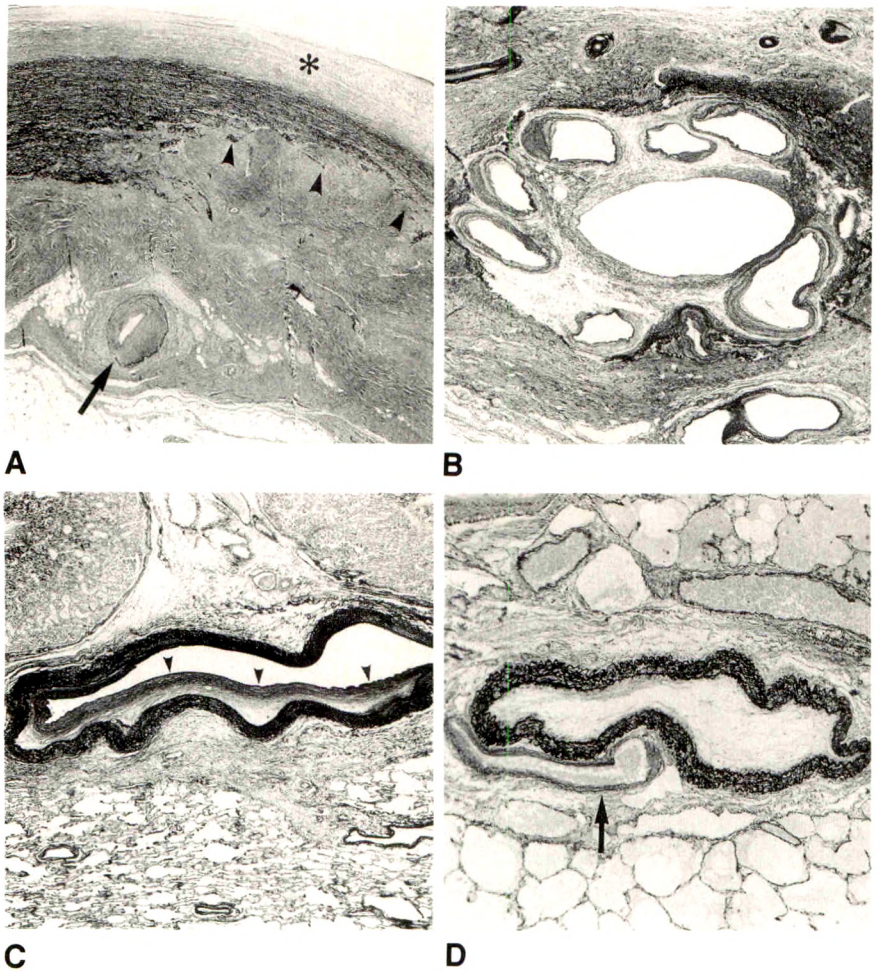


Fig. 6.—Histopathologic findings in autopsy specimens from patients with Takayasu's arteritis.

***A*, Histologic section of thoracic aorta reveals marked fibrotic thickening of adventitia, marked disruption of elastic fibers in media (*arrowheads*), and slight intimal thickening (*asterisk*). Vasa vasorum (*arrow*) are prominent and have increased in number. (Elastica van Gieson stain, original magnification ×32)**

***B*, Occluded lesion of intrapulmonary elastic artery shows marked intimal fibrosis with several small blood vessels, which have circumferential elastic coats (vessel-in-vessel appearance). (Elastica van Gieson stain, original magnification ×100)**

***C*, Stenotic lesion of intrapulmonary elastic artery shows eccentric intimal fibrotic thickening (*arrowheads*). (Elastica van Gieson stain, original magnification ×32)**

***D*, Occluded lesion of intrapulmonary elastic artery shows complete replacement by loose fibrous tissue in lumen. Accompanying muscular artery (*arrow*), which is a branch of bronchial artery, is seen. (Elastica van Gieson stain, original magnification ×80)**

to be indicative of extensive pulmonary artery involvement in Takayasu's arteritis. Further, our pathologic examination revealed an unusual feature of vascular channels within the occluded pulmonary artery (the vessel-in-vessel appearance). We believe that this finding is a histologic manifestation of the systemic to pulmonary artery communication.

In the past, pulmonary arterial lesions were regarded as a rare manifestation of Takayasu's arteritis; however, recent reports suggest that such lesions are more common than had been assumed [6–8, 17]. Our data demonstrate pulmonary arterial abnormalities in 70% of patients. Further, the frequency of pulmonary arterial involvement significantly increased as the lesions in the brachiocephalic vessels advanced. Thus, in Takayasu's arteritis, pulmonary arterial involvement shows a positive correlation with the degree of the brachiocephalic vessel involvement.

Our data also demonstrate that the upper lobe branches are the most frequent site for abnormalities in the pulmonary arterial system. Lupi et al. [8] also have indicated that the upper lobe branches are more frequently involved in Takayasu's arteritis than are the lower lobe branches.

Further, our data demonstrate that in Takayasu's arteritis the segmental and subsegmental branches are the sites in the pulmonary arterial system affected most often. Similarly, Deutsch et al. [4] have also shown that the segmental branches of the pulmonary artery are most often involved in Takayasu's arteritis. Additionally, our limited pathologic study demonstrates stenotic or occluded lesions of the intrapulmonary elastic arteries in the segmental, subsegmental, and more peripheral branches. Although the pulmonary arteriogram in Takayasu's arteritis may resemble that in pulmonary embolic disease, it has been found that in pulmonary embolism the larger pulmonary branches, such as main pulmonary, lobar, and segmental branches, are involved more frequently, particularly the lower lobe branches [18]. Thus, these distinguishing features appear to be useful in excluding pulmonary embolism as causing the angiographic findings. The presence of abnormalities in the aorta and its branches and the systemic artery–pulmonary artery communication will allow a clear distinction between patients with Takayasu's arteritis and those with pulmonary embolism.

To our knowledge, there have been no previous reports of the arteriographic changes in Takayasu's arteritis over time, and our data reveal that stenotic lesions in the aorta and its branches progressed in five (45%) of 11 patients. Further, stenotic lesions in the pulmonary artery were seen to progress in one of three patients. These findings demonstrate the progressive nature of Takayasu's arteritis in arteries of both

the systemic and pulmonary circulations. Recent surveys of Takayasu's arteritis in Japan have revealed that surgical treatments, such as bypass surgery, aortic valve replacement, and aneurysmectomy, were indicated in 10–13% of the patients [19]. Additionally, percutaneous transluminal angioplasty also has been used in cases of Takayasu's arteritis to treat stenoses of the subclavian, carotid, renal, and superior mesenteric arteries, with a relatively high success rate [10]. For appropriate treatment of such patients, therefore, angiography should be repeated to evaluate the need for intervention.

In conclusion, Takayasu's arteritis characteristically involves arteries of the systemic and pulmonary circulations, and the extent of arteritis in the major branches of the aortic arch appears to correlate with pulmonary arterial involvement. Both thoracic and abdominal aortographic studies and pulmonary arteriography are necessary to enable diagnosis and evaluate the extent of the disease, and angiography should be repeated for appropriate follow-up of patients.

REFERENCES

1. Hachiya J. Angiography of pulseless disease: a study of 50 cases. *Nippon Igaku Hoshasen Gakkai Zasshi* **1968**;27:1537–1557
2. Grollman JH Jr, Hanafee W. The roentgen diagnosis of Takayasu's arteritis. *Radiology* **1964**;83:387–395
3. Gotsman MS, Beck W, Schrire V. Selective angiography in arteritis of the aorta and its major branches. *Radiology* **1967**;88:232–248
4. Deutsch V, Wexler L, Deutsch H. Takayasu's arteritis: an angiographic study with remarks on ethnic distribution in Israel. *AJR* **1974**;122:13–28
5. Lande A, Gross A. Total aortography in the diagnosis of Takayasu's arteritis. *AJR* **1972**;116:165–178
6. Kozuka T, Nosaka T, Sato K, Ihara K. Aortitis syndrome with special reference to pulmonary vascular changes. *Acta Radiol* **1968**;7:25–32
7. Suzuki Y, Konishi K, Hisada K. Radioisotope lung scanning in Takayasu's arteritis. *Radiology* **1973**;109:133–136
8. Lupi HE, Sanchez TG, Horwitz S, Gutierrez FE. Pulmonary artery involvement in Takayasu's arteritis. *Chest* **1975**;67:69–74
9. Yamato M, Lecky JW, Hiramatsu K, Kohda E. Takayasu arteritis: radiographic and angiographic findings in 59 patients. *Radiology* **1986**;161:329–334
10. Park JH, Han MC, Kim SH, Oh BH, Park YB, Seo JD. Takayasu arteritis: angiographic findings and results of angioplasty. *AJR* **1989**;153:1069–1074
11. Inada K, Iwashima Y, Okada A, Shimizu Y. Aortitis syndrome: the diagnostic criteria (in Japanese). *Gendai-Iryo* **1976**;8:1183–1188
12. Nasu T. Aortitis syndrome: pathologic aspect (in Japanese). *Gendai-Iryo* **1976**;8:1143–1150
13. Dotter CT, Steinberg I. The angiocardiographic measurement of the normal great vessels. *Radiology* **1949**;52:353–357
14. Tamaki M. The radiographic findings in truncoarteritis (in Japanese). *Nippon Rinsho* **1968**;26:3332–3339
15. Ishikawa T. Systemic artery–pulmonary artery communication in Takayasu's arteritis. *AJR* **1977**;128:389–393
16. Liebow AA, Hales MR, Bloomer WE. Relation of bronchial to pulmonary vascular tree. In: Adams WR, Veith I, eds. *Pulmonary circulation*. New York: Grune & Stratton, **1958**:79–98
17. Umehara I, Shibuya H, Nakagawa T, Numano F. Comprehensive analysis of perfusion scintigraphy in Takayasu's arteritis. *Clin Nucl Med* **1991**;16:352–357
18. Mills SR, Jackson DC, Sullivan DC, et al. Angiographic evaluation of chronic pulmonary embolism. *Radiology* **1980**;136:301–308
19. Ishikawa K. Survival and morbidity after diagnosis of occlusive thromboaortopathy (Takayasu's disease). *Am J Cardiol* **1981**;47:1026–1032

1993 ARRS Scholarship Announcement

The American Roentgen Ray Scholarship for 1993 will be for focused study in a field selected by the Scholar for development of special interests to prepare for advancement in radiology.

The stipend will be $120,000 for one year and will require the candidate to spend 100% of his or her time in the program of study.

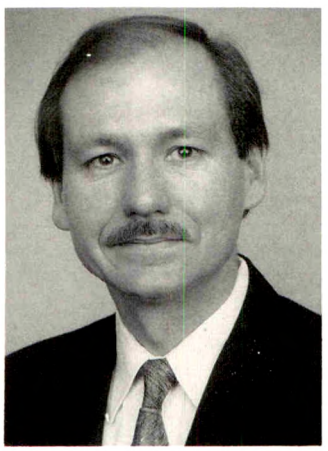
Deadline for submission is September 1, 1992. Further guidelines will be sent to the chairmen of all academic departments of radiology.

Applications should be sent to Mr. Paul Fullagar, Executive Director, American Roentgen Ray Society, 1981 Preston White Dr., Reston, VA 22091.

Announcement of Recipients of 1992 ARRS Scholarships



Felix Chew



Richard Stiles

Felix Chew, of Massachusetts General Hospital, and Richard Stiles, of Emory University School of Medicine, have been selected as the recipients of the first American Roentgen Ray Scholarships.

The Society awards two scholarships each year with the aim of enhancing opportunities in research and professional development for promising staff radiologists. A stipend of up to $60,000 per year for a 2-year period is provided to the winning candidates.

Dr. Chew is an assistant radiologist at the Massachusetts General Hospital and an assistant professor at Harvard Medical School in Boston, MA. He received his M.D. degree from the University of Florida and did an internship there. His residency training was at the State University of New York Health Science Center at Syracuse, NY. After his residency, he joined the radiology staff at Syracuse before accepting his present position. Dr. Chew has been developing multimedia computer-videodisc modules for teaching students, residents, and practicing radiologists, and is evaluating the efficacy of these modules. In 1990, he served as the first Melvin M. Figley Fellow in Radiology Journalism. Dr. Chew plans to use the AARS Scholarship to learn the fundamentals and nuances of clinical research.

Dr. Stiles is a graduate of Vanderbilt University and Vanderbilt University School of Medicine. He had his internship training at Vanderbilt and his residency at Emory University affiliated hospitals. He did a fellowship with Donald Resnick at the University of California, San Diego, and returned to Emory as a staff radiologist. In 1989, he moved to Vanderbilt as an assistant professor of radiology and orthopedics but returned to Emory in 1991. Dr. Stiles wishes to continue his studies in socioeconomic and political issues, with special emphasis on the historical aspects of turf, specialization, and subspecialization. He will also spend a part of his time on a research project involving MR imaging and tendons.

CT Evidence for the "Osseous Pinch" Mechanism of Traumatic Aortic Injury

Alan M. Cohen[1]
Jeffrey R. Crass[1]
Hollis A. Thomas[2]
Richard G. Fisher[3]
David G. Jacobs[4]

OBJECTIVE. Our prior experiments suggested that traumatic laceration of the aorta induced by rapid deceleration results from pinching of the aorta between the spine and the anterior bony complex (manubrium, clavicle, and first rib). This study examines that hypothesis with in vivo CT data.

MATERIALS AND METHODS. In 22 patients with angiographically and surgically proved lacerations of the proximal descending aorta, chest CT scans were obtained before (18) or after (four) surgical repair. The point of impact of the anterior bony complex with the anterior surface of the thoracic spine during compression of the thorax was predicted by simulated rotation of the first rib based on calculations made from the CT scans.

RESULTS. In all 22 patients, the projected site of impact of the anterior bony complex with the spine corresponded to the actual injured aortic segment as determined with angiography.

CONCLUSION. Our data further support the proposed "osseous pinch" mechanism of injury to explain traumatic tears of the aorta.

AJR 159:271–274, August 1992

Previously proposed theories to explain the mechanism of aortic injury in blunt trauma were largely speculative and included differential deceleration of aortic segments (whiplash), torsion forces, hydrostatic forces, or various combinations of these mechanisms [1–13]. Our prior series of experiments suggested that traumatic aortic lacerations could result from compression of the aorta between the anterior bony complex (manubrium, clavicle, and first rib) and the spine [14]. Compressive forces present in blunt thoracic trauma depress the anterior thoracic osseous structures, causing them to rotate posteriorly and inferiorly about the posterior rib articulations. These forces could pinch and shear interposed vascular structures [14].

This article examines the cross-sectional anatomy from CT scans in patients with traumatic aortic lacerations to determine whether the theoretical point of impact between the anterior bony complex and the spine matches the actual site of aortic injury. It provides the first in vivo support for our hypothesis of the "osseous pinch" mechanism of traumatic aortic injury.

Materials and Methods

CT scans of 22 patients admitted to our institutions after high-speed motor vehicle accidents form the data set for this study. Each patient had a CT scan of the chest either before (n = 18) or after (n = 4) surgery for repair of a traumatic tear of the aorta. All had preoperative angiography, which documented traumatic laceration of the aorta.

The CT scans in 21 patients were obtained with contiguous 1-cm-thick sections from the thoracic inlet to below the carina; one patient had similar scans with 1-cm-thick sections at 1.5-cm intervals. The locations and spatial relationships of the spine, ribs, sternum, and aorta found on the CT scans were recorded in a sagittal projection relative to the tabletop on graph

Received November 18, 1991; accepted after revision February 25, 1992.

[1] Department of Radiology, MetroHealth Medical Center, Case Western Reserve University, 2500 MetroHealth Dr., Cleveland, OH 44109. Address reprint requests to A. M. Cohen.

[2] Department of Diagnostic Radiology, Humana Hospital-University, University of Louisville, 530 S. Jackson St., Louisville, KY 40202.

[3] Department of Radiology, Ben Taub Hospital, 1502 Taub Loop, Houston, TX 77030.

[4] Department of Surgery, MetroHealth Medical Center, Case Western Reserve University, Cleveland, OH 44109.

0361–803X/92/1592–0271
© American Roentgen Ray Society

paper by using the following method: (1) each division along the *x*- and *y*-axes of the linear graph paper represented 1 cm; (2) the table was assumed to keep a constant height in relation to the CT gantry so that it could serve as a point of zero reference for the *y*-axis; (3) scan slices were stacked along the *x*-axis at correct (1.0 or 1.5 cm) intervals; (4) each of the noted structures was measured from the tabletop by using the internal ruler present on the CT scan slice; (5) each structure was plotted on its visualized CT scan slice at the proper height on the *y*-axis of the graph paper. Compression of the thorax was simulated by a previously described method [14]: (1) the plotted costovertebral joints of the first rib defined the center point of all rotations; (2) the radius of rotation was defined by the distance from the center point to the anterior structure, first rib, clavicle, or manubrium; (3) the motion of the anterior osseous structures relative to the aorta and anterior surface of the vertebral column was plotted around the axis of rotation by using the defined radius. Since the graph paper was linear and a properly scaled model was plotted on both axes, a compass or calipers could be used for this procedure (Fig. 1). This allowed analysis of the osseous motion in relation to the aorta as well as study of the probable segment of impact of those structures on the aorta.

After the theoretical segment of impact was determined from the above calculation, that region was compared with the actual injured segment shown on the preoperative CT scans or with the segment of aorta replaced shown on the postoperative CT scans. By viewing the vascular anatomy and abnormalities present on each CT scan slice and correlating them with the angiographically defined site of aortic injury, we were able to localize the site of vascular injury to one or at most two contiguous scan slices in the 18 presurgery patients. On postoperative scans, tube grafts were visible for three to four contiguous scan slices so that localization was less precise.

Results

Analysis of the 22 CT scans of the thorax allowed prediction of the theoretical point on the thoracic spine where maximal rib or clavicle rotation would cause the tip of the first rib, clavicle, or manubrium to touch the spine. The points of impact from these structures on the spine had a sagittal spread of 3 cm or less in all instances. The point of impact for the manubrium usually was on the same slice and at the same point as one of the other two structures. In 13 patients, predicted rotation of the first rib/manubrium complex coincided within one scan slice, or 1 cm, with the actual site of aortic injury seen on imaging studies. In five patients, predicted rotation of the clavicle/manubrium complex coincided within one scan slice with the imaged region of aortic injury. The four postoperative patients with tube grafts had longer segments of CT localization. The entire rotated anterior bony complex struck the level of the tube graft in each instance. A typical case is shown in Figure 2.

The region of aortic injury in the proximal descending aorta varied somewhat among 19 patients. In addition, three patients had relatively high lacerations of the aorta, one near the origin of the left carotid artery and two at the top of the aortic arch (Fig. 3). The projected point of osseous pinching of the aorta corresponded to the site of injury in the typical and atypical instances. All 18 preoperative CT scans showed increased mediastinal density indicative of mediastinal hematoma. This ranged from small periaortic density changes without mediastinal distortion to large regions of increased density with marked mediastinal contour changes.

Discussion

In an earlier study [14], we demonstrated in a model that normal thoracic anatomy allows trapping of the aorta between the spine and anterior osseous structures when the thorax is compressed. Calculations made from the cross-sectional anatomy shown on CT scans in our current study provide some support for the osseous pinch hypothesis. We were able to calculate the point of aortic impingement by using the model previously described [14]. The theoretical contact point of the spine with the anterior osseous structures during maximal thoracic compression coincided with the injured aortic segment in each instance. The three cases with unusual sites of aortic laceration, which were accurately predicted with this model, further support the hypothesis and suggest that this mechanism may also account for great vessel injuries from blunt thoracic trauma [14]. Prior theories concerning the mechanism of vascular injury after blunt thoracic trauma never adequately explained these unusual, infrequent sites [1–13].

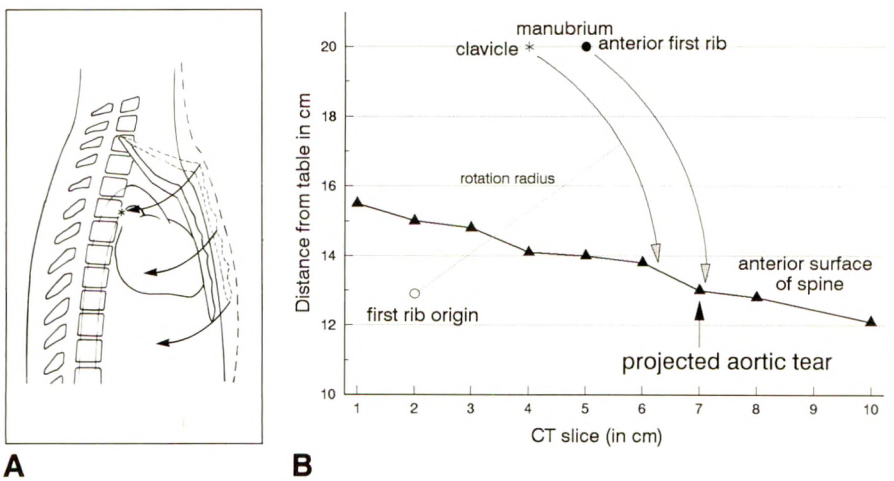


Fig. 1.—*A*, Line drawing (sagittal projection) of area of aortic injury analyzed in *B* shows relationship of aorta to anterior osseous complex and spine. Manubrium, clavicles, and anterior ends of first ribs, when compressed, describe similar arcs around an axis that originates at posterior articulations of first ribs. *Arrows* indicate movement of anterior osseous complex that occurs with full compression. Site of expected aortic impingement is shown by *asterisk*.

***B*, Graph of measurements obtained from set of CT sections of one patient. Measurements for each structure are from CT tabletop. Projected axis of rotation of anterior osseous complex with posterior first rib used as center of rotation is shown by *dotted lines*. Posterior first rib (*open circle*), anterior first rib (*solid circle*), clavicle (*asterisk*), and anterior surface of spine (*triangles*) are recorded. *Solid arrow* marks CT scan of section with actual aortic injury.**

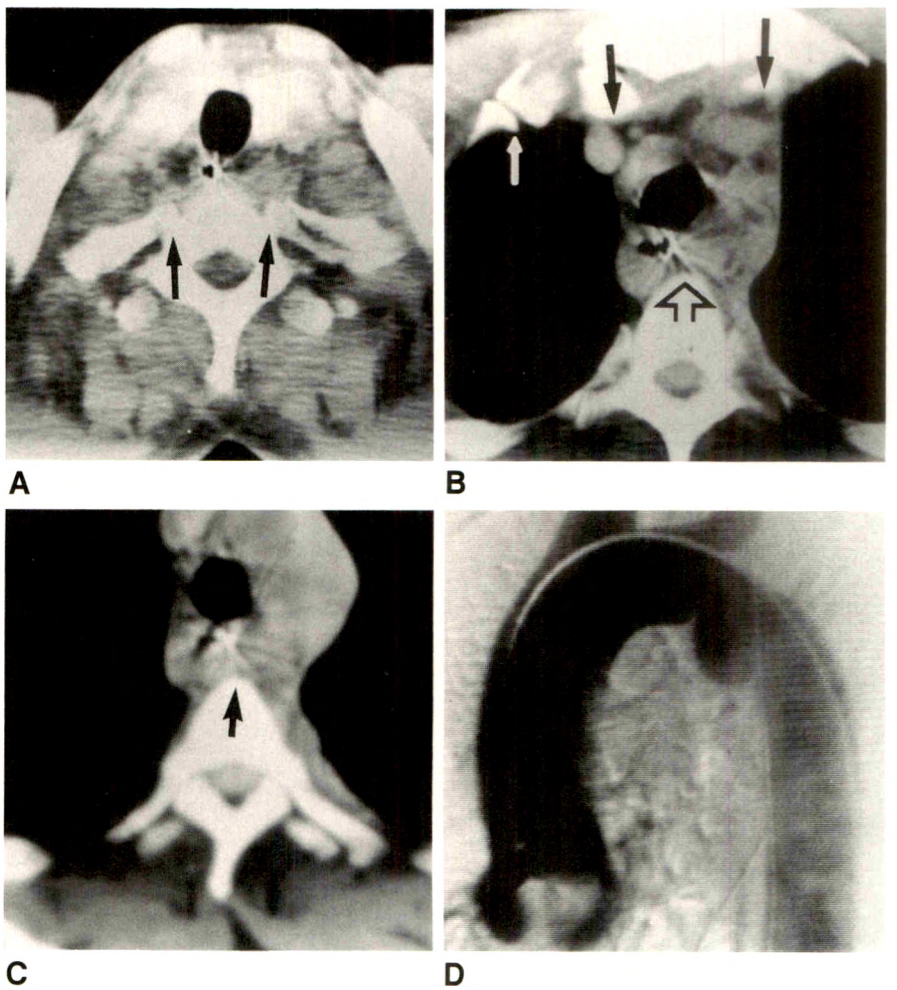
Fig. 2.—CT slices corresponding to sections defined in Fig. 1B of patient whose CT scans were used to create Fig. 1B.

A, CT scan of slice 2 located near thoracic inlet delineates location of posterior insertions for first ribs (*arrows*). Anterior surface of spine was measured but is not marked.

B, CT scan of slice 5 shows location of articulations of anterior end of first rib (*white arrow*) and clavicle (*solid black arrows*) with manubrium. Manubrium was measured on next slice further cephalad (slice 4). Anterior surface of spine (*open arrow*). Increased density in mediastinum is indicative of blood.

C, CT scan of slice 7 at level of aortic arch shows calculated location of impact to anterior osseous complex on anterior surface of spine (*arrow*). Mediastinum is dense, containing blood.

D, Angiogram shows traumatic tear of aorta just distal to great vessels.



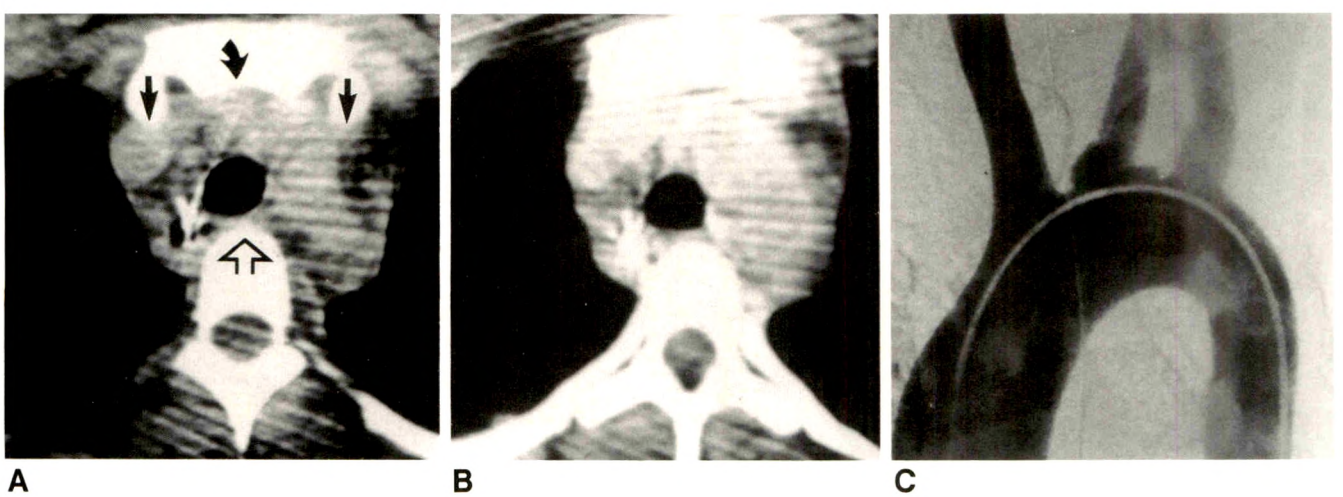


Fig. 3.—CT slices corresponding to sections similar to those graphically depicted in Fig. 1B.

A, CT scan of slice 4 shows posterior surface of manubrium (*curved arrow*), clavicles (*straight solid arrows*), and anterior surface of spine (*open arrow*). Generalized increased density in mediastinum is indicative of blood. Nearly round density to left of trachea may represent a pseudoaneurysm associated with aortic laceration. Projected slice of contact of anterior osseous complex with spine lies between this and next slice further caudad.

B, CT scan of slice 5 shows aortic arch surrounded by blood. Projected point of impact is at this or next level further cephalad.

C, Arteriogram shows a laceration and pseudoaneurysm at junction of aortic arch with left common carotid artery.

Our study indicates that the specific anterior bony structure causing vascular injury may vary. A combination of the manubrium and the clavicle or first rib best fits the geometry in most patients. Differences in patients' anatomy, variations in impact force vectors, and the interaction of these factors suggest a degree of variability in where the anterior and posterior bones will contact. This has some experimental and logical basis. Jackson et al. [15] noted profound movement of the heart and great vessels of up to 8 cm during experimentally controlled thoracic trauma in dogs. Even in these animals and with the profound pectus carinatum of the species, the anterior and posterior bones met. Therefore, our observed variation of osseous compression seems probable.

The osseous pinch theory cannot readily be used to disprove older proposed theories explaining aortic lacerations [1–12, 15, 16]. However, these theories also are unproved, having been created to fit the observed locations of vascular injury. The limitations inherent in previous models become clear after several factors are considered. No experimental model exists to validate those proposed mechanisms of injury. Furthermore, although many currently existing theories suggest that the sudden, extreme mobility of the aorta is the primary pathologic process responsible for the typical isthmic tear, they disagree as to which aortic segment, the aortic arch [12] or descending aorta [9], is mobile on impact. Finally, observations and statements contained in these articles unequivocally show that the postulated forces are insufficient to cause aortic tearing [1, 4, 5, 8, 9, 12]. In contrast, the osseous pinch theory is based on proven anatomic relationships. It even potentially explains why injuries caused by high-speed motor vehicle accidents, vehicles hitting pedestrians, falls from heights, and power tool kickback injuries can produce similar vascular lesions.

Results of the current study support our proposed osseous pinch mechanism to explain aortic lacerations from blunt trauma. Without a human model, absolute proof of this or any theory is probably impossible. Although we had suggested the use of cadavers to test this theory [14], the current medicolegal climate has made that unfeasible. Instead, three-dimensional computer modeling is being considered to provide an alternative method of studying the thorax and the deformities that could occur during blunt chest trauma.

REFERENCES

1. Greendyke RM. Traumatic rupture of aorta. *JAMA* **1966**;195:119–122
2. Klotz O, Simpson W. Spontaneous rupture of the aorta. *Am J Med Sci* **1932**;184:455–473
3. Kuhn LP. Traumatic rupture of thoracic aorta with review of fifty-five abdominal injuries. *Ill Med J* **1925**;47:420–427
4. Lundevall J. The mechanism of traumatic rupture of the aorta. *Acta Pathol Microbiol Scand* **1964**;62:34–46
5. Lundevall J. Traumatic rupture of the aorta with special reference to road accidents. *Acta Pathol Microbiol Scand [A]* **1964**;62:29–33
6. Marsh CL, Moore RC. Deceleration trauma. *Am J Surg* **1957**;93:623–631
7. Oldegard B, Weman PO. Quoted by: Greendyke RM. Traumatic rupture of aorta. *JAMA* **1966**;195:119–122
8. Oppenheim F. Quoted by: Parmley LF, Mattingly TW, Manion WC, Jahnke EJ. Non-penetrating traumatic injury of the aorta. *Circulation* **1958**;17:1086–1101
9. Parmley LF, Mattingly TW, Manion WC, Jahnke EJ. Non-penetrating traumatic injury of the aorta. *Circulation* **1958**;17:1086–1101
10. Stark P. Traumatic rupture of the thoracic aorta: review. *CRC Crit Rev Diagn Imaging* **1984**;21:229–255
11. Strassman G. Traumatic rupture of the aorta. *Am Heart J* **1947**;33:508–515
12. Zehnder MA. Delayed post-traumatic rupture of the aorta in a young healthy individual after closed injury: mechanical-etiological considerations. *Angiology* **1956**;7:252–267
13. Fisher RG, Hadlock F, Ben-Menachem Y. Laceration of the thoracic aorta and brachiocephalic arteries by blunt trauma. *Radiol Clin North Am* **1981**;19:91–110
14. Crass JR, Cohen AM, Motta AO, Tomashefski JF Jr, Wiesen EJ. A proposed new mechanism of traumatic aortic rupture: the osseous pinch. *Radiology* **1990**;176:645–649
15. Jackson FR, Berkas EM, Roberts VL. Traumatic aortic rupture after blunt trauma. *Dis Chest* **1968**;53:577–584
16. Haas GM. Types of internal injuries of personnel involved in aircraft accidents. *J Aviation Med* **1944**;15:77–84

Pictorial Essay

High-Resolution CT of Bronchioloalveolar Carcinoma

Brendan Adler,[1] Simon Padley,[1] Roberta R. Miller,[2] and Nestor L. Müller[1]

Bronchioloalveolar cell carcinoma has a wide spectrum of pathologic and radiologic appearances. Some of the radiologic features are characteristic enough to suggest the underlying pathologic changes. This article illustrates the various manifestations of bronchioloalveolar cell carcinoma on high-resolution CT (1.5-mm collimation reconstructed with a high-spatial-frequency algorithm). Correlations between the CT and pathologic findings are included.

Bronchioloalveolar cell carcinoma typically has one of three radiologic patterns: a solitary nodule, consolidation, and multicentric or diffuse disease. The prevalences of these patterns are 43%, 30%, and 27%, respectively [1]. Pleural effusion has been reported to be present in 32% of cases and hilar or mediastinal lymphadenopathy in 18% [1].

Solitary nodules are typically located in the periphery of the lungs and have spiculated borders previously described as forming a star pattern [2]. Histopathologic correlation shows that the spiculated appearance may be due to infiltrative tumor growth, localized lymphangitic spread, or desmoplastic reaction [3] (Fig. 1). This desmoplastic reaction also accounts for the pleural tags that are frequently seen (Fig. 2).

A characteristic finding of bronchioloalveolar cell carcinoma is the presence of bubblelike lucencies or pseudocavitation

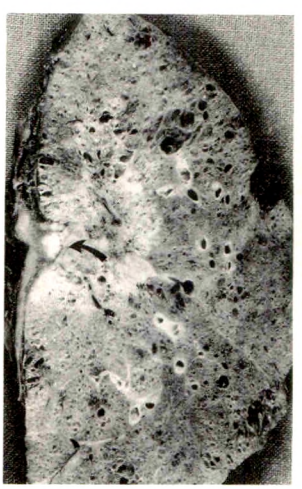
Fig. 1.—*A*, High-resolution CT scan through upper lobe of right lung shows peripheral bronchioloalveolar carcinoma with prominently spiculated borders. Apparent pleural thickening is seen adjacent to mass.

B, Pathologic specimen shows a peripheral solitary mass lesion with infiltrative growth pattern and extensive desmoplastic reaction leading to pleural retraction (*arrow*). Tumor also invades parietal pleura.

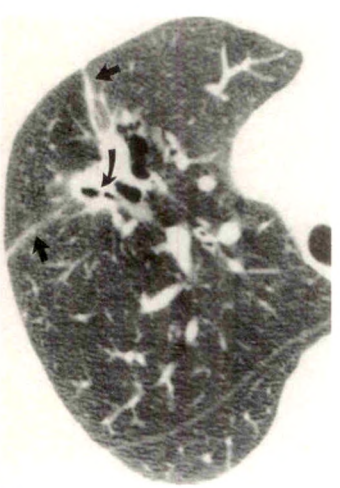
Fig. 2.—High-resolution CT scan through upper lobe of right lung shows a mass with pleural tags (*straight arrows*). These are caused by desmoplastic reaction elicited by bronchioloalveolar carcinoma. Air bronchogram (*curved arrow*) is evident.



1A



1B



2

Received January 13, 1992; accepted after revision February 18, 1992.

[1] Department of Radiology, University of British Columbia and Vancouver General Hospital, 855 W. 12th Ave., Vancouver, B.C., Canada V5Z 1M9.
[2] Department of Pathology, University of British Columbia and Vancouver General Hospital, Vancouver, B.C., Canada V5Z 1M9.

 © American Roentgen Ray Society

(Fig. 3), which corresponds to patent small bronchi or air-containing cystic spaces in papillary tumors [3]. Bubble lucencies are seen more commonly in bronchioloalveolar cell carcinoma (50%) than in acinar adenocarcinomas (31%) or other lung tumors (11%). Overt cavitation occurs in 7% of cases [1] (Fig. 4).

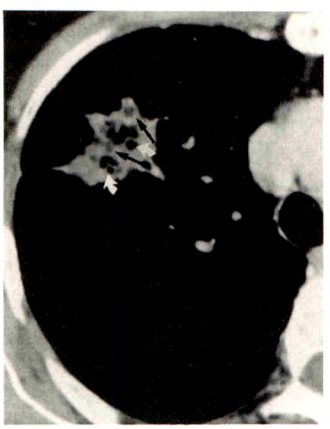
The combination of growth along the alveolar wall and secretion of mucin may cause features of air-space consolidation with air bronchograms (Figs. 2 and 5). The consolidation may be segmental or may involve an entire lobe. Production of mucin can cause swelling of the lobe, leading to bulging of interlobar fissures. The tumor may extend across the fissure into an adjacent lobe (Fig. 6).

Mucin is of lower radiographic density than tumor, so it creates areas of lower attenuation when viewed on mediastinal windows. This causes either heterogeneous attenuation in small masses (Fig. 3) or uniform low attenuation in more confluent consolidation (Fig. 7). The low attenuation allows vessels to be clearly seen, particularly after administration of IV contrast material. This finding, recently described as the CT angiogram sign [4] (Fig. 8), is suggestive but not specific for bronchioloalveolar cell carcinoma.

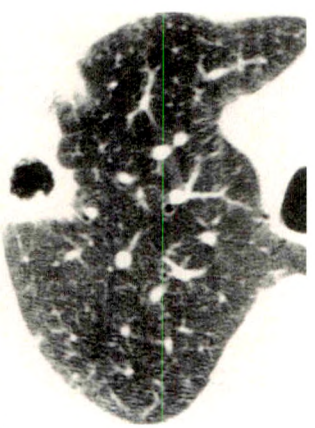
Twenty-seven percent of bronchioloalveolar cell carcinomas are multicentric or diffuse. Although CT is superior to radiography in the detection of lung nodules, the sensitivity of CT in showing pathologically proved multicentricity is only 63–68% [5]. Patients in whom more than one lesion is seen on high-resolution CT scans may have multicentric bronchioloalveolar cell carcinoma (Fig. 5) or bronchioloalveolar cell carcinoma associated with a second, apparently unrelated lesion [4] (Fig. 9). Finally, bronchioloalveolar cell carcinoma may have a widespread multinodular pattern (Fig. 10).

REFERENCES

1. Hill CA. Bronchioloalveolar carcinoma: a review. *Radiology* **1984**; 154:15–20
2. Kuhlman JE, Fishman EK, Kuhajda FP, et al. Solitary bronchioloalveolar carcinoma: CT criteria. *Radiology* **1988**;167:379–382
3. Zwirewich CV, Vedal S, Miller RR, Müller NL. Solitary pulmonary nodule: high-resolution CT and radiologic-pathologic correlation. *Radiology* **1991**; 179:469–476
4. Im J-G, Han MC, Yu EJ, et al. Lobar bronchioloalveolar carcinoma: "Angiogram sign" on CT scans. *Radiology* **1990**;176:749–753
5. Zwirewich CV, Miller RR, Müller NL. Multicentric adenocarcinoma of the lung: CT-pathologic correlation. *Radiology* **1990**;176:185–190



3



4

Fig. 3.—High-resolution CT scan through upper lobe of right lung at level of aortic arch (mediastinal windows) shows heterogeneous attenuation (*straight arrows*) within region of bronchioloalveolar cell carcinoma. This variable attenuation represents areas of mucus secretion, which have lower attenuation than tumor mass has. Note also bubble lucencies (*curved arrows*), which have been shown to correspond to patent small bronchi or air-containing cystic spaces in papillary tumors.

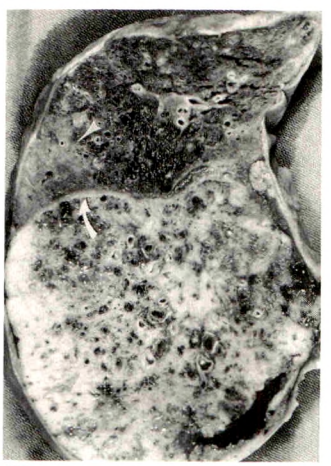
Fig. 4.—High-resolution CT scan through upper lobe of right lung shows a lobulated peripheral bronchioloalveolar carcinoma with a broad pleural attachment. Note cavitation within tumor mass, a feature reported to be present in 7% of cases of bronchioloalveolar carcinoma.



5



6A



6B

Fig. 5.—High-resolution CT scan through left lung at level of bifurcation of main bronchus shows multicentric bronchioloalveolar carcinoma. Segmental malignant consolidation is present in apicoposterior segment of upper lobe, and a nodular opacity is seen within superior segment of lower lobe. Air bronchogram (*arrow*) is evident within segmental consolidation.

Fig. 6.—*A*, High-resolution CT scan through right lung at level of lower lobes shows lobar consolidation of lower lobe, with bulging of major fissure, which is thickened (*arrow*). Tumor extends through fissure (*arrowhead*) into middle lobe.

***B*, Pathologic specimen shows extensive malignant lobar consolidation and confirms presence of a bulging, thickened fissure (*arrow*). Tumor involvement of middle lobe is also shown (*arrowhead*).**



Fig. 7.—*A*, High-resolution CT scan through both lungs at level of left atrium (mediastinal windows) shows confluent consolidation of low attenuation within lingula and another mass (*arrow*) in lower lobe of left lung.
B, Pathologic specimen of lingula shows extensive malignant consolidation by bronchioloalveolar carcinoma. Tumor has a grossly mucoid appearance.
C, Photomicrograph of histologic section from tumor mass shows typical growth of bronchioloalveolar carcinoma along alveolar walls (*arrows*).

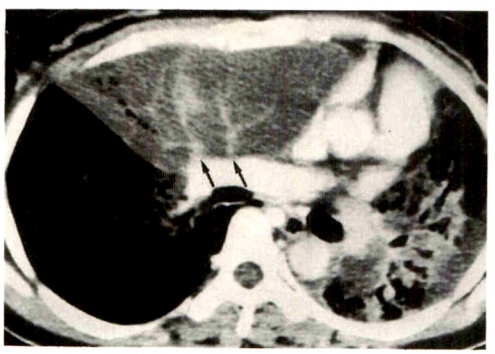
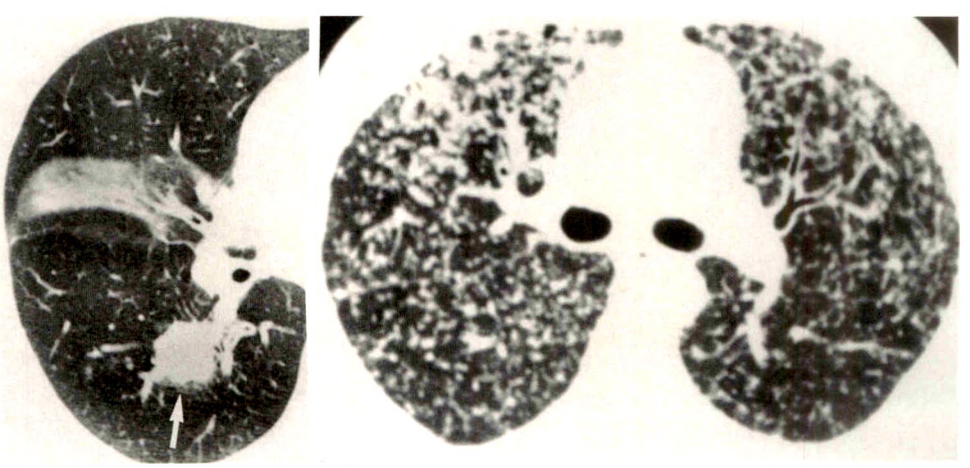


Fig. 8.—Contrast-enhanced 10-mm-collimation CT scan through both lungs at level of right pulmonary artery shows consolidation of right upper, left upper, and left lower lobes. Consolidated right upper lobe is of low attenuation, and contrast-enhanced pulmonary vessels are thus readily visualized (*arrows*) (CT angiogram sign). Note bubble lucencies, air bronchograms, and less well defined angiogram sign in left lung. (Courtesy of J-G. Im, Seoul National University Hospital, Seoul, Korea.)

Fig. 9.—High-resolution CT scan through right lung at level of bronchus intermedius shows segmental confluent bronchioloalveolar carcinoma in middle lobe and a nodular mass (*arrow*) in lower lobe, proved pathologically to be acinar adenocarcinoma.

Fig. 10.—High-resolution CT scan through both lungs at level of left upper lobe bronchus shows widespread extensive multinodular foci of bronchioloalveolar carcinoma.



Radiologic-Pathologic Conferences of the Massachusetts General Hospital

Inverted Papilloma

James H. Brown[1] and Felix S. Chew

A 79-year-old man had a puffy left eyelid. Radiographs showed a poorly aerated nasal cavity and an expanded and opacified left frontal sinus. CT and MR images showed a heterogeneously enhancing mass occupying the left frontal sinus, thinning its bony floor (Fig. 1). The differential diagnosis included benign and malignant tumors, fungal infections, and granulomatous diseases. At surgery, the tumor extended from the nasal cavity into the left frontal sinus. The bony floor was eroded but the periosteum remained intact. The tumor consisted of respiratory surface epithelium invaginated into the underlying stroma, with intact basement membrane. The final pathologic diagnosis was inverted papilloma.

Inverted papilloma is a benign epithelial tumor that arises from the mucous membrane of the nasal cavity and paranasal sinuses, most commonly the lateral nasal wall in the region of the middle meatus. Paranasal involvement most frequently affects the maxillary and ethmoidal sinuses. The term *inverted* is derived from the characteristic proliferation of metaplastic surface epithelium (respiratory, transitional, or squamous type) by inversion into the underlying stroma, resulting in endophytic rather than exophytic growth. Microscopic examination reveals invaginated respiratory, transitional, or squamous type epithelium with orderly maturation. Radiologic findings relate to the bulkiness and slow growth of the tumor. Radiographs may show an opacified nasal cavity. The tumor may enlarge the nasal fossa and remodel the nasal septum and adjacent bones. Opacification of the ipsilateral paranasal sinuses may be due to obstruction or tumor extension. CT and MR imaging provide precise delineation of tumor extension, with CT preferable for showing bone remodeling. The tumor may calcify in punctate, nodular, linear, or circular patterns [1]. MR imaging can be used to distinguish sinonasal tumors, which generally have intermediate T2 signal, from inflammatory tissue, which almost always has high T2 signal [2].

Inverted papilloma constitutes 0.5–0.4% of primary nasal tumors [3] and occurs most frequently in patients in their fifth and sixth decades. Patients typically present with nasal obstruction, epistaxis, or nasal discharge. While the pathogenesis is unknown, the associated conditions include allergy, chronic sinusitis, environmental carcinogens, and viral infection. Malignant change occurs in fewer than 7% of cases [4]. The treatment is surgical; the recurrence rate is high if the lesion is not completely removed.

REFERENCES

1. Lund VJ, Lloyd G. Radiological changes associated with inverted papilloma of the nose and paranasal sinuses. *Br J Radiol* **1984**;57:455–461
2. Som P, Shapiro MD, Biller HF, Sasaki C, Lawson W. Sinonasal tumors and inflammatory tissue: differentiation with MR imaging. *Radiology* **1988**; 167:803–808
3. Lawson W, Lebenger J, Som P, Bernard PJ, Biller HF. Inverted papilloma: an analysis of 87 cases. *Laryngoscope* **1989**;99:1117–1123
4. Phillips PP, Gustafson RO, Facer GW. The clinical behavior of inverting papilloma of the nose and paranasal sinuses: report of 112 cases and review of the literature. *Laryngoscope* **1990**;100:463–469

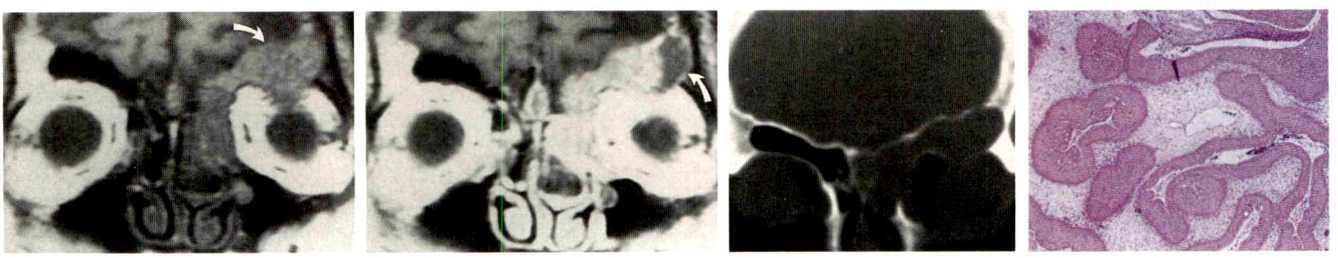


Fig. 1.—Inverted papilloma.
***A* and *B*, Coronal T1-weighted images show tumor (*arrow*) expanding and filling left frontal sinus and nasal cavity (*A*). The tumor enhances after infusion of gadopentetate dimeglumine (*B*). Laterally in sinus is a fluid collection (*arrow*).**
***C*, Coronal CT scan shows expansion and thinning of bone adjacent to tumor.**
***D*, Photomicrograph shows respiratory epithelium with characteristic infolded papillary pattern of proliferation.**

From the weekly radiologic-pathologic correlation conferences conducted by Jack Wittenberg. Pathology editor: Andrew E. Rosenberg. Radiology editors: Felix S. Chew, William E. Palmer, Daniel P. Barboriak, Daniel I. Rosenthal.

[1] Both authors: Department of Radiology, Massachusetts General Hospital and Harvard Medical School, 32 Fruit St., Boston, MA 02114. Address reprint requests to F. S. Chew.

Pictorial Essay

Intrathoracic Neurogenic Tumors: MR-Pathologic Correlation

Fumikazu Sakai,[1] Shusuke Sone,[1] Kunihiro Kiyono,[1] Atsunori Maruyama,[1] Hitoshi Ueda,[1] Jun Aoki,[1] Takashi Kawai,[1] Keiko Ishii,[2] Masami Morimoto,[3] Masayuki Haniuda,[3] and Tomonobu Koizumi[4]

An MR-pathologic correlation of nine intrathoracic neurogenic tumors (three neurofibromas, four schwannomas, and two ganglioneuromas) was performed to characterize their MR appearances. The three types of intrathoracic neurogenic tumor were found to have characteristic appearances on MR images that should be helpful when establishing the differential diagnosis of posterior mediastinal tumors. The MR and histologic features of these tumors are illustrated and described in this essay.

The multiplanar capability and high contrast resolution of MR enable precise definition of the location and extent of intrathoracic neurogenic tumors. The absence of artifacts on MR caused by high-density bone, which often compromise CT scans, facilitates clear visualization of the intracanalicular extension of neurogenic tumors in paraspinal regions. One report [1] has noted characteristic MR findings in paraspinal neurofibromas in patients with neurofibromatosis: that is, high signal intensity in the peripheral zone of the mass and low signal intensity in the central zone on T2-weighted images. The high intensity was attributed to myxoid degeneration seen in pathologic specimens. Although a detailed CT-pathologic correlation of intrathoracic neurogenic tumors has been published [2], a detailed MR-pathologic correlation of intrathoracic neurogenic tumors is lacking. This prompted us to correlate MR features and histologic findings in nine surgically resected intrathoracic neurogenic tumors.

Subjects and Methods

Our study group comprised nine patients with intrathoracic neurogenic tumors (three neurofibromas, four schwannomas, and two ganglioneuromas). The group included seven women and two men. All three patients with neurofibromas had stigmata of neurofibromatosis. The remaining six patients with schwannomas or ganglioneuromas had no evidence of neurofibromatosis. All nine patients had no symptoms related to their tumors, and the mass lesions were incidental findings on their chest radiographs. All nine tumors were resected, and a pathologic diagnosis was established.

MR images were obtained with either a 1.5-T (Signa, General Electric, Milwaukee, WI) or a 0.5-T (MRH-500, Hitachi Medical Co. Ltd., Tokyo, Japan) superconductive imaging unit with ECG gating and respiratory compensation. T1-weighted spin-echo images (RR/20–35 [TR/TE]) and proton density–weighted and T2-weighted multiecho images (2–3 × RR/20–35, 70–80) were acquired in axial planes, and T1-weighted images were acquired in coronal and/or sagittal planes. In two neurofibromas, three schwannomas, and one ganglioneuroma, T1-weighted axial and coronal and/or sagittal images were obtained after IV injection of 0.1 mmol of gadopentetate dimeglumine per kilogram body weight.

Received January 8, 1992; accepted after revision February 28, 1992.
[1] Department of Radiology, School of Medicine, Shinshu University, Asahi, Matsumoto, 390 Japan. Address reprint requests to F. Sakai.
[2] Department of Laboratory Medicine, School of Medicine, Shinshu University, Asahi, Matsumoto, 390 Japan.
[3] Department of Surgery, School of Medicine, Shinshu University, Asahi, Matsumoto, 390 Japan.
[4] Department of Internal Medicine, School of Medicine, Shinshu University, Asahi, Matsumoto, 390 Japan.

AJR **159:279–283, August 1992** 0361–803X/92/1592–0279 © American Roentgen Ray Society

In five tumors (three neurofibromas, one schwannoma, and one ganglioneuroma), MR images of the resected specimens were obtained by using the 1.5-T imaging unit or a 2.0-T chemical-shift imaging unit (General Electric, Fremont, CA). T1-weighted (400–600/20) spin-echo images and T2-weighted (2000–3000/80–120) images were obtained in axial and coronal planes. The resected specimens were cut in the same planes as those used to acquire the ex vivo MR images, and the pathologic findings in the specimens were compared with the corresponding MR images. In five tumors, MR images of resected specimens also were obtained to compare with

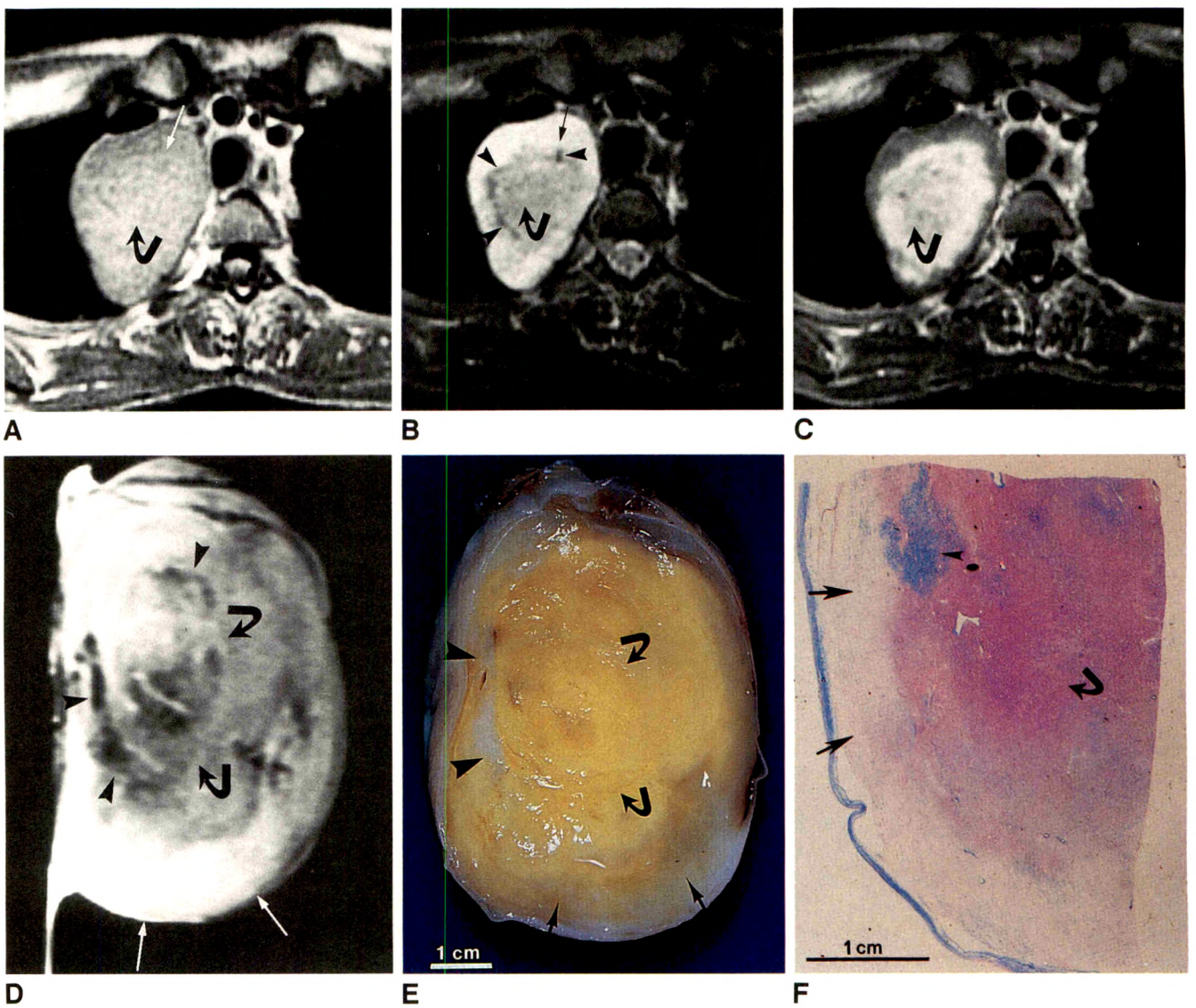


Fig. 1.—Vagal neurofibroma in a 57-year-old woman with neurofibromatosis.

A, T1-weighted (769/20) axial MR image shows a mass lesion in superior portion of mediastinum. Peripheral zone (*straight arrow*) of mass has low signal intensity, and central zone (*curved arrow*) has intermediate signal intensity.

B, T2-weighted (1538/80) axial MR image shows signal intensity of mass lesion is higher than that of fat in the peripheral zone (*straight arrow*). However, central zone (*curved arrow*) remains intermediate in intensity. Curvilinear or nodular low-intensity regions (*arrowheads*) are noted along boundary of central area and peripheral zone of mass.

C, Gadopentetate dimeglumine–enhanced T1-weighted (769/20) axial MR image shows remarkable contrast enhancement in central zone (*curved arrow*) of mass.

D, T2-weighted (2000/80) MR image of resected specimen shows peripheral zone (*straight arrows*) has a higher signal intensity than does central zone (*curved arrows*). Curvilinear or nodular low-intensity regions (*arrowheads*) are noted along boundary of central and peripheral zones.

E, Cut surface of gross specimen shows peripheral zone of resected mass has a gelatinous appearance (*straight arrows*) and central zone appears solid and yellowish (*curved arrows*). Nodular or linear whitish areas (*arrowheads*) are seen predominantly along boundary of central and peripheral zones.

F, Photomicrograph shows peripheral zone (*straight arrows*) has myxoid degeneration with scanty cellular components. Central area (*curved arrow*) has packed cellular components and xanthomatous changes. Linear and nodular areas of collagenous fibrous tissues (*arrowheads*) are seen, mainly along boundary of central area and peripheral zone. (Azan-Mallory stain)

preoperative MR images. In the evaluation of MR images and description of signal intensity, high intensity was defined as equal to or greater than that of fat, intermediate intensity as between the intensities of fat and skeletal muscle, and low intensity as equal to or less than the intensity of skeletal muscle.

Results

Neurofibroma

The three neurofibromas showed low to intermediate signal intensity on T1-weighted images with a slightly higher signal intensity in the central zone than in the peripheral zone (Fig. 1A). On T2-weighted images, the peripheral zone showed a higher intensity than fat and the central zone remained of intermediate intensity, with regional curvilinear or nodular low intensities along the boundaries of the central and peripheral zones (Fig. 1B). On contrast-enhanced MR images, enhancement was seen in the central zones (Fig. 1C).

At surgery, two of three neurofibromas were seen to arise from the vagus nerves, whereas the remaining neurofibroma arose from a thoracic spinal nerve root with extension into the spinal canal through an intervertebral foramen. Correlative study of T2-weighted images of the resected specimens and macroscopic findings disclosed that peripheral high-intensity zones on T2-weighted images corresponded to gelatinous regions, and central zones of intermediate intensity corresponded to solid tissue regions (Figs. 1D and 1E). Microscopically, the peripheral gelatinous regions showed myxoid degeneration and the central solid regions showed packed nerve sheath cells and fibrous tissues with xanthomatous changes (Fig. 1F). The curvilinear or nodular whitish areas seen on T2-weighted images between the central and peripheral zones were composed of collagenous fibrous tissue (Fig. 1F).

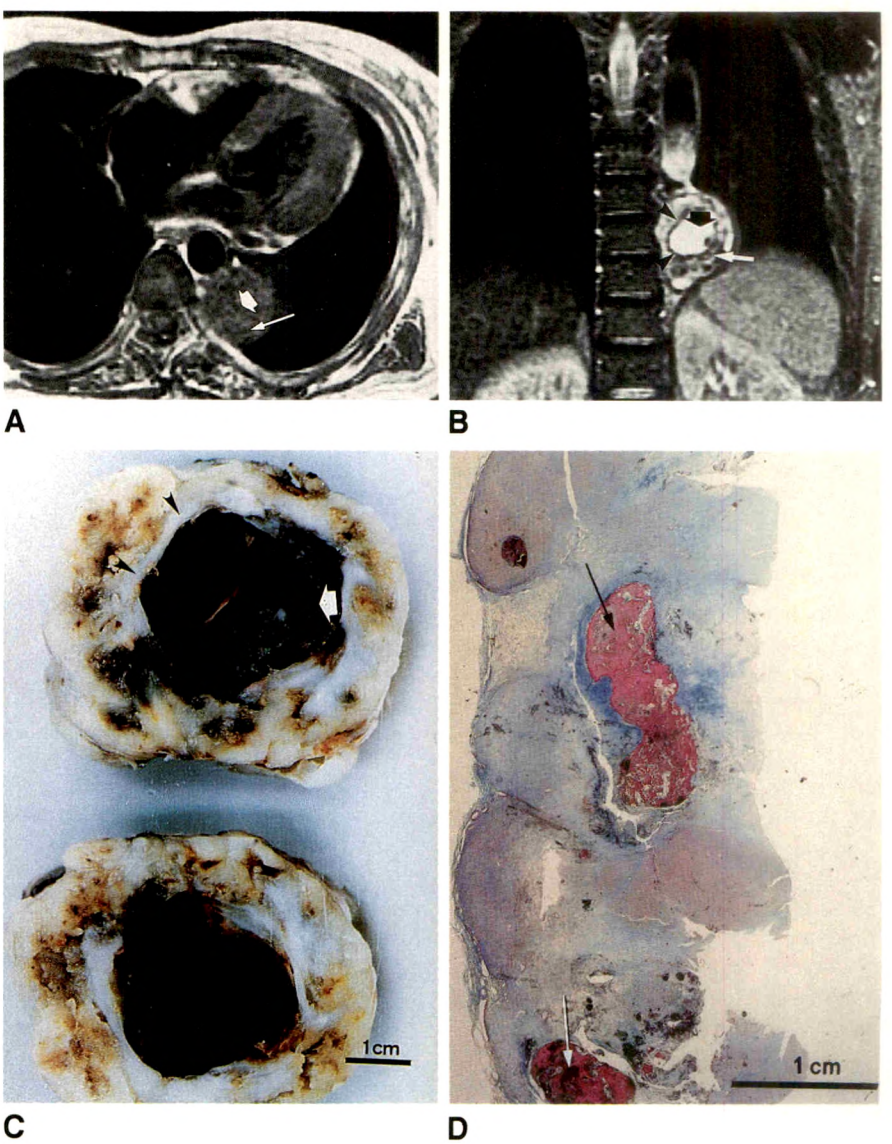


Fig. 2.—Paraspinal schwannoma in a 68-year-old woman.

A, T1-weighted (857/20) axial MR image shows a mass lesion with intermediate signal intensity in paraspinal region. Central portion (*short arrow*) of mass has a somewhat lower intensity than does peripheral portion (*long arrow*).

B, T2-weighted (2571/80) coronal MR image shows signal intensity of central portion (*black arrow*) of mass lesion is higher than that of peripheral portion (*white arrow*). Peripheral portion includes several small high-intensity regions. Linear low intensity (*arrowheads*) encircles central high-intensity portion.

C, Cut surface of resected specimen shows a large region of unilocular cystic degeneration (*arrow*) in mass lesion. This corresponds to central high-intensity region seen on T2-weighted MR images. Collagenous fibrous layer encircles cystic region (*arrowheads*).

D, Photomicrograph shows foci of cystic degeneration scattered in tumor (*arrows*). (Azan-Mallory stain)

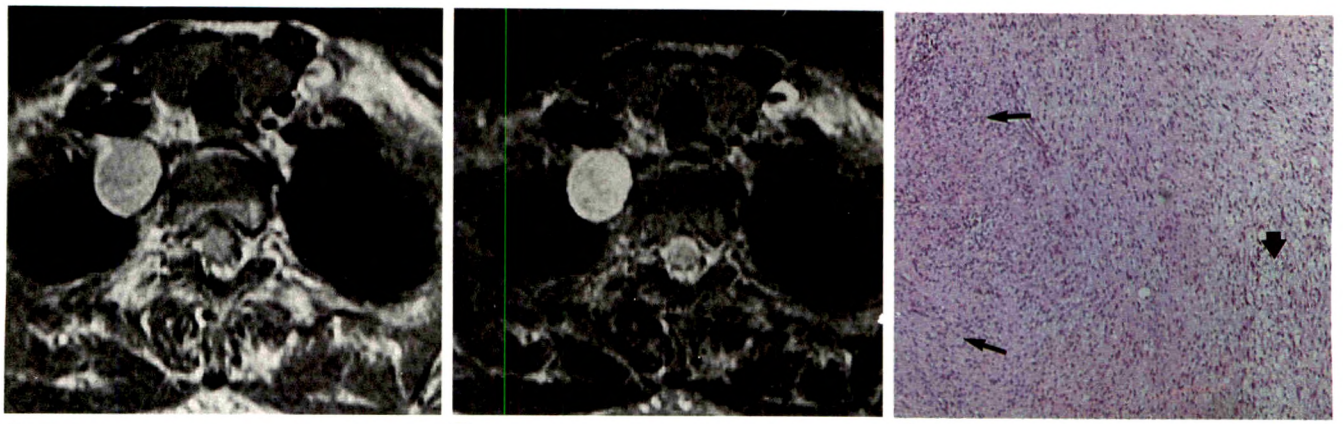


Fig. 3.—Paraspinal schwannoma in a 56-year-old woman.
A, T1-weighted (779/20) axial MR image shows round mass lesion with intermediate signal intensity in paraspinal region.
B, T2-weighted (1667/80) axial MR image shows signal intensity of mass is inhomogeneously high.
C, Tumor was resected transcervically and divided into several pieces. Photomicrograph of resected specimen shows tumor has alternating Antoni type A (*thin arrows*) and type B (*thick arrow*) areas with very little cystic degeneration. (H and E, original magnification ×40)

Schwannoma

Schwannomas showed low to intermediate signal intensity on T1-weighted images (Figs. 2A and 3A). On T2-weighted images, they showed inhomogeneously high intensity (Figs. 2B and 3B). Two of four schwannomas showed very high-intensity regions within the tumor (Fig. 2B). They were found to be of paraspinal origin at surgery. Very high-intensity regions seen on T2-weighted images of two schwannomas corresponded to cystic degeneration with surrounding collagenous fibrous tissue (Figs. 2C and 2D). Two schwannomas that lacked very high-intensity regions on T2-weighted images lacked foci of cystic degeneration on histopathologic specimens (Fig. 3C).

Ganglioneuroma

The two ganglioneuromas showed relatively homogeneous intermediate signal intensity on T1-weighted images (Fig. 4A). On T2-weighted images, the signal intensity was inhomogeneously high (Fig. 4B). A whorled appearance caused by curvilinear or nodular bands of low intensity was noted on both T1- and T2-weighted images (Figs. 4A and 4B). Coronal MR images clearly showed intracanalicular extension (Fig. 4C). At surgery, both ganglioneuromas had a paraspinal origin. The cut surface of the ganglioneuromas showed a whorled appearance, which correlated well with MR images (Figs. 4D and 4E). Ganglion cells, nerve sheath cells, and nerve fibers were seen on microscopic specimens (Fig. 4F). Areas of curvilinear or nodular low intensities on MR images corresponded to collagenous fibrous tissue on pathologic specimens (Fig. 4F).

Discussion

Neurogenic tumors of various histologic types may arise in the thorax. Neurofibromas may manifest as solitary tumors or may be one manifestation of neurofibromatosis. Histologically, neurofibromas show proliferation of nerve sheath cells interspersed with thick wavy collagen bundles and may show variable degrees of myxoid degeneration [3, 4]. Schwannomas arise from nerve sheath cells and occur less commonly than neurofibromas in patients with neurofibromatosis. Schwannomas are divided histologically into two types: Antoni type A shows compactly packed nerve sheath cells, sometimes with palisading of tumor cells, Antoni type B shows scattered tumor cells within myxoid matrices [3, 4]. Both types may be present in a single schwannoma [3]. Inadequate blood supply to the center of the tumor sometimes causes cystic degeneration or hyalinization. Xanthomatous changes also may occur in schwannomas. Ganglioneuromas are composed of large ganglion cells, nerve sheath cells, and nerve fibers. Ganglioneuromas show a typical trabeculated or whorled appearance macroscopically on the cut surface [4].

Our study shows that MR findings correlate well with pathologic findings of intrathoracic neurogenic tumors. On T2-weighted images, high-intensity regions in the periphery of neurofibromas corresponded to myxoid degeneration, as reported by Burk et al. [1]. Curvilinear or nodular areas of low signal intensity corresponded to collagenous fibrous tissue. These fibrous tissues were arranged along the boundaries between the central and peripheral zones in the three neurofibromas. The inhomogeneously high-intensity appearance of schwannomas on T2-weighted images corresponded to alternating Antoni A and B areas. A central very high-intensity region on T2-weighted images of schwannomas corresponded to areas of cystic degeneration. The two ganglioneuromas showed a whorled appearance on MR that corresponded to intermingled neural tissues and collagenous fibrous tissues on histopathologic specimens.

Because our observations are based on a limited number of patients, the true specificity of these MR findings awaits further investigation. However, some of the patterns seen on

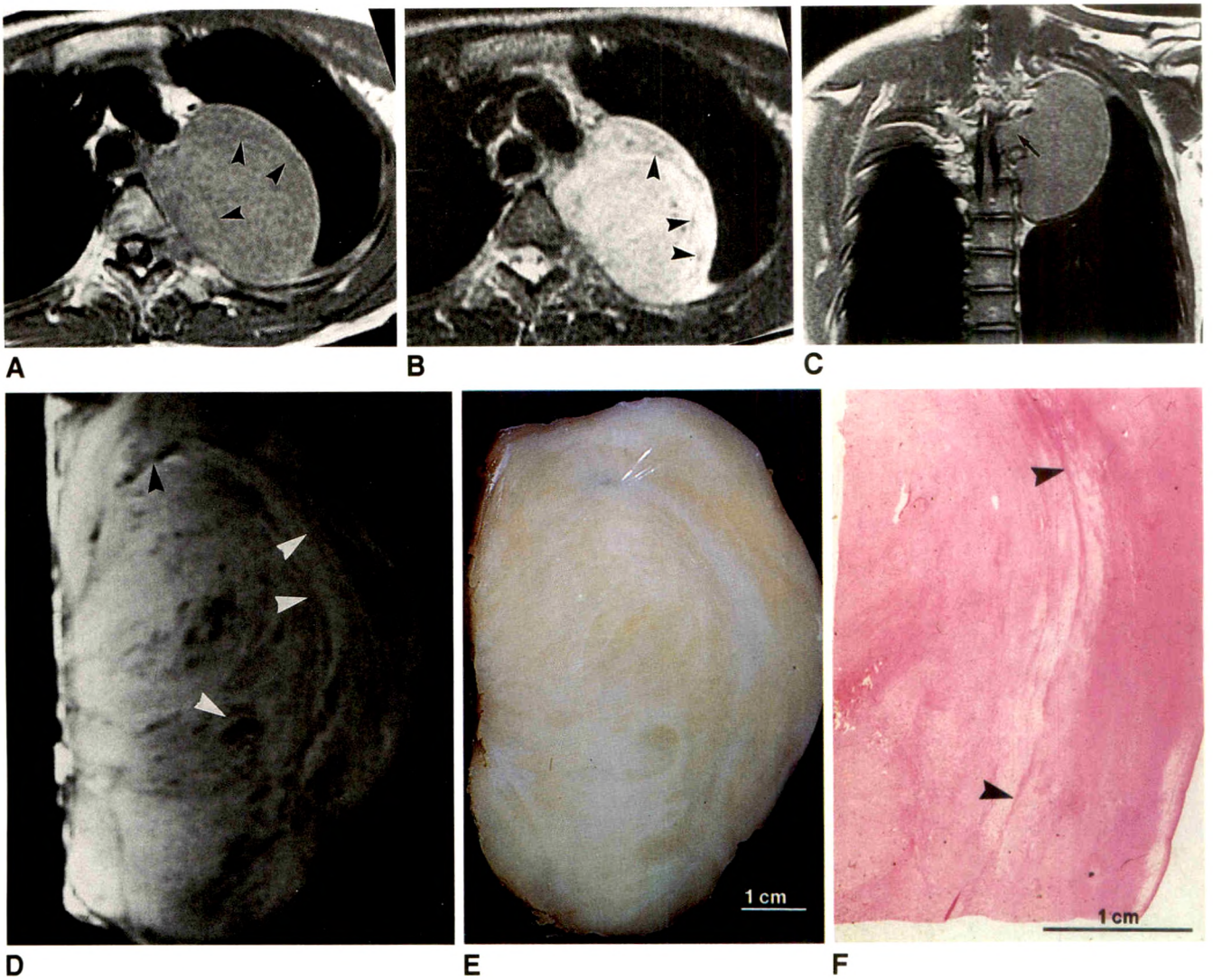


Fig. 4.—Paraspinal ganglioneuroma in a 17-year-old girl.
***A*, T1-weighted (857/20) axial MR image shows intermediate-intensity mass in paraspinal region with curvilinear low-intensity areas (*arrowheads*).**
***B*, T2-weighted (1714/80) axial MR image shows curvilinear or nodular low-intensity areas (*arrowheads*) within high-intensity mass, which has a somewhat whorled appearance.**
***C*, T1-weighted (857/20) coronal MR image shows mass lesion extends into spinal canal through an intervertebral foramen (*arrow*).**
***D*, T2-weighted (2500/100) MR image of resected specimen shows a whorled appearance caused by curvilinear or nodular bands of low intensity (*arrowheads*).**
***E*, On cut surface of resected specimen, same whorled appearance is seen.**
***F*, Photomicrograph shows curvilinear ares of collagenous fibrous tissue (*arrowheads*) within tumor. (H and E)**

MR images may prove to be characteristic of various types of intrathoracic neurogenic tumors.

REFERENCES

1. Burk DL Jr, Brunberg JA, Kanal E, Latchaw RE, Wolf GL. Spinal and paraspinal neurofibromatosis. *Radiology* **1987**;162:797–801
2. Cohen LM, Schwartz AM, Rockoff SD. Benign schwannomas: pathologic basis for CT inhomogeneities. *AJR* **1986**;147:141–143
3. Harkin JC, Reed RJ. Tumors of the peripheral nervous system. In: *Atlas of tumor pathology*, 2nd series, fascicle 3. Washington, DC: Armed Forces Institute of Pathology, **1969**:29–96
4. Enzinger FM, Weiss SW. *Soft tissue tumors*, 2nd ed. St. Louis: Mosby, **1983**

News

Ina L. D. Tonkin, 1992–1993 Distinguished Scientist, Armed Forces Institute of Pathology

James L. Buck[1]



Ina L. D. Tonkin will serve as the Distinguished Scientist in the Department of Radiologic Pathology, the Armed Forces Institute of Pathology (AFIP), from July 1, 1992, to June 30, 1993. Dr. Tonkin is a professor of diagnostic radiology and pediatrics at the University of Tennessee Medical Center and has served as codirector of the Department of Radiology, director of the Vascular and Interventional Laboratory, and codirector of the Cardiac Catheterization Laboratory of LeBonheur Children's Medical Center and St. Jude Children's Research Center in Memphis, TN.

Dr. Tonkin received her B.A. from Depauw University in 1966 and her M.D. from the University of Louisville School of Medicine in 1970. Her internship in pediatrics, residency in diagnostic radiology, and 2-year National Institutes of Health academic cardiovascular fellowship were all at the University of Florida in Gainesville. She is certified by the American Board of Radiology. After serving on the faculty of the University of Arizona and the University of Alabama, she moved to the University of Tennessee in 1979. She has remained at the same institution since that time, earning the rank of professor in 1984.

Her major areas of interest have been the use of angiography and noninvasive imaging techniques for the evaluation of congenital heart disease and the use of vascular and interventional techniques for the diagnosis and treatment of other diseases in infants and children. She has been the author or coauthor of more than 45 publications in the radiologic literature and has served as a visiting professor or invited speaker at innumerable institutions and courses. She serves on the editorial boards of the *Journal of Thoracic Imaging* and *Cardiovascular and Interventional Radiology* and is a reviewer for eight additional journals in the fields of radiology and cardiology. She is the editor of the recently published book *Pediatric Cardiovascular Imaging.* She has been active in numerous local and national medical societies and has served as treasurer of the Society for Pediatric Radiology and president of the North American Society for Cardiac Imaging.

The AFIP is honored to have Dr. Tonkin bring her expertise in pediatric and cardiovascular and interventional radiology to the Department of Radiologic Pathology. Her arrival this year is especially fitting because it coincides with the creation of a new section of pediatric radiology at the AFIP.

The Distinguished Scientist position in radiologic pathology at the AFIP is federally funded through the American Registry of Pathology and is also supported by generous contributions from the American College of Radiology, the Radiological Society of North America, the American Roentgen Ray Society, and the Association of University Radiologists. It is available to established academic radiologists who wish to spend a sabbatical year participating in the teaching and research activities of the Department of Radiologic Pathology. Those interested in applying for the 1994–1995 academic year should submit a letter of interest and a copy of their curriculum vitae to Dr. James L. Buck, Dept. of Radiologic Pathology, Armed Forces Institute of Pathology, Washington, DC 20306-6000. Applications will be accepted until December 31, 1992.

The opinions and assertations contained herein are the private views of the author and are not to be construed as official or as reflecting the views of the Department of Navy or the Department of Defense.

[1] Department of Radiologic Pathology, Armed Forces Institute of Pathology, Washington, DC 20306-6000.

Case Report

Transesophageal Echocardiography for the Evaluation of Atherosclerosis of the Thoracic Aorta

Robert A. Singer,[1] Dean G. Karalis, Pasquale M. Procacci, David Naide, John J. Ross, Jr., and Krishnaswamy Chandrasekaran

Cholesterol embolism can occur spontaneously or after an invasive procedure involving the aorta or peripheral arteries [1]. In a patient with a history of cholesterol embolization, one would expect transfemoral angiography to be associated with a high risk of recurrent embolization. Extensive atherosclerosis is usually less common in the ascending aorta and aortic arch, and therefore, a brachial arterial approach might reduce the risk of cholesterol embolization [2].

However, recent studies have shown that extensive atherosclerosis is common in the ascending thoracic aorta and arch of older patients [3]. In these patients, angiography via the brachial approach may result in a more severe and life-threatening embolism than if the femoral approach had been used. Therefore, knowledge of the extent of atherosclerotic disease would be useful before manipulating a catheter across the proximal aorta. We report a case in which transesophageal echocardiography played an important role in the management of a patient with a history of cholesterol embolization who was referred for angiography.

Case Report

A 68-year-old woman with peripheral vascular disease and hypertension was referred to our institution for aortic and femoral angiography to assess the possibility of peripheral arterial revascularization. Two months earlier, a renal artery angioplasty performed via the femoral artery was complicated by cholesterol embolization to both lower extremities, resulting in gangrene of both feet. For this reason, a brachial arterial approach was planned.

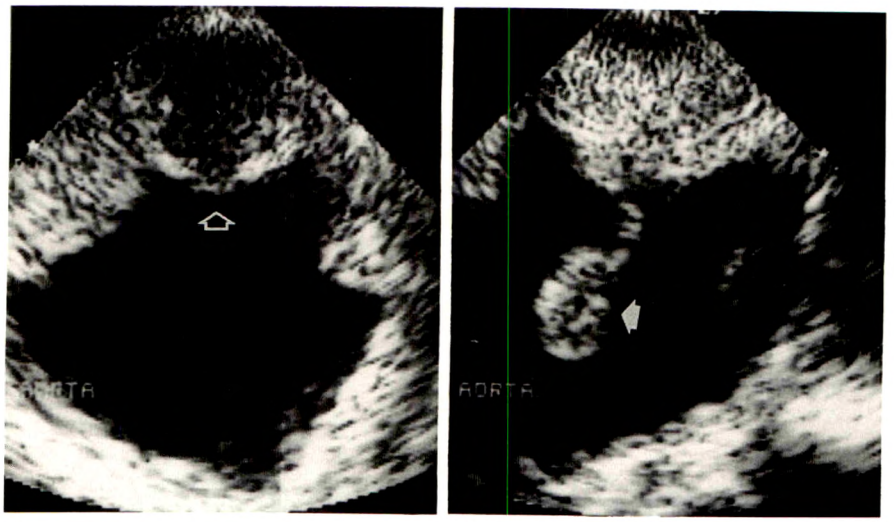
On physical examination, the patient's blood pressure was 178/82 mm Hg in both arms. Carotid bruits were heard bilaterally, although no abdominal bruits were heard. The lower extremities were warm with dry black gangrene involving nine of the 10 toes. No pulses were palpable below the femoral artery bilaterally. No aortic calcifications were seen on chest radiographs. Transesophageal echocardiography was done before angiography to assess the extent of atherosclerosis within the thoracic aorta. Transesophageal echocardiography was performed with a biplane 5.0-MHz phased-array echoscope connected to a Hewlett-Packard Sonos 1000 sonographic imaging system. After obtaining informed consent, we anesthetized the oropharynx with serial applications of an aerosolized 10% solution of lidocaine. Sedation was achieved with IV midazolam hydrochloride. A comprehensive transesophageal echocardiographic examination of the heart and aorta was performed by using previously described standardized scanning planes [4]. Extensive protruding atheromatous plaques with many pedunculated, highly mobile projections were observed diffusely throughout the distal ascending aorta, aortic arch, and descending thoracic aorta (Fig. 1). On the basis of the results of the transesophageal study, we thought that the risk of stroke or major visceral embolism would be high if the aorta were approached from either brachial artery. The patient was therefore managed conservatively with prophylactic foot care and oral pentoxifylline, 400 mg three times a day.

Discussion

Cholesterol embolization is an uncommon but well-recognized complication after angiographic procedures involving the aorta [1]. Atheroemboli are usually thought to originate from atherosclerotic plaques within the lower abdominal aorta. As the thoracic aorta is less commonly involved with atherosclerosis, one would expect that passing a catheter into the descending thoracic aorta from the brachial artery would be less likely to cause cholesterol embolization than

Received January 28, 1992; accepted after revision March 3, 1992.
[1] All authors: Likoff Cardiovascular Institute, Department of Medicine, Hahnemann University, Broad and Vine Sts., Mail Stop 313, Philadelphia, PA 19102-1192. Address reprint requests to D. G. Karalis.

 0361–803X/92/1592–0285 © American Roentgen Ray Society



A B

Fig. 1.—*A* and *B*, Transesophageal echocardiograms of long axis (*A*) and short axis (*B*) of aortic arch. Protruding atheromatous debris (*open arrow*) is extensive. Although not visible on still-frame image, parts of atheromatous debris were pedunculated and highly mobile (*solid arrow*).

when the aorta is approached from the femoral artery. However, in patients with peripheral vascular disease in the Coronary Artery Surgery Study (CASS), catheterization from the brachial approach resulted in embolism and death more often than catheterization from the femoral approach did [5]. This may be because extensive atherosclerosis involving the ascending thoracic aorta and arch is more common than previously thought. In a study of 97 cadaveric specimens of the ascending aorta in adults with clinical coronary artery disease, the prevalence of atherosclerotic plaques greater than 8 mm in diameter was 38% [6]. Intraoperative studies that used sonography to image the ascending thoracic aorta have shown protruding atheromatous plaque in up to 58% of patients undergoing coronary bypass surgery [3].

Transesophageal echocardiography is limited in evaluating the abdominal aorta for atherosclerosis, but it can provide high-quality images of the intimal surface of most of the thoracic aorta [4]. Although semiinvasive, transesophageal echocardiography has been shown to be extremely safe when performed by a skilled echocardiographer [7]; the main contraindication is esophageal disease. We have previously shown that transesophageal echocardiography can easily visualize protruding atheromatous plaque (intraaortic atherosclerotic debris) in the thoracic aorta and that the morphologic characteristics of the atherosclerotic debris are important in predicting embolic risk [8]. Intraaortic atherosclerotic debris that is pedunculated and highly mobile is more likely to embolize than is layered immobile aortic debris. Similar findings have been reported by Tunick et al. [9], supporting the conclusion that atheroscleotic debris in the thoracic aorta is associated with a high risk of embolism.

Risk factors for atherosclerotic debris of the thoracic aorta include advanced age, hypertension, cerebrovascular or peripheral vascular disease, and a history of arterial embolism [10]. Patients with a high-risk profile should be considered for screening transesophageal echocardiography. Transesophageal echocardiography can provide the vascular radiologist with information regarding the extent of atherosclerotic disease in the thoracic aorta before a catheter is advanced into the descending thoracic aorta from the brachial approach. If the ascending thoracic aorta and arch have minimal atherosclerotic disease, then the risk of major visceral embolism or, more importantly, stroke from the brachial approach would probably be low. If atherosclerotic debris is extensive, especially if the aortic debris is pedunculated and highly mobile, then the risk of stroke or major visceral embolization would be expected to be higher.

REFERENCES

1. Dahlberg PJ, Frecentese DF, Cogbill TH. Cholesterol embolism experience with 22 histologically proven cases. *Surgery* **1989**;105:737–746
2. Gaines PA, Reidy JF. Percutaneous high brachial aortography: a safe alternative to the translumbar approach. *Clin Radiol* **1986**;37:595–597
3. Marshall WG, Barzilai B, Kouchoukos WT, Saffitz J. Intraoperative ultrasonic imaging of the ascending aorta. *Ann Thorac Surg* **1989**;487:339–344
4. Seward JB, Khandheria BK, Oh JK, et al. Transesophageal echocardiography: technique, anatomic correlations, implementation and clinical applications. *Mayo Clin Proc* **1988**;63:649–680
5. Davis K, Kennedy JW, Kemp HG, Judkins MP, Gosselin AJ, Killip T. Complications of coronary arteriography from the Collaborative Study of Coronary Artery Surgery (CASS). *Circulation* **1979**;59:1105–1112
6. Tobler HG, Edwards JE. Frequency and location of atherosclerotic plaques in the ascending aorta. *J Thorac Cardiovasc* **1988**;96:304–306
7. Daniel WG, Erbel R, Kasper W, et al. Safety of transesophageal echocardiography: a multicenter survey of 10,419 examinations. *Circulation* **1991**;83:817–821
8. Karalis DG, Chandrasekaran K, Victor MF, Ross JJ, Mintz GS. Recognition and embolic potential of intraaortic atherosclerotic debris. *J Am Coll Cardiol* **1991**;17:73–78
9. Tunick PA, Perez JL, Kronzon I. Protuding atheromas in the thoracic aorta and systemic embolization. *Ann Intern Med* **1991**;115:423–427
10. Amarenco D, Duyckaerts C, Tzourio C, et al. The prevalence of ulcerated plaques in the aortic arch in patients with stroke. *New Engl J Med* **1992**;326:221–225

Interval Carcinomas in the Malmö Mammographic Screening Trial: Radiographic Appearance and Prognostic Considerations

Debra M. Ikeda[1,2]
Ingvar Andersson[1]
Cecilia Wattsgård[1]
Lars Janzon[3]
Folke Linell[4]

OBJECTIVE. Interval carcinoma is the term used to describe malignant breast tumors that are detected in the intervals between mammographic screenings. These tumors are important because they contribute significantly to breast cancer mortality in the screened population.

MATERIALS AND METHODS. Two radiologists retrospectively reviewed the mammograms of the 96 interval carcinomas (17% of all malignant neoplasms in the screened group) that were detected during the 10-year Malmö Mammographic Screening Trial in Malmö, Sweden (average time between screenings, 21 months), including one sarcoma, 75 invasive carcinomas, and 20 noninvasive carcinomas. We recorded the interval between screening and detection, and noted the tumor's appearance on the prior screening mammogram and at the time of diagnosis; these data were correlated with histologic tumor type and the patients' mortality. The doubling time for tumor volume of the invasive carcinomas was estimated.

RESULTS. Excluding the sarcoma, 72 carcinomas (75%) were detected within 18 months of screening. Retrospective review of the available preceding screening mammograms (94 cases) indicated that 10 tumors were missed (observer's error), 63 studies showed no tumor (true interval carcinomas), and 21 studies showed subtle signs of malignancy, mostly nonspecific densities or asymmetries (unrecognized sign). Of 66 invasive carcinomas in which doubling times for tumor volume could be calculated, 27 (41%) had doubling times of less than 100 days. At the end of the study, 20 of the 96 patients had died of breast cancer.

CONCLUSION. Interval carcinomas in this series were dominated by comedo, medullary, and mucinous carcinomas that often had a nonspecific appearance (when present) on prior screening mammograms. The interval carcinomas also contained a subset of rapidly growing tumors with a grave prognosis.

AJR 159:287–294, August 1992

Received October 24, 1991; accepted after revision February 25, 1992.

Presented in part at the annual meeting of the American Roentgen Ray Society, Washington, DC, May 1990.

[1] Department of Radiology, Malmö General Hospital, S-21401 Malmö, Sweden.

[2] Present address: Department of Radiology, University of Michigan Hospitals, 1500 E. Medical Center Dr., Room TC-2910, Box 0326, Ann Arbor, MI 48109-0326. Address reprint requests to D. M. Ikeda.

[3] Department of Epidemiology, Malmö General Hospital, S-21401 Malmö, Sweden.

[4] Department of Pathology, Malmö General Hospital, S-21401 Malmö, Sweden.

0361–803X/92/1592–0287
© American Roentgen Ray Society

The term interval carcinoma describes malignant breast tumors that are detected in the intervals between mammographic screenings. These tumors are important because they contribute significantly to mortality in the screened population [1, 2]. Evaluation of characteristics of interval cancers may suggest interventions to decrease the number of such cancers in future screening programs.

Previous investigations involving a retrospective review of the preceding "negative" screening mammograms, considered not suggestive of malignancy, indicate that some interval cancers can be accounted for by technical or interpretive errors [3–5]. Some mammographically typical tumors are overlooked at screening (observer's error). Other carcinomas show detectable but nonspecific mammographic signs of malignancy that are misinterpreted (unrecognized sign). The remainder of cases without pathologic changes on the preceding screening mammograms have been called "true" interval carcinomas.

A controlled breast cancer screening trial with mammography took place from October 1976 through December 1986 in Malmö, Sweden [1, 6]. At the predetermined end of the study, 100 interval carcinomas had been detected [1, 6]. This

report describes the results of a retrospective review of the mammograms, correlation of radiographic findings with the tumor types, and evaluation of prognostic variables including doubling times for tumor volume of the interval carcinomas from the Malmö Mammographic Screening Trial (MMST).

Materials and Methods

The design of the screening trial has been described previously in detail [1, 6]. Briefly, 50% of a random sample of all women 45–69 years old living in Malmö in 1976 (approximately 21,000) were invited to have mammographic screening. The remaining 50% constituted a control group. Randomization was done on an individual basis, and mammography was the only technique used for screening. The planned interval between screenings was 18–24 months and was, in practice, an average of 21 months. In practice, the first interval between screenings was slightly longer than the subsequent intervals. During the first and second screenings, craniocaudal and mediolateral oblique views were obtained in all patients. During the third and subsequent screenings, two views of each breast were obtained in patients with radiographically dense fibroglandular tissue corresponding to Wolfe's patterns P2 or DY [7]. A single mediolateral oblique view of each breast was obtained in patients with less dense tissue (N1 or P1 Wolfe patterns).

By the predetermined end of the MMST, all of the fifth and most of the sixth screening rounds had been completed. The attendance rate was 74% in the first round and slightly lower in subsequent rounds (70%), and higher among younger women than among older women [1].

The screening mammograms and the mammograms obtained at the time of cancer diagnosis were retrospectively reviewed by two radiologists for signs of malignancy. In order to estimate breast density, each case was categorized into the Wolfe classification [7]. At the time of the design of this project (prior to 1976), the Wolfe classification system [7] was widely used to categorize the mammographic appearances of breast tissue. Although this classification system has been used by others to predict the risk of subsequent development of breast cancer, for the purposes of our study, the Wolfe classifications were used to determine whether patients were to have one- or two-view mammograms for screening on the basis of breast density. Patients with primarily radiodense breasts (Wolfe's DY or P2 classification) had two-view examinations and those with radiolucent breasts (Wolfe's N1 or P1) had single-view examinations, as stated previously. The studies were reviewed together with the clinical history, films of radiographically guided fine-needle aspirations, cytologic results, specimen radiographs, and pathologic reports to ensure that the mammographic finding corresponded to a malignant tumor. A pathologist and the radiologists reviewed the films and histologic slides together if there were discrepancies between the mammographic impression and the pathologic report (seven cases).

Findings on the screening mammograms and mammograms at the time the interval cancers were diagnosed were judged as either normal or abnormal, with abnormalities classified into calcifications, well-circumscribed tumor, poorly defined tumor, spiculated mass, architectural distortion, prominent nodules or ducts, and developing density/asymmetry. Each radiologic finding was classified as nonspecific, atypical but suggestive of cancer, or diagnostic of carcinoma. As a matter of general practice, solitary new circumscribed masses were usually aspirated or a surgical biopsy was done; for five or more irregular, clustered calcifications a surgical biopsy was done; and asymmetric densities were considered benign if they had the appearance of normal overlapping dense fibroglandular breast tissue.

The tumor growth rates of the invasive cancers were estimated by a method described by Fournier et al. [8], in which the size of the tumor is measured on two subsequent mammograms (66 cases). In order to calculate tumor growth rates in patients in whom no abnormality was visible on the previous screening mammogram, an initial 5-mm tumor size was designated for women with less dense breasts (Wolfe's patterns N1 and P1) and a 10-mm initial tumor size was designated for women with denser breasts (Wolfe's patterns P2 and DY); doubling times may have been slightly underestimated in these cases. When an exact measurement of the tumor was not possible on the mammograms obtained when the interval cancer was diagnosed, the tumor size measured at pathologic examination was used. Doubling times for tumor volume were not calculated if the tumor was not reasonably measurable radiographically or pathologically at the time of cancer diagnosis (often the case in extensive breast cancer), if mammograms were not obtained at the time of cancer diagnosis, or if the tumor was not included on the films at screening or before surgery (10 cases).

The average age at detection was younger for the patients with interval carcinoma (60 years) than for patients in whom carcinomas were detected at screening (62 years) and for control subjects (62 years) [1]. The median size of invasive interval cancers was 1.9 cm, that of cancers detected at screening was 1.0 cm, and that of cancers in the control group was 1.9 cm [1].

Axillary metastases were present in 36% of patients with interval invasive carcinoma, 23% of patients with cancers detected at screening, and 44% of control subjects. Forty-two percent of the patients with interval cancer were classified as having stage II cancer or higher, compared with 19% of patients with cancer detected at screening and 52% of control subjects [1]. A proportional hazards analysis, stratified for stage and with adjustment for age at diagnosis, revealed a relative risk of 2.3 of dying from breast cancer for patients with interval cancer as compared with control subjects [1].

Results

Interval Cancer Population Characteristics

In the interval between an initial mammographic examination with normal results and the second screening, breast cancer was detected in 33 women. The corresponding figures for the second through fifth intervals were 18, 17, 11, and 20 cancers, respectively. By the predetermined end of the MMST, part of the sixth round had been completed, and one more interval cancer had been detected, for a total of 100 interval cancers (17% of all cancers in the screened group) [1]. During the same period, breast cancer was diagnosed in 374 screening patients, in 107 women who were invited for mammography but who did not attend the screening, and in 447 women in the control group [1].

Seventy-five of the 100 interval carcinomas were invasive, 24 were noninvasive, and one fibrosarcoma was not classified as invasive or noninvasive. The noninvasive cancers included four cases of lobular carcinoma in situ either found incidentally during pathologic examination of subcutaneous mastectomy material (three cases) or in material excised for a benign palpable mass (one case). These four cases are excluded in the following data analysis.

Excluding the fibrosarcoma, 44 cases (46%) of all interval carcinomas appeared within 12 months of a previous screening, and 72 cases (75%) appeared within 18 months of screening (Table 1). Of the 75 invasive carcinomas, 34 (45%) appeared within 12 months and 55 (73%) appeared before

TABLE 1: Histologic Type of Cancer vs Months Between Screening Mammogram and Diagnosis of Interval Cancer

Histologic Type	No. of Cancers					
	0–6 Months	7–12 Months	13–18 Months	19–24 Months	24+ Months	Total (%)
Tubular	2	2	1	2	1	8 (8)
Tubuloductal	2	3	4	6	0	15 (16)
Invasive comedo, medullary, mucinous	3	15	11	8	0	37 (38)
Lobular	3	4	4	3	0	14 (15)
Carcinoma in situ	6	4	7	1	2	20 (21)
Other	1	0	1	0	0	2 (2)
Total	17	28	28	20	3	96 (100)

Note.—Histologic types were classified according to Linell and Ljungberg [9]. "Other" tumor types were a fibrosarcoma (0–6 months) and invasive tumor, no predominant histologic type (13–18 months).

18 months of screening. Ten (50%) and 17 (85%) of the 20 noninvasive carcinomas were seen within 12 and 18 months of screening, respectively.

The ratio of interval carcinomas to screening-detected carcinomas by age was higher in the younger women than in the older women (Table 2).

Eighty-one women (84%) had clinical signs and symptoms of breast disease, including a palpable mass (57 women), nipple discharge (10 women), or other problems (14 women). Of the remaining 15 women who had no signs or symptoms in the breast, five had a routine physical examination that showed a breast mass, nine had tumors detected on routine mammography outside the screening program, and one had an invasive lobular carcinoma found incidentally in subcutaneous mastectomy material.

Mammographic Findings

In two cases, preceding screening mammograms were not reviewed, as one set of previous screening films was missing and one mammogram did not include the lesion (technical error). The data on these two patients were excluded from the radiologic analysis where appropriate, but are included in the histology and mortality analysis of the entire interval cancer group.

TABLE 2: Interval Cancers as a Proportion of the Women Undergoing Mammography in the Malmö Mammographic Screening Trial

Age at Diagnosis (yr)	No. of Interval Carcinomas/ No. of Screening-Detected and Interval Cancers (%)
45–49	6/22 (27)
50–54	23/83 (28)
55–59	21/76 (28)
60–64	15/95 (16)
65–69	16/113 (14)
70–74	12/59 (20)
75–79	3/22 (14)
Total	96/470 (20)

Note.—Ages of women with screening-detected carcinomas are from the material described in Andersson et al. [1].

In 63 patients (66% of all cases) whose mammographic findings were considered normal at the time of screening, no findings were present to suggest a malignant growth even in retrospect ("true" interval carcinomas) (Fig. 1 and Table 3). These patients included two who had breast biopsy without preoperative mammograms and who had normal findings on previous screening studies at 2 and 21 months, respectively.

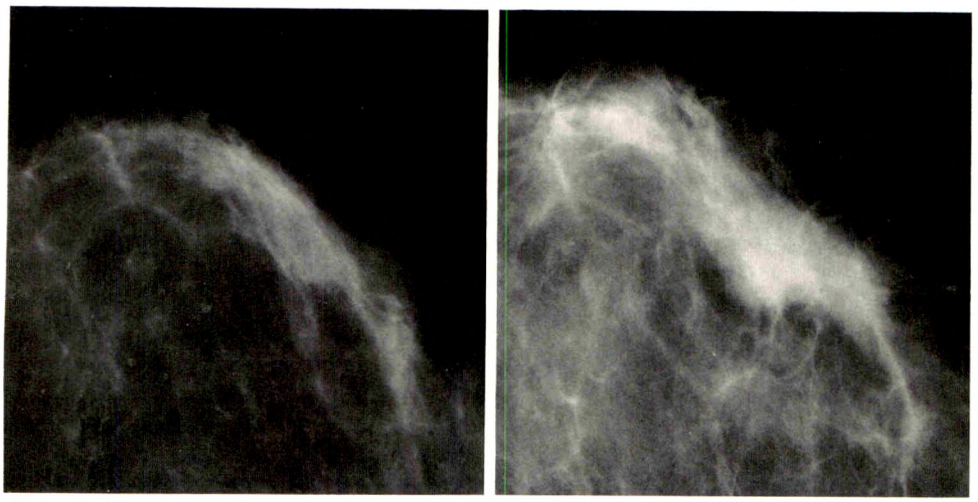
Twenty-one women (22% of all cases) had slight mammographic abnormalities that were evident in retrospect but would not have been selected for further evaluation (nonspecific sign) (Table 4). Seven patients (7% of cases) had clearly abnormal findings that were atypical but suggestive of cancer and likely misinterpreted (unrecognized sign). Three patients (3% of cases) had findings diagnostic for carcinoma that were probably overlooked at screening (observer error). Faulty image quality was not considered a contributing factor in the screening studies unless the lesion was not included on the films (one screening mammogram and one case in which the lesion was growing into the chest wall at the time of diagnosis). Technical factors may have been a contributing factor in two patients who had extremely dense fibroglandular breasts.

When the interval carcinoma was diagnosed, 79 patients (82%) had clearly abnormal findings on mammograms: 21 carcinomas, 42 lesions highly suggestive of cancer, and 16 abnormalities considered atypical but suggestive of cancer. One lesion was incompletely imaged owing to its location near the chest wall. Mammographic findings in 11 patients remained normal and showed slight abnormalities in two patients. In the remaining three cases, one lesion was growing into the chest wall at the time of cancer diagnosis and could not be imaged, and two patients had no films before surgery, as previously discussed.

Of the 96 patients, four, 35, 35, and 22 women were classified as having types N1, P1, P2 and DY breasts, respectively.

No Suggestive Findings on Previous Screening Studies (True Interval Carcinomas)

Of the 63 patients with no suggestive findings on previous screening mammograms in whom cancer developed, two had biopsies without preoperative films and one had a clinically



A B

Fig. 1.—True interval carcinoma in a 56-year-old woman.

***A*, Findings on craniocaudal mammogram (cropped) obtained in baseline screening study were interpreted as normal.**

***B*, Mammogram obtained 20 months after *A*, when patient noticed mass in breast, shows a 2.3-cm mass. Histologic examination showed an invasive ductal carcinoma.**

TABLE 3: Mammographic Findings on Previous Screening vs Histologic Type in 96 Interval Carcinomas

Histologic Type	Normal	Slightly Abnormal	Atypical but Suggestive of Cancer	Typical for Cancer	Total
Tubular	7	0	0	1	8
Tubuloductal	9	3	1	0	13
Invasive comedo, medullary, and mucinous	21	11	4	1	37
Lobular	10	2	1	1	14
Carcinoma in situ	14	5	1	0	20
Other	2	0	0	0	2
Total	63	21	7	3	94

Note.—Because one set of previous films was lost (tubuloductal) and one carcinoma was not included on films (tubuloductal), 94 instead of 96 interval carcinomas are tabulated here.

evident lesion near the chest wall that could not be included on the second set of films. In 25 (40%) of these 63 patients, cancer was diagnosed within 12 months of screening (including one invasive lobular carcinoma discovered at subcutaneous mastectomy); 19 of the 25 cancers were invasive, and nine (four invasive) occurred in women who had normal findings on mammograms at the time of diagnosis. Forty-nine cases (78%) were diagnosed within 19 months of a previous screening with normal results, and of these, 37 were invasive and 11 occurred in women who had normal mammographic findings.

Twenty-one (33%) of the true interval carcinomas were invasive comedo, medullary, or mucinous carcinomas, and 14 (22%) were ductal carcinoma in situ. Other carcinoma types included 10 (16%) invasive lobular, seven tubular, nine tubuloductal, one mixed tumor, and one fibrosarcoma.

The follow-up mammograms obtained when the cancer was diagnosed included a variety of findings: normal (11 cases), circumscribed tumors (15 cases), spiculated tumors (10 cases), suspicious calcifications (nine cases), architectural distortion and nodules (three cases each), nonspecific densities (four cases), nipple retraction (two cases), or other (three cases). Three other patients were not imaged at the time of cancer diagnosis because no preoperative films had been obtained (two cases) or the tumor could not be imaged owing to its location near the chest wall (one case).

Wolfe's patterns in this group included one N1, 27 P1, 22 P2, and 13 DY cases.

Slightly Abnormal Findings on Previous Screening Studies (Nonspecific Sign)

In 21 patients, an attempt was made to further classify the mammographic findings that had been rated as slightly abnormal on the previous screening mammograms. The abnormalities were mostly nonspecific, including 10 densities/asymmetries, four nonspecific calcification clusters, four benign-appearing circumscribed tumors, two poorly defined tumors, and one area of prominent ducts (Figs. 2–4). In some cases, the finding was seen only after the location of the tumor was determined on the follow-up mammograms (Fig. 4). Of note, no spiculated lesions (which are most easily detected at screening) were seen among these 21 cases (Table 4).

In all patients, films obtained when the interval cancer was diagnosed were rated as more suggestive of cancer. In slightly less than 50% of cases (10 patients), the tumor retained the

TABLE 4: Findings on and Interpretation of Preceding Screening Mammograms of 31 Interval Cancers

Finding	Interpretation		
	Slight Abnormality	Not Typical but Suggestive	Highly Suggestive
Calcifications	4	1	1
Circumscribed mass	4	3	0
Spiculated mass	0	0	1
Architectural distortion	0	1	1
Prominent ducts	1	1	0
Nonspecific density	6	1	0
Asymmetry	4	0	0
Poorly defined tumor	2	0	0
Total	21	7	3

same mammographic characteristic but became more suggestive of cancer on the follow-up films because of growth (Fig. 4). In 11 patients, the findings became more apparent because a different major characteristic developed: eight distinct tumors (two of which were spiculated) developed within an area of asymmetry or density, two rounded masses grew into large focal densities, and in one area of asymmetry a prominent duct pattern developed.

More than three quarters of tumors were invasive comedo, medullary, or mucinous carcinomas (11 cases, 52%) or ductal carcinomas in situ (five cases, 24%). Three tubuloductal and two lobular carcinomas accounted for the remaining cases. Fifteen cancers (71%) were diagnosed within 12 months of screening; of these, 12 were invasive.

Wolfe's patterns in this group included three N1, six P1, nine P2, and three DY patterns.

Findings Atypical but Suggestive of Cancer (Unrecognized Sign)

The seven patients with findings atypical but suggestive of carcinoma included three cases of circumscribed tumors and one case each of calcifications, architectural distortion, prominent duct pattern, and density. Six of the seven tumors were invasive, and of the invasive carcinomas, four were subse-

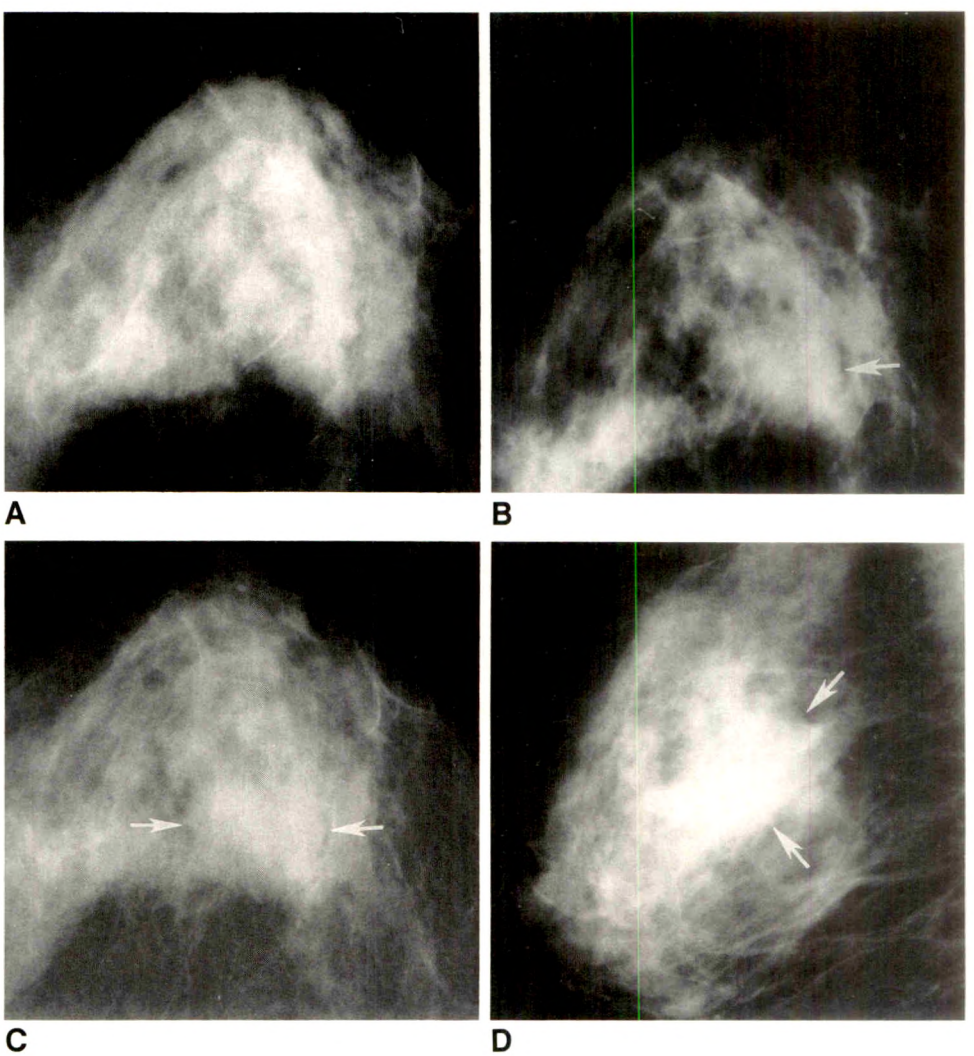


Fig. 2.—Slightly abnormal findings on prior screening study in a 53-year-old woman.

***A*, Craniocaudal mammogram (cropped) obtained in baseline screening study shows fibroglandular tissue with suggestion of multiple benign-appearing nodules. Findings were interpreted as normal.**

***B*, Two screening mammograms (*not shown*) obtained after *A* were unchanged. Craniocaudal mammogram obtained 57 months after *A* was interpreted as unchanged. In retrospect, edge of a nodular density (*arrow*) is seen centrally.**

***C* and *D*, Mammograms obtained 8 months after *B*, when patient noticed mass in breast, shows a nonspecific nodular mass (*arrows*) with one sharp medial edge on craniocaudal (*C*) and mediolateral (*D*) views (images cropped). Histologic examination showed a 3-cm mucinous carcinoma.**

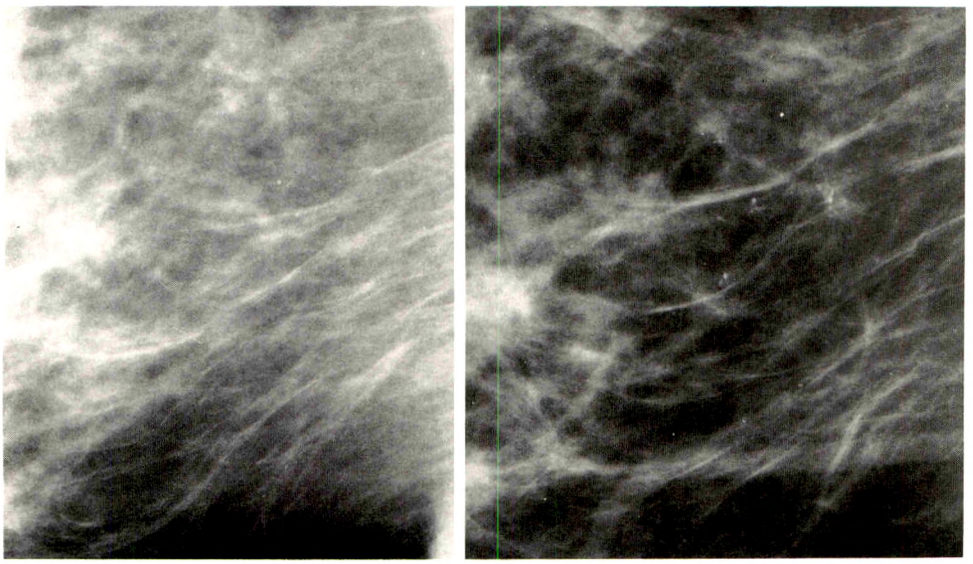


Fig. 3.—Slightly abnormal findings on prior screening study in a 63-year-old woman.

A, Mediolateral oblique screening mammogram (cropped) shows a few nonspecific calcifications.

B, Mammogram obtained 16 months later, outside screening program, shows interval development of suspicious calcifications. Histologic examination showed ductal carcinoma in situ.

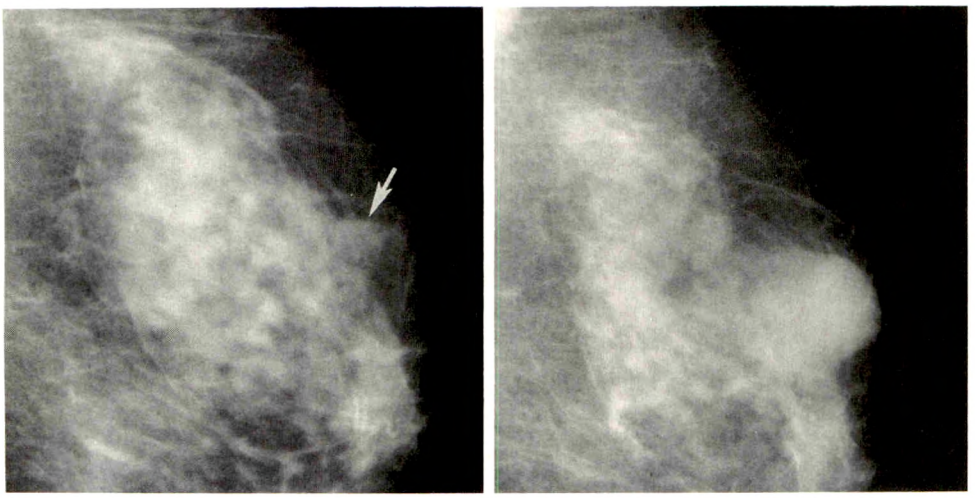


Fig. 4.—Slightly abnormal findings on prior screening study in a 54-year-old woman.

A, Mediolateral oblique mammogram (cropped) obtained in a baseline screening study shows a mixed fatty and glandular breast. Findings were interpreted as normal. In retrospect, a benign-appearing density (*arrow*) is visible in anterior part of breast.

B, Mammogram obtained 19 months after *A*, when patient noticed mass in breast, shows a 2.8-cm mass in region of density seen in *A*. Histologic examination showed mucinous carcinoma.

quently diagnosed within 12 months. On the follow-up studies, the major finding became more suspicious in appearance in six of seven cases. Wolfe's patterns in these cases were mostly dense (one P1, two P2, and four DY), and the main histologic finding was comedocarcinoma (four of seven cases).

Histologic Findings

Comedocarcinoma and medullary and mucinous carcinomas were the main histologic types, representing 38% (37) of all interval carcinomas. The other types of cancer are indicated in Table 1. Fifty (52%) of all interval cancers and a majority of the comedocarcinomas (22 cases) were seen in women less than 60 years old.

Doubling times for tumor volume.—Of the 66 cases in which doubling times for tumor volume could be calculated, 27 (41%) had a doubling time of less than 100 days; these could be considered relatively fast-growing tumors.

Carcinoma in situ.—There were 19 cases of ductal carcinoma in situ and one case of combined ductal carcinoma in situ/lobular carcinoma in situ. Of these 20 patients, eight had nipple discharge, six had a mass, and three had other signs and symptoms in the breast for which they sought advice. Four cancers were detected because suspicious microcalcifications were found on routine mammography outside the screening program. In total, 10 noninvasive cancers were diagnosed at or within 12 months of screening.

In 14 of the 20 cases, findings were normal on the previous screening mammograms, including three cases of Paget's disease of the nipple. Slight abnormalities were shown in five of the other six cases (two cases of benign-appearing calcifications and one case each of density, poorly defined mass, and asymmetry). The remaining patients had a cluster of

calcifications that was atypical but suggestive of cancer and was most likely misinterpreted.

On the follow-up studies, ductal carcinoma in situ was seen as clustered microcalcifications (seven cases), asymmetries and poorly defined tumors (two cases each), and circumscribed tumors and clusters of nodules (one case each). In seven patients with normal mammographic findings, cancers were diagnosed clinically because of Paget's disease of the nipple (three cases), nipple discharge (three cases), or a palpable mass (one case).

Mortality.—By the end of the study, 20 patients in the interval carcinoma group had died of breast cancer and four additional patients had died of other causes. Of those patients who died of breast cancer, the histologic findings included 11 invasive comedocarcinomas, five tubuloductal carcinomas, and four lobular cancers. Fifteen of 20 women who died of breast cancer were considered to have true interval carcinomas when the mammograms were reviewed. Six women had less dense breasts (Wolfe's patterns N1 or P1) and 14 women had denser breasts (Wolfe's patterns P2 or DY).

Discussion

The number of interval carcinomas in a screening program is related to several factors such as the quality of mammography, the experience of the radiologist, the availability of medical care in general and mammography in particular, women's attitudes in seeking advice for breast symptoms, the length of the interval between screenings, and the growth rate of the carcinoma.

The number of true, misinterpreted, and missed carcinomas in our study is similar to the numbers in other series that used review of the mammographic findings of such tumors. The 66% proportion of true interval carcinomas in this study compares favorably with the 44–70% proportion of true interval carcinomas in other series [4, 5, 10]. Observer errors accounted for 10% of interval cancer cases (if the cases of atypical but suggestive mammographic findings are included), compared with observer error ranging from 6% to 30% in other investigations [4, 5, 10–12]. Unrecognized abnormalities constituted 21% of cases in this study, less than the range of 28–34% of such cases elsewhere [4, 5, 10]. The definitions of these errors may vary from study to study, perhaps in part accounting for the different proportions observed in each category. As in other investigations [4, 5, 10, 11], image quality did not play a major role in "missed" cases, except when the carcinoma was not included on the screening films, or on films obtained when the interval cancer was detected.

The number of cancers that develop in the interval between scheduled screening examinations is related to the length of the interval. This is illustrated by a larger number of interval carcinomas detected after the first interval, which, in practice, was slightly longer than the following intervals. Another factor might be more limited experience of the radiologists in the beginning of the study. A third factor might be the absence of comparison films in most cases in the first screening rounds. In the MMST, almost half of the interval tumors were detected within 1 year of screening (46% of all interval carcinomas and 41% of true interval carcinomas). Possibly the remaining 59% of the true interval carcinomas and 54% of all interval cancers in this series would have been detected by mammography had the interval been 12, rather than 21, months. However, some carcinomas would not have been detected, as three patients had no mammographic findings suggestive of cancer despite the clinical signs of breast cancer at the time the interval carcinoma was detected and four had only slightly abnormal findings on the repeat examination. So, although the number of interval carcinomas would be reduced with a shorter screening interval, the exact size of this reduction is not known.

The number of projections has been shown to influence the number of cancers detected, with a slightly larger number of cancers depicted with two-view (mediolateral oblique and craniocaudal projections) than with one-view (mediolateral oblique projection) baseline screening mammography [13, 14]. Two-view screening mammography was performed in the first and second rounds, with a total of 51 interval malignant tumors (including one lobular carcinoma in situ) found in the intervals before the third screening. Thereafter, 49 tumors were detected in the intervals between subsequent screenings; of these, excluding three cases of lobular carcinoma in situ, 23 women had one-view and 23 women had two-view mammography, a distinction based on breast density and the study's design. It is possible that the number of tumors detected might have been increased by two-view, rather than one-view, mammography, but the number of additional tumors that may have been found in these 23 cases is uncertain.

Breast cancer comprises a spectrum of slow- to fast-growing malignant tumors. From a statistical point of view, the probability of detecting a slowly growing tumor at screening is greater than that of detecting a fast-growing one (length-biased sampling) because the former is in a mammographically detectable stage for a longer time. This means that cancers detected at screening should grow more slowiy, on the average, than cancers in the control group, and interval cancers should grow faster than the average tumors. This is supported by the large proportion of tumors with doubling times for tumor volume of less than 100 days and a higher relative risk of dying from breast cancer for the interval cancer group compared with the control group.

Another factor influencing the distribution of cancers between screening detection and interval detection is the so-called detection bias. This refers to the fact that mammography may be more sensitive for detecting the spiculated type of tumor mass than the more nonspecific, circumscribed or nodular type of tumor at an early stage. In the MMST, only a few spiculated masses were missed on the initial screening study (three cases). In contrast, circumscribed nodules, or densities, represented tumor at an early stage when mammographic findings were present, including 17 of 21 cancers with noncalcified, nonspecific signs and five of seven cancers with unrecognized atypical but suggestive signs, indicating that these noncalcified, nonspecific findings may have been more difficult to recognize at screening. The vague morphology of these tumors at an early stage was often compounded by location in a P1 or P2 pattern breast (18 cases).

TABLE 5: Histologic Type of Cancer According to Mode of Detection

Histologic Type	No. (%)	
	Cancers Detected at Screening	Interval Cancers
Tubular	86 (23)	8 (8)
Tubuloductal	101 (27)	15 (16)
Invasive comedo, medullary, mucinous	84 (23)	37 (38)
Lobular	33 (9)	14 (15)
Other	6 (2)	2 (2)
Carcinoma in situ	61 (16)	20 (21)
Total	371 (100)	96 (100)

Note.—Histologic types of screening-detected carcinomas are from the material described in Andersson et al. [1]. Three observations are missing in the screening-detected cancers because data could not be retrieved on three tumor types.

Detection bias was reflected to some extent in the distribution of histologic types among interval carcinomas. Compared with 23% of invasive comedocarcinomas and medullary/mucinous tumors reported in the screening-detected group from this trial [1], the interval cancer group showed a higher proportion (38% or 37/96) of invasive comedocarcinomas and medullary/mucinous tumors (Table 5). These most often had a lumplike appearance or nonspecific density. Although 21 of these histologic types were true interval carcinomas, 16 findings were considered nonspecific (11 cases) or missed (five cases), including seven findings of density or asymmetry, five round tumors or round masses, two prominent ducts/nodules, and two clusters of calcifications.

In contradistinction, a lower percentage of tubular and tubuloductal cancers was found in the interval cancer group (23 cases, or 24%) than in the screening-detected group (50%) [1]. Tubular and tubuloductal cancers are usually characterized by spiculations. In this series, only one such spiculated tubular carcinoma was considered missed on the preceding screening films. Of the others, excluding one set of lost films and one tumor growing near the chest wall, 16 of such tumors were true interval carcinomas. Three other tubular or tubuloductal cancers had nonspecific findings of density (one) or circumscribed mass (two). The last tubular cancer, which appeared as a circumscribed mass on the screening films, was considered missed.

The larger percentage (15%, or 14/96) of interval lobular carcinomas detected in the MMST compared with quoted percentages of lobular carcinomas seen in a general population (10%) is not unexpected because it is difficult to see lobular carcinomas on mammograms [15]. Such tumors constituted 9% of the screening-detected group [1].

In summary, the interval carcinomas in this screening series have a more aggressive behavior compared with the screening-detected carcinomas and contributed considerably to mortality in the screened population. The histologic type of the interval carcinomas was mostly comedo, medullary, or mucinous. In retrospect, the morphology of the tumors at an early stage was characterized by rather nonspecific findings, with a paucity of the spiculated type lesions, which are more easily detected by screening.

ACKNOWLEDGMENTS

We thank Carrie M. Griffith and Melanie L. Shaw for secretarial support.

REFERENCES

1. Andersson I, Aspegren K, Janzon L, et al. Mammographic screening and mortality from breast cancer: the Malmö mammographic screening trial. *BMJ* **1988**;297:943–948
2. Andersson I. What can we learn from interval carcinomas? *Recent Results Cancer Res* **1984**;90:161–163
3. Martin JE, Moskowitz M, Milbrath JR. Breast cancer missed by mammography. *AJR* **1979**;132:737–739
4. Holland R, Mravunac M, Hendriks JHCL, Bekker BV. So-called interval cancers of the breast. *Cancer* **1982**;49:2527–2533
5. Frisell J, Eklund G, Hellstrom L, Somell A. Analysis of interval breast carcinomas in a randomized screening trial in Stockholm. *Breast Cancer Res Treat* **1987**;9:219–225
6. Andersson J. *Mammographic screening for breast carcinoma: a cross-sectional randomized study of 45–69-year-old women* (M.D. thesis). Lund, Sweden: University of Lund, **1980**
7. Wolfe JN. *Xeroradiography of the breast*, 2nd ed. Springfield, IL: Thomas, **1983**:48–126
8. Fournier DV, Weber E, Hoeffken W, Bauer M, Kubli F, Barth V. Growth rate of 147 mammary carcinomas. *Cancer* **1980**;45:2198–2207
9. Linell F, Ljungberg O. *Atlas of breast pathology*. Copenhagen: Munksgaard, **1984**
10. VonRosen A, Erhardt K, Hellstrom L, Somell A, Auer G. Assessment of malignancy potential in so-called interval mammary carcinomas. *Breast Cancer Res Treat* **1985**;6:221–227
11. Holmberg LH, Tabar L, Adami HO, Bergstrom R. Survival in breast cancer diagnosed between mammographic screening examinations. *Lancet* **1986**;2:27–30
12. DeGroote R, Rush FR Jr, Milazzo J, Warden MJ, Rocko JM. Interval breast cancer: a more aggressive subset of breast neoplasias. *Surgery* **1983**;94:543–547
13. Andersson I. Radiographic screening for breast carcinoma: III. Appearance of carcinoma and number of projections to be used at screening. *Acta Radiol* **1981**;22:407–420
14. Sickles EA, Weber WN, Galvin HB, Ominsky SH, Sollitto RA. Baseline screening mammography: one vs. two views per breast. *AJR* **1986**;147:1149–1153
15. Hilleren DJ, Andersson IT, Lindholm K, Linnell FS. Invasive lobular carcinoma: mammographic findings in a 10-year experience. *Radiology* **1991**;178:149–154

Evaluation of Mammographic Image Quality: Pilot Study Comparing Five Methods

Curtis B. Caldwell[1]
Eve K. Fishell[2]
Roberta A. Jong[3]
William J. Weiser[4]
Martin J. Yaffe[1]

A radiograph is considered of high quality when it allows a radiologist to identify abnormalities with high sensitivity and specificity. Although many methods for assessing image quality have been devised, it is not clear which is most meaningful or how well these methods correlate with one another. A pilot study was undertaken to compare five methods of evaluating mammographic image quality. Each of the methods was used to form separate rankings of 11 mammographic system configurations. In two of the methods, observers (three radiologists and three physicists) subjectively ranked the "image quality" of radiographs of phantoms obtained with each configuration. The third method ranked the systems according to contrast as measured densitometrically with an aluminum step wedge, and the fourth, in terms of lowest to highest mean glandular radiation doses to the breast. In the final method, observers based their rankings on mammograms of patients. The intra- and interobserver variabilities of each ranking method were assessed, as well as the correlations between methods, by using standard nonparametric statistical tests. Intraobserver consistency was high with any of the image quality ranking methods; however, image quality rankings based on either of the two phantoms provided better agreement among observers than did rankings based on images of patients. Surprisingly, no significant degree of correlation was found between any two image quality evaluation methods.

Our work may have two implications for the American College of Radiology Mammography Accreditation Program: (1) small variations in phantom scores do not necessarily correlate with subjective variation in image quality in radiographs of patients, and (2) when small numbers of radiographs are used, the assessment of the quality of mammograms of patients may vary considerably among radiologists.

AJR **159:295–301, August 1992**

Received December 16, 1991; accepted after revision February 25, 1992.

This work was supported in part by the Medical Research Council of Canada and the Ontario Cancer Treatment and Research Foundation.

[1] Departments of Medical Biophysics and Radiology, University of Toronto, and Medical Physics Research Group, Sunnybrook Health Science Centre, 2075 Bayview Ave., Toronto, Ontario, Canada M4N 3M5. Address reprint requests to C. B. Caldwell.

[2] Department of Radiology, Women's College Hospital, 76 Greenville St., Toronto, Ontario, Canada M5S 1B2.

[3] Department of Radiology, Mount Sinai Hospital, 600 University Ave., Toronto, Ontario, Canada M5G 1X5.

[4] Department of Radiology, St. Michael's Hospital, 30 Bond St., Toronto, Ontario, Canada M5B 1W8.

0361–803X/92/1592–0295
© American Roentgen Ray Society

Mammography is one of the most technically demanding radiographic procedures. Features characteristic of breast disease are often either small or of low subject contrast. A mammogram is considered of high quality when a radiologist can discern the presence or absence of such features with relative ease and accuracy, that is, when diagnostic sensitivity and specificity are high. Because of the risk of missing cancers owing to inadequate sensitivity or of initiating unnecessary biopsies if specificity is low, mammographic image quality must be optimized. Unfortunately, objective assessment of the quality of mammograms is difficult.

Numerous methods of evaluating image quality have been proposed [1, 2]. It is our goal to determine how these methods correlate with one another and with subjective assessments by radiologists of the quality of mammograms of patients. In this study, we compare five methods of evaluating image quality. These methods are based either on the subjective ranking of the "image quality" of radiographs of either patients or phantoms, or on quantitative indexes derived from images of simple test objects. Both conventional and anthropomorphic phantoms were used. For each subjective method, the observer (either a radiologist or a medical physicist) ranked the quality of the images obtained with 11 mammographic configurations

TABLE 1: Characteristics of Mammographic System Configurations Used in This Study

System Label	Unit Type	Film	Screen	kVp	Half-Value Layer (mm Al)	OD_{typ}	Contrast (at OD_{typ})	Dose (cGy)
1G	Siemens Mammomat	Kodak OM1-(DL)	Kodak MIN-R	33	0.42	1.01	0.535	0.110
1N	Siemens Mammomat	Kodak OM1-(DL)	Kodak MIN-R	31	0.40	1.10	0.525	0.044
2G	Philips Diagnostic U-M	Kodak OM1-(DL)	Kodak MIN-R	32	0.40	0.92	0.520	0.057
2N	Philips Diagnostic U-M	Kodak OM1-(DL)	Kodak MIN-R	30	0.38	0.93	0.435	0.040
3N	CGR 500T	Kodak T-MAT II	Kodak MIN-R Fast	26	0.30	1.11	0.575	0.039
4N	CGR 600T	Kodak T-MAT II	Kodak MIN-R Fast	26	0.30	1.09	0.585	0.033
5G	LoRad	Du Pont SP-150	Kodak MIN-R Medium	27	0.35	1.25	0.630	0.087
6G	Philips Diagnostic U-M	Du Pont SP-150	Kodak MIN-R	30	0.43	1.47	0.550	0.130
7N	CGR 500T	Du Pont SP-150	Kodak MIN-R Medium	28	0.35	0.89	0.440	0.022
7G	CGR 500T	Du Pont SP-150	Kodak MIN-R Medium	28	0.35	1.09	0.497	0.068
8G	CGR 600T	Kodak SO-177	Kodak MIN-R	28	0.37	0.81	0.473	0.109

Note.—System labels refer to units in which grid (G) or nongrid (N) techniques were used. OD_{typ} = gross optical density at the center of the processed image.

from best to worst. We define the ordered set of 11 numbers assigned to the 11 configurations by an observer as a "ranking." Subsequently, the relationships among these rankings were evaluated, in terms of correlation between rankings, internal consistency of rankings, and interobserver variability.

Materials and Methods

Mammographic Systems

Characteristics of the mammographic configurations used in the study are shown in Table 1. Radiographs obtained with eight dedicated mammographic units were collected. For three units, both grid and nongrid techniques were evaluated, resulting in 11 mammographic system configurations. Each unit was equipped with a molybdenum anode tube and had an associated dedicated film processor. All units were located in large diagnostic radiology departments in teaching hospitals and were subject to routine quality control.

At each mammography clinic, a day was chosen during which the technologists recorded details about each craniocaudal mammogram taken. Details recorded included the patient's identification number, kilovoltage, automatic exposure-control setting, and whether a grid was used. Typical grid and nongrid techniques for each configuration were subsequently used when acquiring radiographs of the phantoms and test objects described next.

Phantoms and Test Objects

Our laboratory has been developing an anthropomorphic breast phantom [3, 4], that is, one that yields radiographs similar in appearance to mammograms of patients. The design of the anthropomorphic breast phantom used in the study was based on a mammogram of a patient. The phantom consisted of two numerically milled polymethylmethacrylate (PMMA) layers containing low-spatial-frequency information and one mercury-intensified film layer containing high-spatial-frequency information (Fig. 1A). A radiograph of the phantom is shown in Figure 1B.

The random phantom [5] (Fig. 2A), a three-by-four array of wax blocks, each 1.9 × 1.9 × 0.65 cm, superimposed on a uniform 4.0-cm-thick PMMA base, is a precursor to the current American College of Radiology (ACR) accreditation phantom. The blocks contained either groups of aluminum oxide specks varying from 0.20 to 0.74 mm in diameter or single 1.3-cm-long nylon fibers ranging from 0.40 to 1.56 mm in diameter. The blocks were randomly rearranged between exposures so that observers would not become accustomed to a particular orientation. A combined speck-fiber score (the fraction of the 12 blocks scored correctly as containing a speck or a fiber) was used as a measure of image quality. A typical radiograph is shown in Figure 2B.

For each of the mammographic systems evaluated, a 4.2 × 10 × 10 cm PMMA block, with attenuation characteristic of a typical breast [6], was imaged under automatic exposure control, and the gross optical density at the center of the processed image (OD_{typ}) was measured. A step wedge consisting of 15 0.1-mm-thick steps of type 1100 aluminum was used to estimate system contrast. Optical density was plotted vs step-wedge thickness. Contrast was defined as the slope of the curve measured at OD_{typ}. The half-value layer of the X-ray beam and the entrance exposure to the PMMA block were measured for each configuration by using standard techniques [7]. Mean glandular dose for a craniocaudal view under firm compression was calculated [8] by using the measured half-value layer and entrance exposures (corrected for backscatter [9]). The breast was assumed to be composed of 50% glandular tissue and 50% adipose tissue by weight.

Mammograms of Patients

Two sets of mammograms of patients obtained with each of the 11 mammographic system configurations were assessed. Set A consisted of mammograms of anatomy that appeared to be relatively "easy" (as judged by a radiologist) to image. These images were

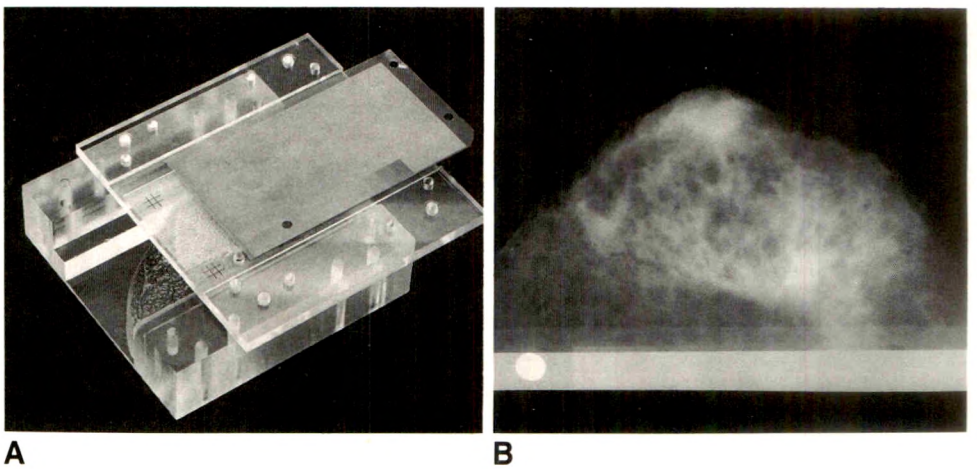


Fig. 1.—*A*, Prototype anthropomorphic breast phantom has layers containing coarse (bottom), intermediate (middle), and fine (top) detail. Bottom and middle layers are composed of polymethylmethacrylate, and top layer consists of mercury-intensified film. Design of phantom is based on a mammogram of a patient and has attenuation properties mimicking those of a human breast.

***B*, Radiograph of anthropomorphic breast phantom taken with exposure factors typically used for patients. Such radiographs are intended to allow radiologists to evaluate image quality subjectively with a realistic "patient-like" image.**

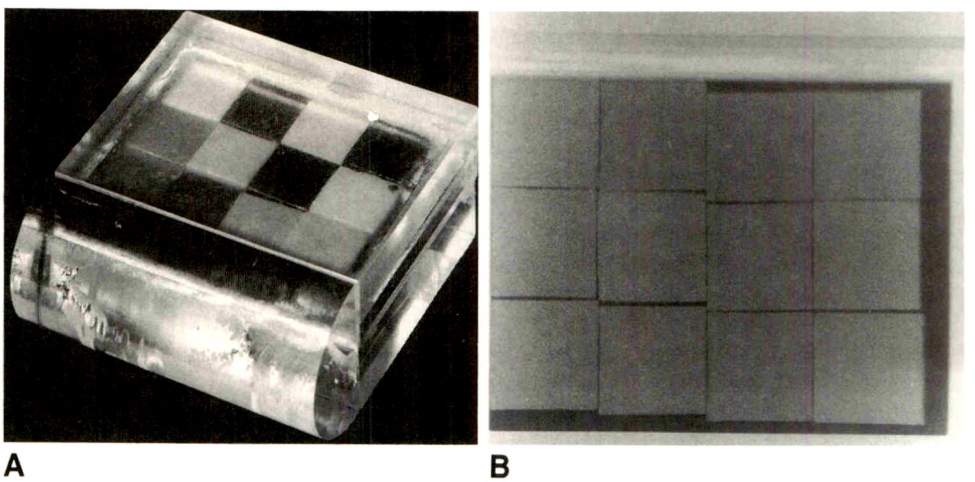


Fig. 2.—*A*, Random phantom is composed of Lucite with wax blocks containing embedded fibers and specks of various sizes. It provides an average attenuation value approximately the same as that of a human breast.

***B*, Radiograph of random phantom taken with exposure factors typically used for imaging patients. Number of specks and fibers detected in this radiograph is taken as a measure of mammographic unit's image quality.**

characterized by primarily fatty breast tissue, with the appearance of a limited amount of fibrous tissue used to assist in the subjective assessment of contrast and resolution. Radiographs of uniformly fatty breasts were rejected from the study as providing insufficient criteria for evaluation of quality. Set B radiographs, in which the anatomy was considered to be "difficult" to image, were mainly characteristic of radiographically dense breasts containing significant amounts of fibrous tissue. On the basis of these criteria, radiographs of the anthropomorphic phantom would have been in the easy category.

Ranking Techniques

The method of paired comparisons [10] was used to obtain rankings of the image quality of the sets of radiographs of patients and of anthropomorphic phantoms. In this method, radiographs are presented side-by-side in pairs to an observer, who records a preference for one of the members of the pair. Observers were told to base their preferences on the criteria they would use in normal clinical practice for assessing mammographic image quality. No attempt was made to establish a consistent set of criteria for all observers (i.e., we attempted not to bias their preferences). Each observer performed the evaluations independently in a darkened room. No limitation was placed on either viewing time or distance. Radiographs were presented in random order and were masked to disguise their place of origin. To rank a set of n radiographs, each observer independently performed all possible pair-wise comparisons for all radiographs from the set (i.e., $n[n-1]/2$ paired comparisons). This method of ranking has been extensively studied [11, 12] and is commonly used when the objects being compared can be judged only subjectively. It has the advantage of making the comparison of any two members of a set independent of comparison with other members of the set. Paired-comparisons testing was done on groups of 12 radiographs, one from each of the 11 systems plus one training radiograph. All possible combinations of two radiographs were compared. The first 11 combinations consisted of the training radiograph compared with each of the other members of the set. The rankings were undertaken by three radiologists experienced in mammography and by three medical physicists experienced in assessing images of phantoms, but with little experience with radiographs of patients.

In the ranking scales, a rank of 1 was assigned to the best system and 11 to the worst. For the contrast and radiation dose scales, the system with the highest contrast or dose was assigned a rank of 1. Systems that tied according to the criteria of the ranking method were assigned averaged ranks. For example, if two systems that would normally have filled the sixth and seventh rank positions were tied, each system was assigned the rank of 6.5.

Statistical Methods

The intraobserver variability of the observers was evaluated with Kendall's coefficient of consistence, ζ [10]. ζ varies between 0 (totally inconsistent) and 1 (totally consistent) and is calculated from the number of "circular triads" that occur during the ranking. A circular triad occurs, for example, if an observer comparing the image quality of radiographs A, B, and C ranks A higher than B, B higher than C, and C higher than A. Interobserver variability was measured by using Kendall's coefficient of concordance, W [10]. W was measured independently for the three radiologists and the three physicists. The mutual agreement among observers is expressed as a number, varying between 0 (no agreement) and 1 (complete agreement). Finally, the correlation between pairs of ranking methods was assessed by using Kendall's τ (rank correlation coefficient) [10]. This coefficient is assigned the value +1 if the agreement is perfect and the value −1 if the disagreement is perfect (i.e., one ranking is the inverse of the other). Near-zero values of τ indicate rankings that are uncorrelated.

Results

System rankings based on phantom and test object data are shown in Table 2. Rankings tabulated are those that used the random phantom (average of three physicist observers), anthropomorphic phantom (averages of three physicist observers and of three radiologists), contrast index, and radiation dose. Table 3 shows individual rankings for each observer with the radiographs of the anthropomorphic and random phantoms. Table 4 gives rankings based on sets A and B of radiographs of patients for each of the three radiologists.

Table 5 illustrates the results of an assessment of intraobserver variation. Coefficients of consistence are tabulated for individual observers' rankings of images of either a patient or the anthropomorphic phantom. Table 5 shows that, in all cases, whether an observer used radiographs of a patient or the anthropomorphic phantom to make a ranking, each ranking showed little intraobserver variation. Interobserver variability is summarized in Table 6. Coefficients of concordance are tabulated for observers ranking radiographs of the anthropomorphic phantom or the random phantom or mammograms of patients. Correlation coefficients of pairs of image quality rankings produced by the different observers (radiologists and physicists) and methods (random phantom, step wedge, dose, anthropomorphic phantom, sets A and B of mammograms of patients) are presented in Table 7.

To investigate the possible effect of the use of an antiscatter grid on imaging performance, we formed two subgroups from the data: one containing the six systems in which an antiscatter grid was used and one containing the five systems in which a grid was not used. The average ranks attained by each group with each ranking method are tabulated in Table 8. Note that when any 11 systems are ranked in this way, the lowest possible average rank (i.e., best possible ranking) for six systems is 3.5 (i.e., $[1 + 2 + 3 + 4 + 5 + 6]/6 = 3.5$), and the highest rank attainable by five systems is 9.0 (i.e., [11 +

TABLE 2: Average Quality Rankings of Phantom-Based Images

System Label	Random Phantom (Physicists)	Anthropomorphic Phantom Films		Contrast (Al Step Wedge)	Radiation Dose
		Physicists	Radiologists		
1G	4.0	4	2	5	2
1N	10.5	7	7	6	7
2G	5.0	9	3	7	6
2N	10.5	10	9	11	8
3N	6.5	3	10	3	9
4N	6.5	8	4	2	10
5G	2.5	6	7	1	4
6G	2.5	1	5	4	1
7N	9.0	11	11	10	11
7G	8.0	5	7	8	5
8G	1.0	2	1	9	3

Note.—Details of systems corresponding to system labels are given in Table 1 (G = grid used, N = no grid used). In assessments of radiographs, a rank of 1 was assigned to the best system and 11 to the worst. If two systems tied, an average of the two ranks was assigned (e.g., if it was not possible to distinguish between 10th and 11th places, a rank of 10.5 was assigned to both systems). For contrast and dose scales, the system with the highest contrast and dose was assigned a rank of 1.

TABLE 3: Individuals' Image Quality Rankings of Radiographs of Phantoms

System Label	Random Phantom (Physicists)			Anthropomorphic Phantom (Physicists)			Anthropomorphic Phantom (Radiologists)		
	P1	P2	P3	P1	P2	P3	R1	R2	R3
1G	3.0	4.0	7	4.0	3.0	5.5	2.0	2.0	1
1N	10.0	11.0	7	7.0	6.5	8.0	7.0	4.5	7
2G	4.5	6.5	4	8.5	8.5	8.0	3.0	3.0	3
2N	10.0	8.0	11	10.0	10.0	10.0	9.5	9.0	7
3N	10.0	4.0	7	4.0	4.0	1.5	9.5	6.5	11
4N	7.0	6.5	7	8.5	6.5	8.0	5.0	8.0	4
5G	1.5	4.0	2	4.0	8.5	4.0	7.0	10.0	7
6G	4.5	1.0	2	1.0	2.0	1.5	4.0	4.5	9
7N	7.0	9.5	10	11.0	11.0	11.0	11.0	11.0	10
7G	7.0	9.5	7	6.0	5.0	5.5	7.0	6.5	5
8G	1.5	2.0	2	2.0	1.0	3.0	1.0	1.0	2

Note.—Details of systems corresponding to system labels are given in Table 1 (G = grid, N = no grid used). Individual rankings were assigned by three physicists (P1, P2, P3) or three radiologists (R1, R2, R3). In assessments of radiographs, a rank of 1 was assigned to the best system and 11 to the worst. If two systems tied, an average of the two ranks was assigned (e.g., if it was not possible to distinguish between 10th and 11th places, a rank of 10.5 was assigned to both systems).

TABLE 4: Radiologists' Rankings of Image Quality of Mammograms of Patients

System Label	Set A			Set B		
	R1	R2	R3	R1	R2	R3
1G	4.0	10.0	2	8	4	3
1N	8.0	4.0	5	5	4	9
2G	5.5	6.0	3	2	2	3
2N	8.0	7.0	7	5	4	7
3N	1.5	8.5	8	3	1	3
4N	10.0	2.0	10	10	7	8
5G	3.0	4.0	1	8	10	5
6G	5.5	8.5	9	5	8	11
7N	11.0	11.0	4	8	6	10
7G	8.0	4.0	11	11	9	6
8G	1.5	1.0	6	1	11	1

Note.—Details of systems corresponding to system labels are given in Table 1 (G = grid used, N = no grid used). Mammograms in set A were of anatomy considered relatively easy (by a radiologist) to image; in set B, the anatomy was considered difficult to image, usually because radiographically dense breasts containing significant amounts of fibrous tissue were present. Individual rankings were assigned by three radiologists (R1, R2, R3). In assessments of radiographs, a rank of 1 was assigned to the best system and 11 to the worst. If two systems tied, an average of the two ranks was assigned (e.g., if it was not possible to distinguish between 10th and 11th places, a rank of 10.5 was assigned to both systems).

TABLE 5: Intraobserver Variability of Paired Comparisons Ranking Methods

Radiographs Assessed/Observer	Coefficient of Consistence
Patient set A	
R1	0.909
R2	0.982
R3	1.000
Patient set B	
R1	0.855
R2	0.982
R3	0.927
Anthropomorphic phantom (radiologists)	
R1	0.909
R2	0.964
R3	0.982
Anthropomorphic phantom (physicists)	
P1	0.964
P2	0.909
P3	0.800

Note.—Mammograms in patient set A were of anatomy considered relatively easy (by a radiologist) to image; in set B, the anatomy was considered difficult to image, usually because radiographically dense breasts containing significant amounts of fibrous tissue were present. Individual rankings were assigned by three radiologists (R1, R2, R3) or three physicists (P1, P2, P3). In all cases, the probability was less than .005 that the degree of consistency in the ranking was arrived at randomly.

10 + 9 + 8 + 7]/5 = 9.0). As expected, the rankings based on dose give these extreme values.

Discussion

The data in Table 5 indicate that little intraobserver variability resulted when radiologists or physicists used radiographs of patients or an anthropomorphic phantom to derive rankings. The rankings either by the three radiologists or by the three physicists of radiographs of the anthropomorphic phantom showed little interobserver variability (Table 6); however, rankings by radiologists and physicists correlated poorly (Table 7). This suggests that clinically experienced and naive observers use different criteria for defining the image quality of realistic images. This difference disappears for the task of differentiating large differences in image quality, such as comparing systems that used a grid with those that did not (Table 8).

TABLE 6: Interobserver Variability of Ranking Methods

Radiographs Assessed	Coefficient of Concordance	*p* Value
Anthropomorphic phantom (three radiologists)	0.839	<.005
Anthropomorphic phantom (three physicists)	0.916	<.005
Random phantom (three physicists)	0.796	.010
Patient set A (three radiologists)	0.507	.130
Patient set B (three radiologists)	0.363	.380

Note.—*p* = Probability of the result being consistent with the null hypothesis (i.e., that the rankings are uncorrelated). Mammograms in set A were of anatomy considered relatively easy (by a radiologist) to image; in set B, the anatomy was considered difficult to image, usually because radiographically dense breasts containing significant amounts of fibrous tissue were present.

Table 6 also indicates good interobserver agreement in rankings based on radiographs of the random phantom. Again, however, rankings based on the anthropomorphic and random phantom images were poorly correlated (Table 7), except when applied to comparison of the grid vs nongrid systems (Table 8). Radiologists and physicists appear to have used different criteria in assessing radiographs of the anthropomorphic phantom. We also retrospectively evaluated data from an independent government survey of mammographic units [13] to assess the correlation between rankings by radiologists and government X-ray inspectors of radiographs of the random phantom. For a set of 40 radiographs, a rank correlation coefficient of 0.733 was found, indicating strong correlation. We think this result reflects the fact that assessment of radiographs of the random phantom (i.e., a phantom containing well-defined objects on a uniform background) is not highly dependent on the observer's subjective criteria for assessing image quality. We would expect similar correlation between radiologists' and physicists' rankings with the random phantom.

A high degree of interobserver variability was found when rankings of image quality based on radiographs of patients were assessed (Table 6). As well, correlation between radiologists' rankings (average of three observers) of set A vs set B mammograms was poor (Table 7). Further evaluation revealed that the rankings by any individual radiologist of set A and set B radiographs were not well correlated. Also, these rankings did not distinguish between configurations in which

TABLE 7: Correlation Between Rankings by Different Image Quality Tests

Parameter	Contrast	Radiation Dose	Radiographs of Anthropomorphic Phantom		Radiographs of Patients (Radiologists)	
			Physicists	Radiologists	Set A	Set B
Radiographs of random phantom (physicists)	0.131	0.224	0.206	0.192	0.154	−0.038
Contrast	0.200	0.200	0.200	−0.112	−0.019	−0.222
Radiation dose			0.309[a]	0.093	0.075	−0.185
Radiographs of anthropomorphic phantom (physicists)				0.150	0.093	0.019
Radiographs of anthropomorphic phantom (radiologists)					−0.077	−0.133
Set A of patients' radiographs (radiologists)						0.095

Note.—Mammograms in set A were of anatomy considered relatively easy (by a radiologist) to image; in set B, the anatomy was considered difficult to image, usually because radiographically dense breasts containing significant amounts of fibrous tissue were present.

[a] For this degree of correlation, $p = .21$.

TABLE 8: Grid vs Nongrid System Rankings

Parameter	Average Rank		p
	All Grid Systems ($n = 6$)	All Nongrid Systems ($n = 5$)	
Radiation dose	3.5	9.0	.0022
Radiographs of random phantom (physicists)	3.8	8.6	.0087
Radiographs of anthropomorphic phantom (radiologists)	4.2	8.2	.026
Radiographs of anthropomorphic phantom (physicists)	4.5	7.8	.063
Set A of patient's radiographs (radiologists)	5.2	7.0	.21
Contrast	5.7	6.2	.47
Set B of patients' radiographs (radiologists)	6.0	6.0	.54

Note.—p = probability that the ranking method in question would fail to distinguish the nongrid subgroup from the grid subgroup. This probability was calculated by using the Mann-Whitney U test applied to the rank sums for the grid and nongrid subgroups. Patients' mammograms in set A were of anatomy considered relatively easy (by a radiologist) to image; in set B, the anatomy was considered difficult to image, usually because radiographically dense breasts containing significant amounts of fibrous tissue were present.

large changes in image quality were expected (i.e., grid vs nongrid systems, Table 8), whereas radiologists' rankings of images of the anthropomorphic phantom in these configurations were significantly different.

It is likely that interobserver variability in assessing the mammograms would have been substantially reduced if we had recruited more observers and if those observers had been given a stricter set of criteria for judging image quality, reinforced with training. One of the goals of the current work, however, was to assess the degree of variability among expert observers in evaluating image quality when using their own evaluation criteria.

One of the problems with the use of mammograms of patients to assess image quality is that of anatomic variation. Only a relatively small number of patients were imaged with each mammographic unit on the days that data were collected. Most of these radiographs fell into the easy category (used for set A). We had few choices for difficult radiographs (used for set B). Thus, the variability in the degree of imaging difficulty (i.e., variations caused by differences in patients' anatomy) was higher in set B than in set A. This may explain the lack of correlation between rankings based on the two sets of radiographs. A higher sample size of set B–type radiographs would have allowed us to select radiographs that reflected similar degrees of imaging difficulty.

As shown in Table 7, the highest correlation between ranking methods was between radiation dose and the anthropomorphic phantom ranking produced by the physicists. This correlation probably occurs because systems with antiscatter grids require higher doses than systems without grids. Even for this comparison, the relatively low rank correlation coefficient of 0.309 had a two-sided significance level of only .21. This result indicates that no value of the correlation coefficient was sufficiently large to allow confident rejection of the hypothesis that the rankings were uncorrelated.

Rankings obtained solely on the basis of either estimated mean glandular dose or contrast as measured with the aluminum step wedge did not correlate strongly with those based on radiographs of the random phantom or of patients. The usefulness of the contrast measurement was limited because the average optical density of the radiographs of patients was often much different from the OD_{typ} value of the PMMA block image. For example, in six of 11 radiographs, the average optical density in uniform areas of the set A of radiographs of patients was at least 0.3 density units greater than the corresponding OD_{typ}. In some cases, the gradient of the film/screen combinations would have been significantly different

at the optical densities seen in the radiographs of patients. These differences in optical density may result from nonlinearities of the automatic exposure control of the mammography machine. Also, contrast was measured under low-scatter conditions. Measurements taken with more realistic scattered radiation levels may have better indicated image quality differences associated with the efficiency of scatter rejection.

The interobserver variability found in this pilot study suggests that different radiologists could select quite different optimal imaging systems if their decisions were based on the image quality of radiographs of patients. Consider the differences in the three systems (3N, 5G, and 8G, which are defined in Table 1) chosen at one time or other as best by a radiologist on the basis of radiographs of patients. Among the three systems, the mean glandular dose per view varied from 0.039 to 0.109 cGy and the kilovoltage varied from 26 to 28 kVp. The half-value layer varied from 0.30 to 0.37 mm of aluminum, and grids were used in two of the systems, but not in the third. We believe that changes of this magnitude would affect "true" image quality in terms of the ability of each system to delineate breast disease.

In the ACR mammography accreditation process [14], both radiographs of a phantom, similar to the random phantom used in this study, and mammograms of patients are used to evaluate image quality. Lack of good correlation between accreditation failures based on images of patients and those based on images of phantoms has already been observed in the ACR program (Wilcox PA, personal communication). It is possible that this lack of correlation is simply due to factors (such as positioning and compression of the breast) that affect radiographs of patients but not those of phantoms. It is also possible, however, that some of this lack of correlation arises from the difficulty of evaluating image quality from a small number of radiographs of patients, especially in the absence of universally accepted criteria for evaluating the quality of mammograms of patients.

Evaluation of mammograms of patients is useful for assessing breast positioning and, possibly, breast compression. Anatomic variation among patients makes it difficult to obtain reliable assessments of overall image quality when using a limited number of radiographs of patients. Subjective assessment of image quality is accomplished more consistently with an anthropomorphic phantom. Objective assessment of image quality is better accomplished with a conventional perceptibility phantom such as the random phantom, although the detection task may be overly simplistic owing to the uniform background. A phantom that combines the features of the anthropomorphic and random phantoms could be designed which would allow a more complete assessment of image quality. More work is required to obtain an index of true image quality (i.e., a parameter correlated with the probability of correct diagnosis) from simple and practical measurements.

ACKNOWLEDGMENTS

We thank R. Nishikawa, N. Robert, N. Bennett, J. Byng, A. Maidment, and G. Mawdsley for assistance; D. Tritchler for advice on statistical methods; and St. Michael's Hospital, Mt. Sinai Hospital, Women's College Hospital, and Toronto Hospital (all located in Toronto, Canada) for cooperation.

REFERENCES

1. Stanton L, Villafana T, Day JL, Lightfoot DA. A breast phantom method for evaluating mammography technique. *Invest Radiol* **1978**;13:291–297
2. McCrohan JL, Thompson WE, Butler PF, Goldstein HA, Phillips PR, Jans RG. *Mammographic Phantom Evaluation Project report of the National Center for Devices and Radiological Health.* Rockville, MD: U.S. Department of Health and Human Services, Food and Drug Administration, **1983**
3. Yaffe MJ, Johns PC, Nishikawa RM, Mawdsley GE, Caldwell CB. Anthropomorphic radiologic phantoms. *Radiology* **1986**;158:550–552
4. Caldwell CB, Yaffe MJ. Development of an anthropomorphic breast phantom. *Med Phys* **1990**;17:273–280
5. DeWerd LA, Wochos JF, Cameron JR. Wisconsin mammographic phantoms. In: Logan WW, Muntz EP, eds. *Reduced dose mammography*. New York: Masson, **1979**:301–306
6. Yaffe MJ, Mawdsley GE, Nishikawa RM. Quality assurance in a national breast screening study. *Proc SPIE* **1983**;419:23–30
7. Yaffe MJ, Barnes GT, Conway BJ, et al. *Equipment requirements and quality control for mammography* (AAPM report no. 29). New York: American Association of Physicists in Medicine, **1990**
8. Rosenstein M, Andersen LW, Warner GG. *Handbook of glandular tissue doses in mammography* (FDA no. 85-8239). Rockville, MD: U.S. Department of Health and Human Services, Food and Drug Administration, **1982**
9. Doi K, Chan H-P. Evaluation of absorbed dose in mammography: Monte Carlo simulation studies. *Radiology* **1980**;135:199–208
10. David HA. *The method of paired comparisons*. London: Griffin, **1963**
11. Cox DR. *The analysis of binary data*. London: Chapman & Hall, **1970**
12. Kendall MG. *Rank correlation methods*, 4th ed. Bristol, Great Britain: Arrowsmith, **1970**
13. Moore RS. *Image quality survey of mammographic facilities in Ontario.* Ontario: X-Ray Inspection Service of the Province of Ontario, Canada, **1989**
14. McLelland R, Hendrick RE, Zinninger MD, Wilcox PA. The American College of Radiology Mammography Accreditation Program. *AJR* **1991**; 157:473–479

AJR

AMERICAN JOURNAL OF ROENTGENOLOGY

MELVIN M. FIGLEY FELLOWSHIPS IN RADIOLOGY JOURNALISM 1993

The American Roentgen Ray Society announces four one-month fellowships in radiology journalism in the La Jolla editorial office of the *AJR*. Board-certified radiologists with special academic promise are invited to apply.

PURPOSE

The purpose of the fellowship is (1) to stimulate bright young radiologists to continue with an academic career, to accelerate their progress, and to stimulate their interest in good radiology journalism and (2) to improve the quality of radiology journals by teaching the fundamentals of medical journalism to academicians, training manuscript reviewers and future editors, and providing core teachers of medical journalism in radiology departments around the country.

CURRICULUM

Through hands-on experience in the editorial office, the fellows will be taught the fundamentals of medical writing, manuscript preparation, peer review, manuscript editing, the ethics of scientific journalism, and journal publication and printing in personal tutorials given by the *AJR* editors and editorial staff. They will visit the ARRS publication office and Waverly Press in Maryland to observe the publication and printing process.

STIPEND

The successful candidates will each be awarded $10,000, which includes the cost of travel to La Jolla and Maryland, living expenses for the month, and an honorarium.

APPLICATIONS

Candidates should apply in writing to Robert N. Berk, M.D., Editor-in-Chief, *AJR* Editorial Office, 2223 Avenida de la Playa, Suite 103, La Jolla, CA 92037. Applications from senior candidates are welcome. The letter must include a curriculum vitae and a description of the candidate's goals during the fellowship. Letters of recommendation from his or her department chairman and one other senior person are required. Deadline for receipt of applications is Sept. 1, 1992. The successful candidates will be notified Oct. 1, 1992.

Duodenal Neoplasms: Predictive Value of CT for Determining Malignancy and Tumor Resectability

Ella A. Kazerooni[1]
Leslie E. Quint
Isaac R. Francis

CT examinations of 25 patients with proved primary or metastatic duodenal neoplasms were retrospectively reviewed to determine if morphologic features seen on CT scans could be used to predict the benign or malignant nature of these neoplasms and to assess the effectiveness of using CT findings to predict tumor resectability. We studied 19 malignant and six benign tumors. Histologic proof was obtained by means of surgery in 20 patients and by endoscopic biopsy in five. CT features of tumor morphology were assessed in the 22 cases in which a duodenal tumor was seen on CT. These features included central necrosis, ulceration or excavation, and the location of the tumor with respect to the bowel wall. The specific morphologic features used to predict that a tumor was malignant included the presence of an exophytic or intramural mass, central necrosis, and ulceration. The only criterion used to predict that a tumor was benign was that the mass be entirely intraluminal. Whenever vascular encasement, invasion of contiguous organs other than the head of the pancreas, distant lymphadenopathy, or metastases were present, the tumor was predicted to be unresectable for cure. With the exception of three benign smooth muscle tumors, all tumors with one or more CT morphologic features indicative of a malignant neoplasm were malignant ($n = 16$). Three of four intraluminal masses were benign. In three cases of polypoid tumors smaller than 2 cm, a duodenal tumor was not seen on CT. Whenever extraduodenal disease was found (15 cases), the neoplasms were malignant. In the 22 cases in which a tumor was detected on CT, the sensitivity of using the presence of one or more morphologic features associated with a malignant neoplasm as a predictor was 94%; the specificity was 50%, and the accuracy was 82%. If the presence of any morphologic feature indicative of a malignant neoplasm was combined with the presence of any finding of extraduodenal disease, CT was 100% sensitive and 86% accurate for predicting that the tumor was malignant. CT appears to be reliable for predicting duodenal tumor resectability. On the basis of CT findings, 10 tumors were correctly predicted as being unresectable for cure, and 12 were predicted as being resectable; no surgery was performed in the remaining three cases.

In conclusion, evaluation of the morphologic features of duodenal neoplasms is a sensitive, but nonspecific, method for predicting that a tumor is malignant. The accuracy of CT findings for predicting that a tumor is malignant improves when morphologic features and the presence of extraduodenal disease are considered together. Although an intraluminal mass without extraduodenal disease will likely be benign, and tumors with extraduodenal disease will likely be malignant, polypoid tumors smaller than 2 cm may not be detected with standard abdominal CT. Last, CT appears to be reliable for predicting whether duodenal tumor resection will be curative.

AJR 159:303–309, August 1992

Received December 20, 1991; accepted after revision February 20, 1992.

[1] All authors: Department of Radiology, University of Michigan Hospitals, Box 30, 1500 E. Medical Center Dr., Ann Arbor, MI 48109-0030. Address reprint requests to E. Kazerooni.

0361–803X/92/1592–0303
© American Roentgen Ray Society

Primary and metastatic neoplasms of the duodenum are uncommon. Traditionally these tumors have been detected and assessed by using barium radiography or endoscopy. More recently, CT has been used to further evaluate and stage duodenal neoplasms detected with these methods. In some cases, duodenal tumors are initially detected on screening CT examinations in patients with nonspecific upper abdominal signs and symptoms [1]. Whereas barium radiography

depicts primarily mucosal involvement by tumor, CT also shows the intra- and extramural extent of the primary tumor, including the presence or absence of vascular encasement, invasion of periduodenal fat or contiguous organs, lymphadenopathy, and visceral organ or bowel metastases [2]. Reportedly, CT is useful in staging duodenal neoplasms and may also be helpful in distinguishing benign from malignant duodenal tumors [3–5]. The aim of our study was to determine if the morphologic features seen on CT scans of 25 duodenal neoplasms examined at our institution could be used to predict whether a tumor was benign or malignant. Additionally, CT findings were assessed to determine the accuracy of CT for predicting whether tumor resection would be curative.

Materials and Methods

A search of our tumor registry for the period 1982–1990 revealed that 29 patients with primary duodenal neoplasms had been seen at our institution. Review of hospital charts and the CT register indicated that CT scans had been obtained in 22 cases. A review of the daily CT logbooks for the same period revealed three cases of distant metastases to the duodenum. The CT appearances of these 25 cases were the basis of this retrospective report. Three of these cases were included in a previous series [3]. Ampullary neoplasms and direct duodenal extension from adjacent neoplasms (renal, adrenal, pancreatic, colonic) were not included in this study. The 25 patients in the study group included 17 men and eight women 42–79 years old (mean, 62 years).

In 21 patients, 10-mm-thick contiguous axial abdominal images were obtained by using either a 9800 Highlite CT/T scanner (19 patients) or an 8800 CT scanner (two patients) (General Electric Medical Systems, Milwaukee). Three patients were imaged by using 8-mm-thick sections at 10-mm intervals and a Somatom DR III scanner, and one was imaged by using 8-mm-thick contiguous sections and a Somatom DRH scanner (Siemens, Iselin, NJ). Dynamic incremental scanning with a bolus administration of 100–150 ml 50–60% urographic IV contrast material was performed in 17 patients. In four patients, contrast material was administered by drip infusion, and in four patients, no IV contrast material was administered. All patients received oral contrast material (1.5% Hypaque) before imaging. No air-contrast or positional techniques were used.

All CT scans were reviewed by two radiologists, and a consensus interpretation was obtained for each case. Scans were interpreted with the knowledge that each case represented a duodenal tumor, but without knowledge of the histologic and surgical findings. Occasionally, interpreters may have had incidental previous knowledge of individual cases. Morphologic features of the duodenal tumor on the CT scans were evaluated. Tumor location was classified as predominantly intramural (if the bowel wall was more than 1 cm thick), intraluminal, or exophytic or extraluminal. The presence or absence of central necrosis, ulceration or excavation, and bowel obstruction and the cross-sectional diameter of each tumor were noted. Scans were also evaluated for findings suggesting extraduodenal tumor spread; these included vascular encasement, invasion of periduodenal fat or contiguous organs, lymphadenopathy (>1 cm in short-axis diameter), and visceral organ or bowel metastases.

For the 22 cases in which a duodenal tumor was detected with CT, morphologic features alone were used to predict whether the tumor was benign or malignant. Features used to predict that a tumor was malignant included the presence of one or more of the following: an intramural mass, an exophytic or extraluminal mass, ulceration, or central necrosis. The only criterion used to predict that a tumor was benign was the presence of a mass that was entirely intraluminal, without additional findings of wall thickening, ulceration, or necrosis. Additionally, using the presence of any morphologic feature indicative of a malignant tumor or any finding of extraduodenal disease, we evaluated whether CT findings could be used to predict that a tumor was malignant.

An assessment of the curative potential of tumor resection was made retrospectively on the basis of the CT findings in all 25 cases. In all patients, a histologic diagnosis was obtained preoperatively by using specimens obtained via endoscopy. Therefore, the questions of disease dissemination and the benefit of resection were raised in all cases, including the three adenocarcinomas not detected on CT. When vascular encasement, direct organ invasion to any site other than the pancreatic head (isolated tumors in the pancreatic head could be resected via a Whipple's procedure), nonregional lymphadenopathy, and/or visceral organ or bowel metastases were found, the tumor was predicted to be unresectable. Periduodenal fat invasion was considered as a separate predictor of resectability.

The CT findings were correlated with surgical and biopsy findings in 19 cases, findings from endoscopic resection in one case (lipoma), and findings from endoscopic biopsy in five cases. Surgery was not performed in the last five cases, which included two patients with biopsy-proved hepatic metastases, one patient with renal cell carcinoma metastatic to the duodenum with additional new pulmonary nodules and retroperitoneal lymphadenopathy, one patient with a leiomyoma, and one patient with lymphoma who decided to have chemotherapy and had subsequent complete remission.

Results

The 25 duodenal neoplasms included 19 malignant and six benign tumors. The malignant tumors were eight primary adenocarcinomas, three primary non-Hodgkin's large-cell lymphomas, three leiomyosarcomas, three metastases (renal, colon, melanoma), one malignant fibrous histiocytoma, and one malignant gastrinoma. Benign tumors included three leiomyomas, two villous adenomas, and one lipoma.

The duodenal tumor was detected on CT scans in 22 (88%) of 25 cases. Three small primary polypoid adenocarcinomas, all 2 cm or smaller, were not seen on CT. In these three patients, the tumors were diagnosed preoperatively on the basis of findings at endoscopy. Four tumors were intraluminal without wall thickening (three benign, one malignant), six were intramural (all malignant), and 12 were exophytic (nine malignant, three benign). Of the 19 malignant tumors, one was intraluminal, three were not identified, and 15 showed wall thickening. The thickening was circumferential in six (Fig. 1) and asymmetric with an exophytic soft-tissue mass in nine (Fig. 2). A metastasis from renal cell carcinoma appeared as an enhancing intraluminal mass in a patient with metastases to other sites (Fig. 3A). One of the primary adenocarcinomas was classified as intramural and another as extraluminal, but each had a smaller intraluminal component.

Three of six benign duodenal neoplasms appeared entirely intraluminal, without associated wall thickening (two villous adenomas, one lipoma). The remaining three benign tumors (leiomyomas) were classified as exophytic, with a smaller intraluminal component present in one case. Three malignant tumors had an intraluminal component. They included the two previously described primary adenocarcinomas that were also

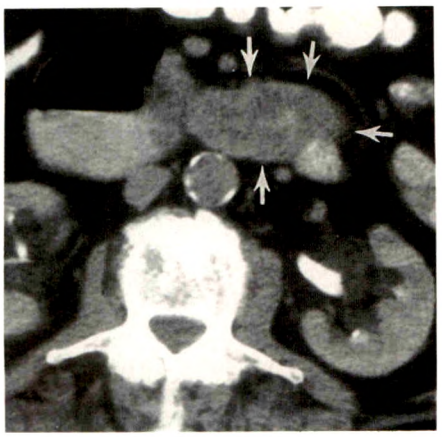


Fig. 1.—Primary duodenal adenocarcinoma. CT scan shows circumferential wall thickening (*arrows*) and proximal bowel dilatation indicative of obstruction.

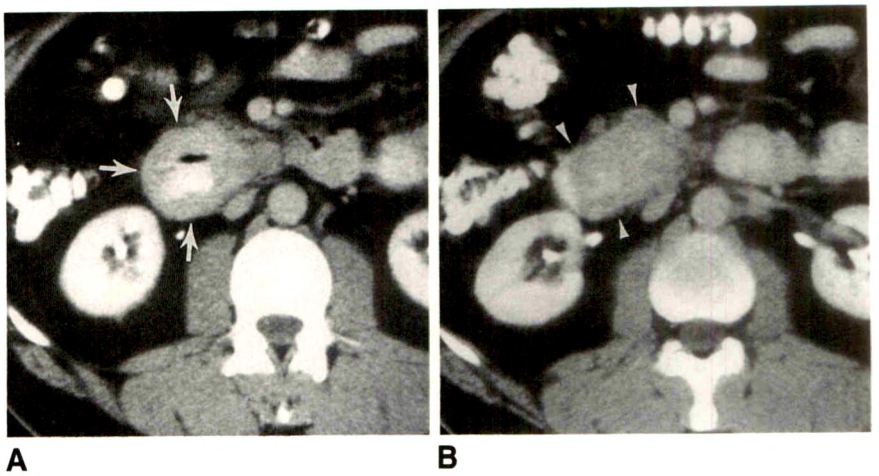


Fig. 2.—Primary duodenal non-Hodgkin's lymphoma.
A and *B*, Contiguous CT scans show circumferential wall thickening (*arrows*, *A*) and exophytic soft-tissue mass (*arrowheads*, *B*) with periduodenal lymphadenopathy.

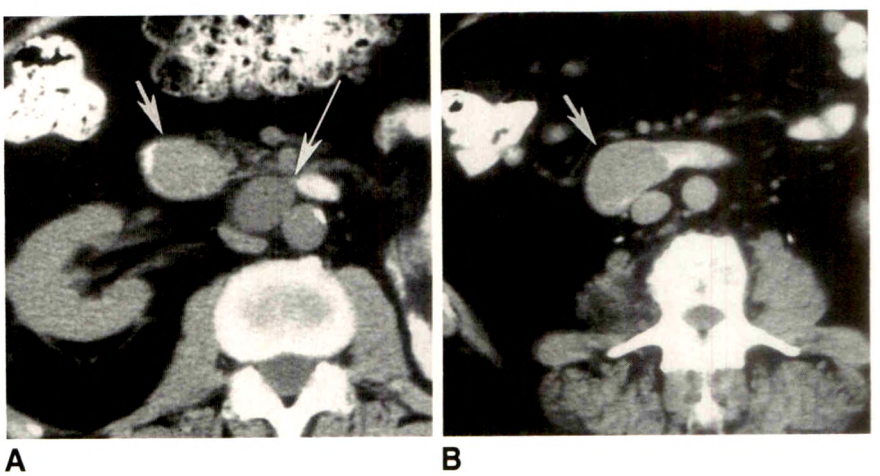


Fig. 3.—Intraluminal duodenal masses.
A and *B*, CT scans show an enhancing metastatic renal cell carcinoma (*short arrow*, *A*) with retroperitoneal lymphadenopathy (*long arrow*) and a benign villous adenoma (*arrow*, *B*).

intramural and a purely intraluminal metastasis from renal cell carcinoma with other distant metastases and lymphadenopathy (Fig. 3A).

Central low attenuation presumably representing tumor necrosis was seen in eight of 25 tumors. Five (26%) of the 19 malignant tumors had this feature, including two leiomyosarcomas (Fig. 4A) and one case each of adenocarcinoma, metastatic melanoma, and malignant fibrous histiocytoma. Although three of six benign tumors also had this feature (Fig. 4C), they were all smooth muscle tumors. Ulceration, as shown by the presence of gas or oral contrast material within the tumor mass, was seen in four malignant tumors, including a leiomyosarcoma (Fig. 4B), a lymphoma, and metastatic colon and renal cell carcinomas. All three tumors causing proximal bowel obstruction were malignant (primary adenocarcinomas).

Considerable overlap was seen in the size of malignant and benign smooth muscle tumors. Of the 16 malignant tumors detected with CT, 13 were 3–10.3 cm (mean, 6 cm), and three were annular lesions with circumferential wall thickening up to 2 cm. The benign tumors were 2–5.3 cm (mean, 3.5 cm). The three leiomyosarcomas were 5, 6, and 10 cm, and the three leiomyomas were 4, 6, and 6 cm. Two 3-cm intraluminal adenocarcinomas each had wall thickening, as did one exophytic 10-cm adenocarcinoma; two annular constricting adenocarcinomas had circumferential wall thickening. Two lymphomas were exophytic masses of 8 and 10 cm; the third case of lymphoma had circumferential thickening of the duodenal wall, up to 2 cm. Pathologic examination showed that the size of the malignant gastrinoma was 0.5 cm, but because of extensive desmoplastic reaction, the size of the soft-tissue mass on CT was 4 cm. The malignant fibrous histiocytoma was a 7-cm exophytic mass.

Extraduodenal abnormality was seen with malignant tumors only. Invasion of the periduodenal fat (Fig. 5) was suggested by CT in 10 of 19 malignant tumors and confirmed surgically in seven. Surgery was not performed in the remaining three patients, including two with biopsy-proved liver

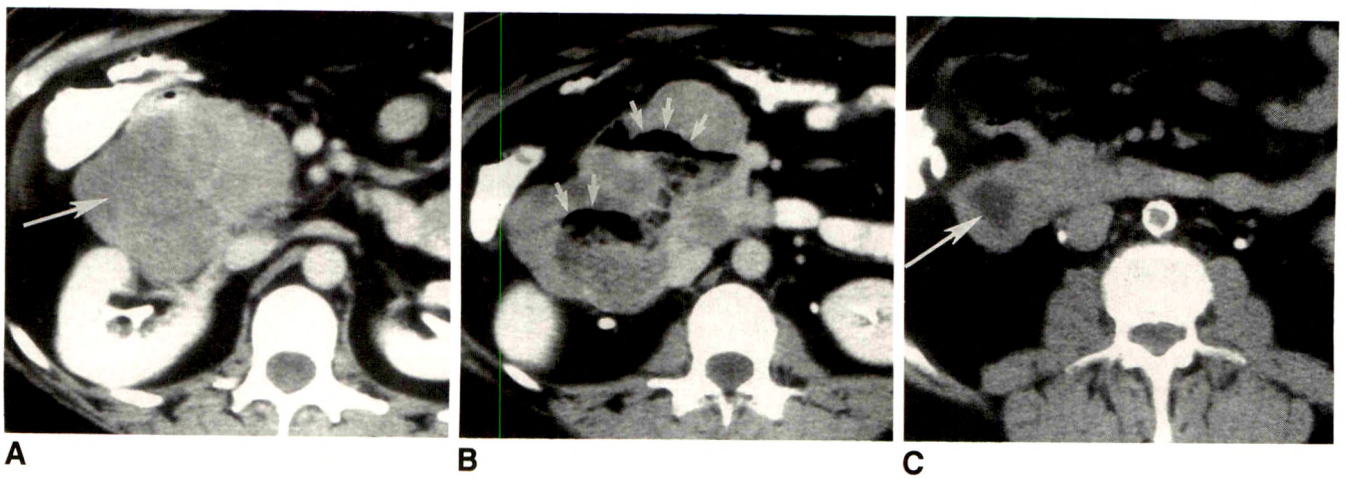


Fig. 4.—Areas of central tumor necrosis and ulceration in two duodenal smooth muscle tumors.
A and *B*, CT scans of leiomyosarcoma show central tumor necrosis (*large arrow*, *A*) and extensive ulceration (*small arrows*, *B*).
C, CT scan of leiomyoma shows central tumor necrosis (*arrow*). (*C* reprinted with permission from Farah et al. [3].)

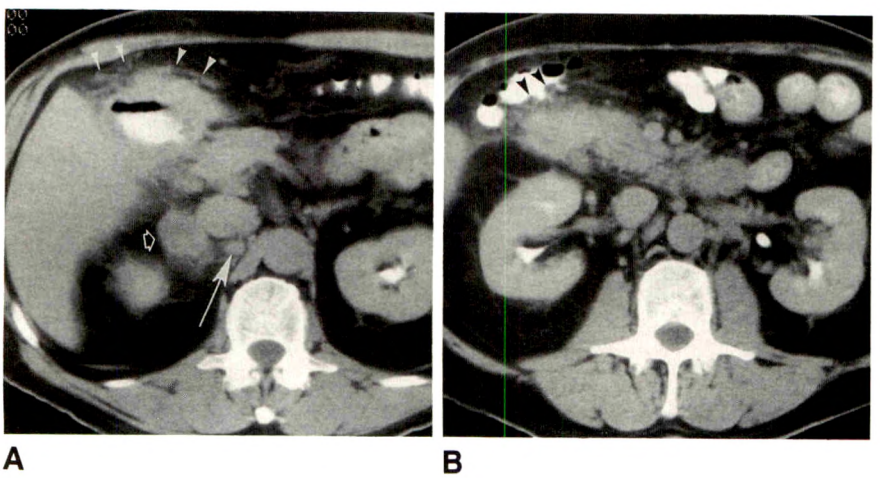


Fig. 5.—Primary duodenal adenocarcinoma.
A and *B*, CT scans show circumferential thickening of duodenal wall, extensive infiltration of periduodenal fat (*white arrowheads*), retroperitoneal lymphadenopathy (*solid arrow*), a mass (*open arrow*) in right adrenal gland (*A*), and direct invasion of scalloped hepatic flexure (*black arrowheads*, *B*).

metastases and one with biopsy-proved lymphoma treated with chemotherapy. CT did not show periduodenal fat (and pancreatic head) invasion that was proved at surgery in one patient with adenocarcinoma; however, this did not preclude surgical resection (Whipple's procedure).

Direct invasion of adjacent organs was confirmed surgically in three cases diagnosed on the basis of CT findings, including two patients with pancreatic invasion and one patient with both pancreatic and colonic invasion (Fig. 5B). In three cases, on CT the tumor was contiguous with adjacent structures, making it difficult to determine if invasion was present. Tumor involvement of the splenic flexure in one case, the pancreas in another, and the liver hilum/common bile duct in a third was surgically confirmed. Surgery was not performed in another patient with tumor contiguous with the pancreatic head and biopsy-proved liver metastases. CT did not show invasion of the pancreas proved by pathologic examination in two cases of primary duodenal adenocarcinoma. Both patients underwent Whipple's procedure. The depth of invasion in one case was 5 mm.

Vascular encasement of the superior mesenteric artery and vein was seen on CT and surgically proved in two of 19 cases (lymphoma, leiomyosarcoma). CT did not show surgically proved encasement of the superior mesenteric artery in one patient with a primary duodenal adenocarcinoma.

Lymphadenopathy was detected with CT in six of 25 patients in a total of eight sites and was always associated with malignancy. The eight sites were localized to the retroperitoneum in three, small bowel mesentery in two, hepatoduodenal ligament in one, peripancreatic region in one, and retrocrural region in one. Only the retrocrural lymphadenopathy was not confirmed by pathologic examination, because of its surgical inaccessibility. In three cases, metastatic lymph node involvement proved by pathologic examination was not seen on CT. This included four retroperitoneal lymph nodes smaller than 1 cm in a patient with primary duodenal adenocarcinoma in whom proved malignant mesenteric lymphadenopathy was seen on CT. In a patient with malignant gastrinoma and CT-detected, hepatoduodenal lymphadenopathy confirmed by pathologic examination, a 1.2 × 0.8 × 0.5 cm anterior pan-

creatic lymph node proved to be malignant. Finally, three of 14 pancreaticoduodenal lymph nodes (size not specified) in a patient with primary duodenal adenocarcinoma and high-grade duodenal obstruction proved to be malignant.

Metastases to visceral organs or the bowel were suspected on the basis of CT findings in five of 19 patients with malignant tumors. Two patients had biopsy-proved liver metastases (adenocarcinoma, leiomyosarcoma), and one patient had a biopsy-proved jejunal mass (lymphoma). Three patients with an adrenal mass (leiomyosarcoma, melanoma, renal cell carcinoma), one of whom also had multiple lung nodules (renal cell carcinoma), had no biopsy proof because of the presence of other sites of metastatic disease. There was one false-negative case of diffuse infiltrative hepatic lymphoma diagnosed on the basis of surgical biopsy findings.

When a duodenal tumor was detected on CT ($n = 22$), if the presence of one or more morphologic features indicative of a malignant tumor (exophytic or intramural mass, central necrosis, ulceration) was used as the sole predictor of whether the tumor was malignant, then CT was 94% sensitive, 50% specific, and 82% accurate for predicting the benign or malignant nature of such masses. The presence of extraduodenal abnormality (vascular encasement, invasion of periduodenal fat or contiguous organs, distant lymphadenopathy, or visceral organ or bowel metastases) was 100% specific as an indication that the tumor was malignant, with a negative predictive value of 67%. If tumor morphology alone was used, three leiomyomas would have been predicted to be malignant. In these cases of a known duodenal tumor, if the presence of any morphologic feature associated with malignant tumors or the presence of any site of extraduodenal abnormality was used as a predictor, CT findings were 100% sensitive and 86% accurate for predicting that a tumor was malignant.

On the basis of CT findings, it was predicted that 15 of 25 cases of duodenal tumors would be resectable and that 10 of 25 cases of duodenal tumors would not be cured if resected. Surgery or percutaneous biopsy confirmed these predictions in 22 patients. Proof of resectability was not obtained in three cases (leiomyoma, lymphoma, metastatic renal cell carcinoma). CT did not show three sites of malignant lymph nodes, invasion of the pancreatic head in two cases of primary adenocarcinoma, diffuse hepatic infiltration in a case of lymphoma, encasement of the superior mesenteric artery in one patient with primary adenocarcinoma, and periduodenal fat invasion in another patient with primary adenocarcinoma; however, the failure to recognize these abnormalities did not alter the surgical determination of resectability or unresectability based on the CT findings in these cases. This was largely because other findings of metastatic disease were present. In the case of invasion of the pancreatic head, the surgical procedure was altered from resection and end-to-end anastomosis to a Whipple's procedure.

Discussion

Tumors of the small bowel account for approximately 5–6% of all neoplasms of the gastrointestinal tract. Of these, about one third are of duodenal origin, making duodenal neoplasms quite rare [6]. Although endoscopy and barium radiography are still the mainstays for the diagnosis of duodenal abnormalities, CT may be useful for evaluating the extraluminal extent of disease [2, 3]. However, recent studies [7–12] suggest that CT findings are not as accurate for predicting the stage of gastrointestinal neoplasms as earlier studies [13, 14] had indicated. Although CT is fairly reliable for detecting metastatic disease to the liver, its findings are not as accurate for assessing nodal involvement and are less reliable for determining the depth of invasion. In most patients, surgical resection and pathologic examination to determine the true extent of the disease are essential for treatment [1]. However, in patients for whom surgery is a risk, CT can be used to guide percutaneous biopsy of suspected metastatic foci.

CT may be useful in suggesting the benign or malignant nature of duodenal masses [3], and may be particularly useful for tumors that do not involve the mucosa and therefore are not detected by endoscopy. Although histologic examination will certainly be required, the ability to distinguish benign from malignant neoplasms may aid in the diagnosis, especially in patients in whom a percutaneous biopsy or laparoscopic open biopsy may be dangerous (bleeding diathesis, surgical risk). In patients at high operative risk for whom a diagnosis cannot be made on the basis of material obtained via an open biopsy, the ability to use CT findings to indicate that a tumor is benign may temper the need for repeated biopsy in favor of radiologic follow-up. The diagnosis of a lipoma can be made accurately and definitively when a round, smooth, homogeneous, intraluminal duodenal mass with an attenuation similar to that of fat is seen [4, 5]. The presence of an intraluminal mass not associated with wall thickening or extraluminal spread favored the finding of a benign tumor in our series. Such an appearance was seen in three of six benign tumors (Fig. 3B). The only malignant neoplasm with this appearance was a metastasis from renal cell carcinoma in a patient with widespread metastatic disease.

Three leiomyomas had features more commonly seen in malignant tumors, including an exophytic component and central tumor necrosis (Fig. 4C). Differentiation between leiomyoma and leiomyosarcoma is difficult even on pathologic examinations. Smooth muscle tumors that have been diagnosed as benign on the basis of pathologic examination have been shown to metastasize [1]. Therefore, it is not surprising that it can also be difficult to distinguish benign from malignant smooth muscle tumors when the morphologic features seen on CT scans are used. Small smooth muscle tumors are usually homogeneous soft-tissue masses that may enhance with IV contrast material [1]. Tumor necrosis, a described feature of larger tumors [15, 16], was seen in two large leiomyosarcomas (Fig. 4A) in this series, but also with all three leiomyomas (Fig. 4C), suggesting that this feature is not a reliable predictor that a tumor is malignant. Although distinguishing leiomyoma from leiomyosarcoma may be impossible with CT, Megibow et al. [17] have suggested that size larger than 6 cm, necrosis, and extensive ulceration or fistulization are morphologic features of a primary tumor that suggest the

tumor is malignant. In our study group, it did not appear that the malignant or benign nature of a tumor could be reliably predicted on the basis of size. The size of one malignant smooth muscle tumor with metastases was 5 cm, whereas two benign smooth muscle tumors were 6 cm.

Malignant tumors typically had an exophytic component or wall thickening or both, as seen in 15 of 19 malignant tumors in this study, in accord with previous reports [3]. One metastatic renal cell carcinoma and two primary duodenal adenocarcinomas were manifested as intraluminal masses, with additional wall thickening or extraduodenal spread.

Duodenal adenocarcinomas are typically small at the time of diagnosis, appearing as either polypoid masses or annular constricting lesions (Fig. 1). Three such tumors in our series, each smaller than 2 cm, were not seen on CT scans. Adenocarcinoma tends to involve a shorter, isolated segment of the bowel than does lymphoma, and commonly is seen associated with bowel obstruction when the primary tumor is still quite small. In one of our cases, duodenal obstruction was obvious on CT, although the obstructing tumor itself was not detected. Bulky lymphadenopathy is less common with adenocarcinoma than with lymphoma [1, 18]. This feature can be helpful in distinguishing between these two entities, especially if a longer segment of small bowel is involved.

Gastrointestinal lymphomas may arise as primary tumors but are usually associated with disseminated disease. Duodenal involvement is rare, as the distribution of lymphoma is proportional to the amount of lymphoid tissue and therefore is more common in the distal ileum [1]. Although the lymphomas seen in this study were bulky masses, they can have a variety of appearances: masses with thickened folds, polypoid masses, or mural nodules [19, 20]. Ulceration and necrosis also have been described [21]; ulceration was seen in one of our cases. Bowel obstruction is uncommon, but sometimes is seen with Hodgkin's disease or is caused by intussusception of a polypoid mass [1]. Aneurysmal dilatation without obstruction may also be seen [21].

The sensitivity of CT for detecting the presence of a duodenal tumor was 88%; small polypoid intraluminal neoplasms accounted for all false-negative cases. When features of tumor morphology were used as predictors, CT had an accuracy of 82% for predicting the benign or malignant nature of a duodenal neoplasm when the tumor could be detected on CT scans. Most malignant tumors had wall thickening or an exophytic component. However, three benign smooth muscle tumors without extraduodenal abnormality also had these features, thereby reducing the accuracy and specificity of tumor morphology as a predictor of whether a tumor is malignant. Although extraduodenal abnormality indicative of tumor spread is a good predictor that a tumor is malignant (positive predictive value, 100%), the lack of such findings (negative predictive value, 67%) cannot be used to reliably predict that a tumor is benign.

The high accuracy rate for predicting tumor resectability in this study group is in sharp contrast to that reported for other studies of tumors of the gastrointestinal tract [7–12, 22–24]; this may be due to the small size of our study group. As all patients in our study were known to have a duodenal neoplasm, likely greater attention was paid to each feature assessed with CT than would have occurred if the diagnosis of a tumor in this region had not been known. Predicting whether tumor involved the adjacent pancreatic head was difficult. Although we detected invasion in three cases, in four others we could only suggest that invasion was possible because of the contiguity of the tumor with the pancreas, colon, or common bile duct. Although knowledge of pancreatic invasion may result in an alteration in the surgical approach, from a simple resection with end-to-end anastomosis to a Whipple's procedure, this decision can be made intraoperatively and the tumor can still be resected. The presence of periduodenal fat invasion alone did not influence the therapeutic approach. Seven of 10 tumors in which periduodenal fat invasion was seen on CT were resected; surgical confirmation was not available in the remaining three cases with widespread metastatic disease.

Conclusions

The morphologic features of duodenal tumors on CT scans can be used as a sensitive, but nonspecific, predictor of whether a tumor is malignant, largely because of the variable appearance of smooth muscle tumors. All tumors with an associated extraduodenal abnormality were malignant. When duodenal tumor morphology and evidence of extraduodenal spread were considered together, both the sensitivity and accuracy of CT for predicting that a tumor was malignant were increased when compared with the use of morphologic criteria alone. Although tumors that are intraluminal and have no associated extraduodenal findings will most likely be benign, small, polypoid adenocarcinomas may occur. Last, CT appears to be reliable for predicting whether the resection of duodenal neoplasms will be curative, by showing sites of metastases, vascular encasement, and possibly contiguous organ invasion.

REFERENCES

1. Hulnick DH, Megibow AJ. CT of small intestine neoplasms. In: Fishman EK, Bronwyn J, eds. *Computed tomography of the gastrointestinal tract: contemporary issues in computed tomography*, vol. 9. New York: Churchill Livingstone, **1988**:205–227
2. Coscina WF, Arger PH, Levine MS, et al. Gastrointestinal tract focal mass lesions: role of CT and barium evaluations. *Radiology* **1986**;158:581–587
3. Farah MC, Jafri SZH, Schwab RE, et al. Duodenal neoplasms: role of CT. *Radiology* **1987**;162:839–843
4. Heiken JP, Forde KA, Gold RP. Computed tomography as a definitive method for diagnosing gastrointestinal lipomas. *Radiology* **1982**; 142:409–414
5. Whetstone MR, Zuckerman MJ, Saltzstein EC, et al. CT diagnosis of duodenal lipoma. *Am J Gastroenterol* **1985**;80:251–252
6. Bockus HL. Duodenal neoplasms. *Gastroenterology* **1985**;2:1428–1438
7. Kleinhaus U, Militianu D. Computed tomography in the preoperative evaluation of gastric carcinoma. *Gastrointest Radiol* **1988**;13:97–101
8. Cook AO, Levine BA, Sirinek KR, et al. Evaluation of gastric adenocarcinoma: abdominal computed tomography does not replace celiotomy. *Arch Surg* **1986**;121:603–606
9. Sussman SK, Halvorsen RA, Illescas FF, et al. Gastric adenocarcinoma; CT versus surgical staging. *Radiology* **1988**;167:335–340

10. Quint LE, Glazer GM, Orringer MB, et al. Esophageal carcinoma: CT findings. *Radiology* **1985**;155:171–175
11. Halvorsen RA Jr, Thompson WM. CT of esophageal neoplasms. *Radiol Clin North Am* **1989**;27:667–685
12. Halvorsen RA Jr, Thompson WM. Gastrointestinal cancer: diagnosis, staging and the follow-up role of imaging. *Semin Ultrasound CT MR* **1989**; 10:467–480
13. Dehn TCB, Reznek RH, Nockler IB, et al. Therapeutic assessment of advanced gastric cancer by computed tomography. *Br J Surg* **1984**; 71:413–417
14. Terrier F, Schapira C, Fuchs WA. CT assessment of operability of carcinoma of the oesophagogastric junction. *Eur J Radiol* **1984**;4:114–117
15. Clark RA, Alexander ES. Computed tomography of gastrointestinal leiomyosarcoma. *Gastrointest Radiol* **1982**;7:127–129
16. Mcleod AJ, Zornoza J, Shirkoda A. Leiomyosarcoma: computed tomographic findings. *Radiology* **1984**;152:133–136
17. Megibow AJ, Balthazar EJ, Hulnick DH, et al. CT evaluation of gastrointestinal leiomyomas and leiomyosarcomas. *AJR* **1985**;144:727–731
18. Ochsner S, Kleckner MS. Primary malignant neoplasms of the duodenum and small bowel. *JAMA* **1957**;163:413–417
19. Hulnick DH. The small intestine. In: Megibow AJ, Balthazar EJ, eds. *Computed tomography of the gastrointestinal tract*. St. Louis: Mosby, **1986**:217–278
20. Megibow AJ, Balthazar EJ, Naidich DP, et al. Computed tomography of gastrointestinal lymphoma. *AJR* **1983**;141:541–547
21. Pagani JJ, Bernardino ME. CT-radiographic correlation of ulcerating small bowel lymphoma. *AJR* **1981**;136:998–1000
22. Moss AA, Schnyder, Mark SW, et al. Gastric adenocarcinoma: a comparison of the accuracy and economics of staging by computed tomography and surgery. *Gastroenterology* **1981**;80:45–50
23. Adalsteinsson B, Glimelius B, Graffman S, et al. Computed tomography in the staging of rectal carcinoma. *Acta Radiol* **1985**;26:45–55
24. Megibow AS. Gastrointestinal lymphoma: the role of CT in diagnosis and management. *Semin Ultrasound CT MR* **1986**;7:43–51

LIST OF BOOK REVIEWS

310 **The Esophagus.** *Castell DO, ed.*
316 **CT & MRI Radiological Anatomy.** *Merran S, ed.*
328 **The Radiologist's Second Reader.** *Fischer HW*
342 **Diagnostic Ultrasound. Physics, Biology, and Instrumentation.** *Bushong SC, Archer BR*
356 **Imaging of Orthopedic Trauma,** 2nd ed. *Berquist TH, ed.*
378 **Radiation Protection in Nuclear Medicine and Pathology.** *Goldstone KE, Jackson PC, Myers MJ, Simpson AE, eds.*
384 **MRI Atlas of the Spine.** *Maravilla KR, Cohen WA*
390 **Human Cross-sectional Anatomy. Atlas of Body Sections and CT Images.** *Ellis H, Logan BM, Dixon A*
394 **Magnetic Resonance Imaging of the Body,** 2nd ed. *Higgins CB, Hricak H, Helms CA*
402 **Ultrasound in Ophthalmologic Diagnosis. A Practical Guide.** *Guthoff R*

Book Review

The Esophagus. Edited by Donald O. Castell. Boston: Little, Brown, 817 pp., 1992. $150

Edited by a prominent gastroenterologist who has special interest in the topic, this textbook covers the esophagus in an encyclopedic fashion. The book consists of 40 chapters: (1) functional anatomy and physiology, (2) overview and symptom assessment, (3) radiology of the oropharynx and esophagus, (4) endoscopy, (5) manometry, (6) ambulatory pH and pressure monitoring, (7) provocative tests for pain, (8) cytology, (9) oropharyngeal dysphagia, (10) achalasia, (11) disorders of increased contractility, (12) neoplasms, (13) surgical cancer therapy, (14) rings and webs, (15) diverticula, (16) esophageal abnormalities in systemic diseases, (17) foreign bodies, (18) surgery for motor disorders, (19–29) various aspects of reflux disease, (30) pill-induced injury, (31) esophagitis in the immunocompromised, (32) caustic injuries, (33) other inflammatory conditions, (34) injury from nonsteroidal antiinflammatory drugs, (35) noncardiac chest pain, (36) rupture and perforation, (37) hiatal hernia and mucosal prolapse, (38) varices and Mallory-Weiss tears, (39) cutaneous diseases, and (40) esophageal diseases in the elderly. The editor is the first or second author of five chapters. Despite this, conflicts of opinion and differences in style are not objectionable. The contributors are largely distinguished. Some are currently at the editor's institution, and many were associates of him at his former institutions.

Radiologic figures are sparse except in chapter 3 and are mostly esophagrams, with some endoscopic sonograms, radionuclide studies, and CT scans. Quality is good to excellent, with a few exceptions. Numerous excellent line drawings and endophotos are present. The book is hardcover with good binding and paper. The price is an unavoidable consequence of the numerous color images. References are given at the end of each chapter but do not seem to be more current than 1990. This is unavoidable in an undertaking of this magnitude.

I can find little to fault in any of the chapters. Clinical esophagology, radiology of the esophagus, esophageal surgery and pathology, and esophageal anatomy and pathophysiology are combined into one encyclopedic textbook. Clearly, the book is geared toward gastroenterologists and trainees in gastroenterology. It has far more information than most radiologists wish to acquire. In comparison, *Radiology of the Esophagus*, by Marc Levine (Saunders, 1989), sells for less (although it is only 365 pages) and has far more comprehensive radiology. It has some clinical, endoscopic, pathologic, and surgical correlation but no endoscopic sonograms. It is, therefore, a much better value for radiologists.

The Esophagus is an excellent encyclopedic monograph that covers all aspects of the esophagus, with a gastroenterologic emphasis. I strongly recommend it to gastroenterologists and to trainees, internists, and surgeons who have an interest in diseases of the esophagus. Gastrointestinal radiologists should have access to this book as a reference, but I can recommend it for purchase only to those radiologists who have a strong interest in diseases of the esophagus.

Arnold C. Friedman
Temple University Hospital
Philadelphia, PA 19140

Pictorial Essay

CT Findings in Patients with Small-Bowel Transplants

D. B. Bach,[1] M. F. Levin,[1] A. D. Vellet,[1] D. B. Downey,[1] P. L. Munk,[1] D. R. Grant,[2] and W. J. Wall[2]

Orthotopic small-bowel transplantation procedures are being performed increasingly often worldwide. CT plays an important role in both the preoperative assessment and the postoperative care of these patients. This pictorial essay serves to acquaint radiologists with the CT findings related to small-bowel transplantation.

Small-bowel transplantation procedures include transplantation of the small intestine only [1, 2]; combined transplantation of the small intestine and liver [3]; and multivisceral transplantation of the small intestine, liver, stomach, duodenum, and pancreas [4]. CT plays a vital role in the postoperative management of patients in whom these procedures are performed. This pictorial essay describes the normal findings on CT, and illustrates the CT appearance of complications that occur in association with these operations.

Procedure

Patients with short-gut syndrome in whom total parenteral nutrition is no longer feasible (usually because of inadequate venous access or total parenteral nutrition–induced intrahepatic cholestasis) are potential candidates for small-bowel

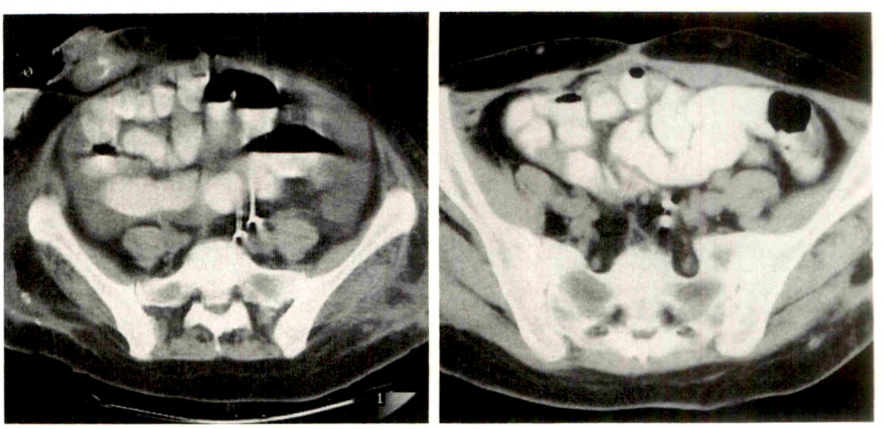


Fig. 1.—36-year-old patient after transplantation of small bowel and liver.

***A*, CT scan at level of ileostomy on day 13. Small-bowel loops have a normal appearance. Note ascites.**

***B*, CT scan obtained 21 months later. Ascites has resolved.**

Received December 18, 1991; accepted after revision February 28, 1992.

[1] Department of Diagnostic Radiology, University Hospital and University of Western Ontario, 339 Windermere Rd., London, Ontario, Canada N6A 5A5. Address reprint requests to D. B. Bach.

[2] Department of Surgery, University Hospital and University of Western Ontario, London, Ontario, Canada N6A 5A5.

AJR **159:311–315, August 1992** 0361–803X/92/1592–0311 © American Roentgen Ray Society

transplantation. The surgical procedure at our hospital has varied depending on the type of graft [5]. For transplantation of the small bowel only, the graft is mobilized on a vascular pedicle consisting of the donor superior mesenteric artery with a segment of aorta, and the superior mesenteric vein with a segment of portal vein. The graft is placed in the recipient in an orthotopic position, with an aortoaortic anastomosis and end-to-side portal anastomosis. The proximal end of the small intestine is anastomosed to the native duodenum; the distal end is brought out as an ileostomy.

In a combined transplantation of small intestine and liver, the vascular pedicle of the graft includes the donor celiac axis and superior mesenteric artery and a short segment of aorta, which is anastomosed to the native infrarenal aorta as an "aortic conduit." The end of the native portal vein is anastomosed to the side of the donor portal vein. In a multivisceral transplantation, the native organs (liver, gastric body and antrum, duodenum, and pancreas) are removed before the graft is placed into the abdominal cavity. Reconstruction includes anastomoses of the supra- and infrahepatic portions

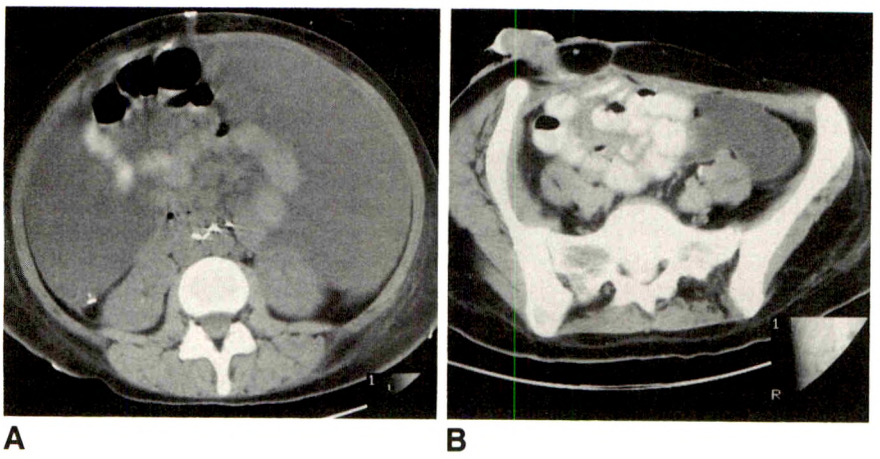


Fig. 2.—27-year-old patient after transplantation of small bowel, liver, stomach, duodenum, and pancreas and removal of colon.

***A*, CT scan of abdomen on day 15. Small bowel loops float centrally in a large amount of ascites fluid.**

***B*, CT scan at level of ileostomy on day 62. Note loculated ascites on left side.**

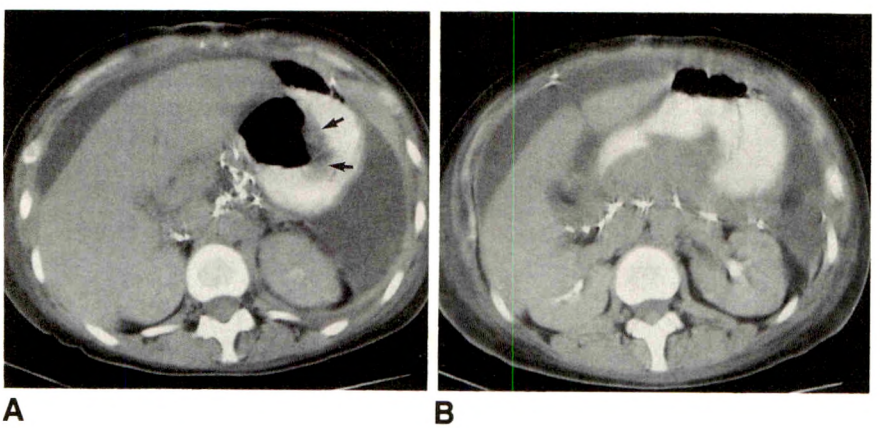


Fig. 3.—27-year-old patient after transplantation of small bowel, liver, stomach, duodenum, and pancreas.

***A*, CT scan through upper abdomen on day 21 shows a thick rind of tissue (*arrows*), which represents gastrogastric anastomosis. Spleen has been removed.**

***B*, CT scan obtained at a level 3 cm inferior to *A*. Transplanted stomach is distended with barium. Note ascites.**

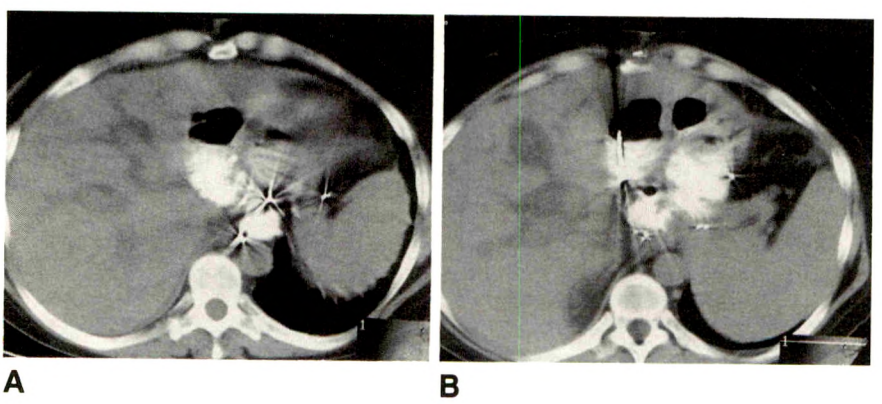


Fig. 4.—36-year-old patient with prior gastrectomy 25 days after transplantation of small bowel and liver.

***A* and *B*, CT scans of upper abdomen show anastomosis between native esophagus and transplanted jejunum, as well as jejunojejunostomy, which was created to serve as a gastric reservoir.**

of the inferior vena cava to the corresponding native vena cava, of the aortic conduit to the native infrarenal aorta, and of the donor stomach to the native gastric fundus. The distal small bowel is again brought out as an ileostomy.

Normal Findings

CT clearly shows the anatomy of the transplanted structures, including the small-bowel graft and its arterial and venous connections. The transplanted small bowel appears

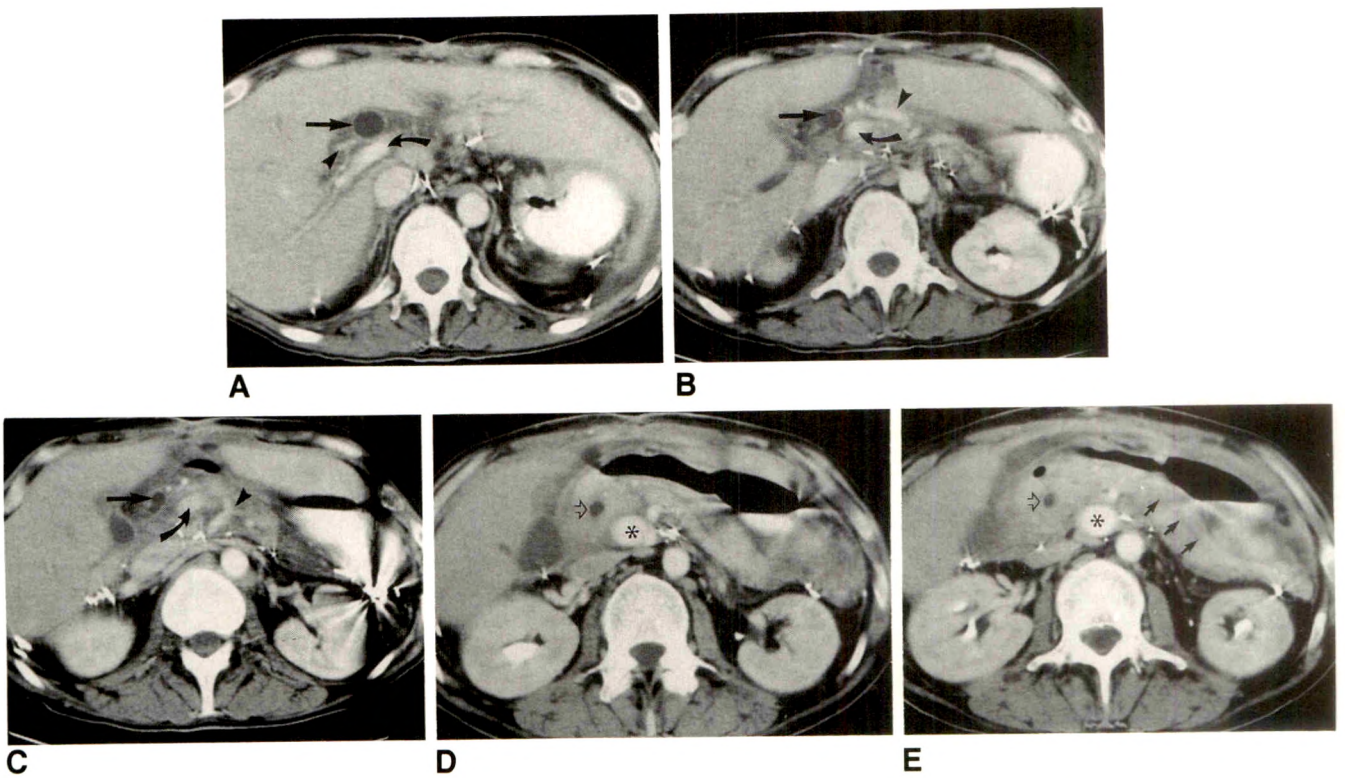


Fig. 5.—31-year-old patient 53 days after transplantation of small bowel, liver, stomach, duodenum, and pancreas. CT scans of upper abdomen obtained during rapid administration of IV contrast material show normal appearance of transplanted liver, stomach, pancreas, portal vein, and aortic conduit with branch vessels.

A, Edema fluid surrounds portal vein (*curved arrow*) and common hepatic duct (*straight arrow*). *Arrowhead* shows right hepatic artery branch.

B, *Curved arrow* shows portal vein, *straight arrow* shows common hepatic duct, *arrowhead* shows hepatic artery.

C, *Curved arrow* shows portal vein, *straight arrow* shows common hepatic duct; note celiac artery division and origin of hepatic artery (*arrowhead*).

D, Branch vessels arise on left side of aortic conduit (*asterisk*). *Open arrow* shows intrapancreatic portion of common bile duct.

E, *Open arrow* shows intrapancreatic portion of common bile duct, *asterisk* shows aortic conduit, three *solid arrows* show pancreatic duct in donor pancreatic body.



Fig. 6.—CT scan of abdomen in a 27-year-old patient 52 days after transplantation of small bowel, liver, stomach, duodenum, and pancreas. Branch vessels (*arrowheads*) exit aortic conduit (*asterisk*) from its right side. Note transplanted pancreas anterior to left kidney.

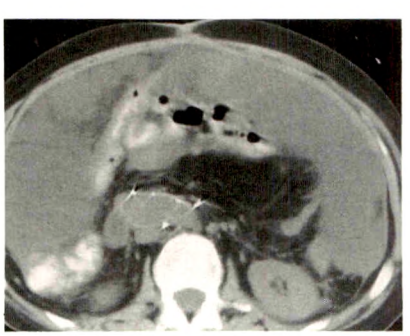


Fig. 7.—CT scan of abdomen in a 36-year-old patient 47 days after transplantation of small bowel and liver. Donor aortic conduit extends anterolaterally to native aorta on right side.

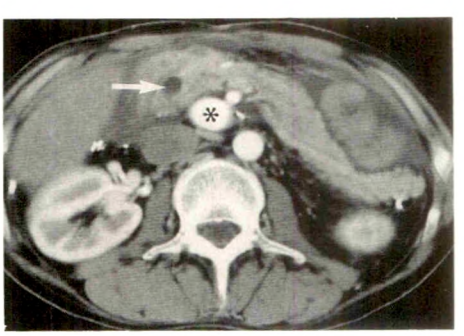


Fig. 8.—CT scan of abdomen in a 31-year-old patient 6.5 months after transplantation of small bowel, liver, stomach, duodenum, and pancreas. Transplanted pancreas lies anterior to lower pole of left kidney. Aortic conduit (*asterisk*); intrapancreatic portion of common bile duct (*arrow*).

similar to the native small bowel (Figs. 1 and 2), and is located in the usual position. The anastomoses, which provide continuity with the recipient's alimentary tract, are well seen (Figs. 3 and 4). The donor aortic conduit and the anastomosis between the conduit and the native aorta are best visualized on contrast-enhanced dynamic CT (Figs. 5 and 6); their appearances vary depending on the orientation of the vascular pedicle (Fig. 7). The body and tail of the transplanted pancreas are located in a more inferior position than normal, and the pancreatic tail curves anterior to the left kidney (Fig. 8).

Abnormal Findings

Ascites, Fluid Collections, and Abscesses

Many patients have prolonged ascites, which persists for many months (Fig. 9). CT is useful in differentiating ascites from loculated fluid collections or possible abscesses (Fig. 10) and in localizing collections for aspiration and drainage (Figs. 11 and 12).

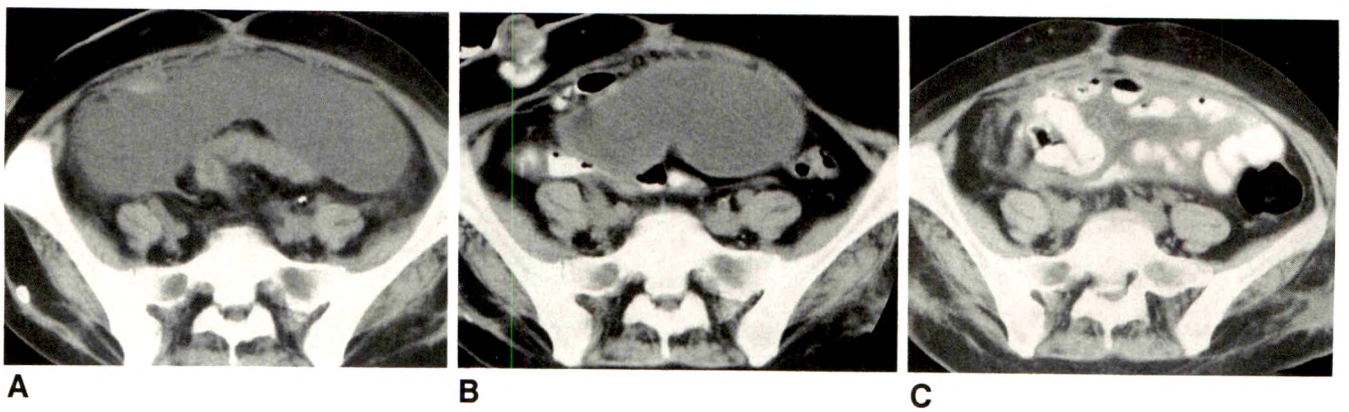


Fig. 9.—36-year-old patient after transplantation of small bowel and liver. Sequential CT examinations over a period of months revealed gradual reduction and eventual resolution of ascites.
A, CT scan of pelvis 47 days after transplantation.
B, CT scan 129 days after transplantation. Ascites is diminished.
C, CT scan 216 days after transplantation. Ileostomy has been closed with restoration of bowel continuity. A small amount of ascites persists.

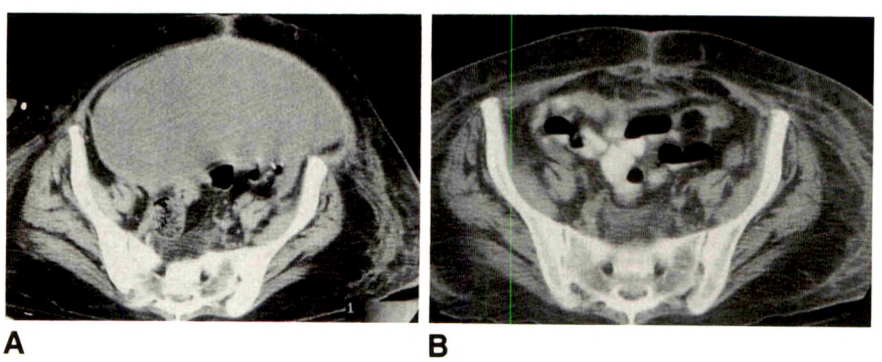


Fig. 10.—41-year-old patient after transplantation of small bowel and liver.
A, CT scan on day 46 shows a large collection of loculated ascites fluid, which extends from left upper quadrant to pelvis. This was drained percutaneously.
B, CT scan 79 days after transplantation. Fluid collection did not recur.

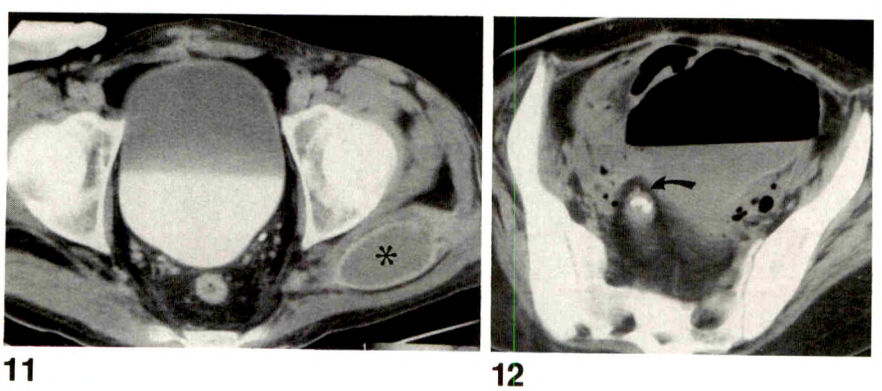


Fig. 11.—CT scan of pelvis in a 31-year-old patient after transplantation of small bowel, liver, stomach, duodenum, and pancreas. Fluid collection (*asterisk*) in left buttock proved to be a sterile hematoma.

Fig. 12.—27-year-old patient who had lymphoma after transplantation of small bowel, liver, stomach, duodenum, and pancreas. CT scan 187 days after transplantation at level of intact rectal stump (*arrow*), which is demarcated by surgical clips and surrounded by fat, shows large collection of air and fluid, representing an abscess related to perforation of small bowel involved by lymphoma.

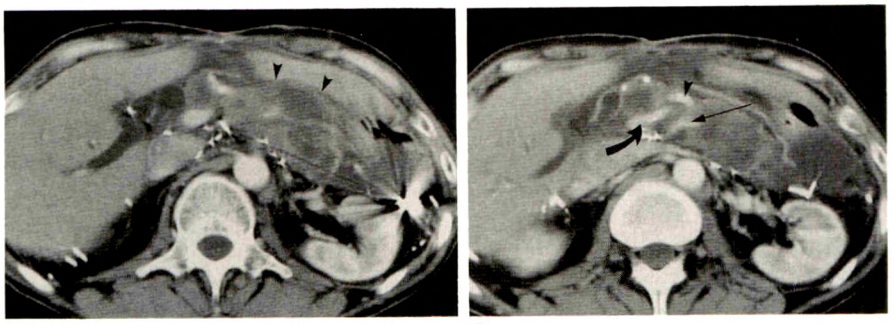


Fig. 13.—31-year-old patient who had lymphoma 6.5 months after transplantation of small bowel, liver, stomach, duodenum, and pancreas (same patient as in Fig. 5). CT scans of abdomen were obtained with IV contrast material.

A, Soft-tissue mass (*arrowheads*) lies inferior to left lobe of transplanted liver. Biopsy showed lymphoma.

B, Mass surrounds portal vein (*curved arrow*), celiac artery (*straight arrow*), and hepatic artery (*arrowhead*).

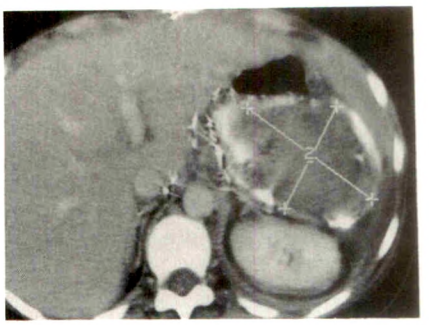


Fig. 14.—27-year-old patient 127 days after transplantation of small bowel, liver, stomach, duodenum, and pancreas. CT scan of abdomen reveals a large mass in stomach that was misdiagnosed as food debris or blood clot. Biopsy revealed lymphoma.

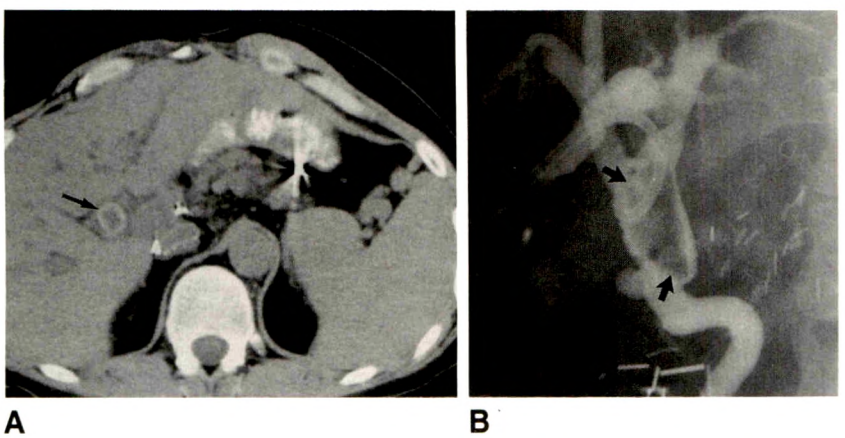


Fig. 15.—36-year-old patient 19 months after transplantation of small bowel and liver, with nonspecific signs of abdominal discomfort and occasional episodes of fever.

A, Unenhanced CT scan of liver shows rim-calcified round structure (*arrow*) at confluence of right and left hepatic ducts, consistent with a calculus.

B, Cholangiogram confirms presence of calculus (*arrows*) in donor common duct. Stricture at choledochocholedochal anastomosis became apparent on a subsequent examination.

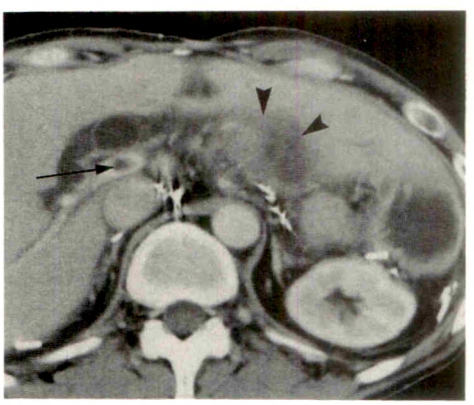


Fig. 16.—31-year-old patient who had lymphoma 6.5 months after transplantation of small bowel, liver, stomach, duodenum, and pancreas. CT scan of abdomen after IV administration of contrast medium shows filling defect in portal vein (*arrow*), which represents thrombus. *Arrowheads* show top of lymphomatous mass.

Lymphoproliferative Disorders

Lymphoma can occur after transplantation. In one case, CT showed a mass at the root of the transplanted small-bowel mesentery (Fig. 13). In another patient, repeated CT examinations did not show lymphadenopathy, and a lymphomatous mass in the transplanted stomach was misdiagnosed as thrombus or food (Fig. 14). In both patients, the transplanted liver maintained a normal appearance, unlike in one patient with intrahepatic lymphomatous masses, reported elsewhere [5].

Other Complications

Patients with combined transplantation of small bowel and liver are subject to the complications of liver transplantation alone. In one patient, a biliary calculus developed in the common hepatic duct proximal to the choledochocholedochal anastomosis. This was diagnosed on the basis of CT findings (Fig. 15) and was treated percutaneously. Nonobstructing thrombus in the portal vein was seen on CT scans in another patient after lymphoma was diagnosed (Fig. 16).

REFERENCES

1. Goulet O, Revillon Y, Brousse N, et al. Two and one-half year follow-up after isolated cadaveric small bowel transplantation in an infant. *Transplant Proc* **1992**; 24:1224–1225
2. Grant D, Sommerauer J, Mimeault R, et al. Treatment with continuous high-dose intravenous cyclosporin following clinical intestinal transplantation. *Transplantation* **1989**;48:151–152
3. Grant D, Wall W, Mimeault R, et al. Successful small bowel/liver transplantation. *Lancet* **1990**;335:181–184
4. Starzl TE, Rowe MI, Todo S, et al. Transplantation of multiple abdominal viscera. *JAMA* **1989**;261:1449–1457
5. Bach DB, Hurlbut DJ, Romano WM, et al. Human orthotopic small intestine transplantation: radiologic assessment. *Radiology* **1991**;180:37–41

Book Review

CT & MRI Radiological Anatomy. Edited by Samuel Merran. (Translated by Adrian Dixon.) Stoneham, MA: Butterworth-Heinemann, 304 pp., 1991. $130

This volume is designed as a comprehensive anatomic atlas of MR imaging and CT. The book is divided into 13 chapters, each dealing with a major anatomic unit: head and skull, sella turcica, orbit, face, ear, neck, vertebral column, thorax, abdomen, peritoneal folds, retroperitoneum, pelvis, and limbs.

The format for all chapters is similar, beginning with suggested imaging techniques and parameters for CT and MR imaging. This is followed by a series of radiologic images, each accompanied by an annotated line drawing in which anatomic structures are numbered, a corresponding figure legend, and, in most cases, an additional image or anatomic drawing to orient the reader to the location of the study section. The number of labeled items per image varies from a few to as many as 25. Most of the images are oriented axially, although effort has been made to include sagittal and coronal images. The chapter on the neck, for example, has 17 axial and two coronal CT scans and four coronal, two sagittal, and one axial MR image. Of the 27 images of the thorax, 13 are axial CT scans, eight are sagittal MR images, and six are coronal MR images. Most of the images deal with normal anatomy, although a few show anatomic variations and the chapter on the peritoneal folds uses images from an obese patient with ascites to better delimit the intra- and retroperitoneal spaces. Inversion recovery MR images are used to show the anatomy of the head, whereas T1-weighted images are used for most other locations.

The chapters are well-illustrated, having a large number of images with corresponding line drawings. The images are, for the most part, of excellent or good quality, though a few are a bit dark. In general both the images and the line drawings are small, together occupying less than half a page, with the figure legend and orientation sketch given the majority of the available page space. The numbering on the drawings is usually self-evident, with, for example, the number keyed to the internal jugular vein placed within the anatomic structure on the drawing. In some instances, lines or arrows are used. However, a few images are busy, and the meaning of a number is not clear until the corresponding legend is read.

The clarity and simplicity of this system is also a drawback in that in some instances, only a few structures are labeled, and labeling tends to relate to major anatomic structures in the region under study. For example, in the section on the neck, labeling centers on the airway, and a search is required to detect the strap muscles. Similarly, areas such as the chest and abdominal walls receive little attention. The section on the limbs is too brief to be of value, covering the shoulder, elbow, wrist, hip, knee, and foot in 16 images. Those specifically interested in the anatomy of the musculoskeletal system will likely not find this adequate.

This text is easy to read and use, although it is somewhat limited in scope. The text is fairly expensive, and the cost of $130 may be prohibitive. The book would be most useful for radiology residents and those involved in general head and body CT and MR imaging.

Mark J. Kransdorf
Armed Forces Institute of Pathology
Washington, DC 20306-6000

Persistence of Portosystemic Collaterals and Splenomegaly on CT After Orthotopic Liver Transplantation

Judith L. Chezmar[1]
Richard D. Redvanly[1]
Rendon C. Nelson[1]
J. Michael Henderson[2]

OBJECTIVE. The appearances of portosystemic collaterals and splenomegaly on CT before and after liver transplantation were evaluated.

MATERIALS AND METHODS. The records of 54 patients undergoing liver transplantation during a 2.5-year period were reviewed retrospectively. Twenty-five of these patients, in whom both a preoperative abdominal CT scan and a follow-up CT scan at least 1 year after transplantation had been obtained, were clinically well and had had no significant episodes of rejection, severe recurrent hepatitis, or other complication at the time of study. A total of 94 abdominal CT scans in these patients were reviewed to assess changes in portosystemic collaterals and splenic volume.

RESULTS. At 6 months after transplantation, portosystemic collaterals at one or more sites were seen in 14 (74%) of the 19 patients scanned at this time in whom collaterals had been seen on CT preoperatively. At 1 year after transplantation, splenic hilar collaterals persisted in 64% of patients, splenocolic ligament collaterals in 50%, retroperitoneal collaterals in 38%, and peripancreatic collaterals in 38% of patients with preoperative varices at these sites who were examined with CT at this interval. Splenic hilar, coronary, and retroperitoneal collaterals were found to persist for up to 4 years after transplantation in the single patient examined at that time. Splenic volume decreased in 94% of patients examined after transplantation, with a mean reduction of 60 ± 19%. However, the spleen remained significantly enlarged in 56% of patients.

CONCLUSION. We conclude that portosystemic collaterals and splenomegaly frequently persist after liver transplantation, but that this finding need not indicate recurrence of hepatic disease or other posttransplantation complications.

AJR 159:317–320, August 1992

The development of collateral channels between the portal and systemic venous systems and the appearance of congestive splenomegaly are two characteristic features of portal hypertension. Orthotopic liver transplantation is now a widely practiced and accepted method of treatment for end-stage liver disease [1]. It has been presumed that variceal collaterals diminish or close after transplantation, either by surgical obliteration during the transplantation procedure or spontaneously by reduction in portal pressure [2]. Congestive splenomegaly is also presumed to resolve. To our knowledge, no reports have addressed the question of the extent and timing of these changes after transplantation. The purpose of our study was to assess the changes in the appearance of collateral varices and splenomegaly on CT after liver transplantation in patients with portal hypertension.

Materials and Methods

We retrospectively reviewed the records of patients who had liver transplantation during a 2.5-year period (January 1987 to July 1989). Of the 54 patients receiving transplants during this period, both a preoperative abdominal CT scan and a follow-up CT scan obtained at least 1 year after transplantation were available in 29 patients. Clinical records and liver biopsy results in these 29 patients were reviewed in order to exclude patients with significant

Received December 26, 1991; accepted after revision February 24, 1992.

[1] Department of Radiology, Emory University School of Medicine, 1364 Clifton Rd., N.E., Atlanta, GA 30322. Address reprint requests to J. L. Chezmar.

[2] Department of Surgery, Emory University School of Medicine, Atlanta, GA 30322.

0361–803X/92/1592–0317
© American Roentgen Ray Society

episodes of rejection, severe recurrent hepatitis, or other posttransplantation complications. This resulted in the exclusion of four patients from the study, two with chronic active hepatitis and cirrhosis, one with venoocclusive disease and hepatocellular necrosis, and one with metastatic cholangiocarcinoma. The study population therefore consisted of 25 patients with a satisfactory clinical course in whom CT examinations were performed as a part of routine postoperative evaluation at approximately 6 months and then at yearly intervals after transplantation. The patients (15 women and 10 men) were 20–64 years old (mean, 43 years). The indications for hepatic transplantation in these patients were as follows: chronic active hepatitis (n = 12), alcoholic cirrhosis (n = 3), primary biliary cirrhosis (n = 3), cirrhosis of other cause (n = 3), Budd-Chiari syndrome (n = 3), and sclerosing cholangitis (n = 1). A total of 94 CT scans were obtained in these 25 patients preoperatively (n = 25) and at intervals of approximately 6 months (n = 20), 1 year (n = 23), 2 years (n = 20), 3 years (n = 5), and 4 years (n = 1) after transplantation.

Patients were scanned with either a Siemens DR-3 (Siemens, Iselin, NJ) or Philips LX or TX (Philips Medical Systems, Shelton, CT) scanner. All images were obtained with either 8- or 10-mm-thick sections with a 0- to 5-mm intersection gap. Oral and IV contrast agents were used for 64 of the 94 CT studies. IV contrast material was administered as a 150-ml bolus of 60% iodinated contrast material. The remaining examinations were performed with oral contrast material only, as dictated by the patients' clinical situation and at the discretion of the attending radiologist.

The posttransplantation CT scans were reviewed by a panel of three abdominal radiologists for evidence of portosystemic collaterals and compared with the preoperative CT scans. Collaterals in the following anatomic areas were specifically noted: esophageal, coronary, splenic hilar, splenocolic ligament, peripancreatic, paraumbilical, mesenteric, retroperitoneal, and subcutaneous. Percentages were calculated that reflected the fraction of patients with preoperative varices who were scanned at the designated interval and were found to have persistent collaterals.

Splenic volumes were calculated for 19 patients on the preoperative scans. With an electronic cursor, the edge of the spleen on each section was traced manually, and the enclosed area was calculated by the computer [3]. The areas from each section were summed and then corrected for intersection gap. These volumes were recorded, as were splenic volumes obtained on postoperative studies, and the percentage of change was calculated.

Results

Portosystemic Collaterals

Portosystemic collaterals at one or more sites were seen on CT in 22 (88%) of 25 patients before hepatic transplantation. The number of patients with varices at each site was as follows: esophageal (n = 13), coronary (n = 20), splenic hilar (n = 16), splenocolic ligament (n = 10), peripancreatic (n = 9), paraumbilical (n = 11), mesenteric (n = 13), retroperitoneal (n = 18), and subcutaneous (n = 3) (Table 1).

Six months after transplantation, portosystemic collaterals at one or more sites were found in 14 (74%) of the 19 patients scanned at this time in whom collaterals were seen on CT preoperatively. The frequency of persistent portosystemic collaterals varied by site. No paraumbilical or subcutaneous varices were detected. Persistent collaterals most frequently detected 6 months after transplantation were peripancreatic (86% of patients), followed by splenic hilar (83%), retroperitoneal (77%), splenocolic ligament (63%), coronary (41%), mesenteric (38%), and esophageal (33%) (Table 1).

Collaterals in the splenic hilum and retroperitoneum persisted for the longest period of time in the largest number of patients. In the splenic hilum, collaterals were still visible in nine (64%) of 14 patients at 1 year, eight (67%) of 12 patients at 2 years, two (67%) of three patients at 3 years, and in the single patient examined 4 years after transplantation (Fig. 1). Retroperitoneal collaterals were still visible in six (38%) of 16 patients at 1 year, five (36%) of 14 at 2 years, three (75%) of four at 3 years, and in the single patient examined 4 years after transplantation. In this patient, coronary varices also were visible 4 years after transplantation. Although the size of collaterals in most cases gradually diminished over time, two patients had no significant change in the size of retroperitoneal and splenic hilar collaterals over time for up to 2 and 3 years, respectively, after transplantation.

Splenic Volume

Splenic volume was measured preoperatively in 19 patients. In three patients the spleen had been removed, and in three others no volume was calculated.

Before transplantation, all measured splenic volumes were outside the normal range (219 ± 76 cm^3) [3], with a mean preoperative splenic volume of 953 ± 468 cm^3. Splenic volumes greater than 5 SD above normal were calculated in 12 patients (63%); the remaining seven patients had splenic volumes greater than 2 but less than 5 SD above normal.

Follow-up CT scans with calculation of splenic volume were obtained in 18 patients; one patient underwent splenectomy

TABLE 1: Detection of Portosystemic Collaterals with CT by Site Before and After Liver Transplantation

Site	No. of Patients with Collaterals Detected/No. Imaged (%)					
	Before Transplantation	Time After Transplantation				
		6 Months	1 Year	2 Years	3 Years	4 Years
Esophageal	13	4/12 (33)	1/12 (8)	0/10 (0)	0/3 (0)	0/0 (0)
Coronary	20	7/17 (41)	6/19 (32)	5/16 (31)	2/5 (40)	1/1 (100)
Splenic hilar	16	10/12 (83)	9/14 (64)	8/12 (67)	2/3 (67)	1/1 (100)
Splenocolic ligament	10	5/8 (63)	4/8 (50)	2/7 (29)	0/1 (0)	0/0 (0)
Peripancreatic	9	6/7 (86)	3/8 (38)	1/8 (12)	1/2 (50)	0/0 (0)
Paraumbilical	11	0/8 (0)	0/10 (0)	0/10 (0)	0/3 (0)	0/1 (0)
Mesenteric	13	3/8 (38)	1/11 (9)	1/10 (10)	0/2 (0)	0/1 (0)
Retroperitoneal	18	10/13 (77)	6/16 (38)	5/14 (36)	3/4 (75)	1/1 (100)
Subcutaneous	3	0/1 (0)	0/3 (0)	0/3 (0)	0/0 (0)	0/0 (0)

at the time of transplantation. One patient had a postoperative increase in splenic volume. This patient had massive pretransplantation splenomegaly (1791 cm^3) and multiple splenic infarcts postoperatively. The remaining patients had a decrease in splenic volume, with a mean volume decrease of 60 ± 19% (range, 35–93%) in a mean follow-up period of 2 years. In seven patients (39%), splenic volumes fell into the normal range after transplantation. These patients had a lesser degree of splenomegaly preoperatively than did the others in the group (mean, 511 ± 138 cm^3; range, 389–777 cm^3). Splenic volumes in these seven patients decreased a mean of 50 ± 12% to an average of 246 ± 58 cm^3 (range, 181–340 cm^3). The remaining 10 patients had a mean decrease in splenic volume of 66 ± 18%, but had persistently markedly enlarged spleens after transplantation (mean, 713 ± 189 cm^3; range, 380–1080 cm^3). This group of patients had massive splenomegaly preoperatively, with a mean pretransplantation volume in this group of 1125 ± 335 cm^3 (range, 562–1858 cm^3).

Two (28%) of the seven patients whose spleen size was in the normal range after transplantation had persistent portosystemic varices; in both cases these were small (Fig. 2). In contrast, seven (70%) of 10 patients with persistent massive splenomegaly had persistent varices, which in some cases were very large (Fig.1).

Discussion

This study is observational in nature but does provide important new information relevant to splanchnic hemodynamics after liver transplantation. Our finding of persistent portosystemic varices in several regions, most frequently the splenic hilum and retroperitoneum, up to 4 years after liver transplantation was unexpected. The previous assumption that all portosystemic collaterals will close after transplantation appears incorrect. These findings have potential significance to radiologists and clinicians involved in the care of patients after hepatic transplantation. The detection of persistent portosystemic collaterals in the absence of other clinical findings does not necessarily mean recurrence of liver disease with portal hypertension; the collaterals may continue

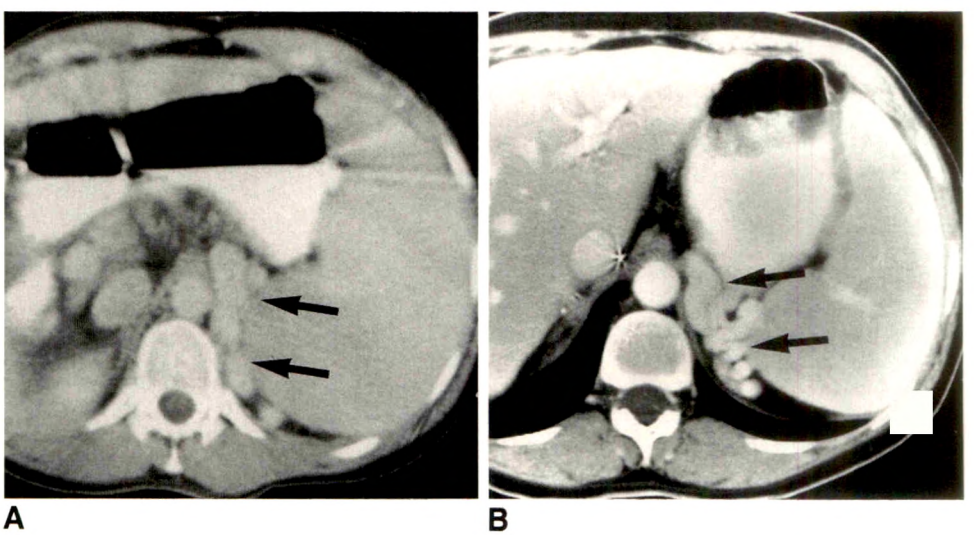


Fig. 1.—37-year-old woman with chronic active hepatitis.
A, CT scan before orthotopic liver transplantation shows large collateral vessels (*arrows*) in retroperitoneum.
B, 4 years after transplantation, large portosystemic collaterals persist (*arrows*). Splenic volume has decreased, but spleen remains markedly enlarged.

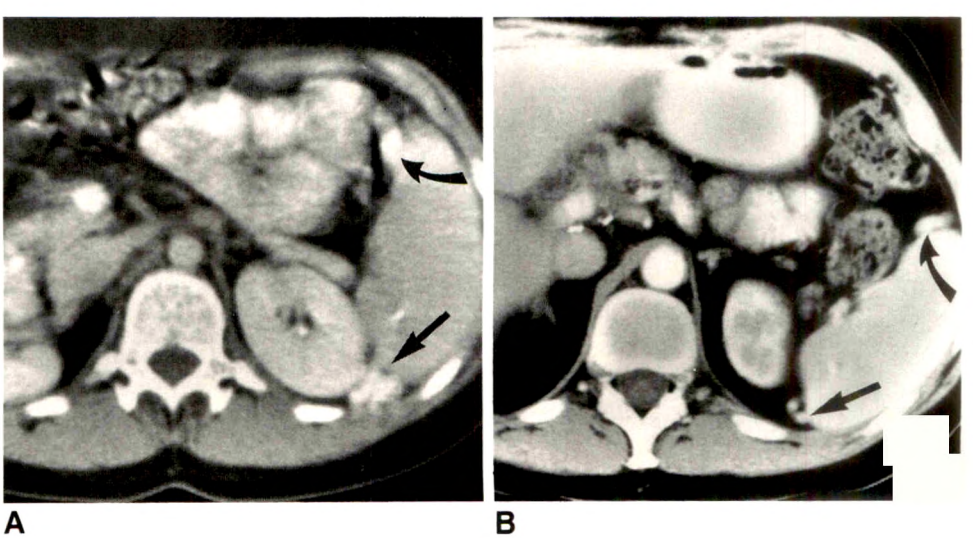


Fig. 2.—46-year-old woman with chronic active hepatitis.
A, CT scan before orthotopic liver transplantation shows portosystemic collaterals in retroperitoneum (*straight arrow*) and splenocolic ligament (*curved arrow*).
B, 2 years after transplantation, retroperitoneal (*straight arrow*) and splenocolic ligament (*curved arrow*) collateral vessels seen before transplantation are small but persistent. Splenic volume has decreased to within normal range.

to be present for months to years after transplantation in patients clinically well and with satisfactory allograft function.

Two recent studies have demonstrated persistence of high azygous flow measured by thermodilution at 3 months [4] and 14 days [5] after transplantation. This flow is a measure of gastroesophageal collateral outflow, and these studies indicate continued flow by this route soon after transplantation. The current study does not point to the gastroesophageal varices as the major persistent collateral route after liver transplantation, but this may reflect differences in methods or time of follow-up. These two studies also documented that portal pressure, measured as hepatic venous pressure gradient, falls to normal after liver transplantation. This suggests that any persistent open collaterals are no longer under the increased pressures associated with portal hypertension.

Although CT scanning has successfully been used to define portosystemic collaterals in the abdomen [6, 7], we recognize that the methods used in this study may not be optimal for defining these collaterals in all cases. Most CT examinations in our study were performed with IV contrast material; however, some of the studies were not contrast enhanced. Therefore, flow through the visualized collateral channels was not documented in all cases. Visceral angiography was not performed in any of these patients, as there was no clinical indication for such an invasive study. Comparison of CT and angiography for detection of varices has shown good correlation, however, and varices in some regions, particularly the retroperitoneum, have been shown to be better depicted with CT than with angiography [8]. This may reflect the fact that to document these collaterals angiographically, large volumes of contrast material would be required.

The reduction in splenic volume seen in this series would be expected after liver transplantation. The reduction in volume parallels that seen after shunt procedures, which decompress the spleen in patients with portal hypertension [9]. In massive splenomegaly, the structural changes in the spleen, including fibrosis, do not allow for complete return to normal size after portal hypertension is relieved; thus, some degree of splenomegaly persists, as was seen in our population of patients. It is noteworthy that the most persistent varices seen at follow-up were in the splenic hilum and retroperitoneum. It could be postulated that the persistent collaterals observed in this study in these regions may, in part, be maintained because of increased flow through the persistently enlarged spleen. This postulate is supported by our data: only two of the seven patients with splenic size in the normal range after transplantation had persistent varices, in contrast to seven of 10 patients with persistent massive splenomegaly.

The potential physiologic significance of the findings in this study are perhaps of greatest interest. Prior studies have shown high blood flow to the liver [10] and persistence of the high cardiac output of end-stage liver disease after transplantation [11]. Persistence of some portosystemic shunting may be a further important finding in the overall pattern of abnormal hemodynamics after transplantation. Persistence of splanchnic hyperemia and the shunting of vasoactive compounds from the splanchnic to the systemic circulation could contribute to these abnormalities.

We conclude that portosystemic collaterals may persist for months to years after liver transplantation despite resolution of portal hypertension. The physiologic significance of the persistent collaterals observed in this study will need to be defined.

ACKNOWLEDGMENT

We thank Shirley Wray for assistance with manuscript preparation.

REFERENCES

1. Starzl TE, Demetris AJ, Van Theil DH. Medical progress: liver transplantation. *N Engl J Med* **1989**;321:1014–1022, 1092–1099
2. Yanaga K, Tzakis AG, Shimada M, et al. Reversal of hypersplenism following orthotopic liver transplantation. *Ann Surg* **1989**;210:180–183
3. Henderson JM, Heymsfield SB, Horowitz J, Kutner MH. Measurement of liver and spleen volume by computed tomography. *Radiology* **1981**;141:525–527
4. Hadengue A, Moreau R, Sogni P, et al. High cardiac output after liver transplantation is due to persistent portosystemic collateral blood flow and elevated hepatic blood flow (abstr). *Hepatology* **1991**;14:57A
5. Navasa M, Feu F, Bosch J, et al. Systemic, splanchnic and humoral changes after orthotopic liver transplantation in cirrhosis (abstr). *J Hepatol* **1991**;13:S55
6. Ishikawa T, Tsukune Y, Ohyama Y, Fujikawa M, Sakuyama K, Fujii M. Venous abnormalities in portal hypertension demonstrated by CT. *AJR* **1980**;143:271–276
7. Clark KE, Foley WD, Lawson TL, Berland LL, Maddison FE. CT evaluation of esophageal and upper abdominal varices. *J Comput Assist Tomogr* **1980**;4:510–515
8. McCain AH, Bernardino ME, Sones PJ, Berkman WA, Casarella WJ. Varices from portal hypertension: correlation of CT and angiography. *Radiology* **1985**;154:63–69
9. Henderson JM, Kutner MH, Millikan WJ, et al. Endoscopic variceal sclerosis compared with distal splenorenal shunt to prevent recurrent variceal bleeding in cirrhosis. *Ann Intern Med* **1990**;112:262–269
10. Henderson JM, Millikan WJ, Hooks MH, Noe B, Kutner MH, Warren WD. Increased galactose clearance after liver transplantation: a measure of increased blood flow through the denervated liver. *Hepatology* **1989**;10:288–291
11. Henderson JM, Mackay GJ, Hooks M, et al. High cardiac output of advanced liver disease persists after orthotopic liver transplantation. *Hepatology* **1992**;15:258–262

Calcifications in the Portal Venous System: Comparison of Plain Films, Sonography, and CT

Carmen Ayuso[1]
Patricio Luburich[1]
Ramón Vilana[1]
Concepción Bru[1]
Jordi Bruix[2]

We describe 10 patients with long-standing portal hypertension and calcifications in the splenoportal and mesenteric venous systems or collateral vessels. The patients were examined with abdominal plain films (n = 10), sonography (n = 10), and CT (n = 9). Calcium was seen on CT scans in nine cases, on sonograms in seven, and on abdominal plain films in five. Calcifications appeared to be located in the wall of the vein in all cases. Sites of detection included the main portal, splenic, superior mesenteric, coronary, and peripancreatic veins.

CT was more sensitive than sonography, and both were more sensitive than plain films, in showing portal venous calcification. Detection of such calcifications may influence surgical or percutaneous therapy of portal hypertension.

AJR 159:321–323, August 1992

Calcification of the portal vein in adults is an uncommon finding on imaging studies. We have found 20 cases reported in the literature [1–16]; five were detected with CT [6, 14–16] and only one was detected with sonography [15]. In these cases, calcifications were located within a portal venous thrombus or in the vein wall.

We performed a study to compare the findings on plain radiographs, sonograms, and CT scans in patients with calcifications of the wall of the portal venous system.

Materials and Methods

We reviewed the imaging findings and medical records of 10 patients with calcifications within the portal vein who were seen over the past 3 years. Included were five men and five women 55–85 years old. Liver studies were performed because of chronic liver disease, including cirrhosis (eight patients), Budd-Chiari syndrome (one), and hepatic fibrosis associated with Caroli's disease (one). The diagnosis of chronic liver disease was made on the basis of clinical, laboratory, and histologic findings. All of the patients had had portal hypertension for 7–18 years (mean, 10.5) and had esophageal varices with or without previous episodes of acute bleeding. Hepatic vein catheterization confirmed the diagnosis of portal hypertension (hepatic venous pressure gradient, >6 mm Hg) in three cases. In one patient, a portocaval shunt had been placed 7 years before the current radiologic evaluation.

Abdominal plain films and abdominal sonograms were obtained in all cases. Sonographic studies were performed with a Sonolayer SSA-270A unit (3.7-MHz transducer) with duplex and color Doppler capabilities or with a Sonolayer SSA-100A unit (3.7-MHz transducer) with duplex Doppler capabilities (Toshiba Medical Systems, Japan). Abdominal CT scans spanning the diaphragm to renal hila were obtained with a Somatom DR3 scanner (Siemens Medical Systems, Erlangen, Germany) in nine patients. Unenhanced CT scans were obtained with 8-mm-thick sections at 10-mm intervals. Dynamic CT scans were obtained with the same technical conditions after a bolus of 100 ml of contrast material (iohexol 64.7% [Omnitrast 300], Schering, Berlin) was injected by hand.

Received December 16, 1991; accepted after revision February 25, 1992.

[1] Department of Radiology, Hospital Clinic, University of Barcelona, Villarroel 170, 08036 Barcelona, Spain. Address reprint requests to C. Ayuso.

[2] Liver Unit, Hospital Clinic, University of Barcelona, 08036 Barcelona, Spain.

0361–803X/92/1592–0321
© American Roentgen Ray Society

Results

In all cases, sonography and CT showed venous abnormalities characteristic of portal hypertension [17, 18], including recanalization of the umbilical vein; coronary gastroesophageal varices; and other collaterals such as dilated perisplenic, mesenteric, retrogastric, or peripancreatic veins. Liver sonography and/or CT showed spontaneous portosystemic shunts in three patients. The presence of portal venous thrombosis was excluded on the basis of Doppler sonographic and contrast-enhanced CT findings in nine patients; in one patient, a filiform portal vein was noted in the hepatic hilum. Cavernous transformation of the portal vein was present in another patient, and multiple periportal sinuous collateral hilar veins were detected on sonography; these enhanced on CT during the portal phase. Calcifications in the splenoportal venous system were seen on abdominal plain films in five of 10 cases, on sonograms in seven of 10 cases, and on CT scans in nine of nine cases. All of the calcifications detected in the portal vein and its tributaries were located in the venous wall. Linear calcifications were observed on plain radiographs of the abdomen in the right upper quadrant and/or in the epigastric area (Fig. 1). Abdominal CT showed linear calcifications located in the wall of the portal vein (eight cases) (Fig. 2A), splenic vein (five cases) (Fig. 3), superior mesenteric vein (six cases), coronary vein (two cases), peripancreatic veins (one case), and retroperitoneal collateral vessels (two cases). Sonograms showed calcifications in the wall of the portal vein in six cases and distal splenic vein in two cases. The sonographic diagnosis was established on the basis of the presence of intense linear echoes along the walls of the veins (Fig. 2B), usually with posterior acoustic shadowing (five cases) of variable intensity (Figs. 2B and 4). In three patients, echogenic nodular material was seen protruding into the lumen (Fig. 5). In one patient, a large number of noncalcified peripancreatic collaterals mimicking a pancreatic mass were detected on sonograms and CT scans obtained 8 years earlier. Calcifications in the walls of the veins were seen on later examinations, with no other morphologic changes in the size and distribution of varices (Fig. 6).

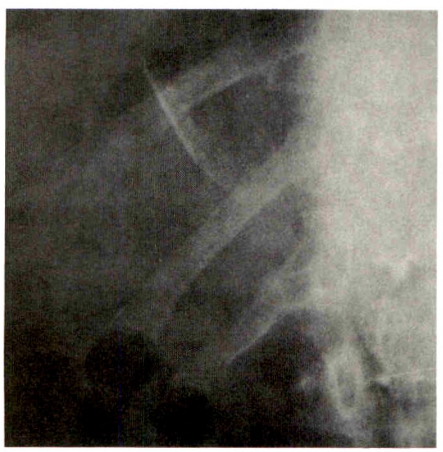
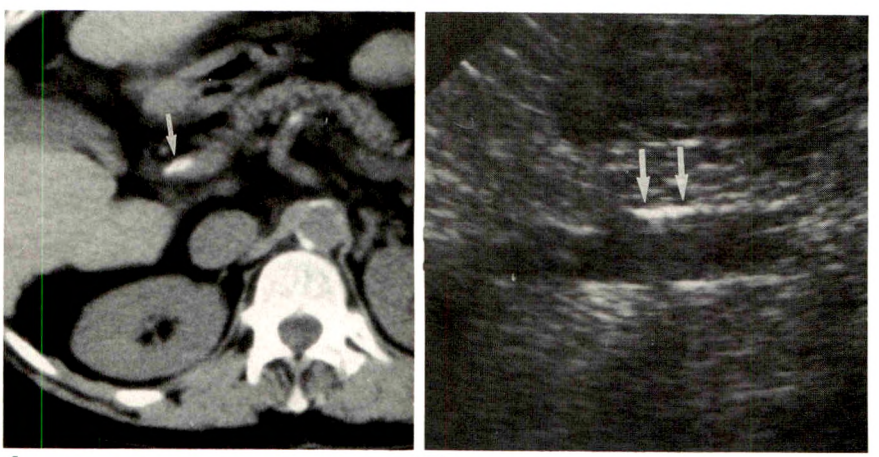


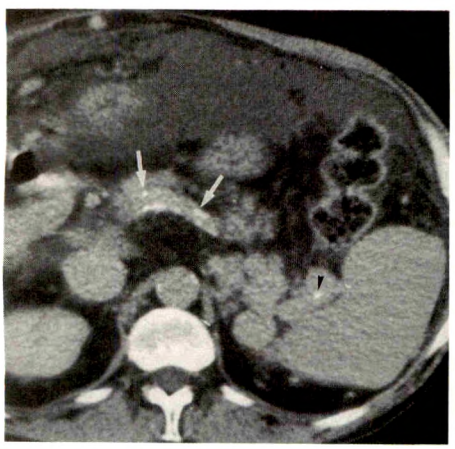
Fig. 1.—Abdominal plain film shows linear calcification directed along expected course of portal vein.



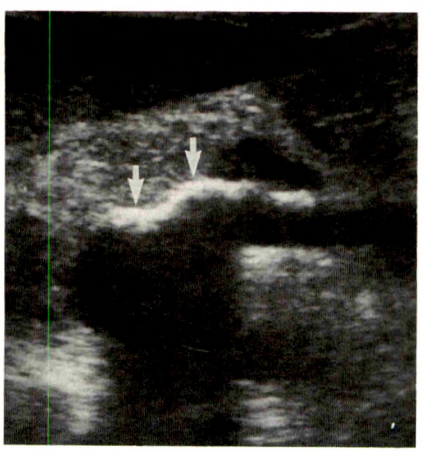
A B

Fig. 2.—*A*, Unenhanced CT scan shows calcification (*arrow*) confined to anterior wall of portal vein.

B, Sonogram shows a linear echogenic focus (*arrows*), in same location noted on *A*, with slight posterior acoustic shadowing.



3



4

Fig. 3.—Delayed contrast-enhanced CT scan shows anterior and posterior calcifications (*arrows*) of distal splenic vein and a small focus of calcification (*arrowhead*) at origin of splenic vein.

Fig. 4.—Transverse sonogram through upper abdomen shows well-defined linear echogenic band (*arrows*) in anterior wall of splenoportal confluence. Intense posterior acoustic shadowing makes it difficult to see lumen and posterior wall of vein.

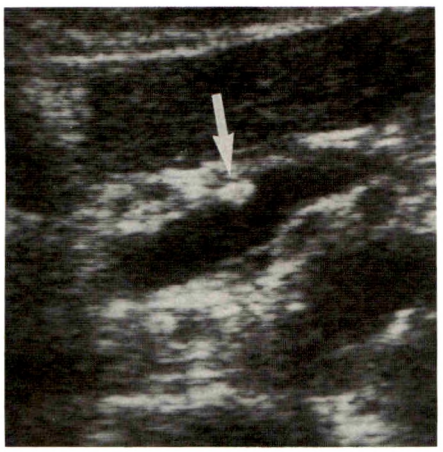
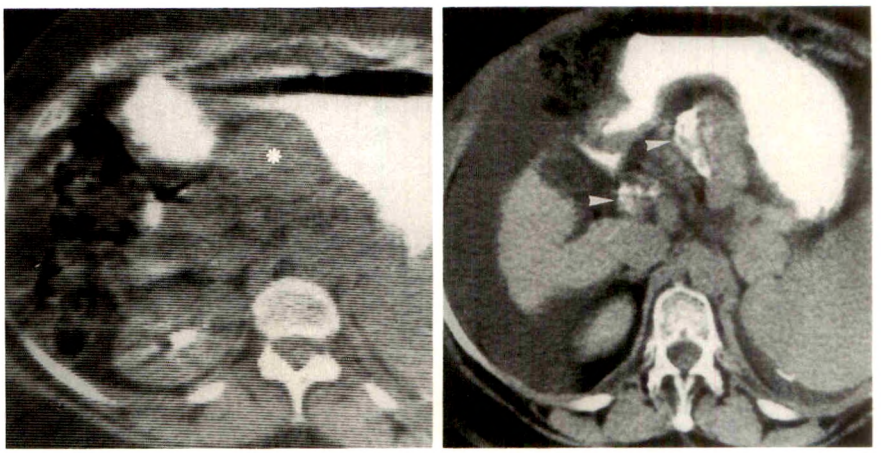


Fig. 5.—Transverse abdominal sonogram through right upper quadrant shows nodular echogenic material (*arrow*) protruding into lumen of portal vein.



A B

Fig. 6.—*A*, Initial contrast-enhanced CT scan shows many epigastric varices mimicking a pancreatic mass (*asterisk*).

B, CT scan obtained 8 years after *A* shows numerous venous calcifications (*arrowheads*) not present on previous study.

Discussion

Calcification of the portal venous system, either in a thrombus or in the vessel wall, has been described in patients with long-standing portal hypertension. Sclerosis and calcification within the thickened intima and media of the vein may result from mechanical stress [19]. Demonstration of calcifications on imaging studies is rare [1–16]. However, calcifications may be slight and found only after exhaustive pathologic examination [5, 19]. Abdominal CT is showing this abnormality with increasing frequency because of its ability to show small amounts of calcium not visible on plain abdominal films. These calcifications may also be seen on abdominal sonograms, particularly when the calcifications are located in the portal vein.

All the patients in our study had long-standing portal hypertension and chronic liver disease. Sonography showed calcifications in the portal vein in six of eight cases when this finding was seen on CT. Calcium deposits in other locations, such as the superior mesenteric vein or collateral vessels, were not seen on sonograms, probably because of the small size of the calcifications or because the interposition of bowel loops made evaluation of the epigastric area difficult. Calcification of the splenic vein was observed on sonograms in two of five cases in which it was detected with CT. The present study demonstrates that CT scans are more sensitive than sonograms, and both are more sensitive than plain films, in showing calcifications in the portal venous system.

The location of calcifications within the walls of the portal venous system is easily shown on abdominal CT. Making the diagnosis on the basis of sonographic findings may be more difficult because the presence of intense posterior acoustic shadowing may hinder evaluation of the lumen. Radiologists should be aware of the possible vascular source of these calcium deposits in order to avoid confusion with chronic pancreatitis, pancreatic ductal calcifications, pancreatic pseudocyst with parietal calcifications, and cystic neoplasms of the pancreas. In addition, the recognition of extensive calcifications in the wall of the portal vein or its tributaries may have therapeutic significance, as their presence may interfere with creation of a venous anastomosis if a portosystemic shunt is planned [19]. The effect of such calcifications on the creation of a percutaneous intrahepatic portosystemic shunt [20] is unknown.

REFERENCES

1. Moberg G. Calcified thrombosis in portal system diagnosed by roentgen examination. *Acta Radiol* (Stockh) **1943**;24:374–383
2. Laws JW, Leight R, Steiner RE. Extrahepatic portal vein obstruction. *Br J Radiol* **1959**;32:774–790
3. Sherrick DW, Kincaid OW, Gambill EE. Calcification in the portal venous system: unusual radiological sign of portal venous thrombosis. *JAMA* **1964**;187:861–862
4. Haddow RA, Kemp-Harper RA. Calcification in the liver and portal system. *Clin Radiol* **1967**;18:225–236
5. Mackenzie RL, Tubbs HR, Laws JW, Dawson JL, Williams R. Obstructive jaundice and portal vein calcification. *Br J Radiol* **1978**;51:953–955
6. Hadar H, Sommer R. Calcification in the portal venous system demonstrated by computed tomography. *Eur J Radiol* **1983**;3:187–188
7. Hirsch M. Portal vein calcification. *Isr J Med Sci* **1983**;19:79–80
8. Marti-Bonmatí L, Menor F, Gil S, Lloret RM. Calcificación de la pared de la vena porta. *Radiología* **1987**;29:337–338
9. Bleich AR, Kipen CS. Venous calcification in Banti's syndrome. *Radiology* **1948**;50:657–660
10. Magovern GJ, Muehsam GE. Calcification of the portal and splenic veins. *AJR* **1954**;71:84–88
11. Smallwood RA, Davidson JS. Calcification in the portal system. *Gastroenterology* **1968**;54:265–269
12. Brambilla G, Colombi C. Calcificazioni della vena splenica e della porta. *Radiol Med* (Torino) **1983**;69:65–67
13. Baker SR, Broker MH, Charnsangavej C, Sitron A. Calcification in the portal vein wall. *Radiology* **1984**;152:18
14. Broker MH, Baker SR. Calcification in the portal vein wall demonstrated by computed tomography. *J Comput Assist Tomogr* **1985**;9:444–446
15. Mata JM, Alegret X, Martinez A. Calcification in the portal and collateral veins wall: CT findings. *Gastrointest Radiol* **1987**;12:206–208
16. Adler J. Venous calcifications associated with cavernous transformation of the portal vein: computed tomographic and angiographic correlations. *Radiology* **1979**;132:27–28
17. Ishikawa T, Tsukune Y, Ohyama Y, Fujikawa M, Sakuyama K, Fujii M. Venous abnormalities in portal hypertension demonstrated by CT. *AJR* **1980**;134:271–276
18. McCain AH, Bernardino ME, Sones PJ, Berkman WA, Casarella WJ. Varices from portal hypertension: correlation of CT and angiography. *Radiology* **1985**;154:63–69
19. Smallwood RA, Davidson JS. Calcification in the portal system. *Gastroenterology* **1968**;54:265–269
20. Richter GM, Noeldge G, Palmaz JC, Roessle M. The transjugular intrahepatic portosystemic stent-shunt (TIPSS): results of a pilot study. *Cardiovasc Intervent Radiol* **1990**;13:200–207

RESIDENTS IN RADIOLOGY AWARDS

The American Roentgen Ray Society

sponsors the

1993 President's Award and the **Executive Council Awards**

RULES AND REGULATIONS

- Papers must be submitted on the clinical application of the discipline of radiology and radiological science.
- The event is open to residents in radiology and radiological sciences. If not the sole author, it is expected that the resident will have performed the majority of the work and be the senior author.
- The submitted manuscript should not exceed 5,000 words and 10 illustrations.
- The winners will be announced by March 16, 1993.
- The papers will be presented at the American Roentgen Ray Society 93rd Annual Scientific Meeting at the San Francisco Marriott, San Francisco, CA, April 25-30, 1993, and be submitted for publication to the *American Journal of Roentgenology.*
- Manuscripts will be returned to candidates not receiving awards.

AWARDS

- The winner of "The President's Award" will be presented a certificate and receive an honorarium of ***$2,000.***
- The two winners of "The Executive Council Award" will each receive a certificate and an honorarium of ***$1,000.***

DEADLINE

- Four copies of the paper and four packages of the illustrations should be submitted no later than **February 12, 1993** to:

Nancy O. Whitley, M.D.
Chairman, Committee on Education & Research
American Roentgen Ray Society
1891 Preston White Drive
Reston, Virginia 22091

Abnormalities of the Gallbladder After Extracorporeal Shock-Wave Lithotripsy: Imaging Findings

William E. Torres[1]
Bruce R. Baumgartner
William J. Casarella

To qualify for treatment with biliary extracorporeal shock-wave lithotripsy (ESWL), patients must have sonograms that show gallstones and oral cholecystograms (OCGs) that show normal opacification (indicating normal function) of the gallbladder. We have noted that sonograms and OCGs made 6 weeks to 6 months after ESWL sometimes show abnormalities that were not visible on these images before ESWL. In these cases, the gallbladder appears contracted on sonograms and is poorly visualized on OCGs. To determine how often this occurs and to study its significance, we analyzed the posttreatment sonograms and OCGs in 174 patients who underwent ESWL. After ESWL, sonograms showed a contracted gallbladder and OCGs showed poor function in 25 (14%) of the 174 patients. One patient (4%) was lost to follow-up. In 17 (68%) of the 25 patients, the abnormalities were transient (findings on sonograms and OCGs returned to normal by 12 months after ESWL). In the other seven patients (28%), the abnormalities persisted (all seven subsequently had a cholecystectomy); this is a cholecystectomy rate twice that in the patients with normal findings on sonograms and OCGs after ESWL (20/149 or 13%). All 25 patients with abnormalities after ESWL had gallstone fragments at 6 weeks, as did 146 of the 149 patients with normal-appearing gallbladders after ESWL. When these abnormalities persist (in approximately one third of patients), cholecystectomy is often required. The cause of the abnormalities is unknown, although chronic cholecystitis, a process that is not detectable by pre-ESWL imaging techniques, seems likely.

AJR **159:325–327, August 1992**

Extracorporeal shock-wave lithotripsy (ESWL) has been used to treat more than 20,000 patients with symptomatic cholelithiasis worldwide. Investigators, using a variety of lithotripters, have shown the safety and efficacy of ESWL in selected patients with cholelithiasis [1–8]. All biliary lithotripsy clinical trials done in the United States require that potential patients meet approved criteria such as having a specified number and size of gallstones. All patients must have a functioning gallbladder shown on oral cholecystograms (OCGs), and the gallstone(s) must be visible on sonograms. All clinical trials require postlithotripsy follow-up at intervals up to 6 months; imaging studies done at the follow-up examinations include sonography, OCG, or both.

As we began to image our patients during their initial follow-up 6 weeks after biliary ESWL, we saw several patients who had contracted gallbladders shown by sonography. It was decided to evaluate gallbladder function specifically in these patients, and thus we added a 6-week OCG examination to the follow-up regimen. This was done in addition to the required follow-up imaging procedures, which are described in the subjects and methods section. The purpose of this study is to evaluate the prevalence of contracted gallbladders shown on sonograms or of faint/nonvisualized gallbladders on OCGs after ESWL and to consider the possible causes and significance.

Received January 21, 1992; accepted after revision February 25, 1992.

[1] All authors: Department of Radiology, Emory University School of Medicine, 1364 Clifton Rd., N.E., Atlanta, GA 30322. Address reprint requests to W. E. Torres.

0361–803X/92/1592–0325
© American Roentgen Ray Society

Subjects and Methods

In 1988, our center began a clinical trial to evaluate the effectiveness and safety of ESWL using the MPL-9000 (Dornier Medizintechnik GmbH, Germering, Germany). In a prospective double-blind manner, we also determined the need for adjuvant chemolysis with ursodeoxycholic acid.

The screening process done before ESWL includes clinical, radiologic, and laboratory testing. Sonography of the gallbladder and biliary tract is done in addition to a double (reinforcement) dose of OCG to evaluate cystic duct patency and gallbladder function.

All 174 patients included in the study were candidates for ESWL using the inclusion and exclusion criteria previously described [3]; in general, a normally functioning gallbladder shown on OCGs and gallstones visible on sonograms were required. Of the 174 patients, 112 were women and 62 were men; the patients ranged in age from 17 to 99 years (mean, 50 years). All patients were randomly selected to receive either ursodeoxycholic acid or placebo for 6 months starting 1 week before ESWL. All ESWL procedures were done as previously described [3, 9]. A maximum of one retreatment was allowed and that only for patients who had fragments 5 mm or larger seen on the sonogram 6 weeks after ESWL.

According to the protocol, all patients had follow-up sonograms 6 weeks, 3 months, and 6 months after ESWL and follow-up OCG 6 months after ESWL. At our institution, we added a 6-week OCG to the follow-up procedure to assess gallbladder concentrating ability; this OCG was added, only at our institution, after seeing several patients whose follow-up sonograms showed contracted gallbladders. This additional 6-week OCG was done in 69 (40%) of the 174 patients; in the group of 25 patients with abnormal gallbladders, 14 patients (56%) had a 6-week OCG. Between 6 weeks and 6 months follow-up, 25 (14%) of the 174 patients had faint/nonvisualized gallbladders on OCGs and contracted gallbladders on sonograms.

Of the entire group of 174 patients, only three patients were free of stones 6 weeks after ESWL. All 25 patients included in the study had gallstone fragments at the time of their gallbladder abnormality.

All patients were evaluated at the time of follow-up with respect to biliary symptoms; additionally, all patients' charts were reviewed. Patients not returning for follow-up were contacted by phone to ascertain their clinical status and to determine if they had had a cholecystectomy.

The follow-up sonograms were done on a variety of sonography units with 3- to 5-MHz transducers, following the guidelines published by the Society of Diagnostic Medical Sonographers [10]. All patients were told to fast for 12 hr before sonography. All patients with a contracted gallbladder shown by sonography were questioned about food intake and reexamined to confirm the contracted gallbladder. All OCG examinations were done by using a 2-day consecutive dose schedule with a total of 12 tablets or 6 g of iopanoic acid (Telepaque, Winthrop Pharmaceuticals, New York, NY) [11]; the patients were instructed to consume a low-fat diet for 2 days before the day of the examination and to take the tablets during a 2-day period as described in the instructions.

Results

None of the 25 patients with a gallbladder abnormality after ESWL had a stone-free gallbladder after treatment. Gallstone fragments were present 6 weeks after ESWL in 146 of the remaining 149 patients. For the first 6 months of the study, 12 of the 25 patients with gallbladder abnormalities were taking ursodeoxycholic acid and 13 of them were given placebo.

The 25 patients were divided into two groups depending on whether or not the abnormalities seen with sonography (contracted gallbladder) or OCG (poor or no visualization) persisted. One patient was lost to follow-up.

A transient gallbladder abnormality was seen in 18 patients during this 12-month period. Of these 18 patients, six had faint or no visualization by OCG and contracted gallbladders shown by sonography; eight patients had abnormal OCG findings alone and four had sonographic abnormalities only. Of the 18 patients, six with an abnormal gallbladder 6 weeks or 3 months after ESWL had normal sonographic and/or OCG findings at 6 months. At 12 months or more after ESWL, 11 of the remaining 12 patients had normal findings on sonograms; therefore, 17 (94%) of 18 patients had a normal gallbladder shown by OCG or sonography at their last follow-up. One patient was lost to follow-up. Two (11%) of the 18 patients in this group were free of stones 12 months after ESWL.

In the seven patients with persistent gallbladder abnormality, three had OCG 6 weeks after ESWL by which there was faint or no visualization of the gallbladder; two patients did not have a 6-week OCG. Cholecystectomy was done in four patients before the 6-month follow-up, with pathologic diagnosis of chronic cholecystitis in three and acute cholecystitis in one; three patients had a cholecystectomy after the 12-month period with the pathologic diagnosis of chronic cholecystitis. All seven patients had residual gallstone fragments found during cholecystectomy.

Of the 25 patients with abnormal findings on imaging studies after ESWL, the seven patients (28%) who had persistently contracted gallbladders all had cholecystectomies. Twenty (13%) of the 149 patients with normal-appearing gallbladders shown by imaging studies underwent cholecystectomy. Only three of the 174 patients were free of stones 6 weeks after ESWL.

Discussion

Few studies on changes in gallbladder appearance or function after ESWL have been reported [1–8, 12, 13]. In an animal study, histologic examination of gallbladders after lithotripsy showed only minimal changes [14]. Spengler et al. [15] showed that gallbladder motility was not altered after ESWL in patients studied with sonography and cholecystokinin. In a multicenter study, Burnett et al. [8] reported "visualization" in 64 of 67 patients examined with OCG 3 months after ESWL. Rawat reported a 12% prevalence of contracted gallbladders shown by sonography in a group of patients after lithotripsy (Rawat B et al., presented at the Third International Symposium on Biliary Lithotripsy, September 1990).

Several investigators [15–20] have suggested that patients with symptomatic gallstones have impaired gallbladder motility. The cause of the gallbladder motility dysfunction in patients with cholelithiasis is unknown, but it may result from gallstones, chronic inflammation, or stone formation. It has been theorized that gallstone disease with gallbladder fibrosis

and wall thickening may be involved [13]. Although no abnormalities have been detected on sonographic examinations, chronic cholecystitis with fibrosis on a histologic level had been suggested as the cause of impaired gallbladder emptying in patients with symptomatic gallstones.

The potential causes of a contracted gallbladder shown by sonography in our patients are many. It is, however, important to distinguish the physiologically collapsed gallbladder (i.e., loss of volume) from a gallbladder that is contracted because of chronic gallbladder disease; this can usually be differentiated on follow-up sonography.

The National Dornier Biliary Lithotripsy Study [5] used sonography to follow up patients 6 weeks, 3 months, and 6 months after ESWL; OCG was used for screening and, subsequently, to evaluate gallbladder function 6 months after ESWL. The 6-week imaging studies performed at our center revealed a group of patients with contracted gallbladders shown by sonography or with a faint or nonfunctioning gallbladder shown by OCG. None of the patients in whom the gallbladder appeared contracted on sonograms had a visible gallbladder on the OCG examination. Conversely, nonvisualization on OCG is not always associated with a contracted gallbladder shown by sonography. We believe that, especially in patients with abnormal gallbladders after ESWL, imaging studies should be done to assess gallbladder function—sonography or OCG following a fatty meal or with cholecystokinin can be used.

The seven patients in our study who had persistent gallbladder abnormality all had cholecystectomy; the overall cholecystectomy rate (28%) in our group of 25 patients with gallbladder abnormalities was much higher than the rate (13%) in the larger group of 149 patients without gallbladder abnormality after ESWL. We postulate partial or complete obstruction of the cystic duct as a cause of the faint or nonvisualization of the gallbladder on OCGs or the contracted bladder shown on sonograms. Of the 25 patients with abnormal gallbladders, almost equal numbers were taking ursodeoxycholic acid or placebo for the first 6 months of the study; the use or nonuse of bile acids is not thought to be a factor in the contracted or faint/nonvisualized gallbladder after ESWL.

The results suggest that in most patients, the abnormal gallbladder after ESWL is a temporary condition—a "stunned gallbladder"—as 17 (68%) of 25 patients had normal findings on sonograms 12 months or more after ESWL. Those patients with persistently abnormal gallbladders after ESWL often require cholecystectomy; in many of these patients, the altered contractility may result from intrinsic gallbladder disease; that is, chronic cholecystitis on a histologic level, not detectable by any imaging method now available.

ACKNOWLEDGMENT

The authors thank Faye Laing, who reviewed and suggested changes to the manuscript.

REFERENCES

1. Sauerbruch T, Delius M, Paumgartner G, et al. Fragmentation of gallstones by extracorporeal shock waves. *N Engl J Med* **1986**;314:818–822
2. Sackmann M, Delius M, Sauerbruch T, et al. Shock-wave lithotripsy of gallbladder stones: the first 175 patients. *N Engl J Med* **1988**;318:393–397
3. Torres WE, Steinberg HV, Davis RC, Baumgartner BR, Nelson RC, Casarella WJ. Shock wave lithotripsy of gallstones: results and 6-month follow-up in 141 patients. *Radiology* **1991**;178:509–512
4. Torres WE, Baumgartner BR, Nelson RC, Morris SJ. Shock wave lithotripsy of gallstones: results and 12 month follow-up in 174 patients. *Radiology* **1991**;179:699–701
5. Schoenfield LJ, Berci G, Carnovale RL, et al. The effect of ursodiol on the efficacy and safety of extracorporeal shock wave lithotripsy of gallstones: The Dornier National Biliary Lithotripsy Study. *N Engl J Med* **1990**;323:1239–1245
6. Ponchon T, Barkun AN, Pujol B, et al. Gallstone disappearance after extracorporeal lithotripsy and oral bile acid dissolution. *Gastroenterology* **1989**;97:457–463
7. Hood KA, Keightley A, Dowling RH, Dick JA, Mallinson CN. Piezo-ceramic lithotripsy of gallbladder stones: initial experience in 38 patients. *Lancet* **1988**;1:1322–1324
8. Burnett D, Ertan A, Jones R, et al. Use of external shock-wave lithotripsy and adjuvant ursodiol for treatment of radiolucent gallstones. *Dig Dis Sci* **1989**;7:1011–1015
9. Steinberg HV, Torres WE, Nelson RC. Gallbladder lithotripsy. *Radiology* **1989**;172:7–11
10. Society of Diagnostic Sonographers. *Educational outline*. Dallas: Society of Diagnostic Sonographers, **1983**
11. Maglinte DDT, Torres WE, Laufer I. The oral cholecystogram in contemporary gallstone imaging: a review. *Radiology* **1991**;178::49–58
12. Brendel W, Enders G. Shock waves for gallstones: animal studies. *Lancet* **1983**;1:1054
13. Johnson AG, Ross B, Stephenson TJ. The short-term effects of extracorporeal shock wave lithotripsy on the human gallbladder. In: Ferrucci JT, Delius M, Burhenne HJ, eds. *Biliary lithotripsy*. Chicago: Year Book Medical, **1989**:59–62
14. Becker CD, Gilks CB, Burhenne HJ. Biological effects of biliary shock wave lithotripsy in swine. *Invest Radiol* **1989**;24:366–370
15. Spengler U, Sackmann M, Sauerbruch T, Holl J, Paumgartner G. Gallbladder motility before and after extracorporeal shock wave lithotripsy. *Gastroenterology* **1989**;96:860–863
16. Shaffer EA, McOrmond P, Duggan H. Quantitative cholescintigraphy: assessment of gallbladder filling and emptying and duodenogastric reflux. *Gastroenterology* **1980**;79:899–906
17. Fisher RS, Stelzer F, Rock E, Malmud LS. Abnormal gallbladder emptying in patients with gallstones. *Dig Dis Sci* **1982**;27:1019–1024
18. Thompson J, Fried GM, Ogden WD, et al. Correlation between release of cholecystokinin and contraction of the gallbladder in patients with gallstones. *Ann Surg* **1982**;195:670–675
19. Forgacs IC, Maisey MN, Murphy GM, Dowling RH. Influence of gallstones and ursodeoxycholic acid therapy on gallbladder emptying. *Gastroenterology* **1984**;87:299–307
20. Pomeranz IS, Shaffer EA. Abnormal gallbladder emptying in a subgroup of patients with gallstones. *Gastroenterology* **1985**;88:787–791

Book Review

The Radiologist's Second Reader. By Harry W. Fischer. Available from Granville Medical Books, Granville, OH. 348 pp., 1992. $18.95, softcover

Professor Fischer has made a mistake again! He has compiled a book to educate radiologists in training. He should know they must spend their full effort on other less important things. The American Board of Radiology has no history examination. How can a former departmental chairman be so wrong?

Harry Fischer has produced an anthology of radiologic treatises that is both entertaining and inexpensive. This volume is for the mature radiologist. Maturity allows time for an interest in history. As we approach the anniversary of the discovery of these "new type of rays" and read or reread some of the notable contributions of the past, it is possible to believe we have a history. The book contains no subspecialty material. It has selections on the initial events in radiology, the problems in the practice of radiology, past giants in radiology, and humor in radiology.

Reread Roentgen's original paper and marvel at the extent of his initial observations. Read Harold Peterson's subtly inflammatory article, "First a Radiologist." It is guaranteed to generate a prolonged philosophical argument. Interpretation of Peterson should be one of the great intellectual challenges for the future. First-class humor is provided by "X-ray Gogs" written by my seriously mysterious colleague Dave Edwards. Personal notes by Jack Campbell about Ben Felson broaden our knowledge of this dynamo of the past. This collection shows the eclecticism of a person whose professional career was notable for his devotion to research in radiology by radiologists. Research is not the emphasis in this book.

Not to be ignored if you missed it is *The Radiologist's First Reader*. This contains Newell's "Mink Coats and Cadillacs." The subtitle is "A Discourse on the Nutrition and Hygiene of the Soul." This advice to the profession is timely and gives remarkable solace in our era of diminishing economic expectations. Also included is Mellins's short, but powerful definition of a diagnostic radiologist. These are two bedside readers for mature radiologists. Enjoy!

John R. Amberg
La Jolla, CA 92037-6407

Case Report

Disappearing "Gallstones": Biliary Pseudolithiasis Complicating Ceftriaxone Therapy

Wanda M. Kirejczyk,[1] Helen M. Crowe,[2] Iain M. Mackay,[1] Richard Quintiliani,[2] and Edward B. Cronin[1]

Ceftriaxone, a parenteral third-generation cephalosporin, is widely used for the treatment of a variety of bacterial infections in both children and adults. Since its release in 1984, more than 20 million patients have received the drug, making it one of the most widely used injectable antibiotics. Ceftriaxone is the treatment of choice for the later stages of Lyme disease and is often prescribed for pulmonary infections and meningitis.

With the growing popularity of ceftriaxone, an unusual complication has been identified in which the drug complexes with calcium in bile salts to form a precipitate that mimics a gallstone on sonograms [1]. With discontinuation of the drug, these "stones" resolve spontaneously, a phenomenon termed "reversible ceftriaxone biliary pseudolithiasis" by Schaad et al. [2].

Although pseudolithiasis has gained the attention of internists and pediatricians, it has not been reported in the imaging literature. We present a case of reversible ceftriaxone-induced pseudolithiasis seen at our institution and discuss the natural history and radiologic manifestations of this complication.

Case Report

A previously healthy 19-year-old woman was referred for evaluation of possible chronic Lyme disease. The patient lived in central Connecticut, a known endemic area for Lyme disease, and during the late summer of 1990 pain, paresthesias, and dysesthesias developed in her back and lower extremities. She had no history of tick bite or rash, but had experienced an influenzalike illness for several days preceding her neurologic symptoms. In June 1991, she was seen by a neurosurgeon for severe thoracic back pain. Results of MR imaging of the thoracic and lumbar spine were normal. Her erythrocyte sedimentation rate was mildly elevated at 29 mm/hr, and serum tests for Lyme disease were positive, as was a Lyme western blot. The patient was given 2 g ceftriaxone IV once daily for 14 days. One week after the therapy was completed, she noted the onset of severe pain in the right upper quadrant and had a temperature of 39.4°C and vomiting.

Sonography showed multiple gallstones (Fig. 1). The patient was not obese, nor was there a family history of gallbladder disease. Because of the recent ceftriaxone use, she was observed without specific therapy. A second sonographic examination 3 weeks later showed a normal gallbladder with complete disappearance of the stones.

At a follow-up visit several months later, the patient's neurologic symptoms and fatigue had improved significantly, and the pain in her right upper quadrant had not recurred.

Discussion

The first case of pseudolithiasis was described by Schaad et al. [3] in 1986. Other investigators have subsequently described similar findings in both adults and children [2–7].

In the study by Schaad et al. [2], gallbladder precipitates developed in 43% of the children treated for serious infections with ceftriaxone, and the precipitates resolved completely with the cessation of therapy. Only 19% of these patients, however, had biliary symptoms [2]. The prevalence of pseudolithiasis was studied in adults by Pigrau et al. [7], who

Received February 7, 1992; accepted March 3, 1992.
[1] Department of Radiology, Hartford Hospital, 80 Seymour St., Hartford, CT 06115. Address reprint requests to E. B. Cronin.
[2] Division of Infectious Diseases, Hartford Hospital, 80 Seymour St., Hartford, CT 06115.

AJR **159:329–330, August 1992** 0361–803X/92/1592–0329 © American Roentgen Ray Society

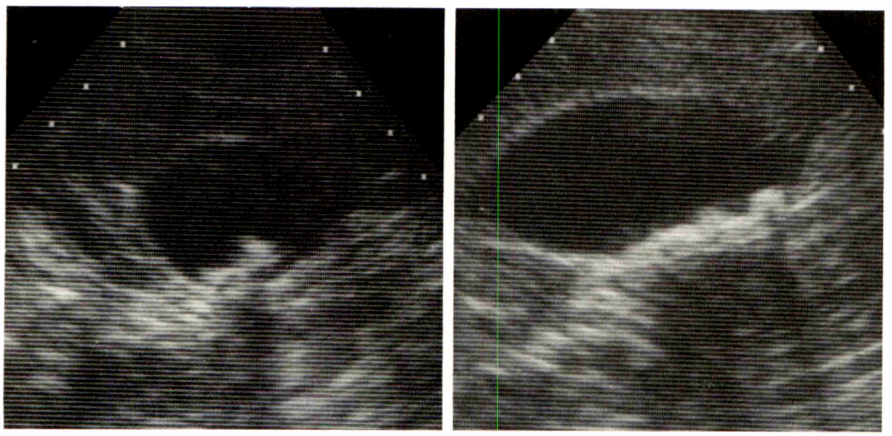


Fig. 1.—Transverse (*A*) and longitudinal (*B*) sonograms of gallbladder show echogenic pseudoliths, which cause posterior shadowing.

found that 25% of their patients had abnormal findings on sonograms of the gallbladder. All the patients remained asymptomatic [7].

The manufacturer of ceftriaxone, Roche Laboratories (Nutley, NJ), has accumulated a total of 73 reports of pseudolithiasis occurring during or after ceftriaxone therapy. Sixteen of these patients underwent cholecystectomy, which revealed a sandlike sediment or semisolid particles in the gallbladder, without stones. Fifty-seven patients were managed conservatively, and of these, 75% had follow-up sonograms that did not show gallstones within 3 months (personal communication, Sudol T, Roche Laboratories).

Although it is not yet clear, it appears that high doses of ceftriaxone and prolonged administration are most likely the major factors in the development of pseudolithiasis [1, 2, 5–7]. Currently, ceftriaxone is the only third-generation cephalosporin to cause these precipitates. The probable reason for this observation is that ceftriaxone is the only cephalosporin that complexes with calcium in bile. Although ceftriaxone is excreted primarily in the urine, 20–40% can be excreted in bile. It appears that with the use of high doses, the solubility of the drug is exceeded, causing the formation of calcium-ceftriaxone salt precipitates. At doses less than 1 g/day, precipitates have not been shown to occur [6].

Sonographically, the concretions seen in ceftriaxone pseudolithiasis are indistinguishable from typical gallstones; they are brightly echogenic with true shadowing posteriorly [1, 6, 8]. They can be mobile in the gallbladder, and range from tiny sludgelike particles to larger concretions. With the widespread use of ceftriaxone, it is likely that the phenomenon of reversible ceftriaxone-induced biliary pseudolithiasis will become more common. The key to the diagnosis of this entity will not lie with the sonographic findings but with the radiologist suspecting that gallstones are unlikely in a particular patient, such as a child or young adult. It is crucial to question the patient or the referring clinician regarding recent ceftriaxone use when making the diagnosis of biliary pseudolithiasis. The correct diagnosis will spare patients needless treatment, such as cholecystectomy, for this spontaneously reversible abnormality.

REFERENCES

1. Park HZ, Lee SP, Schy AL. Ceftriaxone-associated gallbladder sludge. *Gastroenterology* **1991**;100:1665–1670
2. Schaad UB, Wedgwood-Krucko J, Tschaeppeler H. Reversible ceftriaxone-associated biliary pseudolithiasis in children. *Lancet* **1988**;2:1411–1413
3. Schaad UB, Tschappeler H, Lentze MJ. Transient formation of precipitations in the gallbladder associated with ceftriaxone therapy. *Pediatr Infect Dis J* **1986**;5:708–710
4. Jacobs RF. Ceftriaxone-associated cholecystitis. *Pediatr Infect Dis J* **1988**;7:434–436
5. Hein-Duthoy KL, Caperton EM, Pollock R, Matzke GR, Enthoven D, Peterson PK. Apparent biliary pseudolithiasis during ceftriaxone therapy. *Antimicrob Agents Chemother* **1990**;34:1146–1149
6. Shiffman ML, Keith FB, Moore EW. Pathogenesis of ceftriaxone-associated biliary sludge. *Gastroenterology* **1990**;99:1772–1778
7. Pigrau C, Pahissa A, Gropper S, Sureda D, Martinez Vazquez JM. Ceftriaxone-associated biliary pseudolithiasis in adults (letter). *Lancet* **1989**;2:165
8. Lee SP, Lipsky BA, Teefey SA. Gallbladder sludge and antibiotics. *Pediatr Infect Dis J* **1990**;9:422–423

Case Report

Thickened Bile Duct Wall Simulating Ductal Dilatation on Sonography

William D. Middleton[1] and R. Stephen Surratt

Sonography is an accurate noninvasive method of measuring the caliber of the bile ducts. Inaccuracies in ductal measurements generally result when other structures, such as hepatic arteries, tortuous gallbladder necks, or cystic ducts, simulate the bile ducts [1, 2]. We have recently encountered a case of diffuse thickening of the duct wall that simulated a dilated duct despite correct identification of the duct itself. This report describes this potential pitfall and the obliterated luminal reflection sign that ultimately allowed the correct diagnosis to be made.

Case Report

An 84-year-old man with a history of cholecystectomy had painless jaundice and was referred for sonography of the right upper quadrant. Views of the liver showed moderate dilatation of the intrahepatic ducts and bulky periportal lymphadenopathy. Views of the porta hepatis showed the common hepatic duct in its expected location anterior to the right hepatic artery (Fig. 1A). The diameter of the common hepatic duct was measured as 9–10 mm. Subtle low-level echoes in the duct were interpreted as artifactual. Biliary obstruction was diagnosed, and the level of obstruction was determined to be the mid to distal portion of the common bile duct. Because the distal portion of the common bile duct was not visualized, a cause of obstruction was not determined, and the patient was brought back for further sonograms of the biliary tract. These showed a thin linear reflection in the center of the common hepatic duct (Fig. 1B), which was thought to represent the interface between the coapted luminal surfaces of a duct with marked diffuse hypoechoic wall thickening and an obliterated lumen. The diagnosis of cholangiocarcinoma with nodal metastases was made. An ERCP obtained the next day showed a narrowed irregular lumen of the common bile duct, common hepatic duct, and central intrahepatic ducts with dilatation of the peripheral intrahepatic ducts (Fig. 1C). Results of brush biopsy were positive for cholangiocarcinoma.

Discussion

When biliary obstruction is detected sonographically in the jaundiced patient, the next objective is to determine the level and cause of obstruction. The reported sensitivities of sonography in determining the level and the cause of obstruction are 92–95% and 71–88%, respectively [3, 4]. In this case, the obliterated lumen of the duct was not identified initially, and the thickened hypoechoic walls of the duct were interpreted as the lumen. This resulted in the erroneous impression of dilatation of the common hepatic duct and the inappropriate conclusion that the level of obstruction was in the mid to distal portion of the common bile duct. Ultimately, the obliterated lumen of the bile duct was identified as a thin linear reflection in the middle of the duct, and this made it possible to recognize that the duct wall was markedly thickened. This then led to the correct determination of the level of obstruction. Although a number of processes such as sclerosing cholangitis, AIDS cholangiopathy, choledocholithiasis, oriental cholangiohepatitis, and pancreatitis could have produced the thickening of the duct's wall [5], the magnitude of thickening (5 mm) and the associated bulky adenopathy strongly favored cholangiocarcinoma.

Received February 4, 1992; accepted after revision March 5, 1992.

[1] Both authors: Mallinckrodt Institute of Radiology, Washington University School of Medicine, 510 S. Kingshighway Blvd., St. Louis, MO 63110. Address reprint requests to W. D. Middleton.

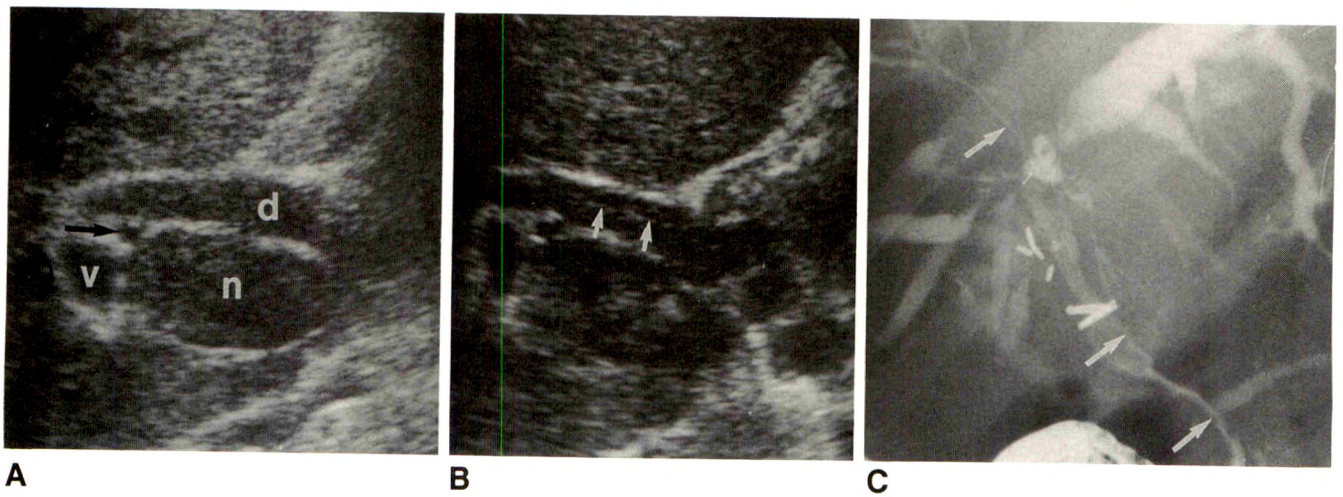


Fig. 1.—*A*, Initial sonogram shows thickening of wall of common hepatic duct (d), simulating ductal dilatation. *Arrow* = right hepatic artery, v = right portal vein, n = enlarged node.
***B*, Second sonogram of common hepatic duct shows obliterated luminal reflection sign (*arrows*).**
***C*, ERCP shows diffuse narrowing of extrahepatic and central intrahepatic ducts (*arrows*) with dilated peripheral intrahepatic ducts.**

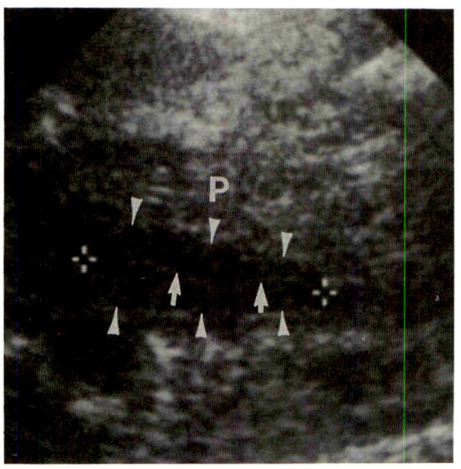


Fig. 2.—Longitudinal sonogram of pancreatic head (P) shows obliterated luminal reflection sign (*arrows*) in distal portion of common bile duct (*arrowheads*).

In most patients with a thickened extrahepatic bile duct, the lumen remains patent. This makes it possible to define the luminal surfaces as two bright linear reflections separated by the intraluminal bile. The thickened wall is then seen as a hypoechoic layer deep to the mucosal surface [6]. A completely obliterated lumen is uncommon. Even when the lumen is completely compressed, we expect it will be difficult to produce the obliterated luminal reflection sign because the reflecting interface is essentially one dimensional. Nevertheless, we have since encountered a second patient with cholangiocarcinoma in whom the sign was present in the distal portion of the common bile duct (Fig. 2).

A finding similar to the obliterated luminal reflection sign has recently been described in renal transplants with thickened urothelium [7]. In their description of the "white line sign," Cunningham and Bacani-Faulls [7] have stressed how useful this sign is in detecting subtle thickening of the renal collecting system and distinguishing it from mild hydronephrosis. These points are equally important in the bile duct. Unlike the bile duct, the obliterated renal collecting system produces flat, two-dimensional interfaces, and therefore, this finding can be expected to be seen more frequently in the kidney than in the biliary tract.

In summary, these two cases illustrate the sonographic appearance of a bile duct with an obliterated lumen due to marked concentric thickening of the ductal wall. Detection and proper interpretation of the obliterated luminal reflection sign should help to avoid potential inaccuracies in the sonographic diagnosis of the level and cause of biliary obstruction.

REFERENCES

1. Callen PW, Mahoney BS. Gallbladder and bile ducts. In: Vogler JB, Helms CA, Callen PW, eds. *Normal variants and pitfalls in imaging.* Philadelphia: Saunders, **1986**:288–297
2. Parulekar SG, Sonography of the distal cystic duct. *J Ultrasound Med* **1989**;8:367–373
3. Laing FC, Jeffrey RB, Wing VW, Nyberg DA. Biliary dilatation: defining the level and cause by real-time US. *Radiology* **1986**;160:39–42
4. Gibson RN, Yeung E, Thompson JN, et al. Bile duct obstruction: radiologic evaluation of level, cause and tumor resectability. *Radiology* **1986**;160:43–47
5. Schulte SJ, Baron RL, Teefey SA, et al. CT of the extrahepatic bile ducts: wall thickness and contrast enhancement in normal and abnormal ducts. *AJR* **1990**;154:79–85
6. Carroll BA, Oppenheimer DA. Sclerosing cholangitis: sonographic demonstration of bile duct wall thickening. *AJR* **1982**;139:1016–1018
7. Cunningham JJ, Bacani-Faulls M. Sonographic "white line sign" for detection of minimal mucosal thickening in renal transplants. *Urology* **1990**;35:367–370

Case Report

Splenosis: Superparamagnetic Iron Oxide–Enhanced MR Imaging

Brett L. Storm,[1] Patricia L. Abbitt, Deborah A. Allen, and Pablo R. Ros

Intraabdominal splenosis is an unusual but well-recognized disease caused by autotransplantation of splenic tissue within the peritoneal cavity. Occasionally, the diagnosis is delayed because the splenic implants are misinterpreted as neoplastic masses or adenopathy [1–5]. We present a case of splenosis that, because of the patient's history of blood transfusions and multiple sexual encounters, was clinically thought to represent adenopathy related to infection with HIV. MR imaging after administration of superparamagnetic iron oxide allowed the diagnosis of splenosis to be made so that biopsy and surgery were avoided.

Case Report

A 28-year-old woman had had fevers, chills, nausea, and pain in her right flank for 2 days. She had been a prostitute and had a history of urinary tract infections. Eight years earlier, she had been in a severe motor vehicle accident and had sustained multiple rib fractures, bilateral pneumothoraces, and bilateral clavicular fractures. She also had had traumatic rupture of the spleen, which had been treated with splenectomy and blood transfusions.

At admission, sonography showed numerous periportal masses (Fig. 1A) and a homogeneous oval mass 2.5 cm in diameter adjacent to the right kidney. CT confirmed the presence of these masses as well as two other soft-tissue nodules in the splenic bed and several other soft-tissue masses in the right hemiabdomen. The periportal masses seen on sonography were not well visualized on CT. The periportal and perirenal masses were thought to be atypical for splenosis and more compatible with adenopathy of unknown cause.

To rule out the possibility of splenosis, we used heat-damaged RBC scintigraphy with 5 mCi (185 MBq) ^{99m}Tc-labeled autologous RBCs (Fig. 1B). This showed uptake of the labeled cells in areas corresponding to the masses seen on CT. MR imaging of the abdomen was performed at 1.0 T with spin-echo and gradient-echo pulse sequences, before and after IV administration (10 μmol Fe per kilogram body weight) of superparamagnetic iron oxide (Feridex or AMI-25, Advanced Magnetics, Cambridge, MA). MR was done to rule out or confirm hepatic involvement by lymphoma related to AIDS and to determine if the periportal masses represented ectopic splenules. T1-weighted (500/30), proton density–weighted, T2-weighted (2000/90), and gradient-echo fast low-angle shot (FLASH, 31/12/15) images were obtained before and after the IV administration of Feridex. The masses in the splenic bed and the celiac and perirenal regions paralleled each other in signal intensity and had decreased signal intensity on T2-weighted and gradient-echo images after IV administration of superparamagnetic iron oxide (Figs. 1C and 1D). These findings were similar to the results obtained with scintigraphy.

Discussion

Splenosis is a well-recognized entity caused by autotransplantation of splenic tissue after trauma or splenectomy [1–7]. The splenic remnants implant on the serosal surfaces of the abdomen and chest, parasitize adjacent blood vessels, and grow into mature splenic tissue that is histologically indistinguishable from normal spleen.

Patients are usually asymptomatic; the splenic implants are found during surgery or during unrelated diagnostic imaging. However, splenosis can cause (1) gastrointestinal hemorrhage when tissue implantation occurs in the stomach or

Received January 21, 1992; accepted after revision February 24, 1992.

[1]All authors: Department of Radiology, University of Florida College of Medicine, P.O. Box 100374, JHMHC, Gainesville, FL 32610-0374. Address reprint requests to B. L. Storm.

AJR **159:333–335, August 1992** 0361–803X/92/1592–0333 © American Roentgen Ray Society

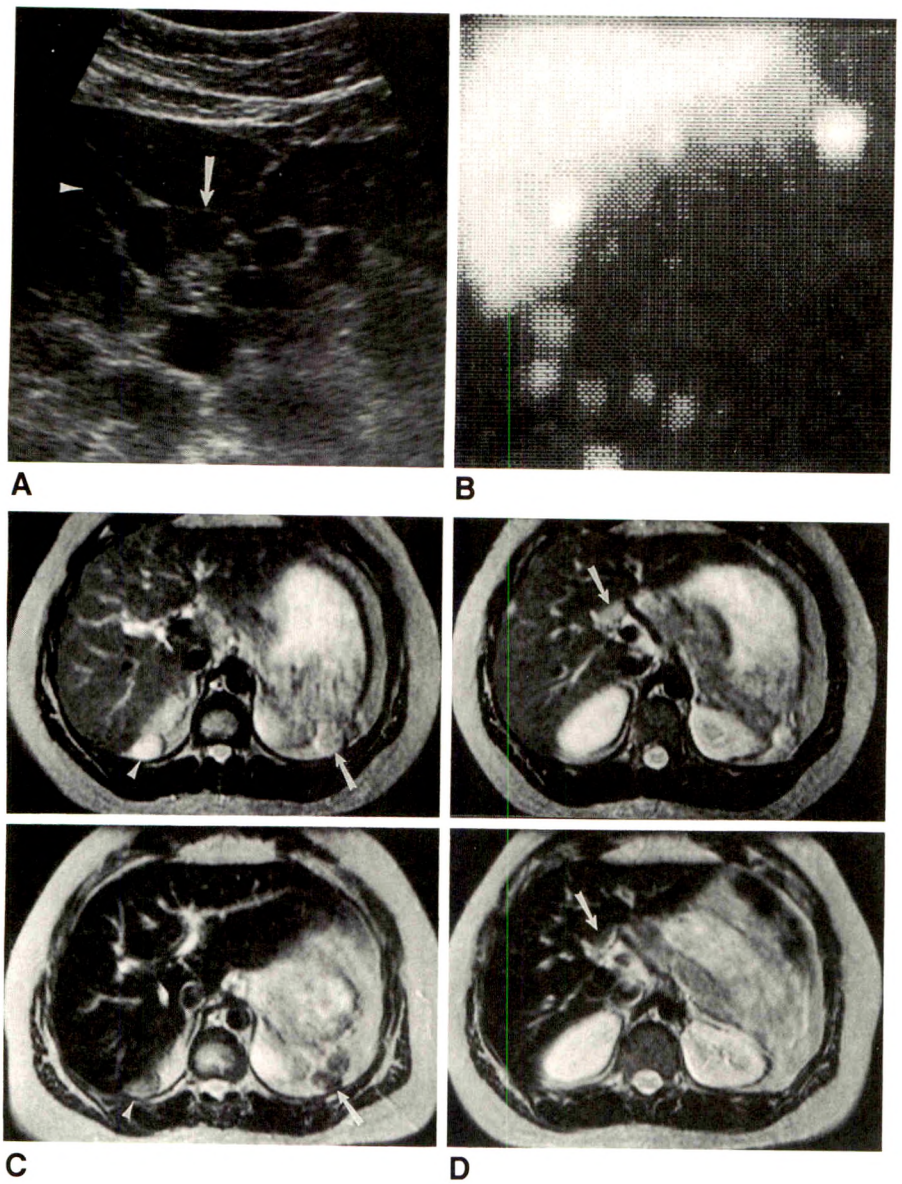


Fig. 1.—Splenosis in a 28-year-old woman.
A, Sonogram shows multiple hypoechoic masses in periportal region (*arrow*). Gallbladder (*arrowhead*).
B, ^{99m}Tc-labeled RBC scintigram shows uptake of labeled cells in splenic bed, in subhepatic region, and down right paracolic gutter, consistent with splenosis of abdomen.
C and *D*, T2-weighted (2000/90) MR images obtained before (*top*) and after (*bottom*) IV administration of superparamagnetic iron oxide show the T2 shortening effect of this contrast agent on liver and on masses within splenic bed (*arrows* in *C*) and right perirenal region (*arrowheads* in *C*). Periportal mass (*arrows* in *D*), which was not well seen on CT, shows decreased signal intensity after addition of superparamagnetic iron oxide.

small bowel; (2) abdominal pain due to intraperitoneal nodule infarction, bowel obstruction, or hematoma from trauma to a preexisting splenic implant; or (3) flank pain from ureteral compression and hydronephrosis. Recurrence of hematologic diseases, previously treated with splenectomy, also may be symptomatic [1–4].

Splenic nodules occur throughout the abdominal cavity, but the most common sites, in order of frequency, are the serosal surface of the small bowel, the greater omentum, the parietal peritoneum, the serosal surface of the large intestine, the mesentery, and the diaphragm [5]. In our case, the distribution of the masses was unusual for splenosis. Our patient had extensive involvement around the celiac axis and many masses in the right paracolic gutter.

Abdominal splenosis can be confused radiologically with numerous diseases such as lymphoma, carcinomatosis, endometriosis, adenopathy, hemangiomatosis, and peritoneal mesothelioma. These diseases can usually be distinguished from one another on the basis of the patient's age, the number and distribution of nodules, and the clinical history.

Because of our patient's sexual history of prostitution and medical history of blood transfusions, causes of neoplastic, reactive, and inflammatory adenopathy were considered. Ultimately, tests for HIV were negative. Biopsy of the masses was postponed until splenosis could be excluded.

The radiologic hallmark of splenosis is uptake of ^{99m}Tc-labeled heat-damaged RBCs in the areas of suspected heterotopic splenic tissue. Sonographic and CT findings are nonspecific in splenosis and show round or oval soft-tissue masses in the various abdominal locations.

Recent literature has described the use of superparamagnetic iron oxide for delineation of hepatic and splenic disease [6, 7]. Feridex is an MR contrast agent composed of superparamagnetic iron oxide particles that show a tissue-specific

biodistribution to phagocytic reticuloendothelial elements of liver and spleen after IV injection. Superparamagnetic iron oxide produces local inhomogeneities in the magnetic field that cause rapid dephasing of transverse magnetization, resulting in a loss of signal intensity on MR images. In our case, the ectopic splenules had signal characteristics similar to those of the liver, because both organs have reticuloendothelial cells. The signal intensity decreases on all pulse sequences after IV administration of ferrite particles. The signal intensity in ectopic splenic tissue after the administration of Feridex is similar to that seen with normal spleen (Ros PR, unpublished data). Normal spleen, as seen in two other patients, shows a 60–70% signal change on T2-weighted images, comparable to a 64% signal change seen in our case of splenosis. The decreased signal intensity is most pronounced on heavily T2-weighted images.

This is the first reported case of superparamagnetic iron oxide–enhanced MR imaging of splenosis. Although nuclear medicine is the mainstay in the diagnosis of splenosis, MR imaging with superparamagnetic iron oxide combines a physiologic test of reticuloendothelial cell uptake with the anatomic detail of MR.

REFERENCES

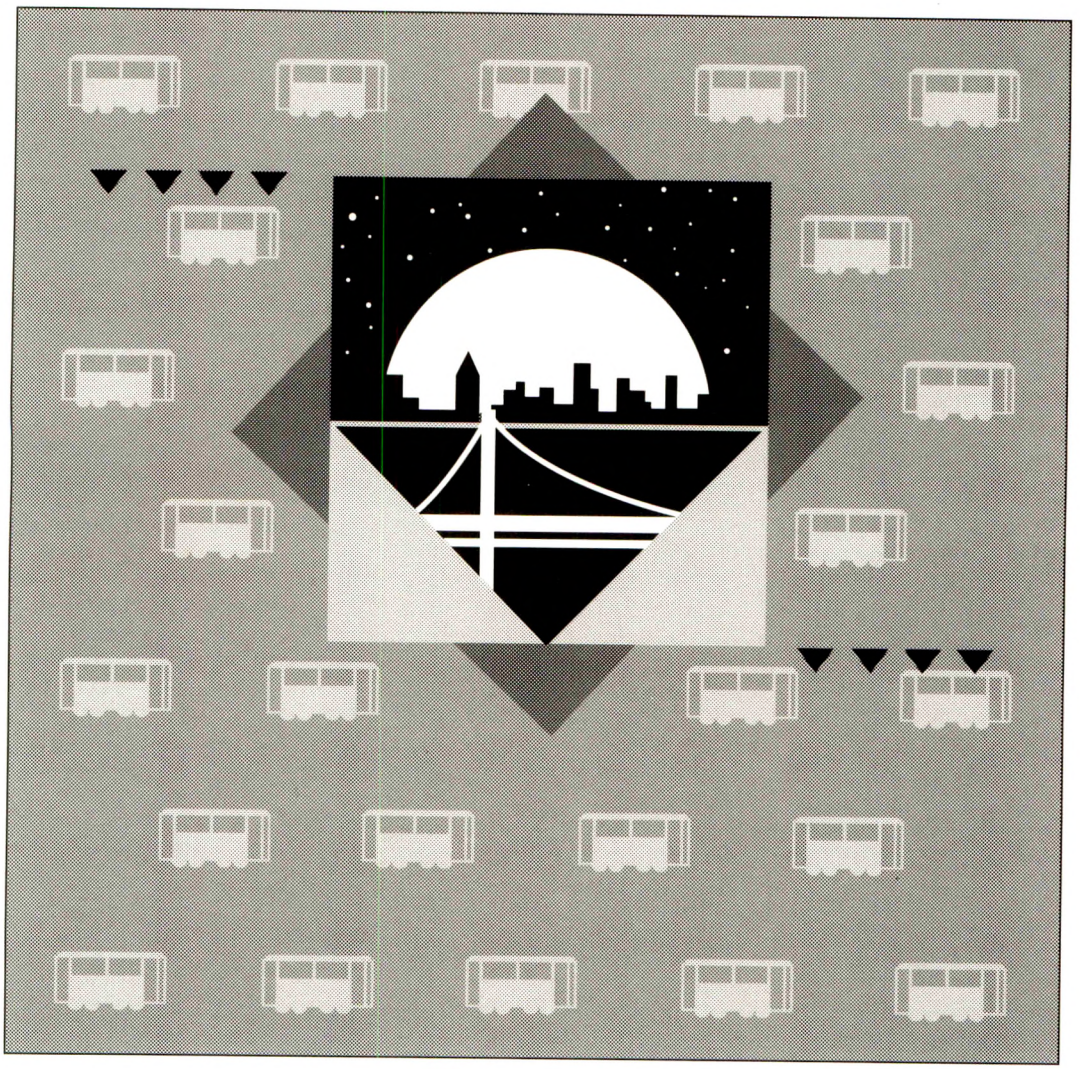
1. Basile RM, Morales JM, Zupanec R. Splenosis: a cause of massive gastrointestinal hemorrhage. *Arch Surg* **1989**;124:1087–1089
2. Delamarre J, Capron JP, Drouard F, Joly JP, Deschepper B, Carton S. Splenosis: ultrasound and CT findings in a case complicated by an intraperitonal implant traumatic hematoma. *Gastrointest Radiol* **1988**;13:275–278
3. Varma DGK, Campeau RJ, Kartchner ZA, Karnik S. Scintigraphic detection of splenosis causing ureteral compression and hydronephrosis (letter). *AJR* **1991**;156:406
4. Gentry LR, Brown JM, Lindgren RD. Splenosis: CT demonstration of heterotopic autotransplantation of splenic tissue. *J Comput Assist Tomogr* **1982**;6:1184–1187
5. Brewster DC. Splenosis: report of two cases and review of the literature. *Am J Surg* **1973**;126:14–19
6. Weissleder R, Hahn PH, Stark DD, et al. Superparamagnetic iron oxide: enhanced detection of focal splenic tumors by MR imaging. *Radiology* **1988**;169:399–403
7. Weissleder R, Elizondo G, Stark DD, et al. The diagnosis of splenic lymphoma by MR imaging: value of superparamagnetic iron oxide. *AJR* **1989**;152:175–180

New Format for Abstracts

Beginning immediately, the *AJR* will publish abstracts of articles in a different format, much like the ones recently adopted by the *New England Journal of Medicine* and the *Journal of the American Medical Asociation*. The purpose of the new design is to have abstracts present the essential elements of articles more clearly and concisely. The contents, organization, and length of the abstracts will be the same as before; however, rather than being all one paragraph except for the conclusion, abstracts will now be divided into four paragraphs, each with a title: objective, subjects (or materials) and methods, results, and conclusion.

The *AJR* Guidelines for Authors, which appears at the front of every issue of the Journal, has been revised to help you write abstracts in this new format. Authors should familiarize themselves with these guidelines and incorporate them into all manuscripts submitted for publication.

Robert N. Berk
Editor-in-Chief



San Francisco

American Roentgen Ray Society

93rd Annual Meeting

April 25–30, 1993

San Francisco Marriott • San Francisco, CA

The Seminal Tract in Patients with Ejaculatory Dysfunction: MR Imaging with an Endorectal Surface Coil

Mitchell D. Schnall[1]
Howard M. Pollack[1]
Keith Van Arsdalen[2]
Herbert Y. Kressel[1]

Twenty-six patients with signs and symptoms of ejaculatory dysfunction (hemospermia, hypospermia, oligospermia, or painful ejaculation) were examined with high-resolution MR imaging with an endorectal surface coil. Findings were abnormal in 15 patients. Abnormalities detected included four cases of müllerian cysts, three cases of wolffian cysts, one case of anaplastic prostatic carcinoma, and various noncystic abnormalities of the seminal vesicles and ejaculatory ducts, including ejaculatory duct obstruction and seminal vesiculitis. In all cases, depiction of both the normal and abnormal anatomy of the entire seminal tract, including the vas deferens, seminal vesicles, and ejaculatory ducts, was excellent. This depiction of the detailed anatomy of the prostatic cysts made it possible to suggest specific diagnoses.

Our results show the value of MR imaging with an endorectal surface coil in the examination of patients with ejaculatory dysfunction.

AJR **159:337–341, August 1992**

Men with ejaculatory dysfunction manifested by painful ejaculation, hemospermia, or reduced seminal volume (hypospermia) often pose a diagnostic challenge. Imaging plays an important role in the detection of anatomic lesions in such patients. In the past, vasovesiculography has been used to visualize the seminal tract in patients with these problems [1]. More recently, transrectal sonography has been used as a noninvasive alternative [2–4], but limitations in the spatial resolution and soft-tissue contrast of sonography may not permit complete evaluation of the ejaculatory ducts and seminal vesicles. The multiplanar capability and high soft-tissue contrast of MR imaging are well suited to the evaluation of the seminal tract [5]. However, the spatial resolution of conventional body-coil techniques used to image the prostate and seminal vesicles is inadequate to reliably provide a detailed portrayal of these structures. It has recently been shown that the resolution of prostatic and seminal vesicular anatomy on MR and the ability to stage prostatic cancer are significantly improved when an endorectal surface coil is used [6, 7]. The purpose of this study was to investigate the normal and pathologic anatomy of the seminal tract by using an endorectal surface coil for MR imaging in patients with ejaculatory disorders.

Subjects and Methods

Twenty-six patients 17–45 years old who had one or more of the following symptoms or signs constituting ejaculatory dysfunction were studied with MR: hemospermia (12 patients), hypospermia (reduced seminal volume, three patients), oligospermia (reduced number of spermatozoa in the ejaculate, three patients), and painful ejaculation (eight patients). Five of the 26 patients were referred because of abnormal findings on a transrectal sonographic or CT examination. These patients underwent MR examination to clarify the abnormal findings.

MR imaging was performed on 1.5-T Signa (General Electric Medical Systems, Milwaukee, WI) system by using an endorectal surface coil provided by Medrad (Pittsburgh, PA). After

Received December 4, 1991; accepted after revision February 18, 1992.

[1]Department of Radiology, Hospital of the University of Pennsylvania, 3400 Spruce St., Philadelphia, PA 19104. Address reprint requests to M. D. Schnall.

[2]Department of Urology, Hospital of the University of Pennsylvania, Philadelphia, PA 19104.

0361–803X/92/1592–0337
© American Roentgen Ray Society

placement of the endorectal coil, sagittal short TR/TE (600/17) images were acquired by using the body coil. This served as a localizing sequence for the subsequent surface-coil images. Surface-coil images were obtained by using a short TR/TE (600/12) and a long TR/short and long TE (2500/40,80) spin-echo sequence in the axial plane. The field of view was 12 cm, and the slice thickness was 4 mm with a 1-mm gap. Images were acquired with a 256 × 128 matrix, and two averages were acquired. A second set of long TR/TE images were obtained in a second (sagittal or coronal) plane with a 14-cm field of view and one acquisition. The entire examination was completed in less than 1 hr and was well tolerated by all of the patients. In some cases, an 11.2-cm round surface coil placed on the anterior aspect of the pelvis was used in combination with the endorectal coil to form an external-endorectal array that used the multicoil array capabilities of the Signa system [8]. In other cases, T2-weighted fast spin-echo images were obtained in lieu of the standard T2-weighted spin-echo images [9].

Results

Images of the normal seminal tract are shown in Figure 1. On MR images made with the endorectal surface coil, the convolutions of the ampulla of the vas deferens and the seminal vesicles are usually seen at the base of the prostate [6] (Fig. 1A). The confluence of the vas deferens and the duct of the seminal vesicles to form the ejaculatory duct is best depicted on sagittal images (Fig. 1B). The course of the ejaculatory ducts can be followed on coronal or axial images. The verumontanum is also routinely seen as a high-signal-intensity crescent in the apical portion of the prostate on long TR/TE axial images.

Of the 26 patients, 11 had transrectal MR images with findings that were thought to be normal. Fifteen patients had abnormal findings: cystic lesions in eight and abnormal, noncystic, seminal vesicle architecture in seven.

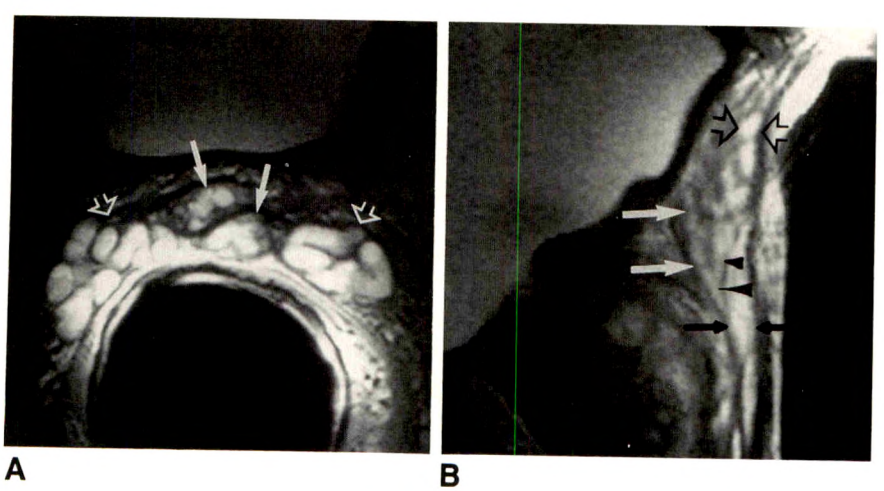
Seven of the eight cystic lesions were classified as wolffian (seminal vesicle, vas deferens, ejaculatory duct) or müllerian (including prostatic utricle) according to their location and imaging appearance. The benign appearance of these lesions obviated histologic confirmation. However, in several cases, analysis of fluid obtained from the cyst helped confirm the diagnosis. In the remaining cases, the diagnosis was made on the basis of the typical clinical course combined with the endoscopic and imaging appearances.

In the four müllerian duct cysts, a midline high-signal mass seen in the prostate on the long TR/TE images was consistent with a cystic structure (Fig. 2A). In three of the four, the cyst had high signal on short TR/TE images as well, presumably because of hemorrhage or high protein content within the cyst (Fig. 2B). In all four patients, the cyst originated just above the verumontanum, most likely in the prostatic utricle. In each case, MR showed that both ejaculatory ducts were displaced laterally on either side of the cyst, differentiating the lesion from ejaculatory duct cysts or simple dilatation of the ejaculatory ducts (Fig. 3). On axial images, the ejaculatory ducts appeared to course in or just lateral to the wall of the cyst. In two cases, the ejaculatory ducts proximal to the cyst were dilated, presumably from obstruction (Fig. 2C). In two of the four cases, the müllerian duct origin of the cyst was confirmed by analysis of fluid from the cyst; a lack of fructose or spermatozoa in the sampled fluid confirmed the diagnosis. Fluid was not available for analysis in the other two cases.

In the three cases thought to represent wolffian duct cysts, a high-signal mass was detected on long TR/TE images also, but the cyst had low to intermediate signal on short TR/TE images (Fig. 4). Unlike müllerian duct cysts, these cysts were often irregular in shape and not midline. In one case, the cyst was inseparable from the seminal vesicle; both structures were incorporated into one cystic mass. In the other cases, the cyst was located at the base of the prostate. When the ipsilateral seminal vesicle could be identified, it appeared small and dysplastic, and the ipsilateral ejaculatory duct was not identified. Presumably, all of these cysts were congenital.

In the eighth patient, a complex mass with both cystic and solid features was detected. It was characterized by mixed high and low signal on short TR/TE images and high signal on long TR/TE images. The wall of the cyst was irregular, and solid masses were seen both in the wall of the cyst and just inferior to it. Biopsy of this lesion revealed a poorly differentiated adenocarcinoma.

The remaining seven patients had some abnormality of seminal vesicle architecture without cyst formation. In three cases, unilateral dilatation of a seminal vesicle and ejaculatory



A B

Fig. 1.—Normal anatomy.

***A*, Axial T2-weighted fast spin-echo MR image of normal seminal vesicles shows high-signal fluid-filled tubules (*open arrows*) of seminal vesicles. Paired ampullae (*solid arrows*) of vas deferens can be seen centrally.**

***B*, Sagittal T2-weighted fast spin-echo MR image shows confluence of vas deferens (*white arrows*) and duct of seminal vesicle (*small arrowhead*) to form ejaculatory duct (*large arrowhead*). Also shown is peripheral zone of prostate (*solid black arrows*) and seminal vesicles (*open arrows*).**

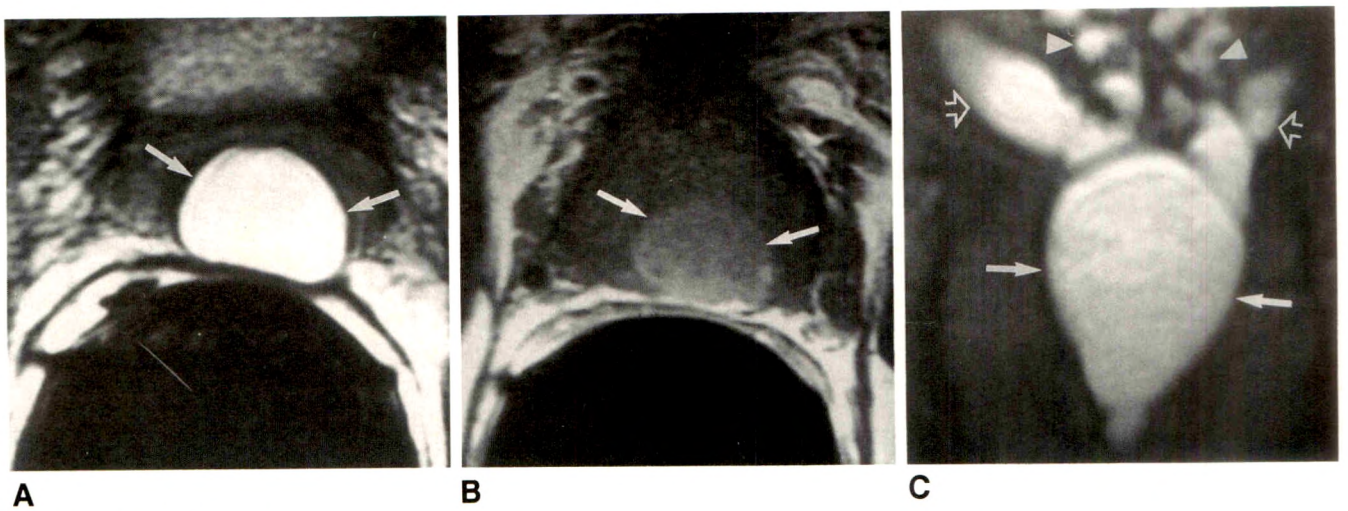


Fig. 2.—Müllerian duct cyst.
A, Axial T2-weighted spin-echo MR image shows large midline high-signal mass (*arrows*) consistent with a midline cystic structure.
B, Axial T1-weighted MR image shows high signal intensity of cystic fluid (*arrows*), indicating presence of hemorrhage or high protein content.
C, Coronal T2-weighted MR image shows dilatation of both ejaculatory ducts (*open arrows*) due to large midline cystic mass (*solid arrows*). Seminal vesicles (*arrowheads*).

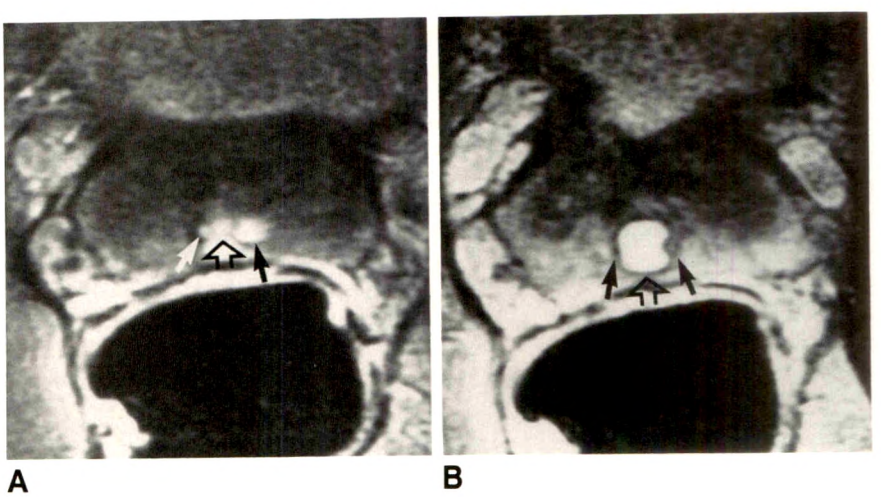


Fig. 3.—Müllerian duct cyst.
A and *B*, Axial T2-weighted spin-echo MR images show midline cystic mass (*open arrows*) that insinuates itself between ejaculatory ducts (*solid arrows*).

duct was detected, presumably the result of obstruction of the ejaculatory duct (Fig. 5). In two of these patients, the area of stricture in the ejaculatory duct was clearly shown. The fluid in the seminal vesicle retained its usual MR signal characteristics. In one of the three cases, however, the fluid in the dilated ejaculatory duct and seminal vesicle had high signal on short TR/TE images, probably because of hemorrhage or high protein content (Fig. 6). In this case, calculi were visualized in the dilated ejaculatory duct.

In three cases, diffuse thickening of the seminal vesicle walls was detected. The walls of the seminal vesicles also had very low signal on long TR/TE images, consistent with chronic inflammatory disease. The fluid, however, had normal signal characteristics. In one case, pathologic proof of tuberculous seminal vesiculitis was available (Fig. 7). In the other two cases, clinical evidence indicated chronic prostatitis.

In one patient with severe hypospermia, very small seminal vesicles were found. The tubular walls were of normal thickness, and the fluid had typical MR signal characteristics. Inasmuch as 85% of the seminal volume originates in the seminal vesicles [10], the finding of diminutive seminal vesicles correlated well with the clinical signs and symptoms. The cause of the abnormality was unclear.

Discussion

Diseases of the seminal tract can lead to signs and symptoms of ejaculatory dysfunction, including painful ejaculation, hemospermia, and infertility (due to azoospermia or hypospermia). Detection of pathologic changes in the seminal tract has been difficult because of the lack of a reliable noninvasive imaging technique with which to evaluate the vasa deferentia, seminal vesicles, and ejaculatory ducts. As a result, many patients with signs and symptoms of seminal tract disease have been considered psychoneurotics or placed into large nonspecific diagnostic categories such as "chronic prostati-

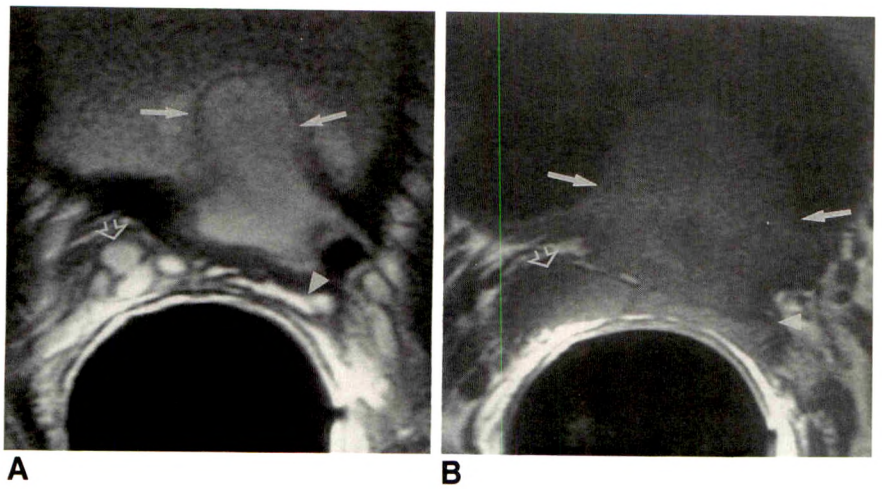


Fig. 4.—Wolffian duct cyst.
A and *B*, Axial T2-weighted (*A*) and T1-weighted (*B*) MR images through region of seminal vesicles show normal right seminal vesicle (*open arrows*) and dysmorphic-appearing left seminal vesicle (*arrowheads*). Large cystic mass invaginating bladder (*solid arrows*) represents wolffian duct cyst. Cyst has intermediate signal intensity on T1-weighted image, indicating a hemorrhagic or protein component. Agenesis of left kidney was associated with these findings.

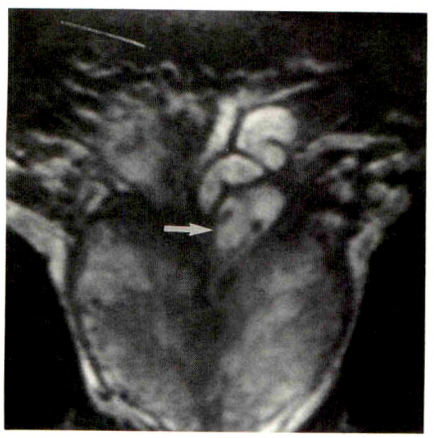


Fig. 5.—Ejaculatory duct obstruction. Coronal T2-weighted spin-echo MR image shows dilatation of proximal left ejaculatory duct, which also appears tortuous (*arrow*). Distal ejaculatory duct appears narrowed.



Fig. 6.—Dilated ejaculatory duct. Coronal T1-weighted MR image shows a midline cystic structure (*arrow*) that subsequently was shown to represent a dilated ejaculatory duct. Fluid within duct has high signal on T1-weighted images, suggesting presence of hemorrhage. Note also several filling defects (*arrowheads*), which represent calculi.

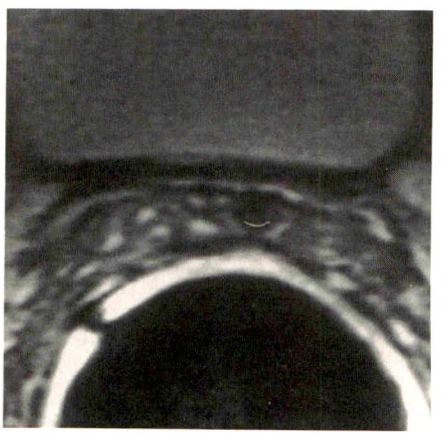


Fig. 7.—Biopsy-proved tuberculous seminal vesiculitis. Axial T2-weighted fast spin-echo MR image of seminal vesicles shows marked thickening of walls of seminal vesicles with narrowing of lumina.

tis." Our study suggests that ejaculatory dysfunction is frequently associated with structural abnormalities of the seminal apparatus. Using MR imaging with an endorectal surface coil, we have shown a variety of abnormalities, including cysts, tumors, inflammation of the seminal vesicles, cysts of the utricle, and obstruction of the ejaculatory ducts in more than half of the patients referred. However, we were generally unable to identify a clear association between the presenting problem and a specific pathologic entity.

High soft-tissue contrast and multiplanar capability make MR an ideal technique for evaluating the seminal tract. Although the seminal vesicles can be detected on MR images made with a conventional body coil, these images do not provide enough resolution for evaluation of the internal architecture of either the seminal vesicles or the ejaculatory ducts and vasa deferentia. We and others have capitalized on the improved resolution of imaging with an endorectal surface coil to study prostatic cancer. The results presented here show that this same technique also can be useful in detecting pathologic changes that can lead to ejaculatory dysfunction.

The anatomic components of the normal seminal tract can be routinely seen on MR images made with an endorectal surface coil. The best pulse sequence for evaluating these structures appears to be T2-weighted spin-echo imaging (2500/80). Images in the axial plane are essential, and additional images in the sagittal or coronal plane are often helpful to follow the course of the ejaculatory ducts.

MR imaging with the endorectal surface coil was extremely sensitive in the detection of cystic masses and dilatation of the seminal tract. The increased resolution of these images allowed not only evaluation of the structure of the cysts but also their relationship to the remainder of the seminal tract.

In particular, the finding of ejaculatory ducts coursing in the wall of a midline cyst was helpful in identifying müllerian duct cysts. These cysts may range in size from almost imperceptible dilatation of the utricle to large pelvic masses. Other features that help in their identification include the presence of seminal vesicles, which, aside from possible displacement, are intrinsically normal. Both kidneys are usually present, and because the cyst does not communicate directly with the seminal tract, it contains no fructose or spermatozoa. The ejaculatory ducts may be displaced or obstructed by these cysts, which course between the ducts in the center of the prostate. The transrectal MR images also were helpful in showing evidence of significant compression or displacement of the nearby ejaculatory ducts in all patients.

Wolffian duct cysts were identified by a constellation of findings in the seminal vesicles. In contrast to müllerian duct cysts, wolffian cysts are usually located laterally, rather than in the midline. As the ipsilateral seminal vesicle is an integral component of the cyst, only one normal seminal vesicle is usually identifiable. Agenesis or severe dysplasia of the ipsilateral kidney is usually present, and aspiration of cystic fluid in postpubertal patients yields fructose and spermatozoa. These cysts also vary in size, and although they do not usually course through the full length of the prostate as müllerian cysts do, the ipsilateral ejaculatory duct can be dysplastic or dilated, permitting confusion with utricular cysts. Cysts of the seminal vesicle frequently protrude into the urinary bladder, giving the appearance of ectopic ureteroceles. In our patients, transrectal MR not only clearly showed the cyst and its relationship to the prostate, bladder, and seminal vesicles but also was useful in evaluating the contralateral seminal vesicle and ejaculatory duct. In one patient, the detection of an irregular wall, irregular signal intensity, and associated solid mass prompted a biopsy, which showed adenocarcinoma.

Although it is possible to detect various types of seminal tract diseases by using body coil MR and transrectal sonography, neither technique, in our view, provides the exquisite detail of the seminal vesicles nor the precise definition of the full course of the ejaculatory ducts and vasa deferentia necessary for diagnosis of ejaculatory dysfunction as defined in this study. MR imaging with an endorectal surface coil is a valuable tool in the management of these frequently neglected and too often improperly treated group of patients.

REFERENCES

1. Wilheim SF. Vaso-seminal vesiculography: clinical and experimental application. *J Urol* **1939**;41:751–757
2. Littrup PJ, Lee F, Mcleary R, Wu D, Lee A, Kamaska GH. Transrectal US of the seminal vesicles and ejaculatory ducts: clinical correlation. *Radiology* **1988**;168:625–628
3. Ngheim HT, Kellman GM, Sandberg SA, Craug BM. Cystic lesions of the prostate. *RadioGraphics* **1990**;10:635–650
4. Carter S, Shinohara K, Lipshultz L. Transrectal ultrasonography in disorders of the seminal vesicles and ejaculatory ducts. *Urol Clin North Am* **1989**;16:773–790
5. Zobel B, Tella S, Confalone D, Passariello R. Male infertility: MRI assessment. In: *Book of abstracts: Society of Magnetic Resonance in Medicine 1989*. Berkely, CA: Society of Magnetic Resonance in Medicine, **1989**:698
6. Schnall MD, Lenkinski RL, Pollack HM, Imai Y, Kressel HY. Prostate: MR imaging with an endorectal surface coil. *Radiology* **1989**;172:570–574
7. Schnall M, Imai Y, Pollack H, Lenkinski R, Kressel H. Local staging of prostate cancer with endorectal surface coil MRI. *Radiology* **1981**;178:797–802
8. Roemer PB, Edelstein WA, Hayes CE, Souza SP, Mueller CM. The NMR phased array. *Magn Reson Med* **1990**;16:192–201
9. Melki PS, Mulkern RV, Panych LP, Jolesz FA. Comparing the FAISE method with conventional dual echo sequences. *J Magn Reson Imaging* **1991**;1:319–326
10. Coffey DS. The biochemistry and physiology of the prostate and seminal vesicles. In: Walsh P, Gittees R, Perlmutter A, Stamey T, eds. *Campbell's urology*. Philadelphia: Saunders, **1986**:233–274

Book Review

Diagnostic Ultrasound. Physics, Biology, and Instrumentation. By Stewart C. Bushong and Benjamin R. Archer. St. Louis: Mosby–Year Book, 177 pp., 1991. $34.95

Diagnostic sonography is one of the most rapidly evolving techniques in medical imaging. Improvements in the performance and capability of commercially available instrumentation are rapid and continuous, primarily because of the advent of microprocessor-controlled machines. The instruments themselves are relatively inexpensive and can produce both qualitative and quantitative information. Thus, demand is increasing for qualified operators who have appropriate training in the principles underlying the use of these instruments. Relatively few formal courses are given, and until recently, few useful textbooks for technologists have been published.

Diagnostic Ultrasound: Physics, Biology, and Instrumentation by Bushong and Archer is written primarily for technologists and is designed to be used as a text for a formal course in sonography. The volume is also useful for medical residents and as an introductory course for physicists.

The book contains 16 chapters. Chapters 1–6 cover the basic physics of ultrasound and include a useful review of the physical quantities involved and the mathematics required to solve problems given later in the book. Chapters 7–13 cover transducer design and performance, including single, multielement, and Doppler transducers and the requirements for imaging instrumentation that uses A, B, and M modes. Chapter 11 is devoted entirely to real-time transducers. Image processing and display are covered in chapter 12, and chapters 14 and 15 cover image analysis and quality assurance. The final chapter is devoted to the biological effects of ultrasound. Each chapter contains worked examples and is followed by review questions, with the answers given in an appendix.

The book is written in a clear and straightforward style, with excellent cartoon illustrations and line diagrams of instrumentation. The clarity of the diagrams is exceptional. As might be expected in the first edition of a new book, a fair number of teething troubles occur, ranging from typographic errors and several unnumbered pages to explanations of several physical concepts that are confusing or wrong. For example, velocity and speed are not synonymous, explanations for the production of side lobes given in chapters 11 and 14 do not agree, and the table giving noise level in terms of decibels should state that this application has a fixed reference level as distinct from the conventional use of decibels throughout the text. None of these items is major, and an alert instructor can guide students past these problems.

For its intended use as a text for students in sonography, this book is highly readable; its abundance of examples makes it an excellent value. It can be used as the major text for a course in sonography and should definitely be available in the library of any ultrasound technology school.

Douglas R. Shearer
Rhode Island Hospital
Providence, RI 02902

Case Report

Use of Transperineal Hydrosonovaginography to Show an Incomplete Vaginal Septum

Les Folio,[1,2] Henrietta Kotlus Rosenberg,[1,3] and Gertrude J. Frishmuth[4,5]

Proving that a communication exists between the two compartments of the vagina in patients with a vaginal septum may be difficult clinically, especially in virgins. Conventional contrast vaginography is generally diagnostic but involves exposure to radiation. Hydrosonovaginography, however, is a nonionizing technique that is diagnostic, especially when it is performed transperineally. We present the case of a 28-year-old woman in whom this method proved useful to show a fenestrated septate vagina.

Case Report

This 28-year-old woman, the larger of inseparable craniopagus Siamese twins, presented with a history of hypermenorrhea. The smaller of the twins had been treated with low-dose birth control pills for the last 1.5 years to suppress formation of ovarian cysts and had normal menstrual cycles. She had had a bicornuate uterus noted during surgical repair of cloacal exstrophy when she was younger. Pelvic examination of the patient in question revealed normal external genitalia. The hymen was excessively thick with an unusually small aperture, making digital examination impossible. A moist Q-tip was used to depress the hymen in the midline, and at this point, a longitudinal septum was noted in the vagina. Long moist Q-tips were then inserted into each vaginal opening; the vagina was noted to be deep and the septum long. On rectal examination, a normal-sized uterus was palpated and no adnexal masses were noted. As the pelvic examination was inconclusive, sonography was requested to better delineate the vaginal anatomy and to evaluate the uterus for congenital anomalies. An Advanced Technology Laboratories (Bothell, WA) UltraMark 9 sonography unit equipped with a 3.0-MHz transducer was used. The uterus appeared normal in size and configuration on routine transabdominal pelvic sonograms, but the vaginal stripe could not be seen (Fig. 1A). Eight-French Foley catheters were placed into each vaginal orifice and attached to syringes filled with sterile water. Water was injected into each vaginal compartment separately during transabdominal sonography, but the vaginal compartments could not be adequately visualized. Therefore, the sector transducer was placed on the perineum at an angle directed toward the vagina. Injections of sterile water into each vaginal compartment were repeated. The sonogram showed that the water passed from the compartment on the side of the injection into the other side, indicating fenestration (Fig. 1B). The water served as a contrast agent, with the microbubbles creating mobile specular reflectors during and after the injections.

Discussion

Congenital anomalies of the vagina include imperforate hymen, which can result in hydrometrocolpos in infants or in hematometrocolpos in mature females [1]; vaginal atresia [2]; vaginal duplications, with either intact or fenestrated septum [3]; ectopic ureter with vaginal terminus; and associated anomalies in the imperforate anus complex (vaginal ectopic terminus, cloacal anomalies). Sonography plays an

Received December 16, 1991; accepted after revision February 5, 1992.

[1] Department of Radiology, The Children's Hospital of Philadelphia, 34th St. and Civic Center Blvd., Philadelphia, PA 19104.
[2] Present address: Ramstein Air Force Base, c/o 86th Medical Group, PSC #1, Box 3763, APO, AE 09009, Ramstein, Germany.
[3] Present address: Department of Radiology, Albert Einstein Medical Center, 5501 Old York Rd., Philadelphia, PA 19141. Address reprint requests to H. K. Rosenberg.
[4] Department of Surgery, The Children's Hospital of Philadelphia, 34th St. and Civic Center Blvd., Philadelphia, PA 19104.
[5] Present address: Department of Obstetrics and Gynecology, University of New Mexico School of Medicine, 2211 Lomas Blvd., Albuquerque, NM 87131-5286.

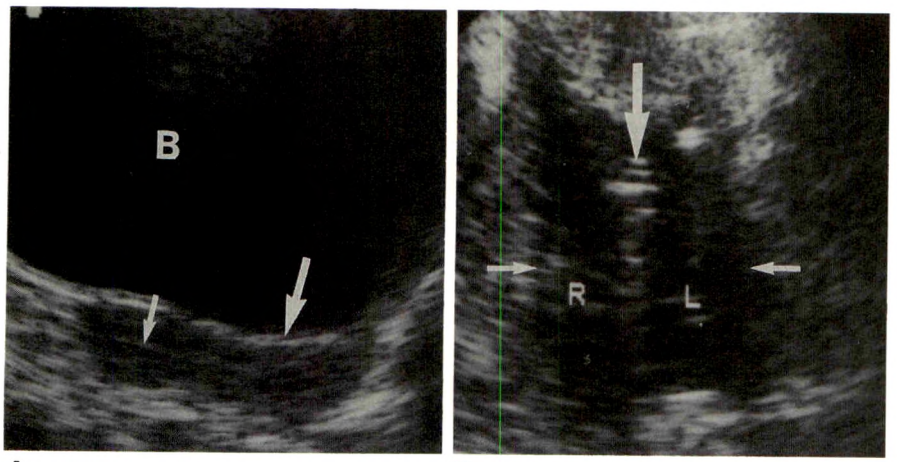


Fig. 1.—*A*, Transabdominal sonogram (sagittal view) shows a single uterus (*large arrow*). *Small arrow* = endometrial stripe, B = bladder.
***B*, Transperineal sonogram (transverse view) shows vaginal septum (*large arrow*) and microbubbles in water outlining each vaginal compartment (*small arrows*). Exact point or number of fenestrae cannot be determined.**

important role in the evaluation of these anomalies and in showing associated urinary tract abnormalities, which can occur on a congenital basis or can result from urinary tract obstruction [4–7].

When clinical examination or conventional sonography is used, it may be impossible to determine the number of vaginal compartments of whether a vaginal septum is complete or incomplete [8]. Sonography is improved if water is injected into the vagina, as long as the orifice can be catheterized and leakage from the vaginal vault to the outside is sufficiently prevented. This is usually not a problem in small children if the legs are kept together, but in older patients it may be necessary to inflate the balloon of the Foley catheter at the introitus to occlude the orifice. However, the transabdominal approach is not always sufficient for sorting out complex vaginal anomalies because of difficulty penetrating the abdominal wall in obese patients, which leads to suboptimal visualization of the deep pelvic structures, or because vaginal distension is inadequate. We found that use of a transperineal approach during hydrosonovaginography allowed us to visualize the vaginal compartments better as soon as the vagina was distended with water.

ACKNOWLEDGMENT

We thank Janet L. Birkmann for secretarial assistance.

REFERENCES

1. Pederson JH, Kuist N, Nielson OH. Hydrometrocolpos: current views on pathogenesis and management. *J Urol* **1984**;132:537–540
2. Griffin JE, Edwards C, Madden JD, Harrod MJ, Wilson JD. Congenital absence of the vagina: the Mayer-Rokitansky-Kuster-Hauser syndrome. *Ann Intern Med* **1976**;85:224–236
3. Kenney PJ, Spirt BA, Leeson MD. Genitourinary anomalies: radiologic-anatomic correlations. *RadioGraphics* **1984**;4:233–260
4. Malini S, Valdes C, Malinek LR. Sonographic diagnosis and classification of anomalies of the female genital tract. *J Ultrasound Med* **1984**;3:397–404
5. Wilson DA, Stacy TM, Smith EI. Ultrasound diagnosis of hydrocolpos and hydrometrocolpos. *Radiology* **1978**;128:451–454
6. Rosenberg HK, Udassin R, Howell C, Betts J, Schnauffer L. Duplication of the uterus and vagina, unilateral hydrometrocolpos and ipsilateral renal agenesis: sonographic aid to diagnosis. *J Ultrasound Med* **1982**;1:289–291
7. Rosenberg HK, Sherman NH, Tarry WF, Duckett JW, Snyder HM. Mayer-Rokitansky-Kuster-Hauser syndrome: US aid to diagnosis. *Radiology* **1986**;161:815–819
8. Graham D, Nelson MW. Combined perineal-abdominal sonography in evaluation of vaginal atresia. *JCU* **1986**;14:735–738

Pictorial Essay

Radiologic Findings of Diseases Involving the Maxilla and Mandible

Thomas E. Underhill,[1] Jerald O. Katz,[2] Thomas L. Pope, Jr.,[3] and Charles L. Dunlap[4]

The purpose of this pictorial essay is to illustrate the radiologic appearances of diseases involving the maxilla and mandible. The high prevalence of dental disease results in inflammatory, infectious, and reactive processes that must be distinguished from more serious conditions with similar radiologic features. Because of their association with odontogenic tissues, lesions of the maxilla and mandible may have radiologic findings not seen in other bones. Furthermore, nonodontogenic cysts and tumors that occur elsewhere in the skeleton may exhibit unique radiologic characteristics when associated with teeth. This pictorial essay presents the radiologic characteristics of inflammatory lesions, developmental abnormalities, fibroosseous lesions, benign cysts and tumors, and malignant lesions of the maxilla and mandible.

Inflammatory Lesions

The lamina dura can be traced on radiographs from the alveolar crest around the roots of the teeth. Loss of continuity of the lamina dura at the apex of a tooth usually indicates the presence of periapical disease. The necrotic pulp of a nonvital tooth can cause infection that destroys periapical bone. The resulting radiographic appearance may be a diffuse (Fig. 1) or well-defined (Fig. 2) apical radiolucency.

Condensing osteitis may appear as a well-defined or diffuse radiopacity often associated with necrotic pulp tissue from a nonvital tooth (Fig. 3). This lesion usually is located in the apical region of the tooth and represents sclerotic bone formed in reaction to chronic inflammation of the pulp. Radiographs also may show widening of the periodontal ligament space, or a larger apical radiolucency between the tooth and the radiopaque lesion.

Osteosclerosis appears as a round or irregular radiopacity, which may or may not be associated with the apices of teeth (Fig. 4). The lesions usually are singular but may be multiple. Their borders may be either well demarcated or diffuse.

Periodontal disease usually begins with erosion of the interdental alveolar crest, followed by vertical bone loss. Teeth that have lost all bone support appear to be "floating." Although the most common cause of floating teeth is severe periodontal disease (Fig. 5), more serious diseases such as osteolytic carcinoma (primary or metastatic) or Langerhans cell granulomatosis (histiocytosis X) also can give this appearance.

Developmental Abnormalities

Variations in the trabecular pattern and marrow space most often are seen in the mandible and may resemble cystlike lesions on radiographs. An early-stage tooth crypt is seen as a well-corticated, singular radiolucency. Its diameter is approximately the same as that of the developing tooth (Fig. 6).

The appearance of retained root tips or unerupted supernumerary teeth (Fig. 7) may resemble that of osteosclerosis. However, the root canal space within the root and the periodontal ligament space and lamina dura surrounding the root differentiate these lesions from inflammatory processes.

Received September 20, 1991; accepted after revision February 25, 1992.
[1] The Bowman Gray School of Medicine, Medical Center Blvd., Winston-Salem, NC 27157-2566. Address reprint requests to T. E. Underhill.
[2] Department of Oral Diagnosis, University of Missouri-Kansas City School of Dentistry, 650 E. 25th St., Kansas City, MO 64108-2795.
[3] Department of Radiology, The Bowman Gray School of Medicine, Medical Center Blvd., Winston-Salem, NC 27157-1088.
[4] Department of Oral Pathology, University of Missouri-Kansas City School of Dentistry, 650 E. 25th St., Kansas City, MO 64108-2795.

AJR **159:345–350, August 1992** 0361–803X/92/1592–0345 © American Roentgen Ray Society

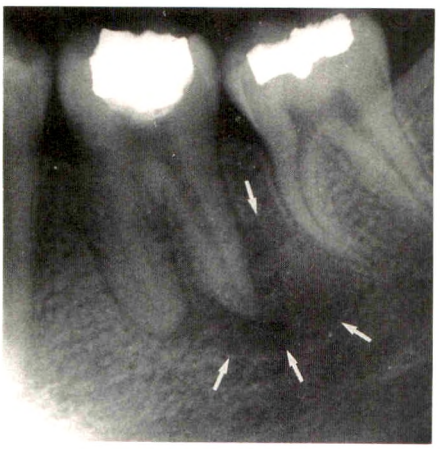


Fig. 1.—Periapical abscess. Intraoral radiograph shows mandibular molar with diffuse radiolucency associated with distal root. Bone destruction was caused by an acute dental abscess (*arrows*).

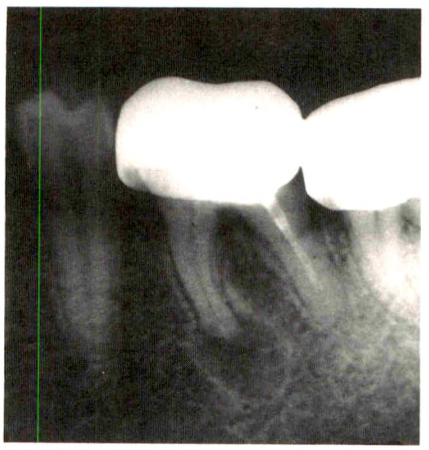


Fig. 2.—Periapical (radicular) cyst. Intraoral radiograph shows mandibular molar with a well-defined periapical radiolucency associated with mesial root. Sclerotic border suggests chronic process unlike that in Fig. 1. Border is continuous with lamina dura. Radicular cyst has formed in response to inadequate endodontic therapy.

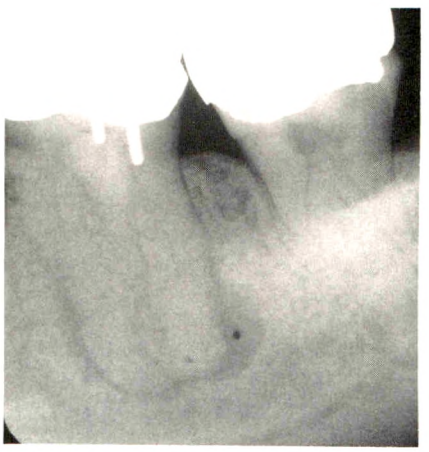


Fig. 3.—Condensing osteitis. Intraoral radiograph shows diffuse radiopacity associated with nonvital mandibular first molar.



Fig. 4.—Osteosclerosis. Intraoral radiograph shows irregularly shaped radiopacity between mandibular first and second premolars.

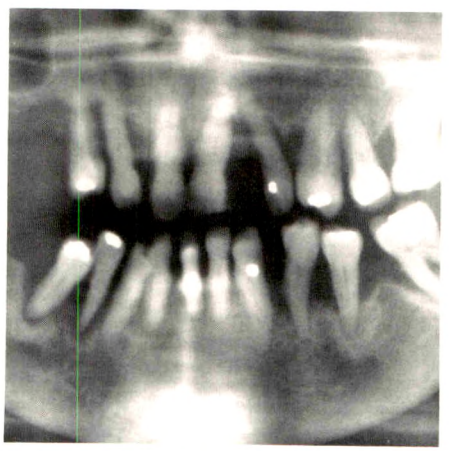


Fig. 5.—Severe generalized periodontal disease. Panoramic radiograph shows "floating teeth." Note smooth, sclerotic, bony appearance indicating a chronic inflammatory response. Compare with ragged borders associated with acute bone destruction in Fig. 23.



Fig. 6.—Early developing tooth crypt. Panoramic radiograph of posterior area of mandible shows well-defined radiolucency distal to second molar.

Developmental salivary gland depression is seen as a well-defined radiolucency in the ramus below the mandibular canal in the region of the second molar. If this depression impinges on the inferior border of the mandible, the inferior cortical plate exhibits a thin, smooth appearance (Fig. 8). It is important not to mistake this anatomic depression for a pathologic lesion.

Fibroosseous Lesions

Benign fibroosseous lesions are relatively common [1]. Hypercementosis, the excess deposition of cementum on the roots of teeth, gives the roots a bulbous appearance (Fig. 9). The periodontal ligament space and lamina dura of the tooth remain intact. Hypercementosis may be idiopathic or may result from pulpal inflammation or excessive occlusal force. Generalized hypercementosis may be associated with Paget disease [2].

Periapical cemental dysplasia (cementoma) is a fibroosseous lesion that develops from the periodontal ligament of the tooth. This periapical lesion may be multiple, often is associated with mandibular anterior teeth, and occurs most frequently in middle-aged black women. The lesion progresses from a radiolucent stage, through a mixed radiolucent-radiopaque stage, and finally to a mostly radiopaque stage, in which the lesion is surrounded by a thin, radiolucent rim (Fig. 10). The associated teeth are asymptomatic, and treatment is not required.

Florid osseous dysplasia has been reported to be the most common cause of generalized radiopacities in the jaws [3]

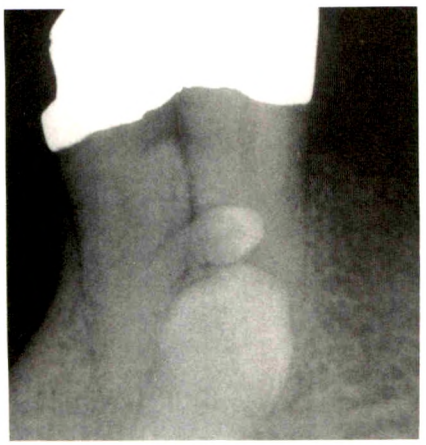


Fig. 7.—Supernumerary teeth. Intraoral radiograph shows small, unerupted supernumerary tooth adjacent to larger, unerupted supernumerary tooth. Enamel, dentin, pulp canal, and characteristic tooth shape help to distinguish smaller tooth from other types of pathologic conditions.

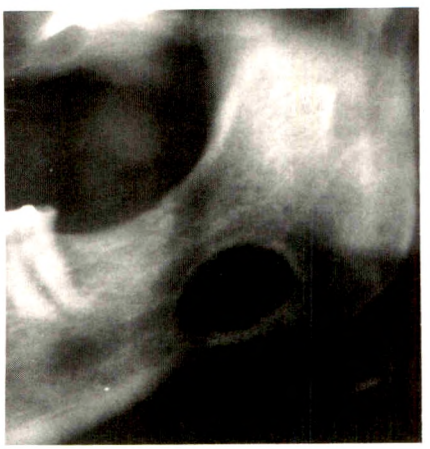


Fig. 8.—Depression of mandibular salivary gland. Panoramic radiograph of posterior area of mandible shows well-defined radiolucency below inferior alveolar canal. Note smooth thinning of inferior cortical border of mandible.



Fig. 9.—Hypercementosis. Intraoral radiograph shows extensive involvement of maxillary premolars. Note bulbous appearance of roots.

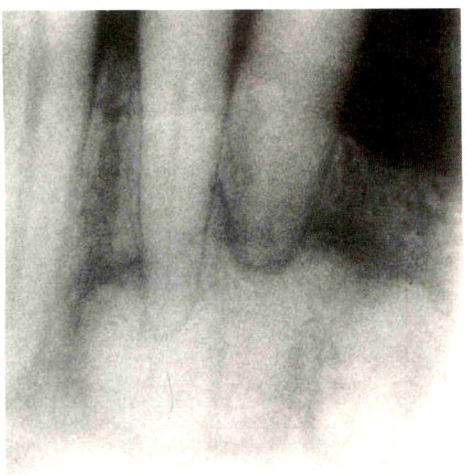


Fig. 10.—Periapical cemental dysplasia. Intraoral radiograph of mandibular anterior teeth shows mature, radiopaque lesions with surrounding radiolucent rims.

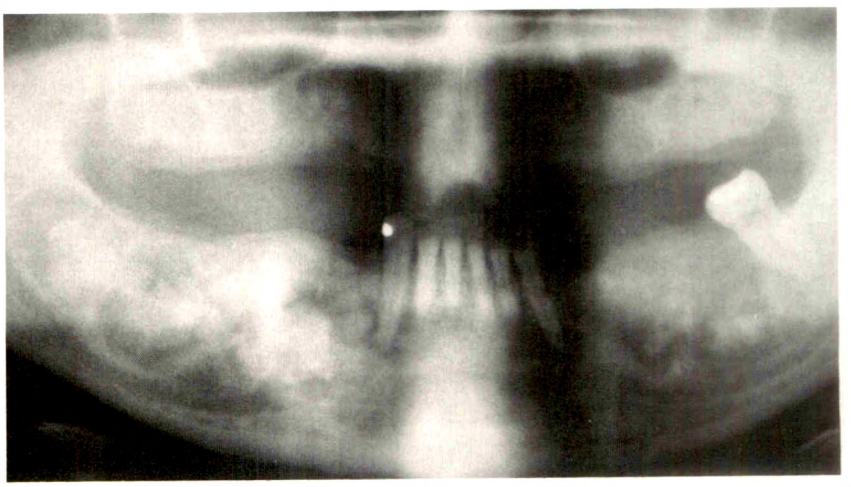


Fig. 11.—Florid osseous dysplasia. Panoramic radiograph shows radiolucent rim or "halo" surrounding opacities. This rim is a common finding with fibroosseous lesions.

(Fig. 11). Some consider florid osseous dysplasia to be a widespread form of periapical cemental dysplasia; others have suggested that it is a chronic sclerosing form of osteomyelitis [4]. Like periapical cemental dysplasia, florid osseous dysplasia often is found in middle-aged black women and progresses through three stages. However, in the final stage of florid osseous dysplasia, the radiolucent border surrounding the radiopaque lesion may be less prominent than in periapical cemental dysplasia.

Central cementifying and ossifying fibromas are rare fibroosseous lesions arising from the periodontal ligament. They may resemble more common lesions such as periapical abscess, periapical cyst, or periapical cemental dysplasia. These lesions progress through radiolucent, mixed, and radiopaque stages of development. Often these lesions are found in young adults, especially in the mandibular premolar and molar region. Lesions usually are well defined and slow growing and may cause expansion and displacement of teeth (Fig. 12).

Fibrous dysplasia, usually discovered during childhood, is a fibroosseous condition that does not originate from the periodontal ligament (Fig. 13). When the jaws are involved, the posterior maxilla is affected most frequently. As lesions mature, radiolucencies with poorly defined borders fill in with dysplastic trabeculae [4]. Lesions may have a dense, granular, radiopaque appearance referred to as "ground glass." Frequently, loss of the lamina dura surrounding the teeth is observed as is expansion of bone with associated facial deformity.

Benign Cysts and Tumors

Torus palatinus, the most common exostosis of the jaws [4], occurs in the midline of the palate. On intraoral radio-

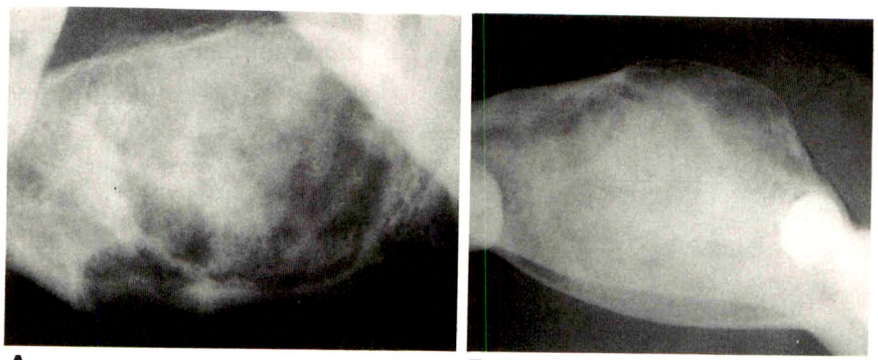


Fig. 12.—Ossifying fibroma.
A, Lateral radiograph of posterior area of mandible shows large, ovoid ossifying fibroma with calcifications. Note expansion of lesion superiorly and inferiorly.
B, Occlusal radiograph of mandible shows expansion of lesion buccally and lingually.

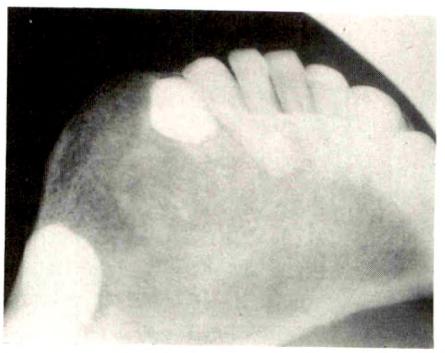


Fig. 13.—Fibrous dysplasia. Occlusal radiograph shows fibrous dysplasia of mandible with buccal expansion. Blending of lesion with surrounding bone differentiates this lesion from an ossifying fibroma.

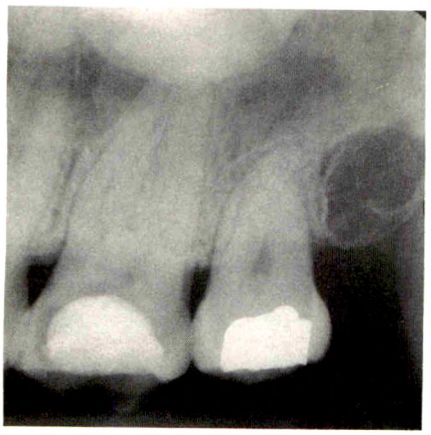


Fig. 14.—Torus palatinus (exostosis). Intraoral radiograph shows torus palatinus superimposed over maxillary sinus and apices of first and second molars. This type of exostosis often has a smooth, lobulated appearance.

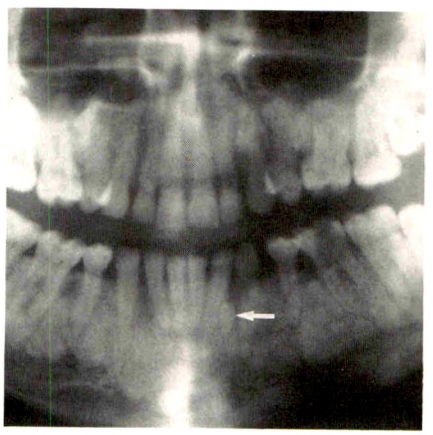


Fig. 15.—Gardner's syndrome. Panoramic radiograph shows multiple osteomas of mandible, possibly involving left posterior area of maxilla. Note small, impacted supernumerary tooth (*arrow*) between mandibular left canine and lateral incisor. Another supernumerary tooth was partially erupted buccal to maxillary right lateral incisor.



Fig. 16.—Compound odontoma. Intraoral radiograph shows compound odontoma between maxillary lateral and central incisors. Note appearance of multiple toothlike structures.

graphs it appears as a well-demarcated radiopacity superimposed over maxillary molar roots and the maxillary sinus (Fig. 14). Torus mandibularis is a similar outward projection of bone, but it occurs on the lingual aspect of the mandible in the premolar region and often is bilateral. Osteomas of the jaws may be periosteal or endosteal. These lesions may appear as well-delineated or diffuse radiopacities of various sizes and shapes. Multiple osteomas of the jaws and unerupted supernumerary teeth are common findings in Gardner's syndrome (Fig. 15).

Reported to be the most common odontogenic tumors [5], odontomas develop concurrently with normal teeth. Compound odontomas resemble single or multiple toothlike structures (Fig. 16), whereas complex odontomas are seen as irregular masses of dental tissues (Fig. 17). Compound odontomas are more common in the anterior maxilla; complex odontomas often are found in the posterior mandible.

The enamel of teeth develops from ameloblasts lining the coronal portion of the developing tooth crypt. Ameloblastoma is a neoplasm of enamel organ-type tissue. Typically, the radiograph shows a multilocular, expansile radiolucency that occurs most often in the posterior mandible (Fig. 18).

The width of the normal follicular space of unerupted teeth may be as large as 3 mm on panoramic radiographs and 2.5 mm on intraoral radiographs [2]. The follicular spaces of the maxillary permanent cuspids normally are larger than those of other teeth. Enlargement of the follicular space suggests a dentigerous cyst or eruption cyst. These cysts are seen as well-demarcated radiolucent lesions around crowns of impacted, embedded, or unerupted teeth (Fig. 19).

Odontogenic keratocyst has a high recurrence rate and may grow rapidly. When small, this lesion is seen as a well-defined radiolucency with an even border. Large lesions have scalloped, usually well-corticated borders; perforation of the



Fig. 17.—Complex odontoma. Panoramic radiograph shows large complex odontoma in posterior area of maxilla. Note displacement of maxillary first molar.

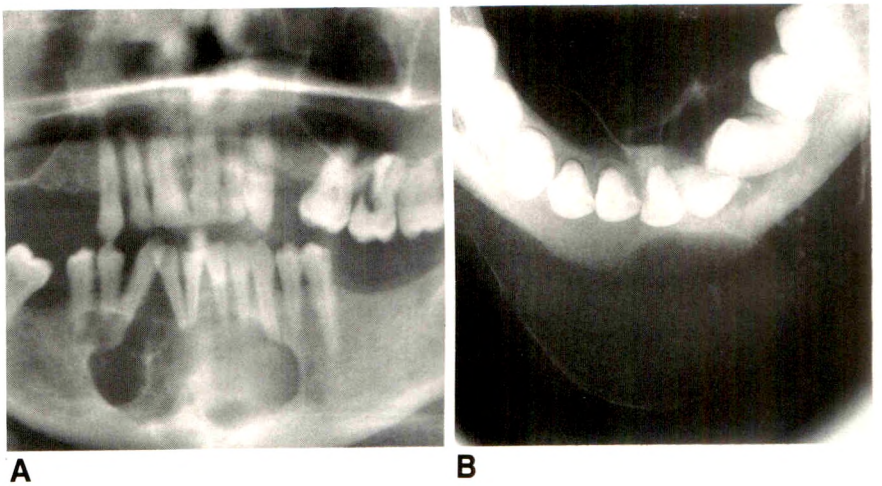


Fig. 18.—Ameloblastoma.
A, Panoramic radiograph shows ameloblastoma in anterior area of mandible with displacement of roots of right canine and lateral incisors.
B, Intraoral cross-sectional occlusal radiograph shows buccal and lingual expansion of cortex.

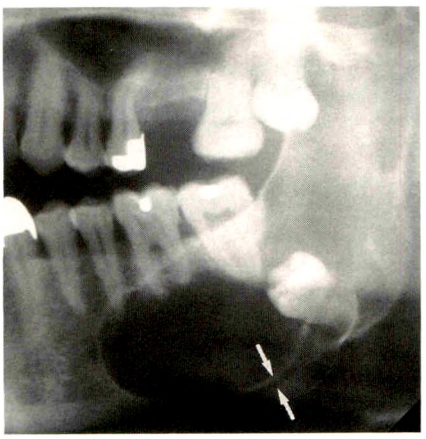


Fig. 19.—Dentigerous cyst. Panoramic radiograph of posterior area of mandible shows large cyst extending from sigmoid notch to premolar area. Note displacement of mandibular third molar and inferior alveolar canal (*arrows*).

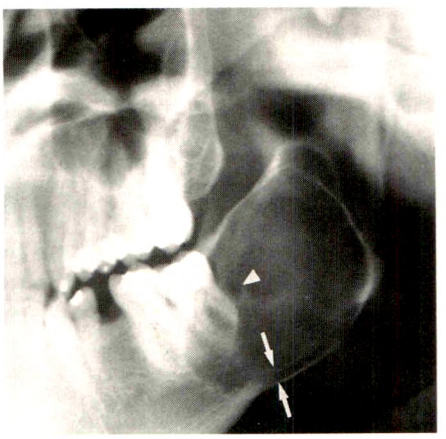


Fig. 20.—Odontogenic keratocyst. Panoramic radiograph shows loculated cyst extending superiorly near coronoid process, expansion and thinning of cortex, and downward displacement of inferior alveolar canal (*arrows*). Note slight resorption of distal root of second molar and possible perforation of cortex distal to second molar (*arrowhead*).



Fig. 21.—Simple bone cyst. Panoramic radiograph shows simple bone cyst in mandibular molar area. Distinguishing feature is scalloped appearance of superior margin of cyst as it spreads between roots of molars.

cortical plate and multiplicity of lesions may be noted (Fig. 20).

Primordial cyst results from degeneration of the developing tooth bud before enamel or dentin formation. On radiographs, it is a well-demarcated radiolucent lesion that can cause expansion of bone and displacement of teeth. Nasopalatine duct cyst is seen as a heart-shaped, well-defined radiolucency in the midline of the anterior maxilla.

Simple (unicameral) bone cyst is 6.5 times more prevalent in the mandible than in the maxilla and usually occurs above the mandibular canal [6] (Figs. 21 and 22).

Malignant Lesions

Although not considered malignant, the histiocytosis X group is included in this section because its appearance on radiographs may be similar to that of a malignant tumor [1]. Involvement of the jaws consists of a generalized alveolar bone loss that resembles advanced periodontal disease and often results in floating teeth (Fig. 23).

Primary osteolytic carcinomas of the jaws cause diffuse bone destruction (Fig. 24). Carcinoma rarely originates in the epithelium of a follicular cyst; when it does, the pericoronal radiolucency has poorly defined borders (Fig. 25). Metastatic carcinoma often appears as a radiolucent lesion with diffuse, ragged borders (Fig. 26).

Jaw involvement is rare, but osteosarcoma is the most common primary sarcoma affecting the jaws [4] (Fig. 27). Both sclerosing and osteolytic variants occur. Mandibular lesions often involve the body of the mandible, whereas maxillary lesions tend to involve the alveolar ridge and antrum.

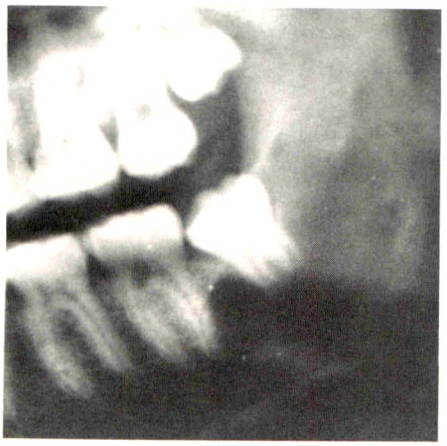


Fig. 22.—Simple bone cyst. Panoramic radiograph shows scalloping around roots of erupting third molar.

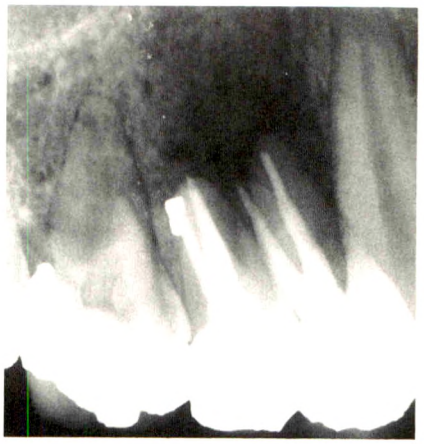


Fig. 23.—Langerhans cell granulomatosis. Intraoral radiograph shows "floating tooth" appearance of maxillary premolars and loss of bone support of maxillary canine and first molar. Bone destruction was thought to be result of infection from a necrotic pulp. When lesion failed to resolve after endodontic therapy, biopsy revealed histologic changes consistent with Langerhans cell granulomatosis.

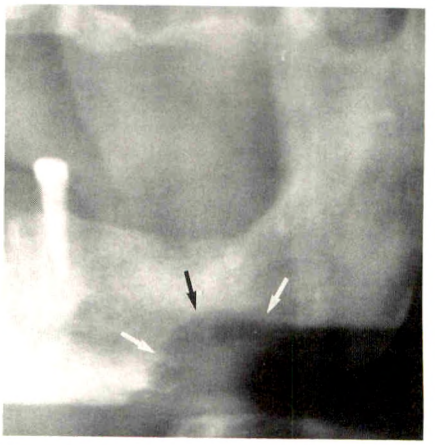


Fig. 24.—Squamous cell carcinoma (floor of the mouth). Panoramic radiograph shows radiolucency with no sclerotic borders (*arrows*) diffusely blending into surrounding bone.



Fig. 25.—Squamous cell carcinoma. Panoramic radiograph of posterior area of mandible shows radiolucency associated with impacted third molar. Compare poorly defined borders of lesion with well-defined borders of dentigerous cyst (Fig. 19). Biopsy disclosed squamous cell carcinoma arising from follicular epithelium.

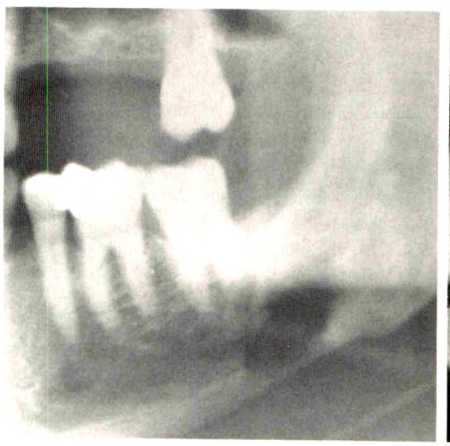


Fig. 26.—Metastasis of prostatic carcinoma. Panoramic radiograph shows lesion similar to that seen in Fig. 8, except that borders are ragged. Biopsy revealed metastatic prostatic carcinoma. This example emphasizes importance of examining integrity of lesion's border.



Fig. 27.—Osteosarcoma. Occlusal radiograph shows radiopaque lesion involving anterior area of maxilla. Note poorly defined margins of lesion and generalized widening of periodontal ligament space of maxillary central and lateral incisors. Fine bony spicules extending beyond cementoenamel junction and widening of periodontal ligament space strongly suggest the diagnosis.

Widening of the periodontal ligament around one or more teeth is an early sign visible on radiographs. Expansion and poorly defined margins are common. The "sun-ray" trabecular pattern occurs at the periphery of the lesion in about one third of cases [4].

ACKNOWLEDGMENTS

The authors acknowledge Donna S. Garrison for her administrative and editorial assistance.

REFERENCES

1. Dahlin DC, Unni KK. *Bone tumors: general aspects and data on 8,542 cases*, 4th ed. Springfield, IL: Thomas, **1986**:440–442
2. Langland OE, Langlais RP, McDavid WD, DelBalso AM. *Panoramic radiology*, 2nd ed. Philadelphia: Lea & Febiger, **1989**:254–380
3. Wood NK, Goaz PW. *Differential diagnosis of oral lesions*, 3rd ed. St. Louis: Mosby, **1985**
4. Goaz PW, White SC. *Oral radiology: principles and interpretation*, 2nd ed. St. Louis: Mosby, **1987**
5. Regezi JA, Kerr DA, Courtney RM. Odontogenic tumors: analysis of 706 cases. *J Oral Surg* **1978**;36:771–778
6. Kuroi M. Simple bone cyst of the jaw: review of the literature and report of case. *J Oral Surg* **1980**;38:456–459

Width of the Articular Cartilage of the Hip: Quantification by Using Fat-Suppression Spin-Echo MR Imaging in Cadavers

Juerg Hodler[1,2]
Debra Trudell[1]
Mini N. Pathria[1]
Donald Resnick[1]

OBJECTIVE. Use of MR imaging to measure the width of the articular cartilage has not been thoroughly investigated. The value of a selective fat-suppression spin-echo sequence in the quantitative assessment of articular cartilage of the hip was studied in cadavers.

MATERIALS AND METHODS. Sagittal and coronal images were acquired in 10 cadaveric hips (age range at time of death, 62–81 years). On the coronal and sagittal MR images that were closest to the center of the femoral head, marks were placed every 30°, with the midpoint of the femoral head used as a reference. Cartilage thickness was measured in 123 resulting locations. Sixty-three positions included both femoral and acetabular cartilages, and 60 positions included femoral cartilage without an acetabular counterpart. The findings were compared with corresponding anatomic sections.

RESULTS. For the 60 locations containing only femoral cartilage, significant correlation between MR and anatomic sections was found (Pearson correlation coefficient = .34, p = .0089). Of the 63 locations containing both femoral and acetabular cartilages, the two cartilage layers could be differentiated on the MR images in 50 locations. In these 50, the MR and anatomic measurements of the femoral cartilage correlated significant (r = .58, $p \leq .0001$). Measurements of the acetabular cartilage in these 50 locations yielded no significant correlation (r = .25, p = .08). When the entire cartilage (femoral plus acetabular) was measured in all 63 locations, the correlation between MR and anatomic measurements was .29 (p = .02). The correlation coefficients obtained in this investigation indicate considerable scattering of the data.

CONCLUSION. Our results show that measurements of articular cartilage thickness of the hip on fat-suppression spin-echo MR images are not sufficiently accurate to be of clinical value.

AJR 159:351–355, August 1992

Previous reports have indicated that fat-suppression MR images provide a high signal-to-noise ratio and good contrast resolution and may be the optimal method for imaging cartilage [1]. Chemical shift is reduced with this technique compared with standard spin-echo sequences, thereby allowing more precise cartilage measurements. Until recently, fat-suppression techniques required time-consuming manual prescanning in order to define the frequency of the fat peak for optimal suppression [2]. Methods of fat suppression that are automated and easy to use have been developed recently.

Few investigations have been published that have evaluated quantitative assessment of articular cartilage [3–5]. In the present investigation, MR measurements of the width of articular cartilage obtained with a commercially available chemical saturation technique were compared with corresponding anatomic sections of cadaveric hip joints.

Materials and Methods

Ten fresh human hip joints (five right and five left) originating from seven cadavers (age range at time of death, 62–81 years; mean, 71 years) were frozen and sectioned to a diameter

Received November 26, 1991; accepted after revision February 24, 1992.

This work was supported in part by Veterans Affairs grant SA 306, a grant from Ciba-Geigy Corp., and a grant from University Hospital, Zurich, Switzerland.

[1] Department of Radiology, Veterans Affairs Medical Center (114), 3350 La Jolla Village Dr., San Diego, CA 92161, and University of California, San Diego, Medical Center (H-756), 225 Dickinson St., San Diego, CA 92103.

[2] Present address: Department of Radiology, University Hospital, Raemistrasse 100, CH-8091 Zurich, Switzerland.

0361–803X/92/1592–0351
© American Roentgen Ray Society

of 7–10 cm in order to fit in the GE (General Electric, Milwaukee, WI) send-receive extremity coil. After they were thawed, the specimens were scanned with a GE Signa 1.5-T MR scanner. Both coronal and sagittal T1-weighted spin-echo images with chemical saturation were acquired. The fat component was suppressed by using a 250-Hz-wide presaturation pulse centered on the fat hydrogen peak. No manual prescanning is required with this technique, and only a few limitations are present compared with standard spin-echo imaging; that is, a slightly reduced number of images available for a specific repetition time, an increase in the specific absorption rate, and dependence on field inhomogeneities. We chose a 600/20 (TR/TE) scanning sequence. Slice thickness was 3 mm and the interslice gap was 1.5 mm. The field of view was 12 cm and the acquisition matrix was 256 × 256. These parameters result in a potential spatial resolution (pixel size) of 0.46 mm. The number of excitations was two and the scanning time per sequence was 5 min 14 sec.

The coronal and sagittal images that were closest to the center of the femoral head were determined by studying the MR images. Marks were placed every 30°, with the midpoint of the femoral head used as a reference point. Cartilage thickness was measured to the closest 0.2 mm by a single observer who used a loupe (Fig. 1). Sixty-three positions that included both femoral and acetabular cartilages were measured. In 50 of these positions, femoral cartilage and acetabular cartilage could be distinguished from each other, and in these 50 cases femoral cartilage, acetabular cartilage, and total cartilage thickness were measured. In the 13 remaining positions, only the total cartilage thickness could be measured. In 60 other positions, femoral cartilage without an acetabular counterpart was measured; that is, in the acetabular fossa and craniolaterally. Therefore, a total of 123 positions were measured.

For anatomic correlation, the midpoint of the frozen femoral head then was determined under fluoroscopy, and a 3-mm-thick coronal section through this midpoint was obtained with a band saw. From the remaining two parts of the specimen, a central sagittal section was obtained (Fig. 1). By using a template containing marks every 30° and the loupe, we were able to measure cartilage thickness to the nearest 0.1 mm at sites corresponding closely to those of the MR images. On the basis of the anatomic sections, two cadaveric hip specimens showed only osteophyte formation, five showed osteophyte formation and focal cartilage damage, and three had diffuse cartilage damage with or without significant osteophyte formation.

Although one observer performed both the anatomic and MR measurements, the MR data were not available to him when the specimens were analyzed. The association between MR and ana-

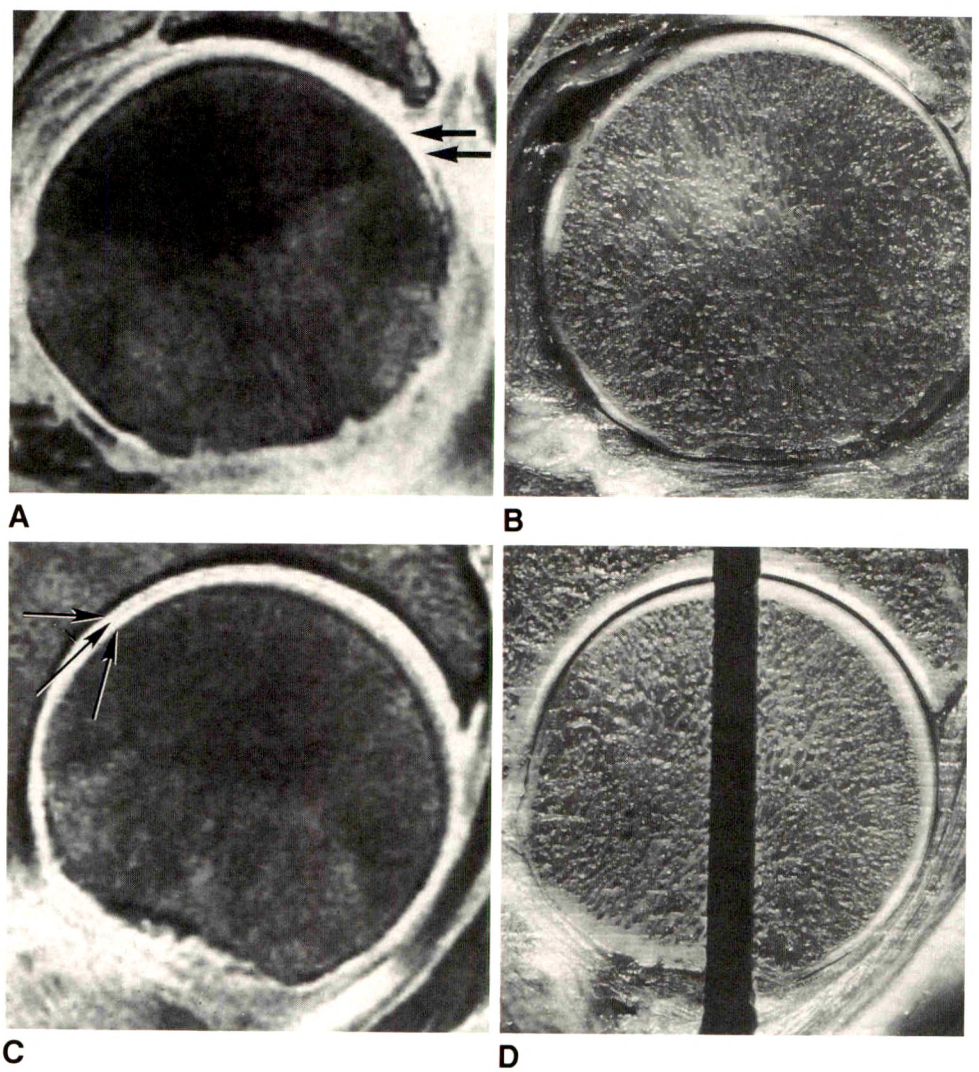


Fig. 1.—*A–D*, Coronal (*A* and *B*) and sagittal (*C* and *D*, left = posterior) MR images (600/20) (*A* and *C*) and corresponding anatomic sections (*B* and *D*) of left hip of a 64-year-old woman. Femoral and acetabular cartilages can be differentiated easily on sagittal image (*C*, *arrows*), but not on coronal image superiorly (*A*). Femoral cartilage may be difficult to differentiate from hyperintense structures within acetabular fossa and superolaterally (presumably related in part to a joint effusion) (*A*, *arrows*).

TABLE 1: MR and Anatomic Measurements of Articular Cartilage

Cartilage Layer	Anatomic (MR) Measurement in mm			r	*p*
	Mean	Range	SD		
Femoral cartilage without acetabular counterpart ($n = 60$)	1.3 (1.8)	0.0–2.3 (0.9–2.3)	0.60 (0.59)	.34	.0089
Femoral cartilage distinguished from acetabular counterpart ($n = 50$)[a]	1.4 (1.5)	0.0–2.4 (0.0–2.6)	0.58 (0.49)	.58	≤.0001
Acetabular cartilage distinguished from femoral counterpart ($n = 50$)[a]	1.2 (1.6)	0.0–2.5 (0.0–2.4)	0.69 (0.50)	.25	.0800
Femoral plus acetabular counterparts ($n = 63$)	2.9 (3.1)	0.4–4.8 (1.2–4.5)	1.10 (0.67)	.29	.0200

[a] Sixty-three positions were measured, but in only 50 of these could femoral cartilage and acetabular cartilage be distinguished from each other.

tomic measurements then was determined by using the Pearson correlation coefficient. The Pearson correlation coefficient is zero when no linear relationship exists between the two variables and 1 when there is a perfect positive linear relationship. The statistical significance of this correlation was calculated. The average measurements were also compared by using the paired t test to determine if MR measurements overestimated or underestimated cartilage thickness. A 5% significance level was used for the statistical evaluations.

Results

The results of the anatomic and MR measurements and their correlation are shown in Table 1 and Figure 2. The highest correlation between the two measurement methods was found for femoral cartilage. In those 50 locations in which the femoral cartilage could be differentiated from acetabular cartilage, measurement of femoral cartilage in contact with acetabular cartilage correlated better with anatomic data than did measurement of isolated femoral cartilage. This difference was related mainly to the fact that part of the surrounding tissue, namely, muscle fibers and loose connective tissue, had an intensity similar to that of hyaline cartilage on the MR sequence used in this study; because of this, depiction of isolated femoral articular cartilage was not ideal (Fig. 3). The same findings probably accounted also for the statistically significant overestimation of femoral cartilage isolated from acetabular cartilage but less so of femoral cartilage combined with acetabular cartilage (paired one-tailed t test: $p \leq .0001$ for isolated cartilage and $p = .02$ for femoral cartilage combined with acetabular cartilage).

Measurements of the acetabular cartilage and the total articular cartilage were less reliable than those of femoral cartilage, as demonstrated by smaller Pearson correlation coefficients. Near the acetabular fossa and craniolaterally near the labrum, the hyperintensity of joint fluid and of surrounding structures (nonfatty content of the acetabular fossa, i.e., loose connective tissue or edema within fat, and degenerated labrum) simulated that of hyaline cartilage (Fig. 1). In one specimen, the cartilage-bone interface was not as well delineated on the acetabular side, presumably owing to edema and/or hemorrhage in the bone marrow.

Despite the significant correlation between anatomic and MR measurements, there was considerable scattering of the data, as shown in Figure 2.

Discussion

There is great interest in developing accurate noninvasive methods for assessing the thickness of hyaline articular cartilage. MR imaging currently is the best noninvasive method for evaluating normal and abnormal hyaline articular cartilages because of its multiplanar capability and inherently high contrast resolution. Problems encountered with MR assessment of cartilage are imprecise delineation of the cartilage-bone interface, which is obscured by a chemical-shift artifact and other factors [3, 4, 6, 7]; limited spatial resolution; and limited contrast between normal and pathologic cartilage and between cartilage and joint fluid. Practical experience with spin-echo imaging has been less than ideal [6, 8] and it seems that standard MR sequences are consistently useful only for the detection of gross cartilage defects. Gradient-echo techniques have been used with some success [9–11].

MR descriptions of cartilage abnormalities include examples of traumatic alterations not visible on plain films [12] and

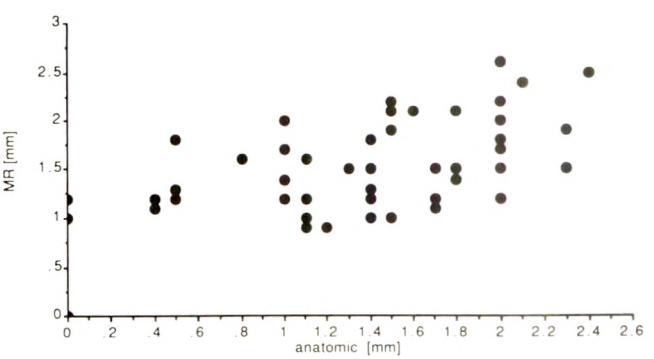


Fig. 2.—Scatterplot shows correlation of MR and anatomic measurements of femoral articular cartilage in contact with acetabular cartilage.

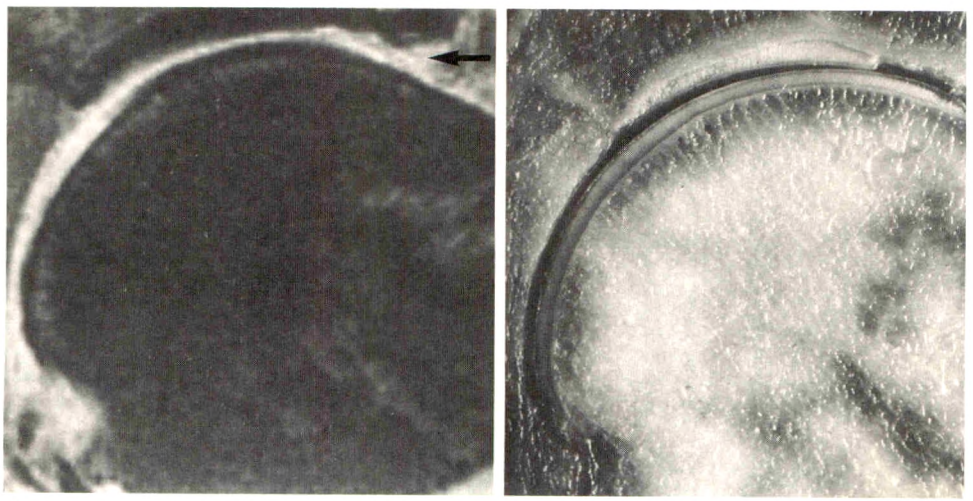


Fig. 3.—*A* and *B*, Coronal MR image (600/20) (*A*) and corresponding anatomic section (*B*) of left hip of a 69-year-old man. Differentiation between superolateral femoral cartilage and parts of labrum (*arrow*), capsule, and surrounding soft tissue is difficult.

of cartilage that is degenerated [13] or destroyed by inflammation [11]. Different MR imaging sequences have been used for cartilage analysis with inconsistent results. In most previous investigations, quantitative assessments are lacking [6, 8], although limited quantitative data in the evaluation of articular cartilage have been reported with parameters such as cartilage thickness [3–5] and signal intensity [10, 13]. A recent article by Chandnani et al. [1] indicated that spin-echo fat-suppression imaging was superior to both the conventional spin-echo technique and MR arthrography (with intra-articular gadopentetate dimeglumine) in the evaluation of hyaline cartilage in the knee. The hybrid technique [14] that these investigators used required manual prescanning with an extended examination time. The fat-suppression technique used in the current investigation is commercially available and simple to use, and the examination time is identical to that of a standard spin-echo sequence, although fewer slices are acquired in one imaging sequence.

The deep hypointense layer of articular cartilage visible during MR examination has been attributed to subchondral bone [1, 9] the deep calcified layer of the cartilage [10, 11], differences in water content [3], susceptibility differences between hyaline cartilage and subchondral bone [7], differences between the T2 relaxation times of different cartilage layers [7], and chemical shift artifacts [4]. Wrazidlo et al. [4] showed a relationship between the visualized cartilage thickness and the direction of frequency encoding. Our own unpublished results indicate that with most imaging sequences this deep layer of signal void is larger than the very thin subchondral bone plate and interferes with precise measurements of articular cartilage thickness. In our unpublished preliminary study, fat-suppression images significantly reduced the thickness of the deep black layer on MR images when compared with standard spin-echo images. On the basis of the investigation of Chandnani et al. [1] and our own preliminary results, we believe that fat-suppression imaging is the simplest and most accurate method for analyzing hyaline cartilage.

The use of cadavers in our investigation probably did not influence our results. Some problems encountered with MR imaging of cadaveric specimens are related to the diffusion of tissue fluid that may reduce image contrast and the introduction of air within the soft tissues or joint. The first of these problems is more prominent in muscles and in loose connective tissue than in dense hyaline cartilage. Intraarticular air leading to secondary susceptibility artifacts did not occur in this study.

Although several of our measurements of cartilage thickness showed a statistically significant correlation between MR imaging and anatomic evaluation, inaccuracies in measurements occurred at specific areas, findings similar to those shown by Chandnani et al. [1]. Although the statistical correlation between anatomic and MR measurements was significant for femoral cartilage with and without contact to acetabular cartilage, and for total articular cartilage thickness, the scatterplots showed considerable scattering of the data and the presence of outlying points. The value of quantitative MR measurements of articular cartilage, therefore, is still questionable, even with the use of optimal experimental conditions (no motion artifacts, use of small specimens and a surface coil). It is likely that the accuracy of the measurements would be improved if a combination of MR sequences were used. For example, a standard T2-weighted sequence added to the fat-suppression technique could be useful for the depiction of joint fluid, and a standard T1-weighted sequence would aid in the differentiation of subchondral edema and articular cartilage.

Our results show that measurements of the thickness of the articular cartilage of the hip joint on fat-suppression spin-echo MR images are not sufficiently accurate to be of value in clinical practice.

REFERENCES

1. Chandnani VJ, Ho C, Chu P, Trudell D, Resnick D. Knee hyaline cartilage evaluated with MR imaging: a cadaveric study involving multiple ir

sequences and intraarticular injection of gadolinium and saline solution. *Radiology* **1991**;178:557–561
2. Dixon WT. Simple proton spectroscopic imaging. *Radiology* **1984**;153:189–194
3. Lehner KB, Rechl HP, Gmeinwieser JK, Heuck AF, Lukas HP, Kohl HP. Structure, function, and degeneration of bovine hyaline cartilage: assessment with MR imaging in vitro. *Radiology* **1989**;170:495–499
4. Wrazidlo W, Schneider S, Richter GM, Kauffmann GW, Bläsius K, Gottschlich KW. Darstellung des hyalinen Gelenkknorpels mit der MR-Tomographie mittels einer Gradientenecho-Sequenz mit Fett-Wasser-Phasenkohärenz. *ROFO* **1990**;152:56–59
5. Braunstein EM, Brandt KD, Albrecht M. MRI demonstration of hypertrophic articular cartilage repair in osteoarthritis. *Skeletal Radiol* **1990**;19:335–339
6. König H, Sauter R, Deimling M, Vogt M. Cartilage disorders: comparison of spin-echo, CHESS, and FLASH sequence MR images. *Radiology* **1987**;164:753–758
7. Cole PR, Jasani MK, Wood B, Freemont AJ, Morris GA. High resolution, high field magnetic resonance imaging of joints: unexpected features in proton images of cartilage. *Br J Radiol* **1990**;63:907–909
8. Hodler J, Berthiaume M-J, Schweitzer ME, Resnick D. Focal changes of the articular cartilage in the femorotibial joint: magnetic resonance (MR)–anatomic correlation and blinded analysis (abstr). *Radiology* **1991**;181(P):301
9. Bongartz G, Bock E, Horbach T, Requardt H. Degenerative cartilage lesions of the hip: magnetic resonance evaluation. *Magn Reson Imaging* **1989**;7:179–186
10. König H, Aicher K, Klose U, Saal J. Quantitative evaluation of hyaline cartilage disorders using FLASH sequence: I. Method and animal experiments. *Acta Radiol* **1990**;31:371–375
11. König H, Aicher K, Klose U, Saal J. Quantitative evaluation of hyaline cartilage disorders using FLASH sequence: II. Clinical applications. *Acta Radiol* **1990**;31:377–381
12. Mink JH, Deutsch AL. Occult cartilage and bone injuries of the knee: detection, classification, and assessment with MR imaging. *Radiology* **1989**;170:823–829
13. Glückert J, Blank-Schäl A, Hofmann G, Kladny B, Willauschus W, Wirtz P. Möglichkeiten der Früherfassung von Arthrosen durch bildgebende Verfahren. *Orthopade* **1990**;19:50–57
14. Suzmowski J, Eisen JD, Vinitski S, Haake PW, Plewes DB. Hybrid methods of chemical-shift imaging. *Magn Reson Med* **1989**;9:379–388

AJR to Use Diskettes Instead of Hard-Copy Manuscripts for Editing and Printing

Beginning with the January 1993 issue, accepted papers to be published in the *AJR* will be edited and printed by using computer diskettes rather than hard copies of the manuscripts. This change will expedite the editing and publication process and result in less delay between submission of manuscripts and their appearance in the Journal. Also, with the new system, authors will receive page proofs rather than galleys before publication. This will enable them to see exactly what their final article will look like.

Effective immediately, upon *acceptance* of manuscripts for publication, authors will be asked to send a copy of their revised manuscript on a 5¼-inch DOS-compatible diskette in WordPerfect or ASCII format along with the hard copy of the revision. Articles will be edited directly on the diskettes. Changes will be highlighted electronically; as before, a hard copy of the edited manuscript and figure proofs will be mailed to authors for approval before publication. Note that hard copies of manuscripts will still be required for the peer-review and revision processes.

The *AJR* already takes great pride in the speed with which the peer-review process is accomplished (mean time, 3.4 weeks) and in the amount of time between submission of manuscripts and their final appearance in print (6 months). This is nearly twice as fast as many other journals. With the new system, these intervals will be even shorter. Authors will see their work in print faster, and the timeliness of the Journal will be greater than ever.

Robert N. Berk
Editor-in-Chief

Book Review

Imaging of Orthopedic Trauma, 2nd ed. Edited by Thomas H. Berquist. New York: Raven, 916 pp., 1992. $140

Imaging of Orthopedic Trauma was written by 21 authors, most from the Mayo Clinic. They are almost all radiologists or orthopedists, and most chapters were written by one or more of each. This is in keeping with the purpose of the book: to bridge the communication gap between radiologists and orthopedic surgeons who treat trauma. This second edition comes just 6 years after the first because of the rapid development of the newer imaging techniques, which are included throughout the book along with all the standard imaging methods such as conventional tomography, angiography, and nuclear medicine.

What does this book cover (and not cover) and how does it compare with others on this topic? The radiology of musculoskeletal trauma can be found in several types of books: Trauma is included in some all-inclusive books on bone radiology such as the second edition of *Diagnosis of Bone and Joint Diseases* (Saunders, 1988), by Resnick and Niwayama (radiologist and pathologist), and *Orthopedic Radiology* (Lippincott, 1988), by Greenspan (a radiologist). Most books on the radiology of emergency medicine cover all organ systems, including musculoskeletal trauma, such as the second edition of *The Radiology of Emergency Medicine* (Williams & Wilkins, 1981), by Harris and Harris (radiologist and orthopedic surgeon). Few books are restricted to the radiology of orthopedic trauma, as *Imaging of Orthopedic Trauma* is. Only one other popular comprehensive book of this type is available: *Radiology of Skeletal Trauma* (Churchill Livingstone, 1982), by Rogers (a radiologist), which is basically a plain film radiology book. *Orthopedic Radiology* (Saunders, 1986), by Weissman and Sledge (radiologist and orthopedic surgeon), comes close to fitting into this class, and it, too, is intended to foster communication between radiologists and orthopedists. It emphasizes the radiology of trauma but includes many nontrauma orthopedic topics such as arthritis and prostheses.

This second edition has added 100 pages (and is virtually the same length as Roger's two-volume text), but the print is slightly larger than that in the first edition and, I think, more pleasing. Some sections have been completely rewritten; others are virtually unchanged. A short chapter on interventional radiology has been deleted, and a short chapter (10 pages) on soft-tissue injuries has been added. This includes just definitions and imaging techniques. Specific musculoskeletal soft-tissue injuries are fully discussed in the 11 chapters on specific anatomic areas, which cover trauma in adults only. Also, the book has no coverage of the skull, face, or chest. Four other chapters include an opening chapter on imaging techniques, written mainly for the orthopedic surgeons, and chapters on fracture healing, posttraumatic infection, and stress fractures.

Each of the chapters on an anatomic area has more than just descriptions of fractures and dislocations. Topics include anatomy; positioning patients for radiography and other imaging techniques, including MR imaging, if appropriate; mechanisms of injury; classifications; treatment; and complications. Many chapters also contain quite a lot on arthrography, including indications, techniques, and findings. Arthroscopy is also presented. Thus, although this book professes to be a book on the radiology of bone trauma, it covers more than imaging of patients with acute trauma and is not unlike Weissman and Sledge's book in this regard. The nontrauma topics are mostly related to joints and arthrography and include such topics as capsulitis in the shoulder, snapping tendon syndrome in the hip, cartilage degeneration disorders, and pigmented villonodular synovitis.

I consider this an academically oriented book, providing more information than is required for quick consultation of a radiologic textbook in the emergency department. This material is to be read slowly and digested to get a detailed perspective of conditions, including results of published series. Many chapters have 300–400 references (although few are more recent than 1988).

The book has a few of the usual typographic errors and inverted figures (Fig. 4-138). At least one table (Table 4-6), correctly done in the first edition, has errors in the second edition. I find only two general faults with this book. First, most of the radiographs are darker than I like, and some are too small to show the intended abnormality. Second, it can be difficult to look up a topic in the index. For example, DISI (dorsal intercalated segment instability) is not under *D* in the index or in the chapter table of contents at the beginning of the chapter on the wrist. It is listed under "collapse deformity" in the index and appears in the anatomic section of the chapter. Similarly, impingement syndrome is found only under "subacromial spur." Many of the nontrauma conditions discussed are not listed in the index at all. Thus, it is difficult to use this as a reference book for other than straightforward traumatic injuries.

How does this book relate to the other books on the radiology of bone trauma, and who should buy it? This is clearly the most up-to-date and complete coverage of the topic with inclusion of the newer imaging techniques. This book and the book by Weissman and Sledge provide the best general orthopedic in-depth coverage. Roger's book is perhaps the easiest to read and the one probably used for quick reference in most emergency departments. For those interested in a more thorough understanding of orthopedic injuries, imaging, and treatments, this new edition of *Imaging of Orthopedic Trauma* is a must. It should be available wherever there are residents in radiology, orthopedics, or emergency medicine. General surgeons who deal with orthopedic injuries might also find this book useful. Finally, as intended by the editor, radiologists who wish to have a better understanding and communication with orthopedic surgeons and orthopedic surgeons who wish to know more about imaging will find this book useful.

Stanley P. Bohrer
Bowman Gray School of Medicine
Winston-Salem, NC 27103

The Cruciate Ligaments of the Knee: Correlation Between MR Appearance and Gross and Histologic Findings in Cadaveric Specimens

Juerg Hodler[1,2]
Parviz Haghighi[3]
Debra Trudell[1]
Donald Resnick[1]

OBJECTIVE. Using anatomic and histologic correlation, we investigated the reasons for differences in the MR signal intensity between the normal anterior and posterior cruciate ligaments and for the focally increased signal intensity within these ligaments occasionally found in elderly patients.

MATERIALS AND METHODS. The MR images of 18 anterior and 20 posterior cruciate ligaments obtained from cadavers (age at death, 56–88 years old; mean, 74 years) were evaluated blindly. Their overall signal intensity and focal regions of increased signal were noted. The findings then were correlated with corresponding anatomic and histologic sections.

RESULTS. The anterior cruciate ligament had greater signal intensity than did the posterior cruciate ligament in 15 of 18 knees and had comparable signal intensity in three knees. No histologic basis to explain the different MR appearances of the anterior and posterior cruciate ligaments was found. Rather, differences in macroscopic anatomy appeared to be the best explanation. In the posterior cruciate ligament, the fibers were parallel, whereas they were diverging and twisted in the anterior cruciate ligament, causing volume-averaging artifacts. A focal area of signal increase was found in 29 of the 38 ligaments. In 17 of these 29 ligaments, mucoid and/or eosinophilic degeneration was found that appeared to have caused the focal MR signal change. In nine ligaments without focally increased signal on the MR images, only one had histologic evidence of degeneration. The predictive value of an abnormal finding on MR was 59%, and the predictive value of a normal finding on MR was 89%. The relationship between increased signal on MR and histologic degeneration was statistically significant (χ^2 test, $p = .0126$).

CONCLUSION. The differences in the MR appearances of the anterior and posterior cruciate ligaments probably are due to differences in gross architecture. Increased MR signal within the cruciate ligaments occurring in elderly patients often can be attributed to degenerative changes.

AJR 159:357–360, August 1992

Received October 21, 1991; accepted after revision February 24, 1992.

This work was supported in part by Veterans Affairs grant SA 306, a grant from Ciba-Geigy Corp., and a grant from University Hospital, Zurich, Switzerland.

[1] Department of Radiology, Veterans Affairs Medical Center (114), 3350 La Jolla Village Dr., San Diego, CA 92161. Address reprint requests to D. Resnick.

[2] Present address: Department of Radiology, University Hospital, Raemistr. 100, CH-8091 Zurich, Switzerland.

[3] Department of Pathology, Veterans Affairs Medical Center, San Diego, CA 92161.

0361–803X/92/1592–0357
© American Roentgen Ray Society

The anterior cruciate ligament (ACL) consistently has a higher signal intensity than the posterior cruciate ligament (PCL) on MR images [1]. To find an explanation for this finding, we compared MR images of cadaveric knee joints with the corresponding anatomic sections and histologic findings.

In elderly patients, focally increased MR signal within the cruciate ligaments can occasionally be found. This same finding was visible in many of our cadaveric specimens and was also correlated with the corresponding histologic sections.

Materials and Methods

Twenty freshly frozen cadaveric knees (10 cadavers from persons 56–88 years old at the time of death; mean, 74 years) were examined by MR imaging after the specimens were thawed. T1-weighted, proton density–weighted, and T2-weighted spin-echo images were acquired. The technical factors for the MR examination included 500–600/20 (TR/TE) for T1-weighted images, 2000/20 for proton density–weighted images, and 2000/70 for T2-weighted

images. A matrix of 256 × 256 or 192 × 256, 16-cm field of view, 3-mm slice thickness, and 1-mm interslice gap were used. All sequences were acquired in the sagittal and coronal planes [2]. The first 10 knee specimens were sectioned in the sagittal plane and the last 10, in the coronal plane. In one specimen, the ACL was completely absent and in another it was completely torn, with only a small residual ligament visible. These two ligaments were excluded from further evaluation. Therefore, eight ACLs and 10 PCLs were examined in the sagittal plane, and 10 ACLs and 10 PCLs were examined in the coronal plane.

The MR images of the 20 knees were evaluated blindly by one of the authors without knowledge of the histologic findings. The overall signal intensity of ACLs and PCLs on T1- and T2-weighted images, the presence of focally increased signal intensity, and the internal pattern (e.g., the depiction and the course of single fascicles) were described. Those T1- and T2-weighted images that contained the largest part of the respective ligament were used for analysis. The anatomic sections then were photographed and prepared for histologic examination (fixation in 10% formalin, embedding in paraffin, and staining with hematoxylin and eosin). The histologic examination was performed by an experienced pathologist who did not know the MR findings or whether either an ACL or a PCL was being examined. Criteria used for the histologic examination were the extent and degree (mild, moderate, or severe) of degenerative changes (e.g., eosinophilic or mucoid degeneration), obvious differences in the fiber thickness of the connective tissue, the cellularity (normal or increased) of the ligament, and the presence or absence of interposed fat within the ligament. Ligamentous degeneration was defined as the presence of eosinophilic and/or mucoid degeneration of any degree. The MR imaging results then were compared with those derived from analysis of the gross anatomy and the histologic findings.

Results

On T1-weighted images, the signal intensity of the ACL was greater than that of the PCL in 13 knees, and the two ligaments had comparable signal intensity in five knees. On T2-weighted images, the ACL had more intense signal than the PCL in 15 knees, and the two ligaments had comparable signal in three knees.

Histologically, no specific finding correlated with these signal differences; fiber thickness and arrangement were identical in the ACL and PCL. Also, no differences were apparent in the size, form, and number of cell nuclei, with the exception of two PCLs and one ACL, in which the cellularity was slightly higher. This last finding was probably explained by accompanying degenerative changes in the ACL and in one of the two PCLs.

The internal architecture of the cruciate ligaments was only partially apparent on MR images. The failure to visualize individual fascicles with MR imaging presumably was related in part to the scarcity of slightly hyperintense fat and loose connective tissue between adjacent fascicles. Also, the diameter of the fascicles (250 μm to several millimeters) [3] was relatively small compared with a theoretical spatial resolution of 0.6 mm accomplished with the imaging parameters used in this study. However, in the distal fanned portion of the cruciate ligaments close to their osseous insertions, single fascicles were identified with significant frequency; these fascicles were more evident in the ACL than in the PCL on MR in 14 cases (seven sagittal and seven coronal), and they were equally apparent on MR in four cases (one sagittal and three coronal). More optimal MR visualization of individual fascicles corresponded to better identification of individual fascicles on anatomic inspection and/or to the presence of interfascicular fat on histologic examination; eight of 18 ACLs and only four of 20 PCLs showed interfascicular fat histologically.

On MR images, the PCL appeared as a homogeneous structure with parallel, well-delineated borders (Fig. 1). Conversely, the ACL had a more complex appearance, with a less homogeneous signal intensity and less well defined borders (Fig. 2). This appearance was more evident on sagittal than on coronal images. Also, anatomically, the PCL consisted mainly of parallel fascicles, whereas the fascicles of the ACL were more twisted, especially the posterior ones. Corre-

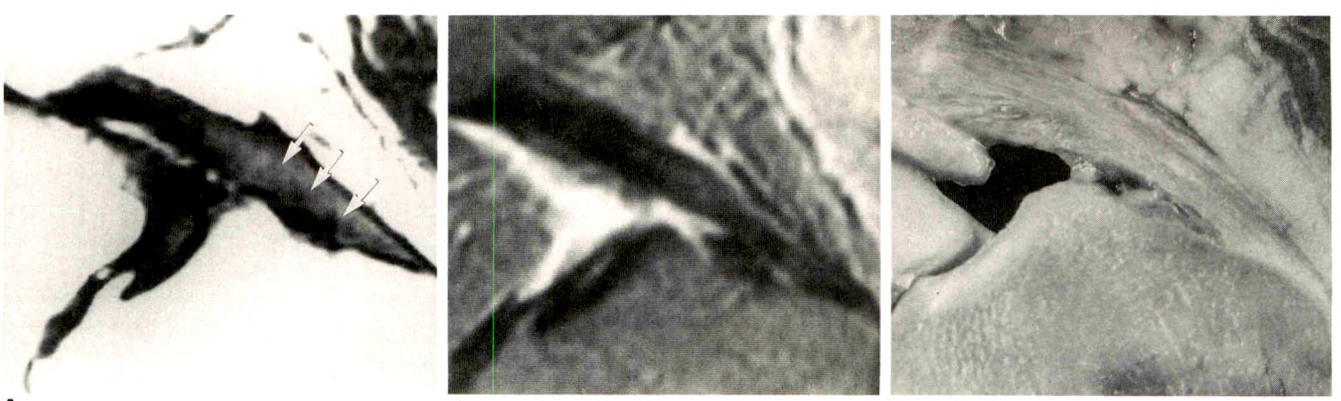


Fig. 1.—Eosinophilic degeneration of posterior cruciate ligament (PCL) in right knee of a 74-year-old woman.
A, Sagittal T1-weighted (500/20) MR image shows borders of PCL are well defined. Normal hypointensity is maintained proximally, with increased signal in middle and distal portions of ligament (*arrows*).
B, Sagittal T2-weighted (2000/70) MR image shows that signal changes appear less extensive than in *A*.
C, Anatomic section shows fibers are parallel to sagittal plane.

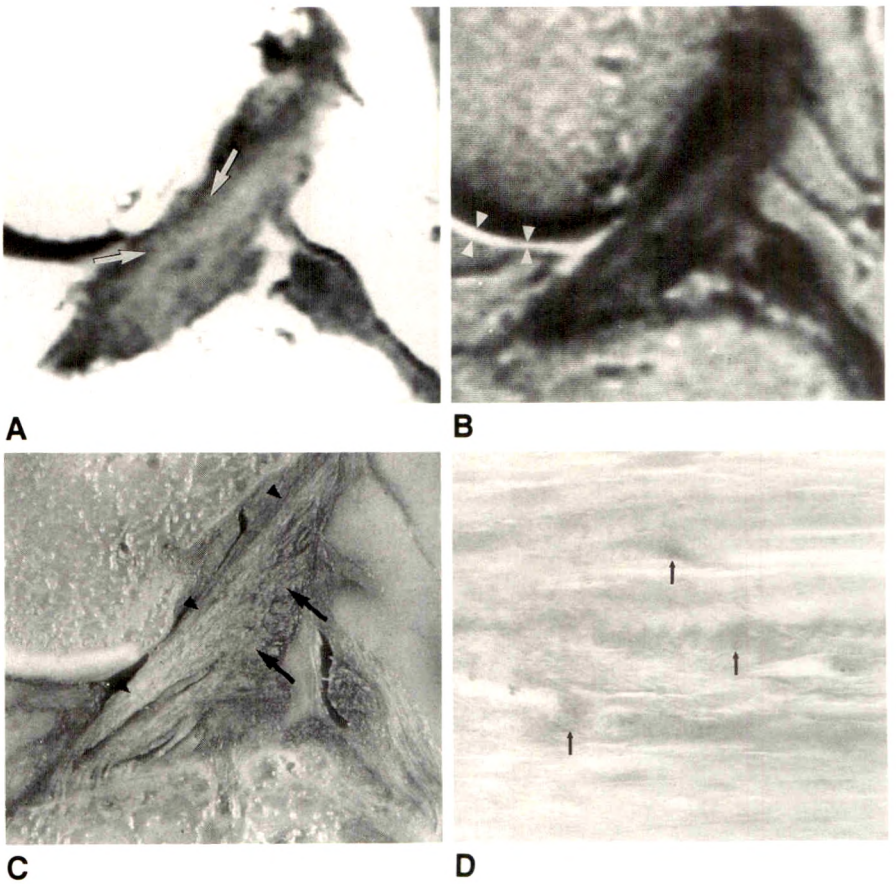


Fig. 2.—Eosinophilic degeneration of anterior cruciate ligament (ACL) in right knee of an 88-year-old man.

***A*, Sagittal T1-weighted (500/20) MR image shows sharply demarcated anterior border and irregular posterior border. Normal hypointensity of anterior portion of ligament is maintained proximally and distally, with increased signal of intermediate part (*arrows*).**

***B*, Sagittal T2-weighted (2000/70) MR image shows less extensive signal than in *A*. Increased signal within ACL is not as intense as that of joint effusion, which is visible anterior to ACL (*arrowheads*).**

***C*, Anatomic section. Whereas anterior fibers are parallel to imaging plane (*arrowheads*), posterior fibers have a less steep course and are more obliquely oriented with regard to sagittal plane (*arrows*).**

***D*, Photomicrograph shows extensive eosinophilic degeneration (*arrows*).**

spondingly, the posterior border of the ACL was not well delineated on all eight sagittal images, whereas the anterior border was well delineated on four of eight sagittal images. Both the anterior and posterior borders of the PCL were well delineated on the sagittal images in all 10 PCLs.

Focal regions of increased signal, which appeared to be more extensive on T1-weighted images than on T2-weighted images, were found in 29 ligaments (14 ACLs and 15 PCLs). In 17 of these 29 ligaments, the MR findings could be explained by eosinophilic degeneration alone (six cases, Figs. 1 and 2), by degeneration that was both eosinophilic and mucoid (seven cases), or by mucoid degeneration alone (four cases) (Fig. 3). Twelve of the 29 ligaments with focal signal changes did not show histologic signs of degeneration, however. Of the remaining nine ligaments with no focal signal changes, one had histologic evidence of degeneration that consisted of focal eosinophilic degeneration alone. The other eight ligaments were normal histologically. The predictive value of normal MR findings was 89%, and the predictive value of abnormal MR findings was 59%. A χ^2 test showed a statistically significant relationship between histologic evidence of degeneration and MR evidence of increased signal ($p = .0126$). The common odds ratio was 11.3 (95% confidence interval = 1.18, 532), indicating that a ligament with focally increased signal on MR is 11.3 times more likely to have histologic degeneration than a ligament with no focally increased signal on MR.

Discussion

Some of the differences in signal intensity that exist between the ACL and the PCL are explained by the oblique course of the ACL with regard to the sagittal plane. The diagnostic value of MR imaging can be improved by altering the imaging plane [4]; the patient's legs either are allowed to rotate into a comfortable position of slight external rotation or a sagittal imaging plane with appropriate anteromedial to posterolateral angulation is chosen on the basis of an axial image. Even when these modifications in MR protocol are used, the ACL has a different appearance than the PCL.

Anatomic studies [3, 5] and the present correlative study indicate that the differences in appearance probably are related to differences in ligament architecture. Although the PCL fascicles have a parallel course, the anatomy of the ACL is more complicated. The ACL has a constant anteromedial bundle, and the remainder of the ligament is more twisted. The amount of twisting depends on the degree of knee flexion [5]. Although investigators disagree on the anatomic characteristics of the ACL, the presence of distinct functional bands [6] seems to be generally accepted [3]. Some of these bands are likely to be obliquely oriented, and therefore cause volume-averaging artifacts during the MR examination. Moreover, the ACL is slightly thinner at its midportion than the PCL is (11.1 vs 13.4 mm [5]), a fact that would increase the probability of volume averaging on MR imaging of the ACL.

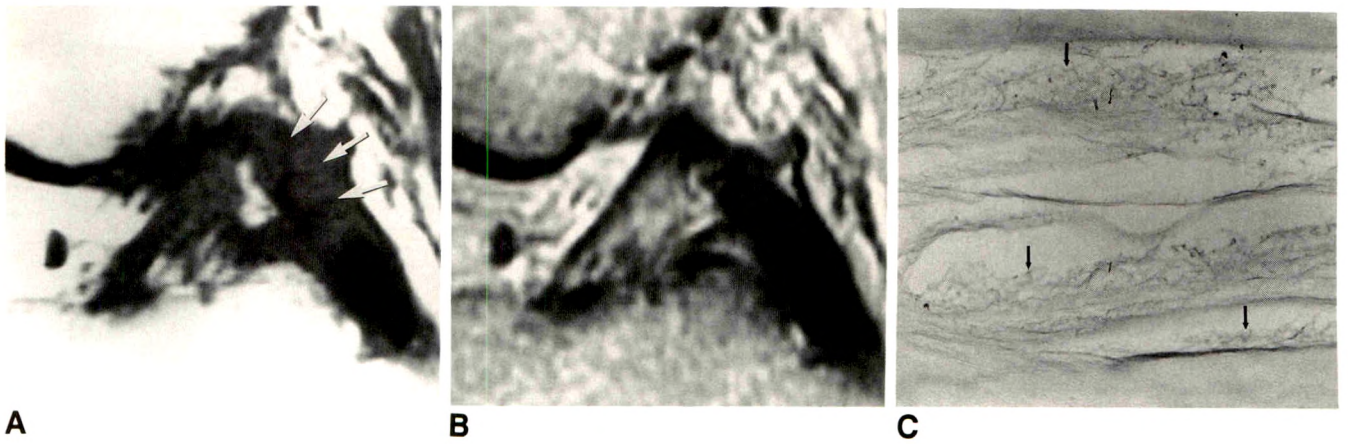


Fig. 3.—Mucoid degeneration of posterior cruciate ligament (PCL) in left knee of a 71-year-old man.
***A*, Sagittal T1-weighted (500/20) MR image shows increased signal intensity, mainly in proximal portion of PCL (*arrows*).**
***B*, Sagittal T2-weighted (2000/70) MR image shows a subtle increase in signal intensity in PCL.**
***C*, Photomicrograph shows extensive mucoid degeneration (*arrows*).**

The fascicles of the ACL have a considerably divergent course distally, and their attachment to the tibial plateau has an average anteroposterior diameter of 30 mm. The fat interposed between the diverging fascicles explains the increased visibility of single fascicles distally.

No significant histologic differences between the ACL and PCL have been found either in this study or by other authors [7, 8]. Both ligaments consist mainly of dense fibrous tissue and therefore should appear hypointense on all MR images. In about 60% of cases with focal signal changes, degenerative findings similar to those described in the rotator cuff [9] and in the menisci of the knee [10] were found.

MR imaging had a high negative predictive value in the analysis of the cruciate ligaments, as only one ligament showed abnormal histologic findings when MR images were interpreted as normal, and the degenerative changes in this ligament were mild. Possible explanations for the low positive predictive value include autolysis, changes that occur during the thawing of the specimen before the MR examination (e.g., diffusion of tissue fluid into the ligament), or architectural alterations due to reduced muscle tension. It is feasible that the positive predictive value of MR imaging in living patients would be improved if such artifacts could be eliminated. Moreover, the radiologist may have overestimated focally increased signal, mainly because of volume-averaging artifacts. Also, the results probably could have been improved by the use of oblique sagittal images, eliminating in part volume-averaging effects.

Another explanation influencing the relationship between MR findings and microscopic abnormalities may be the conservative evaluation of the histologic findings by the pathologist, who wanted to avoid false-positive diagnoses of eosinophilic or mucoid degeneration. Eosinophilic degeneration may be simulated by irregular staining with eosin, and the cystic form of mucoid degeneration may be simulated by the presence of gaps caused by the sectioning process. The clinical importance of degeneration of the cruciate ligaments is probably limited, but degeneration could cause MR abnormalities that simulate those of tears. Indeed, the focal regions of higher signal in a cruciate ligament with intact borders and a normal course could lead to a false diagnosis of a partial tear.

We conclude that the different MR appearances of the ACL and PCL cannot be explained histologically. Variations in macroscopic anatomy leading to volume-averaging artifacts appear to explain these signal differences best. In elderly patients, degenerative changes that are visible on MR images frequently occur in the cruciate ligaments.

ACKNOWLEDGMENT

We thank Sandra J. Underhill for preparing the histologic sections.

REFERENCES

1. Reicher MA, Rauschning W, Gold RH, Bassett LW, Lufkin RB, Glenn W. High resolution MRI of the knee joint: normal anatomy. *AJR* **1985**; 145:895–902
2. Hodler J, Berthiaume M-J, Schweitzer ME, Resnick D. Focal changes of the articular cartilage in the femorotibial joint: magnetic resonance (MR)-anatomic correlation and blinded analysis (abstr). *Radiology* **1991**; 181(P):301
3. Burks RT. Gross anatomy. In: Dale DM, Akeson WH, O'Connor JJ, eds. *Knee ligaments*. New York: Raven, **1990**:59–76
4. Mink JH, Levy T, Crues JV. Tears of the anterior cruciate ligament and menisci of the knee: MR imaging evaluation. *Radiology* **1988**; 167:769–774
5. Girgis FG, Marshall JL, al Monajem ARS. The cruciate ligaments of the knee joint. *Clin Orthop* **1975**;106:216–231
6. Arnoczky SP, Warren RF. Anatomy of the cruciate ligaments. In: Feagin JA, ed. *The crucial ligaments*. New York: Churchill Livingstone, **1988**: 179–195
7. Amiel D, Frank C, Harwood F, Fronek J, Akeson W. Tendons and ligaments: a morphological and biochemical comparison. *J Orthop Res* **1984**; 1:257–265
8. Yao L, Sherwood JW. Ex-vivo MR imaging of the cruciate ligaments. *Comput Med Imaging Graphics* **1991**;15:27–30
9. Kjellin I, Ho C, Haghighi P, et al. MR alterations of the rotator cuff and anterior glenoid labrum: correlation with histopathology (abstr). *Radiology* **1990**;177(P):103
10. Stoller DW, Martin C, Crues JV, Kaplan L, Mink JH. Meniscal tears: pathologic correlation with MR imaging. *Radiology* **1987**;163:731–735

Pictorial Essay

Knee Effusion: Normal Distribution of Fluid

Mark E. Schweitzer,[1] Andreas Falk,[2] Dean Berthoty,[2] Michael Mitchell,[2] and Donald Resnick[2]

Although visualization of articular fluid on MR images of the knee is common, no specific MR criteria that enable assessment of the quantity of the effusion have been established. We performed MR of three cadaveric knee specimens after the instillation of increasingly large volumes of fluid and studied the distribution of the fluid. When 4 ml of fluid was injected, the anteroposterior diameter of the suprapatellar recess was 4 mm on midline sagittal MR images and 10.0–12.5 mm on lateral sagittal MR images, corresponding to the usual routine radiographic criteria for a knee effusion.

Materials and Methods

Knee specimens from three frozen cadavers were obtained by sectioning with a band saw at the levels of the midportion of the femur and the midportions of the tibia and fibula. Routine radiographs were obtained to exclude the presence of significant abnormalities or joint fluid. The specimens subsequently were frozen at −20°C for 12 hr. Before MR imaging, the knees were thawed and heated to approximately 37°C.

After fluoroscopic localization, a 19-gauge needle was inserted into the suprapatellar recess. While the specimen was being rotated, we tried several times to aspirate any joint fluid that was present in order to ensure a "dry" articulation before the instillation of fluid, although little fluid could be aspirated. The knee was progressively distended by using a dilute solution of gadopentetate dimeglumine (1:250, gadopentetate dimeglumine to normal saline). In each cadaveric specimen, MR images were obtained after volumes of 1, 3, 4, 15, and 20 ml had been injected.

The knees were placed in the supine position with 15° of external rotation. Each specimen was imaged with a 1.5-T unit (Signa, General Electric Medical Systems, Milwaukee, WI) in the sagittal plane. Images were obtained with a 14-cm field of view, a 256 × 192 matrix, and two signal acquisitions. The spin-echo technique, 600/20 (TR/TE), was used with a slice thickness of 4 mm and a 1-mm interslice gap.

Two radiologists simultaneously evaluated the MR images and recorded the precise location of the fluid by consensus. In addition, the widest anteroposterior diameter of the suprapatellar recess and the anteroposterior diameter of the suprapatellar recess on a midline image was recorded. The radiologists knew the amount of fluid injected.

Results

Distribution of fluid was nearly identical in the three cadaveric specimens. After the introduction of 1 ml of gadopentetate dimeglumine, MR imaging in each cadaveric knee showed fluid that was barely visible collecting between the femoral condyles and Hoffa's fat pad (Fig. 1). In addition, a small triangular collection of fluid was seen in a recess above the medial meniscus in two of the three knees.

With 3 ml of gadopentetate dimeglumine, fluid consistently accumulated in the suprapatellar recess. The layer of fluid between the condyles and Hoffa's fat pad thickened to approximately 2 mm in the sagittal plane. A small amount of fluid was still noted in the posterior meniscal recesses (greater medially than laterally), and a small amount of fluid was seen posterior and medial to the posterior cruciate ligament.

With 4 ml of fluid, the widest aspect of the suprapatellar recess, the lateral aspect, was 10.0–12.5 mm (Fig. 2A). On

Received December 27, 1991; accepted after revision February 24, 1992.
This work was supported in part by Veterans Affairs grant SA 306.
[1] Department of Radiology, Jefferson Medical College of Thomas Jefferson University, 132 S. 10th St., 1096A Main, Philadelphia, PA 19107. Address reprint requests to M. E. Schweitzer.
[2] Department of Radiology, Department of Veterans Affairs Medical Center, 3350 La Jolla Village Dr., San Diego, CA 92161.

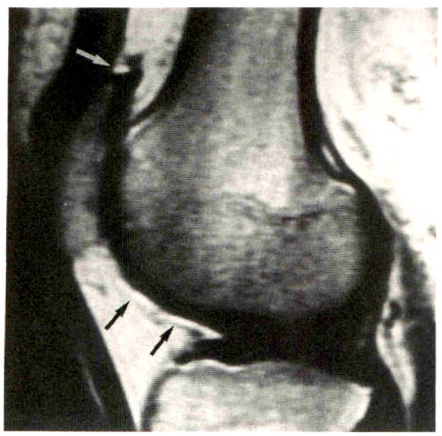
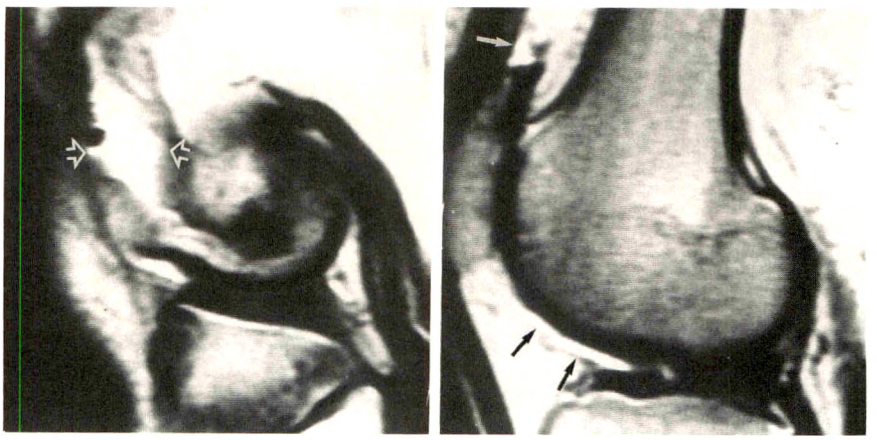


Fig. 1.—Sagittal MR image (600/20) obtained after instillation of 1 ml of dilute gadopentetate dimeglumine into cadaveric knee shows small amount of fluid adjacent to femoral condyles (*black arrows*) and a tiny amount of fluid in suprapatellar recess (*white arrow*).

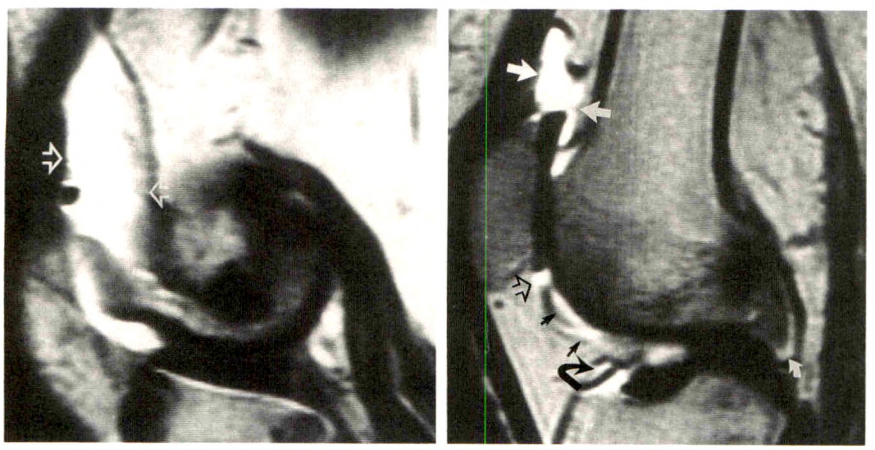


A B

Fig. 2.—Sagittal MR images (600/20) of lateral aspect of cadaveric knee after instillation of 4 ml of dilute gadopentetate dimeglumine.

A, Anteroposterior measurement of widest aspect of suprapatellar recess is 11 mm (*arrows*). Also seen is signal void from injection needle.

B, On midline image, fluid layers about femoral condyles (*black arrows*), in suprapatellar recess (*white arrow*), and in recesses about menisci. Midline width of suprapatellar recess is 4 mm in this specimen.



A B

Fig. 3.—Sagittal MR images (600/20) obtained after instillation of 15 ml of dilute gadopentetate dimeglumine into cadaveric knee.

A, Suprapatellar recess measures 18 mm at its widest aspect (*arrows*).

B, On midline image, increased fluid is seen in suprapatellar recess that is 10 mm in anteroposterior dimension (*straight white arrows*). Small amounts of gadopentetate dimeglumine are seen distending superior vertical cleft in Hoffa's fat pad (*open arrow*), horizontally oriented posterior cleft (*curved black arrow*), between femoral condyle and Hoffa's fat pad (*straight solid black arrows*), and posteriorly about cruciate ligaments (*curved white arrow*).

midline images, the anteroposterior diameter of this fluid averaged around 4 mm (Fig. 2B).

With 15 ml of fluid in the joint, the anteroposterior dimension of the suprapatellar recess was 16–20 mm at its widest aspect (Fig. 3A) and 9.5–15.5 mm at the level of the patellar tendon (Fig. 3B). Fluid was seen between the cartilage of the femoral condyles and Hoffa's fat pad; its dimension averaged about 3 mm in this region. Fluid also was seen in two clefts within this pad. Greater volumes of fluid were seen in the posterior meniscal recesses, and fluid was seen within the popliteal tendon sheath.

The widest aspect of the suprapatellar recess was 18–20 mm with 20 ml of injected fluid (Fig. 4A). The measurement was 11 mm at the level of the quadriceps tendon in all specimens (Fig. 4B). The popliteal tendon sheath was distended and the fluid between the condyles and the fat pad nearly paralleled the cortex of the femoral condyles, although it was slightly convex anteriorly. The widest portion of this fluid was just anterior to the lateral condylar notch. The junction between the fluid and the fat pads was smooth and well marginated.

Two synovial-lined clefts were evident within Hoffa's fat pad. One was located superiorly just posterior to the inferior portion of the patella and had a vertical orientation. The other cleft was anterior to the anterior horns of the menisci and had a horizontal orientation. With large effusions, these clefts distended with fluid and became cigar shaped but retained their characteristic location and orientation (Figs. 3B and 4B). The vertical posterior cleft distended first and to a greater degree. The superior cleft initially distended with 15 ml of fluid.

Discussion

Although articular fluid is commonly recognized on MR images of the knee [1], to our knowledge, the distribution of

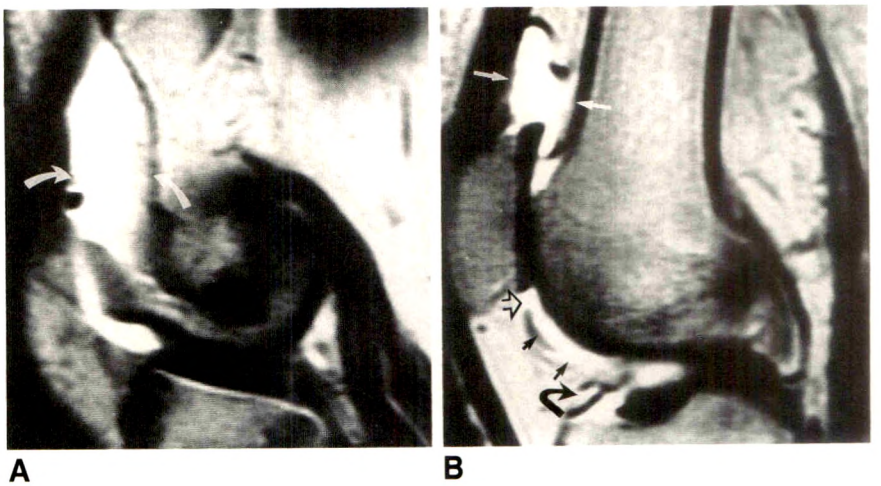


Fig. 4.—Sagittal MR images (600/20) of lateral aspect of knee obtained after injection of 20 ml of dilute gadopentetate dimeglumine into cadaveric knee.

***A*, Suprapatellar recess measures 19 mm at its widest aspect (*arrows*).**

***B*, On midline image, suprapatellar recess measures 11 mm (*white arrows*). Note that Hoffa's fat pad is displaced in anteroinferior direction, and contour of fluid parallels femoral condyles (*straight solid black arrows*). Distension of vertical superior (*open arrow*) and horizontal posterior (*curved arrow*) clefts in Hoffa's fat pad is seen.**

increasing amounts of joint fluid in the knee has not been previously studied. With MR imaging in the sagittal plane, a volume of 1 ml of fluid generally was visible, lying adjacent to the condyles of the femur. The classic plain film radiographic criterion of a joint effusion, a 10-mm soft-tissue density in the suprapatellar recess [2, 3], was seen lateral of midline on sagittal MR images of supine cadaveric knees after 4 ml of fluid had been injected. With this volume of injected fluid, the anteroposterior diameter of the midline suprapatellar recess averaged about 4 mm. This measurement closely corresponds to the 5-mm fat pad separation sign described by Hall [2], which is the distance between prefemoral and quadriceps fat pads as measured on lateral knee radiographs. This volume of fluid also corresponds to the clinical definition of a significant effusion [4]. Although the radiographs in the series of Hall were obtained with mild flexion, fluid should not be significantly displaced because this is a relaxed position. It should be noted that fluid distribution in the lateral-most aspect of the suprapatellar recess will also depend on rotation. To closely simulate the conditions of clinical imaging, we placed the cadaveric knees in slight external rotation.

Because this was a preliminary study of fluid distribution in the knee joint, we were aware of some limitations in the design of the study. First, distribution of fluid in cadaveric knees may not simulate distribution of fluid in living patients. Second, MR may be more sensitive to dilute gadopentetate dimeglumine used to simulate knee effusions than to small volumes of articular fluid found in clinical practice. Third, larger numbers of specimens would be necessary to account for variability in fluid accumulation. Furthermore, despite our vigorous attempts to remove all fluid before the MR study, small amounts may have been present. Although only sagittal images were examined, we think this is the most useful plane for the detection and localization of fluid in the knee.

REFERENCES

1. Beltran J, Noto AM, Herma LJ, et al. Joint effusions: MR imaging. *Radiology* **1986**;158:133–137
2. Hall FM. Radiographic diagnosis and accuracy in knee joint effusions. *Radiology* **1975**;115:49–54
3. Engedstad BL, Friedman EM, Murphy WA. Diagnosis of joint effusion on lateral and axial projections of the knee. *Invest Radiol* **1981**;3:188–190
4. McCarthy DL. Synovial fluid. In: McCarthy OJ, ed. *Arthritis and allied conditions*, 11th ed. Philadelphia: Lea & Febiger, **1989**:70–71

Cerebral Angiography and Egas Moniz

T. Doby[1]

In the early 1920s, Egas Moniz, professor of neurology in Lisbon, Portugal, undertook a task no one really considered possible: the radiographic imaging of the brain in a living human subject. At the time, the only approach to visualizing cerebral abnormalities was Dandy's method of introducing air into the ventricular system. But what a crude method it was. What agony the patient had to endure, strapped to a chair, put in awkward positions, even turned upside down—yet the brain itself could never be seen, only the distorted ventricles. Moniz's supposition was that if he could introduce radiopaque material that would concentrate in the brain, the brain would opacify and be visualized on radiographs.

Bromine, atomic weight 80, had promise of showing up on X-ray film. Because bromides were used as sedatives, it was reasonable to believe that they accumulated in the brain. Moniz gave patients large doses of bromides orally, but the brain was not visualized on radiographs. He then decided to inject the drug into the carotid artery in an effort to outline the artery. The patients had headaches but tolerated the injection. However, the films remained blank. He then injected bromides in dogs. In the 15th dog, ramifications of the cerebral arteries were faintly detected on the films, and Moniz described this as a day of "great enjoyment" [1]; however, the human goal was still distant.

To study the cerebral vasculature, Moniz introduced bromides into the carotid and vertebral arteries of corpses. However, autopsy material was not available to him in sufficient supply to allow him to pursue his studies. The Anatomical Institute, which could have provided the necessary specimens, did not have X-ray facilities. Consequently, he arranged to have decapitated heads transferred in boxes from the Institute to his somewhat distant laboratory in another district of Lisbon by taxicab. The vessels were injected under his supervision, films taken, and then the gruesome cargo sent back to the Anatomical Institute.

Moniz continued to inject bromides into the internal carotid artery of patients, and in the sixth patient the intracranial vessels were faintly visualized for the first time. However, 8 hr later, carotid thrombosis developed and the patient died. Moniz was desperate. He summoned Almeida Lima (his chief associate and later professor of neurosurgery) and his full staff to discuss whether they should continue the investigations. After a long debate, the consensus was to go on, but with the use of iodides rather than bromides. Their thinking was that since iodine has an atomic weight of 127, iodides had a better chance of being seen on films. Also, they took care not to dilute the 5 ml of 22% NaI solution with blood during the injection. They could take only three films in sequence, hand pulled, and the injections were made through cutdown.

In June, 1927, in their third case, portions of the internal carotid artery in the sylvian fissure were distinctly seen. Moniz was triumphant, and he left immediately for a meeting of the Society of Neurology in Paris, where he had done his postgraduate training. His work was greeted with great enthusiasm, and he was invited to present his method a week later in the French Academy of Medicine. Moniz spent the following years evaluating the procedure and supporting the findings with surgical or autopsy proof. Working day and night, he wrote 61 papers in the 4 years between 1927 and 1931 [2]. His first book on cerebral angiography was published in Paris in 1931 [3] with a preface by Babinsky, one of the prestigious neurologists of the day, in which he praised Moniz for his courage, daring, and enthusiasm. In 1949, Moniz received the Nobel prize, not for his work in angiography but for the introduction of frontal lobotomy [4], a procedure that was subsequently discarded.

Contrast materials have changed since Moniz's first intraarterial injections. Modern cassette changers and subtraction techniques are used now, and a number of other advances have been made. Recently, the availability of CT and MR imaging have greatly reduced the need for cerebral angiography, yet it remains indispensable in certain circumstances.

Among Moniz's other achievements, he performed the first pulmonary angiography through a cardiac catheter in 1931 [5], and he encouraged his countryman dos Santos to undertake extensive study of peripheral arteriography [1, 6]. Because his hands were deformed by severe gout, Moniz never made a single injection; yet with his determination and his superior intelligence, he helped launch a new radiologic discipline.

REFERENCES

1. Moniz E. *Confidencias de um investigador cientifico*. Lisboa: Atica, **1949**
2. Moniz E. *Bibliografia cientifica e literaria*. Lisboa: Ediçao do Centro de Estudos Egas Moniz, **1963**
3. Moniz E. *Diagnostic des tumeurs cérébrals et épreuve de l'encephalographie artérielle*. Paris: Masson, **1931**
4. Nobel Foundation. *Nobel lectures in physiology and medicine 1942–1962*. Amsterdam: Elsevier, **1964**
5. Moniz E, de Carvalho L, Almeida Lima P. Angiopneumographie. *Presse Med* **1931**;39:996–999
6. Doby T. *Development of angiography and cardiovascular catheterization*. Preface by H. L. Abrams, Littleton, MA: Publishing Sciences Group, **1976**

In preparation for the 1995 centennial celebration of the discovery of the X-ray, the *AJR* will periodically publish History Pages, which deal with events leading up to and occurring around the time of the discovery.

[1] 22 Cottage Lane, Cape Elizabeth, ME 04107. Address reprint requests to T. Doby.

AJR **159:364, August 1992** 0361–803X/92/1592–0364 © American Roentgen Ray Society

Value of Acute-Phase Angiography in the Detection of Vascular Injuries Caused by Gunshot Wounds to the Head: Analysis of 12 Cases

J. R. Jinkins[1]
M. R. Dadsetan[1]
R. N. Sener[1]
S. Desai[1]
R. G. Williams[2]

A study of the angiographic findings in consecutive civilian patients with cranial gunshot wounds examined in the acute stage has not been done. Most prior clinical studies have evaluated the findings in survivors in the subacute or chronic stages and have often been of war-time casualties. We determined the clinicoradiologic features of six cases of posttraumatic intracranial aneurysm, vascular occlusion, or arteriovenous fistula caused by penetrating missiles among 12 civilian patients who were examined in the acute posttraumatic stage (within 48 hr of injury) during a 1-year period. Three internal carotid/vertebral artery aneurysms, one external carotid artery aneurysm, one combined aneurysm/arteriovenous fistula of the vertebrobasilar circulation, and one cerebral venous occlusion were identified.

The 50% overall prevalence of major vascular lesions in this series of civilian patients with penetrating missile injuries examined in the acute stage suggests these injuries are more common than previously suspected. It may indicate that selective cerebral angiography should be considered in the evaluation of the cranial vascular system of such persons.

AJR 159:365–368, August 1992

Cranial vascular lesions after nonpenetrating head injury, including aneurysms and arteriovenous fistulas, occur rarely. Still rarer are reports of such vascular pathologic changes after injuries by penetrating missiles. However, literature reports largely involve radiologic studies of surviving patients examined in the subacute or even chronic clinical phase. The diagnosis is often delayed or overlooked as the lesion is obscured by the presence of an accompanying hemorrhagic intraparenchymal contusion. With the increasing reliance on CT to supplant cerebral angiography for evaluation of head trauma, these vascular lesions are even more likely to escape detection. Such conditions should be suspected in any patient with a gunshot wound who, after an initial stable period, undergoes sudden clinical deterioration within the first days or weeks after the injury. We report the findings in 12 patients injured by penetrating missiles who were examined angiographically in the acute phase.

Subjects and Methods

During a 1-year period, all patients who had acute gunshot wounds to the head were examined angiographically. All patients (n = 12) had transfemoral selective cerebral angiography within 48 hr of the injury. The type of projectile, trajectory of the bullet, presence or absence of a vascular lesion and its location, and Glasgow coma score on presentation were recorded for each patient. In addition, the treatment, if any, and the clinical outcome at 1 month were also tabulated.

Results

In five (42%) of the 12 patients with acute penetrating gunshot wounds to the head, aneurysms were seen on angiography. Four involved the carotid or vertebral

Received November 13, 1991; accepted after revision February 18, 1992.

[1] Department of Radiology, Neuroradiology Section, The University of Texas Health Science Center at San Antonio, 7703 F. Curl Dr., San Antonio, TX 78284-7800. Address reprint requests to J. R. Jinkins.

[2] Department of Radiology, Methodist Hospital of San Antonio, 7750 F. Curl Dr., San Antonio, TX 78229.

0361–803X/92/1592–0365
© American Roentgen Ray Society

vessels, and one was an aneurysm of the middle meningeal artery (Figs. 1–4). In one patient the traumatic aneurysm was associated with an arteriovenous fistula (Fig. 5). A sixth patient had traumatic occlusion of the transverse venous sinus and internal jugular vein (Fig. 6). Thus, the prevalence of major vascular injuries was 50%. Data on these patients are summarized in Table 1.

Discussion

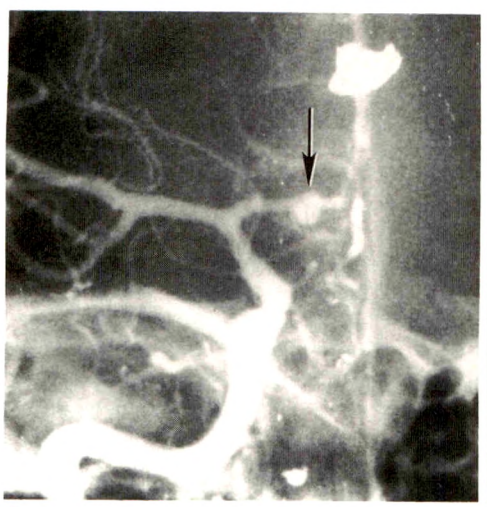
It has been estimated that three of four patients with gunshot wounds to the head survive [1–3]. In the present series, 50% of patients with gunshot wounds had traumatic vascular abnormalities. In view of the approximately 16,500 civilian deaths in the United States that occur each year from gunshot wounds to the cranium, it is conceivable that intracranial vascular injuries may contribute to morbidity or mortality in a significant percentage of these patients.

Traumatic cranial aneurysms, which are responsible for less than 1% of all carotid-vertebral intracranial aneurysms, may be caused by penetrating or nonpenetrating trauma. Nonpenetrating trauma accounts for about two thirds of the reported cases of aneurysm; approximately one third are due to penetrating injuries by missiles and other objects [4–12]. Few or no reports of external carotid aneurysms, intracranial arteriovenous fistulas, or cranial venous occlusions due to penetrating missiles such as those described in this report (Figs. 4–6) could be found in previous reports [12].

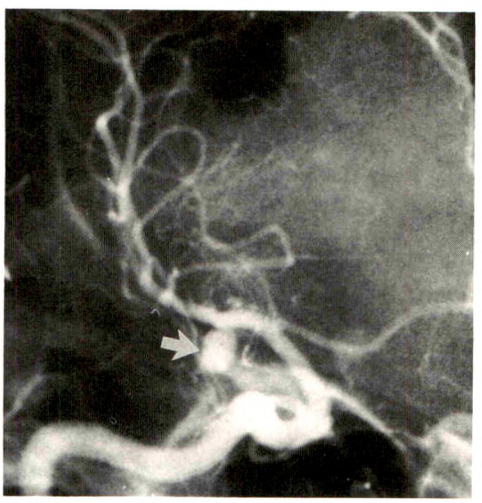
Traumatic intracranial aneurysms due to gunshot wounds typically occur along the main trunks of vessels in the middle or anterior cerebral artery territories. Aneurysms of the vertebrobasilar circulation are less common. Most of these internal carotid/vertebral circulation aneurysms are located at sites other than branching points [3, 6, 12, 13].

The majority of traumatic cranial aneurysms are false aneurysms, although true and mixed aneurysms sometimes occur [2–4, 12]. False aneurysms form by complete disruption of the normal arterial wall, periarterial hematoma accumulation, and cavitation. The resultant aneurysm and clot may come into contact with CSF, which potentially can accelerate autolysis and contribute to delayed intracerebral hemorrhage [4, 10, 14–16].

Early diagnosis is important because a 50% mortality rate is associated with traumatic aneurysms that subsequently rupture [17]. CT can detect a hematoma; however, the only reliable method for diagnosing a traumatic aneurysm is selective cerebral angiography [4, 16–21]. According to previous reports, the interval between the initial traumatic episode and



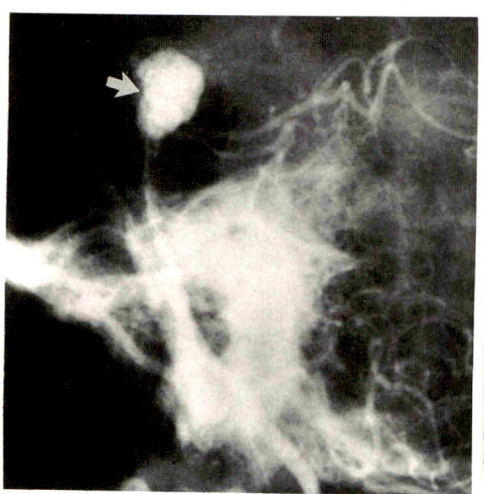
1



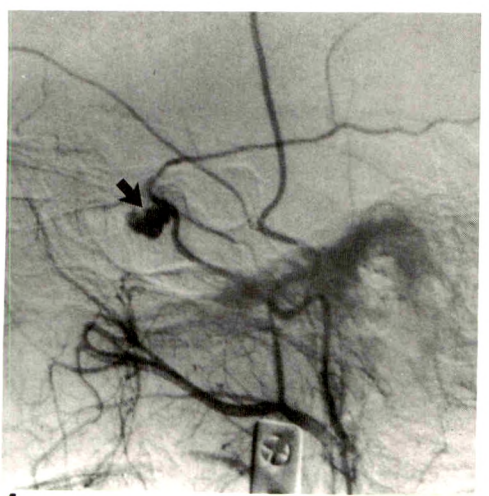
2

Fig. 1.—Right internal carotid angiogram shows traumatic aneurysm (*arrow*) of A1 segment of right anterior cerebral artery in 13-year-old boy.

Fig. 2.—Right internal carotid angiogram shows traumatic aneurysm (*arrow*) of middle cerebral artery in 45-year-old man.



3



4

Fig. 3.—Left vertebral angiogram shows large traumatic aneurysm (*arrow*) of basilar artery in 40-year-old man.

Fig. 4.—Lateral view from left external carotid angiogram shows irregular filling of traumatic aneurysm (*arrow*) from middle meningeal artery in 35-year-old man.

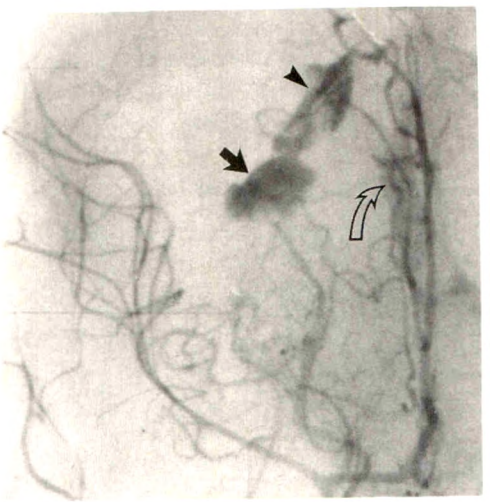


Fig. 5.—Anteroposterior view from right carotid angiogram shows traumatic aneurysm (*solid arrow*) of posterior cerebral artery, arteriovenous fistula (*arrowhead*), and resultant early faint filling of superior sagittal sinus (*open arrow*) in 25-year-old man.

5

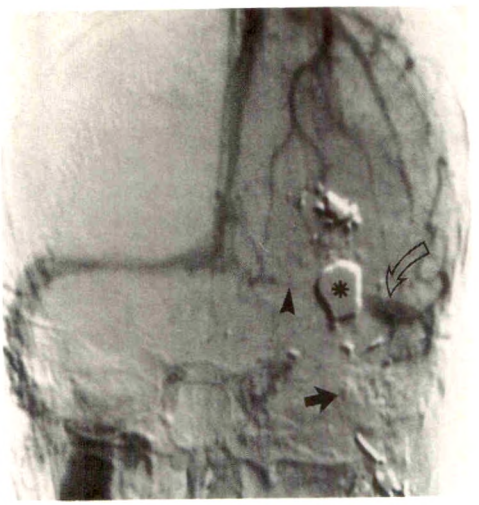


Fig. 6.—Anteroposterior view of venous phase from carotid angiogram shows complete transection (*solid arrow*) of left internal jugular vein along track of bullet in 56-year-old man. Nonopacification of proximal left transverse venous sinus (*arrowhead*) and stagnation distally (*open arrow*) are due to proximal compression by a large bullet fragment (*asterisk*).

6

the late rupture of the aneurysm ranges from 5 days to 10 years; however, more than 50% of the ruptures occur within 3 weeks after the primary injury [4, 12, 22, 23]. Rarely, the initial cerebral arteriogram may appear normal, and the aneurysm is detected only on follow-up examination [17]. More commonly, serial angiography may reveal an increase, a decrease, or even a spontaneous regression of a traumatic aneurysm [4, 6, 10, 14, 18].

Several reports providing data on the formation of intracranial aneurysms caused by penetrating brain injuries during war time give different results. For instance, during the Vietnam conflict, only two cases of aneurysm were noted among 2187 casualties from penetrating head trauma primarily due to gunshot wounds [7]. However, that finding was not the result of a systematic angiographic search. In contrast to this, recent articles on injuries from the Iran-Iraq War and the ongoing Lebanese conflict have reported a slightly increased frequency of intracranial aneurysms associated with primary missile and secondary shrapnel injuries [2, 17, 22, 23]. In a prospective study of the cerebral angiographic findings in 233 patients who sustained missile head wounds during the Iran-Iraq War, Aarabi [17] found that the prevalence of intracranial aneurysms was still only around 4%. In his series, however, angiography was performed at an average of 16.8 days after the injury (median, 15; range, 1–76 days). In another large war-time series [23], the average interval between the injury and angiography was 19.5 days.

The overall prevalence of aneurysms of 42% in our series seems to indicate a higher frequency of cranial aneurysms in this civilian population. One explanation may be that the reported frequency was falsely low in some of the previous reports because of the circumstantial absence of adequate angiographic evaluation. However, this cannot be the reason for the 10-fold difference in occurrence rates between the prospective angiographic study of Aarabi [17] and our study. There are inherent differences between the size, velocity, and jacketing of missiles used in war and those found in civilian situations (e.g., penetrating shrapnel is included in studies of war injuries, but not typically in civilian series) [24, 25]. Thus, the type of trauma incurred in war is likely to be somewhat different from that caused by most missile injuries among civilians. Another explanation is that in war time, many patients with traumatic vascular injuries may not survive long enough to allow proper angiographic examination. In this circumstance, such lesions are likely to be missed on clinical studies when radiologic studies are excluded from the evaluation; thus, the reported rate of occurrence will be falsely low. In civilian populations, however, it is probable that high-technology diagnostic care (e.g., selective angiography) may be offered sooner and more often. The civilian situation, therefore, may represent a more accurate rate of occurrence of traumatic vascular lesions caused by cranial gunshot wounds. It should be recognized, however, that an element of error could exist because of the small number of cases evaluated in our study, and because of errors or differences in the selection of patients.

The appropriate selection of patients for angiographic examination after cranial gunshot wounds is an important consideration. Some patients (e.g., those with brain death) may not substantially benefit clinically from such studies. The risks and benefits of selective cerebral angiography in this setting have not been clarified in the present study and therefore require further elaboration. Our series simply demonstrates the potential range of vascular lesions in a small group of consecutively studied cranial gunshot wounds examined in the acute phase.

In conclusion, previous publications detailing the frequency of vascular lesions associated with penetrating cranial missiles were mostly reports of war-time injuries. These studies were of survivors in whom the examination primarily was done some time after the traumatic incident, and centered on the posttraumatic formation of cerebral aneurysms. The civilians in our series were examined more immediately and generally had injuries from different types and velocities of projectiles than those of many war-time casualties. Our findings indicate that, perhaps because of the timing of the angiographic examination, the frequency of vascular injuries seen at the time of radiologic evaluation in civilians may be higher than that suggested from reports of similar lesions occurring in military populations during war time. The potential cranial vascular injuries and sequelae include not only aneurysms of the internal carotid/vertebrobasilar arterial circulation but also aneurysms of the external carotid artery, traumatic arteriovenous fistulas, and cerebrovascular occlusions. Future studies should focus on corroboration of the high frequency of vascular injuries associated with penetrating mis-

TABLE 1: Summary of Patients with Traumatic Cranial Vascular Lesions Caused by Penetrating Missiles

Age (Years)	Clinical Presentation (Glasgow Coma Score)	Type of Projectile (Caliber)	Trajectory of Bullet	Vessel Involved	Type of Vascular Lesion	Treatment	Clinical Outcome at 1 Month (Glasgow Coma Score)
13	Obtundation (11)	.22	Temporal bone-ipsilateral convexity	Right anterior cerebral artery	Aneurysm	Surgical clipping and entrapment	Stabilization (15)
45	Coma (8)	.45	Temporal bone-contralateral temporal bone	Right middle cerebral artery	Aneurysm	Surgical clipping	Stabilization (15)
40	Coma (9)	.38	Neck-skull base-contralateral occipital bone	Basilar artery	Aneurysm	Surgical clipping	Stabilization (15)
35	Obtundation (11)	.22	Parietal bone-contralateral parietal bone	Left middle meningeal artery	Aneurysm	None	Stabilization (15)
25	Coma (7)	.22	Face-ipsilateral parietooccipital bone	Right posterior cerebral artery	Aneurysm and arteriovenous fistula	None	Brain death
56	Coma (6)	.38	Temporal bone-contralateral occipital bone	Left transverse venous sinus and internal jugular vein	Venous occlusion	None	Brain death

Note.—All patients were males.

siles in civilians, and on the fundamental ballistic causes of these lesions in order that appropriate preventive and potential therapeutic measures for this group of patients might be clarified [26].

ACKNOWLEDGMENT

We thank Joanne M. Murray for manuscript preparation.

REFERENCES

1. Jagger J, Dietz PE. Death and injury by firearms: who cares? *JAMA* **1986**;255:3143–3144
2. Carey ME, Sarna GS, Farrel JB, Happel LT. Experimental missile wound to the brain. *J Neurosurg* **1989**;71:754–764
3. Cockrill HH, Jimenez JP, Goree JA. Traumatic false aneurysm of superior cerebellar artery simulating posterior fossa tumor: case report. *J Neurosurg* **1977**;46:377–380
4. Benoit BG, Wortzman G. Traumatic cerebral aneurysms: clinical features and natural history. *J Neurol Neurosurg Psychiatry* **1973**;36:127–138
5. Bank WO, Nelson PB, Drayer BP, Wilkins RH, Rosenbaum AE. Traumatic aneurysm of basilar artery (case report). *AJR* **1972**;130:957–977
6. Ferry DJ, Kempe LG. False aneurysm secondary to penetration of brain through orbitofacial wounds: report of two cases. *J Neurosurg* **1972**; 36:503–506
7. Hammon WM. Analysis of 2,187 consecutive penetrating wounds of the brain from Vietnam. *J Neurosurg* **1971**;34:127–131
8. Raimondi AJ, Yashon D, Reyes C, Yarza-Garay L. Intracranial false aneurysms. *Neurochirurgia* (Stuttg) **1968**;11:219–233
9. Achram M, Rizk G, Haddad FS. Angiographic aspects of traumatic intracranial aneurysms following war injuries. *Br J Radiol* **1980**;53:1144–1149
10. Buckingham MJ, Crone KR, Ball WS, Tomsick TA, Berger TS, Tew JM. Traumatic intracranial aneurysms in childhood: two cases and a review of the literature. *Neurosurgery* **1988**;22:398–408
11. Kieck CF, deVillers JC. Vascular lesions due to transcranial stab wounds. *J Neurosurg* **1984**;60:42–46
12. Parkinson D, West M. Traumatic intracranial aneurysms. *J Neurosurg* **1980**;52:11–20
13. Stehbens WE. *Pathology of the cerebral blood vessels.* St. Louis: Mosby, **1972**:452–455
14. Fleischer AS, Patton JM, Tindall CT. Cerebral aneurysm of traumatic origin. *Surg Neurol* **1975**;4:233–239
15. Jackson FE, Gleave JRW, Janon E. The traumatic cranial and intracranial aneurysms. In: Vinken PJ, Bruyn GW, eds. *Handbook of cranial neurology.* Amsterdam: North Holland, **1976**:381–398
16. Burton C, Velasco F, Darman J. Traumatic aneurysm of peripheral cerebral artery: review and case report. *J Neurosurg* **1968**;28:468–474
17. Aarabi B. Traumatic aneurysms of brain due to high velocity missile head wounds. *Neurosurgery* **1988**;22:1056–1063
18. Kuhn RA, Kugler H. False aneurysm of the middle meningeal artery. *J Neurosurg* **1964**;21:92–96
19. Thompson JR, Harwood-Nash DC, Fitz CR. Cerebral aneurysm in children. *AJR* **1973**;118:163–175
20. Carothers A. Orbitofacial wounds and cerebral artery injuries caused by umbrella tips. *JAMA* **1978**;239:1151–1152
21. Handel SF, Perpetuo FOL, Handel CH. Subdural hematomas due to ruptured cerebral aneurysms: angiographic diagnosis and potential pitfall for CT. *AJR* **1978**;130:507–509
22. Rahimizadeh A, Abtahi H, Daylami MS, Tabatabei MA, Haddadian K. Traumatic cerebral aneurysms caused by shell fragments. *Acta Neurochir* (Wien) **1987**;84:93–98
23. Haddad FS, Haddad GF, Taha J. Traumatic intracranial aneurysms caused by missiles: their presentation and management. *Neurosurgery* **1991**;28: 1–7
24. Kirkpatrick JB, DiMaio V. Civilian gunshot wounds of the brain. *J Neurosurg* **1978**;49:185–198
25. Hubschmann O, Shapiro K, Baden M, Shulman K. Craniocerebral gunshot injuries in civilian practice—prognostic criteria and surgical management: experience with 82 cases. *J Trauma* **1979**;19:6–12
26. Benzel EC, Day WT, Kesterson L, Willis BK, et al. Civilian craniocerebral gunshot wounds. *Neurosurgery* **1991**;29;67–72

MR Angiography of the Head and Neck: Value of Two-dimensional Phase-Contrast Projection Technique

Gregory R. Applegate[1]
S. Lalith Talagala
Laura J. Applegate[2]

MR angiography is commonly performed by using two- and three-dimensional time-of-flight and three-dimensional phase-contrast techniques. These procedures require long examination times and processing of imaging data by computing maximum intensity projections. Two-dimensional phase-contrast projection angiography has neither of these disadvantages. We analyzed the value of this technique for head and neck MR angiography in 84 patients and 15 control subjects. Patients were examined to resolve specific clinical questions such as the presence of arteriovenous malformations (20 cases), patency of carotid and vertebral arteries (35 cases), patency of the superior sagittal sinus (14 cases), patency of saphenous vein bypass grafts (11 cases), and vascularity of masses (four cases). Conventional angiograms were available for correlation in 22 patients. Two-dimensional phase-contrast projection angiograms were generated by using a gradient-recalled-echo sequence sensitized to flow with the use of flow-encoding gradients. Projection MR angiograms were obtained in approximately 3.5 min by combining images obtained with flow-encoding gradients applied along the axes defining the image plane. MR angiograms were subjectively evaluated by three observers without reference to routine MR images or conventional angiograms. High-quality studies were obtained in 93% of control subjects and 90% of patients examined. The findings based on phase-contrast angiography were confirmed with conventional angiography in 21 of 22 patients for whom conventional angiograms were available.

Evaluation of vascular grafts and of the patency of major cranial vessels was easily done with two-dimensional phase-contrast angiography and was useful in postoperative follow-up examinations. We also advocate its use for superior sagittal sinus thrombosis and follow-up examinations in patients with arteriovenous malformations.

AJR 159:369–374, August 1992

Advances in pulse sequence design and display techniques have enabled diagnostic-quality MR angiographic studies to be performed routinely in a clinical setting. Recent reports indicate that MR angiography can be used to evaluate the cranial vasculature [1–4]. Initial clinical studies so far have illustrated the use of MR angiography in the evaluation of carotid artery disease [5–8], detection of patent intracranial aneurysms [9, 10], assessment of arteriovenous malformations [11, 12], and confirmation of dural sinus occlusion [13].

MR angiography is most commonly performed by using either three-dimensional (3D) time-of-flight (TOF) [14–17] or 3D phase-contrast [18] techniques. Although the two-dimensional (2D) TOF studies [2, 19, 20] are also used in certain situations, the general clinical utility of the 2D phase-contrast technique [21, 22] has not been reported. The main reason for extensive use of 3D TOF, phase-contrast, and 2D TOF techniques is the ability to produce angiographic projections in any desired viewing direction. Even though this can be extremely useful in many situations, in a number of cases the relevant diagnostic information can be obtained by using a projection angiogram that encompasses the vessels in question. A single-slice projection angiogram is most efficiently produced with a 2D acquisition scheme. A variety of techniques have been suggested for generation of projection angiograms

Received December 17, 1991; accepted after revision February 24, 1992.

[1] All authors: Department of Radiology, University of Pittsburgh School of Medicine, Pittsburgh NMR Institute, 3260 Fifth Ave., Pittsburgh, PA 15213. Address reprint requests to S. L. Talagala.

[2] Present address: St. Vincents Medical Center, 2131 W. 3rd St., Los Angeles, CA 90057.

0361–803X/92/1592–0369
© American Roentgen Ray Society

[21, 23–29]. Of these, phase-sensitive techniques [21, 23–25] have the advantage of being able to depict a wide range of in-plane flow velocities in a large anatomic region without signal saturation problems.

In this article, we report our experience with the use of 2D phase-contrast projection MR angiography for evaluation of vessel patency, vascular abnormalities, and masses. We restrict this discussion to head and neck studies.

Subjects and Methods

Fifteen control subjects and 84 patients were prospectively examined with 2D phase-contrast projection MR angiography with a 1.5-T system (General Electric Medical Systems, Waukesha, WI). Twenty patients had arteriovenous malformations, 14 patients were examined for superior sagittal sinus or jugular vein thrombosis, four patients had masses, and 35 patients were examined to determine the patency of the carotid or vertebral artery. In addition, 11 patients had 2D phase-contrast MR angiography to evaluate the patency of saphenous vein bypass grafts that had been placed during skull base surgery. Of this group, 10 patients had intracranial internal carotid artery saphenous vein grafts after sacrifice of the carotid artery, and one patient had a vertebral artery saphenous vein graft after resection of the vertebral artery. Conventional angiograms were available for comparison in 22 patients. Patients without confirmatory conventional angiograms were included in the study in order to assess the technique in a larger and more diverse patient population.

All studies were reviewed together by three observers to determine the image quality subjectively, including definition and clarity in display of the vessels in question, presence of artifacts, and overall scan quality. A consensus was reached by using a scale from 0 to 3 (0 = nondiagnostic, 1 = poor, 2 = good, 3 = excellent) to grade the image quality. In cases of disagreement the scores were averaged. Phase-contrast angiograms were reviewed without reference to routine MR images and conventional angiograms. Before reviewing patient data, phase-contrast MR angiograms of control subjects were examined to identify characteristic features that might impair diagnostic confidence.

Two-dimensional phase-contrast angiograms [21, 22] were generated by using a gradient-recalled-echo sequence sensitized to flow by means of flow-encoding gradients. Two half-period sine wave gradient lobes with equal areas and opposite sign (bipolar gradient) were used for flow encoding. Moving magnetization (e.g., blood) subjected to such a gradient experiences a net phase shift that is proportional to the velocity along the direction of the gradient; the phase shift acquired by magnetization of stationary tissue is zero. This forms the basis for discriminating stationary tissue from flowing blood in phase-contrast MR angiography. The phase shift (ϕ) experienced by magnetization moving at constant velocity is equal to $(2\gamma G v \tau^2)/\pi$, where γ is the gyromagnetic ratio, G is the flow-encoding gradient strength, v is the component of velocity along the direction of the applied gradient, and τ is the duration of each gradient lobe.

In order to eliminate the signal contributed by stationary tissue, two echo signals with inverted bipolar gradients are acquired; that is, the bipolar gradient is applied as a positive and then a negative lobe for the first acquisition, and as a negative and then a positive lobe for the second acquisition [21, 22] (Fig. 1). The phase of magnetization of stationary tissue remains identical in the two echo signals. However, inversion of the bipolar gradient causes the phase angle acquired by moving magnetization to be negative. Thus, subtraction of the two echoes cancels the contribution from the stationary tissue

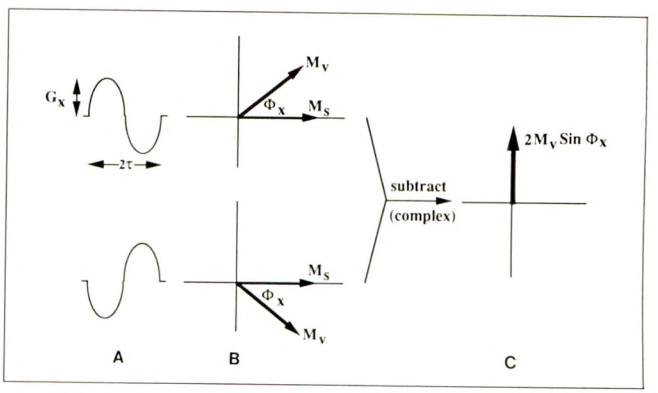


Fig. 1.—Principle of phase-contrast MR angiography. Diagram shows bipolar flow-encoding gradients (*A*) and magnetization vectors (*B*) corresponding to flowing (M_v) and stationary (M_s) magnetization after being subjected to a bipolar gradient. M_v acquires an additional phase shift (ϕ_x) compared with M_s. Inversion of bipolar gradient causes ϕ_x to be negative and leaves M_s unaffected. Subtraction (*C*) of signals corresponding to vector positions shown in *B* cancels contribution from M_s. Magnetization M_v is not completely canceled, and therefore the image generated with subtracted signals corresponds to a "flow" image. G_x = strength of flow-encoding gradient along x direction, 2τ = duration of bipolar gradient lobes.

while retaining a portion of the signal originating from moving magnetization (Fig. 1). An image created by using the subtracted echoes corresponds to a "flow" image, showing the patent blood vessels without interference from stationary tissue. It has been shown that the complex signal subtraction scheme described above is more advantageous than phase-difference methods for thick slab acquisitions because of the lack of "pitting" artifacts and superior stationary tissue suppression [30].

In order to obtain a linear relationship between the intensity of blood on the flow image and blood velocity, the phase angle is constrained to be less than 1 radian for the full range of velocities present in the imaged region [21]. The phase angle is limited to the desired range by using a flow-encoding gradient of appropriate strength calculated according to an estimated maximum average blood velocity within the imaged region.

The 2D phase-contrast projection angiograms presented here were generated by combining two separate flow images obtained by applying the flow-encoding gradients along each axis defining the image plane. For example, coronal projection angiograms were generated by combining individual flow images obtained with flow-encoding gradients applied along the right-left and superior-inferior directions (Fig. 2). For technical limitations, in this study, the composite image was generated by direct summation of the individual flow images. Thus, angiograms are intended to provide anatomic rather than quantitative velocity information.

Angiograms were obtained with slice thicknesses in the range of 20–60 mm, a repetition time of 50 msec, an echo time of 18 msec, and 128 phase-encoding steps. Typically, 16 excitations were acquired for each phase-encoding step with reversal of the bipolar gradient on alternate excitations. A composite angiogram with flow encoding along two directions could be acquired in approximately 3.5 min. The strength of the flow-encoding gradient was adjusted to produce a phase shift of 1 radian for blood moving at 30 cm/sec. When the patency of the vessel in question could not be readily established, a second acquisition was obtained with a stronger flow-encoding gradient to increase the visibility of slow flow. The pulse sequence program code was produced in house for the 3.2 and 4.0 versions of Signa software (General Electric Medical Systems).

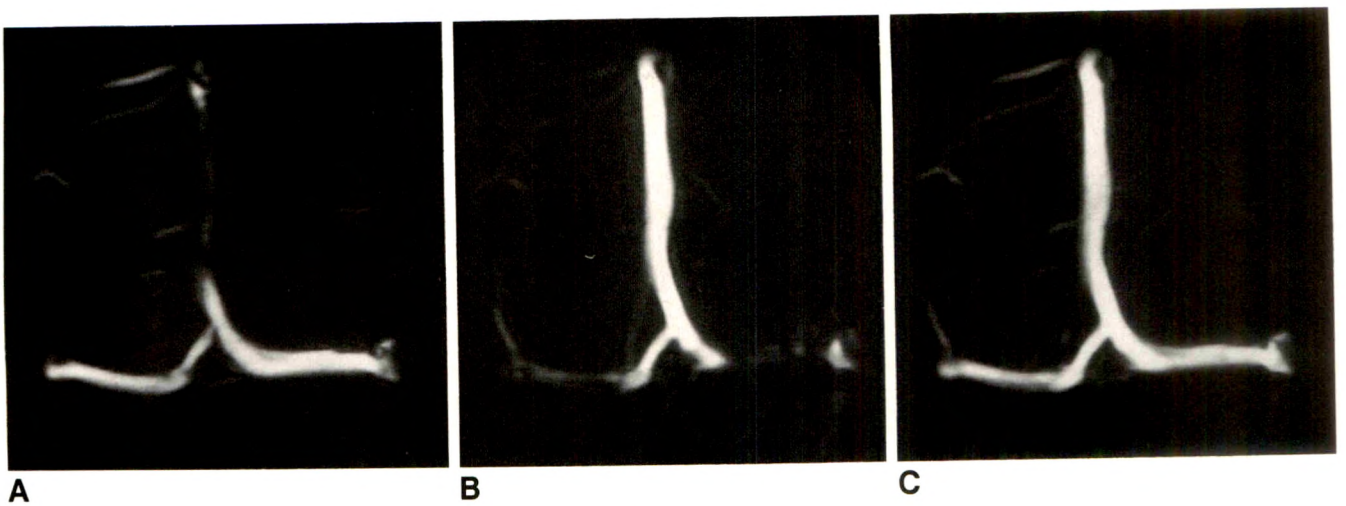


Fig. 2.—Effect of flow-encoding gradient direction in phase-contrast MR angiography.
***A*, Coronal acquisition through posterior fossa with flow-encoding gradient applied to encode flow along right-left direction shows signal intensity within transverse sinuses but poor signal intensity within superior sagittal sinus.**
***B*, Image from same coronal location as *A*, with flow-encoding gradient applied to encode for flow along superior-inferior direction, shows signal within superior sagittal sinus.**
***C*, Summation of *A* and *B* shows complete encoding for flow within imaging plane.**

Results

Review of images by three observers revealed that high-quality studies (score = 2 to 3) were obtained in 14 (93%) of 15 control subjects and 76 (90%) of 84 patients examined. A coronal 2D phase-contrast projection angiogram of a control subject is shown in Figure 3.

Of the 20 patients examined for arteriovenous malformations, residual malformations were detected in 10 patients by 2D phase-contrast MR angiography. Correlative conventional angiographic studies were available in four of the patients with residual malformations (Fig. 4). In all four, the findings of 2D phase-contrast MR angiography were confirmed. In one patient, 2D phase-contrast MR angiography indicated absence of residual arteriovenous malformations after radiosurgery. This observation was confirmed by conventional angiography.

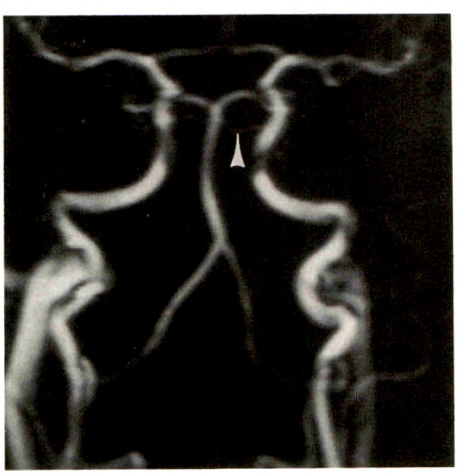


Fig. 3.—Coronal 2D phase-contrast MR angiogram of control subject shows both posterior and anterior circulations, including small branches such as superior cerebellar arteries (*arrowhead*).

Fourteen patients were examined for suspected superior sagittal sinus thrombosis. Patency of the superior sagittal sinus was shown by 2D phase-contrast MR angiography in 10 patients. Of the 10 patients, one patient subsequently had conventional angiography, which confirmed patency of the sinus. In the four patients diagnosed with superior sagittal sinus thrombosis on the basis of 2D phase-contrast MR angiography, the findings were considered conclusive, and conventional angiography was not performed. One of these patients was found to have a partially thrombosed superior sagittal sinus (Fig. 5).

Of 11 patients with saphenous vein bypass grafts, 2D phase-contrast MR angiography demonstrated vessel patency in all cases (Fig. 6). These findings were confirmed by conventional angiography in all cases. One of the patients examined had surgical ligation of the left internal carotid artery for a parasellar aneurysm and also had a superficial temporal artery to middle cerebral artery bypass. Patency of this 2.5-mm-diameter vessel was seen on 2D phase-contrast MR angiography (Fig. 7).

In the examinations performed to confirm patency of the extracranial carotid and vertebral arteries, the vessels in question were patent in 23 of 35 cases. In four of these, findings on conventional angiograms confirmed MR angiographic findings.

Four patients with masses were examined with 2D phase-contrast MR angiography. A significant vascular component to the mass was detected in two cases (Fig. 8).

In one patient, 2D phase-contrast MR angiography showed an abrupt loss of signal in a segment of a middle cerebral artery shown to be normal by conventional angiography. In

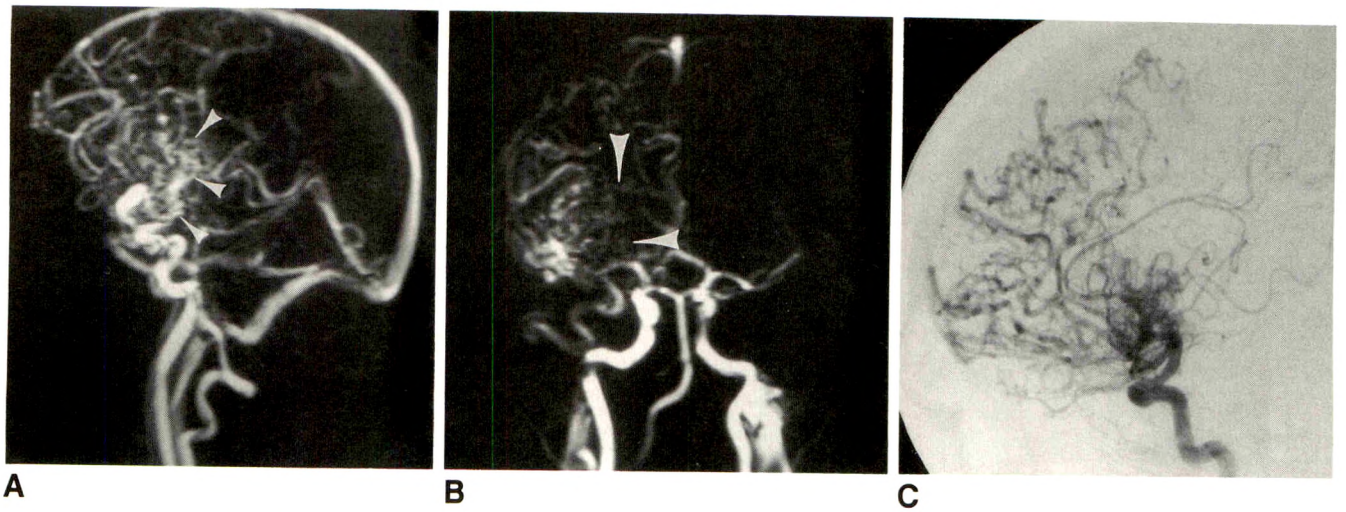


Fig. 4.—Arteriovenous malformation.
A, sagittal 2D phase-contrast MR angiogram shows a large arteriovenous malformation with nidus (*arrowheads*) in region of insular cortex fed primarily by sylvian and cortical branches of middle cerebral artery and branches of pericallosal artery.
B, Corresponding coronal 2D phase-contrast MR angiogram shows large arteriovenous malformation lateral to *arrowheads*.
C, Corresponding right internal carotid artery conventional angiogram.

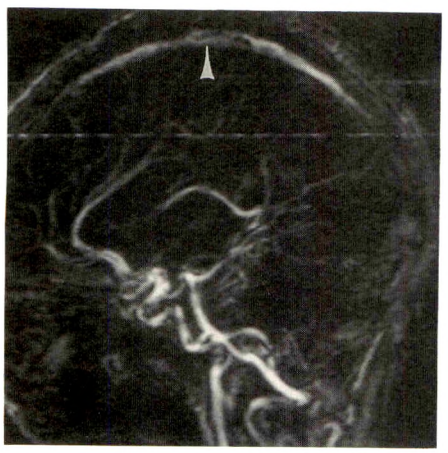


Fig. 5.—Sagittal 2D phase-contrast MR angiogram shows partial thrombosis of superior sagittal sinus. A major portion of superior sagittal sinus is patent (*arrowhead*); however, posterior portion of sagittal sinus and straight sinus are not.

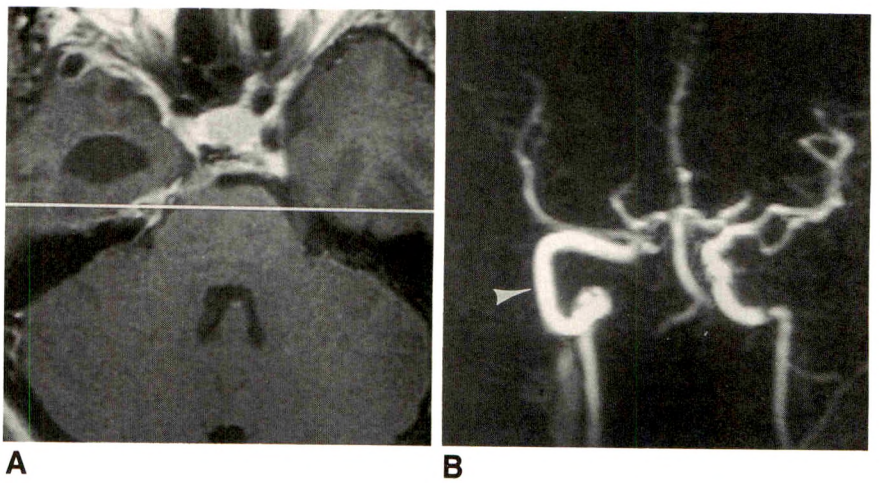


Fig. 6.—Right internal carotid artery saphenous vein bypass graft.
A, Axial short TR/TE spin-echo image shows postoperative changes in right middle cranial fossa. White line outlines slab selected for coronal phase-contrast acquisition.
B, Coronal 2D phase-contrast angiogram shows saphenous vein graft (*arrowhead*) with a more lateral course than normal native carotid artery on contralateral side.

this case, surgical metallic clips were found adjacent to the distal left internal carotid and proximal left middle cerebral arteries (Fig. 9A). Field inhomogeneity arising from local susceptibility differences caused by the clips contributed to artifactual signal loss on the 2D phase-contrast angiogram that mimicked severe stenosis (Fig. 9B). However, a flow void seen on coronal T2-weighted spin-echo images confirmed the patency of the middle cerebral artery. This case stresses the need to correlate MR angiographic findings with those obtained with routine MR imaging.

Discussion

Results obtained with 2D phase-contrast projection MR angiography showed excellent correlation with conventional angiograms in 21 of 22 cases. Patency of native vessels and grafts in the head and neck could be readily assessed with this technique. Although information on vessel patency can also be obtained from routine spin-echo and gradient-echo MR imaging, in our opinion, display of only patent vessels in a single composite image enhances diagnostic confidence and ease of interpretation. Further, abnormally slow flow or absence of flow could be differentiated from normal flow. This differentiation can be difficult with routine spin-echo imaging, as areas of slow flow may be of higher signal intensity and thus mimic thrombus [31]. However, saturation pulses can be used to reduce this problem in spin-echo imaging. With 3D TOF studies, saturation effects encountered with slow flow may make confirmation of vessel patency difficult [7].

In the evaluation of arteriovenous malformations, the loca-

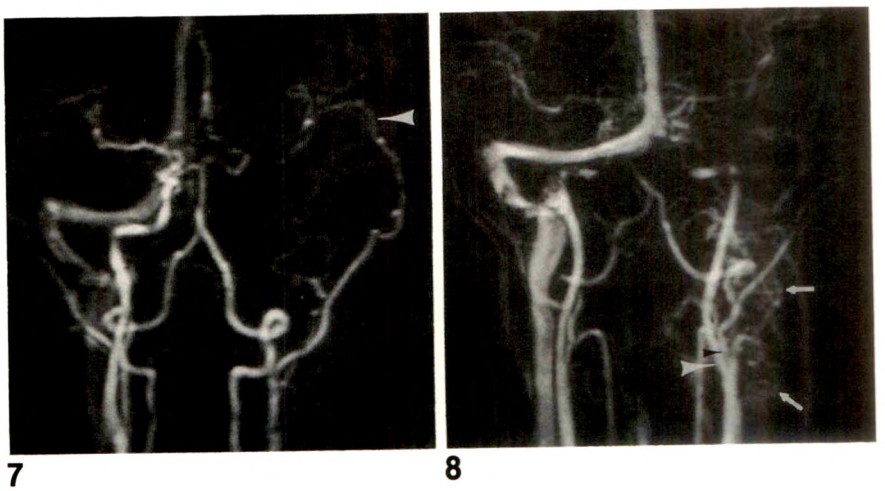


Fig. 7.—External carotid artery to middle cerebral artery bypass. Coronal 2D phase-contrast MR angiogram shows nonpatent left internal carotid artery and patent left superficial temporal artery to left middle cerebral bypass graft (*arrowhead*).

Fig. 8.—Carotid body tumor. Coronal 2D phase-contrast MR angiogram shows medial displacement of left internal carotid artery (*white arrowhead*) and left external carotid artery (*black arrowhead*) by a large paraganglioma (*arrows*).

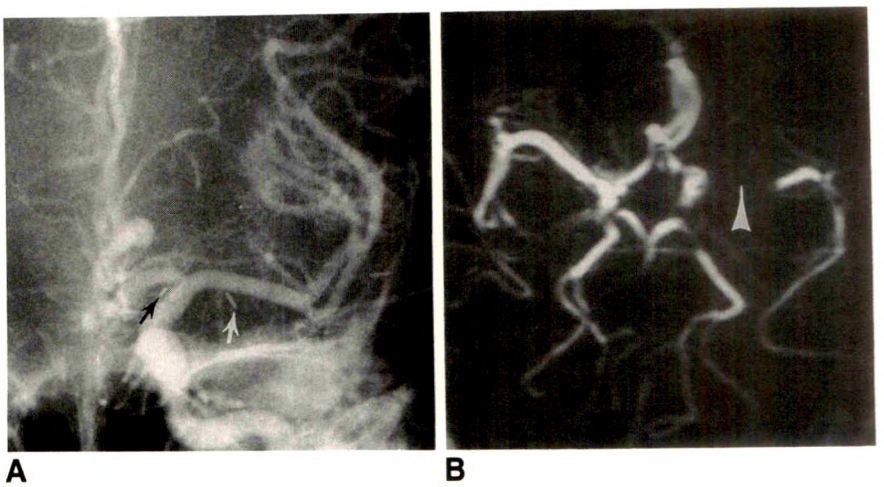


Fig. 9.—Artifactual signal loss.

A, Conventional angiogram of normal left internal carotid artery shows surgical metallic clips adjacent to distal left internal carotid artery (*black arrow*) and proximal left middle cerebral artery (*white arrow*).

B, Axial 2D phase-contrast angiogram shows apparent loss of signal (*arrowhead*) in proximal left middle cerebral artery; this can be misinterpreted as severe stenosis.

tion of the nidus and detection of feeding arteries and possible fistulas must be addressed. Although the location of the nidus is seen with 2D phase-contrast MR angiography, detection of feeding vessels and fistulas is generally difficult with a single acquisition. However, it has been suggested that high-flow feeding vessels can be detected on multiple phase-contrast MR angiographic images with different flow sensitivities (Turski PA et al, presented at the Radiological Society of North America meeting, November 1990).

In the evaluation of dissections, we believe 2D phase contrast can be advocated only as an adjunct to standard spin-echo and gradient-echo imaging, because only the true patent lumen will be evaluated with phase-contrast MR angiography. Frequently, the distortion of the true lumen is quite subtle. Demonstration of thrombus in the false lumen is often more diagnostic than the presence of the deformity of the true lumen and can best be evaluated with conventional spin- and gradient-echo sequences.

Phase-contrast angiograms also depicted some undesirable features that were present in control as well as patient studies. In particular, signal loss was sometimes encountered in tortuous regions of vessels. This is attributed mainly to intravoxel signal phase dispersion caused by complex or turbulent flow [3]. In some of the bypass graft patients, these effects produced signal loss at the graft anastomosis and at vein valves. This can be minimized by using shorter echo times, which can be obtained with better optimized pulse sequence codes. Some areas of hypointensity may also be due to the fact that flow encoding was performed only along the axes defining the image plane. Addition of flow encoding in the slice-selection direction will resolve this issue at a cost of a 50% increase in scan time. The ability to see distal runoff vessels depends on the velocity used to determine the flow-encoding gradient strength. Therefore, sometimes a second acquisition with a higher flow-encoding gradient strength is needed to show distal vessels with slow flow. Another undesirable effect was vessel overlap due to projection of blood vessels along the slice-select direction. This was minimized by selecting the narrowest possible slice thickness to include only the vessels of interest. Other factors contributing to suboptimal images included patient motion and artifacts caused by incomplete suppression of stationary tissue when attempts were made to show lower velocity flow. Incomplete suppression of stationary tissue is attributed to eddy currents generated by switching of large flow-encoding gradients. Finally, susceptibility effects due to metal clips can cause artifactual signal loss (Fig. 9).

Advantages of 2D phase-contrast MR angiography include

the ability to visualize flow in a large anatomic region, relatively short acquisition time, and lack of image processing such as calculation of maximum intensity projections. The individual projection angiograms are immediately accessible, and therefore scan quality and adequate coverage of the region of interest can be determined readily. With TOF techniques, sources of hyperintensity other than flowing blood (e.g., subacute thrombus with methemoglobin) are also depicted in maximum-intensity-projection reconstructions [12]. This problem is not encountered in phase-contrast MR angiography because only the signal from moving magnetization contributes to the final image.

Phase-contrast MR angiography has an advantage over TOF techniques in its improved ability to show slow flow [3]. Flow sensitivity of the phase-contrast images can readily be controlled by changing the flow-encoding gradient strength. Increased visualization of slow flow (greater flow sensitivity) requires greater flow-encoding gradient strength. Thus, the lower limit of flow detection depends on the highest gradient strength available and other considerations such as echo time and artifacts due to eddy currents effects. This flow detection limit is important when vessels with very slow flow are evaluated. We recommend that initial evaluations be performed with the strength of the flow-encoding gradient adjusted assuming a maximum flow velocity of 30 cm/sec. If vessel patency cannot be confirmed, then another acquisition should be obtained with increased flow sensitivity (i.e., flow-encoding gradients adjusted to optimally encode a flow velocity of, for example, 10 cm/sec).

In summary, the 2D phase-contrast technique is a rapid sequence that does not require processing of images after acquisition and in which only flowing blood contributes to image intensity. We advocate the use of 2D phase-contrast MR angiography for rapid evaluation of the patency of major cranial vessels and superior sagittal sinus thrombosis, and for follow-up examinations in patients with arteriovenous malformations. Evaluation of vascular grafts was easily obtained and was useful in noninvasive postoperative follow-up examinations. Future studies with larger patient populations and correlative conventional angiograms will be necessary to fully assess the clinical utility of this technique.

REFERENCES

1. Masaryk TJ, Modic MT, Ross JS, et al. Intracranial circulation: preliminary clinical results with three-dimensional (volume) MR angiography. *Radiology* **1989**;171:793–799
2. Keller PJ, Drayer BP, Fram EK, Williams KD, Dumoulin CL, Souza SP. MR angiography with two-dimensional acquisition and three-dimensional display. *Radiology* **1989**;173:527–532
3. Pericone JR, Siebert JE, Potchen EJ, Pera A, Dumoulin CL, Souza SP. Three-dimensional phase contrast MR angiography in the head and neck: preliminary report. *AJNR* **1990**;11:457–466
4. Blatter DD, Parker DL, Robison RO. Cerebral MR angiography with multiple overlapping thin slab acquisition. *Radiology* **1991**;179:805–811
5. Wagle WA, Dumoulin CL, Souza SP, Cline HE. 3DFT MR angiography of carotid and basilar arteries. *AJNR* **1989**;10:911–919
6. Masaryk TJ, Modic MT, Ruggieri PM, et al. Three-dimensional (volume) gradient-echo imaging of the carotid bifurcation: preliminary clinical experience. *Radiology* **1989**;171:801–806
7. Masaryk AM, Ross JS, DiCello MC, Modic MT, Paranandi L, Masaryk TJ. 3DFT MR angiography of the carotid bifurcation: potential and limitations as a screening examination. *Radiology* **1991**;179:797–804
8. Litt AW, Eidelman EM, Pinto RS, et al. Diagnosis of carotid artery stenosis: comparison of 2DFT time-of-flight MR angiography with contrast angiography in 50 patients. *AJNR* **1991**;12:149–154
9. Ross JS, Masaryk TJ, Modic MT, Ruggieri PM, Haacke EM, Selman WR. Intracranial aneurysms: evaluation by MR angiography. *AJNR* **1990**;11:449–456
10. Sevick RJ, Tsuruda JS, Schmalbrock P. Three-dimensional time-of-flight MR angiography in the evaluation of cerebral aneurysms. *J Comput Assist Tomogr* **1990**;14:874–881
11. Edelman RR, Wentz KU, Mattle HP, et al. Intracerebral arteriovenous malformations: evaluation with selective MR angiography and venography. *Radiology* **1989**;173:831–837
12. Marchal G, Bosmans H, Van Fraeyenhoven L, et al. Intracranial vascular lesions: optimization and clinical evaluations of three-dimensional time-of-flight MR angiography. *Radiology* **1990**;175:443–448
13. Rippe DJ, Boyko OB, Spritzer CE, et al. Demonstration of dural sinus occlusion by the use of MR angiography. *AJNR* **1990**;11:199–201
14. Ruggieri PM, Laub GA, Masaryk TJ, Modic MT. Intracranial circulation: pulse-sequence considerations in three-dimensional (volume) MR angiography. *Radiology* **1989**;171:785–791
15. Schmalbrock P, Yuan C, Chakeres DW, Kohli J, Pelc NJ. Volume MR angiography: methods to achieve very short echo times. *Radiology* **1990**;175:861–865
16. Haacke EM, Masaryk TJ, Wielopolski PA, et al. Optimizing blood vessel contrast in fast three-dimensional MRI. *Magn Reson Med* **1990**;14:202–221
17. Parker DL, Yuan C, Blatter DD. MR angiography by multiple thin slab 3D acquisition. *Magn Reson Med* **1991**;17:434–451
18. Dumoulin CL, Souza SP, Walker MF, Wagle W. Three dimensional phase contrast angiography. *Magn Reson Med* **1989**;9:139–149
19. Kim JH, Cho ZH. 3-D MR angiography with scanning 2-D images: simultaneous data acquisition of arteries and veins (SAAV). *Magn Reson Med* **1990**;14:554–561
20. Brown DG, Riederer SJ, Jack CR, Farzaneh F, Ehman RL. MR angiography with oblique gradient-recalled echo technique. *Radiology* **1990**;176:461–466
21. Dumoulin CL, Hart HR. Magnetic resonance angiography. *Radiology* **1986**;161:717–720
22. Dumoulin CL, Souza SP, Hart HR. Rapid scan magnetic resonance angiography. *Magn Reson Med* **1987**;5:238–245
23. Meuli RA, Weeden VJ, Geller SC, et al. MR gated subtraction angiography: evaluation of lower extremities. *Radiology* **1986**;159:411–418
24. Axel L, Morton D. MR flow imaging by velocity-compensated/uncompensated difference images. *J Comput Assist Tomogr* **1987**;11:31–34
25. Laub GA, Kaiser WA. MR angiography with gradient motion refocussing. *J Comput Assist Tomogr* **1988**;12:377–382
26. Dixon WT, Du LN, Faul DD, Gado M, Rossnick S. Projection angiograms of blood labeled by adiabatic fast passage. *Magn Reson Med* **1986**;3:454–462
27. Nishimura DG, Macovski A, Jackson JI, Hu RS, Stevick CA, Axel L. Magnetic resonance angiography by selective inversion recovery using a compact gradient echo sequence. *Magn Reson Med* **1988**;8:96–103
28. Frahm J, Merboldt K, Hanicke W, Gyngell ML, Bruhn H. Rapid line scan NMR angiography. *Magn Reson Med* **1988**;7:79–87
29. Norris DG, Jones RA, Hutchison JMS. Projective Fourier angiography. *Magn Reson Med* **1988**;7:1–10
30. Bernstein MA, Ikezaki Y. Comparison of phase-difference and complex-difference processing in phase contrast MR angiography. *J Magn Reson Imaging* **1991**;1:725–729
31. Bradley WG. The MR appearance of flowing blood and CSF. In: Brant-Zawadzki M, Norman D, eds. *Magnetic resonance imaging of the central nervous system*. New York: Raven, **1987**:83–96

MR Imaging of the Pituitary Stalk:
Size, Shape, and Enhancement Pattern

Gary E. Simmons[1]
James E. Suchnicki
Kevin M. Rak
Thomas R. Damiano

The size, shape, signal intensity, and enhancement pattern of the normal pituitary stalk were determined retrospectively by review of MR images of 58 patients. The pituitary stalk was measured at the level of the optic chiasm and at its insertion on the pituitary gland. The contour of the stalk was smoothly tapering, measuring 3.25 ± 0.56 mm in transverse diameter at the optic chiasm and 1.91 ± 0.40 mm at its pituitary insertion. The signal intensity of the pituitary stalk on unenhanced T1-weighted images was less than that of the neurohypophysis in all cases and less than that of the optic chiasm in 84% of the cases. After the administration of contrast material, enhancement of the pituitary stalk occurred in all cases. A central area of nonenhancement in an otherwise uniformly enhancing stalk was variably present, depending on the size of the infundibular recess.

Our study defines the size, contour, and MR signal characteristics of the normal pituitary stalk. These criteria can be used to distinguish the normal from the abnormal stalk.

***AJR* 159:375–377, August 1992**

MR imaging is widely accepted as the imaging technique of choice for the evaluation of pituitary and parasellar abnormalities. The high signal intensity of the posterior part of the pituitary gland on T1-weighted images has generated great interest [1–4], but relatively few studies of the pituitary stalk have been published [5, 6]. We retrospectively evaluated MR images in 58 patients to determine the size, shape, and enhancement patterns of the normal pituitary stalk.

Materials and Methods

The study included 168 consecutive patients for whom contrast-enhanced and unenhanced MR images were available. Because the study was designed to evaluate the normal pituitary stalk, patients with conditions that could affect the stalk in any way were excluded. Thus, 15 patients were excluded because of pituitary macroadenomas, 25 because of microadenomas, and 27 because of prior pituitary surgery. Nine patients with a suprasellar mass, seven with empty sellas, and one with an incomplete study also were excluded. Eight of the excluded patients had concurrent hydrocephalus. Because the study was limited to adults, 18 years old or older, 26 additional patients were excluded on the basis of age. Thus, the study was based on findings in 58 patients (17 men, 41 women), 19–71 years old (mean, 40 years).

All images were obtained with a 1.5-T Signa unit (General Electric, Milwaukee, WI). In all 58 patients, a focused pituitary protocol was used: spin-echo (400/12 [TR/TE]) sagittal and coronal images through the sella were obtained before and after injection of gadopentetate dimeglumine. Four excitations, a 16-cm field of view, 3-mm slice thickness, and 1-mm interslice gap were used. In addition, axial spin-echo images at 600/20 with one excitation and a 20-cm field of view were obtained. More heavily T2-weighted axial images (2500/30 and 2500/80) also were obtained. The focused coronal enhanced T1-weighted images were used to evaluate the stalk's size, and the focused sagittal T1-weighted images were used to evaluate the stalk's signal characteristics.

Received November 20, 1991; accepted after revision February 28, 1992.

The opinions and assertions contained herein are the private views of the authors and are not to be construed as official or as reflecting the views of the Department of the Army or Department of Defense.

[1] All authors: Department of Radiology, Fitzsimons Army Medical Center, Aurora, CO 80045-5001. Address reprint requests to K. M. Rak.

0361–803X/92/1592–0377

The MR examinations were reviewed by three radiologists. The stalk was evaluated at two levels: at its insertion on the pituitary gland and at the level of the optic chiasm, near the origin of the stalk from the median eminence (Fig. 1). Specifically noted were the transverse diameter of the stalk, the unenhanced MR signal intensity as compared with those of the neurohypophysis and the optic chiasm, and the pattern of contrast enhancement. The electronic calipers at the physician's console were used to measure the stalk's maximal dimension to the nearest 0.01 mm. Visual comparisons of the signal intensities were made by all three radiologists. Regions of interest for quantitative assessment of signal intensity could not be reliably obtained because the area covered by the cursor was often too large to measure the pituitary stalk without also measuring some of the neighboring CSF.

Results

The maximum transverse dimension of the pituitary stalk at the level of the optic chiasm was 1.56–4.58 mm (mean ± SD, 3.25 ± 0.56). At the level of the stalk's insertion on the neurohypophysis, the maximal transverse dimension at the insertion was 1.04–2.93 mm (mean ± SD, 1.91 ± 0.40). Correlation of the coronal and sagittal images showed that the size differences between the superior and inferior aspects of the pituitary stalk corresponded to a smoothly tapered stalk without abrupt changes in size or contour (Figs. 2 and 3).

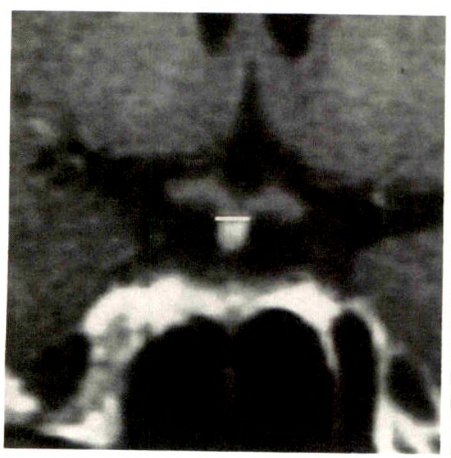
In no case could a change in MR signal intensity be detected along the course of the stalk. When compared with the optic chiasm, the stalk was hypointense on 84% and isointense on 16% of unenhanced images. The stalk was always hypointense relative to the neurohypophysis on the unenhanced images (Fig. 4).

MR in all 58 cases showed contrast enhancement of the pituitary stalk. Contrast-enhanced sagittal images showed that the tuber cinereum, the median eminence of the hypothalamus, and the pituitary stalk enhanced equally in all cases (Fig. 2). The enhanced images showed that the stalk was hyperintense relative to the optic chiasm in all cases. In all cases except one, the enhanced stalk was hypointense compared with the neurohypophysis. On both unenhanced and enhanced images, a variably sized central area of low T1 signal intensity was seen within the stalk, corresponding to the infundibular recess of the third ventricle (Fig. 2).

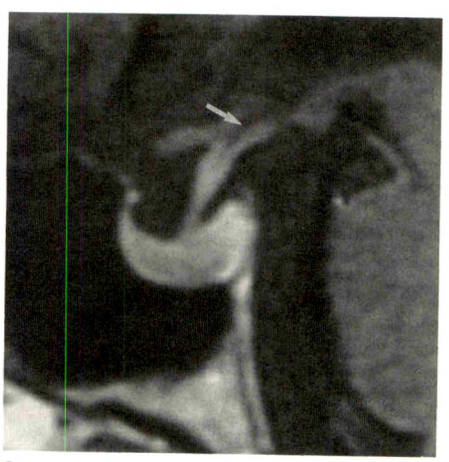
Discussion

Results of CT studies have shown that the diameter of the pituitary stalk is 4.0 mm at the level of the dorsum sella and 4.5 mm above the dorsum [6]. Tien et al. [5] recently determined the size and shape of the pituitary stalk in four patients with Langerhans cell histiocytosis as compared with 20 control subjects. These authors concluded that the upper limit of normal in width of the pituitary stalk is 3.5 mm near the median eminence and 2.8 mm at its midpoint. Our data, based on a larger study population, yielded a mean ± SD of 3.25 ± 0.56 near the optic chiasm and 1.91 ± 0.40 near the insertion on the pituitary gland. Our study shows that the normal stalk on coronal and sagittal images smoothly tapers from superiorly to inferiorly along its course. Increase in size of the stalk or distortion of the contour suggests that an abnormality is present. The normal stalk lacks a blood-brain barrier [7], and in all of our cases the stalk enhanced on contrast-enhanced MR images. Thus, enhancement is normal. Our results show that enhancement may be nonuniform, depending on the size and degree of extension of the infundibular recess of the third ventricle into the pituitary stalk. On axial MR images, in which the continuity of this central CSF-filled recess may not be obvious, this central area of nonenhancement of the stalk should not be considered abnormal. The variation in the size and degree of extension of the infundibular recess also may contribute to the difference in the size and contour of the stalk. As a result, patients with hydrocephalus may have an abnormally large stalk without an intrinsic abnormality of the stalk.

The neurohypophysis has an MR signal intensity similar to that of fat on T1-weighted spin-echo images but brighter than that of fat on T2-weighted images [1, 2]. In our study, the signal intensity of the neurohypophysis on T1-weighted images exceeded that of the pituitary stalk on all of the unen-



1

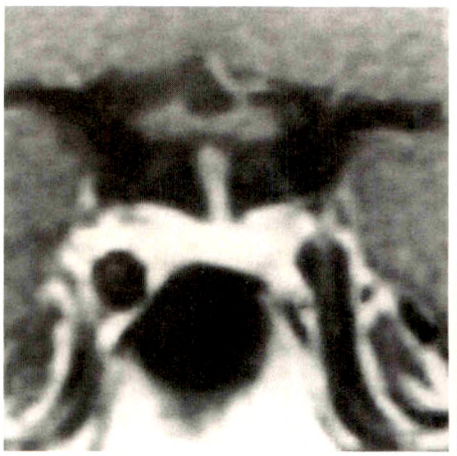


2

Fig. 1.—T1-weighted (SE 400/12) contrast-enhanced coronal MR image of pituitary stalk at level of optic chiasm. Cursor shows how measurements were made in transverse plane.

Fig. 2.—T1-weighted (SE 400/20) contrast-enhanced sagittal MR image shows smooth tapering of pituitary stalk. Note comparable enhancement of stalk, tuber cinereum, and median eminence and low signal of central infundibular recess (*arrow*).

Fig. 3.—T1-weighted (SE 400/12) contrast-enhanced coronal MR image shows tapering appearance of pituitary stalk.



3

Fig. 4.—T1-weighted (SE 400/20) unenhanced sagittal MR image shows pituitary stalk is hypointense relative to optic chiasm (*arrow*) and neurohypophysis.



4

hanced images and all but one of the enhanced images. This is in disagreement with the finding of Fujisawa et al. [8] that the pituitary stalk and posterior lobe had similar signal intensities. In 84% of our cases, the signal intensity of the pituitary stalk on unenhanced T1-weighted images was less than that of the optic chiasm.

In conclusion, we have established criteria for size, contour, and enhancement patterns of the normal pituitary stalk that can be used as baseline values against which pathologic processes can be measured. The stalk is typically hypointense relative to the neurohypophysis on unenhanced and enhanced T1-weighted spin-echo images. Relative to the optic chiasm, the pituitary stalk is typically hypointense on unenhanced images and hyperintense on enhanced images.

ACKNOWLEDGMENT

We thank the Visual Information Branch at Fitzsimons Army Medical Center for the photographic assistance.

REFERENCES

1. Kucharczyk W, Lenkinski R, Kucharczyk J, et al. The effect of phospholipid vesicles on the NMR relaxation of water: an explanation for the MR appearance of the neurohypophysis? *AJNR* **1990**;11:693–700
2. Nishimura K, Fujisawa I, Togashi K, et al. Posterior lobe of the pituitary: identification by lack of chemical shift artifact in MR imaging. *J Comput Assist Tomogr* **1986**;10:899–902
3. Kucharczyk J, Kucharczyk W, Berry I, et al. Histochemical characterization and functional significance of the hyperintense signal on MR images of the posterior pituitary. *AJNR* **1988**;9:1079–1083
4. Fujisawa I, Asato R, Nishimura K, et al. Anterior and posterior lobes of the pituitary gland: assessment by 1.5 T MR imaging. *J Comput Assist Tomogr* **1987**;11:214–220
5. Tien R, Newton TH, McDermott M, et al. Thickened pituitary stalk on MR images in patients with diabetes insipidus and Langerhans cell histiocytosis. *AJNR* **1990**;11:703–708
6. Peyster R, Hoover E, Adler L. CT of the normal pituitary stalk. *AJNR* **1984**;5:45–47
7. Syvertsen A, Haughton V, Williams Cusick J. The computed tomographic appearance of the normal pituitary gland and pituitary microadenomas. *Radiology* **1979**;133:385–391
8. Fujisawa I, Nishimura K, Asato R, et al. Posterior lobe of the pituitary in diabetes insipidus: MR findings. *J Comput Assist Tomogr* **1987**;11:221–225

Book Review

Radiation Protection in Nuclear Medicine and Pathology. (Report No. 63.) Edited by K. E. Goldstone, P. C. Jackson, M. J. Myers, and A. E. Simpson. York, England: The Institute of Physical Sciences in Medicine, 203 pp., 1991. £22.50

For years we instructed our trainees that radiation protection consisted of understanding the three factors of time, distance, and shielding. Alas, no more. It now consists of mastering a long list of governmental agencies, abbreviations, and acronyms. This compact volume presents the British version of the regulations and the alphabetical melange that describes current radiation protection. The editors have put together a glossary, 10 chapters, and seven brief appendixes to accomplish the task. The preface notes that the specialty chapters are self-contained (hence, several topics reappear). The longest chapter (chapter 10) is concerned with transport and movement of radioactive materials. This is especially intriguing because, in addition to the English regulations, requirements of the International Atomic Energy Agency are briefly mentioned.

The three-page glossary, the first substantive portion of the book, refers to "operational" definitions. An initial problem appears for the reader from this side of the Atlantic. Many of the listed terms or abbreviations are related to English law and regulations, and do not have a strict American equivalent. For example, RPS, or radiation protection supervisor, is defined in terms of Ionizing Radiations Regulations 1985. ARSAC and NRPB are important in England, but would only raise an eyebrow here. The problem may be further multiplied as Europe approaches a common policy in many affairs, and likely in radiation safety as well. The term "Euratom" makes its appearance. A brief expression on page 3 perhaps best says it with the phrase "the situation is extremely complex." Of interest is mention of gold-198; this radionuclide is no longer available in the United States. A bit disconcerting is the manner in which the decimal point appears to have a mind of its own. Thus, 1 Gy is defined as 100 rads. However, 1 rad is not simply 0.01 Gy, but emerges as 10 mGy.

After the legal and administrative framework of chapter 1 are chapters on therapeutic uses of unsealed radionuclides, imaging and in vivo procedures, prenatal and pediatric radionuclide protection, unsealed radioactive materials in laboratories, dispensing and manufacture, monitoring, incidents, waste disposal, and transport. The dose review each 13 weeks for the abdomen of female workers might be viewed as being too far from unisex. Workers in nuclear medicine may find particularly helpful appendix III, which lists radiation exposure data for approximately 34 radionuclides. Appendix IV gives radionuclide shielding data and the maximum range of emitted beta particles in water. This slim volume contains much of interest and also should make us aware that regulation of ionizing radiation is not the same on both sides of the Atlantic, and indeed is still changing. Appendix VII gives the addresses of "contact points." However, the reader probably would be delighted to trade the address of HM Inspectorate of Pollution for the presence of an index to the book.

Richard P. Spencer
University of Connecticut Health Center
Farmington, CT 06030-2935

Hypertensive Encephalopathy: Findings on CT, MR Imaging, and SPECT Imaging in 14 Cases

Richard B. Schwartz[1]
Kendall M. Jones
Peter Kalina
Richard L. Bajakian
Michael T. Mantello
Basem Garada
B. Leonard Holman

Hypertensive encephalopathy is a syndrome consisting of headache, seizures, visual changes, and other neurologic disturbances in patients with elevated systemic blood pressure. The purpose of this study was to analyze the imaging findings in 14 patients with hypertensive encephalopathy. CT (n = 13), MR (n = 12), and single-photon emission computed tomography (n = 2) examinations performed in these patients before and after resolution of symptoms were reviewed. Eight had the preeclampsia-eclampsia syndrome, and six had hypertensive encephalopathy due to other causes. CT and MR findings in all patients having these examinations were indicative of edema in the cortex and subcortical white matter in the occipital lobes. Two of the 14 patients also had similar findings in the cerebellum and frontal lobes. Single-photon emission computed tomography showed increased vascular perfusion adjacent to areas that appeared abnormal on CT and MR. The findings on the imaging studies resolved on follow-up examinations performed after the hypertension was corrected.

Our results suggest that the radiologic findings associated with hypertensive encephalopathy may be useful in establishing the diagnosis in the appropriate clinical setting.

AJR 159:379–383, August 1992

Hypertensive encephalopathy is a neurologic syndrome that occurs in patients with elevated blood pressure. It is characterized by rapidly progressive signs and symptoms including headache, seizures, visual disturbances, altered mental status, and focal neurologic signs. Although the syndrome is usually reversible if the hypertension is treated early, it may be fatal if it is unrecognized and treatment is delayed [1, 2]. The clinical findings are sufficiently nonspecific that the diagnosis may be difficult to establish, particularly in patients who have other illnesses. Various neurologic conditions such as stroke, intracranial hemorrhage, venous thrombosis, and encephalitis can mimic hypertensive encephalopathy [3]. Furthermore, the pathophysiologic changes of hypertensive encephalopathy are unclear, being ascribed either to marked vasospasm [4, 5] or to forced vasodilatation [6–8] of the cerebral vasculature.

We reviewed the CT, MR, and single-photon emission computed tomography (SPECT) findings in 14 consecutive patients with this syndrome; 12 patients had CT, 13 had MR, and two had SPECT examinations. The study was performed to determine if these findings can be of value in establishing the diagnosis of hypertensive encephalopathy, in determining the prognosis of this disorder, and in adding to the understanding of the pathogenesis of the syndrome.

Materials and Methods

From September 1989 to August 1991, we saw 14 patients, eight obstetric and six nonobstetric, who had signs and symptoms of hypertensive encephalopathy. All eight obstetric patients, who were 16–44 years old (mean, 28 years old) had the preeclampsia-eclampsia syndrome; one had eclampsia as a result of a molar pregnancy [9], and the other

Received October 28, 1991; accepted after revision February 24, 1992.

[1] All authors: Department of Radiology, Brigham and Women's Hospital and Harvard Medical School, 75 Francis St., Boston, MA 02115. Address reprint requests to R. B. Schwartz.

0361–803X/92/1592–0379
© American Roentgen Ray Society

seven had normal gestations. Six patients, four women and two men 23–70 years old (mean, 36 years old), had hypertensive encephalopathy from other causes. Four of these had chronic renal disease (two idiopathic renal disease, one systemic lupus erythematosus, and one Wegener's granulomatosis). One patient had traumatic aortic transection with resultant renovascular hypertension, and one had acute hypertension associated with chemotherapeutic agents (steroids and cyclophosphamide) used to treat myelodysplasia.

Clinical signs and symptoms included headache (14 patients); seizures, usually with electroencephalographic abnormalities most prominent over the posterior cortex (10 patients); and visual disturbances, including blurred vision, flashing lights, or cortical blindness (nine patients). Focal weakness was noted in those patients with lesions in the basal ganglia and frontal lobe.

All patients were examined with CT or MR within 1 day after the onset of acute signs and symptoms. Thirteen patients had CT; the Siemens Somatom or Somatom Plus scanner (Siemens Medical Systems, Iselin, NJ) with 5-mm-thick axial sections or the GE 9800 unit (General Electric Medical Systems, Milwaukee, WI) with 10-mm-thick axial sections was used. Twelve patients had MR; the GE Signa 1.5-T system or the Siemens Magnetom 1.5-T system was used. In each case, T1-weighted sagittal images (600/25/1 [TR/TE/number of excitations]) and T2-weighted axial images (3000/30,80/1) were acquired, with 3- or 5-mm contiguous sections. Three patients received IV gadopentetate dimeglumine (Magnevist; Berlex Laboratories, Wayne, NJ) during the MR examination. Two patients had SPECT, one during the symptomatic hypertensive crisis and one 1 day after acute signs and symptoms had resolved. The ASPECT brain imager (Digital Scintigraphics, Cambridge, MA) and IV injection of 740–1110 MBq (20–30 mCi) of ^{99m}Tc-hexamethylpropyleneamine oxime (^{99m}Tc-HMPAO) (Ceretec; Amersham Corp., Arlington Heights, IL) were used. Images were obtained with a center resolution of 8.3 mm and reconstructed in 5-mm increments in axial, coronal, and sagittal planes. A superimposition algorithm [10] was used to merge the MR and SPECT data sets obtained within 1 day of each other to allow precise correlation of MR and SPECT findings.

All patients had follow-up CT or MR when their blood pressure had returned to normal. This occurred 5–22 days after the initial imaging examinations. The two patients who had SPECT were examined within 1 day of their first MR examination and then 9 and 14 days, respectively, after resolution of hypertension.

Results

The CT and MR findings in obstetric and nonobstetric cases of hypertensive encephalopathy were identical. All had abnormalities in the occipital lobes bilaterally, involving the subcortical white matter and often extending to the cortical surface. These lesions appeared hypodense on CT (Fig. 1) and showed increased T2 signal on MR (Figs. 2 and 3). Additional abnormalities were noted bilaterally at the parietooccipital junction (three patients), cerebellum (two patients), superior frontal lobes (two patients), and left basal ganglia (one patient). With the exception of this last case, the abnormalities in the occipital lobes were the most significant both radiologically and clinically. Although two patients had no evidence of abnormal contrast enhancement on MR, one had prominent enhancement in the regions of increased T2 signal (Fig. 4); this patient was imaged on the day of admission, whereas the other two patients were imaged on their third day of hospitalization. One patient with thrombocytopenia had evidence of an associated small hemorrhage. In no patient was an infarct or significant intraparenchymal hematoma shown.

In all cases, findings on both CT and MR were abnormal in the acute stage. Abnormalities were always better delineated and often more numerous on the MR images. The abnormalities in all patients resolved within 1–2 weeks after blood pressure was controlled, at which time all neurologic signs and symptoms resolved completely without sequelae.

In the patient in whom SPECT was performed during the symptomatic hypertensive crisis, SPECT showed increased perfusion in the vicinity of the brain that had abnormal signal

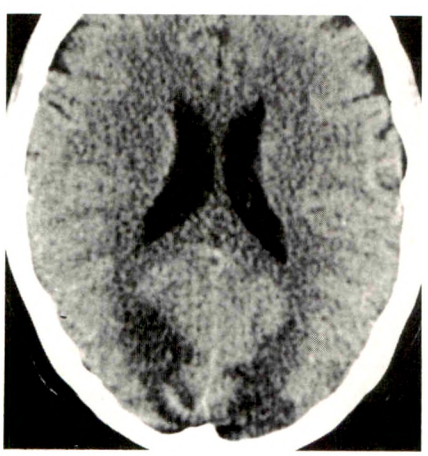


Fig. 1.—CT appearance of hypertensive encephalopathy. Unenhanced CT scan of 25-year-old woman with acute hypertension associated with combined steroid and cyclophosphamide therapy for treatment of myelodysplasia shows decreased attenuation in occipital lobes bilaterally. Findings on CT scan obtained after resolution of hypertension were normal.

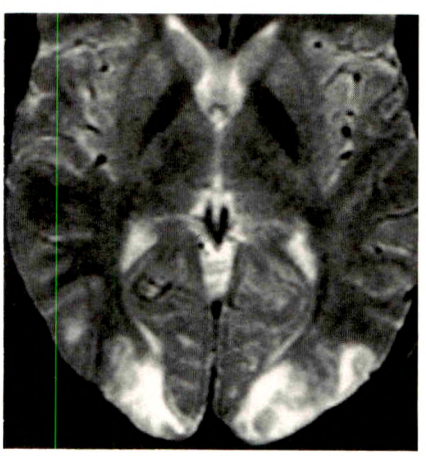


Fig. 2.—MR appearance of hypertensive encephalopathy in renal disease. T2-weighted MR image (3000/80/1) of 24-year-old woman with lupus nephritis shows increased signal in occipital lobes bilaterally. Signal abnormalities resolved 9 days after successful treatment of hypertension.

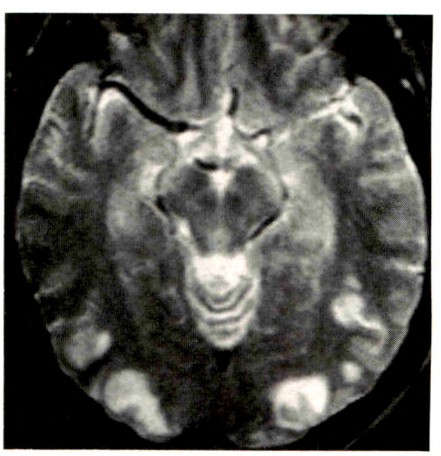


Fig. 3.—MR appearance of hypertensive encephalopathy in preeclampsia-eclampsia syndrome. T2-weighted MR image (3000/80/1) of 17-year-old woman with eclampsia shows increased T2 signal in occipital lobes bilaterally. MR image obtained 1 week after normalization of blood pressure showed complete resolution of these abnormalities.

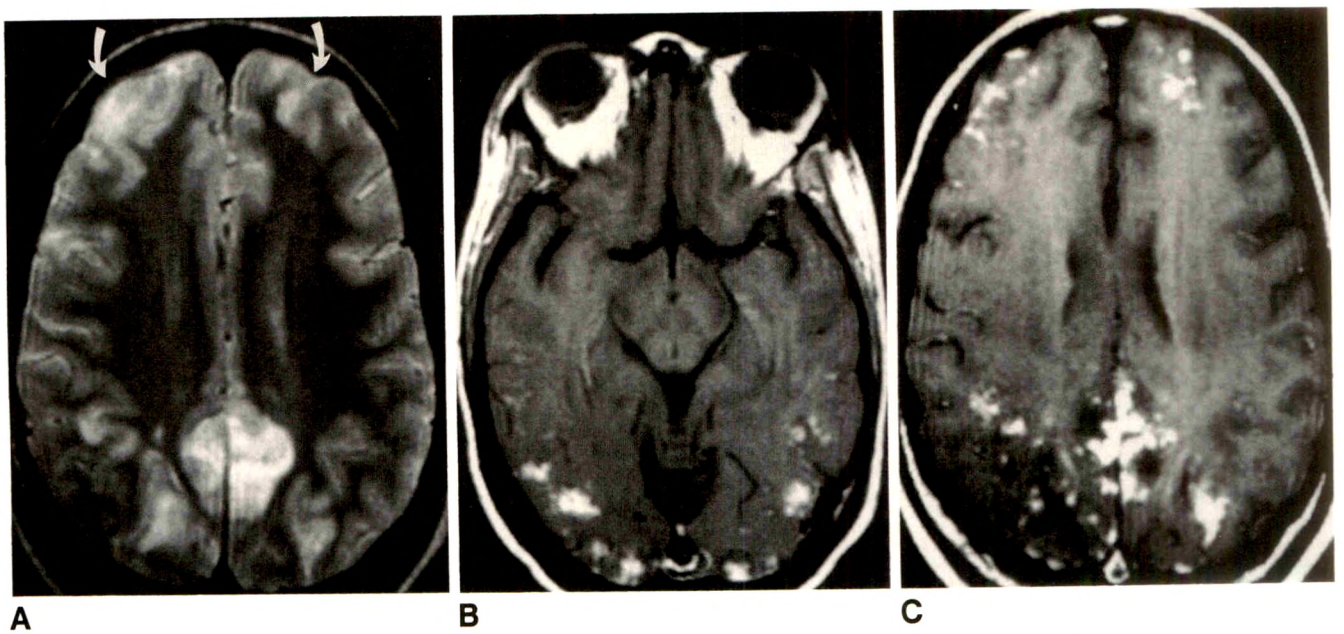


Fig. 4.—Enhancement and unusually extensive distribution of lesions in hypertensive encephalopathy in a 27-year-old woman with preeclampsia.
A, T2-weighted MR image (3000/80/1) shows increased T2 signal in occipital lobes and parietooccipital junction bilaterally. More subtle lesions (*arrows*) are seen in superior frontal lobes bilaterally.
B and *C*, T1-weighted MR images (600/25/1) obtained after IV injection of gadopentetate dimeglumine show enhancement in regions that had increased signal on T2-weighted images. MR images obtained after normalization of blood pressure showed complete resolution of these abnormalities.

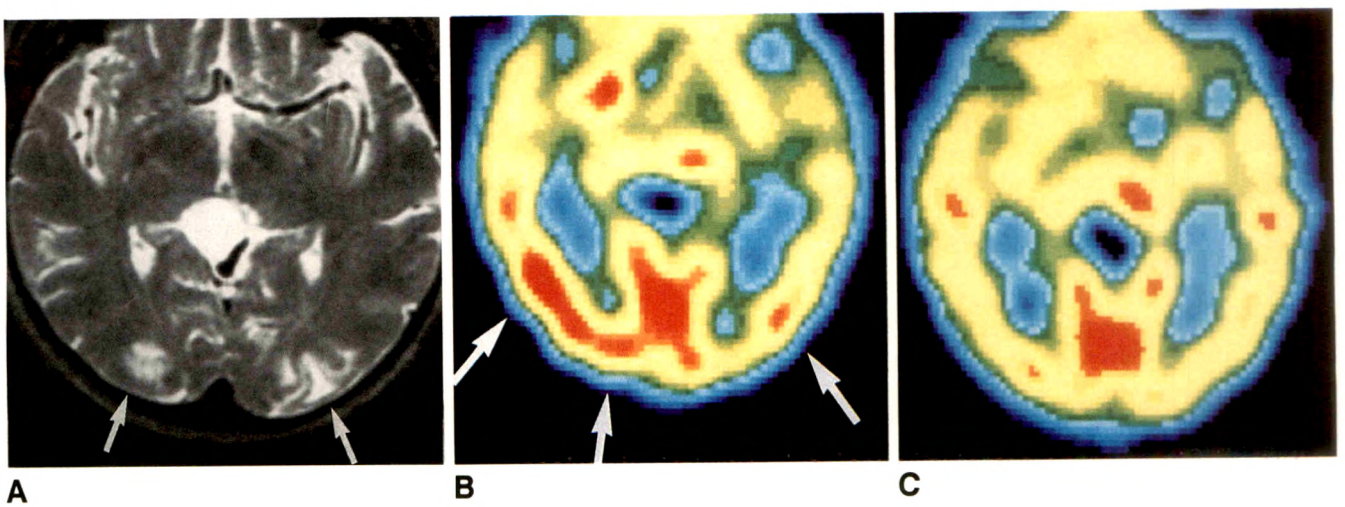


Fig. 5.—Hypertensive encephalopathy in a 23-year-old man with renal failure due to Wegener's granulomatosis.
A, T2-weighted MR image (3000/80/1) shows increased T2 signal (*arrows*) in occipital lobes bilaterally. Note also cyst in pineal region.
B, SPECT image obtained with ^{99m}Tc-hexamethylpropyleneamine oxime (^{99m}Tc-HMPAO) shows increased perfusion (red areas, *arrows*) in occipital poles bilaterally. These perfusion abnormalities are more extensive than corresponding foci of increased T2 signal in *A*.
C, SPECT image obtained with ^{99m}Tc-HMPAO 10 days after normalization of blood pressure shows almost complete resolution of these abnormalities.

on MR (Figs. 5A and 5B). In the second patient in whom SPECT was performed 1 day after the acute signs and symptoms of hypertensive encephalopathy had resolved and when blood pressure was normal, the images showed only mild perfusion abnormalities. In both cases, findings on SPECT scans were entirely normal within 2 weeks after return of normal blood pressure (Fig. 5C).

Discussion

Hypertensive encephalopathy is a syndrome in which headache, seizures, visual changes, and other neurologic disturbances occur in conjunction with elevated systemic blood pressure. In our series, all 14 patients had reversible edema localized mainly to the occipital lobes, as shown by transient

decreased attenuation on CT scans and increased signal on T2-weighted MR images. In addition, nine patients had visual disturbances referable to occipital lobe disease. Consideration of the likely mechanisms of hypertensive encephalopathy may be useful in understanding the radiologic appearance of this syndrome.

The brain normally is protected from extremes of blood pressure by an autoregulation system that ensures constant perfusion over a wide range of systemic pressures. In response to systemic hypotension, cerebral arterioles dilate to maintain adequate perfusion, whereas vessels constrict in response to high pressures. Above the upper limit of autoregulation, hypertensive encephalopathy may occur [7].

Two theories have been proposed to account for the clinical and radiologic abnormalities associated with hypertensive encephalopathy. The first postulates that hypertensive encephalopathy results from spasm of the cerebral vasculature in response to acute hypertension (i.e., overregulation), resulting in ischemia and cytotoxic edema involving mainly the border-zone arterial regions [4, 5]. A more recent hypothesis suggests that the syndrome results from breakthrough of autoregulation, with passive overdistension of cerebral arterioles [6–8]. This would result in interstitial extravasation of proteins and fluid, producing focal vasogenic (hydrostatic) edema in the peripheral vascular distribution of the involved vessel.

Our findings support the existence of a vasodilatory mechanism in the pathogenesis of hypertensive encephalopathy. If vasospasm were an important feature, ischemia with resultant infarction would be likely in some patients. This, however, occurs infrequently both clinically [1, 4–6, 11, 12] and experimentally [8], and was not radiologically evident in any of our patients. Moreover, if the clinical and radiologic abnormalities in hypertensive encephalopathy were due to ischemia, local blood flow in the brain would be decreased, a finding that has not been produced experimentally [8, 13]. In our study, SPECT with ^{99m}Tc-HMPAO was used to investigate regional brain perfusion. We found that during the hypertensive crisis, uptake of the radionuclide was increased in much of the occipital lobe and cerebellum, indicating regional hyperperfusion.

Animal models of hypertensive encephalopathy have shown a "beaded" or "sausage-string" appearance of the cerebral microvasculature intraoperatively; this has been shown experimentally to represent areas of focal forced arteriolar dilatation separated by segments of normally reactive vessel [14]. Disruption of the blood-brain barrier with resultant edema has been found at these dilated arteriolar segments by histologic examination [8, 13]. Breakdown of the blood-brain barrier in hypertensive encephalopathy was suggested in our study by focal enhancement on MR with gadopentetate dimeglumine in the acute stage. Thus, our findings support the view that hypertensive encephalopathy is caused by breakthrough of autoregulation, with focal vasogenic edema.

The susceptibility of the posterior circulation to the lesions of hypertensive encephalopathy is a well-known [6, 11, 15] but poorly understood phenomenon, but one likely explanation involves the regional heterogeneity of the sympathetic vascular innervation. In experimental studies, the sympathetic innervation of the intracranial arterioles has been shown to protect the brain from marked increases in blood pressure [16]. Moreover, ultrastructural studies have shown that the internal carotid system is much better supplied with sympathetic innervation than is the vertebrobasilar system [17]. Acute hypertension would, in this view, stimulate the perivascular sympathetic nerves, which would protect the anterior but not the more poorly innervated posterior circulation. This would result in breakthrough of autoregulation with edema mainly in the occipital lobes, as was seen in our series.

The clinical and radiologic findings in hypertensive encephalopathy are distinct from those of other forms of hypertension. Hypertensive encephalopathy is a subacute phenomenon, requiring several days of increasing pressure to become manifest [2]. All of our patients, for example, had worsening headache or documented increasing blood pressure for 1–10 days before presentation. In more acute hypertensive crises caused by cocaine or other sympathomimetic agents [18, 19], however, abrupt and marked elevations of systemic blood pressures occur, which predispose to intracranial hemorrhage and infarction. Hemorrhages presumably are due to rapid increases in hydrostatic forces that overwhelm autoregulatory mechanisms [7], resulting in vessel rupture, usually at sites of existing vascular pathologic changes [18]. Infarction may be related to intense vasoconstriction caused by the direct effect of these drugs on the sympathetic nerves surrounding intracranial arteries [18].

Our findings also differ from those in patients with chronic hypertension. In these patients, multiple small infarctions and focal hemorrhages involve the basal ganglia, thalamus, centrum semiovale, and less frequently, the pons and cerebellum [1]. In contrast, infarcts or significant hemorrhages did not occur in any of our patients. Petechial hemorrhages and small infarcts have been detected in the postmortem specimens of patients with severe eclampsia [12], but the development of large areas of infarction or hemorrhage in patients with preeclampsia-eclampsia syndrome is uncommon [12, 20] and has not been reported in nonobstetric cases of hypertensive encephalopathy [1, 6].

The radiologic findings and clinical course of the syndrome were identical in obstetric and nonobstetric cases, supporting the clinical impression that regardless of the cause of hypertension, these patients have common pathophysiologic changes [9, 12]. Moreover, the clinical course of the patients in our series suggests that a single episode of hypertensive encephalopathy, irrespective of its cause or signs and symptoms, is associated with an excellent prognosis if treated promptly and requires no further treatment after blood pressures have normalized [20]. Most patients with uncomplicated hypertensive encephalopathy probably do not have radiologic examinations, especially if treatment promptly reverses the syndrome. Nonetheless, awareness of the radiologic appearance of hypertensive encephalopathy should allow radiologists to suggest the correct diagnosis in symptomatic hypertensive patients who have an atypical presentation or clinical course.

In conclusion, hypertensive encephalopathy is a distinct syndrome that differs from other forms of hypertension in its clinical and radiologic manifestations. Characteristic findings

include areas of reversible hypodensity on CT and increased T2 signal on MR, usually localized to the occipital lobes, with increased perfusion to these regions on SPECT. As would be expected, lesions are more conspicuous and more numerous on MR images than on CT scans. Our findings support a vasodilatory mechanism with resultant edema rather than a primary vasospastic mechanism.

ACKNOWLEDGMENTS

We thank Harold M. Tice for advice and Jo-Anne Polak for assistance in manuscript preparation.

REFERENCES

1. Chester EM, Agamanolis DP, Banker BQ, Victor M. Hypertensive encephalopathy: a clinicopathologic study of 20 cases. *Neurology* **1977**;28:928–939
2. Gifford RW. Management of hypertensive crises. *JAMA* **1991**;266:829–835
3. Calhoun DA, Oparil S. Treatment of hypertensive crisis. *N Engl J Med* **1990**;323:1177–1183
4. Trommer BL, Homer D, Mikhael MA. Cerebral vasospasm and eclampsia. *Stroke* **1988**;19:326–329
5. Coughlin WF, McMurdo SK, Reeves T. MR imaging of postpartum cortical blindness. *J Comput Assist Tomogr* **1989**;13:572–576
6. Hauser RA, Lacey DM, Knight MR. Hypertensive encephalopathy: magnetic resonance imaging demonstration of reversible cortical and white matter lesions. *Arch Neurol* **1988**;45:1078–1083
7. Strandgaard S, Paulson OB. Cerebral autoregulation. *Stroke* **1984**;15:413–416
8. Nag S, Robertson DM, Dinsdale HB. Cerebral cortical changes in acute hypertension: an ultrastructural study. *Lab Invest* **1977**;39:150–161
9. Malow BA, Sandson TA, Schwartz RB. Reversible MRI lesions in eclampsia with hydatidiform mole. *Neurology* **1990**;40:1471–1472
10. Holman BL, Zimmerman RE, Johnson KA, et al. Computer-assisted superimposition of magnetic resonance images and high-resolution Tc-99m HMPAO and Tl-201 SPECT images of the brain. *J Nucl Med* **1991**;32:1478–1484
11. Sanders TG, Clayman DA, Sanchez-Ramos L, Vines FS, Russo L. Brain in eclampsia: MR imaging with clinical correlation. *Radiology* **1991**;180:475–478
12. Richards A, Graham D, Bullock R. Clinicopathological study of neurological complications due to hypertensive disorders of pregnancy. *J Neurol Neurosurg Psychiatry* **1988**;51:416–421
13. MacKenzie ET, Strandgaard S, Graham DI, Jones JV, Harper AM, Farrar JK. Effects of acutely induced hypertension in cats on pial arteriolar caliber, local cerebral blood flow, and the blood-brain barrier. *Circ Res* **1976**;39:33–41
14. Kontos HA, Wei EP, Deitrich D, et al. Mechanism of cerebral arteriolar abnormalities after acute hypertension. *Am J Physiol* **1981**;240:H511–H527
15. Aguglia U, Tinuper P, Farnarier G, Quattrone A. Electroencephalographic and anatomo-clinical evidences of posterior cerebral damage in hypertensive encephalopathy. *Clin Electroencephalogr* **1984**;15:53–60
16. Beausang-Linder M, Bill A. Cerebral circulation in acute arterial hypertension: protective effects of sympathetic nervous activity. *Acta Physiol Scand* **1981**;111:193–199
17. Edvinsson L, Owman C, Sjoberg N-O. Autonomic nerves, mast cells, and amine receptors in human brain vessels: histochemical and pharmacologic study. *Brain Res* **1976**;115:377–393
18. Jacobs IG, Roszler MH, Kelly JK, Klein MA, Kling GA. Cocaine abuse: neurovascular complications. *Radiology* **1989**;170:223–227
19. Delaney P, Estes M. Intracranial hemorrhage with amphetamine abuse. *Neurology* **1980**;30:1125–1128
20. Sibai BM, Spinnato JA, Watson DL, Lewis JA, Anderson GD. Eclampsia IV: neurologic findings and future outcome. *Am J Obstet Gynecol* **1985**;152:184–192

Book Review

MRI Atlas of the Spine. By Kenneth R. Maravilla and Wendy A. Cohen. New York: Raven, 456 pp., 1991. $140

As MR continues to develop, new techniques, ideas, and even diagnostic applications have continued to develop also. MR imaging of the spine is an example of an application of this imaging technique in which significant advances have been made over the past few years. In an attempt to keep current with the field, this text is dedicated entirely to the topic of MR imaging of the spine. Organizationally, the text is divided into nine sections. The first two deal mainly with the scientific and technical nature of MR and MR imaging of the spine. The remaining chapters are divided into primarily diagnostic, as opposed to anatomic, chapters and discussions related to MR imaging of the spine. For example, separate chapters are dedicated to MR examinations of neoplastic, degenerative/inflammatory, traumatic, and postinterventional conditions of the spine. Another chapter is devoted to MR imaging of the spine in infants and children and another to imaging of degenerative disk disease. The technical chapters are, as is often the case, highly concise overviews of the MR imaging process, with brief discussions of spin-echo, inversion-recovery, and gradient-echo imaging sequences. Fast spin-echo and three-dimensional Fourier transform techniques are not included in this discussion or, indeed, in the text as a whole. Information on curved reformatting hardware/software, which might be especially relevant for imaging of the scoliotic spine, also is not included. Nevertheless, the technical chapters, seemingly mandatory for texts such as this one, certainly offer a reasonable introduction to the physics of MR imaging of the spine.

The chapters are also interestingly arranged: All figures are grouped at the end of each chapter, after the text and references. Although such an organization may have some positive aspects, my personal preference is to have the figures and images more readily and easily accessible on the pages where they are cited or discussed. However, having the illustrations at the end is only a minor nuisance at worst.

Beginning with the anatomic chapter, the extensive figure captions are an essential part of the book. Although I do not agree with all the accompanying narrative (e.g., describing truncation artifact as central canal in one figure and as central gray matter in another), the captions generally serve as excellent free-standing cases for the points being illustrated. The book has some unusual omissions: Spondylolysis and spondylolisthesis are topics that appear neither in the index nor in the images or text per se. Similarly, the book has several references to short TI inversion recovery sequences but none to chemical-specific fat-saturation sequences. Overall, however, the authors provide multiple cases with copious images for each example, more than adequately highlighting the topic being discussed. Image quality, although somewhat variable, is generally quite good.

In summary, this is not an atlas in the classic sense. The intent of the authors is certainly not to provide simply an atlas of the normal anatomic structures of the spine, although that is a small part of what is included in this work. Rather, this is more of a visual teaching-file type of a reference, with a generous supply of good-quality images illustrating a broad spectrum of normal and abnormal conditions involving the entire spinal column. The organization by disease type and the clear, concise style and detail of the text and the figure captions make this a useful text, especially for those relatively new to the field of diagnostic MR imaging of the spine.

Emanuel Kanal
Pittsburgh NMR Institute
Pittsburgh, PA 15213

Gadopentetate Dimeglumine–Enhanced MR Imaging of the Postoperative Lumbar Spine: Comparison of Fat-Suppressed and Conventional T1-Weighted Images

Scott A. Mirowitz[1]
Kevin L. Shady

OBJECTIVE. Gadopentetate dimeglumine–enhanced T1-weighted MR imaging has been used to distinguish epidural fibrosis from recurrent disk herniation in the postoperative lumbar spine. Potential interpretative difficulties relate to detection of subtle contrast enhancement and distinction of enhanced tissue from surrounding epidural fat. The objective of this study was to evaluate the utility of fat-suppressed T1-weighted imaging in improving the depiction of postoperative abnormalities.

SUBJECTS AND METHODS. Forty-one patients with recurrent signs and symptoms after previous laminectomy and diskectomy were examined with conventional and fat-suppressed T1-weighted imaging before and after IV administration of gadopentetate dimeglumine. MR images were analyzed for the presence or absence of an epidural soft-tissue mass located anterior and/or lateral to the thecal sac. When such masses were identified, their contrast enhancement behavior was characterized according to the volume, intensity, and pattern of enhancement. Epidural fibrosis was diagnosed by using established MR imaging criteria. In patients with evidence of recurrent disk herniation, diagnosis was based on surgery in six patients and on MR imaging findings in the remainder.

RESULTS. Soft-tissue masses were present at 32 of the 43 levels operated on, representing epidural fibrosis (n = 21) or disk herniation (n = 11). Fat suppression improved depiction of contrast enhancement associated with sites of epidural fibrosis. The extent, intensity, and homogeneity of enhancement was greater with fat suppression than with conventional imaging, although the ability to distinguish epidural fibrosis from recurrent disk herniation was not improved.

CONCLUSION. Use of the fat-suppression technique results in increased relative intensity and homogeneity of contrast enhancement associated with sites of epidural fibrosis. However, it does not result in significant improvement in the ability to differentiate fibrotic tissue from recurrent disk herniation. Fat suppression does not appear to be indicated for routine use in imaging of the postoperative lumbar spine, but may be useful as a problem-solving tool in selected patients.

AJR 159:385–389, August 1992

Gadopentetate dimeglumine has been used to assist in the differentiation of postoperative epidural fibrosis from disk herniation in patients who have recurrent pain in the back and/or leg after previous laminectomy. This distinction is based on visualization of enhancement in association with fibrosis, whereas disk material does not significantly enhance [1–4]. Although the accuracy of gadopentetate dimeglumine–enhanced MR imaging is extremely high, potential interpretative difficulties may relate to the detection of subtle degrees of contrast enhancement and the inability to clearly distinguish enhanced tissue from surrounding epidural fat because of their similar signal intensities. We have investigated the potential role of fat-suppressed T1-weighted imaging to improve the detection and distinction of epidural soft-tissue abnormalities in the postoperative lumbar spine.

Received December 19, 1991; accepted after revision February 24, 1992.

[1] Both authors: Department of Radiology, Jewish Hospital at Washington University Medical Center, Washington University School of Medicine, 216 S. Kingshighway Blvd., St. Louis, MO 63110. Address reprint requests to S. A. Mirowitz.

0361–803X/92/1592–0385
© American Roentgen Ray Society

Subjects and Methods

Forty-one consecutive patients (22 men and 19 women 20–76 years old; mean age, 46 years) with recurrent back and leg pain after previous laminectomy and diskectomy were prospectively examined in this pilot study. Imaging was performed with a 1.5-T system (Signa; General Electric Medical Systems, Milwaukee, WI) and a dedicated 5 × 11 in. (13 × 28 cm) surface coil. The postoperative disk levels that were evaluated included the L3–L4 (n = 3), L4–L5 (n = 20), and L5–S1 (n = 20) interspaces. The elapsed time since surgery ranged from 1.5 months to 20 years (mean, 4.6 years).

Initial evaluation was performed with sagittal T1-weighted (400/17/2 [TR/TE/excitations], 192 × 256 matrix, 4-mm slice thickness with 1-mm gap, 24-cm field of view) and spin-density T2-weighted (2000/30, 80/1; 192 × 256 matrix; 4-mm slice thickness with 1-mm gap; 24-cm field of view) pulse sequences. Subsequently, axial T1-weighted imaging was performed with and without application of the fat-saturation technique. The fat-saturation technique uses a chemical shift–selective RF saturation pulse applied at the lipid peak, followed by a spoiler gradient pulse [5, 6]. After the execution of the presaturation and spoiler gradient pulses, a standard spin warp excitation sequence is carried out. The result is that signal intensity from the resonant peak of lipid is suppressed. Imaging parameters were identical for both sets of T1-weighted sequences: 400–600/15, 192 × 256 imaging matrix, 20- to 24-cm field of view, and 4-mm slice thickness with 1-mm interslice gap. Images were acquired parallel to the intervertebral disk spaces. The angle and position of imaging slices were held constant for performance of conventional and fat-suppressed imaging. Imaging time was equivalent for both sets of T1-weighted sequences, although approximately 30% fewer slices were available when the fat-suppression technique was used. Additional images available with conventional T1-weighted sequences were obtained at levels that had not been operated on.

Both sets of axial T1-weighted images were repeated after IV administration of 0.1 mmol of gadopentetate dimeglumine per kilogram body weight; imaging parameters were identical to those described earlier. Imaging commenced immediately after injection of contrast material. Contrast-enhanced conventional T1-weighted images were acquired before enhanced fat-suppressed T1-weighted images in 19 patients and after fat-suppressed images in 22 patients. The mean interval between acquisition of the two sets of contrast-enhanced images was 9 min (range, 5–15 min).

The images obtained were analyzed for the presence or absence of an epidural soft-tissue mass located and/or lateral to the thecal sac. When such masses were identified, their contrast enhancement behavior was characterized according to the volume, intensity, and pattern of enhancement. Images were analyzed by two radiologists, with final determinations made by consensus. The volume of enhancement was judged to be absent, partial, or diffuse. Diffuse enhancement indicated that areas of contrast enhancement were seen throughout the mass, although enhancement may have been heterogeneous. The intensity of enhancement was determined by using the signal intensity of fat on conventional T1-weighted images as a reference. Enhanced tissue that was isointense with fat was regarded as of moderate intensity, whereas enhanced tissue that was hypointense or hyperintense relative to fat was considered of mild or marked intensity, respectively. The enhancement pattern was rated as either homogeneous or heterogeneous. Heterogeneous enhancement was further subdivided according to whether focal nonenhancing or relatively less intensely enhancing portions of the mass were linear and/or nodular in configuration. Other criteria evaluated included the presence or absence of mass effect on the thecal sac and/or adjacent nerve roots, and visualization of enhancement within the parent disk.

Epidural fibrosis was diagnosed by using established criteria, including diffuse contrast enhancement after administration of gadopentetate dimeglumine, linear or irregular contour, and noncontiguity with parent disk [1–4, 7]. In patients with evidence of epidural fibrosis alone, surgical confirmation was not available because of the accepted nonsurgical management of such patients [8, 9]. In patients with evidence of recurrent disk herniation with or without associated fibrosis, MR findings were correlated with surgical results in six patients, and the diagnosis was based on imaging findings in the remainder.

Results

Soft-tissue masses were present at 32 (74%) of the 43 levels examined. Diffuse enhancement due to epidural fibrosis

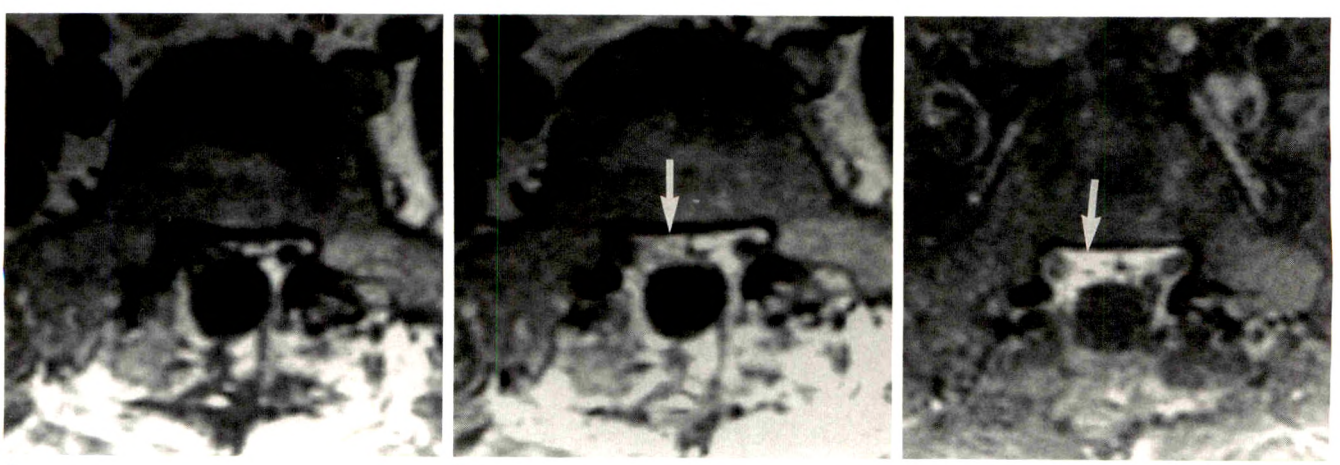


Fig. 1.—45-year-old woman 4 years after L4–L5 diskectomy.
***A–C*, Unenhanced (*A*) and enhanced (*B*) conventional and enhanced fat-suppressed (*C*) T1-weighted MR images. Intensity of contrast enhancement associated with postoperative epidural fibrosis (*arrows*) is considerably greater when fat-suppression technique is used. In addition, fat suppression improves depiction of lesion extent because enhanced tissue and epidural fat are of similar signal intensity on conventional T1-weighted images. Enhancement is also evident within anterior epidural venous plexus.**

was observed on both conventional and fat-suppressed T1-weighted images at 21 levels (Figs. 1–3). Conventional T1-weighted images showed enhancement that was homogeneous at four levels (19%) and heterogeneous at the remaining 17 levels (81%). Among heterogeneously enhancing masses, the enhancement pattern was classified as linear (n = 6), nodular (n = 10), or both (n = 1). Enhanced fat-suppressed images showed homogeneous enhancement at 11 levels (52%) with epidural fibrosis. The remaining 10 levels (48%) with epidural fibrosis showed heterogeneous enhancement in which nodular, linear, or both patterns were present at seven levels, two levels, and one level, respectively. On conventional T1-weighted images, intensity of enhancement was mild at 11 levels (52%) and moderate at 10 levels (48%), whereas on fat-suppressed images, intensity of enhancement was moderate at five levels (24%) and marked at 16 levels (76%). Mass effect due to postoperative epidural fibrosis was shown at three (14%) of 21 levels.

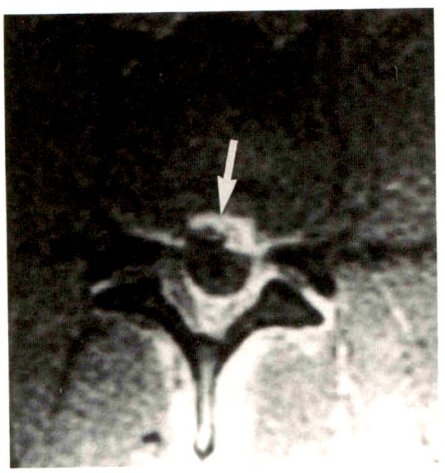


Fig. 2.—34-year-old man 2½ months after diskectomy. Fat-suppressed gadopentetate dimeglumine–enhanced T1-weighted MR image shows prominent enhancement due to epidural fibrosis surrounding thecal sac on left side and extending into outer margin of disk (*arrow*) at site of previous curettage.

A central nonenhancing mass was seen at 11 levels with recurrent disk herniation. Herniated disk material was surrounded by enhancing epidural fibrosis at 10 of 11 levels. The MR appearance of disk herniation correlated with operative findings in all six patients in whom surgery was performed. Peripheral enhancement due to surrounding epidural fibrosis was considerably more conspicuous on enhanced fat-suppressed T1-weighted images than on enhanced T1-weighted images obtained without fat suppression (Fig. 4). Evidence of mass effect on the thecal sac and/or adjacent nerve roots was evident to various degrees at 10 of 11 levels with recurrent disk herniation. The use of fat suppression did not change the diagnosis of recurrent disk herniation vs epidural fibrosis in any patients from that suggested by findings on contrast-enhanced conventional T1-weighted images.

Enhancement of a portion of the adjacent disk, near the curettage site, was seen at 31 (72%) of 43 levels on both sets of T1-weighted images (Fig. 2), although the conspicuousness of this finding was considerably greater when the fat-suppression method was used. In addition, increased conspicuity of contrast enhancement was routinely noted within the dorsal root ganglia and epidural venous plexus on fat-suppressed images.

Discussion

Although recurrence of symptoms after surgical lumbar diskectomy has many causes, two of the most frequent causes are residual or recurrent disk herniation or formation of epidural fibrosis [10]. Both entities offer an explanation for back pain or radicular symptoms, but the distinction between them forms the basis for the treatment approach. Surgical removal of disk fragments is generally undertaken, whereas surgical debridement of epidural fibrosis is usually unsuccess-

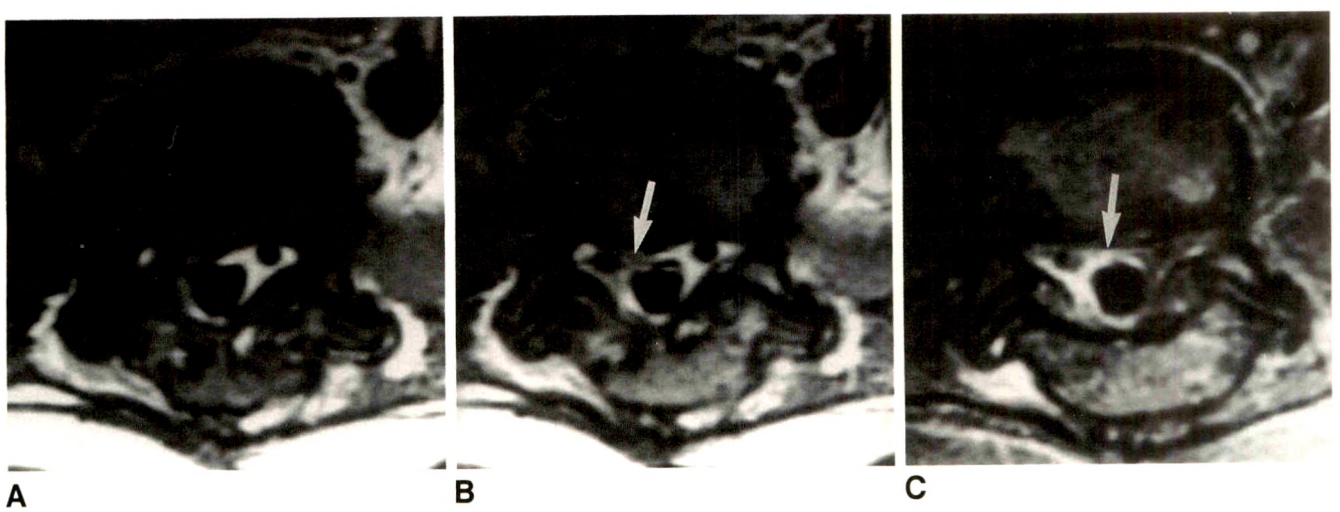


Fig. 3.—30-year-old woman after previous diskectomy.

***A–C*, Unenhanced (*A*) and enhanced (*B*) conventional and enhanced fat-suppressed (*C*) T1-weighted MR images. Epidural fibrosis fills right lateral recess and partially surrounds thecal sac. Intensity of contrast enhancement (*arrows*) is greater on fat-suppressed image, and extent of fibrosis can be more precisely determined because of improved distinction between enhancing tissue and adjacent epidural fat.**

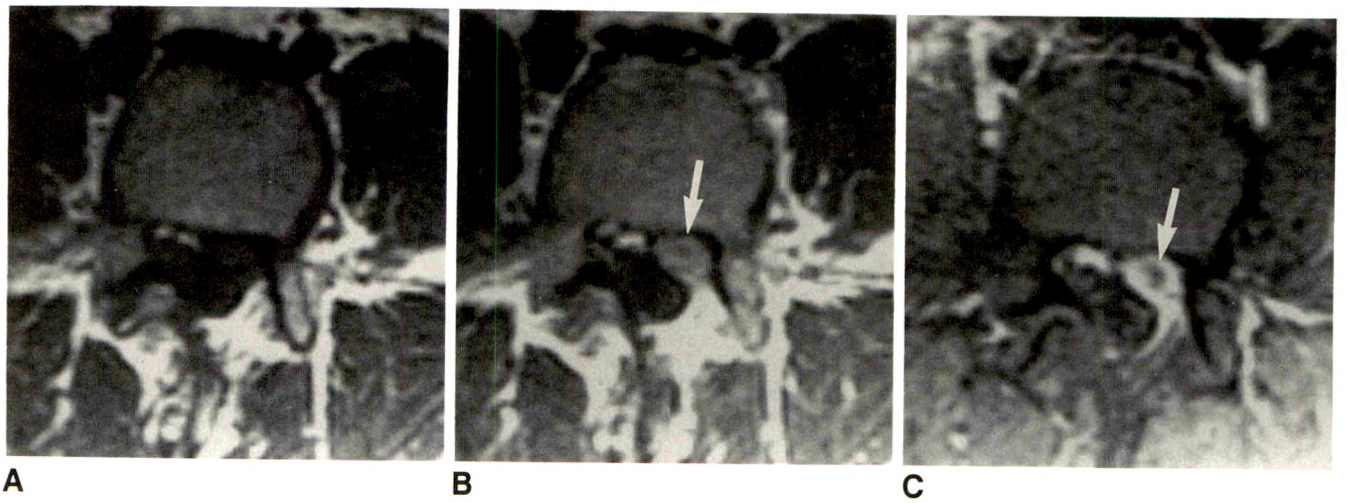


Fig. 4.—35-year-old woman 6 years after L4–L5 diskectomy.
***A–C*, Unenhanced (*A*) and enhanced (*B*) conventional and enhanced fat-suppressed (*C*) T1-weighted MR images. Surgically confirmed recurrent disk herniation (*arrows*) is surrounded by rim of epidural fibrosis. Differential enhancement between disk material and fibrosis is considerably improved with fat-suppression technique, allowing more precise determination of size and location of disk fragment.**

ful, and the approach to such cases is almost invariably conservative [8, 9].

Unenhanced MR images may show signal-intensity patterns on T2-weighted images that allow distinction of disk herniation from epidural fibrosis. Fibrotic tissue located anterior and/or lateral to the thecal sac often shows higher signal intensity than does disk herniation [7, 11]. However, the signal characteristics of herniated disk material and those of fibrosis vary, and the appearances of these tissues may be similar [12]. For example, increased signal intensity may be present in conjunction with extruded disk fragments [11, 13], and the signal intensity of fibrosis may vary considerably over time [2]. Ancillary features such as lesion morphology, contiguity with the parent disk space, and the presence or absence of mass effect also assist in this differentiation. However, these criteria also have been found to be limited in some cases. For example, epidural fibrosis has been noted to result in significant mass effect on the thecal sac and nerve roots in some cases [1, 3].

These limitations have led to the use of contrast-enhanced MR imaging for improved distinction between epidural fibrosis and disk herniation. A number of studies indicate that diagnostic accuracy is significantly improved when gadopentetate dimeglumine–enhanced T1-weighted images, rather than unenhanced T1-weighted or T2-weighted images, are used [1, 3]. Epidural fibrosis enhances because of the presence of vessels and leaky intercellular junctions. Disk material, on the other hand, is largely avascular, and does not enhance within the first 20 min after injection of gadopentetate dimeglumine [3, 14]. Disk material can partially enhance on delayed contrast-enhanced images [1], a phenomenon attributed to growth of granulation tissue into the disk. Such enhancement has been shown on images obtained more than 30 min after administration of gadopentetate dimeglumine [1], although images acquired within 10–20 min of contrast injection have been thought to be unaffected by such disk-related enhancement [3, 14].

Although gadopentetate dimeglumine–enhanced T1-weighted images have shown a high level of accuracy in the evaluation of the postoperative lumbar spine, potential difficulties in interpretation could relate to detection of subtle contrast enhancement and/or an inability to clearly distinguish enhanced fibrotic tissue from surrounding epidural fat owing to similarity in the signal intensities of these structures. These difficulties are usually resolved through close comparison of enhanced and unenhanced T1-weighted images. In this study, we investigated the use of the contrast-enhanced fat-suppression technique in improving the depiction and distinction of soft-tissue abnormalities in the postoperative lumbar spine.

Our findings indicate that fat suppression offers a number of potential advantages in this regard. First, enhancement associated with epidural fibrosis appears considerably more intense when the fat-suppression technique is used. This is primarily attributable to a marked reduction in the signal intensity of surrounding epidural fat, as well as to improvement in the dynamic range for display of tissue contrast [15–18]. In addition to increased relative intensity, increased uniformity of contrast enhancement associated with epidural fibrosis also was observed when the fat-suppression technique was used. This is probably related to improved visualization of enhancement within foci of epidural fibrosis on fat-suppressed compared with conventional images. Depiction of improved homogeneity of contrast enhancement within sites of epidural fibrosis may be diagnostically advantageous, as small nonenhancing or relatively less intensely enhancing fibrotic foci may simulate the presence of disk fragments. These factors allow improved detection of enhancement associated with epidural fibrosis, although in our series they did not increase the accuracy for distinction of epidural fibrosis from recurrent disk herniation.

Although the fat-suppression images showed distinct advantages over conventional T1-weighted images, several important disadvantages also were encountered. Owing to suppression of signal originating from lipid-containing tissues,

fat-suppressed images are of intrinsically lower signal-to-noise ratio than are conventional images that use similar imaging parameters. This is manifested as a grainier appearance, particularly on unenhanced images. Administration of gadopentetate dimeglumine largely alleviates this limitation because of the increased signal intensity contributed by the contrast agent. Unenhanced fat-suppressed images were generally not diagnostically useful, whereas unenhanced conventional images provided considerable anatomic information. Another deficit of the fat-suppression method is a 30% reduction in the number of imaging slices that can be obtained per unit time. Finally, suppression of fat signal could be nonuniform because of intrinsic or extrinsic heterogeneities in the magnetic field [15, 16], although this was not thought to be a significant limitation in this study.

Our frequent observation of contrast enhancement within the disk near the curettage site almost certainly relates to ingrowth of vascularized granulation tissue after surgery. This finding has been shown previously in humans [1] and in an animal model [19], and it should not be interpreted as evidence of infection or other abnormality. Such enhancement is more conspicuous with the fat-suppression technique. Disk enhancement also has been observed in the presence of annular tears, likewise attributed to ingrowth of granulation tissue [20]. In a recent report, Bobman et al. [21] described observation of enhancement within the intrathecal roots of the cauda equina on contrast-enhanced fat-suppressed MR images. This finding, which is presumed to reflect the presence of arachnoiditis, was not evaluated in our study.

In conclusion, use of the fat-suppression technique results in increased relative intensity and homogeneity of contrast enhancement associated with sites of epidural fibrosis. However, no significant improvement was seen in the ability to differentiate fibrotic tissue from recurrent disk herniation. Fat suppression does not appear to be indicated for routine use in imaging of the postoperative lumbar spine, but may be useful as a problem-solving tool in selected patients.

REFERENCES

1. Hueftle MG, Modic MT, Ross JS, et al. Lumbar spine: postoperative MR imaging with Gd-DTPA. *Radiology* **1988**;167:817–824
2. Sotiropoulos S, Chafetz NI, Lang P, et al. Differentiation between postoperative scar and recurrent disk herniation: prospective comparison of MR, CT, and contrast-enhanced CT. *AJNR* **1989**;10:639–643
3. Ross JS, Masaryk TJ, Schrader M, Gentili A, Bohlman H, Modic MT. MR imaging of the postoperative lumbar spine: assessment with gadopentetate dimeglumine. *AJNR* **1990**;11:771–776
4. Djukic S, Genant HK, Helms CA, Holt RG. Magnetic resonance imaging of the postoperative lumbar spine. *Radiol Clin North Am* **1990**;28:341–360
5. Brateman L. Chemical shift imaging: a review. *AJR* **1986**;146:971–980
6. Keller PJ, Hunter WW Jr, Schmalbrock P. Multisection fat-water imaging with chemical shift selective presaturation. *Radiology* **1987**;164:539–541
7. Ross JS, Modic MT, Masaryk TJ, Hueftle MG. The postoperative lumbar spine. *Semin Roentgenol* **1988**;23:125–136
8. Law JD, Lehman RAW, Kirsch WM. Reoperation after lumbar intervertebral disc surgery. *J Neurosurg* **1978**;48:259–263
9. Finnegan WJ, Fenlin JM, Marvel JP, et al. Results of surgical intervention in the symptomatic multiply-operated back patient. *J Bone Joint Surg [Am]* **1979**;61-A:1077–1082
10. Burton CV, Kirkaldy-Willis WH, Yong-Hing K, et al. Causes of failure of surgery on the lumbar spine. *Clin Orthop* **1981**;157:191–199
11. Bundschuh CV, Modic MT, Ross JS, Masaryk TJ, Bohlman H. Epidural fibrosis and recurrent disk herniation in the lumbar spine: MR imaging assessment. *AJR* **1988**;150:923–932
12. Hochhauser L, Kieffer SA, Cacayorin ED, Petro GR, Teller WF. Recurrent postdiskectomy low back pain: MR-surgical correlation. *AJNR* **1988**;9:769–774
13. Glickstein MF, Burke DL Jr, Kressel HY. Magnetic resonance demonstration of hyperintense herniated discs and extruded disc fragments. *Skeletal Radiol* **1989**;18:527–530
14. Ross JS, Delamarter R, Hueftle MG, et al. Gadolinium-DTPA–enhanced MR imaging of the postoperative lumbar spine: time course and mechanism of enhancement. *AJNR* **1989**;10:37–46
15. Semelka RC, Chew W, Hricak H, Tomei E, Higgins CB. Fat-saturation MR imaging of the upper abdomen. *AJR* **1990**;155:1111–1116
16. Mitchell DG, Vinitski S, Saponaro S, Tasciyan T, Burk DL Jr, Rifkin MD. Liver and pancreas: improved spin-echo T1 contrast by shorter echo time and fat suppression at 1.5 T. *Radiology* **1991**;178:67–71
17. Simon JH, Szumowski J, Totterman S, et al. Fat-suppression MR imaging of the orbit. *AJNR* **1988**;9:961–968
18. Simon JH, Szumowski J. Chemical shift imaging with paramagnetic contrast material enhancement for improved lesion depiction. *Radiology* **1989**;171:539–543
19. Nguyen CM, Ho K-C, Yu S, Haughton VM, Strandt JA. An experimental model to study contrast enhancement in MR imaging of the intervertebral disk. *AJNR* **1989**;10:811–814
20. Ross JS, Modic MT, Masaryk TJ. Tears of the anulus fibrosus: assessment with Gd-DTPA–enhanced MR imaging. *AJNR* **1989**;10:1251–1254
21. Bobman SA, Atlas SW, Listerud J, Grossman RI. Postoperative lumbar spine: contrast-enhanced chemical shift MR imaging. *Radiology* **1991**;179:557–562

Book Review

Human Cross-sectional Anatomy. Atlas of Body Sections and CT Images. By Harold Ellis, Bari M. Logan, and Adrian Dixon. Stoneham, MA: Butterworth-Heinemann, 180 pp., 1991. $49.95

This atlas contains superb color photographs of the gross brain and axial sections of both male and female cadavers correlated with CT scans of patients shown on the same or opposing pages. Included are 28 planes through the head and neck; 11 of the thorax, with four additional planes through the superior mediastinum; 10 through the abdomen; 18 of the pelvis (both male and female), 12 selected planes through the lower limb; and 11 selected planes through the upper limb. Diagrams indicating the plane of section and brief anatomic and clinical notes accompany each plane of section. The illustrations are profusely and carefully labeled, with reference numbers on the photographs and on the drawings that accompany the CT scans. Although the text is brief (the anatomic and clinical notes only), it is adequate for an atlas of this type. The anatomic illustrations are large, and the format and organization are both attractive and useful. Both the authors and the publisher are to be congratulated for producing an atlas of such quality.

The book does have a few minor shortcomings. The quality of the CT scans is sometimes less than optimal, as many are dark. This may represent problems in the printing or photographic process, rather than poor quality in the original scans. For example, the CT scan of the head on page 19 and the one on page 27 are of different levels of brightness. Moreover, the differentiation between gray matter and white matter on many of the brain CT scans is less than optimal. The scans of the chest, abdomen, and pelvis were obtained with various amounts of intravascular contrast material and gastrointestinal opacification.

I have a few arguments with the terminology used in the anatomic sections. Dura mater is classified either as "outer endosteal layer" or "inner meningeal layer." Although arachnoid and pia are discussed in the accompanying notes, they are not used in the labeling of the anatomic sections. Similarly, on page 31, cisterna ambiens appears to be the label for what I would call the quadrigeminal cistern. These types of disagreements are minor and certainly do not seriously detract from the quality of this atlas.

The matching of anatomic sections to CT scans is generally good, but inconsistent. For example, on page 57, an anatomic section through the alveolar process of the maxilla, the hard palate, and the cerebellum is matched with a CT scan showing the maxillary sinuses, the nasal turbinates, and the dens. This particular matching of anatomic section and CT scan is the worst in the book. Unfortunately, it has been chosen by the publisher to illustrate the promotional brochure for the atlas.

This atlas is a valuable contribution among a number of publications on this topic and is certainly a valuable book for the modern medical student. It could be somewhat useful for residents in radiology, but the number of sections through some regions of the body and the quality of the CT scans are not sufficient for learning contiguous anatomy as shown on clinical CT scans. This is a suitable atlas, however, for teaching clinical anatomy to first-year medical students. Certainly, its price, $49.95, is a bargain for the color and quality of the anatomic sections.

Robert A. Clark
H. Lee Moffitt Cancer Center and Research Institute
Tampa, FL 33682-0179

Case Report

Ganglioglioma with Leptomeningeal and Subarachnoid Spread: Results of CT, MR, and PET Imaging

Robert D. Tien,[1] Susan L. Tuori,[1] Nathan Pulkingham,[2] and Peter C. Burger[2]

Gangliogliomas of the CNS usually have a nonaggressive MR appearance without extensive spread in the parenchyma, leptomeninges, or subarachnoid space. Most frequently, they occur in children and young adults; 80% of the patients with ganglioglioma are less than 30 years old [1]. Although they are histologically benign lesions, gangliogliomas can cause significant impairment by producing seizures.

Ganglioglioma with leptomeningeal extension has been rarely reported [2, 3]. We describe a case with subarachnoid and leptomeningeal spread in a 12-year-old boy who, to our knowledge, is the first such patient to have MR imaging. This case is important because this histologically benign lesion had a deceptively aggressive MR appearance, mimicking more invasive tumors.

Case Report

The patient is a 12-year-old, right-handed boy with intractable complex partial seizures. His initial seizure occurred without fever at age 11 months after an episode of influenza. At that time the left eye was abducted, and the left upper and lower extremities twitched. The patient had a postepileptic left-sided hemiplegia, which resolved several days later. No further seizures occurred until age 3, at which time the patient had complex partial seizures consisting in staring and sucking movements and twitching of the left side of his face. The patient had approximately three seizures per week; the longest seizure-free period was 2–3 weeks. The patient had never been in status epilepticus, nor had he undergone any imaging studies before these.

Neurologic findings at our institution were normal except for mild dysmetria in the left upper extremity and mirror movements in both upper extremities. Unenhanced CT showed a small cystic mass with calcification in the right medial temporal lobe (Fig. 1A). Contrast-enhanced CT scans showed leptomeningeal enhancement along the proximal portion of the right middle cerebral artery and in the right sylvian fissure (Fig. 1B). Enhancement in the prepontine cistern also was noted (Fig. 1C). Subsequent gadopentetate dimeglumine–enhanced MR images showed a cystic parenchymal mass in the right anteromedial temporal lobe with a minimally enhancing medial component and adjacent abnormal leptomeningeal enhancement (Figs. 1D and 1E). As part of the routine to evaluate patients with seizure before surgery, positron emission tomography (PET) was done. The PET scan (Fig. 1F) showed a diffuse area of mildly decreased activity in the right temporal lobe with one focal area of markedly decreased activity in the uncus. This correlated with the location of the tumor noted on the MR images. Video electroencephalographic monitoring revealed seizures arising from the right temporal lobe. A Wada test located memory and language function in the left hemisphere, with no evidence of language and only minimal memory function in the right hemisphere. Subsequently, the patient underwent an anterior right temporal lobectomy without complications.

The tumor had two components visualized during surgery: (1) a main gelatinous and partially calcified component and (2) a second tougher tissue located in the anterior portion of the right temporal lobe. This tough tissue infiltrated the leptomeninges of the right sylvian fissure and surrounded the right M1 segment of the middle cerebral artery. The portion of the tumor adherent to the middle cerebral artery could not be removed.

The pathologic specimens showed abnormal cluttering of ganglion cells with features typical of a ganglioglioma. These ganglion cell contained a prominent centrally located nucleolus within large round

Received January 24, 1992; accepted after revision February 24, 1992.
[1] Department of Radiology, Duke University Medical Center, Box 3808, Durham, NC 27710. Address reprint requests to R. D. Tien.
[2] Department of Pathology, Duke University Medical Center, Durham, NC 27710.

 0361–803X/92/1592–0391 © American Roentgen Ray Society

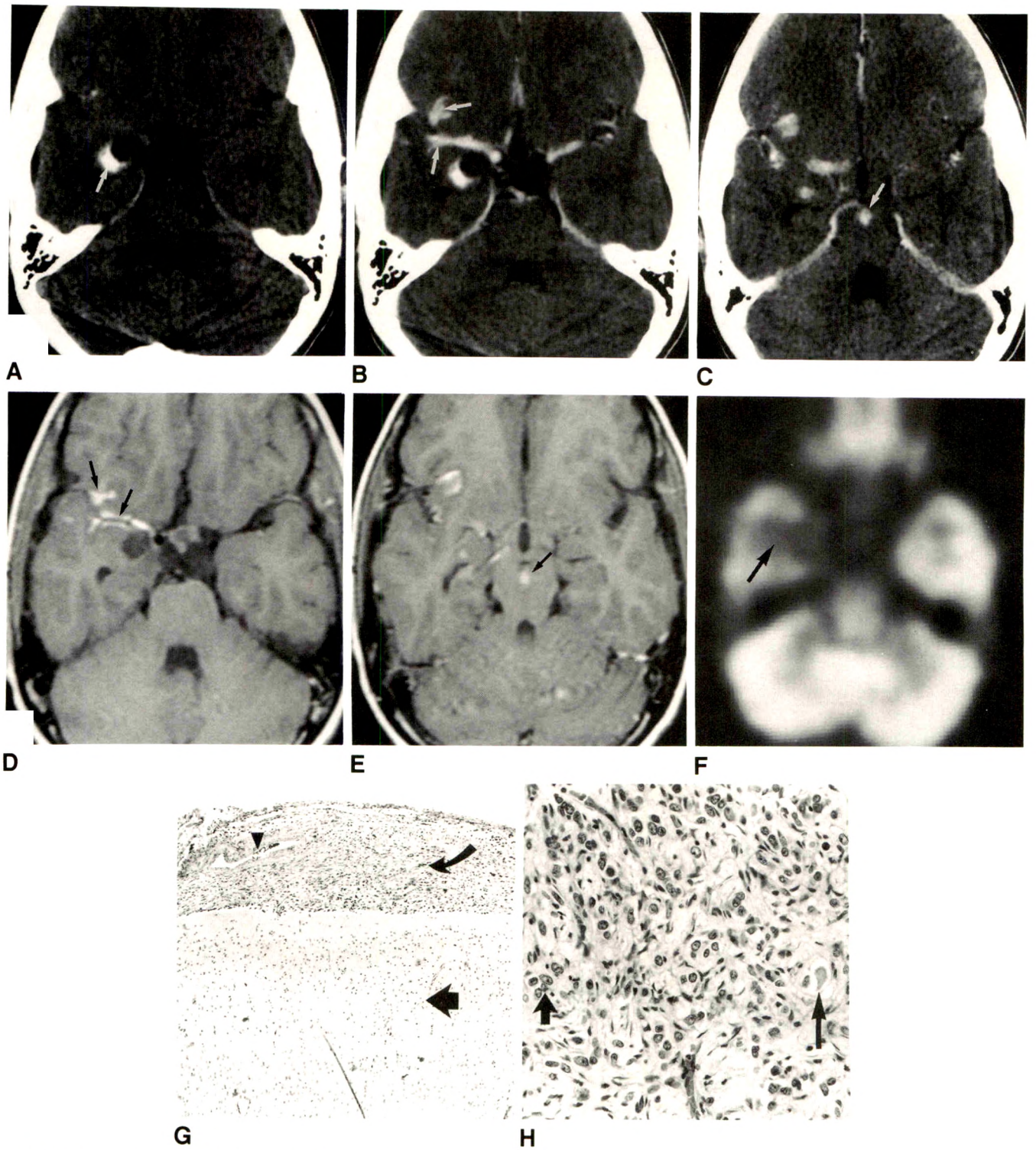


Fig. 1.—*A*, Unenhanced CT scan shows a small cystic mass with calcification (*arrow*) in right medial temporal lobe.

B, Contrast-enhanced CT scan shows abnormal enhancement along right middle cerebral artery and sylvian fissure (*arrows*).

C, Contrast-enhanced CT scan 5 mm below level of *B* again shows abnormal enhancement at right sylvian fissure and prepontine cistern (*arrow*).

D, Gadopentetate dimeglumine–enhanced T1-weighted axial MR image shows abnormal contrast enhancement of right middle cerebral artery and sylvian fissure (*arrows*).

E, Axial MR image 5 mm below level of *A* again shows enhancing tumor in prepontine cistern (*arrow*).

F, ^{18}F-fluorodeoxyglucose positron emission tomography (^{18}F-FDG PET) scan shows markedly decreased uptake of radionuclide in right medial temporal lobe (*arrow*).

G, Photomicrograph of section of normal cortical gray matter (*straight arrow*) shows a hypercellular neoplasm (*curved arrow*) filling and extending throughout leptomeningeal space. Neoplasm totally encases a medium-sized leptomeningeal vessel (*arrowhead*). (H & E, original magnification ×52)

H, Photomicrograph of section of leptomeningeal neoplasm shows abnormal clustering of ganglion cells with nuclear features typical of a ganglion cell neoplasm, including large round to oval nuclei and a vesicular chromatin pattern with a prominent centrally located nucleolus (*short arrow*). Additional evidence of ganglionic origin of neoplasm includes Nissl substance within cytoplasm (*long arrow*). (H and E, original magnification ×400)

or oval nuclei (Fig. 1H). Tumor cells also were seen infiltrating the leptomeninges and encasing the subarachnoid vessels (Fig. 1G).

In the 15 months since surgery, the patient has remained free of seizures and is taking no medications. Results of a postoperative electroencephalogram were normal.

Eight months after surgery, MR images showed postoperative encephalomalacia in the right temporal lobe and the persistent enhancement of the leptomeninges around the right middle cerebral artery and adjacent basilar cisterns. The leptomeningeal enhancement did not change significantly from its preoperative appearance on the MR images and was believed to be residual tumor.

Discussion

Gangliogliomas usually occur in young patients. They are thought to make up between 4.0% and 4.5% of all CNS tumors. The most common sites of occurrence are the temporal lobe, the floor of the third ventricle, and the hypothalamus. These slow-growing tumors are usually small, firm, and well circumscribed. Temporal lobe seizures are common clinical manifestations. The diagnosis of a ganglion cell tumor depends on the microscopic identification of neoplastic neurons. Frequently, these neurons are well differentiated. The presence of Nissl substance identifies these cells as neuronal in origin. Neoplastic neurons are distinguished from normal ganglion cells by their change in distribution, pattern, and cytologic characteristics.

In patients with gangliogliomas, cystic change and calcification are common features detected by CT. Fifty percent of these lesions show some contrast enhancement [4]. On MR the cystic components of these lesions appear heterogeneous, and they mainly have low signal intensity on the T1-weighted images. On T2-weighted images, these tumors have increased signal intensity [5]. These imaging features are nonspecific. Low-grade astrocytoma, pleomorphic xanthoastrocytoma, ganglioglioma, and oligodendroglioma also should be considered. However, in none of these tumors is leptomeningeal spread common. As our case did show leptomeningeal spread, more aggressive tumors (i.e., high-grade astrocytoma and anaplastic oligodendroglioma) were considered. Although lymphoma can typically have leptomeningeal spread, it usually does not have a cystic component with calcification, and therefore, it was not included in our differential diagnosis.

In this case, despite the lesion's aggressive appearance on CT scans and MR images, its hypometabolic nature shown on the subsequent PET scan suggested a slow-growing mass. The pathologic diagnosis of a benign lesion such as a ganglioglioma is compatible with the PET findings.

Leptomeningeal spread of ganglioglioma is exceptionally rare. Wahl and Dillard [2] reported a 15-year-old boy with a ganglion cell tumor of the temporal lobe and multiple cerebrospinal subarachnoid tumors with similar histologic findings. Those tumors were considered to be due to seeding from the primary temporal tumor. During surgery, marked desmoplastic reaction in the leptomeninges was noted. Salazar et al. [3] reported another case of ganglioglioma with leptomeningeal spread in a 50-year-old man. That tumor had a large exophytic growth that extended into the suprasellar and prepontine cisterns.

Although our patient had leptomeningeal tumor extension in the right sylvian fissure and subarachnoid spread to the prepontine cistern, the tumor's benign histologic features and its hypometabolic status shown on the PET scan enabled us to make a favorable prognosis.

REFERENCES

1. Russell DS, Rubinstein LJ. *Pathology of tumors of the nervous system*, 5th ed. Baltimore: Williams & Wilkins, **1989**:260–269
2. Wahl RW, Dillard SH. Multiple gangliogliomas of the CNS. *Arch Pathol* **1972**;94:158–164
3. Salazar FJG, Sanchez-Alarcos S, Gonzalez R, Coca S, Martinez R, Vaquero J. Brain ganglioma with large extension to subarachnoid space. *J Neurosurg Sci* **1990**;34:61–63
4. Castillo M, Davis PC, Takei Y, Hoffman JC Jr. Intracranial ganglioglioma: MR, CT, and clinical findings in 18 patients. *AJR* **1990**;154:607–612
5. Tampieri D, Moumdjian R, Melanson D, Ethier R. Intracerebral gangliomas in patients with partial complex seizures: CT and MR imaging findings. *AJNR* **1991**;12:749–755

Book Review

Magnetic Resonance Imaging of the Body, 2nd ed. By Charles B. Higgins, Hedvig Hricak, and Clyde A. Helms. New York: Raven, 1420 pp., 1992. $169

This book is intended to address the needs of residents, fellows, and practicing radiologists as well as interested clinicians in understanding the physical basis and clinical applications of MR imaging of the body. Since the first edition, published in 1987, the application of MR imaging to nonneurologic disease has grown enormously. The second edition attempts to be a comprehensive text of body MR imaging. In order to accomplish this goal, the size of the book has increased voluminously. It now consists of 55 chapters and has been expanded to 1420 pages with contributions from 71 authors. Growth in MR imaging of the musculoskeletal system has necessitated the adding of a third editor, Clyde A. Helms, who has successfully integrated a much expanded section on this topic.

All the editors and contributors have impeccable credentials, and the images provided are of superb quality. The numerous line drawings, figures, and diagrams throughout the text add much to the readability of this important book.

As in the first edition, the book is organized into an anatomic atlas; principles of MR imaging; clinical applications in the neck, chest, and cardiovascular system; applications in the abdomen, pelvis, and musculoskeletal system; and a sixth section on MR contrast media. One of the strengths of the first edition was the extensive personal experience of the editors, and this remains a strength of the current edition; however, their experience at the University of California, San Francisco, is bolstered by strong chapters by outside contributors. The strongest chapters are still those on the heart, kidneys, female and male pelvis, retroperitoneum, breast, and liver and pancreas. The expanded section on the musculoskeletal system is a welcome addition, and quite successful. The section on the principles of MR imaging has been completely redone and quite easily brings the reader up to date on the latest MR techniques. The chapters present complicated data in a lucid style and add much to the success of this text.

As in the first edition, the section entitled "Anatomic Atlas" is the least successful of the book. These five chapters do not interweave text and figures successfully, and I question their overall usefulness, as much of the anatomy is repeated in individual chapters later on in the book and further duplicated by having the section on MR contrast media again present anatomic detail. A number of anatomic atlases of MR imaging are available, and I think that this part of the book could be eliminated without significant loss.

In conclusion, this is an outstanding, comprehensive text that presents MR imaging of the body better than any other text currently available. I think that the second edition has fulfilled its goals and that it has appropriately added new information, as the field has evolved. I certainly recommend this text as a reference text for every MR imaging laboratory and for those radiologists who specialize in MR imaging of the body. I wish the text were not so large, or that it came in two volumes. The single volume is so large and heavy that it is somewhat cumbersome to use.

Albert A. Moss
University of Washington
Seattle, WA 98195

Pictorial Essay

Fast Spin-Echo High-Resolution MR Imaging of the Inner Ear

Robert D. Tien,[1] Gary J. Felsberg, and James Macfall

Advances in MR imaging continue to improve our ability to evaluate temporal bone anatomy and disease. CT remains the procedure of choice for fine-detail imaging of bone structures such as ossicular anatomy, but it is not the ideal imaging technique for soft-tissue structures (e.g., the membranous labyrinth and neural structures). Conventional spin-echo MR techniques used to image these structures cannot yield excellent contrast and spatial resolution in clinically acceptable time frames. Conventional spin-echo T1-weighted images lack tissue contrast between fluid (e.g., CSF, endolymph, perilymph), neural tissue, otic capsule septa, and surrounding temporal bone. Conventional T2-weighted imaging of the inner ear is needed to reveal the natural contrast between fluid, neural structures, and bone; unfortunately, the use of conventional T2-weighted images is limited by time constraints when large-matrix, thin-section techniques with more than one excitation are used. Fast spin-echo imaging is a recently developed technique that can provide T2-weighted, thin-section (2-mm) high-resolution images with excellent contrast in a fraction of the time needed for conventional spin-echo techniques. This speed advantage allows us to obtain high-resolution images in clinically acceptable time frames. Images produced by this technique are a useful addition, in conjunction with routine T1- and T2-weighted spin-echo images, in the diagnosis of disorders of the inner ear.

Subjects and Methods

Fast spin-echo (FSE) imaging was performed in six normal volunteers and in 11 consecutive patients with a variety of inner ear disorders. The FSE technique we used is a hybrid rapid-acquisition relaxation-enhanced (RARE) technique initially described by Hennig et al. [1]. Thin-section FSE imaging of the temporal bone was prescribed from a sagittal T1-weighted localizer image. Images of subjects were obtained by using FSE techniques with the following parameters: 4000/30,80/1 (TR/TE/excitations), 16-msec bandwidth, echo train length of 16, 20-msec echo space, 18-cm field of view, 512 × 512 matrix, and 2-mm slice thickness. Contiguous slices were obtained by interleaving separate acquisitions. Eleven to 14 such slices were obtained. Images were acquired in both axial and coronal planes with one 5-in. (13-cm) surface coil centered over each ear; both ears were imaged at the same time. Imaging time for this FSE technique was less than 10 min. Conventional spin-echo images with a quadrature head coil were also contained: axial unenhanced T1-weighted images were obtained in all patients, and patients with neurosensory hearing loss also had T1-weighted images after administration of gadopentetate dimeglumine. Imaging parameters were 500/12/2 with 3-mm-thick interleaved slices and a 256 × 192 matrix. In addition, for patients with neurosensory hearing loss, conventional T2-weighted images were obtained of the entire brain (2500/20,70/1) with a 5-mm slice thickness and 2.5-mm gap. The normal anatomy and a variety of inner ear disorders were studied by these methods (Figs. 1–5).

Discussion

The main advantage of FSE imaging is that the scan time is shortened compared with conventional spin-echo images, yet the signal-to-noise ratio is not significantly reduced. Both conventional spin-echo and FSE scan times are determined by the TR, the number of excitations (NEX), and the number of phase-encoding steps (NP). The scan time for a single-echo FSE sequence, however, is reduced by a factor equal to the value of an echo train length (ETL): that is, scan time

Received January 21, 1992; accepted after revision March 3, 1992.
[1] All authors: Department of Radiology, Box 3808, Duke University Medical Center, Durham, NC 27710. Address reprint requests to R. D. Tien.

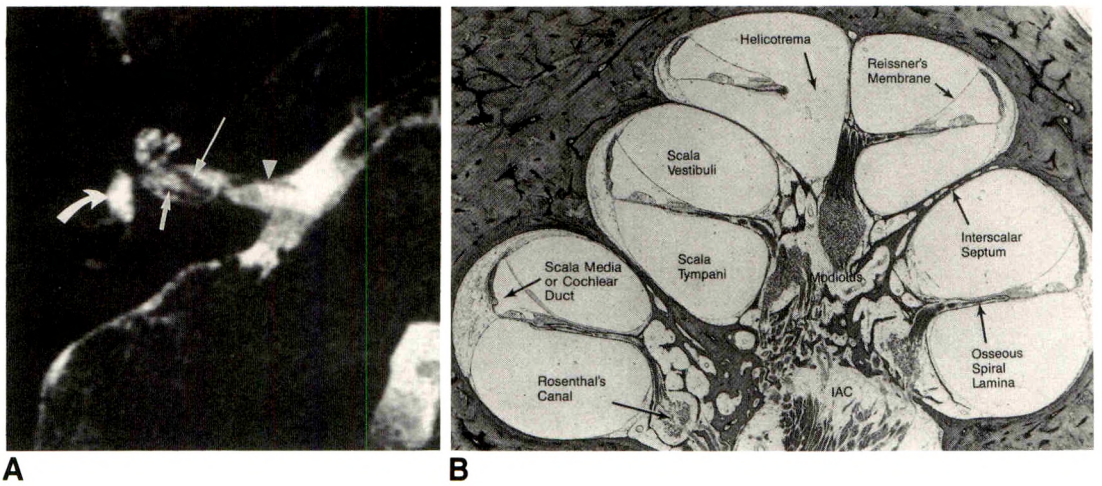


Fig. 1.—*A*, Axial T2-weighted FSE MR image (4000/80) of right inner ear of a 30-year-old healthy male volunteer. Endolymph and CSF have very high signal. Fine detailed anatomy of internal auditory canal and inner ear is seen. Modiolus, osseous spiral lamina, and interscalar septum of cochlea are clearly identified. Cochlear nerve (*long straight arrow*), vestibular nerve (*short straight arrow*), and facial nerve (*arrowhead*) are well visualized in internal auditory canal. High signal from endolymph in vestibule also is well seen (*curved arrow*).

B, Microscopic anatomic photograph of cochlea shows anatomy similar to that imaged in *A*. Modiolus, osseous spiral lamina, and interscalar septum are seen. IAC = internal auditory canal. (Reprinted with permission from Schuknecht and Gulya [2].)



Fig. 2.—Intracanalicular acoustic schwannoma in a 47-year-old woman with left-sided sensorineural hearing loss.

A, Axial surface-coil conventional T1-weighted MR image (500/12) of left ear shows possible poorly defined soft-tissue signal within internal auditory canal (*arrow*).

B, Axial FSE MR image (4000/80) shows complete replacement of normal structures in left internal auditory canal by homogeneous soft-tissue signal (*arrow*).

C, Axial T1-weighted MR image after contrast infusion shows enhancing mass in internal auditory canal and further suggests acoustic schwannoma (*arrow*).

Although both FSE and enhanced T1-weighted images showed the same information, FSE imaging may be useful in patients who refuse or are not eligible for enhanced studies.

= NP × NEX × TR/ETL. Therefore, long TRs (4000–5000 msec) can be used to generate heavy T2 weighting and an improved signal-to-noise ratio without significantly prolonging imaging time. In addition, as each individual echo in this sequence is phase encoded, few excitations are required to determine spatial localization of the signal, and because the inner ear is near the skin surface, surface-coil technology can be used to increase the signal-to-noise ratio. With this improved, diagnostically useful signal-to-noise ratio, images of high resolution (large matrix, 512 × 512) and exquisite detail can be obtained in a clinically acceptable time period.

One drawback of the FSE technique is that we cannot obtain as many slices as with the conventional spin-echo technique for the same TR. In many cases, this reduction in the number of slices is an acceptable tradeoff for the eight- or 16-fold reduction in scan time. In a limited area of interest such as the inner ear, the maximum number of slices with FSE is more than adequate. Also, when a longer TR is used,

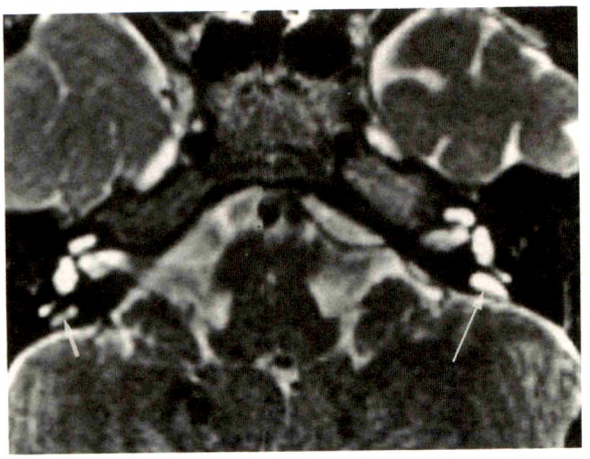


Fig. 3.—Vestibular aqueduct syndrome in a 4-year-old girl with signs and symptoms of Meniere's disease. Conventional T1- and T2-weighted MR images were unremarkable. Axial FSE MR image (4000/80; composite of left and right ears) shows marked dilatation of left vestibular aqueduct (*long arrow*). Right vestibular aqueduct is of normal size (*short arrow*). Size difference between aqueducts was considered beyond the limit of normal variation. No other inner ear structural abnormalities were identified. On the basis of FSE images and clinical symptoms and signs, diagnosis of vestibular aqueduct syndrome was made.

the slice reduction is not as severe. A second potential drawback to the FSE technique is its sensitivity to fluid flow or pulsation, which can result in artifacts on images. This has not been a problem in our experience; because fluid moves relatively slowly through the internal acoustic canal and inner ear, flow-related artifacts on FSE images have been minimal. Last, the known diminished sensitivity to magnetic susceptibility of FSE from osseus structures or paramagnetic material is advantageous in imaging the inner ear because it is surrounded by the temporal bone.

This technique will not replace contrast-enhanced images for evaluation of neuritis (e.g., Bell's palsy) or tumors [3, 4], and it is not as effective as CT in evaluating osseous structures. In cases of intracanalicular acoustic schwannoma, however, this FSE technique will enable visualization of the tumor without contrast injection (Fig. 2). This may benefit patients who are unwilling to receive contrast material or who are allergic to it, those in whom venous access is poor, or those who are in serious renal failure. The main strength of the FSE technique is that it can produce heavily T2-weighted high-resolution images that delineate the fluid-filled otic capsule and internal acoustic canal. This is particularly useful when it is important to diagnose or exclude labyrinthine fistula or cochlear erosion by tumor (Figs. 4 and 5). In most patients, acquisition of a long effective TE FSE image will answer most clinical questions. However, a long effective TE may potentially, by virtue of the extremely high perilymph/endolymph/CSF signal, mask subtle soft-tissue invasion into the cochlea or vestibule. When this is suspected, generation of a short effective TE FSE image (which produces lower intensity CSF analogous to that produced with proton-density conventional spin echo) may be of clinical use (Fig. 4). Thus, this technique can potentially aid in the diagnosis of diseases such as labyrinthine otosclerosis or fibrous labyrinthitis. Conversely, conventional spin-echo images cannot provide the necessary contrast and spatial resolution to delineate these lesions in a reasonable scanning time. Nor does CT furnish adequate contrast resolution to identify confidently the minuscule soft tissue within the otic capsule.

A further application of the FSE technique is for congenital malformations involving the membranous labyrinth. FSE can easily evaluate the size and shape of the fluid-filled otic capsule, vestibule, internal acoustic canal, and aqueducts. Our example of the vestibular aqueduct syndrome (Fig. 3) was elegantly shown by FSE and led to the clinical diagnosis;

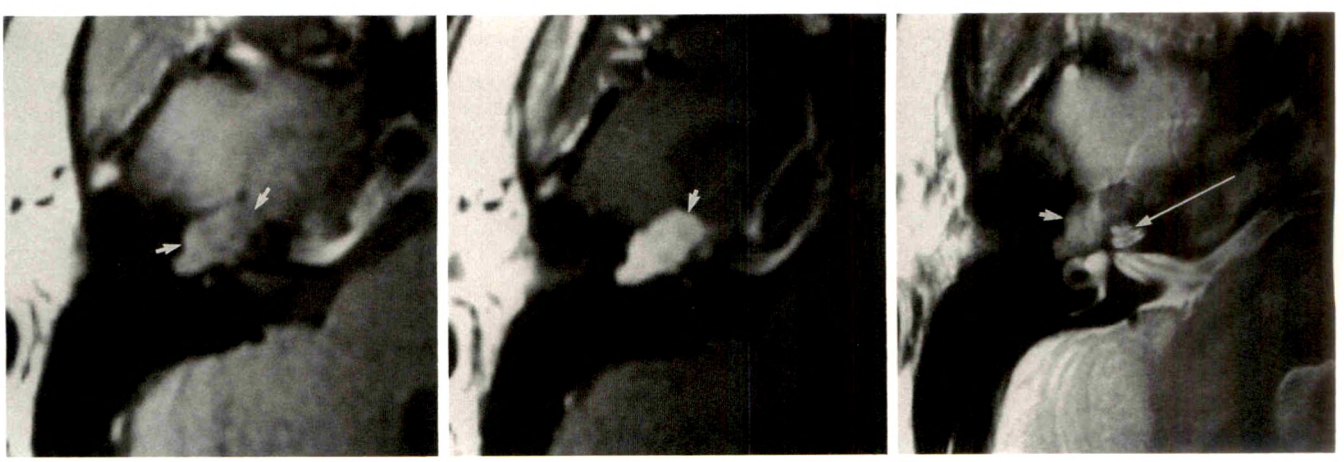


Fig. 4.—Probable facial nerve schwannoma in a 43-year-old woman with gradual onset of mild right-sided facial weakness.

A, Conventional axial T1-weighted MR image (500/12) with surface coil shows isointense soft-tissue mass in right petrous bone (*arrows*). Mass cannot be separated from inner ear structures.

B, Axial T1-weighted MR image after contrast infusion shows intense enhancement of lesion (*arrow*).

C, Axial FSE MR image (4000/30) clearly separates mass in region of geniculate ganglion (*short arrow*) from cochlea (*long arrow*) and vestibule. With FSE image, absence of tumor invasion or erosion into cochlea or vestibule is assured. Patient refused surgery.

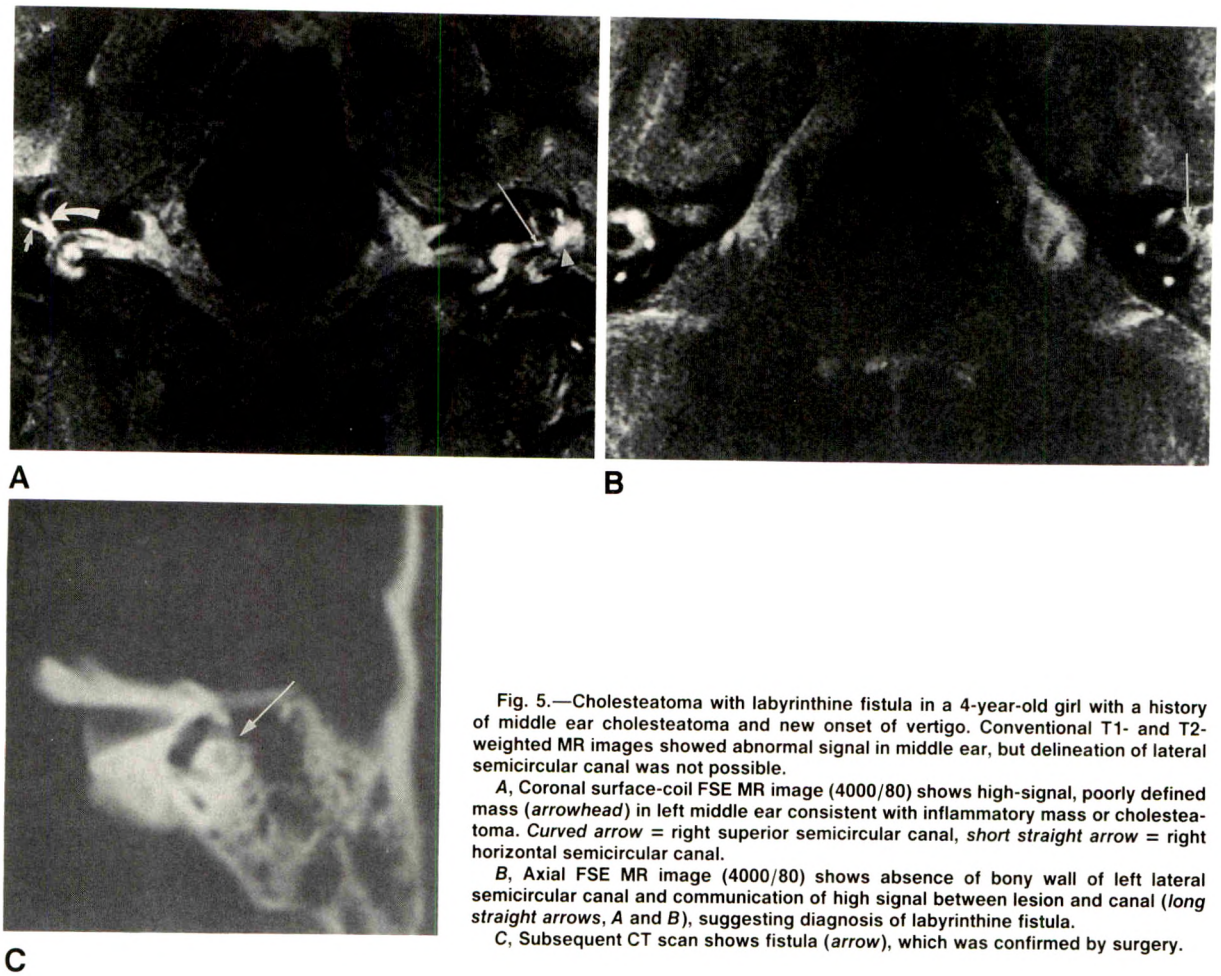


Fig. 5.—Cholesteatoma with labyrinthine fistula in a 4-year-old girl with a history of middle ear cholesteatoma and new onset of vertigo. Conventional T1- and T2-weighted MR images showed abnormal signal in middle ear, but delineation of lateral semicircular canal was not possible.

***A*, Coronal surface-coil FSE MR image (4000/80) shows high-signal, poorly defined mass (*arrowhead*) in left middle ear consistent with inflammatory mass or cholesteatoma. *Curved arrow* = right superior semicircular canal, *short straight arrow* = right horizontal semicircular canal.**

***B*, Axial FSE MR image (4000/80) shows absence of bony wall of left lateral semicircular canal and communication of high signal between lesion and canal (*long straight arrows*, *A* and *B*), suggesting diagnosis of labyrinthine fistula.**

***C*, Subsequent CT scan shows fistula (*arrow*), which was confirmed by surgery.**

on conventional spin-echo imaging this abnormality was missed because of insufficient contrast and spatial resolution. Although high-resolution CT may show the dilated aqueduct or semicircular canal fistula, the radiation exposure to the patient is unnecessary when FSE images can offer the same information without radiation.

In summary, this new FSE technique can show fine contrast and spatial resolution in the inner ear in a reasonable scanning time. In most cases, CT should be performed first for middle ear and labyrinthine disease. Thereafter, we highly recommend application of this new FSE technique in conjunction with conventional spin-echo images for evaluation of certain diseases of the inner ear.

REFERENCES

1. Hennig J, Nauerth A, Friedburg H. RARE imaging: a fast imaging method for clinical MR. *Magn Reson Med* **1986**;3:823–833
2. Schuknecht HF, Gulya AJ. *Anatomy of the temporal bone with surgical implications*. Philadelphia: Lea & Febiger, **1986**:131
3. Tien R, Dillon WP, Jackler RK. Contrast-enhanced MR imaging of the facial nerve in 11 patients with Bell's palsy. *AJNR* **1990**;11:735–741
4. Brogan M, Chakeres DW. Gd-DTPA–enhanced MR imaging of cochlear schwannoma. *AJNR* **1990**;11:407–408

Case Report

Primary Endodermal Sinus Tumor of the Orbit: MR Findings

Barbara A. Appignani,[1] Kendall M. Jones,[1] and Patrick D. Barnes[2]

Endodermal sinus tumors (yolk sac tumors) are rare neoplasms presumed to be of germ cell lineage. They are tumors of childhood that most often arise in the testis or ovary. Cases of primary endodermal sinus tumors in various extragonadal locations have been reported but are unusual. Rarely, endodermal sinus tumors are found in the head and neck. Only five intraorbital cases of endodermal sinus tumors have been reported [1], all of these occurring in children less than 4 years old. We report a case of primary endodermal sinus tumor of the orbit and provide the first description of the MR features of this unusual neoplasm.

Case Report

Progressive exophthalmos and swelling of the left eye developed in a previously healthy 22-month-old girl in a 3-week period. Physical examination showed only a swollen and ecchymotic left eye. Ophthalmologic examination revealed hyperemia and limited ocular motion with preserved vision and pupillary reflex in the left eye. The right eye was normal.

MR imaging examination of the orbits showed a 1.6 × 1.6 cm round mass within the left orbit that was intraconal and retrobulbar. The globe was displaced anteriorly and was deformed posteromedially by the adjacent tumor. The medial rectus muscle was medially deviated and the optic nerve was laterally displaced by the intervening mass. The optic nerve could not be distinguished from the tumor margins.

No evidence of tumor extension through the orbital apex or outside the orbital borders was found. The optic chiasm and tracts appeared normal. Interestingly, the bony margins of the left orbit were expanded, suggesting a chronic process with orbital remodeling.

Signal intensity within the tumor was homogeneous on all MR images (Fig. 1). T1-weighted images showed the mass to be uniformly hypointense relative to surrounding tissue, whereas intermediate signal intensity was seen on proton density–weighted images. The mass appeared relatively hyperintense on T2-weighted images. No flow void or hemorrhage was present within the mass, and no abnormality of the brain was shown. A CT scan done at another hospital reportedly showed similar findings, with a well-demarcated lesion with no calcification in the left orbit.

An excisional biopsy via a left frontal craniotomy yielded tissue for pathologic examination of the tumor. The typical features of an endodermal sinus tumor were seen. The serum level of α-fetoprotein was 2453 ng/ml (2453 μg/l; normal range, 0–6.40 μg/l), providing additional evidence for the diagnosis.

A full metastatic workup including bone marrow biopsy, ovarian and abdominal sonography, chest CT, bone scintigraphy, and CSF analysis showed no evidence of disease outside the orbit. The patient has undergone combined regimen chemotherapy (etoposide/cisplatin/vincristine and vincristine/actinomycin D/cyclophosphamide). To date, no additional disease has been documented. Follow-up evaluation will determine whether adjunctive surgery or radiation therapy is needed.

Discussion

Endodermal sinus tumors are believed to originate from a multipotential primitive germ cell that is also the progenitor of teratomas. Teratomas form from embryogenic tissue derivatives of the primitive germ cell. The undifferentiated germ cell can also give rise to tumors of extraembryonic tissue types, or yolk sac derivatives. These tumors are choriocarcinomas and endodermal sinus tumors [2]. In a 54-year review of

Received January 9, 1992; accepted February 10, 1992.

[1] Department of Radiology, Brigham and Women's Hospital and Harvard Medical School, 75 Francis St., Boston, MA 02115. Address reprint requests to B. A. Appignani.

[2] Department of Radiology, The Children's Hospital and Harvard Medical School, Boston, MA 02115.

AJR **159:399–401, August 1992** 0361–803X/92/1592–0399 © American Roentgen Ray Society

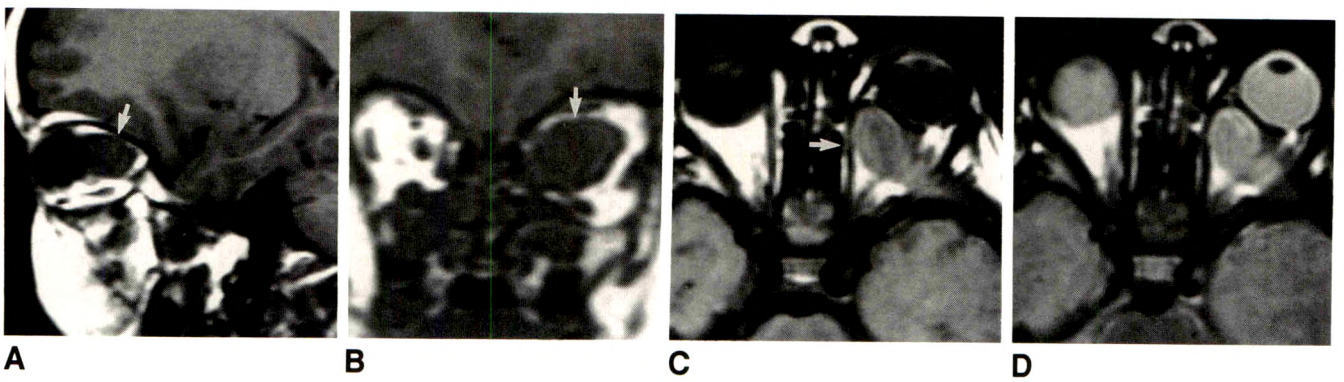


Fig. 1.—*A* and *B*, Sagittal (*A*) and coronal (*B*) T1-weighted MR images show hypointense mass (*arrow*) in left orbit. *C* and *D*, Intraconal mass (*arrow*) appears intermediate in signal intensity on proton density–weighted MR image (*C*) and slightly hyperintense on T2-weighted MR image (*D*). Tumor is fairly sharply demarcated, and orbit appears slightly expanded.

cases of primary extragonadal germ cell tumors by Lack [3], only 16 cases involved the head and neck. Of these, only two tumors, both teratomas, were orbital. Three endodermal sinus tumors of the oropharynx and nasopharynx were diagnosed.

The first published report of an endodermal sinus tumor of the orbit was by Katz et al. [4] in 1982. The diagnosis was made in a 15-month-old boy who was followed up for 8.5 years after therapy. The patient was initially evaluated for progressive exophthalmos and visual loss, with a retrobulbar mass extending into the nasopharynx. The involved orbit had a sclerotic superior margin and expanded superior orbital fissure, suggesting chronicity. Four additional cases of orbital endodermal sinus tumor were reported by the Armed Forces Institute of Pathology in 1983 [1]. These patients were between 3 months and 4 years old, and all had unilateral exophthalmos. Radiologic features were not described. In each case, the tumor was positive for α-fetoprotein. Various therapies were used, with long-term survival in two patients treated with radiation therapy and chemotherapy. In most locations, endodermal sinus tumors are aggressive malignant neoplasms that metastasize widely. The outcome in cases limited to the orbit can, however, be favorable.

Histopathologic examination of endodermal sinus tumors shows a proliferation of tubular and papillary structures with sheets of loose reticular stroma (Fig. 2). Sinusoids are formed from fibrovascular cores lined by tumor cells. Cytoplasm and extracellular spaces contain PAS-positive hyaline globules. The cells also contain large nuclei and prominent nucleoli. Electron microscopy shows dense deposits of basement membrane material, as well as intercellular tight junctions and desmosomal junctions. Microvilli project from these cells to form tubular structures [5]. Additionally, the production of α-fetoprotein helps to distinguish these from other tumors, as in our patient [6].

To our knowledge, the MR appearance of an endodermal sinus tumor of the orbit has not been previously reported, and some of the features of this neoplasm may help to distinguish it from other orbital masses in children. The most common benign orbital mass seen in children is a dermoid or epidermoid. These tumors are well defined and contain fat or fluid, which is usually hyperintense on T1-weighted images.

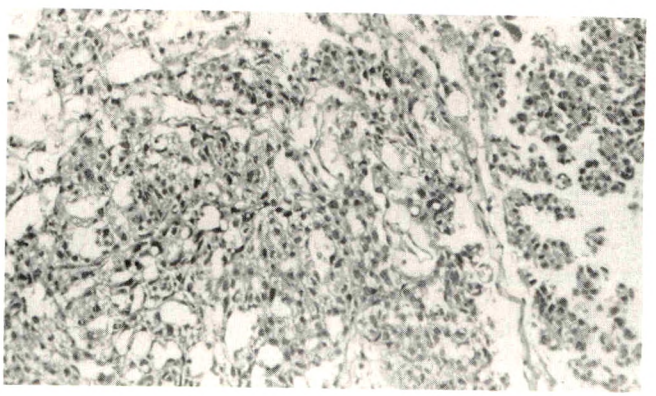


Fig. 2.—Photomicrograph (low power) shows large epithelial cells forming papillary and reticular structures characteristic of endodermal sinus tumor. (Courtesy of M. Aguiar, Dept. of Pathology, Children's Hospital, Boston, MA.)

Orbital venous and lymphatic malformations are typically multilocular masses without well-defined margins that contain "cystic" areas of lymph or hemorrhaged blood. The heterogeneous signal and hemorrhagic contents of these tumors help to differentiate them from other orbital masses. In children, hemangiomas appear as orbital masses with vascular flow voids, a feature that was not present in this case. Orbital pseudotumor is another benign entity that should be considered in the diagnosis of an orbital mass, although it rarely appears as a discrete mass. Neurofibromas and schwannomas also are seen in the orbit of children, especially in children with neurofibromatosis or sphenoorbital dysplasia. These masses have varied appearances and can even simulate a malignant neoplasm.

The most common extraocular malignant tumor occurring in the child's orbit is rhabdomyosarcoma, which is usually an infiltrative and poorly defined mass. Optic gliomas typically produce fusiform enlargement of the optic nerve and may appear as a retrobulbar lobular mass. Metastatic orbital masses seen in children include neuroblastoma, chloroma, Ewing's sarcoma, and lymphoma. These tumors can be indistinguishable from the endodermal sinus tumor, and the knowl-

edge of a primary focus of extraorbital disease aids in the diagnosis of these cases.

In summary, we present a rare case of primary endodermal sinus tumor of the orbit. Characteristics include the occurrence in children and the slow growth as evidenced by bony orbital expansion. The prognosis seems to be better than in extraorbital cases of endodermal sinus tumor. MR features in this case included uniform signal intensity within a well-defined mass, with hypointensity on T1-weighted, intermediate intensity on proton density–weighted, and hyperintensity on T2-weighted images. Awareness of the imaging characteristics and clinical presentation of this tumor, and of the differential diagnosis of orbital tumors in children, may help the radiologist in differentiating an endodermal sinus tumor from other orbital masses.

REFERENCES

1. Margo CE, Folberg R, Zimmerman LE, Sesterhenn IA. Endodermal sinus tumor (yolk sac tumor) of the orbit. *Ophthalmology* **1983**;90:1426–1432
2. Gonzalez-Crussi F. *Extragonadal teratomas*. Washington, DC: Armed Forces Institute of Pathology, **1982**:Fasc. 18, 425
3. Lack E. Extragonadal germ cell tumors of the head and neck region: review of sixteen cases. *Hum Pathol* **1985**;16:56–64
4. Katz NNK, Ruymann FB, Margo CE, Popejoy LA, LaPiana FG. Endodermal sinus tumor (yolk sac carcinoma) of the orbit. *J Pediatr Ophthalmol Strabismus* **1982**;19:270–274
5. Nogales-Fernandez F, Silverberg SG, Bloustein PA, et al. Yolk sac carcinoma (endodermal sinus tumor); ultrastructure and histiogenesis of gonadal and extragonadal tumors in comparison with normal human yolk sac. *Cancer* **1977**;39:1462–1474
6. Teilum G, Albrechtsen R, Norgaard-Pedersen B. Immunofluorescent localization of alpha-fetoprotein synthesis in endodermal sinus tumor. *APMIS* **1974**;82:586–588



Book Review

Ultrasound in Ophthalmologic Diagnosis. A Practical Guide. By Rudolph Guthoff. (Translated from the German by F. C. Blodi.) New York: Thieme, 174 pp., 1991. $59

Most radiologists are not well acquainted with the use of ultrasound in the diagnosis of ophthalmologic disease, because for the most part, this has been considered part of the domain of ophthalmologists. With the increase in nondedicated ultrasound units, radiologists have shown more interest in using this technique to evaluate ophthalmic disease. This is likely to increase as color flow Doppler imaging plays more of a role in this area. For the most part, radiology textbooks make little if any mention of the use of ultrasound in the evaluation of ophthalmic disease. Most of the literature has been written by ophthalmologists, and certainly most textbooks, if not all, have been written by ophthalmologists.

This slim volume is an excellent introduction for radiologists interested in the use of ultrasound in ophthalmologic diagnosis. The book is well written and easily read, and unlike many translated volumes reads quite smoothly. It is divided into seven chapters, the first of which is mainly devoted to the physical principles of sonography, which are familiar to most radiologists. Some useful information about certain aspects of these principles as applied to eye disease is included.

The second chapter is on examination techniques. It provides an introduction to some aspects of A-mode scanning, which is still widely used in the evaluation of eye disease. Chapters 3 and 4 provide a summary of most of the common and some of the uncommon diseases that affect the globe of the eye. The data given are succinct; however, for radiologists who are not familiar with eye disease, many of the entries may be a little difficult to understand, as little information about pathophysiology is provided. The remaining chapters are devoted primarily to evaluation of disease that affects areas behind the globe. The author acknowledges that although much useful information can be obtained by using ultrasound, this anatomic area is still principally the domain of CT and MR imaging.

Many schematic diagrams are included adjacent to the sonograms, making interpretation considerably simpler. Most of the sonograms were obtained by using dedicated ultrasound units, so the quality of the images is in many instances inferior to what most radiologists are accustomed to. However, most of the information can be easily transposed to real-time nondedicated ultrasound units. Fewer than a dozen color flow and duplex Doppler images have been included, consistent with the relatively small amount of work that has been done on the use of Doppler imaging in ophthalmic disease.

A large number of references are given at the end of the book. Most are citations from the ophthalmologic literature; fewer than a dozen references are from the radiologic literature (and most of these refer to CT and MR imaging). Many of the references are also from the German-language literature, reflecting the origin of the author.

In summary, this is an easily read, affordable textbook with a large body of useful information that would be a useful introduction to eye ultrasound for any interested radiologist. I recommend that any ultrasound department interested in entering this area of investigation keep a copy of this book in their departmental library.

Peter L. Munk
University of Western Ontario
London, Ontario, Canada N6A 5A5

Case Report

Diagnosis of von Hippel–Lindau Disease in a Patient with Blindness Resulting from Bilateral Optic Nerve Hemangioblastomas

Brian M. Ginzburg,[1] Walter J. Montanera,[1] Felix J. Tyndel,[2] Jordan A. Griesman,[1] Michael K. McLennan,[1] Karel G. TerBrugge,[1] and Robert A. Willinsky[1]

Hemangioblastomas are uncommon tumors that occur mostly in the cerebellum, medulla, and spinal cord. Supratentorial hemangioblastomas are rare [1], and hemangioblastomas of the optic nerve have, to our knowledge, been reported in only eight previous cases, all of which were unilateral [2, 3]. We report a case of bilateral optic nerve hemangioblastomas, in which the resultant visual loss was the only indication in a patient who had von Hippel–Lindau disease and occult renal cell carcinoma.

Case Report

A 44-year-old man, who had emigrated from Taiwan 1 year previously, had had progressive visual loss for an 8-month period. He had no other neurologic or general signs and symptoms. Examination showed marked reduction of visual acuity, greater in the left eye than in the right, and bilateral optic disk pallor. Contrast-enhanced CT showed two 1-cm round enhancing lesions in the area of the right and left optic nerves immediately anterior to the optic chiasm (Fig. 1A). Marked bilateral white matter edema was present. The most likely diagnosis was optic nerve gliomas with spread of edema or tumor along white matter pathways. Other possibilities included lymphoma, granulomas such as tuberculosis or sarcoidosis, and aneurysms. Contrast-enhanced MR imaging showed enlargement of the optic chiasm and intracranial optic nerves with intensely enhancing prechiasmal masses (Fig. 1B). High signal intensity was seen in the optic tracts and white matter pathways. Again, the most likely diagnosis was optic chiasm and optic nerve gliomas. MR also showed two enhancing nodules, one in the left cerebellar hemisphere and one in the medulla oblongata (Figs. 1C and 1D).

At surgery, an orange-red, highly vascular tumor was completely resected from the right prechiasmal optic nerve. The similar tumor of the left optic nerve could not be completely resected because of its proximity to the internal carotid artery, and a small portion of this tumor was left in situ postoperatively. Both tumors split the optic nerves longitudinally. The optic chiasm was enlarged. The presumptive diagnosis was still optic glioma; however, the initial pathologic examination showed that the optic nerve tumors were hemangioblastomas. This was confirmed on the subsequent pathologic examinations. Examination of the chiasmal biopsy specimen showed reactive gliosis.

Postoperatively, the patient had no light perception in his left eye but was able to distinguish objects with his right eye. On follow-up MR, the optic chiasm and nerves had an almost completely normal appearance, with only minimal residual enhancement of the left optic nerve. The white matter hyperintensity had almost entirely resolved, indicating that it was probably due to edema.

The patient had additional studies because of the possibility of von Hippel–Lindau disease. No retinal angiomas were identified on ophthalmic examination. On sonography and abdominal CT, cysts were detected in the pancreas, liver, and kidneys (Fig. 1E). A large multicentric heterogeneous mass was present in the left kidney; this was proved to be renal cell carcinoma after nephrectomy. MR of the spine did not reveal any spinal hemangioblastomas. This constellation

Received November 25, 1991; accepted after revision February 12, 1992.

[1] Department of Medical Imaging (Radiology), The Toronto Hospital (Toronto Western Division), 399 Bathurst St., Toronto, Ontario, Canada M5T 2S8. Address reprint requests to W. Montanera.

[2] Department of Medicine (Neuro-ophthalmology), The Toronto Hospital (Toronto Western Division), Toronto, Ontario, Canada M5T 2S8.

AJR **159:403–405, August 1992** 0361–803X/92/1592–0403 © American Roentgen Ray Society

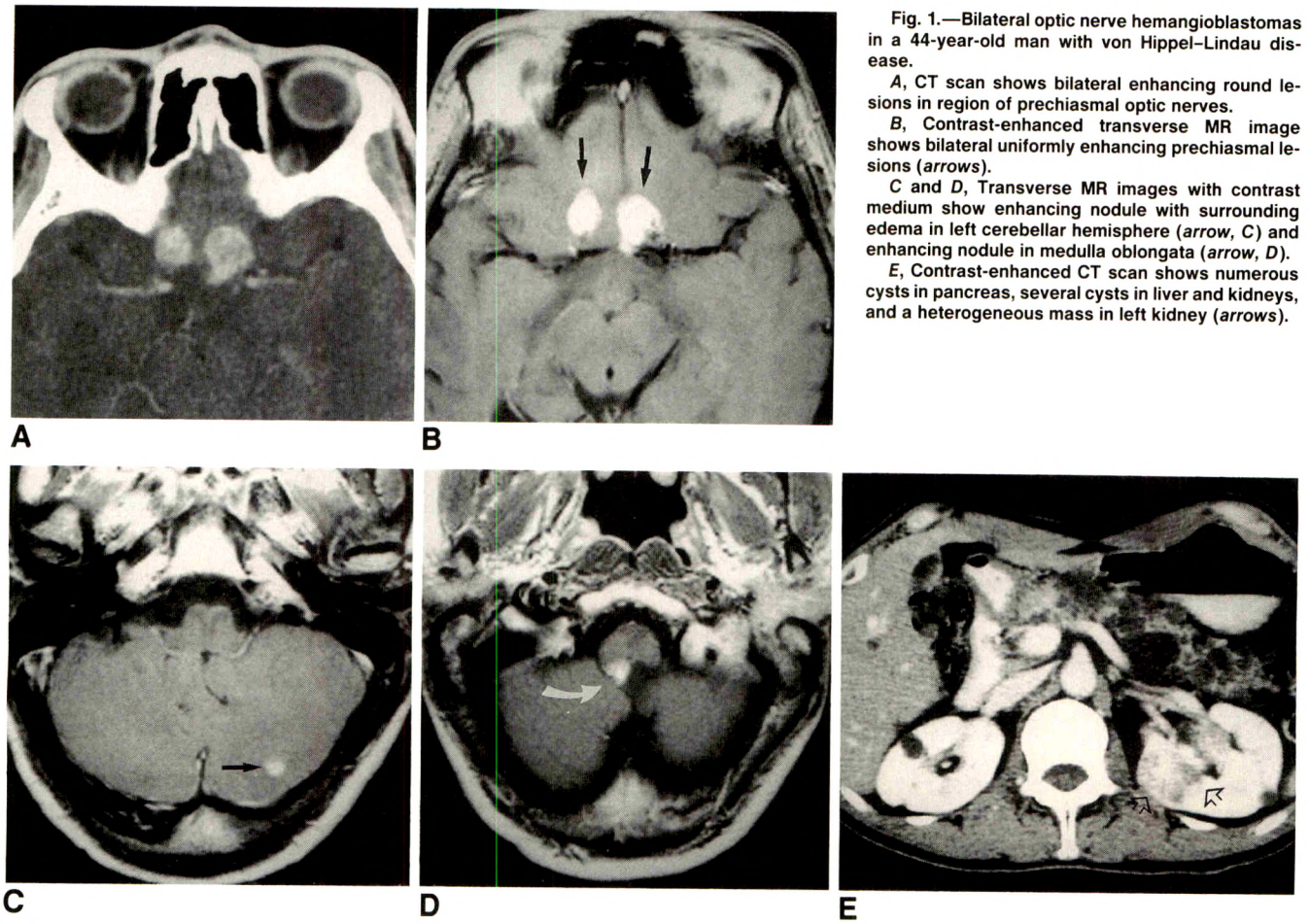


Fig. 1.—Bilateral optic nerve hemangioblastomas in a 44-year-old man with von Hippel–Lindau disease.

***A*, CT scan shows bilateral enhancing round lesions in region of prechiasmal optic nerves.**

***B*, Contrast-enhanced transverse MR image shows bilateral uniformly enhancing prechiasmal lesions (*arrows*).**

***C* and *D*, Transverse MR images with contrast medium show enhancing nodule with surrounding edema in left cerebellar hemisphere (*arrow, C*) and enhancing nodule in medulla oblongata (*arrow, D*).**

***E*, Contrast-enhanced CT scan shows numerous cysts in pancreas, several cysts in liver and kidneys, and a heterogeneous mass in left kidney (*arrows*).**

of CNS hemangioblastomas and abdominal cysts and neoplasms is diagnostic of von Hippel–Lindau disease. The patient was not aware of any family history of von Hippel–Lindau disease.

Discussion

Von Hippel–Lindau disease is an autosomal dominant disorder with variable expression. It confers on those affected a susceptibility to neoplasms and visceral cysts of various types. The prevalence of these lesions varies considerably among affected kindreds. The diagnosis is based on the finding of multiple CNS hemangioblastomas, of a CNS hemangioblastoma in association with at least one other lesion of the von Hippel–Lindau complex, or of a single lesion of the von Hippel–Lindau complex in a patient who has a family member with a proved CNS hemangioblastoma [4,5]. Cerebellar hemangioblastoma and retinal angioma are the most common initial manifestations [4]. Supratentorial hemangioblastomas are rare (more than 90% of intracranial hemangioblastomas occur in the posterior fossa), and optic nerve hemangioblastomas are exceedingly rare [3]. We were able to find only eight documented cases of optic nerve hemangioblastomas [2, 3]. Four of these patients were known to have von Hippel–Lindau disease. In three other cases, the hemangioblastomas were solitary findings with no other manifestations of von Hippel–Lindau disease. In one case, the initial manifestation was an isolated optic nerve hemangioblastoma in a man with a family history of intracranial hemangioblastomas [3]. We could find no case in which bilateral optic nerve hemangioblastomas were reported. Of 10 optic nerve hemangioblastomas (including the two in our case), four were intraorbital, four were intracranial, one involved both the intracranial and intraorbital portions of the nerve, and one was in an unspecified location [2, 3].

Hemangioblastomas are solid vascular tumors composed of both endothelial and stromal cells. Although the cell of origin is unknown, these tumors arise from the optic nerve tissue itself, and not from the nerve sheath [1, 2, 6]. The hemangioblastomas compress and replace the normal nerve tissues, and in our case, even split the nerves.

In the setting of von Hippel–Lindau disease, the differential diagnosis of optic nerve tumors must include hemangioblastoma. Conversely, the diagnosis of von Hippel–Lindau disease must be considered in a patient in whom an atypical CNS lesion, such as an optic nerve tumor, is found in conjunction with a more typical CNS hemangioblastoma. Once the diagnosis of von Hippel–Lindau disease is suspected, a thorough search for other lesions of this complex must follow. This search is directed toward the early detection of renal cell carcinoma, pheochromocytoma, CNS hemangioblastoma,

and retinal angioma; these cause the most morbidity and mortality in von Hippel–Lindau disease [5]. The radiologist plays a pivotal role in this multidisciplinary approach, both in directing subsequent imaging studies and in recommending clinical referrals. Of paramount importance is the examination of family members.

The most sensitive imaging technique for detection of CNS hemangioblastoma is contrast-enhanced MR [1]. The advantages of MR imaging and its depiction of CNS abnormalities associated with von Hippel–Lindau disease have been well described [1]. A careful search of the abdomen is directed toward the detection of occult malignant tumors and other lesions that have the potential for significant morbidity and mortality, but are rarely the presenting problem. CT is the most sensitive technique for detecting small renal cell carcinomas [7], and is thus the screening method of choice. Pheochromocytoma, cysts of the kidneys, liver, and pancreas, and various pancreatic tumors are all readily imaged with CT. Retinal angioma is a frequent and early manifestation of von Hippel–Lindau disease, and if untreated, may result in blindness [4]. This lesion is best detected by the ophthalmologist. Primary screening for pheochromocytoma is best accomplished biochemically, with subsequent imaging directed at the localization of suspected tumors. Genetic counseling is essential, particularly for persons of childbearing age. Screening protocols have been described in more detail elsewhere [1, 8].

REFERENCES

1. Filling-Katz MR, Choyke PL, Patronas NJ, et al. Radiologic screening for von Hippel–Lindau disease: the role of Gd-DTPA enhanced MR imaging of the CNS. *J Comput Assist Tomogr* **1989**;13:743–755
2. Nerad JA, Kersten RC, Anderson RL. Hemangioblastoma of the optic nerve: report of a case and review of literature. *Ophthalmology* **1988**;95:398–402
3. Hotta H, Uede T, Morimoto S, Tanabe S, Hashi K, Takeda M. Optic nerve hemangioblastoma: case report. *Neurol Med Chir* (Tokyo) **1989**;29: 948–952
4. Horton WA, Wong V, Eldridge R. Von Hippel–Lindau disease: clinical and pathological manifestations in nine families with fifty affected members. *Arch Intern Med* **1976**;136:769–777
5. Melmon KL, Rosen SW. Lindau's disease: review of the literature and study of a large kindred. *Am J Med* **1964**;36:595–617
6. In S, Miyagi J, Kojho N, Kuramoto S, Uehara M. Intraorbital optic nerve hemangioblastoma with von Hippel–Lindau disease. *J Neurosurg* **1982**;56:426–429
7. Amendola MA, Bree RL, Pollack HM, et al. Small renal cell carcinomas: resolving a diagnostic dilemma. *Radiology* **1988**;166:637–641
8. Choyke PL, Filling-Katz MR, Shawker TH, et al. Von Hippel–Lindau disease: radiologic screening for visceral manifestations. *Radiology* **1990**;174:815–820



The Radiology Outreach Foundation (ROF) is a nonprofit corporation whose goal is to help disadvantaged countries improve their health care by providing radiology equipment, books, consultation, education, and training to their practitioners. This assistance is on an application basis that is independent of political, ethnic, or religious orientation of the grantee. It depends on the need of the people and the ability of the ROF to meet that need. The ROF is approved by the U.S. Internal Revenue Service as a tax-exempt organization. It is endorsed by the following radiologic societies:

American Association of Women Radiologists
American College of Radiology
American Roentgen Ray Society
Association of University Radiologists
Radiological Society of North America
Society of Chairmen of Academic Radiology Departments
Society for Pediatric Radiology
European Society of Pediatric Radiology

All donations to the ROF are tax deductible. Persons who would like to contribute financially to the ROF, would be interested in being a visiting professor, would like to send books or journals to any of the institutions supported by the ROF, or would like further information about the ROF should write to

Charles A. Gooding, M.D.
President
Radiology Outreach Foundation
3415 Sacramento St.
San Francisco, CA 94118 USA

Influence of the Stopcock on the Efficiency of Percutaneous Drainage Catheters:
Laboratory Evaluation

Horacio B. D'Agostino[1]
Yong Park[1]
J. Philip Moyers[1]
Eric vanSonnenberg[1,2]
Robert B. Sanchez[1]
Brian W. Goodacre[1]
Yun Hwan Kim[1]
Marcelo Vasconcellos Vieira[1]

The effects of stopcocks on percutaneous fluid drainage were tested in a laboratory model by using a standard stopcock (6-French inner diameter) and a prototype stopcock (9-French inner diameter) connected to 8-, 10-, 12-, 14-, and 16-French catheters. Catheters were immersed in water alone or in viscous fluid with particulate matter, and the system was connected to low wall suction or gravity drainage. The average volume of fluid aspirated in a given period with and without a stopcock was compared for each catheter. The standard stopcock decreased drainage efficiency for these catheters by 13–42%. This decreased drainage efficiency was worse with the larger catheters. Particulate fluid blocked the stopcock connection for all catheters. With the prototype stopcock, drainage of water alone was reduced by 0–9% for the catheters of different sizes. Particulate fluid did not obstruct the prototype stopcock with any size catheter. With gravity drainage, the volume of water aspirated was reduced by 12–42% with the standard stopcock and by 3–6% with the prototype stopcock. These data suggest that stopcock connections greatly influence the efficiency of the percutaneous drainage systems. Stopcocks with larger inner diameters may improve drainage over that achievable with the stopcocks that are currently available.

AJR 159:407–409, August 1992

Percutaneous catheter drainage systems include a three-way stopcock and a connecting tube attached to suction or to a drainage bag. Stopcocks are used routinely, regardless of the indication for drainage or the type and size of catheter. Irrigation of the catheter through a stopcock maintains the catheter's patency, and it decreases the risk of occlusion and secondary bacterial contamination of the drainage system [1]. Additionally, the use of a stopcock prevents spillage of fluids while the catheter is being flushed, allowing isolation of body substances, one of the basic universal precautions.

Reduction of flow or obstruction of catheters and stopcocks by particulate matter or stone fragments can hinder drainage of abscesses, biliary or urinary [1, 3–5]. To address these problems, we assessed the effect of the stopcock on the efficiency of catheter drainage systems in an experimental model. We report the results of this study, discuss its potential impact, and recommend ways to improve the efficiency of drainage via catheters.

Materials and Methods

The experimental model used both single-lumen drainage catheters (sizes 8- and 10-French; length, 20 cm) and sump catheters (sizes 12-, 14-, and 16-French; length, 30 cm) (Medi-tech, Watertown, MA). The inner diameter and the number and size of drainage holes for each catheter are given in Table 1. Although double-lumen catheters of sizes 12- to 16-French were used, the sump port was occluded so that we could better address the influence of the stopcock as the sole variable in a single-lumen system.

In the first phase of the experiment, a standard stopcock with a 6-French inner diameter (Baxter, Irvine, CA) was connected in series to both the catheter and continuous low wall

Received November 20, 1991; accepted after revision February 24, 1992.

[1] Department of Radiology, University of California, San Diego, CA 92093. Address reprint requests to H. D'Agostino, Department of Radiology (H-756), UCSD Medical Center, 225 Dickinson St., San Diego, CA 92103.

[2] Department of Medicine, Division of Gastroenterology, University of California, San Diego, La Jolla, CA 92093.

0361–803X/92/1592–0407
© American Roentgen Ray Society

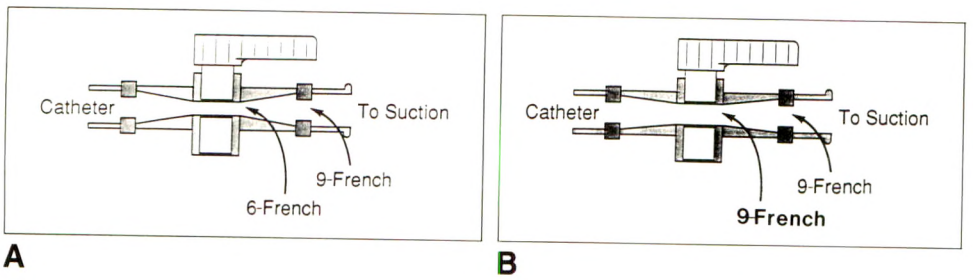


Fig. 1.—*A* and *B*, Diagrams of a stopcock drainage system show standard stopcock with 6-French inner diameter (*A*) and prototype stopcock with 9-French inner diameter (*B*). Three-way stopcock is shown longitudinally and in cross section (third opening has been eliminated for clarity).

TABLE 1: Characteristics of Catheters Studied

Catheter Size (French)	Inner Diameter (mm)	Number of Holes	Size of Holes (mm)
8	1.5	5	2 × 1
10	2.3	4	3 × 2
12	2.3	5	4 × 2
14	2.8	5	5 × 2
16	3.6	5	6 × 2

suction (50 mm Hg) (Fig. 1A). Each catheter was immersed in water alone and then in particulate viscous fluid for three trials of 1 min each. The particulate viscous fluid was prepared by mixing water and ultrasound gel (3:2 v/v mixture) with 10 g of crumbled white bread. The particles of bread were 1–5 mm in size, and the viscosity of the solution was 135 centistokes. The average volumes of the water and the particulate fluid drained with each catheter were noted for each of the three trials. The experiment was repeated after the stopcock was removed from the drainage system. The average volumes drained by each catheter, both with and without the stopcock, were compared, and the percentage of the difference between the two volumes was calculated.

In the second phase of the experiment, an identical catheter drainage system was used with a prototype stopcock that had a 9-French inner diameter (Cook, Inc., Bloomington, IN) (Fig. 1B). As in the first phase, the average volumes drained with each catheter with and without the stopcock were compared, and the percentage of the difference between the two volumes was calculated.

These experiments were repeated with gravity drainage instead of low wall suction. Catheters were again immersed in water and in viscous fluid with particles. The collection container was placed 20 cm below the fluid level. The volumes of fluid drained without a stopcock, with the standard stopcock, and with the prototype stopcock were measured and compared.

Results

The average volumes of fluid aspirated with and without a standard stopcock for both water and particulate viscous solution are shown in Table 2. Incorporating a standard stopcock into the drainage system caused a decrease in performance for all catheters for draining water alone, ranging from a decrease of 13% for 8-French catheters to a decrease of 42% for 16-French catheters. When particulate viscous fluid was drained, the standard stopcock was occluded by particles in one of three trials for 8-French catheters, in two of three trials for 10-French catheters, and in all trials for larger (12- to 16-French) catheters.

A similar comparison of the volumes aspirated with and without the prototype stopcock is shown in Table 3. Drainage efficiency for water decreased by less than 10% for the 14- and 16-French catheters when the prototype stopcock was used. With smaller catheters, practically no difference was seen in the volume of nonparticulate fluid drained with and without the prototype stopcock. Catheter efficiency decreased by less than 10% for all catheters when particulate fluid was drained through the prototype stopcock.

Under gravity drainage, the standard stopcock decreased drainage efficiency by 12–42% (Table 4). The prototype stop-

TABLE 2: Comparisons of Average Volumes Aspirated with and Without Standard Stopcock

Catheter Size (French)	Volume Aspirated (ml)		Drainage Difference (% decrease)[a]
	With Stopcock	Without Stopcock	
		Water	
8	160	183	13
10	290	396	26
12	286	383	25
14	320	460	30
16	356	616	42
		Particulate Fluid	
8	Occluded in 1 of 3 trials	16	—
10	Occluded in 2 of 3 trials	53	—
12	Occluded in 3 of 3 trials	43	—
14	Occluded in 3 of 3 trials	66	—
16	Occluded in 3 of 3 trials	120	—

[a] Drainage difference was not calculated for particulate fluid because of occlusion at stopcock.

TABLE 3: Comparison of Average Volume Aspirated with and Without Prototype Stopcock

Catheter Size (French)	Volume Aspirated (ml)		Drainage Difference (% decrease)
	With Stopcock	Without Stopcock	
		Water	
8	181	183	<1
10	396	396	0
12	380	383	<1
14	460	490	9
16	563	616	9
		Particulate Fluid	
8	16	16	<1
10	43	53	8.1
12	43	43	0
14	63	66	5.1
16	111.6	120	6.9

TABLE 4: Comparison of Average Volumes of Water Drained by Gravity Without and with Standard Stopcock and Prototype Stopcock

Catheter Size (French)	Volume Aspirated (ml)		Drainage Difference (% decrease)	Volume Aspirated with Prototype Stopcock (ml)	Drainage Difference (% decrease)
	Without Stopcock	With Standard Stopcock			
8	90	80	12	85	6
10	155	110	30	150	4
12	170	120	30	170	0
14	175	125	29	170	3
16	250	145	42	250	0

cock reduced drainage by 3–6%. The viscous particulate solution did not flow through the stopcock-catheter systems under gravity drainage alone.

Discussion

The results of our experiment suggest that the inner diameter of standard stopcocks is an important factor that influences the drainage efficiency of catheters ranging in diameter from 8- to 16-French. The efficiency of the catheters decreased when a standard stopcock was incorporated into the system. In the experimental drainage system (and in the clinical setting), the luminal diameter is narrowest at the level of the stopcock. The detrimental effect of the stopcock was accentuated with larger catheters, which have proportionally greater flow. Catheter performance for diverse fluids with different viscosities complies with Poiseuille's law, as has been shown in laboratory studies (Lee SH et al., presented at the annual meeting of the Association of University Radiologists, April 1990).

As would be expected, the effect of the stopcock connection was more critical for particulate fluid than for water alone. It is well known that stone fragments, small pieces of necrotic tissue, particulate debris, and blood clots can block the stopcock in percutaneous drainage of abscesses; nephrostomy; and in percutaneous biliary, pancreatic, chest, or hematoma drainage [1, 3–6]. The particulate matter in our solution similarly occluded the catheter system at the level of the stopcock, irrespective of catheter size. Surprisingly, 8-French catheters performed better in draining particulate fluid than did larger catheters; presumably this was because the drainage holes at the end of the smaller catheter behaved as a filter and prevented larger particles from entering the lumen. In addition, stopcocks became blocked more frequently when they were attached to larger catheters. Larger catheters (12- to 16-French), with proportionally bigger drainage holes, allowed sizable particles to enter and pass through the catheter to the stopcock connection, where they caused occlusion. The importance of the relative sizes of the holes in the catheters in terms of performance was not evaluated in this study.

For efficient drainage, percutaneous drainage systems should not have segments narrower than the inner diameter of the catheter. Thus, standard stopcocks in their current form can be considered impediments to effective drainage. Increasing the diameter by 3-French, as with the prototype stopcock, improved drainage from the 13% reduction seen with standard stopcocks to a less than 1% reduction for 8-French catheters, and from 42% reduction to 9% for 16-French catheters. The inner size of this prototype stopcock is similar to that of the lumen of the female portion of a Luer-Lok connection. Theoretically, the diameter of the Luer-Lok connection could become the limiting factor for efficient drainage of catheters larger than 10-French. In our in vitro experiment, high flow rates were achieved with low wall suction and gravity drainage. The effect of the stopcock connection on the efficiency of the catheter drainage system in clinical cases (in which lower flow rates occur) remains to be studied.

Percutaneous drainage achieves cure in 90–95% of uniocular, well-demarcated abscesses and fluid collections [6]. However, the success rate for percutaneous drainage of collections of higher viscosity or particulate fluid collections (necrotic tumors, hematomas, pancreatic collections) falls to 35–70% [3–5, 6]. Viscosity of organic fluids may vary. We were unable to find any data on viscosity of purulent fluid. Our study suggests that suction is beneficial to drain viscous fluid, as gravity alone may not be sufficient for adequate drainage of this type of fluid.

Because the stopcock is critical in limiting drainage, as shown both by clinical experience and by our laboratory studies, better designed stopcock connections should improve catheter drainage. If care is taken to ensure that the stopcock diameter is not smaller than that of the rest of the system, increased drainage should ensue. In particular, improved drainage of collections with particulate fluid should be expected; this is supported by our comparative results with and without the standard stopcock, and with the larger 9-French prototype stopcock.

ACKNOWLEDGMENTS

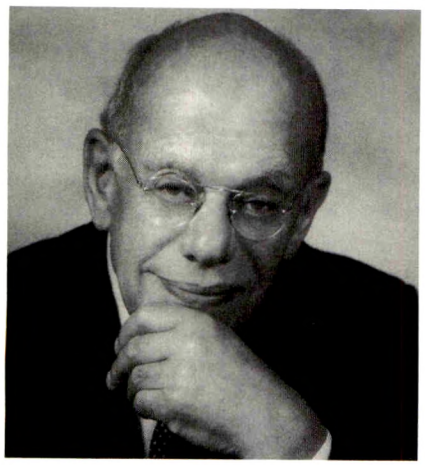
We thank Marcia Earnshaw for her photographic work and Ellen Mower for preparing the illustrations.

REFERENCES

1. Mueller PR, vanSonnenberg E, Ferrucci JT Jr. Percutaneous drainage of 250 abdominal abscesses and fluid collections. Part II: Current procedural concepts. *Radiology* **1984**;151:343–347
2. Wall SD, Olcott EW, Gerberg JL. AIDS risk and risk reduction in the radiology department. *AJR* **1991**;154:911–917
3. Lang EK, Springer RM, Glorioso LW, Cammarata CA. Abdominal abscess drainage under radiologic guidance: causes of failure. *Radiology* **1986**; 159:329–336
4. vanSonnenberg E, Mueller PR, Ferrucci JT. Percutaneous drainage of 250 abdominal abscesses and fluid collections. *Radiology* **1984**;151:337–341
5. Steiner E, Mueller PR, Hahn PF, et al. Complicated pancreatic abscesses: problems in interventional management. *Radiology* **1988**;167:443–446
6. Mueller PR, vanSonnenberg E. Interventional radiology in the chest and abdomen. *N Engl J Med* **1990**;322:1364–1374

Memorial

Richard Schatzki, 1901–1992



Radiology lost one of the pioneers of gastrointestinal radiology January 19, 1992, when Richard Schatzki died after a prolonged illness, 5 weeks before his 91st birthday. Dr. Schatzki made a large number of important contributions to radiology during a career that lasted more than 50 years and will be remembered not only for his contributions to the science of radiology but also for his excellence as a teacher and clinical radiologist.

Richard Schatzki was born on February 22, 1901, in Clafeld, Germany. After attending local schools, he entered medical school at the age of 19, graduating from the University of Berlin in 1925. He received his M.D. after internships in the medical service at the West End Hospital in Berlin and the surgical service of the University Hospital in Frankfort am Main.

Dr. Schatzki spent 1926–1929 at University Hospital in Frankfort am Main. The time included 15 months of radiology study with Hans Heinrich Berg. In 1929, Schatzki became chief of the radiology department at the medical clinic of the University Hospital in Leipzig and professor of radiology. While in Leipzig, he published the first of numerous articles that were to have such a profound effect on gastrointestinal radiology. In 1931, he presented the first detailed discussion of esophageal varices and the initial discussion of gastric varices. In the same year, he published the first of several articles, which included a supplement of *Acta Radiologica*, that emphasized the importance of relief studies in the gastrointestinal tract. In 1933, he described the first fluoroscopic demonstration of erosive gastritis. As was true in later years, he also published a number of articles in other areas, including one of the first descriptions of the radiologic diagnosis of coarctation of the aorta and of calcification of the adrenal gland in tuberculosis.

In 1933, Schatzki left Germany and joined the staff of the Massachusetts General Hospital, where he remained until he entered the army in 1943. In addition to numerous contributions to the literature, he had a profound effect on the trainees in the radiology department, many of whom subsequently became leaders of American radiology. During World War II, Dr. Schatzki served in the army for 3 years, most of which was spent as chief of the radiology department at McGuire Hospital in Richmond, VA. He was discharged in April 1946 with the rank of lieutenant colonel.

Shortly after the end of the war, Schatzki left Massachusetts General Hospital and became chief of the radiology department at the Mount Auburn Hospital in Cambridge, MA. He stayed in that position until 1967 and continued to work as a member of the radiology staff until the age of 82. He was largely responsible for changing Mount Auburn from an unsophisticated community hospital into one of Harvard's teaching hospitals, and he started a residency program in radiology that continues to flourish today. For many years, he offered one of the most popular electives for medical students at Harvard. In 1984, the radiology department was named the Richard Schatzki Department of Radiology.

Starting in 1931, Schatzki made many seminal contributions to radiology. He believed that the recognition of the lower esophageal ring was his most important contribution. In a series of articles between 1953 and 1963, together with John E. Gary, he described this important entity, which is now generally known as the "Schatzki ring." Among other important articles were those that described the face-on demonstration of ulcers in the stomach achieved by using what has become known as the Schatzki position, the first detailed discussion and analysis of intramural extramucosal tumors of the gastrointestinal tract, the description of the small-bowel enema, and the initial description of the gastrointestinal findings in scleroderma. He also continued to make important contributions in other areas of radiology, including the pulmonary findings after the tragic Coconut Grove fire and the osseous changes resulting from frostbite.

Schatzki's emphasis on the "art" of fluoroscopy had a profound influence on several generations of radiologists. Not only in his direct work with residents but also in many postgraduate courses, he stressed that proper fluoroscopic technique was essential to successful gastrointestinal radiology. He thus became revered by many radiologists. His philosophy about fluoroscopy was stated in a 1966 editorial, "You Still Have to Work for It," that discussed the impact of screen intensification. He also was the "physician's radiologist" and was frequently asked to consult on gastrointestinal cases throughout the Northeast.

Dr. Schatzki was an associate clinical professor of radiology at Harvard Medical School, president of the New England Roentgen Ray Society, and vice-president of the American Roentgen Ray Society. In addition to being a member of many national and local radiology societies, he was an honorary member of the radiology societies of Brazil and Colombia. He presented a number of memorial lectures, including those honoring Drs. Caldwell, Holmes, Pancoast, Soule, and Golden. In 1973, the Society of Gastrointestinal Radiologists presented its second Walter B. Cannon Medal to Dr. Schatzki.

Schatzki's towering intellect was joined to an extraordinary curiosity, profound wisdom, and, above all, absolute honesty. He was happiest when surrounded by young physicians and students, playing with young children wherever he met them, or sitting down to play one of his beloved Steinways. He played the piano almost well enough to be a concert artist, and for many years, radiologists recognized that arranging a trio or quartet was an effective way to persuade him to speak outside Boston. He also gave a number of benefit concerts in the Boston area.

Schatzki met a young physician, Greta Stern, in 1929, and they were married shortly after that. For more than 50 years, Richard and Greta Schatzki were inseparable. In 1981, Greta, his wife, best friend, and major source of support, suddenly died. Dr. Schatzki is survived by his sons, Stefan C. Schatzki, of Lexington, MA, and George R. B. Schatzki, of West Hartford, CT. A giant has left us.

Stefan C. Schatzki
Cambridge, MA 02238

Case Report

Percutaneous Extraction of Biliary Stones: Value of Endoluminal Sonography

Steven V. Lossef,[1] Brian S. Garra, Klemens H. Barth, and Robert K. Zeman

During percutaneous retrieval of retained biliary duct calculi, blood clots or focal submucosal hematoma can mimic and sometimes obscure small stones and stone fragments. With the recent availability of catheter-based, miniaturized endoluminal sonography systems, it may be possible to distinguish focal submucosal hematoma and intraluminal clot from an intraluminal stone. This hypothesis was tested in a patient undergoing percutaneous extraction of a stone from the common bile duct via a T-tube track.

Case Report

A 59-year-old woman had a cholecystectomy and exploration of the common bile duct. Subsequent T-tube cholangiography showed a 9-mm retained stone in the common bile duct. Extracorporeal shock-wave lithotripsy fragmented the stone, with subsequent passage of all but one 5-mm particle. After 6 weeks, the stone was extracted percutaneously. A 13-French sheath was placed within the T-tube track, and contrast material was injected into the biliary tree, showing a focal intraluminal filling defect in the common bile duct (Fig. 1A). Endoluminal sonography was performed by using a 20-MHz probe mounted on a 4.9-French catheter (Diasonics, Milpitas, CA), which was inserted over a steerable 0.014-in. (0.37-mm) guidewire. A small echogenic filling defect with acoustic shadowing was detected when the tip of the probe was positioned at the level of the suspected stone (Fig. 1B). No other echogenic structures were seen.

After extraction of the stone with a stone basket, cholangiography showed a new focal filling defect along the medial aspect of the distal portion of the common hepatic duct (Fig. 1C). As the possibility of a residual stone or fragment in this location could not be excluded, the catheter-based sonographic probe was reinserted. It showed a nonechogenic, nonshadowing mural structure at the level of the filling defect (Fig. 1D). This was considered to be more compatible with a focal submural hematoma, presumably from local trauma caused by the catheter, rather than a residual stone fragment. This was later confirmed by sweeping the bile duct with a Fogarty balloon. Intraluminal sonography of the entire biliary tree did not show any other shadowing intraluminal filling defects. Several small, nonshadowing intraluminal defects were present; these were interpreted as small blood clots. An access catheter was inserted at the end of the procedure. A follow-up cholangiogram 2 weeks later showed no residual intraluminal filling defects. The submucosal defect in the distal portion of the common hepatic duct was smaller, consistent with partial resorption of hematoma. The catheter was removed, and the patient has been asymptomatic for 8 months.

Discussion

Percutaneous extraction of stones is typically monitored fluoroscopically by injecting contrast material into the biliary system, and it is usually possible to determine when all fragments have been extracted. The presence of blood clots, submucosal hematoma, or air bubbles or extrinsic compression by vessels can obscure this endpoint. Although air bubbles appear echogenic on intraluminal sonograms, they tend to have more reverberations and less distinct shadows than stones have. Moreover, bubbles can usually be flushed away or removed by gravity drainage, allowing fluoroscopic differentiation from residual stones. Persistent clot or submucosal hematoma may be more difficult to distinguish fluoroscopi-

Received January 2, 1992; accepted after revision March 3, 1992.

[1]All authors: Department of Radiology, Georgetown University Hospital, 3800 Reservoir Rd., N.W., Washington, DC 20007. Address reprint requests to S. V. Lossef.

 0361–803X/92/1592–0411 © American Roentgen Ray Society

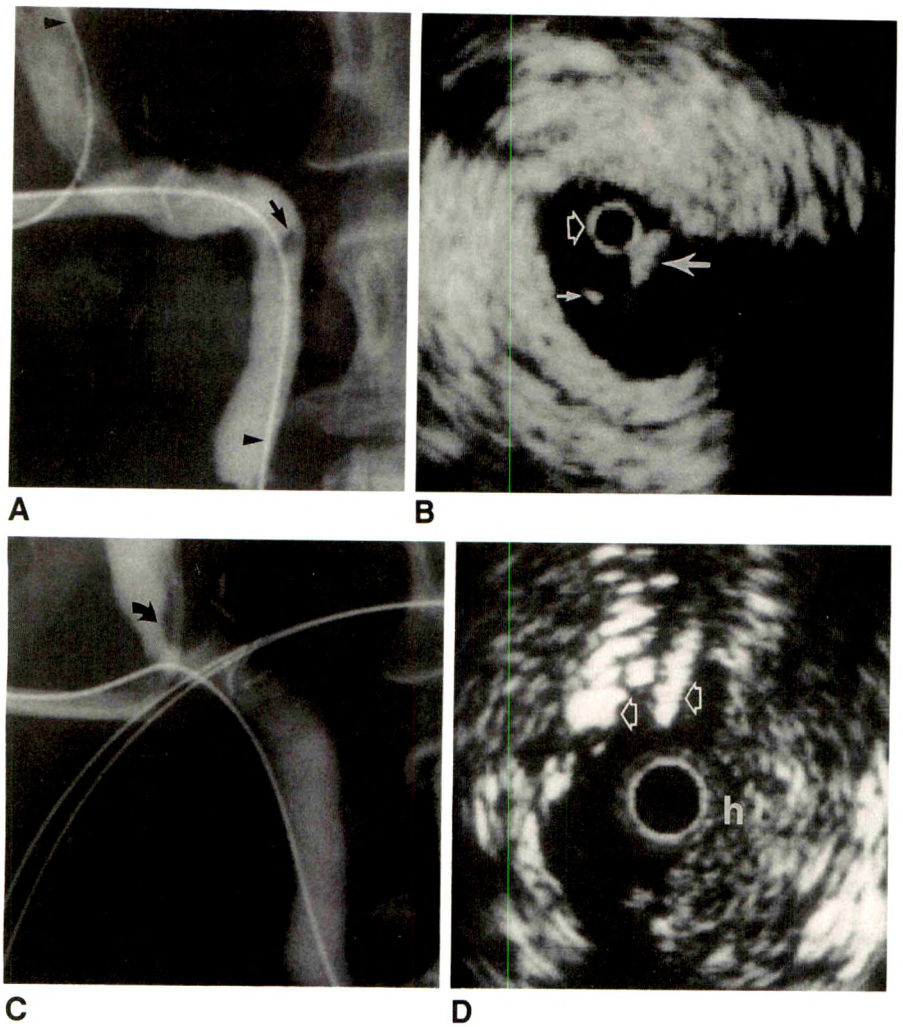


Fig. 1.—Percutaneous extraction of biliary stone in a 59-year-old woman.

***A*, Cholangiogram shows retained stone (*arrow*) in common bile duct. Guidewires (*arrowheads*) were inserted through limbs of T-tube.**

***B*, Intraluminal sonogram shows echogenic, intraluminal calculus with prominent shadowing (*large arrow*), sonographic probe (*open arrow*), and guidewire (*small arrow*).**

***C*, Cholangiogram shows persistent filling defect (*arrow*) after stone extraction.**

***D*, Intraluminal sonogram obtained after *C* shows nonechogenic, nonshadowing structure consistent with intramural hematoma (h). Echoes (*arrows*) are from guidewires.**

cally. In our case, the lack of echogenicity and acoustic shadowing of the residual mural lesion allowed us to terminate the extraction procedure with some assurance that all stone fragments had been retrieved.

Fluoroscopic guidance is recommended during insertion of the sonographic transducer to verify that the tip is inserted beyond any suspicious intraluminal filling defects. Sonograms should then be obtained while pulling the probe back. This should minimize the possibility of inadvertently pushing a stone ahead of the transducer, preventing detection.

Miniaturized probes for endoluminal sonography have been used for intravascular evaluation. Applications have included examination of the lumen of the aorta and iliac arteries [1]; monitoring results of transluminal vascular procedures, including balloon angioplasty, atherectomy, stent insertion, and laser angioplasty recanalization [2]; and evaluation of thrombi in the inferior vena cava [3]. Goldberg et al. [4] reported nonvascular uses of miniaturized endoluminal sonography probes in experimental animals and indicated that the probes could be used to accurately measure luminal thickness and echogenicity of structures such as the ureter, urethra, bile ducts, intestine, and fallopian tubes. Using endoluminal sonography, Goldberg et al. [4] were able to localize renal calculi smaller than the bile duct calculus we imaged.

We conclude that endoluminal sonography may be a useful adjunct to fluoroscopy for evaluating the biliary tree for the presence of residual fragments after extraction of biliary stones.

REFERENCES

1. Nishimura RA, Welch TJ, Stanson AW, Sheedy PF, Holmes DR. Intravascular US of the distal aorta and iliac vessels: initial feasibility studies. *Radiology* **1990**;176:523–525
2. Isner JM, Rosenfield K, Losordo DW, et al. Percutaneous intravascular US as adjunct to catheter-based interventions: preliminary experience in patients with peripheral vascular disease. *Radiology* **1990**;175:61–70
3. McCowan TC, Ferris EJ, Carver DK. Inferior vena caval filter thrombi: evaluation with intravascular US. *Radiology* **1990**;177:783–788
4. Goldberg BB, Liu JB, Merton DA, Kurtz AB. Endoluminal US: experiments with nonvascular uses in animals. *Radiology* **1990**;175:39–43

Perspective

Desperately Seeking Reimbursement

Linda Dickes[1]

A patient with lung cancer who was experiencing visual disturbances and severe headaches underwent CT of the head to evaluate the possibility of metastases. Reimbursement for the CT scan was denied initially by the patient's insurance company because the company's computerized claims-review program could not discern a relationship between lung cancer and a procedure for examining the head. If the claim had been submitted with diagnostic codes for the neurologic symptoms, then the relationship between the procedure and the patient's medical problem would have been clear. In fact, when the claim was recorded and resubmitted, the procedure was reimbursed.

In another instance, a hospital's radiology department entered separate billing charges for the volume of nonionic contrast medium used for each enhanced procedure. The hospital's billing staff, who in the past had not billed separately for contrast media, simply transferred the charges to an inventory control account rather than adding a line item to the claim. As a consequence, the hospital lost revenue for a covered service until a reimbursement specialist from a pharmaceutical company identified the problem and organized a seminar for the hospital's radiology, billing, and medical records departments on insurer policies and required billing information.

Common Reimbursement Problems

Both of these situations exhibit three common reimbursement problems: claim data do not relate the examination to the patient's condition, services covered by insurance are not billed, and nonradiology personnel are not educated as to the technology provided. The tendency is to assume that reimbursement is almost routine, but in fact, considerable effort is required to obtain payments for radiologic procedures.

Insurers have a variety of claims-review mechanisms to limit payments to care that appears necessary for beneficiaries and that meets the policy's requirements. Medicaid programs in most states and health maintenance organizations (HMOs) use prior-approval requirements to limit the use of diagnostic and other health care services. Medicare and most commercial insurers may deny reimbursement if the services provided are not deemed medically necessary. It is the radiologist, not the primary care physician, who risks not being paid when the service provided is not justified or supported by the claim data. If you cannot answer the question "For what medical reason is this diagnostisc procedure necessary?" you probably will not be paid.

Radiologists as Consultants

As noted in a text on quality assurance for radiology departments, "the radiologist's role as a consultant and gatekeeper is critical, avoiding unnecessary and inappropriate tests and directing the rest of the medical staff's access to imaging sources" [1]. As other physicians may be unfamiliar with today's high-technology imaging capabilities, diagnostic specialists must serve as consultants to their referral network. The primary care physician should be educated regarding the type of information about patients that is needed so that the diagnostic physician can select the technology that is most

Received April 22, 1991; accepted after revision February 24, 1992.
Presented in whole or in part at the Economics of Diagnostic Imaging National Symposium, the National Convention of the American Health Care Radiology Administrators, and the meeting of the California Society of Radiology Technologists.
This work was supported by Squibb Diagnostics, a division of Bristol-Myers Squibb Co.
[1] Bristol Myers Squibb Co., Pharmaceutical Group, P. O. Box 4000, Princeton, NJ 08543-4000. Address reprint requests to Public Affairs Dept.

appropriate in making a differentiating diagnosis. Although a referring physician may be familiar with CT scans, MR imaging may be better for imaging the patient's medical problem. Therefore, while the purpose of the examination is set by the patient's physician, the type of examination should be selected by the diagnostic specialist. This is the best way to ensure that the medical necessity for the examination and the procedure performed will be related.

Medical Necessity

Third-party payers will reimburse only for procedures that are defined as medically necessary. The 1988 Medicare Carrier Manual [2], published by the American Medical Association, describes a medically necessary procedure as one that is

> Consistent with the symptoms or diagnoses of the illness or injury under treatment;
> Necessary and consistent with generally accepted professional medical standards (i.e., not experimental or investigational);
> Not furnished primarily for the convenience of the patient, the attending physician, or another physician or supplier; and
> Furnished at the most appropriate level which can be provided safely and effectively to the patient.

Such regulations are not unique in the payers' demand for justification of health care expenditures. Virtually every insurance policy contains some type of clause on medical necessity. They are intended primarily to exclude payment for noncovered services, such as cosmetic surgery. However, they also provide claims reviewers with a mechanism to deny reimbursement for procedures that seem unreasonable, unrelated, or unnecessary with respect to a patient's current health problems. Consequently, it is important for a radiologist's report to include information on why the patient was referred for the procedure, additional services required because of the patient's medical history, and results of the examination that will affect the plan of treatment. These data are later coded on a claim form by billing personnel. The coded information must paint a picture of a health care expense that is clinically necessary in order for the provider to be reimbursed for the services.

Value of Communication

The efforts of referring physicians and radiologists working together are a prerequisite for reimbursement, but their working together does not guarantee it. Accurate and comprehensive coding of the dictated report and effective communication between radiologists and their hospitals' billing departments also are necessary.

Exchange of detailed medical histories benefits everyone. The radiologist is able to select the most effective imaging technique for the examination. The referring physician receives diagnostic data specific to his patient's acute problem, which confirms his medical suspicions or redirects the plan of treatment. The third-party payer can then receive claim data indicating the medical necessity of the examination so that reimbursement can be effectively processed. Such clear communication produces a "win-win" scenario.

Ensuring Reimbursement

Clinical data from journals and health care practitioners and information on utilization patterns of diagnostic procedures have established the use of nonionic contrast media as "consistent with generally accepted professional standards." The usefulness of submitting this information extends beyond the reimbursement of an individual claim. The more clinical data and information on utilization patterns that are submitted with each claim and the more claims submitted for reimbursement for use of nonionic contrast media, the stronger becomes the pattern of use of nonionic media, which creates a foundation for the establishment of future reimbursement based on fee schedules.

By taking an active role as consultants, radiologists can not only enhance reimbursement rates for their medical centers but also influence state and national reimbursement policies. An example of this occurred recently in a Medicare jurisdiction that had a policy of not providing reimbursement for the additional costs involved in using nonionic contrast media. An imaging center in the jurisdiction resubmitted 100 claims on which the charges for nonionic contrast media had been denied. Included with the resubmitted claims were dictated reports explaining the medical necessity for using nonionic contrast media and clinical studies supporting the decision to use such media. At a subsequent meeting with the Medicare hearing officer, a radiologist from the imaging center explained the differences between ionic and nonionic contrast agents, identified medical necessity factors, and described the clinical basis for using nonionic media. The radiologist also categorized patient factors that could be used to classify the various claims according to procedure performed and nonionic contrast agent used.

As a result of this effort, 90% of the previously denied claims were reimbursed immediately. The hearing officer's findings were summarized for the specific claims reviewed and to establish a general application. It was decided that irrespective of general policy, services deemed reasonable and necessary could be reimbursed on a case-by-case basis. Thus, a precedent was set for processing future claims for reimbursement for the use of nonionic contrast media.

This example shows that reimbursement is a dynamic process that can be influenced through better documentation and communication. Radiologists can perform a key role in the team effort to obtain appropriate reimbursement levels by educating referral sources, medical staff, claims reviewers, and policy makers. The net result for radiologists will be increasing acceptance of nonionic contrast media and other radiologic technology and even greater professional stature.

REFERENCES

1. Handmaker H, Sawyer TG, Wilkinson R. *Examples of monitoring and evaluation in diagnostic radiology, radiation oncology, and nuclear medicine services.* Chicago: Joint Commission on Accreditation of Healthcare Organizations, **1988**:9
2. *Medicare carrier review.* Chicago: American Medical Association, **1988**:12

Memo to Readers

Report of the Editor, 1991

Robert N. Berk[1]

This report of the activities of the *AJR* in 1991 was presented to the Executive Council of the American Roentgen Ray Society at its annual meeting on May 10, 1992, in Orlando, FL. It is reproduced here because we believe that the Journal is not solely the property of the Society but rather is a resource for all who are engaged in the practice of radiology. As such, it is accountable to all its readers as well as to the members of the Society.

A statistical overview of the Journal's performance in 1991 is given in Table 1, along with comparative statistics each year since 1982.

Emphasis on publication of original, accurate, and concise major articles continued in 1991. At the same time, efforts were made to provide something of interest for everyone in each issue. As in previous years, such content included review articles, named lectures, case reports and technical notes, meeting summaries, commentaries, pictorial essays, and letters to the editor.

In 1991, additional features were initiated in an attempt to make the Journal more readable—to make it less ponderous without detracting from its nobility. Among the special articles that were published in 1991 that are currently in press or that are being planned are the following:

Historical vignettes. In keeping with the upcoming centennial anniversary celebration, these short articles on the history of radiology will be published with increasing frequency until 1995. Authors include Ronald L. Eisenberg, Philip C. Goodman, Ray Gagliardi, Bobby Nath, T. Doby, and others.

Medicine in American art. These monthly, one-page articles written by Stefan Schatzki concern art as it relates to medicine or artists who were physicians.

Radiologic-pathologic conferences. These monthly case reports are submitted by Felix Chew from the Massachusetts General Hospital and by Beverly Wood from the Los Angeles Children's Hospital.

Memos to authors. These articles, written by the editor, offer advice to authors on crafting manuscripts for publication in the *AJR* and other journals (three to four per year).

Republication of articles from the French journal *Journal de Radiologie* (two or three times per year beginning October 1992).

Vignettes on how to write clearly by Peter Ronai (occasional articles beginning September 1992).

Interventional radiology clinicopathologic conferences from various institutions, edited by Karim Valji (three to four per year beginning September 1992).

The Figley Fellowships in radiology journalism were highly successful again in 1991, the second time they have been offered. Last year's Figley fellows, Jud Gurney of the University of Nebraska and Judith Chezmar of Emory University, served with distinction during the month of March 1991. The goals of the fellowship were achieved in every respect. The recipients of the 1992 fellowships are Gerald D. Dodd III from the University of Pittsburgh and Allen D. Elster of Bowman Gray University. These outstanding radiologists were selected from more than 30 extremely well qualified applicants. They will serve during the month of July 1992 in the editorial office. The number of fellowships will be increased from two to four in 1993, and applicants will not be limited to radiologists who are still early in their careers.

A change in the format of the abstracts of articles published in the Journal is already underway. The abstracts now consist

[1] Editor-in-Chief, *American Journal of Roentgenology*, 2223 Avenida de la Playa, Ste. 103, La Jolla, CA, 92037. Address requests to R. N. Berk.

AJR **159:415–418, August 1992** 0361–803X/92/1592–0415 © American Roentgen Ray Society

TABLE 1: Journal Statistics for January 1, 1982, Through December 31, 1991

	1982	1983	1984	1985	1986	1987	1988	1989	1990	1991	Variance %
Circulation	17,483	17,933	18,770	19,507	20,096	20,565	21,162	21,994	22,517	21,936	(581) (3%)
Cost ($) U.S. individual	60	75	75	90	90	90	100	110	125	125	0 0
Advertising pages	667	579	390	288	412	385	345	360	205	276	71 35%
Text pages	2543	2746	2742	2743	2716	2637	2788	2747	2776	2759	(17) (<1%)
Manuscripts published*	447	481	506	514	496	515	552	593	605	632	27 4%
Pages per published ms.*	–	–	–	–	–	4.2	4.4	4.0	3.8	3.6	(0.2) (5%)
Manuscripts submitted	1205	1207	1191	1208	1200	1301	1240	1270	1370	1516	146 11%
Major papers submitted	646	693	713	764	658	702	684	693	777	864	87 11%
Acceptance % (major papers)	60	53	53	52	41	46	43	44	40	42	2 5%
CR/TN submitted	–	–	–	–	–	508	422	423	408	487	79 19%
Acceptance % (CR/TN)	–	–	–	–	–	27	19	18	17	21	4 24%
Mean time to initial decision (weeks)	8.7	8.6	8.3	8.3	4.8	3.8	3.4	3.6	3.5	3.9	0.4 11%

Note.—Numbers in parentheses are negative variances, CR/TN = Case reports and technical notes, – = not available.
* Includes *AJR* and *AJNR* manuscripts.

of four separate paragraphs entitled objectives, methods, results, and conclusion. This is the same format adopted by *JAMA* and *The New England Journal of Medicine* and is an attempt to make the essence of articles easy for readers to grasp from the abstract.

Circulation Rate, Price, and Advertising

The circulation rate remained essentially constant between 1990 and 1991 (21,936) and the subscription price was unchanged (domestic personal, $125; see Figs. 1 and 2).

The number of commercial advertising pages increased by more than one third from 205 pages in 1990 to 276 pages in 1991 (Fig. 3).

Content

The Journal carried 2759 pages, 59 (2%) more than the contractual allowance of 2700 (Fig. 4). Including the articles reprinted from *AJNR*, 632 articles were published, 27 (4%) more than in 1990 (Fig. 5). The average length of the articles

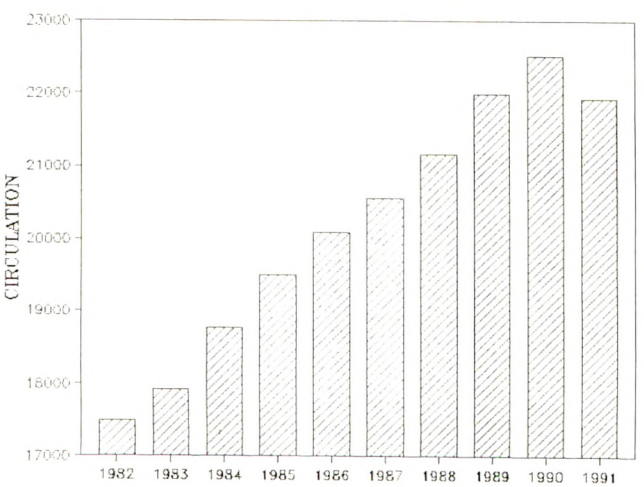


Fig. 1.—Circulation rate.

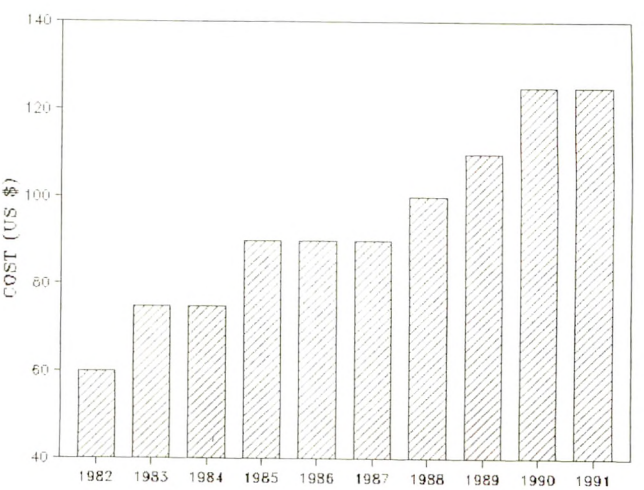


Fig. 2.—Subscription cost.

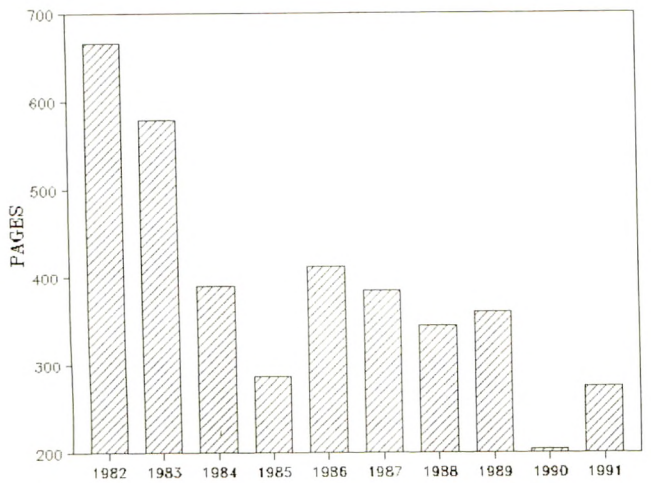


Fig. 3.—Display advertising pages.

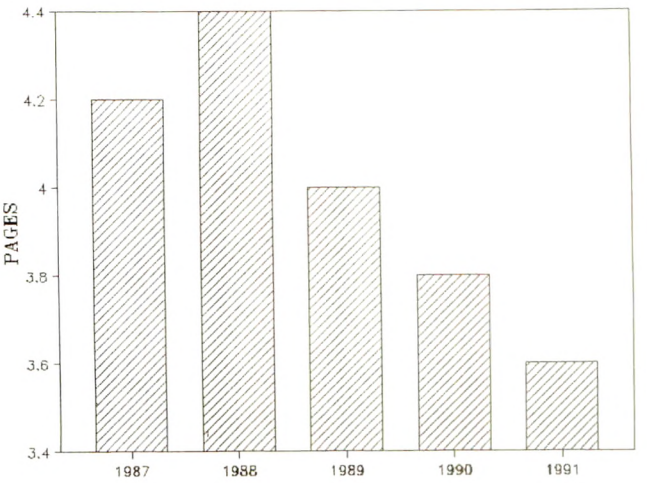


Fig. 6.—Pages per published article.

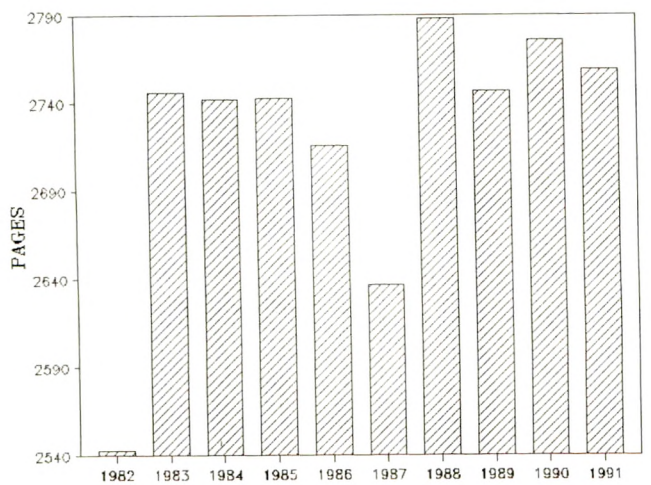


Fig. 4.—Text pages.

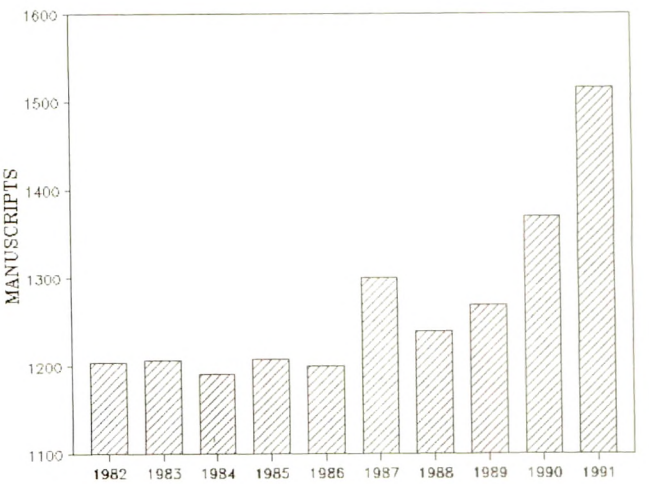


Fig. 7.—Total manuscripts submitted.

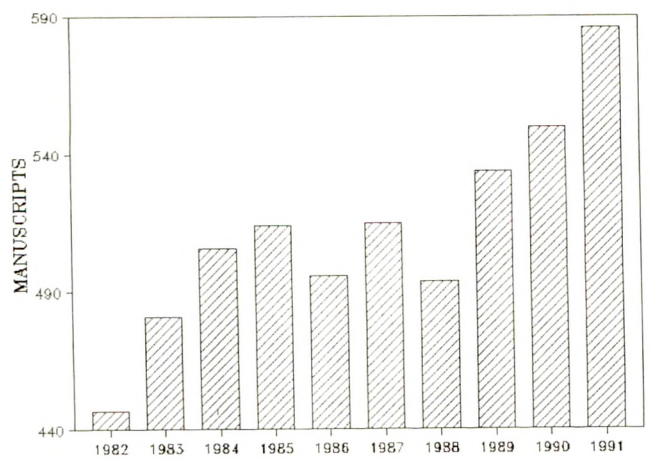


Fig. 5.—Manuscripts published (not including *AJNR* republications).

in 1991 was 3.6 pages compared with 3.8 in 1990, a decrease of 5% (Fig. 6). The editors have succeeded in an effort to make papers more succinct every year since 1987, when the average length was 4.2 pages.

The number of manuscripts received in the year was 1516, 146 (11%) more than in 1990 (Fig. 7). The increase includes (1) neuroradiology manuscripts that would have been submitted to the *AJNR* had the agreement between the ARRS and the ASNR remained in effect and (2) additional review articles invited by the editor. Of the total received, 864 (56%) were major papers and 487 (32%) were case reports and technical notes (Fig. 8).

The acceptance rate for major papers (including reviews and pictorial essays) in 1991 was 42% compared with 40% in 1990 and 44% in 1989. The 1991 acceptance rate for case reports and technical notes was 21%, compared with 17% in 1990 and 18% in 1989 (Fig. 9).

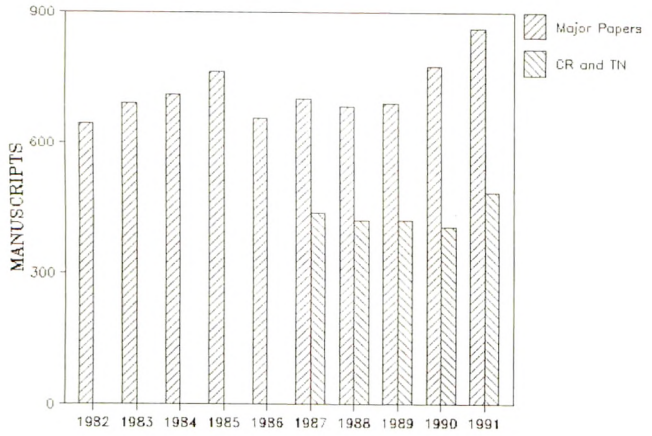


Fig. 8.—Type of manuscripts submitted (major papers and case reports/technical notes).

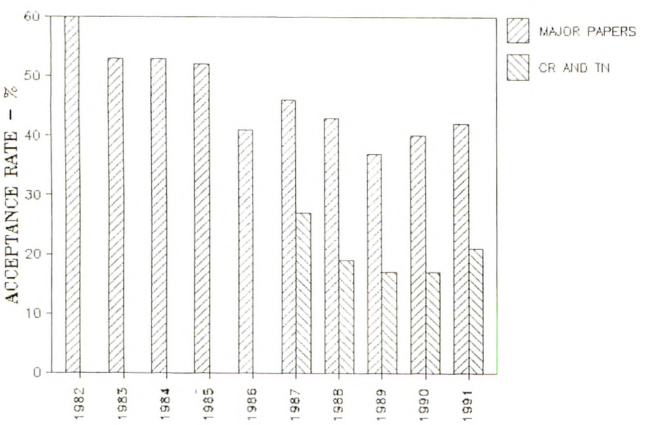


Fig. 9.—Manuscript acceptance rate for major papers and case reports/technical notes.

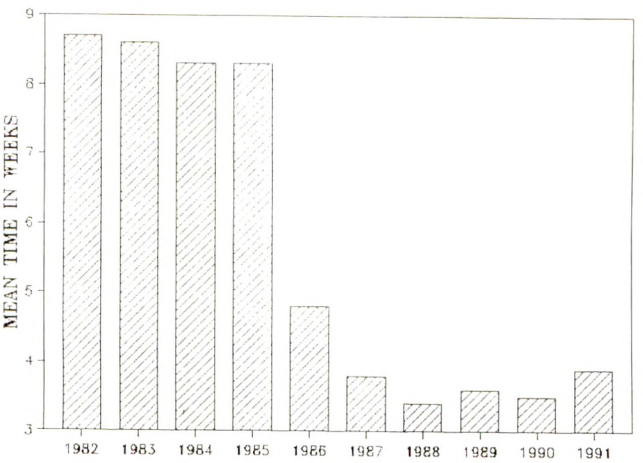


Fig. 10.—Initial editorial decision (mean time in weeks).

Manuscript Flow

In 1991, the mean time required between receipt of a manuscript and an initial editorial decision remained under 4 weeks (Fig. 10). This is nearly twice as fast as many other journals. The average time between final acceptance and publication was 5.3 months, compared with 5.4 months in 1990, 4.2 months in 1989, and 4.4 months in 1988.

The average time between submission and final publication was 7.3 months in 1991 compared with 7.4, 6.4, and 6.3 months in 1990, 1989, and 1988, respectively. The period includes approximately 1 month for peer review, 4–5 months for publication, and 1 month for mailing. The time is proportional to the size of the backlog of accepted articles awaiting publication. Reduction of the backlog requires rejecting substantive articles and risking not having enough accepted articles edited and ready to meet existing publication deadlines. The editors strive to maintain a proper balance so as to achieve an ideal of 5 months between the time a manuscript is received and its date of publication in the Journal.

Meeting News

The American Institute of Ultrasound in Medicine: 36th Annual Convention, March 1992

Elizabeth Whalen[1]

The 36th annual convention of The American Institute of Ultrasound in Medicine (AIUM) was held March 8–12, 1992, at the San Diego Convention Center, San Diego, CA. The goal of the convention was to provide benefits for scientists interested in ultrasound, including physicians, engineers, sonographers, technologists, and veterinarians. In addition to the 31 scientific sessions in which nearly 200 scientific papers were presented, 40 "Meet the Professor" sessions provided participants the opportunity to work in small-group sessions with specialists in different areas of sonography. Eleven categorical courses provided lectures on a wide range of topics, including intraoperative sonography, very high frequency scanning, sonography of HIV-infected patients, fetal echocardiography, neurosonology, advanced ultrasound color-flow techniques, obstetrics/gynecology, pediatric sonography, and instrumentation.

Two special features of the convention were (1) the annual Fry Memorial Lecture, during which awards were presented to Robert C. Waag (the Joseph H. Holmes Basic Science Pioneer Award), Barry B. Goldberg (the Joseph H. Holmes Clinical Pioneer Award), and Peter N. T. Wells (the William J. Fry Memorial Lecture Award) and (2) a discussion by four experts from three countries about the use of ultrasound technology in space ("Human Cardiovascular Adaptation to Space & Ultrasound Technology"). Section meetings also were held, during which professionals with a special interest in a specific application of sonography met to discuss mutual concerns, to determine the significance of their research to other subspecialties and ways to convey the results of this research, and to review proposals for official AIUM statements and policies in terms of their special field. Also, in scanning sessions, manufacturers made presentations and offered hands-on training with the latest sonographic equipment. A huge exhibit hall contained 48 scientific and 178 commercial exhibits.

More than 4000 people attended the 1992 AIUM convention. Because of *AJR* space limitations, we cannot provide coverage of all the activities that took place at this intensive 4-day meeting. However, the following pages do contain summaries of 12 of the presentations of original scientific research, two of the up-to-date reviews given in the categorical courses, and one Meet the Professor session.

Scientific Presentations

Tissue Characterization

Ultrasonic measurements from 100 to 800 MHz.—In this presentation, J. P. Jones (Irvine, CA) described an ongoing study by himself and J. M. C. Gallet in which they investigated medical applications of an acoustic microscope designed for electronic industry applications. Attenuation in the frequency range of 100–800 MHz was measured for liver, kidney, pancreas, brain, and lung. They became interested in this research because very few measurements had been done previously at these frequencies and because this technique

[1] Contributing editor, *American Journal of Roentgenology*, Ste. 103, 2223 Avenida de la Playa, La Jolla, CA 92037.

Editor's note.—"Meeting News" articles report the highlights of important national radiology meetings. The articles will not undergo the peer review usually required of *AJR* publications, nor will they offer a critique of the information provided. The sole purpose of the series is to provide Journal readers with succinct, substantive, and accurate reviews of topics of current interest, written in a readable fashion and published promptly after the meeting.

***AJR* 159:419–425, August 1992** 0361–803X/92/1592–0419 © American Roentgen Ray Society

can eventually be used to make acoustic measurements in vivo. Images are produced as follows: the acoustic lens vibrates at 50 MHz along the *x*-axis; the *x*-axis is divided into 640 pixels; at each pixel point along the *x*-axis, the lens transmits the signal and waits for the returned reflected signal; the echo is envelope-detected; the amplitude of the signal is converted into relative gray-scale values; 500 lines are scanned for a complete sequential image; and an array image of 640 × 500 pixels is drawn. A field of view can be chosen via computer instruction, after which all or part of the image can be selected and a histogram produced from the information in the image.

Using this technique, the researchers studied relative attenuation in three types of skin: skin with no sun damage (normal), with some sun damage, and with definite sun damage. For the dermis of normal skin, relative attenuation was 35; for that of skin with some sun damage, relative attenuation was 41; and for that of skin with definite sun damage, relative attenuation was 46. For the epidermis of normal skin, relative attenuation was 15; for that of skin with some sun damage, relative attenuation was 27; and for that of skin with definite sun damage, relative attenuation was 34. The two main problems with the technique were the tilting of the specimen stage and the unevenness of the specimen; factors affecting attenuation measurement include variation in sample thickness, size of water coupling, and tissue inhomogeneities. In attenuation measurements in skin, the frequency dependency of attenuation normally seen between 10 and 100 MHz continues up through 400 MHz; however, these researchers were surprised to find that a slight *reduction* in frequency dependency occurs between 400 and 800 MHz. Experiments with this technique of attenuation measurement are continuing, particularly in the liver and kidney.

Use of neural nets in ultrasound tissue characterization.—Peter D. Edmonds (Menlo Park, CA) presented the latest results of a current study by J. S. Ostrem and himself; this investigation sought a solution to a problem in an earlier application of training neural nets (i.e., 75% of the data were required for training, so only 25% remained to evaluate after training). In their experiment, freshly excised specimens of breast tissue were placed in a holder mounted on a platform and measured in the 2- to 8-MHz frequency range; the ultrasound data were provided to a self-organizing Kohenen's network (which requires no training set). The samples consisted of tissue from 56 benign lesions, 22 malignant lesions, and 50 normal breasts; pathologic proof was the gold standard in all cases. Typically, interspersion of classes is very obvious from scattered data points on the graph. Input factors included attenuation coefficients at both 5 and 8 MHz, the slope of frequency dependence of the attenuation coefficient (dB/per cm × MHz), sound speed (based on time of flight), and age of patient. To characterize the tissue via the neural nets, they used a back-propagation algorithm with a gradient-descent method to minimize the mean-square error between the actual outputs and the desired outputs of the networks; the networks' weights were iteratively updated according to the back-propagation algorithm. Use of the self-organizing Kohenen's algorithm resulted in a visual separation on the graph between data points corresponding to malignant, abnormal, and normal tissue; however, the researchers are concerned about a substantial overlap between normal and abnormal groupings (including some malignant cases).

Detection of age differences in thrombi.—R. E. Parsons (Philadelphia, PA) discussed the ability of ultrasonic tissue characterization to detect the composition changes that might indicate the age of thrombus (coauthors: B. Sigel, E. J. Feleppa, V. K. Swami, J. Justin, M. C. Rorke, J. Sokil-Melgar, R. M. Golub, H. Kimitsuki, L. Loiacono, A. Can). In 26 pigs, in vivo thrombi of the jugular vein were examined over time. Sonograms were obtained to document thrombus formation, and RF measurements also were obtained. Initially, the thrombi showed mixed histologic findings; however, a marked change was seen by 60 days after thrombus formation. Mean parameters measured by ultrasonic tissue characterization included veins, area, slope and standard deviation, and intercept and standard deviation. Only 7 days after thrombus formation, a marked change in histologic findings was seen. Ultrasonic tissue characterization showed a significant decrease in slope and a significant increase in *y*-intercept (for both, $p < .01$). On color parameter sonograms combining the slope and intercept values, the thrombus color changed from blue to red after 7 days. In this experimental, in vivo model, ultrasonic tissue characterization could be used to distinguish between new and 1-week-old thrombi, probably on the basis of cellularity and fibrin density. Furthermore, ultrasonic tissue characterization can be used to detect changes in the vascular wall that are indicative of intimal hyperplasia and may be applicable to clinical, noninvasive staging and age determination of thrombi.

Acoustic assessment of postmortem autolytic changes in beef longissimus muscle.—Our diet-conscious society may benefit from the results of a study designed to relate acoustic measures to the amount of fat in beef. Felicia Chu (Urbana, IL) and coworkers (J. Novakofski, W. D. O'Brien) studied the longissimus muscles from six steers classified as "choice" by the United States Department of Agriculture (USDA). The muscles were aged at 4°C and evaluated at 1, 6, 13, 20, and 27 days after death. Physical measurements included shear force, yield strength, and free water; acoustic measurements included attenuation coefficient, speed, and heterogeneity index, all obtained in both the parallel and perpendicular orientations. Physical data showed that, as the beef aged, it became more tender, as shown by significant differences in both shear force (day 1 = 5.87 kg, day 27 = 3.28 kg; <4.5 kg is considered meat tender enough for "white-tablecloth restaurant trade") and yield strength (day 1 = 2.52 kg, day 27 = 1.97 kg); 27-day-old beef was also more juicy, according to measures of free water (day 1 = 22.6%, day 27 = 34.5%). In regard to acoustic measurements, the differences between the parallel and perpendicular attenuation coefficients were large at day 1 (3 and 11 dB/mm, respectively), but this difference almost disappeared by day 27 (16 and 15 dB/mm, respectively). However, parallel and perpendicular speed and heterogeneity measures were anisotropic throughout: For both values, the parallel measures were always greater than the perpendicular measures. Parallel speed did correlate positively with shear force. These data indicate that the attenuation coefficient and speed can be used to measure tenderness

in beef. (When a questioner asked Dr. Chu if she could "verify" that all the choice steaks in this study were used for scientific purposes, she replied that she could because she had stopped eating beef when the study began.)

Vascular Sonography

Screening for occult abdominal aortic aneurysm during routine carotid duplex arterial evaluation.—In introducing this study on screening for abdominal aortic aneurysms, Ronald A. Bays (Saginaw, MI: coauthors: G. A. Carty, T. Nachtigal, G. Herzler, R. Magyar) stated that abdominal aortic aneurysms are present in 2% of the elderly population; that elective repair of these aneurysms carries a 2% mortality; and that the operative mortality in emergency repair can be as high as 50%. Despite the high cost and mortality associated with emergency repair of abdominal aortic aneurysms, no current method exists to screen high-risk patients. Therefore, these researchers investigated use of sonography to identify patients at risk for abdominal aortic aneurysms and to determine an appropriate screening method for this disorder. In 131 patients referred for routine carotid duplex evaluation, a rapid sonographic survey also was performed from xiphoid to bifurcation; the entire procedure took about 10 min. Abdominal aortic aneurysms (3.0–7.5 cm) were found in 11 patients (8%); the prevalence of abdominal aortic aneurysms increased to 11% in patients with a stenosis of more than 50% of the internal carotid artery. Regression analyses showed that the presence of abdominal aortic aneurysms correlated significantly with male sex, carotid occlusive changes, and abnormal velocity. The positive predictive value of all these factors together was 82%, with a negative predictive value of 79%: nine of 11 abdominal aortic aneurysms would have been predicted by these factors in this group. Adding screening for these aneurysms to routine sonographic studies and considering the predictive factors mentioned above could significantly reduce both cost and mortality. For example, at the University of Rochester, the cost of one emergency repair of an abdominal aortic aneurysm is equal to the sum of the costs of 54 sonographic studies and one elective repair. These results seem to indicate that rapid sonographic screening for abdominal aortic aneurysms can save lives and money—it is fast, risk free, and reliable; a sonographic study that shows an aneurysm should be followed by a CT examination to determine the best treatment for the patient.

Ultrasonic measurement of the elastic modulus of the common carotid artery.—Ward A. Riley (Winston-Salem, NC; coauthors: R. W. Barnes, G. W. Evans, G. L. Burke) discussed the use of ultrasound to aid in understanding atherosclerosis, including the understanding of how arteries stiffen. Parameters that help specify local arterial stiffness include arterial distensibility, arterial compliance, stiffness index, and pressure-strain elastic modulus; Dr. Riley focused his talk on the last parameter. In regard to pressure-strain elastic modulus, Young's modulus (Y) includes the factor of wall thickness: Y = (pressure-strain elastic modulus)/(ratio of wall thickness to radius). The common carotid artery is a good model for investigating arterial stiffness because it is a superficial, readily accessible vessel, its geometry is relatively simple, and it is located adjacent to the bifurcation, a common site of atherosclerosis. Wall thickness was defined as the combined thicknesses of the intima and media, and the artery diameter was defined as the outer diameter of the vessel (*not* as the diameter of the lumen). Atherosclerosis is being studied in several large multicenter trials with populations as large as 16,000 men and women. Populations being studied include 103 matched pairs of patients with carotid atherosclerosis and control subjects as well as 100 pairs of patients with coronary disease and control subjects. Results so far show that the ratio of wall thickness to radius is the same in men and women in all age groups, although the ratio tends to increase gradually with age. Carotid artery strain decreases with age, and the pressure-strain elastic modulus increases with age in men and women and is slightly higher in men than in women below the age of 50. Understanding the structure of the arterial wall and age-related changes to that structure may help physicians recognize atherosclerosis at an earlier stage.

Abdominal/Gastrointestinal Sonography

Endoluminal esophageal sonography.—A study of a new technique to image and quantitatively assess the detailed anatomy of the normal and abnormal esophageal wall was presented by Ji-Bin Liu (Philadelphia, PA; coauthors: L. S. Miller, B. B. Goldberg, R. I. Feld, A. Alexander, L. Needleman, C. L. Millward). Via a transnasal approach, these researchers inserted 6-French catheters that contained 20-MHz ultrasound transducers through a 16-French nasogastric tube into the esophagi of eight normal subjects and 50 patients with a variety of esophageal disorders (including esophageal varices, scleroderma, achalasia, esophageal carcinoma, and esophagitis). Of the seven echoic layers of the esophagus, four appear hyperechoic and three hypoechoic on sonograms. In the normal subjects, six layers were easily seen with the subject at rest. When the subjects were imaged as they drank water, seven layers were seen. Also, in the normal subjects, the muscles at the lower esophageal sphincter (LES) were significantly thicker than the muscles in the esophageal body. This is the first time these findings have been shown in vivo. In the seven patients with achalasia, the muscle layer thickness at the LES was greater than normal, LES relaxation was incomplete, the esophageal body was dilated above the LES, and the distal esophageal body had no peristaltic activity. Characteristic findings in the 13 patients with scleroderma included increased echogenicity in the muscle layers, normal wall thickness, dilatation of the distal lumen, and peristaltic dysfunction in the distal esophagus. In 15 patients with portal hypertension, multiple anechoic areas representing varices located in the submucosa and periesophageal areas were seen. Communication of varices between the submucosa and periesophageal areas also was shown. In the five patients with esophagitis, the following findings were seen: mucosal and submucosal thickening, dilated vessels in the submucosa, normal muscle thickness, and a normal swallowing pattern. Esophageal carcinoma (five patients) was characterized by the presence of a focal mass, which was either hypoechoic or hyperechoic in appearance. All strictures were easily

passed; however, the ultrasound beam had limited penetration. High-resolution endoluminal esophageal sonography appears to allow detailed imaging of the normal and diseased wall of the esophagus in vivo.

Transabdominal hydrocolonic sonography in diagnosis and staging of colonic tumor.—Dr. Bernd-Limberg (Darmstadt, Germany) presented results of a new technique in diagnosing diseases of the colon. The purpose of the described investigation was to determine if retrograde instillation of water would increase the usefulness of transabdominal sonography in the assessment of colonic polyps and tumors. In 300 patients, both conventional and hydrocolonic sonography were performed and interpreted before colonoscopy was done to verify the diagnosis. The optimal procedure for hydrocolonic sonography involves the following steps: oral lavage of the patient for bowel cleansing; IV injection of 20 mg *N*-butyl-scopolamine bromide for bowel relaxation; placement of the patient supine; retrograde instillation of 1000–1500 ml of water into the colon; and continuous sonographic evaluation of the colon with 3.5-, 5.0-, and 7.5-MHz transducers. The 15-min examination was well tolerated by patients; patients generally felt "pretty comfortable." In 97% of the patients, the entire length of the colon was visualized with hydrocolonic sonography: In optimal cases, the junction of the cecum and ileum was seen. With hydrocolonic sonography, polyps were seen as echogenic structures projecting from the colon wall into the anechoic lumen, and it was possible to tell whether the polyp had invaded the colon. Tumors appeared as echogenic structures projected into the lumen; intramural infiltration could be detected with hydrocolonic sonography. Colonoscopy showed 29 colonic tumors, 28 of which were seen with hydrocolonic sonography and only nine of which were seen with conventional sonography. Colonoscopic results showed polyps larger than 7 mm in 43 patients; 39 polyps were detected with hydrocolonic sonography, but none were detected with conventional sonography. Thus, the sensitivities for the two methods were as follows: for tumors, 97% for hydrocolonic sonography and 31% for conventional sonography; for polyps larger than 7 mm, 91% for hydrocolonic sonography and 0% for conventional sonography. Hydrocolonic sonography also proved helpful in staging the 28 tumors detected: no T1 tumors were detected with either hydrocolonic sonography or colonoscopy; three of four T2 tumors, 17 of 20 T3 tumors, and three of four T4 tumors were correctly staged with hydrocolonic sonography. As mentioned, all polyps were correctly identified with hydrocolonic sonography, which appears to be a potentially useful method to detect and stage polyps and tumors of the large bowel.

Endosonography in the diagnosis of recurrent rectal cancer.—J. Tschmelitsch (Innsbruck, Austria) described a study performed by himself and colleagues (K. Glaser, G, Judmaier, E. Bodner) to evaluate the usefulness of endosonography in detecting local recurrence of rectal cancer. In 85 patients who had undergone curative surgery for rectal cancer, 3-, 6-, and 12-month follow-up examinations included the following: endosonography, rectal/vaginal digital examination, rigid rectoscopy, linear-array sonography, pelvic CT, chest radiography, and pancolonoscopy. All patients were examined at least twice after surgery. Of the 85 postoperative patients studied, 18 (21%) had local recurrences, which occurred 6–27 months postoperatively (mean, 18 months). One recurrence was staged as Duke's A, seven as Duke's B, and 10 as Duke's C. Endosonography showed all 18 recurrences—and, in five cases, endosonography was the only examination to show the recurrence (CT showed 13, digital examination revealed eight, and other tests showed fewer). In 12 cases, the patients underwent surgery again: seven for palliative therapy and five for curative therapy (four of these five cases were early tumors seen only with endosonography). These researchers conclude that endosonography is a very sensitive method to detect postoperative local recurrences of rectal cancer and can show it early enough to allow curative therapy in some patients. Moreover, endosonography, an inexpensive, outpatient procedure, is well tolerated by patients and involves no radiation exposure. As in most cases of radiographic diagnosis, however, the sensitivity of this method depends heavily on the level of expertise of the sonographic operator and interpreter.

Obstetric Sonography

Use of the ovarian pulsatility index to differentiate ectopic pregnancy from spontaneous abortion.—To evaluate the usefulness of the pulsatility index in distinguishing ectopic pregnancy and spontaneous abortion, Mark S. Cartier (Memphis, TN) and colleagues (L. A. Altieri, D. S. Emerson, R. E. Felker, W. C. Smith, A. A. Birch, R. Sellers, T. G. Stovall) reviewed the records of 860 women. These patients had been referred for transvaginal sonography/transvaginal color Doppler studies for suspected ectopic pregnancy. Transvaginal sonography had a sensitivity of 64% in detecting ectopic pregnancy, but a marked increase in sensitivity (to 82%) occurred with the addition of transvaginal color Doppler studies. However, for both types of examinations, "indeterminate" was sometimes the only result of the study (35% of the time for transvaginal sonography, 19% of the time for transvaginal color Doppler studies). These researchers reviewed the cases to look for a method of reducing the number of "indeterminate" calls. Of the 166 cases labeled "indeterminate" on transvaginal color Doppler studies, 8% were ectopic pregnancies, 88% were failed intrauterine pregnancies, and 4% were intrauterine pregnancies. The criteria for "indeterminate" on these studies were (1) "cool to hot" uterus, (2) lack of intrauterine peritrophoblastic flow, (3) presence of contralateral flow, and (4) lack of adnexal mass/flow. Cartier and coworkers investigated whether they could use ovarian pulsatility indexes both to better differentiate complete spontaneous abortion from ectopic pregnancy in the absence of an adnexal mass and to decrease the number of "indeterminate" diagnoses on transvaginal color Doppler studies. Of the 860 original cases, 110 had flow in both ovaries and were reviewed retrospectively from video recordings. The gold standard was either clinical laboratory findings or surgical results. The normal ovarian arterial flow pattern is high resistance and low diastolic flow; the flow is often near the periphery and may be unilateral. On transvaginal color Doppler studies, flow in the corpus luteum has intense color; it is also a low-resistance, high-diastolic

flow, and often is seen around a cyst in the corpus luteum. Flow in the corpus luteum can be unilateral or bilateral in pregnancy. Results showed that the pulsatility index was less than 1 in 16% of women with an intrauterine pregnancy, in 18% of women with an ectopic pregnancy, in 32% of women who experienced an incomplete spontaneous abortion, and in 60% of women who had a complete spontaneous abortion. The pulsatility index was 1 or greater in 32% of women who had an incomplete spontaneous abortion and in 40% of women who had a complete spontaneous abortion; no patient with a pulsatility index of 1 or greater had an ectopic or intrauterine pregnancy. In 81 patients, the pulsatility index was less than 1. Of these, 22% had an intrauterine pregnancy, 25% an ectopic pregnancy, 21% an incomplete spontaneous abortion, and 32% a complete spontaneous abortion. In 29 patients, the pulsatility index was 1 or greater. Of these, 28% had an incomplete spontaneous abortion and 72% had a complete spontaneous abortion. It appears that ovarian pulsatility indexes may enhance diagnostic sensitivity for complete spontaneous abortion; although this study is limited by its retrospective nature, its finding that *no* patients with ectopic pregnancy or intrauterine pregnancy had a pulsatility index of 1 or greater indicates clearly the need for a prospective study to confirm the validity of this potentially important method for differential diagnosis in these cases.

Pregnancy outcome after a first-trimester sonogram with normal findings.—Mary C. Frates (Boston, MA; coauthors: C. B. Benson, P. M. Doubilet) presented a study of the relationship between the outcome of a pregnancy and both the indications and findings of a first-trimester sonogram. In this retrospective study of 1016 cases, the indications for requesting a first-trimester sonogram were as follows: 61% for routine reasons (e.g., uncertain conception date); 29% for symptoms (e.g., vaginal bleeding, pelvic pain); 8% for miscellaneous reasons (e.g., suspected fibroid, uterine abnormality); and 2% for unknown reasons. In 89% of cases, the sonographic results were normal; the abnormal findings included subchorionic hematomas, fibroids, and uterine anomalies. A significant difference was found between the percentage of normal sonographic results in symptomatic (85% normal) and nonsymptomatic (92% normal) patients. The outcome of the pregnancy was known in 562 patients: 92% delivered live neonates, 8% suffered spontaneous abortions. Of all the women with "normal" sonographic studies, 8% eventually had spontaneous abortions; of all those whose sonographic finding were "abnormal," 13% suffered later spontaneous abortions. This difference did not reach statistical significance, possibly because of the small number of patients in this study who had abnormal sonographic results. If the sonographic results were normal, the indication for the sonographic study showed no difference in outcome: In both routine studies and those done in symptomatic patients, the spontaneous abortion rate was about 8%. Fetal loss rate associated with normal sonographic results did decrease significantly as the gestational age increased: In fetuses 6.0–7.9 weeks' gestational age, loss rate was 14%, but that rate decreased to 4% if the fetus was 12–13 weeks' gestational age when the sonographic findings were normal. The data from this retrospective study can be used to provide women in their first trimester of pregnancy with more accurate prognostic information than has previously been available. Possibly the most important information for the physician to remember is that a "normal" sonogram in the first trimester does not guarantee a live birth, but normal sonographic results at 12–13 weeks' gestational age do indicate a good chance for a live birth (only 4% spontaneous abortion rate in this study).

Predictive accuracy of first-trimester abdominal sonography in twin pregnancies.—A study on the use of sonography to determine placental and membrane status of twin pregnancies was presented by A. B. Kurtz (Philadelphia, PA; coauthors: J. Mata, R. Wapner, A. Johnson). A few previous first-trimester studies have indicated the following about the interpretation of abdominal sonographic studies in twin fetuses: (1) a thick dividing membrane is *diagnostic* of dichorionic/diamniotic (DC/DA) twins; (2) a thin membrane *suggests* monochorionic/diamniotic (MC/DA) twins; and (3) lack of a membrane *could represent* monochorionic/monoamniotic (MC/MA) twins. In 166 women carrying twins of 9–12 weeks' gestational age, sonograms were obtained before chorionic villus sampling. For clinical correlation, all twins were followed up until birth. The researchers classified all different-gender twins as DC/DA; for same-gender twins, a follow-up call and pathologic report were used to determine chorionicity and amnionicity. Sonographic criteria for thickness of membrane were as follows: thick = hyperechoic and ≥2 mm; intermediate = ≥1 mm but <2 mm; thin = "wisp" appearance and <1 mm; none = no evidence of membrane. Other features recorded included the number of placentas (one or two) and the presence or absence of the lambda sign (a triangular insert at the insertion of the placenta that is consistent with dichorionicity). Of the 166 twin pairs, follow-up was available in 105: 51 were different-gender twins, therefore, DC/DA; 54 were same-gender twins (34 DC/DA, 16 MC/DA, and four MC/MA). Among the 85 total DC/DA twin pairs, sonographic findings showed a thick membrane in 78 (92%), an intermediate membrane in four (5%), a thin membrane in three (4%), and no membrane in none. In the 16 MC/DA twin pairs, sonography revealed a thick membrane in none, an intermediate membrane in one, a thin membrane in 14, and no membrane in one. No membrane was seen on sonograms in any of the four MC/MA twin pairs. Accuracy of classification for DC/DA was increased when a two-placenta criterion also was considered; 82 of 85 DC/DA twin pairs were then recognized sonographically. However, although identification of two placental sites occurs *only* in DC/DA twin pairs, *it does not occur very often* (in only 22 of 85 cases here). Finally, the lambda sign proved of little use in determining chorionicity and amnionicity sonographically (the lambda sign was seen in six of 85 DC/DA pairs and in two of 16 MC/DA pairs). These researchers concluded that thick membranes always indicate DC/DA twins; the identification of two placental sites is of limited value in recognizing DC/DA twins; thin membrane probably indicates MC/DA twins; no membrane probably indicates MC/MA twins; and the lambda sign has no diagnostic value for the purpose of determining chorionicity and amnionicity in twins.

Categorical Course: Pediatric Sonography

Sonography of the Acute Abdomen in Children

C. Keith Hayden, Jr. (Arlington, TX) presented a 30-min discussion of the usefulness of sonographic evaluation of the acute abdomen in children. Both pediatricians and surgeons request sonography for acute abdominal problems in children, which may be caused by gastroenteritis, appendicitis, intussusception, or (less commonly) pneumonia. Moreover, other diseases (such as mesenteric adenitis, Crohn's disease, Meckel's diverticulitis, or Henoch-Schönlein purpura) can mimic appendicitis and should be considered in these evaluations.

Gastroenteritis is the most common cause of acute abdomen in children. Since sonographic findings are nonspecific for this entity, the radiologist uses sonography only to rule out more serious problems. Moreover, performing sonography in these patients may be frustrating because they have a lot of gas; Dr. Hayden recommended using compression to improve image quality. One possible differential feature of gastroenteritis is that intestinal walls are usually not abnormally thickened in this entity (but sometimes they are). The next most common cause of acute abdomen in children, *appendicitis*, becomes progressively more common with increasing age. The clinical and laboratory findings in appendicitis are extremely nonspecific and sometimes very confusing. In 309 patients with appendicitis suspected on the basis of clinical findings, 110 underwent surgery: 105 had appendicitis and five did not have appendicitis. The sonographic features to look for in suspected appendicitis include the following: a fluid-filled, rigid (noncompressible) appendix; an appendix wall of 2–7 mm (most often 2–3 mm), which may be shaggy or well defined; and anechoic to hyperechoic fluid. If the appendix cannot be visualized on the sonogram, the radiologist should look for localized abscess; free fluid (especially in the right lower quadrant, but many patients have free fluid without appendicitis); diffuse abdominal fluid; and thick intestinal walls. Nonperforated appendicitis can be readily diagnosed (a fluid-filled noncompressible appendix was seen on sonograms in 62/64 patients with nonperforated appendicitis, but in only 13/41 patients with perforated appendicitis). For perforated appendicitis, a decompressed, thick-walled appearance is strongly suggestive of the diagnosis (15/41 patients). Most cases of *intussusception* occur in patients 5–12 months old; as many as 40% of these patients will not have the classic symptoms of this entity. In all patients with intussusception who were studied, variable amounts of free fluid were seen; no patient had necrosis.

Of the diseases that mimic appendicitis, *mesenteric adenitis* (a viral infection) may be the most problematic to diagnose. It cannot be diagnosed clinically, and sonographic diagnosis also can be difficult. *Crohn's disease* occurs more frequently in adults than in children, and patients have a wide variety of symptoms; 20% of patients with Crohn's disease have symptoms that mimic acute appendicitis. An acute inflammatory process of unknown origin, *Henoch-Schönlein purpura* involves the small vessels, and patients frequently have acute abdominal cramping (which precedes the traditional rash). Two sonographic patterns of Henoch-Schönlein purpura have been identified: (1) generalized thickness of abdominal wall and (2) focal thickness of abdominal wall. *Meckel's diverticulitis* also can mimic appendicitis; 30% of these patients have perforation, and the diagnosis is usually made at surgery. Sonographic findings include a short segment of inflamed abnormal bowel; on long axis, a somewhat polypoid lesion (3.0 × 3.5 cm); and on short axis, a persistent thickened mucosal pattern. Gastrointestinal series may or may not confirm the diagnosis of Meckle's diverticulitis.

Dr. Hayden concluded that sonography is an excellent screening method for the acute abdomen in children; it can give the radiologist a specific diagnosis or indicate the next test needed. The take-home message of the lecture was that sonographic screening of these patients is like "opening a box of Cracker Jacks—you never know what you'll find, but if you never look for it, you won't find it."

Pediatric and Adolescent Gynecologic Sonography

In another 30-min lecture, Harris L. Cohen (Manhasset, NY) emphasized the importance of sonography in imaging the pelvis in infants and children. High-quality pelvic sonographic studies require a full bladder (the "window to the pelvis"—water in the bladder displaces air-filled bowel loops). Patients are prepared by having them drink water an hour before the examination. Less commonly, an 8-French feeding tube can be used to fill the bladder of a neonate or young child. Appropriate transducers to use include 7.5- to 5-MHz for infants, 5-MHz for children, and 5- to 3.5-MHz for teenagers (unless the patient is particularly thin). Other sonographic techniques sometimes used include rectal instillation of fluid, transvaginal sonography in nonvirginal patients, transperineal sonography in patients with an intact hymen, and Doppler and color-flow imaging.

Fetal sonographic evaluation may aid interpretation of later pelvic examinations in infants and children by the identification of ovarian cysts or cysts of unknown origin within the pelvis of the fetus or by noting external genitalia (especially in rare cases of conflicting karyotypes). Fetal ovarian cysts represent a universally benign response to maternal hormonal stimuli; they are usually unilocular, and they may become symptomatic after birth. After birth, the presence of large, symptomatic cysts indicates the need for surgery; however, large asymptomatic cysts have been a source of controversy. Although one source claims that the "disappearance" of the fetal cyst is due to torsion in 60% of cases, most authors believe the disappearance is due to involution of a functional cyst. In a study of 101 patients (ages 2–12 years), 68% were found to have ovarian cysts; macrocysts (>9 mm) were seen in 11 patients less than 11 years old. Dr. Cohen reiterated the recommendation that physicians be wary of fetal ovarian cysts that are pedunculated, septated, or that contain retracting clots or fluid-debris levels.

Sonography has shown that the uterus in a neonate is about 3.5 cm long, and the cervix is about two times as thick as the fundus. By 4–12 months, the mean uterine length decreases to 2.6–3.0 cm, and the uterus has a tubelike shape.

Uterine length increases slowly between 3 and 8 years of age, and, by 10–13 years, has an average length of 4.3 cm. After puberty, the normal uterus is pear shaped and ranges from 5 to 8 cm in length. Hydrometrocolpos and hematometrocolpos are the predominant uterine masses seen in neonates and infants. Two types of patients may have these masses, those with no associated abnormalities and those with associated cloacal or urogenital sinus malformation. If hematometrocolpos is not diagnosed at the neonatal stage, it will probably not be discovered until after menarche, when monthly distension of the vagina and uterus may cause pain or mass. Transperineal sonography, in addition to transabdominal sonography, is useful in diagnosing these uterine masses.

Ovarian masses in infants and children may be complex or solid. Complex masses are partly cystic, partly echo-filled, and show decreased through-transmission. This complexity may indicate hemorrhage in functioning cysts or neoplastic, inflammatory, or other noncystic masses. Ovarian teratomas, uncommon before puberty, show echogenicity of various degrees on sonograms: 30–50% are said to be calcified on plain films. Usually asymptomatic, benign ovarian teratomas appear echogenic with a fat shadow and may contain teeth, hair, and so forth; 25% of the benign teratomas are bilateral. Composition of benign ovarian teratomas is said to change with the patient's age: before menarche, 40% are noted to have nodules, and after puberty, 70% are noted to have nodules. Calcification is more common among teratomas noted after puberty, probably because of evolving echogenic elements. Germ cell tumors, including teratomas, make up 67% of all ovarian neoplasms. Of the remaining neoplasms, 25% are epithelial and 10% are of the sex cord or mesenchymal. Fifty percent of hormonally active ovarian tumors in young girls are malignant. Of all ovarian neoplasms in girls, 33% are malignant, but this percentage decreases with age; 85% of these malignant tumors are germ cell neoplasms. After sonography has been used to help diagnose these tumors, CT or MR imaging can provide a more global view of the patient's condition.

Meet the Professor: Interventional Breast Sonography

In this Meet the Professor session, Steve H. Parker (Englewood, CO) led a discussion of the somewhat controversial use of sonography to guide interventional procedures in the breast. Sonography can be an incredibly important tool in this area; placing the ultrasound transducer on an area that is ambiguous on mammograms can reveal the true nature of the abnormality and suggest the best course of action. For all breast interventional procedures under sonographic guidance, Dr. Parker recommends use of local anesthetic because, especially in younger women, the insertion of the 22- or 23-gauge needle into fibrous bands or areas of fibrocystic change will hurt; furthermore, diluting the anesthetic with sodium bicarbonate will eliminate the acidity that causes the sting that occurs on injection of the anesthetic.

Dr. Parker talked specifically about using sonography for cyst aspiration, abscess drainage, localization of lesions for surgery, and biopsy. Cyst aspiration is the easiest interventional procedure in the breast; use of a 21-gauge Vacutainer allows the radiologist to perform a one-handed operation in which, when the cyst is hit by the needle, the red-top tube is popped, and the cyst is thereby aspirated. In patients with multiple cysts, the radiologist can simply advance the Vacutainer from cyst to cyst; Dr. Parker said "zapping" the cysts in this way was somewhat like playing PacMan and that patients enjoyed watching the procedure on the monitor. For abscess drainage, sonographically guided drainage is much less invasive than surgery and can be very helpful in such procedures involving the breast because the abscesses tend to be superficial. Moreover, the mobile sonography unit can be taken to the intensive care unit, and drainage can be performed at the patient's bedside. Sonography also provides pinpoint accuracy for localization of lesions for surgery. Finally, breast biopsies can be performed quickly and easily under sonographic guidance. Dr. Parker recommends use of a Bard Biopty gun with a 14-gauge needle, a *minimum* of five passes to ensure that sufficient tissue has been obtained, and liberal use of local anesthetic. Tissue from sonographically guided core biopsies can provide evidence of infiltrating lesions that cannot be given by fine-needle aspiration biopsy; for benign lesions, core biopsy results can indicate what kind of benign lesion is present and therefore can often obviate surgery. This type of evidence is particularly important in the breast, where 80% of lesions are benign and should not require surgery.

For high-quality breast sonograms to be obtained, good sonographic equipment is needed; Dr. Parker suggested that the participants invite several different manufacturers to their own institutions and perform side-by-side tests with the equipment—then the radiologists can determine which unit will produce the best images of breast abnormalities. Learning to perform these interventions correctly is essential, as they can improve patients' care tremendously. In the future, the routine diagnosis of a breast lesion may take only 1 or 2 days rather than 2 or 3 weeks: A patient referred for a mammographic study may be referred that same day for sonography. If a biopsy is indicated, the biopsy can be done at that time under sonographic guidance, and the patient and physician will know the diagnosis the next day. Radiologists will find some resistance from other radiologists and from surgeons in their attempts to introduce sonographic breast interventions, but data so far have been very encouraging. With precise, reliable sonographic equipment and well-trained radiologists to perform the interventions, the next stage may be needle-directed therapy in the breast.

Forthcoming Articles

REVIEW ARTICLE

MR measurement of blood flow in the cardiovascular system. *Mostbeck GH, Caputo GR, Higgins CB*

CARDIOPULMONARY RADIOLOGY

Diagnosis of obliterative bronchiolitis in heart-lung transplantation patients: importance of bronchial dilatation on CT. *Lentz D, Bergin CJ, Berry GJ, Stoehr C, Theodore J*

Hypersensitivity pneumonitis: sensitivity of high-resolution CT in a population-based study. *Lynch DA, Rose CS, Way D, King TE Jr*

Pulmonary sarcoidosis: changes on follow-up CT examination. *Murdoch J, Müller NL*

Case report. Anomalous left brachiocephalic (innominate) vein: MR demonstration. *Fujimoto K, Abe T, Kumabe T, Hayabuchi N, Nozaki Y*

Case report. Value of MR imaging to detect a peanut causing bronchial obstruction. *O'Uchi T, Tokumaru A, Mikami I, Yamasoba T, Kikuchi S*

BREAST RADIOLOGY

Ductal carcinoma in situ of the breast: correlation between mammographic calcification and tumor subtype. *Stomper PC, Connolly JL*

Solitary breast papilloma: comparison of mammographic, galactographic, and pathologic findings. *Woods ER, Helvie MA, Ikeda DM, Mandell SH, Chapel KL, Adler DD*

Mammography in women with axillary lymphadenopathy and normal breasts on physical examination: value in detecting occult breast carcinoma. *Leibman AJ, Kossoff MB*

GASTROINTESTINAL RADIOLOGY

Pictorial essay. Left-lobe hepatic transplants: spectrum of normal imaging findings. *Caron KH, Strife JL, Babcock DS, Ryckman FC*

Malignant biliary obstruction: efficacy of thin-section, dynamic CT for determining resectability. *Gulliver DJ, Baker ME, Cheng CA, Meyers WC, Pappas TN*

Review. Chronic biliary-type pain in the absence of gallstones: the value of cholecystokinin cholescintigraphy. *Kloiber R, Molnar CP, Shaffer EA*

Membranous obstruction of the inferior vena cava: comparison of findings at sonography, CT, and venography. *Lim JH, Park JH, Auh YH*

Acute lower gastrointestinal hemorrhage: treatment by superselective embolization with polyvinyl alcohol particles. *Guy GE, Shetty PC, Sharma RP, Burke MW, Burke TH*

The density, contour, and thickness of the pancreas in diabetics: a CT study in 57 patients. *Gilbeau J-P, Poncelet V, Libon E, Derue G, Heller FR*

Pictorial essay. Pancreatic disease: findings on state-of-the-art MR images. *Mitchell DG, Shapiro M, Schuricht A, Barbot D, Rosato F*

Diagnosis of acute appendicitis in pregnant women: value of sonography. *Lim HK, Bae SH, Seo GS*

Case report. Pipestem appearance of small bowel in strongyloidiasis is not pathognomonic of fibrosis and irreversibility. *Medina LS, Heiken JP, Gold RP*

Case report. Multiple smooth-muscle tumors of the colon and adrenal gland in an adult with AIDS. *Radin DR, Kiyabu M*

Case report. Inadvertent barium hysterosalpingography. *Carlsen SE, Thurmond AS, Scanlan RM, Patton PE*

GENITOURINARY RADIOLOGY

Pictorial essay. Renal diseases in patients with AIDS: sonographic findings. *Kay CJ*

Submucosal uterine leiomyomas: diagnosis of prolapse into the cervix and vagina based on MR imaging. *Panageas E, Kier R, McCauley TR, McCarthy S*

MUSCULOSKELETAL RADIOLOGY

Temporomandibular joint: relation between MR evidence of effusion and the presence of pain and disk displacement. *Westesson P, Brooks SL*

Injuries of the superior portion of the glenoid labrum involving the insertion of the biceps tendon: MR imaging findings in nine cases. *Hodler J, Kursunoglu-Brahme S, Flannigan B, Snyder SJ, Karzel RP, Resnick D*

Value of unenhanced spin-echo MR imaging in distinguishing between synovitis and effusion of the knee. *Singson RD, Zalduondo FM*

Technical note. Intraarticular sonography for imaging of the knee menisci: evaluation in cadaver specimens. *McDonnell CH III, Jeffrey RB Jr, Björkengren AG, Li KCP*

Elastofibroma: MR and CT appearance with radiologic-pathologic correlation. *Kransdorf MJ, Meis JM, Montgomery E*

NEURORADIOLOGY

Review. Neoplastic diseases affecting the central skull base: CT and MR imaging. *Ginsberg LE*

Review. Diffusion MR imaging: clinical applications. *LeBihan D, Turner R, Douek P, Patronas N*

Pictorial essay. Cystic masses of the head and neck: pitfalls in CT and MR interpretation. *Miller MB, Rao VM, Tom BM*

CT and MR imaging findings in adults with cerebellar medulloblastoma: comparison with findings in children. *Bourgouin PM, Tampieri D, Grahovac SZ, Léger C, Del Carpio R, Melançon D*

Case report. Tortuous vertebral artery: MR and CT demonstration. *Kricun R, Levitt LP, Winn HR*

PEDIATRIC RADIOLOGY

Diagnosis of liver disease in children: value of MR angiography. *Hubbard AM, Meyer JS, Mahboubi S*

Case report. Neonatal hemochromatosis: diagnosis with MR imaging. *Hayes AM, Jaramillo D, Levy HL, Knisely AS*

Case report. AIDS-related cholangitis in children: sonographic findings. *Rusin JA, Sivit CJ, Rakusan TA, Chandra RS*

Case report. Bile nephrosis in a neonate: sonographic findings of rapid kidney enlargement and increased echogenicity. *Bruno MA, Spear GS, Dietrich RB, Pugh PA*

STATISTICS IN RADIOLOGY

0000 Perspective. Strategies for improving power in diagnostic radiology research. *Beam CA*

MEETING NEWS

The Society of Cardiovascular and Interventional Radiology: 17th annual scientific meeting, April 1992. *Whalen E*

ARRS 1992 ANNUAL MEETING

Summary of scientific program
Gold medal recipients
Secretary's report
Administrative report
Award-winning exhibits
New members

Letters

The Selling of a Profession

Increasingly, economic issues dominate the practice of radiology, often overshadowing the more stimulating intellectual challenges that attracted us to the specialty. Vexations such as turf battles, restrictions of third-party payers, and the rampant federal bureaucracy captured our attention and absorbed our energies during the decade of the eighties. Generally, radiology is weathering these trials, as it is a unified society bound to the commitment to abide by the ethical guidelines that best serve the specialty and, most importantly, our patients.

As the centennial of radiology approaches, a little-publicized insidious practice threatens the integrity of our discipline. I refer to the practice of allowing nonradiologists to interpret images and bill for or be paid for their services within radiologic facilities, an abuse that threatens the very core and foundation of the specialty. We witness fellow radiologists laying aside moral principles and medical ethics as they shamelessly sell their rights to imaging to nonradiologists. It is disheartening to see under the letterhead of a radiologist or an imaging group directed by radiologists reports generated by nonradiologists. Such sinister ventures to which radiologists are party foretells a splintering and fragmenting of radiologic care.

Although many of us left the bitter turf battles of the eighties bloodied but resolute, a few compromised their specialty and welcomed the nonradiologist interlopers with open arms and open checkbooks. These radiologists were not coerced into such dangerous liaisons; indeed, some actively sought these arrangements.

Clearly, these self-referral abuses represent the extreme in conflict of interest inasmuch as the nonradiologist who perpetrates the misuse of imaging both requests and interprets the imaging study. In such practices, a spin-off of laissez-faire medicine, the goals are not improvement in the quality of imaging or better service but rather personal financial gain. These ersatz radiologists covet the crown jewels of radiology: MR and CT. The more prosaic and less well compensated plain films do not interest them; and please, paying patients only—no pro bono work. Recent Stark amendments may herald an increase in such practice patterns; the abusers cleverly attempt to bypass the sanctions of kickback regulations. The abusive arrangements, of which the patient is not aware or has been misled about, fall far short of the ideals of practice.

How can organized radiology respond to such perilous intrusions? (1) Recognize that such practice patterns exist and should be discouraged. (2) Adopt more stringent ethical guidelines. The American College of Radiology should take a leadership role in this matter. (3) Let the public know of these practices and how such practices abuse referral patterns. (4) Serve notice on radiologic pretenders that the specialty of radiology is not for sale.

Congressman Stark (D, CA) sent a clear warning to all of medicine when he stated, "Physician ownership/referral arrangements represent an exploding virus which ultimately will erode the trust patients have traditionally placed in their physicians" [1]. A profession is a bond, and trust is the glue that seamlessly holds the profession together and defines its nature. The professional societies in radiology seek to maintain a high level of standards and to promote excellence in imaging; as well, they foster intellectual exchange, encourage collegiality, and defend ethical practice patterns. Those who would shatter the links of that professional bond, who would sully the trust that holds them to professional standards, should make the rest of us fear for the future. Their chilling example reminds us of Gresham's law that the bad drive out the good.

Membership in a society of specialists carries with it an implied contract. Arnold Relman, in a recent Shattuck lecture, wrote, "Most of us believe we are parties to a social contract, not a business contract" [2]. In radiology, that contract, or covenant, charges us to provide quality imaging in an ethical and honest manner. That goal serves best the paramount interests of the patient and eschews those of the self-referring physician. When the boundaries of ethics are trespassed, it is the obligation of the other members of the specialty to condemn such transgressions and to serve notice that the interests of radiology and the patient are being poorly served. If we are to survive as a specialty, the collaboration with self-referring nonradiologist physicians—in essence the selling of the profession—must cease as a viable practice option.

James F. Lally
Christiana Hospital, Medical Center of Delaware
Newark, DE 19718

REFERENCES

1. Iglehart JK. Health policy report: Efforts to address the problem of physician self-referral. *N Engl J Med* **1991**;325:1820–1824
2. Relman AS. Shattuck lecture. The health care industry: where is it taking us? *N Engl J Med* **1991**;325:854–859

Winning the Turf War

It starts early, in medical school. "I'm on radiology next month. I need the vacation to sit back, relax, and enjoy the friendly radiologists." It has been 12 years since my third-year rotations, and I am still hearing the same remarks from today's students.

As a radiologist in private practice (also 2 years as an assistant professor), I know radiology is no vacation, but my nonradiology colleagues do not. This hurts radiologists at the bargaining table from hospital committees to negotiations on Relative Value Schedules. It is time we stop spoon-feeding our medical students and instead give them a dose of the real world as the other specialties do. For example, night call with the emergency department resident, hours of arteriography with lead apron, teaching assignments, and participation in communicating results to referring physicians would do for a start.

I urge my academic colleagues to look beyond the textbooks and consider the political roots of preserving the prestige of our specialty.

Louis A. Friloux III
The Magnetic Resonance Institute of Arlington
Arlington, VA 22206

Mycotic Aneurysm of the Bronchial Artery: a Rare Cause of Hemoptysis

A 34-year-old man whose aortic valve had been replaced 1 year earlier was admitted for treatment of septicemia and acute heart failure. Sonography showed vegetations on the prosthesis, consistent with the endocarditis; blood cultures were positive for *Staphylococcus epidermidis*. The patient was treated with antibiotics. One week later, severe hemoptysis occurred. Selective bronchial arteriography showed a small aneurysm (diameter, <1 cm) of a distal branch of the left bronchial artery (Fig. 1A) and no extravasation of contrast medium. Embolization with small fragments of dura (Totoplast Dura; Pfrimmer Vigo, Erlangen, Germany) controlled the hemoptysis (Fig. 1B). The patient died 4 weeks later of multiple organ failure.

Bleeding from bronchial arteries is usually due to chronic pulmonary infection, pneumoconiosis, or tumor [1, 2]. To our knowledge, rupture of a mycotic aneurysm of the bronchial artery in adults has not been previously reported. Angiographic features of mycotic aneurysm are nonspecific, and congenital aneurysms are difficult to exclude. Rapid growth of the aneurysm is associated with risk of rupture, and prompt treatment is required. Selective embolization of the bronchial arteries is simple and reliable. It results in rapid control of the hemoptysis, even in a patient whose condition is unstable [1–3]. This case emphasizes that mycotic aneurysm of a bronchial artery should be considered as a possible cause of hemoptysis in patients who have septicemia or endocarditis.

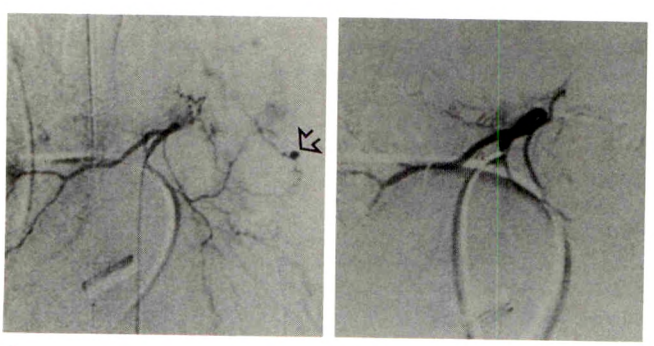


Fig. 1.—Mycotic aneurysm of bronchial artery in a 34-year-old man with hemoptysis.
***A*, Arteriogram shows small aneurysm (*arrow*) on distal part of left bronchial artery and no extravasation of contrast medium.**
***B*, Arteriogram obtained after embolization shows left bronchial artery is occluded.**

Vincent Servois
Alban Denys
Annie Sibert
and colleagues
Hôpital Bichat
75018 Paris, France

REFERENCES

1. Remy J, Arnaud A, Fardou H, Giraud R, Voisin C. Treatment of hemoptysis by embolization of bronchial arteries. *Radiology* **1977**;122:33–37
2. Vujic I, Pyle R, Hungerford GD, Griffin CN. Angiography and therapeutic blockade in the control of hemoptysis. *Radiology* **1982**;143:19–23
3. Rabkin J, Astavjef V, Gothman L, Grigorjev Y. Transcatheter embolization in the management of pulmonary hemorrhage. *Radiology* **1987**;163:361–365

Localized Large Benign Fibroma of the Pleura in Poland's Syndrome

A 31-year-old man had routine chest radiography before sinus surgery. The radiographs showed a large right-sided pleural effusion (Fig. 1A). The patient said he had had progressive exertional dyspnea for 4 years. Axial CT scans showed a large, heterogeneously enhancing soft-tissue mass and pleural effusion occupying much of the right hemithorax and absence of the right pectoralis muscle (Figs. 1B and 1C). Syndactyly of the right hand was noted incidentally. Subsequent bronchoscopy showed only absence of the right bronchus cartilage; no obstructing lesion was found.

At the time of thoracotomy, the right lung was totally collapsed. After drainage of approximately 3 l of serosanguineous fluid, a well-circumscribed, 20 × 12 × 10 cm pleura-based mass was resected. Grossly, the adjacent lung and chest wall were not involved. Histo-

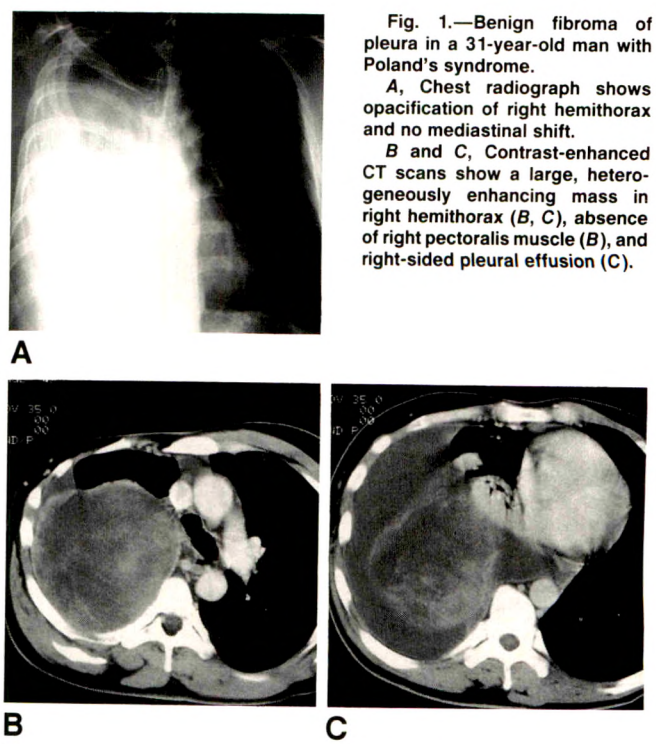


Fig. 1.—Benign fibroma of pleura in a 31-year-old man with Poland's syndrome.
***A*, Chest radiograph shows opacification of right hemithorax and no mediastinal shift.**
***B* and *C*, Contrast-enhanced CT scans show a large, heterogeneously enhancing mass in right hemithorax (*B*, *C*), absence of right pectoralis muscle (*B*), and right-sided pleural effusion (C).**

logic examination of the mass showed a noninfiltrating, benign, pleura-based fibroma and no evidence that it was malignant. With the exception of a small right-sided pneumothorax, the postoperative course was unremarkable.

Poland's syndrome is a congenital anomaly, consisting of hypoplasia or aplasia of the pectoralis major muscle and ipsilateral syndactyly. A localized benign fibroma of the pleura is a rare neoplasm. The large size of the tumor, associated pleural effusion, and the young age of the patient are unusual for this type of tumor. England et al. [1] described findings in a series of 223 localized fibrous tumors of the pleura. In this series, the patients' median age was 57 years. Radiologic findings showed that only six of 58 tumors were larger than 15 cm and only 10 had associated ipsilateral pleural effusion. Seven cases of neoplasm in patients with Poland's syndrome have been reported [2–4]. Four of the cases were acute leukemia in young children, and three were lymphoma in young adults. To the best of our knowledge, a localized benign fibroma of the pleura in a patient with Poland's syndrome has not been previously described. Both Poland's syndrome and the fibroma may arise from a mesodermal defect.

Gregory A. Francken
Robert J. Monette
David J. Czarnecki
Stuart A. Levy
St. Luke's Medical Center
Milwaukee, WI 53215

REFERENCES

1. England DM, Hochholzer L, McCarthy MJ. Localized benign and malignant fibrous tumors of the pleura: a clinicopathologic review of 223 cases. *Am J Surg Pathol* **1989**;13:640–658
2. Mace JW, Kaplan JM, Schanberger JE, Gotlin RW. Poland's syndrome: report of seven cases and review of the literature. *Clin Pediatr* **1972**;11: 98–102
3. Sackey K, Odone V, George SL, Murphy SB. Poland's syndrome associated with childhood non-Hodgkin's lymphoma. *Am J Dis Child* **1984**;138:600–601
4. Hershatter BW, Montana GS. Poland's syndrome and lymphoma. *Am J Dis Child* **1983**;137:1211–1212

Pulmonary Sequestration: Diagnosis Based on MR Angiographic Findings

Pulmonary sequestration, an uncommon congenital pulmonary disorder, is defined as a region of dysplastic and nonfunctioning pulmonary tissue. Usually, no communication to the normal bronchial tree is present. The blind-ending bronchi, which may become distended, trapping mucus secreted by the bronchial glands, are prone to infection. Consequently, cystic degeneration and fibrosis develop [1]. The sequestration either is located within the visceral pleura of a pulmonary lobe (intralobar type) or forms an accessory lobe that has its own visceral pleura (extralobar type). The blood supply is derived from one or multiple systemic arteries that originate from the thoracic or abdominal aorta and enter the lung via the pulmonary ligament. Venous drainage is into pulmonary (intralobar type) or systemic (extralobar type) veins. Surgical intervention, indicated to prevent recurrent infections, requires detailed information on (1) the exact location of the sequestration and the relationship between the affected area and the normal parenchyma, (2) the origin and course of the systemic arterial supply, and (3) the type of venous drainage.

A 23-year-old woman had a mostly cystic process in the lower lobe of the left lung. Findings on chest radiographs and contrast-enhanced CT scans suggested pulmonary sequestration. The results

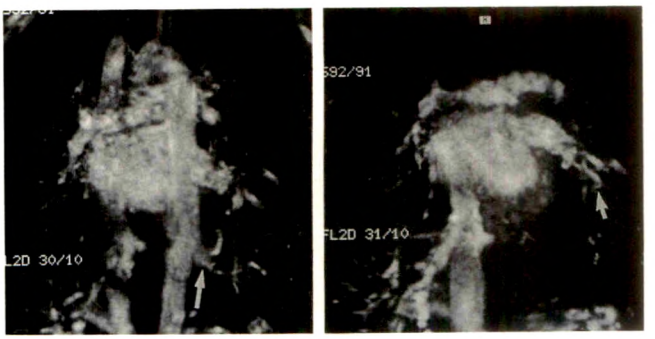


Fig. 1.—Coronal maximum-intensity-projection reconstructions of time-of-flight MR angiograms (30/10, 30° flip angle) of pulmonary sequestration.
***A*, Image obtained without presaturation shows vascular abnormality completely: aortic origin of feeding artery and subsequent branching (*arrow*), intrapulmonary venous drainage (segments 9 and 10).**
***B*, Image obtained with axial presaturation (TR = 31 msec) covering aortic arch shows loss of signal of systemic feeding artery and all its branches. Intrapulmonary vasculature, including venous drainage (*arrow*), is still visible.**

of bronchoscopy were normal. For morphologic evaluation, axial and coronal T1-weighted, ECG-gated MR images were obtained (1.5-T Siemens Magnetom). For MR angiography, sequential coronal two-dimensional fast low-angle shot (FLASH-2D) images (30/10 [TR/TE], 30° flip angle, 5-mm-thick sections, 1-mm overlap) were obtained by using a breath-holding technique in maximum inspiration [2]. FLASH-2D images with axial presaturation covering the aortic arch and a TR of 31 msec were used to saturate spins in the descending aorta, thus proving the origin of the feeding artery of the sequestration. Postprocessing was done by using a maximum-intensity-projection algorithm.

MR imaging showed a well-marginated, irregularly shaped, linearly branching, homogeneous, hyperintense structure within the left lower lobe. The origin of the feeding artery could be delineated. The intrapulmonary course, branching, and the venous drainage of the sequestration were not shown.

MR angiography (Fig. 1A) showed the sequestration as an inhomogeneous hypointense structure. The feeding artery originating from the thoracic aorta was easily detected, and its course could be followed, through the pulmonary ligament into the sequestration, where it divided into several branches. The venous drainage led into the veins of the ninth and tenth segments. These veins had strong flow signals around the sequestration. With axial presaturation, signal in the descending aorta was completely suppressed. No signal was detected from the feeding artery, proving the systemic blood supply to the sequestration (Fig. 1B). The intrapulmonary blood flow remained unchanged. The draining veins were not affected by the presaturation, and their delineation was improved because of the reduced superimposition. All the findings suggested intralobar pulmonary sequestration, which was confirmed by aortography and thoracic surgery; no accessory feeding arteries were detected.

Many different imaging techniques can be used to diagnose pulmonary sequestration: chest radiography, conventional tomography, radionuclide scanning, bronchography, sonography, CT [3], and MR imaging [4]. So far, definitive diagnosis always requires aortography to show the systemic arterial blood supply [1]. MR angiography, including selective vessel display, may complement spin-echo MR imaging in the diagnosis of pulmonary sequestration, as the first technique meeting all the preoperative requirements mentioned earlier. MR angiography is superior to MR imaging for showing the

vascular anatomy: The intrapulmonary vessels, the course of the feeding artery and branches within the sequestration, and the draining veins have high signal intensity (positive contrast) on MR angiograms. In our case, venous drainage into the veins of the ninth and tenth segments suggested intralobar sequestration. Because of its higher spatial resolution and the possibility of using selective catheterization, conventional angiography is superior to MR angiography for showing small accessory feeding arteries.

In summary, preoperative MR angiography and MR imaging can be used together to diagnose and classify pulmonary sequestration in a single noninvasive examination that does not require the use of contrast medium.

Hans-Ulrich Kauczor
Michael V. Knopp
Detlev Branscheid
Wolfhard Semmler
German Cancer Research Center
6900 Heidelberg, Germany

REFERENCES

1. Ferris EJ, Smith PL, Mirza FH, et al. Intralobar pulmonary sequestration: value of aortography and pulmonary arteriography. *Cardiovasc Intervent Radiol* **1981**;4:17–23
2. Edelman RR, Wentz KU, Mattle H, et al. Projection arteriography and venography: initial clinical results with MR. *Radiology* **1989**;172:351–357
3. Neumayer K. X-ray diagnosis of lung sequestration: the value of CT. *Fortschr Rontgenstr* **1989**;151:263–267
4. Naidich DP, Rumancik WM, Lefleur RS, Estioko MR, Brown SM. Intralobar pulmonary sequestration: MR evaluation. *J Comput Assist Tomogr* **1987**;11:531–533

Hair as a Mammographic Artifact

A 44-year-old woman had routine screening mammography. The craniocaudal, but not the mediolateral oblique, mammograms showed bilateral, asymmetric, streaky, curvilinear densities (Fig. 1A). The patient had long, extremely curly hair, and it was suspected that her hair was responsible for the mammographic artifacts. Craniocaudal mammograms obtained after the patient's hair was pulled back with a rubber band showed no curvilinear densities (Fig. 1B). Subsequent comparison with films taken at another site showed similar curvilinear densities in a different pattern and distribution on craniocaudal, but not on mediolateral oblique, mammograms.

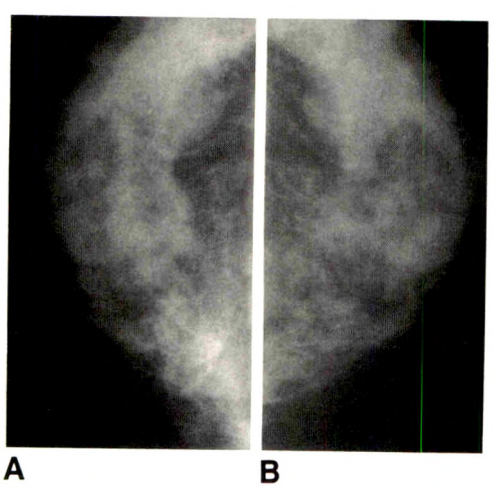


Fig. 1.—*A*, Craniocaudal mammogram shows streaky, curvilinear artifacts caused by hair. Sonograms (*not shown*) indicated that partially visualized masslike density seen here was a cyst.
***B*, Craniocaudal mammogram obtained after hair was moved out of beam shows no artifacts.**

Numerous mammographic artifacts have been reported. They may be particularly troublesome when they mimic findings associated with malignant disease. Reported film-related artifacts include dust or fingerprints on the film and water bubbles in the developer [1]. Dust on the screens also may cause artifacts. Skin-related artifacts can be caused by skin folds, pores, and openings of epidermal glands [1], as well as by powder, medications, and deodorant [2]. Deodorant artifacts are caused by the aluminum salt or powder in the product [3]. On xeroradiographs, sponges containing dirt, powder, or water may cause artifacts [2]. Metallic debris in the X-ray tube head [1] can also cause artifacts simulating calcifications. The appearance of the sternal insertion of the pectoral muscle has been misinterpreted as evidence of carcinoma [4].

Hair artifacts on mammography should be asymmetric, can be unilateral or bilateral, and are more likely to be seen on craniocaudal mammograms than on mediolateral oblique or true lateral mammograms. It is likely that the hair itself rather than the permanent wave used by some patients is the cause of the artifact. Production of this artifact can be avoided by positioning the patient properly; however, in some cases it may be necessary to use a rubber band or hairnet to keep the patient's hair out of the beam. Despite these efforts, occasionally hair-caused artifacts may occur. Experienced mammographers may be aware of this artifact, but it has not been previously reported in the English-language literature, and I wish to bring it to the attention of mammographers who are not yet aware of it.

Burton M. Gold
Winthrop-University Hospital
Mineola, NY 11501

REFERENCES

1. Hoeffken W, Lanyi M. *Mammography: technique, diagnosis, differential diagnosis, results.* Philadelphia: Saunders, **1977**:70, 266
2. Martin JE. *Atlas of mammography: histologic and mammographic correlations.* Baltimore: Williams & Wilkins, **1982**:14
3. Cuomo L. A no sweat artifact. *Radiol Technol* **1988**;59:517–518
4. Britton CA, Baratz AB, Harris KM. Carcinoma mimicked by the sternal insertion of the pectoral muscle. *AJR* **1989**;153:955–956

Low-Cost Screening Mammography

The January 1992 issue of the *AJR* has three consecutive articles [1–3] on low-cost mammography. I think that not one of them actually defines costs. Warren Burhenne et al. [1] report experience in British Columbia, and the abstract includes the words "low cost." The authors have no data on cost, but report that the price paid per examination was U.S.$32.66. Vogel et al. [2] report findings from a screening project of the American Cancer Society in Texas. They also discuss "low-cost mammography," and again cost is not defined or reported. The authors state that the price per examination was $50. Sickles [3] presents a commentary and specifically considers "low-cost mass screening." Again, no data on cost are given.

Appropriate economic ways to evaluate cost are available, and authors should not propose that their articles define costs unless rigid scientific methods have been used to do so. I think my concern not only is important from the scientific standpoint but also may have practical importance. Third-party payers will read these articles and think that mammography can be performed at something less than $50 per examination. I can tell you that in a large department with high volume (>17,000 examinations per year), we cannot break even

economically at a charge of $50 per examination—and our cost is approximately $45 per examination, even with high volume.

Ronald G. Evens
Mallinckrodt Institute of Radiology
Washington University Medical Center
St. Louis, MO 63110

REFERENCES

1. Warren Burhenne LJ, Hislop TG, Burhenne HJ. The British Columbia mammography screening program: evaluation of the first 15 months. *AJR* **1992**;158:45–49
2. Vogel VG, Peters GN, Evans WP, Texas Breast Screening Project Scientific Review Committee. Design and conduct of a low-cost mammography screening project: experience of the American Cancer Society, Texas division. *AJR* **1992**;158:51–54
3. Sickles EA. Low-cost mass screening for breast cancer with mammography (commentary). *AJR* **1992**;158:55–57

In regard to the recent article [1] on the British Columbia mammography screening program, although the concept of low-cost mammography screening certainly has merit, I am not the least bit convinced that this is a truly realistic program as presented. Consider for a moment the concern about breast cancer and think about undergoing a testing procedure knowing that the person who ultimately is responsible for interpreting the results will be paid slightly more than lunch at McDonald's would cost. Persons do get what they pay for, and over a large series of screening examinations, I fear that they might get exactly what they paid for if a program like this were adopted and expanded to a nationwide project.

Charles North
Bakersfield, CA 93302-0119

REFERENCE

1. Warren Burhenne LJ, Hislop TG, Burhenne HJ. The British Columbia mammography screening program: evaluation of the first 15 months. *AJR* **1992**;158:45–49

Replies

We are pleased to respond to the concerns of Drs. Evens and North. Already in 1986, Dr. Evens [1] doubted documentation of low-cost screening mammography [2, 3] in the United States. The low cost of high-volume screening mammography depends, to some extent, on the differences between screening and diagnostic mammography. Diagnostic mammography in a radiology department is time-consuming for the radiologist: he or she must be in the department, ensure that a good history is obtained, be available to consult with the patient, review routine projections and request specialized views, mount the mammograms, and dictate a detailed report. He or she must sign the completed report and contact the referring physician in involved cases. Screening mammography in a free-standing clinic, on the other hand, does not require the presence of a radiologist: He or she comes in the evening to read premounted films with only two views of each breast. No telephone or other interruptions occur while he or she reads the mammograms and pushes one of two buttons on the computer, which generates a paragraph stating either that the mammogram is normal and the patient should return at a specified interval or that the mammograms appear to be abnormal and requesting the patient's physician to proceed to diagnostic mammography. Two technicians have taken, during the daytime, in one room, mammograms at a rate of six to 10 patients per hour, and the patients have filled in a questionnaire. By contrast, diagnostic mammography permits scheduling of no more than three patients per hour in a room with more sophisticated equipment.

Dr. Evens is mistaken when he assumes that U.S.$32.66 was "paid" per examination. We clearly state that this was the "cost" per patient allotted against a government grant, and the breakdown is analyzed in the Results section of our article [4]. The cost includes all expenses (in U.S. dollars) such as salaries and benefits, professional fee, film cost, and equipment maintenance; $4.62 should be added for equipment amortization and $1.08 for office rental. Cost accounting is done in a detailed fashion by the director of finance of the British Columbia Cancer Agency, and annual audits are performed by independent accountants. The unit cost of $32.66 per examination prevailed during the first 15 months of our program. We can now report cost accounting for 3½ years in the same pilot program center with mammography screening of 35,650 patients. The unit cost per woman screened has actually decreased and now amounts to $26.50 per examination. Two additional centers in British Columbia now in operation with more than 10,000 patients screened each year show unit costs of $26.54 for the center in Victoria and $30.24 for the one in Surrey in the Lower Mainland. Again, $4.62 should be added for capital amortization, but office rental is now included in all unit-cost figures. Four additional mammography centers of the provincial screening program opened last year. We should add that the unit cost does not include expenses for promotion, which is done by provincial volunteer organizations such as the Cancer Society. All women who are screened are required to give a physician's name on registration, and the report is sent to this physician, who will then be responsible for follow-up.

We do not understand Dr. Evens's last paragraph in which he states that he cannot break even economically even though he charges $50 for an examination that costs him $45. This runs contrary to his request for defining cost with rigid science. We would also like to put Dr. North at ease, because any one of our 24 radiologist-screeners in seven centers can read and get his professional fees for 100 screening mammograms per hour, the same time that it probably takes Dr. North to have lunch at McDonald's.

L. J. Warren Burhenne
T. G. Hislop
H. J. Burhenne
University of British Columbia
Vancouver, B.C., Canada V5Z 1M9

REFERENCES

1. Evens RG. Mammographic screening: how to operate successfully at low cost (letter). *Radiology* **1986**;161:850
2. Bird RE, McLelland R. How to initiate and operate a low-cost screening mammography center. *Radiology* **1986**;161:43–47
3. Sickles EA, Weber WN, Galvin HB, Ominsky SH, Sollitto RA. Mammographic screening: how to operate successfully at low cost. *Radiology* **1986**;160:95–97
4. Warren Burhenne LJ, Hislop TG, Burhenne HJ. The British Columbia mammography screening program: evaluation of the first 15 months. *AJR* **1992**;15:45–49

Dr. Evens is correct that we did not define cost as an economist would [1]. The low cost refers to fees charged per examination, rather than cost of performing the examination. We also agree that in some instances even with high volume, it is not possible to perform screening mammography and break even economically with a charge of $50. However, others [2, 3] have shown that screening is a financially viable situation provided the examination can be performed in a nonhospital setting.

The 1987 American Cancer Society Texas Breast Screening Project was principally designed as an activity to promote screening mammography. It greatly increased public awareness about breast cancer and the value of early detection. Quality assurance standards

throughout the state were markedly improved, and the project encouraged the development of accreditation standards by the American College of Radiology. Most, if not all, of the 306 participating facilities subsidized the $50 mammogram and, like Dr. Evens, did not break even at that charge. Subsequently, however, we have seen the fees for screening mammography reduced throughout the state. Most high-volume facilities now charge $45 to $75 per examination.

Victor Vogel
The University of Texas, M. D. Anderson Cancer Center
Houston, TX 77030
George Peters
W. Phil Evans
Baylor University Medical Center
Dallas, TX 75246

REFERENCES

1. Vogel VG, Peters GN, Evans WP, Texas Breast Screening Project Scientific Review Committee. Design and conduct of a low-cost mammography screening project: experience of the American Cancer Society, Texas division. *AJR* **1992**;158:51–54
2. Bird RE, McLelland R. How to initiate and operate a low-cost screening mammography center. *Radiology* **1986**;161:43–47
3. Sickles EA, Weber WN, Galvin HB, Ominsky SH, Sollitto RA. Mammographic screening: how to operate successfully at low cost. *Radiology* **1986**;160:95–97

Gastroduodenal Intussusception Due to a Prolapsed Gastric Adenoma

A 63-year-old man with a diagnosis of gastric cancer was referred to our hospital. Intermittent postprandial epigastric discomfort and weight loss had begun 6 weeks before. An upper gastrointestinal barium study performed 1 month before showed a polypoid mass in the antrum of the stomach (Fig. 1A). Endoscopy at admission showed a 7 × 10 cm, ulcerated, polypoid mass arising from the anterior wall of the proximal part of the antrum of the stomach. Biopsy of the mass indicated adenocarcinoma. CT scans obtained 1 month later showed a large mass in the duodenum (Figs. 1B and 1C) and no evidence of a mass in the stomach. Oral contrast medium did not pass beyond the duodenum during CT scanning, even when the patient was in the right lateral decubitus position. An upper gastrointestinal series was not performed at this time.

At laparotomy, a gastroduodenal intussusception caused by a mass in the stomach was found. The intussusception was easily reduced, although the gastric antrum and duodenal bulb were moderately edematous. A subtotal gastrectomy with gastrojejunostomy was performed. The pathologic diagnosis was a sessile type of tubular adenoma of the stomach with early malignant transformation.

Gastric intussusception is usually associated with benign gastric tumors such as leiomyoma, adenoma, and lipoma. CT findings in cases of gastroduodenal intussusception are characteristic. The site of the invagination can be seen as an abnormal targetlike mass in the duodenal region on CT scans. CT also may show foreshortening and beaklike narrowing in the distal stomach. The correct diagnosis can be made on the basis of such findings as an invagination of the greater and lesser omentum. Other CT findings include signs of obstruction of the gastric outlet and multiple concentric layers within a mass.

Hyun K. Ha
Kyung S. Shinn
In C. Kim
Yong W. Bahk
Catholic University Medical College
Seoul 137-701, Korea

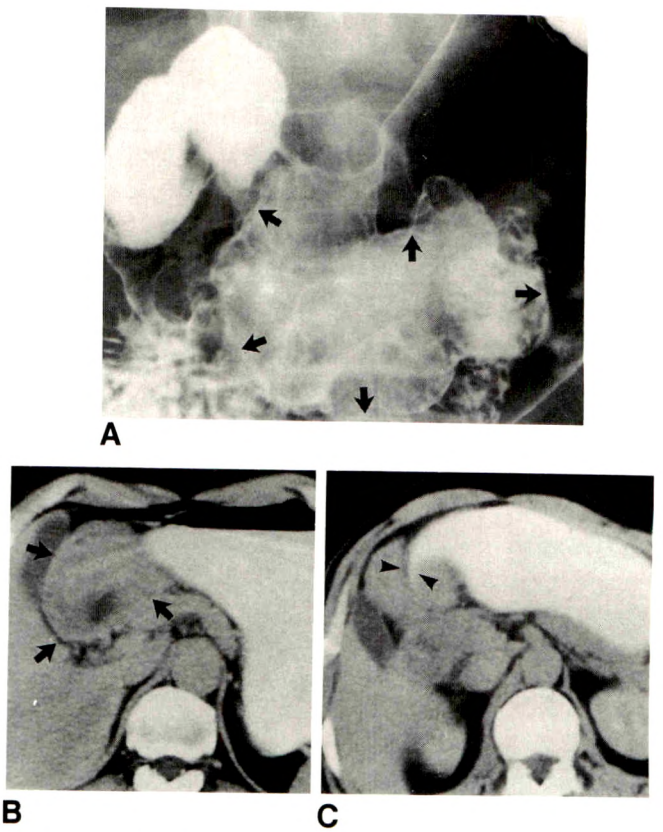


Fig. 1.—Gastroduodenal intussusception due to prolapsed gastric adenoma.

***A*, Radiograph shows large polypoid mass (*arrows*) in antrum of stomach.**

***B* and *C*, CT scans show large soft-tissue mass (*arrows*, *B*) in duodenum and beaklike narrowing in distal stomach (*arrowheads*, *C*). Central low-density area within mass (*B*) represents fluid in duodenal lumen.**

Hepatoma Complicating Byler Disease

Byler disease, a progressive familial intrahepatic cholestasis syndrome, was first described in 1969 [1]. The disease is often diagnosed early in life on the basis of pruritis, hepatomegaly, and elevation of serum levels of bilirubin. Most patients die of hepatic failure in the second decade of life. In older patients with Byler disease, liver biopsies often show progression to biliary cirrhosis [1–4]. We describe a case of Byler disease in a 29-year-old man in whom a hepatocellular carcinoma developed. The patient was being considered for orthotopic liver transplantation for treatment of Byler disease.

At the time of the evaluation for liver transplantation, the patient had had vague pain in the right upper quadrant for several months. Laboratory tests indicated that the patient had lipid-soluble hypovitaminosis, elevated levels of serum alkaline phosphatase, and markedly elevated levels of serum α-fetoprotein. Contrast-enhanced abdominal CT and MR imaging showed a low-attenuation region in the liver that was not present on a previous CT scan (Fig. 1). A sonographically guided percutaneous needle biopsy of the lesion was performed. Pathologic examination showed hepatoma with underlying micronodular biliary cirrhosis. The patient received an orthotopic liver transplant and had no evidence of recurrent or metastatic disease after 1 year.

In 1969, Clayton et al. [1] described a progressive familial intrahepatic cholestasis syndrome in several descendants of an Amish immigrant named Byler, all of whom had elevated serum levels of bile acids. Byler disease is the second most common form of familial

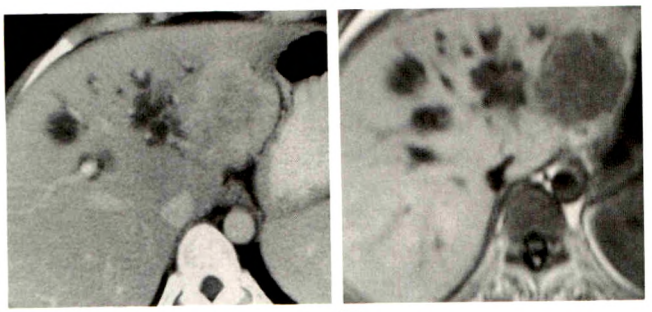


Fig. 1.—Hepatocellular carcinoma in a 29-year-old man with Byler disease.

***A*, CT scan with contrast material shows a peripherally enhancing mass 4 cm in diameter in left lobe of liver that proved to be hepatocellular carcinoma. Note also dilation of intrahepatic biliary ducts, consistent with Byler disease.**

***B*, Corresponding T1-weighted MR image shows area of low signal in lateral segment of left lobe of liver.**

intrahepatic cholestasis that becomes apparent in infancy; the first is Alagille's syndrome. Inheritance of the disorder is presumed to be autosomal recessive [4]. Patients characteristically have jaundice, pruritis, or hepatomegaly in the first year after birth. Laboratory tests show elevated serum levels of bile acids, high serum levels of alkaline phosphatase, and intermittent elevation of serum levels of bilirubin [4]. Pathologic findings initially may be normal or show a giant-cell hepatitis. Later in the course of the disease, micronodular biliary cirrhosis and portal hypertension may occur. Death because of hepatic failure in the second decade of life is the norm. Recently, orthotopic liver transplantation has been used to treat Byler disease.

The neoplastic potential of familial intrahepatic cholestasis is not generally known. Two previous reports [3, 4] of malignant tumor in this disease have been described. Patients with Byler disease likely have an increased risk of hepatocellular carcinoma developing if biliary cirrhosis develops before they die of hepatic failure. Patients with biliary atresia, tyrosinosis, and α-1-antitrypsin deficiency have a similar risk. Frequent radiologic and laboratory examinations may make early diagnosis of complicating hepatoma possible and accelerate therapeutic intervention (transplantation) of this relatively rare complication of Byler disease.

Shawn P. Quillin
James A. Brink
Mallinckrodt Institute of Radiology
Washington University Medical Center
St. Louis, MO 63110

REFERENCES

1. Clayton RJ, Iber FL, Ruebner BH, et al. Byler disease: fatal familial cholestasis in an Amish kindred. *Am J Dis Child* **1969**;117:112–124
2. Dahms BB. Hepatoma in familial cholestatic cirrhosis of childhood. *Arch Pathol Lab Med* **1979**;103:30–33
3. Ugarte N, Gonzales-Crussi F. Hepatoma in siblings with progressive familial cholestatic cirrhosis of childhood. *Am J Clin Pathol* **1981**;76:172–177
4. Riely CA. Familial intrahepatic cholestatic syndromes. *Semin Liver Dis* **1987**;7:119–133

Ligamentous Compression of the Celiac Axis

In their article, "Ligamentous Compression of the Celiac Axis: CT Findings in Five Patients" [1], which appeared in the May 1991 issue of the *AJR*, Patten et al. state that the median arcuate ligament usually passes posterior and inferior to the origin of the celiac axis. This seems to me to be anatomically impossible, unless the celiac axis is an intrathoracic structure, which it is not. The median arcuate ligament of necessity is anterior to the aorta and therefore superior to the origin of the celiac axis.

W. K. Andrew
Eugene Marais Hospitaal
Pretoria 0002, Republic of South Africa

REFERENCE

1. Patten RM, Coldwell DM, Ben-Menachem Y. Ligamentous compression of the celiac axis: CT findings in five patients. *AJR* **1991**;156:1101–1103

Reply

The median arcuate ligament originates as a condensation of the medial fibrous borders of the two crura of the hemidiaphragm as they decussate to form the ventral border of the aortic hiatus. The ligament is a variable structure. In most autopsy specimens, it can be seen as a well-defined round, fibrous cord 1–3 mm wide; however, in others, only an amorphous area of connective tissue can be detected.

Similarly, the relationship of the origin of the celiac axis to the median arcuate ligament of the diaphragm is an extremely variable one, because of multiple factors, including the height and angle of origin of the celiac axis; the height of the ligament; and the body habitus, sex, and age of the subject.

We appreciate Dr. Andrew's confusion about the relationship of the median arcuate ligament to the celiac axis as described in our paper [1]. We refer Dr. Andrew to an excellent 1971 clinicoanatomic analysis of this spatial relationship between the arcuate ligament of the diaphragm and the celiac artery in 75 fresh autopsy specimens [2]. In most cases, the median arcuate ligament resembles an inverted U, passing superior to the origin of the celiac axis in its midportion but extending posterior and inferior to the origin of the celiac axis more laterally. Yet in 36 (48%) of dissections, Lindner and Kemprud [2] found that the ligament sagged inferiorly in its midportion, passing anterior and inferior to at least part of the origin of the celiac artery, and thereby creating the potential for ligamentous compression of the artery against the aorta. Although the clinical syndrome of intestinal ischemia (median arcuate ligament syndrome) related to this entity is controversial, the anatomic relationship discussed here is well documented [3, 4].

R. M. Patten
D. M. Coldwell
Y. Ben-Menachem
University of Washington School of Medicine
Seattle, WA 98195

REFERENCES

1. Patten RM, Coldwell D, Ben-Menachem Y. Ligamentous compression of the celiac axis: CT findings in 5 patients. *AJR* **1991**;156:1101–1103
2. Lindner HH, Kemprud E. A clinicoanatomic study of the arcuate ligament of the diaphragm. *Arch Surg* **1971**;103:600–605
3. Dunbar JD, Molnar W, Beman FF, Marable SA. Compression of the celiac trunk and abdominal angina. *AJR* **1965**;95:731–743
4. Reuter S. Accentuation of celiac compression by the median arcuate ligament of the diaphragm during deep expiration. *Radiology* **1971**;98:561–564

Bilateral Posttraumatic Adrenal Hemorrhage Detected with CT

A 26-year-old man was admitted to our hospital after being in a motor vehicle accident. Abdominal examination showed distension, rigidity, and tenderness. The patient rapidly became hemodynamically unstable. Exploratory laparotomy showed hemoperitoneum and a bleeding splenic laceration, and splenectomy was performed. Abdominal CT scans obtained 24 hr after laparotomy showed a small amount of free intraabdominal fluid, hematoma of the splenic bed, and soft-tissue contusion of the left flank. Both adrenal glands were enlarged and had an unusually high density (Fig. 1). These findings were consistent with bilateral adrenal hemorrhage. The clinical course was not favorable, and 24 hr later the patient died of cardiac arrest.

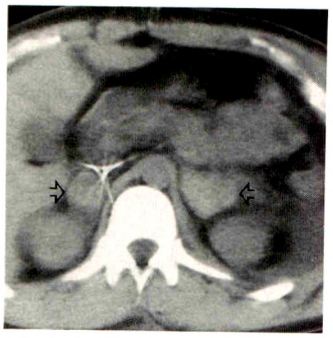


Fig. 1.—Abdominal CT scan shows enlarged, high-density adrenal glands (*arrows*), infiltration of perirenal fat, and hematoma of splenic bed.

Adrenal hemorrhage in adults is uncommon and is usually associated with trauma, septicemia, or anticoagulant therapy [1–3]. The CT findings of this condition have been well described [2, 4]: an adrenal mass with homogeneous hyperdensity and streaky infiltration of the periadrenal fatty tissue. In most cases, the lesions are unilateral, on the right side; approximately 20% of posttraumatic adrenal hemorrhages are bilateral [4]. A susceptibility to massive intraglandular bleeding is probably related to the complex vascular supply of the adrenal glands [1]. They have a rich vascular supply coming from branches of the inferior phrenic artery, the aorta, and the renal artery. Each adrenal gland is drained by a single central vein that emerges from the hilum as a single adrenal vein. Therefore, any acute increase in adrenal venous pressure would result in hemorrhage into the gland.

Traumatic adrenal hemorrhage has three possible mechanisms: direct trauma that compresses the gland against the spine, acute increase in intraadrenal pressure due to compression of the inferior vena cava, and shearing of small vessels as a result of deceleration forces [3, 4]. In our case, hemorrhage as a result of compression of the inferior vena cava seems to be the most likely explanation for hemorrhage in the right adrenal gland, because blunt trauma occurred to the left side only.

Detection of bilateral adrenal hemorrhage in a patient with severe trauma has important clinical implications. This is a life-threatening condition amenable to treatment with corticosteroid therapy, and the clinical manifestations are often serendipitous in the early stages. The adrenal glands must be thoroughly evaluated during CT examination of patients with blunt abdominal trauma, because adrenal hemorrhage is often overshadowed by more spectacular findings elsewhere.

Carlos Valls
Eduard Andia
Isabel Gil
Hospital de Bellvitge
Barcelona, Spain
Isabel Conde
University of Barcelona
Barcelona, Spain

REFERENCES

1. Rao RH, Vagnucci AH, Amico JA. Bilateral massive adrenal hemorrhage: early recognition and treatment. *Ann Intern Med* **1989**;110:227–235
2. Wolverson MK, Kannegiesser H. CT of bilateral adrenal hemorrhage with acute adrenal insufficiency in the adult. *AJR* **1984**;142:311–314
3. Murphy BJ, Casillas J, Yrizarry JM. Traumatic adrenal hemorrhage: radiologic findings. *Radiology* **1988**;169:701–703
4. Wilms G, Marchal G, Baert A, et al. CT and ultrasound features of posttraumatic adrenal hemorrhage. *J Comput Assist Tomogr* **1987**;11:112–115

Meniscal Tears in Marathon Runners

Shellock et al. present an interesting article [1] that gives encouragement to those of us who would call ourselves "runners." The conclusion states, "Our results indicate that the prevalence of meniscal tears in marathon runners is no higher than the prevalence reported for sedentary persons, and the runners have the same amount of meniscal degeneration as do nonrunner athletes." The study was constructed such that the only subjects were asymptomatic marathon runners who volunteered to participate. Therefore, the conclusions can relate to asymptomatic marathon runners only and cannot be extended to include marathon runners in general. It is possible, and in fact likely, that of all marathon runners, the asymptomatic runners make up only a small subset. In order to make a broad, more generalized statement from the data, all marathon runners, symptomatic or asymptomatic, would need to be included in the selection set, even those who have stopped running because of injury. I suggest that the MR meniscal findings in symptomatic runners and injured runners would be quite different when compared with those in asymptomatic runners.

Michael M. Tersegno
Auburn Memorial Hospital
Auburn, NY 13021

REFERENCE

1. Shellock FG, Deutsch AL, Mink JH, Kerr R. Do asymptomatic marathon runners have an increased prevalence of meniscal abnormalities? An MR study of the knee in 23 volunteers. *AJR* **1991**;157:1239–1241

Reply

I agree with Dr. Tersegno that the results of the study [1] specifically pertain to the knees of asymtomatic marathon runners and that further study of symptomatic runners would be necessary in order to make a statement about marathon runners in general. My colleagues and I were particularly explicit with our inclusion criteria for this study so that we could compare our results with those of previous studies that reported MR findings in the knees of asymptomatic populations of athletes and more sedentary persons. We think that our data were of interest because our subjects represent a group who would likely have a higher prevalence of meniscal signal abnormalities on MR images because of their age (average, 40 years) and intense training (average time in training, 10 years; average distance per week training, 41 miles); yet, they did not.

Frank G. Shellock
Tower Musculoskeletal Imaging Center
University of California, Los Angeles, School of Medicine
Los Angeles, CA 90048

REFERENCE

1. Shellock FG, Deutsch AL, Mink JH, Kerr R. Do asymptomatic marathon runners have an increased prevalence of meniscal abnormalities? An MR study of the knee in 23 volunteers. *AJR* **1991**;157:1239–1241

Transfemoral Venous Catheterization Through Inferior Vena Caval Filters

In their recent article [1], Hansen et al. describe their experience with diagnostic and therapeutic procedures in seven patients in which instruments were passed through existing inferior vena caval filters from a femoral vein approach. They advocate the safety and feasibility of this technique, while suggesting that it is a practicable option for radiologists who "may not find the transjugular route a desirable alternative." Notwithstanding their favorable results in these seven patients, we propose that this is a small series on which to base such conclusions. In addition, in our opinion, the probable risk of injuring the inferior vena cava, dislodging thrombus, and damaging or dislodging an inferior vena caval filter during a transfemoral-transfilter

catheterization is greater than the probable risk of performing these same procedures via a jugular vein puncture without traversing an implanted filter.

Percutaneous access to the internal jugular vein should be a standard procedure for interventional radiologists. Landmarks for the vein are easily detected by using inspection and palpation. One approach is to make the puncture posterior to the sternocleidomastoid muscle, just cranial to where the external jugular vein crosses, about midway between the mastoid tip and the clavicle. The needle is then directed toward the sternal notch while the carotid artery is deflected medially. A favored method in our division is a more anterior approach: The needle is advanced with one hand from the apex of the division of the sternocleidomastoid muscle along the medial aspect of the lateral belly of the muscle while the carotid artery is palpated and retracted with the opposite hand. To minimize the risk of injury to adjacent structures in the neck and chest, especially the carotid artery and the apical pleura, we first use a 21-gauge needle (Cook Inc., Bloomington, IN) and a single-wall technique. After venous blood is aspirated, a 0.018 in. (0.46-mm) Cope mandril wire (Cook Inc.) is inserted via the needle and steered into the superior vena cava, across the eustachian valve, and into the inferior vena cava. At this point, the mandril wire is exchanged for a 0.035- or 0.038-in. (0.89- or 0.97-mm) guidewire through a 4-French Desilets-Hoffman introducer (Cook Inc.). Access to the external jugular vein can be obtained with the same equipment and often is easier because most external jugular veins are superficial, visible, and distensible by finger occlusion. The steerability of the 0.018-in. mandril wire is particularly helpful in negotiating the turn from the external jugular vein into the superior vena cava. This approach has been used for placement of titanium Greenfield filters, and it would be expected that the smaller and more flexible Simon nitinol filter, which has been inserted via the internal jugular vein, would also make this turn [2, 3].

From July to November 1991, we performed 25 procedures via the right internal jugular vein. These included placement of 12 vena caval filters (11 titanium Greenfield and one Bird's Nest), placement of six transjugular intrahepatic portosystemic shunts, six transjugular liver biopsies, and placement of one hemodialysis catheter. Ten of the 12 filters were placed by the transjugular route because of iliofemoral or inferior vena caval thrombus, one because of recent bilateral groin surgeries, and one because of recurrent pulmonary emboli presumably from thrombus found partially encasing a Bird's Nest filter. In addition, hepatic venous (free and wedged) contrast studies and manometry were easily performed in conjunction with placement of portosystemic shunts and in conjunction with most of the liver biopsies; access to the hepatic venous system is a particularly direct approach and is much easier than turning sharply into the the hepatic veins from the inferior vena cava.

All 25 procedures were technically successful and without complications; in most cases, jugular access was obtained with the first puncture. In past years, we also have found the transjugular route helpful in performing pulmonary arteriograms in patients who already have jugular venous access (a pigtail catheter from Cook, Inc. with an additional U-shaped secondary curve is used), saving them a separate femoral puncture, and in placing Swan-Ganz catheters (Baxter Health Care Corp., Irvine, CA), which are designed ideally to access the heart from the superior vena cava, although it is possible to insert them with greater difficulty via the inferior vena cava. An additional advantage of jugular vein access is the ease of hemostasis. After the removal of even large filter sheaths, a mild elevation of the patient's upper body and head significantly reduces venous pressure and risk of hematoma.

We acknowledge the limited experience of Hansen et al., which shows that it may be feasible to work through existing inferior vena caval filters. However, we are concerned that use of this technique would be advocated as being as safe as or safer than use of a transjugular approach. Although Figure 3 in the article [1] shows how a 7.1-French catheter could fit between filter elements, it does not show the larger 12-French (outer diameter) filter sheath they passed through implanted filters to place additional Vena-Tech filters in two patients. In addition, although a catheter may fit through a filter and be used to perform pulmonary arteriography, venous sampling, hepatic vein manometry, and right-sided heart catheterization as Hansen et al. advocate, the extensive manipulation of the catheter that frequently is required during these procedures causes us even greater concern. Working through a long sheath may help reduce this risk, but it would also add to the diameter of the system needed to pass through the filter. Finally, Hansen et al. do not discuss the implications of puncturing femoral veins that may have been damaged or become thrombosed during the initial filter placement and the effect repeat puncture might have on the development or worsening of chronic venous stasis disorders that occur in a small percentage of patients with vena caval filters, even the new smaller filter systems [4, 5]. Thrombosis of the jugular vein, on the other hand, is almost never chronically symptomatic [6].

In summary, we think the technique advocated by Hansen et al. should be used in only the most limited circumstances, when no other approach is available. We encourage using jugular vein access for these procedures in order to avoid manipulation through or near a filter and associated caval thrombus. We agree with the authors that clinical judgment should be exercised in each case and that further experience should be obtained. However, in our judgment, transjugular venous catheterization in these patients is technically easier and clinically safer, especially when a small needle is used, than the transfemoral-transfilter approach. We think that interventional radiologists should make the transjugular route a standard technique in their practice.

David J. Eschelman
David M. Hovsepian
Joseph Bonn
Thomas Jefferson University Hospital
Philadelphia, PA 19107

REFERENCES

1. Hansen ME, Geller SC, Yucel EK, Egglin TK, Waltman AC, Transfemoral venous catheterization through inferior vena caval filters: results in seven cases. *AJR* **1991**;157:967–970
2. McCowan TC, Ferris EJ, Carver DK, Harshfield DL. Use of the external jugular vein as a route for percutaneous inferior vena caval filter placement. *Radiology* **1990**;176:527–530
3. Simon M, Athanasoulis CA, Kim D, et al. Simon nitinol inferior vena cava filter: initial clinical experience. *Radiology* **1989**;172:99–103
4. Hicks ME, Middleton WD, Picus D, Darch MD, Kleinhoffer MA. Prevalence of local venous thrombosis after transfemoral placement of a Bird's Nest vena caval filter. *J Vasc Intervent Radiol* **1990**;1:63–68
5. Ricco JB, Crochet D, Sebilotte P, et al. Percutaneous transvenous caval interruption with the LGM filter: early results of a multicenter trial. *Ann Vasc Surg* **1988**;3:242–247
6. Greenfield LJ, Michna BA. Twelve-year clinical experience with the Greenfield vena caval filter. *Surgery* **1988**;104:706–712

Periocular Pseudocyst Caused by a Displaced Contact Lens: CT Appearance

A 21-year-old man was struck in the left eye with a croquet mallet when he was wearing rigid gas-permeable contact lenses composed of pasifocon A and B. The patient subsequently noted that the left contact lens was missing and assumed it had been knocked to the ground. Three years later, he became aware of discomfort about the left eye. Palpation showed a firm, slightly mobile mass deep within the left upper lid. Inspection of the area under the lid did not reveal a contact lens.

Coronal orbital CT showed a cystic-appearing mass contiguous with and superior to the left globe (Fig. 1). With the patient under general anesthesia and with an eyelid traction suture, the upper lid could be pulled away from the globe with more force than was possible during the initial examination. This maneuver revealed a contact lens embedded within the inner surface of the upper eyelid,

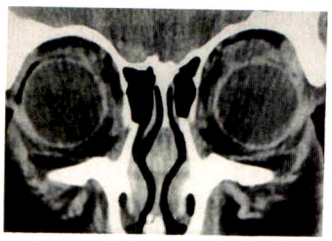


Fig. 1.—Coronal CT scan of orbit shows pseudocyst superior to left globe is bounded by contact lens and posterior surface of eyelid and contains fluid.

near the superior conjunctival fornix, with the convex surface facing the globe. A pair of forceps was used to remove the contact lens.

Contact lenses occasionally may be displaced into the superior conjunctival fornix, either spontaneously or as a result of trauma. The contact lens may become embedded in the upper lid, as in this case, or may migrate into adjacent eyelid or orbital tissues [1, 2]. Although physical examination will sometimes detect a displaced contact lens, this may not always be possible because of the patient's discomfort, lid inflammation, or, in younger patients, relatively tight tissues. A displaced contact lens should be considered in the differential diagnosis of superior periocular cystic-appearing lesions shown by CT.

Herbert J. Glatt
University of Tennessee Medical Center at Knoxville
Knoxville, TN 37920

REFERENCES

1. Hornblass A, Kass L. Contact lenses in the upper eyelid masquerading as lid masses. *Ophthalmic Surg* **1987**;18:438–440
2. Nicolitz E, Flanagan J. Orbital mass as a complication of contact lens wear. *Arch Ophthalmol* **1978**;96:2238–2339

CT of Schizencephaly

A 9-year-old boy had psychomotor retardation and seizures and failure to thrive. CT scans showed moderate dilatation of the lateral ventricles and absence of the septum pellucidum. An apparent umbilication was seen at the border of the left lateral ventricle, and a barely visible one was present on the right side (Fig. 1A). In both hemispheres, abnormal (heterotopic) gray matter extending from the ventricular wall to the periphery was clearly detectable. A cleft was visible on the left side within the heterotopic gray matter, and a localized defect was present near the right ventricular edge, surrounded by heterotopic gray matter (Fig. 1B).

Schizencephaly is one of the migrational disorders of the brain, which include lissencephaly, pachygyria, heterotopia, and polymicrogyria. It is characterized by clefts extending across the hemispheres; the clefts are lined with pial-ependymal tissue and bounded, either totally or in part, by heterotopic gray matter. The cleft may be open (open schizencephaly) or closed (fused-lip schizencephaly). The clefts are commonly seen in the parietal and temporal regions. They are usually bilateral and may be symmetric. Unilateral clefts can also occur and should be distinguished from acquired clefts that can occur after a nonpenetrating contusive injury to the brain. The presence of

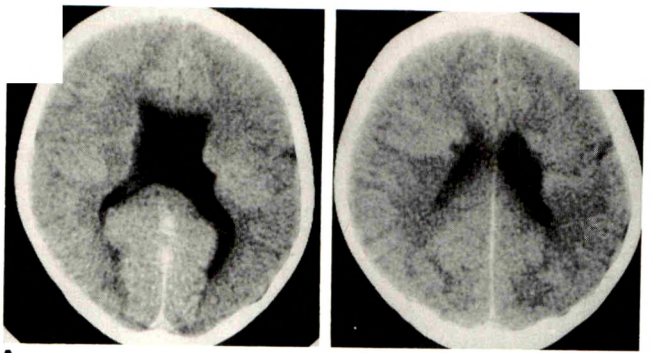


Fig. 1.—Schizencephaly in a 9-year-old boy.
***A*, CT scan shows moderate dilatation of lateral ventricles and absence of septum pellucidum. Note also apparent umbilication at left ventricular border; small CSF-filled cavity adjacent to left parietal bone, representing the peripheral end of a cleft (see *B*); and barely visible umbilication at right ventricular border.**
***B*, CT scan at level higher than *A* shows a cleft on left; surrounding heterotopic gray matter is clearly identifiable. On right, a small cavity connects with ventricle and no cleft is visible; a large amount of heterotopic gray matter surrounds this cavity and extends to cortex.**

heterotopic gray matter around a cleft is considered pathognomonic for schizencephaly, distinguishing it from an acquired condition. This finding can be shown by CT but is best delineated by MR [1–3].

In the present case, the cleft on the left side, which is lined with heterotopic gray matter, is typical for an open schizencephalic defect. On the right side, however, only a small CSF-filled cavity is present surrounded by heterotopic gray matter without an apparent cleft; this represents a closed schizencephalic defect. Therefore, this case represents a simultaneous manifestation of the two forms of schizencephaly. In addition, we think that the apparent umbilication, particularly at the left ventricular border, may be a secondary CT finding signifying the presence of schizencephaly, in the event that a cleft is not visible.

R. Nuri Sener
Güner Bilgin
Ahmet Memis
and colleagues
Hospital of Ege University
Bornova, Izmir, 35100, Turkey

REFERENCES

1. Byrd SE, Osborn RE, Bohan TP, Naidich TP. The CT and MR evaluation of migrational disorders of the brain. Part II. Schizencephaly, heterotopia and polymicrogyria. *Pediatr Radiol* **1989**;19:219–222
2. Zimmermann RA, Bilaniuk LT, Grossman RS. Computed tomography in migratory disorders of human brain development. *Neuroradiology* **1983**;25:257–263
3. Silverman FN. *Caffey's pediatric X-ray diagnosis: an integrated imaging approach*, 8th ed., vol. 1. Chicago: Year Book Medical, **1985**:206

Letters are published at the discretion of the Editor and are subject to editing.

Letters to the Editor must not be more than two *double-spaced*, typewritten pages. One or two figures may be included. Abbreviations should not be used. Limit the number of authors to four, or we will list only the first three and add "and colleagues" to the end of the list. See Author Guidelines.

Material being submitted or published elsewhere should not be duplicated in letters, and authors of letters must disclose financial associations or other possible conflicts of interest.

Letters concerning a paper published in the *AJR* will be sent to the authors of the paper for a reply to be published in the same issue. Opinions expressed in the Letters to the Editor do not necessarily reflect the opinions of the Editor.

Review of Current Literature

Initials and addresses of corresponding authors are provided in parentheses for each article so that the reader can obtain reprints directly. Abstracts are printed verbatim from each journal.

The New England Journal of Medicine

Safety and cost effectiveness of high-osmolality as compared with low-osmolality contrast material in patients undergoing cardiac angiography. Steinberg EP, Moore RD, Powe NR, et al. (EPS, The Johns Hopkins University, 1830 E. Monument St., Rm. 8068, Baltimore, MD 21205). *N Engl J Med* 326(7):425–430, Feb. 1992

Background and Methods. Low-osmolality contrast agents produce fewer hemodynamic and electrophysiologic alterations during cardiac angiography, but they are 20 times more expensive than high-osmolality contrast agents. In a randomized, double-blind trial comparing a nonionic, low-osmolality contrast agent (Omnipaque 350) with a high-osmolality agent that does not avidly bind calcium (Hypaque 76) in 505 patients undergoing cardiac angiography, we determined the incidence of minor, mild, moderate, and severe adverse reactions, identified risk factors for such reactions, and evaluated the cost effectiveness of various strategies for the use of contrast material.

Results. The 253 patients who received a high-osmolality contrast agent were three times more likely to have a moderate adverse reaction (95 percent confidence interval for the relative risk, 1.6 to 5.5) but no more likely to have a severe reaction (95 percent confidence interval, 0.2 to 2.3) than the 252 patients who received a low-osmolality agent. All 10 severe reactions occurred in patients who were older than 60 years or had unstable angina.

Patients with these characteristics were also 3.5 times more likely (95 percent confidence interval, 1.8 to 6.8) to have a moderate reaction (44 of 310 patients, or 14 percent) than those without either characteristic (8 of 195 patients, or 4 percent). We estimated that the incremental cost of each moderate reaction avoided would be $1,698 with a strategy that involved giving a low-osmolality contrast agent only to patients who were over 60 years of age or had unstable angina, instead of giving a high-osmolality agent to all patients. The incremental cost per moderate reaction avoided by giving a low-osmolality contrast agent to all patients rather than only to those over 60 or with unstable angina would be $5,842.

Conclusions. The use of contrast agents with low rather than high osmolality during cardiac angiography reduces the risk of moderate, but not of severe, adverse reactions to the agent used. A strategy of reserving low-osmolality contrast agents for use in patients at high risk for adverse reactions would be more cost effective than one requiring their use in all patients.

Cancer in the contralateral breast after radiotherapy for breast cancer. Boice, JD Jr, Harvey EB, Blettner M, Stovall M, Flannery JT (JDB, Radiation Epidemiology Branch, National Cancer Institute, Executive Plaza N., Rm. 408, 6130 Executive Blvd., Rockville, MD 20852). *N Engl J Med* 326(12):781–795, March 1992

Background. Patients with breast cancer have a threefold increase in the risk that a second breast cancer will develop. Radiation treatment for the initial cancer can result in moderately high doses to the contralateral breast, possibly contributing to this heightened risk.

Methods. We conducted a case–control study in a cohort of 41,109 women diagnosed with breast cancer between 1935 and 1982 in Connecticut. We reviewed the medical records of 655 women in whom a second breast cancer developed five or more years after the initial tumor and compared their radiation exposure with that of 1189 matched controls from the cohort who did not have a second cancer. The dose of radiation to the contralateral breast was estimated from the original radiotherapy records. Among the exposed women, the average radiation dose to the contralateral breast was 2.82 Gy (maximum, 7.10).

Results. Overall, 23 percent of the women who had a second breast cancer and 20 percent of the controls had received radiotherapy (relative risk of a second breast cancer associated with radiotherapy, 1.19). Among women who survived for at least 10 years, radiation treatment was associated with a small but marginally significant elevation in the risk of a second breast cancer (relative risk, 1.33); the risk increased significantly with the dose of radiation. An increase in risk in association with radiotherapy was evident only among women who were under 45 years of age when they were treated (relative risk, 1.59) and not among older women (relative risk, 1.01).

Conclusions. Radiotherapy for breast cancer contributes little to the already high risk of a second cancer in the opposite breast. Fewer than 3 percent of all second breast cancers in this study could be attributed to previous radiation treatment; the risk, however, was significantly increased among women who underwent irradiation at a relatively young age (<45 years). Radiation exposure after the age of 45 entails little, if any, risk of radiation-induced breast cancer.

A comparison of nonionic, low-osmolality radiocontrast agents with ionic, high-osmolality agents during cardiac catheterization. Barrett BJ, Parfrey PS, Vavasour HM, O'Dea F, Kent G, Stone F (PSP, Division of Nephrology, The Health Sciences Centre, St. John's, Newfoundland, Canada A1B 3V6). *N Engl J Med* 326(7):431–436, Feb. 1992

Background. Nonionic low-osmolality radiocontrast agents are used frequently because they are believed to be safer than ionic, high-osmolality agents, but they are also more expensive. We conducted a randomized trial to compare the incidence of adverse events after the administration of ionic, high-osmolality and of nonionic, low-osmolality radiocontrast agents during cardiac angiography.

Methods. We compared the need to treat patients for adverse reactions and the frequency and severity of specific hemodynamic, systemic, and symptomatic side effects in two groups of patients

randomly assigned to receive either ionic, high-osmolality or nonionic, low-osmolality radiocontrast material, and also in 366 patients who could not be randomized.

Results. Treatment for adverse events was required in 213 of 737 patients who received high-osmolality contrast agents (29 percent) but in only 69 of 753 patients who received nonionic agents (9 percent) (95 percent confidence interval for the percent difference, 15.9 to 23.6 percent). Hemodynamic deterioration and symptoms also occurred more often in the high-osmolality group, as did severe or prolonged reactions (2.9 percent, as compared with 0.8 percent in the nonionic group; $P = 0.035$). The severe reactions were largely confined to patients with severe cardiac disease. Multivariate analysis showed that the presence of severe coronary disease and unstable angina were predictors of clinically important adverse reactions. If all the patients in our randomized trial had been given nonionic contrast material, the incremental cost per procedure would have been $89.

Conclusions. Nonionic, low-osmolality contrast material is better tolerated during cardiac angiography than ionic, high-osmolality contrast material. Since cost constraints may prevent the universal use of nonionic contrast material, its selective use in patients with severe cardiac disease could be considered.

Comparison of medical and surgical therapy for complicated gastroesophageal reflux disease in veterans. Spechler SJ, The Dept. of Veterans Affairs Gastroesophageal Reflux Disease Study Group (SJS, Treatment and Research Center for Swallowing and Motility Disorders, Beth Israel Hospital, 330 Brookline Ave., Boston, MA 02215). *N Engl J Med* 326(12):786–792, March 1992

Background. Conventional medical treatment for gastroesophageal reflux disease involves lifestyle modifications and combination drug therapy, but few studies have included these features in their protocols. Antireflux surgery has seldom been studied prospectively, and there have been no trials comparing modern medical and surgical treatments for reflux disease.

Methods. We conducted a long-term, randomized trial of medical therapy (lifestyle modifications and up to four medications) and surgical therapy (Nissen fundoplication) in 247 patients (243 men and 4 women) with peptic esophageal ulcer, stricture, erosive esophagitis, or Barrett's esophagus. They received by random assignment either continuous medical therapy, medical therapy for symptoms only, or surgical therapy. Symptoms were assessed quarterly with a disease-activity index; esophagoscopy was performed at base line and each year for two years. The outcomes evaluated at one and two years included the activity index and the endoscopic grade of esophagitis.

Results. Follow-up data were available for 176 patients at one year and for 106 patients at two years. The mean (±SE) activity-index score (possible range, 74 to 172) decreased in one year from 108 ± 3 to 87 ± 2 in the group receiving continuous medical therapy, from 107 ± 3 to 88 ± 2 in the group receiving medical therapy for symptoms only, and from 109 ± 3 to 78 ± 2 in the surgical-therapy group ($P < 0.0001$ for the change from base line, for all comparisons). The mean (±SE) grade of esophagitis (possible range, 1 to 4) decreased in the respective groups from 2.9 ± 0.1 to 2.0 ± 0.1, from 2.9 ± 0.1 to 2.3 ± 0.1, and from 2.9 ± 0.1 to 1.4 ± 0.1 ($P < 0.005$ vs. base line, for all comparisons). The mean activity-index score and the grade of esophagitis were significantly better in the surgical-therapy group than in either medical-therapy group during the two years of follow-up ($P < 0.003$).

Conclusions. In men with complicated gastroesophageal reflux disease, surgery is significantly more effective than medical therapy in improving the symptoms and endoscopic signs of esophagitis for up to two years, although medical treatment is also effective.

Cancer

The relationship of prostate-specific antigen to digital rectal examination and transrectal ultrasonography: findings of the American Cancer Society National Prostate Cancer Detection Project. Babaian RJ, Mettlin C, Kane R, et al. (CM, Roswell Park Memorial Institute, 666 Elm St., Buffalo, NY 14263). *Cancer* 69:1195–1200, 1992

The participating institutions of the American Cancer Society National Prostate Cancer Detection Project did 520 biopsies on 2425 men over a 3.5-year period. A total of 88 cancers were confirmed pathologically, 93% of which clinically were organ confined. In 324 men (62.3%), a recommendation for biopsy was made based solely on the results of transrectal ultrasonography (TRUS); in 69 patients (13.3%), solely on the digital rectal examination (DRE); in 116 patients (22.3%), on abnormal DRE and TRUS examinations; and in 11 patients (2.1%), in whom DRE and TRUS were normal, on elevated prostate-specific antigen (PSA) levels. The TRUS was abnormal in 80.6% of men found to have cancer, and the PSA level and DRE were abnormal for 67% and 50% of cancers, respectively. The influence of PSA level on cancer detection increased as the serum level increased above 4 ng/ml. The positive predictive values of both the DRE and TRUS were influenced significantly by the presence of an elevated PSA level ($P = 0.044$ and $P < 0.001$, respectively). The results of this ongoing multicenter study support the following statements: (1) the prostate cancer detection rate is influenced by this diagnostic triad and (2) the detection rate of organ-confined disease can be improved substantially by early detection programs.

Reprinted by permission from the American Cancer Society.

Prostate-specific antigen levels in 1695 men without evidence of prostate cancer: findings of the American Cancer Society National Prostate Cancer Detection Project. Kane RA, Littrup PJ, Babaian R, et al. (CM, Roswell Park Memorial Institute, 666 Elm St., Buffalo, NY 14263). *Cancer* 69:1201–1207, 1992

The American Cancer Society National Prostate Cancer Detection Project is a prospective, multidisciplinary, and multicenter trial to assess the potential for early detection of prostate cancer by transrectal ultrasonography (TRUS), digital rectal examination (DRE), and serum prostate-specific antigen assay (PSA). By November 1990, 2805 men between the ages of 55 and 70 years with no known signs or symptoms of prostate cancer were enrolled in the study, which is planned to run for 5 years. Annual TRUS, DRE, and PSA tests were done on these subjects, and biopsies were recommended for suspicious lesions when detected. To study the performance of PSA testing in presumed normal subjects, all men were eliminated who had (1) prostate cancer detected on their initial examinations and proven by biopsy or (2) cancer detected during the year or subsequent examinations. Additionally, all men with TRUS or DRE findings that were interpreted as suspicious for cancer but who are being followed and have not yet had biopsies done were removed from this series. This left a unique, extensively screened group of 1695 men who were free of prostate cancer, as far as could be determined. Analyses of the PSA levels in this large population in the appropriate age range for increasing risk of prostate cancer revealed several important findings. First, there was a direct relationship between serum PSA levels and estimated prostate volume for both the currently available monoclonal and polyclonal PSA assays. Individuals with benign prostatic hyperplasia and larger gland volume have a higher normal limit of PSA than men with normal gland volume. Second, analyses showed no relationship between age and PSA levels or between symptoms of prostatism and PSA levels independent of gland enlargement. It was concluded that volume-adjusted upper limits of normal PSA can be determined for different levels of specificity desired. This information may be applicable to the use of PSA in men not already suspected of having prostate cancer and may increase its effectiveness as a tool for early detection.

Reprinted by permission from the American Cancer Society.

Chest

Ultrasonographic approach to diagnosing hydropneumothorax. Targhetta R, Bourgeois J-M, Chavagneux R, Marty-Double C, Balmes

P (RT, Dept. of Pulmonary Medicine, Gaston Doumergue Hospital, 30006 Nimes, France). *Chest* 101(4):931–934, April 1992

Ultrasound results for 11 patients with HPN confirmed by CXR were compared with those for 100 healthy subjects. The observation of the hyperechogenic line of the pleuropulmonary surface (normal subjects) showed back-and-forth respiratory movements in every case which we call the "gliding sign." Ultrasonographic signs were shown in all patients with HPN. Visualizing the gassy effusion above the pleural fluid, the disappearance of the "gliding sign" ($n = 11$) indicates PN. The image of the HPN allows in addition a "curtain sign" which depicts the movement of air/fluid level (n = 11), the pulmonary collapse being calculated across the lipid window whose echostructure is analyzed. A "polymicrobullous" image (n = 2) caused by air microbubbles within the fluid effusion, is reported. We conclude that echography appears to be a new approach to diagnosing HPN, which is particularly useful during or after ultrasonically guided procedures including pleural drainage, and should be recognized by sonographers.

Gastroenterology

Survival and acquired genetic alterations in colorectal cancer. Laurent-Piug P, Olschwang S, Delattre O, et al. (PLP, Laboratory of Tumor Genetics, Institut Curie, Paris, France). *Gastroenterology* 102:1136–1141, 1992

To set the basis for a precise assessment of new therapeutic approaches, the prognosis of patients with colorectal cancer should be evaluated with the highest precision. The recent discovery, in tumor cells, of somatically acquired genetic alterations believed to be instrumental in tumor behavior may provide new independent prognostic factors. In the present study, the usual prognostic factors and a set of genetic alterations, i.e., Ki-*ras* mutations, DNA content, and allelic losses on chromosome 17p, 18q, 5q, and 1p, were investigated in 109 colorectal carcinomas. Univariate analysis for correlation with 5-year survival showed the following significant associations: histological staging ($P < 0.00001$), preoperative serum carcinoembryonic antigen concentration ($P < 0.002$), DNA content ($P < 0.009$), and allelic loss on the short arm of chromosome 17 ($P < 0.002$) and 1 ($P < 0.03$). In multivariate analysis, only histological staging and allelic loss on the short arm of chromosome 17 were found to be independently associated with shorter survival ($P < 0.0001$ and $P < 0.004$, respectively). Loss of 17p alleles in colorectal carcinoma thus appears to be a marker of tumor aggressiveness. Its monitoring may lead to an improved classification of patients when adjuvant chemotherapy is considered.

Reprinted with permission by the American Gastroenterological Association.

Digestive Diseases and Sciences

Achalasia and hiatal hernia. Goldenberg SP, Vos C, Burrell M, Traube M (MT, Gastroenterology Unit, Yale University School of Medicine, P. O. Box 3333, New Haven, CT 06510). *Dig Dis Sci* 37(4):528–531, April 1992

Several reports have emphasized the rarity of hiatal hernia in achalasia, despite the lack of inherent incompatibility of the two conditions and despite the relatively high frequency of hiatal hernia in the general population. We reviewed the radiographs of 71 of 94 consecutive patients with manometrically proven achalasia referred to Yale-New Haven Hospital. Unequivocal hiatal hernia was seen in 10 (14.1%) patients and was seen in nine of 35 (25.7%) patients 51 years old or more. Review of the radiographic reports from these 10 patients indicated that only two were properly recognized as showing both achalasia and hiatal hernia. All five patients who underwent pneumatic dilatation had excellent results. We conclude that hiatal hernia in achalasia is frequently unrecognized and underreported but is not rare, with a frequency probably similar to that of the general population.

Gastrointestinal Endoscopy

Endoscopic balloon dilation of colonic and ileo-colonic Crohn's strictures: long-term results. Breysem Y, Janssens JF, Coremans G, Vantrappen G, Hendrickx G, Rutgeerts P (GV, Dept. of Medicine, Division of Gastroenterology, University Hospital Gasthuisberg, University of Leuven, Leuven, Belgium). *Gastrointest Endosc* 38:142–147, 1992

The long-term effects of endoscopic dilation of colonic or ileocolonic Crohn's disease strictures were analyzed. In 18 patients with a Crohn's disease-related low gastrointestinal stricture, the stenosis was dilated using through-the-scope (TTS) balloon catheters. A dilation to a diameter of 18 mm was always attempted. Treatment was successfully carried out in 16 patients, and was followed by immediate symptomatic relief in 14 patients. Long-term success was observed in nine patients. There were no complications. Balloon catheter dilation of a colonic stricture or stricture of an ileo-colonic anastomosis was found to be safe and effective. This treatment modality can be an alternative to surgery in a selected group of patients.

The Journal of Bone and Joint Surgery

Medical management compared with operative treatment for osteoid-osteoma. Kneisl J, Simon MA (JSN, 303 E. Chicago Ave., #9-037, Chicago, IL 60611). *J Bone Joint Surg [Am]* 74-A(2):179, Feb. 1992

Twenty-four patients were evaluated and diagnosed, between August 1975 and July 1989, as having probable osteoid-osteoma. Fifteen patients had operative treatment (twelve immediate and three delayed); all fifteen had complete relief of pain. The remaining nine patients were treated with non-steroidal anti-inflammatory medications; all nine had complete relief of pain, and six had resolution of the symptoms without using non-steroidal anti-inflammatory drugs, after an average of thirty-three months (range, thirty to forty months) of treatment. Thus, long-term administration of non-steroidal anti-inflammatory drugs can often be as effective as excision for the treatment of osteoidosteoma, without the morbidity that is associated with the operation, especially in patients in whom operative treatment would be complex or might lead to disability.

Osteosarcoma of the pelvis: a clinical and histopathological study of twenty-five patients. Fahey M, Spanier SS, Vander Griend RA (MF, Dept. of Orthopaedic Surgery, College of Medicine, University of Florida, J. Hillis Miller Health Center, Box J-246, Gainesville, FL 32610-0246). *J Bone Joint Surg [Am]* 74-A(3):321–330, March 1992

Twenty-five patients who had an osteosarcoma of the pelvis were treated at the University of Florida between 1967 and 1990. Two of these patients had underlying Paget disease, and five had received previous radiation therapy to the pelvis. Common problems in this series of patients included delays and errors in establishment of the diagnosis, underestimation of the extent of the tumor on the radiographic staging studies, histopathological findings of local extension next to and into pelvic structures, widespread invasion into major pelvic veins, and microscopic foci of tumor in otherwise normal tissue. These problems led to difficulty in gaining local control of the tumor with any type of operative procedure. Of the eighteen patients who had a resection, only four had a contamination-free wide margin, and a local recurrence developed in thirteen. Only one patient, who had no evidence of disease eleven years after treatment, was alive at the time of writing. Because of the tendency for venous invasion, the radiographic staging studies should include a thorough evaluation of the blood vessels adjacent to the tumor.

The Journal of Pediatrics

Kidney function in very low birth weight infants with furosemide-related renal calcifications at ages 1 to 2 years. Downing GJ,

Egelhoff JC, Daily DK, Thomas MK, Alon U (GJD, Section of Neonatology, Children's Mercy Hospital, 2401 Gillham Rd., Kansas City, MO 64108-9898). *J Pediatr* 120:599–604, 1992

To determine whether long-term renal sequelae follow the use of furosemide in preterm infants, we evaluated renal function in 27 former very low birth weight infants (<1500 gm) at 1 to 2 years of age. Patients were classified into three groups on the basis of status at the time of discharge from the hospital: group 1 (n = 7) had no furosemide treatment or renal calcifications, group 2 (n = 10) had furosemide therapy but no calcifications, and group 3 (n = 10) had furosemide therapy with renal calcifications. Renal ultrasonography at the time of the study demonstrated resolution of the calcifications in six patients in group 3. No differences in renal function were observed between groups 1 and 2. Creatinine clearance (mean ± SEM) in group 3 (83.6 ± 7.8 ml/min per 1.73 m^2) was significantly lower than clearance in groups 1 and 2 (103.2 ± 6.5 and 109.1 ± 5.1, respectively; $p < 0.05$). Children in group 3 had significantly higher urinary calcium/creatinine ratios and fractional excretion of sodium and lower tubular reabsorption of phosphate than children in the two other groups had. Urine-blood difference in carbon dioxide tension after oral acetazolamide load, which indicates the ability of the distal tubule to secrete hydrogen ions, was 8.4 ± 3.4 mm Hg in group 3, significantly lower than values in groups 1 and 2 (22.6 ± 3.1 and 28.0 ± 4.3 mm Hg, respectively, $p < 0.05$). Within group 3 the four children with persistent renal calcifications had significantly lower urine-blood carbon dioxide tension differences than did those with resolution of calcifications ($p = 0.02$). We conclude that furosemide-related renal calcifications in very low birth weight infants may lead to glomerular and tubular dysfunction; further long-term follow-up of this population is recommended.

Journal of Ultrasound Medicine

Multiple criteria in sonographic diagnosis of prostate carcinoma allows identification of all glands harboring clinically significant tumor: an in vitro study with histopathologic correlation. Hardt NS, Kaude JV, Tykochinsky G, Ros PR, Wajsman Z, Hackett RL (NSH, Box J-275, University of Florida College of Medicine, Gainesville, FL 32610). *J Ultrasound Med* 11:117–123, April 1992

Fresh whole prostate glands were examined systematically in a water bath to look for four sonographic criteria for prostatic carcinoma: well-circumscribed hypoechoic regions, external asymmetry of the gland, increase in anterior-posterior diameter ratio, and irregularity of the prostatic capsule. Whole mount sections were examined to correlate the histopathologic and sonographic findings. Using hypoechogenicity alone, 26 of 43 glands harboring tumor were identified correctly. Using all four criteria, 40 of 43 glands harboring tumor were identified, a statistically significant improvement in sensitivity ($P < 0.05$). Specificity of both methods was similar ($P > 0.1$). The three tumors that were missed measured from 0.3 in smallest dimension to 0.9 cm in greatest dimension and were found at autopsy in patients who died of causes unrelated to the prostate. The authors conclude that systematic examination of the gland with attention to multiple criteria for abnormality can improve case finding in prostatic adenocarcinoma.

Reprinted with permission by the American Institute of Ultrasound in Medicine.

Magnetic Resonance Imaging

Bone marrow imaging using STIR at 0.5 and 1.5 T. Jones KM, Unger EC, Granstrom P, Seeger JF, Carmody RF, Yoshino M (KMJ, Dept. of Radiology, Brigham and Women's Hospital, 75 Francis St., Boston, MA 02115). *Magn Reson Imaging* 10:169–176, 1992

We retrospectively examined MR images in 82 patients to evaluate the usefulness of short inversion time inversion recovery (STIR) in bone marrow imaging at 0.5 and 1.5 T. The study included 56 patients at 1.5 T and 26 patients at 0.5 T with a variety of pathologic bone marrow lesions (principally oncological), and compared the contrast and image quality of STIR imaging with spin-echo short repetition time/echo time (TR/TE), long TR/TE, and gradient-echo sequences. The pulse sequences were adjusted for optimal image quality, contrast, and fat nulling. STIR appears especially useful for the evaluation of red marrow (e.g., spine), where contrast between normal and infiltrated marrow is greater than with either gradient-echo or T_1-weighted images. STIR is also extremely sensitive for evaluation of osteomyelitis, including soft tissue extent. In more peripheral (yellow) marrow, T_1-weighted images are usually as sensitive as STIR. Limitations of STIR include artifacts, in particular motion artifact that at high field strength necessitates motion compensation. At 0.5 T, however, motion compensation is usually not necessary. Also, because of extreme sensitivity to water content, STIR may overstate the margins of a marrow lesion. With these limitations in mind, STIR is a very effective pulse sequence at both 0.5 and 1.5 T for evaluation of marrow abnormalities.

News

Cancer Prevention and Early Detection

The American Cancer Society is sponsoring the National Conference on Cancer Prevention and Early Detection, Sept. 10–12, at the Stouffer Riviere Hotel, Chicago. The objective of the meeting is to increase knowledge and skill levels of physicians and other health professionals. Topics to be addressed include scientific concepts of the cause, prevention, risk reduction, and prevention of cancer; feasible approaches to chemoprevention, dietary manipulation, and smoking cessation; current guidelines for cancer detection on asymptomatic persons; research opportunities that can improve cancer prevention and detection; and community-action programs that increase awareness and provide strategies for reaching special populations. Program committee chairman: Walter Lawrence, Jr. Fee (postmarked by Aug. 10/after Aug 10): physicians, $200/$250; all other health professionals, $100/$150. Information: Andy Cannon, Manager, Continuing Medical Education, American Cancer Society, National Conference on Cancer Prevention and Early Detection, 1599 Clifton Rd., N.E., Atlanta, GA 30329; telephone: (404) 329-7604; fax: (404) 636-5567.

Alex Norman Lectureship in Radiology

The 2nd annual Alex Norman Lectureship in Radiology will be held at the Hospital for Joint Diseases Orthopaedic Institute, New York City, Sept. 14. The meeting will cover advanced musculoskeletal imaging, with emphasis on MR imaging. Faculty: D. Resnick, J. Beltran, Z. Rosenberg, and S. Shankman. Seats will be limited RSVP. No registration fee is required. Information: Cathy Smith, Dept. of Radiology, Hospital for Joint Diseases, 301 E. 17th St., New York, NY; telephone: (212) 598-6373; fax: (212) 598-6125.

Advances in CT and MRI

The Dept. of Radiology, The University of Michigan Medical School, is sponsoring Advances in CT and MRI, Sept. 15–17, at the Towsley Center, Ann Arbor. The course will provide up-to-date information on clinically important topics in CT and MR imaging. Technologists may register for a special 1-day program for technologists and pay a special rate or may pay the full technologists' registration fee and participate in the 3-day program. Course directors: Alex M. Aisen, James H. Ellis, and Melvyn T. Korobkin. Category 1 credit: approximately 17 hr. Information: Edwina Borde, Towsley Center for Continuing Medical Education, Dept. of Postgraduate Medicine, The University of Michigan Medical School, P.O. Box 1157, Ann Arbor, MI 48106-9869; (313) 763-1400.

Los Angeles Conference on Musculoskeletal MR Imaging

The 2nd annual Los Angeles Fall Conference, Musculoskeletal Magnetic Resonance Imaging, will be presented Sept. 19–20 at the Century Plaza Hotel, Los Angeles. Program director: Ronald J. Friedman. Faculty: W. G. Bradley, Jr., R. B. Dietrich, M. Brant-Zawadzki, S. Harms, D. L. Resnick, and G. M. Schlesinger. Category 1 credit will be awarded. Fee (through Aug. 1/after Aug. 1): physicians, $295/$325; fellows, residents, interns, and technologists, $195/$225. Information: Musculoskeletal MRI, c/o Medical Seminars International, Inc., 18981 Ventura Blvd., Ste. 303, Tarzana, CA 91356; telephone (818) 774-9077; fax: (818) 774-0244.

Radiology/92: Imaging and Intervention

The Dept. of Radiology, University of Minnesota Medical School, is sponsoring its 55th annual course, Radiology/92: Imaging and Intervention: 1992 and Beyond, Sept. 19–23, at the Mayo Auditorium, University of Minnesota campus, Minneapolis. Category 1 credti: 26.25 hr. Fee: $550. Information: Office of Continuing Medical Education, Radisson Hotel Metrodome, University of Minnesota, 615 Washington Ave., S.E., Ste. 107, Minneapolis, MN 55414; telephone: (612) 626-7600; fax: (612) 626-7766.

Digital Radiography and Image Management Networking Conference

The Dept. of Radiological Sciences, University of California, Los Angeles, will present Digital Radiography and Image Management Networking Conference, Sept. 20–23, at the Miramar Sheraton Hotel, Santa Monica, CA. The course will include the latest clinical and technical information on the digital imaging techniques of digitized fluorography, phosphor storage plates, the AMBER system, and film digitization systems. Course director: Sam Dwyer III. Category 1 credit: 16 hr. Fee: $345. Information: Mila Wayne, Dept. of Radiological Sciences, UCLA Medical Center, 10833 Le Conte Ave., BL-428 CHS, Los Angeles, CA 90024-1721; telephone: (310) 206-7435; fax: (310) 825-9812.

Contemporary MR Imaging

The Dept. of Radiology, University of Wisconsin Medical School, is sponsoring Contemporary MR Imaging, Sept. 24–25, at the Holiday Inn, Madison West Convention Complex, Madison, WI. Topics to be

covered include MR imaging of infants and children, MR imaging of the musculoskeletal system, MR angiography, and fast spin-echo and phased-array multicoil technology. Conference directors: Virgil B. Graves and Patrick A. Turski; Guest faculty: M. Bernstein, P. S. Hinks, T. P. Naidich, and L. E. Swischuk. Category 1 credti: up to 12 hr. Fee: 2 days, $250; 1 day, $125; technologists, $100. Information: Contemporary MRI, Sandy Yost, Dept. of Radiology E3/311, Clinical Science Center, University of Wisconsin, 600 Highland Ave., Madison, WI 53792-3252; telephone: (608) 263-8308; fax: (608) 263-0876.

International Body Imaging Congress

The 17th annual International Body Imaging Congress will be held at the Mauna Lani Bay Resort Hotel, Kona, HI, Oct. 10–17. Topics in MR imaging, CT, interventional radiology, sonography, and correlative techniques will be presented. The program will include a special section on breast imaging. Program director: Ronald J. Friedman. Faculty: W. D. Boswell, W. G. Bradley, Jr., R. B. Dietrich, S. Harms, D. Kumpe, M. L. Manco-Johnson, R. M. Quencer, and M D. Rifkin. Category 1 credit will be awarded. Fee: physicians, $595; fellows, residents, interns, nurses, and technologists, $495 (letter required). Information: Annual Body Imaging Congress, c/o Medical Seminars International, Inc., 18981 Ventura Blvd., Ste. 303, Tarzana, CA 91356; telephone: (818) 774-9077; fax: (818) 774-0244.

MRI: Clinical State of the Art 1992

The Post-Graduate Medical School, NYU Medical Center, will present MRI: Clinical State of the Art 1992, Oct. 12–14, at the NYU Medical Center, New York City. The course will provide a practical, clinically oriented review and analysis of state-of-the-art MR imaging and an introduction to some of the promising new developments in this technique. Anatomy, applications, techniques, and interpretation will be emphasized. Areas to be covered are brain, spine, bones and joints, cardiovascular system, and body. Category 1 credit: 22 hr. Fee: $500. Information: Post-Graduate Medical School, NYU Medical Center, 550 First Ave., New York, NY 10016; telephone: (212) 263-5295; fax: (212) 263-5293.

Symposium on Cardiovascular and Interventional Radiology

The Dept. of Radiology, Brigham and Women's Hospital, and the Dept. of Continuing Education, Harvard Medical School, will present the 1st International Symposium on Cardiovascular and Interventional Radiology: 1992, Oct. 13–16, at the Copley Plaza Hotel, Boston. The emphasis will be on current indications, efficacy of procedures, improvements in technique, useful advances in equipment, and management of patients. Program director: Krishna Kandarpa. Category 1 credit: 31 hr. Fee: physicians, $700; residents, fellows, and technologists, $650. Information: Harvard Med CME, P.O. Box 825, Boston, MA 02117; telephone: (617) 432-1525.

Breast Cancer Diagnosis: State of the Art

The Post-Graduate Medical School, NYU Medical Center, will present Breast Cancer Diagnosis: State of the Art, Oct. 15–17, at the NYU Medical Center, New York City. The focus of the conference will be a comprehensive review of the mammographic detection of small cancers and their further evaluation with interventional methods. Category 1 credit: 18 hr. Fee: $425. Information: Post-Graduate Medical School, NYU Medical Center, 550 First Ave., New York, NY 10016; telephone: (212) 263-5295; fax: (212) 263-5293.

Chest Imaging 1992

The University of Toronto and The Toronto Hospital will present Chest Imaging 1992, Oct. 16. The course will cover high-resolution CT, the solitary pulmonary nodule, AIDS, and other up-to-date topics pertaining to chest imaging in the 1990s. The aim of the course is to provide practical information that radiologists and clinicians can use in day-to-day practice. Guest faculty: D. Naidich. Category 1 credit is pending. Fee: physicians, $120; residents, fellows, and technologists, $70. Information: Rose Baldwin, Dept. of Radiology, The Toronto Hospital, General Division, 200 Elizabeth St., Toronto, Ontario, Canada M5G 2C4; telephone: (416) 340-3372; fax: (416) 340-3900.

Magnetic Resonance Imaging and CT Update

The Dept. of Radiology, Brigham and Women's Hospital, and the Dept. of Continuing Education, Harvard Medical School, will present Magnetic Resonance Imaging and CT Update, Oct. 26–30, at the Hyatt Regency Hotel, Cambridge, MA. The course will emphasize clinical MR imaging and CT, ranging from the basics of methods and interpretation to advanced techniques. Key topics will include fast MR imaging, MR angiography, spiral CT scanning, and high-resolution CT scanning. A comprehensive course on MR physics will be included in the program. Course directors: Steven E. Seltzer, Ferenc A. Jolesz, and Amir A. Zamani. Category 1 credti: 31 hr. Fee: physicians, $600; residents, fellows, and technologists, $400. Information: Harvard Med CME, P.O. Box 825, Boston, MA 02117; telephone: (617) 432-1525.

Interventional Radiology Course

The University of California, San Diego, is sponsoring the 12th annual Interventional Radiology Course, Oct. 30–Nov. 1, at the Hotel Del Coronado, San Diego. Program directors: Eric vanSonnenberg and Horacio D'Agostino. Category 1 credit: 16.5 hr (pending). Fee: physicians, $350; fellows, residents, and technologists, $275. Information: Dawne Ryals, Ryals and Associations, P.O. Box 1925, Roswell, GA 30077-1925; telephone: (404) 641-9773; fax: (404) 552-9859.

Postgraduate Radiology

The University of California, San Diego, is sponsoring Postgraduate Radiology, Nov. 2–6, at the Ritz-Carlton Resort Hotel, Naples, FL. Program director: David S. Feigin. Category 1 credit: 28 hr (pending). Fee: physicians, $600; residents, fellows, and technologists, $400. Information: Dawne Ryals, Ryals and Associates, P.O. Box 1925, Roswell, GA 30077-1925; telephone: (404) 641-9773; fax: (404) 552-9859.

Advanced Seminars in Diagnostic Imaging

The University of California, San Diego, is sponsoring Advanced Seminars in Diagnostic Imaging, Nov. 13–15, at the Ritz-Carlton Laguna Niguel, Laguna Niguel, CA. Program director: David S. Feigin. Category 1 credit: 15 hr (pending). Fee: physicians, $400; residents, fellows, and technologists, $300. Information: Dawne Ryals, Ryals and Associates, P.O. Box 1925, Roswell, GA 30077-1925; telephone: (404) 641-9773; fax: (404) 552-9859.

The American Board of Radiology Examinations

Written examinations for the American Board of Radiology (ABR) are scheduled for Oct. 1–2, 1992, and Sept. 23–24, 1993. Oral examinations will be held at the Executive West Hotel in Louisville, KY, June 7–10, 1993. The ABR will accept applications for admission to the examinations after July 1, but not later than Sept. 30, in the year *preceding* the year in which the examination is to be taken. For application forms and further information: Office of the Executive Director, The American Board of Radiology, 2301 W. Big Beaver Rd., Ste. 625, Troy, MI 48084.

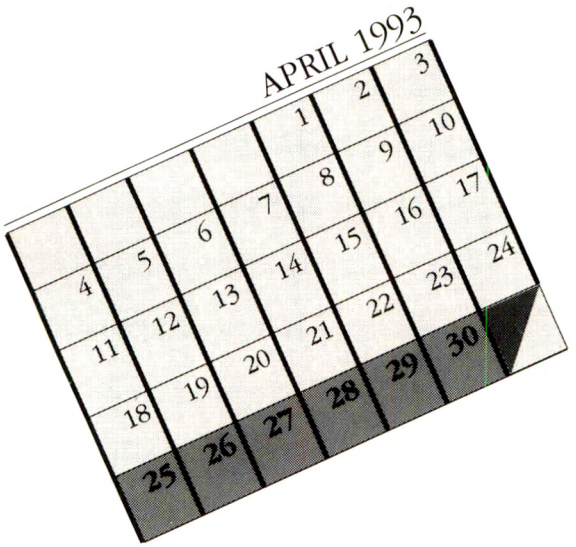
Meeting and Course Review

For the reader's convenience, a summary of upcoming meetings and courses is provided. Detailed listings are given in the *AJR* issue given in parentheses.

MRI and Musculoskeletal Imaging, July 27–Aug. 1, Laguna Niguel, CA (March)
Courses on Prostate Ultrasound, July 31–Aug. 1 and Oct. 16–17, Albany, NY (June)
Mackinac Island Imaging Conference, Aug. 3–6, Mackinac Island, MI (May)
Midwest Interventional Radiology Seminar, Aug. 7–9, Peoria, IL (June)
Northern Imaging 1992 Radiology Seminar, Aug. 7–10, Knee Lake Lodge, Manitoba (June)
Symposium on Diagnostic Imaging, Aug. 8–12, Newport, RI (June)
Contemporary Medical Imaging IX, Aug. 12–16, Hilton Head Island, SC (April)
Summer Practicum Aug. 16–20, Keystone, CO (April)
Barcelona 1992 Post-Games Imaging Conference, Aug. 17–21, Barcelona (April)
European Symposium on Uroradiology, Aug. 24–27, Herlev, Denmark (Aug 1991)
International Skeletal Society Refresher Course, Aug. 26–29, Stockholm (March)
ARDMS Exam Preparation Courses: Ultrasound and Doppler Physics, Aug. 28–29, Washington, DC; Sept. 18–19, Los Angeles; Sept. 26–27, Atlanta; and Oct. 2–3, Chicago; **OB/GYN Ultrasound,** Aug. 30, Washington, DC; Sept. 20, Los Angeles; and Oct. 4, Chicago; **Vascular Technology,** Aug. 30–31, Washington, DC; Sept. 20–21, Los Angeles; and Oct. 4–5, Chicago (July)
Congress of Asian Federation of Societies for Ultrasound in Medicine and Biology, Aug. 30–Sept. 3, Seoul, Korea (Feb)
Cardiovascular and Interventional Radiological Society of Europe Annual Meeting and Postgraduate Course, Aug. 30–Sept. 3, Sitges (Barcelona), Spain (May)
Radiation, Physics, and Biology. Aug. 31–Sept. 4, New York City (May)
Ultrasound Angiography 92, Sept. 2–4, University of Southampton, United Kingdom (Feb)
Radiology in County Kerry, Sept. 6–9, Parknasilla, County Kerry, Ireland (July)
Mammography Update, Sept. 7–11, Santa Fe, NM (June)
Sonography Update, Sept. 9–11, San Diego (July)
Pacific Northwest Diagnostic Ultrasound: OB/GYN Symposium, Sept. 10–12, Seattle (May)
Pittsburgh Breast Imaging Seminar, Sept. 10–13, Pittsburgh (May)
Symposium on Transrectal Ultrasound, Sept. 11–13, Chicago (May)
Ultrasound and Cardiovascular Technology Review Conference, Sept. 11–13, San Diego (June)
Vancouver Imaging Update 1992, Sept. 13–17, Vancouver, B.C. (May)
Mammographic Interpretation, Sept. 14–17 and Oct. 26–29, Boston (April)
MRI Visiting Fellowships at UCLA, Sept. 14–18, Oct. 5–9, and Dec. 7–11, Los Angeles (Sept 1991)
Organ Imaging Review 1992, Sept. 14–18, Toronto (July)
Dose, Time, and Fractionation in Radiation Oncology, Sept. 16–19, Madison, WI (May)
Seminar in Diagnostic Ultrasound, Sept. 17–19, Ann Arbor (July)
Neurologic Complications of Pregnancy, Sept. 17–19, New York City (July)
Musculoskeletal and Neuroradiological MRI, Sept. 21–26, Hilton Head Island, SC (June)
Practicum in Mammography for Technologists, beginning dates, Sept. 28 and Oct 19, San Diego (May)
Update in Film Screen Mammography, Sept. 30–Oct. 2, Richmond, VA (May)
Western Neuroradiological Society Annual Meeting, Oct. 1–4, San Francisco (July)
International Symposium on Vena Cava Filters, Oct. 9–10, Poitiers, France (July)
Fall Foliage Imaging Seminar, Oct. 9–11, Burlington, VT (May)
Practical Radiology, Oct 12–15, Charlottesville, VA (June)
Nuclear Cardiology Symposium and Workshop, Oct. 14–16, Milwaukee (June)
Progress in Magnetic Resonance, Oct. 15–17, Locarno, Switzerland (June)
Michigan Fall Radiology Conference, Oct. 16–17, Birmingham, MI (July)
Breast Imaging Seminar, Oct. 19–21, New York City (July)
Society of Radiologists in Ultrasound Postgraduate Course, Oct. 23–25, Chicago (June)
Musculoskeletal Imaging, Oct. 24–25, San Diego (July)
International Course on MR Imaging, Oct. 25–28, Riyadh, Kingdom of Saudi Arabia (March)
Postgraduate Radiology Course, Oct. 26–30, San Diego (July)
Dysphagia Research Society Inaugural Meeting, Nov. 6–8, Milwaukee (July)

AJR carries announcements of courses, symposia, and meetings of interest to its readers if received a minimum of 5 months before the event. There is no charge; receipt of items by the *AJR* Editorial Office is not acknowledged. Submit items for publication typed double-spaced. Provide title, date, location, brief description, sponsor, course directors, fees, category I credit, and address and telephone number for additional information. Faculty from the host institution will not be listed. Guest faculty names will appear **only** if initials are provided. Mail news items to *AJR* Editorial Office, 2223 Avenida de la Playa, Suite 103, La Jolla, CA 92037-3218.

Mark Your Calendar Now!



The American Roentgen Ray Society will return to San Francisco in 1993, and plans are already underway for what promises to be an educationally fulfilling and socially enjoyable week in the city by the bay. Look for the San Francisco logo in the next several issues of the *AJR* for updated meeting information.

Call for Papers

Abstracts of papers to be considered for the scientific program must be submitted by November 1, 1992. Abstract forms and instructions for submission are included in this issue and will also appear in the July through October issues. The *AJR* has first rights to all papers accepted for presentation at the ARRS meeting.

Call for Scientific Exhibits

The deadline for submission of abstracts to be considered for scientific exhibits is November 1, 1992. Abstract forms and instructions for submission are included in this issue and will also appear in the July through October issues.

Categorical Course

The topic of the 1993 Categorical Course is Ultrasound. A summary of topics and faculty for this course will appear in the February 1993 issue of the *AJR*.

Refresher Courses

Plans are underway to present at least 60 instructional courses on various topics of interest to the radiology community. A summary of these courses will be included in the February *AJR*. Early registration is strongly suggested, as these courses fill up quickly.

Resident Award Papers

The society offers three cash awards for the best scientific papers prepared by residents in radiology. The President's Award has a cash prize of $2,000, and there are two Executive Council Awards with a cash prize of $1,000 each. The winners of these three awards are invited to present their papers during the opening ceremonies at the annual meeting. Papers must be submitted by February 12, 1993, for consideration in this competition. Additional information on these awards will be mailed to all residency program directors in July.

Local Arrangements

The San Francisco area offers many opportunities for sightseeing, shopping and entertainment. Check the February *AJR* for detailed information on local tours developed especially for ARRS meeting attendees.

Registration and Hotel Reservations

All meeting activities will take place in the beautiful new San Francisco Marriott, centrally located on Market Street. The society has negotiated special room rates for meeting attendees, and the February *AJR* will contain meeting registration and hotel reservation forms. As in previous years, early registration is strongly suggested.

Travel

The society will make arrangements with United Airlines and a major car rental firm for preferred rates for meeting attendees. Taking advantage of these special rates benefits both you and the society – you save money on your reservations, and the society receives discounts to send staff and supplies to the meeting. Plan now to check the February issue of the *AJR* for details.

Classified Advertisements

Positions Available

GADSDEN RADIOLOGY ASSOCIATES is a 3-member radiology group seeking a fourth board-certified/eligible radiologist. Gadsden Radiology covers Baptist Memorial Hospital, a 250-bed hospital performing more that 55,000 radiologic exams/yr. All radiologic modalities are available, including state-of-the-art CT, SPECT, nuclear medicine, special procedures, and MRI. Gadsden Radiology Associates also covers their private office, imaging center, and a breast center. Teleradiography is used for call. Gadsden, AL, is a safe, clean city centrally located on the Coosa River approximately 1 hour from Birmingham, 90 Min. from Chattanooga, and 2 hours from Atlanta, GA. Salary and vacation are excellent. Health insurance and malpractice is paid. Interested candidates contact Homer A. Spencer, M.D., 401 Bay Street, Gadsden, AL 35999; (205) 543-3200, or fax (205) 546-7908. 7–1ap

DIAGNOSTIC RADIOLOGIST ON THE ISLAND OF KAUAI with 45 doctors in multispecialty group. Three radiologists in clinic and hospital depts., BC radiologist to perform diagnostic radiology, CT scan, ultrasound, mammography, nuclear medicine, no angiography. Strong FNA service. Island of 50,000 people with moderate subtropical climate. All outdoor sports scuba, snorkeling, fishing, golf, tennis, biking, etc. Incentive formula on becoming stockholder after 1 year, excellent benefits. Congenial group with quality care emphasis. CV by mail or fax (808) 246-1625 welcomed, or call Rex D. Couch, M.D., Medical Director, Kauai Medical Group, Inc., 3420-B Kuhio Highway, Lihue, HI 96766; (808) 245-1077. 7–8a

BC/BE RADIOLOGIST—Busy clinic-and hospital-based practice is seeking to add additional BC/BE radiologists to its staff of 2 neuroradiologists and 7 general radiologists. Special skills or training in pediatrics, MRI, or nuclear medicine would be beneficial. Physician will join a 270-physician multispecialty group representing over 50 specialities. Fargo Clinic is affiliated with St. Luke's Hospitals, a 400-bed level III care center with a NACHRI designated Children's Hospital. Fargo-Moorhead is a tri-college community of 130,000 which supports an opera company, symphony, community theater, and various athletic events. Year-round recreational opportunities abound. Guaranteed first year salary and competitive compensatory arrangements are available. Respond to Kathleen Toft, Physician Recruitment Director, 737 Broadway, Fargo, ND 58123; (800) 437-4010, ext. 2151. 7–10xa

FACULTY POSITIONS IN RADIOLOGY—The Dept. of Radiology and Radiological Sciences of Vanderbilt University School of Medicine has openings in the following areas: neuroradiology, chest, musculoskeletal, and pediatric radiology. Research opportunities are exceptional. Candidates must be board-certified. Please send CV to C. Leon Partain, M.D., Ph.D., Professor and Chairman, Dept. of Radiology and Radiological Sciences, Vanderbilt University, Nashville, TN 37232-2675. An equal opportunity/affirmative action employer. 7–8a

RADIOLOGIST—Established northeastern PA radiology practice seeking fifth radiologist for hospital and private practice. Applicant should have experience in CT, MRI, ultrasound, mammography, nuclear medicine, angiography, and interventional radiology. Potential for partnership. Candidate should be board-certified/eligible and licensed in PA. Address inquiries and current CV to Box E60, AJR (see address this section). 6–8ap

NEURORADIOLOGIST—A faculty position is available in the Dept. of Radiology at the University of Rochester Medical Center, Strong Memorial Hospital, a 725-bed university hospital. An appointment as assistant professor or higher is available at a level appropriate to experience. A fellowship is required. The neuroradiology section consists of 5 faculty members and 1–2 fellows. Research and teaching opportunities are available in a strong academic dept. with state-of-the-art radiologic equipment. Contact John C. Wandtke, M.D., Acting Chair, Dept. of Radiology, Box 648, University of Rochester Medical Center, Rochester, NY 14642; (716) 275-2733. EO/AA/M-F. 6–8a

DIAGNOSTIC RADIOLOGIST, NORTHEAST MICHIGAN—Excellent practice opportunity available for a diagnostic radiologist to commence in the autumn of 1992. Alpena Radiology, P.C,. seeks a BC/BE radiologist to complete our 3-man group. We offer excellent income, early partnership and idyllic lifestyle. We require; a friendly, hard-working individual who will be a team player. The ability to work well with us and our excellent medical staff is a must. Alpena General Hospital is a modern 175-bed facility located on the shores of Lake Huron. The hospital provides all radiology equipment including: new R&F equipment (G.E.), Siemens CT, SPECT nuclear imaging, color flow Doppler, DSA, ACR accredited mammography. Siemens mobile MRI will commence shortly. The hospital administration is very supportive. The Alpena area is a sportsman's paradise. Sailing, boating, golf, fishing, hunting, skiing, etc. are all minutes away. Our moderate winters and Mediterranean summers are ideal. For more information please contact Steven Zweig, M.D. or James Weeks, M.D., Dept. of Radiology, Alpena General Hospital, 1501 W. Chisholm Street, Alpena, MI 49707; (517) 356-7520. 7–9ap

MRI CLINICAL RESEARCH DIRECTOR—Roswell Park Cancer Institute is seeking an MRI clinical research director with interest in oncologic imaging. The Radiology Dept. includes a recently built GE MRI and research center linked with 2 new GE Hi-Light Advantage CT systems. This is part of an MRI, CT, SPECT Cancer Imaging and Research Center. PET collaboration with a nearby university is also possible. At this renowned comprehensive cancer center, opportunity for research and academic activity is outstanding. A faculty appointment will be at the School of Medicine and Biomedical Sciences, State University of New York at Buffalo, according to the level of professional qualifications. Please send CV to Andrew A. Gage, M.D., Deputy Institute Director, Roswell Park Cancer Institute, Elm and Carlton Streets, Buffalo, NY 14263. EOE M/F/H/V. 7–10a

DIAGNOSTIC RADIOLOGY AND BREAST IMAGING—Roswell Park Cancer Institute is seeking board-certified radiologists with interests in oncologic and general radiology, CT/MRI, ultrasound, and breast imaging. The modernization of the entire Radiology and Nuclear Medicine Depts. includes a new multidisciplinary Breast Imaging Center, a new MRI Center, and new CT, ultrasound and fluoroscopy suites. At this renowned comprehensive cancer center, opportunity for multimodality clinical diagnostic imaging, research and academic activity is outstanding. A faculty appointment will be at the School of Medicine and Biomedical Sciences, State University of New York, according to the level of professional qualifications. Please send CV to Andrew A. Gage, M.D., Deputy Institute Director, Roswell Park Cancer Institute, Elm and Carlton Streets, Buffalo, NY 14263. EOE M/F/H/V. 7–10a

NEURORADIOLOGIST—Unique opportunity to join expanding N.Y.C. area practice. Board-certified radiologist with 2-yr fellowship in neuroradiology needed to head section of neuroradiology. This well-established university affiliated practice includes 9 board-certified radiologists practicing in a 487-bed teaching hospital and 2 private offices performing approximately 110,000 procedures/yr. State-of-the-art imaging equipment including 1.5-T GE Signa. Competitive salary leading to full equal partnership. Contact Jorge G. Pardes, M.D/William G. Wolff, M.D. Booth Memorial Medical Center; (718) 670-1594 or 1050. 7–10ap

FAIRBANKS, AK—Four diagnostic radiologists seek fifth partner for diversified practice including general radiology, ultrasound, nuclear medicine, MRI (GE 1.5-T), and CT (GE 9800). Hospital and office practice. Desirable life style advantages in a university town. Unlimited access to the outdoors. Excellent salary, benefits, retirement, and vacation. One yr to full partnership. Contact Douglas Hutchinson, M.D., 1919 Lathrop #5, Fairbanks, AK 99701; (907) 452-5092. 8–1ap

PART-TIME PEDIATRIC/GENERAL RADIOLOGIST, CENTRAL MASSACHUSETTS—Radiologist sought with special competence in pediatric radiology to join an 11-member group. We serve a 550-bed medical center that includes the regional 40-bed neonatal intensive care unit. Position involves sharing general responsibilities including CT, ultrasound, and mammography. Part-time position may become full-time. Please send CV to Richard Danford, M.D., Worcester Radiologists, 121 Lincoln St., Worcester, MA 01605; (508) 753-8151. 6–8ap

VASCULAR/INTERVENTIONAL RADIOLOGIST—Temple University Hospital and School of Medicine is seeking a board-certified vascular/interventional radiologist with fellowship training for a faculty position at the assistant professor rank in the academic yr 1992–1993. This position involves responsibilities in patient care and teaching. Additionally, those candidates with research skills would be preferred. Applicants should contact Francis J. Shea, M.D., Deputy Chairperson, Dept. of Diagnostic Imaging, Temple University Hospital, 3401 N. Broad St., Philadelphia, PA 19140. Temple University Hospital and School of

BC DIAGNOSTIC RADIOLOGIST—Affluent practice. Excellent salary, benefits, and partnership. Investigate now before socialized medicine becomes a reality! This 395-bed hospital, second largest in the beautiful state of Delaware, is centrally located on the East Coast. This is a rapidly expanding, high-powered group practice. Subspecialty training in interventional, imaging, or mammography desired. Open to F/M with 1–2 yr of postgrad experience. Send resume to or contact Ben Hollander, M.D., Dept. of Radiology, St. Francis Hospital, 7th & Clayton Sts., Wilmington, DE 19805; (302) 421-4304. 6–8ap

IMMEDIATE OPENING FOR BC/BE DIAGNOSTIC RADIOLOGIST, NEW ENGLAND, to join a 6-member group, leading to partnership, in an active community, university-affiliated hospital. Over 100,000 exams/yr. Practice includes CT, ultrasound, nuclear medicine, MRI, angiography, and interventional. Locum needed in interval. Located in New England close to boating and skiing, 1 hr from Boston. Contact Allan M. Deutsch, M.D., Dept. of Radiology, The Miriam Hospital, 164 Summit Ave, Providence, RI 02906; (401) 331-8500, ext. 4400. 6–8x

DIAGNOSTIC RADIOLOGIST—Private practice opportunity with 2 radiologists. Senior partner retiring. Excellent salary and early partnership. All imaging modalities including MRI. Angio experience desired. University community of 100,000 with abundant outdoor recreation. CV to Dan Davidson, M.D., 3000 W. Deborah Dr., Monroe, LA 71201; (318) 388-7810. 6–9ap

COASTAL FLORIDA, IMMEDIATE OPENING FOR BC DIAGNOSTIC RADIOLOGIST to join 2-man group in single-site practice at well-equipped 110-bed hospital in small east coast community 60 miles from Orlando and Disney World. Relaxed practice includes all aspects of general radiology, including MRI. Excellent fringe benefits and early partnership. Contact Alan J. Stern, M.D. or Joseph E. Godard, M.D., P.O. Box 933, New Smyrna Beach, FL 32170; (904) 427-3401. 7–10ap

DIAGNOSTIC RADIOLOGIST, ABDOMINAL IMAGING—The University of Missouri– Columbia Hospital and Clinics is seeking a radiologist with expertise in abdominal imaging (GI, CT, ultrasound, and MRI). Board-certification required. Fellowship desirable. Tenure and nontenure tracks available at assistant and associate professor levels. Address inquiries to Robert J. Churchill, M.D., Dept. of Radiology, University of Missouri—Columbia Hospital and Clinics, One Hospital Dr., Columbia, MO 65212. An equal opportunity/affirmative action employer. 5–10ap

DIRECTOR OF PEDIATRIC RADIOLOGY—The Division of Pediatric Radiology, Oregon Health Sciences University, Portland, OR, invites applications for a section director. Completion of an approved fellowship in pediatric radiology and ABR certification is required. Please send CV to Frederick Keller, M.D., Oregon Health Sciences University, Diagnostic Radiology, L340, 3181 S.W. Sam Jackson Park Rd., Portland, OR 97201-3098; (503) 494-4498. The OHSU is an affirmative action, equal opportunity employer. 6–8a

MAMMOGRAPHY FACULTY POSITION—The Dept. of Radiology at the University of Rochester Medical Center has a faculty position available in mammography. The mammography practice is in Strong Memorial Hospital and 2 private offices. One of the offices has over 30,000 exams/yr.The section offers a strong potential for academic growth with emphasis on original research and teaching. Academic time is available for faculty interested in developing a strong academic career. Support, resources, and opportunities are available for research. The radiologist can also participate in other aspects of radiology. Academic rank and salary will be determined by previous experience. Contact John C. Wandtke, M.D., Acting Chair, Dept. of Radiology, Box 648, University of Rochester Medical Center, Rochester, NY 14642; (716) 275-2733. EO/AA/M-F. 6–8a

CENTRAL WISCONSIN—Established radiology group in independent practice is seeking 2 additional radiologists for growing practice in central Wisconsin. All imaging modalities. Competitive first yr salary with full partner status available second yr. Full benefits. Excellent schools, recreation, and quality of life. Contact David E. Enerson, M.D., 900 Illinois Ave., Stevens Point, WI 54481; (715) 346-5140 or Andrew M. Lucas, M.D., 410 Dewey St., Wisconsin Rapids, WI 54495-8080; (715) 423-6060. 8xa

ISRAEL, DIAGNOSTIC RADIOLOGY—Opportunities for 3- to 4-wk or longer working vacations in a number of Israeli medical centers, on a volunteer basis. Positions varied, arrangements flexible. For information contact Jonathan H. Fish, M.D., 1844 San Miguel Dr., #302, Walnut Creek, CA 94596; (510) 947-0560. 8–10xa

PARTNERSHIP POSITION IN PALM SPRINGS, CA—Well-established, 9-member group has openings for 2 board-certified radiologists. A physician with a strong background in MRI is sought as director of the section of MRI. The other position requires a physician with mammography experience to direct imaging in the breast health section of a new comprehensive cancer center. The group covers a 350-bed hospital and 2 offices in a desirable, rapidly expanding area of southern California. MRI facilities include 1.5-T Picker Vista HPQ with MRA package, ViStar imaging computer, and 1.5-T GE Signa. Other equipment includes 3 CT, a Cemax image processor, 2 Acuson color-flow Doppler ultrasound, 4 nuclear cameras including 2 SPECT, and all other diagnostic modalities. Ground has just been broken on a new 25,000 sq. ft. radiology wing, which will be furnished with state-of-the-art equipment. New trauma center, cancer center, and rehab hospital being built. Excellent compensation and benefits package leading to full partnership. Beaches and large-city amenities of Los Angeles only 2 hr away. Yr-round sunny weather. Ample free time to enjoy southern California and the unparalleled recreational opportunities offered by the resort community of Palm Springs. Direct inquiries to Marvin J. Friedenberg, M.D., Desert Hospital, Dept. of Radiology, 1150 N. Indian Canyon Dr., Palm Springs, CA 92262. 8xa

BOSTON—Expanding private-practice group. No night or evening call. Need experience in mammography. Great lifestyle. Salary leading to equal partnership. Send letter and CV to Box E49, AJR (see address this section). 5–10a

DIAGNOSTIC RADIOLOGIST FOR TOP-5 CITY (MONEY MAGAZINE OCTOBER '91)—Progressive, well-established group of 9 board-certified radiologists has position immediately available for a recently trained BC diagnostic radiologist. Fellowship training preferred, but will consider qualified individual with special expertise in body imaging; angiographic experience is optional. Practice includes 2 tertiary hospitals (850 and 350 beds), private office, and 2 imaging centers. State-of-the art equipment includes 2 GE 1.5-T MRI units; ATL, Toshiba, and Acuson duplex color ultrasound; and 5 GE 9800 CT. High plains offer moderate climate, and surrounding area is ideal for outdoor interests, including skiing, hunting, boating, and fishing. Excellent compensation and benefits package leading to full partnership. Please reply with CV to Todd R. Samuels, M.D., Lubbock Radiology Associates, 3707 21st St., Lubbock, TX 79410. 5–8ap

TWO DIAGNOSTIC RADIOLOGISTS, WASHINGTON—Prominent, 100-physician multispecialty clinic in Pacific Northwest seeks both a diagnostic radiologist and an interventional radiologist. Interventional radiologist should have fellowship training and/or extensive experience in interventional radiology. Diagnostic radiologist should have general radiology experience to include all full-scope imaging services. Guaranteed salary and partnership track available. Excellent benefit package. Abundant 4-season recreational opportunities. Send CV to Fred Bockenstedt, M.D., P. O. Box 489, Wenatchee, WA 98807. 5-10ap

SUPERB PARTNERSHIP POSITION IN LAS VEGAS—Rapidly expanding 7-member group practice covering 2 full-service imaging centers and a small hospital has an immediate opening. We are looking for an additional board-certified radiologist with an uncommon dedication to excellence in patient care. Our outpatient facilities include 2 MR, 2 CT, angio with a 4-bed recovery area, 5 ultrasound, 5 mammography, 3 SPECT, plus R&F. This is an excellent opportunity for a partnership position with a well-respected group in a growing community. Please send CV to Dr. Mark Winkler, SDMI, 2950 S. Maryland Pkwy., Las Vegas, NV 89109. 3–2ap

RADIOLOGIST—A 4-physician group seeks a fifth to join our well-established and growing practice. We are located in east-central Illinois, with a 4-yr college, Jr. college, and a farming economy enhanced by numerous growing industries. We serve a rural but very modern 230-bed hospital ($25 million expansion underway) and several other sites, performing more than 80,000 exams/yr. Mattoon-Charleston is a great place to raise a family while still having access to big-city amenities. Please be BC/BE, skilled in interventional or MRI, and able to handle general diagnostic modalities competently. Please reply to Bruce Fluesmeier, Lakeland Radiologists, Ltd., 1221 Broadway, Mattoon, IL 61938; (800) 745-7701. 3–8ap

THE DEPT. OF RADIOLOGY, VIRGINIA COMMONWEALTH UNIVERSITY/MEDICAL COLLEGE OF VIRGINIA, AND THE MCGUIRE VA MEDICAL CENTER, RICHMOND VIRGINIA seek faculty for positions in diagnostic radiology (chest, GI, mammography, CT/US/MR, musculoskeletal, ER, angio/interventional, neuroradiology). MCV is a 1,058-bed facility and a level 1 trauma center. The McQuire VAMC is an 800-bed facility. ABR certification or eligibility required. Individual should have experience working in a culturally diverse environment. Academic rank and salary commensurate with experience. For position description, or to submit CV, write or phone A.V. Proto, M.D., Dept. of Radiology, MCV Box 470, Richmond VA 23298-0470; (804) 786-7212. VCU/MCV is an equal opportunity/affirmative action employer. Women and minorities are encouraged to apply. 7–8a

SAN ANTONIO, TEXAS—Large group covering multiple hospitals and outpatient facilities seeks radiologists with angiography skills. Send CV to Search Committee, M&S X-Ray Associates, P.O. Box 15920, San Antonio, TX 78212-9510. 7–12ap

SOUTH CENTRAL FLORIDA—Immediate opening for board-certified (or eligible with intention to certify), Florida licensed general diagnostic radiologist. Four radiologists are now covering 3 hospitals totaling 250 beds as well as private diagnostic office with mammography. Onsite MRI at 1 hospital and mobile unit at another. Expertise in all modalities including interventional and angiography. Competitive package including early partnership. Send CV to Lawrence S. Ross, M.D., Radiology Consultants, P.A., 114 Medical Center, Sebring, FL 33870. 8xa

CALIFORNIA, CENTRAL COAST (POP 60K)—BC radiologist sought for a small hospital with an active outpatient service. Routine radiology with mammography and ultrasound. Solo position. Relief coverage available. Generous salary. Full-time or 6-8 mo/yr. Write Box D44, *AJR* (see address this section). 7–8a

MEDICAL COLLEGE OF VIRGINIA - DEPARTMENT OF RADIOLOGY—Chief of section and section member, angiography/interventional radiology. An excellent opportunity is available for a dynamic individual interested in building an outstanding program already established on a strong foundation. Currently there are 2 full-time faculty members in the section plus the services of additional faculty members equaling a third full-time faculty equivalent. We are seeking to add another fellowship-trained full-time junior faculty member and a section chief to form a 5-faculty section in charge of angiography/interventional radiology at the Medical College of Virginia and its affiliated Hunter Holmes McGuire VA Medical Center. Together the 2 institutions comprise 1,800-beds. ABR certification or eligibility required. Individual should have experience working in a culturally diverse environment. Academic rank and salary commensurate with experience. Anyone interested should send CV to or phone Anthony V. Proto, M.D., Professor and Chairman, Dept. of Radiology, P.O. Box 470, Richmond, VA 23298-0470; (804) 786-7212, fax (804) 371-6129. VCU/MCV is an equal opportunity/affirmative action employer. Women and minorities are encouraged to apply. 7–8a

IMMEDIATE OPENING, DIAGNOSTIC RADIOLOGIST, NEW YORK STATE—Expanding, progressive and innovative 26-radiologist group seeking BC/BE university trained radiologist with experience in body CT and body MRI. Private practice opportunity in university affiliated tertiary teaching hospitals as well as smaller suburban and rural hospitals and multiple comprehensive freestanding imaging centers. Practice includes 4 MRI units, 5 CT scanners and complete range of current ultrasound, mammography, diagnostic, interventional and nuclear medicine technology. The practice is centered in an Upstate New York community of approximately 1 million with full cultural, educational and sports opportunities. Excellent compensation and job security. Send CV to Dr. Steven Herbert, 2273 South Clinton Ave., Rochester, NY 14618. 8–9a

CENTRAL NEW JERSEY, IMMEDIATE OPENING—Radiologist with fellowship training or equivalent experience in vascular/interventional and/or in MR imaging to join 6-member group. Must be willing to do other aspects of diagnostic radiology, mammography, ultrasound, CT, and nuclear medicine. Practice includes a 340-bed community hospital, a private radiology office, and an MRI facility. Area is within a 10-mi. radius of Princeton and is near New York City and Philadelphia. Competitive salary, excellent benefits, and partnership opportunity. Send CV or call Margaret M. Beck, Business Manager, 2127 Hamilton Ave., Trenton, NJ 08619; (609) 587-9410. 8xa

MAMMOGRAPHER—Dartmouth-Hitchcock Medical Center is seeking radiologist to lead mammographic program with strong interest in new techniques and teaching. Dept. consists of 18 staff, 12 residents, 2 fellows, with a full range of modern radiologic practice. A new dept. in a new 420-bed medical center. Separate mammography section with state-of-the-art equipment. Opportunity exists to collaborate with Jack Wennberg in Outcomes Research. Seeking senior assistant, full professor level to be member of a 200-physician academic multispecialty group which forms the clinical faculty of Dartmouth Medical School. Write to Peter K. Spiegel, M.D. Chairman, Dept. of Diagnostic Radiology, Dartmouth-Hitchcock Medical Center, One Medical Center Dr., Lebanon, NH 03756. 7–9ap.

LIVE WHERE YOU CAN PLAY, THE SMOKY MOUNTAINS OF WESTERN NC—A 5-person group seeks a BC/BE diagnostic radiologist with experience in all modalities. Special interest in angio/interventional or nuclear medicine desired. Competitive salary leading to early full partnership. State-of-the-art equipment. Friendly, small-town atmosphere in 75,000+ population county. Plentiful amenities and diverse recreational activities in the immediate area. Moderate 4-season climate. Position available at this time, but would hold for suitable candidate. Send CV or call Dr. Ronald Liljedahl, Hendersonville Radiological Consultants, 807 N. Justice, Hendersonville, NC 28739; (704) 696-1046, work; (704) 697-6741, home. 6–9ap

FACULTY POSITION IN ABDOMINAL IMAGING—Dartmouth-Hitchcock Medical Center is seeking a faculty member at the senior assistant, full professor level with experience and interest in abdominal imaging. Clinical responsibility will be in an entirely new 420-bed clinical facility opening in Oct. 1991 with state-of-the-art instrumentation. Position will involve responsibility for residency training in GI/GU area. Proven record of academic performance including research and teaching with an interest in providing academic guidance for energetic staff of younger radiologists. Interested candidates write with CV to Peter K. Spiegel, M.D., Chairman, Dept. of Diagnostic Radiology, Dartmouth-Hitchcock Medical Center, Hanover, NH 03756. AA/EOE. 7–9ap

CARDIOVASCULAR RADIOLOGIST wanted for clinical care, teaching and research at the New England Deaconess Hospital (NEDH), a 450-bed adult tertiary-care hospital. NEDH is an equal opportunity/affirmative action employer and is fully affiliated with Harvard Medical School. Submit CV to Melvin Clouse, M.D., Chairman, Dept. of Radiology, New England Deaconess Hospital, 185 Pilgrim Rd., Boston, MA 02215. 8–9a

ACADEMIC BC/BE DIAGNOSTIC RADIOLOGIST wanted at the New England Deaconess Hospital (NEDH), a 450-bed adult tertiary-care hospital. NEDH is an equal opportunity/affirmative action employer and is fully affiliated with Harvard Medical School. Applicants should have training experience in body imaging, CT, MRI and ultrasound. Preference will be given to candidates who have experience in resident training and managing a teaching program. Submit CV to Melvin Clouse, M.D., Chairman, Dept. of Radiology, New England Deaconess Hospital, 185 Pilgrim Rd., Boston, MA 02215. 8–9a

RESEARCH ASSOCIATE—Position available to perform research projects in therapy of vascular lesions of the brain and spinal cord. Position will microsurgically create experimental aneurysms in pigs and will then treat them with various embolic materials via transfemoral catheterization. Position requires M.D. or equivalent foreign degree with 2 yrs residency in radiology and 2 yrs of experience in a similar position. Knowledge of all necessary methods for animal research, specimen preparation, etc., and elementary knowledge in vascular surgery. Experience with diagnostic and interventional procedures in neurosurgical disorders and basic skills in the use of personal computers required. Starting salary will be $24,000. Submit CV to Georgia Dept. of Labor, 1275 Clarendon Ave., Avondale Estates, GA 30002, or to the nearest Georgia Job Placement Center. Job order GA 5545038. 8a

ASSISTANT/ASSOCIATE PROFESSOR OF RADIOLOGY, NON-TENURE TRACK POSITION—The Dept. of Radiology, University of Cincinnati Medical Center is seeking qualified applicants to fill the following position: Diagnostic radiologist at the assistant/associate professor level. The candidate must be board-certified in diagnostic radiology and have either a fellowship in pulmonary radiology or demonstrated experience in an academic center in pulmonary radiology. The candidate must participate in the teaching, research activities and patient care and must have an Ohio license. Send CV, at lease 3 letters of recommendation or names and addresses of at least 3 references to Jerome F. Wiot, M.D., Chairman, Dept. of Radiology 234 Goodman St., M.L. 742, Cincinnati, OH 45267. An equal opportunity employer. 8a

HUDSON VALLEY—Private practice radiology group seeking board-certified seventh partner interested in first rate hospital-based and outpatient radiology, all modalities. Excellent benefits and time off. Contact Dr. Victor Gaines; (914) 454-4950. 8a

PROFESSOR/DIRECTOR, PEDIATRIC RADIOLOGY CHILDREN'S HOSPITAL MEDICAL CENTER AFFILIATED WITH THE UNIVERSITY OF CINCINNATI, CINCINNATI, OH—Applications are being accepted for the position of director of pediatric radiology at the Children's Hospital Medical Center, Cincinnati, Ohio. Candidates must be board-certified radiologists with special training in pediatric radiology. Must have demonstrated administrative abilities and academic credentials must indicate scholarly productivity and must have involvement in national pediatric radiology activity. To apply submit a letter of application, a current CV and at least 3 letters of recommendation to Thomas A. Tomsick, M.D. Chairman, Pediatric Radiology Search Committee, University of Cincinnati, Dept. of Radiology, 234 Goodman Street, M.L. 742, Cincinnati, OH 45267. Deadline date for applications is July 31, 1992. The University of Cincinnati is an equal opportunity affirmative action employer. Deadline date for applications is Aug. 31, 1992. 8a

CT/ULTRASOUND/MRI, VASCULAR/INTERVENTIONAL, NEURORADIOLOGISTS — The Medical College of Pennsylvania is seeking BC/BE radiologists with expertise in the above specialty areas. Responsibilities involve clinical work, teaching (resident and medical students), and research as desired. Competitive salary and benefits. Immediate full/part-time openings. Please contact Mindy M. Horrow, M.D., Dept. of Radiologic Sciences, Medical College of Pennsylvania, 3300 Henry Ave., Philadelphia, PA 19129; (215) 842-6578. 8–9a

PART-TIME/LOCUM TENENS DIAGNOSTIC RADIOLOGIST NEAR NORTH CAROLINA COAST—High quality, amiable, hospital-based 2-man practice seeks well-trained BC/BE radiologist. Practice encompasses all imaging modalities but expertise in all modalities not required. Work schedule flexible. One hour to beautiful beaches. Send CV, inquiries to *AJR* Box 80 (see address this section). 8xap

LAKE PLACID-SARANAC LAKE, NY—Director of Radiology. State-of-the-art radiology dept. seeks BC director skilled in all imaging modalities. Angiography essential. Modern, 90-bed medical center in beautiful Adirondack region. Send CV to New England Health Search, 63 Forest Ave., Orono, ME 04473; (207) 866-5680. 8–9a

DIAGNOSTIC RADIOLOGIST, NUCLEAR MEDICINE—500-bed hospital Midwest-based private practice radiology group seeking applications for a BE/BC radiologist with nuclear medicine competency and interest. Successful applicant will devote 50% of their time to nuclear medicine and remaining involved in diagnostic radiology. Nuclear medicine dept. utilizes state-of-the-art SPECT and planar equipment to support a wide range of imaging studies including nuclear cardiology. Equipment includes a majority of Siemens cameras and computers as well as a Trionix Triad camera. Imaging studies available include new heart agents and monoclonal antibodies. Excellent salary, benefits, retirement and vacation. Interested candidates should send CV and references to James E. Call, M.D., Radiology Nuclear Medicine, Inc., 622 Doctors Building, 4239 Farnam St., Omaha, NE 68131. 8–10ap

PEDIATRIC RADIOLOGIST-CHILDREN'S HOSPITAL OF LOS ANGELES—Several faculty positions are available in pediatric radiology including ultrasound, MR, CT, and angiography/interventional radiology, and a position as a second pediatric neuroradiologist. CHLA is a 331-bed primary and tertiary-care hospital with pediatric and surgical programs. Faculty appointments are at the University of Southern California. The dept. is fully equipped with modern equipment including color Doppler ultrasound, CT, and a 1.5-T magnet. Approximately 100,000 radiologic studies are performed annually. Residency training and a fellowship training program are in place with an active teaching program. CHLA is a EOE/AA employer. For information write to Beverly P. Wood, M.D., Radiologist-in-Chief, Dept. of Radiology MS #81, Children's Hospital Los Angeles, 4650 Sunset Blvd., Los Angeles, CA 90027. 8–10a

MUSCULOSKELETAL RADIOLOGIST—University of Arkansas for Medical Sciences, University Hospital, and McClellan Veterans Administration Hospital. This 14-person group in a large tertiary-care medical center seeks musculoskeletal radiologist. The 800-bed complex, receiving referrals from the entire state of Arkansas and from surrounding states, offers full service radiology depts., including digital fluoroscopy, nuclear medicine (with SPECT), Acuson ultrasound with color Doppler, GE 1.5-T MRI, and GE, Picker, and Phillips CT scanners. Position is for director of the musculoskeletal radiology division and includes musculoskeletal MR, CT, and interventional/biopsy cases, as well as 1 academic day per week. A 1- or 2-yr fellowship in musculoskeletal radiology is suggested; salary and academic intensity are negotiable. Little Rock is a medium-sized city in the foothills of the Ouachita Mountains with little traffic and clean air and water. Please send letters and CV to Richard E. Leithiser, Jr., M.D., Associate Professor of Radiology, University of Arkansas for Medical Sciences, 4301 West Markham, Little Rock, AR 72205. 8–10a

PHILADELPHIA—Full- or part-time opportunity for diagnostic radiologist at an outpatient clinic affiliated with the Medical College of Pennsylvania. Modalities include general radiology, mammography, and ultrasound. This individual would rotate through the main dept. with teaching responsibilities for the residency program. Send CV or call Mindy M. Horrow, M.D., Dept. of Radiologic Sciences at the MCP, Main Clinical Campus, 3300 Henry Ave., Philadelphia, PA 19129; (215) 842-6578. 8–9a

MRI RESEARCHER wanted by Radiological Science Research Center, New England Deaconess Hospital. NMR physicist (postdoctoral) with expertise in 3-D vascular imaging and post-prcocessing techniques. Must have strong background in computers, ability to program pulse sequences, and have experience in fast magnetic resonance imaging. NEDH is an affirmative action and equal opportunity employer. Send CV to Melvin E. Clouse, M.D., Dept.of Radiology, New England Deaconess Hospital, 185 Pilgrim Rd, Boston, MA 02215. 8a

THE DEPT. OF RADIOLOGY AT THE UNIVERSITY OF MASSACHUSETTS MEDICAL CENTER in Worcester has a full-time position available in the musculoskeletal division at the rank of assistant, associate or full professor beginning July 1, 1992. The medical center is a 370-bed university hospital and medical school located approximately 40 miles west of Boston. The dept. consists of 25 staff, 15 residents and 2–4 fellows and does approximately 140,000 exams/yr. The dept. is well-equipped with 2 GE 9800 HiLite CT scanners as well as 2 GE 1.5-T MRI scanners and a 2.0-T small-bore unit for animal research in a stand-alone facility. The hospital is a Level 1 trauma center maintaining a full-time trauma service and an active emergency room with an associated emergency medicine residency of approximately 36 residents. The hospital is serviced by 2 Life Flight helicopters. A strong interest in teaching and collaborative clinical research is desired. Rank and salary are commensurate with experience. For further information contact Edward H. Smith, M.D., Chairman, Dept. of Radiology, University of Massachusetts Medical Center, 55 Lake Ave. North, Worcester, MA 01655; (508) 856-3252. UMMC is an equal opportunity/affirmative action employer. 8–9ap

FLORIDA, STAFF RADIOLOGIST—Opportunity for board-certified/eligible diagnostic radiologist with experience in reading plain films, fluoroscopy, ultrasound, CT, nuclear medicine, and some angiography, in the radiology service at this Dept. of Veterans Affairs (VA) Medical Center. Affiliation in surgery with the University of Florida. Excellent employment benefits including 30 days paid vacation and 15 days paid sick leave per yr; liberal life and health insurance benefits; malpractice insurance; and retirement program. Moving expenses paid. Lake City, Fl., is located in northern Florida with a mild climate yr-round. Extensive outdoor recreational activities, reasonable cost of living no state income tax, fine schools, local community college, and nearby universities provide opportunities for continuing education and cultural diversion. Licensure in any state acceptable. Contact or send CV to Richard Parker, M.D., Chief of Radiology, VA Medical Center, Lake City, FL 32055-5898; (904) 705-3016, ext. 2543. An equal opportunity employer. 8–9a

FACULTY POSITIONS—The University of Colorado Health Sciences Center, Denver, Colorado, is recruiting for faculty in the following positions: Angiography/interventional radiology, body imaging/ultrasound. The level of faculty appointment depends upon prior experience. Candidates interested in working in a stimulating academic and clinical environment are encouraged to send their CV to Michael L. Manco-Johnson, M.D., Professor and Chairman, Dept. of Radiology, University of Colorado Health Sciences Center, Campus Box C-277, 4200 E. Ninth Ave., Denver, CO 80262; (303) 270-7719. The University of Colorado Health Sciences Center is committed to equal opportunity and affirmative action. 8-9a

MAINE—BC/BE diagnostic radiologist with MRI and/or interventional skills. Join well-established multidimensional group. Associate leading to partnership. Competitive financial package. Family oriented small city. Business and cultural center. Major university. One hour to coast. Easy access to ski areas. Send CV to New England Health Search, 63 Forest Ave., Orono, ME 04473; (207) 866-5680.

DIAGNOSTIC RADIOLOGIST with skills in CT, MR, interventional, ultrasound, and nuclear medicine needed to join group of 8 board-certified radiologists. Growing practice in eastern Washington at a 228-bed hospital, a new multimodality imaging center and 1 private office. Potential for long-term practice is excellent. Top-notch school system, including 3 first-rate universities. Excellent hunting, fishing, boating and skiing. Contact Eric W. Koelsch, N. 5901 Lidgerwood, Ste. 18B, Spokane, WA 99207; (509) 487-1264. 8-1ap

THE UNIVERSITY OF CHICAGO has an unexpected opening for a radiology resident with 1 yr of prior residency training. Interested parties should forward their CV to Dr. Larry B. Dixon, Chairman Residency Selection Committee, University of Chicago Hospitals, MC 2026, 5841 S. Maryland Ave., Chicago, IL 60637. You may call for information at (312) 702-3550 or fax your CV to (312) 702-1161. Affirmative action/equal opportunity employer. 8a

WORK HARD AND PLAY HARD IN BEAUTIFUL SANTA FE, NM—Medical director position available at state-of-the-art outpatient imaging center with a 1.5-T Siemens SP MRI, DRH CT scanner, Acuson ultrasound, with R&F and mammography to fill in the gaps. Excellent salary and benefits for the individual willing to be proactive and competitive. Neuroradiologist with extensive MRI training MANDATORY. Call Jim Lester at (505) 983-9350 for more details or send CV to Santa Fe Imaging Center, 1640 Hospital Dr., Santa Fe, NM 87501. 8a

ASSISTANT PROFESSOR RADIOLOGY/CHEMISTRY—The MGH-NMR Center of the Massachusetts General Hospital and Harvard Medical School has an opening for a physician/scientist at the assistant professor level with experience in medical imaging, chemical synthesis and immunology. Candidates should hold the degree of M.D. or M.D., Ph.D., board-certification in radiology, and should have sufficient research experience to demonstrate significant accomplishments and strong promise. Resources are available to develop a strong research program addressing problems in imaging contrast agent design and application. Letters of application should include CV, bibliography, a brief statement (less than 500 words) indicating research activities, 3 letters of recommendation and a notarized copy of degree to be sent to Thomas J. Brady, M.D., Director, MGH-NMR Center, Building 149, 13th St., Charlestown, MA 02129. The Massachusetts General Hospital and Harvard Medical School is an equal opportunity affirmative action employer. Qualified women and minority members are encouraged to apply. 8a

MANCHESTER, KY—Excellent opportunity for BC/BE radiologist to take over existing solo practice at rural hospital in east Kentucky. Call sharing available with radiologist in adjacent community. Adventist Health System Sunbelt, 2400 Bedford Rd., Orlando, FL 32803; (800) 327-9290. 8a

VASCULAR/INTERVENTIONAL RADIOLOGIST—The University of Arizona Dept. of Radiology is recruiting a fellowship-trained vascular/interventional radiologist to join the faculty at the assistant associate professor level. Facilities at the University Hospital (300-bed) and Tucson Veteran's Hospital (300-bed) are state-of-the-art. Income is based on AAMC guidelines, but is negotiable. Contact Gerald D. Pond, M.D., Head, Section of Vascular and Interventional Radiology, University of Arizona Health Sciences Center, Tucson, AZ 85724; (602) 626-6794. Women and minorities are encouraged to apply. The University of Arizona is an EEO/AA employer. Applications will be accepted until position is filled. 8xa

BETH ISRAEL HOSPITAL - BOSTON/HARVARD MEDICAL SCHOOL—Beth Israel Hospital and Harvard Medical School are seeking a professor of radiology to serve as radiologist-in-chief at Beth Israel Hospital. The successful candidate should be a distinguished clinician and investigator in the field of radiology, with recognized achievements as a leader and administrator. The radiologist-in-chief must be capable of organizing and administering a complex hospital dept. including directing a very large clinical service, leading a major scientific research program and directing a radiology training program for medical students, residents and fellows. Reply with CV and statement of research interests to Robert M. Glickman, M.D., Chairman, Dept. of Medicine, Beth Israel Hospital, 330 Brookline Ave., Boston, MA 02215. Harvard Medical School and Beth Israel Hospital are affirmative action equal opportunity employers. Women and minority candidates are encouraged to apply. 8a

CHAIRPERSON DEPT. OF IMAGING CEDARS-SINAI MEDICAL CENTER LOS ANGELES, CA—Cedars-Sinai Medical Center, a 1,120-bed, full-service, acute tertiary-care hospital affiliated with the UCLA School of Medicine, is seeking a chairperson for the dept. of imaging. The dept. of imaging currently has 21 hospital-based physicians, an approved residency and fellowship training program, and major research activity under the direction of the full-time chairperson. The dept. of imaging provides the full range of sophisticated imaging services. Cedars-Sinai Medical Center is seeking an individual with nationally demonstrated leadership capabilities and experience in academic imaging, including research, qualifying for a full-time faculty appointment at the rank of professor at the UCLA School of Medicine. The successful candidate will have demonstrated management ability in an academic health center and knowledge of managed care programs. Excellent communication and collaboration skills are required. Interested applicants should forward a CV to James R. Klinenberg, M.D., Chairman, Search Committee Cedars-Sinai Medical Center, 8700 Beverly Blvd., Rm. 2211, Los Angeles, CA 90048-1869. 8a

RADIOLOGY—Marshfield Clinic Dept. of Radiology is seeking a fellowship-trained or experienced abdominal imager to join its 16 members. Interest in high risk OB ultrasound is desirable. The dept. is subspecialized and provides services to more than 380 clinic physicians in all branches of medicine and surgery. This challenging, state-of-the-art practice opportunity is located in a friendly, small town atmosphere. For additional information, please send CV to William Manor, D.O., Dept. of Radiology, Marshfield Clinic, 1000 North Oak Ave., Marshfield, WI 54449 or call collect at (715) 387-5261. An equal opportunity/affirmative action employer. 8a

VASCULAR/INTERVENTIONAL RADIOLOGIST—Two positions available at the staff level. The practice is based at Boston City Hospital and The University Hospital. The appointment will be at the assistant or associate professor level. The candidate should be interested in teaching; research will be encouraged. Must be eligible for Massachusetts state license. Please send CV and letter of inquiry to Dr. Jerome Shapiro, Chairman, The University Hospital, Dept. of Radiology, 88 E Newton St., Boston, MA 02118; (617) 638-6610. An equal opportunity employer. 8a

EXCELLENT OPPORTUNITY FOR FULL-TIME BREAST IMAGING RADIOLOGIST—The Dept. of Diagnostic Radiology of Henry Ford Hospital in Detroit is seeking a board-certified radiologist with subspecialty training or expertise and experience in breast imaging. The Henry Ford Health System in the Metropolitan Detroit area performs over 35,000 mammograms annually. The Breast Imaging Division also performs breast sonography and fine needle aspiration cytology. We are a subspecialized dept. with large residency and fellowship programs, including mammography. There is opportunity for clinical research. Eligibility for or licensure by the State of Michigan is required. Please contact Murray Rebner, M.D., Director of Breast Imaging, Dept. of Diagnostic Radiology, Henry Ford Hospital, 2799 W. Grand Boulevard, Detroit, MI 48202-2689; (313) 876-1331, fax (313) 876-9134. The Henry Ford Health System is an equal opportunity institution. 8-10 ap.

DIRECTOR, MAMMOGRAPHY—Columbia-Presbyterian Medical Center is offering an outstanding opportunity for a director in mammography in a large and growing program in a major academic center. The mammography suite contains 3 recent vintage GE-CGR units that are ACR accredited. The suite is located near the main lobby of the new Milstein Hospital building where it can conveniently serve outpatients and occasional inpatients. The area is undergoing a major expansion to allow ultrasound, stereotactic biopsy, on-site offices and an expanded film review area to be added. The expanded suite will be virtually adjacent to our new multi-unit MRI suite. There is an active mammography fellowship program, 1 additional staff physician specialized in mammography and a large, excellent residency program. Responsibilities include management of the mammography service, clinical work, teaching and clinical research. Board certification in diagnostic radiology and suitable experience in mammography are required. A NYS medical license is required to practice; narcotics license desirable. Salary and academic rank will be commensurate with qualifications and experience. Please send resume to Philip O. Alderson, M.D., Dept. of Radiology, Columbia-Presbyterian Medical Center, 622 West 168th St., New York, NY 10032. Columbia University is an affirmative action/equal opportunity employer. 8a

NW ROCKY MOUNTAINS—Highly respected 8-person group with strong subspecialty interests seeks highly qualified radiologist. Fellowship or academic experience preferred. Body imaging/MRI or nuclear medicine with boards or ABR special competency strongly desired. Position includes all aspects of radiology. Practice is located in Boise, ID , which has many recreational and cultural amenities. Reply to Paul Traughber, M.D., or J. Tim Hall, M.D., Dept. of Radiology, St Alphonsus Regional Medical Center, 1055 No. Curtis Rd., Boise, ID 83706; (208) 378-2161. 8-1a

GROWING HOSPITAL/OFFICE PRACTICE IN BEAUTIFUL COEUR D' ALENE, ID, 40 MILES EAST OF SPOKANE, WA, is seeking a general radiologist to join 5-man group. All modalities available including MRI. Experienced individuals with subspecialty preferred. Send CV to Peter Semogas, M.D., 1104 Ironwood Dr., Coeur d'Alene, ID 83814. 8-9a

UCSD SCHOOL OF MEDICINE—The Dept. of Radiology is seeking an ultrasonologist to direct clinical service, medical student and resident teaching, and research projects. Participation in other diagnostic subspecialties is available. Qualifications required: Board-eligibility/certification; California medical license; and 1-yr fellowship in ultrasound. Title Series: Associate or full professor (in-residence or clinical series - not currently a tenure-track position); level based on years experience; salary commensurate with rank and step of appointment based on the established salary schedule of the UCSD School of Medicine Faculty Compensation Plan. The University of California, San Diego is an equal opportunity/affirmative action employer. All CV's received prior to September 30, 1992 or thereafter until position is filled will be given full consideration. Send to George R. Leopold, M.D., Professor and Chairman, Dept. of Radiology, 8756, UCSD Medical Center, 225 Dickinson St. San Diego, CA 92103 . 8a

UCSD SCHOOL OF MEDICINE—The Dept. of Radiology at the VA Medical Center is seeking an angio/interventional radiologist to participate in clinical, teaching, and research programs. Qualifications required: Board-eligibility/certification; California medical license; 1-yr fellowship in angio/interventional radiology. Title Series: Assistant/associate professor (in-residence or clinical series - not currently a tenure-track position); level based on years experience; salary commensurate with rank and step of appointment based on the established salary schedule of the UCSD School of Medicine Faculty Compensation Plan. The University of California, San Diego is an equal opportunity/affirmative action employer. All CVs received prior to September 30, 1992, or thereafter until position is filled will be assured full consideration. Send to Lee B. Talner, M.D, Professor of Radiology, Dept. of Radiology -8756, UCSD Medical Center, 225 Dickinson St., San Diego, CA 92103-1990. 8a

Fellowships and Residencies

IMAGING (ULTRASOUND, BODY CT, AND MRI) FELLOWSHIP TO BEGIN JULY 1993—The Dept. of Radiology at The Western Pennsylvania Hospital (a 578-bed advanced, tertiary-care teaching hospital), Pittsburgh, PA, offers a 1-yr imaging fellowship. The fellowship emphasizes diagnostic ultrasound with rotations in body magnetic resonance imaging and computed body tomography. Examinations in all areas of sonography are performed and include obstetrics and gynecology, vascular/Doppler, abdominal, prostate, pediatrics, breast, and small parts. State-of-the-art equipment in all areas of the dept. Fellows will participate in procedures guided by ultrasound and computed tomography. Fellows have ample opportunity to participate in conference presentations and research projects, many of which culminate in publications. Inquiries should be addressed to Marcela Bohm-Velez, M.D., Director of Imaging Fellowship Program, Dept. of Radiology, The Western Pennsylvania Hospital, 4800 Friendship Ave., Pittsburgh, PA 15224. 5–12c

FELLOWSHIPS AT THOMAS JEFFERSON UNIVERSITY HOSPITAL—The Dept. of Radiology at Thomas Jefferson University Hospital in Philadelphia offers the following fellowship programs each yr: (1) Ultrasound/CT/MRI—Jefferson's ultrasound division is one of the largest in the world and performs all currently available exams, including obstetric, vascular, lithotripsy, invasive, and endoluminal. We also operate 4 GE 1.5-T MRI units and 3 CT scanners. Contact Barry Goldberg, M.D. regarding this program. (2) Cardiovascular/interventional—This division is housed in a new suite containing Philips angio units with DSA and performs the full range of vascular and nonvascular interventional procedures. Contact Geoffrey Gardiner, Jr., M.D. (3) Neuro/ENT radiology—very active clinical services supply a wealth of material to this division, which is housed in a neurosciences imaging center containing all imaging modalities. Contact Carlos Gonzales, M.D. (4) Breast imaging—Jefferson's new breast-imaging center performs approximately 85 studies/day including ultrasound and needle localizations. Contact Stephen Feig, M.D. (5) Chest—includes biopsies and CT. Contact Robert Steiner, M.D. (6) MRI—a dedicated body MRI program including excellent research opportunities in addition to a large clinical case load. Contact Donald Mitchell, M.D. (7) Ultrasound—a dedicated ultrasound program. Contact Barry Goldberg, M.D. (8) Musculoskeletal—includes MRI of the musculoskeletal system. Contact David Karasick, M.D. All program directors listed above can be contacted at the Dept. of Radiology, Thomas Jefferson University Hospital, Philadelphia, PA 19107. Jefferson is an equal opportunity/affirmative action employer. 8xc

FELLOWSHIP POSITION: WOMEN'S IMAGING—High-volume breast imaging (mammography, breast ultrasound, interventional procedures) and ultrasound with emphasis on obstetrical and gynecologic sonography. State-of-the-art mammographic and sonographic equipment including stereotactic table and digital capability. Using stereotactic, ultrasound, or mammographic guidance, all breast interventional procedures are performed, including fine needle and core biopsies, cyst aspirations, presurgical localizations, and galactography. Elective time in MRI, CT, and related clinical specialties (surgery, pathology, obstetrics-gynecology). One-year fellowship to start in July 1993. Fellows also have the opportunity to participate in teaching, conference presentations, and research projects, many of which culminate in publications. Inquiries should be addressed to Ellen B. Mendelson, M.D., Chief, Mammography and Women's Imaging, The Western Pennsylvania Hospital, 4800 Friendship Ave., Pittsburgh, PA 15224. 5–12c

ADVANCED IMAGING FELLOWSHIP—The Dept. of Radiology and The Graduate Hospital Imaging Center are offering a 1-yr advanced imaging fellowship to include MR, CT and ultrasound. Positions are available for July 1993 and July 1994. MR and CT imaging time will be spent performing both body and neuro studies. Facilities include 2 state-of-the-art GE 1.5-T MR scanners with phased array coils, endorectal MR and MRA. Ultrasound includes color flow Doppler. CTs include Elscint 2400 Elite and GE 9800. Candidates must have completed an approved 4-year residency prior to commencing the fellowship. Board-eligibility is a requirement. Salary will be at a PGY-5 level. Interested candidates should apply to Jerome G. Jacobstein, M.D., Chairman, Dept. of Radiology, The Graduate Hospital, One Graduate Plaza, Philadelphia, PA 19146; (215) 893-2050. 7–8cp

FELLOWSHIPS AT ALBANY MEDICAL CENTER—The newly-renovated and equipped Dept. of Radiology at the Albany Medical College and Center in Albany, NY, offers the following fellowship positions each yr: (1) Abdominal Imaging—This fellowship encompasses all aspects of MRI, ultrasound, CT, and other advanced techniques in imaging the abdomen. Four state-of-the-art MRI and 4 CT scanners as well as 5 color Doppler ultrasound units are utilized daily. Contact James C. Peters, M.D. regarding this program. (2) Neuroradiology—This fellowship encompasses the full range of advanced neuro imaging including MRI, CT, angiography, and myelography. Contact William A. Wagle, M.D. (3) Angiography and interventional radiology—Three advanced angiographic suites are utilized daily for a full range of vascular and interventional procedures. Contact Mohammad S. Sarrafizadeh, M.D. All program directors listed above may be contacted at the Dept. of Radiology, A-113, Albany Medical Center, Albany, NY 12208; (518) 445-3277 or contact Matthew D. Rifkin, M.D., Chairman, Dept. of Radiology, A-113, at the above address. Albany Medical Center is an equal opportunity/affirmative action employer. 1–12c

ONCORADIOLOGY/MAMMOGRAPHY FELLOWSHIP—The Dept. of Radiology at the Dana-Farber Cancer Institute and Brigham and Women's Hospital, which are Harvard Medical School affiliates, offers a 1-yr fellowship position beginning July 1, 1993. All imaging modalities involved in the diagnosis, staging, and follow-up of patients with malignant disease are integrated into this program. An additional feature is a concentrated experience in the performance of interventional breast diagnostic procedures. Please contact Jack E. Meyer, M.D., Director of Diagnostic Radiology, Brigham and Women's Hospital and Dana-Farber Cancer Institute, 75 Francis St., Boston, MA 02115; (617) 732-6269. Brigham and Women's Hospital/Dana Farber Cancer Institute/Harvard Medical School is an affirmative action/equal opportunity educator and employer. 5–4c

FELLOWSHIP IN VASCULAR AND INTERVENTIONAL RADIOLOGY—The University of Arizona is sponsoring a 1-yr fellowship in vascular and interventional radiology beginning July 1, 1994. In depth clinical experience and training in all aspects of interventional radiology will be offered. Facilities at the University Hospital (300-bed) and Tucson Veterans Hospital (300-bed) are state-of-the-art. Interested applicants should submit a current CV and 3 letters of recommendation (including one from their program director) to Gerald D. Pond, M.D., Head, Section of Vascular and Interventional Radiology, University of Arizona Health Sciences Center, Tucson, AZ 85724. For further information please contact Ruth Kneup at (602) 626-6794. 8xc

FELLOWSHIP POSITIONS—The Dept. of Radiology of the Brigham and Women's Hospital-Harvard Medical School has 1- or 2-yr fellowship positions in the following areas: (1) cardiovascular and interventional, (2) neuroradiology, (3) CT/ultrasound/MR/interventional, (4) oncoradiology, (5) chest, (6) bone, (7) nuclear medicine, and (8) computer science. For more information, please send CV specifying your area of interest to B. Leonard Holman, M.D., Chairman, Dept. of Radiology, Brigham and Women's Hospital, 75 Francis St., Boston, MA 02115. Harvard Medical School and Brigham and Women's Hospital are equal opportunity, affirmative action employers. 5–4c

VASCULAR/INTERVENTIONAL RADIOLOGY FELLOWSHIP—Temple University Hospital and School of Medicine has available a 1-yr fellowship beginning July 1, 1992. The candidate will have exposure to all areas of vascular and interventional radiology including noninvasive techniques and MRI/A. Applicants should contact, David S. Ball, D.O., Chief, Section of Vascular/Interventional Radiology, Dept. of Diagnostic Imaging, Temple University Hospital, 3401 N. Broad St., Philadelphia, PA 19140. Temple University Hospital and School of Medicine is an affirmative action/equal opportunity employer. 8xc

FELLOWSHIP IN IMAGING/ANGIO-INTERVENTIONAL—A 1-yr fellowship program at Lehigh Valley Hospital in Allentown, PA., is available. LVH is a 492-bed acute-care, university affiliated hospital. The fellowship program offers training in CT (head and body), ultrasound, MR, angiography, and interventional radiology. For further information contact Robert Kricun, M.D., Dept. of Radiology, Lehigh Valley Hospital P.O. Box 689, Allentown, PA. 18105-1556. 7–9c

ACCREDITED FELLOWSHIPS IN PEDIATRIC RADIOLOGY AND PEDIATRIC NEURORADIOLOGY—Dept. of Radiology, Children's Hospital Medical Center, Cincinnati, OH, offers 1- or 2-yr accredited (Residency Review Committee for Radiology of ACGME) fellowships in pediatric radiology beginning July 1, 1994. A 1-yr pediatric neuroradiology fellowship program is also offered and may be taken separately or combined with 1 yr of adult neuroradiology fellowship at the University of Cincinnati Medical Center. Children's Hospital Medical Center (CHMC) is a 355-bed institution. The dept. performs over 105,000 radiological exams/yr in the largest children's hospital and ambulatory practice in the U.S. The dept. has 14 full-time faculty pediatric radiologists, 1 full-time research faculty, 7 fellows, and many resident trainees. Six pediatric radiology and 1 pediatric neuroradiology fellowship positions are available annually. Training includes all aspects of pediatric imaging neonatal radiology; neuroimaging; musculoskeletal radiology; cardiovascular and thoracic imaging; abdominal imaging; oncologic imaging; ultrasonography; nuclear medicine; computed tomography; MRI; and vascular/interventional procedures. The dept. has an active clinical service with state-of-the-art equipment as follows: digital fluoroscopy; Acuson and ATL ultrasound units with Doppler and color flow Doppler capabilities; planar SPECT gamma cameras; GE 9800 Quick CT scanner; 1.5-T GE MRI with spectroscopy, and cardiac catheterization/angiographic suite with digital vascular imaging. The fellowship provides a broad clinical experience in pediatric radiology as well as numerous opportunities to participate in both clinical and basic research. Candidates must be board-certified or board-qualified in diagnostic radiology and must obtain an Ohio medical license. Salary and fringe benefits are highly competitive. Applications are due prior to February 1993 with interviews scheduled during the fall and winter of 1992–93. There are numerous career opportunities in pediatric radiology and pediatric neuroradiology in both academic and private practice settings. To receive more information about the fellowships at CHMC or careers in pediatric radiology, please contact Director, Dept. of Radiology, Children's Hospital Medical Center, Cincinnati, OH 45229-2899; (513) 559-8058. Children's Hospital Medical Center and the University of Cincinnati College of Medicine are affirmative action/equal opportunity employers. 7–1cp

FELLOWSHIP IN VASCULAR/INTERVENTIONAL RADIOLOGY—Boston University Dept. of Radiology has an opening for a fellowship in vascular/interventional radiology to begin July 1993. The dept. is based at Boston City Hospital and The University Hospital. The candidate must be eligible for Massachusetts state license and must be interested in teaching research. This is a full academic program, providing training and experience in all aspects of vascular interventional radiology. Send a CV and letter of inquiry to Dr. Anthony Carter, The University Hospital, Dept. of Radiology, 88 E. Newton St., Boston, MA 02118; (617) 638-6610. An equal opportunity employer. 8c

EXCITING RADIOLOGIST OPPORTUNITIES NATIONWIDE!—Now is the time to make your move! ABSOLUTELY NO COST TO YOU. We specialize in RADIOLOGY only, so we understand your needs. Positions from Sunbelt to Northern-most regions. Both salaried and private practice opportunities with top money offered. Utilizing the Snelling Search Computer Network. We know of the positions first and give you the inside tracks! Fax your CV to (214) 258-1092, or mail to Snelling Search Medical Group. 1303 Walnut Hill Lane, Ste. 103, Irving, TX 75038. For information on specific positions call toll free (800) 259-5973. Ask for Roman. 8a

FELLOWSHIP PROGRAM IN INTERVENTIONAL RADIOLOGY—The fellowship offered is a 1-yr training program in interventional radiology. A high volume of studies provides excellent experience for the fellowship training program. The 1-yr appointment is intensive, supervised, and allows for graded responsibility in performance and interpretation of studies including angioplasty, atherectomy, arterial and biliary stents, and all drainage procedures. The fellowship training involves performance of interventional procedures under sonographic and CT guidance as well as fluoroscopy. Inquiries should be addressed to Gordon K. McLean, M.D., Director, Interventional Radiology, The Western Pennsylvania Hospital, 4800 Friendship Ave., Pittsburgh, PA 15224. 5–12c

MRI FELLOWSHIP—One-yr position is available in 1993 for fellow in MRI. The fellowship encompasses all phases of MR (musculoskeletal, body and neuro) as well as magnetic resonance angiography (including phase contrast, time-of-flight and magnitude phase contrast MRA). Over 12,000 MRIs are performed and interpreted annually as a part of this fellowship with direct one-on-one supervision. The fellowship also includes 20–30% CT; additionally, the option to obtain independent, full American Board of Nuclear Medicine certification is available. MR studies are divided between approximately 45% neuro and 55% body and musculoskeletal, including all joints and body parts. For further information contact Stephen J. Pomeranz, M.D; (513) 281-3400, and ask for Chris or Jill. 7–9cp

FELLOWSHIP IN NEURORADIOLOGY—One fellowship position in neuroradiology is available July 1, 1993, in the Dept. of Radiology at New England Medical Center Hospitals, Boston, MA. The hospital is the teaching unit of Tufts University School of Medicine. The program is for 1 or 2 yrs, and includes both adult and pediatric case material. The fellowship is accredited by the Accreditation Council for Graduate Medical Education. The fellow will be trained in the technique and interpretation of carotid and vertebral angiography as well as myelography. Computed tomography and MRI of the head and spine form major components of the neuroradiology service, as does interventional neuroradiology. Neuroradiological services at the New England Medical Center Hospitals are carried out in liaison with the Depts. of Neurology, Neurosurgery, and Pediatric Neurology. Joint radiological and clinical conferences are held frequently and, within a short time, the applicants will have considerable exposure to an array of neuroradiological material. The Dept. of Neuropathology also runs conferences, allowing correlation to be made between radiological interpretation and pathology. Interested applicants should call (617) 956-6333, or write to Samuel M. Wolpert, M.D., Professor of Radiology & Neurology, Director, Neuroradiology Fellowship Program, Dept. of Radiology, 750 Washington St., Boston, MA 02111. 7–8cp

UNEXPECTED OPENING FOR FELLOWSHIP IN CARDIOVASCULAR-INTERVENTIONAL RADIOLOGY—Available July 1, 1992, 1-yr fellowship program is available at a 750-bed teaching hospital. Extensive clinical experience involving all aspects of cardiovascular imaging, interventional vascular, and nonvascular procedures. Availability for clinical or animal research. Send CV and inquiries to Oscar H. Gulierrez, M.D., Dept. of Radiology, Box 648, University of Rochester Medical Center, Rochester, NY 14642. AA/EO/M-F employer. 8–10c

FELLOWSHIP IN PEDIATRIC RADIOLOGY—University of Arkansas for Medical Sciences offers a 1-yr fellowship in pediatric radiology at Arkansas Children's Hospital. Training includes all aspects of pediatric imaging including: plain films, digital fluoroscopy, neonatal radiology (ECMO); a very active neuroradiology service (GE 9800 Quick Highlight CT Scanner, GE 1.5-T MRI with MRA), nuclear medicine (with SPECT); interventional procedures; angiography; and state-of-the-art ultrasound with color flow Doppler. There is opportunity to participate in clinical or basic research if desired. Arkansas Children's Hospital is a 300-bed hospital which serves as the only pediatric tertiary referral care facility for the community. Little Rock/Central Arkansas provides ample recreational and cultural opportunities. UAMS is an equal opportunity employer. Please direct inquiries to Joanna Seibert, M.D., Director, Dept. of Radiology, Arkansas Children's Hospital, 800 Marshall St., Little Rock, AR 72202; (501) 320-1175. 8,10,12c

Tutorials/Courses

FOURTH ANNUAL CONFERENCE ON ADVANCED INTERVENTIONAL TECHNIQUES FOR PERIPHERAL VASCULAR DISEASE—SEPT. 16–19, 1992; Hyatt Regency Oak Brook, Oak Brook, IL. Course Director is Amir Motarjeme, M.D. Contact Karin Bodenhagen, R.N., Midwest Vascular Institute of Illinois, 3815 Highland Ave., Downers Grove, IL 60515; (708) 963-0660, (708) 963-8348 (fax). 8d

KONA, HI 1992—Seventeenth Annual International Body Imaging Congress, Oct. 10–17. CME 1. Mauni Lani Bay Hotel. Contact Medical Seminars International, Inc., 18981 Ventura Blvd., Ste. 303, Tarzana, CA 91356; (818) 774-9077, fax (818) 774-0244. 5–10d

MUSCULOSKELETAL MRI, SECOND ANNUAL LOS ANGELES CONFERENCE, SEPT. 19–20, 1992—Faculty: Drs. Bradley, Brant-Zawadzki, Dietrich, Friedman, Harms, Resnick, Schlesinger. Medical Seminars International, Inc., 18981 Ventura Blvd., #303, Tarzana, CA 91356; (818) 774-9077, fax (818) 774-0244. 4–9d

DIAGNOSTIC IMAGING IN ARUBA—The Dept. of Radiology, Cornell University Medical College and The New York Hospital will present the 18th annual postgraduate course, Diagnostic Imaging, January 31 – 5, 1993 at the Hyatt Regency Hotel in Aruba. Category I credit: 30 hrs. Fee: Physicians, $495; residents, fellows and technologists $295. Information: Ms. Julia Anne Mala, Radiology, Cornell University Medical College, 1300 York Ave., New York, NY 10021; (212) 746-2522. 8d

New Business Office for AJR

All inquires and correspondence regarding classified ads should be sent to:

AJR Classifieds
1891 Preston White Drive
Reston, VA 22091
Attn: Terry Fitterer
Phone: (703) 648-8992
FAX: (703) 264-8863

General Information

The American Roentgen Ray Society, founded in 1900, has been a forum for progress in radiology since shortly after the discovery of the x-ray. From its beginning and continuing today, the ARRS has been guided by dedication to the goal of the advancement of medicine through the science of radiology and its allied sciences.

The goal of the ARRS is maintained through an annual scientific and educational meeting and through publication of the *American Journal of Roentgenology*.

The annual meeting consists of instructional courses, scientific sessions, a symposium, scientific exhibits, and commercial exhibits. A special categorical course is also offered. Category I CME credits are available on an hour-for-hour basis.

The monthly *American Journal of Roentgenology* is a highly respected peer review journal with a worldwide circulation of more than 23,000. For more than 75 years the AJR has been accepted as one of the best specialty journals available in the world.

The quarterly ARRS *Memo* newsletter keeps members informed of annual meeting plans and general Society information.

Application Instructions

Candidates for Active Membership

An Active member must be a graduate of an approved medical school or hold an advanced degree in one of the physical, chemical, or biological sciences and be certified by the American Board of Radiology, the American Osteopathic Board of Radiology, or the Royal College of Physicians of Canada or document training and credentials that are adequate to qualify for membership. Active members must actively practice radiology or one of its branches in the United States or Canada. Such members are eligible to participate in all activities of the Society, including membership on committees, and have full voting privileges.

Application must be on an official form signed by the applicant. Applications will be received and processed by the administrative office of the Society throughout the year. Processing of applications will include review of credentials and verification of board certification by the appropriate American medical specialty board or the Secretary of the Royal College of Physicians and Surgeons of Canada. A list of candidates for Active membership whose applications have been received and processed during the preceding three months will be published quarterly by the Society. Members of the Society may voice objections to such applicants to the administrative office by mail within 30 days of such publication. If no objections are received by the administrative office within the 30-day period, such applicants will become Active members on the following January 1, April 1, July 1, or October 1.

Annual dues are currently $150, payable on January 1 of each year. Of this amount, $50 is allocated for subscription to the *AJR*; $5 is allocated for subscription to the *Memo*. Annual dues for new Active members will be prorated for whatever portion of the calendar year remains after membership becomes effective. In subsequent years annual dues will be assessed and payable on January 1 of each year.

Candidates for International Membership

An International member must meet the qualifications of Active membership but reside and practice in a foreign country. International members have special consideration in fees and subscription rates to the *AJR*. International members cannot hold Society offices or vote. Dues are payable in U.S. funds.

Candidates for In-Training Membership

In-Training members must be serving in a radiology residency or a post-residency fellowship program approved by the Radiology Residency Review Committee of the American Council of Graduate Medical Education or the American Osteopathic Board of Radiology or be a postgraduate student in an allied science. In-Training members have special consideration in fees and subscription rates to the *AJR*. In-Training members cannot hold Society offices or vote.

Application must be on an official form signed by the applicant, with training status verified by the program director. Applications will be processed by the administrative offices of the Society throughout the year, and membership will become effective on January 1 or July 1, whichever date is closest to the date the application is received.

In-Training member status will be limited to a maximum of six years, starting with the entrance date into the radiology residency. In the sixth or final year, In-Training members will receive an application for transfer to Active membership. Those who do not respond with a completed application to transfer by October 1 of the year their residency or fellowship is completed will be dropped from membership but may later apply as a new member through the process outlined for Active membership.

There is no application fee for In-Training members. Annual dues are $25. Membership includes a subscription to the *AJR* and admission to the annual meeting without payment of the registration fee.

Candidates for International In-Training Membership

An International In-Training member must meet the qualifications of In-Training membership but reside and practice in a foreign country. International In-Training members have special consideration in fees and subscription rates to the *AJR*. International In-Training members cannot hold Society offices or vote. Dues are payable in U.S. funds.

Candidates for Introductory In-Training Membership

Introductory In-Training members must be first year residents serving in an approved radiology residency program. Candidates must meet the same criteria as In-Training members. Introductory In-Training members have special consideration in fees and subscription rates to the *AJR*. Introductory In-Training members cannot vote or hold elective office.

Candidates for Introductory In-Training membership must submit a completed membership application to the administrative office during the enrollment period held each year between July 1 and September 30. At the completion of the first year of residency, the Society will send each Introductory In-Training member an invitation to transfer to regular In-Training membership. Introductory In-Training members who do not respond to this invitation to transfer will be dropped from the roll of membership but may reapply at any time during their residency.

ALL APPLICANTS

1. **Do not remit application fee or dues until requested.**
2. **Send completed form to:** **American Roentgen Ray Society**
   1891 Preston White Drive
   Reston, VA 22091

For ARRS Office Use
Date Received _____
I.D.# _____

American Roentgen Ray Society
APPLICATION FOR MEMBERSHIP

Date _____

Category of Membership: ❑ Active ❑ In-Training ❑ International ❑ International In-Training ❑ Introductory In-Training

Name (Please Print) _____ Degree(s) _____
(First) (Initial) (Last)

Mailing Address _____ Date of Birth _____
(Street/Box)

_____ Telephone _____
(City/State/Country) (Zip Code)

DETACH HERE

A Education (List name of institution, years attended, and degree and type received.)

Undergraduate: _____

_____

Graduate (Medical School, Graduate School, etc.):

_____

_____

Postgraduate (Internship, Residency, Fellowship, etc.):

_____

_____

_____

B Licensure

Licensed to practice _____ in _____ since _____
(Type) (State, Province, etc.)

C. Appointments/Memberships (In-Training applicants: skip to Section E on reverse.)

Present Appointments: Academic _____

_____

Hospitals _____

_____

Membership in Scientific Societies: _____

_____

Offices or Committee Assignments: _____

_____

Government Service (Military or Civilian): _____
(Position) (Years)

Active Member candidates on active military service or full time in Veterans Administration hospitals can obtain reduced dues. Do you qualify? ❑ Yes ❑ No

DETACH HERE

CONTINUED ON REVERSE SIDE

D. Credentials: (To be completed by Active and International applicants only.)

I hereby certify that I was issued a certificate of qualification in _____ (Specialty)

in _____ (Year) by the _____ (Name of Qualifying Board)

Other Credentials: _____

Signature: _____

E. In-Training applicants must complete this section.

I certify that I am serving as a Resident/Fellow in _____ (Specialty)

at _____ (Name of Institution) Date program began (begins): _____

Date program to end _____ I understand that in-traing membership is limited to a maximum of 6 yrs.

Applicant Signature: _____

Verification: (Program Director of Department Chairman only)

I certify that this applicant is in training at the institution named and qualifies for enrollment as a member-in-training of the American Roentgen Ray Society.

Name (Please Print) _____

Address _____

_____

Signature _____

Send completed form to:

American Roentgen Ray Society • 1891 Preston White Drive • Reston, Virginia 22091

Call for Scientific Papers

American Roentgen Ray Society
1993 Annual Meeting
April 25 – 30, 1993
San Francisco, CA

Final No.

Date Received

Tracking No.

ADDRESS OF PRESENTING AUTHOR

Department

Institution

Street

City State Zip

Phone

Type title, authors, and abstract in the space provided below. (Instructions are on reverse side of this page. Abstract should not exceed 300 words.)

Select one category: ❑ Angio/Interventional ❑ Breast ❑ Sonography ❑ CT ❑ Gastrointestinal Tract ❑ Genitourinary Tract
❑ Neuroradiology ❑ Skeletal ❑ Chest ❑ MR ❑ Pediatrics ❑ Medical Physics

Projection Requirements: ❑ 35mm– single or double (circle one) ❑ 16mm silent film ❑ VHS (½") ❑ VHS (¾")

Has this been presented elsewhere? ❑ Yes ❑ No If yes, where? _____

Instructions for Scientific Paper Abstracts

1. Type information single-spaced. Underline the name of the presenting author. Append as a last line of the abstract any research grant support, if applicable (e.g. Supported by USPHS Grant HE-80144). If the abstract is accepted, it will appear in the program book exactly as typed. Use the following format:

    MR IMAGING OF THE SPINE AND NECK
    F.S. Lau, M.D., A.N. Kirk, M.D., R.A. Beck, Ph.D.
    University of California, Bakersfield, Bakersfield, CA 92338

2. Abstracts should include four paragraphs devoted sequentially to the following topics: (1) object or purpose of the study; (2) materials, methods and procedures; (3) results; and (4) significance of the results and conclusions. The text should not exceed 300 words. Specific data are essential. The abstract should be a succinct summary of work done rather than a promissory note.

3. The Scientific Program Committee will grade each abstract and determine acceptance. Letters indicating acceptance or rejection will be mailed to all applicants in mid-January, together with meeting registration information.

Deadline for submission of abstracts is November 1, 1992. Mail **one** copy of abstract to

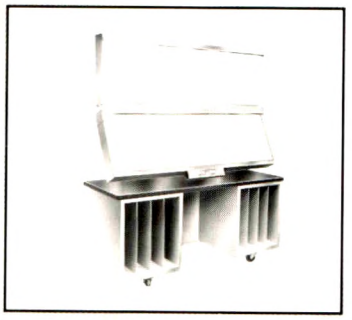
ARRS President-Elect
c/o Susan Roberts, Projects Manager
American Roentgen Ray Society
1891 Preston White Drive
Reston, VA 22091

Although mail submission is preferable, abstracts will be accepted by fax at (703) 264-8863. When faxing an application, **do not** mail a confirmation copy, as this results in unnecessary duplication of paper work.

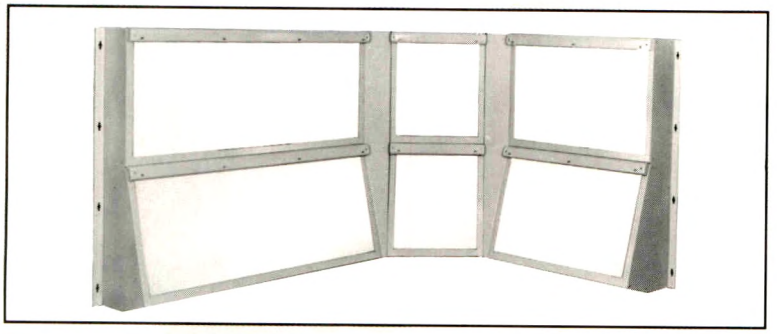
X-RAY ACCESSORIES

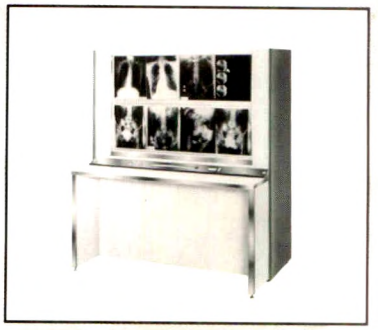
The Difference is Clear



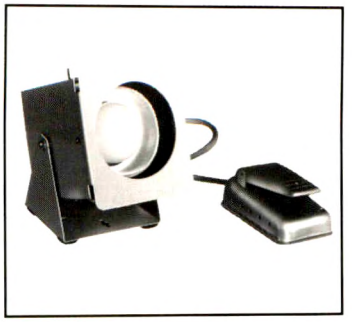


Tried, tested and trusted for over 40 years, S & S x-ray products deliver maximum proficiency and economy -- backed by quality, dependability and innovation.









- **X-RAY** Film Viewers
- **X-RAY** Protection
- **X-RAY** Files
- **X-RAY** Darkroom Equipment
- **X-RAY** Cabinets
- **X-RAY** Accessories

For a FREE copy of our fully illustrated, 100+ page catalog, contact S & S directly or your local x-ray dealer.



1101 Linwood Street
Brooklyn, N.Y. 11208

Phone: 718/649-8500
FAX: 718/257-0219
Toll Free: 800/347-XRAY

S&S X-RAY PRODUCTS
Factories in NY, NC, PA, TX

Volume 159 American Journal of Roentgenology August 1992

REVIEW ARTICLES

245 **Stress fractures: current concepts.** *Daffner RH, Pavlov H*

253 **Infertility in women: diagnostic evaluation with hysterosalpingography and other imaging techniques.** *Krysiewicz S*

CARDIOPULMONARY RADIOLOGY

263 **Pulmonary artery disease in Takayasu's arteritis: angiographic findings.** *Yamada I, Shibuya H, Matsubara O, et al.*

271 **CT evidence for the "osseous pinch" mechanism of traumatic aortic injury.** *Cohen AM, Crass JR, Thomas HA, Fisher RG, Jacobs DG*

275 **Pictorial essay. High-resolution CT of bronchioloalveolar carcinoma.** *Adler B, Padley S, Miller RR, Müller NL*

279 **Pictorial essay. Intrathoracic neurogenic tumors: MR-pathologic correlation.** *Sakai F, Sone S, Kiyono K, et al.*

285 **Case report. Transesophageal echocardiography for the evaluation of atherosclerosis of the thoracic aorta.** *Singer RA, Karalis DG, Procacci PM, Naide D, Ross JJ Jr, Chandrasekaran K*

BREAST RADIOLOGY

287 **Interval carcinomas in the Malmö mammographic screening trial: radiographic appearance and prognostic considerations.** *Ikeda DM, Andersson I, Wattsgård C, Janzon L, Linell F*

295 **Evaluation of mammographic image quality: pilot study comparing five methods.** *Caldwell CB, Fishell EK, Jong RA, Weiser WJ, Yaffe MJ*

GASTROINTESTINAL RADIOLOGY

303 **Duodenal neoplasms: predictive value of CT for determining malignancy and tumor resectability.** *Kazerooni EA, Quint LE, Francis IR*

311 **Pictorial essay. CT findings in patients with small-bowel transplants.** *Bach DB, Levin MF, Vellet AD, et al.*

317 **Persistence of portosystemic collaterals and splenomegaly on CT after orthotopic liver transplantation.** *Chezmar JL, Redvanly RD, Nelson RC, Henderson JM*

321 **Calcifications in the portal venous system: comparison of plain films, sonography, and CT.** *Ayuso C, Luburich P, Vilana R, Bru C, Bruix J*

325 **Abnormalities of the gallbladder after extracorporeal shock-wave lithotripsy: imaging findings.** *Torres WE, Baumgartner BR, Casarella WJ*

329 **Case report. Disappearing "gallstones": biliary pseudolithiasis complicating ceftriaxone therapy.** *Kirejczyk WM, Crowe HM, Mackay IM, Quintiliani R, Cronin EB*

331 **Case report. Thickened bile duct wall simulating ductal dilatation on sonography.** *Middleton WD, Surratt RS*

333 **Case report. Splenosis: superparamagnetic iron oxide–enhanced MR imaging.** *Storm BL, Abbitt PL, Allen DA, Ros PR*

GENITOURINARY RADIOLOGY

337 **The seminal tract in patients with ejaculatory dysfunction: MR imaging with an endorectal surface coil.** *Schnall MD, Pollack HM, Van Arsdalen K, Kressel HY*

343 **Case report. Use of transperineal hydrosonovaginography to show an incomplete vaginal septum.** *Folio L, Rosenberg HK, Frishmuth GJ*

MUSCULOSKELETAL RADIOLOGY

345 **Pictorial essay. Radiologic findings of diseases involving the maxilla and mandible.** *Underhill TE, Katz JO, Pope TL, Dunlap CL*

351 **Width of the articular cartilage of the hip: quantification by using fat-suppression spin-echo MR imaging in cadavers.** *Hodler J, Trudell D, Pathria MN, Resnick D*

357 **The cruciate ligaments of the knee: correlation between MR appearance and gross and histologic findings in cadaveric specimens.** *Hodler J, Haghighi P, Trudell D, Resnick D*

361 **Pictorial essay. Knee effusion: normal distribution of fluid.** *Schweitzer ME, Falk A, Berthoty D, Mitchell M, Resnick D*

NEURORADIOLOGY

365 **Value of acute-phase angiography in the detection of vascular injuries caused by gunshot wounds to the head: analysis of 12 cases.** *Jinkins JR, Dadsetan MR, Sener RN, Desai S, Williams RG*

369 **MR angiography of the head and neck: value of two-dimensional phase-contrast projection technique.** *Applegate GR, Talagala SL, Applegate LJ*

375 **MR imaging of the pituitary stalk: size, shape, and enhancement pattern.** *Simmons GE, Suchnicki JE, Rak KM, Damiano TR*

379 **Hypertensive encephalopathy: findings on CT, MR imaging, and SPECT imaging in 14 cases.** *Schwartz RB, Jones KM, Kalina P, et al.*

385 **Gadopentetate dimeglumine–enhanced MR imaging of the postoperative lumbar spine: comparison of fat-suppressed and conventional T1-weighted images.** *Mirowitz SA, Shady KL*

391 **Case report. Ganglioglioma with leptomeningeal and subarachnoid spread: results of CT, MR, and PET imaging.** *Tien RD, Tuori SL, Pulkingham N, Burger PC*

395 **Pictorial essay. Fast spin-echo high-resolution MR imaging of the inner ear.** *Tien RD, Felsberg GJ, Macfall J*

399 **Case report. Primary endodermal sinus tumor of the orbit: MR findings.** *Appignani BA, Jones KM, Barnes PD*

403 **Case report. Diagnosis of von Hippel–Lindau disease in a patient with blindness resulting from bilateral optic nerve hemangioblastomas.** *Ginzburg BM, Montanera WJ, Tyndel FJ, et al.*

INTERVENTIONAL RADIOLOGY

407 **Influence of the stopcock on the efficiency of percutaneous drainage catheters: laboratory evaluation.** *D'Agostino HB, Park Y, Moyers JP, et al.*

411 **Case report. Percutaneous extraction of biliary stones: value of endoluminal sonography.** *Lossef SV, Garra BS, Barth KH, Zeman RK*

ECONOMICS

413 **Perspective. Desperately seeking reimbursement.** *Dickes L*

MEMO TO READERS

415 **Report of the Editor, 1991.** *Berk RN*

MEETING NEWS

419 **The American Institute of Ultrasound in Medicine: 36th annual convention, March 1992.** *Whalen E*

OTHER CONTENT

262 **Medicine in American art.** *Schatzki SC*

269 **1993 ARRS scholarship announcement**

270 **Announcement of recipients of 1992 ARRS scholarships**

278 **Radiologic-pathologic conference.** *Brown JH, Chew FS*

284 **Ina L. D. Tonkin, AFIP Distinguished Scientist.** *Buck JL*

302 **Figley Fellowship announcement**

309 **List of book and videotape reviews**

324 **ARRS 1993 residents' award papers information**

364 **History page.** *Doby T*

410 **Memorial. Richard Schatzki**

426 **Forthcoming articles**

427 **Letters**

437 **Review of current literature**

441 **News**

444 **1993 ARRS meeting information**

445 **Classified advertisements**

452 **ARRS membership information and application**
Call for papers and exhibits for 1993 ARRS meeting

A-4 ***AJR* business and subscriber information**

A-13 **Guidelines for authors**